VISIT…

DRUGS AND THE PHARMACEUTICAL SCIENCES VOLUME 192

SECOND EDITION

Polymorphism in Pharmaceutical Solids

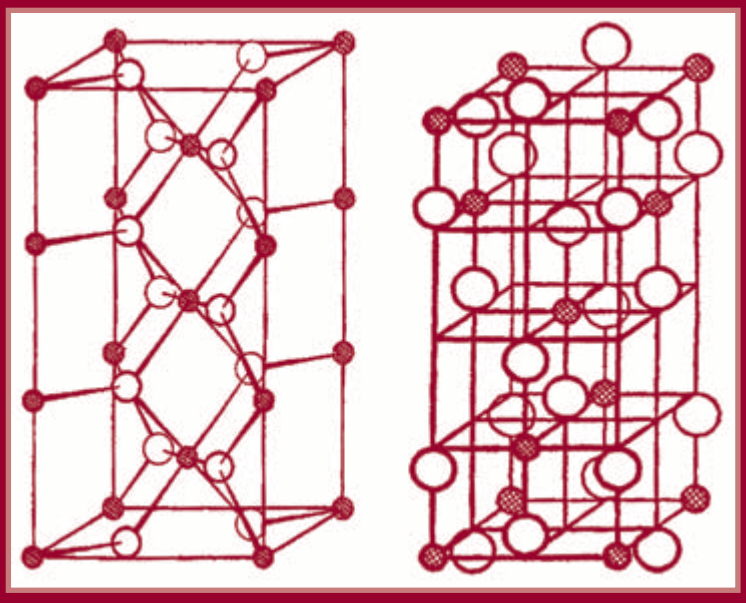

edited by

Harry G. Brittain

informa
healthcare

Polymorphism in Pharmaceutical Solids

DRUGS AND THE PHARMACEUTICAL SCIENCES
A Series of Textbooks and Monographs

Executive Editor

James Swarbrick
PharmaceuTech, Inc.
Pinehurst, North Carolina

Advisory Board

Larry L. Augsburger
University of Maryland
Baltimore, Maryland

Jennifer B. Dressman
University of Frankfurt Institute of
Pharmaceutical Technology
Frankfurt, Germany

Anthony J. Hickey
University of North Carolina
School of Pharmacy
Chapel Hill, North Carolina

Ajaz Hussain
Sandoz
Princeton, New Jersey

Joseph W. Polli
GlaxoSmithKline
Research Triangle Park
North Carolina

Stephen G. Schulman
University of Florida
Gainesville, Florida

Yuichi Sugiyama
University of Tokyo, Tokyo, Japan

Geoffrey T. Tucker
University of Sheffield
Royal Hallamshire Hospital
Sheffield, United Kingdom

Harry G. Brittain
Center for Pharmaceutical Physics
Milford, New Jersey

Robert Gurny
Universite de Geneve
Geneve, Switzerland

Jeffrey A. Hughes
University of Florida College
of Pharmacy
Gainesville, Florida

Vincent H. L. Lee
US FDA Center for Drug
Evaluation and Research
Los Angeles, California

Kinam Park
Purdue University
West Lafayette, Indiana

Jerome P. Skelly
Alexandria, Virginia

Elizabeth M. Topp
University of Kansas
Lawrence, Kansas

Peter York
University of Bradford
School of Pharmacy
Bradford, United Kingdom

For information on volumes 1–149 in the *Drugs and the Pharmaceutical Science* Series, please visit www.informahealthcare.com

150. Laboratory Auditing for Quality and Regulatory Compliance, *Donald Singer, Raluca-loana Stefan, and Jacobus van Staden*
151. Active Pharmaceutical Ingredients: Development, Manufacturing, and Regulation, *edited by Stanley Nusim*
152. Preclinical Drug Development, *edited by Mark C. Rogge and David R. Taft*
153. Pharmaceutical Stress Testing: Predicting Drug Degradation, *edited by Steven W. Baertschi*
154. Handbook of Pharmaceutical Granulation Technology: Second Edition, *edited by Dilip M. Parikh*
155. Percutaneous Absorption: Drugs–Cosmetics–Mechanisms–Methodology, Fourth Edition, *edited by Robert L. Bronaugh and Howard I. Maibach*
156. Pharmacogenomics: Second Edition, *edited by Werner Kalow, Urs A. Meyer, and Rachel F. Tyndale*
157. Pharmaceutical Process Scale-Up, Second Edition, *edited by Michael Levin*
158. Microencapsulation: Methods and Industrial Applications, Second Edition, *edited by Simon Benita*
159. Nanoparticle Technology for Drug Delivery, *edited by Ram B. Gupta and Uday B. Kompella*
160. Spectroscopy of Pharmaceutical Solids, *edited by Harry G. Brittain*
161. Dose Optimization in Drug Development, *edited by Rajesh Krishna*
162. Herbal Supplements-Drug Interactions: Scientific and Regulatory Perspectives, *edited by Y. W. Francis Lam, Shiew-Mei Huang, and Stephen D. Hall*
163. Pharmaceutical Photostability and Stabilization Technology, *edited by Joseph T. Piechocki and Karl Thoma*
164. Environmental Monitoring for Cleanrooms and Controlled Environments, *edited by Anne Marie Dixon*
165. Pharmaceutical Product Development: In Vitro-ln Vivo Correlation, *edited by Dakshina Murthy Chilukuri, Gangadhar Sunkara, and David Young*
166. Nanoparticulate Drug Delivery Systems, *edited by Deepak Thassu, Michel Deleers, and Yashwant Pathak*
167. Endotoxins: Pyrogens, LAL Testing and Depyrogenation, Third Edition, *edited by Kevin L. Williams*
168. Good Laboratory Practice Regulations, Fourth Edition, *edited by Anne Sandy Weinberg*
169. Good Manufacturing Practices for Pharmaceuticals, Sixth Edition, *edited by Joseph D. Nally*
170. Oral-Lipid Based Formulations: Enhancing the Bioavailability of Poorly Water-soluble Drugs, *edited by David J. Hauss*
171. Handbook of Bioequivalence Testing, *edited by Sarfaraz K. Niazi*
172. Advanced Drug Formulation Design to Optimize Therapeutic Outcomes, *edited by Robert O. Williams III, David R. Taft, and Jason T. McConville*
173. Clean-in-Place for Biopharmaceutical Processes, *edited by Dale A. Seiberling*
174. Filtration and Purification in the Biopharmaceutical Industry, Second Edition, *edited by Maik W. Jornitz and Theodore H. Meltzer*
175. Protein Formulation and Delivery, Second Edition, *edited by Eugene J. McNally and Jayne E. Hastedt*
176. Aqueous Polymeric Coatings for Pharmaceutical Dosage Forms, Third Edition, *edited by James McGinity and Linda A. Felton*
177. Dermal Absorption and Toxicity Assessment, Second Edition, *edited by Michael S. Roberts and Kenneth A. Walters*
178. Preformulation Solid Dosage Form Development, *edited by Moji C. Adeyeye and Harry G. Brittain*
179. Drug-Drug Interactions, Second Edition, *edited by A. David Rodrigues*

180. Generic Drug Product Development: Bioequivalence Issues, *edited by Isadore Kanfer and Leon Shargel*
181. Pharmaceutical Pre-Approval Inspections: A Guide to Regulatory Success, Second Edition, *edited by Martin D. Hynes III*
182. Pharmaceutical Project Management, Second Edition, *edited by Anthony Kennedy*
183. Modified Release Drug Delivery Technology, Second Edition, Volume 1, *edited by Michael J. Rathbone, Jonathan Hadgraft, Michael S. Roberts, and Majella E. Lane*
184. Modified-Release Drug Delivery Technology, Second Edition, Volume 2, *edited by Michael J. Rathbone, Jonathan Hadgraft, Michael S. Roberts, and Majella E. Lane*
185. The Pharmaceutical Regulatory Process, Second Edition, *edited by Ira R. Berry and Robert P. Martin*
186. Handbook of Drug Metabolism, Second Edition, *edited by Paul G. Pearson and Larry C. Wienkers*
187. Preclinical Drug Development, Second Edition, *edited by Mark Rogge and David R. Taft*
188. Modern Pharmaceutics, Fifth Edition, Volume 1: Basic Principles and Systems, *edited by Alexander T. Florence and Jurgen Siepmann*
189. Modern Pharmaceutics, Fifth Edition, Volume 2: Applications and Advances, *edited by Alexander T. Florence and Jurgen Siepmann*
190. New Drug Approval Process, Fifth Edition: Global Challenges and Solutions, *edited by Richard A. Guarino*
191. Drug Delivery Nanoparticulate Formulation and Characterization, *edited by Yashwant Pathak and Deepak Thassu*
192. Polymorphism in Pharmaceutical Solids, Second Edition, *edited by Harry G. Brittain*

SECOND EDITION

Polymorphism in Pharmaceutical Solids

edited by
Harry G. Brittain
Center for Pharmaceutical Physics
Milford, New Jersey, USA

informa
healthcare
New York London

Informa Healthcare USA, Inc.
52 Vanderbilt Avenue
New York, NY 10017

© 2009 by Informa Healthcare USA, Inc.
Informa Healthcare is an Informa business

No claim to original U.S. Government works
Printed in the United States of America on acid-free paper
10 9 8 7 6 5 4 3 2 1

International Standard Book Number-10: 1-4200-7321-4 (Hardcover)
International Standard Book Number-13: 978-1-4200-7321-8 (Hardcover)

This book contains information obtained from authentic and highly regarded sources. Reprinted material is quoted with permission, and sources are indicated. A wide variety of references are listed. Reasonable efforts have been made to publish reliable data and information, but the author and the publisher cannot assume responsibility for the validity of all materials or for the consequence of their use.

No part of this book may be reprinted, reproduced, transmitted, or utilized in any form by any electronic, mechanical, or other means, now known or hereafter invented, including photocopying, microfilming, and recording, or in any information storage or retrieval system, without written permission from the publishers.

For permission to photocopy or use material electronically from this work, please access www.copyright.com (http://www.copyright.com/) or contact the Copyright Clearance Center, Inc. (CCC) 222 Rosewood Drive, Danvers, MA 01923, 978-750-8400. CCC is a not-for-profit organization that provides licenses and registration for a variety of users. For organizations that have been granted a photocopy license by the CCC, a separate system of payment has been arranged.

Trademark Notice: Product or corporate names may be trademarks or registered trademarks, and are used only for identification and explanation without intent to infringe.

Library of Congress Cataloging-in-Publication Data

Polymorphism in pharmaceutical solids / edited by Harry G. Brittain. — 2nd ed.
p. ; cm. — (Drugs and the pharmaceutical sciences ; v. 192)
Rev. ed. of: Polymorphism in pharmaceutical solids / edited by Harry G. Brittain. 1999.
Includes bibliographical references and index.
ISBN-13: 978-1-4200-7321-8 (hb : alk. paper)
ISBN-10: 1-4200-7321-4 (hb : alk. paper) 1. Solid dosage forms. 2. Polymorphism (Crystallography) 3. Solvation. 4. Hydration. I. Brittain, H. G. II. Polymorphism in pharmaceutical solids. III. Series: Drugs and the pharmaceutical sciences ; v. 192.
[DNLM: 1. Chemistry, Pharmaceutical. 2. Crystallization. 3. Molecular Structure. W1 DR893B v.192 2009 / QV 744 P7833 2009]
RS201.S57P64 2009
615'.19—dc22

2009015389

For Corporate Sales and Reprint Permissions call 212-520-2700 or write to: Sales Department, 52 Vanderbilt Avenue, 16th floor, New York, NY 10017.

Visit the Informa Web site at
www.informa.com

and the Informa Healthcare Web site at
www.informahealthcare.com

Preface

It is now just about 10 years since the publication of the first edition of *Polymorphism in Pharmaceutical Solids*, which certainly received a positive reaction from workers in drug development. Since then, Joel Bernstein and Rolf Hilfiker have published their books on polymorphic phenomena, and the field has continued to expand both in the number of works published and also in the depth of their coverage. Some things have not changed, however, and the effects of crystal structure on the solid-state properties of a given system remains of paramount importance. As I stated in the preface to the first edition, the heat capacity, conductivity, volume, density, viscosity, surface tension, diffusivity, crystal hardness, crystal shape and color, refractive index, electrolytic conductivity, melting or sublimation properties, latent heat of fusion, heat of solution, solubility, dissolution rate, enthalpy of transitions, phase diagrams, stability, hygroscopicity, and rates of reactions are all strongly influenced by the nature of the crystal structure.

The content of the present edition of *Polymorphism in Pharmaceutical Solids* has expanded to reflect the larger scope of topics having interest to development scientists. The book is now divided into six main sections, the first dealing with thermodynamic and theoretical issues. Within this initial section, one will find updated chapters from the first edition, "Theory and Principles of Polymorphic Systems" and "Application of the Phase Rule to the Characterization of Polymorphic and Solvatomorphic Systems." Reflecting the growing trend in predictive science, a new chapter entitled "Computational Methodologies: Toward Crystal Structure and Polymorph Prediction" is now featured in this section.

The second section of the new edition features preparative methods for polymorphs and solvatomorphs, and the single chapter of the first edition has been split into two chapters entitled "Classical Methods of Preparation of Polymorphs and Alternative Solid Forms" and "Approaches to High-Throughput Physical Form Screening and Discovery." In the next section, one will find chapters relating to the structural properties of polymorphs and solvatomorphs, updating the chapters from the first edition, "Structural Aspects of Polymorphism" and "Structural Aspects of Solvatomorphic Systems." With greater interest developing about the advantageous properties of co-crystal systems, it was appropriate to expand the structural section to include a new chapter entitled "Pharmaceutical Co-crystals: A New Opportunity in Pharmaceutical Science for a Long-Known but Little-Studied Class of Compounds."

In the first edition, topics related to the characterization methods for polymorphs and solvatomorphs were covered in two chapters, but the growth in the field that has taken place in the past 10 years required far greater coverage of these

areas. Hence, the four chapters of the next section are entitled, "Thermoanalytical and Crystallographic Methods," "Vibrational Spectroscopy," "Solid-State Nuclear Magnetic Resonance Spectroscopy," and "Effects of Polymorphism and Solid-State Solvation on Solubility and Dissolution Rate." The chapter on solubility and dissolution is especially poignant, as it retains timeless and consequential contributions written by the late Professor David Grant for the analogous chapter in the first edition.

In the first edition, the phase interconversion of polymorphs and solvatomorphs was covered only from a processing viewpoint, but in the present edition, this important topic is now covered in two chapters, "Solid-State Phase Transformations" and "Effects of Pharmaceutical Processing on the Solid Form of Drug and Excipient Materials."

As in the first edition, the last section contains chapters that have been grouped together as special topics. The chapter "Structural Aspects of Molecular Dissymmetry" concerns structural variations that can arise from the existence of molecular dissymmetry, manifested primarily in marked differences in solid-state properties between solids composed of racemates relative to solids composed of separated enantiomers. Finally, as the amorphous state represents one polymorphic form potentially available to all compounds, this extremely important field is covered in great depth in a chapter entitled "Amorphous Solids."

Even though the scope of the second edition of *Polymorphism in Pharmaceutical Solids* is substantially increased relative to that of the first edition, there is simply no way that all developments in the field could have been covered in depth in a single volume. Beginning with a survey of papers published during 2004, I am writing annual reviews of polymorphism and solvatomorphism that attempt to summarize the state of the field during a given calendar year. Interested readers can easily find these in the literature.

In the present edition of *Polymorphism in Pharmaceutical Solids*, I have once again tried to bring together a single volume that contains a comprehensive view of the principles, practical concerns, and consequences of the existence of polymorphism and solvatomorphism. As with the previous edition, I hope that the new chapters will continue to suggest approaches that will stimulate work and encourage additional growth in this area of solid-state pharmaceutics.

Harry G. Brittain

Contents

Preface . . . vii
Contributors . . . xi

PART I THERMODYNAMIC AND THEORETICAL ISSUES

1. Theory and Principles of Polymorphic Systems *1*
Harry G. Brittain

2. Application of the Phase Rule to the Characterization of Polymorphic and Solvatomorphic Systems *24*
Harry G. Brittain

3. Computational Methodologies: Toward Crystal Structure and Polymorph Prediction *52*
Sarah (Sally) L. Price

PART II PREPARATIVE METHODS FOR POLYMORPHS AND SOLVATOMORPHS

4. Classical Methods of Preparation of Polymorphs and Alternative Solid Forms *76*
Peter W. Cains

5. Approaches to High-Throughput Physical Form Screening and Discovery *139*
Alastair J. Florence

PART III STRUCTURAL PROPERTIES OF POLYMORPHS AND SOLVATOMORPHS

6. Structural Aspects of Polymorphism *185*
Harry G. Brittain, Stephen R. Byrn, and Eunhee Lee

7. Structural Aspects of Solvatomorphic Systems *233*
Harry G. Brittain, Kenneth R. Morris, and Stephan X. M. Boerrigter

8. **Pharmaceutical Co-crystals: A New Opportunity in Pharmaceutical Science for a Long-Known but Little-Studied Class of Compounds** *282*
Kapildev K. Arora and Michael J. Zaworotko

PART IV CHARACTERIZATION METHODS FOR POLYMORPHS AND SOLVATOMORPHS

9. **Thermoanalytical and Crystallographic Methods** *318*
Sisir Bhattacharya, Harry G. Brittain, and Raj Suryanarayanan

10. **Vibrational Spectroscopy** *347*
Harry G. Brittain

11. **Solid-State Nuclear Magnetic Resonance Spectroscopy** *381*
Patrick A. Tishmack

12. **Effects of Polymorphism and Solid-State Solvation on Solubility and Dissolution Rate** *436*
Harry G. Brittain, David J. R. Grant, and Paul B. Myrdal

PART V INTERCONVERSION OF POLYMORPHS AND SOLVATOMORPHS

13. **Solid-State Phase Transformations** *481*
Harry G. Brittain

14. **Effects of Pharmaceutical Processing on the Solid Form of Drug and Excipient Materials** *510*
Peter L. D. Wildfong

PART VI SPECIAL TOPICS RELATED TO POLYMORPHISM AND SOLVATOMORPHISM

15. **Structural Aspects of Molecular Dissymmetry** *560*
Harry G. Brittain

16. **Amorphous Solids** *587*
Lynne S. Taylor and Sheri L. Shamblin

Index . . . 631

Contributors

Kapildev K. Arora Department of Chemistry, University of South Florida, Tampa, Florida, U.S.A.

Sisir Bhattacharya* Department of Pharmaceutics, University of Minnesota, Minneapolis, Minnesota, U.S.A.

Stephan X. M. Boerrigter SSCI, an Aptuit Company, West Lafayette, Indiana, U.S.A.

Harry G. Brittain Center for Pharmaceutical Physics, Milford, New Jersey, U.S.A.

Stephen R. Byrn Department of Industrial and Physical Pharmacy, Purdue University, West Lafayette, Indiana, U.S.A.

Peter W. Cains Avantium Technologies BV, Amsterdam, The Netherlands

Alastair J. Florence Solid-State Research Group, Strathclyde Institute of Pharmacy and Biomedical Sciences, University of Strathclyde, Glasgow, U.K.

David J. R. Grant College of Pharmacy, University of Minnesota, Minneapolis, Minnesota, U.S.A.

Eunhee Lee Department of Industrial and Physical Pharmacy, Purdue University, West Lafayette, Indiana, U.S.A.

Kenneth R. Morris College of Pharmacy, University of Hawaii at Hilo, Hilo, Hawaii, U.S.A.

Paul B. Myrdal College of Pharmacy, University of Arizona, Tucson, Arizona, U.S.A.

Sarah (Sally) L. Price Department of Chemistry, University College London, London, U.K.

Sheri L. Shamblin Pfizer Global Research and Development, Pfizer, Inc., Groton, Connecticut, U.S.A.

Raj Suryanarayanan Department of Pharmaceutics, University of Minnesota, Minneapolis, Minnesota, U.S.A.

Lynne S. Taylor Department of Industrial and Physical Pharmacy, School of Pharmacy and Pharmaceutical Sciences, Purdue University, West Lafayette, Indiana, U.S.A.

Patrick A. Tishmack SSCI, an Aptuit Company, West Lafayette, Indiana, U.S.A.

Peter L. D. Wildfong Duquesne University, Pittsburgh, Pennsylvania, U.S.A.

Michael J. Zaworotko Department of Chemistry, University of South Florida, Tampa, Florida, U.S.A.

Current affiliation: Forest Laboratories, Inc., Commack, New York, U.S.A.

1 Theory and Principles of Polymorphic Systems

Harry G. Brittain
Center for Pharmaceutical Physics, Milford, New Jersey, U.S.A.

INTRODUCTION

With the discovery by Bragg that one could use the angular dependence of scattering of X rays from a crystalline solid to determine the structure of that solid (1), structural science has played a large role in the fields of chemistry and physics. Very early in the 19th century, it had become known that many compounds were capable of exhibiting the phenomenon of *dimorphism*, and could be crystallized into solids having different melting points and crystal habits. For example, the α- and β-forms of potassium ethyl sulfate were found to exhibit different solubilities and eutectic temperatures in their phase diagram (2). The existence of a thermally induced phase transition between the anhydrous and monohydrate forms of 5-nitrosalicylic acid was deduced from the temperature dependence of its solubility (3).

As the techniques of structure elucidation grew in their sophistication, the crystallographic basis of dimorphism became firmly established. The X-ray crystallographic technique enabled workers to determine the dimensions and angles associated with the fundamental building blocks of crystals, namely, the unit cell. At the same time it also became recognized that crystalline solids were not limited to one or two crystal forms, and that many solids were capable of being isolated in multitudes of crystalline forms.

During the very first series of studies using single-crystal X-ray crystallography to determine the structures of organic molecules, Robertson reported the structure of resorcinol (1,3-dihydroxybenzene) (4). This crystalline material corresponded to that ordinarily obtained at room temperature, and was later termed the α-form. Shortly thereafter, it was found that the α-form underwent a transformation into a denser crystalline modification (denoted as the β-form) when heated to about 74°C, and that the structure of this newer form was completely different (5). A summary of the unit cell parameters reported for both forms is provided in Table 1. The α-form features a relative open architecture that is maintained by a spiraling array of hydrogen bonding that ascends through the various planes of the crystal. The effect of the thermally induced phase transformation is to collapse the open arrangement of the α-form by a more compact and parallel arrangement of the molecules in the β-form. This structural change causes an increase in crystal density on passing from the α-form (1.278 g/cm^3) to the β-form (1.327 g/cm^3).

The term *polymorphism* has come to denote those crystal systems for which a substance can exist in structures characterized by different unit cells, but where each of the forms consists of exactly the same elemental composition. For a long time, the term *pseudopolymorphism* was used to denote other crystal variations where the crystal structure of the substance is defined by still other unit cells where these unit cells differ in their elemental composition through the inclusion of one or more

TABLE 1 Summary of the Unit Cell Parameters Associated with the two Polymorphs of Resorcinol (4,5)

Polymorphic form	α-form	β-form
Crystal class	Orthorhombic	Orthorhombic
Space group	P*na*	P*na*
Number of molecules per unit cell	$Z = 4$	$Z = 4$
Unit cell axis lengths	a =10.53 Å	a = 7.91 Å
	b = 9.53 Å	b = 12.57 Å
	c = 5.66 Å	c = 5.50 Å
Unit cell angles	$\alpha = 90°$	$\alpha = 90°$
	$\beta = 90°$	$\beta = 90°$
	$\gamma = 90°$	$\gamma = 90°$

molecules of solvent, and more recently this term has become replaced by the term *solvatomorphism*. The crystallographic origins and consequences of polymorphism and solvatomorphism have been the focus of several monographs and reviews (6–12), recent annual reviews (13–15), and will be discussed in great detail in one of the later chapters in this book.

The existence of different crystal structures of the various polymorphs of a substance often causes these solids to exhibit a variety of different physical properties, many of which are listed in Table 2. Because of differences in the dimensions, shape, symmetry, capacity (number of molecules), and void volumes of their unit cells, the different polymorphs of a given substance have different physical properties arising from differences in molecular packing. Such properties include molecular volume, molar volume (i.e., molecular volume multiplied by Avogadro's number), density, refractive index along a given crystal axis, thermal conductivity, electrical conductivity, and hygroscopicity. Differences in melting points of the various polymorphs arise from differences of the cooperative interactions of the molecules in the solid state compared with the liquid state. Also observed are differences in spectroscopic properties, kinetic properties, and some surface properties. Differences in packing properties and in the energetics of the intermolecular interactions (i.e., thermodynamic properties) among polymorphs give rise to differences in mechanical properties.

These differences in physical properties among the crystal forms of a polymorphic system have become extremely interesting to pharmaceutical scientists because their manifestation can sometimes lead to observable differences that have implications for processing, formulation, and drug availability (16–21). For such situations, the regulatory concerns can often become critically important, and can determine the path of development for a given drug substance (22). Consequently, an entire field of characterization techniques for the evaluation of pharmaceutical solids has arisen, and its degree of sophistication continues to grow (23–29).

Once the phase space of a substance has been determined, and the scope of possible polymorphic or solvatomorphic forms is established, it becomes critical to determine the boundaries of stability for the different forms and how they might be interconverted. At the very least, one must determine which crystal form is the most stable state, because unless mitigating circumstances dictate otherwise, that form would be the one to be chosen for continued development.

TABLE 2 Physical Properties that Differ Among Crystal Forms of a Polymorphic System

Packing properties	Molar volume and density
	Refractive index
	Conductivity: electrical and thermal
	Hygroscopicity
Thermodynamic properties	Melting and sublimation temperatures
	Internal or structural energy
	Enthalpy
	Heat capacity
	Entropy
	Free Energy and Chemical Potential
	Thermodynamic Activity
	Vapor Pressure
	Solubility
Spectroscopic properties	Electronic state transitions
	Vibrational state transitions
	Nuclear spin state transitions
Kinetic properties	Dissolution rate
	Rates of solid-state reactions
	Stability
Surface properties	Surface free energy
	Interfacial tensions
	Crystal habit
Mechanical properties	Hardness
	Tensile strength
	Compactibility, tabletting
	Handling, flow, and blending

THERMODYNAMICS OF POLYMORPHIC SYSTEMS

Before a discussion of the thermodynamics associated with systems capable of being crystallized in more than one form can be undertaken, a number of fundamental principles regarding the interactions that can take place in solid systems must be set out. In such discussions, one often uses thermodynamics to treat an *ideal* system, which may be taken as approximating some type of limiting condition. Real systems are often difficult to treat, but ideal systems are useful in that their boundaries can be used to deduce simple laws that are often sufficiently accurate to be practically useful. The following discussion has been distilled from several standard texts on thermodynamics and chemical equilibrium (30–34).

Systems are said to possess *energy*, and interacting systems exhibit simultaneous changes in observable properties that are accompanied by changes in energy. The energy of a system therefore implies the power to interact but also is a description of the results of interaction in terms of changed properties. To the thermodynamic scientist, these properties are usually descriptions in which the system exchanges energy with some standard system, although the properties can also be defined with respect to another member of the system. The changes of interest most pertinent to the present discussion involve changes in *potential* energy, or energy stored in a system as a result of how it came into that state. For example, the transformation of a substance from one physical phase to another involves the transfer of energy in the form of heat. Only changes or differences in energy are empirically measurable, because the

absolute energy of a system depends critically on the standard from which that energy might be measured.

Properties are identified as being *extensive* (dependent on the quantity of mass present) or *intensive* (independent of the amount of mass present), and the latter properties express a quality of the system rather than a quantity of something. For example, one may measure the amount of heat required to vaporize one gram of water, but dividing that amount of heat by that amount of water yields an intensive property that defines the substance called water. For every type of energy, there is a property whose difference between two systems determines whether energy will be exchanged and over which direction that energy will flow. Temperature, for example, is a measure of the intensity of heat in a system, and the value of this property with respect to the temperature of another system determines how much heat will flow and which system will be the donor of that heat.

It is concluded that the relative intensities of the various forms of energy in different systems determine whether interactions of exchanges of energy can take place between them. For a series of systems isolated from the universe, energy must flow until total equality in all forms of energy is attained. Consequently, to define a system one must be able to state the intensities of all significant forms of energy contained within that system. When this situation has been reached, the intensities of these energies existing within the system are grouped together in a class of properties denoted as *conditions*.

The conditions of a system can be controlled by manipulating the surroundings of the system. For example, unless a system is contained in a closed vessel, the pressure of ordinary chemical and physical transformations is fixed as the same as atmospheric pressure by virtue of the interaction of the system with open surroundings. As will be seen in the next chapter dealing with the Phase Rule, this stipulation results in reduced degrees of freedom and a limitation on the number of equilibria available to a system. In partly isolated systems, one may vary conditions by the deliberate introduction of one type of energy in order to observe the consequences of that addition in a linear manner.

In numerous experiments, it has been demonstrated that although energy can be converted from one form to another, it cannot be created or destroyed. This finding is the basis for the law of conservation of energy, which in turn, is the basis for the *first law of thermodynamics*: "The total energy of a system and its surroundings must remain constant, although it may be changed from one form to another." The energy of a system is seen to depend upon its pressure, volume, temperature, mass, and composition, with these five quantities being related by the *equation of state* for the system. Therefore, it is possible to assign a definite amount of energy to any given state of a system, which is determined only by the state itself and not by its previous history. If E_A represents the energy of the state A, and E_B is the energy of the state B, then the change in energy that accompanies the transformation of the system from A to B is independent of the path taken, and is given by:

$$\Delta E = E_B - E_A \tag{1}$$

The *internal energy* of the system, E, is a function of pressure, volume, and temperature, and includes all forms of energy other than those resulting from the position of the system in space. The actual magnitude of the internal energy is usually not known, but because thermodynamics is concerned primarily with changes in energy, the actual value of the internal energy is not significant.

When a system changes from one state to another, it may perform some type of external work, the magnitude of which is represented by w. If the work is done by the system, then w is positive, but if work is not done in the system, then w is negative. In addition, the system may absorb or evolve an amount of heat equal to q during the change, and q will always be positive if the system absorbs heat. According to the first law of thermodynamics, in order for the total energy of the system and surroundings to remain unchanged during the transition, it follows that the change in energy (ΔE) must be exactly equivalent to the heat q absorbed from the surroundings less the energy w lost to the surroundings in the from of external work:

$$\Delta E = q - w \tag{2}$$

For non-electrical thermodynamic processes that take place at constant pressure, the work term in equation (2) can be replaced by an expansion term, where P is the constant external pressure and ΔV is the increase of volume. If the amount of heat absorbed at constant pressure is represented as q_P, then with a slight rearrangement, one obtains:

$$q_P = \Delta E + P\Delta V \tag{3}$$

Because P and V are thermodynamic properties of the system, and because E depends only on the state of the system and not on its previous history, it follows that the quantity ($E + PV$) is also dependent only the state of the system. This latter quantity is called the *enthalpy* (H) of the system:

$$H = E + PV \tag{4}$$

At constant pressure:

$$\Delta H = \Delta E + P\Delta V \tag{5}$$

Comparison of equations (3) and (5) indicates that the increase ΔH in the enthalpy of the system at constant pressure equals the heat absorbed under these conditions.

Thermochemistry deals with the changes in heat of a system that accompany chemical or physical transformations where reactants transition into products. Because different substances have different amounts of internal energy in the form of chemical energy, the total energy of the products of a reaction will differ from the total energy of the reactants. As a result, the reaction will be accompanied either by the liberation or consumption of heat. An *exothermic* reaction is one where heat is produced as a product of the reaction, while an *endothermic* reaction is one where hear is consumed as a reactant in the reaction.

If a system transformation is run under constant atmospheric pressure, then the amount of heat absorbed is identified as the *enthalpy of reaction*, and this quantity represents the difference in the enthalpies of the reaction products and the reactants. For example, the combustion of solid elemental graphite with gaseous elemental oxygen at 25°C (i.e., 298 K) to yield gaseous carbon dioxide is endothermic:

$$C_{(S)} + O_{2\,(G)} \rightarrow CO_{2\,(G)} \tag{6}$$

and the enthalpy of combustion equals –94.05 kcal/mol. It is generally postulated that elements are in their standard states (i.e., the stable forms at ambient conditions), and

therefore their respective enthalpies are set to zero. Because equation (6) depicts the formation of CO_2 from its constituent elements, the enthalpy of that reaction is termed the enthalpy of formation for CO_2.

When the reaction under consideration involves a phase change, then the change in enthalpy is indicative of that reaction. For example, the *enthalpy of vaporization* of a substance is defined as the amount of heat required at constant pressure to vaporize one mole of that substance. One may determine the difference in enthalpy between two polymorphic forms of a compound by applying Hess's Law of constant heat summation, if the enthalpies of combustion for the two forms are known. The enthalpy of combustion for the reaction of diamond with oxygen equals –94.50 kcal/mol, and therefore the enthalpy of transition accompanying the conversion of diamond into graphite equals –0.45 kcal/mol.

Although the majority of chemical reactions that are exothermic in character will spontaneously go to completion under ordinary conditions, a number of reactions are known to require the absorption of heat and are still spontaneous. For example, the dissolution of most salts is endothermic, and yet their dissolution proceeds spontaneously as long as the equilibrium solubility is not exceeded. This simple observation demonstrates that enthalpy considerations are not sufficient to determine the spontaneity of a reaction, and that the definition of another parameter is required.

This additional state function is known as the *entropy* of the system, and has been given the symbol, S. One often encounters the explanation that entropy is a measure of disorder in a system, and that a spontaneous reaction is accompanied by an increase in entropy. Although apart from statistical mechanics it is difficult to define entropy, it is easier to define changes in entropy. Even though it is clear that spontaneous reactions are irreversible in nature, one can still break down the overall irreversible process into a series of infinitely small processes, each one of which is reversible in nature. The increase in entropy, dS, that accompanies an infinitesimal change equals the heat absorbed when the change is carried out in a reversible manner divided by the absolute temperature, T:

$$dS = \delta(q_{REV})/T \tag{7}$$

Because $\delta(q_{REV})$ has a definite value for a reversible, isothermal change, one can integrate equation (7) between the temperature limits of the initial and final states to obtain the entropy change for the process, ΔS.

It has proven expeditious to define other functions where the entropy is part of the determinant of spontaneity, one of these being:

$$A = E - TS \tag{8}$$

where the *work function*, A, equals the maximum amount of work obtainable when a system undergoes a change under reversible conditions. More useful to pharmaceutics and issues of polymorphism is the *free energy*:

$$G = H - TS \tag{9}$$

It is not difficult to show that combination of equations (4), (8), and (9) yields the relation:

$$G = A + PV \tag{10}$$

When a system undergoes a transformation, that change takes place at constant temperature and then the free energy of the transition is given by:

$$\Delta G = \Delta H - T\Delta S \tag{11}$$

If the transformation is also conducted at constant pressure, then equation (5) can be substituted into equation (11) to yield:

$$\Delta G = \Delta E + P\Delta V - T\Delta S \tag{12}$$

Figure 1 shows the energy relationships for a hypothetical system where the enthalpy and the entropy of the system increase with increasing absolute temperature. According to the Third Law of Thermodynamics, the entropy of a perfect, pure crystalline solid is zero at absolute zero, enabling one to set the zero-point entropy of the system. The ($T \cdot S$) product is seen to increase more rapidly with increasing temperature than does the enthalpy, and therefore the free energy will decrease with increasing temperature. This decrease also corresponds to the fact that the slope ($\delta G/\delta T$), of the plot of G against T is negative according to the equation:

$$(\delta G/\delta T)_P = -S \tag{13}$$

Each polymorphic form of a substance will yield an energy diagram similar to that of Figure 1, and because each polymorph has its own distinctive crystal lattice, it is to be anticipated that the values of enthalpy, entropy, and free energy at a given temperature would be different among the various polymorphs. In discussions of the relative stability of polymorphs and the driving force for polymorphic transformations at constant temperature and pressure, the difference in free energy between the forms is the decisive factor, with the form exhibiting the lowest free energy being the most stable.

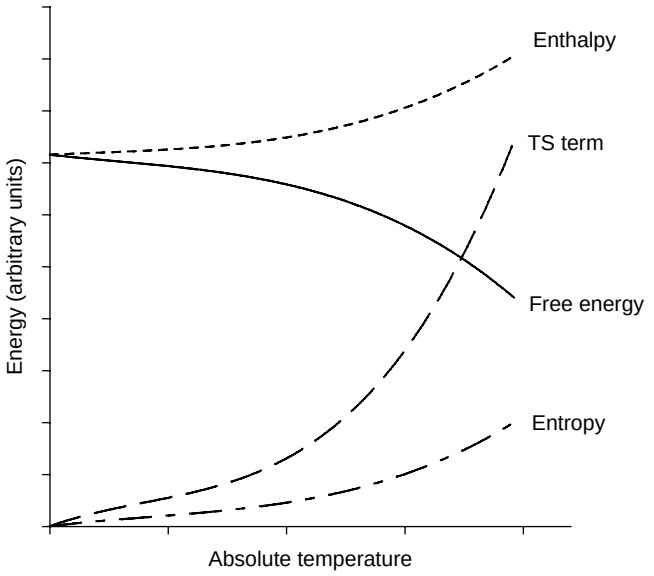

FIGURE 1 Temperature dependence of various thermodynamic functions.

Figure 2 shows the temperature dependence of the enthalpy and free energy for two different polymorphs, identified as Form-1 and Form-2. Because the temperature dependence of the free energies of the forms differs, at some temperature the respective curves cross and the two forms become isoenergetic. If the intersection point is determined under ambient conditions, the temperature is referred to as the *ordinary transition point* (T_{TR}). The fact that the free energies of the two polymorphs are equal implies that Form-1 and Form-2 are in equilibrium at that temperature.

Figure 2 shows Form-2 having an enthalpy that is higher than that of Form-1, so that the difference in enthalpies has the order $H_2 > H_1$ (i.e., ΔH is positive and the transition is endothermic in nature). Because at the transition temperature the difference in free energies of the forms equals zero, it follows that the difference in entropies will have the order $S_2 > S_1$. Equating the free energies of the two forms leads to the useful relation:

$$\Delta H_{TR} = T_{TR}\Delta S_{TR} \tag{14}$$

where $\Delta H_{TR} = H_2 - H_1$ and $\Delta S_{TR} = S_2 - S_1$ at the transition point. Through the use of differential scanning calorimetry, one may measure the enthalpy of the transition, and therefore calculate the entropy of the transition as long as the transition point is accurately determined. For this measurement to be accurate, the rate of temperature increase must be slow enough to allow Form-1 to completely transform into Form-2 over a span of a few degrees so as to achieve reversible conditions as closely as possible.

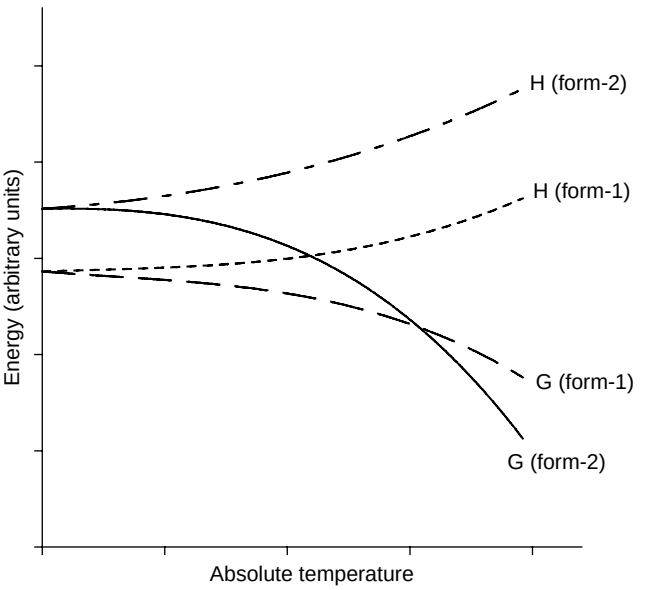

FIGURE 2 Temperature dependence of the enthalpy (*H*) and free energy (*G*) for two polymorphic crystal forms.

Figure 2 also shows that below the transition temperature, Form-1 has the lower free energy (i.e., $G_2 > G_1$), and therefore is more stable within that temperature range. On the other hand, above the transition temperature, Form-2 now has the lower free energy and is therefore more stable (i.e., $G_2 < G_1$). One concludes that under defined conditions of temperature and pressure, only one polymorph can be stable, and that all other polymorphs must be unstable. It is important to note that thermodynamics speaks to the relative energies and stabilities of polymorphs, but as will be discussed shortly, has nothing to say regarding the rates of these phase transformations. Diamond is thermodynamically unstable with respect to graphite, but the kinetics associated with that phase change are so infinitesimally slow that one refers to diamond as a metastable phase.

Equation (10) applies to the ideal systems discussed thus far, and differentiating both sides of the equation yields:

$$dG = dA + PdV + VdP \tag{15}$$

But dA is the maximum work of the expansion and must therefore be numerically equal to $-P$dV, so equation (15) reduces to:

$$dG = VdP \tag{16}$$

In order to integrate equation (16), one requires an equation of state defining V in terms of P. For one mole of an ideal gas, the law is simply:

$$V = nRT/P \tag{17}$$

where n is the number of moles of gas and R is the gas constant. Substitution of equation (17) into (16) and integrating yields:

$$\Delta G = G_2 - G_1 = RT \ln(P_2/P_1) \tag{18}$$

Equation (18) applies to any change of state or isothermal transfer of a substance from a region in which it has a vapor pressure P_1 to another region where its vapor pressure is P_2.

Practically all substances do not behave as ideal gases, so the concept of *fugacity* has been developed for real materials. One way to understand fugacity is to see it as the tendency manifested by a substance to leave the phase where it exists and pass into every other phase to which it has access. Because for an ideal gas, the partial pressure equals the fugacity, it is clear that equation (18) is a limiting instance of a more general equation. One may therefore substitute the fugacities (f_i) of the substance in each phase for the partial pressures to obtain:

$$\Delta G = RT \ln(f_2/f_1) \tag{19}$$

As is typically the case for thermodynamics, it is useful to define the fugacity of a substance with respect to the fugacity of some standard state, which can be taken as f^0. The ratio of the fugacity of a substance to that of the substance in the standard state has been termed the *activity* (a):

$$a = f/f^0 \tag{20}$$

so that:

$$G - G^0 = RT \ln(a) \tag{21}$$

As long as the reference state used to define G^0 and f^0 is the same, the quantities may be used interchangeably, so it follows that:

$$\Delta G = G_2 - G_1 = RT \ln(a_2/a_1) \tag{22}$$

The tendency of any one substance to be transferred from one phase or state to another at the same temperature depends on the properties of that substance, on the states involved, and on the temperature in question. However, neither the fugacity nor the activity are dependent upon the path or mechanism of transfer. At any specified temperature, these quantities can be considered to be governed by a property of the substance in the separate states. For many purposes, they are satisfactorily measured by the free energy of transfer or difference in molal free energy between the states. The molal free energy in any individual phase therefore comprises a measure of the escaping tendency of the substance in that phase relative to a standard state.

For dilute solutions, the activity is approximately proportional to the solubility, *s*, in any given solvent. One can then write an expression approximating the free energy difference between two polymorphic forms in terms of their respective equilibrium solubilities, or:

$$\Delta G \sim RT \ln(s_2/s_1) \tag{23}$$

If the dissolution of the polymorphic forms is conducted under transport-controlled sink conditions and under conditions of constant hydrodynamic flow, then the dissolution rate per unit surface area, *J*, is proportional to the solubility according to the Noyes–Whitney equation. One then can write another approximation for the free energy difference of two polymorphs as:

$$\Delta G \sim RT \ln(J_2/J_1) \tag{24}$$

Because the most stable polymorph under defined conditions of temperature and pressure has the lowest free energy content, it must therefore have the lowest values of fugacity, vapor pressure, thermodynamic activity, and solubility, and dissolution rate per unit surface area in any solvent.

ENANTIOTROPY AND MONOTROPY

In the preceding section, the general thermodynamics associated with systems was discussed, and methods were developed for determining the degree of spontaneity of a potential change were outlined. Implicit to the discussion was the understanding that the thermodynamic relations applied to systems undergoing reversible changes. In real crystals, however, a multitude of complicating factors introduce a degree of irreproducibility into the thermodynamic relations, thus limiting the scope of exact calculations in the understanding of real systems (35). Consequently, a number of more empirical concepts and rules have been developed to deal with actual polymorphic systems.

As described above, it is possible for polymorphic crystal forms to exhibit an ordinary transition point where one form can reversibly transform into another. Obviously, the temperature of this transition point must be less than the melting point of either polymorph or else the system would pass into the liquid state and no phase transition could be detected. For such systems, one polymorph will be

characterized by a definite range of conditions under which it will be the most stable phase, and the other form will be characterized by a different range of conditions under which it is the most stable phase. Polymorphic systems of this type are said to exhibit *enantiotropy*, and the two polymorphs are said to be enantiotropes of each other.

The free energy relationships between two enantiotropic polymorphs is illustrated in Figure 3, where now the enthalpy and free energy curves of the liquid (molten) state have been added. In the figure, Form-1 is shown as having a lower free energy content over the lower temperature range, while Form-2 is shown to have a lower free energy over a higher temperature range. For such an enantiotropic system, a reversible transition between forms can be observed at the transition temperature where the free energy curves cross and the forms are isoenergetic. The existence of enantiotropism in the system is indicated by the fact that the free energy curve for the liquid phase intersects the free energy curves for both polymorphs at a temperature that is higher than the temperature of the transition point.

Other systems exist where only one polymorph is stable at all temperatures below the melting point. As a result, all other polymorphs have no region of stability anywhere on a pressure–temperature diagram, and must be unstable with respect to the stable form. Polymorphic systems of this type are said to exhibit *monotropy*, and the two polymorphs are said to be monotropes of each other. The polymorph having the lowest free energy curve and solubility at any given temperature will necessarily be the most thermodynamically stable form.

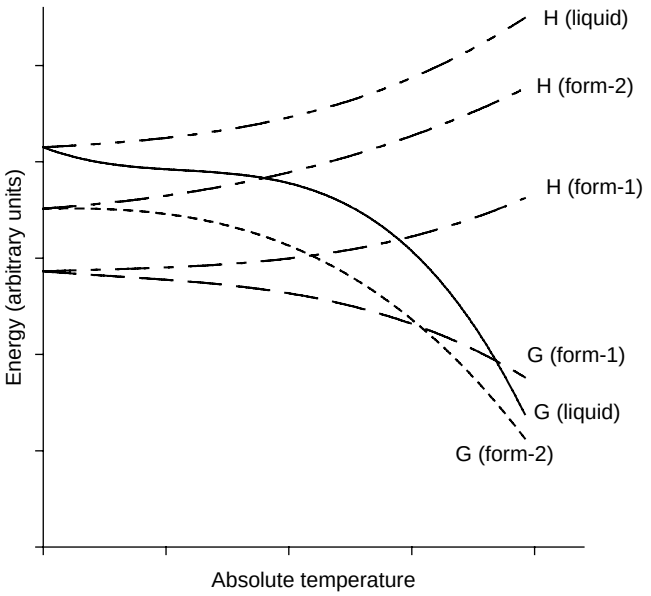

FIGURE 3 Temperature dependence of the enthalpy (*H*) and free energy (*G*) for two enantiotropic polymorphic crystal forms and their liquid (molten) state.

The free energy relationships between two monotropic polymorphs is illustrated in Figure 4, including the enthalpy and free energy curves of the liquid (molten) state. In this figure, Form-1 is shown as always having a lower free energy content over the entire accessible temperature range, and Form-2 has a higher free energy over the same temperature range. The free energy curve of the liquid state crosses the free energy curves of both polymorphs at temperatures less than that of the transition point, and hence, there can be no temperature at which the two polymorphs would exhibit a reversible phase transition. For a monotropic system the free energy curves do not cross, so no reversible transition can be observed below the melting point.

The isolation of polymorphs that form an enantiotropic system requires careful control over the isolation conditions. For enantiotropic materials, one can always identify a set of conditions where one polymorph or the other is the most thermodynamically stable form, and if crystallization is performed under those conditions one can usually obtain the desired form. Owing to its superior stability under all accessible temperature and pressure conditions, the isolation of the most stable polymorph in a monotropic system can usually be achieved without great difficulty. Isolation of the less stable form, however, requires a kinetic trapping of the system under conditions where the polymorph is characterized as being metastable at best.

A number of rules have been developed that serve to aid in the elucidation of the relative order of stability of polymorphs, and to facilitate determination of the existence of enantiotropism or monotropism in a polymorphic system (36–41). Although a summary of these many thermodynamic rules is provided in Table 3, it should be noted that the most useful and generally applicable rules are the Heat of Fusion rule and the Heat of Transition rule.

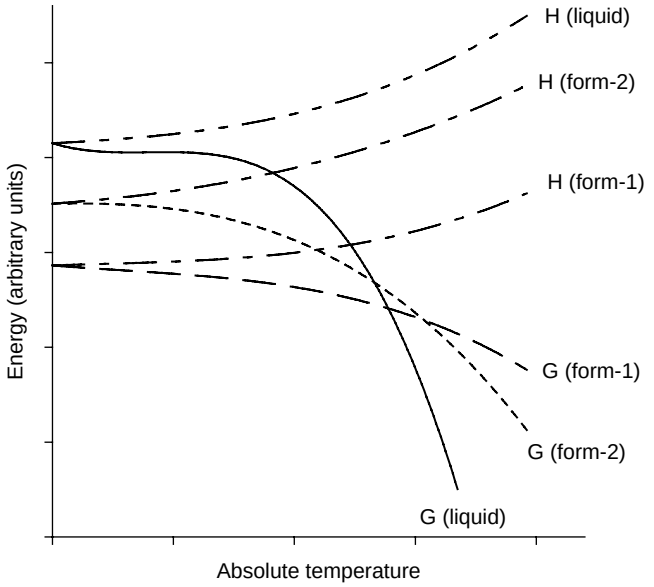

FIGURE 4 Temperature dependence of the enthalpy (*H*) and free energy (*G*) for two monotropic polymorphic crystal forms and their liquid (molten) state.

TABLE 3 Empirically Based Rules for Assigning the Nature of Phase Relationships in Polymorphic Systems[a]

Rule	Enantiotropic system	Monotropic system
Fundamental definition	Form-1 is the most stable polymorphic form at temperatures below the transition point, while Form-2 is the most stable polymorphic form at temperatures above the transition point	Form-1 is the stable polymorph at all temperatures below that of the melting point
Heat of fusion	The enthalpy of fusion of Form-1 is less than the enthalpy of fusion of Form-2	The enthalpy of fusion of Form-1 is more than the enthalpy of fusion of Form-2
Heat of transition	The phase transition of Form-2 to Form-1 is endothermic	The phase transition of Form-2 to Form-1 is exothermic
Entropy of fusion	The melting points of both Form-1 and Form-2 is less than the temperature of the transition point	The melting point of the most stable polymorph is higher than the temperature of the transition point
Phase transformation reversibility	The phase transformation at the transition point is reversible	The phase transformation of Form-2 into Form-1 is irreversible
Solubility	Form-1 is the most soluble polymorphic form at temperatures below the transition point, while Form-2 is the most soluble polymorphic form at temperatures above the transition point	Form-1 is the most soluble polymorph at all temperatures below that of the melting point
Density	The density of Form-1 is less than the density of Form-2	The density of Form-1 is more than the density of Form-2

[a]In the table, the convention where Form-1 has a higher melting point relative to that of Form-2 has been used.

The *Heat of Transition Rule* states that, if the transition between polymorphic forms is endothermic in nature, then the two forms are related by enantiotropy. Conversely, if the phase transformation is exothermic, then the two polymorphic forms are related by monotropy. Burger and Ramberger based this rule on the fact that because ΔH and ΔS are ordinarily positive for a spontaneous reaction, the enthalpy curves will not intersect and the free energy curves can intersect only once (36). In favorable circumstances, the sign and magnitude of the enthalpy change can be determined using differential scanning calorimetry (DSC).

When the enthalpy of transition cannot be measured by DSC, the *Heat of Fusion Rule* should be applied next. This rule states that if the higher melting polymorph has the lower enthalpy of fusion, then the two forms are enantiotropes. Conversely, if the higher melting polymorph has the higher enthalpy of fusion, then the two forms are monotropes. Burger and Ramberger have pointed out that the difference between the enthalpies of fusion of a polymorphic pair does not

exactly equal the enthalpy of transition, and have provided an improvement to the difference in enthalpies of fusion based on the difference in heat capacities of the two forms (36).

The *Entropy of Fusion Rule* states that if the polymorph having the higher melting point has a lower entropy of fusion, then the two forms are related by enantiotropy (38). One may calculate the entropy of fusion (ΔS_F) from the enthalpy of fusion (ΔH_F) measured for a reversible phase transformation taking place as the transition point (T_{TR}) by applying equation (7) to the melting process:

$$\Delta S_F = \Delta H_F / T_{TR} \tag{25}$$

Equation (25) cannot properly be applied to the calculation of ΔS_F for a monotropic system, because monotropy is fundamentally irreversible in nature. However, if the form having the higher melting point had a higher entropy of fusion, then the two polymorphic forms would be related by monotropy. Yu has developed a method for inferring thermodynamic stability relationships from melting data, calculating the free energy difference and the temperature slope of ΔG between two polymorphs (40).

The *Solubility Rule* proceeds directly from equation (23), which relates the free energy difference between two polymorphic forms to the solubility ratio of these. Because the solubility of a solid phase is directly determined by its free energy, it follows that if one polymorph is the most soluble form at temperatures below the transition point, and the other form is the most soluble form at temperatures above the transition point, then the two polymorphs must be enantiotropes. Conversely, if one polymorph is the most soluble form at all temperatures below that of the melting point of either form, then the two polymorphs must be monotropes.

The *Density Rule* is probably the least reliable of the Burger and Ramberger rules (36), and states that the polymorph having the highest true density will be the more stable crystal form. The basis for this rule is the assumption that the most stable polymorphic form would have the most efficient crystal packing, and hence, the greatest amount of lattice energy. A number of exceptions have been observed to the density rule, among them the instance of resorcinol that was discussed earlier (4,5).

As an example of how the thermodynamic rules are used, consider the enantiotropically related system constituted by the two non-solvated polymorphs of auranofin (i.e., 5-triethylphosphine-gold-2,3,4,6-tetra-*o*-acetyl-1-thio—*D*-glyucopyranoside) (42). Form-A was found to melt at 112°C, with the enthalpy of fusion being determined as 9.04 kcal/mol. Form-B was found to melt at 116°C, and its enthalpy of fusion was found to be 5.84 kcal/mol. According to the heat of fusion rule, because the higher melting form has the lower heat of fusion, the two polymorphs must be enantiotropically related and the difference in fusion enthalpies was calculated to be 3.20 kcal/mol. Using solution calorimetry, the enthalpy of solution for Form-A in 95% ethanol was found to be 12.42 kcal/mol, whereas the enthalpy of solution for Form-B in the same solvent system was found to be 9.52 kcal/mol. In dimethylformamide, the enthalpy of solution of Form-A was found to be 5.57 kcal/mol, whereas the enthalpy of solution for Form-B was found to be 2.72 kcal/mol. Thus, the enthalpy difference between the two forms was found to be 2.90 kcal/mol in 95% ethanol and 2.85 kcal/mol in dimethylformamide. The equilibrium solubility of Form-A in 25% aqueous polyethylene glycol 200 was found to be 0.65 mg/mL, whereas the equilibrium solubility of Form-B in the same

solvent system was found to be 1.30 mg/mL. The enantiotropic nature of the auranofin system is demonstrated that at room temperature Form-A is the most stable, whereas at elevated temperatures Form-B is the most stable.

NUCLEATION AND CRYSTAL GROWTH

Among the various methods one may use to prepare different polymorphs are crystallization from liquid solutions of various pure and mixed solvents, crystallization from the molten liquid state, suspension of less-soluble substances in pure and mixed solvents, thermal treatment of crystallized substances, exposure of solids to various relative humidities, sublimation, and crystallization from supercritical fluids. Typically, the first experiments performed in a preformulation study entail the attempted crystallization of polymorphic solids from solutions using various solvents and various temperature regimes (43,44). In these experiments, initially supersaturated solutions are prepared, and then the supersaturation is discharged by either slow or rapid cooling of the solution, evaporation of the solvent, addition of an anti-solvent to induce precipitation, chemical reaction between two or more soluble species, or variation of pH to produce a less soluble acid or base.

The crystallization process begins with the aggregation of molecules into clusters, and the continued addition of molecules to the clusters eventually results in the formation of tiny crystallites (45–48). The *critical nucleus* is obtained when the clusters of molecules have the smallest size capable of independent existence in the supersaturated phase, with these particles existing in a reversible state where they have an equal probability of growing into larger crystals or dissolving back in the solution phase. These critical nuclei are too small to be observed directly, and their structure is not known. Mullin has stated that the structure of a critical nucleus could be anything from a diffuse agglomeration of molecules to a miniature crystal that is perfect in form (46).

The typical theory of nucleation is based on the theory developed for the condensation of vapor into a liquid that has been extended to crystallization from the molten state. The formation of a liquid droplet or a solid particle in a homogeneous fluid requires the performance of work to obtain the end product. The total amount of work required to form a crystal nucleus, W_{TOT}, equals the amount of work required to form the surface (W_S) plus the amount of work needed to form the bulk of the particle (W_V):

$$W_{TOT} = W_S + W_V \tag{26}$$

Using the geometrical equations known for spherical particles, it can be shown that total work of equation (26) equals:

$$W_{TOT} = \tfrac{4}{3}\pi\sigma r^2 \tag{27}$$

where r is the radius of the particle and σ is the surface energy of the particle per unit area.

The increase in vapor pressure resulting from the decrease in size of a droplet can be estimated from the Gibbs–Thompson equation:

$$\ln(P_R/P^*) = \frac{2M\sigma}{RT\rho r} \tag{28}$$

where P_R is the vapor pressure over a droplet of radius r, P^* is the equilibrium vapor pressure of the liquid, M is the molecular weight, ρ is the liquid density, T is the absolute temperature, and R is the universal gas constant.

For solid particles, the pressure terms of equation (28) can be replaced by concentration equivalents. However, the ratio of the concentration of a particle having a radius equal to r (C_R) to the equilibrium solubility (C^*) is a measure of the degree of supersaturation (D) in the system:

$$D = C_R / C^* \tag{29}$$

In that case, equation (28) can be written as:

$$\ln(D) = \frac{2M\sigma}{RT\rho r} \tag{30}$$

or more usefully as:

$$r = \frac{2M\sigma}{RT\rho \ln(D)} \tag{31}$$

Substitution of equation (31) into equation (27) yields the important relationship:

$$W_{TOT} = \frac{16\pi M^2 \sigma^3}{3[RT\rho \ln(D)]^2} \tag{32}$$

According to equation (32), a saturated solution cannot spontaneously nucleate, because $\ln(D) = 0$, and the work required for nucleation would be infinite. The equation also indicates that any supersaturated solution can undergo spontaneously nucleation as long as a sufficient amount of energy is supplied to the system. Nucleation may be primary (not requiring pre-existing crystals of the crystallizing substance) or secondary (nucleation is induced by pre-existing crystals of the substance). Primary nucleation may be homogeneous (the nuclei of the crystallizing substance arise spontaneously in the medium), or heterogeneous (the nuclei comprise foreign solid matter, such as particulate contaminants, dust particles, or the walls of the container.

The change in free energy associated with the process of nucleation (ΔG_{TOT}) from a homogeneous solution is given by:

$$\Delta G_{TOT} = \Delta G_S + \Delta G_V \tag{33}$$

where ΔG_S is the excess free energy between the surface of the particle and the bulk of the particle, whereas ΔG_V is the excess free energy between a very large particle having $r = \infty$ and the solution in solution. ΔG_S is a positive quantity known as the surface excess free energy, ΔG_V is a negative quantity known as the volume excess free energy, and both quantities are functions of the radius of the particle.

Because the ΔG_S and ΔG_V terms contribute opposing contributions to the total free energy change as the radius of the nucleus increases, the free energy passes through a maximum (ΔG_{CRIT}) at a particle radius equal to the radius (r_{CRIT}) of the critical nucleus. This behavior has been illustrated in Figure 5, and the free energy of the critical nucleus can be calculated as:

$$\Delta G_{CRIT} = 4\pi\sigma r_{CRIT}{}^{2}/_{3} \tag{34}$$

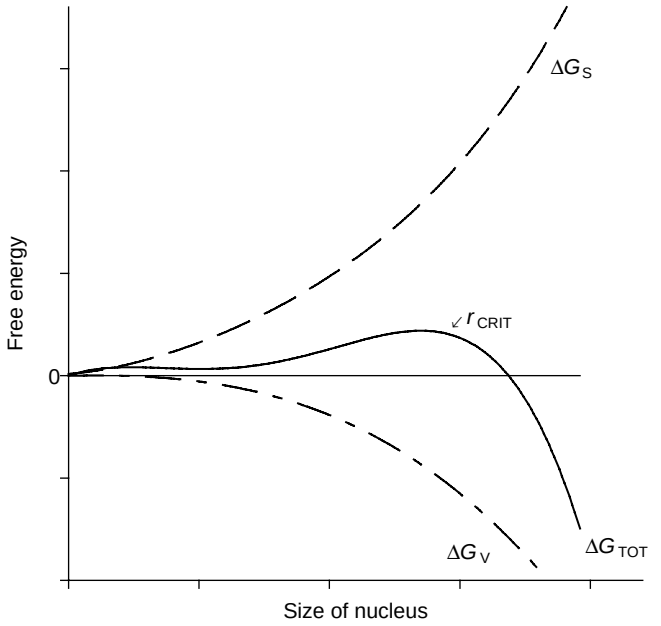

FIGURE 5 Dependence of the surface excess free energy (ΔG_S) and the volume excess free energy (ΔG_V), illustrating the existence of a critical nucleus having a diameter equal to r_{CRIT}.

Spontaneous nucleation is therefore seen to be governed by the algebraic opposition of a volume term that favors the accretion of additional molecules from the supersaturated medium and a surface term that favors the dissolution of the molecular aggregates that would otherwise form nuclei (45–48). The molecules of the crystallizing substance tend to aggregate in the supersaturated medium under the influence of the volume term that tends to reduce the Gibbs free energy of the system.

For a substance capable of existing in two or more polymorphic forms, each polymorph would have its own characteristic ΔG_{TOT} as determined by its particular ΔG_V and ΔG_S properties, as well as its own characteristic value of r_{CRIT} and ΔG_{CRIT}. Within the limits imposed by their characteristic curves, the aggregates or embryos of the various polymorphs would compete for molecules in their relative attempts to grow into crystallites so that their free energies could decrease. Depending on the characteristics of the free energy curves and the properties of the solution, it is to be anticipated that the aggregate for which the critical activation energy is the lowest will form the first nucleus, and continued deposition of molecules on that nucleus would eventually yield the crystallization of that particular polymorph.

In order to form crystals from the nuclei, molecules of the crystallizing substance attach onto the nuclei until the crystallization medium is no longer supersaturated and the equilibrium solubility of the substance is reached. The small but definite increase of solubility with decreasing particle size for microscopic solid particles predicted by equation (30) does, however, account for the increase in the average particle size when crystals of various sizes are allowed to age in constant

with a saturated solution. This phenomenon, known as *Ostwald ripening*, occurs because a smaller particle, having a higher solubility, will dissolve in the unsaturated solution that is saturated with respect to a larger particle of lower solubility. Conversely, a larger particle having a lower solubility will grow in the supersaturated solution that is actually saturated with respect to a smaller particle of higher solubility. Larger particles will therefore grow at the expense of smaller particles and the concentration of the "saturated" solution will decrease asymptotically.

Because the most easily nucleated polymorph is the one whose critical nuclei are the easiest to form (i.e., they have the most favorable free energy characteristics), one frequently finds that a phase transformation accompanies an Ostwald ripening process. As the science of crystallization developed during the 19th century and workers learned that compounds could be obtained in more than one solid state form, a number of cases were documented where a metastable form of a compound crystallized first and subsequently transformed into a more stable form. These findings led Ostwald to propose his *Law of Stages*, which stated that a supersaturated state does not spontaneously transform directly into that phase that is the most stable of the possible states, but instead, transforms into the phase that is next more stable than itself (49). In thermodynamic terms, the crystal form most likely to be initially crystallized would be the one whose free energy was closest to the free energy of the dissolved state.

Stranski and Totomanov provided an explanation for this phenomenon developed in terms of the kinetics of transformation (50). In this model, the determining factors are the relative rates of nucleation and crystal growth for the stable and metastable forms. The differences between the various parameters may be such that at the working temperature, the rate of nucleation is greater for the metastable product. This situation would cause the metastable phase to preferentially nucleate. In another scenario, the rates of nucleation may be more or less the same for the two forms, but if the metastable phase has a higher rate of growth, then this form would eventually predominate in the isolated product.

One may also encounter the situation where nucleation of the stable form may have taken place to a small extent along with the nucleation and growth of the metastable form. Because the stable form would necessarily have a lower solubility, a process of solution-mediated phase transformation is set up where over time the metastable phase transforms into the stable phase. For the situation where no nuclei of the stable phase were formed, then for a phase transformation to occur nuclei of the stable form would have to be created. The most likely situation for formation of these nuclei would be that they would not be generated within the bulk solution, but would instead be formed on the surfaces of the metastable crystals.

One typically identifies those situations where two crystal forms are obtained in an isolated product as *concomitant crystallization*, the products as *concomitant polymorphs*, and the thermodynamics and kinetics of the phenomenon have been discussed in detail (51). For example, two orthorhombic polymorphs of 1-deoxy-α-D-tagatose have been crystallized from a mixed methanol/ethyl acetate solvent system (52). Form-II was obtained as hexagonal places after allowing the mother liquor to stand for 16 hours, while Form-I crystallized as needles from the same solution after 72 hours. The two polymorphic forms were collected in approximately equal amounts from the crystallizing solution, and the single-crystal structures of these forms indicated that the polymorphism was derived from differences in hydrogen-bonding patterns.

Probably the best way to avoid the generation of concomitant polymorphs is through the introduction of seed crystals into a slightly supersaturated solution. As long as the seed crystals do not undergo a solution-mediated phase transformation of their own, the supersaturation in the crystallization medium is then discharged through growth onto the seeds. The implementation of this process requires knowledge of the temperature dependence of the equilibrium solubility and the spontaneous nucleation curve, and seeding is conducted in the concentration region between these boundaries (i.e., the *metastable zone*). The techniques for seeding a desirable polymorphic form during crystallization have been discussed in detail (46–48,53).

Another possibility where one may obtain stable or metastable crystal forms is where nucleation and subsequent crystal growth takes place on foreign surfaces, a process known as *epitaxial crystallization*. When surfaces, foreign nuclei, or appropriate seed crystals are present in a solution, these may favor the formation of a different form when the surfaces of the epitaxial agents present interfaces for which the structure closely matches the structure that would exist in a crystal of the new form (54,55). For example, Form-III of anthranilic acid was obtained by crystallization on glass coated with trimethoxysilane, Form-II was obtained when the crystallization took place on glass coated with chloro-triisobutlysilane, and a mixture of Form-II and Form-III was obtained if the crystallization was conducted on uncoated glass (56). It was concluded that the availability of hydrogen-bonding functionality at the nucleation surface played an important role in the polymorphic selectivity.

The various phenomena discussed in the preceding paragraphs amply demonstrate that one must exercise a considerable degree of control over the nucleation process and succeeding crystal growth processes if one seeks to obtain phase-pure materials. The crystal nucleation process has been discussed in detail (57), as has been the significance of controlling crystallization mechanisms and kinetics (58). These phenomena have also been critically examined with a view toward polymorph selection, and the crystal engineering that would be desirable in obtaining bulk drug substances having appropriate structures (59).

DISAPPEARING AND REAPPEARING POLYMORPHS

Over the years, stories have accumulated that summarize the failed attempts to reproduce previously reported crystallization products. When observed, the phenomenon is simultaneously frustrating and infuriating because modern physical science is often judged on the basis of its reproducibility. Dunitz and Bernstein addressed systems where a particular crystal form could not be obtained despite heroic efforts, concluding that control over nucleation and crystal growth processes was required (60). Crystallographers and preformulation scientists recognize the role of seeding in initiating nucleation, and many consider the disappearance of a metastable form to be a local and temporary phenomenon. These authors concluded that, "once a particular polymorph has been obtained, it is always possible to obtain it again; it is only a matter of finding the right experimental conditions."

In a subsequent work, Bernstein and Henck returned to the subject of transient polymorphs, examining this time certain systems where polymorphs had become elusive after a new polymorphic form was isolated (61). Through studies of the benzocaine:picric acid, *p*′-methylchalcone, benzophenone, and N-(N′-methylanilino) phthalimide systems, hot-stage microscopy was demonstrated to be of great use in the design of further experimentation that would yield the elusive polymorph.

The monoclinic polymorph of paracetamol (i.e., acetaminophen) is a commercially important form of the drug substance, despite its unsuitability in direct compression formulations. An orthorhombic crystal form of the drug substance had been characterized (62), but this polymorph could not be reproduced by several groups even though they followed the reported method of isolation. Eventually the experimental difficulties were overcome and a scalable process was reported that yielded the orthorhombic form in sufficient quantities for its characterization and formulation (63). The key to the successful process came through the use of appropriate seeding techniques to suppress the nucleation of the unwanted monoclinic polymorph, and rapid isolation of the product at low temperatures to suppress any phase transformation.

One example where a metastable polymorph was replaced by a more stable crystal form is that of meso-xylitol. In the early 1940s, two polymorphs of xylitol were described, with one being a metastable, hygroscopic, monoclinic form, melting at 61–61.5°C (64) and the other a stable orthorhombic form melting at 93–94.5°C (65). After a sample of the orthorhombic form was introduced into a laboratory in which the monoclinic polymorph had been prepared, the metastable spontaneously transformed into the stable form on exposure to the ambient environment. As part of a structural study of the orthorhombic polymorph, it was noted that "Attempts to obtain the lower melting monoclinic form from alcoholic solutions either at room temperature or close to 0°C have hitherto been unsuccessful. We invariably grow the orthorhombic crystals. It is interesting to note that although xylitol was first prepared as a syrup in 1891 there was no report of crystallization until 50 years later, when it was the metastable hygroscopic form that was prepared first. Having now obtained the stable form, it is difficult to recover the metastable crystals" (66).

The existence of two new polymorphic forms of 3-aminobenzenesulfonic acid (orthorhombic needles and monoclinic plates) have been reported, one of which had not been previously known (67). Form-I was suggested to be a disappearing polymorph, and the serendipitous discovery of Form-III resulted from the attempt to use tailor-made additives in order to re-obtain Form I. Although the attempt to prepare Form-I did not succeed, the study demonstrated the necessity to explore the polymorphic phase space as fully as possible even in simple systems.

A metastable form of benzamide was identified by Liebig and Woehler in 1832, but the structure of this unstable modification was determined much later (68). During reproductions of the historical experiments, rapid phase transformation was observed of the metastable form to the stable form, with the phase transformation being complete within 800 seconds. Ultimately, a high-resolution powder diffraction pattern of the metastable form was obtained by performing the crystallization in a sealed capillary, and subtracting the diffraction peaks of the stable form. Detailed evaluation of the structures of the stable and metastable polymorphs indicated that the phase transformation involved little structural rearrangement, and this fact was deduced as contributing to the difficulty of preparing phase-pure metastable crystals.

Three concomitant polymorphs of 1,3-bis(*m*-nitrophenyl)urea were reported in 1899 as yellow prisms (the α-form), white needles (the β-form), and yellow tablets (the γ-form), and a more detailed investigation of the system has been conducted (69). During work designed to prepare the γ-form, a new δ-form (that had the same color and habit as the β-form) and a monohydrate form were discovered, and the analysis suggested that the monohydrate was actually the reported γ-form.

It was also observed that despite the existence of considerable conformational differences in the molecules constituting the various crystal forms, the small degree of difference in the solid-state ^{13}C-NMR spectra of these forms indicated the existence of comparable environments for the NMR-active nuclei.

In their review, Dunitz and Bernstein pointed out that their examples of disappearing polymorphs involved molecules capable of adopting different conformations (60). These molecules would possess significant degrees of conformational freedom and molecular configurations that would facilitate the existence of equilibrium amounts of the different conformations in the solution, and solid-state effects would dictate which of these could be best able to build up into a crystal. It was noted that the rate of formation of nuclei of a stable polymorph could be significantly reduced by a low concentration of the required conformer, whereas another conformer might be incorporated in the nuclei of a metastable polymorph, which then underwent rapid growth. The phase interconversions accessible to systems of these types must be considered in the context of their enantiotropic or monotropic character, and therefore correctly designed preformulation studies of pharmaceutical compounds should resolve these kinetic and thermodynamic issues.

REFERENCES

1. Bragg WH, Bragg WL. X-Rays and Crystal Structure. London: G. Bell and Sons, Ltd., 1918.
2. Hammick DL, Mullaly JM. The dimorphism of potassium ethyl sulfate. J Chem Soc London 1921: 1802–6.
3. Chattaway FD, Curjel WRC. The crystalline forms of 5-nitrosalicylic acid and of related compounds. J Chem Soc London 1926: 3210–15.
4. Robertson JM. The structure of resorcinol: A quantitative X-ray investigation. Proc Royal Soc London 1936; A157: 79–99.
5. Robertson JM, Ubbelohde AR. A New Form of Resorcinol. I. Structure Determination by X-Rays. Proc Royal Soc London 1938; A167: 122–35.
6. McCrone WC. Polymorphism, chapter 8 in Physics and Chemistry of the Organic Solid State, volume II. In: Fox D, Labes MM, Weissberger A, eds. New York: Interscience Pub, 1965: 725–67.
7. Verna AR, Krishna P. Polymorphism and Polytypism in Crystals. New York: John Wiley & Sons, 1966.
8. Byrn SR, Pfeiffer RR, Stowell JG. Solid State Chemistry of Drugs, 2nd edn. West Lafayette: SSCI Inc., 1999.
9. Brittain HG. Polymorphism in Pharmaceutical Solids. New York: Marcel Dekker, 1999.
10. Vippagunta SR, Brittain HG, Grant DJW. Crystalline solids. Adv Drug Del Rev 2001; 48: 3–26.
11. Bernstein J. Polymorphism in Molecular Crystals. Oxford: Clarendon Press, 2002.
12. Hilfiker R. Polymorphism in the Pharmaceutical Industry. Weinheim: Wiley-VCH, 2006.
13. Brittain HG. Polymorphism and solvatomorphism 2004, Chapter 8 in Profiles of Drug Substances, Excipients, and Related Methodology, volume 32. In: Brittain HG, ed. Amsterdam: Elsevier Academic Press, 2005: 263–83.
14. Brittain HG. Polymorphism and solvatomorphism 2005. J Pharm Sci 2007; 96: 705–28.
15. (a) Brittain HG. Polymorphism and solvatomorphism 2006. J Pharm Sci 2008; 97: 3611–36. (b) Brittan HG. Polymorphism and solvatomorphism 2007. J Pharm Sci 2008; 98: 1617–42.
16. Haleblian JK, McCrone WC. Pharmaceutical applications of polymorphism. J Pharm Sci 1969; 58: 911–29.
17. Haleblian JK. Characterization of habits and crystalline modification of solids and their pharmaceutical applications. J Pharm Sci 1975; 64: 1269–88.

18. Bernstein J. Conformational Polymorphism, in Organic Solid State Chemistry. In: Desiraju GR, ed. Amsterdam: Elsevier, 1987: 471–518.
19. Morris KR, Rodriguez-Hornado N. Hydrates, in Encyclopedia of Pharmaceutical Technology, volume 7. In: Swarbrick J, Boylan J, eds. New York: Marcel Dekker, 1993: 393–440.
20. Byrn SR, Pfeiffer RR, Stephenson G, Grant DJW, Gleason WB. Solid-state pharmaceutical chemistry. Chem Mat 1994; 6: 1148–58.
21. Brittain HG. Effects of mechanical processing on phase composition. J Pharm Sci 2002; 91: 1573–80.
22. Byrn SR, Pfeiffer RR, Ganey M, Hoiberg C, Poochikian G. Pharmaceutical solids: a strategic approach to regulatory considerations. Pharm Res 1995; 12: 945–54.
23. Brittain HG, Bogdanowich SJ, Bugay DE, et al. Physical Characterization of Pharmaceutical Solids. Pharm Res 1991; 8: 963–73.
24. Bugay DE. Solid-state nuclear magnetic resonance spectroscopy: theory and pharmaceutical applications. Pharm Res 1993; 10: 317–27.
25. Threlfall TL. Analysis of organic polymorphs. Analyst 1995; 120: 2435–60.
26. Brittain HG. Spectral methods for the characterization of polymorphs and solvates. J Pharm Sci 1997; 86: 405–12.
27. Brittain HG. Solid-state analysis, Chapter 3, in the Handbook of Pharmaceutical Analysis. In: Ahuja S, Scypinski S, eds. New York: Marcel Dekker, 2001: 57–84.
28. Brittain HG, Medek A. Polymorphic and solvatomorphic impurities, chapter 3 in Handbook of Isolation and Characterization of Impurities in Pharmaceuticals. In: Ahuja S, Alsante KM, eds. Academic Press, 2003: 39–73.
29. Brittain HG. Spectroscopy of Pharmaceutical Solids. New York: Taylor and Francis, 2006.
30. Lewis GN, Randall M. Thermodynamics and the Free Energy of Chemical Substances. New York: McGraw-Hill Book Co, 1923.
31. Denbigh K. The Principles of Chemical Equilibrium. Cambridge: University Press, 1955.
32. Klotz IM. Chemical Thermodynamics. New York: W.A. Benjamin, 1964.
33. Vanderslice JT, Schamp HW, Mason EA. Thermodynamics. Englewood Cliffs: Prentice-Hall, 1966.
34. Sonntag RE, van Wylen GJ. Introduction to Thermodynamics: classical and statistical. New York: John Wiley & Sons, 1971.
35. Westrum EF, McCullough JP. Thermodynamics of crystals, chapter 1 in Physics and Chemistry of the Organic Solid State, volume I. In: Fox D, Labes MM, Weissberger A, eds. New York: Interscience Pub, 1963: 1–178.
36. Burger A, Ramberger R. On the polymorphism of pharmaceuticals and other molecular crystals: I, Mikrochim. Acta [Wien] 1979; II: 259–71.
37. Burger A, Ramberger R. On the polymorphism of pharmaceuticals and other molecular crystals: II, Mikrochim. Acta [Wien] 1979; II: 273–316.
38. Burger A. Thermodynamic and other aspects of the polymorphism of drugs. Pharm Int 1982: 158–63.
39. Giron D. Thermal analysis and calorimetric methods in the characterization of polymorphs and solvates. Thermochim Acta 1995; 248: 1–59.
40. Yu L. Inferring thermodynamic stability relationship of polymorphs from melting data. J Pharm Sci 1995; 84: 966–74.
41. Grunenberg A, Henck J-O, Siesler HW. Theoretical derivation and practical application of energy/temperature diagrams as an instrument in preformulation studies of polymorphic drug substances. Int J Pharm 1996; 129: 147–58.
42. Lindenbaum S, Rattie ES, Zuber GE, Miller ME, Ravin LJ. Polymorphism of auranofin. Int J Pharm 1985; 26: 123–32.
43. Newman AW, Stahly GP. Form selection of pharmaceutical compounds, chapter 1 in Handbook of Pharmaceutical Analysis. In: Ohannesian L, Streeter AJ, eds. New York: Marcel Dekker, 2001: 1–57.

44. Brittain HG. Preparation and identification of polymorphs and solvatomorphs, Chapter 3.3, in Preformulation in Solid Dosage Form Development. In: Adeyeye MC, Brittain HG, eds. New York: Informa Healthcare Press, 2008: 185–228.
45. Strickland-Constable RF. Kinetics and Mechanism of Crystallization. London: Academic Press, 1968: 74–129.
46. Mullin JW. Crystallization, 2nd edn. London: Butterworth & Co, 1972: 136–200.
47. Mersmann A. Crystallization Technology Handbook, 2nd edn. New York: Marcel Dekker, 2001: 45–79.
48. Myerson AS. Handbook of Industrial Crystallization, 2nd edn. Boston: Butterworth Heinemann, 2002: 33–65.
49. Ostwald W. Z Phys Chem 1897; 22: 289–330.
50. Stranski IN, Totomanov D. Z Phys Chem 1933; A163: 399.
51. Bernstein J, Davey RJ, Henck J-O. Concomitant polymorphs. Angew Chem Int Ed 1999; 38: 3441–61.
52. Jones NA, Jenkinson SF, Soengas R, et al. The concomitant crystallization of two polymorphs of 1-deoxy-α-D-tagatose. Acta Cryst 2007; C63: o7–o10.
53. Beckmann W. Seeding the desired polymorph: background, possibilities, limitations and case studies. Org Process Res Dev 2000; 4: 372–83.
54. Carter PW, Ward MD. Topographically directed nucleation of organic crystals on molecular single-crystal substrates. J Am Chem Soc 1993; 115: 11521–35.
55. Bonafede SJ, Ward MD. Selective nucleation and growth of an organic polymorph by ledge-directed epitaxy on a molecular crystal substrate. J Am Chem Soc 1995; 117: 7853–61.
56. Carter PW, Ward MD. Directing polymorph selectivity during nucleation of anthranilic acid on molecular substrates. J Am Chem Soc 1994; 116: 769–70.
57. Weissbuch I, Lahav M, Leiserowitz L. Toward stereochemical control, monitoring, and understanding of crystal nucleation. Cryst Growth Design 2003; 3: 125–50.
58. Rodriguez-Hornedo N, Murphy D. Significance of controlling crystallization mechanisms and kinetics in pharmaceutical systems. J Pharm Sci 1999; 88: 651–60.
59. Blagden N, Davey RJ. Polymorph selection: challenges for the future. Cryst Growth Design 2003; 3: 873–85.
60. Dunitz JD, Bernstein J. Disappearing polymorphs. Acc Chem Res 1995; 28: 193–200.
61. Bernstein J, Henck J-O. Disappearing and reappearing polymorphs – an anathema to crystal engineering. Cryst Engineer 1998; 1: 119–28.
62. Haisa M, Kashino S, Maeda H. The orthorhombic form of p-hydroxyacetanilide. Acta Cryst 1974; B30: 2510–12.
63. Nichols G, Frampton CS. Physicochemical characterization of the orthorhombic polymorph of paracetamol crystallized from solution. J Pharm Sci 1998; 87: 684–93.
64. Wolfrom ML, Kohn EJ. Crystalline xylitol. J Am Chem Soc 1942; 64: 1739.
65. Carson JF, Waisbrot SW, Jones FT. A new form of crystalline xylitol. J Am Chem Soc 1943; 65: 1777–8.
66. Weissbuch I, Zbaida D, Addadi L, Leiserowitz L, Lahav M. Design of polymeric inhibitors for the control of crystal polymorphism. Induced enantiomeric resolution at racemic histidine by crystallization at 25°C. J Am Chem Soc 1987; 109: 1869–71.
67. Rubin-Preminger JM, Bernstein J. 3-Aminobenzenesulfonic acid: a disappearing polymorph. Cryst Growth Design 2005; 5: 1343–9.
68. Blagden N, Davey R, Dent G, et al. Woehler and Liebig revisited: a small molecule reveals its secrets – the crystal structure of the unstable polymorph of benzamide solved after 173 years. Cryst Growth Design 2005; 5: 2218–24.
69. Rafilovich M, Bernstein J, Harris RK, et al. Groth's original concomitant polymorphs revisited. Cryst Growth Design 2005; 5: 2197–209.Theory and Principles of Polymorphic Systems

2 Application of the Phase Rule to the Characterization of Polymorphic and Solvatomorphic Systems

Harry G. Brittain
Center for Pharmaceutical Physics, Milford, New Jersey, U.S.A.

INTRODUCTION TO THE PHASE RULE

Bancroft has stated that the two expressions describing in a qualitative manner all states and changes of equilibrium are the Phase Rule and the Theorem of Le Chatelier (1). One of these principles describes the possibilities that might exist among substances in equilibrium, and the other describes how such equilibrium systems would react to an imposed stress. These changes may entail alterations in chemical composition, but could just as well involve transitions in the physical state. There is no doubt that thermodynamics is the most powerful tool for the characterization of such equilibria. Consider the situation presented by elemental sulfur, which can be obtained in either a rhombic or monoclinic crystalline state. Each of these forms melts at a different temperature, and is stable under certain well-defined environmental conditions. An understanding of this system would entail knowing under what conditions these two forms could equilibrate with liquid sulfur (either singly or together), and what would be the conditions under which the two could equilibrate with each other in the absence of a liquid phase.

These questions can, of course, be answered with the aid of chemical thermodynamics, the modern practice of which can be considered as beginning with publication of the seminal papers of J. Willard Gibbs (2). Almost immediately after the Law of Conservation of Mass was established, Gibbs showed that all cases of equilibria could be categorized into general class types. His work was perfectly general in that it was free from hypothetical assumptions, and immediately served to show how different types of chemical and physical changes actually could be explained in a similar fashion. Gibbs began with a system that needed only three independent variables for its complete specification, these being temperature, pressure, and the concentration of species in the system. From these considerations, he defined a general theorem known as the Phase Rule, where the conditions of equilibrium could be specified according to the composition of that system.

The following discussion of the Phase Rule, and its application to systems of polymorphic interest, has primarily been distilled from the several classic accounts published in the first half of this century (1,3–10). It may be noted that one of the most fractious disagreements that took place early in the development of physical chemistry took place between the proponents of pure computational thermodynamics and those seeking a more qualitative understanding of physical phenomena. The school of exact calculations prevailed (11), and this view has tended to dominate how workers in the field treat experiment and theory. Nevertheless, having a qualitative understanding about phase transformation equilibria can provide

one with a clearer grasp regarding a particular system, and the Phase Rule is still valuable for its ability to predict what is possible and what is not in a system that exists in a state of equilibrium.

Phases

A heterogeneous system is composed of various distinct portions, each of which is in itself homogenous in composition, but which are separated from each other by distinct boundary surfaces. These physically distinct and mechanically separable domains are termed phases. A single phase must be chemically and physically homogeneous, and may consist of single chemical substance or a mixture of substances.

Theoretically, an infinite number of solid or liquid phases may exist side by side, but there can never be more than one vapor phase. This situation arises from the fact that all gases are completely miscible with each other in all proportions, and will therefore never undergo a spontaneous separation into component materials. It is important to remember, however, that equilibrium is independent of the relative amounts of the phases present in a system. For instance, once equilibrium is reached, the vapor pressure of a liquid does not depend on either the volume of the liquid or vapor phases. As another example, the solubility of a substance in equilibrium with its saturated solution does not depend on the quantity of solid material present in the system.

In a discussion of simple polymorphic systems, one would consider the vapor and liquid phases of the compound as being separate phases. In addition, each solid polymorph would constitute a separate phase. Once the general rule is deduced and stated, the Phase Rule can be used to deduce the conditions under which these forms could exist in an equilibrium condition.

Components

A component is defined as a species whose concentration can undergo independent variation in the different phases. Another way to state this definition is that a component is a constituent that takes part in the equilibrium processes. For instance, in the phase diagram of pure water, there is only one component (water), despite the fact that this compound is formed by the chemical reaction of hydrogen and oxygen. Because according to the Law of Definite Proportions the ratio of hydrogen and oxygen in water is fixed and invariable, it follows that their concentration cannot be varied independently, and so they cannot be considered as being separate components.

For the specific instance of polymorphic systems, the substance itself will be the only component present. The situation complicates for solvatomorphs because the lattice solvent will compromise a second component, and hence, different phases will not have the same composition. The general rule is that the number of components present in an equilibrium situation is to be chosen as the smallest number of the species necessary to express the concentration of each phase participating in the equilibrium.

Degrees of Freedom

The number of degrees of freedom of a system is defined as the number of variable factors that must be arbitrarily fixed to completely define the condition of the system at equilibrium. Gibbs (2) demonstrated that the state of a phase is completely

determined if the temperature, pressure, and chemical potentials of its components are known. For a system of one component, there are no chemical potentials involved, so the system becomes specified only through knowledge of the temperature and pressure. One often speaks of the *variance* of a system, which is defined by the number of degrees of freedom required to specify the system.

For example, consider the situation of a substance forming an ideal gas in its vapor phase. The equation of state for ideal gases is given by the familiar equation:

$$PV = nRT \tag{1}$$

where P is the pressure, V is the volume, n is the number of moles present, T is the absolute temperature, and R is the gas constant. For a given amount of gas, if two out of the three independent parameters are specified, then the third is determined. This type of system is then said to be bivariant, or one that exhibits two degrees of freedom. If the gaseous substance is then brought into a state of equilibrium with its condensed phase, then empirically one finds that the condition of equilibrium can be specified by only one variable. The system exhibits only one degree of freedom, and is now termed univariant. If this system is cooled down until the solid phase forms, and the liquid and vapor remain in an equilibrium condition, one empirically finds that this equilibrium condition can only be attained if all independent parameters are specified. This latter system exhibits no degrees of freedom, and is said to be invariant.

The Phase Rule

For a substance capable of existing in two different phases, the state of equilibrium is such that the relative amounts of substance distributed between the phases in the absence of stress appears to be unchanging over time. This can only occur when the Gibbs chemical potential is the same in each phase, so equilibrium is defined as the situation where the chemical potential of each component in a phase is the same as the chemical potential of that component in the other phase.

Consider the system that consists of C components present in P phases. In order to specify the composition of each phase, it is necessary to know the concentrations of $(C - 1)$ components in each of the phases. Another way to state this is that each phase possesses $(C - 1)$ variables. Besides the concentration terms, there are two other variables (temperature and pressure), so that altogether the number of variables existing in a system of C components in P phases is given by:

$$\text{Variables} = P(C - 1) + 2\text{Variables} \tag{2}$$

In order to completely define the system, one requires as many equations as variables. If for some reason there are fewer equations than variables, then values must be assigned to the variables until the number of unknown variables equals the number of equations. Alternatively, one must assign values to undefined variables or else the system will remain unspecified. The number of these variables that must be defined or assigned to specify a system is the variability, or the degree of freedom of the system.

The equations by which the system is to be defined are obtained from the relationship between the potential of a component and its phase composition, temperature, and pressure. If one chooses as a standard state one of the phases in which all of the components are found, then the chemical potential of any component in another phase must equal the chemical potential of that component in the standard

state. It follows that for each phase in equilibrium with the standard phase, there will be a definite equation of state for each component in that phase. One concludes that if there are P phases, then each component will be specified by $(P - 1)$ equations. Then for C components, we deduce that the maximum number of available equations is given by:

$$\text{Equations} = C(P - 1) \tag{3}$$

The variance (degrees of freedom) in a system is given by the difference between the number of variables and the number of equations available to specify these. Denoting the number of degrees of freedom as F, this can be stated as:

$$F = \text{Variables} - \text{Equations} \tag{4}$$

Substituting equations (2) and (3) into equation (4), and simplifying, yields:

$$\text{F} = C + 2 - P \tag{5}$$

which is often rearranged to yield the popular statement of the Phase Rule:

$$P + F = C + 2 \tag{6}$$

One can immediately deduce from equation (5) that for a given number of components, an increase in the number of phases must lead to a concomitant decrease in the number of degrees of freedom. Another way to state this is that with an increase in the number of phases at equilibrium, the condition of the system must become more defined and less variable. Thus, for polymorphic systems where one can encounter additional solid-state phases, the constraints imposed by the Phase Rule can be exploited to obtain a greater understanding of the equilibria involved.

SYSTEMS OF ONE COMPONENT

In the absence of solvatomorphism or chemical reactions, polymorphic systems consist of only one component. The complete phase diagram of a polymorphic system provides the boundary conditions for the vapor state, the liquid phase, and the boundaries of stability for each and every polymorph. From the Phase Rule, it is concluded that the maximum amount of variance (two degrees of freedom) is only possible when the component is present in a single phase. All systems consisting of one component in one phase can therefore be perfectly defined by assigning values to a maximum of two variable factors. However, this bivariant system is not of interest to our discussion.

When a single component is in equilibrium between two phases, the Phase Rule predicts that it must be a univariant system exhibiting only one degree of freedom. Consequently, it is worthwhile to consider several univariant possibilities, because the most complicated phase diagram of a polymorphic system can be broken down into its component univariant systems. The Phase Rule applies equally to all of these systems, and all need to be understood for the entire phase diagram to be most useful.

Characteristics of Univariant Systems

When a single component exists in a state of equilibrium between two phases, the system is characterized by only one degree of freedom. The types of observable

equilibria can be of the liquid/vapor, solid/vapor, solid/liquid, and (specifically for components that exhibit polymorphism) solid/solid types. We will consider the important features of each in turn.

Liquid/Vapor Equilibria

A volatile substance in equilibrium with its vapor constitutes a univariant system, which will be defined if one of the variables (pressure or temperature) is fixed. The implications of this deduction are that the vapor pressure of the substance will have a definite value at a given temperature. Alternatively, if a certain vapor pressure is maintained, then equilibrium between the liquid and vapor phase can only exist at a single definite temperature. Each temperature point therefore corresponds to a definite pressure point, and so a plot of pressure against temperature will yield a continuous line defining the position of equilibrium. Relations of this type define the *vaporization curve*, and are ordinarily plotted to illustrate the trends in vapor pressure as a function of system temperature. It is generally found that vaporization curves exhibit the same general shape, being upwardly convex when plotted in the usual format of pressure–temperature phase diagrams.

As an example, consider the system formed by liquid water, in equilibrium with its own vapor. The pressure–temperature diagram for this system has been constructed over the range of 1–99°C (12), and is shown in Figure 1. The characteristics of a univariant system (one degree of freedom) are evident in that for each definite temperature value, water exhibits a fixed and definite vapor pressure.

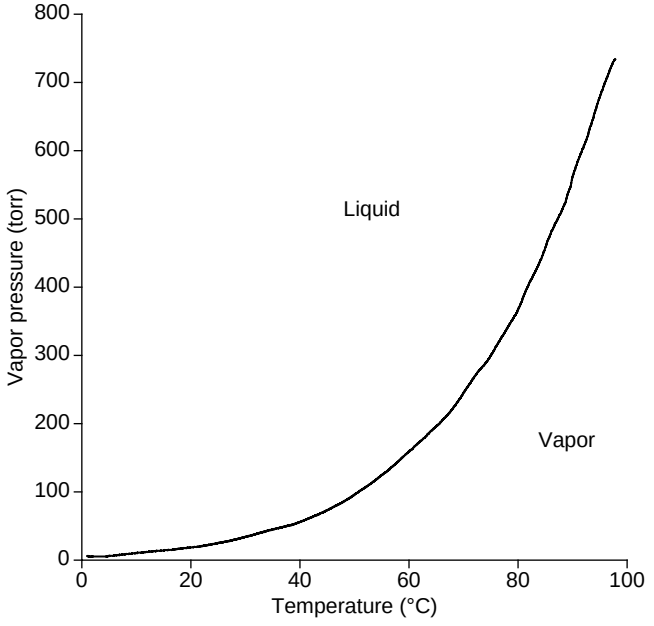

FIGURE 1 Vapor pressure of water as a function of temperature. The data were plotted from published values (12).

In a closed vessel, the volume becomes fixed. According to Le Chatelier's Principle, an input of heat (i.e., an increase in temperature) into a system consisting of liquid and vapor in equilibrium must result in an increase in the vapor pressure. It must also happen that with the increase of pressure, the density of the vapor must increase, whereas with the corresponding increase in temperature the density of the liquid must decrease. At some temperature value, the densities of the liquid and vapor will become identical, and at that point the heterogeneous system becomes homogeneous. At this *critical point* (defined by a critical temperature and a critical pressure), the entire system passes into one homogeneous phase, and the vaporization curve terminates at this critical point. As evident in Figure 1, the vapor pressure of a liquid approaches that of the ambient atmospheric pressure as the boiling point is reached.

Continuing with the principle of Le Chatelier, if an equilibrium system is stressed by a force that shifts the position of equilibrium, then a reaction to the stress that opposes the force will take place. Consider, therefore, a liquid/vapor system that is sufficiently isolated from its surroundings so that heat transfer is prevented (i.e., an adiabatic process). An increase in the volume of this system results in a decrease in the pressure of the system, causing liquid to pass into the vapor state. This process requires the input of heat, but because none is available from the surroundings, it follows that the temperature of the system must fall.

Although qualitative changes in the position of liquid/vapor equilibrium can be predicted by Le Chatelier's principle, the quantitative specification of the system is given by the Clausius–Clapeyron equation:

$$\frac{\mathrm{d}P}{\mathrm{d}T} = \frac{q}{T(v_2 - v_1)} \tag{7}$$

where q is the quantity of heat absorbed during the transformation of one phase to the other, v_2 and v_1 are the specific volumes of the two phases, and T is the absolute temperature at which the change occurs. Integration of equation (7) leads to useful relations that permit the calculation of individual points along the vaporization curve.

Solid/Vapor Equilibria

As a univariant system, a solid substance in equilibrium with its vapor phase will exhibit a well-defined vapor pressure for a given temperature, which will be independent of the relative amounts of solid and vapor present. The curve representing the solid/vapor equilibrium conditions is termed a *sublimation curve*, and generally takes a form similar to that of a vaporization curve. Although the sublimation pressure of a solid is often exceedingly small, for many substances it can be considerable.

One example of a solid that exhibits significant vapor pressure is camphor, for which a portion of its sublimation curve is shown in Figure 2. This compound exhibits the classic pressure–temperature profile (13), finally attaining a vapor pressure of 422.5 torr at its melting point (179.5°C). When heated above the fusion temperature, only a short vaporization curve is possible because the boiling point of camphor is reached at 207.4°C.

The sublimation curve of all substances will have its upper limit at the melting point, and a theoretical lower limit of absolute zero. However, because

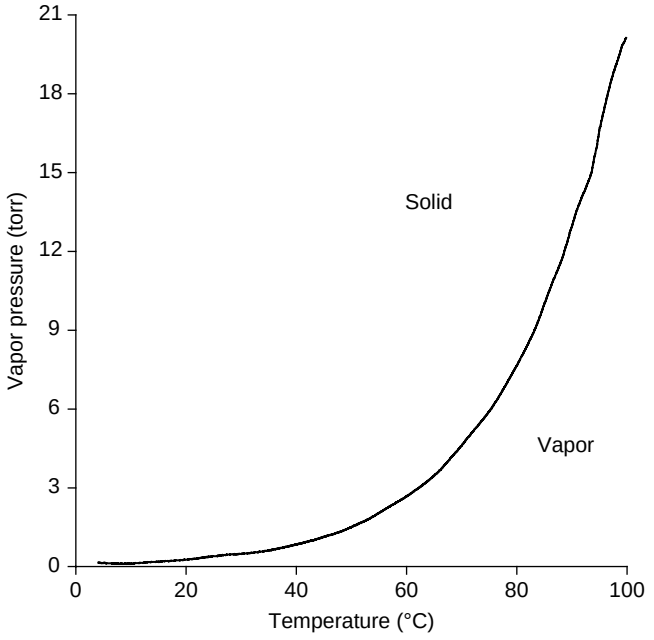

FIGURE 2 Vapor pressure of camphor as a function of temperature. The data were plotted from published values (13).

low-temperature polymorphic transitions can be encountered, one often encounters considerable complexity in sub-ambient phase diagrams. One need only consider the example of water, where at least seven crystalline forms are known.

If the sublimation pressure of a solid exceeds that of the atmospheric pressure at any temperature below its melting point, then the solid will pass directly into the vapor state (sublime) without melting when that substance is stored in an open vessel at that temperature. In such instances, melting of the solid can only take place at pressures exceeding ambient. Carbon dioxide is one of the best known materials that exhibits sublimation behavior. At the usual room temperature conditions, solid "dry ice" sublimes easily. Liquid carbon dioxide can only be maintained between its critical point (temperature of +31.0°C and pressure of 75.28 atm) and its triple point (temperature of –56.6°C and pressure of 4.97 atm) (14).

The direction of changes in sublimation pressure with temperature can be qualitatively predicted using Le Chatelier's principle, and quantitatively calculated by means of the Clausius–Clapeyron equation.

Solid/Liquid Equilibria

When a crystalline solid is heated to the temperature at which it melts and passes into the liquid state, as long as the two phases are in equilibrium, the solid/liquid system is univariant. Consequently, for a given pressure value, there will be a definite temperature (independent on the quantities of the two phases present) at which the equilibrium can exist. As with any univariant system, a curve representing the

equilibrium temperature and pressure data can be plotted, and this is termed the melting point or *fusion curve*. Because both phases in a solid/liquid equilibrium are condensed (and difficult to compress), the effect of pressure on the melting point of a solid is relatively minor unless the applied pressures are quite large.

Using Le Chatelier's principle, one can qualitatively predict the effect of pressure on an equilibrium melting point. The increase in pressure results in a decrease in the volume of the system. For most materials, the specific volume of the liquid phase is less than that of the solid phase, so that an increase in pressure would have the effect of shifting the equilibria to favor the solid phase. This shift will have the observable effect of raising the melting point. For those unusual systems where the specific volume of the liquid exceeds that of the solid phase, then the melting point will be decreased by an increase in pressure.

An example of a fusion curve is provided in Figure 3, which uses benzene as the example (15). It can be seen that to double the melting point requires an increase in pressure from 1 atm to approximately 250 atm. The fusion curve of Figure 3 is fairly typical in that in the absence of any pressure-induced polymorphic transformations, the curve is essentially a straight line.

The quantitative effect of pressure on the melting point can be calculated using the inverse of the Clausius–Clapeyron equation:

$$\frac{dT}{dP} = \frac{T(v_2 - v_1)}{q} \tag{8}$$

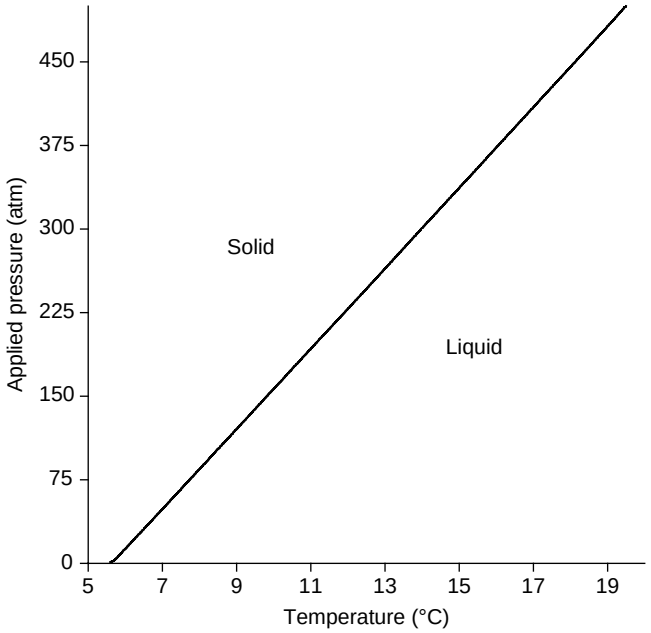

FIGURE 3 Effect of pressure on the melting point of benzene. The data were plotted from published values (15).

However, the magnitude of such shifts of the melting point with pressure are relatively minor, because the differences in specific volumes between the liquid and solid phases are ordinarily not great.

According to equation (8), for a fusion curve to exhibit a positive slope (as was the case for the one illustrated in Fig. 3), the specific volume of the liquid must be greater than the specific volume of the solid. In such systems, the substance would expand upon melting. Other systems are known where the specific volume of the liquid is less than the specific volume of the solid, so that these substances contract upon fusion. The classic example of the latter behavior is that of ice, which is known to contract upon melting. For example, although the melting point of water is 0°C at a pressure of 1 atm, the melting point decreases to –9.0°C at a pressure of 9870 atm (16).

Triple Points

When one component is present in three phases that co-exist in a state of equilibrium, the Phase Rule states that the system is invariant and therefore possesses no degrees of freedom. This implies that such a system at equilibrium can only exist at one definite temperature and one definite pressure, which is termed the *triple point*. For example, the solid/liquid/vapor triple point of water is found at a temperature of 273.16 K and a pressure of 4.58 torr.

Although the solid/liquid/vapor triple point is the one most commonly considered, the existence of other solid phases yields additional triple points. The number of triple points possible to a polymorphic system increases very rapidly with the number of potential solid phases. It has been shown that the number of triple points in a one component system is given by (17):

$$\#\,TP = \frac{P(P-1)(P-2)}{6} \tag{9}$$

Thus, for a system capable of existing in two solid-state polymorphs, a total of four phases would be possible, which would then imply that a total of four triple points are theoretically accessible. Denoting the liquid phase as L, the vapor phase as V, and the two solid phases as S_1 and S_2, the triple points correspond to:

$$\begin{aligned} &S_1\text{–}L\text{–}V \\ &S_2\text{–}L\text{–}V \\ &S_1\text{–}S_2\text{–}L \\ &S_1\text{–}S_2\text{–}V \end{aligned} \tag{10}$$

The S_1–S_2–V point is the *transition point* of the substance, the S_1–L–V and S_2–L–V points are *melting points*, and the S_1–S_2–L point is a *condensed transition point* (7). Whether or not all of these points can be experimentally attained depends on the exact details of the phase diagram of the system, and the temperatures and pressures at which these points exist.

To the scientist interested in polymorphic phenomena, the S_1–S_2–L triple point is of particular interest. Because the Phase Rule requires that triple points for systems of one component be invariant and devoid of degrees of freedom, it follows that crystallization from the melt could only yield two polymorphic solids at a

single pressure and temperature. In other words, the possibility that one could encounter simultaneous formation of two polymorphs from the molten phase (i.e., concomitant crystallization) at ordinary ambient pressure is exceedingly remote.

It has already been established that each S_i–V curve ends at the melting point. At this point, liquid and solid are each in equilibrium with vapor at the same pressure, so they must also be in equilibrium with each other. It follows that the particular value of temperature and vapor pressure must lie on each S_i–V curve(s) as well as on the L–V curve. Applying the Clausius–Clapeyron equation to both transitions, one concludes that a discontinuity must take place on passing from the S_i–V curve(s) to the L–V curve. This arises that because the change in specific volume for each transition is essentially the same, and because the heat required to transform a solid into its vapor must necessarily exceed the heat required to transform a liquid into its vapor, it must follow that the value of dP/dT for the solid/vapor transition must exceed that for the liquid/vapor transition. Therefore, the S_i–V curve(s) must increase more rapidly than does the L–V curve, with the curves intersecting at a triple point. Using a similar argument, it can be deduced that each S_i–L curve must also pass through a triple point. One therefore deduces that the triple point is a point of intersection of three univariant curves. These relationships are illustrated in Figure 4, which provides the phase behavior for a typical substance for which the specific volume of the liquid exceeds that of the solid.

The triple point differs from the ordinary melting point, because the latter represents the transition point that is determined at atmospheric pressure. At the triple point, the solid and liquid are in a state of equilibrium under a pressure that equals their vapor pressure.

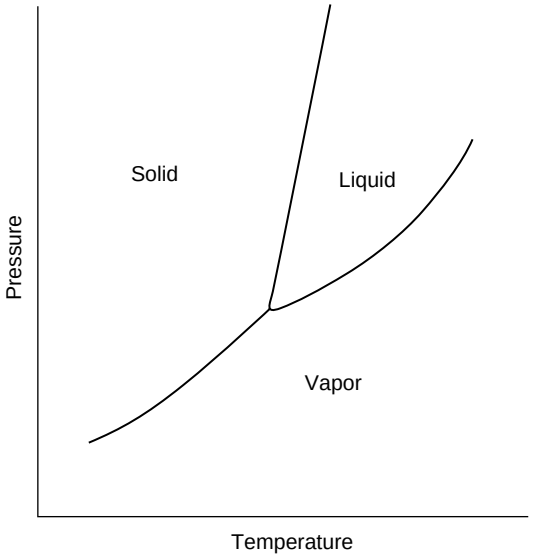

FIGURE 4 Phase diagram of a hypothetical substance for which the specific volume of the liquid exceeds that of the solid. The triple point is defined by the intersection of the three univariant curves describing the solid–vapor, liquid–vapor, and solid–liquid equilibria.

Interesting conclusions can be reached if one considers the consequences of applying Le Chatelier's principle to a system in equilibrium at its triple point. Stressing the system through a change in either pressure or temperature must result in an opposing effect that restores the equilibrium. However, because the system is invariant, the position of equilibrium cannot be shifted. Therefore, as long as the system remains in equilibrium at the triple point, the only changes that can take place are changes in the relative amounts of the phases present. For the specific instance of polymorphic solids, this deduction must apply to all other triple points of the system. It should be emphasized that at the triple point, all three phases must be involved in the phase transformations.

SOLID-STATE POLYMORPHISM AND THE PHASE RULE

That a given solid can exist in more than one crystalline form was first established by Mitscherlich for the specific instance of sodium phosphate (18). The phenomenon has been shown to be very widespread for both inorganic and organic systems, with compilations (19–21) and annual reviews (22–24) having been published regarding compounds of pharmaceutical interest that exhibit polymorphism. Throughout the following discussion, one must remember that these structural differences exist only in the solid state, and that the liquid and vapor phases of all polymorphs of a given component must necessarily be identical.

According to the preceding definition, each solid-state polymorphic form constitutes a separate phase of the component. The Phase Rule can be used to predict the conditions under which each form can co-exist, either along or in the presence of the liquid or vapor phases. One immediate deduction is that because no stable equilibrium can exist when four phases are simultaneously present (i.e., at a quadrupole point), it cannot happen that two polymorphic forms exist in equilibrium with each other as well as being in equilibrium with both their solid and vapor phases. However, when the two crystalline forms (denoted as S_1 and S_2) are in equilibrium with each other, then the two triple points (S_1–S_2–V and S_1–S_2–L) become exceedingly important.

The Transition Point

The S_1–S_2–V triple point is obtained as the intersection of the two univariant sublimation curves, identified as S_1–V and S_2–V. Below this triple point only one of the solid phases can exist in stable equilibrium with the vapor (i.e., being the stable solid phase), and above the triple point only the other phase can be stable. The S_1–S_2–V triple point therefore provides the pressure and temperature conditions at which the relative stability of the two phases inverts, and hence, is referred to as the *transition point*.

The S_1–S_2–V triple point is also the point of intersection for the S_1–S_2 curve, which delineates the conditions of equilibrium for the two polymorphic forms with each other. Because the S_1–S_2 curve defines a univariant system, it follows that the temperature at which the two phases can be in equilibrium will depend on the pressure. In common practice, workers make use of the ordinary transition point (defined as the temperature of equal phase stability at atmospheric pressure), but this point in the phase diagram must be distinguished from the S_1–S_2–V triple point. The ordinary transition point bears the same relationship to the S_1–S_2–V triple point that the ordinary melting point bears to the S–L–V triple point.

The transition point, like the melting point, is affected by pressure. Depending on the relative values of the specific volumes of the two polymorphs, an increase in pressure can either raise or lower the transition temperature. However, because this difference in specific volumes is ordinarily very small, the Clausius–Clapeyron equation predicts that the magnitude of dT/dP will not be great.

To illustrate the phase behavior of a substance at the S_1–S_2–V triple point, we will return to the example of camphor whose sublimation curve was shown in Figure 2. The pressure dependence of the S_1–S_2 (Form-1/Form-2) phase transformation is known (25), and the phase diagram resulting from the addition of this data to the sublimation curve is shown in Figure 5. Because the data used to construct the S_1–S_2 curve were obtained at pressure values ranging up to 2000 atm, the location of the triple point must be deduced from an extrapolation of the S_1–S_2 curve to its intersection with the S–V curve. One finds that the triple point is located at a temperature of 87°C and a pressure of 0.017 atm (13 torr). This finding would imply that the S–V sublimation curve reported for camphor actually represents the composite equilibrium of the two phases with their common vapor phase.

The Condensed Transition Point

For the sake of this argument, let us assume that phase S_1 is more stable than is phase S_2 at ordinary ambient conditions. If one increases the pressure on the system, the position of equilibrium will be displaced along the S_1–S_2 transition curve, which will

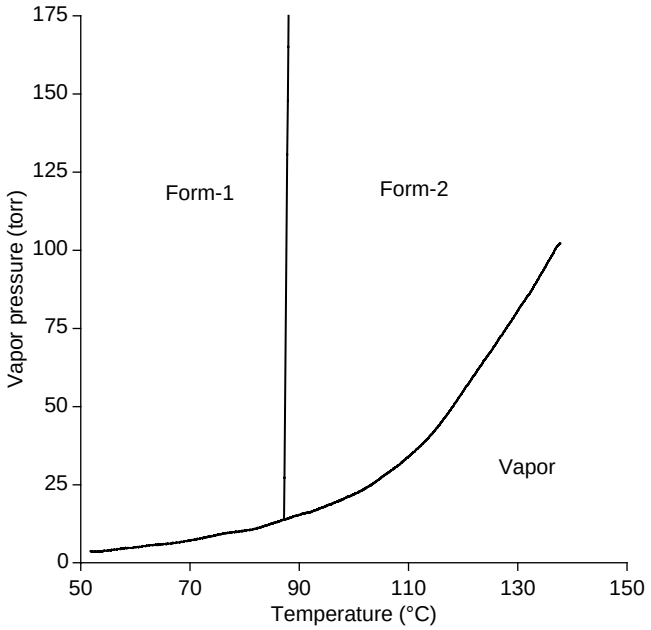

FIGURE 5 Location of the Form-1/Form-2/vapor triple point in the phase diagram of camphor. The triple point is deduced from the extrapolated intersection of the S_1–S_2 transition curve with that of the S–V sublimation curve. The data were plotted from published values (13,25).

have the effect of raising the transition temperature. At some point, the univariant S_1–S_2 curve will intersect with the univariant S_1–L fusion curve, producing a new triple point S_1–S_2–L, which is denoted the *condensed transition point*. The S_1 phase ceases to exist in a stable condition above this triple point, and the S_2 phase will be the only stable solid phase possible.

When observable, the S_1–S_2–L triple point is encountered at extremely high pressures. For this reason, workers rarely determine the position of this triple point in a phase diagram, but focus instead on the S_1–S_2–V triple point for discussions of relative phase stability.

To illustrate a determination of an S_1–S_2–L triple point, we will return to the example of benzene, for which the low-pressure portion of the S–L fusion curve was shown in Figure 3. When the full range of pressure–temperature melting point data is plotted (15), one finds that the pressure-induced volume differential causes a definite non-linearity to appear in the data. Adding the S_1–S_2 transition data (26) generates the phase diagram of benzene, which is shown in Figure 6, where the triple point is obtained as the intersection of the S–L fusion curve and the S_1–S_2 transition curve. The S_1–S_2–L triple point is deduced to exist at a temperature of 215°C and a pressure of 11,500 atm. Such pressures are only attainable through the use of sophisticated systems, which explains why the S_1–S_2–L triple point is only rarely determined during the course of ordinary investigations.

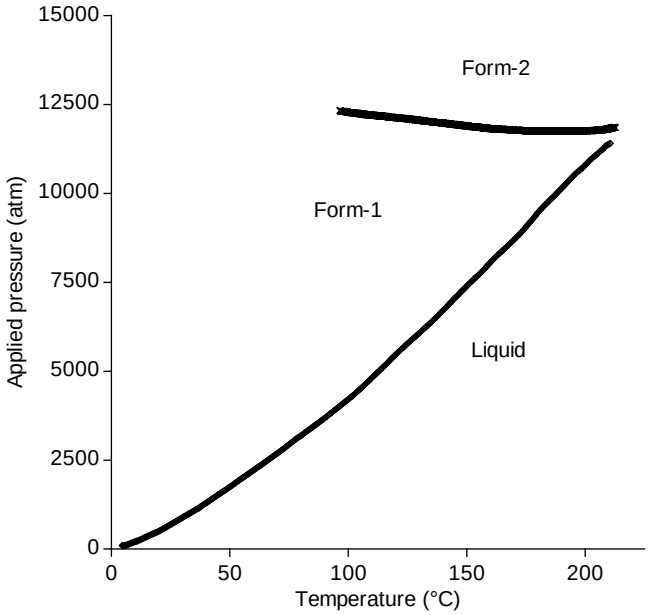

FIGURE 6 Location of the Form-1/Form-2/liquid triple point in the phase diagram of benzene. The triple point is deduced from the extrapolated intersection of the S_1–S_2 transition curve with that of the S–L fusion curve. The data were plotted from published values (15,26).

Enantiotropy and Monotropy

The S_1–S_2–V triple point is one at which the reversible transformation of the crystalline polymorphs can take place. If both S_1 and S_2 are capable of existing in stable equilibrium with their vapor phase, then the relationship between the two solid-state forms is termed *enantiotropy*, and the two polymorphs are said to bear an enantiotropic relationship to each other. For such systems, the S_1–S_2–V triple point will be a stable and attainable value on the pressure–temperature phase diagram. A phase diagram of a hypothetical enantiotropic system is shown in Figure 7. Each of the two polymorphs exhibits an S–V sublimation curve, which cross at the same temperature at which they intersect the S_1–S_2 transition curve. The S_2–V curve crosses the stable L–V fusion curve at an attainable temperature, which is the melting point of the S_2 phase. The S_1–S_2 transition and the S_2–L fusion curves eventually intersect with the S_1–L fusion curve, forming the condensed transition point.

It should be noted that the ordinary transition point of enantiotropic systems (which is measured at atmospheric pressure) must be lower than the melting point of either solid phase. Each polymorph will therefore be characterized by a definite range of conditions under which it will be the most stable phase, and each form is capable of undergoing a reversible transformation into the other.

The melting behavior of an enantiotropic system is often interesting to observe. If one begins with the polymorph that is less stable at room temperature (i.e., the metastable phase) and heats the solid up to its melting point, the S_2–L melting phase transformation is first observed. As the temperature is raised further, the melt is often observed to re-solidify into the more stable polymorph (S_1) because the liquid

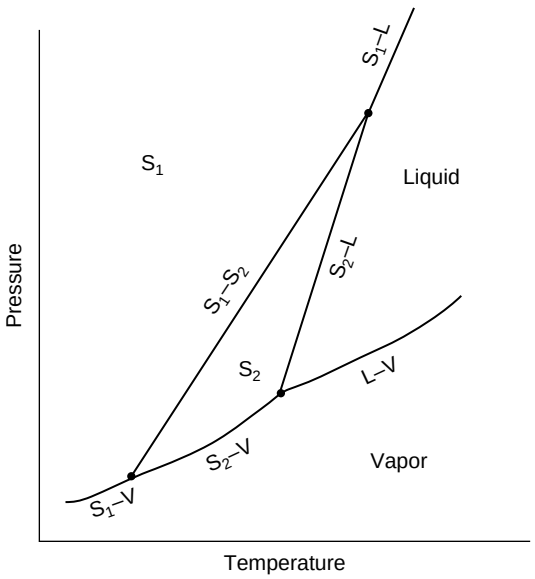

FIGURE 7 Idealized phase diagram of a substance whose two polymorphs exhibit an enantiotropic relationship.

now exists in a metastable state with respect to S_1. Continued heating then results in the S_1–L phase transformation. If one allows this latter melt to re-solidify and cool back to room temperature, only the S_1–L melting transition will be observed.

Other systems exist where the second polymorph (S_2) has no region of stability anywhere on a pressure–temperature diagram. This type of behavior is termed *monotropy*, and such polymorphs bear a monotropic relationship to each other. For a monotropic system, the S_1–S_2–V triple point will not be an attainable value on the pressure–temperature phase diagram because melting of one of the forms takes place before the triple point can be reached.

The melting point of the metastable S_2 polymorph will invariably be less (in terms of both pressure and temperature) than will the melting point of the stable form (S_1). This, in turn, has the effect of causing the S_1–S_2–V triple point to exceed the melting point of the stable S_1 phase. Monotropy therefore differs from enantiotropy in that the melting points of an enantiotropic pair are higher than the S_1–S_2–V triple point, whereas for monotropic systems one or both of the melting points is less than the S_1–S_2–V triple point.

The phase diagram of a hypothetical monotropic system is illustrated in Figure 8. The S_1–S_2–V triple point (transition point) point is clearly virtual in that fusion of all solid phases takes place before the thermodynamic point of phase stability can be attained. The phase diagram indicates that only one of the polymorphs can be stable at all temperatures up to the melting point, and the other polymorph must be considered as being a metastable phase. For such systems, there is no transition point attainable at atmospheric pressure, and the transformation of polymorphs can take place irreversibly in one direction only.

Very complicated phase diagrams can arise when substances can exist in more than two crystalline polymorphs. In certain cases, some of the forms may be enantiotropic to each other, and monotropic to yet others. For instance, of the eight polymorphs of elemental sulfur, only the monoclinic and rhombic modifications exhibit

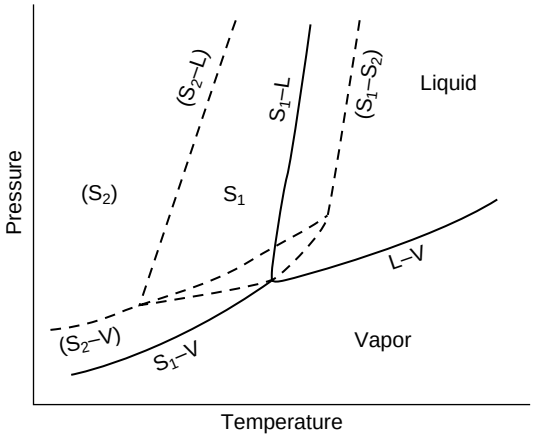

FIGURE 8 Idealized phase diagram of a substance whose two polymorphs exhibit a monotropic relationship.

enantiotropy and the possibility of reversible interconversion. All of the other forms are monotropic with respect to the monoclinic and rhombic forms, and remain as metastable phases up to the melting point.

KINETICALLY IMPAIRED EQUILIBRIA

Using the computational tools of quantitative thermodynamics, one can predict the course of an equilibrium process and determine what will be the favored product. Unfortunately, classical thermodynamics has nothing to say about the velocity of reactions, so a short discussion as to the possible kinetics associated with phase transformation reactions is appropriate.

Suspended Phase Transformations

It is well established that certain phase transformations, predicted to be spontaneous on the basis of favorable thermodynamics, do not take place as anticipated. For instance, the diamond phase of carbon is certainly less stable than the graphite phase, but under ordinary conditions (i.e., in a gemstone setting) one does not observe any evidence for phase transformation. The diamond polymorph of carbon is metastable with respect to the graphite phase of carbon, but the phase interconversion can only take place if appropriate energy is added to the system.

Fahrenheit found that pure liquid water, free from suspended particles, could be cooled down to a temperature of –9.4°C without formation of a solid ice phase (27). If the temperature of the supercooled water was decreased below –9.4°C, solidification was observed to take place spontaneously. However, if a crystal of solid ice was added to supercooled water whose temperature was between 0 and –9.4°C, crystallization was found to take place immediately. Fixing the system pressure as that of the atmosphere, one can define the metastable region of stability for supercooled water as 0 to –9.4°C. Supercooled water is unstable with respect to phase transformation at temperatures less than –9.4°C.

Suspended phase transformations are those phase conversions that are predicted to take place at a defined S_1–S_2–V triple point, but do not owing to some non-ideality in the system. One can immediately see that only through the occurrence of a suspended transformation could one obtain a metastable polymorph in solid form. In the case of two solids, slow conversion kinetics can permit the transition point to be exceeded when moving in either direction along the S_1–S_2 transition curve, permitting the isolation of the otherwise unobtainable metastable phase.

One of the best-known examples of suspended transformation is found with the polymorphs formed by quartz (28). The three principal polymorphic forms are quartz, tridymite, and cristobalite, which are enantiotropically related to each other. The ordinary transition point for the quartz/tridymite transition is 870°C, whereas the ordinary transition point for the tridymite/cristobalite transition is 1470°C. The melting point of cristobalite is at 1705°C, which exceeds all of the solid phase transition points. However, the phase transformations of these forms are extremely sluggish, and consequently, each mineral form can be found in nature existing in a metastable form.

Ordinarily, the rate-determining step during phase conversion is the formation of nuclei of the new phase. If suitable nuclei cannot be formed at the conditions of study, then the phase transformation is effectively suspended until the nuclei either form spontaneously or are added by the experimenter. Synthetic chemists

have made use of these phenomena by introducing "seed" crystals of their desired phase into a supersaturated solution to obtain a crop of material in that solid-state form, and to suppress the formation of unwanted by-products. This procedure is especially important during the resolution of enantiomers and diastereomers by direct crystallization.

For example, the inclusion of seed crystals of chloramphenicol palmitate Form-A to a mass of Form-B was found to lead to accelerated phase transformation during a simple grinding process (29). The same type of grinding-induced conversion was obtained when seed crystals of Form-B were added to bulk Form-C prior to milling. In this study, the conversion kinetics were best fitted to a two-dimensional nuclear growth equation, but the parameters in the fitting were found to depend drastically on the quantity of seeds present in the bulk material. The practical import of this study was that Form-A was the least desirable from a bioavailability viewpoint, and that milling of phase-impure chloramphenicol palmitate could yield problems with drug products manufactured from overly processed material.

Pressure–Temperature Relations Between Stable and Metastable Phases

It has already been mentioned that in the vicinity of the S–L–V triple point, the S–V sublimation curve increases more rapidly than does the L–V vaporization curve. If follows that if the L–V curve is to be extended below the triple point (as would have to happen for a supercooled liquid), the continuation of the curve must lie above the S–V curve. This implies that the vapor pressure of a supercooled liquid (a metastable phase) must always exceed the vapor pressure of the solid (the stable phase) at the same temperature.

For solids capable of exhibiting polymorphism, in the vicinity of the S_1–S_2–V triple point, the sublimation curve for the metastable phase (S_2–V) will always lie above the sublimation curve for the stable phase (S_1–V). It therefore follows that the vapor pressure of a metastable solid phase will always exceed the vapor pressure of the stable phase at a given temperature. This generalization was first deduced by Ostwald, who proved that for a given temperature of a one component system, the vapor pressure of any metastable phase must exceed that of the stable phase (30). This behavior was verified for the rhombic and monoclinic polymorphs of elemental sulfur, where it was found that the ordinary transition point of the enantiotropic conversion was 95.5°C (31). The vapor pressure curve of the rhombic phase was found to invariably exceed that of the monoclinic phase at all temperature values above 95.5°C, whereas the vapor pressure of the monoclinic phase was higher than that of the rhombic phase below 95.5°C. This behavior provided direct evidence that the rhombic phase was the most stable phase below the transition point, and that the monoclinic phase was more stable above the transition point.

Owing to the experimental difficulties associated with measurement of the families of S_i–V sublimation curves required for the use of Ostwald's rule of relative phase stability, a variety of empirical rules (not based on the phase rule) have been advanced for the deduction of relative phase stabilities. However, when the pertinent data can be measured, application of the rule can yield unequivocal results. The pressure–temperature diagram for the α-, β-, and γ-phases of sulfanilamide was constructed using crystallographic and thermodynamic data, and by assigning the temperatures of the experimentally observed phase transitions to triple points involving the vapor phase (32). At temperatures below 108°C, the order of vapor pressures was $\beta < \alpha < \gamma$, which indicated that the β-phase was more stable than the α-phase, which

is itself more stable than the γ-phase. Between 108°C and 118°C, the order of vapor pressures was determined to be $\beta < \gamma < \alpha$, so that within this range the β-phase remained the most stable, and that the γ-phase was more stable than the α-phase. At temperatures exceeding 118°C, the order of vapor pressures was $\gamma < \beta < \alpha$, indicating that the γ-phase became the most stable, and that the α-phase remained the least stable. The data clearly indicate that the β- and γ-phases are enantiotropically related, having a transition point of 118°C. It was further concluded that because no stability region could be identified for the α-phase (it only became less metastable as the temperature increased), it bore a monotropic relationship to the other two phases.

SYSTEMS OF TWO COMPONENTS

When the substance under study is capable of forming a hydrate or solvate system and can therefore exhibit solvatomorphism, the number of components must necessarily increase to at least two. The two components are the substance itself and the solvent of solvation, because any other compound can be described as some combination of these. The various phases that can be in equilibrium will generally not exhibit the same composition, so that the usual variables of pressure, volume, and temperature must be augmented by the inclusion of the additional variable of concentration (thermodynamically through the chemical potential). In fact, it is a general rule that if the composition of different phases in equilibrium varies, then the system must contain more than one component.

Two components present in a single phase constitute a tervariant system, characterized by three degrees of freedom. The equilibrium condition between two phases is a bivariant system, whereas three phases in equilibrium would be univariant. For a system of two components to be invariant, there must be four phases in equilibrium. From the Phase Rule, one immediately concludes that there cannot be more than four phases in equilibrium under any set of environmental conditions. Owing to the difficulties in expressing phase diagrams on a two-dimensional surface, the graphical expression of these phase relationships requires the a priori specification of some of the conditions. Fortunately, for the two component systems of most interest to pharmaceutical scientists (hydrates and their anhydrates), studies are usually conducted at atmospheric pressure, and this specification immediately fixes one of the variables, enabling the construction of planar diagrams.

Solid/Vapor Equilibria

One two-component system is where one or more solid phases exists in a state of equilibrium with a single vapor phase. This type of situation would exist for solvation/desolvation equilibria whose transition temperatures are substantially less than the fusion point corresponding to generation of a liquid phase, and is certainly a commonly encountered type of solvate system of pharmaceutical interest. For most compounds, the solid substance in question has no appreciable vapor pressure, so that the sole component of the vapor phase will be essentially that of the volatile solvent. The usual occurrence where the evolved solvent passes entirely into the vapor phase will be assumed, where it does not form a discrete liquid phase of its own.

Upon heating, the solvate species can dissociate either into a solvate of lower solvation, or into an anhydrous phase. Each stage of such equilibria represents a

system of two components (substance and solvent) present in three phases (initial solvate, solvate product, and solvent vapor). According to the Phase Rule, this constitutes a univariant system, so a definite vapor pressure must correspond to each temperature. This is termed the *dissociation pressure*, and will be independent on the relative or absolute amounts of phases present.

Single Solvation State Systems

Copper chloride dihydrate is an example of simple dehydration, which upon simple heating below the melting point, is capable of losing its water of hydration:

$$CuCl_2 \cdot 2H_2O \rightarrow CuCl_2 + 2H_2O \tag{11}$$

At atmospheric pressure, the dehydration of the dihydrate is essentially complete by 75°C (33). The pressure–temperature curve of the dihydrate consists of a simple dissociation curve, having the form illustrated in Figure 9.

When dehydrating the dihydrate phase at constant temperature, the pressure would be maintained at the value corresponding to the dissociation pressure of the dihydrate until the complete disappearance of that phase. At that point, the pressure would fall to that characteristic (and negligible) vapor pressure of the anhydrate phase. If the external pressure on the dihydrate is reduced below its dissociation pressure at a given temperature, then the solid will undergo spontaneous efflorescence and will lose the requisite water of hydration to the atmosphere.

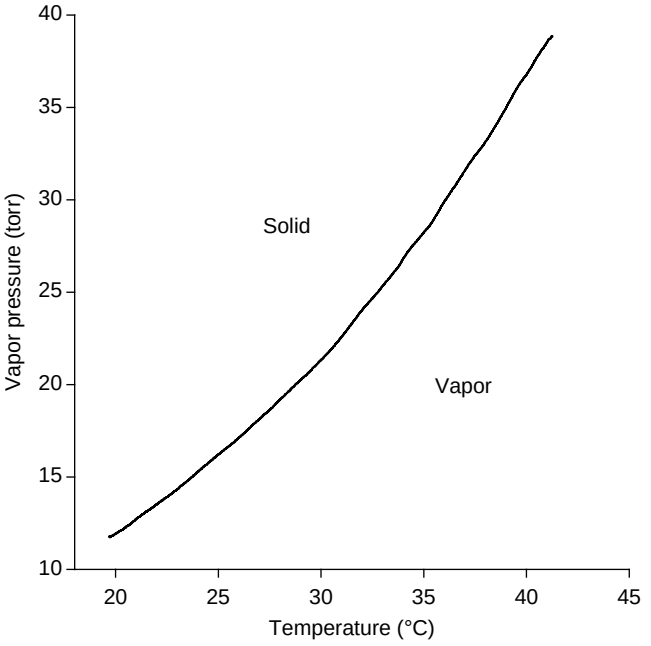

FIGURE 9 Vapor pressure of water over copper chloride dihydrate as a function of temperature. The data were plotted from published values (33).

Conversely, if one begins with the anhydrous phase, and exposes the solid to water vapor, as long as the vapor pressure is less than that of the dissociation pressure at that temperature, no hydrate phase will form. This does not imply that adventitious water will not be absorbed, however, but simply that the crystalline dihydrate cannot be formed. This situation arises because according to the phase diagram, only the anhydrate phase is stable below the lowest dissociation pressure. At the dissociation pressure, however, a univariant system is obtained because with formation of the hydrate phase there are now three phases in equilibrium. With the experiment being conducted at constant laboratory temperature, the pressure must also be constant. Continued addition of water vapor can only result in an increase in the amount of dihydrate phase, and a decrease in the amount of anhydrate phase present. When the anhydrate is completely converted, the system again becomes bivariant pressure and the pressure increases again with the amount of water added. Because no higher hydrate forms are possible for copper chloride, only adventitious water can be absorbed. Of course, if sufficient water is absorbed, the solid can presumably dissolve in the extra water, a phenomenon which is known as *deliquescence*.

Multiple Solvation State Systems

When substances are capable of forming multiple solvated forms, it is observed that the different solvates will exhibit different regions of stability and the pressure–temperature phase diagram becomes much more complicated. Each solvate will be characterized by its own dissociation curve, and these families of curves mutually terminate at points of intersection. Each dissociation curve will exhibit an initial increase, then plateaus as conversion to another solvation state begins, and then decreases as the vapor pressure of the solvate product becomes established. At temperature values slightly above the intersection point of two dissociation curves, the solvate product would have a higher vapor pressure than the solvate reactant, and would therefore be metastable with respect to the higher solvate. However, once the temperature is allowed to rise beyond the plateau value, the solvate product becomes the stable phase.

The hydrate system formed by lithium iodide will be used to illustrate the stepwise dehydration process. When heated at temperature values below the melting point of anhydrous lithium iodide (446°C), the trihydrate is capable of losing its water of hydration, to form a dihydrate and a monohydrate on the way to the anhydrate phase:

$$\begin{aligned} \mathrm{LiI \cdot 3H_2O} &\rightarrow \mathrm{LiI \cdot 2H_2O + H_2O} \\ \mathrm{LiI \cdot 2H_2O} &\rightarrow \mathrm{LiI \cdot 1H_2O + H_2O} \end{aligned} \tag{12}$$

At atmospheric pressure, the transition point for the trihydrate/dihydrate conversion is 72°C, and the transition point for the dihydrate/monohydrate conversion is 87°C (34). As illustrated in Figure 10, the pressure–temperature phase diagram of the system consists of three discrete dissociation curves, which intersect at the ordinary transition points.

When dehydrating the trihydrate phase at constant temperature, the pressure would be maintained at the value corresponding to the dissociation pressure of the trihydrate until the complete disappearance of that phase. At that point, the pressure would fall to that characteristic pressure of the dihydrate phase. Continued dehydration would take place at the dissociation pressure of the dihydrate phase until it

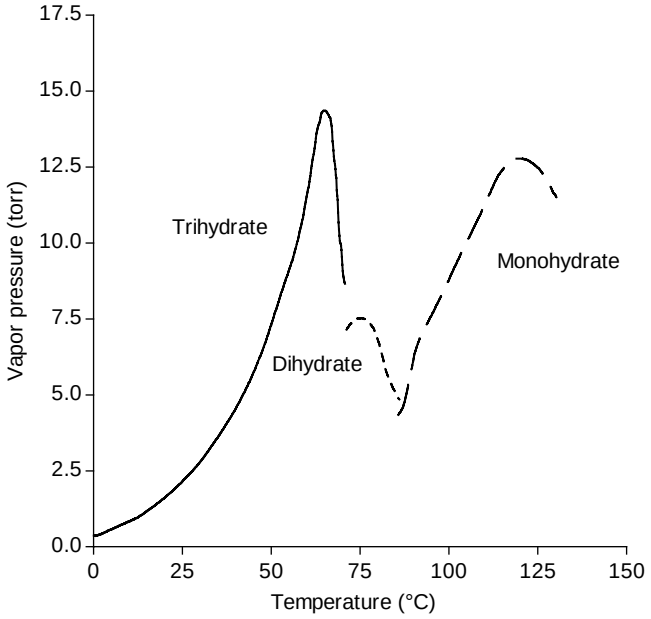

FIGURE 10 Vapor pressure of water over the trihydrate (solid trace), dihydrate (short dashed trace), and monohydrate (long dashed trace) phases of lithium iodide as a function of temperature. The data were plotted from published values (34).

was completely transformed to the monohydrate, whereupon the pressure would immediately fall to the dissociation pressure of the monohydrate. As previously discussed, once the external pressure on a given hydrate is reduced below its characteristic dissociation pressure, then the solid will undergo spontaneous efflorescence to a lower hydration state and will evolve the associated water of hydration.

Conversely, if one begins with the anhydrous lithium iodide, and exposes the solid to water vapor, as long as the vapor pressure is less than any of the dissociation pressures, no hydrate phase can form. At the lowest dissociation pressure a univariant system is obtained, because upon formation of the hydrate phase there must be three phases in equilibrium. Because the experiment is being conducted at constant laboratory temperature, the pressure must also be constant. Continued addition of water vapor can only result in an increase in the amount of hydrate phase, and a decrease in the amount of anhydrate phase present. When the anhydrate is completely converted, the system again becomes bivariant pressure and the pressure increases again with the amount of water added. The higher hydrate forms are, in turn, produced at their characteristic conversion pressures in an equivalent manner.

Desolvated Solvates

A desolvated solvate is the species formed upon removal of the solvent from a solvate. Depending on the empirical details of the system, the desolvated solvate may be produced as either a crystalline or an amorphous phase. These materials are not equivalent, possessing different free energies, and the amorphous phase

will ordinarily be the less stable of any of the crystalline forms. For example, the thermal dehydration product of theophylline monohydrate could be formulated into tablets, which then exhibited different dissolution rates than tablets formed from either the monohydrate or anhydrate phases (35).

However, from a Phase Rule viewpoint, a completely desolvated solvate, from which the solvent vapor has been totally removed from the residual solid, is simply a system of one component. The characteristics and phase equilibria of such systems have been amply described earlier in the section "Systems of One Component," and all of the deductions reached about systems of one component must necessarily hold for solids produced by the desolvation of a solvate species.

Solid/Liquid/Vapor Equilibria

This system exists when the solid phase containing the solvated compound is in equilibrium with both its liquid and vapor phase. This system would result from the congruent melting of the solid phase, which was in turn accompanied by the simultaneous volatilization of the included solvation molecules. The equilibrium therefore consists of two components (substance and solvent) present in three phases (initial solvate, fused liquid, and solvent vapor). According to the Phase Rule, this constitutes a univariant system, so just as for the system described previously, for each temperature there will correspond a definite vapor pressure. This is still a dissociation pressure, and will be independent on the relative or absolute amounts of phases present.

Examples of this type of behavior are not commonly encountered for compounds of pharmaceutical interest, because the melting points of drug substances generally lie at considerably higher temperatures than do the dehydration points. Even for excipients characterized by low melting points, the dehydration steps take place at lower temperatures than do the fusion transitions. One of the closest pairs of dehydration and melting temperatures was noted for the crystalline dihydrates of magnesium stearate and palmitate, but even here the melting transition occurred approximately 20°C higher than the dehydration transition (36). As a result, the crystalline hydrates could be completely dehydrated prior to the onset of any melting.

Nevertheless, the Phase Rule can be used to deduce some conclusions about systems where a congruently melting solid remained in equilibrium with the vapor phase. One deduction is that one would not expect to encounter a condition where, in addition to being in equilibrium with liquid and vapor phases, the solvate phase was in equilibrium with any other type of solid phase. Such a system would constitute an invariant system, and could only exist at a characteristic quadrupole point. Because it is hardly likely to encounter a quadrupole point at ambient temperature or pressure, the possibility can be effectively discounted from ordinary experience.

The power of the Phase Rule is immediately evident in that the solid/liquid/vapor system is characterized by the same amount of variance as was the solid/vapor system. As a result, the arguments made regarding the pressure–temperature curves of the former system can be extended to apply to the latter system, except that the liquid phase takes the place of the anhydrate phase.

Solid/Solution Equilibria

Given that most polymorph screening studies entail crystallization of solids out of a solution, it follows that the equilibria existing between solid phases and a liquid phase containing dissolved solute would be of prime interest. This area, of course, relates to

the solubility of materials in solvents, which has been the subject of in-depth reviews (37–42).

For simple unsaturated solutions, as long as the saturation solubility is not exceeded, all components in the liquid phase will be completely miscible, and therefore the number of phases equals one. Because the number of components equals two, the number of degrees of freedom available to the system is calculated to be three. Considering that experimental work is normally conducted at atmospheric pressure, the variability is further reduced down to two. These two variables are temperature and the chemical potential of the dissolved component, which is more commonly expressed as a solution concentration. As long as the solvent is capable of completely dissolving added solute, the variance of the system will remain effectively equal to two because the effect of pressure is generally not significant for a condensed phase.

Once the ability of the solvent to dissolve solute is exceeded, the number of phases increases to two and the variance (at constant pressure) decreases to one. It follows that for a solute in equilibrium with its saturated solution, the specification of either temperature or concentration fixes the other value. One may then plot the *equilibrium solubility* of a substance as a function of temperature to obtain the solubility curve that defines the solute concentrations existing in a the saturated solution that is in a state of equilibrium with pure solid solute.

For most substances, the dissolution process is endothermic, and therefore the equilibrium solubility of solute will increase with temperature. As an example, the equilibrium solubility of malic acid (43) as a function of temperature is plotted in Figure 11. However, for a much smaller number of compounds, the dissolution of solute is an exothermic process, which causes the solubility to decrease with increasing temperature. Calcium acetate (44) is one such example, as the solubility curve of Figure 11 illustrates.

Of course, the temperature of a solution cannot be varied indefinitely because temperatures will exist where phase transitions will occur. The equilibrium phase diagram of a simple aqueous binary system that does not form a hydrate is shown in Figure 12. The unbroken liquidus line represents the equilibrium between the solid solute and its saturated solution, and is the *solubility* curve discussed above. The broken liquidus line represents the equilibria between ice and the saturated solution, and is termed the *freezing point* curve. The region bounded by these liquidus lines defines the unsaturated solution condition that was discussed in detail earlier. The horizontal dashed line is termed the *eutectic* line, and at all temperatures below the eutectic temperature the system would be entirely solid.

If one prepares a dilute solution of the solute and initiates cooling, one would find that pure ice would crystallize out of the solution when the temperature reached a point along the freezing point curve. As one decreased the temperature further, the solution would become more concentrated up to the point where the freezing point curve intersects with the eutectic line. Alternatively, if one began with a concentrated solution of the solute and initiated cooling, solid solute would crystallize out of the solution when the temperature equaled a point along the solubility curve. Continued cooling of the solution would result in the crystallization of more solute, thus decreasing the solution concentration, until the temperature equaled the same point along the solubility curve.

The eutectic point is therefore the condition where ice and solid solute separate out together in the form of a conglomerate mixture, and the system freezes at

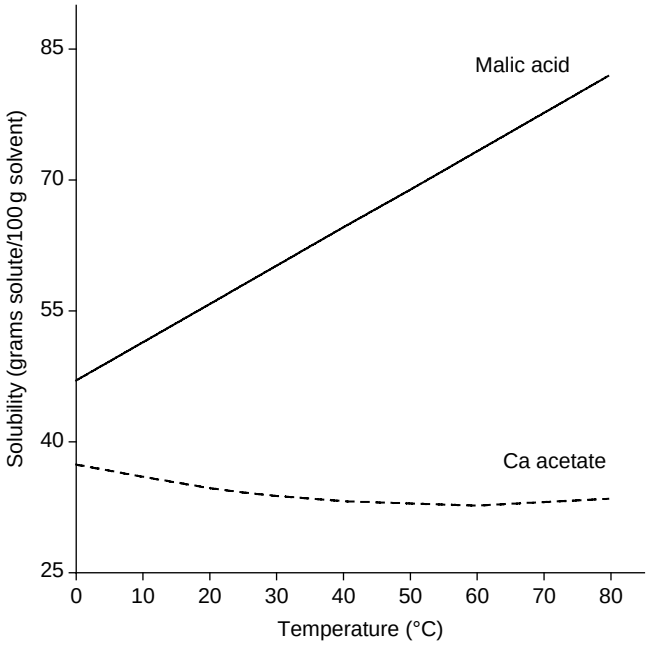

FIGURE 11 Equilibrium solubilities of malic acid (solid trace) and calcium acetate (dashed trace) as a function of temperature. The malic acid data were plotted from published values (43), as were the calcium acetate values (44).

constant temperature without change in composition. At the eutectic point, the number of phases equals three, and for a system of two components this reduces the variance to one. However, because the pressure of the system has been fixed at atmospheric, the system is actually invariant and possesses no degrees of freedom.

When the solute is capable of exhibiting polymorphic or solvatomorphic behavior, the phase diagram summarizing the various equilibria existing between solutions of dissolved solute and its solid phases is of much greater interest. For example, the temperature dependence of the solubilities of ampicillin anhydrate and trihydrate have been studied, with both solvatomorphs exhibiting good linearity in their van't Hoff plots (45). The solubility data from this study have be reformatted and plotted in Figure 13, and the break noted in the solubility curve at 42°C indicates the existence of a phase transition. It was determined that the anhydrate phase was the stable phase at temperatures above the ordinary transition point, whereas the trihydrate was the stable phase below this temperature. The data also indicate that the enthalpy of solution for the trihydrate phase is endothermic, whereas the enthalpy of solution of the anhydrate phase is exothermic.

Kinetically Impaired Equilibria

Although thermodynamics and the Phase Rule are rigorous in defining equilibrium conditions, its frequently happens that a system can become kinetically trapped in a metastable state and remain outside a condition of true equilibrium. For instance,

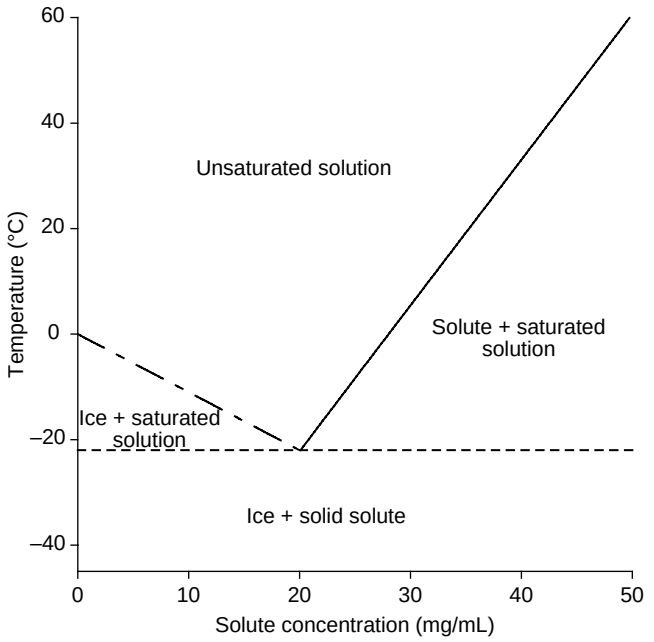

FIGURE 12 Phase diagram for a binary system consisting of a hypothetical solute in equilibrium with water at fixed pressure.

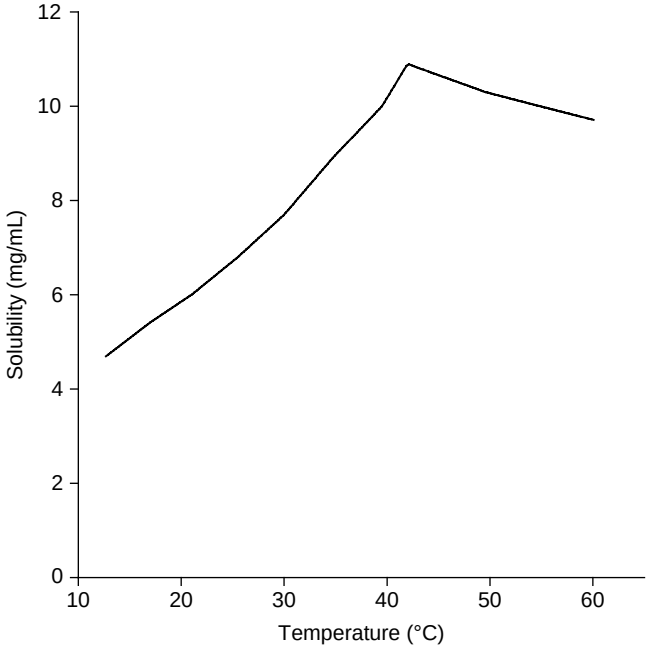

FIGURE 13 Solubility curve for ampicillin in water as a function of temperature. The data were plotted from published values (45).

efflorescence of a hydrate may not occur immediately once the pressure is reduced below the dissociation pressure, and will, in fact, take place only when a suitable nucleus for growth is formed. Michael Faraday noted that the decahydrate phase of sodium sulfate is unstable with respect to open air, because the vapor pressure of the salt exceeds the vapor pressure of water vapor at room temperature (46). However, the system only dehydrates upon contact with the anhydrate phase, demonstrating the metastable nature of the decahydrate phase.

The instability of many anhydrate phases with respect to water has been long known. For instance, it was shown by Shefter and Higuchi that hydrate phases of cholesterol, theophylline, caffeine, glutethimide, and succinyl sulfathiazole would spontaneously form during dissolution studies (47). Similar behavior has been reported for metronidazole benzoate (48) and carbamazepine (49). In each of these systems, the integrity of the anhydrous phases can be maintained only as long as the relative humidity is kept below the dissociation pressure of the hydrate species.

As discussed above, ampicillin is known to form crystalline anhydrate and trihydrate phases, which exhibit an ordinary transition point of 42°C when in contact with bulk water (45). The anhydrate phase is found to be the stable phase above the transition point, and the trihydrate is the stable phase below this temperature. The trihydrate is the phase of pharmaceutical interest, and can be maintained in a stable condition as long as contact with the anhydrate phase is minimized and the substance maintained at temperatures below the transition point. When milled in contact with anhydrate phase, or when placed in contact with bulk water at room temperature, the anhydrate phase forms from the trihydrate with great velocity.

SUMMARY

Even though the conclusions that can be reached through its use are mainly of a qualitative nature, the Phase Rule is still extremely useful for providing a physical understanding of polymorphic and solvatomorphic systems in a short amount of time. It also is very useful in providing a physical interpretation of phase transformation phenomena, and is especially useful in its ability to rule out the existence of simultaneous multiple equilibria that violate its fundamental equation. Judicious use of the Phase Rule permits one to rule out implausible systems, freeing up one to focus on more quantitative questions relating to the signs and magnitudes of free energy changes associated with accessible systems.

REFERENCES

1. Bancroft WD. The Phase Rule, the Journal of Physical Chemistry. New York: Ithaca, 1897.
2. Willard Gibbs J. Collected Works, Volume 1. New York: Longmans, Green and Co, 1928: 96–144.
3. Clibbens DA. The Principles of the Phase Theory. London: Macmillan and Co, 1920.
4. Rivett ACD. The Phase Rule. London: Oxford University Press, 1923.
5. Rhodes JEW. Phase Rule Studies. London: Oxford University Press, 1933.
6. Marsh JS. Principles of Phase Diagrams. New York: McGraw-Hill, 1935.
7. Bowden ST. The Phase Rule and Phase Reactions. London: Macmillan, 1938.
8. Findlay A, Campbell AN. The Phase Rule and its Applications. New York: Dover Publications, 1938.
9. Ricci JE. The Phase Rule and Heterogeneous Equilibrium. New York: D. Van Nostrand, 1951.

10. Denbigh K. The Principles of Chemical Equilibrium. Cambridge: Cambridge University Press, 1955: 180–210.
11. Lewis GN, Randall M. Thermodynamics and the Free Energy of Chemical Substances. New York: McGraw-Hill, 1923: 185–6.
12. Washburn EW. International Critical Tables, volume 3. In: Washburn EW, ed. New York: McGraw Hill, 1928: 210–12.
13. Dean JA. Lange's Handbook of Chemistry, 12th edition. New York: McGraw Hill, 1979: 10–38.
14. Weast RC, ed. Handbook of Chemistry and Physics, 50th edition. Cleveland: Chemical Rubber Co, 1969: D–139.
15. Bridgeman PW. Proc Am Acad 1912; 47: 441.
16. Merrill L. J Phys Chem Ref Data 1977; 6: 1205.
17. Riecke E. Phys Z Chem 1890; 6: 411.
18. Mitscherlich E. Ann Chim Phys 1821; 19: 414.
19. Kuhnert-Brandstätter M. Thermomicroscopy in the Analysis of Pharmaceuticals. Oxford: Pergamon Press, 1971.
20. Borka L, Haleblian JK. Crystal polymorphism of pharmaceuticals. Acta Pharm Jugosl 1990; 40: 71–94.
21. Borka L. Review on crystal polymorphism of substances in the European Pharmacopeia. Pharm Acta Helv 1991; 66: 16–22.
22. Brittain HG. Polymorphism and solvatomorphism 2004. Chapter 8, in Profiles of Drug Substances, Excipients, and Related Methodology, Volume 32. In: Brittain HG, ed. Amsterdam: Elsevier Academic Press, 2005: 263–83.
23. Brittain HG. Polymorphism and Solvatomorphism 2005. J Pharm Sci 2007; 96: 705–28.
24. (a) Brittain HG. Polymorphism and Solvatomorphism 2006. J Pharm Sci 2008; 97; 3611–36. (b) Brittain HG. Polymorphism and Solvatomorphism 2007. J Pharm Sci 2008; 98: 1617–42.
25. Bridgeman PW. In International Critical Tables, volume 4. In: Washburn EW, ed. New York: McGraw Hill, 1928: 16.
26. Bridgeman PW. In International Critical Tables, volume 4. In: Washburn EW, ed. New York: McGraw Hill, 1928: 15.
27. Fahrenheit GD. Phil Trans 1724; 39: 78.
28. Winchell AN, Winchell H. The Microscopic Characters of Artificial Inorganic Solid Substances. New York: Academic Press, 1964: 63–4.
29. Otsuka M, Kaneniwa N. Effect of seed crystals on solid-state transformation of polymorphs of chloramphenicol palmitate during grinding. J Pharm Sci 1986; 75: 506–11.
30. Ostwald W. Z Phys Chem 1897; 22: 313.
31. Ruff G, Graf R. Z Anorg Chem 1908; 58: 209.
32. Toscani S, Dzyabchenko A, Agafonov V, Dugué J, Céolin R. Polymorphism of sulfanilamide: stability hierarchy of α, β, and γ forms from energy calculations by the atom-atom potential method and from the construction of the P, T phase diagram. Pharm Res 1996; 13: 151–4.
33. Kracek FC. International Critical Tables, volume 3. In: Washburn EW, ed. New York: McGraw Hill, 1928: 366.
34. Kracek FC. International Critical Tables, volume 3. In: Washburn EW, ed. New York: McGraw Hill, 1928: 369.
35. Phadnis NV, Suryanarayanan R. Polymorphism in anhydrous theophylline – implications on the dissolution rate of theophylline tablets. J Pharm Sci 1997; 86: 1256–63.
36. Sharpe SA, Celik M, Newman AW, Brittain HG. Physical characterization of the polymorphic variations of magnesium stearate and magnesium palmitate hydrate species. Struct Chem 1997; 8: 73–84.
37. Hildebrand JH, Scott RL. Solubility of Nonelectrolytes, 3rd edn. New York: Reinhold Pub, 1950.
38. Hildebrand JH, Prausnitz JM, Scott RL. Regular and Related Solutions. New York: Van Nostrand Reinhold, 1970.

39. Dack MRJ. Solutions and Solubilities. New York: John Wiley & Sons, 1975.
40. Grant DJW, Higuchi T. Solubility Behavior of Organic Compounds. New York: John Wiley & Sons, 1990.
41. Grant DJW, Brittain HG. Solubility of pharmaceutical solids, Chapter 11 in Physical Characterization of Pharmaceutical Solids. In: Brittain HG, ed. New York: Marcel Dekker, 1995: 321–86.
42. Gong Y, Grant DJW, Brittain HG. Principles of solubility, Chapter 1, in Solvent Systems and Their Selection in Pharmaceutics and Biopharmaceutics. In: Augustins P, Brewster ME, eds. Arlington, VA: Springer-AAPS Press, 2007: 1–27.
43. Seidell A. Solubilities of Organic Compounds, volume 2. New York: D Van Nostrand Co, 1941: 232.
44. Seidell A. Solubilities of Inorganic and Metal Organic Compounds, volume 1. New York: D. Van Nostrand Co, 1940: 245.
45. Poole JW, Bahal CK. Dissolution behavior and solubility of anhydrous and trihydrate forms of ampicillin. J Pharm Sci 1968; 57: 1945–8.
46. Findlay A, Campbell AN. The Phase Rule and its Applications. New York: Dover Publications, 1938: 85.
47. Shefter E, Higuchi T. Dissolution behavior of crystalline solvated and nonsolvated forms of some pharmaceuticals. J Pharm Sci 1963; 52: 781–91.
48. Hoelgaard A, Møller N. Hydrate formation of metronidazole benzoate in aqueous suspensions. Int J Pharm 1983; 15: 213–21.
49. Laine E, Tuominen V, Ilvessalo P, Kahela P. Formation of dihydrate from carbamazepine anhydrate in aqueous conditions. Int J Pharm 1984; 20: 307–14.

3 Computational Methodologies: Toward Crystal Structure and Polymorph Prediction

Sarah (Sally) L. Price
Department of Chemistry, University College London, London, U.K.

INTRODUCTION

A computational method of predicting all polymorphs of a given pharmaceutical molecule, and the conditions under which they could be found, requires a fundamental understanding of the causes of polymorphism. A computational model would only be reliable if it incorporated all the factors that can affect which polymorphs can be found. Given the diversity of methods that can generate new polymorphs (1), and the disappearance of polymorphs due to changes in impurity profiles (2), modelling all relevant factors currently seems almost impossible. At the moment, we can aspire to compute the crystal energy landscape, the set of structures that are thermodynamically feasible, for a specific compound (3). We can predict the most thermodynamically stable structure that should exist at specified thermodynamic conditions, if we have performed the calculation of the relative energies sufficiently accurately. Currently, this is the only crystal structure that can be predicted, by assuming thermodynamic control of crystallization. However, comparing the other low-energy structures on the computed crystal energy landscape with each other and with the known polymorphs can provide considerable insight into the possible solid form diversity (4). Using computational modelling in conjunction with the experimentally determined crystal structures can help provide an atomic level picture of the factors that are influencing the crystallization of a molecule, from guiding the experimental search to seek polymorphs with alternative packing motifs, to using the similarity between predicted structures to suggest the likely forms of disorder or crystal growth problems. Gaining a molecular level of understanding of crystallization presents challenges to both experimental characterization of solids and nucleation processes (5), and computational chemistry (6). Thus, this chapter seeks to demonstrate the types of insight into polymorphism that can come from combining various computational tools with experimental work, with due allowance for the limitations of the complementary techniques.

STRUCTURE COMPARISON TOOLS

Many visualization tools are available for viewing organic crystal structures, but their three-dimensional nature often makes even qualitative comparison difficult, and quantifying similarity is a challenge. Some methods are demonstrated by comparing pairs of structures of acetaminophen, aspirin, and eniluracil. In all three cases the two structures have the same types of hydrogen bonds, and the same

graph sets (7). In acetaminophen (paracetamol), the two polymorphs (8) are held together by O–H···O=C C(9) and N–H···O(H) C(7) hydrogen-bonded chains, but form I has highly undulating sheets, whereas the sheets are almost flat in form II. An attempt to overlay the 15 molecule coordination sphere of the two structures, using the Compack methodology (9) (incorporated in the CalculateSimilarity facility in Mercury (10)), shows that only one molecule can be overlaid within the default tolerance of 20% in the atom–atom distances and 20° in the angles. The relative orientations of the other molecules are very different (Fig. 1A) despite having the same hydrogen bonding pattern. The conformations are very similar, as shown by the $RMSD_1$ value. [$RMSD_n$ is the minimum root-mean-square difference in the non-hydrogen atom positions for the n molecules that can be overlaid of the 15 (default value) coordination cluster of the two structures]. These differences in the packing are also evident in the Hirschfield (11,12) surfaces (Fig. 1B), which are defined by the surface where the molecule contributes half of the model for the electron density in the crystal (11). These shapes, particularly when color coded to show the nearest intermolecular atom distances, quickly show up the differences in packing. Other derived plots can assist the structure comparison (11). As would be expected, the simulated powder patterns of the two crystal structures are obviously different (Fig. 1C). The similarity in some peaks can be quantified (13) using the program CalculateSimilarity (14).

Aspirin illustrates a case where the differences between the two structures are more subtle. Eleven of the 15 molecule coordination group of the recently published structure for form II (15) can be overlaid with form I (16) to give an $RMSD_{11}$ of 0.07 Å (Fig. 2A). The two structures have the same hydrogen bonded layers (15), but these stack with different C–H···O interactions, which can be seen as small differences in the acetyl region of the Hirschfield surfaces (Fig. 2B). The comparison of the energetic fingerprints (17) (the center of mass distance, symmetry relationship, and the components of the interaction energy between a central molecule and each of its coordinating molecules) of the crystal structures adds further clarity to the debate as to whether these two structures should be considered as polymorphs (18). In this case, the simulated powder patterns are very similar (Fig. 2C), with a CalculateSimilarity (14) index of 0.96. It is therefore difficult to discriminate between the two structures by powder or single crystal X-ray diffraction work (19). This value of 0.96 is also in the gray area where this index does not clearly distinguish (20) between polymorphs and redeterminations of the same structure. This calibration of the powder pattern similarity index was established (20) using the polymorphs and redeterminations from different samples in different laboratories at different temperatures (with an approximate correction for thermal expansion), in the Cambridge Structural Database (CSD) (21). The dangers of just comparing powder patterns are illustrated by two structures proposed for eniluracil (5-ethynyluracil) from powder X-ray data (22). Both structures are based on $R_2^2(8)$ N–H···O=C hydrogen bonded ribbons, but only five molecules of the 15 molecule coordination sphere can be overlaid (Fig. 3A) with an $RMSD_5$ of 0.045 Å. The entire coordination sphere would overlay if C4=O was chemically identical to C6–H, providing an almost identical coordination environment (Fig. 3B). Distinguishing between this oxygen and hydrogen, one structure is comprised of polar ribbons and the other of non-polar ribbons. Their simulated diffraction patterns are very similar (Fig. 3C) with a CalculateSimilarity index of 0.98 Å, a value more in keeping with different determinations of the same structure, although the structures would normally be classified as polymorphs.

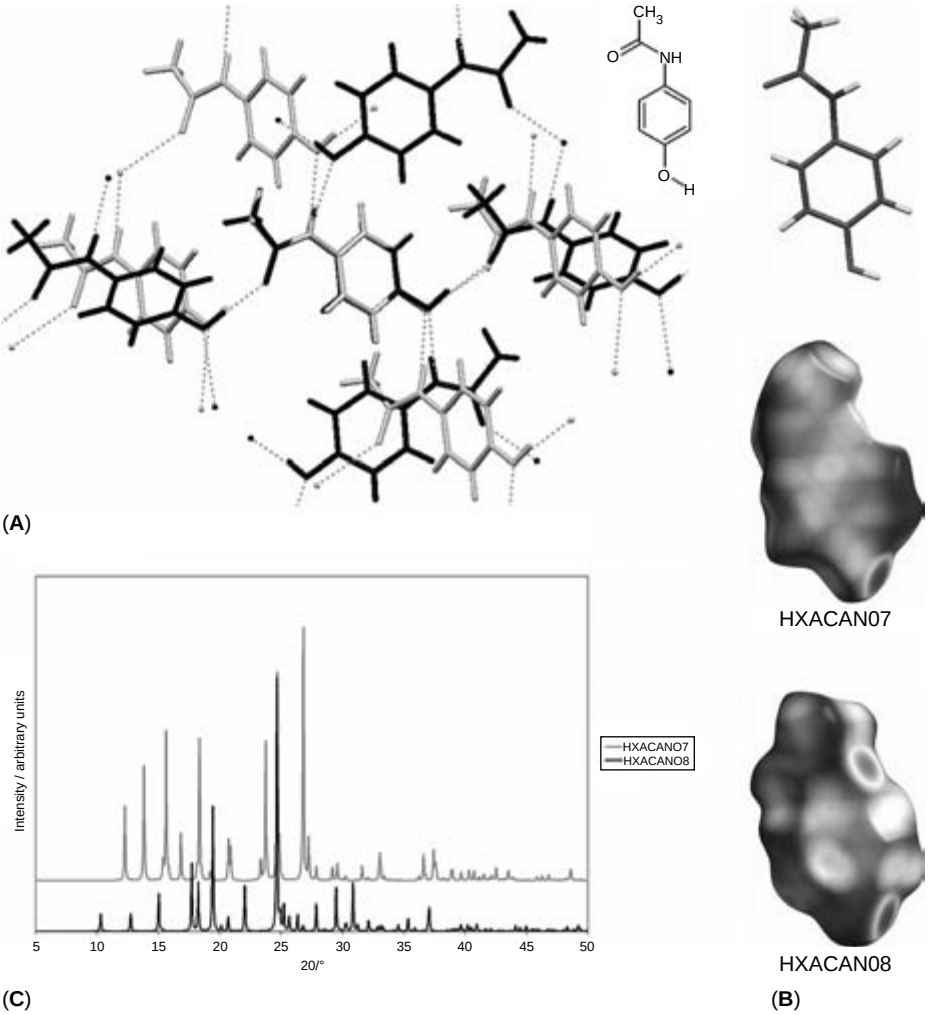

FIGURE 1 Different methods of comparing the two polymorphs of acetaminophen (paracetamol) (8): (**A**) optimal overlay of central molecule, showing the hydrogen-bonded coordinating molecules in the two forms [form I HXACAN07 (gray); form II HXACAN08 (black); $RMSD_1$ = 0.096]; (**B**) Hirshfeld surfaces, which emphasize the differences in the stacking in the two forms; and (**C**) the simulated powder patterns (CalculateSimilarity index = 0.75). *Abbreviation*: $RMSD_1$, root-mean-square difference in overlay of the molecule.

Other methods of comparing crystal structures are being developed, for example, the Xpac (23) methodology, which helps avoid the tendency to concentrate on hydrogen bonding, and look at the importance of molecular shape. This approach demonstrated the relationship between the packing in 25 crystal structures of carbamazepine and close analogues (24).

As experimental screening methods produce more crystal structures containing the same or closely related molecules, the use of complementary comparison

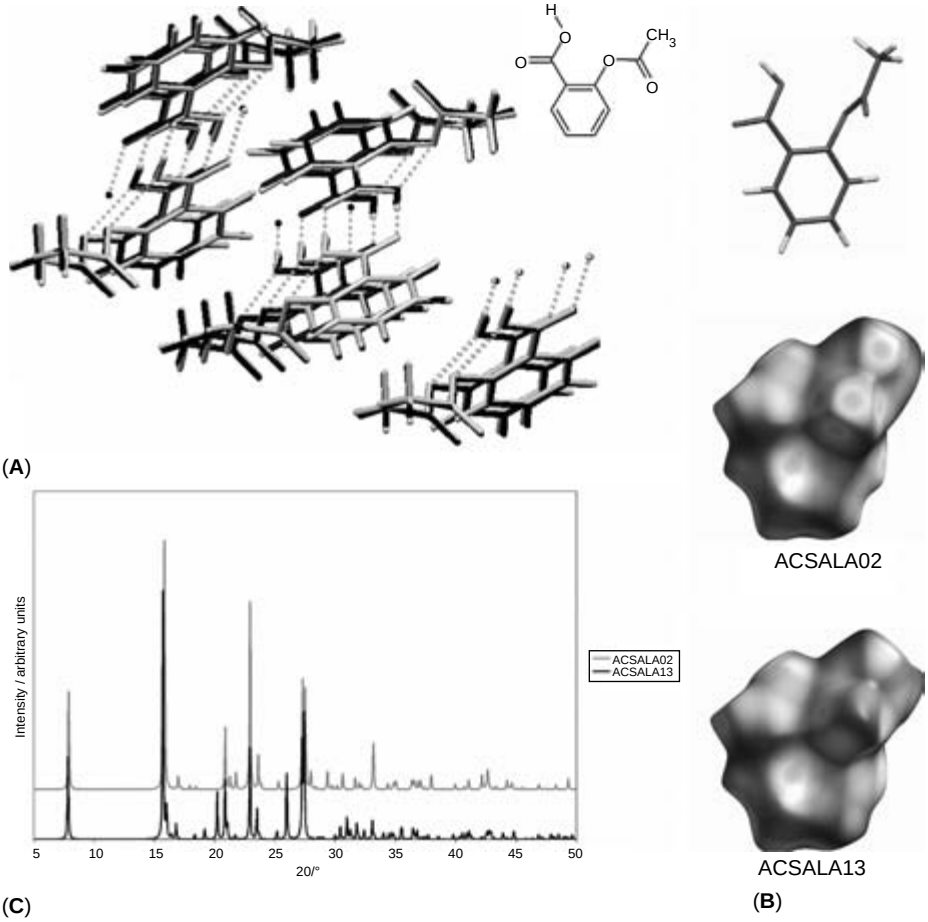

FIGURE 2 Different methods of comparing the two experimental structures of aspirin represented by ACSALA02 (gray), a 100 K determination of form I (16) and the form II structure ACSALA13 (black) (15): (**A**) optimal overlay of the 11 molecule cluster in common ($RMSD_{11}$ = 0.07 Å); (**B**) Hirshfeld surfaces aligned to show the difference in packing of the acetyl groups; and (**C**) the simulated powder patterns (CalculateSimilarity index = 0.96). *Abbreviation*: $RMSD_{11}$, root-mean-square difference in overlay of the 11 molecule cluster.

tools will become more widespread. Because computed crystal energy landscapes often generate huge numbers of thermodynamically feasible structures, further automation and development of comparison methods will be needed to obtain the real benefits of comparing known and computer-generated crystal structures. The ability to differentiate different types of polymorphism and solid-form diversity helps assess the implications for quality control of possible pharmaceutical products, as will be exemplified by these three examples in the section "Interpretation of Crystal Energy Landscapes."

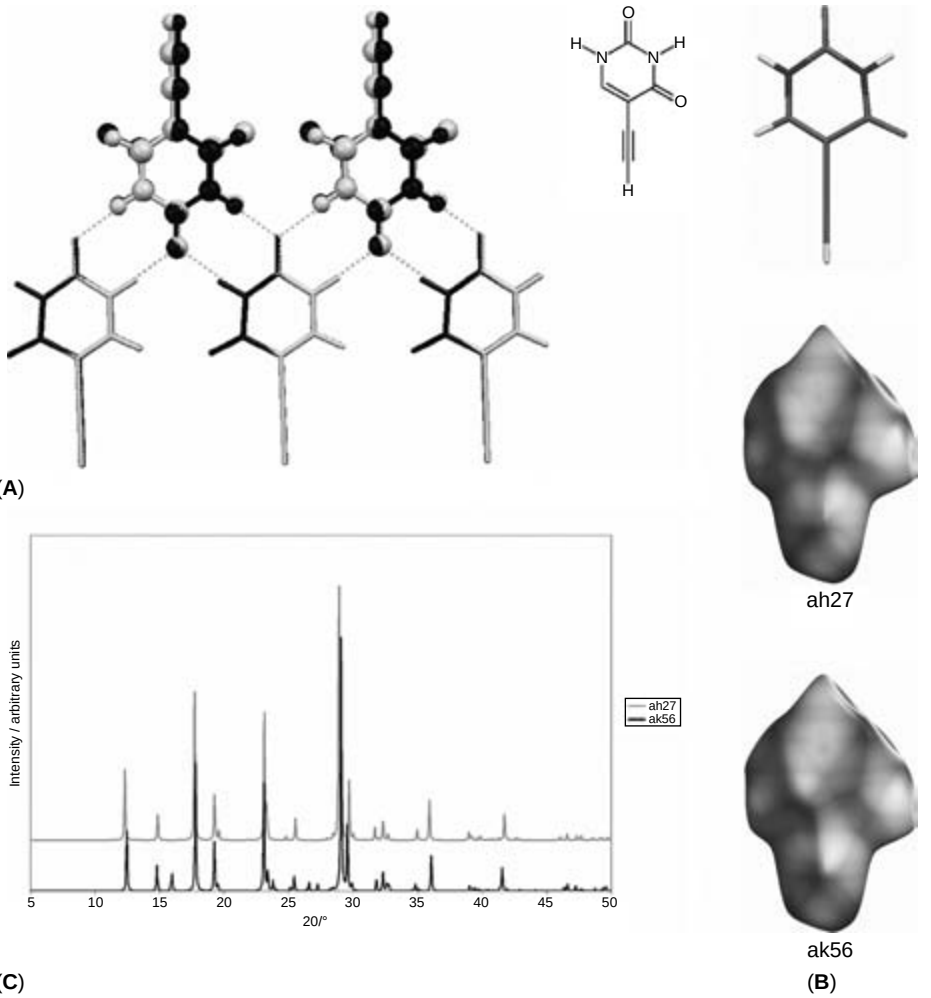

FIGURE 3 Different methods of comparing the two idealized crystal structures of eniluracil (22), based on polar (ah27 in black) and non-polar hydrogen bonded ribbons (ak56 in gray): (**A**) the ribbon portion of the optimal overlay of the five molecule cluster in common, showing how the ribbon is completed by molecules that differ in the position of C4=O and C6–H; the other two molecules that overlay are in the sheet above ($RMSD_5$ = 0.045); (**B**) Hirshfeld surfaces, which show the very slight differences from the O/H distinction in the packing of the layer above; and (**C**) the simulated powder patterns (CalculateSimilarity index = 0.98). *Abbreviation*: $RMSD_5$, root-mean-square difference in overlay of the five molecule cluster.

CALCULATION OF CRYSTAL ENERGIES

The calculation of the relative energies of polymorphs provides a major challenge to computational chemistry. There is currently no method that can be considered reliable for all pharmaceutical molecules for all purposes, although this is an objective of considerable research because it is closely related to other fields such as

computational drug design. However, there can be a choice of methods that could be applied to a given molecular system, and a key question is whether any one is accurate enough for your purposes. Very crude models, such as a computationally generated space-filling model, can readily deal with questions such as whether a structure is plausibly close-packed or sterically implausible. At the other extreme, periodic electronic structure methods are beginning to be evaluated for calculating organic crystal energies. The traditional approach to modelling organic crystals (25,26) sums the energy of the interactions between all the molecules in the crystal as evaluated from a model intermolecular potential. The molecules are either modelled as rigid or the energy penalty for the change in conformation is added. Organic crystal structure modelling is challenging because the energy differences between polymorphs are so small compared with the covalent bond energies.

A straightforward evaluation of the energy difference between two or more experimental crystal structures, by even the most expensive computational method, could be very misleading for several reasons. First, computed lattice energies are extremely sensitive to the location of the protons involved in hydrogen bonding. X-ray determinations have a systematic error in hydrogen atom positions, and so the position of all protons must be adjusted so the X–H bond length is more realistic, by using average neutron values (27) or ab initio optimization. Also, the hydrogen charge density may have been carefully located in the published structure, but often the crystallographer has to make assumptions to include the proton positions. If, for example, a planar conformation had been assumed for an amine group, which in reality distorts to a pyramidal conformation to form better hydrogen bonds, the hydrogen bonding energy would be significantly underestimated.

Second, the crystal structure should be optimized using the computational model for the energy. The van der Waals contacts within crystals are where the attractive and repulsive forces balance, and so small changes in these distances can lead to large energy differences because of the exponential distance dependence of the repulsion. Temperature affects organic crystal structures in an anisotropic fashion, reflecting the nature of the intermolecular interactions in the different directions. Hence, modelling based on low-temperature structures is always preferred, and mixing structures determined at different temperatures can lead to significant uncertainties. For example, the lattice energy of form I acetaminophen, after rigid-body lattice energy optimization, differs by 2.1 kJ mol^{-1}, depending on whether the molecular conformation determined at 20 K or 330 K is used (28). This is greater than the 1.0 kJ mol^{-1} difference between the two polymorphs, using the conformations in structures determined at 123 K, and the same as the polymorphic energy difference using the molecular conformations determined at room temperature (28). An ab initio estimate of the difference in energy due to the change in the molecular conformation between conformational polymorphs can be affected by experimentally insignificant variations in, for example, the C=O bond lengths. A more realistic estimate would be made by fixing the degrees of freedom that have been affected by the crystal packing, such as torsions around single bonds, to those determined in the crystal structures, and optimizing all other bond lengths and angles.

Finally, computational work can reveal "errors" in the crystal structure, such as the diffraction experiment not detecting a small amount of disordered solvent. Recent computational analyses of form II of carbamazepine, by either Hirshfeld surfaces (29) or energy calculations (30), prompted investigations that showed that this polymorph is being stabilized by solvent.

Thus, the development of accurate methods of computing polymorphic energy differences is very dependent on the quality of the crystallography used for validation, although it is not unknown for modelling work to raise questions about the accuracy of a published structure.

Lattice Energy Evaluation

Most crystal structure modelling only considers the lattice energy, that is, the energy of the static crystal lattice relative to infinitely separated molecules, both nominally at 0 K and neglecting zero-point vibrational motion. There are many programs that can calculate the energy of an infinite static perfect lattice by using various mathematical techniques to sum up all the contributions. These range from electronic structure methods, which explicitly model the electrons in the structure by an approximate solution of the quantum mechanical equations, through to atom–atom force fields that use an equation for the energy as a function of the nuclear positions. These empirically parameterized equations represent the energy penalties for various conformational distortions as well as the intermolecular interactions. The current state-of-the-art method for most organic crystal structures is the intermediate "monomer + model" approach, in which ab initio calculations on the isolated molecule are used to model the molecular structure, energy, and charge density as a function of conformation, and then this charge density is used to construct a model for the intermolecular potential. These three approaches to evaluating lattice energies are outlined, before the additional requirements to include the effect of temperature on the relative thermodynamics of pharmaceutical polymorphs are described in the section "Free Energies and Other Properties."

Electronic Structure Modelling

Modern electronic structure methods are increasingly being applied to the solid state. However, organic crystals provide a particular challenge for an approximate solution of the Schrödinger equation, because the importance of modelling the dispersion forces adequately can vary significantly between polymorphs. Because the dispersion forces arise from the correlation of electron motions, they are not described at all by routine molecular orbital methods, such as the Hartree–Fock approximation, which as the alternative name of Self-Consistent-Field indicates, only allows each electron to respond to the average field of all the other electrons. There are a variety of methods that include electron correlation under development, including many variants of density functional theory. However, correctly predicting the most stable gas phase conformations of flexible molecules, such as polypeptides, where there is a significant dispersion contribution between the different functional groups, challenges all currently widely available methods (31). The problem in modelling dispersion also produces very variable results for organic crystals, often producing unphysical expansion of the crystal in the directions where the dispersion interaction provides the bonding. For example, one polymorph with hydrogen bonds in all three dimensions may be well reproduced, whereas a polymorph based on a hydrogen bonded sheet will have the stacking separation overestimated. This has been demonstrated (32) by applying several types of periodic density functional theory to the two polymorphs of *o*-acetamidobenzamide and the five polymorphs of oxalyl dihydrazide. The structures and relative energies are much more reasonably modelled (32) by a new empirically dispersion-corrected density functional, where the damping function for adding a C_6/R^6 model for the

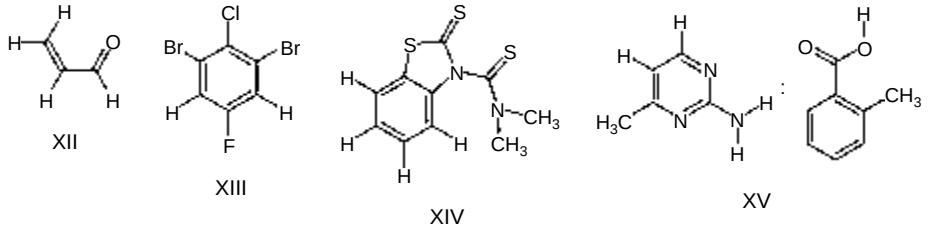

FIGURE 4 The four molecules used in the 2007 Cambridge Crystallographic Data Centre's international blind test of crystal structure prediction, with Roman numerals defined by this series of tests (35). These represent a simple rigid molecule, one with less common functional groups, a flexible molecule and a cocrystal, believed to be within the claimed capabilities of many of the available methodologies. All these crystal structures were correctly predicted by methods based on the monomer + model approach and the dispersion-corrected density functional method (36). The success of these lattice energy-based predictions implies that the target crystal structures were the most stable for all compounds and monotropically related to any polymorphs.

long-range dispersion to the electronic energy had been empirically fitted to organic crystal structures (33). This model was successful in the international blind test of crystal structure prediction (34) held in 2007 (35), correctly predicting all four target structures (Fig. 4) as the most stable (36).

Force Fields

The simplest force fields, which are useful for organic crystal structure modelling, are the isotropic atom–atom exp-6 model intermolecular potentials of the form:

$$U = \sum_{i \in M, k \in N} A_{\iota\kappa} \exp(-B_{\iota\kappa} R_{ik}) - C_{\iota\kappa} / R_{ik}^6 \qquad (1)$$

where atom i in rigid molecule M and atom k in rigid molecule N are of atom types ι and κ, respectively, and are separated by a distance R_{ik}. This potential is only explicitly modelling the repulsion between the atoms as their charge clouds overlap, and the dispersion force. The parameters for atomic types ι = C, N, O, Cl, S, and separate parameters for H bonded to C, N, and O, have been derived (37,38) by fitting to heats of sublimation and the crystal structures of rigid molecules. There is no explicit electrostatic term, so the lattice energies can be quickly evaluated by direct summation. This results in the hydrogen bonding potentials having particularly deep wells to absorb the missing electrostatic term. This *exp-6* model does remarkably well for its simplicity, and can be used for approximate comparisons with the molecule held rigid at the experimental conformation.

Most commercial modelling programs use one of the many force fields that are being developed for biomolecular modelling, where the molecular flexibility is represented by bond stretching, bond bending, and torsional terms, and the intermolecular forces are modelled in the same way as the intramolecular interactions between atoms separated by a few covalent bonds. These non-bonded interactions are usually of the form of equation (1), or the Lennard–Jones 12-6 model, with the addition of an atomic point-charge electrostatic model. There are many force fields available (39) and the choice for a particular study should be dictated by the properties

and types of molecules used in the parameterization and validation. The essential preliminary test of a force field for crystal structure modelling is whether it gives a minimum in the lattice energy reasonably close to the experimental crystal structure for a range for similar molecules. There are cases where the intramolecular forces cause a change in the conformation of a flexible molecule that ensures that the optimized crystal structure is qualitatively wrong (40). A prediction that aspirin should have a more stable polymorph with the molecule in a planar conformation (41) arose from the use of a force field that predicted that the isolated molecule should be planar. Ab initio calculations show that the planar conformation is a transition state, although the conformation observed in the crystal is close to a local rather than the global minimum in the conformational energy (42). A general limitation of such force fields is that the same atomic charges are simultaneously modelling the intermolecular interactions and determining the conformation of the molecule, and are unable to represent the changes in charge distribution with conformation sufficiently realistically (43).

Monomer + Model

The approach that has proved adequate for a wide range of organic crystal structures, including those in the 2007 blind test of crystal structure prediction (Fig. 4), is to concentrate on the obtaining the best possible model for the intermolecular interactions (44,45). The energy penalty for any significant change in conformation from the ab initio-optimized molecular structure, ΔE_{intra}, is evaluated by the best affordable ab initio calculations on monomers. The lattice energy is then given by $E_{latt} = U_{inter} + \Delta E_{intra}$, where U_{inter} is the intermolecular lattice energy.

Atom–atom models for U_{inter} explicitly model at least the electrostatic and repulsion–dispersion contributions. The electrostatic model is usually derived from the charge density of the molecule, preferably calculated for every distinct conformation to represent the redistribution of charge with changes in the intramolecular interactions. The electrostatic model can use the atomic charges that give the best possible reproduction of the electrostatic potential in the van der Waals contact region around the molecule (46). However, modelling organic crystal structures satisfactorily often requires (47) additional point charges on non-nuclear sites to represent the electrostatic forces arising from lone pair and π electron density. These non-spherical features in the atomic charge distribution can be more effectively and automatically represented (44,45) by a distributed multipole model obtained by analyzing (48) the ab initio charge density of the molecule. Figure 5 shows the electrostatic potential around a fairly spherical molecule, and the errors from using an atomic point charge representation of the same charge density relative to the more complete distributed multipole representation. There are significant differences even around the saturated hydrocarbon rings. The differences are more marked for molecules that form stronger hydrogen bonds (49). A survey of the computed lattice energy landscapes for 50 rigid molecules containing only C, H, N, and O (50,51) concluded that the 64 known structures were significantly more likely to be found at or near the global minimum in the lattice energy when a distributed multipole model was used rather than an atomic point-charge model.

The electrostatic interactions mainly determine the directionality of the hydrogen bonding and π–π stacking, whereas the repulsion between atoms is critical in determining the van der Waals contact distances and the dispersion favors dense, close-packed crystals. Thus, in addition to the electrostatic interactions, U_{inter} has to

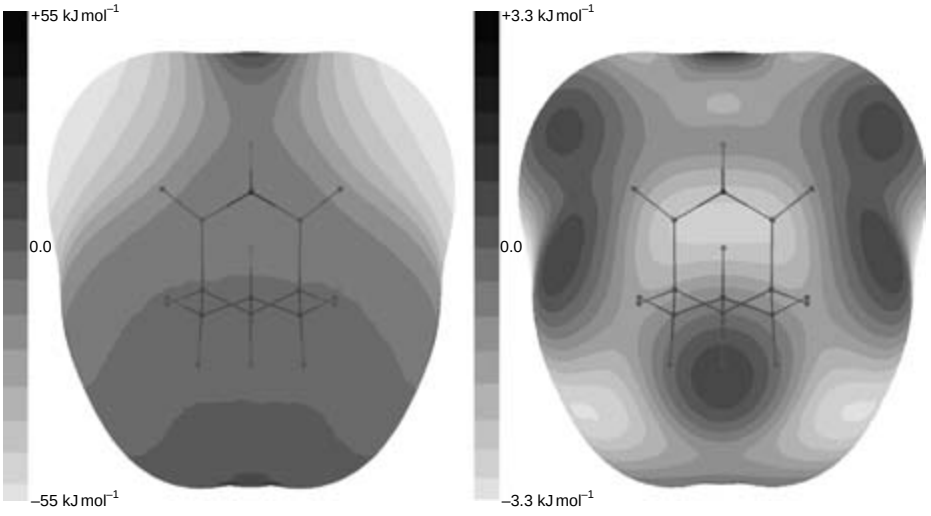

FIGURE 5 (**A**) The electrostatic potential on the water-accessible surface of 3-azabicyclo(3.3.1) nonane-2,4-dione, with the imide group at the top, in the plane of the paper, as calculated from the distributed multipole representation of the MP2 6-31G(d,p) charge density. The electrostatic potential minimum of $-55\,kJ\,mol^{-1}$ is near the carbonyl groups, and the maximum of $39\,kJ\,mol^{-1}$ is in the hydrocarbon region. (**B**) The error in the same electrostatic potential when atomic point charges derived from the same charge distribution are used. The atomic charges underestimate the potential near the hydrogen bond donor by $3.1\,kJ\,mol^{-1}$.

include a model for all the other intermolecular contributions, which is usually an isotropic atom–atom potential [equation (1)]. Two such models have been developed specifically for modelling organic crystal structures by having the parameters in equation (1) determined by fitting to a range of crystal structures and heats of sublimation. The FIT potential has evolved from a series of studies of different types of molecules (52,53). The more recent WILL01 potential (54) has different parameters for H, C, N, and O, depending on their covalently bonded neighbors, and was specifically developed and tested for nucleoside and peptide crystals. Table 1 contrasts the two sets of parameters and the larger range of atomic types used in WILL01. The marked differences emphasize that equation (1) is a crude approximation, so that the parameters reflect the optimum values for reproducing the close contacts in crystal structures used in the fitting.

These two model intermolecular potentials have been successfully used for modelling a wide range of organic crystal structures, in conjunction with realistic electrostatic models derived from the molecular charge density. However, there are many cases where it is clear that more accurate models are needed for the relative lattice energies. This can occur when the low-energy structures contain very different hydrogen-bonding arrangements (55) to those sampled in the crystal structures used in the potential derivation. This can be attributed to the empirically fitted model potentials absorbing the induction (also called polarization) energy into the parameters in a way that does not extrapolate very accurately to unusual geometries. The induction energy, the additional stabilization due to the distortion of the

TABLE 1 Comparison of the FIT Potential and WILL01 Potential Parameters for the Atom–Atom exp-6 Potential [equation (1)] in Conjunction with an Explicit Electrostatic Model. The interactions between unlike atoms are generated by the combining rules: $A_{ik} = \sqrt{A_{ii}A_{kk}}$, $B_{ik} = (B_{ii} + B_{kk})/2$, $C_{ik} = \sqrt{C_{ii}C_{kk}}$

Potential	Atom pair	Description	A_{ii}/(kJ mol^{-1})	B_{ii}/(Å^{-1})	C_{ii}/(kJ mol^{-1} Å^6)
FIT	C ···C	Any C atom	369746	3.60	2439.82
WILL01	C(2) ···C(2)	C bonded to two atoms	103235	3.60	1435.09
WILL01	C(3) ···C(3)	C bonded to three atoms	270363	3.60	1701.73
WILL01	C(4) ···C(4)	C bonded to four atoms	131571	3.60	978.36
FIT	H_C···H_C	H bonded to C	11971	3.74	136.40
WILL01	H(1)···H(1)	H bonded to C[a]	12680	3.56	278.37
FIT	H_O···H_O	H bonded to O	2263	4.66	21.50
WILL01	H(2)···H(2)	H in alcoholic group[a]	361	3.56	0
WILL01	H(3)···H(3)	H in carboxyl group[a]	116	3.56	0
FIT	H_N···H_N	H bonded to N	5030	4.66	21.50
WILL01	H(4)···H(4)	H bonded to N[a]	765	3.56	0
FIT	N···N	Any N atom	254531	3.78	1378.41
WILL01	N(1)···N(1)	N in triple bond	96349	3.48	1407.57
WILL01	N(2)···N(2)	other N with no bonded H	102369	3.48	1398.15
WILL01	N(3)···N(3)	N bonded to one H atom	191935	3.48	2376.55
Will01	N(4)···N(4)	N with two or more bonded H	405341	3.48	5629.82
FIT	O···O	Any O atom	230066	3.96	1123.60
WILL01	O(1)···O(1)	O bonded to one other atom	241042	3.96	1260.73
WILL01	O(2)···O(2)	O bonded to two other atoms	284623	3.96	1285.87

[a]WILL01 has the hydrogen interaction sites shifted 0.1 Å into the bond from the proton positions, representing the effect on the intermolecular forces of shift of the hydrogen electron density into the bond that also gives rise to a systematic error in the location of protons by X-ray diffraction.

charge density of a molecule by the electrostatic field of surrounding molecules, gives a significant reordering of the relative stability of the catemer and dimer-based structures of carbamazepine (56). The induction energy can account for the otherwise unrealistic energy differences between polymorphs that differ in the number of intermolecular and intramolecular hydrogen bonds (32). Another approximation in empirically fitted potentials is that the molecular charge distribution is modelled as a superposition of spherical atoms for all contributions (except the electrostatic contribution when distributed multipoles are used instead of atomic point charges). This is clearly a bad approximation for chlorine, bromine, iodine, and some sulphur atoms, where the wide range of orientations in crystal structures sample the differences in the repulsive wall produced by the lone pair density. Such anisotropy in the repulsion is best derived from the molecular charge distribution, as illustrated by the nearly non-empirical anisotropic atom–atom potentials that have been used for modelling the chlorobenzene crystal structures and their properties (57) and rationalizing the complex polymorphism of chlorothalonil (58). Thus,

the application of the theory of intermolecular forces is allowing very accurate models for U_{inter} to be derived for specific molecules (6). Indeed, the 2007 international blind test of crystal structure prediction saw the first entry and successful prediction by a model intermolecular potential that had been derived with no solid-state input (59), for $C_6Br_2ClFH_2$.

The importance of intramolecular dispersion unfortunately implies that the larger and more flexible the molecule, the greater the importance of using an accurate and expensive wavefunction to evaluate the intramolecular energy penalty ΔE_{intra}. The optimization of the lattice energy $E_{latt} = U_{inter} + \Delta E_{intra}$ for small variations in specified molecular conformational parameters simultaneously with the crystal structure can be performed by DMAflex (60). The conformational parameters that have to be optimized are the low energy-barrier torsion angles that will be affected by the packing forces and could differ in conformational polymorphs. However, the sensitivity of the lattice energy to the geometry of hydrogen bonds means that the torsion angles defining every polar proton need to be optimized (i.e., two angles for every NH_2 group). Work on reducing the computational cost of the optimization of molecular conformations within organic crystal structures is in progress (61) to increase the range of pharmaceuticals that can be studied.

Free Energies and Other Properties

The prediction of the relative stability of polymorphs at ambient temperatures, and whether they are monotropically or enantiotropically related, represents a major challenge to theoretical modeling. The comparison of total lattice energies, E_{latt}, completely neglects the effects of temperature and pressure on the relative stability of the crystal structures. Although enthalpy differences dominate entropy differences in known polymorphs (62), the relative lattice energies only provide a first estimate of the stability order for monotropically related systems.

Most entropy estimates are based on lattice dynamical calculations for rigid molecules (63), as the second derivatives of the lattice energy with respect to changes in the relative orientations and positions of the molecules (or cell parameters) are quite readily calculated. (Realistic second derivatives for conformational variations of flexible molecules are generally too demanding of the balance between the inter- and intramolecular forces.) Estimates of the lattice frequencies (63) can be used for assigning the low-energy lattice modes sometimes measured in the far-infrared, Raman, and terahertz spectra (64), which can be used for polymorphic identification. The phonon frequencies generally correlate with structure, for example, the sheet structure of acetaminophen form II has its lowest frequency around 20 cm^{-1} for relative motion of the sheets, almost half the frequency for the lowest energy mode of form I. The second derivatives can also be used to estimate the elastic tensor for the infinite perfect crystal (65), and again, the lowest eigenvalue of the shear tensor for form II acetaminophen (~0.8 GPa) is much lower than the ~3.5 GPa estimated for form I, consistent with its compaction properties. Form II of aspirin is estimated to be so susceptible to shear (~0.2 GPa), that it would be surprising if it did not transform readily. (Both second-derivative properties provide a very worthwhile check that a structure is a true minimum, rather than a transition state between lower energy structures in a lower symmetry space group.) Thus, computational estimates of the elastic tensor and the phonon modes are useful in identifying marked differences between idealized crystal structures of the same molecule. The resulting differences in harmonic estimates of the thermal contributions to the energy

are usually small; for example, the relative stability of the two polymorphs of either acetaminophen or aspirin at room temperature differs by less than about 0.5 kJ mol^{-1} from the lattice energy estimate.

The motions in organic crystal structures are not always well approximated by the harmonic model, even for rigid molecules, although this depends on the forces in the crystal structure. Molecular Dynamics studies can model the motions of molecules in a solid at finite temperature by using Newtonian mechanics and the forces derived from the model intermolecular potential. Such Molecular Dynamics studies (66) on 5-azauracil and imidazole crystals were able to reproduce the significantly greater thermal expansion in the cell directions that did not contain hydrogen bonds. A comparison of the lattice modes from the two simulation methods (with the same model for the forces) had differences of less than 20 cm^{-1} despite the lattice dynamic harmonic estimates being nominally at 0 K and the Molecular Dynamics simulating 5-azauracil at room temperature. A major disadvantage of the harmonic model is that it does not reveal when a structure is thermally unstable. In contrast, a Molecular Dynamics simulation can show, for example, that cyclopentane transforms from an ordered crystal structure, through an intermediate phase, to a rotationally disorder high symmetry phase with increasing temperature (67). However, the periodic boundary conditions on the Molecular Dynamics simulation cell generally prevent the simulations showing first-order transformations involving nucleation and growth. Nevertheless, Molecular Dynamics simulations can reveal when the vibrational motion at the simulated temperature is such that it overcomes the small energy barriers between lattice energy minima. Thus, some lattice energy minima are not free energy minima at ambient conditions. A successful application of the metadynamics method to exploring the free energy surface for benzene (68) suggested that there were only seven free energy minima corresponding to the known phases. However, for 5-fluorouracil, only a quarter of the 60 low-energy lattice energy minima proved to be unstable in free energy simulations at ambient temperature (69). This qualitative difference relates to the experimental tendency to change intermolecular contacts: benzene readily undergoes solid-state transformations and rotates in the solid, whereas there is no observed transformation between the two polymorphs of 5-fluorouracil, and other computed hydrogen bonding motifs are observed in solvates and cocrystals. Molecular Dynamics studies are so computationally demanding that, even in the future, they are only likely to be applied in special cases. Thus, although the crystal energy landscape should use free energies as a function of the temperature and pressure in the range of practical interest, the lattice energy landscape is generally a worthwhile first approximation.

CRYSTAL STRUCTURE PREDICTION OR COMPUTING THE CRYSTAL ENERGY LANDSCAPE

Crystal structure prediction is based on assuming that the molecule will crystallize in the most thermodynamically stable structure, although other structures that are close in energy may be observed as polymorphs. This requires an adequate search through the space-groups that the molecule could crystallize in. This is often restricted to the most common orthorhombic, monoclinic, and triclinic space groups with one molecule in the asymmetric unit ($Z' = 1$). Most of the older methods of generating trial crystal structures for lattice energy minimization use crystallographic

insight to efficiently sample the huge range of possible crystal structures. PROMET (70) looks for strong interactions between molecules related by the symmetry operators, and MOLPAK (71) seeks dense packings within common coordination patterns. As more extensive searches became possible, various types of simulated annealing explored the lattice energy surface (72), and systematic searches were developed to perform a complete search in specified space groups for a given value of Z'. Analysis of the 2005 blind test results (73) suggests that some of these computationally demanding methods (74) are close to ensuring a complete search of the approximate lattice energy surface for a wide range of space-groups and $Z' = 1$ or 2 .

The search effort increases very quickly with the number of conformational degrees of freedom (such as torsion angles), or independent units in the asymmetric unit cell, as this increases the dimensionality of the lattice energy surface. Most of the search methods that consider flexible molecules cannot be sure of crossing significant conformational barriers, and so would start from all the low-energy conformational minima of the molecule. The conformation would then be refined by the energy minimization method. Searches for co-crystals, monohydrates, and salts, where there are necessarily two independent molecular fragments in the asymmetric unit, are becoming feasible. A fairly general search method correctly predicted that the acetone solvate of dihydrocarbamazepine could be isostructural with that of carbamazepine (75), and new methods (61) are being developed that can be applied to co-crystals (76) and other demanding multi-component systems, trying to optimize the balance between the significant computational cost of the search and evaluating the final crystal energies sufficiently accurately. The more restricted approach of using a range of plausible hydrogen-bonded structures for the asymmetric unit cell contents to generate initial structures, and then allowing their relative positions to adjust on lattice energy minimization, has been successfully applied to 5-azauracil monohydrate (77) and simple diastereomeric salts (78). A preliminary search for plausible crystal structures of a rigid non-chiral molecule, restricted to one molecule in the asymmetric unit, would require about 3000 lattice energy minimizations using MOLPAK, but for more confidence that structures with unusual packings would be found, a Crystal Predictor (74) search would minimize about 10^5 crystal structures.

It is the molecule itself that determines the types of structures that are low in energy and their relative energies, and so determines the type of search and energy evaluation required to order the low-energy structures correctly. For example, Figure 6A shows the lattice energy landscape for 2,3-dichloronitrobenzene, calculated with a simple MOLPAK search in common space-groups with $Z' = 1$ and using the molecule held rigid in the ab initio optimized "gas phase" conformation. The known structure is clearly predicted to be the most stable. However, its isomer, 3,5-dichloronitrobenzene does not have such a good way of packing (Fig. 6B), with many alternatives to its most stable structure being so close in energy that a more accurate energy evaluation is clearly desirable. The lattice energy landscape for 2,4-dichloronitrobenzene (Fig. 6C) appeared to be clearly predicting some favorable packings. Later, the crystal structure was found to have two molecules in the asymmetric unit, with different torsional distortions of the nitro group, thereby producing a structure that was somewhat more stable. The observed structure could have been predicted by a far more demanding search allowing both conformational flexibility and extending to two molecules in the asymmetric unit cell.

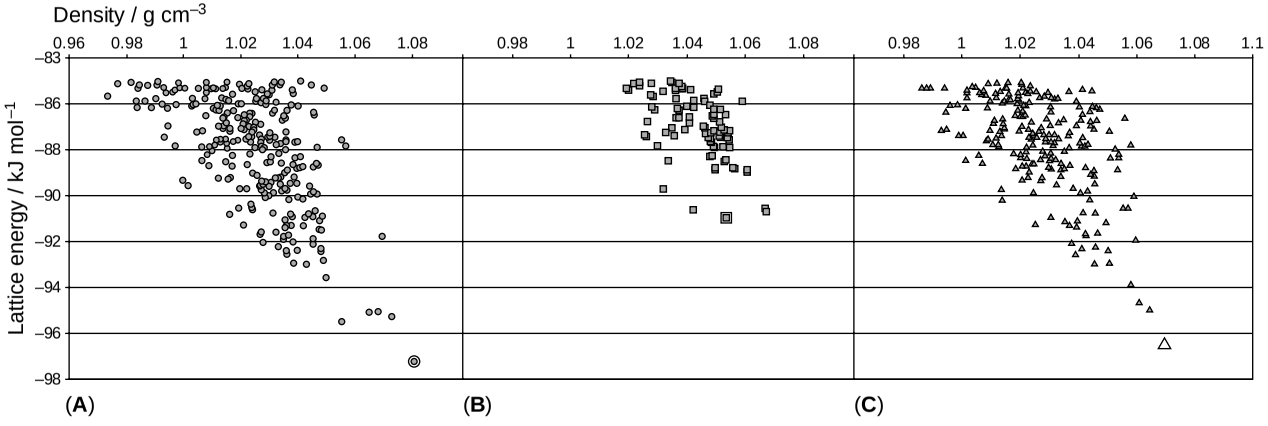

FIGURE 6 The lattice energy landscapes for (**A**) 2,3-dichloronitrobenzene, (**B**) 3,5-dichloronitrobenzene, and (**C**) 2,4-dichloronitrobenzene. Each symbol denotes the lattice energy and density of an optimized crystal structure, with the open symbol denoting the lattice energy of the experimental structure calculated with the corresponding computational model.

The requirement for $Z' = 2$ searches is also shown by the polymorphs of 7-fluoroisatin (55). One polymorph corresponded to the minimum in a simple $Z' = 1$ search, and the most metastable polymorph is $Z' = 2$ but also based on the $R_2^2(8)$ hydrogen bonded dimer, and can be viewed as an "arrested crystallization." However, the most thermodynamically stable polymorph is intrinsically $Z' = 2$, using different hydrogen-bonding donors and acceptors in a $R_4^4(18)$ motif.

Because different initial structures can minimize to essentially the same structure, it is necessary to remove duplicates from the crystal energy landscape. This raises some interesting questions as to which criteria will not eliminate structures that would be experimentally described as polymorphs, and yet not include structures where the differences would be eliminated by thermal motion. For example, a new low-temperature orthorhombic form of alloxan (79) is a slightly better match to the global lattice energy minimum (80) ($RMSD_{15} = 0.16$ Å) than the high-temperature, tetragonal structure ($RMSD_{15} = 0.18$ Å for the 42 K determination) (81). The examples of aspirin and eniluracil in Figures 2 and 3 demonstrate why it is safer only to eliminate as duplicate structures those with both a low $RMSD_{15}$ and a high similarity index for the simulated powder patterns.

Comparison of the simulated powder patterns of the low-energy structures with experimental powder X-ray diffraction patterns can aid solving structures when crystals suitable for single-crystal X-ray diffraction cannot be grown, and the powder pattern cannot be indexed. Several successes have been reported, particularly for pigments (82). However, the combination of typical errors of a few percent in the computed cell dimensions with the variations in the powder pattern with temperature, let alone the possibility of disorder in structures with growth problems, means that an automated comparison of an experimental powder pattern with those simulated from hundreds of low-energy structures is not trivial. However, analyzing the range of packing motifs among the low-energy structures can support or correct qualitative crystal engineering assumptions (80) in interpreting powder and other experimental data in terms of possible structures.

INTERPRETATION OF CRYSTAL ENERGY LANDSCAPES

A few idealized types of crystal energy landscape are shown in Figure 7, showing the relative free energies of different crystal structures denoted by similarities in the crystal packing, such as similar hydrogen-bonded sheets. The interpretation of each type is given below (3,4), based on comparing the energy differences between structures and the plausible energy difference between different polymorphs. More experimental studies may allow a better definition of this quantity, which is generally taken as less than 10 kJ mol^{-1} (83), although it is likely to be determined by the barriers to polymorphic transformations for the specific molecule. Each type of crystal energy landscape is illustrated by a few systems that have been found to approximate this type of landscape, although the distinction is rarely clear cut. In the illustrative examples, the lattice energy landscape has been computed and used, with a tentative allowance made for the likely effects of temperature and other inaccuracies in the computational model.

Monomorphic Crystal Energy Landscapes

The monomorphic crystal energy landscape (Fig. 7A) is where one structure is more thermodynamically stable than any other, by more than the plausible energy

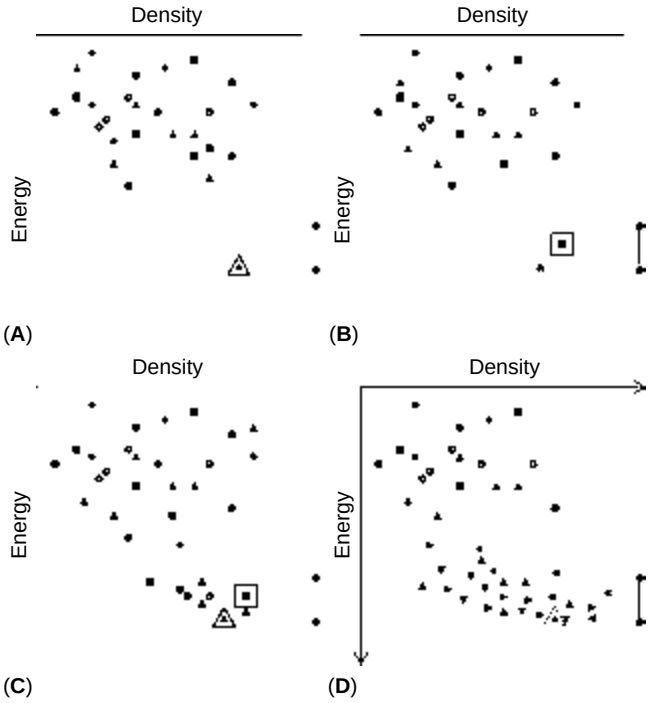

FIGURE 7 Schematic examples of crystal energy landscapes. Each point denotes a crystal structure that is a local energy minimum, with the symbols representing significantly different types of packing, such as different hydrogen bonding motifs. The experimentally known structures are denoted by open symbols. The plausible energy range of polymorphism is marked on the right.

difference between polymorphs. The molecule should only crystallize in this structure (unless there is a particularly thermodynamically advantageous multicomponent crystal). Once this crystal structure is obtained, such a crystal energy landscape would add confidence to a limited polymorph screen that there are unlikely to be any practically significant polymorphs (84). A monomorphic crystal energy landscape arises when the molecules can pack densely in a unique manner in all three dimensions with translational symmetry. This is rare, explaining the challenge of designing new materials by crystal engineering.

The degree of choice in solid form development in pharmaceuticals, while maintaining the medicinal effect and chiral purity, is so limited that clearly monomorphic crystal energy landscapes are likely to be exceptional. However, we could find a situation where there was a significant energy gap between the global minimum and the other structures, which are probably within the energy range of possible polymorphism. If these metastable structures are related to the global minimum structure in a way that suggests that it will be impossible to trap the molecules into these free energy minima during nucleation and growth, then the system is probably monomorphic. As illustrated by 3-oxauracil (85), such calculations would add considerable confidence to a solid form screen that had not shown any signs of polymorphism.

Predictive Crystal Energy Landscapes

A predictive energy landscape (Fig. 7B), where an alternative polymorph is predicted to be more stable than the known form, would motivate a careful search to find it or establish that there is no route to nucleating it. Because seeds of the more stable form could be used to develop a practical crystallization route, any method (1) that might force nucleation of the predicted form could be used. Two cases where the lattice energy landscape predicted more stable structures than the known $Z' = 4$ structures have resulted in the finding of a new $Z' = 1$ polymorphs, although neither for pyridine (86) nor 5-fluoruracil (87) is it established that the new forms are more thermodynamically stable. The new polymorph of 5-fluorouracil was crystallized from dry nitromethane. Molecular Dynamics (88) simulations show how this solvent promotes the formation of the doubly hydrogen-bonded $R_2^2(8)$ dimer motif in form II, whereas water hydrates the molecule so strongly that it promotes the close F···F contacts in form I. This is just one example how analyzing the variety of hydrogen bonding motifs in the low-energy structures can suggest (89) solvents to target the formation of each motif. Similarly, analysis of the predicted structure could suggest polymer, surface, or additive templates that would be worth trying to nucleate the predicted structure. The prediction that a catemer-based polymorph of carbamazepine would be competitive with the known $R_2^2(8)$ dimer polymorphs led to the discovery of catemeric carbamazepine in a solid solution with the attempted template, dihydrocarbamazepine (90).

A case where a lattice energy landscape made a very clear prediction, which required considerable effort to validate because of the kinetic barrier to rearrangement to the most stable form, was the predicted structure of racemic progesterone (91). Although natural progesterone is a case where an established polymorph appears stabilized by impurities (2), the racemate can adopt a structure that has an ideal interaction between the carbonyl groups. The predicted crystal structure was found by crystallizing progesterone with its synthetic mirror image (91).

Of course, once all the polymorphs have been found, the "predictive" energy landscape becomes one with the known polymorphs as the lowest energy structures. Acetaminophen approximates this, in that forms I and II were the lowest energy structures on the crystal energy landscape (92); however, there are alternative structures that are only slightly less stable. One of these has been proposed (93) as a possible structure for form III, but the complexity of the metastable region of the crystal energy landscape suggests the possibility of form III being disordered.

Complex Crystal Energy Landscapes

When there are many distinct crystal structures within a small energy range, as shown in Figure 7C, then there are many ways of packing the molecule that are energetically competitive. Which ones are actually seen will depend on kinetic factors that influence which structures can nucleate and grow most readily and not transform into a slightly more stable structure. For example, the discussion of the 2001 blind test of crystal structure prediction (94) concluded the 3-azabicyclo(3.3.1) nonane-2,4-dione should form an $R_2^2(8)$ dimer-based structure as well as the know hydrogen-bonded catemer form. An extensive search (95) found two solvates, a $Z' = 2$ "fossil relic" chain polymorph, and a plastic phase. The latter implied that the barrier to disrupting the hydrogen bonding was very low, and computational

modeling confirmed that the hydrogen bonding motif could readily change in small clusters. This was because the hydrogen bonding is atypically weak and non-directional for this rather spherical imide (Fig. 5) Thus, it is probably not possible to trap the dimer-based motif as a metastable polymorph because it will rearrange to the catemer structure during nucleation and growth.

The type of crystal energy landscape in Figure 7C indicates that multiple solid forms are likely. The molecule has a packing problem, which may result in polymorphism or be solved by solvate or cocrystal formation. For example, the low-energy structures of 5-fluorocytosine all contain the same ribbon motif that appears to have no preferred way of packing, and was later found (96) in both polymorphs and the four stable solvates. In contrast, hydrochlorothiazide had a wide range of bimolecular hydrogen bonding motifs in the low-energy landscape (97), and the problem of packing these dimers results in many of these distinct motifs being found in the two polymorphs and seven solvates. Thus, a complex crystal energy landscape can help interpret the molecular self-association processes that can lead to solvate formation.

Interchangeable Crystal Energy Landscape and Disorder

A particular type of complex crystal energy landscape is when the low-energy structures are related in an interchangeable fashion (Fig. 7D), for example, when there are two or more ways of stacking the same hydrogen-bonded sheet with effectively the same energy. This implies that a multitude of structures based on different combinations of the stackings of these sheets will be very similar in energy. Thus, depending on the barrier to rearrangement to correct the inevitable growth mistakes, such a crystal energy landscape may result in disorder or multiple stacking faults, polytypism, or incommensurate structures. Aspirin provides an example of this. The two alternative stackings of the same sheet (Fig. 2) were predicted to be so close in energy (42) at the global minimum of the lattice energy landscape, that it rationalizes the later discovery of form II (15) and the observation of the intergrowth of polymorphic domains within the same single crystal (18). Although the metastable form II of aspirin readily transforms to the more stable form I, other forms of disorder arising from interchangeable motifs may be less readily corrected and lead to problems in devising a robust production process. The crystal energy landscape of eniluracil (22) contains several structures built up of the polar and non-polar ribbons illustrated in Figure 3, which are very close in energy and would be identical if C4=O and C6–H were indistinguishable. It seems highly likely that growth mistakes would occur, such as the non-polar ribbons interdigitating in a parallel rather than anti-parallel fashion, which, once formed, would be difficult to reverse. Thus, the eniluracil crystal energy landscape rationalizes the variable disorder seen in different single crystals by detailed diffraction analyses (22). This understanding of the variety of possible disordered structures would have facilitated the development of a production process. A further case of the complexity of the solid state being apparent in the lattice energy landscape is chlorothalonil, where five structures within 1.25 kJ mol^{-1} of the global minimum have been related to the observed polymorphs (58): the ordered form I corresponded to the global minimum, two predicted $Z' = 1$ ribbon structures could be recognized in the $Z' = 3$ form III, and two $Z' = 1$ predicted layer structures rationalize the apparent disorder in form II. Thus, examining the types of crystal packings on a complex crystal energy landscape, such as those illustrated in Figure 7C and D, warns

of the possibility of a complex solid state, and can complement the experimental characterization.

SUMMARY

Comparing the crystal structures of pharmaceutical polymorphs, solvates, and co-crystals can help generate an understanding and means of control of their physical properties. This is illustrated by Figures 1–3 showing the differences between (a) clearcut polymorphism in the case of acetaminophen, (b) the debated borderline case of aspirin, and (c) eniluracil, which has recently been demonstrated to be better described as a case of variable disorder than polymorphism. If the comparison is extended to include the crystal structures that are predicted to be competitive in thermodynamic stability to the known forms, then this will complement the experimental screening (4). It may just provide confidence that all practically significant polymorphs are known, as in the case of 3-oxauracil, or allow the targeting of specific novel polymorphs, for example, for 5-fluorouracil. It can determine the type of potential complexity in the solid state. At the time of this writing, calculating the crystal energy landscape with a worthwhile relative accuracy in the thermodynamic stability and range of crystal structures considered is restricted to the smaller pharmaceutical molecules with limited flexibility. It requires considerable computational infrastructure and expertise in computational chemistry to select and test whether a given approach to calculating the crystal energy landscape is likely to be "good enough" for purpose. However, this field has advanced sufficiently in the last decade for the use of computational modelling to be a complementary tool in multidisciplinary studies of polymorphism in industrial as well as academic research.

REFERENCES

1. Llinas A, Goodman JM. Polymorph control: past, present and future. Drug Discover Today 2008; 8: 198–210.
2. Lancaster RW, Karamertzanis PG, Hulme AT, et al. The polymorphism of progesterone: stabilization of a 'disappearing' polymorph by co-crystallization. J Pharm Sci 2007; 96: 3419–31.
3. Price SL. From crystal structure prediction to polymorph prediction: interpreting the crystal energy landscape. Phys Chem Chem Phys 2008; 10: 1996–2009.
4. Price SL. Computed crystal energy landscapes for understanding and predicting organic crystal structures and polymorphism. Accounts Chem Res 2009; 42: 117–26.
5. Davey RJ, Allen K, Blagden N, et al. Crystal engineering – nucleation, the key step. CrystEngComm 2002; 4: 257–64.
6. Price SL. Computational prediction of organic crystal structures and polymorphism. Int Rev Phys Chem 2008; 27: 541–68.
7. Bernstein J, Davies RE, Shimoni L, et al. Patterns in hydrogen bonding: functionality and graph set analysis in crystals. Angew Chem Int Ed Engl 1995; 34: 1555–73.
8. Nichols G, Frampton CS. Physicochemical characterization of the orthorhombic polymorph of paracetamol crstallized from solution. J Pharm Sci 1998; 87: 684–93.
9. Chisholm JA, Motherwell S. COMPACK: a program for identifying crystal structure similarity using distances. J Appl Crystallogr 2005; 38: 228–31.
10. Macrae CF, Edgington PR, McCabe P, et al. Mercury: visualization and analysis of crystal structures. J Appl Crystallogr 2006; 39: 453–7.

11. McKinnon JJ, Fabbiani FPA, Spackman MA. Comparison of polymorphic molecular crystal structures through hirshfeld surface analysis. Cryst Growth Des 2007; 7: 755–69.
12. Wolff SK, Grimwood DJ, McKinnon JJ, Jayatilaka D, Spackman MA. CrystalExplorer. [2.1]. University of Western Australia, 2007.
13. de Gelder R, Wehrens R, Hageman JA. A generalized expression for the similarity of spectra: application to powder diffraction pattern classification. J Comput Chem 2001; 22: 273–89.
14. van de Streek J, de Gelder R. CalculateSimilarity: a program to calculate the similarity of two crystal structures. Cambridge UK: Cambridge Crystallographic Data Centre, 2005.
15. Vishweshwar P, McMahon JA, Oliveira M, et al. The predictable elusive form II of aspirin. J Am Chem Soc 2005; 127: 16802–3.
16. Wilson CC. Interesting proton behaviour in molecular structures. Variable temperature neutron diffraction and ab initio study of acetylsalicylic acid: characterising librational motions and comparing protons in different hydrogen bonding potentials. New J Chem 2002; 26: 1733–9.
17. Gavezzotti A. A solid-state chemist's view of the crystal polymorphism of organic compounds. J Pharm Sci 2007; 96: 2232–41.
18. Bond AD, Boese R, Desiraju GR. On the polymorphism of aspirin: crystalline aspirin as intergrowths of two polymorphic domains. Angew Chem Int Ed 2007; 46: 618–22.
19. Bond AD, Boese R, Desiraju GR. On the polymorphism of aspirin. Angew Chem Int Ed 2007; 46: 615–7.
20. van de Streek J, Motherwell S. Searching the cambridge structural database for polymorphs. Acta Crystallogr Sect B 2005; 61: 504–10.
21. Allen FH. The cambridge structural database: a quarter of a million crystal structures and rising. Acta Crystallogr Sect B 2002; 58: 380–8.
22. Copley RCB, Barnett SA, Karamertzanis PG, et al. Predictable disorder versus polymorphism in the rationalization of structural diversity: a multi-disciplinary study of eniluracil. Cryst Growth Des 2008; 8: 3474–81.
23. Gelbrich T, Hursthouse MB. A versatile procedure for the identification, description and quantification of structural similarity in molecular crystals. CrystEngComm 2005; 7: 324–36.
24. Gelbrich T, Hursthouse MB. Systematic investigation of the relationships between 25 crystal structures containing the carbamazepine molecule or a close analogue: a case study of the XPac method. CrystEngComm 2006; 8: 448–60.
25. Pertsin AJ, Kitaigorodsky AI. The Atom-Atom Potential Method. Applications to Organic Molecular Solids. Berlin: Springer-Verlag, 1987.
26. Gavezzotti A. Molecular Aggregation: Structure Analysis and Molecular Simulation of Crystals and Liquids. Oxford: Oxford University Press, 2007.
27. Allen FH, Kennard O, Watson DG. Tables of bond lengths determined by X-ray and neutron diffraction. Part 1. Bond lengths in organic compounds. J Chem Soc Perkin T 1987; 2: S1–S19.
28. Beyer T, Price SL. The errors in lattice energy minimisation studies: sensitivity to experimental variations in the molecular structure of paracetamol. CrystEngComm 2000; 2: 183–90.
29. Fabbiani FPA, Byrne LT, McKinnon JJ, et al. Solvent inclusion in the structural voids of form II carbamazepine: single-crystal X-ray diffraction, NMR spectroscopy and hirshfeld surface analysis. CrystEngComm 2007; 9: 728–31.
30. Cabeza AJC, Day GM, Motherwell WDS, et al. Solvent inclusion in form II carbamazepine. Chem Commun 2007: 1600–2.
31. van Mourik T, Karamertzanis PG, Price SL. Molecular conformations and relative stabilities can be as demanding of the electronic structure method as intermolecular calculations. J Phys Chem A 2006; 110: 8–12.

32. Karamertzanis PG, Day GM, Welch GWA, et al. Modeling the interplay of inter- and intra-molecular hydrogen bonding in conformational polymorphs. J Chem Phys 2008; 128: art–244708.
33. Neumann MA, Perrin MA. Energy ranking of molecular crystals using density functional theory calculations and an empirical van der waals correction. J Phys Chem B 2005; 109: 15531–41.
34. Day GM, Motherwell WDS, Ammon HL, et al. A third blind test of crystal structure prediction. Acta Crystallogr Sect B 2005; 61: 511–27.
35. Day GM, Cooper TG, Cruz Cabeza AJ, et al. Significant progress in predicting the crystal structures of small organic molecules – a report on the fourth blind test. Acta Crystallogr Sect B 2009; 65: 107–25.
36. Neumann MA, Leusen FJJ, Kendrick J. A major advance in crystal structure prediction. Angew Chem Int Ed 2008; 47: 2427–30.
37. Filippini G, Gavezzotti A. Empirical intermolecular potentials for organic-crystals: the '6-exp' approximation revisited. Acta Crystallogr Sect B 1993; 49: 868–80.
38. Gavezzotti A, Filippini G. Geometry of the intermolecular X-H…Y (X, Y=N, O) hydrogen-bond and the calibration of empirical hydrogen-bond potentials. J Phys Chem 1994; 98: 4831–37.
39. Goodman JM. Chemical Applications of Molecular Modelling. Cambridge, UK: Royal Society of Chemistry, 1998.
40. Brodersen S, Wilke S, Leusen FJJ, et al. A study of different approaches to the electrostatic interaction in force field methods for organic crystals. Phys Chem Chem Phys 2003; 5: 4923–31.
41. Payne RS, Rowe RC, Roberts RJ, et al. Potential polymorphs of aspirin. J Comput Chem 1999; 20: 262–73.
42. Ouvrard C, Price SL. Toward crystal structure prediction for conformationally flexible molecules: the headaches illustrated by aspirin. Cryst Growth Des 2004; 4: 1119–27.
43. Gourlay MD, Kendrick J, Leusen FJJ. Rationalization of racemate resolution: predicting spontaneous resolution through crystal structure prediction. Cryst Growth Des 2007; 7: 56–63.
44. Stone AJ. The Theory of Intermolecular Forces. Oxford: Clarendon Press, 1996.
45. Price SL. Quantifying intermolecular interactions and their use in computational crystal structure prediction. CrystEngComm 2004; 6: 344–53.
46. Wiberg KB, Rablen PR. Comparison of atomic charges derived via different procedures. J Comput Chem 1993; 14: 1504–18.
47. Williams DE, Cox SR. Nonbonded potentials for azahydrocarbons: the importance of the coulombic interaction. Acta Crystallogr Sect B 1984; 40: 404–17.
48. Stone AJ. Distributed multipole analysis: stability for large basis sets. J Chem Theory Comput 2005; 1: 1128–32.
49. Price SL, Richards NGJ. On the representation of electrostatic fields around ab initio charge distributions. J Comput Aid Mol Des 1991; 5: 41–54.
50. Day GM, Chisholm J, Shan N, et al. Assessment of lattice energy minimization for the prediction of molecular organic crystal structures. Cryst Growth Des 2004; 4: 1327–40.
51. Day GM, Motherwell WDS, Jones W. Beyond the isotropic atom model in crystal structure prediction of rigid molecules: atomic multipoles versus point charges. Cryst Growth Des 2005; 5: 1023–33.
52. Coombes DS, Price SL, Willock DJ, et al. Role of electrostatic interactions in determining the crystal structures of polar organic molecules. A distributed multipole study. J Phys Chem 1996; 100: 7352–60.
53. Beyer T, Price SL. Dimer or catemer? Low-energy crystal packings for small carboxylic acids. J Phys Chem B 2000; 104: 2647–55.
54. Williams DE. Improved intermolecular force field for molecules containing H, C, N, and O atoms, with application to nucleoside and peptide crystals. J Comput Chem 2001; 22: 1154–66.

55. Mohamed S, Barnett SA, Tocher DA, et al. Discovery of three polymorphs of 7-fluoroisatin reveals challenges in using computational crystal structure prediction as a complement to experimental screening. CrystEngComm 2008; 10: 399–404.
56. Welch GWA, Karamertzanis PG, Misquitta AJ, et al. Is the induction energy important for modeling organic crystals? J Chem Theory Comput 2008; 4: 522–32.
57. Day GM, Price SL. A nonempirical anisotropic atom-atom model potential for chlorobenzene crystals. J Am Chem Soc 2003; 125: 16434–43.
58. Tremayne M, Grice L, Pyatt JC, et al. Characterization of complicated new polymorphs of chlorothalonil by X-ray diffraction and computer crystal structure prediction. J Am Chem Soc 2004; 126: 7071–81.
59. Misquitta AJ, Welch GWA, Stone AJ, et al. A first principles solution of the crystal structure of $C_6Br_2ClFH_2$. Chem Phys Lett 2008; 456: 105–9.
60. Karamertzanis PG, Price SL. Energy minimization of crystal structures containing flexible molecules. J Chem Theory Comput 2006; 2: 1184–99.
61. Karamertzanis PG, Kazantsev AV, Issa N, et al. Can the formation of pharmaceutical co-crystals be computationally predicted? 2. Crystal structure prediction. J Chem Theory Comput 2009; in press: DOI: 10.021/ct8004326.
62. Gavezzotti A, Filippini G. Polymorphic forms of organic-crystals at room conditions – thermodynamic and structural implications. J Am Chem Soc 1995; 117: 12299–305.
63. Day GM, Price SL, Leslie M. Atomistic calculations of phonon frequencies and thermodynamic quantities for crystals of rigid organic molecules. J Phys Chem B 2003; 107: 10919–33.
64. Day GM, Zeitler JA, Jones W, et al. Understanding the influence of polymorphism on phonon spectra: lattice dynamics calculations and terahertz spectroscopy of carbamazepine. J Phys Chem B 2006; 110: 447–56.
65. Day GM, Price SL, Leslie M. Elastic constant calculations for molecular organic crystals. Cryst Growth Des 2001; 1: 13–26.
66. Gray AE, Day GM, Leslie M, et al. Dynamics in crystals of rigid organic molecules: contrasting the phonon frequencies calculated by molecular dynamics with harmonic lattice dynamics for imidazole and 5-azauracil. Mol Phys 2004; 102: 1067–83.
67. Torrisi A, Leech CK, Shankland K, et al. The solid phases of cyclopentane: a combined experimental and simulation study. J Phys Chem B 2008; 112: 3746–58.
68. Raiteri P, Martonak R, Parrinello M. Exploring polymorphism: the case of benzene. Angew Chem Int Ed 2005; 44: 3769–73.
69. Karamertzanis PG, Raiteri P, Parrinello M, et al. The thermal stability of lattice energy minima of 5-fluorouracil: metadynamics as an aid to polymorph prediction. J Phys Chem B 2008; 112: 4298–308.
70. Gavezzotti A. Generation of possible crystal-structures from the molecular-structure for low-polarity organic-compounds. J Am Chem Soc 1991; 113: 4622–9.
71. Holden JR, Du ZY, Ammon HL. Prediction of possible crystal-structures for C-, H-, N-, O- and F-containing organic compounds. J Comput Chem 1993; 14: 422–37.
72. Verwer P, Leusen FJJ. Computer Simulation to Predict Possible Crystal Polymorphs. In: Lipkowitz KB, Boyd DB, eds. Reviews in Computational Chemistry Volume 12; Vol. 12. New York: Wiley-VCH, 1998: 327–65.
73. van Eijck BP. Comparing hypothetical structures generated in the third cambridge blind test of crystal structure prediction. Acta Crystallogr Sect B 2005; 61: 528–35.
74. Karamertzanis PG, Pantelides CC. Ab initio crystal structure prediction – I. rigid molecules. J Comput Chem 2005; 26: 304–24.
75. Cabeza AJC, Day GM, Motherwell WDS, et al. Prediction and observation of isostructurality induced by solvent incorporation in multicomponent crystals. J Am Chem Soc 2006; 128: 14466–7.
76. Issa N, Karamertzanis PG, Welch GWA, et al. Can the formation of pharmaceutical co-crystals be computationally predicted? I comparison of lattice energies. Cryst Growth Des 2009; 9: 442–53.

77. Hulme AT, Price SL. Towards the prediction of organic hydrate crystal structures. J Chem Theory Comput 2007; 3: 1597–608.
78. Karamertzanis PG, Price SL. Challenges of crystal structure prediction of diastereomeric salt pairs. J Phys Chem B 2005; 109: 17134–50.
79. Ibberson RM, Marshall WG, Budd LE, et al. Alloxan – a new low-temperature phase determined by neutron powder diffraction. CrystEngComm 2008; 10: 465–8.
80. Lewis TC, Tocher DA, Price SL. Investigating unused hydrogen bond acceptors using known and hypothetical crystal polymorphism. Cryst Growth Des 2005; 5: 983–93.
81. Swaminathan S, Craven BM, McMullan RK. Alloxan – electrostatic properties of an unusual structure from X-ray and neutron diffraction. Acta Crystallogr Sect B 1985; 41: 113–22.
82. Schmidt MU, Dinnebier RE, Kalkhof H. Crystal engineering on industrial diaryl pigments using lattice energy minimizations and X-ray powder diffraction. J Phys Chem B 2007; 111: 9722–32.
83. Bernstein J. Polymorphism in Molecular Crystals. Oxford: Clarendon Press, 2002.
84. Price SL. The computational prediction of pharmaceutical crystal structures and polymorphism. Adv Drug Deliver Rev 2004; 56: 301–19.
85. Copley RCB, Deprez LS, Lewis TC, et al. Computational prediction and X-ray determination of the crystal structures of 3-oxauracil and 5-hydroxyuracil – an informal blind test. CrystEngComm 2005; 7: 421–8.
86. Anghel AT, Day GM, Price SL. A study of the known and hypothetical crystal structures of pyridine: why are there four molecules in the asymmetric unit cell? CrystEngComm 2002; 4: 348–55.
87. Hulme AT, Price SL, Tocher DA. A new polymorph of 5-fluorouracil found following computational crystal structure predictions. J Am Chem Soc 2005; 127: 1116–17.
88. Hamad S, Moon C, Catlow CRA, et al. Kinetic insights into the role of the solvent in the polymorphism of 5-fluorouracil from molecular dynamics simulations. J Phys Chem B 2006; 110: 3323–9.
89. Blagden N, Cross WI, Davey RJ, et al. Can crystal structure prediction be used as part of an integrated strategy for ensuring maximum diversity of isolated crystal forms? The case of 2-amino-4-nitrophenol. Phys Chem Chem Phys 2001; 3: 3819–25.
90. Florence AJ, Leech CK, Shankland N, et al. Control and prediction of packing motifs: a rare occurrence of carbamazepine in a catemeric configuration. CrystEngComm 2006; 8: 746–7.
91. Lancaster RW, Karamertzanis PG, Hulme AT, et al. Racemic progesterone: predicted in silico and produced in the solid state. Chem Commun 2006: 4921–3.
92. Beyer T, Day GM, Price SL. The prediction, morphology and mechanical properties of the polymorphs of paracetamol. J Am Chem Soc 2001; 123: 5086–94.
93. Peterson ML, Morissette SL, McNulty C, et al. Iterative high-throughput polymorphism studies on acetaminophen and an experimentally derived structure for form III. J Am Chem Soc 2002; 124: 10958–9.
94. Motherwell WDS, Ammon HL, Dunitz JD, et al. Crystal structure prediction of small organic molecules: a second blind test. Acta Crystallogr Sect B 2002; 58: 647–61.
95. Hulme AT, Johnston A, Florence AJ, et al. Search for a predicted hydrogen bonding motif – a multidisciplinary investigation into the polymorphism of 3-azabicyclo[3.3.1] nonane-2,4-dione. J Am Chem Soc 2007; 129: 3649–57.
96. Hulme AT, Tocher DA. The discovery of new crystal forms of 5-fluorocytosine consistent with the results of computational crystal structure prediction. Cryst Growth Des 2006; 6: 481–7.
97. Johnston A, Florence AJ, Shankland N, et al. Crystallization and crystal energy landscape of hydrochlorothiazide. Cryst Growth Des 2007; 7: 705–12.

4 Classical Methods of Preparation of Polymorphs and Alternative Solid Forms

Peter W. Cains
Avantium Technologies BV, Amsterdam, The Netherlands

SOLID FORMS AND THEIR CHARACTERISTICS

An awareness of the properties of the solid form in which drug substances (APIs) are manufactured and isolated today plays an important role in pharmaceuticals development. In the majority of cases a crystalline form is preferred, which enables the substance to be produced reliably and reproducibly with well-defined and characterized physical properties. However, a recent trend in pharmaceuticals development is a move toward APIs that are more lipophilic, hydrophobic, and insoluble in nature (1), and in these cases limitations in bioavailability may favor the development of amorphous or metastable forms with higher solubilities and dissolution rates (2). Whatever solid form is chosen will provide the starting point for the formulation of the drug, and the formulation and means of delivery will conversely exert requirements and restrictions on the solid form selection (3). For example, an amorphous API is not desirable for administration via a conventional dry powder inhaler.

The phenomenon of polymorphism has focused minds on identifying the optimal solid form for development. Polymorphs are essentially different crystalline forms of a solid resulting from different crystal packings of the same molecules, or of the same ions. Because polymorphs also represent different and distinct solid phases, their physical properties will differ. Some of these properties, in particular solubility and dissolution rate, are important in determining the uptake rate of the drug, and must be taken into account in developing an appropriate formulation. A survey in 2005 (4) showed that the solubility ratios between polymorphs generally lie in the range 1 to 4.5, with the majority of cases (90%) within a factor of two.

The facility to manufacture the selected polymorphic form reliably will also be a key factor in determining the success of the drug product. There have been a number of cases in the past where this has not been achieved, notably with the anti-HIV agent ritonavir where a second and less soluble polymorphic form appeared in manufacture in the summer of 1998 (5,6). Today, regulatory bodies such as the FDA (7) recommend that some kind of polymorph screen be carried out to establish the reliability of a specified solid form and its stability under stress conditions, and the robustness of the process by which it is manufactured. Furthermore, patent protection is normally granted only on individual polymorphic forms that have been identified, characterized, and differentiated (8), so there is a powerful incentive to identify and protect alternative forms that may otherwise be identified and developed by a competitor or a generics manufacturer.

From a manufacturing point of view, a procedure to prepare and work with the ground-state polymorph that is most stable thermodynamically will always be

the preferred option. With no driving force to transform, these products are least likely to come up with surprises either in manufacturing or in subsequent storage. However, in practice, the possibility of another, less stable form arising in manufacture can never be entirely ruled out, particularly if there are variations in procedure or if the production process is operated under conditions that are far from equilibrium. On the other hand, the ground-state polymorph will always exhibit the lowest solubility because its chemical potential is lowest by definition. Moreover, dissolution rates of less stable forms are also invariably higher because the less stable solid forms are more labile, and the ground-state crystalline form will usually have the highest packing density and the highest activation energy barriers to dissolution.

Manufacturers are thus presented with the challenge of balancing solubility, dissolution rate, and bioavailability against reliability of manufacture, to choose the product most suitable for development as a drug. It is also incumbent on them to demonstrate in registering the drug that no alternative crystalline or amorphous forms outside the specifications of manufacture are likely to arise in their processes, and it is in their interests to identify all the alternative solid forms that the compound in question may adopt and the conditions under which they arise. The question arises as to how far to go. One of the many often quoted statements of W.C. McCrone from the 1950s and 1960s states, "Those who study polymorphism are rapidly reaching the conclusion that all compounds, organic and inorganic, can crystallize in different forms and polymorphs. In fact, the more diligently any system is studied the larger the number of polymorphs discovered" (9). In other words, the more time and effort spent searching, the more polymorphs will be discovered. Then there is the reported phenomenon of "disappearing polymorphs," where a particular solid form suddenly ceases to be obtainable by the method employed hitherto for its preparation (10).

Today, a search for polymorphs is an integral part of any drug development process, and can run from early pre-clinical to the advanced development stages of phases 2 and 3. In the early stages, the emphasis is on finding suitable (and usually stable) forms for development, and feeding such information into the decision processes for selecting a suitable formulation. Here, both the quantities of material available and the funding available for searches will be limited, and a successful outcome in terms of a form suitable to take forward into further development is required on a short time scale. At later stages, the searches become more exhaustive, with a view toward optimization of the solid form and the process by which it is manufactured, and toward protecting the product against the predations of competitors and generics manufacturers who may wish to exploit an alternative and unprotected solid form. In this chapter, the different methods by which solid forms can be prepared will be outlined, along with discussion of which methods are most suitable for which outcomes in terms of form stability. Polymorph and other solid form screening is often carried out in high-throughput arrangements whereby large numbers of experiments can be undertaken with designed variations in conditions using the methods described herein. These high-throughput systems are covered in the following chapter.

Crystallizations carried out close to equilibrium conditions are likely to produce the ground-state polymorph, or forms that are relatively stable. More stable polymorphs are generally less labile and more closely packed than less stable ones, and require longer time periods under moderate conditions to acquire the correct

molecular ordering and orientation in the solid state. Also, for enantiotropic substances the order of stability and the ground state will change with temperature, and thus the outcomes may be temperature dependent. On the other hand, crystallizing under stress conditions far from equilibrium, for example by crash-cooling a solution, is more likely to produce unstable polymorphs, for two reasons. First, crystallization kinetics rather than thermodynamics will determine the crystal form under stress conditions, and the formation of the more labile unstable solid forms will be kinetically favored. Second, and critically, the high supersaturations induced by crash cooling set up the driving forces whereby the unstable and more soluble forms can crystallize. The formation of metastable forms under conditions of kinetic control was expressed in the 1890s in Ostwald's "Rule of Stages" (11), which states that "an unstable system does not necessarily transform into the most stable state, but into one which most closes resembles the starting condition with the smallest loss of free energy." However, Ostwald himself recognized that this "Rule" does not always apply, and many more cases have been discovered subsequently. More recent theoretical descriptions involve a combination of kinetics with thermodynamic (12) or structural (13) factors.

The formation of solvates of a compound may complicate both its polymorphic landscape and the methods by which it is prepared and formulated. The term "solvate" generally denotes any solid form that includes solvent molecules in its structure, and can be ambiguous in terms of the nature of the form. Figure 1 illustrates the types of solvate commonly encountered. In "true" solvates, or "solvatomorphs" (Fig. 1A), solvent molecules form an integral part of the unit cell of the crystal, are in a stoichiometric ratio to the principal substrate, and are bound into the crystal lattice by hydrogen bonding or other binding arrangements that can hold multi-component crystals together (14). Removal of the solvent cannot occur without structural disruption, and the conversion of the substrate to either an amorphous or a re-ordered, non-solvated crystalline form. In these cases, the temperature at which solvent removal occurs, measured thermogravimetrically, is usually well above the boiling point of the solvent, and is determined by the energy input required to bring about disruption of the lattice structure.

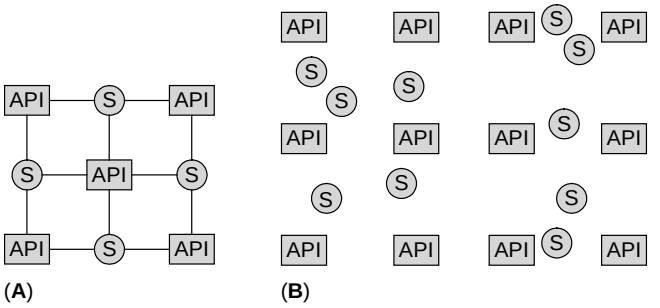

FIGURE 1 Solvates: solid forms incorporating solvent molecules. (**A**) "True" solvate or "solvatomorph," stoichiometric. Solvent molecule(s) form part of the unit cell of the crystal. (**B**) Solvent molecules are trapped in void spaces (*left*) or channels (*right*), non-stoichiometric. Capillary and steric effects may retain the solvent way above its boiling point. *Abbreviations*: API, active pharmaceutical ingredients; S, solvent.

Solvates also include crystal structures where the solvent is not incorporated stoichiometrically into the crystal structure, but is accommodated by affinity at the surface, or in voids or channels in the structure (Fig. 1B). Where solvent is located at the surfaces, it may usually be driven off at temperatures slightly above the solvent boiling point, and the thermal stability will be the primary factor determining whether or not the structure is disrupted. Solvation by incorporation into voids or channels is more akin to solid solution formation, whereby the solvent acts as a solute in the host matrix of the crystalline substrate. In these cases, desolvation may or may not result in structural disruption, depending on both the thermal stability and the extent of the mechanical effects of removing solvent molecules from the depths of the lattice structure. In these cases, desolvation usually occurs at temperatures considerably higher than the solvent boiling point (often up to 30 K higher), because of capillary effects in channels and geometric blocking of solvent release. It should be noted, however, that the arrangement of solvent molecules in channels also occurs quite commonly in stoichiometric solvatomorphs (15), by virtue of the crystallographic geometry, and the identification of solvent molecules within channels does not, in itself, characterize the solvate type.

"True" solvates are not polymorphic with the corresponding non-solvated forms, because the chemical constitutions are different. The term "solvatomorph" can be used to designate the fact that they represent alternative structures that are not polymorphic (14). As a general rule, solvates are not favored for pharmaceutical development, except for hydrates and occasionally ethanolates, because of the toxicity and undesirability of ingesting most solvents. Hydrates are often, although by no means universally, less soluble in aqueous media than the corresponding anhydrous forms (4).

Salt forms of drug substances are often employed to enhance their aqueous solubilities. Table 1 shows published data on the number of drug salts available in the 1990s (16). It can be seen that the number of salts with acidic counter-ions (anions) represents about 75% of the total from both sources. There are several reasons for this. First, most APIs contain basic nitrogen functions in their free base forms. Second, the list of anions that are suitable in terms of both appropriate pK_a values and pharmacological safety is much more extensive than the corresponding list of bases. Many nitrogenous bases exert biological and pharmacodynamic effects, and most inorganic cations are either toxic or exert essential biological functions, and in this latter case the dosing of additional quantities may restrict the scope of administration of the drug. Even so, the proportion of cations that are inorganic is considerably higher than the corresponding ratio for anions in both data sets recorded in Table 1. Table 2 gives the frequency distribution of the most common

TABLE 1 Reported Number of Drugs Available as Salts, and the Distribution of Acidic (Anionic) and Basic (Cationic) Counter-ions (16)

Source	No. of drug salts		No. of counter-ions (CIs)	
	with acid CI	with basic CI	Acidic	Basic
Index Nominum, 1995	1346	474	108	37
Rote Liste, 1999 (Germany)	612	208	55	21

TABLE 2 Distributions of Salts with the Most Frequently Occurring Acidic (Anionic) and Basic (Cationic) Counter-ions

Acidic (anionic) counter-ions			Basic (cationic) counter-ions		
Anion	**Percentage of total**		**Cation**	**Percentage of total**	
	Ref. (16)	**Ref. (17)**		**Ref. (16)**	**Ref. (17)**
Hydrochloride	36.2	42.1	Sodium	14.8	17.5
Sulfate	5.2	10.1	Potassium	2.9	4.9
Tartrate	3.3	2.6	Calcium	3.6	1.7
Hydrobromide	4.4	1.4	Magnesium	1.6	
Maleate	3.3	2.3	Meglumine	1.0	
Mesylate	3.3	1.2	Ammonium	0.9	
Phosphate	2.0	3.1	Aluminium	0.8	
Acetate	1.8	3.2	Zinc	0.5	
Citrate	3.0	0.8	Piperazine	0.5	
Pamoate	1.5	0.3	Tromethamine (Tris)	0.5	
Nitrate	1.3	0.8	Lithium	0.5	
Lactate	1.1	1.0	Choline	0.4	
Fumarate	1.1	0.6	Diethylamine	0.4	
Hydroiodide	1.3		4-Phenylcyclohexylamine	0.3	
Methylsulfate	1.1		Benzathine	0.3	
Succinate		1.1			
Propionate		1.0			
Carbonate		0.5			
Gluconate		0.5			
Aspartate		0.3			
Saccharate		0.3			
Besylate		0.3			
Valerate		0.3			

salt-forming acidic and basic counter-ions, as percentages of the total (acids + bases), calculated using data from two sources (16,17). It is clear from these data which counter-ions are used predominantly, although the detailed figures vary according to the data that has been sampled for the two compilations.

Figure 2 shows examples of the solubilization by salt formation of two candidate drug compounds, both of which were virtually insoluble as free bases, with data points effectively lying on the baselines of the charts (18). On solubility grounds alone, Figure 2A shows a clear preference for the edisylate (ethanedisulfonate) salt, although the solubility of 1.7 mg/mL is not high in absolute terms. Much higher solubilities are exhibited by the salts in Figure 2B, up to 10 mg/mL for the three most soluble forms. A recent investigation of salts with the saccharate anion has identified solubility enhancements of 600, 40, and 3, respectively, for halperidol, mirtazepine, and quinine (19). However, it cannot be assumed that all salts will confer enhanced solubility, and salts can often have lower solubilities than the corresponding free bases. Salt screens are frequently carried out to identify the most suitable counter-ions, as will be described below.

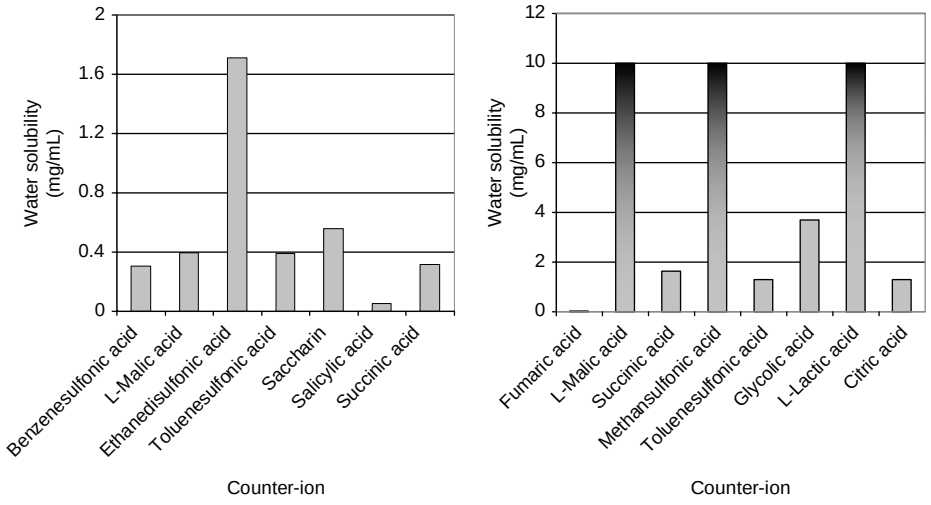

FIGURE 2 Examples of increased water solubility from salt formation: solubility data for salt forms of two virtually insoluble (off-scale) free bases (18).

In recent years, the development and use of co-crystals as alternative solid forms for APIs has received much attention in the scientific literature. Co-crystals are covered in more detail in Chapter 8. The idea of using co-crystals for pharmaceutical products appeared as a serious point of discussion in 2003–2004 (20), although the concept of combining multiple molecular entities in a single crystal has been around for very much longer (21). Terminology has also evolved with time, and what is today designated a "co-crystal" might in the past have been called an "adduct" or an "inclusion compound." There has been some debate about how a co-crystal should be defined. "A mixed crystal that contains two different molecules, made from reactants that are solids at ambient temperature" (22) is now widely accepted, although alternatives such as "a molecular recognition event between two different molecular species" (23) are also sometimes used. The first of these is intended to exclude salts, which contain ions rather than molecules, and solvates in which the second "reactant" is not usually a solid at room temperature. Both of these definitions are restricted to two molecular components or "reactants," which could be too narrow in that co-crystallized forms containing three or more molecular entities may also exist, either as isomorphic substitutions (24) or as three of more molecular entities within the unit cell. There can also be structural ambiguities between salts and co-crystals, as illustrated by the pyridinium benzoate salt structure and the strong hydrogen bond of pyridine–benzoic acid shown in Figure 3; in these cases the structural difference arising from a single proton transfer can give rise to marked differences in the physical properties of the crystalline product (25).

In the 1990s and the early 2000s, the commercial applications of co-crystals centered on two types of materials development; materials with non-linear optical properties, and host–guest complexes that may be used for purposes of separation

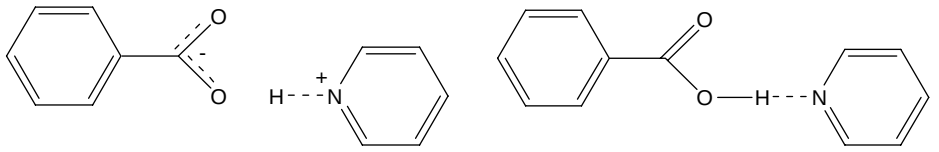

(**A**) (**B**)

FIGURE 3 Structural ambiguity between (**A**) a salt (proton transfer) and (**B**) a co-crystal (proton sharing). Transfer of a single proton can change the form and properties of the crystalline product (25).

or purification. Non-linear optical materials have been designed by combining ionic and hydrogen bonding, for example, in a number of phenol–pyridine co-crystalline structures (26) to form a crystal in a non-centrosymmetric space group. The lack of centrosymmetry accounts for the anisotropic optical properties of this and similar materials. Host–guest complexes usually involved the construction of hosts with channels, often including urea (27), which is well known for forming channel-like solid structures and also for its extensive application as a co-crystal former on account of its multiple hydrogen donor and acceptor sites.

For pharmaceuticals, the potential advantages of co-crystals include the enhancement of solubility and dissolution rate, but also the prospect of improving stability and other physical properties over a range of options that are far more extensive than what is available using salt formation. The co-crystal of caffeine and oxalic acid, unlike crystalline caffeine, is non-hygroscopic and resists hydration at all relative humidities (28), and a similar result was obtained with theophylline (29) where the 2:1 co-crystal with oxalic acid also resisted hydration at relative humidities up to 98%. Co-crystallization with dicarboxylic acids has been shown to increase the solubility and the dissolution rate of both itraconazole (20,30) and fluoxetine hydrochloride (Prozac) (31). Co-crystallization of the slowly dissolving drug carbamazepine with lactamide or glycolamide resulted in marked increases in dissolution rate; data for the glycolamide co-crystal are shown in Figure 4 (32). A co-crystal of a sodium channel blocker with glutaric acid showed considerable enhancement in blood plasma concentration in dogs (33), and a phosphodiesterase-IV inhibitor showed plasma levels in Rhesus monkeys a factor of 20 higher when the API was "complexed" with L-tartaric acid (34).

Despite the intense research and development efforts, no co-crystal form of a drug is known to be approaching the advanced stages of development, and the regulatory challenges associated with licensing and releasing a drug as a co-crystal remain to be fully explored. In the context of drug development timeframes, the interest in co-crystals has been relatively short lived, and it will probably be a few years yet before co-crystal products are available.

The development of amorphous APIs as drug products has also received much attention in recent years, largely driven by the question of bioavailability. Table 3 gives some examples of drugs that have been licensed in amorphous, or partially amorphous, forms in recent years, taken from their manufacturers' literature. Methods by which amorphous forms are prepared and stabilized will be briefly discussed in the section "Preparation and Stabilization of Amorphous Forms." In most of the cases in Table 3, limited bioavailability related to low

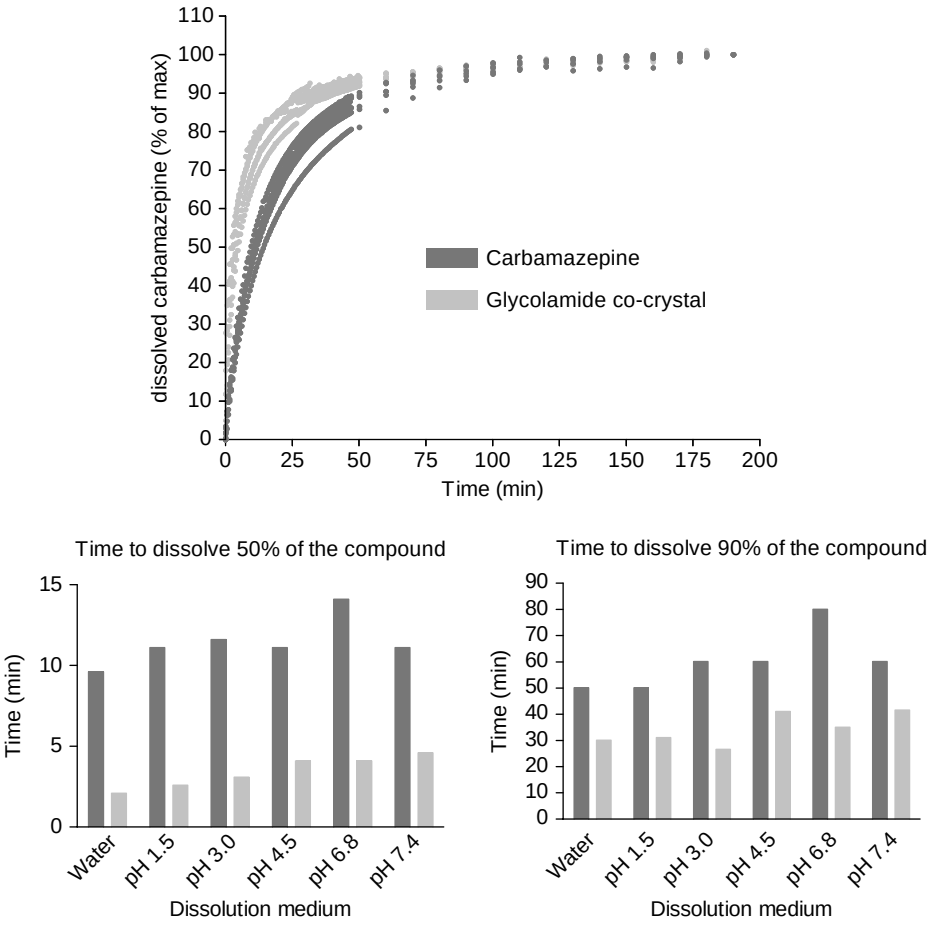

FIGURE 4 Dissolution rate data in water for the co-crystal of carbamazepine with glycolamide (32). Comparison is made with carbamazepine form III, the most stable polymorph at room temperature.

solubility and slow dissolution is the key driver to formulate the therapy using the amorphous form.

Figure 5 shows a series of instantaneous dissolution measurements for amorphous indomethocin and the crystalline forms, carried out over two-hour periods, at temperatures of 5, 25, and 45°C (2). These may be taken to represent the solubilities at each particular time instance, although the lack of equilibration time means that these measurements cannot necessarily be read as accurate solubility values. At 5°C, the solubility of the amorphous form is around four times that of the crystalline (γ-)form, with neither showing substantial variation over the two-hour period. At 25°C, the amount of amorphous material dissolved initially increases sharply to maximum at 15 minutes, which is presumably dissolution proceeding toward equilibrium over this time period. Over the following 35 minutes, however,

TABLE 3 Examples of Drug Products that Have Been Licensed in Amorphous, or Partially Amorphous, Forms in Recent Years

Compound (discoverer/manufacturer)	Year licensed	Comments
Lopinavir (Abbot) 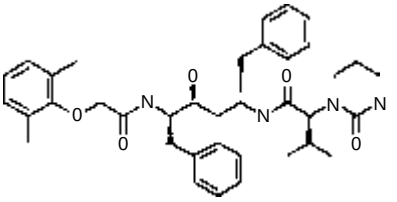	USA 2000 Europe 2001	Co-formulated with ritonavir as Kaletra to treat HIV/AIDS. Lopinavir exists as an amorphous form and 4 crystalline forms. The commercial material is a mixture of the amorphous form and Form I crystals.
Cefuroxime axetil (GSK) 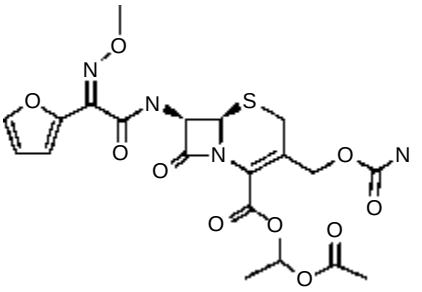	USA 1977	Second generation cephalosporin antibiotic, trade names Ceftin, Zinacef, Zinnat. Crystalline form is a mixture of two diastereomers. Amorphous form recently dispersed with HPMC 2910/ PVP K-30 to increase dissolution rate.
Zafirlukast (Astra-Zeneca) 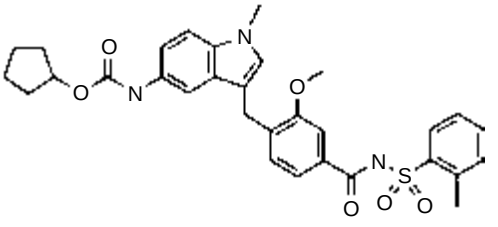	1999	Oral leukotriene receptor agonist for maintenance treatment of asthma, trade names Accolate, Accoleit, Vanticon. Forms A (amorphous), B (unstable crystal), X (stable crystal) discovered, also ethanol and methanol solvates. X has poor bioavailability, B is difficult to prepare reliably. A is used in formulations.

(*Continued*)

TABLE 3 Examples of Drug Products that Have Been Licensed in Amorphous, or Partially Amorphous, Forms in Recent Years (*Continued*)

Compound (discoverer/manufacturer)	Year licensed	Comments
Rosuvastatin calcium (Astra-Zeneca) 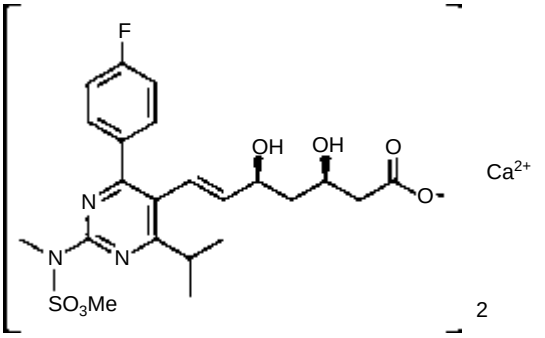	USA 2003 154 other countries 2004	High potency statin for reducing high blood cholesterol levels, trade name Crestor. Amorphous solid, slightly soluble in water (7.8 mg/mL @ 37°C).
Itraconazole (Janssen Pharmaceutica) 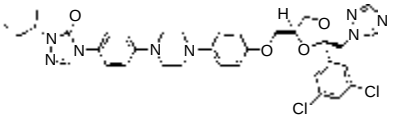	Europe 1987 USA 1992	Triazole antifungal agent, trade name Sporanox. Solid formulation consists of a dispersion of amorphous itraconazole, HPMC, and PEG coated on sugar spheres; these are filled into a capsule for oral administration.
Quinapril hydrochloride (Pfizer) 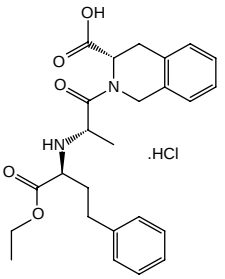	1989	ACE (angiotensin converting enzyme) inhibitor for treating hypertension and congestive heart failure, trade name Accupril. Amorphous powder, freely soluble in water and organic solvents.

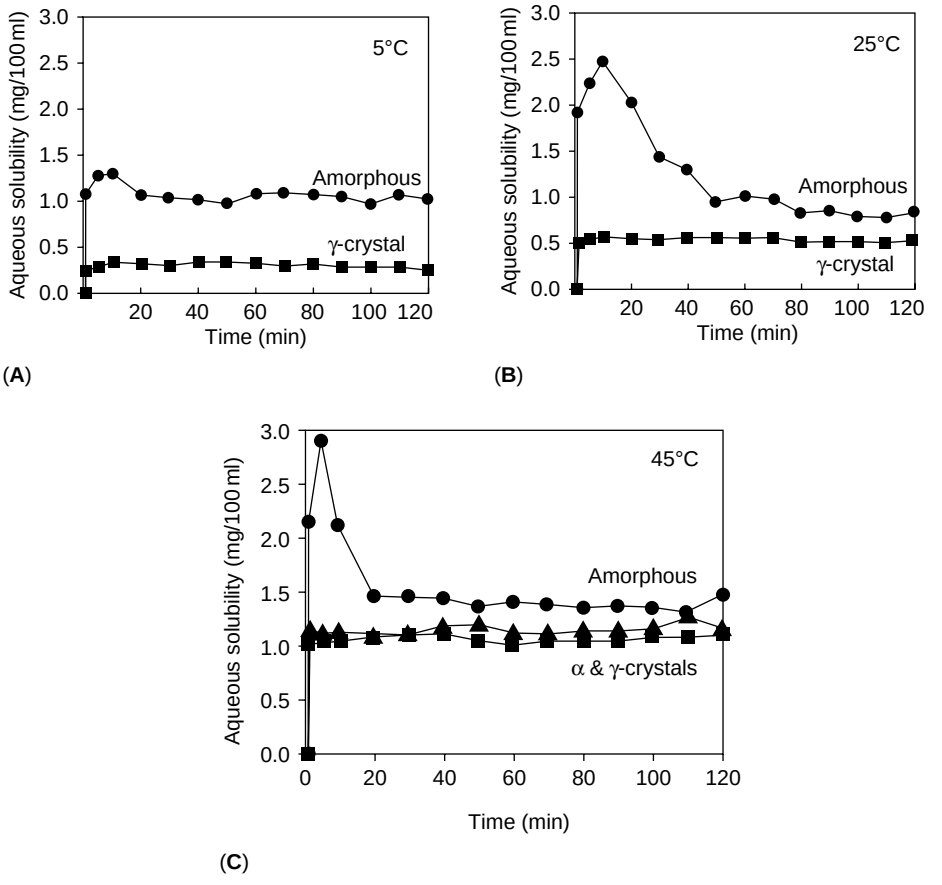

FIGURE 5 Aqueous dissolution of amorphous indomethacin over a two-hour period at different temperatures (2): (**A**) 5°C, (**B**) 25°C, and (**C**) 45°C.

the quantity dissolved decreases sharply, eventually to around a third of its maximum value and to a factor only 1.5 times that of the crystalline material. What is probably happening here is that crystalline material is separating from solution, and the observed solubility is therefore moving toward the solubility of the crystalline form, with the solution at equilibrium with the crystalline solid. The fact that the quantity dissolved remains higher for the amorphous material throughout the two-hour period probably indicates that the conversion is not complete over this time period, and in any case the solution containing the dissolved amorphous material will require time to come to equilibrium with the crystalline solid form by crystallizing out excess solute. At 45°C, these effects occur more rapidly, and at the end of the two-hour period measurements starting with the amorphous form show solubility similar to those starting with the crystalline forms.

These measurements highlight some of the difficulties that arise in working with amorphous forms, that derive from the fact that they are unstable and tend to

revert to crystalline forms over a period of time. The rate at which such changes occur is of critical importance, and methods developed for stabilizing and formulating amorphous drugs are usually designed to minimize and slow down such interconversions, both in storage and in use. A result such as that in Figure 5C, with interconversion over 20 minutes at 45°C, indicates that such reductions in solubility could occur in vivo (37°C) over the time scale of absorption of the drug, which could end up deposited in the digestive tract as a poorly soluble and slowly absorbed crystalline form.

OVERVIEW OF METHODS FOR PRODUCING SOLID FORMS

The ways in which the various solid forms above may be prepared will be outlined in the following sections in a method-based structure, whereby those methods employed most extensively will be described first and in most detail. The last 10 years or so has seen an explosion in the range and types of method used to prepare solid forms that has been fuelled by the burgeoning interest in polymorphism and solid form diversity and the consequent requirement to prepare and manufacture targeted solid forms consistently and reliably. The traditional crystallization methods have been developed by understanding and controlling their functions, and have been augmented by a number of innovative new techniques to improve both their form selectivity and the range of polymorphs and other solid forms that can be prepared (35).

For preparing crystalline forms, crystallization from solution is by far the commonest method used in the pharmaceutical industry today. Crystallization from melts is rarely employed, mainly because of the limitation of thermal stability of API compounds and the small scales of production. Pharmaceutical production is usually at relatively small scale, with processes carried out batchwise in multipurpose plants under conditions that are specific for a given product and manufacturing process. Furthermore, synthesized organic compounds are usually prepared in a solution, and crystallization is most commonly employed as the method by which solid material is recovered from the solution of the final synthesis step. Although the logistics and procedural details are different, the same underlying principles govern crystallization as a production method and its use in investigative work, including polymorph searching and single-crystal preparation for X-ray structure determination. Moreover, the production of a specific polymorph identified in such investigations may require the method by which it was obtained to be translated to a preparative or production environment, and this knowledge transfer will be greatly assisted by a sound understanding of the principles that underlie the method by which it was obtained.

As a general principle, slow crystallization and transformation processes operated under mild conditions with moderate driving forces are more likely to produce stable crystalline polymorphs, whereas rapid processes employing dynamic and extreme conditions with large driving forces will produce metastable and unstable crystalline forms and amorphous solids. This principle is illustrated in Figure 6 for a selection of preparation methods, compiled by the author based on a recent similar idea (35,36). The relationship between the speed at which a process operates and the outcome is well represented by the antisolvent mediated processes, using bulk addition and diffusion. These operate on the same principle, but with very different rates of antisolvent addition. Diffusion is a method that introduces

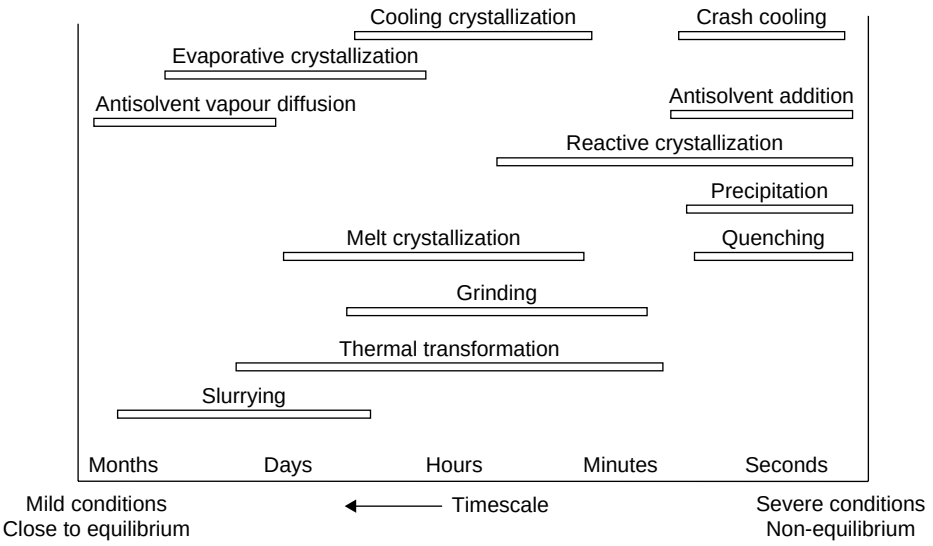

FIGURE 6 A selection of methods for producing crystalline forms. Longer running procedures favor stable polymorphs, whereas more rapid methods are more likely to yield less stable forms (35,36).

the antisolvent slowly, that is used in the slow growth of single crystals, whereas bulk antisolvent addition will cause a solute to crash out of solution, and is often used where other milder crystallization methods fail.

CRYSTALLIZATION FROM SOLUTION

As mentioned above, crystallization from solution is by far the commonest crystallization method used as a process for product recovery in the pharmaceutical industry. In this context, it simultaneously fulfills two essential functions:

1. Purification of the high-value pharmaceutical product, and separation from reaction by-products.
2. Consolidation of the product into a specified crystalline form with consistent and well-characterized physical properties.

Ideally, crystallization will be carried out starting with the solution from the final reaction step of product preparation or manufacture. Often, however, isolation of crude product is carried out using a method that maximizes yield but does not crystallize well, which does not purify effectively or give rise to a good crystalline form. In these cases, recrystallization is often employed to carry out the purification and consolidation functions.

Crystallization to produce specific polymorphs follows the same set of principles as those used in designing processes to manufacture crystalline products, and a basic understanding of these principles can greatly aid the design of a crystallization screen for polymorphs or of a process by which a particular polymorph,

stable or metastable, can be prepared consistently. Some of the general principles, applying to all solution crystallizations, will be outlined in the section "Cooling Crystallization," for which they are easiest to formulate and understand. In the following sections, we will show how they can be extended to alternative methods of crystallization from solution.

Although following the same principles, crystallizations carried out for investigative purposes such as polymorph screening are subject to fewer constraints and limitations than processes in manufacture, although these limitations may subsequently come to bear if the process has to be adapted for production of the identified polymorph. For example, investigative crystallizations do not need high yields, because small quantities of a polymorph product can usually be isolated and identified. Also, it is possible to employ a diversity of methods in investigative work that are not scaleable and adaptable to larger scale, or for which such adaptations may be expensive. Conversely, there are also methods that are operated much more conveniently at larger scale, such as processes involving supercritical fluids.

Cooling Crystallization

Cooling crystallization from solution is usually the method of first choice, both for investigative crystallization in the laboratory and for manufacture at large scale. Its advantages are that it is easy to carry out and reproduce, it is generally well understood, and it may be reasonably scaled up in most cases. In practice, there are often limitations to cooling crystallization at large scale, in particular, the preference for natural cooling limits the rate at which cooling can be applied. In the laboratory, however, cooling rates can be set flexibly and accurately, depending on the purpose for which the crystallization is carried out and the product properties that are required.

There are a number of excellent texts that cover the principles of cooling crystallization comprehensively (37–39), and they are only outlined briefly here to serve the matter in hand, viz. the use of cooling crystallization to prepare polymorphs and other variable solid forms. Nevertheless, a sound understanding of the principles of crystallization is essential if solid-form searching is to be designed in an efficient and comprehensive manner. For a given crystallizing compound and solvent, the first requirement is knowledge of the solubility curve. This is best illustrated by reference to Figure 7, which shows the aqueous solubilities of some common inorganic salts as a function of temperature, from readily available data (40). $CuSO_4$ shows a steady increase in solubility with temperature, and may be crystallized by cooling the solution to give blue crystals of the stable pentahydrate $CuSO_4 \cdot 5H_2O$. Examination of the curve reveals that cooling a solution from 90°C to 10°C could result in recovery of 64% of the dissolved solid, if the crystallization proceeds to equilibrium. On the other hand, NaCl shows only a very slight increase in solubility with temperature, and cooling from 90°C to 10°C could produce only a maximum of 5% of the dissolved solute as solid. Cooling crystallization from water is unsuitable for NaCl, and industrial processes for its preparation rely on other methods, principally evaporative crystallization. The solubility curve for Na_2SO_4 shows a discontinuity at 32°C, which corresponds to the transition of the most stable solid phase at equilibrium with the solution from the decahydrate $Na_2SO_4 \cdot 10H_2O$ to the anhydrous salt. Although the most stable phase at the crystallization temperature will be favored thermodynamically under these conditions, it will not necessarily be obtained for the reasons discussed below.

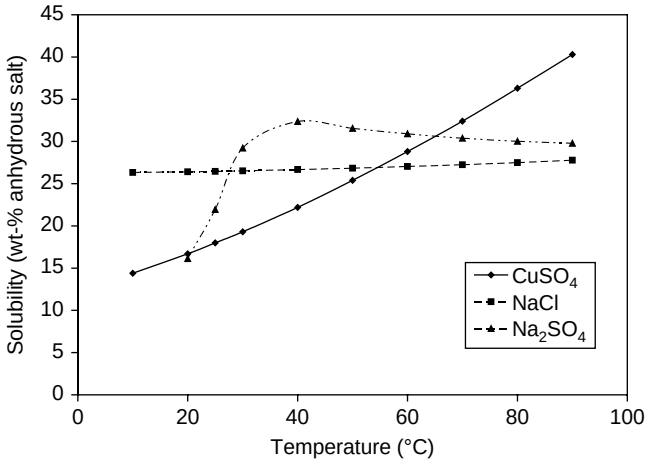

FIGURE 7 Solubility curves for the dissolution of simple inorganic salts in water (40). $CuSO_4$ may be crystallized from water by cooling, whereas NaCl may not. Na_2SO_4 exhibits a change in the most stable solid phase at 32°C, which is manifested as a discontinuity in the solubility curve.

Extensive solubility data is not usually available when approaching the crystallization of a new compound in form screening, but an indication as to whether cooling crystallization is a feasible option can be obtained from two data points corresponding to the solubilities at low and high temperature for the solvents under consideration. A compound that shows a marked solubility increase at the higher temperature may, in principle, be crystallized by cooling. For form screening purposes, the crystallization yield does not have to be high, and cooling crystallization may be employed provided that a reasonable supersaturation level, say 15% to 20%, can be achieved by cooling the solution. For production, yields will normally need to be higher than this, and in such cases cooling will have to be supplemented by other means of removing solid from solution, such as evaporation or an antisolvent.

The solubility curve is fixed by the thermodynamic relationship between the solid and the solution, and represents the condition that the chemical potentials of the dissolved solute and the solid at equilibrium with the solution are equal. The Gibbs Phase Rule stipulates that, for any given temperature, there will be a unique and determined concentration corresponding to equilibrium. The other component of the route map for a cooling crystallization is the metastable zone width (MZW), illustrated in Figure 8. An initially undersaturated solution at point A is cooled at a constant rate of temperature decrease, following the horizontal arrow. On crossing the solubility line at B the solution becomes supersaturated, but no solid separates at this point. At C, crystal nucleation occurs. Substantial crystallization occurs beyond this point by both the growth of the nuclei formed at C and by further nucleation and growth, and the conditions return toward equilibrium on the solubility line at D. Taking a range of temperature–concentration starting points A, represented as points below and to the right of the solubility curve in Figure 8, the supersolubility curve represents the locus of the points at which nucleation first

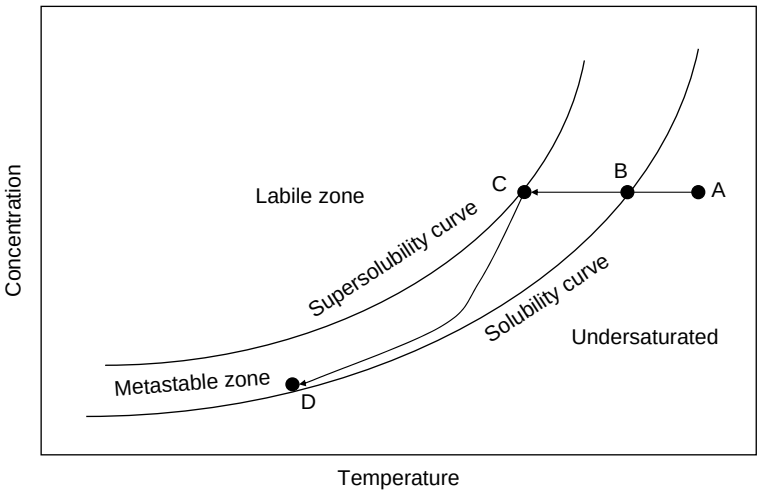

FIGURE 8 The metastable zone in cooling crystallization. Cooling a solution from A induces supersaturation at B, and nucleation at C. The region BC in which the solution is supersaturated but no nucleation occurs is the metastable zone. Beyond the nucleation point, crystal growth and further nucleation occurs until equilibrium is attained at D.

occurs for a given set of crystallization conditions, including cooling rate. The width of the metastable zone (MZW), represented by BC, is a measure of the difficulty in crystallizing a given substance due to the kinetics of inducing nucleation.

Unlike the solubility curve, the supersolubility curve and MZW are dependent on the conditions employed for crystallization, in particular, the cooling rate. Because crystal nucleation has a kinetic component associated with the ordering of molecular clusters into structured crystal nuclei, higher rates of cooling will give rise to wider metastable zones. MZW can vary from 2 to 5K for simple inorganic salts to tens of degrees for complex organic molecules. The MZW represents the level of supersaturation driving force and departure from equilibrium at which nucleation and crystallization take place, and this can substantially affect polymorph selectivity. Operation close to equilibrium with narrow metastable zones will favor the formation of relatively stable solid forms, because stable crystalline solids are generally less labile than unstable and amorphous forms, and the lower driving forces and more extended timescales associated with working close to equilibrium generally favor their formation.

A further factor that can affect polymorph selectivity in cooling crystallization is enantiotropy, and this is illustrated in Figure 9 for the simple case of a dimorphic system in which the transition temperature T_t lies within the operating temperature range of the crystallization (41). Form II is stable below T_t, form I above T_t. Cooling from point A, the metastable zone of form I is traversed and crystallization is nucleated while the solution remains undersaturated with respect to form II. Point B represents the limit of this condition; the nucleation of form I occurs at the saturation point of form II. At C, the solution first becomes supersaturated with respect to form I, but in this case saturation with respect to form II occurs before the form I

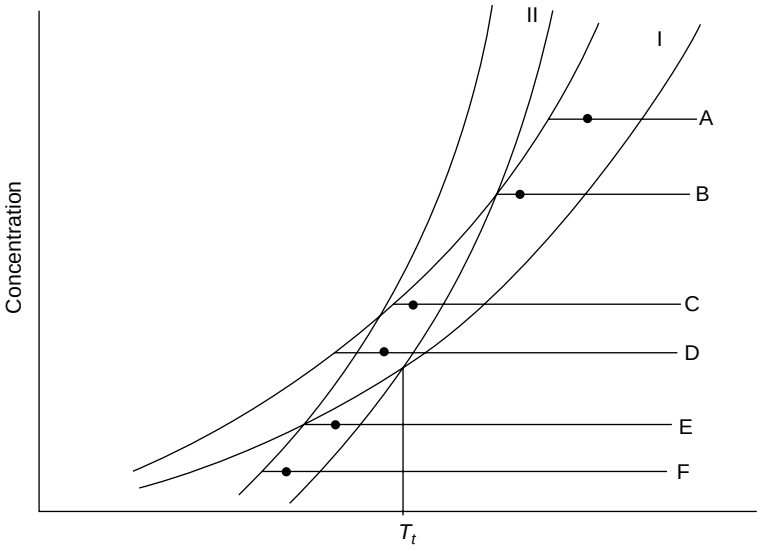

FIGURE 9 Solubility and metastable zones for the cooling crystallization of a dimorphic compound with a transition temperature within the crystallization region. Selecting the start and end temperatures A–F will determine the crystal forms obtained. *Source*: Adapted from Ref. (41). *Abbreviation*: T_t, transition temperature.

metastable zone limit is reached. Thus, crystallization of form I will occur from a solution that is also supersaturated with respect to form II, and there is the possibility of cross-seeding and producing a mixture of the two forms. At D, a mixture of forms is even more likely. Points E and F represent the converse of B and A, respectively, and indicate the conditions under which form II may be prepared. Figure 9 illustrates the importance of varying the crystallization conditions, in this case the temperature, in any search for polymorphs. Given that such searches are usually conducted to discover what forms can be prepared, the existence of characteristics such as enantiotropy will not be known at the time such searches are undertaken.

Figure 10 illustrates a situation where further unstable polymorphs exist along with the enantiotropic dimorphic relationship of Figure 9, and how these forms may be accessed by using extreme crystallization conditions, in this case cooling rate (41). Under slow cooling, forms III and IV will never occur because the solute will crystallize as forms I and/or II depending on the temperature conditions. Increasing the cooling rate will "stretch" the metastable zone to encompass a larger area of the concentration–temperature continuum. Unstable forms will have high solubilities, and this extension of the metastable zone, as shown in Figure 10, will eventually lead to the conditions for their crystallization falling within the metastable zones of the more stable forms. Under these conditions, the unstable forms are more likely to form because they are generally more labile than the more stable forms, as is reflected in their relatively narrow metastable zones within this area of the concentration–temperature plane.

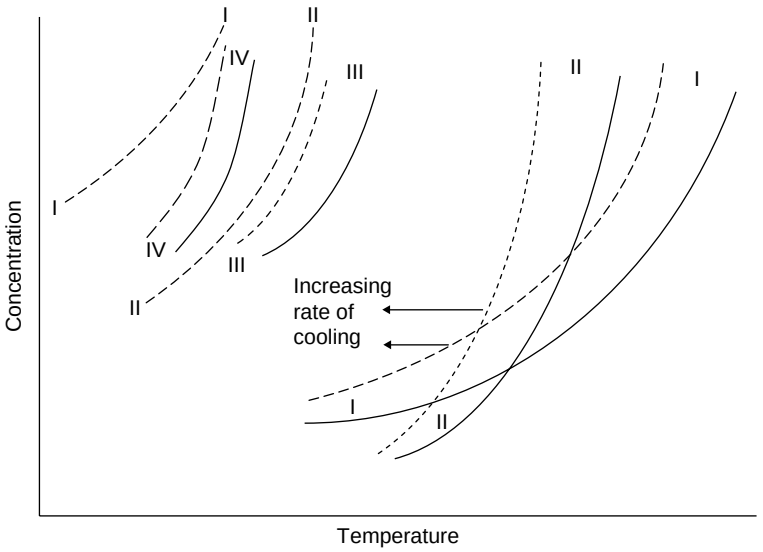

FIGURE 10 Crystallizing unstable polymorphs by crash-cooling. Increasing the rate of cooling broadens the metastable zones of the stable forms I and II, as shown by the dashed curves. This may eventually span the crystallization regions of unstable forms III and IV. Under these conditions, the unstable forms are more likely to occur because of their lability. *Source*: Adapted from Ref. (41).

Figures 9 and 10 demonstrate the importance of diversity in any polymorph screening program. Within the confines of a single crystallization method, variations in the conditions employed—temperature and cooling rate—can lead to different outcomes. Crystallizing under conditions close to equilibrium generally results in the more stable polymorphs; such conditions are usually "mild" in that they employ moderate driving forces sustained over longer periods. More "extreme" conditions induce crystallization further from equilibrium under large driving forces and generally favor unstable polymorphs and amorphous forms. Such extreme conditions are inherently unstable and often cannot be sustained over extended periods. The less labile and more stable polymorphs are thus denied the time scales of structural organization that they require, which works in favor of the less stable forms.

Effects of Solvent

Moderate solubilities with a steep increase with increasing temperature are the optimum conditions for cooling crystallization, with solubilities typically in the range 5 to 200 mg/mL at room temperature. If the solubility exceeds 200 mg/mL, the viscosity of the solution is likely to be high, and a glassy amorphous product may be obtained in preference to crystals. A useful preliminary test can be performed on 25 to 50 mg of sample, adding a few (5–10) drops of solvent: if the solid completely dissolves the solubility is probably too high. Also, highly viscous solvents are not usually conducive to efficient crystallization. Solvents with very low vapor pressures, such as DMSO or glycerol, are not good for process applications because of the difficulty of removing residues from the isolated products.

Table 4 lists solvents commonly used in the crystallization of pharmaceuticals, in decreasing order of their boiling points. Comprehensive polymorph screening will involve a larger and wider range of solvents that are not necessarily safe and suitable for use in processing but rather give the maximum range and diversity of interactions and effects on the solute that is being crystallized. Data from a search of the CCDC database (in March 2008) of their frequency of occurrence is also given, but this information must be treated with some caution. Although the searches were carried out using the common synonyms of the solvents (e.g., 2-butanone/methyl ethyl ketone/MEK, chloroform/trichloromethane), the "hits" include structures in which the "solvent" moiety forms part of the crystal structure, and in these cases may or may not be considered part of the solvent. For pyridine and cyclohexane, these structures or their derivatives occur very frequently in the crystal structures prepared, and their categorization as a "solvent" does not seem appropriate. THF (tetrahydrofuran) also occurs frequently in this way, and most of the solvents in Table 4 participate in at least a few of the structures reported. The distinction between this type of structure and a solvate, where the solvent molecule forms part of the crystal structure but is deemed to constitute a distinct and separate molecular species, can be a fine one. Also, Table 4 has been compiled using all entries in the database, many of which are organometallic, and how representative this selection is of pharmaceutical products is difficult to judge. Searching with exclusions does not seem to be justified, as organometallics arise quite often as therapeutic compounds, for example, as cytotoxic compounds used in cancer chemotherapy.

The need to utilize a diversity of solvents in polymorph and other solid-form screening was recognized early on (42), and the selection of suitable lists of solvents has now become a matter of considerable scientific sophistication. In the 1990s, the selection of suitable solvents was approached predictively using group contribution methods such as UNIFAC (43), and this has now evolved into more sophisticated packages (44) such as the NRTL–Segment Activity Coefficient (SAC) model that is now implemented in commercially available software (45). Mixtures of solvents are commonly employed to modify and optimize the solvent properties, including solute solubility, polarity, and hydrogen-bonding donor and acceptor properties.

Several effects on crystallization and polymorph selection can be mediated by the solvent selection, the simplest of which is an effect of temperature. The temperature range in which a solvent can be used is limited by its boiling point (Table 4), and by the solubility profile of the solute. In enantiotropic systems, the polymorph that is crystallized may depend on the crystallization temperature by the principles discussed in the section "Cooling Crystallization" and Figure 9. McCrone, writing in 1957 (9), describes the use of high-boiling solvents such as benzyl alcohol and nitrobenzene for the recrystallization of metastable forms on a hot stage. For the API buspirone hydrochloride, a higher or a lower melting form resulted according to whether the crystallization was carried out above or below 95°C (46). Recrystallization from xylene (boiling point 137–140°C) converted the lower boiling form to the higher boiling form. This can be explained by enantiotropy, whereby the lower melting form becomes the more stable below the transition temperature, but crystallization is strongly influenced by the kinetics of nucleation and crystal growth and does not always give rise to the most stable form.

The freeze-crystallization of mannitol was found to be influenced by both the initial mannitol concentration and by the rate of freezing (47). In the range of 2.5–15%, the δ-polymorph was favored by higher concentrations, whereas the

TABLE 4 Common Crystallization Solvents and Their Frequency of Occurrence in the CCDC Database, in Order of Decreasing Boiling Point

Solvent	Boiling point (°C)	ICH class (17)	Occurrences in the CCDC database			
			As solvents		As solvates	
			Occurrences	Percentage of total	Occurrences	Percentage of total
Dimethyl sulfoxide (DMSO)	189	3	737	0.34	73	0.07
N,N-dimethylformamide (DMF)	153	2	3079	1.41	1524	1.52
Acetic acid	118	3	1821	0.83	204	0.20
Pyridine	116	2	N/A[a]			
Toluene	111	2	11482	5.26	4576	4.57
1,4-Dioxane	102	2	1188	0.54	341	0.34
Water	100	–	11350	5.20	41283[b]	41.20
1-Propanol	97	3	192	0.09	31	0.03
2-Propanol	83	3	1406	0.64	220	0.22
Acetonitrile	82	2	14447	6.62	5769	5.76
Cyclohexane	81	2	N/A[a]			
2-Butanone	80	3	169	0.08	13	0.01
Benzene	80	1	19784	9.07	4596	4.59
Ethanol	78	3	30462	13.96	8380	8.36
Ethyl acetate	77	3	5346	2.45	438	0.44
n-Hexane	69	2	26305	12.05	1903	1.90
Methanol	65	2	17881	8.19	5916	5.90
Tetrahydrofuran (THF)	65	2	12359	5.66	4115	4.11
Chloroform	62	2	9328	4.27	3892	3.88
Acetone	57	3	8127	3.72	2671	2.67
Dichloromethane	40	2	29696	13.61	11909	11.89
Diethyl ether	35	3	12611	5.78	2292	2.29

[a]Data was not extractable from the CCDC because a large proportion of structures contained moieties of the substance within the crystal structure. It was not possible to quantify the proportion of cases in which the substance constituted a solvent, rather than a reactant in synthesizing the compound crystallized.
[b]The search term used was "hydrate." There are many examples of hydrates prepared in non-aqueous solvents, or in solvent mixtures containing small amounts of water. Hence, the number of hydrates exceeds those that cite water as a solvent.

β-polymorph was favored at lower concentrations. At constant mannitol concentration (10%), the α-polymorph was favored by a slow freezing rate, whereas a fast freezing rate favored the δ-form. Also, for the crystallization of stearic acid from *n*-hexane (48), both the cooling rate and the initial concentration of stearic acid influenced the proportion of polymorphs A, B, C, and E that could be isolated.

The solvent can also determine polymorph selectivity via chemical intervention in the formation of the crystalline solid at the point of nucleation. Different polarities (49) and hydrogen-bonding characteristics (50) of the solvent are believed to promote or inhibit the cluster precursors of particular forms in supersaturated

solutions. For example, the crystallization of diflunisal from polar solvents gave polymorph form III, whereas the alternative forms I and IV were obtained from apolar solvents (51). Moricizine hydrochloride (52) recrystallized as form I from ethanol, acetone, and acetonitrile, whereas the alternative form II was obtained from dichloromethane, either alone or as a mixture with ethyl acetate.

The effects of the solvent hydrogen-bonding characteristics on polymorph selectivity via the processes of molecular self-assembly that precede crystal nucleation has been demonstrated for the crystallization of 2,6-dihydroxybenzoic acid (50,53). This compound can crystallize as two polymorphic forms shown in Figure 11. The monoclinic form I is based on centrosymmetric carboxylic acid dimers paired via $R_2^2(8)$ ring structures, whereas the more stable form II is non-centrosymmetric and made up of a catemer motif formed by intra- and intermolecular interactions involving both the carboxylic acid functions and the phenolic hydroxyl groups in the *o*-positions. Form I nucleates from solutions in toluene, where there is a preferential assembly of dimers. Form II was prepared from solutions in chloroform, in which the phenolic catemer motifs were strongly solvated. A further example of hydrogen bonding with the solvent affecting polymorph selectivity is provided by 2-amino-4-nitrophenol (54). This compound has a wealth of donor and acceptor sites for hydrogen bonding, and structure predictions showed up to 250 possible crystal structures. The choice of solvent in this case can either promote or deactivate particular interactions to influence the crystal product, as illustrated in Figure 12. Nitromethane tends to solvate the amine functions, which directs the packing toward nitro–hydroxy interactions. Similarly, methanol will solvate the hydroxy groups, favoring nitro–amine bonded structures. Toluene tended to promote hydrogen-bonding interactions non-specifically, giving rise to both NH_2–NO_2 dimers and chains made up of OH–NO_2 linkages.

The interference of solvents in hydrogen-bonding interactions as above can also affect crystal habit, and this has led to the use of specific solvents or solvent types as growth and habit modifiers. An example is in the crystallization of acetanilide (55). Acetanilide tends to crystallize as needles, a pattern of behavior common among simple secondary amides where a hydrogen-bonded molecular chain in a *trans*-conformation, with the carbonyl acceptor and –NH donor *anti*- to each other, forms along the axis of the needle. Solvents that do not interact with the formation of these chains, such as benzene and tetrachloromethane, give rise to needles. Proton donors (such as methanol) and acceptors (such as acetone) compete for the hydrogen-bonding sites and thus slow the crystal growth along this axis. Crystallization from these solvents gives a rod-like crystal shape in which the aspect ratio is less extreme. Impurities that have similar molecular structures to the crystallizing substance can have similar habit-modifying effects by blocking or otherwise interfering with crystal growth in a particular direction. Traces of benzoic acid have been shown to inhibit the growth of benzamide crystals in the c-direction, by bonding into the chain of $R_2^2(8)$ amide dimers and exerting a repulsion on the next incoming benzamide growth unit (56). In a similar way, "impurities" of 2- and 4-toluamide retard growth respectively in the a- and b-directions by interfering with the stacking of the growth units.

Seeded Crystallization

Seeding is a method that is commonly used as a control measure in crystallization processes, usually to improve reproducibility and to obtain better quality crystals

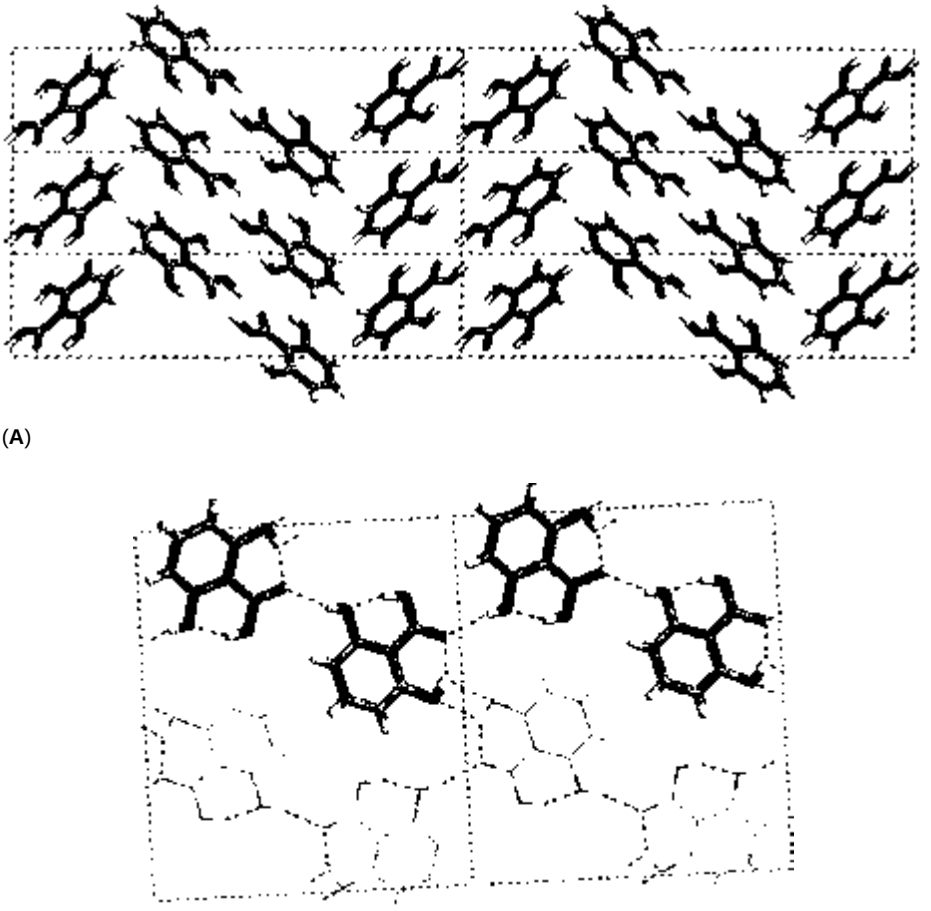

FIGURE 11 Polymorphs of 2,6-dihydroxybenzoic acid: **(A)** form I, monoclinic, formed from centrosymmetric carboxylic acid dimers; **(B)** form II, catemer motif involving carboxylic acid and *o*-hydroxy interactions. Crystallization from solution is influenced by the hydrogen-bonding interactions of the solvent, which can exert polymorphic selectivity by promoting or inhibiting specific solid-state bonding patterns (50). Reproduced by permission of the Royal Society of Chemistry.

and a more favorable particle size distribution. Essentially, nucleation is induced by the introduction of a small quantity of product crystals at some pre-determined point within the metastable zone. The principle and effect of seeding in this respect is illustrated for a cooling crystallization in Figure 13. Introduction of seeds at point B enables crystal growth to start at moderate supersaturation levels, and prevents the creation of very extensive and uncontrolled nucleation at the higher supersaturation of point C. However, this also illustrates the importance of introducing the seed material at the right point in the cooling profile. If the seeds are added too

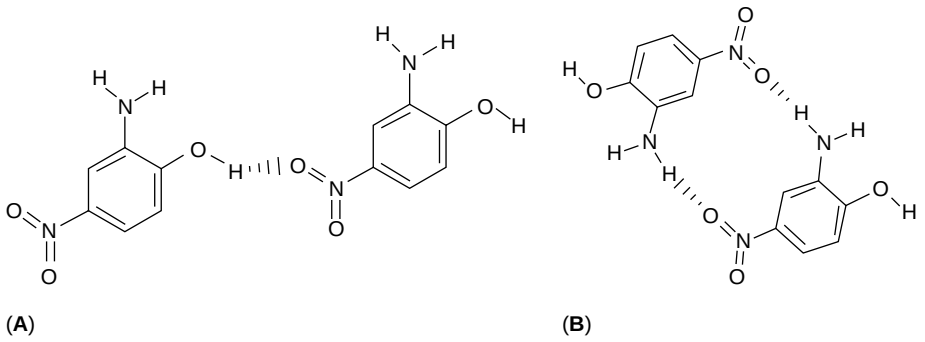

FIGURE 12 2-Amino-4-nitrophenol, a polyfunctional molecule with many possible hydrogen-bonding interactions between OH, NH_2, and NO_2 groups: (**A**) OH–NO_2 interactions, favored in nitromethane; (**B**) H_2N–NO_2 interactions, favored in methanol. Solvents can direct polymorphic selectivity by interacting with and "switching off" particular groups or bond types (54). Reproduced by permission of the PCCP Owner Societies.

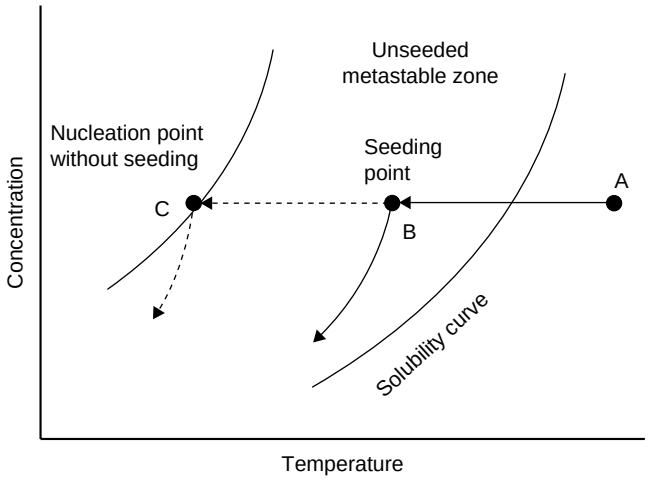

FIGURE 13 Seeding as a means of narrowing the metastable zone. Seed material provides nuclei to enable crystal growth at more moderate supersaturation levels.

early before the solution is supersaturated they will dissolve. If they are introduced too late when point C has already been attained, their effects will be much diminished. A recent investigation (57) recommends that, in general, seeds should optimally be added at a point of supersaturation 30–40% of the unseeded metastable zone width.

Recent investigations of seeding have focused entirely on the effects on the product size distributions. Seeding is effective if sufficient material is added to

prevent random nucleation, and its success is indicated by a unimodal size distribution (58,59). If insufficient seed is added, a bimodal distribution is obtained, because part of the product derives from the growth of seeds and the remainder arises as smaller particles from random nucleation and the growth of these nuclei. Conventionally, the surface area of the seeds is believed the critical parameter in determining the effectiveness of seeding (60), but some investigations contradict (58) this in showing that seeds above a certain critical size are more effective. It is also common practice to wash seed material with a slightly undersaturated solution of the substance being crystallized, which both dissolves out fine material and activates the surfaces by removing adsorbed impurities and other passivating effects.

In crystallizing polymorphic substances, seeding can also influence the solid form obtained by templating a particular polymorph at the expense of others. Because the seed nucleates the crystallization into its own crystalline form, with crystal growth as the dominant mechanism, it should be possible, in principle, to direct the crystallization to the required product by a judicious choice of seed material. In practice, this works on some occasions but not on others, and there are many cases where seeding with one polymorph leads to crystallization that gives an alternative form as the dominant product. This is because seeding is never perfect in that it can completely replace the nucleation step, and nucleation of other polymorphs can occur as in an unseeded process. Also, solvent-mediated transformation (see the section "Slurrying") is a very common mechanism by which less stable forms transform to more stable ones, and a crystallizing solution is a very effective medium for such transformations. Seeding with an unstable polymorph can thus give rise to a more stable product form at the point of isolation.

Seeding also underlies cases of "disappearing polymorphs" (10), whereby the crystallization of a new form in a process, either serendipitously or by design, has effectively prevented the form previously obtained from being produced again in the same equipment and process. Usually, the new form is more stable than the form previously obtained, and the reason postulated for its repeated formation is that plant and equipment remains contaminated with small quantities of seed of the new form that cannot be removed by cleaning procedures. There are also reports of different forms occurring at different laboratories and locations using nominally identical processes and procedures. The credibility of these seeding theories depends on the fact that most crystal nucleation is believed to occur heterogeneously, which is supported by the observations that crystallizations carried out in clean environments, such as sterile pharmaceutical areas, are often reluctant to nucleate. The presence of small traces of dirt and impurities are therefore believed to be important in initiating crystallizations, and the presence of residual material from previous batches may well exert a significant effect on crystallization and form selectivity.

The application of seeding to polymorph control also presupposes that a small quantity of seed material is available as a starting point at the beginning of the development. This is often obtainable from a set of polymorph screening experiments, but if these have been carried out at very small scale (~μg), there may have to be two or three scale-up stages before gram quantities of material can be prepared. Seed crystals generally have to be of good quality in terms of their size, shape, and morphological integrity. Hence, the preparation of suitable seed material is very often at a premium, and can be a major area of difficulty.

The principles of seeding also underlie the preparation of single crystals by growing a small, well-formed crystal from a moderately supersaturated solution.

Here, a relatively low supersaturation level is generated slowly, to maximize the growth of the crystal and minimize the probability of nucleation occurring. Nucleation not only takes away the supersaturation from the solution itself, but the nuclei generated provide competing growth sites, and a growth experiment in which significant nucleation has occurred will very often have to be discarded and started again.

Evaporative Crystallization

Evaporative crystallization is used in bulk chemicals production in cases where the temperature dependence of solubility renders cooling crystallization non-viable, the classical example being sodium chloride (Fig. 7). The evaporation of brines in shallow ponds has been practiced in arid areas for thousands of years as a means of recovering salts (37). In temperate climates, energy costs can be a limiting factor in the production of bulk commodities (61). Evaporative crystallization is also used to isolate sucrose from cane syrups (62).

Evaporative crystallization can be studied and understood in terms of the metastable zone, as shown in Figure 14, for a case where it would be favored because of a relatively flat solubility curve. Isothermal evaporation, which reduces volume and increases concentration, reaches the nucleation point C via the vertical trajectory BC. In this case, cooling induces only low levels of supersaturation, giving rise to the wide metastable zone AC and a small yield of solid. In reducing the volume, evaporative crystallization also increases the solid yield by reducing the amount of saturated solution that remains at the isolation temperature. In pharmaceutical applications, evaporation is often combined with cooling crystallization to increase product yields, usually using partial vacuum to induce evaporation. Most volatile solvents are recovered in operational applications, partly for reasons of economy but also for environmental reasons. The option of evaporation may influence solvent choice in such operations.

Evaporation is used extensively in polymorph screening and searching, often as a default option for recovering solids from experiments where cooling or other

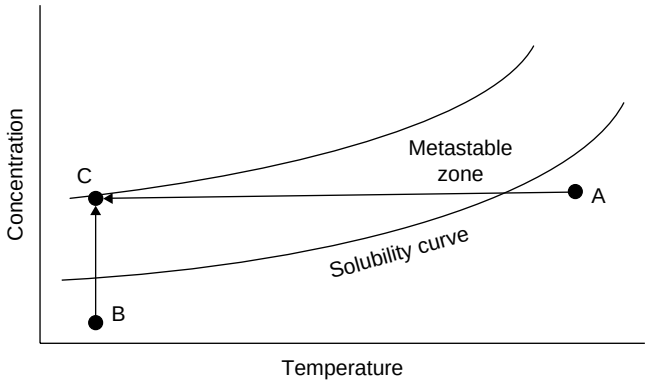

FIGURE 14 Evaporative crystallization and the metastable zone. Isothermal evaporation at point B increases concentration to the nucleation point C. The relatively flat solubility curve gives small driving forces on cooling, requiring a large degree of undercooling.

methods of inducing crystallization do not work. However, a comprehensive and well-designed polymorph screen will usually include evaporative crystallization as a designed-in option, as part of its diversity. It can sometimes be difficult to eliminate evaporation from experiments investigating other crystallization methods, particularly when working at very small scale in well-plates where very high levels of seal integrity would be required to eliminate it, particularly when working with volatile solvents. It is common to evaporate residual solutions to dryness even in cases where solids have been crystallized by other methods such as cooling, and have been isolated from the crystallizing solutions by filtration or centrifugation. Extra information, and in some cases even new polymorphs and other solid forms, can often be gleaned from analysis of the solid recovered from such evaporations.

Antisolvent Crystallization

In antisolvent crystallization, supersaturation is generated by adding a second liquid to a solution of the substance to be crystallized, which is miscible with the solvent and in which the crystallized substance is insoluble or sparingly soluble. The solid is less soluble in the mixture than in the original solvent, and therefore comes out of solution. Antisolvent crystallization is used extensively today in pharmaceutical developments and perhaps less extensively in other fine chemicals manufacturing. It is very rare in commodity chemicals processing, where its closest equivalent is in "salting out" (37), whereby salt addition is used to induce crystallization by reducing solvent activity.

Antisolvent crystallization in the pharmaceuticals context has been investigated fairly extensively in recent years, but has received very little coverage to date in conventional texts on industrial crystallization (37–39). As such, there has been very little discussion of its dynamics in terms of solubility curves and metastable zones. We suggest the representation in Figure 15 as a means of understanding

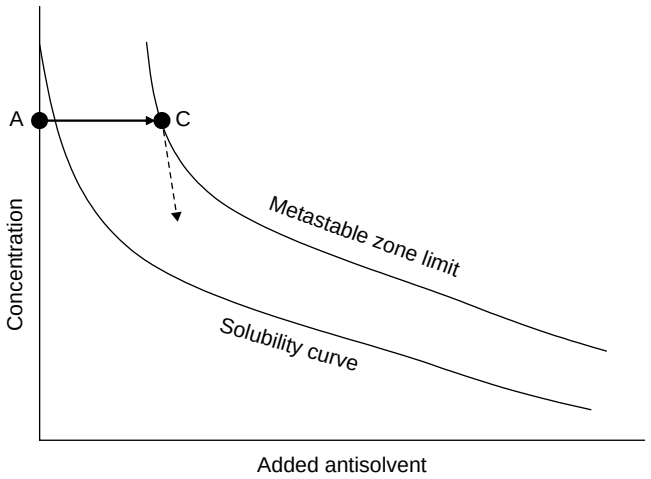

FIGURE 15 Antisolvent crystallization and the metastable zone, in a representation analogous to Figure 8. Here, solubility decreases with antisolvent addition, but a metastable zone is also created, and its width will depend primarily on the antisolvent addition rate.

these processes and comparing them with other modes of crystallization. For an isothermal addition of antisolvent, the solubility will decrease, although antisolvent addition will also increase the volume of the (mixed) solvent, and quantitative work needs to take this into account. However, the performance of antisolvent crystallization will also depend markedly on the rate at which the antisolvent is added, which is reflected in the width of the metastable zone. For fast antisolvent additions, separation of solid is usually instantaneous, and under these conditions the metastable zone width will often not be measurable. This is the phenomenon of "crashing out" that is commonly used to obtain solid products on a first pass from the final stages of synthesis. Material that is precipitated in this way may be crystalline, but the crystal quality of the product particles will be poor, consisting of agglomerated small particles with a large surface area. Substances that are crashed out of solution in this way are often recrystallized using more conventional and moderate crystallization methods in order to purify and consolidate the solid form of the product.

Figure 6 shows that antisolvent crystallization can be carried out over widely ranging time scales by methods that promote greater or lesser degrees of dis-equilibrium in the crystallizing mixture. Very slow addition of antisolvent will give rise to very gradual supersaturation, and crystallizations operated in this way will exhibit narrow metastable zones. Diffusion of an antisolvent into a solution is used extensively in the preparation of single crystals for X-ray diffraction analysis, where low supersaturation levels are required to promote growth and avoid nucleation. Addition of bulk antisolvent will give rise to conditions that are much more forced with wide metastable zones. Here, the rate of antisolvent addition and the dynamics of mixing of the solution and antisolvent will be the critical factors in influencing the crystallization behavior.

In some cases, a differentiation is also made between forward addition, where the antisolvent is added to the solution, and reverse addition, where the procedure is reversed and solution containing the dissolved solid is added to a batch of antisolvent. Reverse addition might be expected to produce the largest driving forces for solute to come out of solution, because the higher transient ratio of antisolvent to solvent will create very low transient solubility. However, in practice, mixing of antisolvent with solvent is usually rapid, and any control over an antisolvent addition is usually exercised by regulating the rate at which the antisolvent is added. In normal laboratory work, antisolvents are usually added and mixed rapidly, and the conditions created will deviate only slightly from those of reverse addition. From a point of view of creating diverse conditions in form screening, therefore, the differentiation of forward and reverse addition is not that important, and a better experimental design would vary the rate at which antisolvent is added, preferably with some knowledge of how the solubility varies with the composition of the solvent mixture. In this way, a slow antisolvent addition could complement the usual rapid addition and mixing to give a more gradual development of supersaturation.

Examples of the use of antisolvent crystallization for the preparation of metastable polymorphs include indomethacin, where the α-form was obtained on the addition of water as the antisolvent to a solution in methanol (63). The stable γ-form can be obtained on recrystallization from diethyl ether at room temperature. The insolubility of crystalline forms of indomethacin in water is the reason it is usually formulated in its amorphous form (2). The metastable form II of midodrine hydrochloride has been prepared by the addition of ethyl acetate or dichloromethane to a

solution in methanol (64). There is also more recent evidence that more extreme conditions of supersaturation created during an antisolvent addition lead to a greater preponderance of metastable forms. In the crystallization of abecarnil from solution in isopropyl acetate by the addition of hexane antisolvent, the stable form C was predominant at low supersaturation, whereas metastable form B occurred at higher supersaturation levels (65). A similar result was obtained for the crystallization of L-histidine from aqueous solutions using ethanol as the antisolvent (66). Here, a mixture of the stable form A and the metastable form B was obtained at relatively low supersaturation ratios (ratio of actual concentration to saturation concentration) ≤2, although at higher supersaturations ≥2.3 only the metastable form was observed. The supersaturation in this case was controllable by varying both the concentration of the starting solution and the antisolvent addition. There was also interconversion of the metastable to the stable form in the product slurry, on a time scale significantly slower than the crystallization observed. The principal reason postulated for the predominance of the metastable form at high supersaturation is its enhanced growth rate compared with the A form under these conditions.

The antisolvent crystallization of 2-aminobenzoic acid from ethanol solution with water also yields different polymorphic ratios according to the degree of supersaturation that is induced (67). The polymorphism of 2-aminobenzoic acid is well understood; there are three non-solvated forms I, II, and III. The system is enantiotropic with form I stable below 354 K and form II stable above this temperature. Form I contains two unlike molecules in the unit cell: one zwitterion and a molecule in the non-zwitterionic form. Forms II and III are made up of molecules that are not zwitterions. Form III only arises by condensation from the gas phase or in melt crystallization. Selectivity between the other two forms was dependent on the supersaturation levels generated, as is shown by the polymorphs first observed as the solids began to crystallize out as summarized in Table 5. These results show clearly that the high supersaturation forcing rapid removal of solid from solution favors the metastable form, whereas more moderate and gentle conditions favor the stable form.

Form II also showed a tendency to transform into form I via a solvent-mediated process over periods of 30–35 minutes. Forms I and II exhibited a large difference in solubility, which is indicative of a large free energy difference between them and may explain why this transformation occurs rapidly. However, growth rate measurements of the two forms show that in the intermediate supersaturation region of ratios

TABLE 5 Polymorphs of 2-Aminobenzoic Acid Obtained on First Crystallization from Ethanol Solutions Using Water as the Antisolvent (67)

Supersaturation ratio (C/C_0)	Polymorph first crystallized	Induction time[a]
1.2	I	15–95 min
1.4–1.6	I + II	70–260 sec
1.9–2.3	II	10–20 sec
3.1–4.5	II	<10 sec

[a]Time elapsed between antisolvent addition and the appearance of crystals.

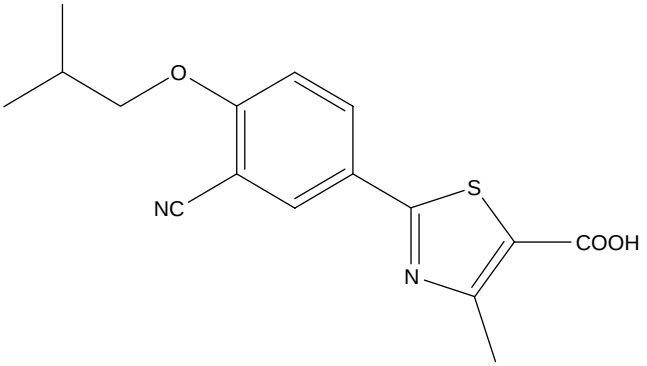

FIGURE 16 Enzyme inhibitor BPT, 2-(3-cyano-4-isobutyloxyphenyl)-4-methylthiazole-5-carboxylic acid. BPT can crystallize from methanol–water as three non-solvated forms A, B, C, a hydrate BH, and a methanol solvate D. Antisolvent crystallization with water never produces the most stable form C (68,69).

1.4–1.6 the mixture of forms arises from a concomitant crystallization of the two forms and not from an initial formation of form II followed by a transformation.

Antisolvent crystallization of the enzyme inhibitor BPT, Figure 16, from methanol solution by the addition of water in the temperature range of 40–60°C gave rise to different polymorphs at different temperatures (68). The experiments were carried out by dissolving BPT in a mixture of 38 mL methanol and 2 mL water at the temperature of the experiment, and then adding 14 mL of water to induce crystallization dropwise at rates between 0.2 and 2.0 mL/min while stirring with an impeller. Under these conditions, BPT has three non-solvated polymorphs A, B, and C, a hydrate (BH), and a methanol solvate (D). The most stable form C was not obtained in these experiments. At the higher temperature (60°C) close to the methanol boiling point (65°C, cf. Table 4) forms A and BH crystallized competitively, with form A favored at low initial concentrations and low water addition rates and the hydrate BH predominant at high concentrations and high addition rates. At 50°C, the hydrate BH crystallized, with the methanolate D forming additionally at the higher rates of water addition (69). At 40°C, form D was dominant and form BH crystallized also at low concentrations, and there was evidence that BH transformed to D at this temperature. There were clear indications that BPT exhibits enantiotropy within the temperature range investigated, and that the methanol–water solvent composition also affected the transformations between the solvated forms.

The examples above illustrate that antisolvent addition can be a very effective method in screening for polymorphs, and that in general, the more extreme the crystallization conditions in terms of their departure from equilibrium, the greater the probability of preparing unstable and metastable forms. The principles of antisolvent crystallization can also be used to create moderate supersaturation levels under conditions where cooling and evaporative crystallization are difficult or inappropriate, for example, where the solubility curve does not favor cooling and the solvent is not sufficiently volatile for evaporation. The use of vapor diffusion in single crystal growth has been mentioned above, where very slow antisolvent

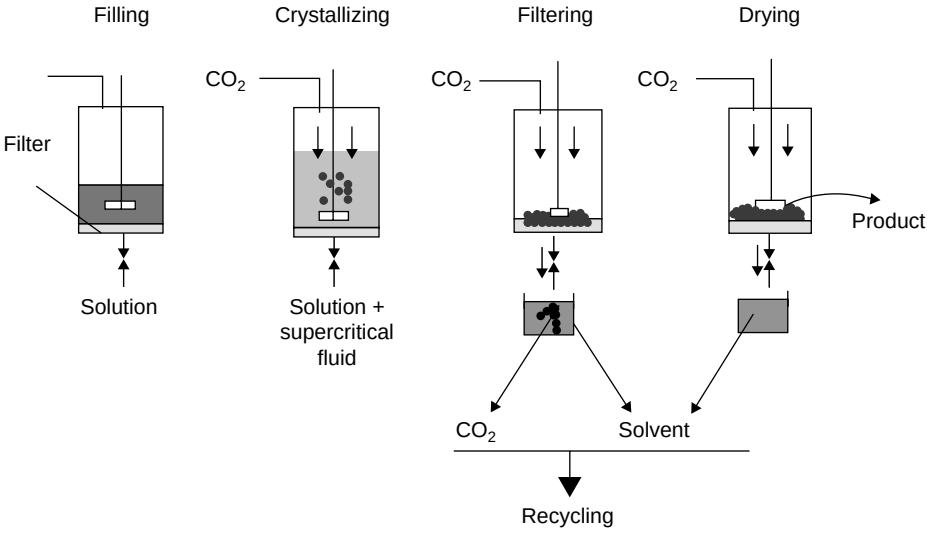

FIGURE 17 Principles of gas antisolvent (GAS) crystallization. Crystallization is induced by the addition of supercritical CO_2 which is subsequently drawn off after filtration. Antisolvent and solvent can often be recycled (70).

addition is limited by the rate of diffusion of the antisolvent through a particular geometric arrangement that can be designed to further slow the rate of antisolvent addition.

Another variant of antisolvent crystallization that produces milder supersaturation conditions involves the addition of a supercritical fluid or a gas under near-critical conditions as the antisolvent, most commonly CO_2. This technique is known as Gas Antisolvent Crystallization, abbreviated GAS, and is most commonly used to produce better quality crystals than those obtained by a conventional antisolvent crystallization. The principle of operating the method is shown in Figure 17 (70). The substance to be crystallized is dissolved in a solvent at the filling stage, and the antisolvent added under pressurization. The crystallized suspension is filtered and the pressure subsequently reduced to release the antisolvent gas and the solvent, both of which can be recycled. The final step involves the drying of the product crystals. The method has been used to isolate the antiarthritic agent lobenzarit in preference to conventional antisolvent crystallization with alcohols to produce small crystals with an acceptable size distribution (71). Here CO_2 and ethane were used as antisolvents, and a small amount of co-solvent (methanol, ethanol, isopropanol, or acetone) was added to the aqueous solution to promote the solubility of the antisolvent. The method has also been used to crystallize amoxicillin from DMSO and N-methylpyrrolidone (NMP) (72), and paracetamol from ethanol (70).

A systematic investigation of three sulfanilamide drug substances that exhibit polymorphism (73) showed no polymorphic changes occurring during crystallization using water and supercritical CO_2 as antisolvents, although substantial changes in crystal size and habit occurred under different conditions, particularly where

alternative solvents were used. For example, the habit of crystals of sulfathiazole, known to be highly polymorphic, prepared from acetone and methanol solvents using CO_2 were respectively granular and acicular, although no change in form was apparent. Similar habit changes with different solvents were observed for sulfamethizole and sulfabenzamide. Generally, crystal size increased with the temperature at which the crystallization was carried out, and smaller crystals were obtained using CO_2 as the antisolvent compared with a conventional antisolvent crystallization with water.

Reactive Crystallization

Reactive crystallization occurs where two chemical entities react in solution to give a product species that is less soluble than the reactants from which it is formed. Supersaturation is generated by the formation of the new product compound, and the rate at which it develops is determined by the rate of reaction and the solubility of the product species relative to the reactants and the conditions employed. Reactive crystallizations are common in the manufacture of commodity chemicals, and occur quite often in pharmaceuticals manufacture, in particular, where a final synthesis stage yields a product that is less soluble than the reactants and any by-products such that isolation can be carried out simply by crystallization or precipitation from the solution in which the reaction has been carried out.

The principles by which reactive crystallizations may be analyzed and developed in general have been reviewed recently, in the light of increased interest in this type of process over several years (74). According to this review, the above description of a reactive crystallization is incomplete because it does not include the situation where a solid reactant dissolves and reacts to form the crystallizing product within the reactor vessel. In the present author's experience, this type of process is not often used in the final stages of manufacture of pharmaceutical products; the reaction of two species in solution is much more common. Even within this more limited range of possibilities, there is a great deal of scope for variations depending on reaction rates and the solubilities of the reactants and products. Figure 18 shows two illustrative cases. In Figure 18A, rapid isothermal reaction leads to very high supersaturation and crash-crystallization, conditions analogous to rapid antisolvent

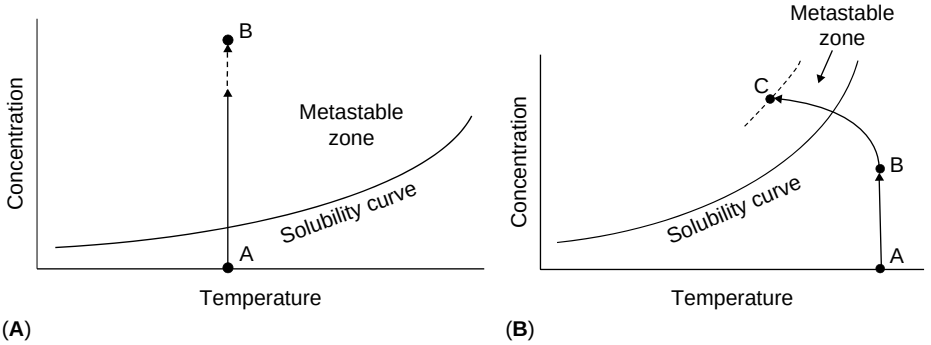

FIGURE 18 Reactive crystallization and the metastable zone. (**A**) The case of rapid reaction inducing a very high supersaturation, leading to precipitation or crash-crystallization. (**B**) Combination of reaction and cooling crystallization leading to mild crystallization conditions.

addition (section "Antisolvent Crystallization"). This condition occurs commonly in precipitations, for example, in the well-known precipitation of insoluble inorganic compounds by double decomposition, where non-crystalline material is usually required. Figure 18B shows the opposite extreme of a reaction leading to a product concentration below saturation, and continuing reaction and cooling leading to crystallization under moderate conditions. All combinations of reaction with heating and cooling, that may be influenced by exothermic or endothermic reaction, are possible in principle.

A very common method of reactive crystallization in the pharmaceutical industry is via the alteration of pH. Many drug substances are slightly soluble weak acids or bases, whose anionic or cationic salt forms are much more soluble in water. Adjustment of the pH can thus lead to the crystallization or precipitation of the free acid or base, and this can be used to purify and consolidate the final product. Proton-transfer reactions associated with pH shifts are generally rapid, and the condition of Figure 18A often arises in these preparations. It is fairly common for a time gap of several hours to elapse before nucleation and crystallization are observed in these cases, the delay being due to the energy barrier associated with nucleation. The combination of rapid reaction and delayed nucleation usually results in conditions analogous to a very wide metastable zone, promoting the formation of amorphous materials, unstable and metastable polymorphs, and crystals of poor quality.

Simple, early examples of this technique for polymorph discovery include form I of the X-ray contrast agent iopanoic acid, which was prepared by the adjustment of a solution prepared at pH 12.5 (in 0.1 M NaOH) to pH 2.15 by HCl addition (75). Similarly, form III of the diuretic hydrochlorothiazide, which as its name indicates is a hydrochloride salt, was precipitated from an aqueous NaOH solution via HCl addition (76). More recently, piretamide form C was precipitated on adjusting a solution in 0.1 M NaOH to pH 3.3 by a 1:1 stoichiometric acid addition (77). In this case, a slight deviation in the acid:base stoichiometric ratio to 0.95:1, presumably leading to a different pH value, gave rise to mixture of amorphous piretamide and crystalline form C. It appears in this case that acidification was sufficient to form the protonated species (as determined by pKa values), but the final pH influenced the morphological form of the product.

CRYSTALLIZATION FROM MELTS

Melt crystallization is not commonly employed in pharmaceuticals manufacture, unlike in the production of commodity chemicals where it is often employed as a purification technique (37). Many pharmaceutical compounds decompose on approaching their melting points, and the melting and recrystallization of a new compound in development, for which many physical and stability properties remain unknown, would carry a high risk of degradation. However, there will be cases where melt crystallization will give rise to polymorphs that are not accessible by other solution-based methods. The highly polymorphic compound ROY, 5-methyl-2-[(2-nitrophenyl)amino]-3-thiophenecarbonitrile, yielded a form Y04 on crystallization from the melt at room temperature that was not found by crystallization from solution (78). This subsequently transformed to a further, more stable new polymorph YT04 over several hours. Despite being unobtainable by solution methods, YT04 was found to be the densest known polymorph at room temperature,

and is believed to be the second most stable in terms of its lattice energy (at 0 K). As a further example, form I of *p*-(I*R*,3*S*)-3-thioanisoyl-1,2,2-trimethylcyclopentane carboxylic acid was obtained from form II by melting the latter and recrystallizing in vacuo (79).

Generally, melt crystallization is governed by the same principles as crystallization from solution, in terms of kinetics versus thermodynamics and of a supercooling driving force in the place of solution supersaturation. Forced solidification by rapid or quench cooling is analogous to crashing out of solution by rapid antisolvent addition. Quench cooling a melt can sometimes result in formation of an amorphous solid that, on subsequent heating (annealing), undergoes a glass transition followed by crystallization (80).

There is considerable interest recently in the use of thermal fusion methods for the preparation of co-crystals. As discussed in the sections "Solid Forms and Their Characteristics" and "Preparation of Different Types of Solid Forms," co-crystals have attracted much interest as new solid forms in recent years, and the development of new methods for their preparation has strongly influenced thinking on polymorph preparation. A method attracting much interest for the preparation of co-crystals is the Köfler mixed fusion method (81), in which two (or more) substances are heated separately on the hot stage of a microscope until at least one melts, and then contacted by mixing with a coverslip. The method has traditionally been employed to determine the thermal phase properties of melts, in particular, the formation of eutectics (9). Several variants have been employed in recent years. Under favorable conditions the thermal behavior of a binary mixture can be observed across a gradation of compositions between 100% of each component.

The sodium channel blocker 2-[4-(4-chloro-2-fluorophenoxy)phenyl]pyrimidine-4-carboxamide has been screened in this way for co-crystal formation with 26 carboxylic acid co-formers (33), and the glutaric acid adduct exhibited much improved bioavailability compared with the original API. Here the API was rendered as a liquid phase below its melting point by dissolution in high-boiling solvents such as methyl salicylate and methyl benzoate, with the liquid composition and concentration used to tailor the conditions to suit the co-former under test. A similar method using methyl benzoate was used to screen for co-crystals of imprimine hydrochloride (82), by which a co-crystal with (+)-camphoric acid was prepared.

In a very recent investigation (83), the Köfler method has been employed in conjunction with solution crystallization to search for new solid co-crystals of nicotinamide with a number of small-molecule APIs containing carboxylic acid or amide functions. Visual images were created by viewing under crossed polar filters that mapped the eutectic melting points with respect to changes in composition. Five out of eight potential co-crystals were identified in this way by the presence of three distinct eutectics, and in one case, with flurbiprofen, polymorphism of nicotinamide was observed in addition to co-crystal formation. Also, form III of flurbiprofen was identified (by powder X-ray diffraction) in the material recovered from the Köfler melt. Form III flurbiprofen is unstable, and usually transforms to form I over periods of minutes. Evidence of two co-crystal phases that could not be prepared by solution crystallization, of fenbufen–nicotinamide and flurbiprofen–nicotinamide, were also found in the melts, and in principle, the possibility exists of using such materials as seed to prepare such normally inaccessible solid forms from solution.

Similar principles underlie a further recent report (84) of the use of differential scanning calorimetry (DSC) for identifying co-crystal formation from binary melts. The presence of a co-crystal is indicated by the presence of a second fusion endotherm, in addition to the one associated with the binary eutectic. Tests using 20 API–co-former combinations gave results confirming the formation of seven co-crystals already identified, and indicating a further nine new co-crystal phases that were confirmed by variable-temperature powder X-ray diffraction. In all cases, the new co-crystal fusion event was recorded at a higher temperature than the melting of the eutectic, and was distinguishable from the known fusion characteristics of the components.

Although the above investigations were focused on co-crystal preparation, the accessibility of new forms to these methods will undoubtedly stimulate interest in their use for discovering polymorphs that are not accessible by solution crystallization, as has already happened with mechanochemical methods of preparation (section "Mechanochemical Methods"). There is evidence from these investigations (83) that polymorphs that are unstable and difficult to prepare from solution can be observed in melt systems, and it is probable that the different conditions promote the formation of some polymorphs and co-crystal phases at the expense of others. Further investigations of methods based on melt crystallization for polymorph discovery can be expected in the near future.

MECHANOCHEMICAL METHODS

Mechanochemical methods, more commonly and usefully described as grinding, have been employed extensively in the preparation of co-crystals in recent years, and, as with the thermal methods above, this activity is generating interest in their use more generally in solid form preparations. The first reference to the use of grinding to produce adducted materials dates back to the late 19th century (85). In the early 1990s, grinding was employed alongside solution crystallization methods in the preparation of co-crystals of 2-aminopyrimidine with carboxylic acids (86), and also of pairs of nucleotide bases (86,87). For the latter, the formation of co-crystal phases was found to depend on the method employed. 9-methyladenine and 1-methylthymine formed a co-crystal on grinding together in the solid state that could not be prepared from solution, while the exact converse was true for mixtures of 9-ethylguanine and 1-methylcytosine (87). Grinding here was carried out over a 20-minute period in a "mechanical amalgamator" using a 25-mm steel capsule fitted with a single 3-mm ball bearing. At around the same time, there were also some reports of polymorphic transformations being induced by grinding. Metastable forms B and C of chloramphenicol palmitate were transformed into stable form A upon grinding at room temperature (88). The stable β-caffeine was converted into the metastable α-form in a 95% phase conversion on grinding for 60 hours (89), showing that phase transformations up the free energy ladder are also possible. Depending on the material and the conditions employed, grinding can also result in conversion to an amorphous substance, as discussed below.

More recently, the use of so-called "solvent-drop" grinding has been developed, in which a small quantity of a solvent is added to the solid substance or mixture prior to grinding. Grinding cyclohexane-*cis*,*cis*-1,3,5-tricarboxylic acid (CTA) with 4,4′-bipyridine (Bipy) for one hour in a Retsch MM200 Mixer Mill with an oscillation frequency of 15 Hz resulted in partial conversion to the 1:1 co-crystal, whereas the

TABLE 6 Solvent-Drop Grinding: the Promotion of Co-crystal Formation from CTA (Cyclohexane-*cis*,*cis*-1,3,5-tricarboxylic acid) and fPh (4,7-Phenanthroline) in Relation to Solvent Choice and the Solubility of the Components (90)

Solvent	Solubility of		Enhancement	Comments
	CTA	fPh		
None (dry grinding)	–	–	–	Low yield after long period
Methanol	v	v	yes	Complete conversion in 10 min
Water	v	s	yes	Accelerated reaction
Ethyl acetate	i	v	yes	Accelerated reaction
Acetonitrile	s	s	yes	Accelerated reaction
Cyclohexane	i	i	no	No reaction after 1.5 hr

Abbreviations: v, very soluble; s, slightly/partially soluble; i, insoluble.

addition of a small quantity of methanol (50 µL to 200 mg of solid) accelerated the process to completion in 20 minutes (90). A more extended investigation (90) of the formation of the 1:2 CTA co-crystal with 4,7-phenanthroline (fPh) showed that acceleration of the reaction was associated with solubility of one or more of the components, as summarized in Table 6. In this case, the co-crystal in question can be readily obtained by solution crystallization from methanol.

Grinding with and without solvent present has been applied to the preparation of the dimorphic 1:1 co-crystal of caffeine and glutaric acid (91). Slow evaporative crystallization from chloroform results in a mixture of the two polymorphs; monoclinic form I crystallizes as rods mixed with block-shaped crystals of the triclinic form II. The forms have very similar densities (1.486 and 1.482 g/cm^3) and the packing architectures are similar, suggesting that the lattice energies and free energies of formation are probably very similar. Solvent drop grinding with *n*-hexane, cyclohexane, and *n*-heptane gave a predominance of form I in the product, although with cyclohexane there was still some unreacted caffeine present after 60 minutes. Grinding with chloroform, dichloromethane, acetonitrile, and water led to a predominance of form II. It is suggested that the effect of solvent polarity in determining the polymorphic outcome may arise from packing differences between the two forms. Form I includes a non-polar cleavage plane (200) with exposed methyl and methylene groups between stacks of ribbons along the *b*-axis that is not exhibited in form II. It is suggested that non-polar solvents may favor form I by stabilizing these planes upon grinding-induced cleavage.

Co-crystals of caffeine with trifluoroacetic acid (TFA) were found to be only accessible by grinding (28). Attempts to co-crystallize 1:1 caffeine + TFA from a number of solvents gave rise to either crystalline caffeine or occasionally to materials with alternative powder diffraction patterns that could not be reproduced. Evaporation of a solution of caffeine with excess TFA led to a viscous liquid from which no crystals could be obtained. Dry grinding the components together in a 1:1 ratio gave rise to two apparent polymorphic 1:1 co-crystals, designated D and E, depending on the quantities of material used. Starting with 140 mg caffeine + equivalent TFA, form D was produced, whereas a similar experiment with 320 mg caffeine + equivalent TFA produced form E. The grinding was carried out in a Retsch MM200 Mixer Mill at 30 Hz in a 10 mL stainless steel grinding jar with two 7 mm stainless steel

grinding balls. Seeding the viscous liquid prepared by evaporating a solution in excess TFA as above with crystals of either form D or form E from grinding led to crystallization and growth of the seeded form, from which single-crystal structure determinations were obtained. Form D was stable on storage for six months, whereas form E transformed completely to form D in as little as three days. As with the β- to α-phase conversion of caffeine discussed above (89), no explanation was offered (28) for the appearance of a metastable form depending on experimental scale, and there is a great deal still to be discovered about transformation mechanisms during grinding.

Crystallization of a saturated solution of caffeine in excess acetic acid resulted in a 1:2 caffeine–acetic acid co-crystal (28), which could also be prepared by grinding caffeine and acetic acid together in a 1:2 molar ratio. The co-crystal form produced was stable on storage for six months. Grinding caffeine and acetic acid together in a 1:1 ratio resulted in a new 1:1 co-crystal that could not be prepared by solution crystallization. However, residual caffeine was also found in the product, and this could not be eliminated by further grinding, whereas the addition of excess acetic acid gave rise to contamination with the 1:2 co-crystal form. Solvent drop addition of *n*-heptane reduced the residual caffeine. The 1:1 co-crystal was unstable, and dissociated to crystalline caffeine and acetic acid vapor within one day of storage at ambient temperature.

There is now ample evidence that grinding methods can be used to identify and access solid forms that would not be found if solution crystallization methods alone were to be used in screening for them. There is also evidence that small amounts of materials prepared by grinding can be used to seed more extensive batches of solution to obtain both crystals for structure determination and for subsequent manufacture. What is lacking at present is a complete understanding of the mechanisms by which grinding promotes phase transformation and co-crystal formation, and in particular, why some positive results can be obtained by grinding that are not obtainable by solution methods. We can examine this in two ways: first, by looking at the effects of shearing and other disruptive mechanical forces on the materials under test, and second, by making comparisons with solution crystallization via phase diagrams.

Mechanical trauma will both break down macroscopically ordered structure and introduce local heating and pressurization effects. An early source (92) summarizes this by describing a molecular "loosening," or separation from the lattice, that is the first stage of any solid-state transformation. Grinding is extensively used in pharmaceuticals processing to reduce particle size, and extreme breakdown effects may ultimately result in amorphous material. Breakdown of crystalline structure in this way can be explained mechanically, in terms of increasingly anharmonic lattice vibrations (phonons) under stress, eventually violating the Born stability criteria of the lattice, above which it collapses to yield an amorphous structure (93). An alternative view based on thermodynamics asserts that continuous mechanical energy input increases the concentration of defects to a critical limit, beyond which the amorphous phase has greater stability than the disrupted crystal (94).

Transformation to a new crystalline phase, polymorph or co-crystal, will take place if the "loosened" material can be nucleated in some way and subsequently grow in to form the new solid. The mobility of the amorphous intermediate toward this type of reordering will be determined, among other factors, by whether it is above or below its glass transition temperature, T_g. Above T_g, the amorphous material

may be expected to re-order itself much more readily because of its higher lability and lower viscosity. Cryogenic grinding is commonly employed in producing amorphous materials, to keep the amorphous material at a low temperature and prevent re-ordering and recrystallization.

A detailed investigation of the cryogenic grinding of indomethacin (93) produced amorphous material starting from all of the non-solvated polymorphs, namely γ (stable), α, and δ (alternatively designated forms I, II, and IV, respectively). Amorphous indomethacin has been well characterized, and has a T_g of around 43°C. Previous work on the grinding of indomethacin at around the T_g (95) yielded only partially amorphous material, and the physical stability of this product was dependent on the initial crystal form. Cryogenically grinding the methanol solvatomorph (93) also produced amorphous material, but this had to be desolvated subsequently because the methanol released destabilized the product, probably by acting as a plasticizer. This provides an interesting parallel with solvent drop grinding, where a small amount of solvent is introduced expressly to promote transition to a crystalline form. Another indomethacin solvatomorph, the *t*-butanolate, was unaffected by cryogenic grinding and retained its original structure.

The grinding of ursodeoxycholic acid (USDA) with either phenanthrene or anthrone at ambient temperature led to an inclusion structure that contained both compounds (96). Lower temperature grinding did not yield this structure, but a mixture of amorphous USDA and the original crystalline phenanthrene or anthrone. Subsequent heat treatment of this mixture did not form the inclusion structure. It was concluded that interplay of mechanical and thermal factors were responsible for the adduction, but an argument based on the transient production of a labile amorphous phase could also explain these observations.

A recent investigation of the preparation of the carbamazepine (CBZ)–saccharin (SAC) co-crystal by grinding under wet and dry conditions (97) bears out the principles established above. Amorphous CBZ has a well-established T_g around 41°C, and grinding the anhydrous components together gave a much faster rate of co-crystal formation when operated at room temperature, where the temperature in the mill was established as 45°C, than under cryogenic conditions. Thermal analysis of a mixture of dry, amorphous CBZ and SAC showed a crystallization event (exotherm) at 69°C, followed by an endotherm at 174°C that corresponds with the melting of the CBZ–SAC co-crystalline phase. Storage experiments at 0% and 75% relative humidity showed a greater tendency for co-crystals to form under humid conditions, and co-crystals also formed more readily when CBZ dihydrate was ground with SAC in place of the anhydrous material. This indicates that water is acting as a plasticizer in increasing the lability of the amorphous components to form new crystalline phases.

A mechanism of breakdown of crystalline form during grinding followed by the recrystallization of the amorphous phase explains many facets of polymorphic transformation and co-crystal formation under these conditions. The enhancements brought about by the addition of small quantities of solvent as a plasticizer, and the effect of temperature in determining whether the amorphous phases are above or below their T_gs are also explained. However, the correspondence between the efficacy of particular solvents in promoting transformations and the solubilities of the components as indicated in Table 6 suggests that dissolution effects may also be playing a part in enhancing transformations with small quantities of solvent present. This could be analogous to the commonly reported polymorph transformation

occurring in the storage of damp materials, where traces of solvent provide a pathway via which transformation from a metastable to a stable polymorph may occur.

Recent investigations of the preparation of co-crystals by solution crystallization (98,99) have emphasized the importance of the phase diagram in indicating the composition conditions under which co-crystals are most likely to form, and have shown that the intuitive use of a ratio of components corresponding to the stoichiometry of the co-crystal is not necessarily optimum. Also, solvent-mediated transformations have been used (100) both to prepare new co-crystalline phases and also to investigate the relative stabilities of polymorphs. In these, the solvent is introduced to provide a mechanistic pathway, and the quantities used are much less than is required to completely dissolve any of the components present. Solvent drop grinding may work in a similar way by providing a small volume solution pathway for changes to take place. It is possible that both solvent-mediated transformation and solvent drop grinding may be "sampling" a wide range of compositional variation, and thus locating at some point in space the region of the phase diagram in which the desired phase transition is most favored. Such small-scale variations will not be apparent in the design of the experiment, which will be worked out in terms of the macroscopic ratios of reactants and solvents. This notion of "sampling" compositional variation is analogous to the Köfler method for melts, in that the latter allows for a continuous variation in the proportions of the reactants in the region where they interact.

There are at least two modes of mechanical action within a grinding process, impact, and shear, and there appears to have been no systematic study of the effects of these on amorphization or phase transformation, nor any attempt to investigate them separately. Most investigations today take place in small ball-milling devices such as a Retsch Mill, but, for example, the different caffeine–TFA co-crystals (28) obtained starting with different amounts of reactant material may be due to the samples experiencing different mechanical disturbances. A more thorough understanding of milling and grinding processes seems to be required to explain more fully some of the unusual and anomalous outcomes that are reported.

OTHER METHODS FOR INDUCING CRYSTALLIZATION AND POLYMORPHIC TRANSFORMATION

Mechanochemistry, described above, differs from the other methods discussed so far in this chapter in starting immediately from and transforming solid phases, rather than starting with the supersaturated liquid phases of a solution or a melt. However, the weight of evidence that crystallization by grinding proceeds via an intermediate amorphous phase tends to place mechanochemistry into the same category, with the outcome determined by the nucleation and growth of specific solid phases in a process of crystallization. This can also be said about a number of other, long-standing, methods that induce solid-phase transformations, usually via an intermediate phase in which the original crystalline structure is either transiently destroyed or seriously disrupted. These will be reviewed in this section.

Thermal Methods

Thermally induced phase transformations in the solid state can arise because of changes in stability ordering with temperature, as in cases exhibiting enantiotropy,

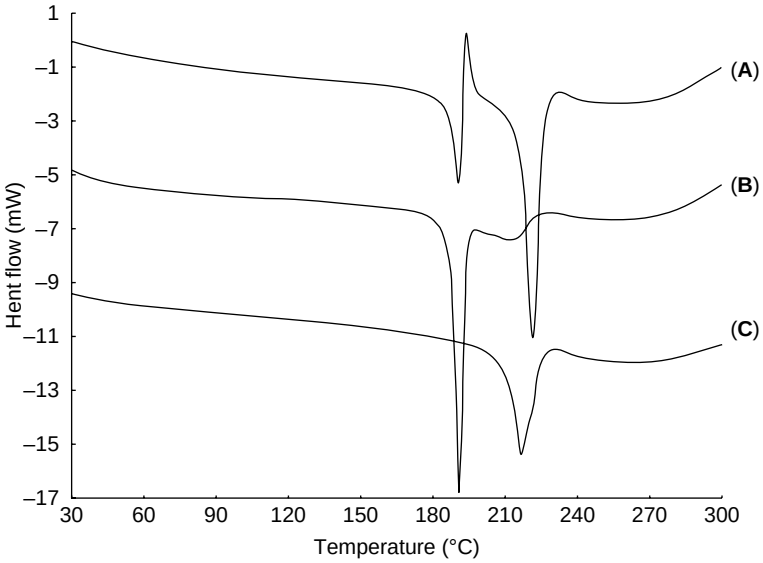

FIGURE 19 Melting–recrystallization as recorded as an endotherm–exotherm by DSC (101): (**A**) the less stable tiotropium fumarate form II (1:1) salt melts at 186°C; (**B**) the melt immediately recrystallizes to the more stable form IV (tiotropium fumarate–fumaric acid (2:1:1) co-crystal); (**C**) form IV subsequently melts at 216°C.

or occasionally because of kinetic factors favoring formation of an alternative form at higher temperature. Phase transitions also occur on melting a less stable solid form, which then immediately recrystallizes as a more stable, higher melting form. Differential scanning calorimetry (DSC) will show such a melting–recrystallization event as an endotherm associated with the melting immediately followed by an exotherm corresponding to recrystallization. An example from the author's recent work (101) is given in Figure 19. The stable phase formed by recrystallization will subsequently melt at a higher temperature, giving rise to a further endotherm. In such cases, it should be possible in principle to prepare the recrystallized form by thermal treatment, although practical difficulties such as degradation and the need for accurate temperature control will often make such preparations difficult.

There are many examples of thermally induced phase transformations in the literature. Chlorpropamide form C was prepared by heating form A, crystallized from ethanol solution, in an oven at 100°C for three hours (102). Similarly, the γ-form of tegafur was obtained by heating the β-form at 130°C for one hour (103). Heating β-caffeine, the stable form at room temperature, for 10 hours at 180°C resulted in formation of the α-form (89). However, the quoted sublimation temperature for caffeine is 178°C (below the melting point), and it is possible that this transformation may have been mediated via the vapor rather than by the melt. Sulfathiazole form I was obtained by heating form III crystals at 170°C for 30–40 minutes (104). On a larger scale, a vacuum drying pistol has been used with a high boiling liquid such as chlorobenzene, enabling the generation of *p*-(I*R*,3*S*)-3-thioanisoyl-1,2, 2-trimethylcyclopentane carboxylic acid form I by the melting of form II with this

arrangement (79). Temperature dependence of the obtained solid forms was observed in the thermally induced crystallization of anhydrous indomethacin (105). When an amorphous solidified melt of indomethacin was stored at 40°C, it partly crystallized as the thermodynamically stable γ-form, while at 50°C, 60°C, and 70°C, mixtures of the α- and the γ-form were obtained.

The other route for thermal phase transformation often employed is sublimation. This is commonly used for the preparation of single crystals for X-ray structure determination, where the sublimed vapor is both condensed and nucleated by a small nucleus crystal in a cooled environment. A 1971 source (106) estimated that approximately two-thirds of all organic compounds were converted at least partially from the solid to the gaseous state on heating and back to the solid on cooling. How relevant this is today, and how applicable it is to pharmaceutical active ingredients, many of which are not particularly stable at elevated temperature, is questionable. Although, strictly speaking, the term sublimation refers only to the phase change from solid to vapor without the intervention of the liquid phase, it is quite common that crystals are formed on surfaces in close proximity to the melt, whereas no crystals are formed at lower temperatures well below the melting point.

The sublimation temperature and the distance of the collecting surface from the material undergoing sublimation have a great influence on the form and size of the crystals produced, and these experimental variables are usually optimized in single-crystal preparation. The occurrence of polymorphic modifications depends on the temperature of sublimation. In general, it may be assumed that unstable crystals form preferentially at lower temperatures, whereas at higher temperatures stable forms are to be expected. This is because lower temperatures induce quench-cooling, and the solid structure will adopt the form closest to the melt condition, in accordance with Ostwald's Law of Stages. At higher temperatures cooling will be less rapid, and the condensed solid will have more relaxation time to adopt more stable, and less labile, configurations. Also, mixtures containing several forms are frequently found together.

A simple test has been recommended (9) to determine whether a material sublimes and is suitable for crystallization or recrystallization by sublimation. A small quantity (10–20 mg) of solid is placed in a Petri dish and covered with an inverted watch glass. The dish is heated gently on a hot plate and the watch glass is observed to determine if crystals are growing on it. When the sublimate is well formed, the cover glass is removed to a clean slide for examination. It may also be possible to form good crystals by sublimation from one microscope slide to a second held above it, with the upper slide also being heated so that its temperature is only slightly below that of the lower slide. Controlled cooling of the coverslip by placing drops of various low-boiling solvents on the top surface will cause condensation, the lower temperatures leading to the most unstable forms. On a larger scale, a glass cold finger can be employed. Once crystals of various modifications have been obtained they can be used as seeds for the solution phase crystallization of larger quantities, as described for the methods in previous sections.

As examples of crystallization by sublimation, form I of 9,10-anthraquinone-2-carboxylic acid has been obtained as needle-like crystals upon sublimation at temperatures exceeding 250°C (107). Sublimation has also been employed to purify theophylline by recrystallization for vapor pressure studies (108). Stable phases of both 1,3-dimethyluracil and malonamide have been be prepared by vacuum sublimation (109).

In previous sections, the use of temperature as a variable in determining the polymorphic outcome of crystallization for compounds exhibiting enantiotropy has already been discussed, as for example, for the enzyme–inhibitor compound in Figure 16 (68). There are also cases where heat treatments can be used to convert an enantiotropic compound to the form more stable at higher temperature, although this may not always be the best method to obtain the form reliably (110), and it is also likely that the form stable at lower temperature (i.e., room temperature) may be the form preferred.

The technique of thermocycling is sometimes employed in solid form screening. This consists of alternately raising and lowering the temperature of a sample several times, usually between room temperature and a temperature close to the melting point of the solid. The thinking behind this is that the cycling will allow any transient "memory effects" of conversion built up in the solid during individual cycles to mature, and eventually to produce a new solid form. However, there are no statistics as to the success of this technique in preparing and discovering new forms, and it would seem that the cycling would serve to perpeptuate a non-equilibrium condition in a sample exhibiting enantiotropy or other variations in crystallization behavior with temperature.

Slurrying

Slurrying is a method in which a sample of a solid material is suspended, usually for an extended period, in a quantity of solvent that is insufficient to dissolve it completely. Its primary function in polymorph and solid form screening is to allow a pathway via the medium of the solvent for the solid to transform to more stable forms, thus ultimately providing a "ladder" down the stability order. Depending on the technique used, and the information that it is required to generate, the formation of the new solid form(s) may or may not be seeded.

Unseeded slurrying is used to seek more stable and hitherto undiscovered polymorphs of a compound, and has also been employed in the preparation of co-crystals. The primary process occurring is a solvent-mediated transformation, which is characterized by the dissolution of the starting material and the nucleation and growth of the new form. A detailed investigation using a range of solvents has been carried out for sulfamerazine in terms of these stages (111). Sulfamerazine is dimorphic and enantiotropic, with form II stable below and form I above the transition temperature of 51–54°C. The rate of the solvent-mediated transformation of form I to form II was determined primarily by the nucleation rate of form II, and this in turn was related to the solubility and the strength of the solute–solvent interactions, particularly those associated with hydrogen bonding. To facilitate the crystallization of the more stable polymorph, a solvent should be selected to give high solubility of the starting material with moderately strong hydrogen-bonding interactions. It was also shown that agitation rates and conditions may be adjusted to optimize the nucleation conditions of the new, more stable, form, although it is not possible at present to set out general principles to guide this. Solvent-mediated transformations relying on the same principles have also been employed in the preparation of co-crystals (100,112); these involve conversion of a less stable mixture of components to a more stable co-crystal form, and proceed through similar, sequential stages of dissolution, nucleation, and growth.

The success of an unseeded solvent-mediated transformation in searching for new and more stable polymorphs is ultimately dependent on the nucleation

process from a supersaturated solution, and the uncertainties and difficulties associated with this have been discussed above (section "Crystallization from Solution"). As nucleation is a stochastic process, and events are usually expressed as a rate or the number of events occurring in unit time, the probability of such an event occurring increases with time, and slurrying is therefore most effective if continued over an extended period. The use of an extended period of slurrying is also desirable for other reasons. Solubility differences between less stable and more stable polymorphs can often be small, and the supersaturation of solutions formed from the less stable form with respect to the more stable form will also be small. Under these conditions, crystallization will be slow and produce small amounts of the more stable form, which can then subsequently seed the crystallization of supersaturated solutions created by further dissolution of the metastable form. Slurrying experiments are usually carried out over periods of 2–4 weeks, or even longer.

Another type of slurrying experiment, carried out in polymorph screening for different reasons, is seeded or competitive slurrying. This method is used where several polymorphic forms are already known, and the requirement is the identification of the most stable form. Here, a quantity of all the known forms are slurried together in a solvent, again for an extended period. In theory, all will eventually transform to the most stable form by a series of processes of re-dissolution and crystallization. According to Ostwald's Law of Stages (11), each metastable or unstable polymorph should dissolve and recrystallize as the form immediately below it on the stability scale; experience tells that this happens in some cases but not in others. Nevertheless, periodic sampling of a slurry may identify transient enrichments that indicate forms of intermediate stability, and particularly forms that crystallize readily because of favorable kinetics. In the subsequent development of crystallization processes, such kinetically favored forms are likely to be encountered, either as the desired product or possibly as a polymorphic impurity.

Crystallization in the Presence of Additives

The use of additives to modify and control crystal growth has been investigated over several decades. Additives can enhance or, more commonly, inhibit growth, and the effect is often specific to a crystal face or group of faces that serves to modify the habit of the crystal. This has been an important direction of research in this area, to modify crystal properties by altering the aspect ratios of their faces. For example, the presence of benzoic acid inhibits the growth of benzamide crystals along the c-direction, while *o*- and *p*-toluamide, respectively, retard growth along the *b*- and *a*-axes (56) (cf. section "Effects of Solvent"). In a more recent example (113), a low level of octanoic acid inhibits the growth of crystalline adipic acid, a common excipient, on the hydrophilic (100) face.

Another effect of growth modification and inhibition has been to change the polymorph selectivity of a crystallization process. It has been suggested that additives bind specifically to the surfaces of particular polymorphs at the development of nucleation, and so inhibit their achieving the critical size (114). This will allow an alternative phase to grow without competition. Although the α-form of glycine is normally obtained by recrystallization from water, addition of 3% of racemic hexafluorovaline leads to the precipitation of the γ-polymorph as trigonal pyramids (115). This additive was designed to be strongly adsorbed at the four (011)

faces of α-glycine and to bind at only one pole (NH_3^+) of the polar crystal, thus leaving the crystal free to grow at the opposite CO_2^- pole.

Additives at levels as low as 0.03% have been shown to inhibit nucleation and crystal growth of a stable polymorph, thus favoring the growth of a metastable form (116). This presents a possibility in principle of designing crystal nucleation inhibitors to direct the formation of particular polymorphs. Crystals of form I terephthalic acid could be obtained by crystallization only in the presence of *p*-toluic acid, while the form II polymorph, more stable at ambient temperatures, was obtained from a hydrothermal recrystallization (117). The transformation of crystallized, metastable α-indomethacin to the stable γ-form was inhibited by the presence of hydroxypropyl methylcellulose (118).

The use of synthetic polymers and polymer mixtures to nucleate particular polymorphs selectively has been investigated with some success in recent years (119). It is generally accepted that most crystallizations are induced by heterogeneous nucleation events, and this work aims to bring this principle together with a control and understanding of the relationship between the chemical and structural properties of the nucleus and the forms obtained. The fourth polymorph of carbamazepine was discovered using this method (120), and differentiation of the polymer compositions has been employed to control the crystallization of the two polymorphs of acetaminophen (121). The metastable orthorhombic form of the latter, hitherto inaccessible via solution crystallization, was prepared by nucleation with a "library" mixture of commercially available polymers. The correlation of the polymorph obtained with the polymers used appears to be a complex matter involving both chemical functionalities and the crystallinity of the polymer. Tests with the highly polymorphic intermediate 5-methyl-2-[(2-nitrophenyl)amino]-3-thiophenecarbonitrile (ROY) (121) showed that polymer heteronuclei could be used to generate all six structurally characterized forms of this substance, and to prepare good quality single crystals suitable for structural determinations.

Desolvation of Hydrates and Solvatomorphs

Desolvation of solvatomorphs and solvates is used as a method to discover and prepare polymorphic forms that are inaccessible via ordinary crystallization techniques. Often, these "desolvated solvates" retain the crystal structure of the original solvate form, and exhibit relatively small changes in lattice parameters. However, there are also cases where the solvent plays an essential role in stabilizing the lattice, and the process of desolvation may give rise to a new crystal form, an amorphous material, or at least a change in the lattice parameters. Examples of polymorphs prepared uniquely by the dehydration of hydrates include caffeine form II, which was prepared by recrystallizing caffeine from water, drying for eight days at 30°C, and then heating for four hours at 80°C (89). Chloroquine diphosphate 3:1 hydrate was converted to a crystalline anhydrous form by heating to temperatures above 188°C (122).

A more complicated pattern of interconversion is exhibited by etoposide (123). The monohydrate form I underwent a dehydration in the temperature range of 85–115°C to yield etoposide form la. This form melted at 198°C and recrystallized immediately to etoposide form IIa, which itself re-melted and subsequently recrystallized at 206°C to yet another polymorph, form IIb. Form IIb melted at 269°C, and converted to a hydrate (form II) when exposed to the atmosphere at room

temperature. This latter hydrate was also found to dehydrate at 90–120°C to yield its corresponding anhydrate form IIa.

DSC of levofloxacin hemihydrate measured under various conditions showed different patterns of thermal behavior (124). This was attributed to a dehydration process that resulted in a multiple-phase transition. Dehydration at higher temperatures (above 70°C) gave a sharp endothermic peak corresponding to the melting of the γ-form, whereas dehydration at a lower temperature (50°C) gave a peak corresponding to the melting of the α-form. However, the thermal behavior of levofloxacin monohydrate was not affected by the conditions under which the dehydration was carried out.

The solvent-free form II of iopanoic acid was prepared via desolvation of the benzene solvate (75). The benzene solvate was prepared by rapidly freezing a warm benzene solution of iopanoic acid in a dry ice–acetone mixture. The solid obtained was permitted to melt at room temperature, yielding crystals of the solvate suspended in benzene. When these were vacuum filtered and stored for 12 hours at 500 mbar and 70°C, form II was obtained free of benzene.

Zanoterone form II was prepared by recrystallization from ethanol and vacuum drying at 45°C (125). Form III was isolated similarly by desolvating the acetonitrile solvate at 80°C under vacuum, and was the form chosen for clinical development due to the good reproducibility of its isolation during manufacture. Similarly, forms I and II of stanozolol were obtained by heating solvates of the compound to 205°C and 130°C, respectively (126).

Crystallization with Ultrasound

The application of power ultrasound in the frequency range 20–100 kHz has been employed as means of inducing nucleation in solution crystallization (127). It has been successful in controlling nucleation and the consequent particle size distribution for a range of model compounds (128) and of some substances that are conventionally difficult to nucleate, such as sugars (129), but its use as a crystallization technique for pharmaceutical products does not appear to be widespread at present. The nucleating effect appears related to the phenomenon of ultrasonic cavitation (130), which occurs above a well-defined intensity threshold. A theoretical connection of cavitation to nucleation events is still lacking, although the most plausible suggestion has been that the pressure transient associated with cavitational collapse corresponds to a smaller critical cluster size to give rise to a viable nucleus (131).

The induction of crystal nucleation by ultrasonic cavitation has been compared with the phenomenon of seeding (127,128), which raises the interesting question of its selectivity with respect to polymorphs. Ultrasound lacks the structural templating effect of a seed crystal, and therefore, its selectivity may be expected to follow the principles that usually underlie homogeneous nucleation, such as Ostwald's rules. However, there is some evidence that ultrasound can affect polymorph selectivity, although there appear to be no consistent trends and no means of establishing the causal relationship. The formation of a metastable polymorph of 4-aminobenzoic acid has been enhanced by the application of ultrasound (132). The purity of α-glycine obtained by crystallization from water and ethanol with respect to the contaminant γ- and β-forms has been altered by the application of ultrasound in the temperature ranges 20–30°C and 40–50°C, although the effects are neither systematic nor consistent (133). There remains much work to

be done in understanding the relationship of ultrasonic cavitation to nucleation and polymorph selectivity.

Crystallization in Capillaries

Crystallization in capillary tubes is a technique often employed by crystallographers to produce a sample in situ for powder X-ray diffraction. Crystallization from solution in capillaries may also give rise to conditions that are not attained in more conventional crystallization vessels, owing to the effects of the capillary in lowering the rate of evaporation of the solvent, due to both the restricted escape path for vapor and the meniscus effect of the capillary in reducing the effective vapor pressure. It has been suggested (134) that the very slow evaporation rate in a capillary, together with the absence of nucleating agents, allows the metastable zone width to expand, providing access to metastable and unstable forms.

A polymorph screen using capillaries has been used to prepare a new metastable form of the antihyperglycemic API metformin hydrochloride (134). A screen consisting of a matrix of 28 solvents by eight evaporation conditions in capillaries was carried out. Forty-five percent of the capillary experiments resulted in powder X-ray diffraction patterns corresponding to the new metastable form B. No preferences based on solvent identity were observed; however, form B was predominant in crystallizations carried out at elevated temperature. Furthermore, capillaries of diameter 0.7 mm and 1.0 mm were tested, and the tendency to form B was more marked in the narrower bore tubes where the inhibition of solvent evaporation would be most marked. Form B remained stable for several weeks while contained in the capillary tubes, but any mechanical action such as removal of the solid appeared to promote a transition to the stable form A.

Capillary crystallization has also been employed to identify a new polymorph of nabumetone (135). The growth of high-quality single crystals of proteins has been reported (136) using methods that employ slow counter diffusion in the geometry of a capillary.

PREPARATION OF DIFFERENT TYPES OF SOLID FORMS

Solvatomorphs

As a general rule, the preparation of APIs and other pharmaceutical products as solvatomorphs is not favored. The exception to this is where the solvent is water, producing hydrates, but even here the presence of water in a product that may become labile under the conditions of the formulation is generally undesirable. Relatively few solvates with other solvents are acceptable because of the toxicity of the solvent. There are occasional exceptions where the non-solvated compound is not obtainable, has unacceptable physical properties, or may be difficult to handle and process. However, solvatomorphs may occasionally be prepared as intermediates, for example, in cases where the desired form may be produced by desolvation as described in the section "Desolvation of Hydrates and Solvatomorphs."

Compounds that exhibit a rich polymorphic landscape, that is, are able to form many polymorphs, will generally also exhibit a high propensity to form solvates. Solvate formation can sometimes be controlled by careful selection of crystallization solvents to avoid those that form the undesired solvates, but it is not at all unusual for a substance to form solvates will all viable solvents. For example,

the semi-synthetic macrolide antibiotic dirthromycin crystallizes in at least nine stoichiometric solvate forms (137), six of which are isomorphic. With water, it is not unknown for hydrates to form from water present as impurity in a different solvent, as is illustrated by the large number of hydrates reported in Table 4 (for discussion, see section "Effects of Solvent"). Also, pharmaceutical solids may come into contact with water during a wide range of processing steps including lyophilization, wet granulation, aqueous film coating, or spray drying. They may be exposed to water during storage in an atmosphere containing water vapor, or in a dosage form consisting of materials that contain water (e.g., excipients) that are capable of transferring it to other ingredients. Water may be adsorbed onto the solid surface and/or may be absorbed in the bulk solid structure.

Hydrates can exhibit polymorphism, and some substances form a series of hydrates with differing levels of hydration. Nitrofurantoin forms two monohydrates with different packing arrangements and temperatures and enthalpies of dehydration (138), and amiloride hydrochloride dihydrate has been obtained as two polymorphic forms (139). Scopolamine hydrobromide has been isolated as a hemihydrate, a sesquihydrate, and a trihydrate, all with the same molecular geometries and unit cell parameters (140). Ouabaine has been crystallized at a range of hydration levels, with the most stable form changing with temperature (141).

Hydrates are can be prepared most simply by recrystallization from water, or from a solvent mixture that contains water. For example, trazodone hydrochloride tetrahydrate has been prepared by dissolving the anhydrate in hot distilled water, allowing the solution to remain at room temperature overnight, and storing the collected crystals at 75% relative humidity and 25°C until they reached constant weight (142). Sorbitol provides another example where slow cooling of a saturated aqueous solution yields long thin needles of sorbitol hydrate (143). Acemetacin monohydrate has been obtained by slow evaporation from a mixture of acetone and water at room temperature (144).

Stable hydrates can also be obtained by suspending the anhydrous material in water. Aqueous suspensions of anhydrous metronidazole benzoate are metastable, and storage at temperatures lower then 38°C leads to monohydrate formation accompanied by crystal growth (145). When suspended in water, anhydrous carbamazepine is transformed to the dihydrate (146).

Simply exposing an anhydrous powder to high relative humidity can sometimes lead to formation of a hydrate. On exposure to a relative humidity of 100%, dexmedetomidine hydrochloride is converted to the monohydrate (147). Droloxifene citrate is an example of a compound that is not very hygroscopic and yet still forms a hydrate (148). Sorption of water only occurs when the anhydrate form is exposed to atmospheres with relative humidity above 85%. However, the monohydrate can be formed by exposing the anhydrous form to 98% relative humidity for 10 days at 24°C.

Investigations of the formation of co-crystal hydrates of theophylline and caffeine by grinding methods (149) have demonstrated different outcomes according to the methods used. The methods were: (1) grinding together "neat" solids using hydrated form(s) of one or both reactants, and (2) liquid-assisted grinding of anhydrous starting materials in the presence of liquid water. The first method can either result in an anhydrous co-crystal, as with caffeine, or steer the reaction to a co-crystal hydrate, as with theophylline. The ability to prepare an anhydrous co-crystal from a hydrated starting material may be valuable if the co-crystal has

more favorable physical or formulation characteristics. However, there are also cases where a hydrated from will be preferred, and may offer better stability and resistance to further hydration.

Techniques used for the preparation of non-aqueous solvates are generally similar to those for preparing hydrates, viz. crystallization from either the solvent forming the solvate or a mixture containing it. In some cases, it may be possible to exchange the solvating solvent by recrystallization from solution in the new solvating medium. There are also cases of "mixed" solvates in which more than one solvent is incorporated, usually of roughly comparable polarity. An exception to this is the sodium salt of the antibiotic K-41 4-bromobenzoate monohydrate *n*-hexane solvate (150), crystallized from *n*-hexane saturated with water.

As discussed in the section "Desolvation of Hydrates and Solvatomorphs," there are cases where the inclusion of a solvent is necessary to build up a stable crystal structure. For example, numerous crystallization tests on 11β-[4-(dimethylamino) phenyl-17β-hydroxy-17α-(1-propynyl)estra-4,9-diene-3-one] indicated that crystals were only obtainable in the presence of *n*-butyl acetate or *n*-propyl acetate (151). A structure determination showed that the solvent molecule had no strong interactions with the rest of the structure, and was necessary to fill empty space in the molecular packing. There are also cases of solvent molecules strengthening the crystal lattice and improving stability to solid-state decomposition, for example, the solvated structures of prenisolone *t*-butyl acetate affect the flexibility of the steroid nucleus, and hence the structure-dependent degradation of the compound when exposed to air and light (152).

Salts

Salt preparation and screening is very often carried out in drug development, for the reasons discussed in the section "Solid Forms and Their Characteristics." Table 2 lists the counter-ions most commonly encountered. It is common practice to screen a new API for suitable salt forms, particularly when the API is a free base and there is a possibility of improving its properties by combination with an anion. In principle, salt screening is usually carried out together with crystallization of the salt product, for which solution crystallization methods are by far the most common. This offers the prospect of a "one-pot" salt preparation and crystallization process, in which the free-base API and anion are combined in solution and the salt product subsequently crystallized by one of the methods described in the section "Crystallization from Solution."

Salt screening usually consists of testing the API with a selection of appropriate counter-ions in a limited range of solvents. In practice, the solvent selection is limited by compatibility with the API and the counter-ion to enable a reasonable prospect of the salt being able to form. If both the API and the counter-ion (as its acid or other suitable compound) are both soluble, then the salt will form in solution and may be crystallized by any of the methods in section "Crystallization from Solution" according to its solubility profile. Salt preparation may also be carried out in a solvent where one component (usually the counter-ion) and the salt are soluble, provided adequate contact can be made (e.g., by stirring) between the solution and the insoluble component for the latter to react and pass into solution as its salt. Generally, counter-ion acids dissolve in polar solvents, in which many recently developed APIs are not very soluble (cf. section "Solid Forms and Their Characteristics"), so this latter situation is quite common today.

In selecting suitable counter-ions, the "rule of thumb" commonly employed is that a difference in the pK_a values for the basic function of the API and the acid of the counter-anion (or vice versa) should be at least two pH units. A recent investigation of the formation of salts of the base (1R,2S)-(–)-ephedrine (153) has shown that this kind of logic can only really be applied to aqueous solvents, for which pK_a values are readily available. pK_a values for common acids in other polar solvents such as methanol can be up to five pH units higher, which will at least severely restrict the range of conditions under which salt formation can take place. The principle is shown in Figure 20 for the combination of ephedrine (pK_a 9.74) and acetic acid, a comparatively weak acid (pK_a in water 4.76). Furthermore, pK_a values for non-aqueous solvents are much less readily available and are rarely quoted. Strong acids with aqueous pK_a values less than two are generally more suitable for salt formation in non-aqueous solvents.

There are cases where salt preparation and screening cannot be carried out by simple acid-base contact, for example, APIs that have been prepared as quaternary ammonium salts. Methods employing ion exchange are usually employed in such cases. A salt screen starting from the quaternary ammonium salt tiotropium hydrobromide was carried out by initially exchanging the Br^- anion for HCO_3^- in aqueous solution using a Dowex 1x8-100Cl exchanger previous loaded with bicarbonate, and then immediately contacting the exchanged solution with the acids of the counter-ions (101). The product solutions were evaporated and the solids recrystallized from suitable solvents.

Co-crystals

In recent years, much of the research that has been carried out on the preparation of pharmaceutical solid forms has been directed to the preparation of co-crystals, as has been discussed in previous sections. Basically, there are two methods by which co-crystals may be prepared: solution-based crystallization and grinding. Opinions differ as to which is the more effective. Details of these methods and of the outcomes have been discussed in the previous four sections.

There are numerous examples of co-crystals prepared by grinding that were not obtainable by solution methods (see section "Mechanochemical Methods") (86–89), and the reasons for this are still far from clear. Also, the range of grinding conditions has been extended by the addition of solvents in the "solvent-drop" method (90), and this may represent the introduction of solution conditions on a limited scale to the grinding process. There are a number of recent developments in solution crystallization, principally in identifying the optimum region of the phase diagram to work in (98,99). Improvements in the predictability of co-crystal formation as well the development of more reliable and better understood ways in which they may be prepared are development priorities for the near future.

Preparation and Stabilization of Amorphous Forms

The option of preparing and formulating an API in its amorphous form can be preferable to its use in a crystalline form, for the reasons discussed in the section "Solid Forms and Their Characteristics." Amorphous forms invariably have higher free energies of formation than crystalline forms, and there is therefore always a thermodynamic driver toward crystallization. Given that an API is required to withstand a wide range of conditions during processing, formulation, storage, and use, it is necessary to take whatever measures are necessary to prevent crystallization. Hence,

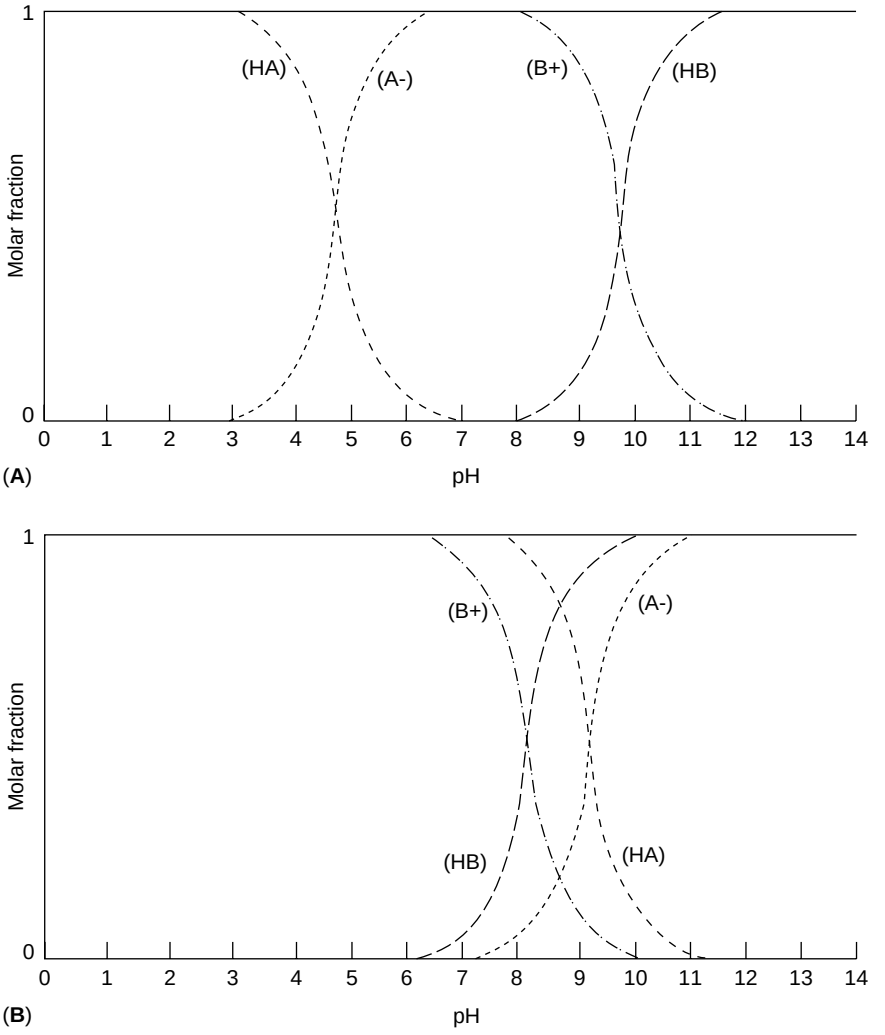

FIGURE 20 Formation of the acetate salt of (1*R*,2*S*)-(–)-ephedrine in solution in (**A**) water and (**B**) methanol. In water, the "rule" of 2 pH units works, and both cation and anion are stable in the pH range 6–9. In methanol, the pKa value of the acid is much higher (8.74) and there is no pH region in which the cation and anion are simultaneously stable (153).

there is a challenge to prevent the formation of crystalline forms of the substance, both during their preparation and also subsequently. This section will briefly outline methods that have been employed to produce pharmaceutical materials in their amorphous form, and also methods by which an amorphous active can be stabilized against subsequent crystallization.

The conditions generally required to produce an amorphous form are those that create large deviations from equilibrium during solidification. In terms of

Figures 6 and 10, they are also the conditions most likely to give rise to less stable polymorphs. These principles are consistent, because amorphous forms are less stable than crystalline forms, and also the action of forcing the solid rapidly out of its liquid phase precursor (solution or melt) will minimize the possibilities of the solid attaining an ordered structure prior to its separation. Thus, one set of methods for producing amorphous materials is to induce rapid separation or precipitation. The second type of method involves the mechanical disruption of an ordered structure using methods such as milling. Table 7 lists some examples from the literature of amorphous APIs that have been prepared by various methods within these two categories.

The method of solidification from the melt also serves to illustrate some general principles about the properties and behavior of amorphous forms. Figure 21 shows the enthalpy (or, interchangeably, specific volume) of a hypothetical substance against temperature as it cools from the melt to form either a crystalline or an amorphous solid. For the crystalline form, there is a definite enthalpy change, the enthalpy of fusion, on passing through a definite melting point T_m, following the dashed vertical line ΔH_m in Figure 21, and the crystalline form exhibits its ordered structure that is very distinct from the liquid phase. This distinction is reflected in the specific heat, corresponding to the gradient of the line for the crystalline solid, which is considerably lower than that of the liquid melt.

For transition from the liquid melt to an amorphous solid, there is no definite melting point corresponding to T_m at which a discontinuity in structure and physical properties occurs. The changes in the physical properties of the liquid as the temperature falls occur continuously and the substance becomes a supercooled liquid, following the solid line in Figure 21. Thus the viscosity increases continuously, typically to a value of around 10^{-2} poise in the supercooled liquid region. This is sufficiently high for the material to take on some of the appearances of a solid, but molecular motion still occurs and associated changes in physical form can take place over moderate timescales. Continued cooling leads to a change in physical properties when the glass transition is reached. At the glass transition T_g, the amorphous material transforms from a supercooled liquid to a glassy solid, at which point it exhibits a lower specific heat and a very much higher viscosity (typically in the region of 10^{13} poise). Under the conditions of the glassy solid, molecular motion is very much slower, and the material is much less susceptible to physical or chemical transformation.

A key objective in preparing and working with amorphous forms is to maintain the material in its glassy state, where the probability of crystallization and other changes are minimized. In practice, this means keeping the material below its T_g. T_g can be detected by DSC, where it appears as a step change in the heat capacity on heating or cooling. However, this feature indicates that the transition has already taken place, and the measured temperature often varies with the conditions of the experiment such as the heating rate. Ageing experiments on sucrose, PVP, and indomethacin (171) showed that it was necessary to lower the temperature to 50 K below T_g in order for molecular motion to be slowed to a point where it will give rise to no changes over the lifetime of a pharmaceutical product. This temperature, 50 K below T_g, appears to be the Kauzmann temperature T_k (Fig. 21), below which the time scale for molecular motion is of the order of years (172). Measured T_g values for many common drug substances are within the range of 0°C to 100°C, often in the range of ambient and body temperature, 20°C to 40°C (173). This means that the

TABLE 7 Some Examples of Drug Substances Prepared in the Amorphous State

API	Preparation method	Ref.
(1) Separation/precipitation of solid from liquid		
(1a) Solidification from the melt		
Indomethacin	Quench cooling with liquid N_2; slow cooling from the melt over 30 min.	(105)
Felodipine	Cooling in liquid N_2 or at ambient temperature.	(154)
Nifedipine	Melting at 180°C, immersion in liquid N_2.	(155)
Lovostatin	Melting under N_2, rapid cooling to 20°C below glass transition.	(156)
(1b) Spray drying		
4″-O-(4-methoxyphenyl) acetyltylosin	Spray drying a dichloromethane solution.	(157)
Salbutamol sulfate	Spray-drying aqueous solution in a Buchi 90 spray dryer.	(158)
Furosemide	Spray-drying a 4:1 chloroform:methanol solution.	(159)
Digoxin	Spray-drying an aqueous solution with hydroxypropyl methylcellulose.	(160)
(1c) Freeze drying (Lyophilization)		
Dirithromycin	Freeze drying from dichloromethane solution.	(137)
Aspirin	Freeze drying an aqueous solution with 1% hydroxypropyl-β-cyclodextrin.	(161)
Sodium ethacrynate	Rapid freezing of an aqueous solution to –50°C, freeze-drying.	(162)
Cephalothin sodium; Cefamandol sodium	Freeze-drying from a 25% aqueous solution.	(163)
(2) Mechanical disruption of an ordered structure		
(2a) Milling		
Cimetidine	Ball milling.	(164)
Calcium gluceptate	Milling in a Pulverisette 2 grinder (Fritsch) for 4 hr.	(165)
Chloramphenicol palmitate	Milling in a Pulverisette 0 grinder (Fritsch) for 85 hr.	(166)
Digoxin	Milling in a Glen Creston Model M270 ball mill for 8 hr.	(167)
(2b) Desolvation		
Tranilast anhydrate	Dehydration of the monohydrate over P_2O_5.	(168)
Erythromycin	Heating the dihydrate for 2 hr at 135°C, and then cooling to room temperature.	(169)
Calcium DL-pantothenate	Drying the methanol:water 4:1 solvate in vacuo at 50–80°C.	(170)

question of destabilization via transformation to a supercooled liquid needs to be considered in the formulation and use of the drug.

The preparation methods (1) in Table 7 aim to create amorphous materials in their glassy state by rapid transitions to the required conditions from the melt or solution, by quench-cooling the melt, by rapid evaporation of the solvent, or by freeze-drying with a combination of solvent removal and the maintenance of a low temperature both to inhibit molecular motion toward the crystalline state and to maintain the amorphous solid formed below T_g. The methods (2) in Table 7 rely on a mechanical disruption of the crystalline structure, either by externally applied mechanical means or via the disruption of a solvate and the release of solvent.

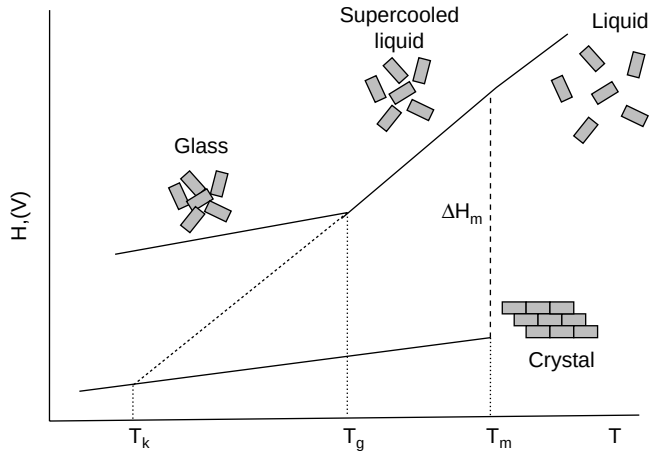

FIGURE 21 Enthalpy (or specific volume) of a substance versus temperature as it cools from the melt (*gray dashed line*) to form a crystalline solid (*gray solid and dotted line*) or an amorphous solid (*black solid*, *dashed*, *and wavy line*). The amorphous solid exists as a supercooled liquid (*wavy line*) down to the glass transition temperature T_g, below which it becomes a glassy solid. *Abbreviations*: H, enthalpy; T_g, glass transition temperature; T_k, Kauzmann temperature; T_m, melting point, V, specific volume.

The presence of impurities or additives in an amorphous solid can raise or lower the T_g significantly. In particular, the presence of water commonly acts as a plasticizer and lowers T_g, potentially undermining stability. Hygroscopicity is thus an important consideration in dealing with amorphous solids. Mixing the amorphous solid intimately with a benign substance or an excipient that can increase its T_g is a method that is often used to stabilize amorphous APIs, particular those with low T_g around room and body temperature. A number of polymers used as excipients, such a poly(N-methylpyrrolidone) (PMP) and hydroxypropylmethylcellulose (HPMC) can exert this effect, and are therefore used to confer stability on amorphous API formulations.

Mixing an amorphous API with a polymer or other stabilizer will, under favorable conditions, result in a mixture with a T_g between the values for the API and the stabilizer. The Gordon–Taylor equation is often used to identify suitable combinations of API and stabilizer. This states that the T_g of a mixture will be given as the average of the two components weighted by their proportions on a volumetric basis. Figure 22 shows some measured values for mixtures of the API itraconazole (T_g of 58°C) and HPMC (T_g of 147°C) in comparison with such predictions (174). The measured T_g values clearly deviate from the predictions in an unfavorable direction. For the Gordon–Taylor equation to be applicable, very intimate mixing of the two components is required, and the prediction takes no account of any interactions between the API and its stabilizer. The results of Figure 22 almost certainly show that mixing is imperfect, and that regions of the mixture that are enriched in itraconazole are undergoing the phase transition at temperatures closer to the T_g of the API than the prediction for the mixture.

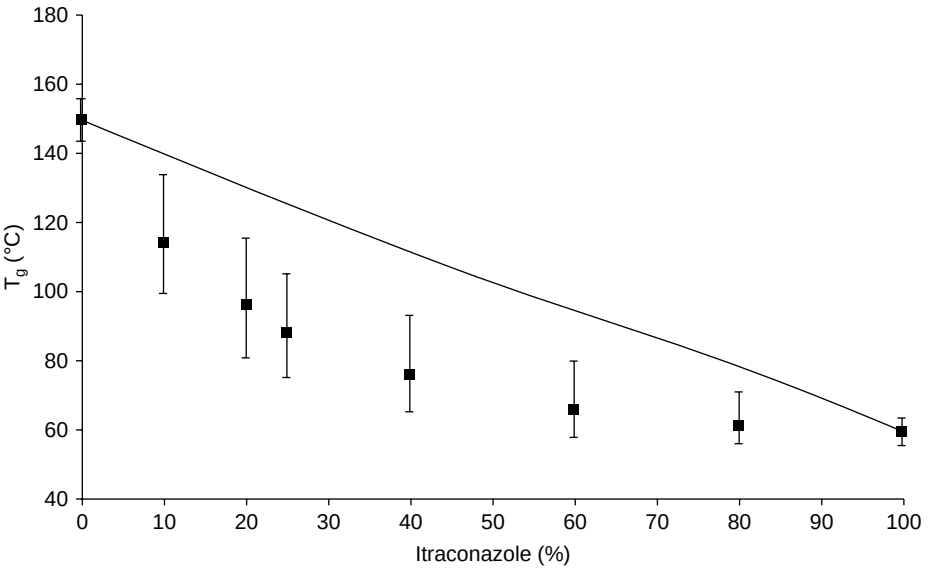

FIGURE 22 Glass transition temperatures of mixtures of itraconazole (T_g of 58°C) and HPMC (T_g of 147°C). The line indicates the predictions of the Gordon–Taylor equation. Unfavorable deviations can arise from imperfect mixing or interactions between the API and the stabilizer (174).

Figure 23 shows spatially resolved Raman mappings of mixtures of the amorphous API felodipine with the stabilizer PVP at 10, 30, and 50% API loadings (175). The maps show the ratio of the API signal at 1643 cm^{-1} to the PVP signal at 934 cm^{-1}, and indicate the efficacy of mixing of the two components, with the API-rich regions darker and the PVP-rich regions lighter. It may be seen that as the API loading increases, the number and extent of the dark regions increases. This kind of segregation, occurring particularly at high API loadings, is likely to give rise to results like those in Figure 22, where API-rich regions of the mixture undergo phase transitions at temperatures well below those predicted by the Gordon–Taylor calculation.

A comparison of mixtures of griseofulvin–PVP and indoprofen–PVP at 10–30% API loadings indicated that the tendency to disaggregate was hindered in the latter case by chemical interaction between the two components (176). Rate constants for phase separation were an order of magnitude lower than for the griseofulvin–PVP mixture where no interaction took place. Infrared spectra showed interaction between indoprofen and the PVP carbonyl function, which appeared to stabilize the composite against disaggregation.

Figure 24 shows (A) an unsuccessful and (B) a successful dispersion of an amorphous API in different types of PVP as a means of preventing crystallization (18). The API can exist in either a crystalline or an amorphous form, and powder X-ray diffraction has been used to detect any crystallinity developing within the mixture. In both cases, the mixture is amorphous on preparation and up to five days thereafter, as shown by the amorphous halo in the diffraction pattern. However, in case (A), the diffraction pattern of the crystalline API is evident after 12 days,

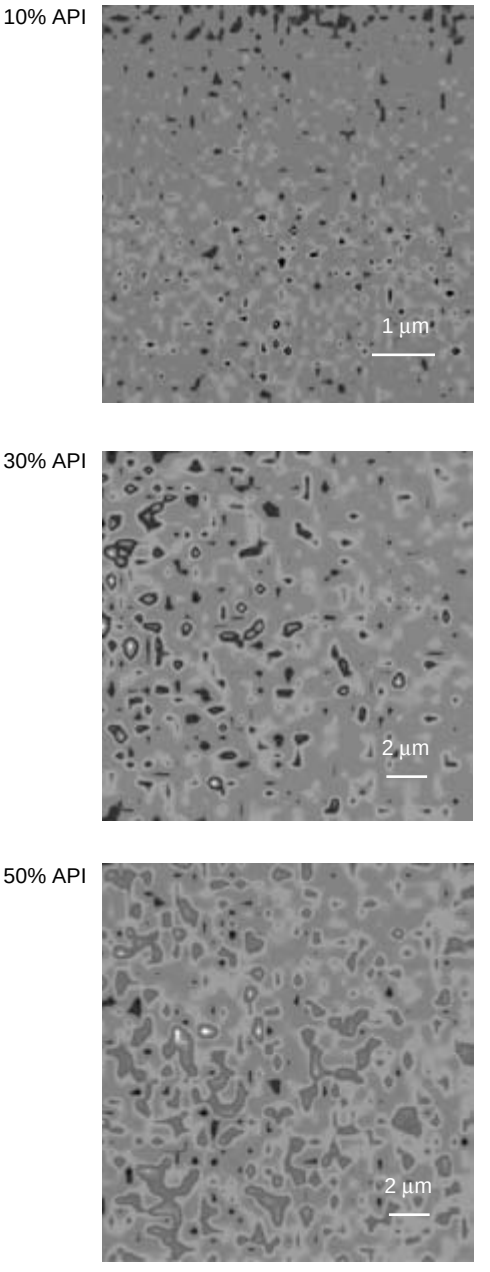

FIGURE 23 Raman mappings of mixtures of the amorphous API felodipine with PVP. The dark regions represent high levels of API, and their number and extent increases with the API loading. The presence of these enriched regions lowers the effectiveness of the stabilizer (175).

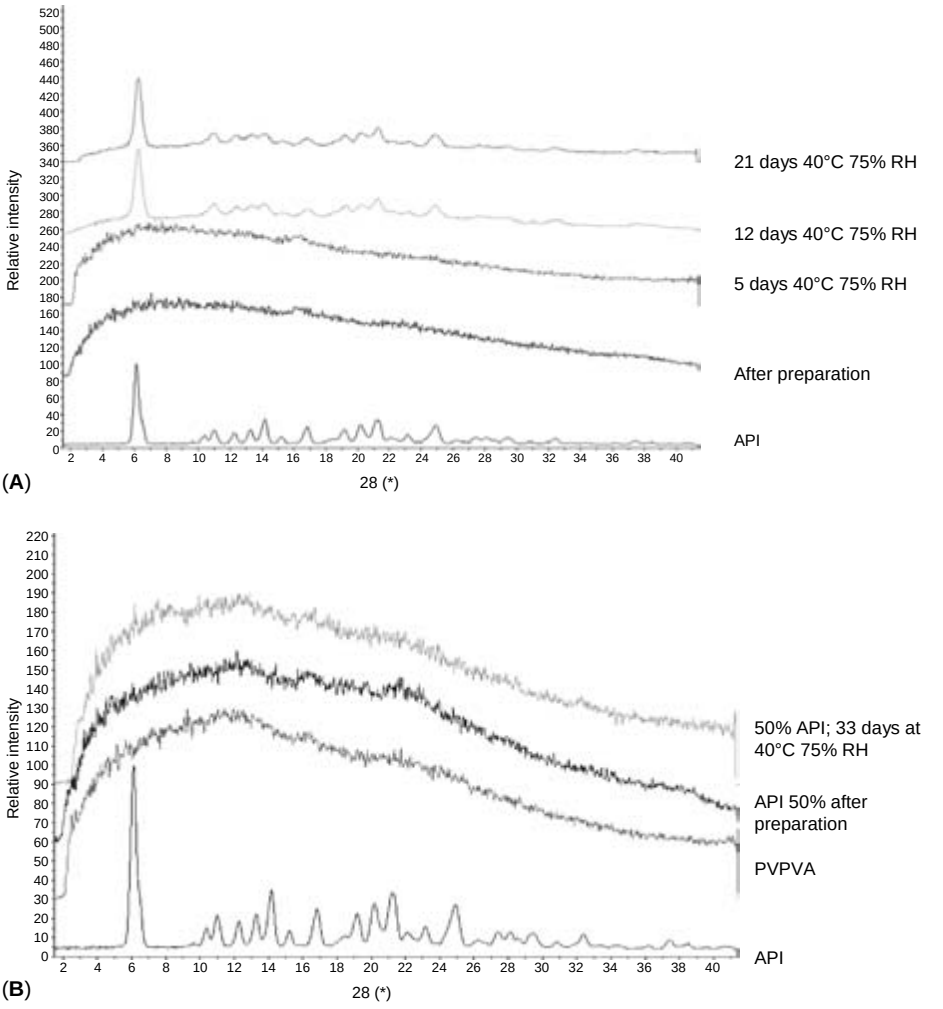

FIGURE 24 An unsuccessful (**A**) and a successful (**B**) dispersion of an amorphous API in different types of PVP, as demonstrated by powder X-ray diffraction (18). Both mixtures are amorphous on preparation, but (**A**) shows the diffraction pattern of the crystalline API after 12 days of storage. *Abbreviations*: API, active pharmaceutical ingredients; PVPVA, poly(vinylpyrrolidone) modified with vinyl acetate; RH, relative humidity.

indicating both disaggregation and crystallization of the API. In case (B), there is no evidence of the crystalline API at 33 days and beyond, and the mixture appears to remain amorphous.

ACKNOWLEDGMENTS

The author thanks Dr. Rita Ramos for supplying information on amorphous forms, and Dr. Eva Dova and Dr. Michael Millan for reading and commenting on the text.

REFERENCES

1. Lipinski CA. Drug-like properties and the causes of poor solubility and poor permeability. J Pharm Tox Methods 2000; 44: 235.
2. Hancock BC, Parks M. What is the true solubility advantage for amorphous pharmaceuticals? Pharm Res 2000; 17: 397.
3. Horspool KR, Lipinski CA. Advancing new drug delivery concepts to gain the lead. Drug Delivery Tech 2003; 3: 34.
4. Pudipeddy M, Serajuddin ATM. Trends in solubility of polymorphs. J Pharm Sci 2005; 94: 929.
5. Chemburkar SR, Bauer J, Deming K, et al. Dealing with the impact of ritonavir polymorphs on the late stages of bulk drug process development. Org Proc Res Dev 2000; 4: 413.
6. Bauer J, Spanton S, Rodger H, et al. Ritonavir. An extraordinary example of conformational polymorphism. Pharm Res 2001; 18: 859.
7. DeCamp W. FDA presentation Regulatory Issues Relating to Polymorphism. See http://www.fda.gov/cder/ondc/Presentations/WilsonDeCamp.ppt#305,9
8. Correa CM. Pharmaceutical inventions: when is the granting of a patent justified? Int J Intell Prop Mgt 2006; 1: 4.
9. McCrone WC. Fusion Methods in Chemical Microscopy. New York: Interscience, 1957.
10. Dunitz JD, Bernstein J. Disappearing polymorphs. Acc Chem Res 1995; 28: 193.
11. Ostwald W. Lehrbuch der allgemeinen Chemie. 1896; 2: 444; Engelmann, Leipzig. Studien über die Bildung und Umwandlungen fester Körper Z. Phys Chem 1897; 22: 289.
12. Cardew PT, Davey RJ. Kinetic Factors in the Appearance and Transformation of Metastable Phases. In Symp. on the Tailoring of Crystal Growth. London: Institution of Chemical Engineers, 1982: 1.1–1.9.
13. Anwar J, Boateng PK. Computer simulation of crystallization from solution. J Am Chem Soc 1998; 120: 9960.
14. Brittain HG. Polymorphism and Solvatomorphism 2004. 'Profiles of Drug Substances. Excipients, and Related Methodology'. 2005; 32: 263.
15. Hosokawa T, Datta S, Sheth AR, et al. Isostructurality among five solvates of phenylbutazone. Cryst Growth Des 2004; 4: 1195.
16. Stahl PH, Wermuth CG, eds. International Union of Pure and Applied Chemistry (IUPAC). Handbook of Pharmaceutical Salts. Properties, Selection and Use. Zürich, Wiley VCH: Verlag Helvetica Chimica Acta, 2002.
17. FDA Orange Book. See http://www.fda.gov/cder/ob/default.htm
18. Avantium Technologies BV. 2009, Unpublished data.
19. Bhatt PM, Ravindra NV, Banerjee R, et al. Saccharin as a salt former. Enhanced solubilities of saccharinates of active pharmaceutical ingredients. Chem Commun 2005: 1073.
20. Almarsson O, Bourghol Hickey M, Peterson M, et al. PCT Int Pat Appns WO 2004078161, WO 2004078163, 2004.
21. Pfeiffer P. Organische Molekülverbindungen. Stuttgart: Ferdinand Enke, 1922.
22. Vishweshwar P, McMahon J, Bis JA, et al. Pharmaceutical co-crystals. J Pharm Sci 2006; 95: 499.
23. Desiraju GR. Crystal and co-crystal. CrystEnggComm 2003; 5: 466; Dunitz JD. Crystal and co-crystal: a second opinion. CrystEnggComm 2003; 4: 506.
24. Scoppettuolo L, Peterson M, Almarsson O, et al. PCT Int Pat Appn WO 2005118577, 2005.
25. Aakeröy CB, Fasulo ME, Desper J. Cocrystal or salt: does it really matter? Mol Pharm 2007; 4: 317.
26. Huang K-S, Britton D, Etter MC, et al. A novel class of phenol – pyridine co-crystals for second harmonic generation. J Mater Chem 1997; 7: 713.
27. Videnova-Adrabinska V, Janeczko E. Urea–picoline N-oxide (4:2) cocrystal: an unusual channel inclusion compound. Chem Commun 1999: 1527.

28. Trask AV, Motherwell WDS, Jones W. Pharmaceutical cocrystallization: engineering a remedy for caffeine hydration. Cryst Growth Des 2005; 5: 1013.
29. Trask AV, Motherwell WDS, Jones W. Physical stability enhancement of theophylline via cocrystallization. Int J Pharm 2006; 320: 114.
30. Remenar JF, Morisette SL, Peterson ML, et al. Crystal engineering of novel cocrystals of a triazole drug with 1,4-dicarboxylic acids. J Am Chem Soc 2003; 125: 8456.
31. Childs SL, Chyall LJ, Dunlap JT, et al. Crystal engineering approach to forming cocrystals of amine hydrochlorides with organic acids. Molecular complexes of fluoxetine hydrochloride with benzoic, succinic and fumaric acids. J Am Chem Soc 2004; 126: 13335.
32. Dova E, Ras E-J, van Langen S, et al. Synthesis and Properties of Co-crystals of Carbamazepine with Primary Amides. Poster to Am Assoc of Pharm Scientists (AAPS) Annual Meeting & Exposition, San Diego, 11th – 15th Nov. 2007.
33. McNamara DP, Childs SL, Giordiano J. Use of a glutaric acid cocrystal to improve oral bioavailability of a low solubility API. Pharm Res 2006; 23: 1888.
34. Vanankaval N, Wenslow R, Murry J. Preparation and solid-state characterization of non-stoichiometric cocrystals of a phosphodiesterase-IV inhibitor and L-tartaric acid. Cryst Growth Des 2006; 6: 690.
35. Llinàs A, Goodman JM. Polymorph control: past, present and future. Drug Discov Today 2008; 13: 198.
36. Anderton C. Raman – a valuable technique for polymorph screening. Eur Pharm Rev 2005: 68.
37. Mullin JW. Crystallization, 4th ed. Butterworth-Heinemann, 2001.
38. Mersmann A. Crystallization Technology Handbook, 2nd ed. Marcel Dekker Inc, 2001.
39. Davey R, Garside J. 'From Molecules to Crystallizers. An Introduction to Crystallization.' (Repr. 2002), OUP, 2000.
40. CRC Handbook of Chemistry and Physics, 81st edition. CRC Press, 2000–2001: 8-102–8-110.
41. Threlfall T. Crystallization of polymorphs: thermodynamic insight into the role of solvent. Org Proc Res Dev 2000; 4: 384.
42. Bavin M. Polymorphism in process development (crystal structure transformation). Chem & Ind 1989; 21: 527.
43. Nass KK. Rational solvent selection for cooling crystallizations. Ind Engg Chem Res 1994; 33: 1580.
44. Kolář P, Shen J-W, Tsuboi A, et al. Solvent selection for pharmaceuticals. Fluid Phase Equilibria 2002; 194: 771.
45. Chen C-C, Song Y. Solubility modelling with a non-random two-liquid-segment activity coefficient model. Ind Engg Chem Res 2004; 43: 8354.
46. Behme RJ, Kensler TT, Mikolasek DG, et al. U.S. Patent 4,810,789 (to Bristol-Myers Co), 1989.
47. Kim AJ, Nail SL. AAPS Annual Meeting: Invited and Contributed Paper Abstracts. Seattle, WA: 1996: Abstract PDD7443.
48. Kaneko F, Sakashita H, Kobayashi M, et al. Infrared spectroscopic and chemical etching study on the crystallization process of the B and E forms of stearic acid – roles of dislocations in single crystals. J Phys Chem 1994; 98: 3801.
49. Byrn SR, Pfeiffer RR, Stephenson G, et al. Solid-state pharmaceutical chemistry. Chem Mater 1994; 6: 1148.
50. Davey RJ, Allen K, Blagden N, et al. Crystal engineering – nucleation, the key step. CrystEngComm 2002; 4: 257.
51. Martinez-Oharriz MC, Martin MC, Goni MM, et al. Polymorphism of diflusinal: isolation and solid-state characteristics of a new crystal form. J Pharm Sci 1994; 83: 174.
52. Wu L-S, Torosian G, Sigvardson K, et al. Investigation of moricizine hydrochloride polymorphs. J Pharm Sci 1994; 83: 1404.

53. Davey RJ, Blagden N, Righini S, et al. Crystal polymorphism as a probe for molecular self-assembly during nucleation from solutions: the case of 2,6-dihydroxybenzoic acid. Cryst Growth Des 2001; 1: 59.
54. Blagden N, Cross WI, Davey RJ, et al. Can crystal structure be used as part of an integrated strategy for ensuring maximum diversity of isolated crystal forms: the case of 2-amino-4-nitrophenol. Phys Chem Chem Phys 2001; 3: 3819.
55. Etter MC, Jahn DA, Donahue BS, et al. Growth and characterization of small molecule organic crystals. J Cryst Growth 1986; 76: 645.
56. Berkovitch-Yellin Z, Addadi L, Idelson M, et al. Gezielte Veränderungen des Kristalhabitus durch "maßgeschneiderte" Verunreinigungen: Anwendungen auf Benzamid. Angew Chem 1982; 94: 640.
57. Warstat A, Ulrich J. Optimierung von Batch-Kühlungskristallisationen. Chem Ing Tech 2007; 79: 272.
58. Kubota N, Doki N, Yokota M, et al. Seeding policy in batch cooling crystallization. Powder Tech 2001; 121: 31.
59. Doki N, Yokota M, Nakamura H, et al. Seeded batch cooling crystallization of adipic acid from ethanol solution. J Chem Engg Japan 2003; 36: 1001.
60. Loï Mi Lung-Somarriba B, Moscosa-Santillan M, Porte C, et al. Effect of seeded surface area on crystal size distribution in glycine batch cooling crystallization: a seeding methodology. J Cryst Growth 2004; 270: 634.
61. Zijlema TG, Geertman RM, Wittkamp G-J, et al. Antisolvent crystallization as an alternative to evaporative crystallization for the production of sodium chloride. Ind Engg Chem Res 2000; 39: 1330.
62. Martins PM, Rocha FA, Rein P. Modelling sucrose evaporative crystallization. Part 2. Investigation into crystal growth kinetics and solubility. Ind Engg Chem Res 2005; 44: 8865.
63. Kaneniwa N, Otsuka M, Hayashi T. Physicochemical characterization of indomethacin polymorphs and the transformation kinetics in ethanol. Chem Pharm Bull 1985; 33: 3447.
64. Burger A, Ratz AW. Polymorphie und Auflösungsverhalten von Midodrinhydrochlorid. Pharm Ind 1988; 50: 1186.
65. Beckmann W. Nucleation phenomena during the crystallization and precipitation of abercarnil. J Cryst Growth 1999; 198/9: 1307.
66. Roelands CPM, Jiang S, Kitamura M, et al. Antisolvent crystallization of the polymorphs of L-histidine as a function of supersaturation ratio and of solvent composition. Cryst Growth Des 2006; 6: 955.
67. Jiang S, ter Horst JH, Jansens PJ. Concomitant polymorphism of o-aminobenzoic acid in antisolvent crystallization. Cryst Growth Des 2008; 8: 37.
68. Kitamura M, Hironaka S. Effect of temperature on antisolvent crystallization and transformation behaviors of thiazole-derivative polymorphs. Cryst Growth Des 2006; 6: 1214.
69. Kitamura M, Sugimoto M. Antisolvent crystallization and transformation of thiazole-derivative polymorphs.–I. Effect of addition rate and initial concentrations. J Cryst Growth 2003; 257: 177.
70. Weber A, Yelash LV, Kraska T. Effect of the phase behavior of the solvent – antisolvent systems on the gas – antisolvent crystallization of paracetamol. J Supercrit Fluids 2005; 33: 107.
71. Amaro-González D, Mabe G, Zabaloy M, et al. Gas antisolvent crystallization of organic salts from aqueous solutions. J Supercrit Fluids 2000; 17: 249.
72. Reverchon E, Della Porta G, Fallivene MG. Process parameters and morphology in amoxicillin micro and submicro particles generation by supercritical antisolvent precipitation. J Supercrit Fluids 2000; 17: 239.
73. Park S-J, Yeo S-D. Antisolvent crystallization of sulfa drugs and the effect of process parameters. Separ Sci Tech 2007; 42: 2645.

74. Ulrich J, Heinrich J. Reaktivkristallisation. Chem Ing Tech 2005; 77: 1759.
75. Stagner WC, Guillory JK. Physical characterization of solid iopanoic acid forms. J Pharm Sci 1979; 68: 1005.
76. Kim BH, Kim JK. Pharmaceutical studies on the polymorphism of hydrochlorothiazide. Arch Pharm Res 1984; 7: 47.
77. Chikaraishi Y, Otsuka M, Matsuda Y. Preparation of amorphous and polymorph piretanide and their physicochemical properties and solubilities. Chem Pharm Bull 1996; 44: 1614.
78. Chen S, Guzei IA, Yu LJ. New polymorphs of ROY and new record for coexisting polymorphs of solved structures. Am Chem Soc 2005; 127: 9881.
79. Rambaud J, Bouassals A, Pauvert B, et al. Comparative study of the two polymorphic forms of p-(1R,3S)-thioanisoyl-1,2,2-trimethylcyclopentane carboxylic acid. J Pharm Sci 1993; 82: 1262.
80. Perrenot B, Widmann G. Polymorphism by differential scanning calorimetry. Thermochim Acta 1994; 234: 31.
81. Köfler L, Köfler A. Thermomikromethoden. Weinheim: Verlag Chemie, 1954.
82. Childs SL. PCT Int Pat Appn WO/2007/067727, 2007.
83. Berry DJ, Seaton CC, Clegg W, et al. Applying hot-stage microscopy to co-crystal screening: a study of nicotinamide with seven active pharmaceutical ingredients. Cryst Growth Des 2008; 8: 1697.
84. Lu E, Rodriguez-Hornedo N, Suryanarayanan R. A rapid thermal method for co-crystal screening. CrystEngComm 2008; 10: 665.
85. Ling AR, Baker JL. Halogen derivatives of quinone. Part III. Derivatives of quinhydrone. J Chem Soc 1893; 63: 1314.
86. Etter MC, Adsmond DA. The use of cocrystallization as a method of studying hydrogen bond preferences of 2-aminopyrimidine. J Chem Soc Chem Commun 1990: 589.
87. Etter MC, Reutzel SM, Choo CG. Self-organization of adenine and thymine in the solid state. J Am Chem Soc 1993; 115: 4411.
88. Otsuka M, Otsuka K, Kaneniwa N. Relation between polymorphic transformation pathway during grinding and the physicochemical properties of bulk powders for pharmaceutical preparations. Drug Dev Ind Pharm 1994; 20: 1649.
89. Pirttimaki J, Laine E, Ketolainen J, et al. Effects of grinding and compression on crystal structure of anhydrous caffeine. Int J Pharm 1993; 95: 93.
90. Shan N, Toda F, Jones W. Mechanochemistry and co-crystal formation: effect of solvent on reaction kinetics. Chem Commun 2002, 2372.
91. Trask AV, Motherwell WDS, Jones W. Solvent-drop grinding: green polymorph control of crystallization. Chem Commun 2004: 890.
92. Byrn SR. Solid State Chemistry of Drugs. New York: Academic Press, 1982; See also same title by Byrn SR, Pfeiffer RR, Stowell JG. West Lafayette: SSCI Inc, 1999.
93. Crowley KJ, Zografi G. Cryogenic grinding of indomethacin polymorphs and solvates: assessment of amorphous phase formation and amorphous phase physical stability. J Pharm Sci 2002; 91: 492.
94. Fecht HJ. Defect-induced melting and solid-state amorphization. Nature 1992; 356: 133.
95. Otsuka M, Kaneniwa N. A kinetic study of the crystallization process of noncrystalline indomethacin under isothermal conditions. Chem Pharm Bull 1988; 36: 4026; Otsuka M, Matsumoto T, Kaneniwa N. Effect of environmental temperature on polymorphic solid-state transformation of indomethacin during grinding. Ibid 1986; 34: 1784.
96. Oguchi T, Kazama K, Fukami T, et al. Specific complexation of ursodeoxycholic acid with guest compounds induced by co-grinding. II. Effect of grinding temperature on the mechanochemical complexation. Bull Chem Soc Japan 2003; 76: 515.
97. Jayasankar A, Somwangthanaroj A, Shao ZJ, et al. Cocrystal formation during cogrinding and storage is mediated by amorphous phase. Pharm Res 2006; 23: 2381.
98. Chiarella RA, Davey RJ, Peterson ML. Making co-crystals – the utility of ternary phase diagrams. Cryst Growth Des 2007; 7: 1223.

99. Ter Horst JH, Deij MA, Cains PW. Discovering new co-crystals. Cryst Growth Des 2009; 9: 1531.
100. Ter Horst JH, Cains PW. Co-crystal polymorphs from a solvent mediated transformation. Cryst Growth Des 2008; 8: 2537.
101. Pop M, Sieger P, Cains PWJ. Tiotropium fumarate: an interesting pharmaceutical co-crystal. J Pharm Sci 2009; 98: 1821.
102. Otsuka M, Effects of environmental temperature and compression energy on polymorphic transformation during tabletting. Drug Dev Ind Pharm 1993; 19: 2241.
103. Uchida T, Yonemochi E, Oguchi T, et al. Polymorphism of tegafur: physicochemical properties of four polymorphs. Chem Pharm Bull 1993; 41: 1632.
104. Shakhtshneider TP, Boldyrev VV. Phase transformations in sulfathiazole during mechanical activation. Drug Dev Ind Pharm 1993; 19: 2055.
105. Yoshioka M, Hancock BC, Zografi G. Crystallization of indomethacin from the amorphous state below and above its glass transition temperature. J Pharm Sci 1994; 83: 1700.
106. Kuhnert-Brandstätter, M. Thermomicroscopy in the Analysis of Pharmaceuticals. Oxford: Pergamon Press, 1971.
107. Tsai S-Y, Kuo S-C, Lin S-Y. Physicochemical characterization of 9,10-anthroquinone-2-carboxylic acid. J Pharm Sci 1993; 82: 1250.
108. Fokkens JG, van Amelsfoort JGM, de Blaey CJ, et al. A thermodynamic study of the solubility of theophylline and its hydrate. Int J Pharm 1983; 14: 79.
109. Sakiyama M, Imamura A. Thermoanalytical characterization of 1,3-dimethyluracil and malonamide crystals. Thermochim Acta 1989; 142: 365.
110. Sun C. Solid-state properties and crystallization behavior of PHA-739521 polymorphs. Int J Pharm 2006; 319: 114.
111. Gu C-H, Young V, Grant DJW. Polymorph screening: influence of solvents on the rate of solvent-mediated polymorphic transformation. J Pharm Sci 2001; 90: 1878.
112. Zhang GGZ, Henry RF, Borchardt TB, et al. Efficient co-crystal screening using solution-mediated phase transformation. J Pharm Sci 2007; 96: 990.
113. Keel TR, Thompson C, Davies MC, et al. AFM studies of the crystallization and habit modification of an excipient material, adipic acid. Int J Pharm 2004; 280: 185.
114. Addadi L, Berkovitch-Yellin Z, Weissbuch I, et al. Growth and dissolution of organic crystals with "tailor-made" inhibitors – implications in stereochemistry and materials science. Angew Chem Int Engl Ed 1985; 24: 466.
115. Weissbuch I, Leiserowitz L, Lahav M. "Tailor-made" and charge transfer auxiliaries for the control of the crystal polymorphism of glycine. Adv Materials 1994; 6: 952.
116. Weissbuch I, Addadi L, Leiserowitz L, et al. Molecular recognition at crystal interfaces. Science 1991; 253: 637.
117. Davey RJ, Maginn SJ, Andrews SJ, et al. Morphology and polymorphism in molecular crystals: terephthalic acid. J Chem Soc Farad Trans 1994; 90: 1013.
118. Ikeda K, Saitoh I, Oguma T, et al. Effect of hydrophobically-modified hydroxypropylmethylcellulose on the crystallization from supersaturated solutions of indomethacin. Chem Pharm Bull 1994; 42: 2320.
119. Lang MD, Grzesiak AL, Matzger AJ. The use of polymer heteronuclei for crystalline polymorph selection. Am Chem Soc 2002; 124: 14834.
120. Lang MD, Kampf JW, Matzger AJ. Form IV of carbamazepine. J Pharm Sci 2002; 91: 1186.
121. Price CP, Grzesiak AL, Matzger AJ. Crystalline polymorph selection and discovery with polymer heteronuclei. J Am Chem Soc 2005; 127: 5512.
122. Bjerga-Bjaen A-K, Nord K, Furuseth S, et al. Polymorphism of chloroquine diphosphate. Int J Pharm 1993; 92: 183.
123. Jasti BR, Du J, Vasavada RC. Characterization of thermal behavior of etoposide. Int J Pharm 1995; 118: 161.

124. Kitaoka H, Wada C, Moroi R, et al. Effect of dehydration on the formation of levofloxacin pseudopolymorphs. Chem Pharm Bull 1995; 43: 649.
125. Rocco WL, Morphet C, Laughlin SM. Solid-state characterization of zanoterone. Int J Pharm 1995; 122: 17.
126. Rocco WL, Winthrop S. Solid state characterization of stanozolol. Drug Dev Ind Pharm 1994; 20: 1831.
127. Ruecroft G, Hipkiss D, Ly T, et al. Sonocrystallization: the use of ultrasound for improved industrial crystallization. Org Proc Res Dev 2005; 9: 923.
128. McCausland LJ, Cains PW, Maxwell M. Sonocrystallization – the use of power ultrasound to control and manipulate the nucleation of crystals. Chem-Ing-Tech 2001; 73: 717.
129. McCausland LJ, Cains PW. Power ultrasound – a means to promote and control crystallization in biotechnology. Biotech & Genet Engg Revs 2004; 21: 3.
130. Young FR. Cavitation. McGraw-Hill, 1989.
131. Virone C, Kramer HJM, van Rosmalen GM, et al. Primary nucleation induced by ultrasonic cavitation. J Cryst Growth 2006; 294: 9.
132. Gracin S, Uusi-Penttilä M, Rasmuson ÅC. Influence of ultrasound on the nucleation of polymorphs of p-aminobenzoic acid. Cryst Growth Des 2005; 5: 1787.
133. Louhi-Kultanen M, Karlajainen M, Rantanen J, et al. Crystallization of glycine with ultrasound. Int J Pharm 2006; 320: 23.
134. Childs SL, Chyall LJ, Dunlap JT, et al. A metastable polymorph of metformin hydrochloride: isolation and characterization using capillary crystallization and thermal microscopy techniques. Cryst Growth Des 2004; 4: 441.
135. Chyall LJ, Tower JM, Coates DJ, et al. Polymorph generation in capillary spaces: the preparation and structural analysis of a metastable polymorph of nabumetone. Cryst Growth Des 2002; 2: 505.
136. Biertumpfel C, Basquin J, Suck D, et al. Crystallization of biological macromolecules using agarose gel. Acta Cryst D 2002; 58: 1657.
137. Stephenson GA, Stowell JG, Toma PH, et al. Solid-state analysis of polymorphic, isomorphic and solvated forms of dirithromycin. J Am Chem Soc 1994; 116: 5766.
138. Caira MR, Pienaar EW, Lotter AP. Polymorphism and pseudopolymorphism of the antibacterial nitrofurantoin. Mol Cryst Liq Cryst 1996; 279: 241.
139. Jozwiakowski MJ, Williams SO, Hathaway RD. Relative physical stability of the solid forms of amiloride HCl. Int J Pharm 1993; 91: 195.
140. Michel A, Drouin M, Glaser R. Solid-state stereochemistry of (-)-scopolamine hydrobromide sesquihydrate, a new polymorph of the anticholinergic drug. J Pharm Sci 1994; 83: 508.
141. Giron D. Thermal analysis and calorimetric methods in the characterization of polymorphs and solvates. Thermochim Acta 1995; 248: 1.
142. Sasaki K, Suzuki H, Nakagawa H. Physicochemical characterization of trazodone hydrochloride tetrahydrate. Chem Pharm Bull 1993; 41: 325.
143. Cammenga HK, Steppuhn ID. Polymorphic status of sorbitol: solution calorimetry versus DSC. Thermochim Acta 1993; 229: 253.
144. Burger A, Lettenbichler A. Polymorphie und Pseudopolymorphie von Acemetacin. Pharmazie 1993; 48: 262.
145. Caira MR, Nassimbeni LR, van Oudtshoorn B. X-ray structural characterization of anhydrous metronidazole benzoate and metronidazole benzoate monohydrate. J Pharm Sci 1993; 82: 1006.
146. Young WWL, Suryanarayanan R. Kinetics of transition of anhydrous carbamazepine to carbamazepine dihydrate in aqueous suspensions. J Pharm Sci 1991; 80: 496.
147. Rajala R, Laine E, Örn G. Characterization and hygroscopic properties of dexmedetomidine hydrochloride, a new drug substance. Eur J Pharm Sci 1994; 1: 219.
148. Burger A, Lettenbichler A. Preformulation studies in droloxifene citrate pseudopolymorphism and hygroscopicity. Eur J Pharm Biopharm 1993; 39: 64.

149. Karki S, Friščić T, Jones W, et al. Screening for pharmaceutical cocrystal hydrates via neat and liquid-assisted grinding. Mol Pharm 2007; 4: 347–54.
150. Shiro M, Nakai H, Nagashima K, et al. X-ray determination of the structure of the polyether antibiotic K-41. J Chem Soc Chem Commun 1978: 682.
151. van Geerestein VJ, Kanters JA, van der Sluis P, et al. Structure of the n-butyl acetate solvate of 11β-[4-(dimethylamino)phenyl]-17β-hydroxy-17α-(1-propynyl)estra-4,9-dien-3-one. Acta Cryst C 1986; 42: 1521.
152. Byrn SR, Sutton PA, Tobias B, et al. Crystal structure, solid-state NMR spectra, and oxygen reactivity of five crystal forms of prednisolone tert-butylacetate. Am Chem Soc 1988; 110: 1609.
153. Black SN, Collier EA, Davey RJ, et al. Structure, solubility, screening and synthesis of molecular salts. J Pharm Sci 2007; 96: 1053.
154. Srcic S, Kerc J, Urleb U, et al. Investigation of felodipine polymorphism in its glassy state. Int J Pharm 1992; 87: 1.
155. Aso Y, Yoshioka S, Otsuka T, et al. The physical stability of amorphous nifedipine determined by isothermal microcalorimetry. Chem Pharm Bull 1995; 43: 300.
156. Elder JP. A new accelerated oxidative stability test for glass-forming organic compounds. Thermochim Acta 1990; 166: 199.
157. Yamaguchi T, Nishimura M, Okamoto R, et al. Glass formation of 4''-O-(4-methoxyphenyl)acetyltylosin and physicochemical stability of the amorphous solid. Int J Pharm 1992; 85: 87.
158. Buckton G, Darcy P, Greenleaf D, et al. The use of isothermal microcalorimetry in the study of changes in crystallinity of spray-dried salbutamol sulphate. Int J Pharm 1995; 116: 113.
159. Matsuda Y, Otsuka M, Once M, et al. J Pharm Pharmacol 1992; 44: 627.
160. Nimberg E, Dolle B, Bafort JM. Pharm Ind 1982; 44: 630.
161. Suryanarayanan R, Mitchell AG. Phase transitions of calcium gluceptate. Int J Pharm 1986; 32: 213.
162. Yarwood RJ, Phillips AJ, Collett JH. Processing factors influencing the stability of freeze dried sodium ethacynate. Drug Dev Ind Pharm 1986; 12: 2157.
163. Pikal MJ, Dellerman KM. Stability testing of pharmaceuticals by high-sensitivity isothermal calorimetry at 25°C: cephalosporins in the solid and aqueous solution states. Int J Pharm 1989; 50: 233.
164. Bauer-Brandl A. Polymorphic transitions of cimetidine during manufacture of solid dosage forms. Int J Pharm 1996; 140: 195.
165. Suryanarayanan R, Mitchell AG. Evaluation of two concepts of crystallinity using calcium gluceptate as a model compound. Int J Pharm 1985; 24: 1.
166. Fomi F, Iannuccelli V, Cameroni R. J Pharm Pharmacol 1987; 39: 1041.
167. Florence AT, Salole EG. Changes in crystallinity and solubility on comminution of digoxin and observations on spironalactone. J Pharm Pharmacol 1976; 28: 637.
168. Kawashima Y, Niwa T, Takeuchi H. Characterization of polymorphs of tranilast monohydrate when crystallized by two solvent change spherical crystallization techniques. J Pharm Sci 1991; 80: 472.
169. Laine E, Kahela P, Rajala R. Crystal forms and bioavailability of erythromycin. Int J Pharm 1987; 38: 33.
170. Inagaki ME. Crystal forms and optical resolution by preferential crystallization of calcium DL-pantothenate. Chem Pharm Bull 1977; 25: 1001.
171. Hancock BC, Shamblin SL, Zografi G. Molecular mobility of pharmaceutical solids below the glass transition temperature. Pharm Res 1995; 12: 799.
172. Shamblin SL, Tang X, Chang L, et al. Characterization of the time scales of molecular motion in pharmaceutically important glasses. J Phys Chem 1999; 103: 4113.
173. Fukuoka E, Makita M, Yamamura S. Glassy state of pharmaceuticals. III. Thermal properties and stability of glassy pharmaceuticals and their binary glass systems. Chem Pharm Bull 1989; 37: 1047.

174. Six K, Berghmans H, Leuner C. Characterization of solid dispersions of itraconazole and hydroxypropylmethylcellulose prepared by melt extrusion. Part II. Pharm Res 2003; 20: 1047.
175. Karavas E, Georgarakis M, Docoslis A, et al. Combining SEM, TEM, and micro-Raman techniques to differentiate between the amorphous molecular level dispersions and nanodispersions of a poorly water-soluble drug within a polymer matrix. Int J Pharm 2007; 340: 76.
176. Vasanthavada M, Tong W-Q, Yatindra J, et al. Phase behavior of amorphous molecular dispersions. II. Role of hydrogen bonding on solid solubility and phase separation kinetics. Pharm Res 2005; 22: 440.

5 Approaches to High-Throughput Physical Form Screening and Discovery

Alastair J. Florence

Solid-State Research Group, Strathclyde Institute of Pharmacy and Biomedical Sciences, University of Strathclyde, Glasgow, U.K.

INTRODUCTION

The development of experimental methods for increasing the throughput and efficiency of all stages of drug discovery and development is an important area of research within the pharmaceutical industry. In the context of physical form discovery of pharmaceuticals, the fundamental aim when establishing a rigorous experimental crystallization search strategy is to achieve as wide a coverage of crystallization conditions and methods as possible within the constraints of available time, material, and resources. For the purposes of this chapter, physical form will be taken to mean any solid form of the compound being examined, whether crystalline (polymorphs, solvates, salts, and co-crystals) or non-crystalline (amorphous). Automated crystallization approaches allow the basic process steps involved in a typical manual solution recrystallization method (Fig. 1) to be efficiently replicated over large numbers of parallel experiments. In principle, this enables the routine implementation of search strategies designed to maximize the diversity of crystallization conditions tested, allowing the experimental search to be carried out over a finer grid (e.g., a larger solvent library).

A significant driver for the development and application of automated crystallization approaches has come from the need during pre-clinical drug development of a new chemical entity to identify the complete range of solid forms, and their associated properties, as quickly and efficiently as possible (1–4). It is also necessary to control polymorphism in generic product development and manufacture (5). However, the selection of effective approaches for finding polymorphs can also be complicated by the limited, sometimes milligram, amounts of compound available during the earliest stages of drug development for the initial assessment of polymorphism (4,6). In this context, automated and parallel crystallization methodologies offer distinct advantages.

A comprehensive knowledge of solid-state diversity can add considerable value to the product development cycle, informing the control of raw material crystallization, scale-up, formulation and product manufacturing processes, and minimizing the risk of unexpected polymorphs appearing during later stages in the compound's development and production. The enumeration of all solid forms of a novel active pharmaceutical ingredient (API) at an early stage in its development also adds significant value by supporting robust intellectual property (IP) protection (7).

In one high-throughput crystallization study summarized in Table 1, the authors estimated a 120-fold increase in efficiency over manual approaches alone realized through a combination of the increased number of trials carried out in parallel and the increased speed at which individual experiments were implemented (9).

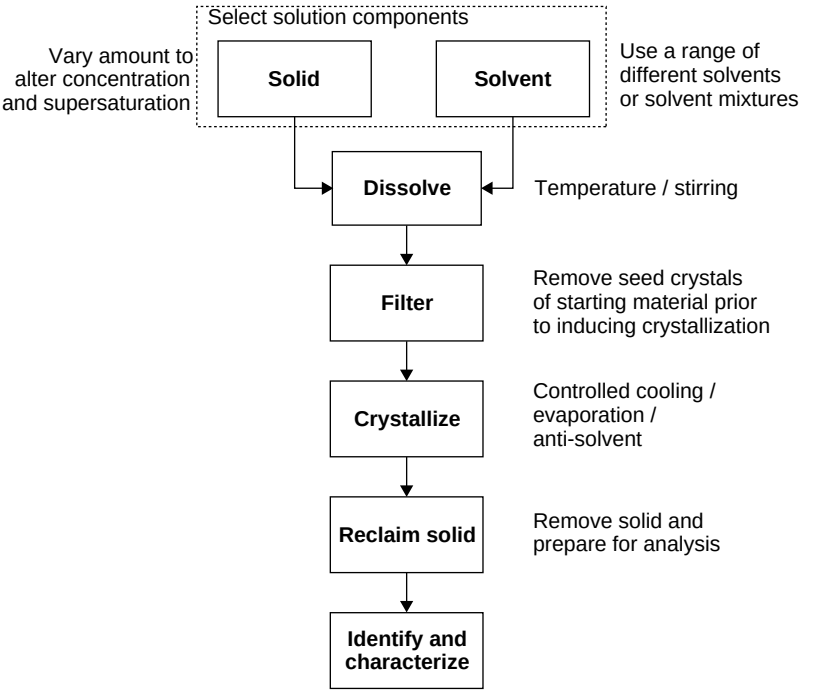

FIGURE 1 Process steps and variables in a typical manual solution crystallization experiment. In the context of an experimental physical form search, the aim is to explore factors that may influence the thermodynamic and/or kinetic control of nucleation and crystal growth.

The results in Table 1 highlight some important issues when considering the value of developing and implementing automated or high-throughput crystallization technologies. For example, the high-throughput approach was significantly more effective in finding diverse crystalline forms of MK-996 within a much shorter period of time than with manual methods. This was due to the greater search-space accessed using the high-throughput approach. The use of parallel approaches also enabled the entire study to be completed in an eighth of the time compared with manual methods and from only half the total amount of compound. The increased scale of the investigation also increases confidence that all forms have been observed and provides information on the reproducibility with which specific polymorphs can be obtained. The search on MK-996 (9) also generated one form, form D, that the original study (8) identified as being difficult to obtain once a more stable form I had been produced. High-throughput studies on acetaminophen (10) and ritonavir (11) also demonstrate the benefit of high-throughput methods for identifying multiple sets of conditions that produce each specific form.

High-throughput crystallization studies rely on large numbers of small-scale individual crystallizations (e.g., microliter scale crystallizations utilizing micrograms of API) carried out in parallel using multi-well plate or rack formats. These approaches rely on the extensive use of automation to carry out thousands of crystallizations as part of the screen, utilizing robotics and computer control to implement some or all

TABLE 1 A Comparison of Performance Criteria for Manual and High-Throughput Crystallization Studies on the Compound MK-996 (8)

	Manual methods	**High-throughput methods**
Number of crystallizations implemented	100	1500
Time scale of study	Approximately 32 weeks	4 weeks
Total amount of compound used	More than 10 grams	Less than 5 grams
Number of crystalline forms observed	9	18

Source: Data taken from Ref. (9).

aspects of each crystallization process. Many systems are available for automated liquid handling, for example, and these have been applied to great effect in structural biology to screen protein nucleation and crystal growth conditions for the production of diffraction quality samples (12). Whatever the type of solute being studied, the development of high-throughput methods has focused on crystallization techniques that are well suited to automation, miniaturization, and parallelization. For small molecule pharmaceuticals, automated solution crystallization has been the most widely applied to date. This section will outline methods and strategies based on high-throughput, automated, or parallel technologies that have been developed to increase the throughput and efficiency of crystallization searches for solid forms of APIs.

THE EXTENT OF PHYSICAL FORM DIVERSITY

The crystal energy landscape describes all possible crystal structures that a molecule may adopt (13). To isolate all of the possible forms requires an extensive experimental survey, and the more rigorous the search, the more confident we can be that all relevant forms have been observed. For practical purposes, "relevant forms" might only include the most stable form (14) and those that may be produced during the specific synthetic, bulk crystallization, and product manufacturing processes to which the compound will be exposed or, perhaps only those forms that are stable at ambient temperature. Unfortunately, it is not currently possible to know at the outset of any experimental search exactly how many polymorphs a given compound will actually produce. Indeed, some molecules may not display polymorphism, Pigment Yellow 74 (15), for example, regardless of the number and type of crystallizations that are carried out, although others may produce many polymorphs and solvates.

Although methods for crystal structure prediction (CSP) have advanced considerably in recent years, they are not currently able to cope routinely with the molecular complexity of many large, conformationally flexible pharmaceutical APIs. However, as CSP technologies continue to advance so there is increased potential to exploit theoretical structure prediction as a tool to inform and interpret experimental searches. For example, a CSP study may indicate that a molecule is likely to be polymorphic, establishing the need to implement a rigorous search. Or, where an experimental search finds the most probable predicted form(s), this would increase confidence that all of the likely forms that fall within the scope of the CSP search had been observed (e.g., $Z' < 1$ structures, most common space groups). Experimental searches can also locate forms that typically lie outside the scope of typical CSP

searches (e.g., $Z' > 1$ structures, less common space groups, disordered solids, solvates). Alternatively, if the most probable forms from the CSP are not actually observed by experiment, this may suggest that kinetic, rather than thermodynamic, factors determine which of the energetically feasible crystal structures are observed. The potential value of CSP is not restricted to polymorphs but can also be used to provide a more complete view of the favorable motifs that underpin solvate formation. For example, an automated parallel crystallization study of the thiazide diuretic, hydrochlorothiazide, found two polymorphs and seven solvates (16). An associated CSP study generated ca. 60 energetically feasible crystal structures, including both polymorphs. The study identified, a range of recurrent bimolecular hydrogen-bonded motifs in the predicted structures that were also observed among the experimental solvate crystal structures.

Maximizing the Number of Physical Forms Observed

The actual number of solid forms identified by an experimental screen may represent only a subset of all thermodynamically feasible structures. The temperature, pressure, and supersaturation (solubility) ranges that are practically accessible in an experimental search, as well as the chemical stability of the compound, all limit the diversity of crystallization conditions to which a given molecule can be exposed, and so potentially restrict the range of forms that can be observed.

Figure 2 shows a schematic representation of an idealized "experimental space" for a physical form search that combines several crystallization techniques. The outer box represents all possible structures that the molecule could adopt under all conditions, and the inner box represents the subset of all forms that are of direct relevance to pharmaceutical applications. The shaded areas represent experimental space accessible by each crystallization technique. Some forms may be observed only by one particular method, whereas others may be produced by several different techniques. Thus, the total number of forms observed may, in principle, be increased by maximizing the total shaded area, or diversity of crystallization conditions, covered in the screen. This can be achieved by (i) combining multiple crystallization techniques and (ii) maximizing the scope, or breadth of conditions tested, by each technique. Automated parallel approaches to crystallization can help to achieve these aims.

For example, the anti-epileptic compound carbamazepine has four known polymorphic forms (17–20) in addition to a wide variety of solvates (21–23) and co-crystals (24–28) (Table 2). Although the compound has been subjected to a wide range of crystallization studies with thousands of individual crystallizations, the *C*-centered polymorph form IV, has only been recovered by recrystallization from solution in the presence of polymers (19,29).

Crystallization Methods

There are many ingenious means of recrystallization that have been demonstrated to be effective for exploring solid-state diversity. These include vapor (30) or liquid–liquid (31) diffusion, sublimation (32), thermal analysis (33) and hot-stage microscopy (34), slurrying (35), contact line crystallization (36), potentiometric cycling (37), neat and solvent-assisted grinding (38,39), high-pressure crystallization (40,41), epitaxial growth on crystalline substrates (42) or templating using various materials (29,43–48), supercritical fluids (49), laser-induced nucleation (50), and capillary crystallization (51). Clearly, with such considerable variety of experimental approaches to choose from, it is not logistically possible to cover all possibilities

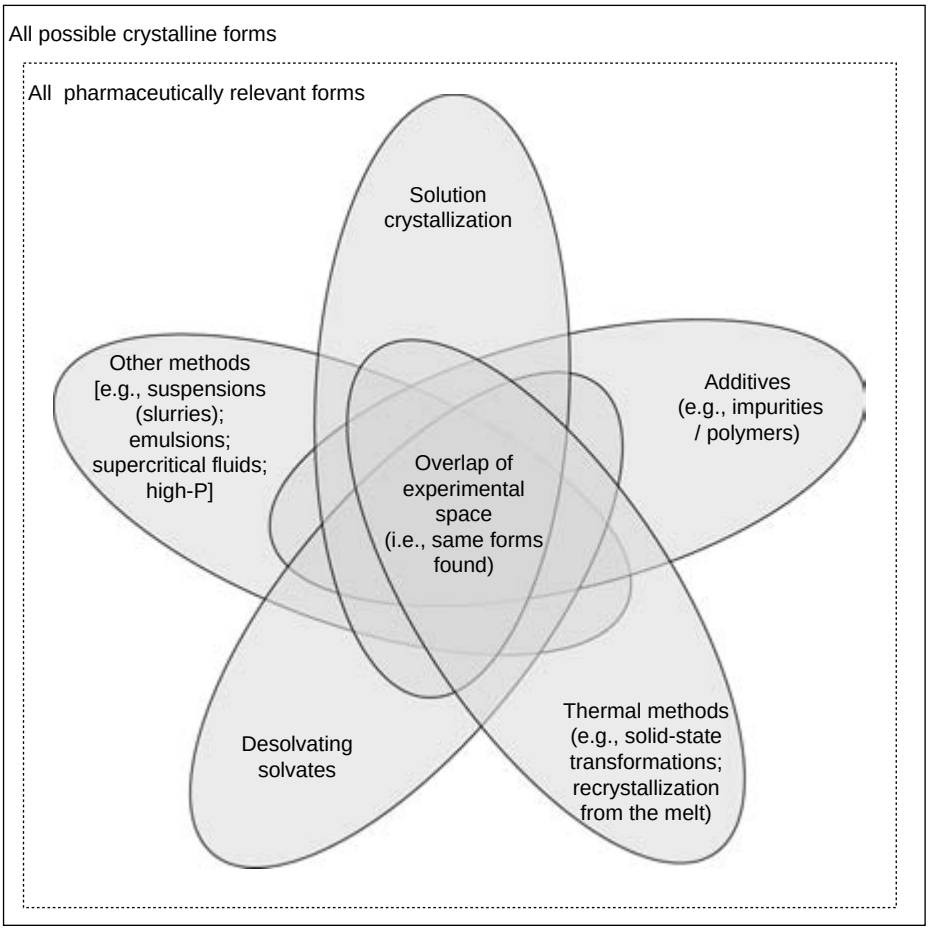
All possible crystalline forms
All pharmaceutically relevant forms
Solution crystallization
Other methods [e.g., suspensions (slurries); emulsions; supercritical fluids; high-P]
Additives (e.g., impurities / polymers)
Overlap of experimental space (i.e., same forms found)
Desolvating solvates
Thermal methods (e.g., solid-state transformations; recrystallization from the melt)

FIGURE 2 Schematic illustration of the relationship between all possible crystalline forms and the coverage of experimental space using different techniques.

TABLE 2 Structural Parameters for the Four Reported Polymorphic Forms of Carbamazepine [5H-dibenzo(b,f)azepine-5-carboxamide; $C_{15}H_{12}N_2O$, Mol. Wt. = 236.3]

Form	Crystal system/ space group	*a*, *b*, *c* (Å)	α, β, γ (°)
I	Triclinic,	5.171(1), 20.574(2), 22.245(2)	84.12(4), 88.01(4), 85.19(4)
II	Trigonal, $R\bar{3}$	35.454(3), 35.454(3), 5.253(1)	90, 90, 120
III	Monoclinic, $P2_1/n$	7.537(1), 11.156(2), 13.912(3)	90, 92.86(2), 90
IV	Monoclinic, $C2/c$	26.609, 6.927, 13.957	90, 109.72, 90

systematically in a grid-type search. So, although the application of multiple experimental techniques remains an important aspect of comprehensive polymorph screening, crystallization from solution remains the most widely employed method in automated large-scale crystallization studies. The majority of typical steps in solution crystallization (Fig. 1) are readily amenable to automation, allowing various parameters that may influence nucleation and crystal growth from solution to be rigorously tested using efficient parallel experimental approaches.

Automated Parallel Crystallization

The inherent challenges of implementing large numbers of experiments under different conditions in a comprehensive search can be addressed by carrying out experiments in parallel. This is at the core of high-throughput polymorph screening methods that combine parallel experiments with automation and miniaturization to maximize efficiency and provide an early indication of the extent of polymorphism and solvate formation in the compound being studied (3,9–11,52,53). Figure 3 shows an overview of the main components of a physical form search strategy, spanning the selection of crystallization methods and experimental variables, the implementation of individual crystallizations and identification of samples to the complete characterization of all solid forms that are discovered.

The design phase involves the selection of specific methods and diverse conditions to be used in the screen. Once crystallization protocols have been established, these are translated into instrument controls to allow the robotic platform to implement the required experiments. Visual, or optical, inspection of individual crystallizations allows the presence of recrystallized solid to be detected, often triggering a sample preparation or retrieval step (e.g., removal of solution). Samples are next subjected to physical analysis to identify each specific form produced from the experiments performed. Finally, once sufficient sample is available, each novel form produced can then be subjected to further characterization of physicochemical properties, allowing the relationships between them to be established. Given the potential scope of these activities, electronic data management tools are essential to deal with the large volumes of data generated during each of the above stages of the screen. The successful application of high-throughput, automated, and parallel crystallization methods combined with various design strategies has been demonstrated for a range of organic compounds over the last decade (1,54–56) and some examples are highlighted in Table 3.

Parallelization does not necessarily require sophisticated and expensive automated instruments; small-scale formats utilizing multi-well plates combined with manual multi-channel pipettes for liquid dispensing can also provide a versatile platform for crystallization screening (Fig. 4). Simple quartz glass plates with individual wells can be used for crystallization screening, giving good chemical resistance to organic solvents. Accurate dosing of solute can be achieved by dispensing stock solution onto the plate and drying. Solvents can then be dispensed in a combinatorial manner across the well to produce the crystallization solutions. In Figure 4, for example, in direction 1 a series of 12 solvents with increasing polarity may be used, whereas in direction 2, the amount of solid introduced can be reduced sequentially in each row to vary concentration. The plate containing 96 individual crystallizations can then be stored in a controlled environment to allow cooling or evaporation and on the appearance of solid; the plate can be analysed by microscopy, Raman, or X-ray powder diffraction (XRPD).

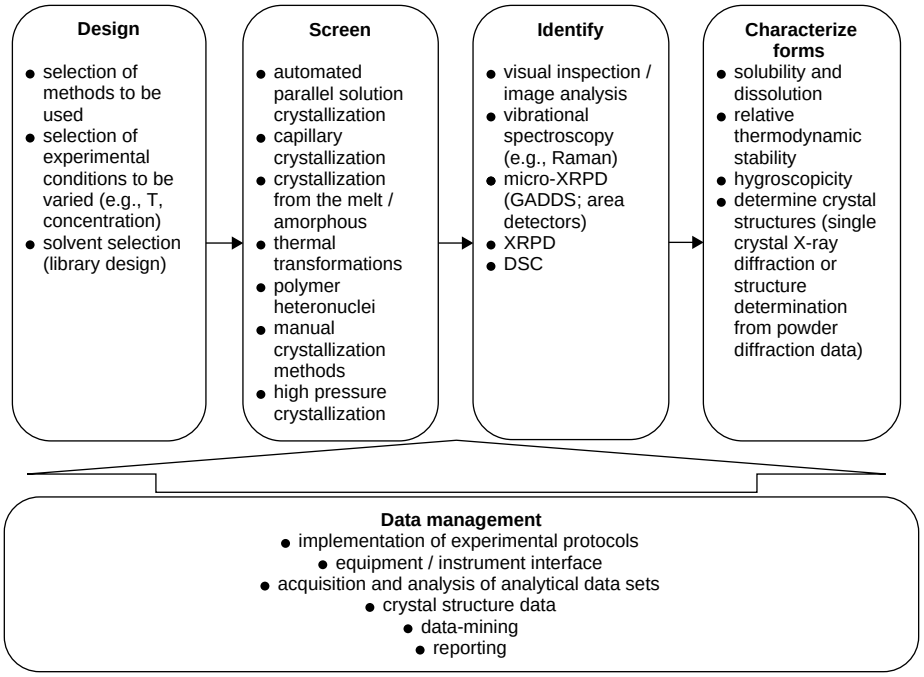

FIGURE 3 An overview of the main process elements in a comprehensive physical form discovery approach. *Abbreviations*: DSC, differential scanning calorimetry; GADDS, general area diffraction detector system; XRPD, X-ray powder diffraction.

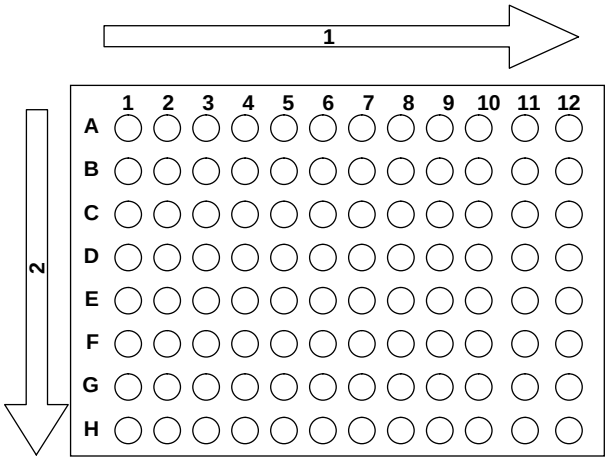

FIGURE 4 A typical 96-position plate/rack format capable of supporting parallel crystallizations (54).

TABLE 3 Examples of High-Throughput, Automated, and/or Parallel Crystallization Studies on Pharmaceutical Compounds

Compound	Methodology	Analytical methods	Forms observed	Notes
Acetaminophen (10)	Solution (evaporation) and melt crystallization 24 solvents in mixtures	Optical imaging Raman XRPD	3 polymorphs	2592 crystallizations (varying solvent, concentration, and temperature in triplicate) Identified reproducible conditions for producing form II
3-azabicyclo (3.3.1) nonane-2,4-dione (57)	Solution crystallization (controlled cooling and evaporation) Thermal transformations	Microscopy XRPD DSC/variable-temperature capillary XRPD	2 polymorphs 1 plastic crystalline phase 2 solvates	182 crystallizations 67 solvents
Carbamazepine (29)	Polymer heteronuclei in methanol solutions (evaporation)	Raman	Form IV	84 different polymers over 3 trials
Carbamazepine (45)	Solution crystallization on polymer microarrays	Microscope Raman	2 polymorphs	128 crystallizations Carbamazepine printed in DMSO onto polymer spots 6.5 mg of active used in total
Carbamazepine (22)	Solution crystallization (controlled cooling and evaporation)	XRPD	3 polymorphs 9 solvates	594 crystallizations (3–5 mL) 66 solvents 5 conditions
3,4-dichloro nitrobenzene (58)	Solution crystallization (controlled cooling)	XRPD	1 polymorph 2 solvates	224 crystallizations 64 solvents Controlled cooling
5-HT4 antagonist (59)	96-well plate (no automation) polymorph and salt screening Solution evaporation (salt selection) with slurrying	Microscopy Raman	2 polymorphs 2 hydrates (total of 16 crystalline forms of 5 salts)	12 solvents, 15 acids Solids dispensed in methanol solution. Upon drying 200 µL of each crystallization solvent added to each well
Hydrochlorothiazide (16)	Solution crystallization (controlled cooling and evaporation)	XRPD	2 polymorphs 7 solvates	642 crystallizations (3–5 mL) 67 solvents 4 conditions used
Mefenamic acid (60)	Crystallization by evaporation of nano- and picoliter solution droplets on self-assembled monolayers	Microscope Raman XRPD	2 polymorphs	Supports high-supersaturation levels and concomitant crystallization of forms from confined volumes

MK-996 (potassium salt) (9)	Solution crystallization in blocks of 96 capillary tubes by cooling	Raman XRPD	9 polymorphs 9 solvates	1–3 mg of compound per crystallization 1440 crystallizations 96 slurry experiments 21 solvents (in mixtures)
2-[(2-nitrophenyl) amino]-3-thiophenecarbonitrile (ROY) (45)	Solution crystallization on polymer microarrays	Microscope Raman	4 polymorphs	128 crystallizations 1 solvent ROY printed in NMP/acetone solution onto polymer spots
2-[(2-nitrophenyl) amino]-3-thiophenecarbonitrile (ROY) (9)	Solution crystallization in blocks of 96 capillary tubes (cooling)	Raman XRPD	4 polymorphs	3100 solution crystallizations 24 solvents alone or in mixtures; 2 concentrations; 2 temperatures 1–2.5 mg of ROY per crystallization
Ritonavir (11)	Solution crystallization using 24 solvents in mixtures (cooling)	Optical imaging Raman	3 polymorphs 2 solvates	~2000 crystallizations, 2 g of material used for entire screen Individual solution volumes used = 50 µL
Sertraline (61)	96-well blocks for capillary crystallizations Controlled cooling	Raman XRPD	18 crystalline salts Polymorphs of HCl, HCBr, benzoate, and mesylate salts	3456 crystallizations with sertraline dispensed in methanol in solution. Salt formers added in solution form and then solutions evaporated Crystallization solvents added using a 32-channel liquid dispenser
Sulfamethoxazole (45)	Polymer microarrays 768 crystallizations	Microscope Raman	2 polymorphs	Compound printed in methanol or ethanol onto polymer spots Individual solution volumes used = 50 µL
Sulfathiazole (60)	Solution evaporation on self-assembled monolayers	Microscope Raman XRPD	4 polymorphs	Crystallization of nano- and picoliter solution droplets on self-assembled monolayers
Tamoxifen (62)	Salt section and polymorphism study 96-well plate using 12 solvents and 6 acids in different stoichiometries Solution crystallization (evaporation)	Raman	12 crystalline salt forms identified including polymorphs	25–50 µL volumes of API (100 mg used) and acid solutions mixed in wells, heated, and allowed to evaporate

Abbreviations: API, active pharmaceutical ingredient; DMSO, dimethyl sulfoxide; DSC, differential scanning calorimetry; XRPD, X-ray powder diffraction.

Other multi-position formats are also in use including heating blocks for capillary crystallization and, for example, 96-position racks with individual crystallization inserts in each position. Robotics can be used to prepare each sample solution, monitor wells, and transfer either entire plates or individual inserts for analysis once crystallization has occurred. Although automation may not be suitable for all types of crystallization, in general, it can support improved throughput, more accurate control of conditions, and greater reproducibility of conditions compared with manual techniques. A summary of various pros and cons of automated crystallization systems is listed in Table 4.

Experimental Variables for Solution Crystallization

The sections below highlight several experimental variables that may influence the thermodynamic and kinetic control of solution crystallizations, and are therefore commonly utilized in the automated parallel crystallization searches.

Solvent and Solvent Selection

Variation of solvent identity can be a relatively straightforward means of designing diversity into the crystallization screen and manipulating physical form outcome (63,64). Solvent properties such as viscosity, surface tension, and density are key parameters in nucleation and crystal growth (65), and can be readily varied by using a diverse solvent library comprising many individual solvent types and/or solvent mixtures (1,3,56). Mixed solvent systems or co-solvents can be dispensed to increase the variety of solution properties and to address poor solubility. Chemical compatibility with the solute may also need to be taken into account during solvent selection.

In pharmaceutical development the safety of solvents can also be an important consideration. For example, the International Conference on Harmonization

TABLE 4 Potential Disadvantages and Advantages of Automated Crystallization Approaches

Disadvantages	Advantages
• High initial costs of hardware, varies with the extent of control and integration offered (initial hardware costs can range from £20,000–£500,000) • Need for bespoke software if multiple platforms used incombination (for experimental design; instrument control; data analysis; information management) • Difficulties in miniaturizing key steps (e.g., filtration of suspensions under temperature control) • Potentially high maintenance costs • High cost of development or implementation of new or bespoke features to pre-existing systems	• Repeatability of steps under direct computer control: implement multiple protocols (e.g., controlled cooling or evaporation across a large solvent library, isothermal crystallization using anti-solvent) • Manageability: ease of implementation of combinatorial experiments with integrated data management • Reduced wastage of materials • Integration with information management systems and data repositories • Increased productivity: greater number and throughput of crystallizations • Reduced labor for equivalent numbers of experiments • Increased scale of experimental search and diversity of conditions • Increased efficiency

of Technical Requirements for Registration of Pharmaceuticals for Human Use (www.ich.org) has published solvent classifications largely based on the safety of each group for administration to humans (Table 5). Although class 1 solvents such as benzene can, in principle, be used in drug substance manufacture as long as strict limits are followed on the level of residual solvent in the final product, generally these solvents will be avoided completely, and solvents selected from classes 2 or 3.

A number of statistical techniques can be applied to grouping solvents according to their bulk and molecular properties, providing a basis for rational selection. Such analyses attempt to quantify the similarity and dissimilarity of solvents in a given library based on various experimental or calculated physicochemical descriptors that, ideally, are directly relevant to the influence a solvent may have over the nucleation and growth of the solute. In addition to published resources (67,68), modern computational methods can also provide a wide range of electronic and structural molecular properties that can be included in clustering methods. Given that the relationship between solvent, nucleation and growth of a crystal is generally poorly defined, and may involve factors other than solvent identity, the selection of appropriate solvent descriptors remains a challenge.

In one study, 96 solvents were classified into 15 distinct groups using a hierarchical clustering method (69). Eight descriptors were used for each solvent that included hydrogen bond acceptor propensity, hydrogen bond donor propensity, polarity/dipolarity, dipole moment, dielectric constant, viscosity, surface tension, and cohesive energy density. In another screen, principal components analysis (PCA) was applied to 15 calculated and experimental descriptors describing each of 67 solvents used in an automated parallel crystallization screen on carbamazepine (22). The PCA analysis quantified the diversity of solvents being utilized. Solution crystallizations were then implemented for the compound from all solvents in the library under five separate conditions, selected on a qualitative basis, to explore the effect of temperature and supersaturation. The two dimensional score plots from the PCA analysis on the solvent library also provided a useful means of visualizing the results for each set crystallizations (Fig. 5).

PCA and self-organizing maps (SOM) have been applied to assess physicochemical diversity in a library of 218 organic solvents using 24 descriptors (70). Both methods confirmed the extent of diversity in the library, and the SOM also

TABLE 5 Some Examples of Solvents and Their Classifications According to ICH Q3C (66)

ICH Class	Solvent	Risks
Class 1	Benzene 1,2-Dichloroethane 1,1,1-Trichloroethane	Carcinogenic, toxic or environmentally hazardous. Concentration limits based on toxicity range from 2 to 8 ppm
Class 2	Acetonitrile 1,4-Dioxane Methanol	Should be limited in pharmaceutical products due to inherent toxicity. Concentration limits for class 2 solvents range from 50 to 3880 ppm
Class 3	Acetone Ethanol Methyl ethyl ketone	Up to 5000 ppm acceptable without justification

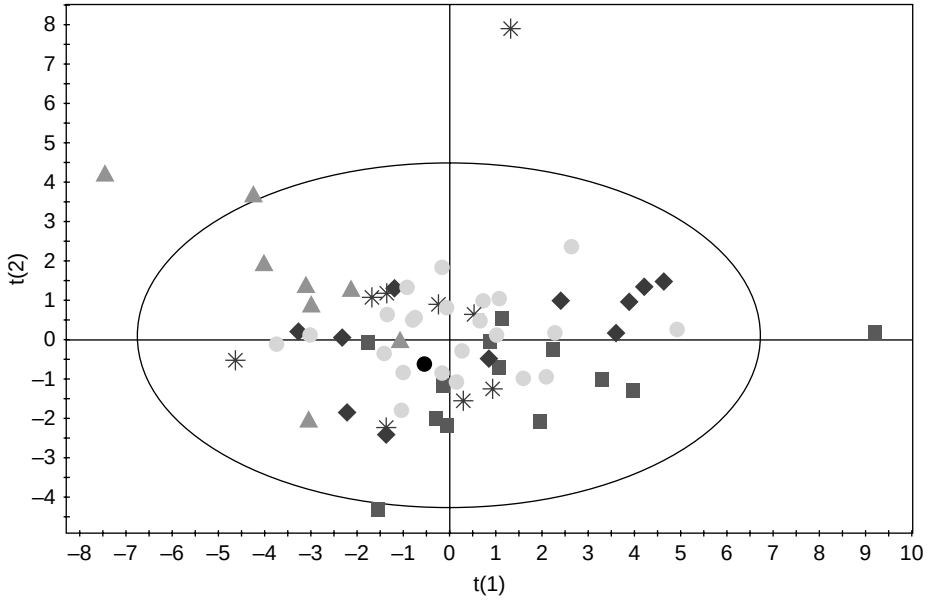

FIGURE 5 Scatter plot for solvent library with symbol positions obtained from a PCA score plot derived from 15 solvent property descriptors (22). The ellipse represents the Hoteling T2 with 95% confidence. The symbols indicate individual physical form outcomes determined by XRPD from each solvent under the tested conditions. Square, no sample obtained; black circle, form I; diamond, form II; asterisk, form III; grey circle, a mixture of anhydrous forms; triangle, solvated form.

provides a convenient method to visualize the solvent clusters, enabling straightforward selection of diverse subsets of solvents from the entire library. Calculated partial charge distributions for solute and solvents have also been assessed as potential tools to explore the influence of solvent on polymorphic forms of ranitidine hydrochloride and stearic acid (71).

Although the application of clustering and related methods for assessing solvent diversity cannot guarantee that multiple forms of a solute will be obtained from solution, they are still of considerable value in the selection of solvent libraries. When used with appropriate descriptors, they provide a means to quantify the range and type of diversity of solvents included in a screen, and so increase confidence that a suitably broad set of conditions has been incorporated. Analysis of the solvent properties can be used to identify under-represented regions of property space within the library that would benefit from the addition of new solvents or, identify solvents that may have largely similar properties and so may be considered for exclusion. An effective clustering approach can also be used to select subsets of solvents that encompass the same overall diversity as a larger library in an attempt to minimize the number of experiments carried out.

Supersaturation

Although solvent identity is often important, the crystalline form produced can also be essentially independent of solvent identity and be more closely related with solubility and supersaturation (72). The supersaturation achieved during each

crystallization can be a major factor determining the nucleation and growth kinetics of different forms (65). For example, a solution crystallization screen on carbamazepine using only one solvent, cumene, successfully found three of the four known polymorphs of this compound by varying only temperature and concentration in the screen (73). Limiting the number of solvents used in the search will, however, also limit the possibility of producing novel crystalline solvates. The rate and extent of supersaturation achieved can easily be varied by using different initial concentrations and temperatures of solutions and then applying different rates of cooling, evaporation, or addition of anti-solvents.

Temperature

Temperature plays a very important role in automated approaches and robotic platforms provide for dynamic temperature control, both heating and cooling, of samples either individually or in zones covering multiple samples. This allows a wide range of control during both sample preparation (dissolution) and crystallization. Controlled cooling of saturated solutions is a relatively straightforward means of inducing crystallization, and is widely used. The accessible temperature ranges for individual crystallizations will depend on the boiling point, vapor pressure, and freezing point of the solvent as well as the hardware specifications of the platform (solvent compatibility, temperature ranges). Isothermal crystallizations at different temperatures can return different outcomes where, for example, they are carried out above and below a transition temperature between two thermodynamic forms. Evaporative and anti-solvent techniques are particularly useful for isothermal solution crystallization at elevated temperatures. Lower crystallization temperatures can also favor solvate formation. Temperature ramps can also be applied to achieve parallel crystallization from molten material in arrays of glass capillaries (10).

Time Scales and Rate of Crystallization

Parallel experimentation aims to secure many results simultaneously; however, this can be frustrated by the difficulty in controlling the specific time it takes for a solid product to be formed by any individual crystallization. It is also desirable to include methods for both rapid and slow rates of nucleation and crystallization in a screen. Rapid cooling of a saturated solution or fast evaporation under vacuum, for example, may favor the production of metastable forms, although can also lead to oiling out or amorphous products. Longer crystallization processes may favor stable forms, in the absence of solvent interactions that stabilize a specific polymorph or solvate. However, in some circumstances supersaturated solutions may exist for weeks without nucleation occurring. Clearly in such cases, a decision must be made between waiting for all experiments to yield results and discarding all crystallizations that have not produced solid within a fixed time scale. With high-throughput screens involving several thousand crystallizations, the latter approach can often be safely adopted whilst still yielding significant numbers of recrystallized samples (56). Alternatively, the original crystallization conditions can be altered, by the addition of anti-solvent, for example, to accelerate the rate of crystallization. Once crystallization has occurred, it is desirable to identify the sample as quickly as possible to reduce the risk of rapid transformation of metastable forms that could otherwise be missed in the search.

Evaporation

Evaporative crystallization under temperature control is another effective means of inducing crystallization and can be achieved by pulling a vacuum in the sample

chamber (55) or by using a controlled gas flow over the samples. Evaporative methods are less effective in achieving rapid crystallization from solvents with a low vapor pressure or high boiling point. With either method, it is important to minimize the risk of cross-contamination by solvents vapors where they come into contact with other solutions in the array. Although this may give rise to interesting results (e.g., a novel form) such uncontrolled conditions complicate analysis of the screening results and potentially limit the success of subsequent attempts to reproduce particular conditions.

Agitation

Stirring or agitation of solution is often applied during the preparation of solutions to facilitate rapid dissolution of solute in the crystallization solvent. However, agitation can also influence nucleation kinetics (74). Crystallization from agitated solutions can be achieved either using individual magnetic stirrers or by placing the vessels or crystallization plates on large orbital shakers, with the latter approach being appropriate for automated parallel systems.

Anti-solvent Addition

Dispensing anti-solvents into solutions is easy to automate, and provides a rapid and reliable means of producing recrystallized samples within short time scales (3,56). Variation in the identity of anti-solvent, temperature of addition, volume of anti-solvent added, and rate of addition are all potential variables that may be included in the screening protocol.

Use of Additives

The addition of specific additives (or the presence of impurities) of different identities or concentrations can also influence the outcome of crystallization, possibly by templating or preferentially stabilizing particular forms (75,76). This can be readily assessed using automated parallel crystallization methods. For example, both the monoclinic and orthorhombic polymorphs of acetaminophen were obtained from trials in which 84 different polymers were used as heteronuclei during crystallization from aqueous solutions by slow evaporation (29). The selective crystallization of a metastable polymorph of tolbutamide from aqueous solutions containing 2,6-di-O-methyl-β-cyclodextrin has also been attributed to the inhibition of a solution-mediated transformation to the stable form by the cyclodextrin additive (77).

Suspensions

Suspension crystallizations, or slurries, are generally aimed at finding the most stable form in the absence of impurity effects, solvate formation, or other specific solvent effects that may stabilize a metastable form (76,78). Solvent identify, temperature, incubation time, and temperature cycling can all influence the solid-form retrieved.

Desolvation of Solvates

The occurrence of solvated crystalline forms may not always be of direct significance to a particular pharmaceutical product. A labile acetonitrile solvate, for example, is unlikely to be selected for use in the manufacture of a new tablet formulation. However, where solvates are identified it is always worth confirming the identity of the desolvated form, as this can lead to the production of novel non-solvated

forms. The product of desolvation should therefore be routinely assessed during parallel screens by analyzing all solvated samples before and after desolvation (1).

IMPLEMENTATION OF AUTOMATED PARALLEL CRYSTALLIZATION

With automated systems it becomes possible to produce large numbers of individual crystallizations in a short period of time. For example, one compound crystallized from 64 solvent systems using two different supersaturation levels and two temperatures each carried out in duplicate could lead to 512 samples requiring analysis. Of course, the larger the search, the larger the experimental/analytical overhead incurred and the more time-consuming and costly the exercise becomes. The following sections provide an overview of the main process steps and methodologies used to accomplish efficient and effective automated parallel crystallization searches (Table 6).

Before embarking on a systematic crystallization screen, it is important to collate as much information as possible about the raw material (Table 7). A single a crystal structure, or details on chemical and physical purity of the sample as well as initial physical properties and straightforward tests for thermal or solution-mediated transformations, can generate novel forms at the outset. At the very least, this preliminary inspection will provide reference data that can be used for identification of samples produced during the screen.

TABLE 6 Typical Hardware Components for Automated Crystallization Systems

Component	Objective and methods
• Solid dispensing	• Accurate dispensing of raw compound for dissolution • Addition of multiple solid components for salt and co-crystal screening • Achieved by dispensing stock solution followed by evaporation or manual or automated solid-dosing
• Liquid dispensing	• Prepare solutions for accurate dispensing of single or mixed solvent systems • Addition of buffer solutions to control/vary pH • Addition of anti-solvent • Readily achieved by accurate liquid handling systems comprising single or multi-channel pumps under computer control. Many systems have robotic arms to enable complex manipulations to be carried out
• Temperature control	• Control of solution temperature during dissolution and crystallization
• Agitation	• Facilitate dissolution using magnetic stirring, orbital shaking, or sonication under temperature control
• Filtration	• Remove undissolved solid to prevent seeding by starting form. • Retrieve recrystallized solid
• Sample retrieval and transfer	• Identify presence of solid (e.g., turbidity/optical inspection) • Transfer samples for analysis/identification
• Sample analysis	• Collect characteristic data to distinguish between solid forms • Methods used include microscopy, spectroscopy and XRPD

TABLE 7 An Overview of Initial Investigations on Raw Material to Establish Initial Form and Related Properties

Crystal structure	Determine crystal structure; useful for subsequent identification of forms
XRPD	Obtain reference powder data for known forms; confirm single crystal structure is representative of polycrystalline sample
Raman/FT-IR	Obtain reference data/fingerprints
DSC/TGA	Determine melting points and identify transformations
VT-XRPD	Structural characterization of polycrystalline phases obtained from thermal transformations in situ using SDPD
Dynamic vapor sorption/slurrying	Assess hydrate/solvate formation
Solubility/dissolution	Characterize form and assess solution meditated transformations

Abbreviations: DSC, differential scanning calorimetry; FT-IR, Fourier transform-infrared spectroscopy; SDPD, structure determination from powder data methods; TGA, thermogravimetric analysis; VT-XRPD, variable temperature X-ray powder diffraction; XRPD, X-ray powder diffraction.

Experimental Design

Armed with appropriate techniques to implement a systematic experimental search strategy, the challenge is to ensure that the widest possible diversity of crystallization techniques and conditions can be carried out within the constraints of available material, equipment, manpower and time. In general, Design of Experiments (DOE) approaches aim to establish experimental models that relate the experimental variables (factors) to the experimental outcome (responses) and so inform the execution of experiments aimed at maximizing the information returned from a minimum number of experiments. Significantly, owing to the complexity of the processes involved in crystallization, reliable models that can predict the experimental conditions under which a new polymorph will be found are not available. However, DOE can be used to assist in the selection of diverse experimental conditions, and the application of D-optimal designs and other methods for diversity generation have been described in this context (3,56). DOE applications can be used to select diverse experimental variables from the accessible range of solvents, temperature, concentration, techniques, and amount of material, and therefore maximize the spread of experimental conditions that are sampled during a search and avoid unintentional overlap of experiments. The design matrix may incorporate any relevant data such as solubility data and measured or calculated solvent properties. Any constraints on the experiment, such as hardware limitations (e.g., maximum achievable cooling rate), chemical incompatibilities, or toxicity issues can also be factored in to remove certain experimental conditions from consideration.

Information Management and Process Control

Information and data management software are of particular value in high-throughput and automated systems. These will often combine process, chemical, and analytical databases that are used to inform and control the design, implementation, and analysis of the screen (56,79). The experimental variables selected

in the design stage are mapped onto the instruments to create workflows defining the conditions and sequence of all steps. This may involve a single integrated platform or separate hardware systems (e.g., for solid dispensing, liquid dispensing, and incubation under controlled temperature) integrated via system control software. Instrumental control interfaces typically utilize a graphical user interface that illustrates the hardware configuration with simple user control commands to describe tasks such as liquid or solid dosing, and sample retrieval. Upon initiating the experimental sequence, solute and solvent are dispensed using the conditions required by the combinatorial design. The platform records parameters, such as actual weights and volumes of material dispensed, the times at which each step occurred, temperature profiles, and pressure or gas flows, throughout each process step. Thus, the performance of the hardware can be monitored and the actual conditions used can be easily checked against the original protocol. Crystallizations are monitored for the presence of solid, and once sample is observed, the solid is retrieved and analyzed. The experimental database then collates process data and analytical results collected during the experiment. The user can then view results, carry out cluster analysis, and ultimately identify all physical forms crystallized in the study.

Automated Preparation of Solutions

The first step to be automated is the preparation of the individual crystallization solutions, and a number of systems have been described (3,80) for high-throughput experiments using small-scale crystallizations on multi-well plate designs or capillary tubes. Crystallization in capillaries has been reported to be particularly useful for obtaining metastable forms through inhibition of nucleation (51). In such small-scale studies, it is convenient to dispense the API into each well or vessel in the form of fixed volume of a bulk solution, whereupon evaporation of the solvent, a specific mass of API (microgram to milligram range) is left. With larger scale crystallizations (3–5 mL), automatic weighing stations can also be used to accurately dose solid directly into the vessels (55). Next, the crystallization solvent or solvent mixtures are dispensed combinatorially and dissolution facilitated either through heating or via a combination of heating and agitation (55) or heating and sonication (3).

It is desirable that crystallization occurs from a seed free solution so that the outcome is determined by the specific solution conditions. Visual or optical inspection of individual solutions can identify whether residual undissolved solid remains after the addition of solvent. These solutions can be left to run, and treated as slurries rather than solution crystallizations (3). Alternatively, after dissolution, primary solutions may be passed through filters that remove undissolved solids and transferred into fresh crystallization vessels. A post-filtration heating ramp can be applied to dissolve any residual seeds that may have passed through the filters (55). In the context of automated crystallization, filtration is typically better suited to milliliter scale experiments than the very low (microliter) solution volumes utilized in high-throughput multi-well plate experiments. Although hardware for automated liquid dispensing and aspiration is widely available, it can be difficult to ensure temperature control of solutions held at non-ambient temperatures during liquid transfer steps such as filtration. For example, a hot saturated solution coming into contact with a filter or transfer needle at a lower temperature risks crystallization occurring within the needle that may lead to blockages or the production of seed crystals.

Inducing Crystallization

As outlined in the section "The Extent of Physical Form Diversity," there are a variety of means of inducing supersaturation and crystallization that can be easily implemented on automated crystallization systems. Whether controlled cooling, evaporation, or anti-solvent methods are used, once the necessary conditions have been imposed, solutions should be monitored to identify the appearance of recrystallized solid.

Isolation of Solid Sample

Rapid isolation of solid can be achieved by filtration (55), aspiration of the supernatant (10), and/or evaporation using a nitrogen gas flow (61), and is desirable in order to minimize the opportunity for sample transformations to occur prior to analysis. For example, over time, metastable polymorphs may transform to more stable forms via solution-mediated transformation. However, drying may also lead to desolvation of solvates, so it is advisable to collect data from wet as well as dried samples (1). XRPD is well suited for the analysis of wet samples, as scattering from the liquid will not affect the position or intensities of the diffraction peaks required for phase identification. Imaging of samples during the retrieval and analysis process may also enable the occurrence of desolvation to be identified from any change in appearance of the sample. Rapid sample analysis is also desirable to avoid secondary crystallization from trace solution left in the well or vessel after filtration or solution aspiration. For example, where the supernatant is aspirated from a suspension, evaporation of trace amounts of residual solution may yield a different solid form from the primary product. Once each sample has been separated from solution they are subjected to primary analysis to attempt identification of the physical form(s) present. Details on methods of physical form identification in the context of high-throughput and parallel crystallization searches are provided in the section "Analytical Methods in Physical Form Screening."

Assessment of Completeness

An effective screening approach should obtain samples of all forms accessible within the scope of the search, and provide some information on the factors that influence the occurrence of those forms (3). Importantly, having identified the individual growth conditions for each form, these can be replicated to obtain further samples for additional physical characterizations including crystal structure determination, measurement of thermal properties (transformations and melting point), hygroscopicity, solubility, and dissolution rate.

Multivariate analysis techniques can be applied to assess the completeness of the experimental search and attempt to identify correlations between the conditions tested and the outcomes observed. For example, a retrospective Random Forest (81) analysis of the results from a solution crystallization screen on carbamazepine (23) used a variety of parameters to describe each crystallization (solvent and conditions) and each outcome (polymorph or solvate) identified in the screen. These results were used to train a classification model (81) that identified three solvents (Fig. 6) as being likely to form solvates, despite the fact they had produced non-solvated forms in the original screen. The predictions were confirmed by subsequent recrystallization of carbamazepine from each solvent. The model could not specify the crystallization conditions that would produce the solvates, so the recrystallizations were carried out at 5°C, that is, outside the temperature range of the

original search. The analysis also identified several solvent descriptors that correlated with carbamazepine solvate formation. Although it may have been possible to crystallize these new solvates by having implemented a more extensive crystallization search at the outset, solvates can still be missed in a search where they are labile and desolvate prior to analysis.

Examples of Automated Systems for Parallel Crystallization

A range of systems capable of automating crystallization screening for small organic molecules have been developed in recent years. These range from complete integrated systems with full automation of liquid and solid handling, real-time monitoring of crystallizations with automatic analysis and data capture with sophisticated experimental design, instrument control, informatics, and data mining capabilities, to small-scale semi-automated bench-top systems that do not offer automation of material transfer, but provide accurate, dynamic control of parallel crystallizations. A selection of platforms capable of supporting experimental searches for physical form diversity are described below.

The CrystalMax platform is a proprietary, highly integrated system that utilizes automated technologies for high-throughput crystallization combined with experimental design and instrument control systems plus support for data capture, analysis, and mining (56). It features full automation with support for over 10,000 individual parallel crystallizations using between 0.25 and 1 mg of API. Access to diverse crystallization parameters is achieved with automated dispensing of liquids into crystallization tubes combined with cooling, evaporation, or anti-solvent addition to induce crystallization. Each crystallization tube can be monitored using a vision station to identify those containing recrystallized solids. These can then be removed from the array and the supernatant removed by aspiration and drying under a gas flow prior to analysis. If no solid is present, the sample is returned to the crystallization station. Recrystallized solids are initially assessed using optical inspection and in situ Raman spectroscopy. Several examples of polymorph screens using this technology are included in Table 3. A screen of ritonavir using the CrystalMax system implemented over 2000 individual crystallizations with API concentrations varying

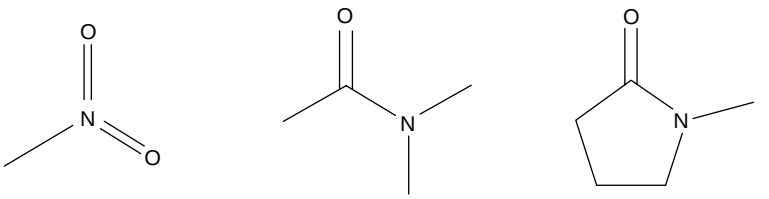

Nitromethane | *N*,*N*-dimethyl acetamide | N-methylpyrrolidone

FIGURE 6 Molecular structures of solvents that produced non-solvated carbamazepine forms in a prior crystallization study, yet were classified by Random Forest analysis alongside other solvate forming solvents. Subsequent recrystallization at 5°C produced three novel carbamazepine solvates with each solvent.

between 20 and 100 mg mL^{-1} (11). In-house experimental design software was used to select diverse solvent selections using single and binary mixtures selected from across a library of 24 pharmaceutically acceptable solvents. Controlled cooling was used to induce supersaturation and crystallization. Fifty-one recrystallized samples were returned from the screen, and Raman spectra for each dried sample identified a total of five forms. Both forms I and II of ritonavir were produced in addition to a new polymorph, a hydrate, and formamide solvate.

The Crissy platform is a scalable, customizable system for automated parallel crystallization (82). In addition to automated liquid handling, temperature control, and weighing, it can accommodate a range of different reactor block sizes and configurations (Fig. 7). A common plate format is used that allows rapid interchange between 8, 24, 48, or 96 position standard format plates/vials or proprietary reactor block designs, depending on the requirements of the screen. A computer-controlled balance can record the amounts of solid dosed into each well, and solvents are automatically added from the library by a liquid dispensing arm. Containers are then transferred to stations that enable combined heating, drying, or vortexing on the platform (shown) or to separate external incubators to bring about dissolution or crystallization as required. The various stations on the platform configuration shown in Figure 7 (from *left* to *right*) are: (1) reagent rack for holding solutions or solvents; (2) hot and cold vortexing stations; (3) pipetting positions; (4) filtration box; (5) and (6) are heating and cooling plates for dissolution or crystallization steps. With certain block designs, recrystallized solids are left on the glass base-plate of each reactor, allowing the entire plate to be transferred without further intervention onto an XRPD or Raman instrument for analysis.

Although the SpecScreen xHTS (Fig. 8) system is primarily designed for automated stability testing on solids, it is also capable of supporting polymorph screening (83). The self-contained automated platform system consists of temperature-controlled racks (5–80°C) that can accommodate up to 1000 samples in 96- or 24-well plate format racks holding individual glass vials. The platform can be configured with an integral orbital shaker and Raman/NIR spectrometers with robotic transfer of samples between the racks and the spectrometers. The system software enables instrument control, and experimental and analytics databases provide support for classification of spectra and the generation of reports.

Another automated parallel crystallization platform, configured for 32 crystallizations per day, has also been described (55) and applied in a range of polymorph screens (16,22,57,58). The platform is well suited to sample volumes of 3–8 mL with between 10 and 500 mg of API per crystallization using evaporation, controlled cooling, or anti-solvent addition. The larger scale of individual crystallizations allows for significant flexibility in the crystallization conditions that can be explored and is well suited to application during later stages of development where API is available in greater quantities (4). The platform layout is shown in Figure 9. Crystallization solutions are held in double-jacketed glass vessels, allowing temperature control for isothermal crystallization (5–250°C) or controlled cooling (5°C min^{-1}). Pairs of vessels are connected by a filtration system to remove any undissolved solid from solutions prior to crystallization. The vessels are mounted in blocks that utilize motorized ceramic plates to either open each glass vessel (e.g., to allow liquid and solid dosing) or close it (e.g., to prevent evaporation). The platform stores up to six 2.5-L solvent vessels (e.g., for washing cycles) plus a library of over 60 crystallization solvents.

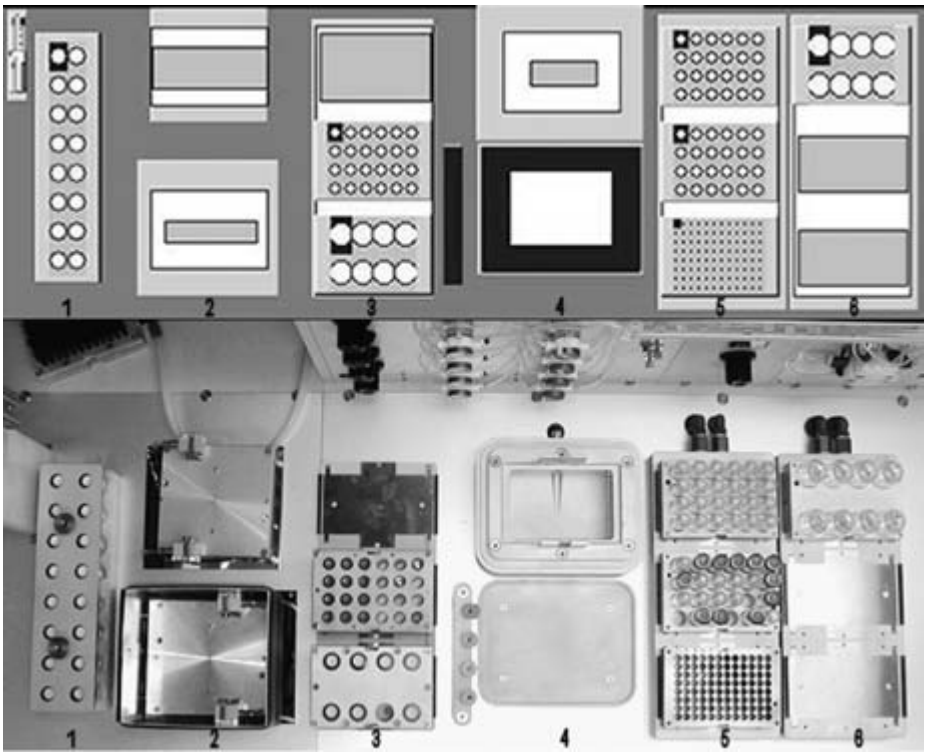

FIGURE 7 View showing the instrument software control interface (*top*) in relation to the hardware configuration (*bottom*) on a Zinsser Crissy platform. The view illustrates various plate formats that can be utilized for different crystallization volumes and scales of experiment (see text for detailed description).

Automation of both solid and liquid dispensing is enabled by a robotic arm allowing the programmed exchange of a solid dispensing unit and a four-channel liquid handling head. The parameter log file for a controlled cooling crystallization protocol is illustrated in Figure 10, summarizing the key steps of dissolution, filtration, and supersaturation. With this system, the recrystallized samples must be retrieved manually from vessels by filtration. The solution volume used is typically sufficient to produce enough polycrystalline sample for analysis using transmission foil XRPD (84), even from solvents in which the solute has a relatively low solubility. Experimental design and XRPD data analysis is achieved using third-party software.

Small-Scale Semi-automated Crystallization

There are various small-scale bench-top systems available that can support accurate, dynamic control of multiple crystallizations, and an example is shown in Figure 11. Although this type of parallel reactor block does not provide automation of material dosing into wells, they do provide enhanced control of temperature (heating and cooling) and stirring throughout a crystallization cycle compared with

FIGURE 8 SpecScreen xHTS platform housing (*top right*) the automation system for transfer of sample vials between racks and analysis, underneath which sits the temperature-controlled racks for housing multiple 96-position racks containing individual sample vials, (*middle left*) NIR and Raman spectrometers, and (*bottom right*) instrument control PCs.

typical manual approaches. This type of device is therefore well suited to support small-scale semi-automated crystallization searches on milligram quantities of API. The Crystal16 system (79), for example, can continuously monitor 16 × 1-mL solutions using integrated turbidity probes, for example, to monitor dissolution, solubility, and crystallization (85,86).

Small-scale semi-automated devices are also ideal for scaling-up the production of specific forms, by replicating conditions identified from a high-throughput screen. Parallel slurrying experiments are also straightforward to implement, with stirred samples in contact with a range of solvents in individual sealed vessels under temperature control. The application of slow cooling rates to saturated solutions into which seed crystals have been introduced can also be of value when attempting to grow single crystal samples of novel forms for crystal structure determination (87). Semi-automated methods can be used as a complement to other

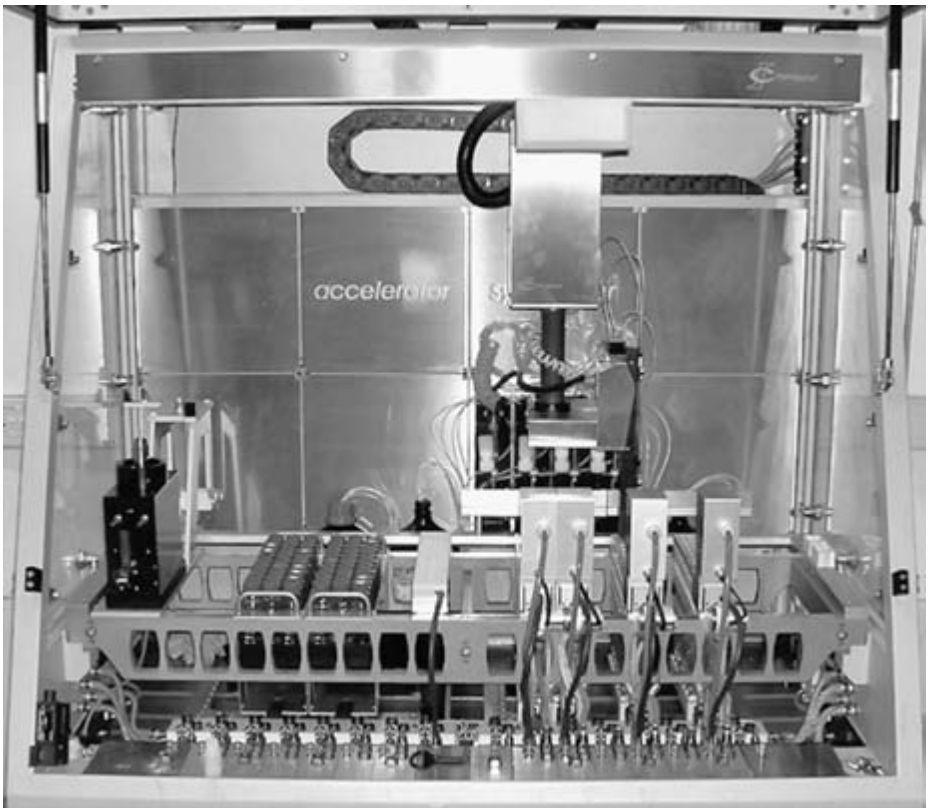

FIGURE 9 Chemspeed Accelerator SLT100 parallel synthesizer configured as an automated parallel crystallization platform. The system enables the automation of basic crystallization steps with automated solid and liquid dispensing, in-line filtration, and controlled cooling or evaporation with or without agitation.

approaches, exploring conditions that lie outside the normal range accessible using automated or high-throughput systems (e.g., low-temperature).

ANALYTICAL METHODS IN PHYSICAL FORM SCREENING

The analytical tools applied to the primary analysis of samples must be able to distinguish between a range of possible outcomes that include identifying whether the sample is:

- crystalline or amorphous
- a single form or mixed solid phases
- a known form (i.e., matches a reference)
- a novel form
- chemically different from the raw material (degradation product, adduct, solvate, salt, or co-crystal)

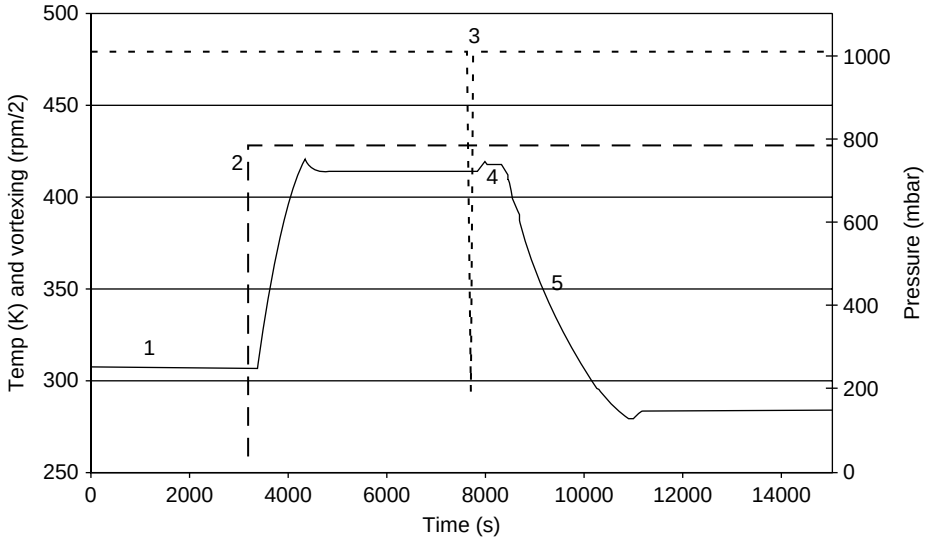

FIGURE 10 Graphical representation of the key parameters during a typical crystallization protocol. T (K), jacket temperature (—); ω (rpm/2), vortex frequency (-----); P (mbar), pressure (·····). Crystallization steps are indicated as follows: 1, solid and solvent(s) dosed into vessels (ω = 0 rpm, T = 306 K, P = 1006 mbar); 2, solution agitated at 850 rpm, while heating to 413 K, to facilitate solid dissolution; the suspension is held under these conditions for about 60 minutes; 3, suspensions are vacuum-filtered into post-filtration vessels on right-hand side of block; 4, the temperature of the filtered solutions is increased by 5 K for ca. 10 minutes to promote dissolution of any seed crystals that may remain post-filtration; 5, crystallization is induced, in this example, by cooling the solutions to 283 K, at a rate of ca. 3 K/min, while vortexing at 850 rpm. *Source*: Data from Ref. (55).

The large sample numbers, small sample amounts (perhaps only a few micrograms), and often random disposition of sample in the crystallization vessel present significant challenges to physical form analysis. For primary analysis, the analytical technique used must be able to collect usable data at a rate commensurate with the production of samples by the parallel crystallization methods used. Once primary identification has been carried out, further characterization steps will typically include determination of crystal structure, measurement of characteristic physical properties such as melting point, solubility and hygroscopicity, and establishing relative thermodynamic favorability of forms (Fig. 12). The following sections will discuss microscopy, spectroscopy, and diffraction as tools for primary analysis.

Microscopy and Imaging

Optical microscopy has wide application in the study and characterization of the organic solid state, and its various applications have been described in detail (88). In the context of screening, an important advantage is that can be relatively straightforward to implement for small-scale crystallizations with multi-well plates (62) or capillaries (10), to monitor the progress of crystallization automatically, and provide confirmation on the presence of recrystallized solid. Plane-polarized light microscopy

FIGURE 11 An example of a small-scale, bench-top parallel crystallization device (Reactarray RM2) with 12 independent wells able to accommodate solution volumes in the range <1 to 30 mL. A computer interface enables individual control of temperature (–30 to 150°C) and stirring in each crystallization vessel.

can also provide an indication as to whether samples are crystalline. Machine imaging systems for automated image acquisition and analysis can capture images from digital video cameras, allowing particle size and morphology information to be recorded and the automated assessment of samples for further analysis (10,89). Optical imaging systems can also locate the specific area within an individual well where solid particles are deposited and guide automatic location of sample and data collection (4).

Raman Spectroscopy

A variety of spectroscopic methods, including solid-state NMR (90), NIR (91,92), FT-IR (93), and terahertz (94) spectroscopy have been applied to the investigation of polymorphism in pharmaceuticals. However, Raman spectroscopy has been widely adopted as a primary analytical tool for rapid sample characterization in high-throughput polymorph screening (1,3,10,95). For a detailed account of the basis of Raman spectroscopy and its application to pharmaceuticals, see, for example (96,97). Raman lends itself well for distinguishing polymorphs, salts, solvates, and co-crystals as spectra typically display sharp, well-resolved bands whose position and intensities are sensitive to both the physical and chemical composition of the sample (98). Particular advantages of the technique, relevant to its application as an identification tool in polymorph screening, include the availability of microprobes that enable individual Raman spectra to be collected in around one minute from very small sample amounts (down to the nanogram level) spread over very small areas (approximately 1 μm) without sample orientation effects or the need for sample preparation (98,99). High spatial resolution microprobes also allow several spectra to be collected from different locations in a single sample well, increasing the chances

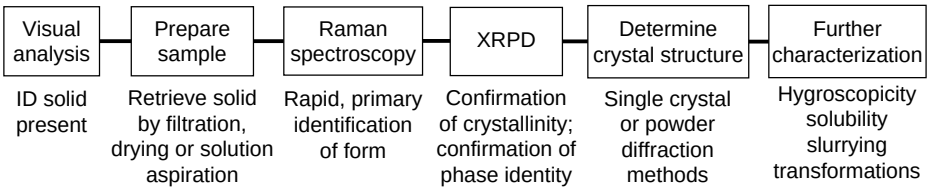

FIGURE 12 Outline of an analytical workflow suitable for physical form screening outlining typical process steps and individual objectives.

of detecting mixed-phase samples. Spectra can also be collected from samples in contact with water or held on glass substrates, as neither material gives rise to significant Raman scattering. Sample fluorescence can, however, restrict the use of Raman for certain compounds.

Commercial Raman microprobe systems are available with integrated multiwell plates readers that enable automated alignment of each sample (100). Individual 96-well plates are simply transferred onto the instrument, and each well is automatically scanned in sequence, with multiple individual spectra collected and collated for further analysis. Raman immersion probes also enable in situ measurement of spectra from suspended solid in larger vessels (101).

A microprobe system was used for a salt formation and polymorph screen of tamoxifen using quartz 96-well plates. After dispensing 25–50-μL stock solutions of tamoxifen and different acids into each well to give the desired stoichiometry, the initial solvent was evaporated before 300-μL aliquots of 12 different aqueous solvent mixtures were dispensed, sealed, stirred, and heated before being evaporated under nitrogen. Based on the Raman spectra, it was concluded that tamoxifen has a tendency to form 1:1 salts with polybasic acids, and that several of the salts formed were polymorphic (62). Although Raman is widely used for primary identification in high-throughput screening, different polymorphs of a compound may yield similar Raman spectra, with the result that novel forms produced in the screen can be missed (80). Often, therefore, multiple techniques are used, for example, with Raman spectra, forming the basis of the initial sample identification and XRPD data used to confirm the sample assignments (11,102).

Classification of the large number of spectra that can be generated from comprehensive screens is impractical using manual inspection alone, and techniques to automate this process are required. Multivariate data analysis methods capable of identifying individual samples or groups of samples that yield the same characteristic Raman spectrum amongst large numbers of spectra, have become widely adopted. For example, PCA analysis has been used to distinguish between Raman/NIR spectra of nitrofurantoin polymorphs produced during a polymorph screen (103). Tanimoto matrices, obtained from similarity coefficients calculated for each pair of spectra collected during a screen (i.e., an $n \times n$ matrix is produced for n spectra) have also been applied as a convenient method of grouping spectra from similar solid forms together in an easily visualized form (10,56).

XRPD

Many of the crystallization techniques employed in experimental searches for physical forms will result in polycrystalline samples. XRPD is therefore a vital

element in the arsenal of analytical techniques used to support physical form screening. XRPD can be used alone (80) or in conjunction with spectroscopic methods for the primary identification of large numbers of recrystallized samples. It is also applied as a secondary technique to confirm the identification of samples based on initial Raman analysis. However, in addition to sample identification, XRPD also affords the opportunity to extract valuable structural information from the sample.

XRPD data can be used for a wide range of analyses on individual samples including (i) characterizing samples as crystalline or amorphous, (ii) identification, "fingerprinting" and pattern comparison, (iii) comparison of XRPD data from individual samples with single crystal structures for the purposes of identification, and (iv) providing direct access to unit cell, space group, and crystal structure information in the absence of suitable single-crystal samples. The following sections will provide a brief overview of each application in turn. However, first we shall consider general instrumental requirements.

XRPD Instrumentation for Screening Applications

Developments in instrument technology in recent years have lead to the availability of commercial laboratory XRPD instruments capable of collecting powder diffraction data from very small sample amounts on similar time scales to Raman spectroscopy, making them suitable for application in high-throughput screens. For example, the Bruker-AXS General Area Diffraction Detector System (GADDS™) combines an X-ray source with small focal point (50–300 μm), automated *x*-*y*-*z* sample stage with video and laser-guided sample alignment and a large two-dimensional area detector enabling the rapid assessment of samples (4). Many instruments can also record digital images of each sample at the start of the XRPD data collection. These are stored along with the raw powder data and enable individual samples to be visualized during subsequent analysis steps. For example, where a pattern does not display any XRPD peaks, the image can be checked to confirm that the well contained sufficient solid sample. Area detectors enable a wide range of 2θ (typically up to 35° 2θ) to be collected simultaneously, reducing data collection times significantly compared with standard laboratory instruments employing one-dimensional position-sensitive detectors (PSD) (104,105). However, although area detectors enable rapid data acquisition, they have some disadvantages compared with modern PSDs. These include a significant reduction in angular resolution of the integrated XRPD pattern, variable peak shapes, low signal-to-noise ratios, high backgrounds, and preferred orientation effects that can be problematic for pattern comparison (106).

Where larger amounts of sample are available (around 10 mg per sample), alternative instrument configurations enable higher quality data to be collected, albeit at the expense of sample throughput. The combination of primary monochromator, transmission foil geometry, and PSDs allows high-quality data acquisition on about 30 samples per day (84) (Fig. 13). Data collected from such systems have been demonstrated to yield high-quality data that are important in pattern recognition and imperative in indexing. Reflection geometry is also widely used, often in combination with PSD and sample changer. Utilization of $K\alpha_{1,2}$ radiation provides greater beam intensity compared to standard monochromated systems and is beneficial for sample throughput. Reflection geometry also allows the use of controlled humidity and temperature chambers.

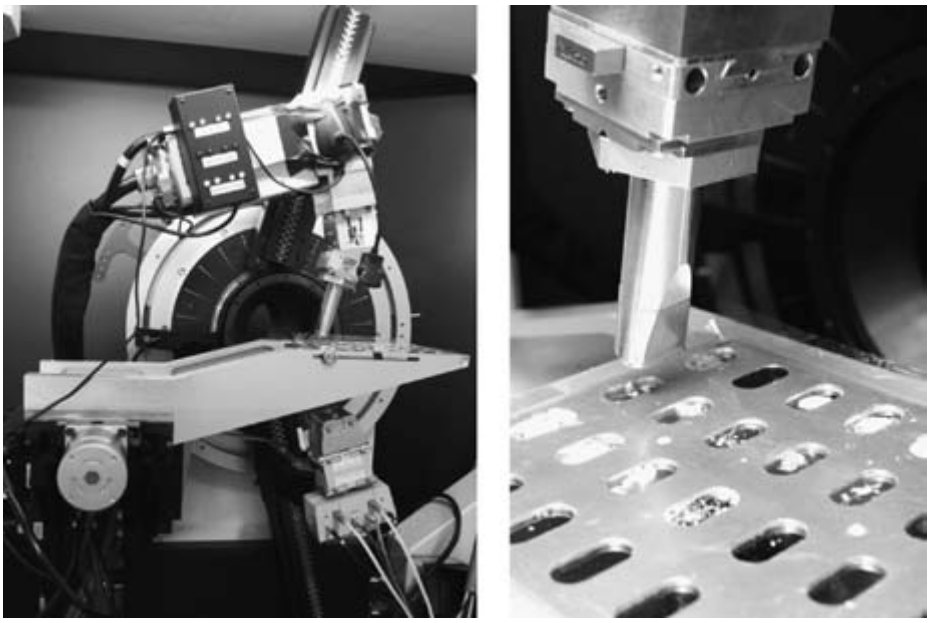

(**A**) (**B**)

FIGURE 13 (**A**) A transmission multi-sample XRPD instrument utilizing primary monochromated Cu Kα_1 radiation, automated *x-y* stage, and PSD. The system is also fitted with a camera to collect images of each sample during data collection. (**B**) A 28-well plate for multiple data collections. Samples are held on an X-ray transparent 7.5-μm Kapton support. Crystallization can be implemented in situ on the plates or samples manually transferred from crystallization vessels.

Capillary transmission instrument geometry can be used where there is a need to obtain both accurate reflection positions and intensities, such as for structure determination from powder data (SDPD) methods. Capillary measurements are also advantageous to protect sensitive samples from air or humidity, for example. For SDPD applications, an effective instrumental configuration includes primary monochromated radiation, capillary sample holder, and PSD. The sample is filled into a glass capillary (typically 0.5–1.0-mm diameter, borosilicate or quartz glass) and rotated continuously during data collection. This effectively reduces preferred orientation effects and maximizes the number of crystallites contributing to the diffraction pattern during data collection. Although laboratory capillary XRPD instruments provide high-quality diffraction data from individual samples, this is typically at the expense of long data collection times.

Sample Characterization

Crystalline solids give rise to Bragg diffraction of X-rays, whereas amorphous solids, lacking long-range internal order, produce only a diffuse scattering halo with no Bragg diffraction peaks. The term "diffraction amorphous" is often used to describe such samples, indicating that the sample contains no crystalline material within the limits of detection of the method. Amorphous samples are worth further

investigation, as in some instances, although a particular set of conditions in the screen has given rise to a non-crystalline solid, crystallization of different polymorphs has been described from amorphous samples of indomethacin (107) and carbamazepine–nicotinamide co-crystals (108), for example.

Sample Identification

The position of each peak in an XRPD pattern corresponds to the interplanar *d*-spacing from a set of planes within the lattice. Hence, any change in the lattice resulting from different crystal packing will result in changes in the diffraction peak positions and intensities observed for that sample. With relatively small numbers of patterns, fingerprinting can be easily done by direct visual comparison of the each pattern; however, once large numbers of patterns are involved, automated means of assessing pattern similarity are highly desirable.

Diffraction pattern quality (i.e., accurate measurement of peak positions, either degrees 2θ or *d*-spacings, Å, and intensities, *I*) is important, as with improved quality of the available XRPD patterns, so the process of pattern recognition becomes easier (109). Low full-width half maximum (FWHM) values are also advantageous, as good angular resolution improves the ability to distinguish individual diffraction peaks in the observed pattern (Fig. 14). It is clearly desirable, if data quality permits, to go beyond pattern matching and recognition by additionally securing structural information for each novel form found in the search. However, even more than with pattern recognition, meeting these ambitious demands requires routine high-quality XRPD data collections as an integral part of the physical form screen.

Traditional, search/match methods rely on comparing *d*-spacings and/or intensities of prominent peaks in the experimental patterns against reference values (109,111). Such approaches require accurate peak positions and intensities, and as stated above, data from high-throughput micro-XRPD instruments can be sub-optimal in this regard. Automatic similarity checking and cluster analysis can, however, be achieved using software packages developed to deal with high-throughput XRPD data. For example, the program PolySNAP (112) allows various corrections (e.g., background subtraction, data scaling, and sample displacement) to be applied automatically to individual patterns as they are read into the program database. The program can compare up to 1500 XRPD data sets simultaneously, and also has provision for additional data types (e.g., DSC, Raman), and for example, quantitative and categorical descriptors about crystallization conditions. The program includes a range of powerful statistical and visualization tools to facilitate rapid clustering and interrogation of large numbers of data and facilitate the identification of new forms among large numbers of individual data sets (106). Rather than rely on individual peak positions or intensities, PolySNAP carries out a full-profile comparison of each pattern with all other patterns. The correlation matrix obtained from these comparisons are used as the basis of subsequent similarity and cluster analyses (Fig. 15). The visual interface allows users to select members of each cluster and check that the automated analyses are accurate, and also to retrieve representative data for any new forms identified.

Comparison of XRPD Data with Single-Crystal Structure

Where one or more reference crystal structures are available, these can be used to identity samples produced from the crystallization screen. The identity of any sample may be confirmed by comparison of the experimental XRPD pattern with

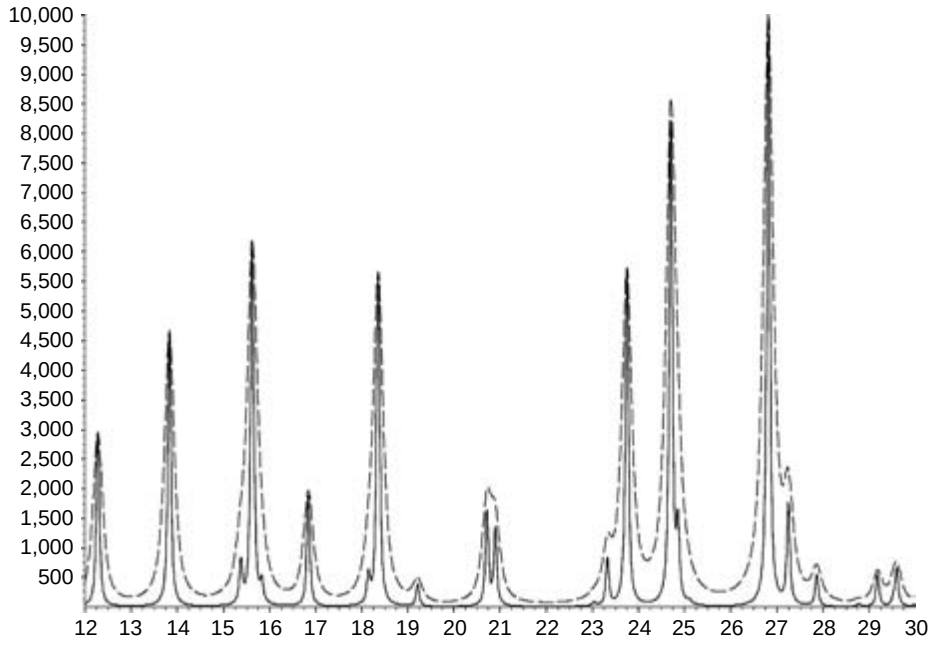

FIGURE 14 Overlaid XRPD patterns simulated using Mercury CSD 2.0 (110) for the monoclinic polymorph of acetaminophen in the range 12–30° 2θ. The patterns are calculated using identical parameters except for the peak full-width at half-maximum value (FWHM), which is set at 0.25° 2θ (*dashed line*) and 0.08° 2θ (*solid line*). Note the considerable loss of detail available at ca. 15.5, 18, 21, and 25° 2θ in the low-angular resolution pattern calculated with 0.25° 2θ FWHM value.

simulated powder data generated from reference single-crystal structures (113,114). However, as single-crystal structures are normally determined from data collected at low temperature, this can lead to significant shifts in the calculated reflection positions in the simulated data. The effects of thermal expansion can therefore complicate the pattern comparison process (115). A more robust approach is to allow the low temperature single-crystal structure unit cell parameters to vary in a Pawley-type fit (116) to the data. The experimental unit cell parameters and space group from the known single-crystal structure are used as the starting values for the refinement. The Pawley fit involves a least-squares refinement of parameters describing the background, instrumental zero-point error, lattice parameters, peak shapes, and peak areas to obtain the best fit to the observed XRPD pattern. Where the calculated profile accounts for all of the observed diffraction peaks and a good fit is achieved, it can be concluded that the single-crystal structure is representative of the sample (Fig. 16). Careful inspection of the final fit to the data can also reveal the presence of contaminant polycrystalline phases.

An additional level of analysis would be to use a Rietveld refinement (117) in which the peak intensities are calculated from the atomic co-ordinates of atoms within the single-crystal structure, rather than being fitted by refining peak area, as in a Pawley fit. However, Pawley refinement is well suited where the aim is to identify

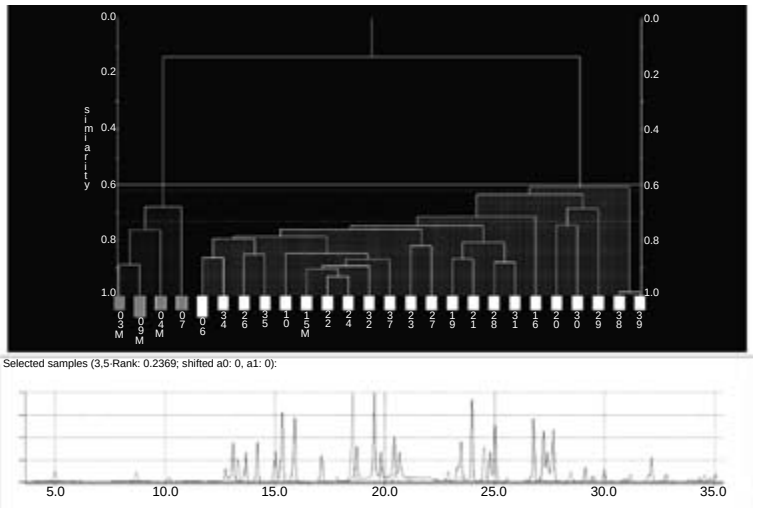

(**A**)

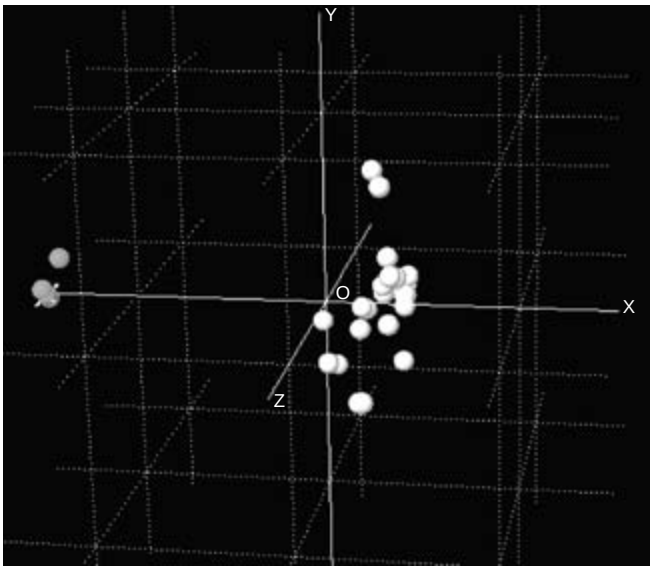

(**B**)

FIGURE 15 (**A**) A dendrogram generated using PolySNAP showing the results of a cluster analysis on a sample of 26 XRPD patterns collected from samples produced from an automated parallel crystallization search on carbamazepine (22). The program has identified two clusters comprising four (gray markers on *left hand side*) and 22 (*white markers*), respectively. The panel at the *bottom* of the plot shows an overlay of two representative patterns from each cluster. (**B**) A 3D metric multi-dimensional scaling (MMDS) plot for the cluster analysis. Each sphere represents an experimental XRPD pattern and is colored according to the cluster to which it belongs in the dendrogram plot. Similar patterns are plotted close together, and outliers are easily identified and can be checked to confirm the assignment.

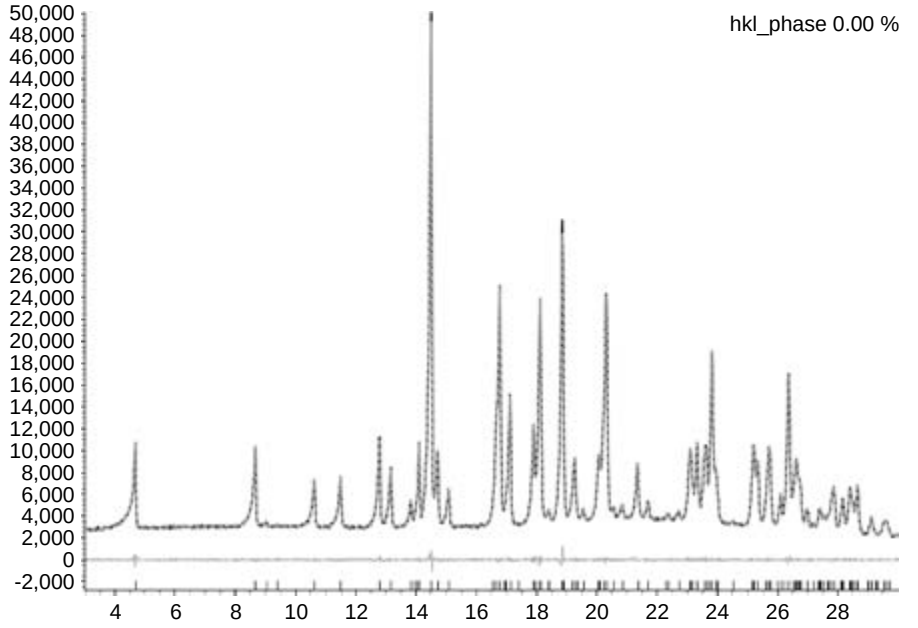

FIGURE 16 A Pawley fit to room temperature capillary XRPD data from a polycrystalline sample of verapamil hydrochloride in the range 3–30° 2θ carried out in TOPAS Academic v4.1. The plot shows the observed (*black*), calculated (*gray-dashed*), and difference (*bottom*) profiles for the final fit. The tick marks along the *bottom* of the plot show the calculated reflection positions. The published unit cell parameters (CSD refcode: CURHOM) were used as the starting point for the refinement. The fit to the data are excellent as indicated by a low R_{wp} value (0.018) and flat difference profile. The refined lattice parameters at room temperature for the triclinic structure ($P\bar{1}$, $Z = 2$) are *a*, *b*, *c* (Å) = 7.0931(1), 10.5950(2), 19.2056(5), α, β, γ (°) = 100.073(1), 93.723(2), 101.569(1).

whether observed diffraction peaks arise from a particular crystalline phase with a known unit cell and space group.

Structure Determination from Powder Data

Although single-crystal methods remain the method of choice for crystal structure determination, in the absence of a suitable single-crystal samples of a particular form, SDPD, using global optimization methods, can often be used (118). SDPD has been successfully applied to determine the crystal structures of a wide range of pharmaceutical polymorphs (119–121), solvates (122–124), salts (125–128), and cocrystals (129), as well as natural products (130) and excipients (131–133). The increased use of SDPD has been facilitated by the wide range of software packages that have become available for implementing global optimization (Table 8). Table 8 also highlights some of the sample, instrumental, data, and software requirements for successful SDPD. The application of global optimization to SDPD has been described in detail elsewhere (118), and the following section will provide a brief overview of this powerful technique for structure analysis.

TABLE 8 A Range of Values of M_n and F_n Returned by the Indexing Program DICVOL for the Correct Unit Cells Obtained from the First 20 Reflection Positions Measured from the Laboratory Capillary XRPD Data

Compound	M(20)	F(20)
Creatine monohydrate	41.9	83.4
Diltiazem.HCl	37.6	103.1
Famotidine (form B)	32.3	88.6
Hydrochlorothiazide (form I)	87.1	160.8

The higher the value the more probable the unit cell is correct. From laboratory data, F(20) values of 30–40 and above often merit close inspection.

SDPD Using Global Optimization

To maximize the chances of successfully and accurately solving crystal structures from laboratory XRPD data, the following data requirements should be met: accurate measurement of reflection positions and intensities, high angular resolution (i.e., small FWHM) and spatial resolution (approximately 2 Å or better), good signal-to-background ratios across the full pattern and minimal preferred orientation effects. These requirements are best achieved in the laboratory with the sample mounted in a rotating glass capillary using data collected in transmission geometry with monochromatic Cu $K\alpha_1$ radiation. Once high-quality accurately measured data have been collected, the next step is to attempt to determine the unit cell parameters. Indexing methods generally use the first 20 peak positions of the pattern to determine the crystal system and unit cell dimensions of the sample. Indexing algorithms use various strategies to search for combinations of lattice parameters that give the best match to the observed peak positions. With accurately measured peak positions, indexing programs tend to work extremely well (Table 8). However, if peak positions arising from the presence of impurities in an XRPD pattern are also used in the search, this will often reduce the chances of successful pattern indexing.

With the cell parameters known, the space group symmetry can be determined by visual comparison of observed peak positions with reflection positions calculated from the unit cell parameters and systematic absences of each space group. Probabilistic methods for identifying the correct space group that effectively automate the process have also been implemented (134). A Pawley refinement to the experimental pattern using the unit cell and space group can then be used to provide confirmation that the correct cell and symmetry settings have been selected.

The next step in the structure determination process is to extract the individual intensities associated with each reflection from the observed diffraction peaks. The Le Bail (169) and Pawley (116) methods are most widely applied to dealing with intensity extraction from overlapped peaks, and whichever method is used, once a good fit has been obtained to the data, the extracted intensities can then be used as the basis for the global optimization.

Global optimization strategies are used to find the trial crystal structure (position, orientation, and conformation of molecular components in the unit cell) that gives the lowest possible *R*-factor (or best fit) between the observed intensities and those calculated from the trial structure, that is, locate the global minimum. Various

search methods have been applied in this context with simulated annealing in particular being widely implemented (Table 9). Global optimization approaches are also amenable to parallelization, and so can also take advantage of modern multicore processors or distributed computing grids. This can significantly reduce the time required to solve complex structures or assess multiple models, for example, when dealing with potentially disordered structures. With simulated annealing, many runs (typically several hundred) are implemented to confirm that the global minimum has been correctly identified in the search.

In single-crystal diffraction, each atomic position is generally determined independently using direct methods (153). This is routinely possible, as a typical experiment will yield several thousand independent reflection intensities. A typical powder experiment, however, provides access to only a few hundred reflections as a result of reflection overlap arising from the collapse of the three dimensions of reciprocal space onto a single dimension in the powder pattern. Global optimization approaches can effectively overcome this loss of information by using prior chemical knowledge, typically in the form of the atomic connectivity of the molecular fragments in the structure; thereby significantly reducing the number of parameters that need to be determined. A three-dimensional model, in the form of a z-matrix, is constructed for each structural fragment in which the bond lengths and angles defining the connectivity of atoms are constrained to standard values. The parameters that define the location of atoms in the unit cell and optimized during the search, comprise six variables describing the position (x, y, z) and orientation (θ, ϕ, ψ) of each molecular fragment in the asymmetric unit plus an additional variable for each flexible torsion angle describing the molecular conformation.

For example, a single-crystal structure determination attempt for verapamil hydrochloride would need to determine 219 fractional co-ordinates to describe the location of all 73 atoms in the asymmetric unit. In contrast, a global optimization search need only determine 22 parameters (3 degrees of freedom for the position of the chloride ion, 6 describing the position and orientation of the verapamil cation, and 13 degrees of freedom describing each of the flexible torsion angles in the molecule; Fig. 17). During the global optimization search, the position, orientation, and

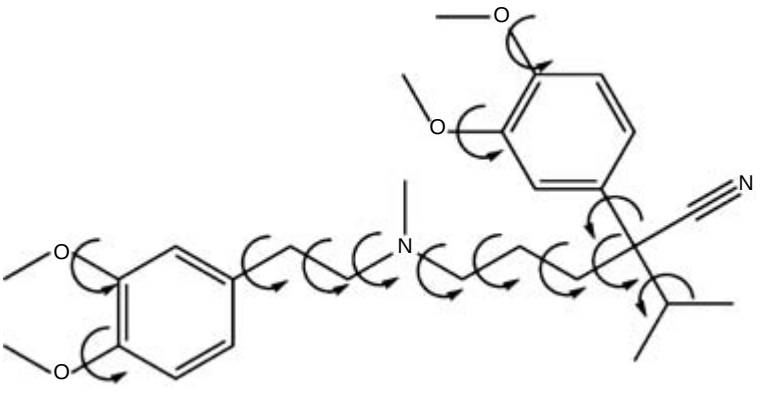

FIGURE 17 Molecular structure of verapamil with 13 flexible torsion angles highlighted (*curved arrows*).

TABLE 9 Various Factors for the Successful Application of SDPD Using Laboratory XRPD Data to Polycrystalline Pharmaceuticals

Requirements	Comments
Sample	
• ca. 10 mg sample	• Know molecular connectivity, relative stereochemistry, solvate, or salt
• Known chemical composition	
• Minimal preferred orientation	• Lightly grind sample or recrystallize
• Known unit cell and space group	• From powder pattern indexing
• Accurate 3D models of the molecular geometry	• Generated from related structures, for example, known polymorph, or from molecular modeling
Instrument	
• Transmission capillary geometry	• Sample in rotating 0.7-mm diameter borosilicate capillary
• Primary monochromatic radiation	• Single wavelength simplifies data analysis
• Position sensitive detector	• Yields good counting statistics and angular resolution
• Sample temperature control	• Cryostream devices: 80–500 K
Data	
• Good signal-to-noise ratio	• Apply variable counting time (VCT) scheme (135,136) and/or low-temperature data collection
• Good angular resolution	• ca. 0.08° 2θ FWHM typical for organic molecular solids using instrumentation described above
• Indexing and global optimization	• Capillary XRPD data to ~2 Å resolution using relatively long step times (5–10 seconds) to identify weak reflections in low 2θ range
• Rietveld refinement	• Capillary XRPD data to at least 1.3 Å resolution using VCT
Software	
• Indexing	• e.g., DICVOL (137,138), ITO (139), TREOR (140,141), TOPAS (142), McMaille (143), and X-Cell [144]
• Structure determination	• e.g., DASH (145), Endeavour (146), ESPOIR (147), FOX (148), PowderSolve (149), PSSP (150) and TOPAS (151)
• Structure (Rietveld) refinement	• e.g., GSAS (152), TOPAS

Abbreviations: FWHM, full-width at half-maximum; XRPD, X-ray powder diffraction.

conformation of the model are varied, and the calculated intensities from each trial structure compared to those extracted from the experimental XRPD pattern. As the search progresses, the model is varied in such a way as to try and improve the fit. When the best possible match to the data is identified, the global minimum has been found and the crystal structure solved.

The structure is then finalized by carrying out a Rietveld refinement in which the model returned from the global optimization is varied to obtain the best possible fit to the experimental data while retaining good chemical sense.

Variable Temperature XRPD

Just as DSC is widely used to identify thermal transformations in organic solids, so XRPD can be combined with variable temperature and/or %R.H. to identify the conditions under which structural changes may occur. Capillary XRPD with temperature control is a particularly effective technique for tracking structural transformations in polycrystalline samples. Temperatures in the range 80–500 K are accessible using standard cryostream systems enabling samples to be heated or cooled in situ to monitor structural transitions such as desolvations or solid–solid transitions. High-resolution capillary XRPD data can then be collected from the emergent form, enabling the crystal structure to be solved and refined using the procedures outlined above. Structural transformations cannot usually be monitored effectively using single-crystal diffraction as the structural re-arrangement associated with the transition frequently results in a polycrystalline sample.

The structure determination of form II cytenamide ($C_{16}H_{13}NO$; Fig. 18) is an example of the application of variable-temperature XRPD, SDPD, and Rietveld refinement to good effect in physical form discovery (154). A polycrystalline sample of form I cytenamide, an analogue of carbamazepine, was obtained by recrystallization from chloroform, placed in a rotating 0.7-mm borosilicate glass capillary and mounted on a Bruker AXS D8 Discover TXS X-ray powder diffractometer. The sample transformed to form II on heating the sample to 498 K. The sample of form II cytenamide was then cooled to room temperature, where it remained stable, and data collected using a VCT scheme to 70° 2θ (12 kW; Cu $K\alpha_1$, $\lambda = 1.54056$ Å; step size 0.017° 2θ). The diffraction pattern indexed to a triclinic unit cell using DICVOL, and the structure was solved using simulated annealing in DASH with a *z*-matrix constructed from the cytenamide form I single-crystal structure. The $Z' = 4$ triclinic structure required 28 degrees of freedom to describe the position, orientation, and confirmation of four independent molecules. A rigid-body Rietveld refinement of the structure obtained by simulated annealing included a total of 72 parameters (22 profile, 6 cell, 1 scale, 1 isotropic temperature factor, 14 preferred orientation, 4 torsion angles, 12 position, 12 rotation) yielded a final $R_{wp} = 0.041$ (Fig. 18).

Single Crystal diffraction

Single-crystal X-ray diffraction is the definitive method for crystal structure determination, and is responsible for over 430,000 experimental crystal structure determinations available as of January 2008 in the Cambridge Structural Database (CSD) (155). Modern laboratory instruments are widely available, and offer automated collection of high-quality data to atomic resolution (<1 Å) as required by the direct methods approach commonly applied to structure determination of organic materials. Crystal structures (unit cell parameters, space group, and atomic co-ordinates) are of considerable value for the unambiguous identification of novel crystalline forms and structural analysis of molecular packing in different polymorphs produced in experimental searches.

Although SDPD can be used for crystal structure determination in the absence of suitable single-crystal samples, single-crystal X-ray diffraction is the technique of choice for crystal structure determination. Hence, where crystals of suitable size

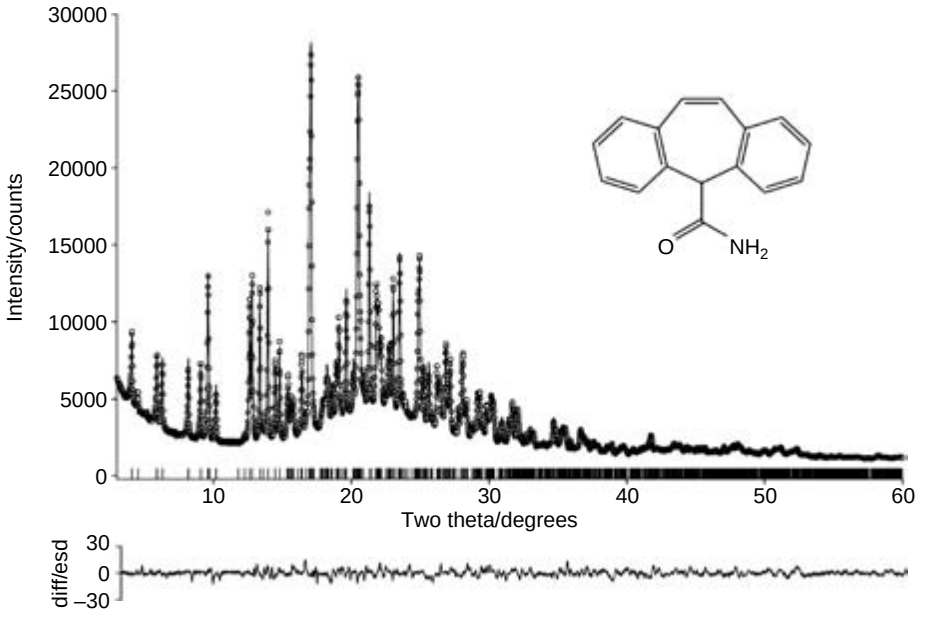

FIGURE 18 Final observed (*points*), calculated (*line*), and difference $[(y_{obs} - y_{calc})/\sigma(y_{obs})]$ profiles for the rigid-body Rietveld refinement of cytenamide (inset) form II (refined lattice parameters a = 5.8100(2), b = 19.6315(5), c = 21.7087(6) Å, α = 85.918(2), β = 86.164(2), γ = 84.482(2), V = 2453.82(13) Å^3, triclinic, $P\bar{1}$, Z' = 4) using laboratory XRPD data collected at 293 K to a resolution of 1.3 Å. The final fit to the data is excellent yielding a final R_{wp} = 0.041.

and quality are not obtained from an initial crystallization, it is always desirable to employ further recrystallizations in an attempt to obtain more suitable samples of the particular form of interest. Controlled cooling or slow evaporation of solutions are often useful in this context, with the best results obtained from unstirred solutions aimed at reducing rates of nucleation and slowing crystal growth (e.g., slow evaporation or controlled cooling). Recrystallization may also, however, give rise to alternative polymorphs or solvates to the intended form. Seeding the solution with small amounts of the original sample can be an effective way to ensure the correct form is obtained and increase crystallite size. Other approaches that alter the nucleation and growth environment in such a way as to favor improved quality single-crystal samples include trying different solvents, solvent mixtures, and temperatures or other methods such as vapor diffusion (31,156), liquid–liquid diffusion (157), thermal gradients (158), sublimation (33,159), growth from the melt (159,160), and crystallization from gels (161,162). If these attempts fail, at least within the time scales imposed by the experiment, then SDPD can be attempted. Single-crystal samples of at least 100 μm are usually required for modern laboratory instruments, although smaller crystals may be used in some cases. For small, weakly scattering microcrystals, high powered rotating anode laboratory sources or synchrotron instruments can also be used to collect data of sufficient quality to allow structure determination (163).

A consequence of the increasing use of parallel crystallization in physical form discovery, either in high-throughput or semi-automated, smaller scale modes, is the increasing number of samples being produced that require crystal structure determination. This poses considerable challenges for traditional laboratory single-crystal diffraction facilities. It is perhaps a logical consequence that, where the demand for large numbers of novel crystal structures continues to grow, innovative approaches to high-throughput chemical crystallography are required (164).

Crystal Packing Analysis

With the increasing rate at which novel organic molecular crystal structures can be produced, crystal structure analysis has arguably become a new bottleneck in the study of polymorphism and multi-component crystal formation. In recent years a variety of techniques including Mercury (110), d-SNAP (165), XPac (166), and CrystalExplorer (167) have been developed to enable efficient structural classification of different crystalline structures and to investigate the interplay between molecular structure, intermolecular interactions, and crystal packing. In combination with developments in CSP and other computational methods for studying crystalline solids, these tools are providing new opportunities to explore the basic science underpinning polymorphism and physical form diversity in pharmaceutical solids.

Physicochemical Characterization

In keeping with the drive to increase the efficiency of all stages in the discovery and development of new pharmaceuticals, high-throughput approaches to physicochemical characterization of pharmaceutical solids have also been developed in recent years (2). A variety of automated systems are commercially available to support thermal analysis, solubility, hygroscopicity, drug-excipient compatibility, and chemical stability on small amounts of material. However, as with automated crystallization methods these characterization technologies require careful deployment and effective data management and informatics tools to ensure their productive use in solid form development.

CONCLUDING REMARKS

Control and prediction of the structure and properties of pharmaceutical solids remains a significant challenge for those involved in the commercial development and manufacture of pharmaceuticals. Phenomena such as polymorphism and solvate formation continually test our understanding of the basic science underpinning crystallization and the organic solid state. Thus, in the absence of reliable predictive models, rigorous experimental investigation remains the best means to establish the extent of structural diversity a particular molecule can display, the crystal structure of each form, the conditions under which they can be produced, and their physicochemical properties. Parallel crystallization techniques therefore have a valuable role to play in these endeavors, providing a more detailed and accurate view of the extent of solid-state diversity in molecular solids. That said, high-throughput crystallization screening does not offer a complete solution to understanding physical form diversity (1,80,168). Rather, automated methods offer a powerful set of tools that complement the arsenal of other approaches, described elsewhere in this book,

that can profitably increase the coverage of experimental space included during any investigation.

REFERENCES

1. Hilfiker R, Berghausen J, Blatter F, et al. Polymorphism – integrated approach from high-throughput screening to crystallization optimization. J Therm Anal Calorim 2003; 73: 429–40.
2. Kumar L, Amin A, Bansal AK. An overview of automated systems relevant in pharmaceutical salt screening. Drug Discov Today 2007; 12: 1046–53.
3. Morissette SL, Almarsson O, Peterson ML, et al. High-throughput crystallization: polymorphs, salts, co-crystals and solvates of pharmaceutical solids. Adv Drug Delive Rev 2004; 56: 275–300.
4. Storey R, Docherty R, Higginson PD, et al. Automation of Solid Form Screening Procedures in the Pharmaceutical Industry – How to Avoid the Bottlenecks Crystallography Reviews. 2004; 37: 243–52.
5. Snider DA, Addicks W, Owens W. Polymorphism in generic drug product development. Adv Drug Delive Rev 2004; 56: 391–5.
6. Balbach S, Korn C. Pharmaceutical evaluation of early development candidates the 100 mg-approach. Int J Pharm 2004; 275: 1–12.
7. Bernstein J. Polymorphism and Patents from a Chemist's Point of View, in Polymorphism in the pharmaceutical industry. In: Hilfiker R, ed. Wiley-VCH; Weinheim, 2006: 365–82.
8. Jahansouz H, Thompson, KC, Brenner GS, et al. Investigation of the polymorphism of the angiotensin II antagonist agent MK-996. Pharm Dev Technol 1999; 4: 181–7.
9. Almarsson O, Hickey MB, Peterson ML, et al. High-throughput surveys of crystal form diversity of highly polymorphic pharmaceutical compounds. Crys Growth Des 2003; 3: 927–33.
10. Peterson ML, Morissette SL, McNulty C, et al. Iterative high-throughput polymorphism studies on acetaminophen and an experimentally derived structure for form III. J Am Chem Soc 2002; 124: 10958–9.
11. Morissette SL, Soukasene S, Levinson D, et al. Elucidation of crystal form diversity of the HIV protease inhibitor ritonavir by high-throughput crystallization. P Nat Acad Sci USA 2003; 100: 2180–4.
12. Chayen NE. Protein crystallization for genomics: throughput versus output. J Structural Functional Genomics 2003; 4: 115–20.
13. Price SL. From crystal structure prediction to polymorph prediction: interpreting the crystal energy landscape. Phys Chem Chem Phys 2008; 10: 1996–2009.
14. Miller JM, Collman BM, Greene LR, et al. Identifying the stable polymorph early in the drug discovery-development process. Pharm Dev Technol 2005; 10: 291–7.
15. Schmidt MU. In Crystal Engineering: From Molecules and Crystals to Materials. In: Braga D, Grepioni F, Orpen AG, eds. Kluwer: Dordrecht, 1999: 331–48.
16. Johnston A, Florence AJ, Shankland N, et al. Crystallization and crystal energy landscape of hydrochlorothiazide. Crys Growth Des 2007; 7: 705–12.
17. Bandoli G, Nicolini M, Ongaro A, et al. X-ray crystallographic Characterization of 10,11-dihydro-5H-dibenz[B,F]azepine-5-carboxamide. J Cryst Spectrosc 1992; 22: 177–83.
18. Grzesiak AL, Lang MD, Kim, K, et al. Comparison of the four anhydrous polymorphs of carbamazepine and the crystal structure of form I. Pharm Sci 2003; 92: 2260–71.
19. Lang MD, Kampf JW, Matzger AJ. Form IV of carbamazepine. J Pharma Sci 2002; 91: 1186–90.
20. Rustichelli C, Gamberini G, Ferioli V, et al. Solid-state study of polymorphic drugs: carbamazepine. J Pharmaceu Biomed 2000; 23: 41–54.

21. Lohani S, Zhang YG, Chyall LJ, et al. Carbamazepine-2,2,2-trifluoroethanol (1/1). Acta Crystallographica Section E-Structure Reports Online 2005; 61: O1310–O1312.
22. Florence AJ, Johnston A, Price SL, et al. An automated parallel crystallisation search for predicted crystal structures and packing motifs of carbamazepine. J Pharm Sci 2006; 95: 1918–30.
23. Johnston A, Johnston BF, Kennedy AR, et al. Targeted crystallization of novel carbamazepine solvates based on a retrospective random forest classification. CrystEngComm 2008; 10: 23–5.
24. Fleischman SG, Kuduva SS, McMahon JA, et al. Crystal engineering of the composition of pharmaceutical phases: multiple-component crystalline solids involving carbamazepine. Crys Growth Des 2003; 3: 909–19.
25. Almarsson O, Zaworotko MJ. Crystal engineering of the composition of pharmaceutical phases. Do pharmaceutical co-crystals represent a new path to improved medicines? Chem Commun 2004: 1889–96.
26. Childs SL, Rodriguez-Hornedo N, Reddy LS, et al. Screening strategies based on solubility and solution composition generate pharmaceutically acceptable cocrystals of carbamazepine. CrystEngComm 2008; 10: 856–64.
27. McMahon JA, Bis JA, Vishweshwar P, et al. Crystal engineering of the composition of pharmaceutical phases. 3. Primary amide supramolecular heterosynthons and their role in the design of pharmaceutical co-crystals. Z Kristallogr 2005; 220: 340–50.
28. Porter WW, Elie SC, Matzger AJ. Polymorphism in carbamazepine cocrystals. Crys Growth Des 2008; 8: 14–6.
29. Lang MD, Grzesiak AL, Matzger AJ. The use of polymer heteronuclei for crystalline polymorph selection. J Am Chem Soc 2002; 124: 14834–5.
30. Toro R, de Delgado GD, Bahsas A, et al. The presence of polymorphism in oxytetracycline hydrochloride shown by X-ray powder diffraction techniques. Z Kristallogr 2007: 563–8.
31. Vandersluis P, Hezemans AMF, Kroon J. Crystallization of Low-molecular-weight Organic-compounds for X-ray Crystallography. J Appl Crystallogr 1989; 22: 340–4.
32. Ceolin R, Toscani S, Gardette MF, et al. X-ray characterization of the triclinic polymorph of carbamazepine. J Pharma Sci 1997; 86: 1062–5.
33. van Hoof P, Lammers R, von Puijenbroek R, et al. Polymorphism of the CNS active drug Org 13011: the application of high temperature analysis to detect new polymorphs. Int J Pharm 2002; 238: 215–28.
34. Vitez IM, Newman AW, Davidovich M, et al. The evolution of hot-stage microscopy to aid solid-state characterizations of pharmaceutical solids. Thermochim Acta 1998; 324: 187–96.
35. Gong YC, Collman BM, Mehrens SM, et al. Stable-form screening: overcoming trace impurities that inhibit solution-mediated phase transformation to the stable polymorph of sulfamerazine. J Pharm Sci 2008; 97: 2130–44.
36. Capes JS, Cameron RE. Contact line crystallization to obtain metastable polymorphs. Crystal Growth & Design 2007; 7: 108–12.
37. Llinas A, Box KJ, Burley, JC, et al. A new method for the reproducible generation of polymorphs: two forms of sulindac with very different solubilities. J Appl Crystallogr 2007; 40: 379–81.
38. Trask AV, van de Streek J, Motherwell WDS, et al. Achieving polymorphic and stoichiometric diversity in cocrystal formation: importance of solid-state grinding, powder X-ray structure determination, and seeding. Crystal Growth & Design 2005; 5: 2233–41.
39. Trask AV, Shan N, Motherwell WDS, et al. Selective polymorph transformation via solvent-drop grinding. Chem Commun 2005: 880–2.
40. Fabbiani FPA, Allan DR, David WIF, et al. High-pressure recrystallisation – a route to new polymorphs and solvates. CrystEngComm 2004; 6: 504–11.

41. Fabbiani FPA, Pulham CR. High-pressure studies of pharmaceutical compounds and energetic materials. Chem Soc Rev 2006; 35: 932–42.
42. Mitchell CA, Yu L, Ward MD. Selective nucleation and discovery of organic polymorphs through epitaxy with single crystal substrates. J Am Chem Soc 2001; 123: 10830–9.
43. Grzesiak AL, Matzger AJ. New form discovery for the analgesics flurbiprofen and sulindac facilitated by polymer-induced heteronucleation. J Pharma Sci 2007; 96: 2978–86.
44. Price CP, Grzesiak AL, Matzger AJ. Crystalline polymorph selection and discovery with polymer heteronuclei. J Am Chem Soc 2005; 127: 5512–17.
45. Liberski AR, Tizzard GJ, Diaz-Mochon JJ, et al. Screening for polymorphs on polymer microarrays. J Comb Chem 2008; 10: 24–7.
46. Dressler DH, Hod I, Mastai Y. Stabilization of alpha-L-glutamic acid on chiral thin films – A theoretical and experimental study. Salt Lake City, UT: In 15th International Conference on Crystal Growth, 2007.
47. Hiremath R, Basile JA, Varney SW, et al. Controlling molecular crystal polymorphism with self-assembled monolayer templates. J Am Chem Soc 2005; 127: 18321–7.
48. Lee T, Hung ST, Kuo CS. Polymorph farming of Acetaminophen and Sulfathiazole on a chip. Pharmaceu Res 2006; 23: 2542–55.
49. Edwards AD, Shekunov BY, Kordikowski A, et al. Crystallization of pure anhydrous polymorphs of carbamazepine by solution enhanced dispersion with supercritical fluids (SEDS™). J Pharm Sci 2001; 90: 1115–24.
50. Zaccaro J, Matic J, Myerson AS, et al. Nonphotochemical, laser-induced nucleation of supersaturated aqueous glycine produces unexpected gamma-polymorph. Crys Growth Des 2001; 1: 5–8.
51. Hilden JL, Reyes CE, Kelm MJ, et al. Capillary precipitation of a highly polymorphic organic compound. Crys Growth Des 2003; 3: 921–6.
52. Hilfiker R, Berghausen J, Blatter F, et al. High-throughput screening for polymorphism. Chim Oggi 2003; 21: 75.
53. Peterson ML, Hickey MB, Zaworotko MJ, et al. Expanding the scope of crystal form evaluation in pharmaceutical science. J Pharm and Pharm Sci 2006; 9: 317–26.
54. Cima MJ, Levinson D, Lemmo AV et al. High-Throughput Formation, Identification, and Analysis of Diverse Solid-Forms USPTO, Pub No. US2002/0048610 A1, 2002.
55. Florence AJ, Johnston A, Fernandes P, et al. An automated platform for parallel crystallization of small organic molecules. J Appl Crystallogr 2006; 39: 922–4.
56. Gardner CR, Almarsson O, Chen HM, et al. Application of high throughput technologies to drug substance and drug product development. Comp Chem Eng 2004; 28: 943–53.
57. Hulme AT, Johnston A, Florence AJ, et al. Search for a predicted hydrogen bonding motif – a multidisciplinary investigation into the polymorphism of 3-azabicyclo[3.3.1] nonane-2,4-dione. J Am Chem Soc 2007; 129: 3649–57.
58. Barnett SA, Johnston A, Florence, AJ, et al. A systematic experimental and theoretical study of the crystalline state of six chloronitrobenzenes. Crys Growth Des 2008; 8: 24–36.
59. Kojima T, Sugano K, Onoue S, et al. Solid form selection of zwitterionic 5-HT4 receptor agonist. Int J Pharm 2008; 350: 35–42.
60. Lee IS, Lee AY, Myerson AS. Concomitant polymorphism in confined environment. Pharmaceu Res 2008; 25: 960–8.
61. Remenar JF, MacPhee JM, Larson BK, et al. Salt selection and simultaneous polymorphism assessment via high-throughput crystallization: the case of sertraline. Org Process Res Dev 2003; 7: 990–6.
62. Kojima T, Onoue S, Murase N, Katoh, F.; et al. Crystalline form information from multiwell plate salt screening by use of Raman microscopy. Pharmaceu Res 2006; 23: 806–12.

63. Rohani S, Horne S, Murthy K. Control of product quality in batch crystallization of pharmaceuticals and fine chemicals. Part 1: design of the crystallization process and the effect of solvent. Org Process Res Dev 2005; 9: 858–72.
64. Miller J, RodrÍGuez-Hornedo N, Blackburn A, et al. Solvent systems for crystallization and polymorph selection, in solvent systems and their selection in pharmaceutics and biopharmaceutics 2007: 53–109.
65. Mullin JW. Crystallization, 4th ed. Oxford; Boston: Butterworth-Heinemann, 2001: xv, 594.
66. Pinto SS, Diogo HP. Thermochemical study of two anhydrous polymorphs of caffeine. J Chem Thermodyn 2006; 38: 1515–22.
67. Lide DR, ed. Properties of Organic Solvents, Version 2.0. Boca Raton: Taylor & Francis Ltd, 1996: 48.
68. Reichardt C. Solvents and solvent effects in organic chemistry. 3rd updated and enl. ed. Weinheim: Wiley-VCH, 2003: xxiv, 629.
69. Gu CH, Li H, Gandhi RB, et al. Grouping solvents by statistical analysis of solvent property parameters: implication to polymorph screening. Int J Pharma 2004; 283: 117–25.
70. Alleso M, Van Den Berg F, Cornett C, et al. Solvent diversity in polymorph screening. J Pharma Sci 2008; 97: 2145–59.
71. Mirmehrabi M, Rohani S. An approach to solvent screening for crystallization of polymorphic pharmaceuticals and fine chemicals. J Pharma Sci 2005; 94: 1560–76.
72. Threlfall T. Crystallisation of Polymorphs: thermodynamic insight into the Role of Solvent. Org Process Res Dev 2000; 4: 384–90.
73. Getsoian A, Lodaya RM, Blackburn AC. One-solvent polymorph screen of carbamazepine. Int J Pharma 2008; 348: 3–9.
74. Roelands CPM, ter Horst JH, Kramer HJM, et al. Precipitation mechanism of stable and metastable polymorphs of L-glutamic acid. Aiche J 2007; 53: 354–62.
75. Poornachary SK, Chow PS, Tan RBH. Influence of solution speciation of impurities on polymorphic nucleation in glycine. Crys Growth Des 2008; 8: 179–85.
76. Mukuta T, Lee AY, Kawakami T, et al. Influence of impurities on the solution-mediated phase transformation of an active pharmaceutical ingredient. Crys Growth Des 2005; 5: 1429–36.
77. Sonoda Y, Hirayama F, Arima H, et al. Selective crystallization of the metastable form IV polymorph of tolbutamide in the presence of 2,6-di-O-methyl-beta-cyclodextrin in aqueous solution. Crys Growth Des 2006; 6: 1181–5.
78. Gu CH, Young V, Grant DJW. Polymorph screening: influence of solvents on the rate of solvent-mediated polymorphic transformation. J Pharma Sci 2001; 90: 1878–90.
79. Hilfiker R, De Paul SM, Szelagiewicz M. Approaches to Polymorphism Screening, in Polymorphism in the pharmaceutical industry. In: Hilfiker R, ed. Wiley-VCH: Weinheim, 2006: 287–308.
80. Stahly GP. Diversity in single- and multiple-component crystals. The search for and prevalence of polymorphs and cocrystals. Crys Growth Des 2007; 7: 1007–26.
81. Liaw A, Wiener M. Classification and Regression by randomForest. R News 2002; 2: 18–22.
82. Nollenberger K, Gryczke A, Meier CH, et al. Pair distribution function X-ray analysis explains dissolution characteristics of felodipine melt extrusion products. J Pharma Sci 2008; 98: 1476–86.
83. Perlovich GL, Surov AO, Hansen LK, et al. Energetic aspects of diclofenac acid in crystal modifications and in solutions – mechanism of solvation, partitioning and distribution. J Pharma Sci 2007; 96: 1031–42.
84. Florence AJ, Baumgartner B, Weston C, et al. Indexing powder patterns in physical form screening: instrumentation and data quality. J Pharma Sci 2003; 92: 1930–8.
85. Birch M, Fussell SJ, Higginson PD, et al. Towards a PAT-Based strategy for crystallization development. Organic Process Res Dev 2005; 9: 360–4.
86. ter Horst JH, Cains PW. Co-crystal polymorphs from a solvent-mediated transformation. Crys Growth Des 2008; 8: 2537–42.

87. Florence AJ, Shankland N, Johnston A. Crystallization in Final Stages of Purification, in Natural products isolation. In: Sarker SD, Latif Z, Gray AI, eds. Totowa, NJ: Humana Press, 2006: 275–95.
88. Nichols G. Light Microscopy. Polymorphism in the pharmaceutical industry. In: Hilfiker R, ed. Wiley-VCH: Weinheim, 2006: 167–209.
89. Mayo CJ, Diprose JM, Walter TS, et al. Benefits of Automated Crystallization Plate Tracking, Imaging, and Analysis. Structure 2005; 13: 175–82.
90. Harris RK. Applications of solid-state NMR to pharmaceutical polymorphism and related matters. J Pharm and Pharmacol 2007; 59: 225–39.
91. Norris T, Aldridge PK, Sekulic SS. Near-infrared spectroscopy. Analyst 1997; 122: 549–52.
92. Aaltonen J, Rantanen J, Siiria S, et al. Polymorph screening using near-infrared spectroscopy. Anal Chem 2003; 75: 5267–73.
93. Chan KLA, Kazarian SG, Vassou D, et al. In situ high-throughput study of drug polymorphism under controlled temperature and humidity using FT-IR spectroscopic imaging. Vib Spectros 2007; 43: 221–6.
94. Taday PF, Bradley IV, Arnone DD, et al. Using terahertz pulse spectroscopy to study the crystalline structure of a drug: a case study of the polymorphs of ranitidine hydrochloride. J Pharma Sci 2003; 92: 831–8.
95. Rodriguez-Spong B, Price CP, Jayasankar A, et al. General principles of pharmaceutical solid polymorphism: a supramolecular perspective. Adv Drug Deliver Rev 2004; 56: 241–74.
96. Sasic S. Pharmaceutical applications of Raman spectroscopy. Wiley series on technologies for the pharmaceutical industry. Ames, Iowa: Wiley-Interscience, 2008, 1–258.
97. Bugay DE, Brittain HG. Raman Spectroscopy, in Spectroscopy of pharmaceutical solids. In: Brittain HG, ed. New York: Taylor & Francis, 2006: 271–312.
98. Auer ME, Griesser UJ, Sawatzki J. Qualitative and quantitative study of polymorphic forms in drug formulations by near infrared FT-Raman spectroscopy. J Mol Struct 2003; 661–2: 307–17.
99. Bugay DE, Findlay WP. Vibrational spectroscopy, in Handbook of pharmaceutical analysis. In: Ohannesian L, Streeter AJ, eds. New York: Marcel Dekker, 2002.
100. Adar F, Whitley A, Geiger R. A Raman Microprobe Optimized for Microarrays and Multiple-Well Plates. American Genomic/Proteomic Technology, 2001.
101. Yang X, Jie Lu, Xiujuan Wang, et al. In situ monitoring of the solution-mediated polymorphic transformation of glycine: characterization of the polymorphs and observation of the transformation rate using Raman spectroscopy and microscopy. J Raman Spectros 2008; 39: 1433–9.
102. Remenar JF, MacPhee JM, Larson BK, et al. Salt selection and simultaneous polymorphism assessment via high-throughput crystallization: the case of sertraline. Org Process Res Dev 2003; 7: 990–6.
103. Aaltonen J, Strachan CJ, Pöllänen K, et al. Hyphenated spectroscopy as a polymorph screening tool. J Pharmaceut Biomed 2007; 44: 477–83.
104. Reibenspies JH, Bhuvanesh NSP. Combinatorial screening employing nylon loops and micro-X-ray powder diffraction. J Pharmaceut Biomed 2005; 37: 611–4.
105. Ning G, Flemming RL. Rietveld refinement of LaB6: data from μXRD. J Appl Crystallogr 2005; 38: 757–9.
106. Barr G, Dong W, Gilmore CJ. High-throughput powder diffraction II. Applications of clustering methods and multivariate data analysis. J Appl Crystallogr 2004; 37: 243–52.
107. Bhugra C, Shmeis R, Pikal MJ. Role of mechanical stress in crystallization and relaxation behavior of amorphous Indomethacin. J Pharm Sci 2008; 97: 4446–58.
108. Seefeldt K, Miller J, Alvarez-Nunez F, et al. Crystallization pathways and kinetics of carbamazepine-nicotinamide cocrystals from the amorphous state by in situ thermomicroscopy, spectroscopy and calorimetry studies. J Pharm Sci 2007; 96: 1147–58.
109. Faber J, Fawcett T. The powder diffraction file: present and future. Acta Crystallogr B 2002; 58: 325–32.

110. Bruno IJ, Cole JC, Edgington PR, et al. New software for searching the Cambridge Structural Database and visualizing crystal structures. Acta Crystallogr B 2002; 58: 389–97.
111. Faber J. ICDD's new PDF-4 organic database: search indexes, full pattern analysis and data mining. Crystallogr Rev 2004; 10: 97–107.
112. Barr G, Dong W, Gilmore CJ. PolySNAP: a computer program for analysing high-throughput powder diffraction data. J App Crystallogr 2004; 37: 658–64.
113. Leech CK, Florence AJ, Shankland K, et al. 10,11-dihydrocarbamazepine (form III). Acta Crystallogr E-Structure Reports Online 2007; 63: O675–O677.
114. Karami S, Li Y, Hughes DS, et al. Further errors in polymorph identification: furosemide and finasteride. Acta Crystallographica Section B-Structural Science 2006; 62: 689–91.
115. Stephenson GA. Anisotropic lattice contraction in pharmaceuticals: the influence of cryocrystallography on calculated powder diffraction patterns. J Pharm Sci 2006; 95: 821–7.
116. Pawley GS. Unit-cell refinement from powder diffraction scans. J Appl Crystallogr 1981; 14: 357–61.
117. Rietveld HM. A profile refinement method for nuclear and magnetic structures. J Applied Crystallogr 1969; 2: 65–71.
118. Shankland K, David WIF. Global optimisation strategies, in Structure Determination from Powder Diffraction Data. In: David WIF, et al, eds. Oxford: Oxford University Press, 2002: 252–85.
119. Fernandes P, Shankland K, Florence AJ, et al. Solving molecular crystal structures from X-ray powder diffraction data: the challenges posed by gamma-carbamazepine and chlorothiazide N,N,-dimethylformamide (1/2) solvate. J Pharm Sci 2007; 96: 1192–202.
120. Shankland N, David WIF, Shankland, K, et al. Structural transformations in zopiclone. Chem Commun 2001: 2204–5.
121. Florence A, Johnston A, Fernandes P, et al. Powder study of hydrochlorothiazide form II. Acta Crystallogra E-Structure Reports Online 2005; 61: O2798–O2800.
122. Burley JC, van de Streek J, Stephens PW. Ampicillin trihydrate from synchrotron powder diffraction data. Acta Crystallogr E-Structure Reports Online 2006; 62: O797–O799.
123. Fernandes P, Florence AJ, Shankland K, et al. Powder study of chlorothiazide N,N-dimethyl-formamide solvate. Acta Crystallographica Section E-Structure Reports Online 2006; 62: O2216–O2218.
124. Florence AJ, Johnston A, Shankland K. Powder study of hydrochlorothiazide-methyl acetate (1/1). Acta Crystallogra E-Structure Reports Online 2005; 61: O2974–O2977.
125. Chernyshev VV, Stephens PW, Yatsenko AV, et al. Structural characterization of prazosin hydrochloride and prazosin free base. J Pharm Sci 2004; 93: 3090–5.
126. Stephenson GA. Structure determination from conventional powder diffraction data: application to hydrates, hydrochloride salts, and metastable polymorphs. J Pharm Sci 2000; 89: 958–66.
127. Lewis GR, Steele G, McBride L, et al. Hydrophobic vs. hydrophilic: ionic competition in remacemide salt structures. Crys Growth Des 2005; 5: 427–38.
128. Nishibori E, Ogura T, Aoyagi S, et al. Ab initio structure determination of a pharmaceutical compound, prednisolone succinate, from synchrotron powder data by combination of a genetic algorithm and the maximum entropy method. J Appl Crystallogr 2008; 41: 292–301.
129. Remenar JF, Peterson ML, Stephens PW, et al. Celecoxib: nicotinamide dissociation: using excipients to capture the cocrystal's potential. Molecular Pharmaceutics 2007; 4: 386–400.
130. Pagola S, Tracanna MI, Amani SM, et al. Sideroxylin from Miconia ioneura: Monohydrate crystal structure from high resolution X-ray powder diffraction. Natural Product Communications 2008; 3: 759–64.

131. Nunes C, Suryanarayanan R, Botez CE, et al. Characterization and crystal structure of D-mannitol hemihydrate. J Pharm Sci 2004; 93: 2800–9.
132. Platteau C, Lefebvre J, Affouard F, et al. Ab initio structure determination of the hygroscopic anhydrous form of a-lactose by powder X-ray diffraction. Acta Crystallogr B 2004; 60: 453–60.
133. van Mechelen JB, Peschar R, Schenk H. Structures of mono-unsaturated triacylglycerols. III. The beta-2 polymorphs of trans-mono-unsaturated triacylglycerols and related fully saturated triacylglycerols. Acta Crystallogr B 2008; 64: 240–8.
134. Markvardsen AJ, David WIF, Johnson JC, et al. A probabilistic approach to space-group determination from powder diffraction data. Acta Crystallogr A 2001; 57: 47–54.
135. Madsen IC, Hill RJ. Collection and analysis of powder diffraction data with near-constant counting statistics. J Appl Crystallogr 1994; 27: 385–92.
136. Shankland K, David WIF, Sivia DS. Routine ab initio structure determination of chlorothiazide by X-ray powder diffraction using optimised data collection and analysis strategies. Journal of Mater Chem 1997; 7: 569–72.
137. Boultif A, Louer D. Indexing of Powder Diffraction Patterns for Low-Symmetry Lattices by the Successive Dichotomy Method. J Appl Crystallogr 1991; 24: 987–93.
138. Boultif A, Louer D. Powder pattern indexing with the dichotomy method. J Appl Crystallogr 2004; 37: 724–31.
139. Visser J. A Fully Automatic Program for Finding the Unit Cell from Powder Data. J Appl Crystallogr 1969; 2: 89–95.
140. Werner PE, Eriksson L, Westdahl M. TREOR, A Semi-Exhaustive Trial-and-Error Powder Indexing Program for all Symmetries. J Appl Crystallogr 1985; 18: 367–70.
141. Altomare A, Giacovazzo C, Guagliardi A, et al. New techniques for indexing: N-TREOR in EXPO. J Appl Crystallogr 2000; 33: 1180–6.
142. Coelho AA. Indexing of powder diffraction patterns by iterative use of singular value decomposition. J Appl Crystallogr 2003; 36: 86–95.
143. Le Bail A. Monte Carlo indexing with McMaille. Powder Diffraction 2004; 19: 249–54.
144. Neumann MA. X-Cell: a novel indexing algorithm for routine tasks and difficult cases. J Appl Crystallogr 2003; 36: 356–65.
145. David WIF, Shankland K, van de Streek J, et al. DASH: a program for crystal structure determination from powder diffraction data. J Appl Crystallogr 2006; 39: 910–15.
146. Putz H, Schon JC, Jansen M. Combined method for ab initio structure solution from powder diffraction data. J Appl Crystallogr 1999; 32: 864–70.
147. Le Bail A. ESPOIR: a program for solving structures by Monte Carlo analysis of powder diffraction data, in Epdic 7: European Powder Diffraction, Pts 1 and 2. 2001: 65–70.
148. Favre-Nicolin V, Cerny R. FOX, 'free objects for crystallography': a modular approach to ab initio structure determination from powder diffraction. J Appl Crystallogr 2002; 35: 734–43.
149. Engel GE, Wilke S, Konig O, et al. PowderSolve - a complete package for crystal structure solution from powder diffraction patterns. J Appl Crystallogr 1999; 32: 1169–79.
150. Pagola S, Stephens PW, Towards the solution of organic crystal structures by powder diffraction. in European Powder Diffraction, Eds. Delhez, R., Mittemeijer, EJ, Parts 1 and 2, Materials Science Forum, 2000; 321-3: 40–5.
151. Coelho AA. Whole-profile structure solution from powder diffraction data using simulated annealing. J Appl Crystallogr 2000; 33: 899–908.
152. Larson AC, Von Dreele RB. General Structure Analysis System (GSAS). Report LAUR 86–748. New Mexico, USA: Los Alamos National Laboratory, 2004.
153. Glusker JP, Trueblood KN. Crystal Structure Analysis: A primer. 2nd ed., New York; Oxford: Oxford University Press, 1985, 102–12.
154. Florence AJ, Bedford CT, Fabbiani FPA, et al. Two-dimensional similarity between forms I and II of cytenamide, a carbamazepine analogue. CrystEngComm 2008; 10: 811–13.

155. Allen FH. The Cambridge Structural Database: a quarter of a million crystal structures and rising. Acta Crystallogr Section B 2002; 58: 380–8.
156. Field JS, Ledwaba LP, Munro OQ, et al. Crystal structures and photoluminescent properties of the orange and yellow forms of [Pt{4 '-(o-ClC6H4)trpy}(CN)]SbF6: an example of concomitant polymorphism. CrystEngComm 2008; 10: 740–7.
157. Weatherhead-Kloster RA, Selby HD, Miller WB, et al. Organic crystal engineering with 1,4-piperazine-2,5-diones. 6. Studies of the hydrogen-bond association of cyclo[(2-methylamino-4,7-dimethoxyindan-2-carboxylic acid) (2-amino-4,7-dimethoxyindan-2-carboxylic acid)]. J Org Chem 2005; 70: 8693–702.
158. Watkin DJ. A simple small-scale recrystallization apparatus. J Appl Crystallogr 1972; 5: 250.
159. Sarma B, Roy S, Nangia A. Polymorphs of 1,1-bis(4-hydroxyphenyl) cyclohexane and multiple Z ' crystal structures by melt and sublimation crystallization. Chem Communications, 2006: 4918–20.
160. Bleay J, Hooper RM, Narang RS, et al. Growth of single-crystals of some organic-compounds by czochralski technique and assessment of their perfection. J Cryst Growth 1978; 43: 589–96, 1–112.
161. Henisch HK. Crystal growth in gels. New York: Dover Publications, 1996.
162. Ramachandran E, Natarajan S. Gel growth and characterization of beta-DL-methionine. Cryst Res Technol, 2006; 41: 411–15.
163. Clegg W, Teat SJ. Tetracycline hydrochloride: a synchrotron microcrystal study. Acta Crystallogr C 2000; 56: 1343–5.
164. Hursthouse MB. High-Throughput Chemical Crystallography (HTCC): meeting and greeting the combichem challenge. Crystallogr Rev 2004; 10: 85–96.
165. Barr G, Dong W, Gilmore CJ, et al. dSNAP: a computer program to cluster and classify Cambridge Structural Database searches. J Appl Crystallogr 2005; 38: 833–41.
166. Gelbrich T, Hursthouse MB. A versatile procedure for the identification, description and quantification of structural similarity in molecular crystals. Crystengcomm 2005; 7: 324–36.
167. McKinnon JJ, Mitchell AS, Spackman MA. Hirshfeld surfaces: a new tool for visualising and exploring molecular crystals. Chem-Euro J 1998; 4: 2136–41.
168. Llinas A, Goodman JM. Polymorph control: past, present and future. Drug Discov Today 2008; 13: 198–210.
169. Le Bail A, Duroy H, Fourquet JL. Ab-initio structure determination of $LiSbWO_6$ by X-ray powder diffraction. Mater Res Bull 1988; 23: 447–52.

6 Structural Aspects of Polymorphism

Harry G. Brittain
Center for Pharmaceutical Physics, Milford, New Jersey, U.S.A.
Stephen R. Byrn and Eunhee Lee
Department of Industrial and Physical Pharmacy, Purdue University, West Lafayette, Indiana, U.S.A.

INTRODUCTION

A century ago, the study of crystals was only concerned with examinations of their external form and with the physical properties, as these varied along the different crystal directions. The regularity of the appearance and of the external form of naturally occurring crystals led observers to believe that these materials were formed by the regular repetition of identical building blocks. It was deduced that when a crystal grows in a constant environment, the shape remains unchanged while the mass is built up from the continuous addition of fundamental units. Mineralogists made the important discovery that the faces of a crystal could be indexed to exact integers, and in 1784 Haüy showed that only the arrangement of identical particles in a three-dimensional periodic array could account for the law of rational indices (1). It was subsequently suggested by Seeber that the elementary building blocks of crystals were small spheres, held together in a lattice array through the balance of attractive and repulsive forces (2). Different crystal structures were believed to arise from the various ways spheres could be packed into alternate motifs. Shrewd guesses about the structures of a number of crystals were made by Barlow, who argued from considerations of symmetry and the packing of spheres (3).

The modern study of the physical properties of the solid state essentially began in 1912 with the publication of a paper by Laue and coworkers on the diffraction of Röntgen rays (now known as x-rays) (4). In the first part of the paper, Laue developed an elementary theory for the diffraction of x-rays by a periodic array of atoms, whereas in the second part Friedrich and Knipping reported the first experimental observations of X-ray diffraction by crystals. This work demonstrated simultaneously that x-rays must possess a wave character (because they could be diffracted), and that solids were composed of a regular network of atoms. These experimental proofs are considered to mark the beginning of the field of solid state physics. W.L. Bragg reported the first determinations of crystal structures in 1913, deducing the structures of KCl, NaCl, KBr, and KI (5).

LATTICE THEORY OF CRYSTAL STRUCTURE

An ideal crystal is constructed by the infinite regular repetition in space of identical structural units. In the simplest crystals formed by monatomic elements, the basic structural unit consists of a single atom. For the organic molecules of pharmaceutical interest, the structural unit will contain one or more molecules. One may describe the structure of all crystals in terms of a single periodic lattice, which represents the translational repetition of the fundamental structural unit. For elemental or

ionic crystal structures, each point in the lattice may be a single atom. For organic molecules, a group of atoms is often attached to a lattice point, or situated in an elementary parallelepiped.

A *lattice* is defined as a regular periodic arrangement of points in space, and is by definition a purely mathematical abstraction. The nomenclature is in allusion to the fact that a three-dimensional grid of lines can be used to connect the lattice points. It is important to note that the points in a lattice may be connected in various ways to form an infinite number of different lattice structures. The crystal structure is formed only when a fundamental unit is attached identically to each lattice point, and extended along each crystal axis through translational repetition.

The points on a lattice are defined by three fundamental translation vectors, **a**, **b**, and **c**, such that the atomic arrangement looks the same in every respect when viewed from any point **r** as it does when viewed at point **r′**:

$$\mathbf{r}' = \mathbf{r} + n_1\mathbf{a} + n_2\mathbf{b} + n_3\mathbf{c} \quad (1)$$

where n_1, n_2, and n_3 are arbitrary integers. The lattice and translation vectors are said to be *primitive* if any two points from which an identical atomic arrangement is obtained through the satisfaction of equation (1) with a suitable choice of the n_1, n_2, and n_3 integers. It is common practice to define the primitive translation vectors to define the axes of the crystal, although other non-primitive crystal axes can be used for the sake of convenience. A lattice translation operation is defined as the displacement within a lattice, with the vector describing the operation being given by:

$$\mathbf{T} = n_1\mathbf{a} + n_2\mathbf{b} + n_3\mathbf{c} \quad (2)$$

The Unit Cell

The crystal axes, **a**, **b**, and **c**, form three adjacent edges of a parallelepiped. The smallest parallelepiped built upon the three unit translations is known as the *unit cell*. Although the unit cell is an imaginary construct, it has an actual shape and definite volume. The entire crystal structure is generated through the periodic repetition, by the three unit translations, of matter contained within the volume of the unit cell. A unit cell does not necessarily have a definite absolute origin or position, but does have the definite orientation and shape defined by the translation vectors. A cell will fill all space under the action of suitable crystal translation operations, and will occupy the minimum volume permissible. By elementary vector analysis, the volume of a unit cell is defined by the magnitude of the cell axes:

$$V_c = |\,\mathbf{a} \times \mathbf{b} \cdot \mathbf{c}\,| \quad (3)$$

The unit cell is defined by the lengths of the lengths (*a*, *b*, and *c*) of the crystal axes, and by the angles (α, β, and γ) between these. The convention is that α defines the angle between the *b* and *c* axes, β defines the angle between the *a* and *c* axes, and γ defines the angle between the *a* and *b* axes. There are seven fundamental types of primitive unit cell, whose characteristics are provided in Table 1. These same unit cell characteristics define the seven *crystal classes*. As stated earlier, each unit cell will occupy one lattice point in the structure.

Unit Cell Symmetry Operations

Crystal lattices can be carried into themselves not only by the lattice translation defined in equation (2), but also by the performance of various point symmetry

TABLE 1 The Seven Crystal Classes, Defined From the Fundamental Unit Cells

System	Relationship between cell edges	Relationship between cell angles
Cubic	$a = b = c$	$\alpha = \beta = \gamma = 90°$
Tetragonal	$a = b \neq c$	$\alpha = \beta = \gamma = 90°$
Orthorhombic	$a \neq b \neq c$	$\alpha = \beta = \gamma = 90°$
Monoclinic	$a \neq b \neq c$	$\alpha = \gamma = 90° \beta \neq 90°$
Triclinic	$a \neq b \neq c$	$\alpha \neq \beta \neq \gamma \neq 90°$
Hexagonal	$a = b \neq c$	$\alpha = \beta = 90° \gamma = 120°$
Trigonal	$a = b = c$	$\alpha = \beta = 90° \gamma \neq 90°$

operations. A *symmetry operation* is defined as an operation that moves the system into a new configuration that is equivalent to and indistinguishable from the original one. A *symmetry element* is a point, line, or plane with respect to which a symmetry operation is performed. There are a total of five symmetry operations of import to the solid state.

The simplest operation is the *identity*, which leaves the system unchanged, and hence, in an orientation identical with that of the original. Although the performance of the identity operation does not yield any translation, it is a mathematical requirement of the theory of groups necessary to handle the ensemble of symmetry operations. Its presence also serves to distinguish between identical and equivalent orientations.

The second symmetry operation is that of *reflection* through a plane, and is denoted by the symbol "σ." Using Cartesian coordinates, the effect of reflection is to change the sign of the coordinates perpendicular to the plane, while leaving unchanged the coordinates parallel to the plane. The third symmetry operation is that of *inversion* through a point, and is denoted by the symbol "i." In Cartesian coordinates, the effect of inversion is to change the sign of all three coordinates that define a lattice point in space.

The fourth type of symmetry operation is the *proper rotation*, which represents the simple rotation about an axis that passes through a lattice point. Only rotations by angles of 2π (360°), $2\pi/2$ (180°), $2\pi/3$ (120°), $2\pi/4$ (90°), and $2\pi/6$ (60°) radians are permissible. These operations are referred to as one-fold (symbol C_1), two-fold (symbol C_2), three-fold (symbol C_3), four-fold (symbol C_4), and six-fold (symbol C_6) proper rotation axes. Rotations by other angles will not bring a three-dimensional lattice system into an equivalent configuration, and are therefore not permissible symmetry operations in the solid state.

The final type of symmetry operation is the *improper rotation*, which represents the combination of a proper rotation axis followed by the performance of a reflection operation. Once again, only improper rotations by angles of 2π (360°), $2\pi/2$ (180°), $2\pi/3$ (120°), $2\pi/4$ (90°), and $2\pi/6$ (60°) radians are permissible, and are denoted as one-fold (symbol S_1), two-fold (symbol S_2), three-fold (symbol S_3), four-fold (symbol S_4), and six-fold (symbol S_6) proper rotation axes.

The 14 Bravais Lattices

Bravais (6) proved that if the contents of a unit cell have symmetry, the number of distinct types of space lattices becomes 14. These are the only lattices that can fill

all space, and are commonly termed the 14 Bravais lattices. Because there are seven crystal systems, it might be thought that by combining the seven crystal systems with the idea of a primitive lattice a total of seven distinct Bravais lattices would be obtained. However, it turns out that the trigonal and hexagonal lattices so constructed are equivalent, and therefore only six lattices can be formed in this way. These lattices, which are given the label P, define the primitive unit cells (or P-cells) in each case.

The other eight Bravais lattices are derived by taking each of the six P-lattices and considering what happens when other lattice points are added through the use of certain centering conditions. This operation yields eight centered lattices, seven of which are given a name (body-centered, all-face-centered, one-face-centered) and a new symbol (I, F, and A, B, or C). The last new lattice is a specially centered hexagonal lattice that can be regarded after appropriate redefinition of axes of reference as a primitive rhombohedral lattice.

One crystal system can have all four space lattices (P, I, F, and C), whereas some crystal systems can have only the P-lattice. For each crystal system, the I-, F-, or C-lattices have unit cells that contain more then one lattice point, because we have added lattice points in various centered positions. Cells with more than one lattice point are sometimes known as multiple-primitive unit cells. The same axes refer to all the space lattices in a given crystal system, so all of these conventional, centered unit cells will display exactly the same rotational symmetry as does the corresponding P-cell in a given crystal system.

The assignation of axes of reference in relation to the rotational symmetry of the crystal systems defines six lattices which, by definition, are primitive or P-lattices. To determine if new lattices can be formed from these P-lattices, one must determine if more points can be added so that the lattice condition is still maintained, and whether this addition of points alters the crystal system. For example, if one starts with a simple cubic primitive lattice and adds other lattice points in such a way that a lattice still exists, it must happen that the resulting new lattice still possesses cubic symmetry. Because the lattice condition must be maintained when new points are added, the points must be added to highly symmetric positions of the P-lattice. These types of positions are (a) a single point at the body center of each unit cell, (b) a point at the center of each independent face of the unit cell, (c) a point at the center of one face of the unit cell, and (d) the special centering positions in the trigonal system that give a rhombohedral lattice.

In the triclinic system, there are no restrictions on the magnitudes of the lengths of the unit cell axes or on their inter-axial angles. One can therefore always take a triclinic lattice and center it, to produce a new lattice that will be compatible with the conditions of the triclinic crystal system. However, there is nothing new about this lattice, because a smaller primitive cell can be determined with the same complete arbitrariness of the cell edges and angles. Thus, for the triclinic crystal system there can be only one Bravais lattice: the primitive or P-lattice.

For the monoclinic system, a new lattice can be obtained by centering a monoclinic P-cell along the face defined by the plane formed by the intersection of the a and b crystal axes. This is because it is not possible to maintain the fundamental monoclinic conditions and yet describe this lattice as a P-lattice. There are therefore two unique monoclinic Bravais lattices.

The primitive orthorhombic lattice can be thought of as arising from a primitive monoclinic lattice with the added restriction that the third angle is also 90°. In that

case, all the unit cell translation vectors are 90° to one another but have different lengths. In the orthorhombic system, one may construct a C-centered cell, which can also be described as an A- or B-lattice by an interchange of the orthogonal axes. In addition, there can also be an all-face-centered F-lattice structure and a body-centered I-lattice. Thus, for the orthorhombic crystal system, there are four unique Bravais lattices, P, I, F, and C.

In the tetragonal system, centering any of the P-cell faces results only in a lattice equivalent to the P-lattice itself. It happens that the only new lattice that can be generated in the tetragonal system in the one formed through body-centering of the P-cell. The surroundings of every point in this cell are still identical, with each point having eight nearest neighbors at the same distance and in the same directions, which preserves the four-fold symmetry. It is concluded, therefore, that for the tetragonal crystal system there are only two distinct Bravais lattices.

Placing a lattice point at the body-center position of a cubic P-cell yields a new lattice. Each point is surrounded by eight other nearest-neighbor points, all in the same relative positions regardless of the observation point. The I-cell type remains cubic because the four three-fold axes are preserved. This structure is frequently denoted as the body-centered-cubic cell. One may also add points at the face centers of the primitive cubic unit cell to obtain another new lattice. Twelve nearest-neighbor points surround every lattice point in the F-cell, still preserving the four three-fold axes. This F-lattice is often denoted as being the face-centered-cubic cell. It is clear that the cubic crystal system cannot have a single face-centered lattice, because centering only one face would destroy the four three-fold axes of symmetry. Thus, one concludes that there are three cubic Bravais lattices.

The hexagonal and trigonal systems yield special complications owing to the relationship between crystal axes and angles. One finds that face-centering or body-centering the primitive lattice types with simultaneous preservation of the three- or six-fold axes is not possible. It shall suffice to say that only the two Bravais lattices of Figure 1 are possible, and readers seeking additional information on this question are referred to the literature (7).

The 230 Space Groups

The structure of a given crystal might be assigned to one of the seven crystal systems, or to one of the 14 Bravais lattices. In those classification schemes, one can state with certainty the crystal system as well as the type of lattice. On a deeper level, one could deduce the molecular point group of the molecules in the unit cell, which would then pinpoint to which of the 32 point groups the crystal belongs. This latter classification would yield both the crystal system as well as the relationships between the tensors that describe the macroscopic behavior and the properties of the crystal.

In a further development of detail, one can take into account how the atoms of the solid are distributed spatially. The issue of symmetry in context with a fixed point in the crystal, and the symmetry of Bravais lattices has been addressed, but in order to describe the entire crystal the effects of two new types of symmetry operation must be included. A *space group* determined in this way describes the spatial symmetry of the crystal. By definition, a crystallographic space group is the set of geometrical symmetry operations that take a three-dimensional periodic crystal into itself. The set of operations that make up the space group must form a group in

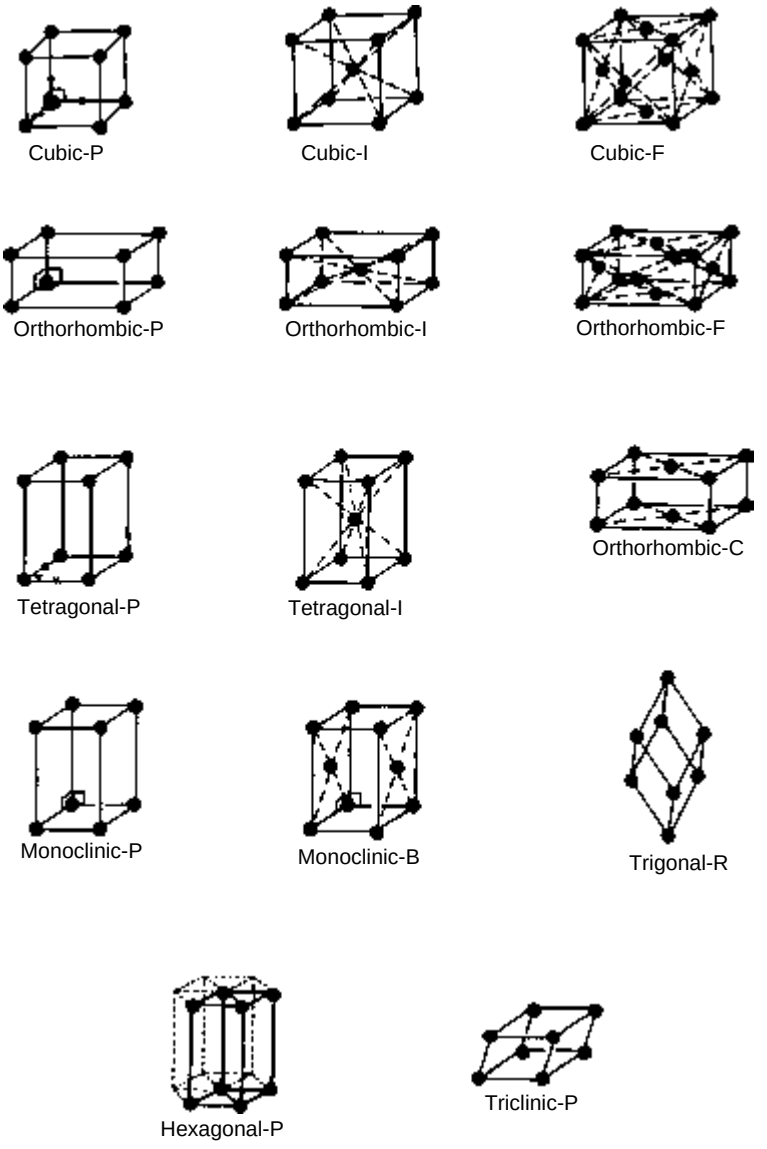

FIGURE 1 The 14 Bravais lattices.

the mathematical sense, and must include the primitive lattice translations as well as other symmetry operations.

Bravais also showed that when the full range of lattice symmetry operations are taken into account, there are a maximum of 230 distinct varieties of crystal symmetry. The ensemble of these 230 configurations are the space groups, and the structure of any given crystal must be described by one of these. A detailed

description of all 230 space groups is beyond the scope of this discussion, but such treatments are available (7).

The set of symmetry operations is ordinarily divided into two main classes. The product of the symmetry operations with the identity of the translation group (zero translation) yields the category termed essential space group operations. The other products of the symmetry operations with primitive lattice translations are termed non-essential space group operations. Operations obtained by the product of the identity of the symmetry operations with the primitive lattice translations are simply the translation symmetry operations.

Space group symmetry operations may involve a translation, which is smaller than a primitive lattice translation and which is coupled with a rotation or reflection operation. These symmetry operations are known as glide or screw operations. This leads to an important classification of space groups as being either symmorphic or nonsymmorphic. A symmorphic space group is one that is entirely specified by symmetry operations acting at a common point, and that do not involve one of the glide or screw translations. The symmorphic space groups are obtained by combining the 32 point groups with the 14 Bravais lattices. This generates the ensemble of symmorphic space groups, which account for 73 space groups out of the total of 230.

When it is necessary to specify a space group by at least one operation involving a glide or screw translation, the space group is said to be nonsymmorphic. The *screw operation* is a symmetry operation derived from the coupling of a proper rotation with a non-primitive translation parallel to the axis of rotation, which is called the screw axis. The combination of a reflection operation plus a translation operation yields a *glide plane*. Three types of glide plane are known in crystals, and these are termed the axial glide, the diagonal glide, and the diamond glide. In all of these glides, one reflects across a plane and translates by some distance that is a fraction of the unit cell. In the *axial glide*, the magnitude of the translation vector is one half of a unit-cell translation parallel to the reflection plane. One refers to the axial glide as an *a*-, *b*-, or *c*-glide according to the axis along which the translation is carried out. The reflection that accompanies this translation can be across any of the planes defined by the intersection of two of the translation axes. The *diagonal glide* involves translations along two or three directions, which are usually $(a + b)/2$, $(b + c)/2$, or $(c + a)/2$. In the case of tetragonal and cubic crystal systems the diagonal can also include a translation of $(a + b + c)/2$. The *diamond glide* operation consists of a translation having a magnitude of $(a \pm b)/4$ or $(b \pm c)/4$ or $(a \pm c)/4$ and $(a \pm b \pm c)/4$ in tetragonal and cubic crystals.

The nonsymmorphic space groups are specified by at least one operation that involves a non-primitive translation. Taking such operations into account, it is found that there are a total of 157 nonsymmorphic space groups. These, taken together with the 73 symmorphic space groups, produce the entire 230 space groups originally derived by Bravais.

The best description of the properties of individual space groups uses the ensemble of symmetry operations, which give rise to the fundamental structure. One must explain the coordinates of the general equivalent positions, and the positions and occurrence of all the symmetry elements (both essential and non-essential) with respect to any particular choice of origin. The procedure is to consider the point group of any space group, and to ascertain the number of essential symmetry operations. This will automatically yield the number of general equivalent positions

in the primitive unit cell. Crystallographers use matrix operator methods to determine the coordinates of the entire general equivalent positions, and the presence and positions of all symmetry elements.

CRYSTAL STRUCTURES DERIVED FROM THE CLOSE PACKING OF SPHERES

The first crystal structures to be solved were those of inorganic compounds, for which great help was found through considerations of how one could pack spheres into structures that minimized the magnitude of interstitial space (8). In this approach, the crystal is built up from spherical structural units that make contact with one another. Alternatively, one could consider the points of a lattice network to be inflated into spheres. As a result, all individual symmetry is removed from the individual particles, and the symmetry of the lattice structure follows from the fashion in which the spheres are arranged.

The model of sphere packing requires no definition as to the nature of the bonding holding the spheres together, and in fact, requires that no directionality be exhibited in the bonding. This model does not work well when applied to structures built up of covalently bonded organic molecules, but does work reasonably well for the crystals formed by ionic or metallic solids.

Spheres of Equivalent Size

If spheres of equal size are packed together in a plane, they will arrange themselves in one of the patterns shown in Figure 2. The sphere centers will lie at the corners of equilateral triangles, and each sphere will be in contact with six others. The three-dimensional structure of closely packed spheres of equal sizes will consist of such. The conditions that must be satisfied are that the space occupied per sphere is a minimum, and that the spheres all have the same environment. The relative orientation of the spheres is disregarded if it is assumed that they possess full spherical symmetry, and that there is no way of determining their orientations.

There are two ways to arrange equivalent spheres in a regular array that minimizes the interstitial volume. If the positions of the atoms in a layer are labeled as A, then an exactly similar layer can be superimposed on the first so that the centers of the atoms in the upper layer are vertically placed above the positions B. When the third layer is placed above the second layer, the centers of the atoms may lie above either the C or the A positions. In the latter, case one obtains the layer sequence of ABABAB, etc., which is the simplest form and is denoted as hexagonal close packing. In the former case, the sequence of layers is ABCABC, etc., and is denoted as cubic close packing. The terms hexagonal and cubic refer to the symmetry of the resulting aggregate.

The highest axial symmetry of hexagonal close packing consists of six-fold axes perpendicular to the layers. In cubic close packing, there are three-fold axes of symmetry in four directions, inclined to one another as are the body-diagonals of a cube. This structure requires that the close-packed layers of the planes are perpendicular to any body-diagonal of the cube. The unit cell of cubic close packing is a group of atoms situated at the corners and mid-points of the faces of a cube, which leads to the alternative name of face-centered cubic for a cubic close-packed structure.

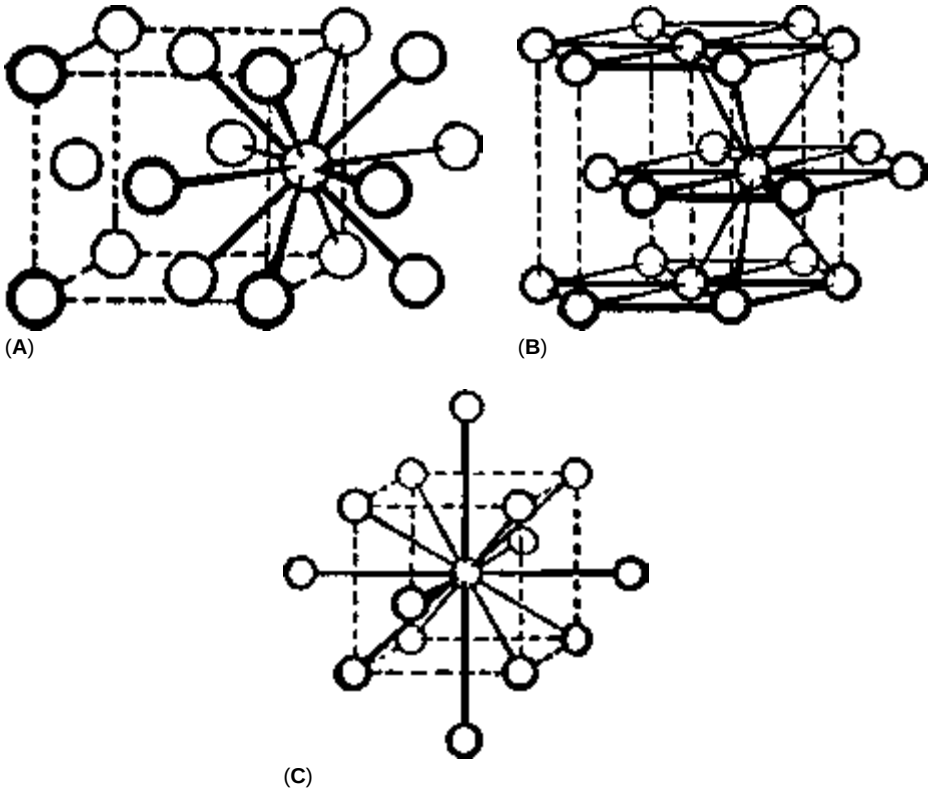

FIGURE 2 Close-packing arrangements of spheres of equal sizes. Shown are (**A**) cubic close packing, (**B**) hexagonal close packing, and (**C**) body-centered cubic packing.

In both of these close-packed arrangements each atom has 12 equidistant nearest neighbors, six in its own plane and three in each adjacent layer. The next nearest neighbors are, however, differently arranged in the two cases. It is apparent that any sequence of close-packed layers must lead to a close-packed structure, for any atom will always have 12 equidistant nearest neighbors. Any other sequences of layers, however, differ from the sequences ABABAB … and ABCABC … in that the environment of all the atoms is not the same. Although the arrangement of the nearest neighbors is identical, the arrangement of the next nearest neighbors the atoms fall into is two or more sets. For example, in the sequence ABACABAC … ("double" hexagonal close packing) there are two types of non-equivalent spheres.

There are numerous examples of cubic and hexagonal close packing. Metallic solids are known to exhibit both cubic and hexagonal structures, whereas the inert gases are found to form solids characterized by cubic packing. The structures of many simple diatomic molecules can also be described in terms of cubic close packing.

It is evident that even the simplest model for the packing of spheres of equivalent size permits the possibility of polymorphism. Most of the metals of the

lanthanide series exist in the hexagonal close-packed structure at room temperature, but transform into the body-centered cubic form at temperatures exceeding 800°C (9). For the most part, these transitions appear to be enantiotropic in nature.

Spheres of Differing Sizes

As soon as spheres of different sizes (i.e., different species) are considered, the number of possibilities for packing arrangements increases significantly. Such situations arise most often for ionic solids, formed by the interactions of positively charged (cations) and negatively charged (anions) spheres.

For this approach, monatomic ions may be considered as incompressible spheres that are only slightly polarized by the ions of opposite charge around them. The two conditions for an arrangement of ions in space to have minimum potential energy are that (a) the larger ions (usually the anions) around a smaller ion of opposite sign must all be in contact, and (b) the coordination number of an ion must be as large as possible (subject to the first condition being observed). Thus, coordination numbers of 5, 7, 9, 10, and 11 are excluded by geometry if the ionic arrangement is to form a regular spatial pattern. In addition, the coordination number of 12 is excluded by the requirement that positive and negative charges balance one another.

For instance, in the well-known sodium chloride structure (body-centered cubic packing), only six chloride ions can be accommodated around a sodium ion so that they all "touch" the cation, even though the available space would accommodate more sodium ions. But because electrical neutrality must be achieved, and as the system is stable only when the cation touches all the anions surrounding it, the coordination in sodium chloride must be six. Thus, any single sodium ion has six octahedrally arranged chlorides as its nearest neighbors, whereas each chloride ion similarly has a corresponding arrangement of sodium ions around it.

For a compound having a 1:1 stoichiometry of cations and anions, the number of anions surrounding a cation in a given structure will depend on the ratio of the cationic (r_c) and anionic (r_a) radii. For instance, the smallest radius ratio (r_c/r_a) that permits four anions to surround a single cation in the same plane is 0.414. This value therefore represents the smallest radius ratio for which six-coordination of the cation is possible. In addition to the four anions within the plane, one anion can be accommodated above and one below the cation. For lower values of r_c/r_a, six-coordination of the cation is not possible because the anions touch one another but not the cation. The limiting values of radius ratios for various coordination numbers are given in Table 2.

The situation becomes complicated for stoichiometries other than 1:1. In crystals of an AB_2 compound, the coordination number of A is twice that of B and the structure is determined by the coordination number of the smaller ion. The radius ratio rule is clear-cut only with simple ions, and polymorphism is much more prevalent when complex ions are involved. For example, the commonly employed pigment titanium dioxide is known to exist in two polymorphs, anatase and rutile, whose structures are each built up from different arrangements of octahedral coordination. As shown in Figure 3, the coordination polyhedron of rutile is essentially ideal, whereas for anatase there are very distorted octahedra of oxygen atoms about each titanium ion. Although rutile is ordinarily assumed to be the most stable form owing to its common occurrence, anatase is actually more stable by approximately 8–12 kJ/mol (10).

TABLE 2 Limiting Radius Ratios, Cation Coordination Numbers, and Ionic Arrangements in Ionic Solids

Radius ratio (r_c/r_a)	Cation coordination number	Arrangement
$1 \rightarrow 0.73$	8	At cube corners
$0.73 \rightarrow 0.41$	6	Octahedral
$0.41 \rightarrow 0.22$	4	Tetrahedral
For anisodesmic crystals		
$0.73 \rightarrow 0.41$	4	Square
$0.22 \rightarrow 0.16$	3	Triangular
0.16	2	Linear

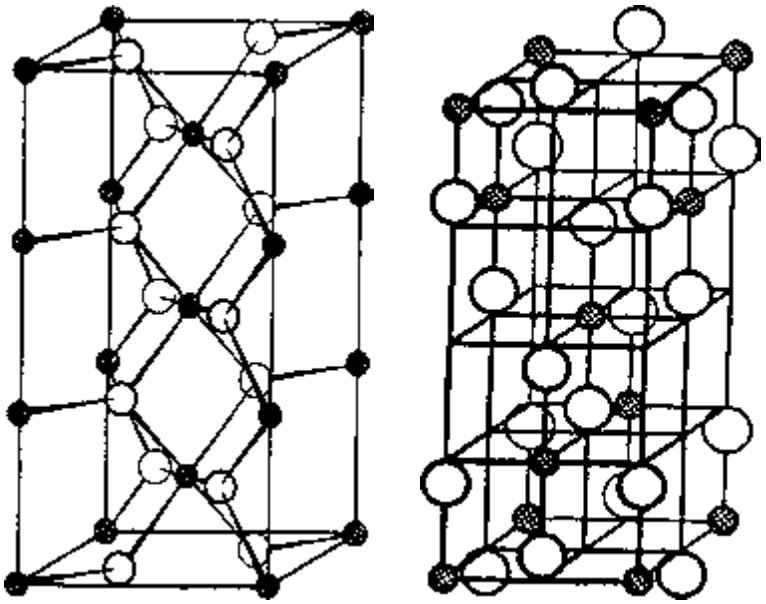

(**A**) (**B**)

FIGURE 3 Solid-state structure adopted by titanium dioxide in the (**A**) rutile and (**B**) anatase structures. The titanium atoms are indicated by the cross-hatched circles, and the oxygen atoms are indicated by the open circles.

STRUCTURAL THEORY OF POLYMORPHISM

The problem with thermodynamics is that the rate of formation of individual polymorphic modifications is not determined solely on the basis of energetics through a reduction in their free energy. Entering into the picture are other structural factors that play a part and that, under given circumstances, may even prove to be quite decisive. One often encounters apparent kinetic obstacles to thermodynamic predictions, which lead to the observation of metastable states. This situation has been pointed out in the first two chapters of this book, and indicates the need for

supplementing the thermodynamic approach by structural considerations based on atomic and molecular theory.

The classification of polymorphic substances into monotropic and enantiotropic classes from the standpoint of observed phenomena is not appropriate as a basis for the lattice theory of polymorphism. In the lattice theory, one begins with a consideration as to whether the lattices of the polymorphic forms are related in structure or not. Only in the case of lattices that are structurally related will it be possible for mutual transformation to take place at a transition point fixed by the temperature and pressure of the system. If the lattices differ in such a way that atoms or molecules must be completely regrouped during the transformation (changing their state of bonding), no point of contact for mutual reversible transformation will exist.

Generally speaking, the concepts of monotropy and enantiotropy in phase theory appear to coincide with the structural concepts of unrelated and related lattices. Nevertheless, one must avoid equating the two, for it is certainly possible that one of two related lattices of the same substance be less stable than is the other under all conditions of temperature and pressure. This would indicate the existence of monotropy in spite of the existence of related lattices. This situation becomes especially important for polymorphic organic compounds, which form molecular lattices.

Polymorphism Among Structurally Unrelated Lattices

The most striking differences in properties are exhibited by those polymorphic modifications for which the lattices have a completely different arrangement. Frequently, a complete change in the arrangement of the lattice particles is also accompanied by a change in the state of bonding. For example, completely different chemical bonding exists for the diamond/graphite or white/red phosphorus polymorphic pairs. The difference in energy between polymorphs may be quite considerable (as with the modifications of phosphorus or arsenic), but also can be surprising small (as with diamond and graphite). In almost all instances, polymorphic changes that require the breaking of primary bonds and the re-joining of atoms into a different arrangement necessitate the existence of monotropy.

The modifications of various non-metals usually differ drastically in their structure and bonding. Systems are known where one or more non-metallic modifications form molecular lattices in which a definite small number of elementary atoms are closely united to form a structural grouping, while other semi-metallic modifications exist that do not exhibit such a grouping in the lattice. A classic example of this type of behavior is provided by white phosphorus (with a P_4 structural grouping), and black phosphorus (which exhibits a layered structure (11).

Even where there is not such a marked difference in the kind of bonding, pronounced differences in the structural arrangement are able to stipulate very different physical and chemical properties. This type of behavior is typified by elemental sulfur. The "plastic" modification consists of long disordered chains of sulfur atoms, whereas the two crystalline modifications contain the structural group S_8 as molecule in the lattice (12).

An explanation for the existence of the very different kinds of lattices that are observed for the various non-metals demands a profound knowledge of the possible ways in which the valence electrons of these elements can be arranged.

This information is only available from the performance of suitable molecular orbital calculations, which yield detailed information about the distribution of electron density in the components of a unit cell. For instance, only such computational methods can provide the basis as to why phosphorus forms P_4 molecules in the vapor phase, and why these same molecular species are again encountered in the lattice of white phosphorus.

Polymorphism in Structurally Related Lattices

Any structural theory of polymorphism as applied to lattice structures must deal with three issues. One is first required to establish the structural relationships between the different lattice types on the basis of the lattice theory. Next, one must explain why a particular substance is able to arrange its structural units in two closely related lattices. The last issue deals with the manner and conditions under which a rearrangement of the units from one lattice type to another may occur.

The structural relations existing between the 230 space groups have been dealt with adequately, and a very detailed summary of these relationships is available (7). Hückel has provided an exhaustive summary of the structural causes of polymorphism among related crystal lattice types, and has provided the entire range of mechanisms whereby a polymorphic transition may take place (13).

Three-dimensional lattices of the same symmetry class characterize the two polymorphic forms, but the unit cells exist with different coordination numbers and different coordination polyhedra. The classic example of this type of behavior is given by cesium chloride, which undergoes a reversible transformation from a cubic body-centered lattice to a cubic face-centered lattice at 445°C (14). On the body-centered modification, two simple primitive cubic lattices (one of Cs cations and one of Cl anions) are placed inside one another so that the corners of one kind of cube are situated at the centers of cubes of the other kind. The face-centered modification is built up from face-centered ionic lattices situated inside one another.

The two polymorphs are characterized by three-dimensional lattices with the same coordination scheme, but with different arrangements of the more remote lattice points. The structures are related to one another in a manner that finds expression in twin-formation at the plane of twinning. Examples of this category are the two polymorphs of zinc sulfide, zinc blende, and wurtzite (15). At ambient temperatures, zinc blende is the stable modification, but changes enantiotropically into wurtzite at 1024°C. For both forms, the zinc occupies a site of tetrahedral symmetry. In zinc blende, all the tetrahedra are situated inversely with respect to each other, so that all the Zn and S atoms respectively are structurally equivalent. In wurtzite, three tetrahedra are situated inversely with respect to each other and the fourth as a mirror image. The one structure follows from the other by rotating alternate layers formed by buckled six-membered rings through 180°.

The lattices of the two polymorphs are related by symmetry changes in the lattice, associated with changes of symmetry of the lattice particles through rotation. One example of this type of behavior is given by sodium nitrate, which at 250–275°C transforms from the trigonal modification into a regular modification (16). This phase change takes place as a result on the onset of rotation of the nitrate ions about the trigonal axis. A considerable elongation of the lattice in the direction of the trigonal *c*-axis takes place at the same time, leaving essentially unchanged the

magnitudes of the two basal axes. This dilatational change forces the trigonal lattice to transform into a lattice of hexagonal symmetry.

Different polymorphs may exist under certain conditions as a result of varying coordination schemes that become possible when the radius ratio for the particles lies close to one of the limits shown in Table 2. Examples of this behavior are the calcite and aragonite modifications of calcium carbonate (17). In the rhombohedral structure of calcite, each calcium ion has the six oxygen atoms of two carbonate ions as neighbors, whereas in aragonite, the nine oxygen atoms of three carbonates are nearest neighbors. It happens that the radius ratio for the calcium ion in the two forms is close to 0.73, which places it at the cusp, which separates eight-coordination from six-coordination. The thermal expansion of the lattice that accompanies heating a sample of calcite is sufficient to cause the phase transformation to aragonite.

Polymorphs may arise from the displacement of atomic layers or groups of layers in layer lattices. Examples from this class are the red tetragonal and yellow rhombic modifications of mercuric iodide, which are enantiotropically transformable at 127°C (18). The red phase consists of a layered lattice, in which the mercury ions possess the unusual coordination number of four and a pseudo-tetrahedral configuration. This coordination number arises as a result of the very tight binding of the stable modification, and the close packing of alternate layers of mercury and iodine atoms. In the high-temperature yellow form, the mercury atoms assume a coordination number of six in a pseudo-octahedral structure. The transformation arises from a shift in the relationship between the alternate layers of mercury and iodine atoms, originating from both a lattice expansion and a lateral shift. The transition is enantiotropic in nature because the phase change only requires that each mercury atom shift from the center of a pseudo-tetrahedron to the center of a structurally related pseudo-octahedron.

In other systems, new polymorphs may originate in the migration of atoms within a lattice in which the lattice particles have a relatively high mobility due to the fact that the lattice can be regarded as one with unoccupied positions. This can also take the form of a change from a rigid lattice to one with mobile lattice particles. For instance, in the α and γ forms of aluminum oxide, the substance is able to crystallize in an open lattice with unoccupied positions (γ-alumina) (19) or in a compact lattice (α-alumina) (20). In the most stable α-form, the oxygen atoms in the lattice form a hexagonal close packing, the gaps of which are filled by a regular arrangement of aluminum atoms. The structure of the γ-phase is much more open, being a spinel lattice in which one-third of the spaces available for the metal atoms are unoccupied. The arrangement of the oxygen atoms in the γ-form approximates that of cubic close packing, possessing both octahedral and tetrahedral sites for the aluminum atoms.

Finally, new polymorphic structures can arise from different ways of assembling closely related coordination polyhedra. Three possibilities are known, which lead to polymorphism of this type, which are most commonly found in oxidic lattices. First, the coordination polyhedron of one lattice particle is the same, whereas that of the other is only slightly changed (e.g., silicon dioxide). Second, the coordination polyhedron of one lattice particle is the same, and that of the other is considerably changed (e.g., titanium dioxide). Finally, the coordination polyhedra are both deformed to varying degrees, with the basic lattice type being the same but the type of distortion different (e.g., zirconium dioxide).

POLYMORPHISM IN MOLECULAR CRYSTALS

The survey given above does not represent a complete exposition of the structural aspects of polymorphic substances, but the examples chosen from the range of inorganic structural possibilities do serve to provide an insight into the underlying causes of polymorphism. The systems become more complex when one considers the structural causes of polymorphism in crystals formed by the hydrogen-bonded molecules that are of pharmaceutical interest, where it becomes essential to develop the structural considerations by a closer examination of the states of bonding of the atoms in the different structures.

When considering the structures of organic molecules, one finds that different polymorphic crystal forms can be formed along two distinguishable routes. Should the molecule be constrained to exist as a rigid grouping of atoms that lacks conformational lability, these may be packed in different motifs to occupy the points of different lattice types. Because this variety of polymorphism is attributable to packing phenomena, it is usually termed packing polymorphism. On the other hand, if the molecule in question is not rigidly constructed and can exist in distinct conformational states, then it may transpire that each of these conformationally distinct modifications may pack into its own characteristic structure. This latter behavior has been termed conformational polymorphism (21,22).

Polymorphism Resulting from the Packing of Conformationally Similar Molecules

General principles of packing polymorphism will be illustrated through a discussion of representative examples where polymorphs have originated through the assembly of different modes of conformationally equivalent molecules. One theme that will be encountered throughout this section is that differing packing modes are readily available to compounds for which hydrogen bonding is important, and for which there exist multiple possibilities to achieve the necessary intramolecular and intermolecular interactions.

Resorcinol

During the early development of single-crystal X-ray crystallography for the determination of the structures of organic molecules, Robertson reported the structure of the stable α-polymorph of resorcinol (1,3-dihydroxybenzene) (23):

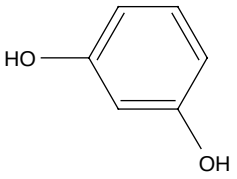

This crystal form was characterized by the orthorhombic space group of P*na*2_1, and unit cell lengths of $a = 10.53$ Å, $b = 9.53$ Å, and $c = 5.66$ Å. It was subsequently learned that the α-form underwent a phase transformation into a denser crystalline modification (the β-form) when heated at about 74°C (24), and that although this form also crystallized in the orthorhombic P*na*2_1 space group, the unit cell dimensions of the β-form were quite different ($a = 7.91$ Å, $b = 12.57$ Å, and $c = 5.50$ Å).

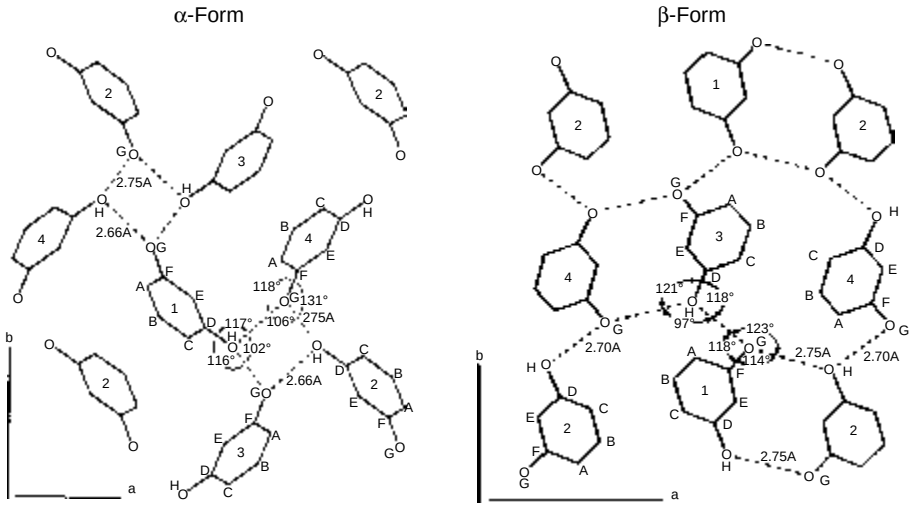

FIGURE 4 Crystal structures of the α- and β-forms of resorcinol, as viewed down the *c*-axis (001 plane). The figure was adapted from data given in Refs. (23) and (24).

The crystal structures of the α- and β-forms (viewed down the *c*-axis, or (001) crystal plane) are illustrated in Figure 4, where it may be noted that each form is characterized by a different motif of hydrogen bonding. In particular, the α-form is characterized by a relatively open architecture that is maintained by a spiraling array of hydrogen bonding that ascends through the various planes of the crystal. In the view illustrated (defined by the *ab*-plane), the apparent closed tetramic grouping of hydroxyl groups is actually a slice through the ascending spiral.

The effect of the thermally induced phase transformation is to collapse the open arrangement of the α-form by a more compact and parallel arrangement of the molecules in the β-form. This structural change causes an increase in crystal density on passing from the α-form (1.278 mg/m^3) to the β-form (1.327 mg/m^3). After the open structure of the α-form has collapsed into the β-form structure, the molecules adopt a more parallel packing array that results in the generation of indefinite chains, as opposed to the infinite helices of the α-form.

Sulfamerazine

Sulfamerazine [4-amino-*N*-(4-methyl-2-pyrimidinyl)benzene-sulfonamide]:

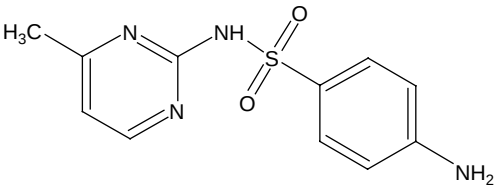

is known to exist in a polymorph (Form-I) that is stable at high temperatures and another polymorph (Form-II) that is stable at ambient conditions, and the

TABLE 3 Crystallographic Data for the Polymorphs of Sulfamerazine

Crystal class	**Form I (27)**	**Form II (26)**	**Form II (28)**
	Orthorhombic	**Orthorhombic**	**Monoclinic**
Space group	P$n2_1a$	Pbca	P$2_1/c$
Unit cell lengths	a = 14.474 Å	a = 9.145 Å	a = 11.0966 Å
	b = 21.953 Å	b = 11.704 Å	b = 8.3152 Å
	c = 8.203 Å	c = 22.884 Å	c = 13.9640 Å
Unit cell angles	$\alpha = 90°$	$\alpha = 90°$	$\alpha = 90°$
	$\beta = 90°$	$\beta = 90°$	$\beta = 99.327°$
	$\gamma = 90°$	$\gamma = 90°$	$\gamma = 90°$
Molecules in unit cell	8	8	4
Cell volume	2606.5 Å^3	2449.3 Å^3	1271.43 Å^3
Density	1.347 g/cm^3	1.43 g/cm^3	1.381 g/cm^3

temperatures at which these forms can be interconverted has been discussed (25). The existence of two orthorhombic polymorphic forms of sulfamerazine has been demonstrated and the physical properties of these studied (26,27), and more recently the crystal structure of an additional monoclinic form has been published (28). The crystallographic data reported for all three forms are found in Table 3, and the hydrogen-bonding motifs existing in sulfonamide structures has been discussed in depth (29).

In the orthorhombic forms, the repeating motif is a molecular dimer, assembled through the formation of two N(amide)–H–N(pyrimidinyl) hydrogen bonds, that is pseudo-centrosymmetric in Form-I and centrosymmetric in Form-II. The extent of hydrogen bonding is equivalent in the two structures, which accounts for the relatively low energy required to cause the solid-solid phase transition of Form-II into Form-I. In the monoclinic form, the molecules adopt a *gauche* conformation when viewed along the S–N axis, and the bond angles in the tetrahedral sulfur atom were found to be significantly distorted from 109°.

Even though the solid-state phase transition between Form-I and Form-II is enantiotropic in nature, modulated differential scanning calorimetry studies have shown that the endothermic transition is observed in both the reversing and non-reversing heat flow thermograms (30). The results were interpreted as requiring the existence of a first-order phase transition that was kinetically irreversible, although still being thermodynamically reversible. The kinetics of the solution-mediated Form-I to Form-II phase transformation were studied as a function of solvent composition and temperature, and the rates correlated with hydrogen bonding between the dissolved solute molecules and the ease with which nucleation to the new form might take place (31). The effect of impurities on the solution-mediated phase transformation have also been studied, where it was discovered that the acetyl derivative of sulfamerazine strongly inhibited the transition, even when it was present at very low levels in solvent systems known to favor the phase transformation (32).

Iodoanilinium Picrate

Crystals of 2-iodoanilinium picrate:

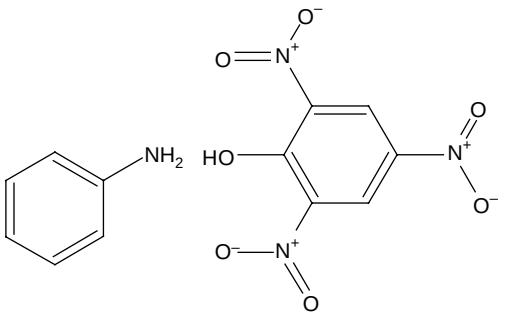

have been obtained in three distinct polymorphic forms, and each of these has been found to exhibit a characteristically different color (33). The structures of yellow Form-I and green Form-II have been obtained, but the structure of the red Form-III could not be solved owing to its instability. Crystals of Form-II were only somewhat more stable, and were found to transform into Form-I within a day. The crystallographic data obtained on the two characterized structures may be found in Table 4.

In Form-I and Form-II, the iodoanilinium cations and picrate anions form nearly planar ion pairs, with the iodoanilinium ion being hydrogen bonded to the picrate ion by a N–H···O hydrogen bond. As illustrated in Figure 5, the pairs related by translational symmetry in Form-I are stacked to form segregated columns, in which the same ion types are stacked with each other. In addition, all the nitro groups lie essentially in the plane of the benzene ring. This structure may be contrasted with that of Form-II, where the anions and cations are alternatively stacked along the *a*-axis to form continuous columns. In Form-II, the oxygen atoms of the nitro groups at the *ortho*-positions deviate from the plane of the benzene ring.

TABLE 4 Crystallographic Data for the Polymorphs of Iodoanilinium Picrate (33)

Crystal class	**Form-I**	**Form-II**
	Monoclinic	**Triclinic**
Space group	$P2_1/n$	$P\bar{1}$
Unit cell lengths	$a = 14.492$ Å	$a = 7.323$ Å
	$b = 4.3733$ Å	$b = 8.245$ Å
	$c = 24.153$ Å	$c = 13.656$ Å
Unit cell angles	$\alpha = 90°$	$\alpha = 75.71°$
	$\beta = 98.81°$	$\beta = 74.05°$
	$\gamma = 90°$	$\gamma = 75.64°$
Molecules in unit cell	4	2
Cell volume	1512.6 Å^3	753.7 Å^3
Density	1.968 g/cm^3	1.974 g/cm^3

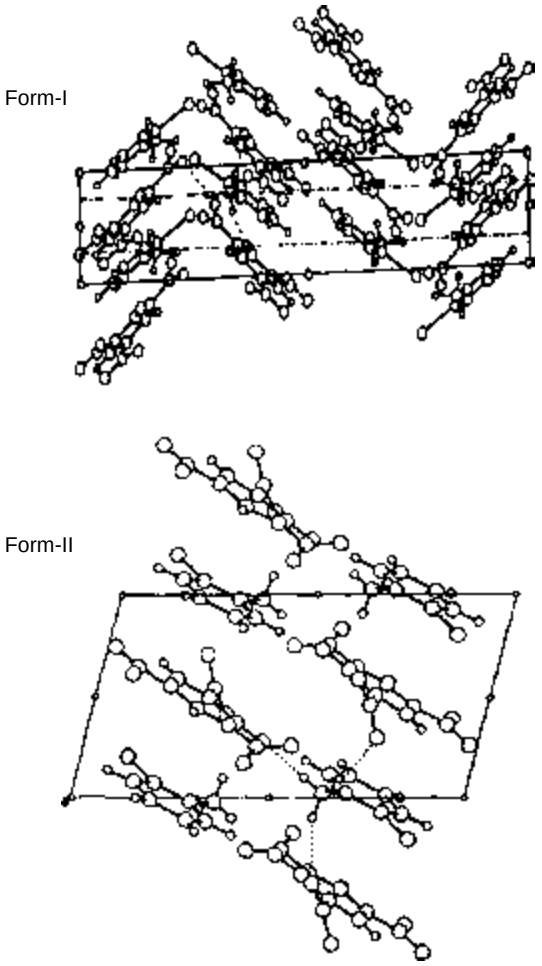

FIGURE 5 Hydrogen bonding motifs in the two polymorphs of iodoanilinium picrate, and how these affect molecular packing in the crystal forms. The projection of Form-I is down the *a*-axis, whereas the projection of Form-II is down the *b*-axis. The figure was adapted from data presented in Ref. (33).

The iodoanilinium picrate system was found to exhibit thermochromism for both polymorphs. Form-I crystals changed from yellow to red upon heating to 60°C, while Form-II crystal changed from green to red at temperatures above 60°C. The thermochromism is due to the polymorphic transformation to the red form (Form-III), which is only stable at elevated temperatures. The changes in stacking mode alter the nature of the charge-transfer transitions between 2-iodoaniline and picric acid, which are responsible for the observed color. In yellow Form-I, only the local excitation band at 400 nm is observed. However, in the green Form-II, the local excitation band (400 nm) is superimposed with the charge-transfer band observed at

500–700 nm. Upon passing into the red Form-III, the charge-transfer band shifts toward higher energies (wavelength of 500 nm), and its combination with the local excitation band (400 nm) results in the observed change in color.

Sulfathiazole

Sulfathiazole [4-amino-N-(2,3-dihydro-2-thiazolylidene)benzenesulfonamide]:

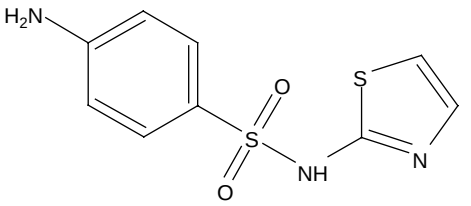

has been found to crystallize in five polymorphic forms (34–38), with the identity of these being the subject of some confusion in their nomenclature and in their ability to be obtained on a consistent basis (39). The polymorphic space of this system has been examined in great detail, establishing the absolute identity and existence of the first four polymorphs, modes for their isolation, and the solid-state spectroscopic properties of these crystal forms (40). A summary of the crystallographic data reported for the five polymorphs is provided in Table 5.

Form-I appears to be unique in the system, consisting of two independent and interwoven hydrogen-bonded chain networks, one of which is a two-dimensional network and the other which is a three-dimensional network. Forms II, III, and IV have been found to be based on a single dimeric chain network that is packed into sheets of different and unique motifs. Form-I can be distinguished from the other forms primarily on the basis of the difference in hydrogen bonding at the aniline functionality, and it was also reported that this contact is associated with a significant difference in the degree of hydrogen bonding on the fastest growing face of Form-I

TABLE 5 Crystallographic Data for the Polymorphs of Sulfathiazole

Crystal class	Form-I (35)	Form-II (34)	Form-III (36)	Form-IV (36)	Form-V (37)
	Monoclinic	Monoclinic	Monoclinic	Monoclinic	Monoclinic
Space group	$P2_1/c$	$P2_1/c$	$P2_1/c$	$P2_1/n$	$P2_1/n$
Unit cell lengths	a = 10.554 Å b = 13.220 Å c = 17.050 Å	a = 8.235 Å b = 8.550 Å c = 15.580 Å	a = 15.570 Å b = 8.570 Å c = 15.583 Å	a = 10.867 Å b = 8.543 Å c = 11.456 Å	a = 10.399 Å b = 15.132 Å c = 14.280 Å
Unit cell angles	α = 90° β = 108.06° γ = 90°	α = 90° β = 93.67° γ = 90°	α = 90° β = 112.93° γ = 90°	α = 90° β = 88.13° γ = 90°	α = 90° β = 91.21° γ = 90°
Molecules in unit cell	2	1	2	1	8
Cell volume	2261.3 Å^3	1093.2 Å^3	2162.0 Å^3	1063.0 Å^3	2246.6 Å^3
Density	1.50 g/cm^3	1.55 g/cm^3	1.57 g/cm^3	1.60 g/cm^3	1.51 g/cm^3

relative to the other forms (39). Specifically, in Form-I only one aniline hydrogen is involved, whereas in the other polymorphic forms II, III, and IV the hydrogens of both aniline groups are used.

Differential scanning calorimetry has been used to study the thermally induced phase transformation of Form-I into Form-II, and the technique used as a quantitative method for levels of Form-I in bulk Form-II (41). A study of isothermal reaction rates indicated that the transition kinetics could be explained by a model that was similar to that of diffusion-controlled crystal growth from solution. In another study, the melting points of Forms I, II, and III were reported to be 201.0°C, 196.5°C, and 173.6°C, but that complete melting of Forms I and II could only be achieved if the polymorphic purity of the forms was very high (42). Forms I and II were shown to undergo a solution-mediated phase transformation to Form-III in aqueous suspensions.

The five polymorphs of sulfathiazole have been shown to exhibit clearly distinguishable solid-state ^{13}C-NMR spectra, and the spectra fully interpreted and rationalized in terms of the crystal structures (43). Somewhat in contradiction with the crystallographic interpretations, the spectra of Forms III, IV, and V were found to be qualitatively similar but substantially different from the spectra of forms I and II. The thermally induced interconversion of all five polymorphs have been studied using differential scanning calorimetry and pulsed terahertz spectroscopy (44). Here, Form-I was determined to be the stable polymorph at high temperatures (melting point of 202°C), and Form-II was noted to melt around 197°C and subsequently recrystallize to Form-I at slightly higher temperatures. In this work, Forms III, IV, and V were all observed to undergo a thermally induced phase transformation at temperatures less than 177°C.

Sulfathiazole has been found to exhibit a remarkable ability to form solvates with practically any organic solvent, and one group has detected the existence of over 100 structurally distinct solvatomorphs and many related two-component systems (45).

Nitrofurantoin

Nitrofurantoin [*N*-(5-nitro-2-furfurylidene)-1-aminohydantoin]:

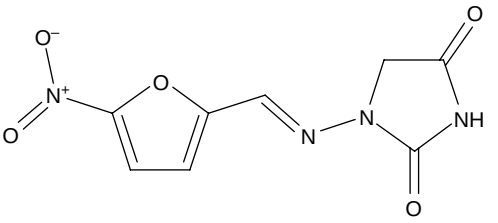

is widely used as a urinary tract antibacterial agent, but the compound is characterized by poor water solubility, and consequently, its dissolution rate is the main factor that determines its bioavailability (46). Two non-solvated polymorphic forms have been reported for the compound, with the α-form being crystallized from a hot acetic acid–water solution and the β-form being obtained from acetone (47,48).

TABLE 6 Crystallographic Data for the Polymorphs of Nitrofurantoin

Crystal class	α-Form (47)	β-Form (47,48)
	Triclinic	Monoclinic
Space group	$P\bar{1}$	$P2_1/n$
Crystal habit	Tabular	Plates
Unit cell lengths	a = 6.774 Å	a = 7.840 Å
	b = 7.795 Å	b = 6.486 Å
	c = 9.803 Å	c = 18.911 Å
Unit cell angles	α = 106.68°	α = 90°
	β = 104.09°	β = 93.17°
	γ = 92.29°	γ = 90°
Molecules in unit cell	2	4
Cell volume	477.6 Å^3	960.2 Å^3
Density	1.656 g/cm^3	1.648 g/cm^3

A summary of the crystallographic data reported for the polymorphs is found in Table 6.

In both polymorphs, the nitrofurantoin molecules pack in layers that are held together by van der Waals forces. The molecules associate to form centrosymmetric dimers through two identical intermolecular N–H····O hydrogen bonds. These dimers are themselves linked by a weaker C–H····O hydrogen bond in both of the non-solvated crystal structures. There is a considerable amount of intra-layer hydrogen bonding that dictates the packing modes of the β-form, and this degree of hydrogen bonding is less extensive in the structure of the α-form. These structural details account for the very slight difference in crystal densities between the two forms.

What complicates the dissolution behavior of nitrofurantoin and its formulations is the propensity of the compound to form solvates and hydrates. Two polymorphic monohydrate forms have been, one crystallizing in the monoclinic $P2_1/n$ space group and the other in the orthorhombic P*bca* space group (49). In both structures, water molecules stabilize the structures primarily through different modes of O–H···O (carbonyl) and N–H···O (water) hydrogen bonding. The existence of a dimethylformamide solvate and a dimethylsulfoxide solvate have also been reported, where the solvent molecules in the solvatomorphs appear to have been clathrated into the structure (50).

Because the solubility of the anhydrous forms of nitrofurantoin could not be determined with accuracy owing to the tendency of the solids to convert into one of the monohydrates, the dissolution profiles obtained using a rotating-disk method based on a kinetic model were used to obtain apparent solubility values (51). Because the solution-mediated phase transformation of the compound proceeds efficiently with a fair degree of velocity, nitrofurantoin has been one of the phase transformation models of choice in studies seeking to determine mechanisms for the conversion (52–54).

Carbamazepine

Carbamazepine (5*H*-dibenzo[*b*,*f*]azepine-5-carboxamide)

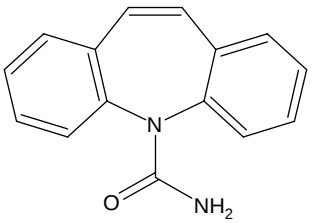

is used as an anticonvulsant and in treatment of pain associated with trigeminal neuralgia. The compound has been obtained in a triclinic polymorph crystallizing in the $P\bar{1}$ space group (55–56), one in a trigonal polymorph having the $R\bar{3}$ space group (57), and the most stable polymorph in the monoclinic $P2_1/n$ space group (58–60). More recently, another monoclinic polymorphic form has been reported, crystallizing in the $C2/c$ *C*-centered space group (61). A summary of the unit cell parameters for these four polymorphs is found in Table 7. Although Form-II is crystallized from apolar solvents, Form-III by the slow crystallization from polar solvents, and Form-I by the heating of the other forms, all three polymorphs could be obtained using appropriately controlled solution-enhanced dispersion with supercritical fluids (62).

Matzger and coworkers have discussed the structural variations that exist between the non-solvated polymorphs (56), noting that the differences arise entirely in the packing of the carboxamide dimer units, manifested in the pattern of weak C–H···O interactions. The monoclinic forms were both reported to contain infinite chains formed by the interaction of a vinylic hydrogen of the azepine ring and an oxygen acceptor. The triclinic and trigonal polymorphs were found to be similar in their patterns of weak hydrogen bond patterns, where each oxygen atom acted as an acceptor to hydrogen atoms from two nearby carbons.

TABLE 7 Crystallographic Data for the Polymorphs of Carbamazepine

Crystal class	**Form-I (55,56)**	**Form-II (57)**	**Form-III (58–60)**	**Form-IV (61)**
	Triclinic	**Trigonal**	**Monoclinic**	**Monoclinic**
Space group	$P\bar{1}$	$R\bar{3}$	$P2_1/n$	$C2/c$
Unit cell lengths	a = 5.1705 Å	a = 35.454 Å	a = 7.534 Å	a = 26.609 Å
	b = 20.574 Å	b = 35.454 Å	b = 11.150 Å	b = 6.927 Å
	c = 22.245 Å	c = 5.253 Å	c = 13.917 Å	c = 13.957 Å
Unit cell angles	α = 84.12°	α = 90°	α = 90°	α = 90°
	β = 88.01°	β = 90°	β = 92.94°	β = 109.70°
	γ = 85.19°	γ = 120°	γ = 90°	γ = 90°
Molecules in unit cell	4	18	4	8
Cell volume	2366.4 Å^3	5718.32 Å^3	1167.5 Å^3	2572.6 Å^3
Density	Not reported	1.235 g/cm^3	1.35 g/cm^3	1.31 g/cm^3

The thermodynamic relationships among the different polymorphic forms of carbamazepine have been the focus of a number of studies, all of which agree that Form-III is the most stable crystal form under ambient conditions. Forms I and III have been reported to bear an enantiotropic relationship to each other (63), while forms I and II were determined to be monotropes (64). Using solid-state infrared absorption and the "infrared rule" it was confirmed that Forms I and III were enantiotropes, whereas a similar relationship was demonstrated for Forms II and III (65).

During an automated screening study covering 66 solvents and five crystallization protocols, one hydrate and eight organic solvates were discovered in addition to the non-solvated Forms I, II, and III (66). The anhydrate-to-dihydrate (and vice versa) phase transition of carbamazepine has been the focus of a large number of studies investigating both solution-mediated and thermally initiated phase transformations (67–73).

Paracetamol (Acetaminophen)

It has been found that paracetamol (*p*-hydroxyacetanilide, and also known as acetaminophen):

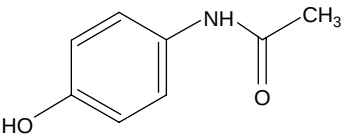

is capable of being crystallized in an orthorhombic polymorph having the P*cab* space group (74) and a monoclinic polymorph having the $P2_1/a$ space group (75). Structural details of another relatively unstable monoclinic polymorph having the $P2_1/c$ space group were deduced from the X-ray powder diffraction pattern (76). A summary of the unit cell parameters reported for these three forms is found in Table 8.

TABLE 8 Crystallographic Data for the Polymorphs of Paracetamol

Crystal class	Form-I (75)	Form-II (74)	Form-III (76)
	Monoclinic	Orthorhombic	Monoclinic
Space group	$P2_1/a$	P*cab*	$P2_1/c$
Unit cell lengths	$a = 12.93$ Å	$a = 11.805$ Å	$a = 16.05$ Å
	$b = 9.40$ Å	$b = 17.164$ Å	$b = 5.07$ Å
	$c = 7.10$ Å	$c = 7.393$ Å	$c = 9.65$ Å
Unit cell angles	$\alpha = 90°$	$\alpha = 90°$	$\alpha = 90°$
	$\beta = 115.9°$	$\beta = 90°$	$\beta = 79.1°$
	$\gamma = 90°$	$\gamma = 90°$	$\gamma = 90°$
Molecules in unit cell	4	8	Not reported
Cell volume	862.9 Å^3	1498.0 Å^3	785.3 Å^3
Density	1.296 g/cm^3	1.342 g/cm^3	Not reported

In the monoclinic Form-I structure, the molecules are linked together by two kinds of hydrogen bonds to form a pleated sheet that runs parallel to the *ac*-plane and along the *b*-axis, and the dihedral angle between the benzene ring and the amide group is 21.2° (75). In the orthorhombic Form-II structure, two kinds of hydrogen bonds form two-dimensional molecular sheets that run parallel to the *ab*-plane and along the *c*-axis (74). In this structure, the carbonyl group adopts an *endo* conformation relative to the benzene ring, and the dihedral angle between the benzene ring and the amide plane is 17.7°. The structure for the unstable Form-III polymorph is proposed to compose of bilayers where each bilayer is held together by O–H···O(H) hydrogen bonds in the *bc*-plane, and this hydrogen bonding pattern was noted to be strikingly different from the patterns observed in the other polymorphic forms (76).

The thermodynamic relationships between Forms I and II have been studied by several groups, with Form-I being stable under ambient conditions and Form-II stable under conditions of high pressure. The relative stabilities of the two polymorphs have been evaluated through pressure-temperature and temperature-volume phase diagrams, and the I-II-liquid triple point has been identified at a temperature of approximately 230°C and a pressure of 234 MPa (77). At atmospheric pressure Form-I melts at 169°C and Form-II melts at 157°C, but both melting points increase with pressure until the equalize at a pressure of approximately 250 MPa (78). A systematic crystal structure prediction search has been conducted for paracetamol, which identified Form-I as the global lattice-energy minimum and at least a dozen additional energetically feasible structures (79).

A real interest in the polymorphism of paracetamol arose when it was shown that the orthorhombic Form-II was much more suitable in direct compression formulations than was the monoclinic Form-I (80), and the compaction qualities of the metastable form have been studied in detail (81,82). Given that Form-II is metastable under ambient conditions, and that it can undergo a solution-mediated phase transformation to Form-I during ordinary production conditions, a substantial amount of work has gone into deducing routes whereby the metastable form can be reliably produced in bulk quantities (83–86).

Paracetamol has also been shown to form a wide range of solvatomorphic structures, such as a monohydrate (87), a trihydrate (88), adducts with 1,4-dioxane, N-methylmorpholine, morpholine, N,N-dimethylpiperazine, piperazine, and 4,4'-bipyridine (89), as well as two dioxane solvates (90).

Polymorphism Resulting from the Packing of Conformationally Different Molecules

Organic molecules can exist in a variety of conformations that have similar energies, and the multiple functional groups of pharmaceutically active compounds can lead to the existence of different conformers under the right conditions. In many cases, the molecule adopts a particular conformation that was determined by the nature of its interaction with the crystallizing solvent, and maintains this conformation when it packs into a crystal. The packing-type polymorphism discussed in the previous section usually represents different modes by which molecules in their most favorable conformational state have been assembled into alternate solid structures. In some cases, however, a molecule for which different conformational states are possible yields a different polymorph when its different conformations are packed.

This conformational polymorphism is therefore defined as the existence of different conformers of the same molecule in different polymorphic modifications.

Bernstein has provided a comprehensive explanation for the polymorphism that can arise from the packing of molecules in different conformational states (91). One can define conformations that are those various contortions of molecules that arise by rotation about single bonds, and that correspond to potential energy minima. Because the crystal structure of a molecule will yield information about the preferred conformation of that molecule in a given polymorph, it follows that the various arrangements of atoms or conformation cannot differ too significantly in free energy content from the equilibrium structure of the molecule. It is important to emphasize that both the crystal structure and molecular conformation represent potential energy minima that are not necessarily unique, and there may exist a number of possible molecular geometries of very nearly the same energy for both the molecular conformation and the crystal structure. It is this proximity of molecular conformational energies that makes possible the existence of different molecular conformations in a single crystal structure, or conformational polymorphism when they are in different crystal structures.

The differences in lattice energy among different crystal forms of an organic compound can be expected to be in the range of 1–2 kcal/mol, especially when van der Waals interactions dominate the structure. From estimates of the magnitudes of intermolecular interactions, this is within the range of energy required to bring about changes in molecular torsional parameters about single bonds. However, the energy required to significantly perturb bond lengths and bond angles far exceeds this range. Therefore, for those molecules that possess torsional degrees of freedom, various polymorphs may exhibit significantly different molecular conformations. This represents the rationale accounting that crystal forces may play a role in determining the conformation of a molecule, and yielding the phenomenon of conformational polymorphism.

p-*(*N-*chlorobenzylidene)*-p-*chloroaniline*

Bernstein has described methodology suitable for the study as to how crystal forces can influence molecular conformation, and elucidated the basic tenets of conformational polymorphism. (92). A combination of quantitative analysis of the molecular packing in different space groups along with ab initio molecular orbital calculations was used. Choosing the model system of *N*-(*p*-chlorobenzylidene)-*p*-chloroaniline:

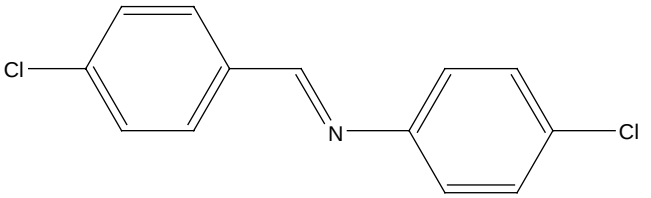

lattice energy calculations involving minimization of the energy of the triclinic and orthorhombic crystal forms of this molecule were performed. The results of

these calculations were able to explain the stability of the lattice structure in which the unstable planar conformation of the molecule is obtained. Three different potential functions were evaluated, with all potential functions yielding lower energies for the triclinic lattice (in agreement with experimental observation).

The crystallographic data for the two forms is summarized in Table 9, whereas the crystal packing and molecular conformations are illustrated in Figure 6. The molecule was found to adopt a planar conformation in the triclinic phase, but in the orthorhombic phase the phenyl rings were rotated by 24.8° about the N-phenyl and CH–phenyl bonds. Both structures may be described as being composed of blocks of molecules between two neighboring parallel planes. For the triclinic polymorph the blocks are stacked along the *b*-axis, whereas in the orthorhombic structure the stacking is due to a glide along the *c*-axis (rather than a simple translation. Within the blocks, the stacks are related by a translation along the *a*-axis in the triclinic structure, and a translation along the *b*-axis in the orthorhombic form. In the triclinic form, disorder was noted about a center of symmetry, whereas in the orthorhombic form the disorder was about a two-fold crystallographic axis.

Subsequently, additional studies on the effect of crystal forces on molecular conformations was reported for various methyl analogues of *N*-(*p*-chlorobenzylidene)-*p*-chloroaniline (93). The ab initio calculations were able to predict the relative stability of the various polymorphs, and by using a number of potential functions the authors were able to demonstrate the ruggedness of the method. Taken together, the two works demonstrate that use of partial atomic energies for the analysis of changes in molecular environments in crystals is valid, even when the energy differences involved are small in magnitude.

TABLE 9 Crystallographic Data for the Polymorphs of *N*-(*p*-chlorobenzylidene)-*p*-chloroaniline (92)

Crystal class	**Form-I**	**Form-II**
	Orthorhombic	**Triclinic**
Space group	P*ccn*	$P\bar{1}$
Crystal habit	prisms	needles
Unit cell lengths	$a = 24.503$ Å	$a = 5.986$ Å
	$b = 6.334$ Å	$b = 3.933$ Å
	$c = 7.326$ Å	$c = 12.342$ Å
Unit cell angles	$\alpha = 90°$	$\alpha = 87.38°$
	$\beta = 90°$	$\beta = 78.40°$
	$\gamma = 90°$	$\gamma = 89.53°$
Molecules in unit cell	4	4
Cell volume	284.2 Å^3	284.3 Å^3
Density	Not reported	Not reported

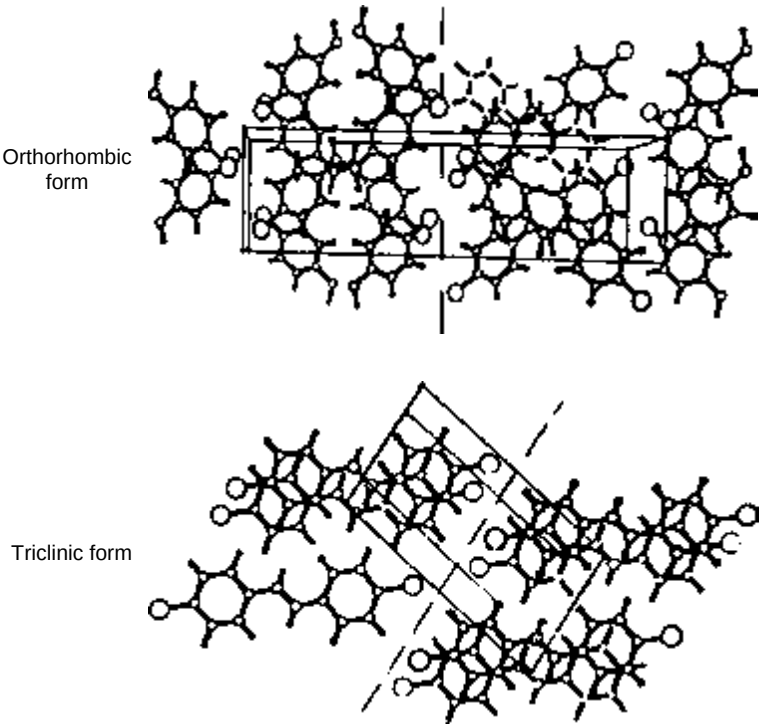

FIGURE 6 Views of the molecular packing for the triclinic and orthorhombic polymorphs of *N*-(*p*-chlorobenzylidene)-*p*-chloroaniline. The figure is adapted from data presented in Ref. (92).

p-*methyl*-N-*(*p-*methylbenzylidine)aniline*

Bar and Bernstein continued their work on conformational polymorphism, using lattice energy minimization techniques to characterize the influence of crystal forces (as well as orientational and positional disorder) on the molecular conformation of *p*-methyl-*N*-(*p*-methylbenzylidine) aniline (94):

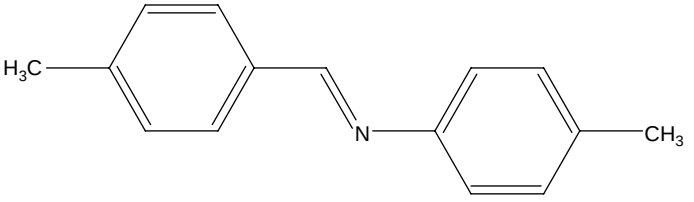

This compound was obtained in three polymorphic forms, in which the title molecule was found to adopt different conformations in each form. A summary of the reported crystallographic data is found in Table 10.

TABLE 10 Crystallographic Data for the Polymorphs of *p*-methyl-*N*-(*p*-methylbenzylidine) aniline (94)

Crystal class	Form-I	Form-II	Form-III
	Monoclinic	Monoclinic	Monoclinic
Space group	$P2_1/c$	$P2_1$	$P2_1/c$
Crystal habit	Not reported	Not reported	Not reported
Unit cell lengths	$a = 6.089$ Å	$a = 6.891$ Å	$a = 9.878$ Å
	$b = 7.751$ Å	$b = 7.153$ Å	$b = 4.884$ Å
	$c = 26.766$ Å	$c = 12.600$ Å	$c = 12.018$ Å
Unit cell angles	$\alpha = 90°$	$\alpha = 90°$	$\alpha = 90°$
	$\beta = 103.16°$	$\beta = 102.70°$	$\beta = 90.48°$
	$\gamma = 90°$	$\gamma = 90°$	$\gamma = 90°$
Molecules in unit cell	4	2	2
Cell volume	1230.07 Å^3	605.88 Å^3	579.78 Å^3
Density	Not reported	Not reported	Not reported

Form-I was found to crystallize in the monoclinic space group $P2_1/c$, with four molecules in the unit cell. This form exhibited a positional disorder, and it was found that there were two orientations of the bridge atoms with non-equivalent occupancy. The observed disorder led to fairly large displacements of the bridge atoms, but significantly less displacements for the ring atoms and methyl groups. Form-II was found to crystallize in a non-disordered chiral monoclinic space group ($P2_1$), and hence, would exhibit optical activity within this crystalline state. Finally, Form-III also crystallizes in the monoclinic space group $P2_1/c$, but contains only two molecules per unit cell. Although disorder was observed at the bridge atoms, this phenomenon was different in character than that noted for Form-I.

Lattice energy calculations were performed on the three polymorphs in order to account for the relative stability of Forms I and III, where the unstable planar conformation is prevalent. The minimizations were carried out with three different potential functions, and it was found that Form-II was characterized by the highest energy. The energies of the other two forms were found to be somewhat comparable, and were considerably less than the energy of Form-II. The minimized lattice energies were analyzed in terms of partial atomic energy contributions to the total energy, and it was shown that the relative contribution of various groups to the total energy was the same for the three polymorphs. The stability of Form-I and Form-III with respect to Form-II was attributed to the relatively favorable environment of the bridge atoms, demonstrating the important role of disorder in the stabilization of the energetically less favorable planar conformation.

Probucol

The lipid-lowering antioxidant drug probucol (4,4′-[(1-methylethylidene)bis(thio)]-bis-[2,6-bis(1,1-dimethylethyl)phenol]):

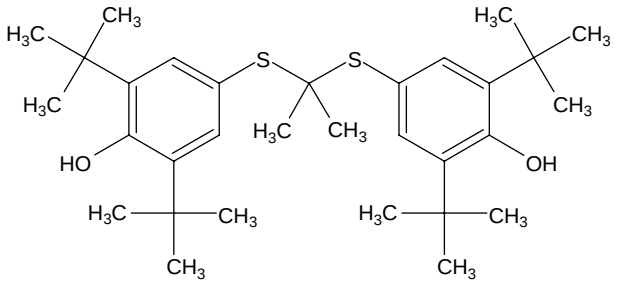

has been reported to exist either as a white crystalline solid obtained from ethanol that has a melting point of 124.5–126°C, a yellow crystalline solid obtained from isopropanol that has a melting point of 125–126.5°C, or a third form having an onset of melting of 116°C (95).

The rapid crystallization at room temperature from saturated ethanol or isopropanol solutions was found to yield a crystalline solid having an onset of melting at 116°C, which was identified as Form-II (96). When suspensions of Form-II in the crystallizing solution were allowed to stand for at least two months, a solution-mediated phase transformation took place that yielded a new crystalline solid (identified as Form-I) that was characterized by a melting onset of 125°C. The phase transformation of Form II into Form I could also be accelerated by grinding of the crystals.

Crystals of Forms I and II were obtained in sufficient quality to have their structures determined using single-crystal X-ray diffraction (96), and a summary of the reported unit cell parameters is provided in Table 11. The conformations of the probucol molecule in each form were found to be quite different, and the molecular conformations are contrasted in Figure 7. In Form-II, the C–S–C–S–C chain is extended, and the molecular symmetry approximates C_{2v}. This symmetry is lost in Form-I, where the torsional angles around the two C–S bonds deviate significantly

TABLE 11 Crystallographic Data for the Polymorphs of Probucol (96)

Crystal class	**Form-I**	**Form-II**
	Monoclinic	**Monoclinic**
Space group	$P2_1/c$	$P2_1/n$
Crystal habit	Not reported	Not reported
Unit cell lengths	a = 16.972 Å	a = 11.226 Å
	b = 10.534 Å	b = 15.981 Å
	c = 19.03 Å	c = 18.800 Å
Unit cell angles	$\alpha = 90°$	$\alpha = 90°$
	$\beta = 113.66°$	$\beta = 104.04°$
	$\gamma = 90°$	$\gamma = 90°$
Molecules in unit cell	4	4
Cell volume	3116.0 Å^3	3272.0 Å^3
Density	1.102 g/cm^3	1.049 g/cm^3

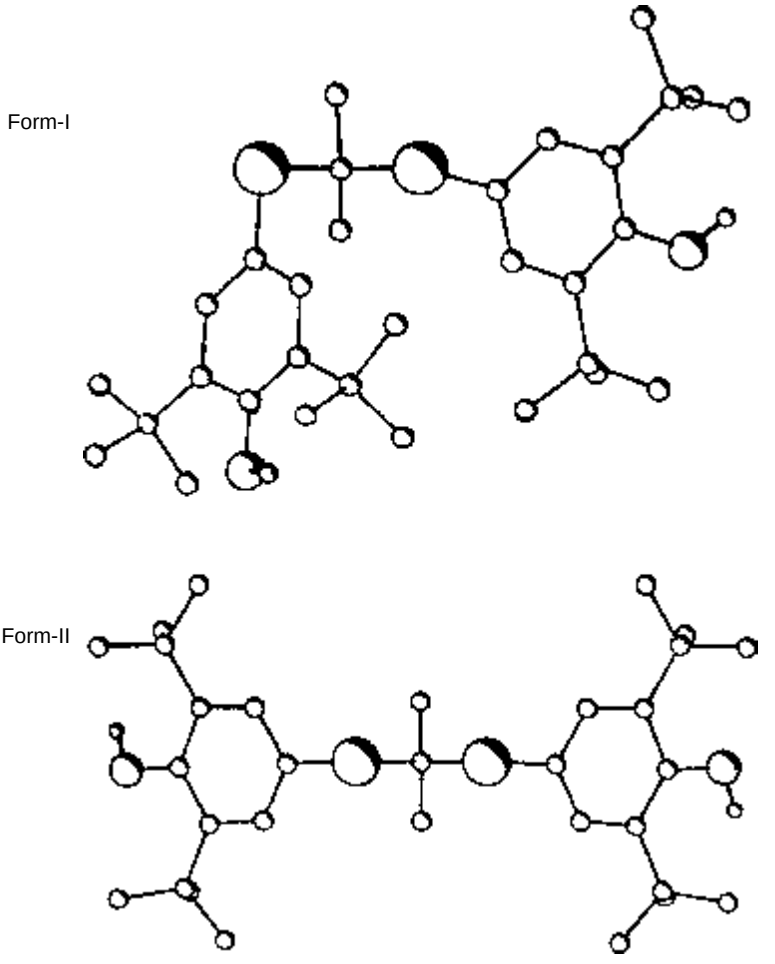

FIGURE 7 Molecular conformations adopted by probucol in its two polymorphic forms. The figure is adapted from data presented in Ref. (96).

from 180°. Steric crowding of the phenolic groups by the *t*-butyl groups was evident from deviations from trigonal geometry at two phenolic carbons in both forms. Using a computational model, the authors found that the energy of Form-II was 26.4 kJ/mol higher than was the energy of Form-I, indicating that the less symmetrical conformer is more stable. The Form-I conformer packs into a crystal whose density is 5% higher than that of Form-II, which may be taken as being indicative of more efficient packing.

The authors examined space-filling models of the two conformers, and concluded that the phenolic groups were poorly exposed on the molecular surface. The inaccessibility of the phenolic groups was taken to explain both the low solubility of the drug in water and the absence of hydrogen bonding in either of the two crystal forms.

Spironolactone

It has been established that the diuretic steroidal aldosterone agonist spironolactone (17-hydroxy-7α-mercapto-3-oxo-17α-pregn-4-ene-21-carboxylic acid):

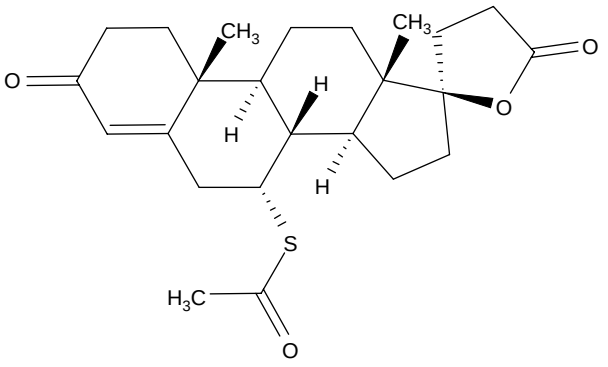

is capable of being obtained in a number of crystalline modifications, and that the variable and incomplete oral absorption that is associated with its poor water solubility and slow dissolution rate is complicated by the existence of polymorphism and solvatomorphism (97,98).

The crystal structure of orthorhombic Form-I has been reported, with the compound crystallizing in the non-centrosymmetric $P2_12_12_1$ space group (99). In this structure, the *A*-ring is highly distorted owing to the presence of the Δ^4 double bond and the ketone group, the *B*-ring and the *C*-ring adopt a chair conformation, the *D*-ring is a distorted half-chair, and the *E*-ring is a half-chair. The hydrophobic nature of the compound is manifested in the observation that the molecules are held together entirely by van der Waals forces. The unit cell parameters reported for Form-I are found in Table 12.

TABLE 12 Crystallographic Data for the Polymorphs of Spironolactone

Crystal class	**Form-I (99)**	**Form-II (100)**
	Orthorhombic	**Orthorhombic**
Space group	$P2_12_12_1$	$P2_12_12_1$
Crystal habit	Needle-like	Prisms
Unit cell lengths	$a = 9.979$ Å	$a = 10.584$ Å
	$b = 35.573$ Å	$b = 18.996$ Å
	$c = 6.225$ Å	$c = 11.005$ Å
Unit cell angles	$\alpha = 90°$	$\alpha = 90°$
	$\beta = 90°$	$\beta = 90°$
	$\gamma = 90°$	$\gamma = 90°$
Molecules in unit cell	4	4
Cell volume	2209.8 Å^3	2213 Å^3
Density	Not reported	1.25 g/cm^3

The crystal structure of the other non-solvated polymorphic Form-II has been reported as well, also crystallizing in the non-centrosymmetric $P2_12_12_1$ space group (100). The unit cell parameters reported for Form-II are also found in Table 12. In this structure, the *A*-ring conformation was described as being that of a sofa, the *B*-ring and the *C*-ring were chair-shaped, the *D*-ring was a distorted 13β envelope, and the *E*-ring was almost planar. As in the case of Form-I, the molecules in the structure were held together by van der Waals forces.

Examination of the intermolecular distances in the various forms indicates that the predominant cohesive forces are van der Waals interactions, and all crystals are characterized by close molecular packing (101). The steroid nuclei are almost planar in all forms, and perpendicular to the *E*-ring and to the 7-α-acetylthio side-chain. A comparison of torsional angles confirmed the existence of conformational polymorphism. Differences in carbon–carbon bond angles were noted in the flexible *A*-rings of all non-solvated forms, with this ring being in a "half-chair" conformation in Form-I and a "sofa" conformation in Form-II. The conformation of the rigid *B*-ring and *C*-ring is relatively fixed in the various forms, while the conformation of the flexible *D*-ring and *E*-ring varies significantly in the various forms.

In this latter study, the structures of additional solvated crystalline forms were disclosed as well (101). Form-III is a 2:1 acetonitrile solvate, Form-IV is a 2:1 ethanol solvate, Form-V is a 4:1 ethyl acetate solvate, and Form-VI is a 1:2 methanol solvate. Interestingly, a definite formula could only be obtained for Form-III, which agreed with the results of the crystallographic study. The solvent content of the other solvates was in conflict with the determined space group, and may be indicative of disorder in the solid. The crystal structure of the acetonitrile solvate has been discussed in more detail (102).

Flufenamic Acid

Flufenamic Acid (2-{[3-(trifluoromethyl)phenyl]amino}benzoic acid):

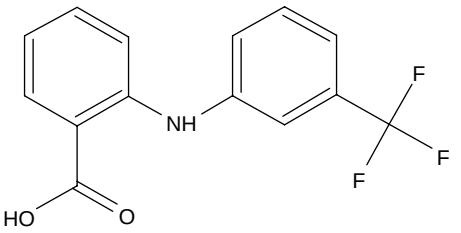

has been found to exist in at least three different monoclinic polymorphic forms (103), of which Form-I (104) and Form-III (105) have been the subject of additional investigation owing to the stability and metastability under ambient conditions. The details of the reported unit cells of the polymorphs are collected in Table 13. Form-III can be obtained by crystallization from ethanol, and the enantiotropically related Form-I can be obtained by simple thermal means. A significant amount of thermodynamic information about the thermally induced phase transformations among flufenamic acid polymorphs can be found in the compilation of Burger and Ramberger (106).

The difference between the two polymorphs of flufenamic acid has been reported to exist in the geometrical disposition of the [3-(trifluoromethyl)phenyl]

amino moiety with respect to the benzoic acid moiety. As in other fenamate structures, the carboxyl group and the nitrogen atom of the imino group are connected through an intramolecular hydrogen bond. In addition, pairs of centro-symmetrically related molecules are connected through hydrogen bonds involving carboxyl groups. A more detailed discussion of the structural elements of compounds in the fenamate class is available (107).

Raman spectroscopy has been used as an on-line tool to quantitatively monitor the crystallization of flufenamic acid from solution (108). The crystallization was monitored as a function of temperature and time using an immersion probe coupled to a Raman spectrometer, with data regarding the species existing in the solution phase and in the crystallized solids being obtained. It was shown that one could identify the polymorphic form initially crystallizing from solution, and the kinetics of the conversion of the metastable form to the stable form could be readily followed. In a subsequent work, information regarding the phase transformation kinetics was obtained using in situ Raman spectroscopic studies (109). On-line X-ray powder diffraction has also been used to monitor the polymorphic state of flufenamic acid in formulations undergoing wet granulation (110).

Lomeridine Dihydrochloride

Lomeridine dihydrochloride (1-[bis(4-fluorophenyl)methyl]-4-(2,3,4-trimethoxygenzyl)-piperazine dihydrochloride):

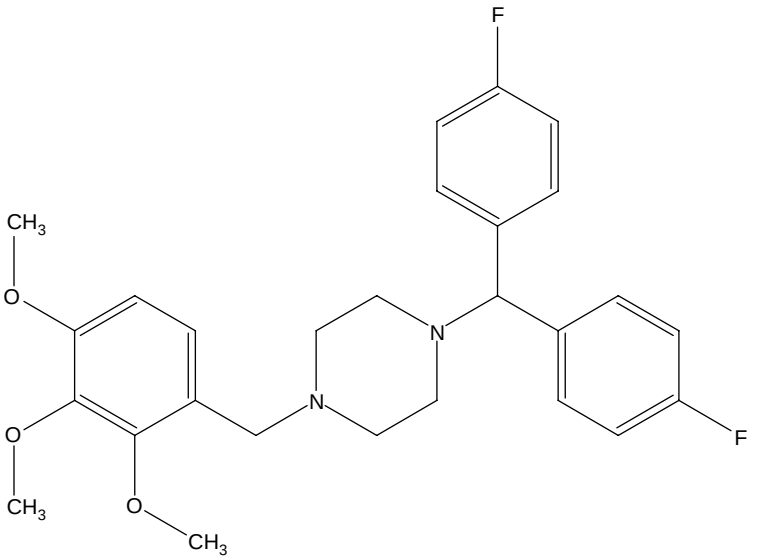

has been developed as a calcium entry blocker in cerebral and peripheral circulation, being potentially useful as an agent against migraine. The compound has been shown to be capable of existing in two polymorphic forms, for which the structures have been reported (111). Form-I was obtained from acetonitrile solution, whereas Form-II was crystallized from either the methanol, ethanol, *n*-propanol, *i*-propanol, *n*-butanol, or methyl ethyl ketone solvent systems. The reported unit cell parameters for the two forms is found in Table 14.

TABLE 13 Crystallographic Data for the Polymorphs of Flufenamic Acid

Crystal class	**Form-I (104)**	**Form-II (103)**	**Form-III (105)**
	Monoclinic	**Monoclinic**	**Monoclinic**
Space group	$P2_1/c$	$P2_1/a$	$C2/c$
Unit cell lengths	$a = 12.523$ Å	$a = 11.850$ Å	$a = 39.848$ Å
	$b = 7.868$ Å	$b = 10.425$ Å	$b = 5.107$ Å
	$c = 12.874$ Å	$c = 11.220$ Å	$c = 12.240$ Å
Unit cell angles	$\alpha = 90°$	$\alpha = 90°$	$\alpha = 90°$
	$\beta = 95.20°$	$\beta = 112.83°$	$\beta = 92.47°$
	$\gamma = 90°$	$\gamma = 90°$	$\gamma = 90°$
Molecules in unit cell	4	4	8
Cell volume	1263.27 Å^3	1277.49 Å^3	2488.57 Å^3
Density	1.47 g/cm^3	Not reported	Not reported

TABLE 14 Crystallographic Data for the Polymorphs of Lomeridine Dihydrochloride (111)

Crystal class	**Form-I**	**Form-II**
	Triclinic	**Trigonal**
Space group	$P\bar{1}$	$R\bar{3}$
Crystal habit	Not reported	Not reported
Unit cell lengths	$a = 19.487$ Å	$a = 20.060$ Å
	$b = 11.930$ Å	$b = 20.060$ Å
	$c = 6.920$ Å	$c = 20.060$ Å
Unit cell angles	$\alpha = 118.27°$	$\alpha = 90°$
	$\beta = 90.99°$	$\beta = 90°$
	$\gamma = 97.35°$	$\gamma = 117.30°$
Molecules in unit cell	2	6
Cell volume	1399.6 Å^3	4504 Å^3
Density	1.285 g/cm^3	1.198 g/cm^3

Although the molecular conformations of the lomeridine molecule in the two polymorphic structures are somewhat similar in many respects, torsion about one bond was sufficient to yield the conformational polymorphism. The two conformations of the lomeridine unit are illustrated in Figure 8, where it may be seen that the main conformational difference consists in the rotation about a single C–N bond. At the same time, Form-I exhibits head-to-head and tail-to-tail packing toward the diagonal axis of the *ab*-plane. In Form-II, a three-fold screw axis passes by one of the *p*-fluorobenzenes, which stacks continuously, and the other *p*-fluorobenzene lies along the axis.

It was also reported that the averaged isotropic atomic displacement parameter of Form-II was larger by about 0.4 Å relative to that of Form-I, and

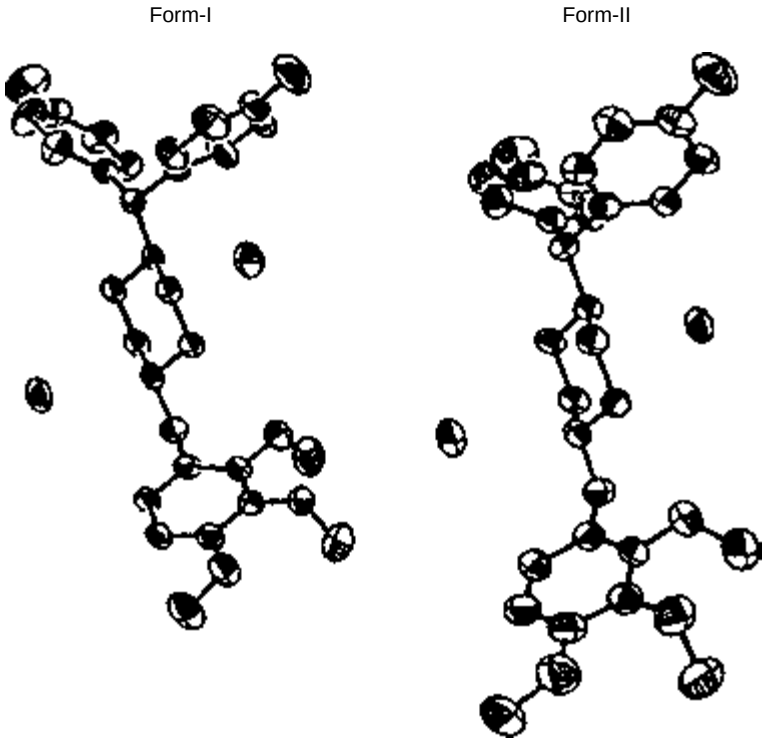

FIGURE 8 Views of the molecular conformations adopted by lomeridine dihydrochloride in its two polymorphic forms. The figure is adapted from data presented in Ref. (111).

hence, the molecular packing in the Form-I structure was judged to be more thermodynamically stable than that of Form-II. The difference in the averaged isotropic atomic displacement parameter for the trimethoxybenzene group was found to be larger in Form-II is larger relative to that of Form-I, whereas the difference in the averaged atomic displacement parameter for the *p*-fluorobenzene groups in the polymorphic structures was small. It was therefore concluded that the difference in the packing stability between the polymorphs was mainly determined by the stability of the packing of the trimethoxybenzene groups in the two structures.

The different polymorphs were found to exhibit different moisture sorption profiles, with Form-II tending to form a stable trihydrate when exposed to high levels of relative humidity. Form-I, on the other hand, appeared to form a monohydrate under similar conditions, but underwent deliquescence at a relative humidity of 90%. X-ray powder diffraction patterns obtained for the high-humidity forms were consistent with the presence of a phase change for both polymorphs, and the diffraction patterns of the resulting hydrate crystal forms differed from each other as well.

5-Methyl-2-[(2-nitrophenyl)amino]-3-thiophenecarbonitrile (ROY)

5-Methyl-2-[(2-nitrophenyl)amino]-3-thiophenecarbonitrile (usually known as ROY):

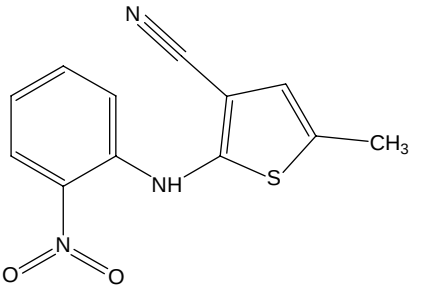

represents a system that exhibits both conformational and color polymorphism (112,113), and is currently the organic compound with the greatest number of determined polymorphic crystal structures in the Cambridge Structural Database. Crystallographic data for this polymorphic system is collected in Table 15, and Figure 9 shows the conformation of ROY in its orange needle, yellow, red, orange plate, yellow needle, orange–red plate, and YT04 (transformed) crystal forms.

The red, orange, and yellow forms differ in the angle between the plane of the phenyl and thiophene ring, with values of 104.7° (yellow form), 104.1°(yellow needle), 52.6° (orange needle), 46.1°(orange plate), 39.4°(orange–red plate), and 21.7° (red form) being reported. The different colors of the solids arise from perturbation of the energies of the molecular orbitals of the compound associated with the different degrees of overlap of the double bonds in these two rings. This hypothesis is consistent with calculations of the overlap and absorption spectra of 5-methyl-2-[(2-nitrophenyl)amino]-3-thiophenecarbonitrile.

The history of the discovery of the various forms of ROY provides a fascinating case study in polymorph research. ROY was originally obtained by Dr. Chuck Bunnell at Tippecanoe Labs (Eli Lilly, Indianapolis, Indiana, U.S.A.) as either a red or yellow solid. ROY was then subjected to an abbreviated polymorph screen by Dr. Greg Stephenson at Purdue University, who discovered a third form, which he named Form-ON. Dr. Lian Yu and coworkers at Eli Lilly subsequently discovered three additional forms of ROY, which they named forms OP, YN, and ORP. The seventh polymorph, Form-RPL, was discovered by selective epitaxial nucleation on the (010) face of a succinic acid crystal (114). Energy temperature diagrams among ROY polymorphs, forms Y, OP, ON, R, and YN, were constructed using melting and eutectic melting data by Dr. Yu, who found that Form-Y is the most stable form at room temperature, forms YN and R are the two most metastable forms and are monotropically related to other forms he also established that forms ON, OP, and Y are enantiotropically related to one another (113). Then in 2005, Yu et al. reported the discovery of the eighth and ninth forms of 5-methyl-2-[(2-nitrophenyl)amino]-thiophene-carbonitrile, learning that Form-YT04 was the second most stable form of ROY (115).

A new set of conceptual elements and computational methods have been developed for a quantitative view of packing in organic crystal structures, and the

TABLE 15 Crystallographic Data for the Polymorphs of 5-methyl-2-[(2-nitrophenyl)amino]-thiophenecarbonitrile (112)

Crystal class	Yellow form (Y)	Orange needle (ON)	Red form (R)	Yellow needle (YN)	Orange plate (OP)	Orange-red plate (ORP)
	Monoclinic	Monoclinic	Triclinic	Triclinic	Monoclinic	Orthorhombic
Space group	$P2_1/n$	$P2_1/c$	$P\bar{1}$	$P\bar{1}$	$P2_1/n$	$Pbca$
Crystal habit	Plates	Needles	Plates	Needles	Plates	Plates
Unit cell lengths	a = 8.5001 Å	a = 3.9453 Å	a = 7.4918 Å	a = 4.5918 Å	a = 7.9760 Å	a = 13.177 Å
	b = 16.413 Å	b = 18.685 Å	b = 7.7902 Å	b = 11.249 Å	b = 13.319 Å	b = 8.0209 Å
	c = 8.5371 Å	c = 16.3948 Å	c = 11.9110 Å	c = 12.315 Å	c = 11.676 Å	c = 22.801 Å
Unit cell angles	α = 90°	α = 90°	α = 75.494°	α = 71.194°	α = 90°	α = 90°
	β = 91.767°	β = 93.830°	β = 77.806°	β = 89.852°	β = 104.683°	β = 90°
	γ = 90°	γ = 90°	γ = 63.617°	γ = 88.174°	γ = 90°	γ = 90°
Molecules in unit cell	4	4	2	2	4	8
Cell volume	1190.463	1205.891	598.885	601.825	1199.862	2409.870
Density	1.447 g/mL	1.428 g/mL	1.438 g/mL	1.431 g/mL	1.435 g/mL	1.429 g/mL

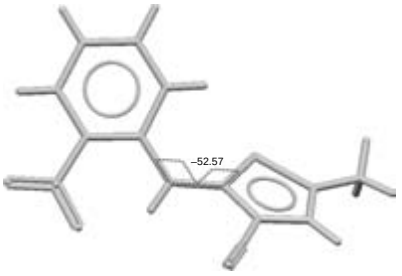

ON (orange needle)

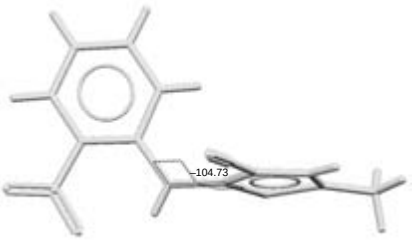

Yellow form

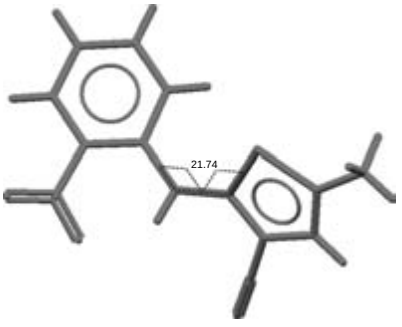

Red form

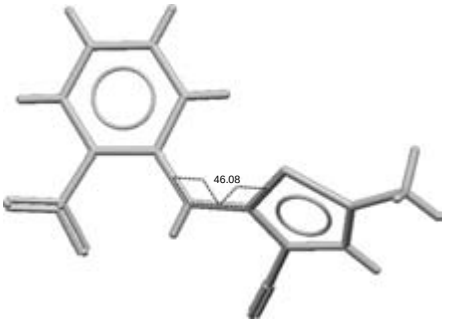

OP (orange plate)

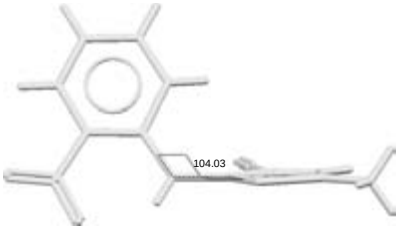

YN (yellow needle)

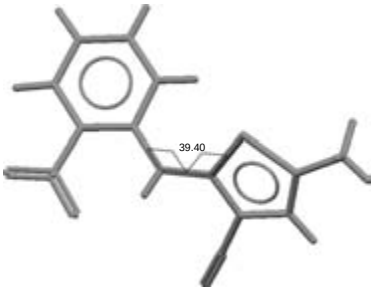

ORP (orange–red plate)

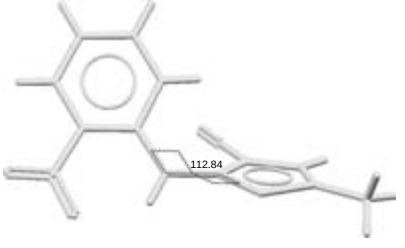

YT04 (Y04 transformed)

FIGURE 9 Conformation of the various forms of 5-methyl-2-[(2-nitrophenyl)amino]-thiophene-carbonitrile (ROY) in the crystal.

method was illustrated by the six known polymorphs of ROY (116). Cross-nucleation of polymorphs has been studied in the spontaneous and seeded melt crystallization of ROY, where it was shown that certain of the polymorphs could not nucleate without the aid of another and where the new form grew at a faster rate relative to the existing form (117).

A summary of methods of preparation for the various forms of ROY are outlined in Table 16. Although polymorph interconversions abound at high temperature for ROY, the red, orange, and yellow polymorphs have been found to be stable at ambient conditions for many years. The observations made by these various workers are consistent with experience at SSCI/Aptuit for a number of polymorphic systems. Typically, the most stable form is found early in the screening study, and less stable forms are found during subsequent studies. For both the ROY example and others, it is clear that many polymorphic forms do not crystallize from solution, and therefore, solution-based crystallizations will undoubtedly miss other metastable crystal forms.

Other Conformational Polymorphic Systems Structurally Related to ROY

Polymorphic derivatives of 5-methyl-2-[(2-nitrophenyl)amino]-thiophenecarbonitrile have been synthesized, and polymorphic transformation in these systems studied as well by Dr. Thomas Borchardt and Dr. Hui Li at Purdue University. 5-Methyl-2-[(4-methyl-2-nitrophenyl]amino]-3-thiophenecarbonitrile and 2-[(2-nitrophenyl)amino]-3-thiophenecarbonitrile are among the derivatives exhibiting both conformational and color polymorphism.

Five polymorphs of 5-methyl-2-[(4-methyl-2-nitrophenyl)amino]-3-thiophenecarbonitrile:

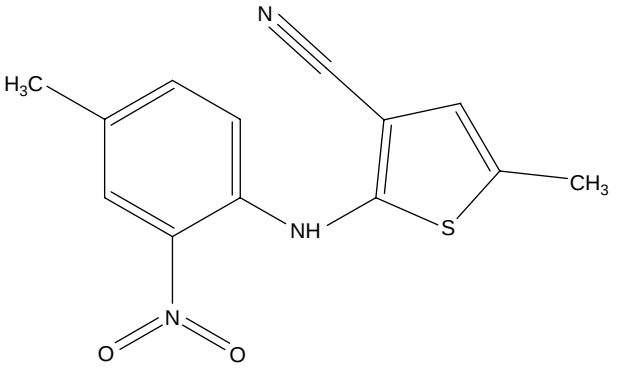

have been observed, with the solids being colored red (R), dark red (DR), light red, deep red, and orange (O) (118). The solid-to-solid phase transformation from the DR form to the R form was investigated, and it was observed that at 85°C large particles underwent faster phase transitions than did small particles. Milling and the presence of moisture increased the rate of the phase transformation, whereas ethanol vapor annealing reduced the rate. It was concluded that defects on the surface were responsible for the solid-to-solid transition for this compound, and that larger crystals had more defects that facilitated their phase transformation relative to the rates of small crystals.

TABLE 16 Outline of Methods of Preparation for Most of the Polymorphic Forms of 5-methyl-2-[(2-nitrophenyl)amino]-thiophenecarbonitrile

Polymorphic form	Method of preparation
Y	Solution mediated conversion of any other from near room temperature, also solution crystallization
ON	Fast crystallization from a variety of solvents
R	Fast crystallization from a variety of solvents
YN	Fast crystallization from a variety of solvents
OP	Required seeding or by heating R
ORP	Crystallized from a melt
RPL	Crystallized from vapor through epitaxy
Y04	New yellow form crystallized from a melt
YT04	Obtained from transformation of Y04

2-[(2-nitrophenyl)amino]-3-thiophenecarbonitrile:

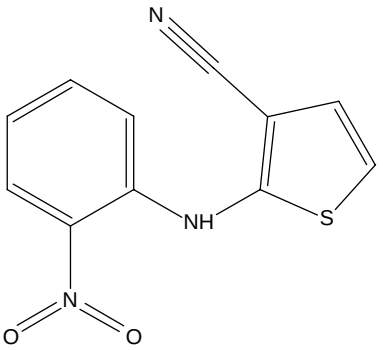

has been shown to exist in three polymorphic-colored forms so far, with these being identified as yellow (Y), R, and O (119). In addition, an "appearing/disappearing polymorph" has also been detected for Form-Y. Energy temperature diagrams for the R and O forms were constructed, and free energy differences were calculated as well.

Crystallographic data for the R and O forms are shown in Table 17. Based on slurry conversion and solubility studies, Form-R was found to be the stable form before melting. Based on the normalized energy-temperature diagram, it was concluded that the free energy difference between forms R and O was small (~0.2 kJ/mol). A polymorphic transformation from Form-O to Form-R was not observed unless the process was seeded with crystals of Form-R in both the solution as well as in the solid state.

Significant differences between the structures of the R and O forms were identified in torsional angles between the thiophene and phenyl rings. The torsion angle of Form-R (5.01°) is much higher than that of Form-O (53.8°), and this difference results in a higher degree of planarity in the molecular conformation of Form-R. Increased planarity allows for stronger overlap of the nitrogen in the amino group

TABLE 17 Crystallographic Data for the Polymorphs of 2-[(2-nitrophenyl) amino]-3-thiophenecarbonitrile

Crystal class	Red form	Orange form
	Monoclinic	Triclinic
Space group	C2/*c*	P1
Crystal habit	Plates	Needles
Unit cell lengths	*a* = 13.8617 Å	*a* = 3.9331 Å
	b = 8.7921 Å	*b* = 7.1080 Å
	c = 17.511 Å	*c* = 10.154 Å
Unit cell angles	α = 90°	α = 75.949°
	β = 96.1°	β = 78.08°
	γ = 90°	γ = 87.372°
Molecules in unit cell	8	1
Cell volume	2121	269.43
Density	1.535 g/cm^3	1.510 g/cm^3

with the thiophene π-orbital, which in turn, shortens the distance between the nitrogen in the amino group and the thiophene ring. In addition, the torsional angles found in the polymorphs are consistent with those of original ROY polymorph, for which the R form has lowest torsion angle and the O form has a torsional angle around 50°.

SUMMARY

It is apparent that the molecules are capable of adopting multiple solid-state forms upon crystallization, and that the rationales for the existence of different polymorphic states are wide and varied. Understanding the origins of such phenomena becomes the first step in prediction, and prediction, in turn, should yield mechanisms for the control of polymorphs. Approaches to identifying the most stable polymorphs are important, and must be used in order to guide the selection of the best form for development.

In recent years, approaches to the calculation of the crystal structure of various polymorphs have been introduced and discussed. Such methods were introduced in Chapter 1 of this book. If crystal structures can be calculated with certainty it would, of course, be possible to predict the polymorphism of a compound and use this information to guide experimental studies. This remains a difficult goal to achieve, and requires the development of better force fields. However, Desiraju has recently presented a very balanced view of the possibility of calculating crystal structures (120). In some cases it is possible to calculate crystal structures, especially if the space group is known. The calculation is more difficult for other cases, particularly those involving salts and when several molecules are present in an asymmetric unit. However, it will be interesting to observe the developments in this area as force fields improve, and the speed of computation increases.

The Cambridge Crystallographic Database had held four blind tests of crystal structure prediction, with the results of the third test being summarized in a 2005 publication (121). Eighteen groups participated in this test, which involved

attempting to predict the structures of three molecules. Only one of the 18 groups participating was able to predict the structure of only one molecule. These results show that as of 2005 better energy models and improved search procedures are needed. Interestingly, preliminary information from the fourth blind in 2008 test show that one group was able to successfully predict the crystal structures of all of the test molecules. This is an impressive improvement that will no doubt lead to additional research in this important area.

Compounds under pharmaceutical development will continue to adopt structures differing in their free energy, and it will probably be true that the most thermodynamically favored form will only appear after some time has elapsed. However, if the research teams have done their job properly, the full details of the polymorphism will be known long before the drug reaches Phase 3, and then there would be no surprises to encounter.

REFERENCES

1. Haüy RJ. Essai d'une Théorie sur la Structure des Crystaux. Appliquée à Plusieurs Genres de Substances Crystallisées. In: Traité de Cristallographie, volume 1. Paris: Gogué et Née de La Rochelle, 1784: 206–30.
2. Seeber AL. Versuch einer erklarung des inneren baues der festen körper. Ann Phys 1824; 76: 229–49.
3. Barlow W. Probable nature of the internal symmetry of crystals. Nature 1883; 29: 186–8.
4. Friedrich W, Knipping P, von Laue M. Interference phenomena with roentgen rays. Sber bayer Math Phys Klasse (Kgl.) Akad Wiss 1912: 303–22.
5. Bragg WL. The structure of some crystals as indicated by their diffraction of X-rays. Proc Roy Soc (London) 1913; A89: 248–77.
6. Bravais A. Etudes Crystallographiques. Paris: Gautier-Villars, 1866.
7. Burns G, Glazer AM. Space Groups for Solid State Scientists. New York: Academic Press, 1978.
8. Wells AF. Structural Inorganic Chemistry, 5th Edition. Oxford: Clarendon Press, 1984.
9. Gschneider KA. Crystallography of the rare-earth metals, chapter 14 in The Rare Earths. In: Spedding FH, Daane AH, eds. New York: Robert E. Krieger Publishing Co, Huntington, 1961: 190–214.
10. Cotton FA, Wilkinson G. Advanced inorganic chemistry, 5th Edition. New York: John Wiley & Sons, 1988: 654–5.
11. Hultgren R, Gingrich NS, Warren BE. The atomic distribution in red and black phosphorus and the crystal structure of black phosphorus. J Chem Phys 1935; 3: 351–5.
12. Warren BE, Burwell JT. The structure of rhombic sulfur. J Chem Phys 1935; 3: 6–8.
13. Hückel W. Structural chemistry of inorganic compounds, volume II. Amsterdam: Elsevier, 1951: 687–8.
14. Wagner G, Lippert L. Z Physik Chem 1936; B31: 263.
15. Bragg WL. The analysis of crystals by the X-ray spectrometer. Proc Roy Soc (London) 1913; A89: 468.
16. Kracek FC, Posnjak E, Hendricks SB. Gradual transition in sodium nitrate. II. The structure at various temperatures and its bearing on molecular rotation. J Am Chem Soc 1931; 53: 3339–48.
17. Bragg L, Claringbull GF. Crystal Structures of Minerals. New York: Cornell University Press, Ithaca, 1965: 127–34.
18. Bijvoet JM, Claassen A, Karssen A. Proc K Acad Wetensch. Amsterdam 1926; 29: 529.

19. Hägg G, Söderholm G. Crystal structure of Mg-Al spinels with Al_2O_3: surplus and γ-Al_20_3. Z Physik Chem 1935; B29: 88–94.
20. Topping J. On the form and potential energy of the isomorphous crystals. Ruby (Al_2O_3) and hoematite (Fe_2O_3). Proc Roy Soc (London) 1928; A122: 251–73.
21. Bernstein J. Conformational polymorphism, Chapter 13 in Organic Solid State Chemistry. In: Desiraju GR, ed. Amsterdam: Elsevier, 1987: 471–518.
22. Bernstein J. Conformational polymorphism: intra- and intermolecular energetics, Chapter 5 in Polymorphism in Molecular Crystals. Oxford: Clarendon Press, 2002: 151–87.
23. Robertson JM. The structure of resorcinol: a quantitative X-ray investigation. Proc Royal Soc (London) 1936; A157: 79–99.
24. Robertson JM, Ubbelohde AR. A new form of resorcinol. I. Structure Determination by X-Rays. Proc Royal Soc (London) 1938; A167: 122–35.
25. Zhang GGZ, Gu C, Zell MT, et al. Crystallization and transitions of sulfamerazine polymorphs. J Pharm Sci 2002; 91: 1089–100.
26. Acharya KR, Juchele KN, Kartha G. Crystal structure of sulfamerazine. J Cryst Spectrosc Res 1982; 12: 369–76.
27. Caira MR, Mohamed R. Positive identification of two orthorhombic polymorphs of sulfamerazine ($C_{11}H_{12}N_4O_2S$), their thermal analyses and structural comparison. Acta Cryst 1992; B48: 492–92.
28. Hossain GMG. A new polymorph of sulfamerazine. Acta Cryst 2006; E62: o2166–o2167.
29. Adsmond DA, Grant DJW. Hydrogen bonding in sulfonamides. J Pharm Sci 2001; 90: 2058–77.
30. Kawakami K, Ida Y. Application of modulated-temperature DSC to the analysis of enantiotropically related polymorphic transitions. Thermochim Acta 2005; 427: 93–9.
31. C-Hui Gu, Young V, Grant DJW. Polymorph Screening: Influence of solvents on the rate of solvent-mediated polymorphic transformation. J Pharm Sci 2001; 90: 1878–90.
32. Gong Y, Collman BM, Mehrens SM, et al. Stable-form screening: overcoming trace impurities that inhibit solution-mediated phase transformation to the stable polymorph of sulfamerazine. J Pharm Sci 2008; 97: 2130–44.
33. Tanaka M, Matsui H, Mizoguchi J-I, et al. Optical properties, thermochromism, and crystal structures of the dimorphs of 2-iodoanilinium picrate. Bull Chem Soc Jap 1994; 67: 1572–9.
34. Kruger GJ, Gafner G. The crystal structure of sulfathiazole II. Acta Cryst 1971; B27: 326–33.
35. Kruger GJ, Gafner G. The crystal structures of polymorphs I and III of sulfathiazole. Acta Cryst 1972; B28: 272–83.
36. Blagden N, Davey RJ, Lieberman HF, et al. Crystal chemistry and solvent effects in polymorphic systems: sulfathiazole. J Chem Soc Faraday Trans 1998; 94: 1035–44.
37. Hughes DS, Hursthouse MB, Threlfall T, et al. A new polymorph of sulfathiazole. Acta Cryst 1999; C55: 1831–3.
38. Chan FC, Anwar J, Cernik R, et al. ab initio structure determination of sulfathiazole polymorph V from synchrotron X-ray powder diffraction data. J Appl Cryst 1999; 32: 436–41.
39. Blagden N, Davey RJ, Rowe R, et al. Disappearing polymorphs and the role of reaction by-products: the case of sulfathiazole. Int J Pharm 1998; 172: 169–77.
40. Anwar J, Tarling SE, Barnes P. Polymorphism of sulfathiazole. J Pharm Sci 1989; 78: 337–42.
41. Shami EG, Bernardo PD, Rattei ES, et al. Kinetics of polymorphic transformation of sulfathiazole form I. J Pharm Sci 1972; 61: 1318–20.
42. Lagas M, Lerk CF. The polymorphism of sulfathiazole. Int J Pharm 1981; 8: 11–24.
43. Apperley DC, Fletton RA, Harris RK, et al. Sulfathiazole polymorphism studied by magic-angle spinning NMR. J Pharm Sci 1999; 88: 1275–80.

44. Zeitler JA, Newnham DA, Taday PF, et al. Characterization of temperature-induced phase transitions in five polymorphic forms of sulfathiazole by terahertz pulsed spectroscopy and differential scanning calorimetry. J Pharm Sci 2006; 95: 2486–98.
45. Bingham AL, Hughes DS, Hursthouse MB, et al. Over one hundred solvates of sulfathiazole. Chem Comm 2001: 603–4.
46. Gouda HW, Moustafa MA, Al-Shora HI. Effect of storage on nitrofurantoin solid dosage forms. Int J Pharm 1984; 18: 213–15.
47. Pienaar EW, Caira MR, Lötter AP. Preparation and X-ray crystal structures of two anhydrous forms of nitrofurantoin. J Cryst Spectrosc Res 1993; 23: 785–90.
48. Bertolasi V, Gilli P, Ferretti V, et al. Structure and crystal packing of the antibacterial drug 1-{[(5-nitro-2-furanyl)methylene]amino}-2,4-imidazolidinedione (Nitrofurantoin). Acta Cryst 1993; C49: 741–4.
49. Pienaar EW, Caira MR, Lötter AP. Preparation and X-ray crystal structures of two monohydrated forms of nitrofurantoin. J Cryst Spectrosc Res 1993; 23: 739–44.
50. Caira MR, Pienaar EW, Lötter AP. Polymorphism and pseudopolymorphism of the antibacterial nitrofurantoin. Mol Cryst Liquid Cryst 1996; 279: 241–64.
51. Otsuka M, Teraoka R, Matsuda Y. Rotating-disk dissolution kinetics of nitrofurantoin anhydrate and monohydrate at various temperatures. Pharm Res 1992; 9: 307–11.
52. Rodríguez-Hornedo N, Murphy D. Significance of controlling crystallization mechanisms and kinetics in pharmaceutical systems. J Pharm Sci 1999; 88: 651–60.
53. Aaltonen J, Heinänen P, Peltonen L, et al. In situ measurement of solvent-mediated phase transformations during dissolution testing. J Pharm Sci 2006; 95: 2730–7.
54. Wikström H, Rantanen J, Gift AD, et al. Toward an understanding of the factors influencing anhydrate-to-hydrate transformation kinetics in aqueous environments. Cryst Growth Des 2008; 8: 2684–93.
55. Ceolin R, Toscani S, Gardette M-F, et al. X-ray characterization of the triclinic polymorph of carbamazepine. J Pharm Sci 1997; 86: 1062–5.
56. Grzesiak AL, Lang M, Kim K, et al. Comparison of the four anhydrous polymorphs of carbamazepine and the crystal structure of form I. J Pharm Sci 2003; 92: 2260–71.
57. Lowes MMJ, Caira MR, Lötter AP, et al. Physicochemical properties and X-ray structural studies of the trigonal polymorph of carbamazepine. J Pharm Sci 1987; 76: 744–52.
58. Reboul JP, Cristau B, Soyfer JC, et al. 5H-Dibenz[b,f]azépine-carboxamide-5 (Carbamazépine). Acta Cryst 1981; B37: 1844–8.
59. Himes VL, Mighell AD, De Camp WH. Structure of carbamazepine: 5H-dibenz[b,f] azepine-5-carboxamide. Acta Cryst 1981; B37: 2242–5.
60. Lisgarten John N, Palmer Rex A, Saldanha Jose W. Crystal and molecular structure of 5-carbamyl-5H-dibenzo[b,f]azepine. J Cryst Spectrosc Res 1989; 19: 641–9.
61. Lang M, Kampf JW, Matzger AJ. Form IV of carbamazepine. J Pharm Sci 2002; 91: 1186–90.
62. Edwards AD, Shekunov BY, Kordikowski A, et al. Crystallization of pure anhydrous polymorphs of carbamazepine by solution enhanced dispersion with supercritical fluids (SEDSTM). J Pharm Sci 2001; 90: 1115–24.
63. Behme RJ, Brooke D. Heat of fusion measurement of a low melting polymorph of carbamazepine that undergoes multiple-phase changes during differential scanning calorimetry analysis. J Pharm Sci 1991; 80: 986–90.
64. Edwards AD, Shekunov BY, Forbes RT, et al. Time-resolved X-ray scattering using synchrotron radiation applied to the study of a polymorphic transition in carbamazepine. J Pharm Sci 2001; 90: 1106–14.
65. Rustichelli C, Gamberini G, Ferioli V, et al. Solid-state study of polymorphic drugs: Carbamazepine. J Pharm Biomed Anal 2000; 23: 41–54.

66. Florence AJ, Johnston A, Price SL, et al. An automated parallel crystallization search for predicted crystal structures and packing motifs of carbamazepine. J Pharm Sci 2006; 95: 1918–30.
67. Young WWL, Suryanarayanan R. Kinetics of transitiotn of anhydrous carbamazepine to carbamazepine dihydrate in aqueous suspensions. J Pharm Sci 1991; 80: 496–500.
68. McMahon LE, Timmins P, Williams AC, et al. Characterization of dihydrates prepared from carbamazepine polymorphs. J Pharm Sci 1996; 85: 1064–9.
69. Brittain HG. Fluorescence studies of the transformation of carbamazepine anhydrate form-III to its dihydrate phase. J Pharm Sci 2004; 93: 375–83.
70. Tian F, Zeitler JA, Strachan CJ, et al. Characterizing the conversion kinetics of carbamazepine polymorphs to the dihydrate in aqueous suspension using raman spectroscopy. J Pharm Biomed Anal 2006; 40: 271–80.
71. Qu H, Louhi-Kultanen M, Rantanen J, et al. Solvent-mediated phase transformation kinetics of an anhydrate/hydrate system. Cryst Growth Des 2006; 6: 2053–60.
72. Qu H, Louhi-Kultanen M, Kallas J. Additive effects on the solvent-mediated anhydrate/hydrate phase transformation in a mixed solvent. Cryst Growth Des 2007; 7: 724–9.
73. Tian F, Saville DJ, Gordon K, et al. The influence of various excipients on the conversion kinetics of carbamazepine polymorphs in aqueous suspension. J Pharm Pharmacol 2007; 59: 193–201.
74. Haisa M, Kashino S, Kawai R, et al. The monoclinic form of p-hydroxy-acetanilide. Acta Cryst 1976; B32: 1283–5.
75. Haisa M, Kashino S, Maeda H. The orthorhombic form of p-hydroxyacetanilide. Acta Cryst 1974; B30: 2510–12.
76. Peterson ML, Morissette SL, McNulty C, et al. Iterative high-throughput polymorphism studies on acetaminophen and an experimentally derived structure for form III. J Am Chem Soc 2002; 124: 10958–9.
77. Espeau P, Céolin R, Tamarit J-L, et al. Polymorphism of paracetamol: relative stabilities of the monoclinic and orthorhombic phases inferred from topological pressure-temperature and temperature-volume phase diagrams. J Pharm Sci 2005; 94: 524–39.
78. Ledru J, Imrie CT, Pulham CR, et al. High pressure differential scanning calorimetry investigations on the pressure dependence of the melting of paracetamol polymorphs I and II. J Pharm Sci 2007; 96: 2784–94.
79. Beyer T, Day GM, Price SL. The prediction, morphology, and mechanical properties of the polymorphs of paracetamol. J Am Chem Soc 2001; 123: 5086–94.
80. Di Martino P, Guyot-Hermann A-M, Conflant P, et al. A new pure paracetamol for direct compression: the orthorhombic form. Int J Pharm 1996; 128: 1–8.
81. Garekani HA, Ford JL, Rubinstein MH, et al. Formation and compression characteristics of prismatic polyhedral and thin plate-like crystals of paracetamol. Int J Pharm 1999; 187: 77–89.
82. Garekani HA, Ford JL, Rubinstein MH, et al. Highly compressible paracetamol: II. compression properties. Int J Pharm 2000; 208: 101–10.
83. Nichols G, Frampton CS. Physicochemical characterization of the orthorhombic polymorph of paracetamol crystallized from solution. J Pharm Sci 1998; 87: 684–93.
84. Garekani HA, Ford JL, Rubinstein MH, et al. Highly compressible paracetamol: I: crystallization and characterization. Int J Pharm 2000; 208: 87–99.
85. Al-Zoubi N, Kachrimanis K, Malamataris S. Effects of harvesting and cooling on crystallization and transformation of orthorhombic paracetamol in ethanolic solution. Eur J Pharm Sci 2002; 17: 13–21.
86. Al-Zoubi N, Malamataris S. Effects of initial concentration and seeding procedure on crystallization of orthorhombic paracetamol from ethanolic solution. Int J Pharm 2003; 260: 123–35.

87. Parkin A, Parsons S, Pulham CR. Paracetamol monohydrate at 150 K. Acta Cryst 2002; E58: o1345–o1347.
88. McGregor PA, Allan DR, Parsons S, et al. Preparation and crystal structure of a trihydrate of paracetamol. J Pharm Sci 2002; 91: 1308–11.
89. Oswald IDH, Allan DR, McGregor PA, et al. The formation of paracetamol (acetaminophen) adducts with hydrogen-bond acceptors. Acta Cryst 2002; B58: 1057–66.
90. Vrcelj RM, Clark NIB, Kennedy AR, et al. Two new paracetamol/dioxane solvates: a system exhibiting a reversible solid-state phase transformation. J Pharm Sci 2003; 92: 2069–73.
91. Bernstein J. Conformational polymorphism, chapter 13. In Organic Solid State Chemistry. In: Desiraju GR, ed. Amsterdam: Elsevier, 1987: 471–518.
92. Bernstein J, Hagler AT. Conformational polymorphism: the influence of crystal structure on molecular conformation. J Am Chem Soc 1978; 100: 673–81.
93. Hagler AT, Bernstein J. Crystal energetics by computational substitution: further evidence for the sensitivity of the method. J Am Chem Soc 1978; 100: 6349–54.
94. Bar I, Bernstein J. Crystal energetics of a trimorphic system including disorder. J Phys Chem 1982; 86: 3223–31.
95. Neuworth MB, Laufer RJ, Barnhart JW, et al. Synthesis and hypocholesterolemic activity of alkylidenedithio bisphenols. J Med Chem 1970; 13: 722–5.
96. Gerber JJ, Caira MR, Lötter AP. Structures of two conformational polymorphs of the cholesterol-lowering drug probucol. J Cryst Spectrosc Res 1993; 23: 863–9.
97. El-Dalsh SS, El-Sayed AA, Badawi AA, et al. Studies on spironolactone polymorphic forms. Drug Dev Indust Pharm 1983; 9: 877–94.
98. Salole EG, Al-Sarraj FA. Spironolactone crystal forms. Drug Dev Indust Pharm 1985; 11: 855–64.
99. Dideberg O, Dupont L. La structure cristalline et moléculaire de la spironolactone (7-acétylthio-3-oxo-17–4-pregnène-21,17 carbolactone). Acta Cryst 1972; B28: 3014–22.
100. Agafonov V, Legendre B, Rodier N. A new crystalline modification of spironolactone. Acta Cryst 1989; C45: 1661–3.
101. Agafonov V, Legendre B, Rodier N, et al. Polymorphism of spironolactone. J Pharm Sci 1991; 80: 181–5.
102. Agafonov V, Legendre et B, Rodier N. Structure cristalline du solvate spironolactone-acétonitrile (2:1). Acta Cryst 1991; C47: 365–9.
103. Krc J. Crystallographic properties of flufenamic acid. Microscope 1977; 25: 31–45.
104. Krishna Murthy HM, Bhat TN, Vijayan M. Structure of a new crystal form of 2-{[3-(trifluoromethyl)phenyl]amino}benzoic acid (flufenamic acid). Acta Cryst 1982; B38: 315–17.
105. McConnell JF. Structure flufenamic acid form III. Cryst Struct Comm 1973; 2: 459–61.
106. Burger A, Ramberger R. On the polymorphism of pharmaceuticals and other molecular crystals. II. applicability of thermodynamic rules. Mikrochim Acta [Wien] 1979; II: 273–316.
107. Dhanaraj V, Vijayan M. Structure and interactions of anti-inflammatory fenamates: a concerted crystallographic and theoretical conformational study. Acta Cryst 1988; B44: 406–12.
108. Hu Y, Liang JK, Myerson AS, et al. Crystallization monitoring by raman spectroscopy: simultaneous measurement of desupersaturation profile and polymorphic form in flufenamic acid systems. Ind Eng Chem Res 2005; 44: 1233–40.
109. Hu Y, Wikström H, Byrn SR, et al. Estimation of the transition temperature for an enantiotropic polymorphic system from the transformation kinetics monitored using raman spectroscopy. J Pharm Biomed Anal 2007; 45: 546–51.
110. Davis TD, Morris KR, Huang H, et al. In situ monitoring of wet granulation using online X-ray powder diffraction. Pharm Res 2003; 20: 1851–7.

111. Hiramatsu Y, Suzuke H, Kuchiki A, et al. X-ray structural studies of lomeridine dihydrochloride polymorphs. J Pharm Sci 1996; 85: 761–6.
112. Stephenson GA, Borchardt TB, Byrn SR, et al. Conformational and color polymorphism of 5-methyl-2-[(2-nitrophenyl)amino]-3-thiophenecarbonitrile. J Pharm Sci 1995; 84: 1385–6.
113. Yu L, Stephenson GA, Mitchell CA, et al. Thermochemistry and conformational polymorphism of a hexamorphic crystal system. J Am Chem Soc 2000; 122: 585–91.
114. Mitchell CA, Yu L, Ward M. Selective nucleation and discovery of organic polymorphs through epitaxy with single crystal substrates. J Am Chem Soc 2001; 123: 10830–9.
115. Chen S, Guzei IA, Yu L. new polymorphs of ROY and new record for coexisting polymorphs of solved structures. J Am Chem Soc 2005; 127: 9881–5.
116. Dunitz JD, Gavezzotti A. Toward a quantitative description of crystal packing in terms of molecular pairs: application to the hexamorphic crystal system, 5-methyl-2-[(2-nitrophenyl)amino]-3-thiophenecarbonitrile. Cryst Growth Des 2005; 5: 2180–9.
117. Chen S, Hanmi X, Yu L. Cross-nucleation between ROY polymorphs. J Am Chem Soc 2005; 127: 17439–44.
118. Li H, Stowell JG, He X, et al. Investigations on solid-solid phase transformation of 5-methyl-2-[(4-methyl-2-nitrophenyl]amino]-3-thiophenecarbonitrile. J Pharm Sci 2007; 96: 1079–89.
119. Li H, Stowell JG, Borchardt TB, et al. Synthesis, conformational polymorphism, and construction of a G–T diagram of 2-[(2-nitrophenyl)amino)-3-thiophenecarbonitrile. Cryst Growth Des 2006; 6: 2469–74.
120. Desiraju GR. Crystal gazing: structure prediction and polymorphism. Science 1997; 278: 404–5.
121. Day GM, Motherwell WDS, Ammon HL, et al. A third blind test of crystal structure prediction. Acta Cryst 2005; B61: 511–27.

7 Structural Aspects of Solvatomorphic Systems

Harry G. Brittain
Center for Pharmaceutical Physics, Milford, New Jersey, U.S.A.
Kenneth R. Morris
College of Pharmacy, University of Hawaii at Hilo, Hilo, Hawaii, U.S.A.
Stephan X. M. Boerrigter
SSCI, an Aptuit Company, West Lafayette, Indiana, U.S.A.

INTRODUCTION

Whereas polymorphism has been defined in other chapters as crystal systems for which a substance can exist in structures characterized by different unit cells, but where each of the forms has exactly the same elemental composition, the term solvatomorphism refers to those systems where the crystal structures of the substance are also defined by different unit cells, but where these unit cells differ in their elemental composition through the inclusion of one or molecules of solvent. Another definition of a solvatomorph is that it is a crystalline solid in which solvent molecules have become included in the structure through positional substitution at positions that are site-specific and that are related to other solvent molecules through translational symmetry.

Solvatomorphs may be broadly classified as to the ratio of drug substance, namely, that they are either stoichiometric (where a definite ratio of solvent to molecule exists) or non-stoichiometric (where the ratio of solvent to molecule may vary continuously over a given range). Griesser has further identified non-stoichiometric solvatomorphs as being solid solutions where the solvent can be present in either an interstitial or substitutional mode (1). It has been pointed out that the definitions of solvatomorphs and cocrystals are not mutually exclusive (2), and so the use of the latter term might eventually supersede the use of the former.

In his solvatomorph chapter, Byrn (3) has tabulated a list of solvents known to form solvatomorphs with organic compounds, namely, water, methanol, ethanol, *n*-propanol, isopropanol, *n*-butanol, *sec*-butanol, isobutanol, *tert*-butanol, acetone, methyl ethyl ketone, acetonitrile, diethyl ether, tetrahydrofuran, dioxane, acetic acid, butyric acid, phosphoric acid, hexane, cyclohexane, benzene, toluene, xylene, ethyl acetate, ethylene glycol, dichloromethane, chloroform, carbon tetrachloride, l,2-dichloroethane, *N*-methylformamide and *N*,*N*-dimethyl-formamide, *N*-methylacetamide, pyridine, and dimethyl sulfoxide. Although the presence of most of these solvents in a therapeutically indicated drug substance might raise toxicity concerns, Byrn (3) has provided a number of reasons for which solvatomorphs of organic solvents would be of interest:

- The solvatomorph could be the penultimate solid form of the drug substance.
- The solvatomorph could be specifically chosen for recovery or purification.
- The solvatomorph could be characterized by a crystal morphology that facilitates performance of a step in a manufacturing process.

- The solvatomorph could be the only crystalline form suitable for crystal structure determination of the drug substance by means of single-crystal X-ray diffraction study.
- The solvatomorph could be useful in a desolvated form that facilitated its dissolution.
- The solvatomorph could constitute new intellectual property, and thus be patentable.

Without a doubt, water is the solvent that forms the largest number of pharmaceutically useful solvatomorphic solids, and it has been estimated that approximately one-third of drug substances are capable of forming crystalline hydrates (4). Owing to its small size that enables it to fill structural voids and because of its multidirectional hydrogen-bonding capability, water is an ideal agent for the linking of drug molecules into stable crystal structures (3). The mere presence of water in a system is not a sufficient reason to anticipate formation of a hydrate species, because the activity of water in the crystallizing medium determines whether a given hydrate species will form (5). Because water is such a ubiquitous substance, it is not surprising that the most important type of solvatomorphism involves the incorporation of water into crystal lattices.

The potential pharmaceutical impact of changes in hydration state of crystalline drug substances and excipients exists throughout the development process. The behavior of hydrates has become the object of increasing attention over the last decades, primarily due (directly or indirectly) to the potential impact of hydrates on the development process and dosage form performance. Substances may hydrate or dehydrate in response to changes in environmental conditions, processing, or over time, if they exist in a metastable thermodynamic state (6).

Often it may turn out not be practical or possible to maintain the same hydrate species of a compound during scale-up activities that was originally isolated during the discovery "bench" scale synthesis. The choice of counterions required to produce a more soluble salt form may also be dictated by the extent and type of hydration observed for a given salt, and/or by the moisture level that may be safely accommodated by the dosage form (7).

The physicochemical stability of the compound may raise issues during preformulation. Some hydrated compounds may convert to an amorphous form upon dehydration, and some may become chemically labile. This is true of cephradine dihydrate, which dehydrates to become amorphous and then undergoes subsequent oxidation. Other compounds may convert from a lower to higher state of hydration yielding forms with lower solubility. In any case, the resulting "new" forms would represent unique entities that, depending on the dosage form, might have to be maintained throughout the manufacturing process and in the clinic, and would impact on the regulatory status of the compound. Most often this demands that the form (usually crystalline) be identified and characterized with respect to handling conditions during the early pre-IND stage of the development process.

As dosage form development proceeds, changes in hydration state can result in variable potencies depending on handling conditions during weighing steps, the kinetics of the hydration/dehydration process, and the environmental conditions during processing. Differences in powder flow can result from changes in crystal form and/or morphology that may accompany the hydration/dehydration process. This can affect content uniformity in solid processing either in the mixing process or during

transfer to other processing equipment such as tablet presses. Aqueous granulation, particle size reduction, film coating, and tablet compression, all provide opportunities to "trap" a compound in a metastable form that may "relax" to a more stable form at some unpredicted point in the life of a dosage form. Alternately, a kinetically favored but thermodynamically unstable form may be converted during these processes to a more stable and less soluble form.

During and after manufacturing, moisture from the environment or that sealed in the package may redistribute throughout the dosage form and change the hydration state(s). These changes can, in turn, visit the negative consequences discussed above for the bulk drug on the dosage form. These may be manifest as: changes in tablet/capsule dissolution rates (and perhaps bioavailability), changes in lyophile reconstitution times, tablet capping, chemical instability, discoloration, and more. Of course, the potential for changes in hydration state also exists for many pharmaceutical excipients (such as lactose or magnesium stearate).

Such problems are typically magnified as both synthetic and dosage form production is scaled up. This may be caused by solvent limitations, heat transfer differences in production equipment, changes in raw materials and/or raw material suppliers, changes in processing times, and time and control constraints on product storage, to name a few.

The arguments just provided detail the potential issues around hydrates in the development process, but the question is how often hydrates are encountered during the conduct of "real-life" drug development. A quick search of the Cambridge Structural Database (version 5.29) shows that 56,940 out of a total 42,3752 crystal structures (i.e., 13.4%) contain molecular water (8). Interestingly, when organometallic compounds are excluded from the analysis, it turns out that only 15,390 out of 181,370 structures contain water (i.e., 8.5%). However, if the search is further limited to those structures that are marked as being biologically active, the percentage is 14.4% (i.e., 1552 out of 10,722 compounds). The difference in the last two percentages suggests that hydrates are more common among pharmaceutically relevant compounds. It is to be noted that these statistics cannot be completely accurate, as the Cambridge Crystallographic Data Centre (CCDC) cannot guarantee that all active compounds have been identified as such, and not all compounds tagged as being active are actually used as pharmaceutical agents. Nevertheless, the current subset of biologically active compounds is still a better representation of pharmaceutical compounds than is the full ensemble of structures in the Cambridge Structural Database (CSD).

It must also be noted that a considerable number of crystal structures that are **solved** during pharmaceutical development do not ever become published. In other circumstances, one may obtain evidence for the formation of a hydrate or hydrates, but the actual crystal structures are never elucidated. This situation can arise either because of a simple lack of interest or because the hydrate crystals are deemed to be of insufficient quality to perform single-crystal X-ray analysis. Finally, even when hydrates are found and their crystal structures determined, in many instances the details of the structural analysis are never published for intellectual property concerns. It is highly likely that the actual occurrence of hydrates is much higher than database statistics suggest, and that the estimate of one-third of drug substances forming hydrates is probably valid.

When the hydrated compounds that have been identified as being active are evaluated for their stoichiometry, the breakdown of these according to hydration

number is that shown in Figure 1. Monohydrates are by far the most common, followed by dihydrates. The frequency of higher hydration numbers rapidly declines beyond the trihydrates. It is interesting to note the relatively frequent occurrence of hemihydrates (0.5 water molecules per drug substance molecule) and sesquihydrates (1.5 water molecules per drug substance molecule). Apparent fractional hydration states can also be encountered, representing either the existence of complicated unit cells (such as a unit cell containing one water molecule and two drug substance molecules), or the sharing of water molecules between unit cells in the structure.

Other occurrences with frequencies of one represent non-stoichiometric hydrated compounds, but a word of caution is due when such hydrates are encountered. An apparent stoichiometry of 0.6 water molecules could correspond to a partially dehydrated monohydrate, or to a hemihydrate having sorbed additional water due to defects or amorphous content. It could also be a partially dehydrated hydrate that was characterized by a true 2/3 stoichiometry. The conditions to which crystals are typically exposed during single-crystal X-ray analysis (i.e., a flux of dry nitrogen close to its evaporation temperature) particularly tend to dehydrate crystals during analysis.

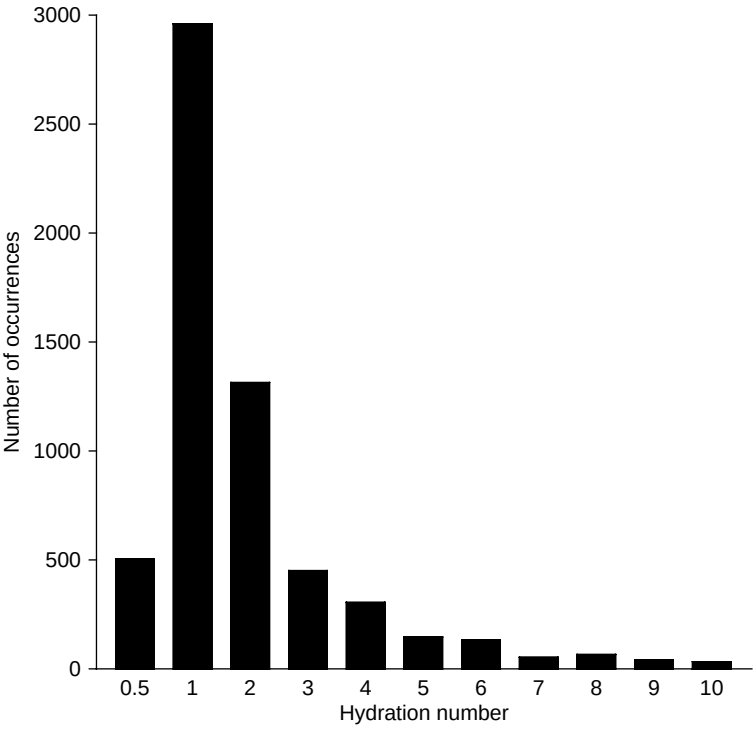

FIGURE 1 Occurrence of various crystalline hydrate stoichiometries.

The symmetry of these hydrate crystals follows fairly closely with that reported for organic structures overall. Table 1 shows the breakdown for space groups, organized by crystal system, accounting for the top approximately 90% of the structures. Space group $P2_1/c$ (number 14) is the most commonly encountered group, as with the general population of organic molecules contained in the CSD.

THERMODYNAMICS OF SOLVATOMORPHIC SYSTEMS

As discussed in a previous chapter, a solvatomorphic system will consist of at least two components (the substance itself and the solvent of solvation), and to describe the various phases one must invoke the variables of pressure, volume, temperature, and composition. For the two component systems of interest to pharmaceutical scientists (typified by hydrates and their anhydrates), studies are usually conducted at atmospheric pressure, and this specification immediately fixes one of the variables and enables the construction of ordinary phase diagrams.

Two important considerations related to biphasic equilibria are of importance during the development of solvatomorphs for pharmaceutical purposes. The first concerns the environmental conditions associated with the vapor pressure of solvate species, as these are associated with the ability of a solvate to become desolvated. The other concerns the solubility of solvatomorphs in solvent systems, and how the different physical properties of a solvatomorph may be exploited during development. As hydrates are of most importance to the pharmaceutical community, the discussion will focus largely on issues associated with water, but from a thermodynamic viewpoint, the content applies equally well to solvatomorphs that contain organic solvents.

TABLE 1 Ten Most Common Space Groups for Compounds Marked as being Active in the Cambridge Structural Database[a]

Space group	Percentage of active compounds having the indicated space group	Percentage of active hydrates having the indicated space group
$P2_1/c$	28.0	19.0
$P2_12_12_1$	21.1	22.1
$P2_1$	15.7	18.8
$P\bar{1}$	13.9	13.2
$C2/c$	4.3	4.8
$Pbca$	3.4	1.9
$C2$	2.3	4.5
$P1$	2.2	3.5
$Pna2_1$	1.2	1.0
$P2_12_12$	0.9	2.3
	93.0	91.1

[a]Organometallic compounds were excluded from these statistics.

One solvatomorphic system of interest to the present discussion is where a solid phase exists in a state of equilibrium with a single vapor phase, such as would be encountered for solvation/desolvation equilibria at temperatures less than the fusion temperature of the desolvated solid. Upon heating, the solvatomorph can dissociate either into a solvate of lower solvation, or into an anhydrous phase.

Consider the hydration/dehydration equilibrium associated with the hypothetical monohydrate, C–H_2O:

$$C\text{–}H_2O \rightleftharpoons C + H_2O \tag{1}$$

When C–H_2O is present in equilibrium with its desolvated form and liberated water vapor, this system consists of two components and three phases, and according to the Phase Rule is characterized by one degree of freedom. If one were to perform the equilibration at fixed pressure (e.g., atmospheric pressure), then the system becomes invariant, and the condition of equilibrium could only exist at a fixed temperature. Alternatively, if one were to place the monohydrate in a vessel maintained at constant temperature, then the pressure would equilibrate at the dissociation pressure of the monohydrate and remain at that pressure until the dehydration process is complete.

Experimentally, it has been found that the vapor pressure curve of a hydrate system is the same type as that of liquid water (9). In terms of the temperature–pressure phase diagram depicted in Figure 2, the B–O curve portion is the vapor pressure curve of ice, O–A is that of liquid water, and O–C is the effect of pressure on the melting point. The S–H curve provides the vapor pressures of saturated solutions of the monohydrate at various temperatures, and must lie below the O–A curve because the vapor pressure is lowered by the presence of dissolved solute. In addition, the amount of dissolved substance (and consequently the depression in vapor pressure) will increase with temperature, so the solution curve will gradually recede from the water curve. The solution curve intersects with the ice curve at the point S, where four phases (ice, monohydrate, solution, and vapor) will coexist in equilibrium. This point is known as a cryohydric point.

It is to be emphasized that the vapor pressure of a hydrate is not a pressure of water vapor with which the hydrate alone is in equilibrium. According to the Phase Rule, before a system can be univariate there must be three phases present, namely, two solid phases and the vapor phase. In the context of our hypothetical monohydrate, the correct use of the term "vapor pressure of a hydrate" would be that of the vapor pressure of the system C/C–H_2O. Bowden (9) has summarized the significance of vapor pressure, and this is found in Table 2.

The equilibrium thermodynamics of stoichiometric hydrates has been described by several authors, which tend to follow the same general outline (10,11). The equilibrium constant, K_h, between an anhydrous crystal and a hydrate whose stoichiometry is given by the number m, A (solid) + $m$$H_2O$ ↔ A · $m$$H_2O$ (solid), is defined as

$$K_h = \frac{a[\mathrm{A} \cdot m\mathrm{H_2O}\ (\mathrm{solid})]}{a[\mathrm{A}\ (\mathrm{solid})]a[\mathrm{H_2O}]^m} \tag{2}$$

Here, a represents the activity of the hydrate [a(A · $m$$H_2O$ (solid))] and anhydrate [a(A (solid))], respectively. Besides the anhydrous form on one side, this equilibrium relation can easily be adapted to any system with different levels of hydration,

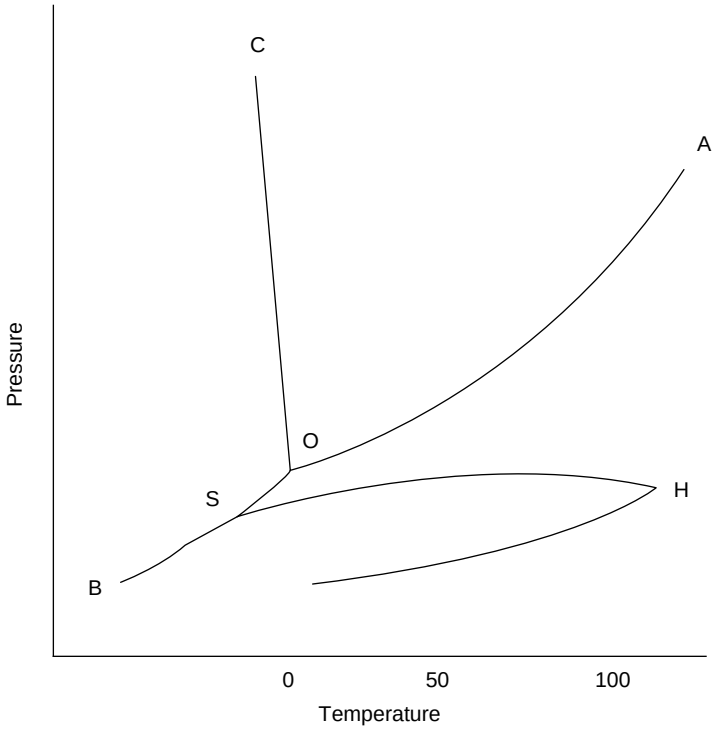

FIGURE 2 Vapor pressure curve for water and a hypothetical monohydrate.

TABLE 2 The Significance of Vapor Pressure (9)

	Property of a pure liquid	**Property of an aqueous solution**	**Property of a crystalline hydrate**
Number of components	1	2	2
Number of phases	2	2	3
Degrees of freedom	1	2	1
Composition of phases	Invariant	Variable (function of concentration)	Invariant
Definition of vapor pressure	The pressure of vapor in equilibrium with the liquid	The pressure of aqueous vapor in equilibrium with the solution	The pressure of aqueous vapor in equilibrium with the hydrate and the hydrate of next lowest stoichiometry (or anhydrate)

but for the sake of brevity we will consider only this case. In equilibrium the water activity, $a(H_2O)$, is defined as the partial vapor pressure in equilibrium, p/p_0, and can thus be written as

$$p/p_0 \equiv a[H_2O] = \left(\frac{a[A \cdot mH_2O\ (solid)]}{a[A\ (solid)]K_h} \right)^{1/m} \quad (3)$$

The partial vapor pressure of water is typically expressed as a percentage and referred to as the relative humidity (RH), that is, RH = $p/p_0 \times 100\%$. The hydrate/anhydrous system gives rise to a specific critical RH at which these phases are in equilibrium. When a substance is subjected to a RH below the critical RH the anhydrous phase is more stable; above it, the hydrate is more stable. This means phase transitions typically occur when materials are kept outside their respective stable RH regions.

Figure 3 shows the water adsorption behavior of levothyroxine sodium, which shows the equilibrium between the anhydrous and the pentahydrate forms. The sudden jump in weight at about 12% RH shows the phase transition. The material continues to slightly gain weight at higher RH because of surface adsorption. When materials go through several hydration states, such as a monohydrate followed by a dihydrate, two individual sharp jumps in height are observed.

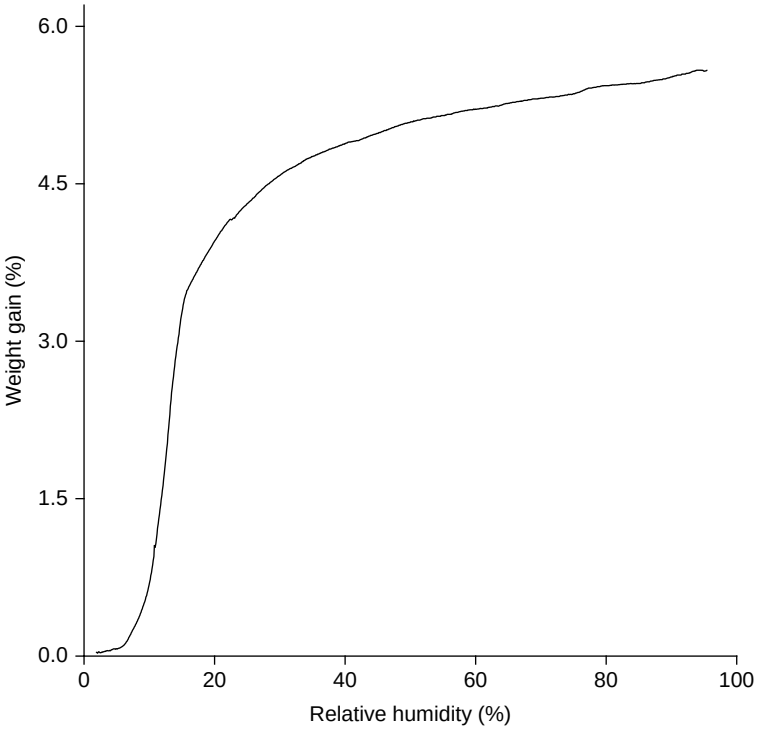

FIGURE 3 Vapor adsorption behavior of previously dehydrated levothyroxine sodium that shows a phase transition to the pentahydrate at an RH of approximately 12%.

When kept in a closed system and allowed to equilibrate, the air above a mass of crystals will attain the RH value that stems from equation (3). These microenvironmental RH values are important to keep in mind when considering the shelf life of dosage forms and their packaging, because the water content of any free volume of air will equilibrate with the drug product. What makes matters worse is the exponential temperature dependence of the RH. As a general rule of thumb, the partial vapor pressure of water drops by a factor of two for every 11.1°C. Therefore, in a closed system, the RH rises by a factor of two for the same drop in temperature.

Although for polymorphs, phase interconversions are mostly temperature controlled, solvatomorphs are also highly sensitive to the activity of the solvents involved, as well as to the phase identity of the solvent. Even though thermodynamics might favor a solid–solid phase transition, it frequently happens that the reaction is kinetically unfavorable, and hence, some metastable polymorphs can be maintained for years without any evidence for formation of the stable polymorph. However, when these metastable forms are exposed to even the smallest amounts of solvent, the interconversion process can take place very rapidly.

Nývlt discussed the kinetics of this mechanism, and called it a solid–liquid–solid phase transformation (12). Boerrigter et al. encountered this process in their investigations on their research of epitaxial polymorphic growth of a model steroid compound and showed that a tiny amount of acetone present in the system catalyzed recrystallization of the metastable phase. To emphasize that the molecules involved must pass through a temporary state of dissolution rather than a melt they redubbed the term to be more specifically a solid–solute–solid phase transition (13). In short, the mechanism is explained as a molecular level layer of solution that traverses through the crystal. Keeping this in mind, when a certain crystalline form undergoes a phase transition after a solvent is introduced that does not necessarily mean that a solvatomorph was formed. It is equally possible that a metastable form recrystallized into a more stable solvent-free form.

Hydrates represent a special case of solvatomorphs because water raises no issues regarding toxicity and is usually of no concern in the approval of drug products. On the other hand, water is the only solvent that is present in ambient conditions, and its uptake and possible equilibria between hydrate forms represents a concern for processing, packaging, and storage. For practical purposes it is therefore important to determine the relative stabilities of solvatomorphs. Relative stability studies for solvatomorphic systems are no different than those for anhydrous polymorphic systems, except that the activity of the solvent must be taken into account.

By far the most instructive information about the relative stability of polymorphs and solvatomorphs can be gathered from a *G–T* diagram (free energy vs. temperature). Figure 4 shows such a diagram taken from a recently published paper in which Griesser and coworkers diligently analyzed the behavior of three polymorphs of (*R*)-cinacalcet hydrochloride using a plethora of analytical techniques (14). *G–T* cannot, of course, be measured directly, and it must be determined from data gathered from various experiments, typically a combination of differential scanning caliometry (DSC) and hot-stage microscopy that identify the thermal energy exchange during phase transitions. Because the solid forms cannot be forced to interconvert between all phases at any given temperature actual data can only be measured on a limited number of events. The thick arrows represent actual data of temperature and enthalpy exchange, whereas the curves were later deducted from

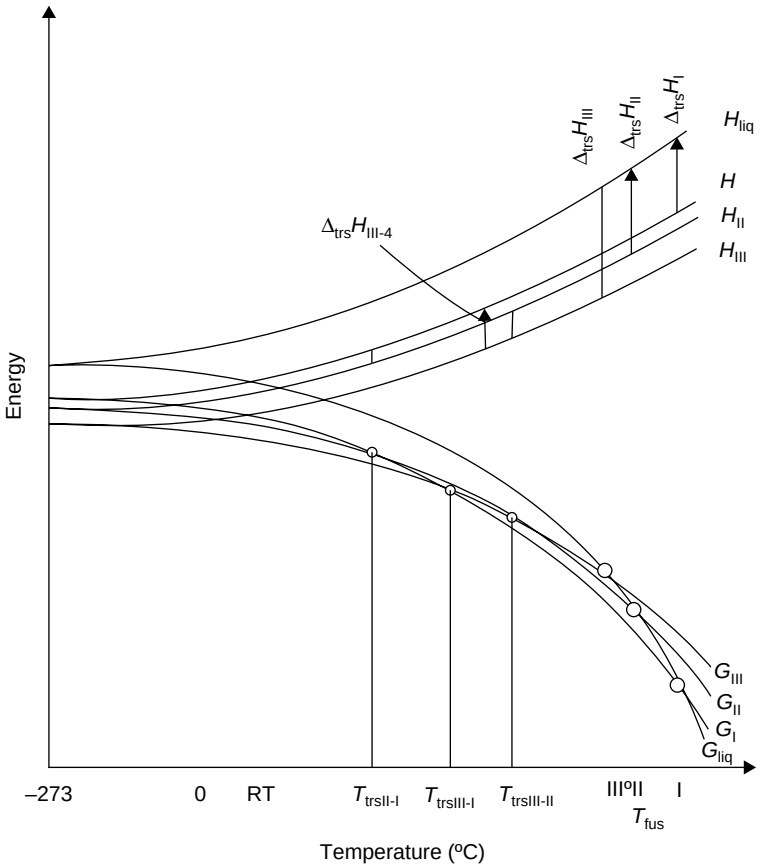

FIGURE 4 Semi-schematic energy/temperature diagram of the crystal forms of (*R*)-cinacalcet hydrochloride polymorphs, where the bold vertical arrows mark the measured enthalpies. In the figure, T_{fus} is the melting point, *G* is the Gibbs free energy, *H* is the enthalpy, $\Delta_{fus}H$ is the enthalpy of fusion, T_{trs} is the transition point, $\Delta_{trs}H$ is the transition enthalpy, and liq is the liquid phase (melt). The figure has been adapted from Ref. (14).

the interpretation of the other data presented in the work. In the figure, one sees the *H*–*T* curves, which go up with increasing temperature. On this scale they appear to go up in parallel, but in reality they tend to diverge slightly, causing the difference in enthalpy between the curves to increase slightly with increasing temperatures. On the lower side of the *G*–*T* diagram one sees the Gibbs free energy of the polymorphs. These curves necessarily have a negative slope, because $(\partial G/\partial T)_p = -S$, and entropy is always positive. The form that has the lower Gibbs free energy at a given temperature is the more stable form at that temperature, and thus it is immediately obvious which form is the most stable for any given temperature from this type of diagram. Very important is the Gibbs free energy curve of the liquid. The temperature where a polymorph curve crosses the liquid curve represents a melting temperature.

Because of the differences between polymorphs in how their entropies increase with temperature, the Gibbs free energy curves may cross. The temperature at which a pair of curves crosses is called the transition temperature. To avoid the confusion that typically arises from the various types of nomenclatures of the polymorphs (typically using Greek letters or Roman numerals), the form that is more stable below the transition temperature is often referred to as the low-temperature form and the other form as the high-temperature form. In this example we can see that Form-III is the low-temperature form, stable up to 148.5°C, whereas Form-I is the most stable from 148.5°C to its melting point at 179.5°C. Even though the Form-II curve crosses both that of Forms I and III, it is never the lowest, so Form-II is metastable at any given temperature.

When materials crystallize from aqueous solution, they are effectively exposed to unit activity. If the phase is anhydrous (assuming no specific interaction between the molecule and the water), when the phase is removed from the solvent it is usually stable at that temperature, because the free energy of the phase is independent of the solvent of origin. If the phase is hydrated, when it is removed from the solvent the RH it is exposed to necessarily drops significantly. Once removed from the water, the activity of water needed to maintain the form (the critical activity) can be determined by several methods. These may include water vapor sorption analysis and Karl Fischer titrimetry (11). Alternatively, the critical activity can be assessed by crystallizing the material at different water activities by using mixtures of solvents, such as from various aqueous alcohol systems (15,16). The percentage water in solution is directly related to the RH, as will become obvious in the following discussion.

For ideal solutions the change in Gibbs free energy ($\Delta G = \Delta H_f - T\Delta S_f$) is related to the solubility, x, by $\Delta G = -RT \ln x$. These two relations can easily be combined into

$$\ln x = \frac{\Delta H_f}{R}\frac{1}{T} + \frac{\Delta S_f}{R} \tag{4}$$

where ΔS_f and ΔH_f are the entropy and enthalpy of fusion at the melting point, respectively, and R is the gas constant. For each phase, $\ln x$ can be plotted against $1/T$, which should yield a straight line with a slope equal to $-\Delta H_f/R$ and an intercept of $\Delta S_f/R$. In this so-called Van't Hoff plot, the equilibrium temperature of different phases is found at the intersection of their lines. Non-ideal dissolution behavior is observed as a curvature in these otherwise straight lines. In addition, this relation assumes that the enthalpy of solution is equal to the enthalpy of melting at the melting point. A more general expression may be derived, but the reciprocal dependence of solubility and temperature is preserved. Just as with a G–T plot, the intersection of curves generated for two different crystalline phases represents a point of equal free energy and a transition temperature.

When substituted in equation (3) the identical role of water activity as that of solubility becomes immediately obvious from Raoult's law:

$$x = p/p_0 \tag{5}$$

Again, water is unique in that ambient conditions provide a counter-pressure to the loss of water in a hydrated crystal form. For any other solvated crystal, the ambient vapor pressure is zero, which stresses the material to a maximum. This stability issue demonstrates another grave concern against using solvates in drug formulations.

ORGANIC MOLECULE SOLVATES

As discussed above, a wide variety of organic solvents are able to co-crystallize with compounds having pharmaceutical interest, and for reasons discussed earlier, these solvatomorphs should not necessarily be excluded from consideration as viable crystal forms during development. Generally, the role of a solvent molecule is to lend stability to a crystal lattice, primarily by fostering stronger interactions between molecules or between planes of molecules. This can be accomplished in two primary ways: one where the solvent molecules occupy isolated positions in the crystal structure, and the other where the lattice positions group the solvent molecules along channels in the structure.

Discrete Position Solvates

During the course of a polymorph screening study conducted on the fumarate salt of formoterol:

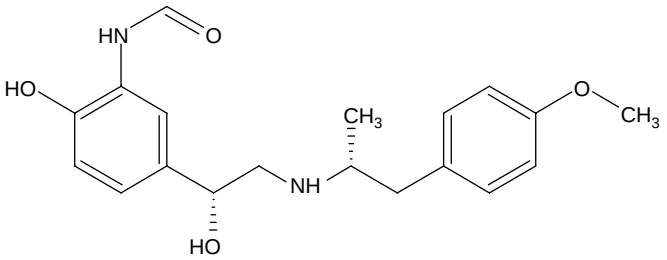

the drug substance was crystallized from 12 solvents (17). In addition to three non-solvated forms and a dihydrate, crystalline disolvates were obtained from ethanol, isopropanol, and benzyl alcohol. The ethanol and isopropanol disolvates were found to be isostructural, where the formoterol cations and fumarate anions hydrogen bond into sheets and the methoxy-substituted benzene rings pack into hydrophobic layers between the molecular sheets. The solvent molecules reside in the hydrophobic layers, but do interact with the fumarate anions via their hydroxyl groups.

Studies on crystalline forms of paracetamol (acetaminophen):

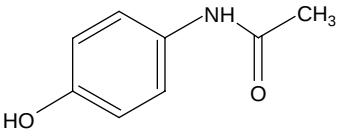

are ordinarily concerned with the non-solvated monoclinic and orthorhombic polymorphic forms, but the compound has also been shown to form solvatomorphs and co-crystals with hydrogen-bond acceptor molecules (18). In this work, structures of the 1,4-dioxane, dimethylpiperazine, *N*-methylmorpholine, piperazine, 4,4′-bipyridine, and morpholine adducts have been reported. In the monoclinic dioxane structure, the chains of paracetamol molecules are sinusoidal in nature, where the –NH groups form hydrogen bonds with the oxygen atoms of the solvent molecules. Because the dioxane

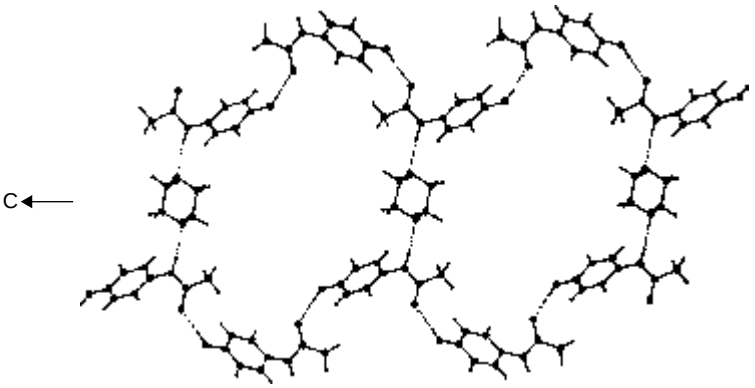

FIGURE 5 Molecular interactions in the 1,4-dioxane solvatomorph with paracetamol, viewed perpendicular to the (210) plane and along the *c*-axis. The figure has been adapted from Ref. (18).

molecules reside on inversion centers, two-dimensional molecular sheets are assembled where chains of paracetamol are linked by dioxane bridges. This type of structure is illustrated in Figure 5. The dioxane solvatomorph has itself shown to exhibit polymorphism, as a high-temperature orthorhombic form has also been reported (19).

Without a doubt, sulfathiazole:

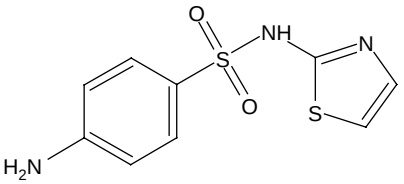

holds the record for forming the largest number of solvatomorphs, with the existence of over 100 solvates being known (20). The structure of the tetragonal 1:1 adduct between sulfathiazole and pyridine has been reported; however, with the solid being crystallized from an *n*-propanol/pyridine solution (21). The solvatomorph was found to be stable only in pyridine vapor, and decomposed into sulfathiazole Form-I under ambient conditions. The structure of a disappearing solvatomorph was reported in a separate study, where the described monoclinic 1:1 adduct with pyridine could no longer be obtained after the tetragonal polymorph had been previously crystallized (22).

The thiazide diuretic compound hydrochlorothiazide:

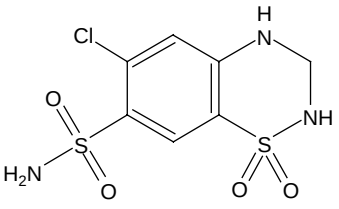

has been found to exhibit a rich solvatomorphic landscape, and the structures of the 1:1 solvates with aniline (23), methyl acetate (24), 1,4-dioxane (25), *N*,*N*-dimethylformamide (26), and dimethyl sulfoxide (27) having been reported. The structures of the 1:2 solvates with *N*,*N*-dimethylacetamide (28) and *N*-methyl-2-pyrrolidone (29) have been reported as well. The hydrochlorothiazide compound was found to be capable of existing in a variety of conformational states in the different structures, with the solvent molecules playing key roles in determining the particular conformation adopted in a given solvatomorph structure.

Carbamazepine:

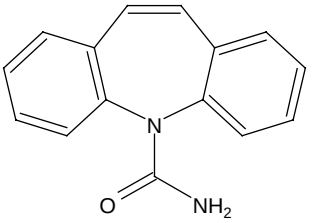

is known to crystallize in four polymorphic forms and in number of co-crystal structures, and the structures of the 1:1 solvate with 2,2,2-trifluoroethanol (30), *N*,*N*-dimethylformamide (31), and trifluoroacetic acid (32) have been reported, as well as the structure of the hemisolvate with furfural (33). In these structures, the carbamazepine molecules form the same centrosymmetric hydrogen-bonded $R_2^2(8)$ dimer motif that exists is all of the polymorphs, and the solvent molecules serve to link the dimers through hydrogen-bond bridges.

Channel-Type Solvates

Besides structures where the solvent molecules are effectively isolated from each other and bridge individual molecules or sheets of molecules, other structural types exist where the solvent molecules included in the lattice are located in proximity to other solvent molecules in adjoining unit cells along an axis of the lattice. This structural feature can be envisioned as being that of a solvent channel that exists through the crystal, and hence, this type of solvatomorph will be identified as a channel-type solvate. For example, in the tetrahydrofuran, *tert*-butanol, toluene, and *p*-xylene solvatomorphs of *N*,*N*′-dithiobisphthalimide, the highly disordered solvent molecules lie within continuous channels created by sequences of π···π stacking interactions and very weak C–H···O hydrogen bonds (34).

The crystal structures of the 2:1 solvates of phenylbutazone:

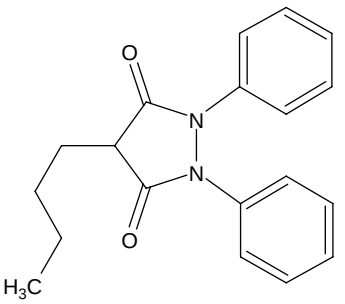

with benzene, cyclohexane, 1,4-dioxane, tetrahydrofuran, tetrachloromethane, and chloroform have been published, where it was found that almost all of the solvatomorphs were isostructural (35). In these structures, the solvent molecules were located in channels that ran along the (010) direction that was formed by the molecular framework of the phenylbutazone molecules. It was also found that the free volume available to the solvent molecules in the channels was related to their geometry in addition to the strength of the drug–solvent interactions.

The crystal structures of several solvates of erythromycin A:

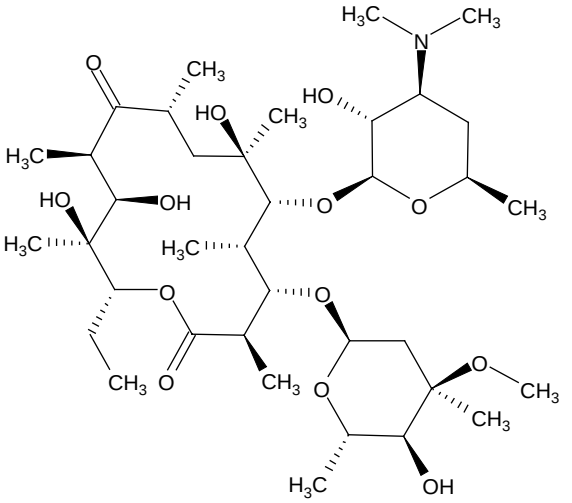

have been reported, and the hydrogen-bonding patterns and packing motifs of the included solvent molecules in these solvatomorphs discussed in detail (36). Although the solvent molecules in the tetrahydrofuran, dioxane, and isopropanol solvates resided in channels in the structure, the solvent molecules in the methanol solvatomorph (whose structure was found to be isomorphic with that of clarithromycin) resided in discrete pockets that were not connected to form a continuous solvent space. As illustrated in Figure 6, the weak fluorescence of the methanol solvatomorph of erythromycin A was found to undergo a drastic reduction in intensity when the substance was subjected to thermal dehydration (37).

Triamcinolone diacetate:

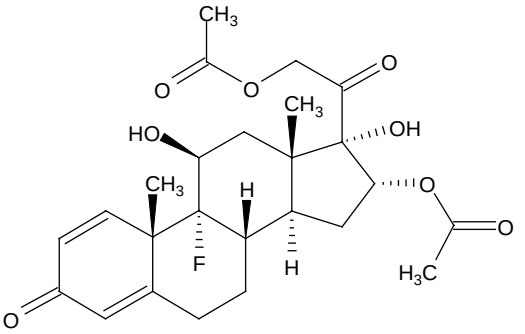

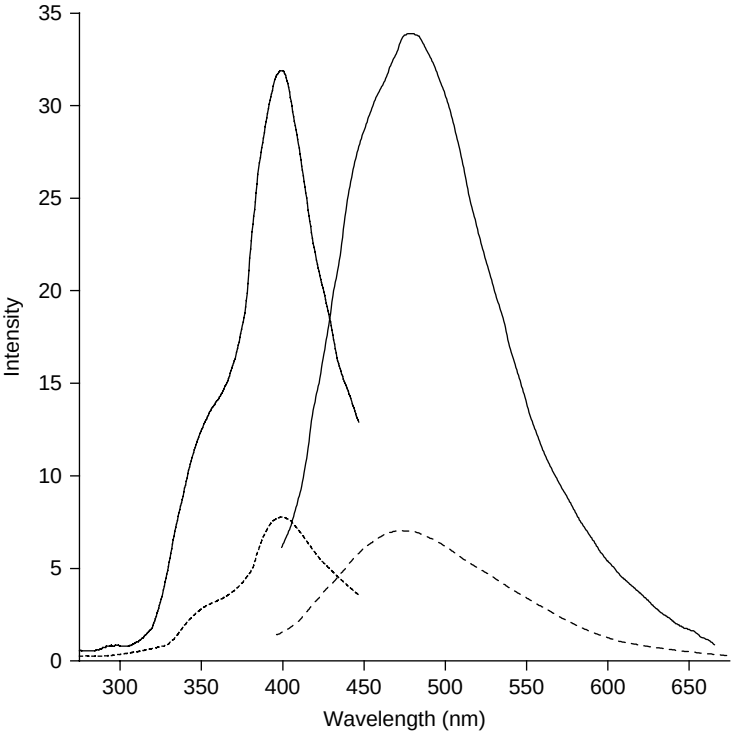

FIGURE 6 Excitation (*fine traces*) and emission (*heavy traces*) spectra obtained for the methanol solvatomorph of erythromycin A (*solid traces*), and its thermally dehydrated product (*dashed traces*) (H.G. Brittain, unpublished results).

was found to crystallize in an orthorhombic structure that contained channels along the crystallographic *a*-axis in which a number of different solvent molecules could be included in a 1:1 molecule–solvent ratio (38). Essentially, isostructural solvatomorphs were obtained from ethanol, 1-propanol, 2-propanol, 1-butanol, 2-butanol, acetone, 2-butanone, and methyl acetate. On the other hand, triamcinolone acetonide:

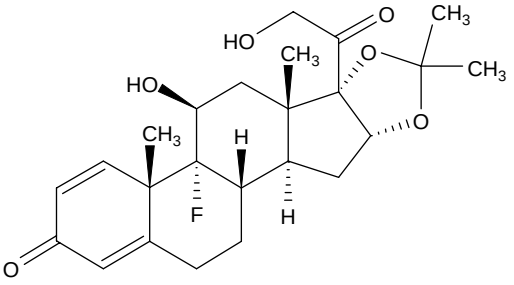

was found to form a solvatomorph where the unit cell contained two methanol molecules and three drug substance molecules (39). In this structure, the solvent molecules were located in channels formed along the crystallographic *c*-axis.

HYDRATES

As discussed above, water is known to form a large number of solvatomorphs that have pharmaceutical significance, and the lack of toxicity issues associated with hydrates makes them the most appropriate type of solvatomorphic solid, if one is going to be used. Water is characterized by an abundant range of hydrogen-bonding possibilities, and because it is characterized by a small size that enables it to fill structural, a considerable number of pharmaceutical compounds have been investigated for their tendency to form hydrate structures. In addition, the crystallization of a hydrate during the course of a complicated synthetic route can sometimes offer advantages not possible in a purely non-aqueous environment (40).

One way to classify crystalline hydrates is on the basis of their energetics (41). In this view, one looks at the strength of the hydrogen bonds that the water molecules have formed in the crystal structure. Hydrogen bonds span a wide variety of interaction energies that can range from being extremely weak, all the way to being extremely strong. Much debate can be made as to when to call a hydrogen bond a hydrogen bond, but the fact is that the strength of hydrogen bonds is a sliding scale, and everything strongly depends on other features of a crystal structure to determine whether a hydrogen bond is a significant contribution to the crystallographic arrangement. The only objective way to proceed is to calculate the energies of interaction using some reasonable level quality method (such as density functional theory), but oftentimes empirical methods can perform better.

Closely related to the interaction energy view is the role of the water molecules in the solid-state chemistry of the crystal. Hence, one may advance a rudimentary classification of crystalline hydrates, where the water of crystallinity is either stoichiometric (i.e., having a well-defined water content and a different crystal structure than the anhydrous drug or other hydrates) or non-stoichiometric (i.e., having continuously variable composition within a certain range that is not associated with any significant corresponding change in the crystal structure, except for some anisotropic expansion of the crystalline network to accommodate the additional water molecules) (5). The entropic state of the water molecules in the solid, as observed in a single-crystal structure determination, can often indicate their behavior. When no clear hydrogen bonding is present in the crystal, the molecules will usually appear to be disordered and/or non-stoichiometric.

A more important supramolecular aspect is the motifs of hydrogen bonding that the water molecules form. When observing crystal structures it can readily be seen that water molecules can have very different roles in this respect, which can therefore greatly influence the stability of the three-dimensional crystal. At one end of the spectrum, water can play a minor role where it appears to merely decorate the structure by clinging onto the three-dimensional arrangement of the host molecules. In many other cases, however, the multiple hydrogen-bonding capability of water can cause it to act as a bridge between the host molecules in a host–water–host type of arrangement. In those cases the water is typically found to be stoichiometric and rigidly incorporated in the structure. All sorts of higher order motifs can be found where multiple water molecules cooperate to form a stable link between the host molecules (host–water–water–host, and so on).

It is clear that these types of supramolecular arrangements strongly define the stability of the crystal structure. The three-dimensional structure of these cooperative systems can be quite complex, and can really only be fully appreciated by studying them on a computer workstation. However, a mistake often made is to qualify crystal structures by looking only at the hydrogen-bonding motifs. Because of their cooperative nature and larger numbers, Van der Waals contacts typically account for the majority of the lattice energy for less polar molecules, and Coulomb interaction for more polar molecules. The relative contributions can again only be objectively studied by performing proper calculations, and visualization of a crystal graph can be extremely helpful in these matters.

Perhaps a more practical classification is that of stability. As discussed in previous sections, both temperature and RH determine the stability of crystalline hydrates. These concerns will usually be of primary importance when drug products are developed for eventual commercialization.

Although having limitations, a highly successful classification scheme is that proposed by Morris and Rodríguez-Hornedo (6). In this approach, the following three categories of crystalline hydrates are recognized:

- Isolated site hydrates: The structure where water molecules are isolated from direct contact with other water molecules by intervening drug molecules.
- Channel hydrates: The water molecules included in the lattice lie next to other water molecules of adjoining unit cells along an axis of the lattice, forming "channels" through the crystal.
- Metal ion-associated hydrates: The water molecules are bound directly to a metal ion, either as part of a coordination complex in the case of transition metal ions, or through strong ionic bonds as in the case of alkali metal and alkaline earth ions.

Isolated Site Hydrates

These hydrate species represent the structures with water molecules isolated from direct contact with other water molecules by intervening drug molecules. To illustrate some of the characteristics of this hydrate class, consider the dihydrate of cephradine:

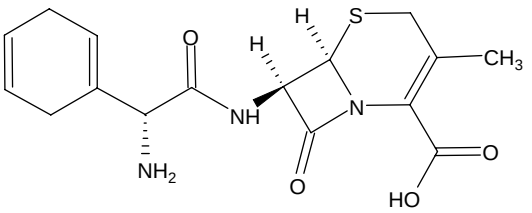

Determination of the crystal structure of cephradine dihydrate was of particular importance because when the compound is dehydrated, it becomes amorphous and very unstable (42). Figure 7 shows the molecular connectivity diagram of cephradine dihydrate, where it may be observed that each unit cell contains two molecules of cephradine and four molecules of water. The two water molecules hydrogen bond with each other, and with the carbonyl, carboxyl, and amide groups on the

two cephradine molecules. No axis can be drawn between separate water pairs without passing through an intervening portion of the cephradine molecule. This means that a pair of water molecules on the surface may be easily lost, but the creation of the hole does not leave other water molecules accessible.

As an isolated site hydrate type of structure, the thermal analysis of cephradine dihydrate should be characterized by a sharp differential scanning calorimetry endotherm and a narrow thermogravimetric weight loss range. This is demonstrated in Figure 8, where the DSC thermogram shows two incompletely resolved, but sharp, endotherms around 100°C, and the TG thermogram shows the anticipated sharp weight loss over a similar range. In addition, the onset of dehydration observed in the DSC thermogram is quite sharp.

Olanzapine:

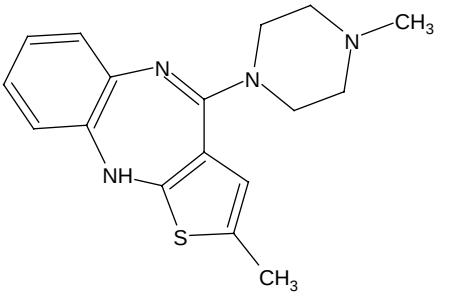

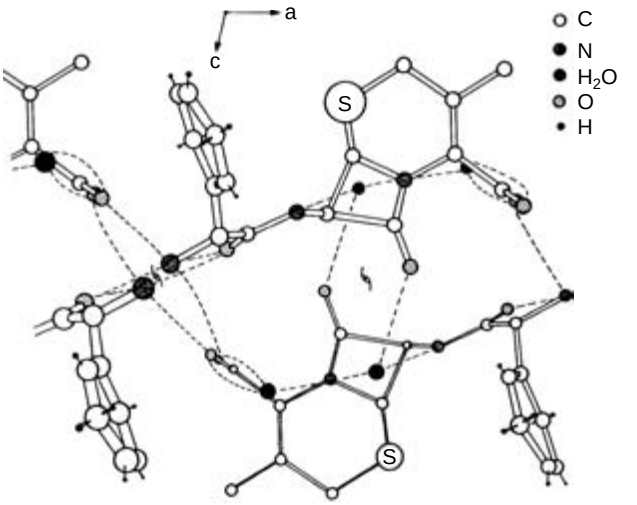

FIGURE 7 Distribution of the water molecules in the cephradine dihydrate structure, where the pairs of water molecules are seen to reside in isolated lattice sites. The figure has been adapted from Ref. (42).

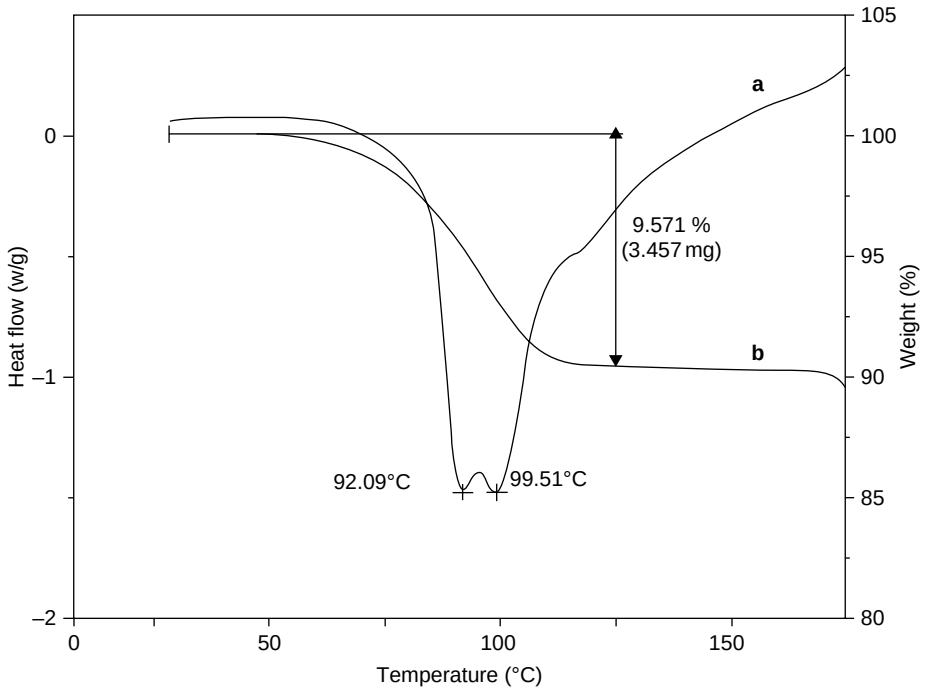

FIGURE 8 (**a**) Differential scanning calorimetry and (**b**) thermogravimetric analysis thermograms obtained for cephradine dihydrate.

has been found to crystallize in more than 25 crystal forms, among which are three polymorphic dihydrates that are pharmaceutically relevant, and whose structures have been reported (43). The basic crystal building block was a centrosymmetric dimer of olanzapine molecules, stabilized by the complementary surfaces of the most stable conformational enantiomers. In all of the hydrate structures, the water molecules were held by two or three hydrogen-bonding interactions, with the main difference in the structures being the relative orientation of adjacent two-dimensional layers of olanzapine molecules.

The 5-HT_3 receptor antagonist cilansetron hydrochloride:

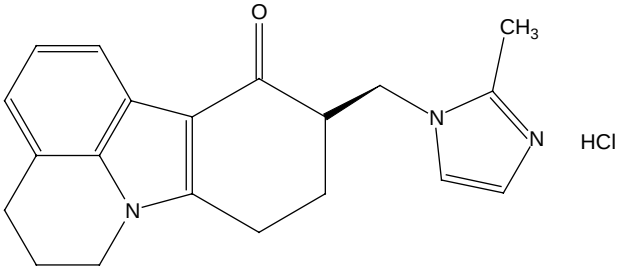

have been reported to crystallize in two polymorphic monohydrate solvatomorphs: one crystallizing in a monoclinic space group (44), and the other in an orthorhombic (45) modification. Both structures feature helical chains of alternating water and chloride ions, with these running parallel to the crystallographic *b*-axis in the monoclinic structure and attached laterally to the drug molecules through a network of N–H···Cl contact interactions. In the orthorhombic structure, the helices run parallel to the crystallographic *a*-axis, but these are now connected to the drug molecules by means of N–H···O_{water} contacts. As one might suspect, these structural similarities give rise to similar X-ray powder diffraction patterns for the two monohydrate crystal forms, but as illustrated in Figure 9, the differences in powder patterns confirms the polymorphic nature of the two forms.

Channel Hydrates

Hydrates in this class contain water in channels that form wormholes through the structure, where the water molecules included lie next to other water molecules of adjoining unit cells along an axis of the lattice. When channels empty upon dehydration of the crystals, the crystals are expected to relax some of the stress related to the resulting low-density structure by some changes in the lattice parameters.

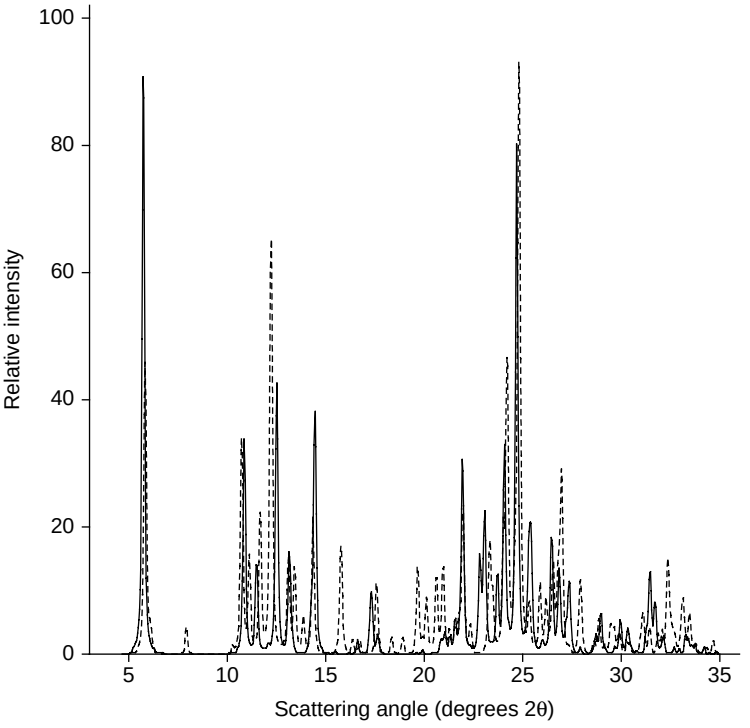

FIGURE 9 X-ray powder diffraction pattern of the monoclinic (44) form of cilansetron hydrochloride monohydrate (*solid trace*) and of the orthorhombic (45) form (dashed trace). The patterns were generated from data contained in the Cambridge Structural Database (version 5.29) using the CSD program Mercury (version 2.0).

The channel water in ampicillin trihydrate:

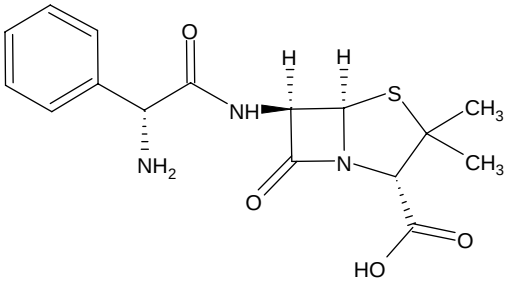

exhibits characteristics of this class, and whose structure has been detailed in the literature (46). The packing diagram of ampicillin trihydrate is shown in Figure 10, which contains four unit cells. The water molecules can be seen to line up with the screw axis along the crystallographic *c*-axis, where a channel having a diameter of 3.5 Å would be formed if the water molecules were to be removed without changing the structure. The water molecules are hydrogen bonded to four (or more)

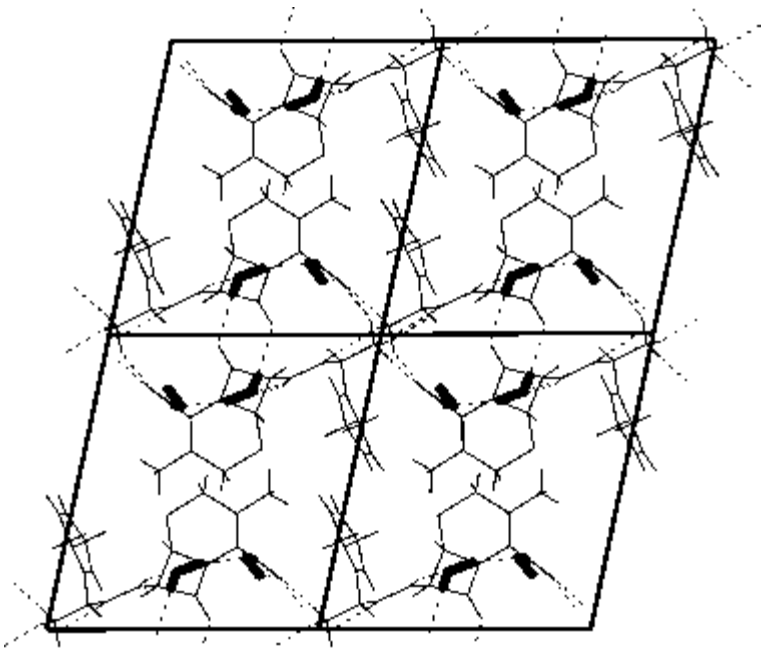

FIGURE 10 Packing diagram for ampicillin trihydrate deduced from the single-crystal structural data. The van der Waals radii are included for the water hydrogens and oxygen, and the "channels" are along the screw axes.

other water molecules and at least two ampicillin molecules through the carboxylate ion, the carbonyl on the β-lactam, the amino group, or through the ammonium group.

Results of thermal analysis performed on ampicillin trihydrate demonstrate some of the interesting characteristics of channel hydrate dehydration. As shown in Figure 11, the water contained in the channels ampicillin trihydrate begins to evolve at a much lower temperature than the water contained in the isolated lattice sites of cephradine dihydrate. Ampicillin trihydrate is found to lose water continuously at temperatures up to 125°C, whereas the dehydration endotherms of cephradine dihydrate (Fig. 8) are very narrow. Interestingly, the dehydration temperature of ampicillin trihydrate is higher than that of cephradine dihydrate, which can be understood using a stepwise model. Dehydration begins at the surface of the crystal, and continues toward the center along the channels. As the temperature increases, so does the probability of losing the first water molecules on the surface at the channel ends. The loss of these water molecules leaves a channel for the next and sets up a thermodynamic gradient in the same direction. The drug molecules need not reorganize to lose many water molecules from the crystal. This phenomenon has been observed visually, with Byrn and coworkers observing that crystals were heated on a microscope hot stage, and the dehydration appeared as a progressive darkening (increasing opacity) from the surface of the crystal that traveled toward the center along the crystallographic *c*-axis (47).

The anhydrate and monohydrate phases of mometasone furoate:

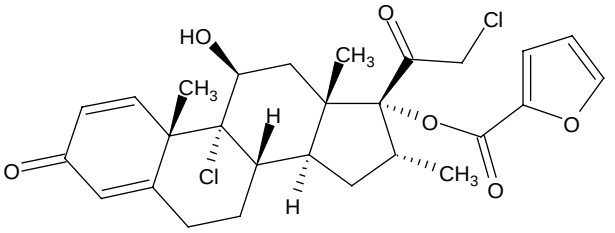

were found to exhibit distinctly different modes of crystal packing even though the constituent molecules exhibited similar conformations (48). The anhydrate was found to crystallize in an orthorhombic space group, with the drug substance molecules being packed tightly in the form of interlocked molecules. The monohydrate form crystallized in a triclinic space group, where the water molecules formed channels along the *a*-axis and the mometasone furoate molecules packed in layers along the same direction. When heated above 90°C, the monohydrate could be dehydrated to yield a metastable anhydrous form, which could then be transformed to the known anhydrate when heated above 150°C. The metastable anhydrate could also be converted to the monohydrate form after short exposure to an RH of 45%.

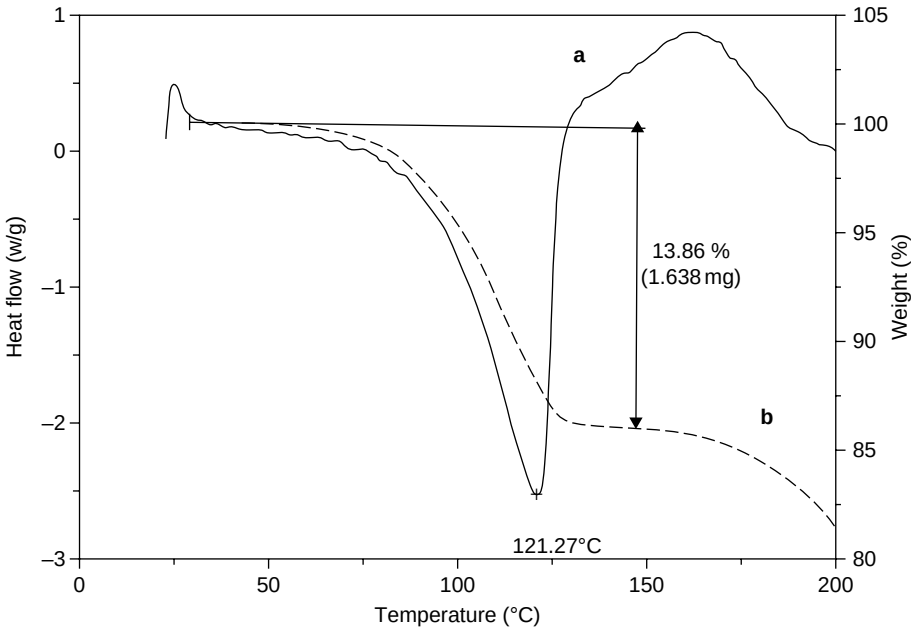

FIGURE 11 (**a**) Differential scanning calorimetry and (**b**) thermogravimetric analysis thermograms for ampicillin trihydrate.

When samples of topetecan hydrochloride:

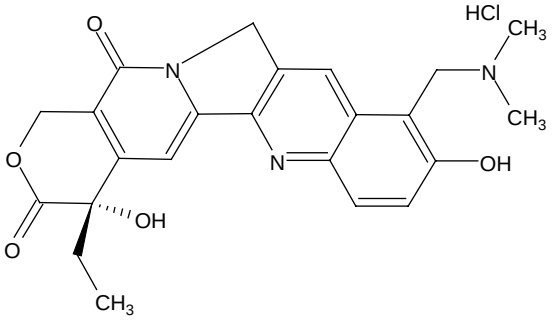

were equilibrated under a series of different RH conditions, it was found that the substance formed a trihydrate solvatomorph that could adsorb an additional two equivalents of water without forming a pentahydrate phase (49). X-ray diffraction studies were used to demonstrate that although the crystal structure of the trihydrate was broken by its dehydration, adsorption into or removal of the additional two equivalents of water from this form did not lead to changes in the crystal structure. Performance of a series of solid-state NMR studies enabled the deduction that although the water molecules of the trihydrate were intrinsic parts of the crystal

lattice, the trihydrate possessed additional structural channels where water could hydrogen bond to specific portions of the topotecan molecules.

Another characteristic of some channel hydrates structures is that the solids may reversibly gain or lose significant quantities of water in the channels as a result of equilibrium with various RH conditions. These hydration or dehydration reactions do not cause alterations in the overall crystal structure, but are instead accompanied by expansions or contraction in the crystal lattice that change the dimensions of the unit cell. Such effects were shown qualitatively for the disodium salt of cromolyn:

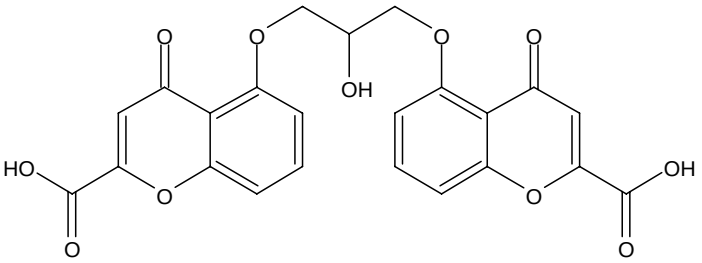

where it was found that as crystals absorbed additional moisture, the lattice expanded to accommodate the additional water (50). It was proposed that increases in hydration caused the crystal expand to the limit of the structure to sustain such change.

Grant and coworkers determined the single-crystal structure of cromolyn disodium containing 6.44 water molecules per cromoglycate anion (51), which was found to correspond to the previously studied structure. As shown in Figure 12, the structure contained large sodium ion and water channels that ran parallel to the crystallographic *a*-axis and perpendicular to the plane of cromoglycate anions, and which occupied approximately 50% of the unit cell volume. It was noted that the existence of these large channels in the structure facilitated easy passage of water molecules with a minimal energy expenditure and disruption to the packing arrangements. Interestingly, the structure could not be solved for crystals equilibrated at relative humidities of 0%, 11.4%, and 21.6%, indicating that a certain minimum amount of water was required to sustain the crystal structure.

Channel hydrate structures featuring channels that extend along the full width of the crystal are often termed planar hydrates. The structures of the dihydrate forms of the sodium salt of racemic and enantiomerically resolved ibuprofen:

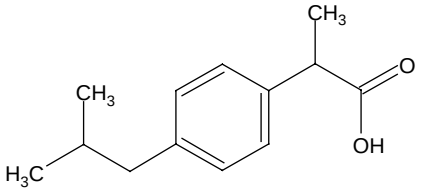

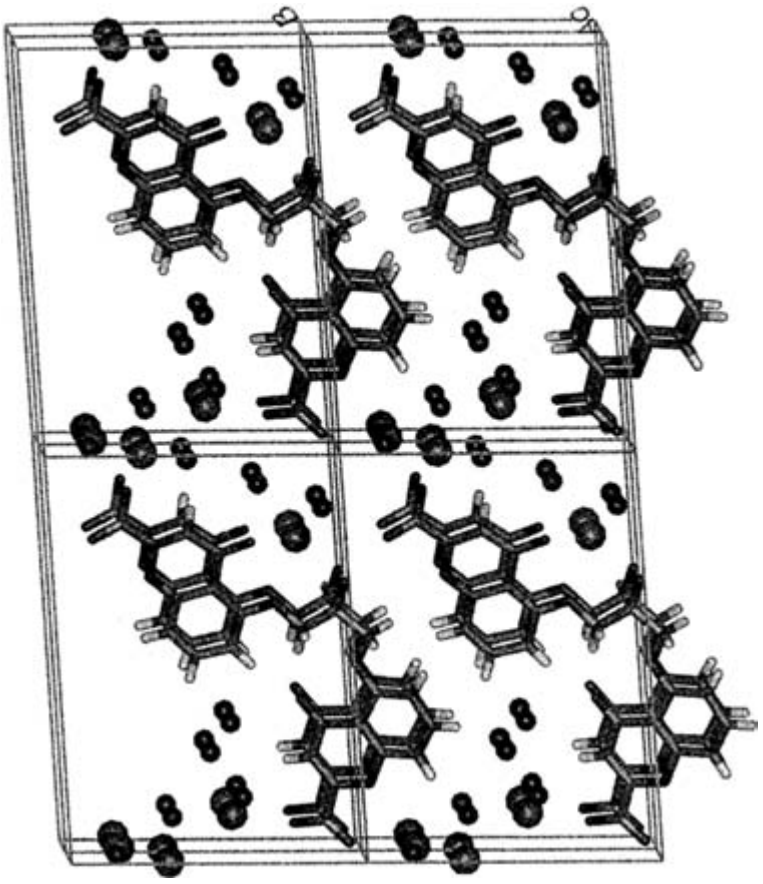

FIGURE 12 Crystal packing diagram of cromolyn disodium, viewed down the crystallographic *a*-axis. The small balls represent the oxygen atoms of the water molecules and the large balls represent the sodium ions in the channels. The figure has been adapted from Ref. (51).

have been found to bear a strong degree of similarity to each other, with the dominance of interaction between oxygen atoms and the sodium cations overcoming the fact that one structure is heterochiral and the other homochiral (52). Figure 13 shows the packing diagram for sodium ibuprofen, where the waters of hydration are seen to be associated with the sodium ions localized in the *a*–*c* plane of the lattice.

It is worth noting that not all hydrates associated with a given drug substance will necessarily be characterized by the same type of hydrate structure. For example, the existence of four hydration states (an anhydrate, a monohydrate,

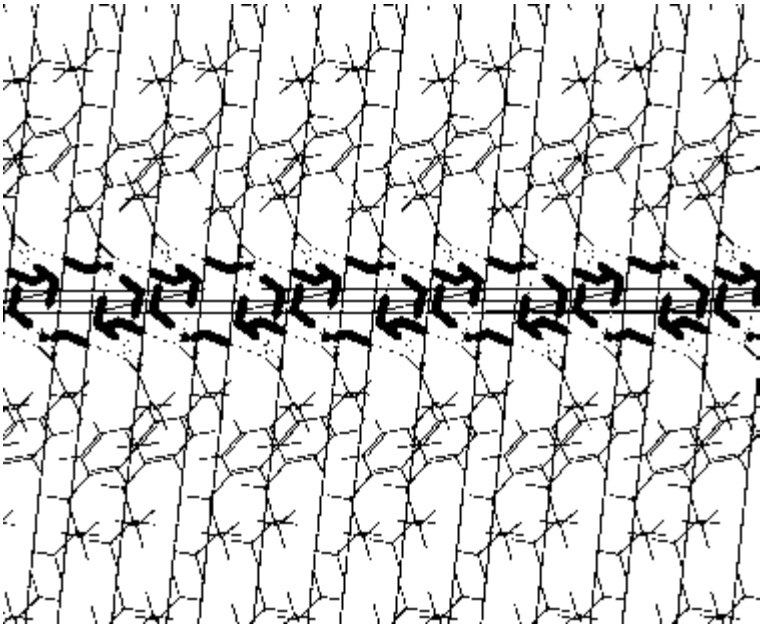

FIGURE 13 Packing diagram for sodium ibuprofen, with waters of hydration and sodium ions being shown as van der Waals spheres. The figure is unpublished, and courtesy of Jack Z. Gougoutas.

a hemi-pentahydrate, and a variable hydrate containing four to six waters) have been reported for the sodium salt of risedronate (53):

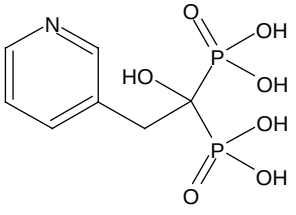

Although the variable hydrate form exclusively contained channel water, the hemi-pentahydrate form appeared to contain both lattice and channel water. In contrast, the monohydrate was determined to contain lattice water that could only be lost at high temperatures.

Metal Ion-Associated Hydrates

Hydrate structures of this type contain water molecules that are directly coordinated to a metal ion. The resulting interactions between a metal cation and the lone-pair electrons of the oxygen atoms of the bound water molecules are so strong

that they to dominate the experimental characteristics of the material. For example, dehydration of these bound water molecules typically takes place only at very high temperatures (54).

Nedocromil:

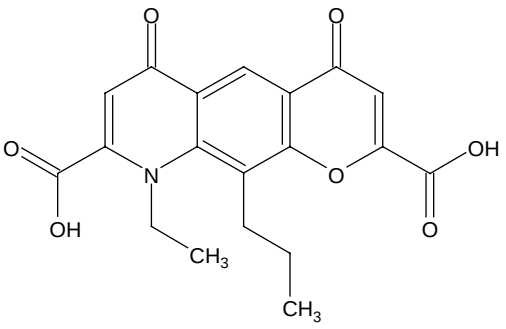

has been found to form complexes with a number of bivalent metal ions, and the crystal structures of the hydrated salts with magnesium (55), zinc (56), calcium (57), and nickel (58) have been reported. As illustrated in Figure 14 for the instance of the zinc salt, the six directed valences of the metal ion are satisfied by the coordination

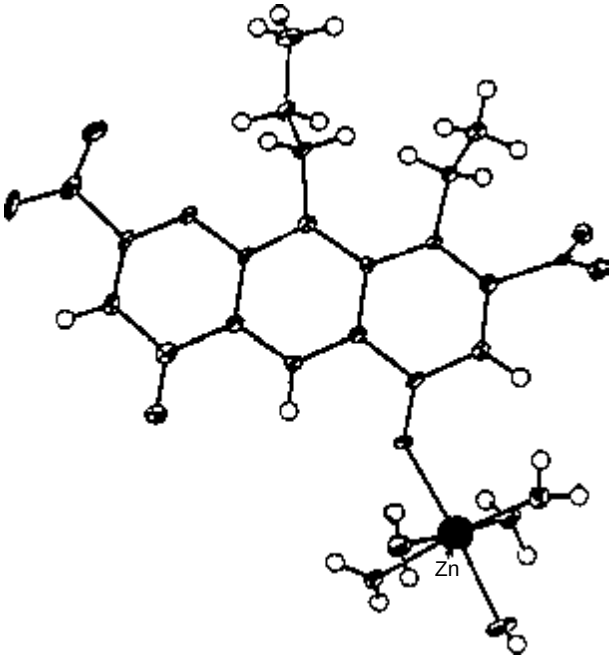

FIGURE 14 Molecular structure of nedocromil zinc heptahydrate, showing only the water molecules bound in the inner coordination sphere of the Ni(II) ion. The figure has been adapted from Ref. (56).

of five water molecules and one ionic linkage to the nedocromil molecule. Additional water molecules, not bound to the metal ion, can be present in the structure (and would be for the instance of nedocromil zinc heptahydrate), but the ion-associated water is seen to constitute the inner coordination sphere of the metal ion.

The calcium salt of [10-(2-hydroxypropyl)-1,4, 7,10-tetraazacyc1ododecane-1,4,7-triacetato]calciate:

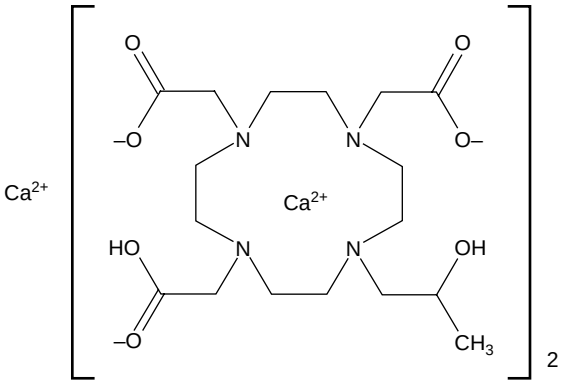

is also known as calteridol calcium, and is used as a stabilization aid in the formulation of the Gd(III) imaging agent, ProHance®. The compound has been obtained in a tetra-decahydrate and in a tetra-dihydrate form, both of which crystallize in the $C2/c$, space group, but which are characterized by significantly different unit cell dimensions. Molecular packing diagrams are shown in Figure 15 for the two hydrates of calteridol calcium.

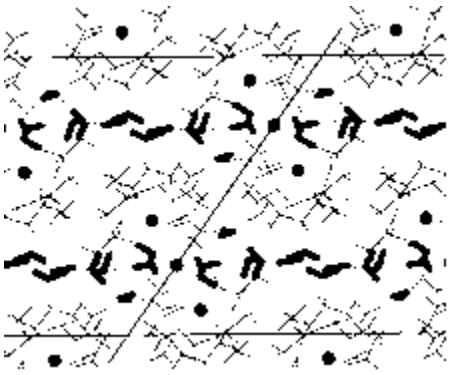

Calteridol calcium,
tetra-decahydrate crystal form

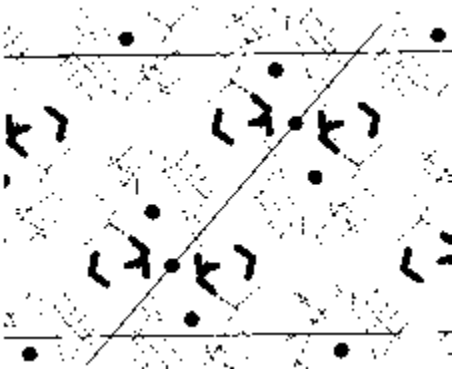

Calteridol calcium,
tetra-dihydrate crystal form

FIGURE 15 Packing diagrams derived from single-crystal data results obtained for the two hydrates of calteridol calcium, the tetra-decahydrate and the tetra-dihydrate (obtained after six-hour dehydration at room temperature).

For the tetra-decahydrate form, there are four water molecules associated with each central calcium ion, and 10 lattice water molecules located in each channel that run perpendicular to the plane of the figure (the crystallographic *b*-axis). One would anticipate that the channel water would be lost more easily than would be the water associated with the cation. One reason for this is that the energy of association of water with calcium through the lone pair electrons on oxygen is greater than that of hydrogen bonding in water, and the other reason is that the loss of water in channels occurs more easily than would be expected by its interaction energy alone. Also shown in Figure 15 is the structure of the crystal after dehydration at room temperature has been conducted for six hours. Most of the channel water (eight molecules per unit cell) has been lost, leaving the four calcium-associated water molecules and two water molecules in the secondary sphere of hydration of the calcium.

Figure 16 contains the thermal analysis results obtained for the initial tetra-decahydrate solvatomorph. The DSC thermogram exhibits a large broad endotherm beginning at ambient temperature and peaking at approximately 75°C, which is associated with a weight loss of 13.56% (based on dry weight) or eight moles of water per mole of calteridol (the theoretical water content is calculated to be 13.96%). Further heating leads to the observation of a smaller endotherm and a weight loss corresponding to two moles of water. As the heating continues, a sharper endotherm is seen at approximately 179°C, and a weight loss corresponding to the four

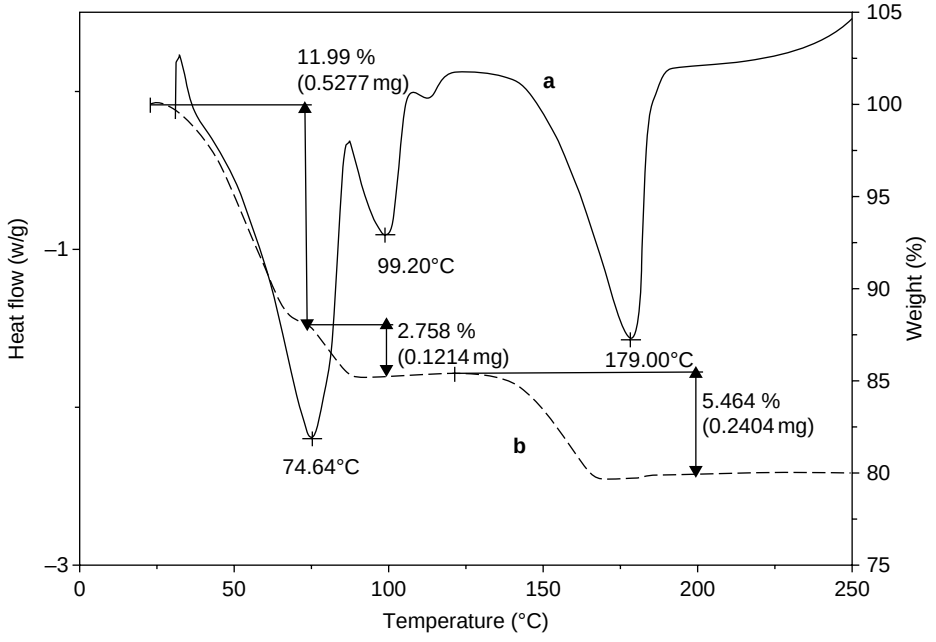

FIGURE 16 (**a**) Differential scanning calorimetry and (**b**) thermogravimetric analysis thermograms for the tetra-decahydrate solvatomorph of calteridol calcium.

moles of water directly associated with the calcium ion. The molar heat of dehydration is between two and three times larger for the loss of the calcium-bound water than for the channel or lattice water.

DESOLVATION AND DEHYDRATION PHENOMENA

If one has made the decision to pursue the development of a solvatomorph as the crystal form of a drug substance, one of the more critical issues that arise concerns the conditions under which the solvatomorph might become desolvated. That the mechanism of desolvation of an organic solvate might differ from the mechanistic pathway of dehydration of a hydrate was demonstrated in kinetic studies of the monohydrate and ethyl acetate solvatomorphs of fluconazole (59). Isothermal thermogravimetric analysis was used to monitor thermally induced weight changes of fluconazole monohydrate and ethyl acetate solvate, and the results analyzed using model-dependent and model-independent methods. It was determined that a three-dimensional phase boundary reaction model provided the best fit to the monohydrate data, whereas a three-dimensional diffusion model provided the best fit for the ethyl acetate solvate data. In addition, the activation energy associated with the monohydrate dehydration was determined to be significantly smaller that the activation energy of the ethyl acetate solvate desolvation.

However, because the majority of solvate forms that achieve pharmaceutical importance are actually hydrates, most of the discussion that follows will be concerned with the dehydration of hydrates. Many models have been developed to account for the dehydration kinetics of crystalline hydrates (60,61). Generally, these assume a certain geometry, and rely on some consistency of the system as the process proceeds. Often these models are indistinguishable for a given system due to experimental variation, and the fact that many structures (and, therefore, mechanisms) change during dehydration. The change in structure may also contribute to the hysteresis observed upon re-hydration of a dehydrated structure.

When regarding the structural aspects of hydration/dehydration it is worth considering the classification proposed by Galwey (61), who based his scheme on observations made of the behavior of crystals during dehydration. In this model, the processes include:

- Crystal structure maintained.
- Diffusion across an adherent barrier layer.
- Interface advance/nucleation and growth or contracting envelope.
- Homogeneous reactions in crystals.
- Melting and formation of impervious outer layer.
- Comprehensive melting.

This classification scheme is especially useful when the process is being observed using microscopy, and provides a guideline that may serve to understand the mechanism. If proceeding from a crystallographic point of view, one can arrive at a somewhat simplified scheme, anticipating one of three situations (62):

1. The crystal structure of the resulting anhydrous substance is nearly identical to that of the original hydrate.

2. The crystal collapses resulting in an amorphous phase, a mixed system of unidentifiable crystallites, or, in general, a very poor crystallinity.
3. The crystal transforms into a new crystal structure.

The practical consequences of dehydration kinetics may be found in the activities associated with determining boundary conditions for allowable exposure of bulk drug substances during development and processing, selection of proper packaging, determination of allowable temperature ranges for shipping, storage, and labeling of final product, and for the initial selection of a form for development.

Dehydration and Hydrate Class

We have already implied two aspects of dehydration in previous sections, namely, the thermodynamic and the kinetic. Obviously the onset of dehydration will strongly be related to the enthalpy of interaction of water in the system, but in addition, the rate of dehydration will be strongly related to the geometrical arrangement of the water in the crystal structure. For isolated site hydrates, dehydration rates would be anticipated to be low even when the substance is heated nearly to the dehydration temperature. Once the dehydration temperature is achieved, the kinetics would be expected to become very rapid unless the structure collapsed and presented a barrier to loss of the last water. This type of behavior is due to the fact that the waters would be in similar energetic environments (i.e., hydrogen bonded to drug molecules), so that when sufficient energy is supplied to free one water, there is enough to liberate them all.

For example, in the structure of inosine dihydrate (which can classified as an isolated site hydrate type), the purine rings are hydrogen bonded together to form ribbons running along the crystallographic *b*-axis, and the water molecules hydrogen bond with the amino hydrogen atoms and the carbonyl oxygen atoms of the base (63). During studies conducted on the thermally induced thermal dehydration of inosine dihydrate, three types of water loss were detected (64). One water molecule bridging the furan ends of the molecules was lost separately, and the waters found to the carbonyl group and those bridging the aromatic planes were lost in separate processes. The loss of the water of hydration leads to conformational and packing changes that are required for the final transformation into the α-anhydrate structure.

The dehydration kinetics of channel hydrates are anticipated to be different relative to those of isolated site hydrates because the hydrogen-bonding network is dominated by water–water interactions. It is a generally accepted idea that all the hydrogen bonds of a given water molecule may get stronger as subsequent hydrogen bonds are formed. This suggests that when one water molecule is taken away from this arrangement, the remaining water molecules become less strongly bound to the host system. This explains both the continuous dehydration observed with an onset at relatively low temperatures for channel hydrates, and the relatively discrete water loss associated for the isolated site and the ion associated hydrates that are not subject to this cascade effect.

As mentioned before, the kinetics of dehydration appear to be strongly influenced by the role of the water in the lattice and its geometrical arrangement. When channel or planar hydrates are concerned, there is a conceivable reversibility in the process accompanied by well-behaved departure and re-entrance of the water molecules in the system. Hence, hysteresis in the vapor sorption analysis may be expected to be relatively small and the impact on the crystals is expected to be relatively low.

Several studies of the multi-step dehydration of the channel hydrate theophylline monohydrate have been reported. In the crystal structure of the monohydrate, theophylline molecules form chains of dimers, and the water molecules form infinite hydrogen-bonded chains that run through tunnels parallel to the crystallographic *a*-axis (65). The water chains are hydrogen bonded to the theophylline dimers, and this arrangement results in the formation of two-dimensional hydrogen-bonded layers that run parallel to the *ab*-plane.

The mechanistic pathway of theophylline monohydrate dehydration has been shown to be a function of experimental conditions, where in a closed system the phase transition consisted only of a dehydration step (i.e., molecular loosening and breaking of hydrogen bonds) because evaporation of the water to the vapor phase was inhibited (66). However, when the dehydration was conducted in an open system, the reaction proceeded first by a dehydration step that was followed by a second step of evaporation of the loosened crystal water.

The dehydration of theophylline monohydrate has also been studied from the viewpoint of the crystallographic identity of the dehydration products. Using two-dimensional X-ray powder diffraction studies (acquired with a time resolution of 40 milliseconds using synchrotron radiation), Suryanarayanan and coworkers showed that the products of the two-step dehydration of theophylline monohydrate were a metastable anhydrous crystal form and the stable anhydrate (67). The dehydration kinetics were also studied by means of Raman spectroscopy, where the two-step dehydration process going through the two anhydrate crystal forms was confirmed (68).

Although thermal analysis and X-ray crystallography represent the typical methods for studying dehydration processes, spectroscopic methods can sometimes reveal steps in the mechanism not readily evident. For example, although thermal analysis and X-ray powder diffraction studies indicated that cefadroxil monohydrate appeared to undergo a relatively simple thermally induced dehydration, solid-state fluorescence spectroscopy studies pointed toward the existence of a cefadroxil hemihydrate that could be obtained by appropriate thermal dehydration (69). The fluorescence spectral results indicated the existence of two major photophysical pathways for delocalization of excitation in the cefadroxil monohydrate crystal, each of which could be selectively activated by irradiation with the proper excitation wavelength. One of the photophysical systems appeared to dominate the spectroscopy of the monohydrate, but was eliminated once the monohydrate was dehydrated to a hemihydrate. The other photophysical pathway existed in the monohydrate structure, and became the sole mechanism for observable fluorescence once the cefadroxil monohydrate was partially dehydrated to the hemihydrate. The fact that the different species exhibited widely differing fluorescence intensities enabled a spectral evaluation of the decomposition pathway, which is illustrated in Figure 17.

Impact of Particle Size and Crystal Morphology

More often than not, one can go by the general rule that the smaller is the particle size, the more rapid will be the rate of dehydration. Assuming bulk diffusion in the material to be the rate-limiting step, the general assumption can be justified on the basis of surface area. A secondary contribution to this effect is seen for materials that have been milled, where the resulting crystal defects contribute to an increased

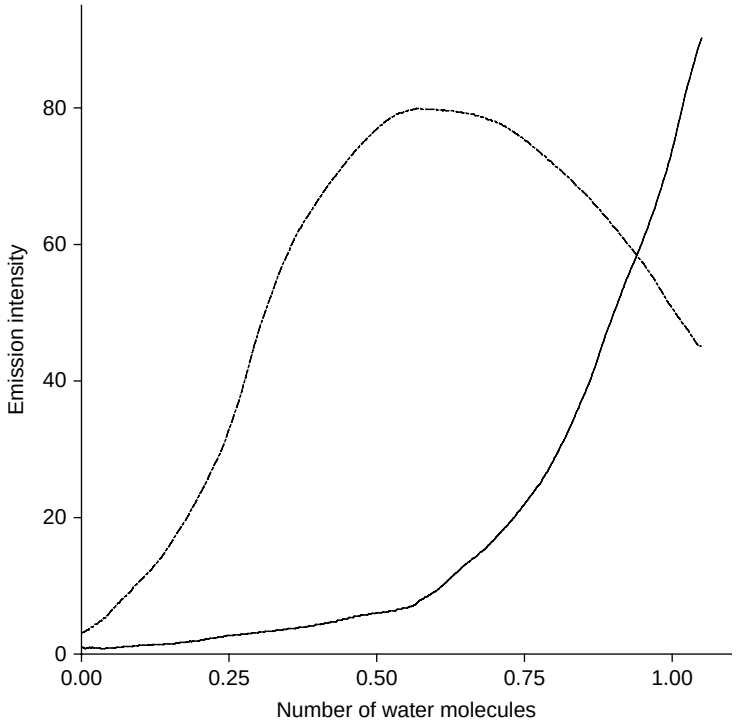

FIGURE 17 Cefadroxil fluorescence intensity as a function of the number of water molecules per molecule of cefadroxil in isothermally heated samples (69). The intensity of the excitation = 360 nm/emission = 460 nm system is shown as the solid trace, whereas the intensity of the excitation = 390 nm/emission = 540 nm system is shown as the dashed trace.

degree of bulk diffusivity, as well as an apparently larger surface-to-bulk ratio due to cracks and porosity.

In one study, the dehydration mechanism and activation energy of dehydration of theophylline monohydrate were found to be dependent on both the particle size and on the sample weight used (70). For large sample weights, the dehydration process was best described by the Avrami-Erofeev equation for both non-fractionated samples and for sieve cuts smaller than 500 μm. On the other hand, a two-dimensional phase boundary mechanism proved to be the most consistent to describe the dehydration of samples having passed through a 150-μm sieve. For smaller sample weights, the Avrami-Erofeev model proved satisfactory to describe dehydration in both the non-fractionated samples and in the <150-μm sieve cut. It was suggested that both the mechanism and the activation energy associated with the dehydration of a hydrate could be significantly influenced by sample pre-history, and that factors such as particle size, sample weight, crystal defects, and surface characteristics needed to be taken into account.

The impact of crystal morphology on dehydration kinetics is seen to be somewhat be more subtle, and is hardly ever independent of particle size considerations.

Nevertheless, it can easily be conceived that (especially for instances of channel hydrates) bulk diffusion would be highly anisotropic, and that morphologies that have shorter and more channels per unit of bulk will result in faster dehydration.

This topic is complicated by the reality that particle size analysis is a very subjective measurement, and the issue of proper sampling can introduce additional error (71). This makes it difficult to know how to approach the problem of obtaining a crystalline hydrate in the form of two different morphologies that have the same particle size. Another complication has to do with the dehydration rate measurements themselves. As discussed earlier, the stability of the hydrated form cannot be specified without knowledge of the partial pressure (or RH) of water at each temperature of interest. Most dehydration experiments are performed against very low values of RH, and the conditions/results may not be very realistic or revealing. The literature does contain some interesting studies of dehydration at various RH values that clearly show the expected trends (72,73). The use of moisture sorption/desorption data is also becoming more common, although most workers still use only the equilibrium values even though the kinetic data is usually available from the same experiments.

The discussion on dehydration characteristics of the different classes suggests that, for equivalent particle size, channel hydrate dehydration kinetics should be more sensitive to changes in morphology than would be the other classes. For ampicillin trihydrate (a channel hydrate), the water lies on the crystallographic *c*-axis. For crystals that are more elongated along this axis, the relative density of dehydration sites on the crystal surface is smaller. This should lead to slower dehydration (at least early in the process before structural changes can occur) due to the increase in the average distance a water molecule must travel before it becomes liberated.

BEHAVIOR OF SOLVATOMORPHS DURING PROCESSING, HANDLING, AND STORAGE

It is well established that the mechanical forces encountered by polymorphs and solvatomorphs during the processing of drug substances into drug products can often cause phase transitions from metastable into more stable crystal forms (74–76). Although such topics will be discussed in considerable detail in other chapters in this book, it is appropriate at this time to explore where in the dosage form development process one might encounter phase transformations of solvatomorphs, and especially of hydrate species. The discussion naturally divides itself into those situations where a stage during secondary processing induces a phase transition and those situations where transitions take place in the final drug product subsequent to its manufacture. Although the majority of published works are concerned with the transformations among polymorphs, a sufficient number of studies have been discussed for transitions among states of hydration systems.

Processing Induced Transitions

Of particular interest in pharmaceutical development is the induction of phase transitions during processing, which can occur for several possible reasons. If the crystalline state of the bulk drug substance is a metastable polymorph or solvatomorph, the introduction of sufficient energy to overcome any activation energy barrier may cause a phase transformation into a more stable form during processing. The same may be said about amorphous drug substances, which will always be metastable with respect to any crystalline form. At the end of the phase transformation process, the final state

may either be a more stable polymorph or a different hydration state, and the processing may kinetically trap a metastable form in the dosage form. It is also possible, that a new form may appear that is only stable in the formulation matrix.

Solution-Mediated Transformations

During any manufacturing process that entails contact of a non-solvated crystal form of a drug substance with any kind of bulk solvent, the possibility of a phase transformation into a solvated or hydrated crystal form must be considered. In suspensions of solid crystal forms, the higher free energy of a metastable form will cause it to exhibit a higher degree of solubility than its more stable forms. Consequently, a saturated solution of the less stable form would be supersaturated with respect to the more stable form, which would then crystallize during processing. These situations are termed solution-mediated phase transformations, and depend upon the solution phase to provide the mobility necessary to rearrange in the most stable form. Perhaps carbamazepine and theophylline constitute the best known systems of this type, and shall be more fully discussed in Chapter 13.

Although the anhydrous crystal form of metronidazole benzoate is the commercially available substance, the monohydrate has been shown to the thermodynamically stable form in water at temperatures less than 38°C (77). The phase transformation of the anhydrate to the monohydrate was found to be accompanied by a drastic increase in particle size, which in turn, led to instabilities in suspension formulations intended for oral administration. In subsequent work, it was found that the aqueous solutions of the drug substance would form an inclusion complex with β-cyclodextrin, and that formation of this complex drastically impeded the course of the solution-mediated phase transformation (78). In addition, cyclodextrin complexation also served to decrease the rate of hydrolysis and to protect the drug substance against photochemical degradation.

The ability of polyvinylpyrrolidone to inhibit the humidity-induced phase conversion of anhydrous theophylline into its monohydrate has been studied in physical mixtures of varying proportions (79). The excipient was found to retard the degree of hydrate formation by competing with the drug substance for water molecules, while at the same time promoting formation of monohydrate by delivering water in close proximity to theophylline crystals. However, the second mechanism only became significant at high levels of excipient and/or RH, indicating that the protective action of polyvinylpyrrolidone in the mixtures could be attributed to the action of an internal desiccant.

Carbamazepine represents another well-known system where suspension of any of the anhydrous polymorphic forms in aqueous media results in the solution-mediated phase transformation of the substance into its dihydrate form. This phase transformation is illustrated in Figure 18, where the tabular crystals of the anhydrate Form-III convert into the needle-like crystals of the dihydrate over time. The effect of excipients that could be grouped into functional classifications on this transition has been evaluated, and it was determined that hydrogen-bonding interactions and solubility interactions played the dominant roles in inhibition of the phase transformation (80).

The chemical and physical stability of aqueous and non-aqueous suspensions of the anhydrate, two polymorphic monohydrates, the 1:1 *N*,*N*′-dimethylformamide solvatomorph, the 1:1 dimethyl sulfoxide solvatomorph, the 1:1 methanol solvatomorph, and the 2:1 tetraethylene glycol hemisolvate of niclosamide has been

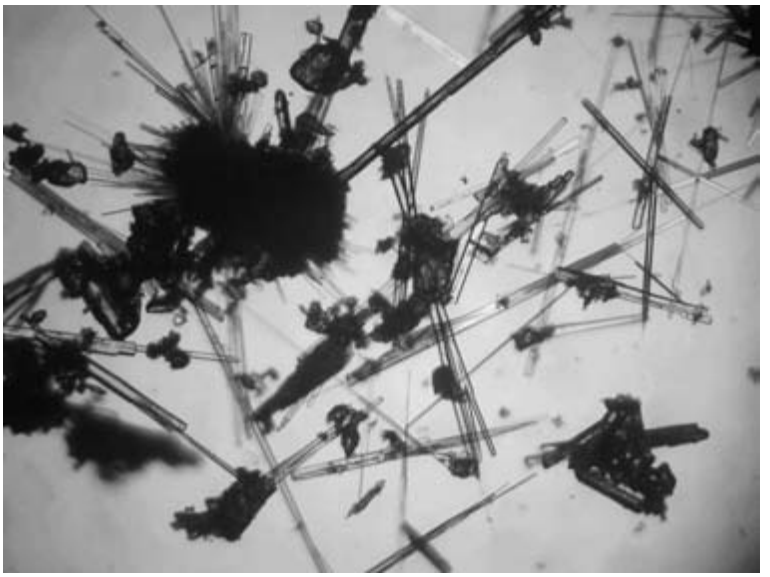

FIGURE 18 Photomicrograph taken at a magnification of 40×, illustrating the growth of carbamazepine dihydrate needles on equant crystals of carbamazepine anhydrate Form-III during an aqueous solution-mediated phase transformation (H.G. Brittain, unpublished results).

evaluated in an effort to develop pharmaceutically acceptable suspension formulations (81). All of the solvatomorphs were found to convert initially to one of the polymorphic monohydrates, and over time all of the initially formed metastable monohydrates converted to the more stable monohydrate phase. The various solvatomorphs could be readily desolvated, but these were unstable and became re-hydrated or re-solvated upon exposure to the appropriate solvent.

Ciprofloxacin anhydrate was shown to rapidly convert to its hydrated form upon exposure to water, but it was found that premixing the anhydrate with hydroxypropyl methylcellulose in the presence of water or ethanol would inhibit the processing-induced phase transition, and that proper choice of excipients would allow formulation without phase transformation via wet granulation (82). Extended-release tablets of containing hydroxypropylmethylcellulose (HPMC) that were prepared with the solvatomorphs were found to exhibit different dissolution rates, which was interpreted to indicate that the anhydrate-to-hydrate transition was significantly inhibited by the excipient in the gel layer of hydrated tablets.

Particle Size Reduction

Considering the amount of energy that accompanies the processing, unit operations of particle size reduction (i.e., grinding and milling) have considerable potential to induce changes in the solvation or hydration state of a drug substance. Often the process of milling (especially if the energy input into the system is high) can result in the formation of a considerable percentage of amorphous content in the ground substance. The formation of a high-energy amorphous material is usually undesirable

in that it must be thermodynamically metastable, and will tend to spontaneously transform either to a crystalline hydrate or anhydrate.

Extended performance of a milling operation will serve to lower the degree of crystallinity in the solid, and this phenomenon is especially important for solvatomorphs having lower degrees of lattice energy. As the degree of crystallinity in a solid steadily decreases, a level can be reached where the crystal structure of a hydrate is sufficiently disrupted so as the lattice water can no longer be retained, and the solid collapses into an amorphous product. This phenomenon was most clearly demonstrated during studies conducted on cephalexin monohydrate (83,84), where samples were ground using a variety of methods and the degree of crystallinity determined using a calibrated X-ray powder diffraction method. As illustrated in Figure 19, solids that had been milled to degrees of crystallinity less than 20%

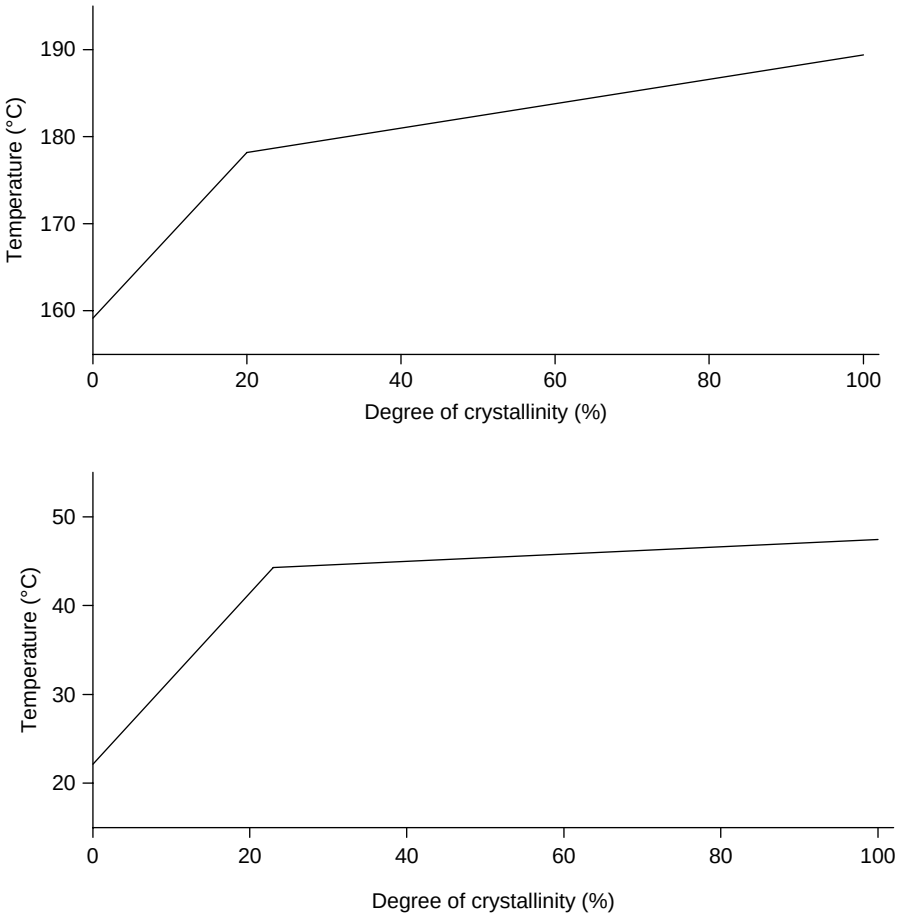

FIGURE 19 Relationship between the degree of crystallinity in ground cephalexin samples and the dehydration temperature (*lower trace*) and the decomposition temperature (*upper trace*). The figure is adapted from data contained in Ref. (84).

were significantly less stable than the more crystalline solids, as evidenced by the precipitous decreases in dehydration and decomposition temperatures.

The phenomenon of loss of crystalline water upon extensive grinding of a hydrate solvatomorph is not limited to cephalexin. Cefixime trihydrate could be transformed into an amorphous state after four hours of mechanical processing in an automated mortar, although no sharply defined critical degree of crystallinity could be identified in this study (85). On the other hand, the grinding of cyclophosphamide monohydrate was shown to proceed through a new metastable phase on the way to a stable anhydrous phase (86). Lactitol monohydrate became easier to dehydrate upon grinding, even though an analogous grinding process was not found to influence the dehydration temperature of the dihydrate phase (87).

The effects of particle size reduction, granulation, consolidation, and compression on celecoxib and its solvatomorphs have been studied, establishing that the non-solvated drug substance retained its crystalline identity without formation of any amorphous material during processing (88). On the other hand, milling the *N,N'*-dimethylacetamide solvatomorph generated crystal defects that initiated further changes, and milling the *N,N'*-dimethylformamide solvatomorph yielded partial transformation to the non-solvated phase. These solvatomorphs were found to become desolvated upon wet granulation, and additionally, compaction forces also served to desolvate the solvatomorphs.

Wet Granulation and Subsequent Drying

Wet granulation is a particularly efficient process for kinetic trapping of metastable crystal forms. During one mode of this processing methodology, one prepares a highly concentrated solution of the drug substance by using hot solvent to dissolve the dry substance, and possibly additional excipients, and then the mixture is rapidly dried onto other solids using an evaporative cooling process. The resulting product can exhibit a range of characteristics that vary from no change in crystal form, to a mixture of forms, to a metastable crystalline form, or to a metastable amorphous form. This aspect of processing-induced phase transformation will be illustrated through a discussion of the anhydrate-monohydrate phase transitions of theophylline during granulation processing and subsequent drying because a substantial body of work has developed concerning such processes.

The influence of the degree of wetting during the granulation step of the pelletization process on the drug release from several blends of micro-crystalline cellulose with theophylline anhydrate has been studied (89). The differences in release rate were correlated with the anhydrate-to-monohydrate phase crystal transition, where the degree of conversion was quantitatively influence by the percentage of anhydrous theophylline, the choice of excipient, and the degree of wetting during the granulation step. In another study of micro-crystalline cellulose blends with theophylline, it was confirmed that wet granulation caused a decrease in the rate of drug release rate that was caused by the conversion of theophylline anhydrate into theophylline monohydrate (90). Additionally, it was found that oven drying the products at 400°C did not restore the anhydrate state, and that a decrease in dissolution rate could be obtained for dry compacts of theophylline anhydrate and micro-crystalline cellulose that were stored at high humidity levels.

The influence of lactose monohydrate or silicified micro-crystalline cellulose on the anhydrate-to-monohydrate phase transformation during wet granulation has been studied with the specific aim of determining whether the highly water

absorbing cellulosic excipient could retard the transition (91). It was determined that lactose exerted no effect on the phase transformation, and that the silicified micro-crystalline cellulose only inhibited the transition at low levels of moisture and not the levels needed to form granules. The processing-induced phase transformations of theophylline was further investigated with the aim of studying the formation of a metastable anhydrate form that was produced after wet massing and drying of theophylline with poly(vinylpyrrolidone) (92). Different amounts of stable and metastable theophylline could be produced depending on the granulation method, and these and subsequent phase transitions had a significant effect on product performance.

The effect of a number of pharmaceutical excipients on the kinetics of theophylline monohydrate formation during high-shear wet granulation has been studied, where mixtures of theophylline anhydrate and the excipient were wet granulated in a high-shear granulator using water as the granulation fluid (93). The kinetics of the solution-mediated phase transformation was also evaluated in slurries where theophylline and excipients were added to the aqueous phase. It was found that at typical levels of excipient in the granulations, the of phase transformation theophylline were effectively unchanged, but that when granulation was conducted using low concentrations of certain polymeric binders the transformation kinetics could be significantly retarded. For example, when 0.3% w/w of hydroxypropyl methylcellulose was added to a formulation containing 30% w/w theophylline anhydrate, the formation of the monohydrate could be completely prevented over the time period of the granulation experiment, without significantly affecting the granular properties.

Near infrared (NIR) spectroscopy has been used to study the solution-mediated phase transformation of anhydrous theophylline to the monohydrate during an aqueous-based wet granulation process (94). As shown in Figure 20, the NIR spectra of theophylline anhydrate and its monohydrate are sufficiently different so as to permit their ready identification. It was reported that at low levels of granulation fluid (corresponding to 0.3 moles of water per mole of theophylline), the water absorption maxima observed the NIR spectra corresponded to those of theophylline monohydrate, but at higher levels of granulation fluid (i.e., 1.3–2.7 moles of water per mole of theophylline) spectral contributions to free water were identified. In a subsequent study, the abilities of NIR and Raman spectroscopies to follow the species in a theophylline wet granulation process were evaluated, and it was concluded that although NIR spectroscopy provided information regarding the state of water in the solids, Raman spectroscopy yielded information related to the drug molecule itself (95).

The utility of Raman spectroscopy as a probe technique was evaluated as to its potential use for in-line monitoring of the transformation of theophylline anhydrate to theophylline monohydrate during high-shear wet granulation (96). The transformation kinetics observed during wet granulation were compared with those generated by a simple model describing the solvent-mediated transformation of theophylline in solution, and it was concluded that a simple solvent-mediated transformation model could be useful for estimating the time scale for hydrate formation during high-shear wet granulation.

Because it was known that theophylline monohydrate can be thermally dehydrated to generate either the stable Form-I or the metastable Form-I*, the effect of different drying methods on the phase composition was studied (97). When using either a multi-chamber micro-scale fluid bed dryer or the hot-stage of a variable

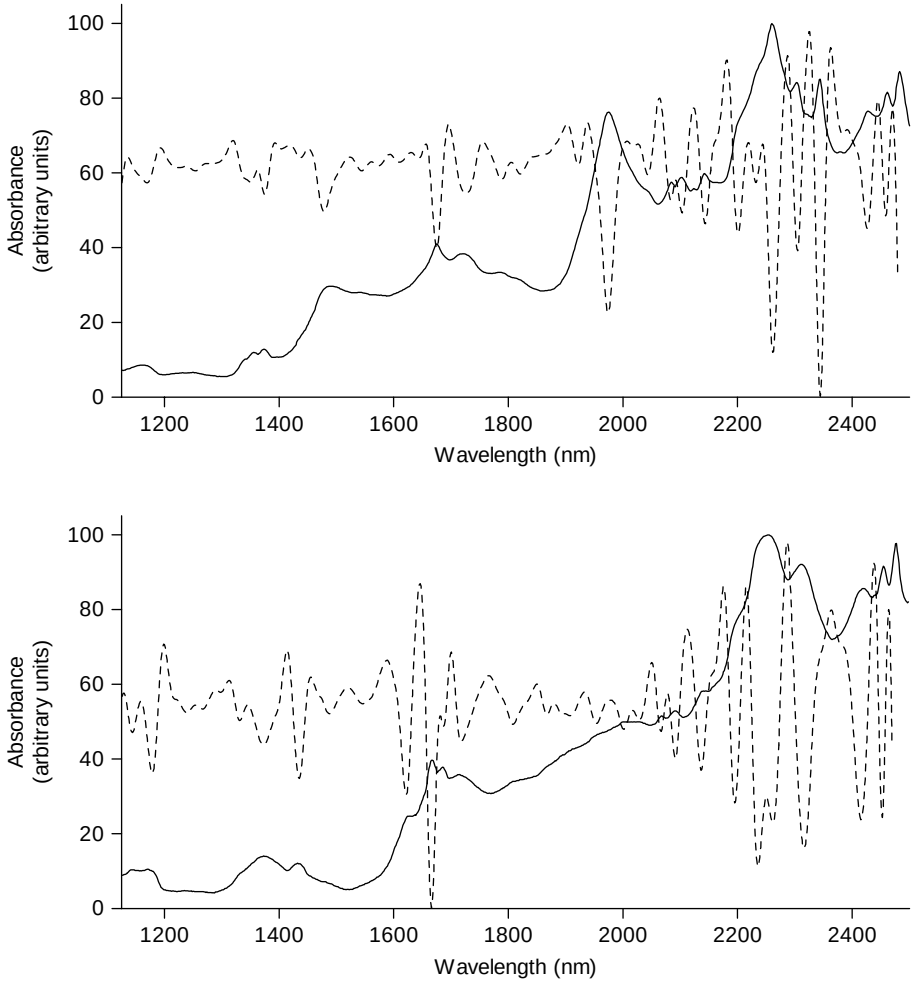

FIGURE 20 Near-infrared spectra obtained for theophylline monohydrate (*upper spectra*) and theophylline anhydrate (*lower spectra*), showing both the raw absorption spectrum (*solid traces*) and the corresponding second derivative spectrum (*dashed traces*) for each. The spectra are shown in arbitrary units, and have been adapted from Ref. (94).

temperature X-ray powder micro-diffraction (XRPD) diffractometer, Form-I* was produced when the drying was conducted at 40–50°C. Drying at 60°C in the VT-XRPD unit yielded only Form-I, whereas mixtures of products were produced in the micro-scale fluid bed dryer even at temperatures as high as 90°C.

Transitions in the Final Product

Once a final dosage form has been produced, there remains the possibility of in situ phase transitions. These can happen either because a metastable form was produced,

or because the ambient conditions have forced the transition. These changes can be either hydration or dehydration, alterations in the polymorphic state, or amorphous-to-crystalline phase transitions. A transformed drug substance in a dosage form could exhibit an altered solubility or dissolution rate that might produce an undesirable profile, and this effect would be particularly pronounced when developing a metastable form of the drug substance.

Processes that kinetically trap a metastable phase in a solid dosage form are not unusual. To entrap a phase, one must restrict its molecular mobility once it forms, and this situation is easier to accomplish in a solid dosage form. Once a metastable phase is formed, it may achieve a fair degree of stability in the dosage form, and can even represent a marketing advantage where one takes advantage of the potentially higher solubility, dissolution rate, and bioavailability. If the phase transformation results in a polymorphic or solvatomorphic form other than the desired one, a considerable degree of concern will arise. One need only recollect the example of Abbott's Ritonavir, where the initially marketed drug product became unacceptable upon crystallization of a less available, more stable polymorph (98).

The effect of high degrees of RH on tablets prepared containing anhydrous theophylline has been studied in considerable detail. For example, when such tablets were stored under conditions of high RH, needle-like crystals of the monohydrate phase appeared on the surface of the tablets that resulted in a decrease of the dissolution rate (99,100). The problem was found to be more pronounced for tablets containing hygroscopic materials such as polyethylene glycol 6000, magnesium chloride, potassium acetate (illustrated in the dissolution curves of Fig. 21), or sodium chloride. In a latter study, it was found that unless tablets prepared from theophylline anhydrate were stored at relative humidities less than 52%, phase transformation of the drug substance into its monohydrate and additional hydration of the magnesium stearate lubricant would take place (101). The rate of drug release was found to bear an inverse relationship to the compression pressure, but the degree of compaction was not found to affect the rates of moisture sorption or phase transformation.

The effects of tableting pressure and various geometric factors on the hydration kinetics tablets prepared using the various polymorphs of theophylline anhydrate have been studied (102,103). Tablets were stored at 35°C and 95% RH, and the effects of these storage conditions on tablet expansion and hydration were studied as a function of tablet thickness and diameter. In these works, it was found that hydration of the tablets decreased with increased tableting pressure, suggesting that the role of the tablet excipients, and their effect on tablet porosity, played a dominant role in the hygroscopicity. In a related study, the dehydration kinetics of theophylline monohydrate in compressed tablets was studied as a function of tableting pressure and tablet geometric factors (104). It was determined that like the hydration kinetics of tablets containing theophylline anhydrate, the dehydration kinetics of theophylline monohydrate in tablets was largely determined by the tablet porosity and thickness.

It has been established that dehydration of theophylline monohydrate first yields a metastable anhydrous phase that, in turn, undergoes a further phase transformation to the most stable polymorphic state. In one study, tablet formulations containing either the metastable or stable anhydrate form were prepared and stored at ambient temperature and RH conditions of 33% and 52% (105). It was found that the drug substance in tablets prepared beginning with the metastable anhydrate

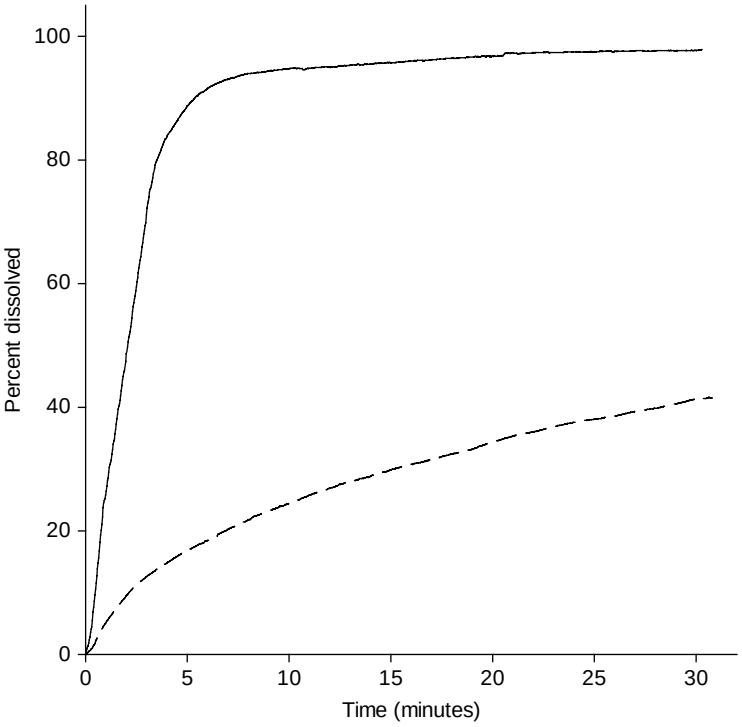

FIGURE 21 Dissolution data obtained for an initially produced theophylline tablet formulation that contained potassium acetate in addition to conventional excipients (*solid trace*) and for the same formulation stored for four weeks at 37°C and 90% RH (*dashed trace*). The curves have been adapted from data contained in Ref. (100).

completely converted to the stable anhydrate in less than 10 days, and the dissolution rate of the tablets stored at 52% RH failed the USP dissolution test. In another study, anhydrous theophylline was wet massed with different molecular weight grades of polyvinylpyrrolidone to effect conversion to the monohydrate, the products dried, and the resulting levels of metastable and stable anhydrate determined (106). It was determined that the physical form of theophylline in the tablets was influenced by the molecular weight of the binding agent, the granulation method, and the drying temperature.

During an investigation of dissolution failures encountered for tablets containing erythromycin dihydrate indicated that an isomorphic desolvated form of the dihydrate phase was responsible for the observed decreases in the dissolution rates, specifically because the dehydrated dihydrate would become bound with formulated $Mg(OH)_2$ (107). Interestingly, the phenomenon could be reversed by exposing tablets to water vapor for a relatively short period of time. On the other hand, the process-induced transformation of erythromycin dihydrate to its dehydrated form was demonstrated to take place during oven tray drying at higher temperatures (60°C) than at lower temperatures (60°C), suggesting that erythromycin does not tend to transform easily during processing (108).

Kinetics of Transformation

Only a few generalities can be advanced regarding the kinetics of phase transformations that take place during processing, but it is true that constant-temperature solution-mediated transformations typically proceed much faster than do those in the solid state. Some transformations that proceed rapidly and are apparently occurring in the solid state may actually be taking place in an absorbed water layer, or in the amorphous fractions of the solid. Hydrate transformations can be thought of as reactions that are not necessarily occurring in the solid state, because the water may be in the vapor phase. These may even be considered as being solution mediated, consistent with the relative rapidity with which many hydration/dehydration reactions occur.

If the thermodynamics of a system indicate that free energy differences represent only a small driving force for a solid-state polymorphic transformation, even favorable kinetics may be insufficient to allow the transition to occur rapidly. In general, the existence of favorable kinetics has more effect on the transformation rate than does a relatively large driving force, so increasing temperature and/or pressure conditions become the main controllable factors. The degree of RH can be the main factor in a hydrate transformation, and here a large driving force represented by the partial pressure of water may enhance the kinetics by inducing mobility in the system.

The kinetics of phase transformation can become problematic for accelerated stability studies for several reasons. Stress testing conditions may exceed the temperature of a polymorphic phase transition or dehydration, and the use of accelerated conditions may make a relaxation of a metastable phase more rapid due to the increased molecular mobility in the solid. In addition, the RH of the station may be in the range sufficient to cause a solvatomorphic transition associated with a dehydration or a hydration process. If such transformations are possible under stress conditions, then it is equally possible that they may also be observed during excesses in storage and handling.

It is easy to see from the phase diagram of an enantiotropic polymorphic system that if the storage condition of the stable phase of drug exceeds the transition temperature, the order of stability changes and a new phase will form if the kinetics permits. A more common problem is the exceeding of the glass transition temperature of amorphous compounds (or coatings), which then may induce crystallization and/or other mobility related problems. A crystal form that is metastable at a given temperature can convert to the stable form if the conditions and kinetics become favorable. As the temperature is increased, even though the free energy gradient decreases, the conversion kinetics becomes more favorable.

REFERENCES

1. Griesser UJ. The importance of solvates, chapter 8 in Polymorphism in the Pharmaceutical Industry. In: Hilfiker R, ed. Weinheim: Wiley-VCH, 2006: 211–33.
2. Vishweshwar P, McMahon JA, Bis JA, et al. Pharmaceutical cocrystals. J Pharm Sci 2006; 95: 499–516.
3. Byrn SR, Pfeiffer RR, Stowell JG. Hydrates and solvates, chapter 11 in Solid State Chemistry of Drugs, 2nd edn. West Lafayette: SSCI Inc, 1999: 233–47.
4. Stahl HP. The Problems of Drug Interactions with Excipients, in Towards Better Safety of Drugs and Pharmaceutical Products. In: Braimar DD, ed. Elsevier/North-Holland: Biomedical Press, 1980: 265–80.

5. Vippagunta SR, Brittain HG, Grant DJW. Crystalline solids. Adv Drug Del Rev 2001; 48: 3–26.
6. Morris KR, Rodríguez-Hornedo N. Hydrates, in Encyclopedia of Pharmaceutical Technology. In: Swarbrick J, Boylan J, eds, volume 7. New York: Marcel Dekker, 1993: 393–440.
7. Morris KR, Fakes MG, Thakur AB, et al. An integrated approach to the selection of optimal salt form for a new drug candidate. Int J Pharm 1994; 105: 209–17.
8. Cambridge Structural Database, version 5.29. Cambridge, UK: Cambridge Structural Data Centre, release of 2007.
9. Bowden ST. Two-component systems, chapter 3 in The Phase Rule and Phase Reactions. London: MacMillan and Co, 1950: 63–86.
10. Grant DJW, Higuchi T. Solubility Behavior of Organic Compounds. New York: John Wiley & Sons, 1990: 38–9.
11. Khankari RK, Grant DJW. Pharmaceutical hydrates. Thermochim Acta 1995; 248: 61–79.
12. Nývlt J. On the kinetics of solid–liquid–solid phase transformation. Cryst Res Technol 1997; 32: 695–9.
13. Boerrigter SXM, van den Hoogenhof CJM, Meekes H, et al. In situ observation of epitaxial polymorphic nucleation of the model steroid methyl analogue 17 norethindrone. J Phys Chem B 2002; 106: 4725–31.
14. Braun DE, Többens DM, Kahlenberg V, et al. Structural and thermodynamic features of crystal polymorphs of R-cinacalcet hydrochloride. Cryst Growth Des 2008; 8: 4109–19.
15. Zhu H, Yuen C, Grant DJW. Influence of water activity in organic solvent + water mixtures on the nature of the crystallizing drug phase. 1. Theophylline. Int J Pharm 1996; 135: 151–60.
16. Zhu H, Grant DJW. Influence of water activity in organic solvent + water mixtures on the nature of the crystallizing drug phase. 2. Ampicillin. Int J Pharm 1996; 139: 33–43.
17. Jarring K, Larsson T, Stensland B, et al. Thermodynamic stability and crystal structures for polymorphs and solvates of formoterol fumarate. J Pharm Sci 2006; 95: 1144–61.
18. Oswald IDH, Allan DR, McGregor PA, et al. The formation of paracetamol (acetaminophen) adducts with hydrogen-bond acceptors. Acta Cryst 2002; B58: 1057–66.
19. Vrcelj RM, Clark NIB, Kennedy AR, et al. Two new paracetamol/dioxane solvates: a system exhibiting a reversible solid-state phase transformation. J Pharm Sci 2003; 96: 2069–73.
20. Bingham AL, Huches DS, Hursthouse MB, et al. Over one hundred solvates of sulfathiazole. Chem Comm 2001: 603–4.
21. Drebushchak TN, Mikhailenko MA, Boldyreva EV, et al. Tetragonal polymorph of the 1:1 adduct of sulfathiazole with pyridine. Acta Cryst 2006; E62: o2669–o2671.
22. Drebushchak TN, Mikhailenko MA, Boldyreva EV, et al. Monoclinic polymorph of the 1:1 adduct of sulfathiazole with pyridine. Acta Cryst 2006; E62: o2707–o2709.
23. Johnson A, Florence AJ, Kennedy AR. Hydrochlorothiazide–aniline (1/1). Acta Cryst 2005; E61: o2520–o2522.
24. Florence AJ, Johnson A, Shankland K. Powder study of hydrochlorothiazide–methyl acetate (1/1). Acta Cryst 2005; E61: o2974–o2977.
25. Johnson A, Florence AJ, Kennedy AR. Hydrochlorothiazide–1,4-dioxane (1/1). Acta Cryst 2005; E61: o2573–o2575.
26. Johnson A, Florence AJ, Kennedy AR. Hydrochlorothiazide N,N-dimethyl-formamide solvate. Acta Cryst 2006; E62: o1730–o1732.
27. Johnson A, Florence AJ, Kennedy AR. Hydrochlorothiazide dimethyl sulfoxide solvate. Acta Cryst 2006; E62: o2288–o2290.
28. Johnson A, Florence AJ, Kennedy AR. Hydrochlorothiazide N,N-dimethyl-acetamide disolvate. Acta Cryst 2006; E62: o2926–o2928.

29. Johnson A, Florence AJ, Kennedy AR. Hydrochlorothiazide N-methyl-2-pyrrolidone disolvate. Acta Cryst 2006; E62: o5169–o5171.
30. Lohani S, Zhang Y, Chyall LJ, et al. Carbamazepine–2,2,2-trifluoroethanol (1/1). Acta Cryst 2005; E61: o1310–o1312.
31. Johnson A, Florence AJ, Kennedy AR. Carbamazepine N,N-dimethylformamide solvate. Acta Cryst 2005; E61: o1509–o1511.
32. Fernandes P, Bardin J, Johnson A, et al. Carbamazepine trifluoroacetic acid solvate. Acta Cryst 2007; E63: o4269.
33. Johnson A, Florence AJ, Kennedy AR. Carbamazepine furfural hemisolvate. Acta Cryst 2005; E61: o1777–o1779.
34. Farrell DMM, Glidewell C, Low JN, et al. Polymorphs and pseudopolymorphs of N,N'-dithiobisphthalimide. Acta Cryst 2002; B58: 289–99.
35. Hosokawa T, Datta S, Sheth AR, et al. Isostructurality among five solvates of phenylbutazone. Cryst Growth Des 2004; 4: 1195–201.
36. Henry R, Zhang GGZ. Crystallographic characterization of several erythromycin a solvates: The Environment of the Solvent Molecules in the Crystal Lattice. J Pharm Sci 96: 1251–7.
37. Brittain HG. Unpublished solid-state fluorescence excitation and emission spectra obtained using a modified Perkin-Elmer LS 5B luminescence spectrometer.
38. Suitchmezian V, Jess I, Nather C. Investigations on the polymorphism and pseudopolymorphism of triamcinolone diacetate. Int J Pharm 2006; 323: 101–9.
39. Jess I, Nather C. Triamcinolone acetonide methanol 0.67-solvate at 107 K. Acta Cryst 2006; E62: o960–o962.
40. Black SN, Cuthbert MW, Roberts RJ, et al. Increased chemical purity using a hydrate. Cryst Growth Design 2004; 4: 539–44.
41. Falk M, Knop O. In Water, A Comprehensive Treatise, volume 2. In: Franks F, ed. Water in Crystalline Hydrates. New York: Plenum Press, 1973: 55–113.
42. Florey K. Cephradine, in Analytical Profiles of Drug Substances, volume 5. In: Florey K, ed. New York: Academic Press, 1976: 21–59.
43. Reutzel-Edens SM, Bush JK, Magee PA, et al. Anhydrates and hydrates of olanzapine: crystallization, solid-state characterization, and structural relationships. Cryst Growth Des 2003; 3: 897–907.
44. Jones PG, Möller H, Finner E. Cilansetron hydrochloride monohydrate, modification a (monoclinic). Acta Cryst 2003; E59: o38–o40.
45. Jones PG, Möller H, Finner E. Cilansetron hydrochloride monohydrate, modification b (orthorhombic). Acta Cryst 2003; E59: o41–o43.
46. Burley JC, van de Streek J, Stephens PW. Ampicillin trihydrate from synchrotron powder diffraction data. Acta Cryst 2006; E62: o797–o799.
47. Lin CT, Byrn SR. Desolvations of solvated organic crystals. Mol Cryst Liq Cryst 1979; 50: 99–104.
48. Chen X, Carillo M, Haltiwanger RC, et al. Solid-state characterization of mometasone furoate anhydrous and monohydrate forms. J Pharm Sci 2005; 94: 2496–509.
49. Vogt FG, Dell'Orco PC, Diederich AM, et al. A study of variable hydration states in topotecan hydrochloride. J Pharm Biomed Anal 2006; 40: 1080–8.
50. Cox JSG, Woodard GD, McCrone WC. Solid-state chemistry of cromolyn sodium (disodium cromoglycate). J Pharm Sci 1971; 60: 1458–65.
51. Chen LR, Young VG D, Lechuga-Ballesteros, et al. Solid-state behavior cromolyn sodium hydrates. J Pharm Sci 1999; 88: 1191–200.
52. Zhang Y, Grant DJW. Similarity in structures of racemic and enantiomeric ibuprofen sodium dihydrates. Acta Cryst 2005; C61: m435–m438.
53. Redman-Furey N, Dicks M, Bigalow-Kern A, et al. Structural and analytical characterization of three hydrates and an anhydrate form of risedronate. J Pharm Sci 2005; 94: 893–911.

54. Dzidic I, Kebarle P. Hydration of the alkali ions in the gas phase: enthalpies and entropies of reactions M+(H2O)n–1 + H2O = M+(H2O)n. J Phys Chem 1970; 74: 1466–74.
55. Zhu H, Khankari RK, Padden BE, et al. Physicochemical characterization of nedocromil bivalent metal salt hydrates. 1. Nedocromil Magnesium. J Pharm Sci 1996; 85: 1026–34.
56. Zhu H, Padden BE, Munson EJ, et al. Physicochemical characterization of nedocromil bivalent metal salt hydrates. 2. Nedocromil Zinc. J Pharm Sci 1997; 86: 418–29.
57. Zhu H, Halfen JA, Young VG, et al. Physicochemical characterization of nedocromil bivalent metal salt hydrates. 3. Nedocromil Calcium. J Pharm Sci 1997; 86: 1439–47.
58. Zhu H, Young VG, Grant DJW. Crystal structure and thermal behavior of of nedocromil nickel octahydrate. Int J Pharm 2002; 232: 23–33.
59. Alkhamis KA, Salem MS, Obaidat RM. Comparison between dehydration and desolvation kinetics of fluconazole monohydrate and fluconazole ethyl acetate solvate using three different methods. J Pharm Sci 2006; 95: 859–70.
60. Byrn SR, Pfeiffer RR, Stowell JG. Loss of solvent of crystallization, chapter 14 in solid state chemistry of drugs, 2nd edn. West Lafayette: SSCI Inc, 1999: 279–303.
61. Galwey AK. Structure and order in thermal dehydrations of crystalline solids. Thermochim Acta 2000; 355: 181–238.
62. Garner WE. Chemistry of the solid state. New York: Academic Press, 1955.
63. Thewalt U, Bugg CE, Marsh RE. The crystal structure of guanosine dihydrate and inosine dihydrate. Acta Cryst 1970; B26: 1089–101.
64. GilIon AL, Davey RJ, Storey R, et al. Solid state dehydration processes: mechanism of water loss from crystalline inosine dihydrate. J Phys Chem B 2005; 109: 5341–7.
65. Sun C, Zhou D, Grant DJW, et al. Theophylline monohydrate. Acta Cryst 2002; E58: o368–o370.
66. Suihko E, Ketolainen J, Poso A, et al. Dehydration of theophylline monohydrate: a two step process. Int J Pharm 1998; 158: 47–55.
67. Nunes C, Mahendrasingam A, Suryanarayanan R. Investigation of the multi-step dehydration reaction of theophylline monohydrate sing 2-dimensional powder X-ray diffractometry. Pharm Res 2006; 23: 2393–404.
68. Amado AM, Nolasco MM, Ribeiro-Claro PJA. Probing pseudopolymorphic transitions in pharmaceutical solids using raman spectroscopy: hydration and dehydration of theophylline. J Pharm Sci 2007; 96: 1366–79.
69. Brittain HG. Fluorescence studies of the dehydration of cefadroxil monohydrate. J Pharm Sci 2007; 96: 2757–64.
70. Agbada CO, York P. Dehydration of theophylline monohydrate powder: effects of particle size and sample weight. Int J Pharm 1994; 106: 33–40.
71. Brittain HG. Evaluation of the Particle Size Distribution of Pharmaceutical Solids chapter 7 in Profiles of Drug Substances, Excipients, and Related Methodology, volume 31. In: Brittain HG, ed. Amsterdam: Elsevier Academic Press, 2004: 379–419.
72. Galwey AK, Laverty GM, Baranov NA, et al. The solid-state dehydration of lithium potassium tartrate monohydrate is completed in two rate processes. II. The nucleation and growth second reaction and dehydration mechanism. Phil Trans Royal Soc London 1994; A347: 139–56.
73. Galwey AK, Laverty GM, Baranov NA, et al. The solid-state dehydration of lithium potassium tartrate monohydrate is completed in two rate processes. I. The deceleratory diffusion controlled first reaction. Phil Trans Royal Soc London 1994; A347: 157–84.
74. Brittain HG, Fiese EF. Effects of pharmaceutical processing on drug polymorphs and solvates, Chapter 8, in Polymorphism in Pharmaceutical Solids, 1st edn. In: Brittain HG, ed. New York: Marcel Dekker, 1999: 331–61.
75. Brittain HG. Effects of mechanical processing on phase composition. J Pharm Sci 2002; 91: 1573–80.

76. Govindarajan R, Suryanarayanan R. Processing-induced phase transformations and their implications on pharmaceutical product quality, Chapter 13, in Polymorphism in the Pharmaceutical Industry. In: Hilfiker R, ed. Weinheim: Wiley-VCH, 2006: 333–64.
77. Hoelgaard A, Møller N. Hydrate formation of metonidazole benzoate in aqueous suspensions. Int J Pharm 1983; 15: 213–21.
78. Andersen FM, Bundgaard H. Inclusion complexation of metonidazole benzoate with β-cyclodextrin and its depression of anhydrate-hydrate transition in aqueous suspensions. Int J Pharm 1984; 19; 189–97.
79. Kesavan JG, Peck GE. Solid-state stability of theophylline anhydrous in theophylline anhydrous – polyvinylpyrrolidone physical mixtures. Drug Dev Indust Pharm 1996; 22: 189–99.
80. Tian F, Saville DJ, Gordon KC, et al. The influence of various excipients on the conversion kinetics of carbamazepine polymorphs in aqueous suspension. J Pharm Pharmacol 2007; 59: 193–201.
81. de Villiers MM, Mahlatji MD, van Tonder EC, et al. Comparison of the physical and stability of niclosamide crystal forms in aqueous versus nonaqueous suspensions. Drug Dev Ind Pharm 2004; 30: 581–92.
82. Li X, Zhi F, Hu Y. Investigation of excipient and processing on solid phase transformation and dissolution of ciprofloxacin. Int J Pharm 2007; 328: 177–82.
83. Otsuka M, Kaneniwa N. Effect of grinding on the degree of crystallinity of cephalexin powder. Chem Pharm Bull 1983; 31: 4489–95.
84. Otsuka M, Kaneniwa N. Effect of grinding on the physiochemical properties of cephalexin powder. Chem Pharm Bull 1984; 32: 1071–9.
85. Kitamura S, Miyamae A, Koda S, et al. Effect of grinding on the solid-state stability of cefixime trihydrate. Int J Pharm 1989; 56: 125–34.
86. Ketolainen J, Poso A, Viitasaari V, et al. Changes in solid-state structure of cyclophosphamide monohydrate induced by mechanical treatment and storage. Pharm Res 1995; 12: 299–304.
87. Yajima K, Okhira A, Hoshino M. Transformation of lactitol crystals and dehydration with grinding. Chem Pharm Bull 1997; 45: 1677–82.
88. Chawla G, Bansal AK. Effect of processing on celecoxib and its solvates. Pharm Dev Tech 2004; 9: 419–33.
89. Herman J, Remon JP, Visavarungroj N, et al. Formation of theophylline monohydrate during the pelletization of microcrystalline cellulose-anhydrous theophylline blends. Int J Pharm 1988; 42: 15–8.
90. Herman J, Visavarungroj N, Remon JP. Instability of drug release from anhydrous theophylline-microcrystalline cellulose formulations. Int J Pharm 1989; 55: 143–6.
91. Airaksinen S, Luukkonen P, Jørgensen A, et al. Effect of excipients on hydrate formation in wet masses containing theophylline. J Pharm Sci 2003; 92: 516–28.
92. Tantry JS, Tank J, Suryanarayanan R. Processing-induced phase transitions of theophylline: implications on the dissolution of theophylline tablets. J Pharm Sci 2007; 96: 1434–44.
93. Wikström H, Carroll WJ, Taylor LS. Manipulating theophylline monohydrate formation during high-shear wet granulation through improved understanding of the role of pharmaceutical excipients. Pharm Res 2008; 25: 923–35.
94. Räsänen E, Rantanen J, Jørgensen A, et al. Novel identification of pseudopolymorphic changes of theophylline during wet granulation using near infrared spectroscopy. J Pharm Sci 2001; 90: 389–96.
95. Jørgensen A, Rantanen J, Karjalainen M, et al. Hydrate formation during wet granulation studied by spectroscopic methods and multivariate analysis. Pharm Res 2002; 19: 1285–91.
96. Wikstrom H, Marsac PJ, Taylor LS. In-line monitoring of hydrate formation during wet granulation using raman spectroscopy. J Pharm Sci 2005; 94: 209–19.

97. Airaksinen S, Karjalainen M, Räsänen E, et al. Comparison of the effects of two drying methods on polymorphism of theophylline. Int J Pharm 2004; 276: 129–41.
98. Bauer J, Spanton S, Henry R, et al. Ritonavir: an extraordinary example of conformational polymorphism. Pharm Res 2001; 18: 859–66.
99. Ando H, Ishii M, Kayano M, et al. Effect of moisture on crystallization of theophylline in tablets. Drug Dev Indust Pharm 1992; 18: 453–67.
100. Ando H, Ishii M, Kayano M, et al. Effect of crystallization of theophylline on physical properties of tablets. Drug Dev Indust Pharm 1995; 21: 2227–37.
101. Adeyeye CM, Rowley J, Madu D, et al. Evaluation of crystallinity and drug release stability of directly compressed theophylline hydrophilic matrix tablets stored under varied moisture conditions. Int J Pharm 1995; 116: 65–75.
102. Otsuka M, Kaneniwa N, Kawakami K, et al. Effects of tableting pressure on hydration kinetics of theophylline anhydrate tablets. J Pharm Pharmacol 1991; 43: 226–31.
103. Otsuka M, Kaneniwa N, Otsuka K, et al. Effect of geometric factors on hydration kinetics of theophylline anhydrate tablets. J Pharm Sci 1992; 81: 1189–93.
104. Otsuka M, Kaneniwa N, Otsuka K, et al. Effect of tableting pressure and geometrical factor of tablet on dehydration kinetics of theophylline monohydrate tablets. Drug Dev Indust Pharm 1993; 19: 541–57.
105. Phadnis NV, Suryanarayanan R. Polymorphism in anhydrous theophylline – implications on the dissolution rate of theophylline tablets. J Pharm Sci 1997; 86: 1256–63.
106. Tantry JS, Tank J, Suryanarayanan R. Processing-induced phase transitions of theophylline – implications on the dissolution of theophylline tablets. J Pharm Sci 2007; 96: 1434–44.
107. Bauer JF, Dziki W, Quick JE. Role of an isomorphic desolvate in dissolution failures of an erythromycin tablet formulation. J Pharm Sci 1999; 88: 1222–7.
108. Römer M, Heinämäki J, Miroshnyk I, et al. Phase transformations of erythromycin a dihydrate during pelletization and drying. Eur J Pharm Biopharm 2007; 67: 246–52.

8 Pharmaceutical Co-crystals: A New Opportunity in Pharmaceutical Science for a Long-Known but Little-Studied Class of Compounds

Kapildev K. Arora and Michael J. Zaworotko

Department of Chemistry, University of South Florida, Tampa, Florida, U.S.A.

INTRODUCTION

Active pharmaceutical ingredients (APIs) are typically orally delivered as solid dosage forms that contain a single crystalline form of the API. This is an artifact of crystalline solids tending to be more stable and reproducible in the context of purification and processing when compared to other types of solid forms such as amorphous solids and solid solutions. Interestingly, the importance of crystal form selection during development of APIs has probably never been higher, and in the past five years pharmaceutical co-crystals have become part of a landscape that was previously occupied only by polymorphs, salts, and solvates/hydrates (Fig. 1) (1–4). Nevertheless, whereas there is a clear need for better understanding and control of crystalline forms in the context of drug development, the concepts of supramolecular synthesis (5–8) and crystal engineering (9–18) remain largely underexploited, and there are many basic questions about pharmaceutical co-crystals that remain unanswered, including their tendency to form polymorphs (19). Furthermore, a number of factors that are critically important in making an API viable as an oral dosage form remain difficult to predict or even control:

- *Dissolution rate and intrinsic solubility* of different crystal forms of an API are variable, and can strongly influence bioavailability. This is a particularly salient factor in light of the increasing prevalence of "BCS Class II" drugs (i.e., low-solubility, high-permeability APIs) (20).
- *Stability toward temperature and humidity* of an API is critically dependent upon crystal packing.
- *The unpredictability (i.e., lack of obviousness) of crystal structures* and physical properties means that there are opportunities and challenges in terms of obtaining and maintaining patent protection for an API.

In such a context, scientific developments that afford greater diversity in terms of the number of crystalline forms available for a given API and, therefore, an opportunity to customize the physical properties of an API with a process or clinical need, are obviously of profound relevance to the pharmaceutical industry. This chapter highlights how crystal engineering can afford such an opportunity to diversify the number of crystal forms known for an API, and to fine tune their physical properties of clinical relevance by reviewing the emerging field of pharmaceutical co-crystals. Particular emphasis is placed upon their history, their design, and

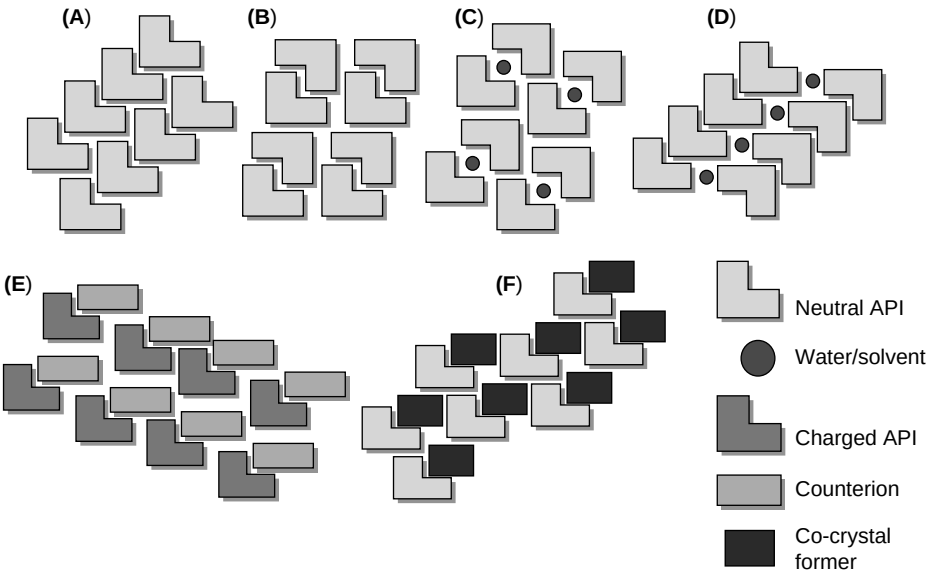

FIGURE 1 A schematic illustration of the classes of crystal form that might be exhibited by active pharmaceutical ingredients (APIs) (**A**) single component API; (**B**) polymorph of single component API; (**C**) hydrate or solvate of API; (**D**) polymorph of solvate or hydrate of API; (**E**) salt of API; (**F**) co-crystal of API.

their recent impact on preformulation strategies for development of dosage forms of APIs.

WHAT IS A CO-CRYSTAL?

That there is not yet a recognized definition of the term "co-crystal" has engendered a topical debate on the subject (21–27). In the Zaworotko research group we have been using the following operating definition: *A co-crystal is a stoichiometric multiple component crystal in which all components are solid under ambient conditions when in their pure form. These components consist of a target molecule or ion and a molecular co-crystal former(s) and when in a co-crystal they coexist at the molecular level within a single crystal* (28). This perspective has also been taken by Aakeröy (29). That all components are solids under ambient conditions has important practical considerations because synthesis of co-crystals can be achieved via solid-state methods, and chemists can execute a certain degree of control over the composition of a co-crystal because they can invoke molecular recognition, especially hydrogen bonding, during the selection of co-crystal formers. These features distinguish co-crystals from another broad group of multiple component compounds, solvates, and it should be noted that most molecular compounds are amenable to formation of co-crystals as they exist as solids under ambient conditions (30). An increasingly important subset of co-crystals is pharmaceutical co-crystals, that is, *co-crystals in which the target molecule or ion is an active pharmaceutical ingredient, API, and it bonds to the co-crystal former(s) through*

hydrogen bonds (31). The recent and rapid emergence of pharmaceutical co-crystals can be attributed to a number of factors including the following:

- *Design.* Our scientific understanding of the noncovalent forces that sustain molecular organic crystals, in particular co-crystals, has recently advanced to the extent that control over the stoichiometry and composition of co-crystals can be asserted, that is, by exploiting the strategy of crystal engineering (9–18,32–35) in the context of understanding and predicting hydrogen-bonding interactions. Crystal engineering is facilitated by the Cambridge Structural Database (CSD) (36), and the nature of APIs, that is, molecules or ions with exterior functional groups that engage in hydrogen bonding, makes all APIs inherently predisposed to formation of pharmaceutical co-crystals (31,37–39). This is not ordinarily the case for polymorphs and solvates for which high-throughput screening, which to a certain extent relies upon serendipity, tends to be relied upon rather than design, or for salts, which require an ionizable functional group.
- *Discovery.* That mechanochemistry can be utilized to synthesize co-crystals has been known since the first co-crystals were discovered in the 1840s by dry grinding (40), but it has only recently been realized and accepted that "solvent-drop" or "liquid-assisted" grinding are preferred methodologies (41–44). Indeed, it is fair to assert that co-crystals are readily accessible through solvent-free or solvent-reduced methods, although other techniques such as slurrying (45) and solution (46) are complementary.
- *Diversity.* It has become apparent that pharmaceutical co-crystals exhibit different physical properties compared to the pure crystal form(s) of APIs, that a given API might form co-crystals with dozens of co-crystal formers, and that some of these co-crystals might exhibit enhanced solubility (47–50) or stability to hydration (51). Therefore, pharmaceutical co-crystals represent an opportunity to significantly diversify the number of crystal forms of an API, and in turn, fine tune or even customize its physicochemical properties without the need for chemical (covalent) modification.
- *Development.* Whereas pharmaceutical co-crystals can be designed using crystal engineering strategies, this does not mean that details of their crystal structures or physical properties can be predicted before they have been measured. Therefore, there is no reason to assume that it will not be possible for pharmaceutical co-crystals of existing APIs to be patented as new crystal forms and, if they exhibit clinical advantages, then they are open to be developed as new drugs (52). This has potentially important implications for drug development because it abbreviates some aspects of drug development time lines and mitigates costs and risks related to discovery and toxicology of new APIs.
- *Delivery.* As mentioned earlier, being able to fine tune solubility can be a critical factor that influences the clinical performance of an API if its bioavailability is controlled by rate of dissolution. This is generally considered to be important for BCS Class II APIs (53), the most common classification (20,54–55) for the current generation of APIs.

History of Co-crystals

If one uses the criterion that all components of a co-crystal must be solid under ambient condition, then co-crystals represent a long known class of compounds.

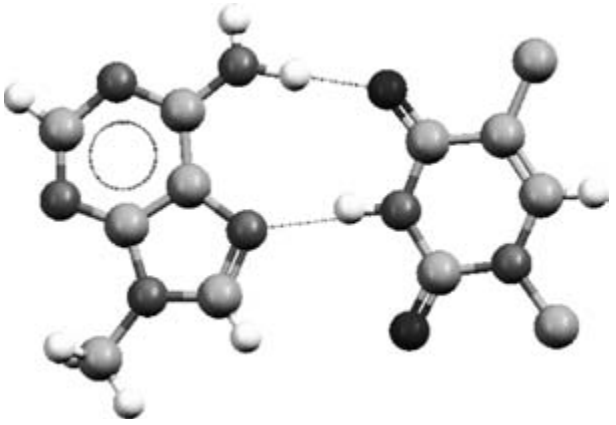

9-Me-adenine 1-Me-thymine

FIGURE 2 The Hoogsteen base-pairing that occurs in the 1:1 co-crystal of 9-methyladenine and 1-methylthymine.

The prototypal co-crystal is quinhydrone, which was reported in 1844 (40), and was further studied during the late 1800s (56). Co-crystals were subsequently described as *organic molecular compounds* (57). However, structural information on co-crystals was largely absent until the 1960s, when the term *complexes* was coined, and most recently, the term *heteromolecular crystals* was coined to describe a co-crystal formed between two hydrocarbons: cubane and fullerenes (58).

That complexes form readily via molecular recognition between complementary nucleic bases (59–60) is not just of relevance to biochemistry. Such interactions are key to understanding existing co-crystals and designing new co-crystals. Figure 2 illustrates the crystal structure of the co-crystal that forms when 9-methyladenine is crystallized in the presence of 1-methylthymine. This compound can be regarded as a prototypal co-crystal that illustrates how molecular recognition (i.e., hydrogen bonding) can indeed govern the existence and the composition of a co-crystal. It is therefore somewhat surprising, especially given the broad relevance and even application of interactions between nucleobases (61), that even today there is relatively little structural information on base pairing. Indeed, the August 2008 release of the CSD (36) contains structural information on 456,628 organic, metal–organic, and organometallic crystal structures and, if salts and solvates are excluded, there are less than 100 crystal structures involving nucleobases. Furthermore, there is essentially no information concerning the stability of base pairing in a competitive environment (i.e., when other hydrogen bonding groups are present). The situation with nucleobases represents a microcosm of co-crystals in general because there is not a great deal of structural information in the CSD on co-crystals. There are only two entries prior to 1960, and even today there are only ca. 2083 (0.46% of the CSD) hydrogen bonded co-crystals versus 50,019 hydrates (10.95% of the CSD). Therefore, it would be fair to summarize co-crystals as being a long known but little studied class of compounds.

History of Pharmaceutical Co-crystals

Pharmaceutical companies are always in search of a crystal form that is stable during handling, processing, and storage. However, such stability is not always at hand because APIs are prone to the formation of polymorphs that could be metastable or less soluble. Furthermore, it is at best difficult to predict beforehand how many polymorphs of an API might exist and under what experimental conditions these polymorphs will appear. The other commonly developed forms of active pharmaceutical ingredients include salts, solvates, hydrates and multi-component crystalline phases, pharmaceutical co-crystals, and of course, polymorphs can also occur with all these entities. The availability of multiple co-crystal formers for a given API is what makes pharmaceutical co-crystals special. The co-crystal former is a compound that is pharmaceutically acceptable or approved. The scope of available co-crystal formers is not yet set but even if it is limited to "generally regarded as safe" (GRAS) compounds or compounds that have already been approved by the FDA for use in formulation such as a "salt formers," there could be 100 or more possible co-crystal formers for an API. However, pharmaceutical co-crystals are not only of interest because they can afford crystal form diversity and improve physical properties of clinical relevance. They also represent an opportunity to patent and market clinically improved crystal forms of existing APIs, possibly as a new drug. It should therefore be unsurprising that much of the currently available literature on the subject is found in patents. Indeed, perhaps the earliest example of a pharmaceutical co-crystal was reported in a 1934 French patent that disclosed co-crystals of barbiturates with 4-oxy-5-nitropyridine, 2-ethoxy-5-acetaminopyridine, *N*-methyl-α-pyridone and α-aminopyridine (62). In 1995, Eli-Lilly patented complexes of cephalosporins and carbacephalosporins, a class of β-lactam antibiotics, with parabens and related compounds (63). Sildenafil citrate, the active pharmaceutical ingredient in Viagra®, a $1.5 bn/year drug that is used for the treatment of male erectile dysfunction and pulmonary arterial hypertension, is a BCS class II drug with low solubility. The co-crystal of sildenafil with acetyl salicylic acid (aspirin) was patented in 2007 (64), and it exhibits higher solubility under acidic conditions compared to the commercially available crystal form sildenafil citrate (Fig. 3). A more detailed discussion of this pharmaceutical co-crystal is presented in the section "Case Studies of Pharmaceutical Co-crystals."

In terms of the scientific literature there were few reports of pharmaceutical co-crystals until the past decade. However, Caira, demonstrated that "old" drugs such as sulfonamides could form co-crystals (65), and suggested their potential in pharmaceutical development. Pharmaceutical co-crystals have received much more attention in recent years, as evidenced by several review articles (28,31,38,39) and a feature article in the June 18th 2007 issue of *Chemical & Engineering News* (66). This cover story focused upon various aspects of active pharmaceutical ingredients including polymorphs, solvates, hydrates, pharmaceutical co-crystals, and patentability.

Design of Co-crystals

It is evident that many of the early co-crystals reported in the literature appear to have been the result of serendipity rather than design. However, the emergence of crystal engineering has changed this situation, and in recent years several groups have successfully exploited crystal engineering principles for design and synthesis of co-crystals, with particular emphasis upon exploitation of hydrogen bond

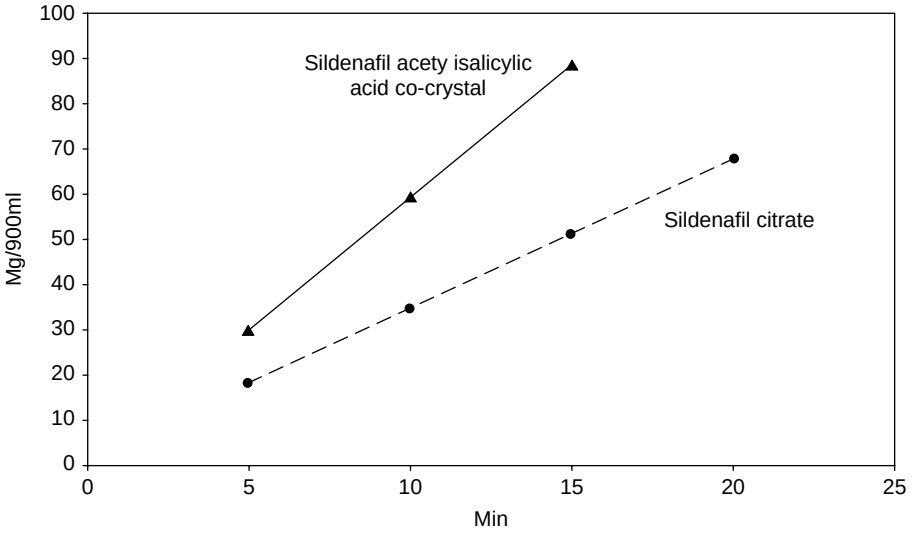

FIGURE 3 Intrinsic dissolution rate of the 1:1 sildenafil citrate:aspirin co-crystal versus sildenafil citrate.

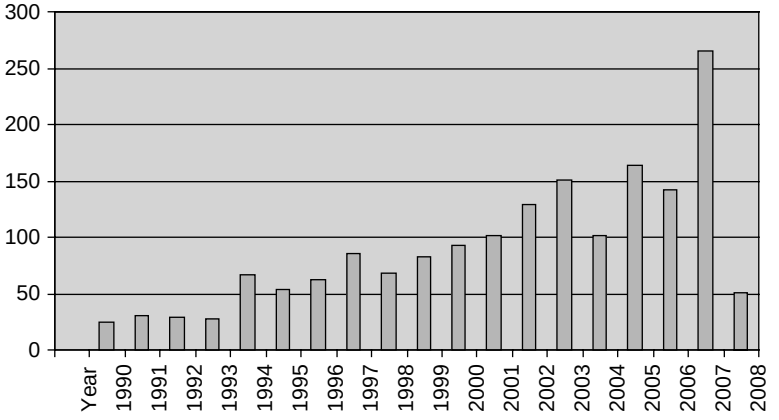

FIGURE 4 Hydrogen-bonded co-crystals formed between two or more compounds that are solid under ambient conditions deposited in the CSD from 1990 to 2008 [CSD Conquest 1.10 (August 2008 update)].

motifs (29,33,34,67–69). Figure 4 reveals that there has been a steady increase in the number of co-crystals reported from 1990–2008, a time period that coincided with the emergence of the paradigm of crystal engineering. Pepinsky introduced the concept of crystal engineering as far back as 1955 (32), and it was first implemented by Schmidt in the context of organic solid-state photochemical reactions (9). It is fair to assert that Etter popularized the term "co-crystal" in the 1980s (33), and at around

the same time Desiraju defined crystal engineering as "the understanding of intermolecular interactions in the context of crystal packing and in the utilization of such understanding in the design of new solids with desired physical and chemical properties" (11). Crystal engineering has now matured into a widely accepted paradigm for the preparation or supramolecular synthesis of new compounds. A salient feature of crystal engineered structures is that they are designed from first principles using the concepts of supramolecular chemistry and self-assembly (16,70–73).

A crystal engineering experiment typically involves CSD surveys followed by experimental work to prepare and characterize new compounds that are sustained by molecular recognition events or *supramolecular synthons* (5). A detailed understanding of the supramolecular chemistry of the functional groups present in a given molecule is a prerequisite for designing a co-crystal because it facilitates selection of appropriate co-crystal formers. However, when multiple functional groups are present in a molecule, the CSD rarely contains enough information to address the hierarchy of the possible supramolecular synthons. Furthermore, the role of solvent in nucleation of crystals and co-crystals remains poorly understood, and solvent can play a critical role in obtaining a particular co-crystal. However, the hierarchy of the supramolecular synthons that can occur for common functional groups such as carboxylic acids, amides, and alcohols with emphasis upon *supramolecular heterosynthons*, that is, non-covalent bonds between different but complementary functional groups (29,47,67b,e,f,74) is becoming better defined. Furthermore, it is becoming evident that such interactions are key to implementing a design strategy for co-crystals in which a target molecule forms co-crystals with a series of co-crystal formers that are carefully selected for their ability to form supramolecular heterosynthons with the target molecule.

How Are Co-crystals Prepared?

Synthesis of a co-crystal from solution might be thought of as counter-intuitive because crystallization is such an efficient and effective method of purification. However, if different molecules with complementary functional groups result in hydrogen bonds that are energetically more favorable than those between like molecules of either component, then co-crystals are likely to be thermodynamically (although not necessarily kinetically) favored. Supramolecular heterosynthons that seem to favor formation of co-crystals are exemplified by carboxylic acid–pyridine (29a,67b,e,75), carboxylic acid–amide (67g,76), and alcohol–pyridine (67f,77) (Fig. 5).

Single crystals involving these supramolecular heterosynthons are commonly discovered via slow evaporation from a solution containing stoichiometric amounts

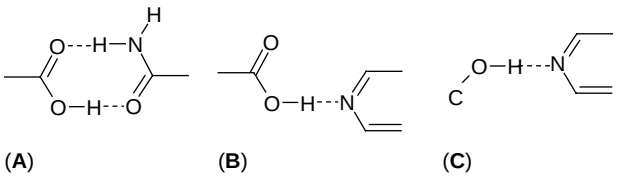

FIGURE 5 (**A**) Acid–amide, (**B**) acid–pyridine, and (**C**) alcohol–pyridine supramolecular heterosynthons.

of the components (co-crystal formers); however, sublimation, growth from the melt, slurrying, and grinding of two or more solid co-crystal formers in a ballmill are also suitable methodologies. Indeed, dry grinding was used as far back as the 19th century (40,56), and the recently developed technique of solvent-drop grinding, addition of a small amount of suitable solvent to the ground mixture to accelerate co-crystallization, appears to be a particularly fruitful methodology (41–44). The crystal form that is obtained is typically (45,74a), but not always, (4a) independent of the synthetic methodology. However, that co-crystals can often be prepared in a facile one-step manner using "green chemistry" approaches (78) does not mean that their synthesis and isolation is routine:

- As mentioned above, a detailed understanding of the supramolecular chemistry of the functional groups present in a given molecule is a prerequisite for designing a co-crystal because it facilitates selection of appropriate co-crystal formers. However, when multiple functional groups are present in a molecule the CSD rarely contains enough information to address the hierarchy of the multiple possible supramolecular synthons.
- Mismatched solubility between the components of a co-crystal can preclude their generation from solution if the co-crystal formers are present in a stoichiometric ratio.
- The role of solvent in nucleation of crystals and co-crystals remains poorly understood, and choice of solvent can be crucial in obtaining a particular co-crystal.

Why are Co-crystals Broadly Relevant?

Co-crystals are attractive to solid-state chemists because they offer opportunities to modify the composition of matter and the chemical and/or physical properties of a molecular species without the need to make or break covalent bonds. Thus far, there are several notable applications for co-crystals, all of which have direct or indirect relevance to pharmaceuticals:

- *Non-covalent derivatization* (79,80) was coined in the context of modifying the stability of Polaroid film (80,81). In this particular context, reduced solubility of a co-crystal reduced solubility and diffusion of an active ingredient. The net effect was greater stability and shelf life. Such a situation could be relevant to drug formulation, especially transdermal formulations, but has not to our knowledge yet been applied as such.
- *Solid-state synthesis*. Crystal engineering was first implemented in the context of photodimerization in the solid-state (9), and there are multiple examples of co-crystal formers having been used as templates to control the orientation of photoreactive molecules (Fig. 6) (67d,77c). Such a situation affords a level of control that cannot be achieved in the absence of the co-crystal former or in solution, and can lead to 100% yield and no waste. Co-crystals in which both co-crystal formers are reactants have also been exploited for solid-state synthesis. Etter et al. reported the first example of such a reaction in 1989 (82), a nucleophilic substitution reaction, and more recently, Cheney et al. have reported co-crystal controlled solid-state synthesis of imides, C^3S^3, via condensation of amines and acid anhydrides (83).
- *Chiral resolution.* Whereas spontaneous resolution of racemic mixtures into racemic conglomerates, "Pasteur crystallization," represents one of the best

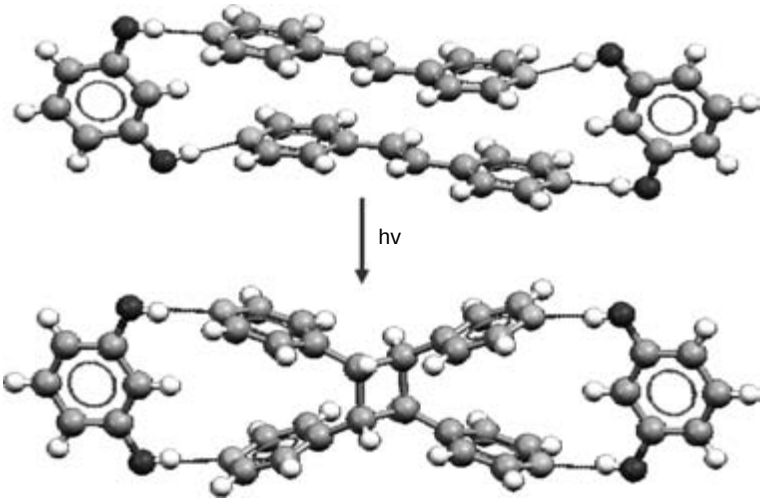

FIGURE 6 The co-crystal controlled (2+2) photodimerization of a resorcinol co-crystal of a substituted olefin.

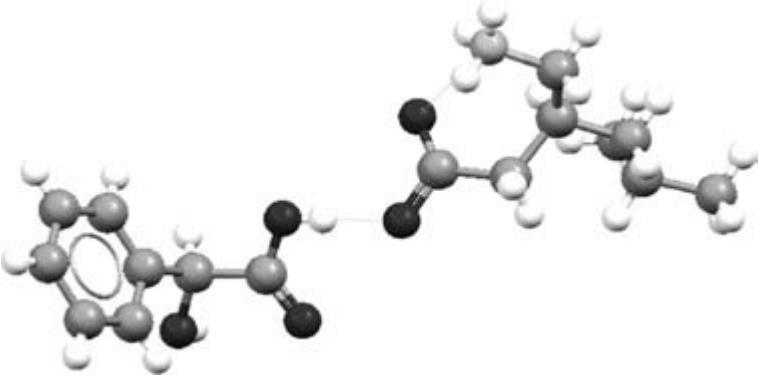

FIGURE 7 1:1 co-crystal of (*S*)-3-(ammonionmethyl)-5-methylhexanoate and (*S*)-mandelic acid.

known crystallization experiments (84), it is not the typical outcome to such an experiment. Rather, racemates are generally considered to be the outcome in around 90% of crystallizations of racemic mixtures (85). Chiral co-crystal formers offer an enhanced possibility of separating enantiomers by fractional crystallization because the resulting co-crystals are diastereomeric in nature. For example, (*S*)-mandelic acid has been used to resolve racemic pregabalin on an industrial scale (86), and it is able to resolve racemic 2-aminobutyric acid (87a) and phenylalanine (87b) through fractional crystallization. On the other hand, racemic mandelic acid can be resolved by (*S*)-alanine and *R*-cysteine (88). A diastereomeric co-crystal of (*S*)-mandelic acid is illustrated in Figure 7.

- Many of the crystal engineering principles and protocols that have been exploited for the generation of pharmaceutical co-crystals might also be invoked for the design and isolation of other types of co-crystal. In this context, molecular targets that would be particularly attractive and amenable for study because of technological opportunities and their hydrogen-bonding capabilities include the following: nucleobases (drug design and detection of oligonucleotides), molecules with high polarizability (new classes of NLO material), explosives/propellants (reformulation, enhanced thermal stability, enhanced properties), agrichemicals (reformulation, enhanced properties), renewable substrates (solid-state, polymer, and green chemistry), and volatile organics (air pollution).

CASE STUDIES OF PHARMACEUTICAL CO-CRYSTALS

An early example of studies that are related to pharmaceutical co-crystals was a series of studies conducted in the 1950s by Higuchi and his coworkers, who studied complex formation between macromolecules and certain pharmaceuticals (89). For example, complexes of polyvinylpyrrolidone (PVP) with sulfathiazole, procaine hydrochloride, sodium salicylate, benzylpenicillin, chloramphenicol, mandelic acid, caffeine, theophylline, and cortisone were isolated (89–90). However, these compounds would not be classified as pharmaceutical co-crystals according to the criteria applied herein. Whitesides et al. addressed the use of substituted barbituric acid, including barbital and melamine derivatives, to generate supramolecular "linear tape," "crinkled tape," and "rosette" motifs sustained by robust supramolecular synthons with three-point hydrogen bonding (34). Despite their success in co-crystal formation, the focus of these studies was not so much the physical properties of the resulting co-crystals but rather the supramolecular functionality of barbitals and their complementarity with melamine. Nevertheless, these studies illustrated the potential diversity of crystal forms that can exist for a particular API, as more than 60 co-crystals were structurally characterized in this series of studies. Herein we shall focus upon case studies that exemplify the formation of pharmaceutical co-crystals with altered physical properties of clinical relevance.

Pharmaceutical Co-crystals of Carbamazepine (Tegretol®)

Carbamazepine (CBZ) has been in use for over three decades for the treatment of epilepsy and trigeminal neuralgia even though it has multiple challenges associated with its oral drug delivery, including a small therapeutic window, autoinduction of metabolism, and dissolution limited bioavailability. A CSD analysis on CBZ reveals that it has 45 entries that include four fully characterized polymorphs (91), a dihydrate (92), 14 solvates (acetone, furfural, DMSO, trifluoroethanol, DMF, NMP, nitromethane, acetic acid, formic acid, butyric acid, formamide, trifluroacetic acid, tetrahydrofuran, *N*,*N*′-dimethyl acetamide) (93,96a), two ammonium salts (94), a solid solution with dihydrocarbamazepine (95), and 16 co-crystals including co-crystal hydrate/solvates and co-crystal polymorphs (67g,96). Most recently, Hilfiker et al. (97), at Solvias AG, identified three new forms and a dioxane solvate using high-throughput screening and Childs et al. (45) demonstrated the preparation of 27 unique solid phases of carbamazepine utilizing 18 carboxylic acids as co-crystal formers and four different screening methods. CBZ probably has more reported co-crystals than any other API, and some of these co-crystals have also been studied in terms of their dissolution and bioavailability. CBZ is therefore an

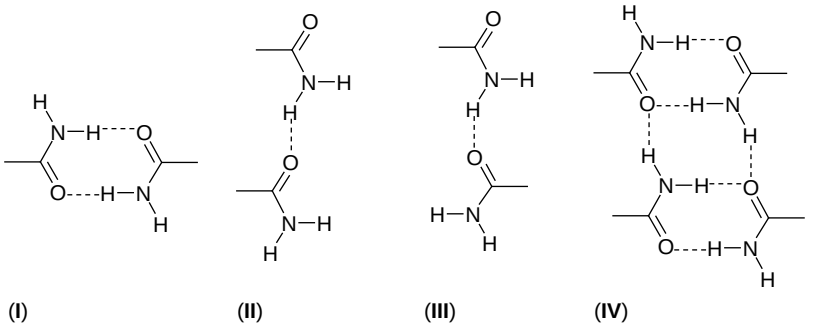

FIGURE 8 The four supramolecular homosynthons typically exhibited by primary amides.

appropriate starting point for case studies. CBZ exhibits a simple molecular structure in terms of its hydrogen-bonding capabilities because it possesses a single hydrogen-bonding moiety, a primary amide. The supramolecular homosynthons typically exhibited by primary amides are presented in Figure 8.

The primary amide dimer, I, like the carboxylic acid dimer, is a well-documented supramolecular homosynthon. A survey of the CSD reveals that there are 1,464 crystal structures that consist of at least one primary amide functional group, and I is exhibited in 589 of these structures even in the presence of competing hydrogen bond donors/acceptors. However, this represents a raw set of data, and a more refined search of the occurrence of this moiety in the absence of competing hydrogen bond donors and/or acceptors revealed 61 crystal structures that contain an amide moiety in the absence of other hydrogen bond donor or acceptor groups. Fifty-two (85 %) of these structures exhibit I and 9 (15 %) exhibit catemer motif II, suggesting that I is favored over II when no competing groups are present. Once the dimer is formed between the amide moiety, the anti-hydrogen atom either forms a hydrogen bond to an adjacent amide so as to form molecular tapes or sheets or it hydrogen bonds to a different functional group via a supramolecular heterosynthon. However, this is not the case with CBZ, in which the anti-hydrogen atom is not involved in hydrogen bonding, presumably due to steric constraints imposed by the azepine ring of CBZ (Fig. 9). That the CBZ dimer does not engage its peripheral hydrogen-bonding capabilities represents one avenue for crystal engineering and makes CBZ an excellent candidate for formation of pharmaceutical co-crystals. A second strategy involves breakage of the dimer motif and formation of supramolecular heterosynthons. Both strategies have been successful, and have afforded a number of CBZ co-crystals that exhibit improved physicochemical properties. Several of these co-crystals are described herein.

Carbamazepine:Nicotinamide 1:1 Co-crystal (1a) (96a)

In the pharmaceutical co-crystal of CBZ and nicotinamide, **1a**, CBZ molecules form supramolecular homosynthon **I** around a crystallographic inversion center. These CBZ dimers H-bond to the *syn* positions of nicotinamide amide groups, and the aromatic nitrogen atoms of the nicotinamide molecules are not involved in hydrogen bonding (Fig. 10).

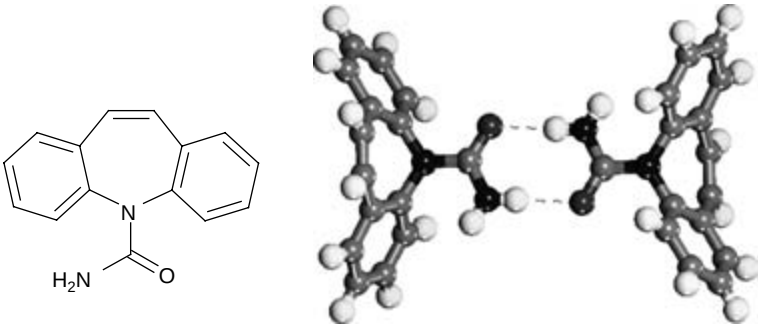

FIGURE 9 Molecular structure of carbamazepine (CBZ; *left side*) and the amide dimer (**I**; *right side*) that occurs in pure CBZ polymorphs.

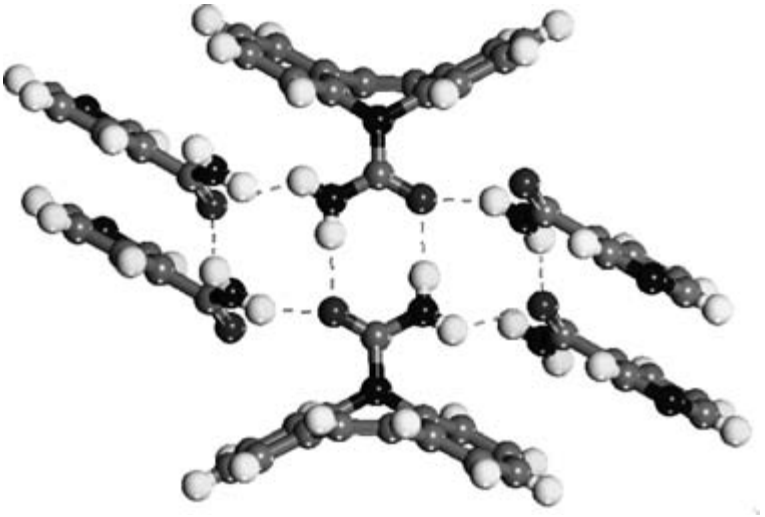

FIGURE 10 Illustration of the interaction between CBZ dimers and nicotinamide. Nicotinamide links the CBZ dimers by forming hydrogen-bonded tapes.

Rodriguez-Hornedo and coworkers have studied CBZ to develop an approach called reaction crystallization for the rapid formation of co-crystals in microscopic and macroscopic scales under ambient conditions (40). Reaction crystallization exploits solubility differences between the API, co-crystal former and co-crystal, and involves analysis of the ternary phase diagram. **1a** was selected as a model system to study the reaction pathways and kinetics in both aqueous and organic media. The phase solubility diagram for **1a** as a function of the concentration of co-crystal former in EtOH was reported, and the co-crystallization process of **1a** using anhydrous CBZ form III and nicotinamide in EtOH was monitored by Raman spectroscopy (Fig. 11). This formation of **1a** was the result of dissolution of

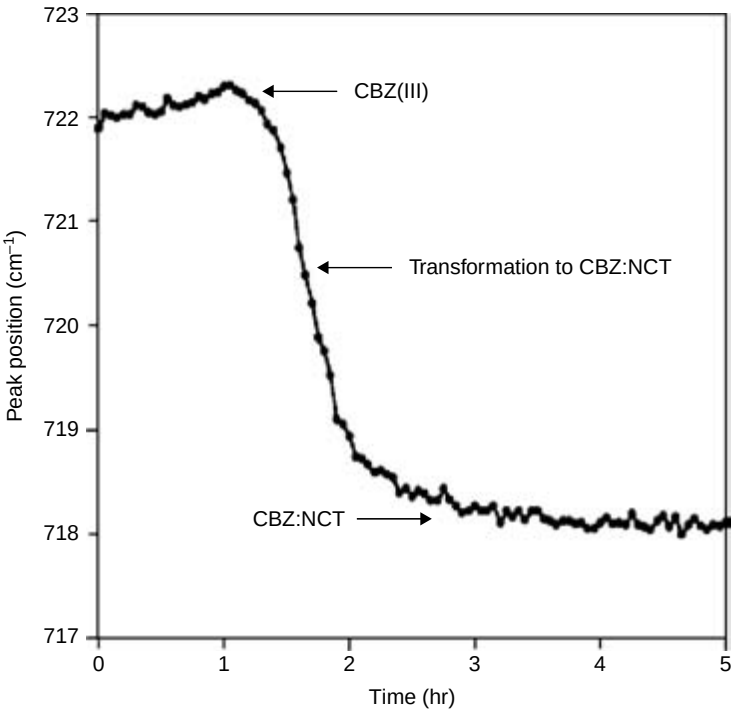

FIGURE 11 Raman peak position with respect to time showing the slurry conversion or transformation of solid phase CBZ(III) to co-crystal **1a** at 25°C after adding 0.16 M solution of nicotinamide in ethanol to CBZ(III).

anhydrous CBZ form III, leading to supersaturation of co-crystal **1a**. In situ preparation of **1a** using covered depression slides on a polarizing optical light and Raman microscope by addition of a few drops of solvent such as ethanol, ethyl acetate, or 2-propanol to the solid API and co-crystal former was also described. This study suggests broadly applicable screening methods for the preparation of co-crystals.

The factors that can control amorphous phase-mediated co-crystallization using **1a** as a model system were also addressed in order to evaluate whether amorphous phases lead to co-crystal formation and if there is a relation between temperature and crystallization pathways (98). The results suggested that amorphous phases can indeed generate co-crystals, and that temperature affects the crystallization pathways in significant ways. A new phase of **1a** (Form II) was identified during the thermal analysis.

Rodriguez-Hornedo et al. also developed a mathematical model to describe the solubility of co-crystals by taking into consideration the equilibria between co-crystal, co-crystal components, and solution complexes with **1a** as a model [Fig. 12(A)] (99). Nicotinamide solutions with varying concentrations were prepared using solvents such as ethanol, 2-propanol, or ethyl acetate [Fig. 12(B)]. The co-crystal solubility was measured by suspending co-crystals in these solutions, and it was observed that the solubility of co-crystal decreases with the increase in nicotinamide concentration.

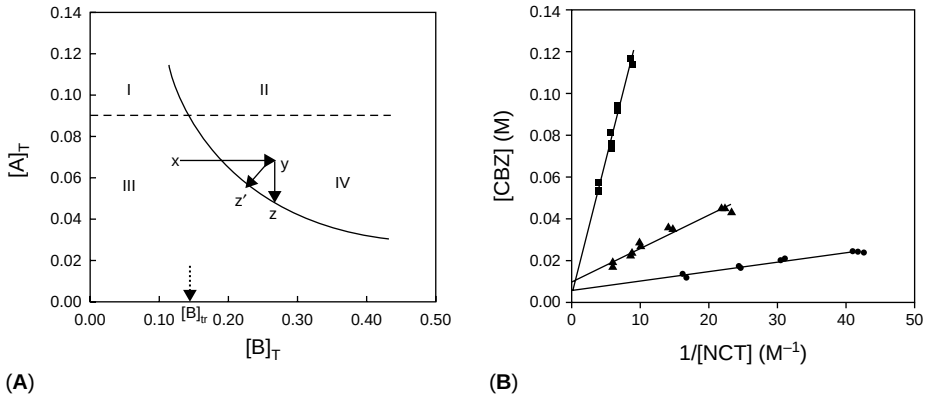

FIGURE 12 (**A**) Effect of co-crystal former B concentration on the solubility of co-crystal AB (*solid line*) and the solubility of single-component crystal (for instance API) A (*dashed line*). The transition of the co-crystal former concentration $[Br]_{tr}$ occurs when the solubility of A equals the solubility of AB. (**B**) Total CBZ concentration in equilibrium with co-crystal, **1a**, at 25°C as a function of the inverse total nicotinamide concentration in ethanol (*top*), 2-propanol (*middle*), and ethyl acetate (*bottom*), showing the linear dependence as per the prediction.

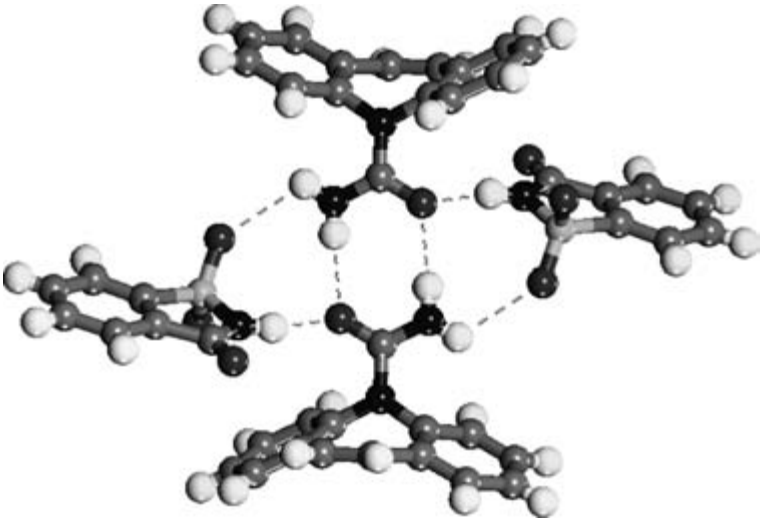

FIGURE 13 Illustration of the interactions between CBZ dimers and saccharin (**1b**).

Carbamazepine:Saccharin 1:1 Co-crystal (1b) (96a)

1b exhibits a structure similar to that of **1a** in that CBZ molecules form supramolecular homosynthon I related by inversion symmetry. The saccharin molecules serve as both hydrogen-bond donors (N–H moiety) and acceptors (S=O group) by forming hydrogen bonds with both the carbonyl and N–H moieties of CBZ. The carbonyl and the second S=O of saccharin molecules are not involved in hydrogen bonding (Fig. 13).

Almarsson and coworkers (50) studied **1b** with regard to multi-gram scale-up, propensity for crystal polymorphism, physical stability, in vitro dissolution, and oral bioavailability in comparison with the marketed form III of CBZ (Tegretol®). **1b** was scaled up to 30 g with a conventional cooling crystallization process from alcohol solution without seeding. The physical stability of the co-crystal **1b** was found to be superior compared to that of solvates of CBZ and similar to that of the marketed form of CBZ. It was also found that co-crystal **1b** is resistant to hydrate formation over a period of 15 days under direct exposure to ICH storage conditions. The oral pharmacokinetics (PK) of co-crystal **1b** were studied in dogs and compared with the marketed form of Tegretol®. The study was conducted at a dose equivalent to 200 mg of anhydrous CBZ, and was administered orally in a two-way cross-over design to four fasted beagle dogs. The study suggested that co-crystal could serve as a practical alternative to anhydrous CBZ in oral formulation because the bioavailability appears to be improved. Other benefits of the co-crystal **1b** include the following: (i) it has better solubility compared to the CBZ dihydrate or pure CBZ forms; (ii) it is stable in water for >24 hours; (iii) it has similar chemical stability compared to other forms of CBZ; (iv) although pure CBZ has four polymorphs co-crystal is not overtly polymorphic (1200 screen CRYSTALMAX experiments that include high-throughput screening, neat grinding, solvent-drop grinding with various solvents, and slurry conversion in different solvents). In general, if CBZ represents a microcosm of issues related to crystal form selection of APIs then pharmaceutical co-crystals could indeed represent a viable approach for improving the diversity and performance of API crystal forms.

Polymorphs of 1a and 1b (96d)

Utilization of functionalized cross-linked polymers as heteronuclei has been used as effective strategy for polymorph discovery of active pharmaceutical ingredients, and CBZ co-crystal polymorphs have been discovered using such an approach. Matzger and coworkers demonstrated that **1a** and **1b** are polymorphic when grown from solution in the presence of polymer heteronuclei. The single-crystal X-ray structure of form II of **1b** revealed the formation of supramolecular heterosynthons between CBZ and saccharin molecules as shown in Figure 14, in contrast to the amide–amide dimers observed in Form I.

Polymorphs of the Carbamazepine:Isonicotinamide 1:1 Co-crystal (1c) (100)

Horst and coworkers investigated two polymorphs of **1c** through a solvent-mediated transformation process in which a dry mixture of the pure components was suspended in ethanol. Co-crystals with two different morphologies and stabilities were obtained. Metastable, needle-like crystals (Form II) were obtained first followed by stable plate-like single crystals (Form I). Single-crystal X-ray structure determination revealed that Form I is constituted of chains of alternating dimers of CBZ and dimers of isonicotinamide, whereas the powder X-ray diffraction pattern of Form II suggests that it is isostructural to the known 1:1 stoichiometric co-crystal of CBZ and nicotinamide (i.e., centrosymmetric CBZ dimers hydrogen bonded to chains of nicotinamide molecules). Figure 15 compares the crystal structures of the two polymorphs of **1c**.

The ternary phase diagram reveals that excess isonicotinamide favors formation of co-crystals, whereas 1:1 stoichiometry affords either CBZ crystals or mixtures of CBZ and co-crystals. Generally APIs are slightly or moderately soluble

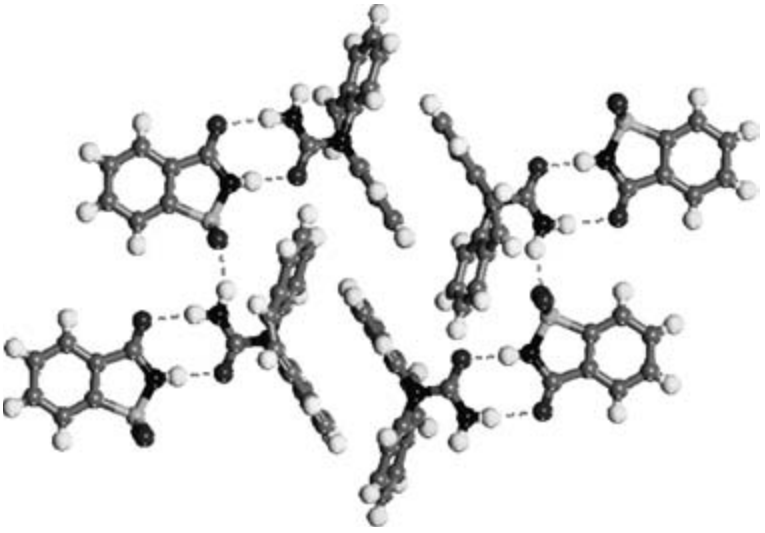

FIGURE 14 Molecular packing in CBZ:saccharin form II co-crystal.

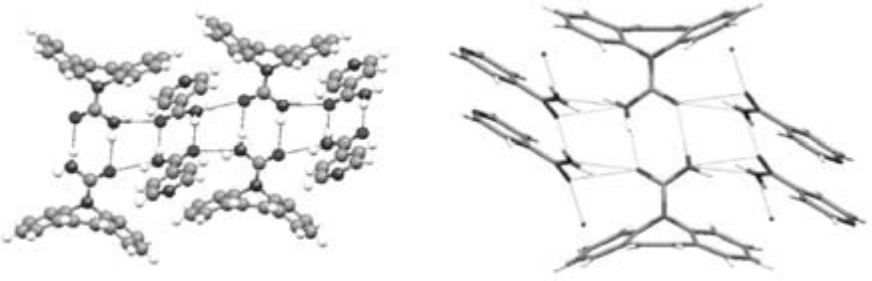

(**A**) (**B**)

FIGURE 15 Single-crystal X-ray structure of CBZ:isonicotinamide co-crystals: (**A**) Form I; (**B**) proposed structure of Form II, showing the principal hydrogen bonding synthons.

in solvents acceptable in pharmaceutical industries. Taking this into consideration a typical schematic phase diagram for an API (A), a co-crystal former (B), and solvent is as shown in Figure 16. This phase diagram highlights how solvent-mediated transformations such as reaction crystallization can offer a simple, flexible, and adaptable method for identifying the presence of co-crystal polymorphs.

Pharmaceutical Co-crystals of Fluoxetine Hydrochloride (Prozac®) (48)

Fluoxetine hydrochloride (fluoxetine HCl) is the API found in the common antidepressant drug Prozac®. It is a solid under ambient conditions, and only one crystalline phase is known. Childs et al. (48) demonstrated the preparation of co-crystals of

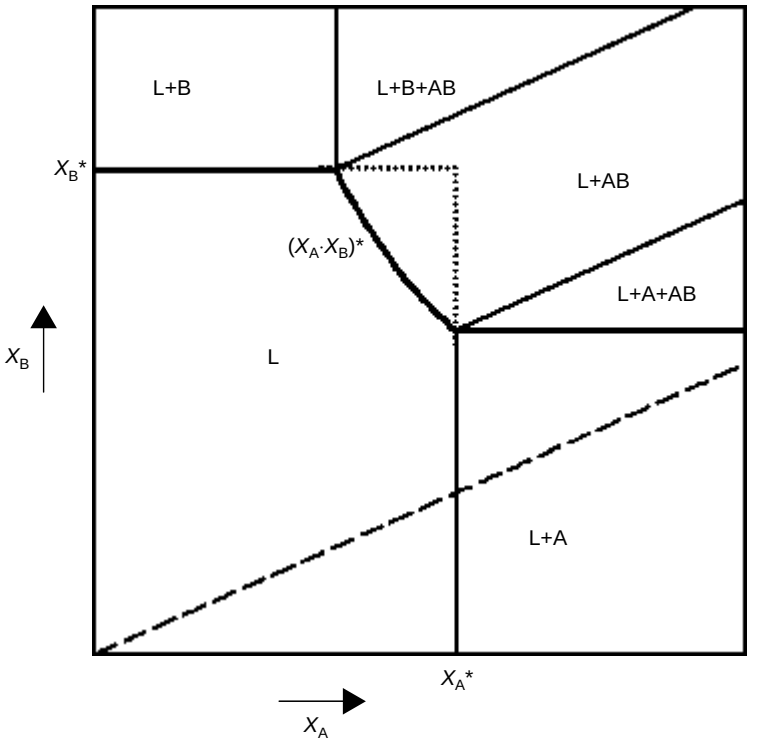

FIGURE 16 A schematic phase diagram for slightly soluble components and co-crystal. In the region L+AB co-crystallization occurs and ultimately equilibrium is reached between the AB co-crystal and the solution. In the regions L+A+AB and L+B+AB both the co-crystal and a pure component crystal phase are formed and the system moves to the three-phase equilibrium point where the two solubility lines meet. The dashed line indicates a 1:1 stoichiometric solution.

fluoxetine HCl using pharmaceutically acceptable carboxylic acids that form hydrogen bonds with the chloride ions. That chloride is perhaps the most preferred anion for generating salts of APIs makes co-crystals of fluoxetine HCl prototypal for many APIs. Fluoxetine HCl was co-crystallized with benzoic acid (1:1), succinic acid (2:1), and fumaric acid (2:1) via traditional evaporation techniques. For all three co-crystals, the carboxylic acid was found to hydrogen bond to the chloride ion, which in turn, interacted with the protonated amine. Powder dissolution experiments were carried out in water for the three novel co-crystals, resulting in a spread of dissolution profiles (Fig. 17). The fluoxetine HCl:benzoic acid co-crystal was found to have a decrease in aqueous solubility of ca. 50%, and the fluoxetine HCl:fumaric acid co-crystal had only a slight increase in aqueous solubility. However, the fluoxetine HCl:succinic acid co-crystal exhibited an approximately two-fold increase in aqueous solubility after only five minutes. The dissolution profile is consistent with the complex between succinic acid and fluoxetine HCl falling apart in solution to generate its pure components after about one hour. An intriguing aspect of this study is that by simply hydrogen bonding a hydrochloride salt of an API with similar

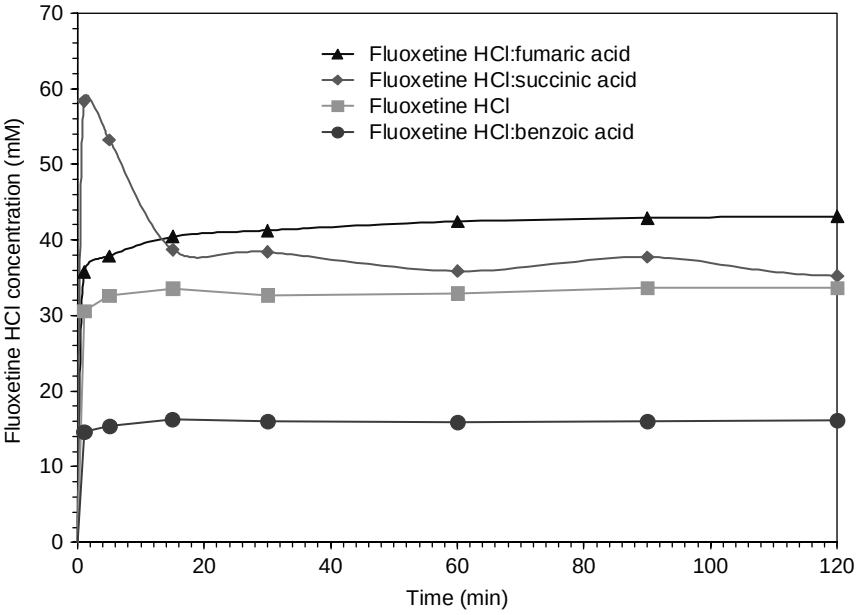

FIGURE 17 Powder dissolution profile for various forms of fluoxetine HCl illustrate how intrinsic dissolution can be modified through co-crystallization.

co-crystal formers one can generate distinctively different dissolution profiles in a manner that could not be achieved through, for example, particle size control.

Pharmaceutical Co-crystals of Itraconazole (Sporanox®) (47)

Itraconazole (Fig. 18) is an extremely water-insoluble (aqueous solubility is estimated at ~1 ng/mL at neutral pH and ~4 μg/mL at pH 1) (101) triazole antifungal agent. It is administered both orally and intravenously. The oral administration is formulated with the amorphous form of itraconazole coated on the surfaces of sucrose beads of 0.4–0.5-mm diameter and marketed as Sporanox® capsules. In addition, co-administration of acidified HP-β-cyclodextrin beverages with Sporanox® capsules is required to achieve the maximal absorption of the API, even though such a co-administration can cause diarrhea.

Intriguingly, a survey of the patent literature revealed that there is no data available on crystalline salts of itraconazole, even though salt formation using itraconazole and an acidic salt former would seem to be a logical approach to improve the absorption properties of the API. Crystalline phases of itraconazole can be crystal engineered by introduction of additional molecules to match hydrogen-bond donors and acceptors. The 2:1 co-crystal of itraconazole and succinic acid is shown in Figure 19, and it reveals hydrogen bonding via carboxylic acid-triazole supramolecular heterosynthons. The aqueous dissolution of itraconazole co-crystals was studied; two of the co-crystals exhibit a dissolution profile more akin to the Sporanox® form than to the crystalline form of pure API. In a further pharmacokinetic study of itraconazole co-crystals, it was revealed that the co-crystal formulation of the API

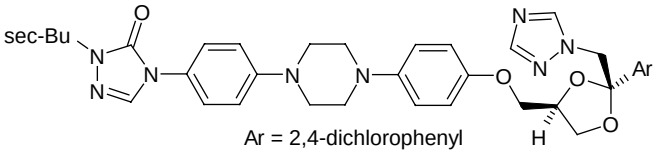

FIGURE 18 Molecular structure of itraconazole.

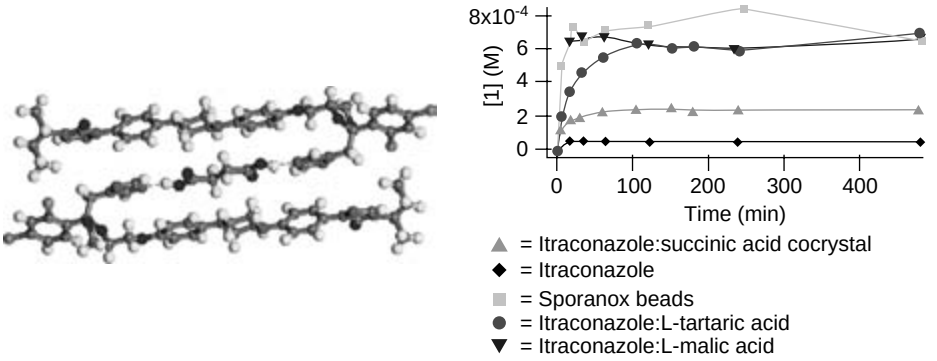

FIGURE 19 (**A**) The 2:1 co-crystal of itraconazole and succinic acid forms a trimeric unit. (**B**) Dissolution profiles in 0.1 N HCl at 25°C.

gives similar oral bioavailability to the Sporanox® form in the animal trial using a dog model.

Pharmaceutical Co-crystals of Sildenafil (Viagra®) (64)

Sildenafil, 1-[[3-(6,7-dihydro-1-methyl-7-oxo-3-propyl-1*H*-pyrazolo[4-3-*d*]pyrimidin-5-yl)-4-ethoxyphenyl]sulphonyl]-4-methylpiperazine [Fig. 20(A)] is a drug utilized in the treatment of a number of disorders including pulmonary arterial hypertension, stable, unstable, and variant angina, congestive heart failure, atherosclerosis, conditions of reduced blood vessel patency, peripheral vascular disease, bronchitis, chronic and allergic asthama, as well as male erectile dysfunction and female sexual disorders. Sildenafil is available as a citrate salt form, and has been commercially developed and marketed by Pfizer under the trademark Viagra®. Although it is available as a salt form it is moderately soluble in water and thus exhibits erratic or incomplete absorption, low bioavailability, and slow onset of action. It has been observed that sildenafil in a pharmaceutical co-crystal form could provide an improved solubility of the API under acidic conditions. In addition, such an improvement of solubility of sildenafil could be particularly advantageous for its orally administrable formulation. Sildenafil has been successfully co-crystallized with acetylsalicylic acid (1:1 molar ratio) by slurry or under reflux conditions. The crystal structure of the co-crystal of sildenafil and acetylsalicylic acid has been determined

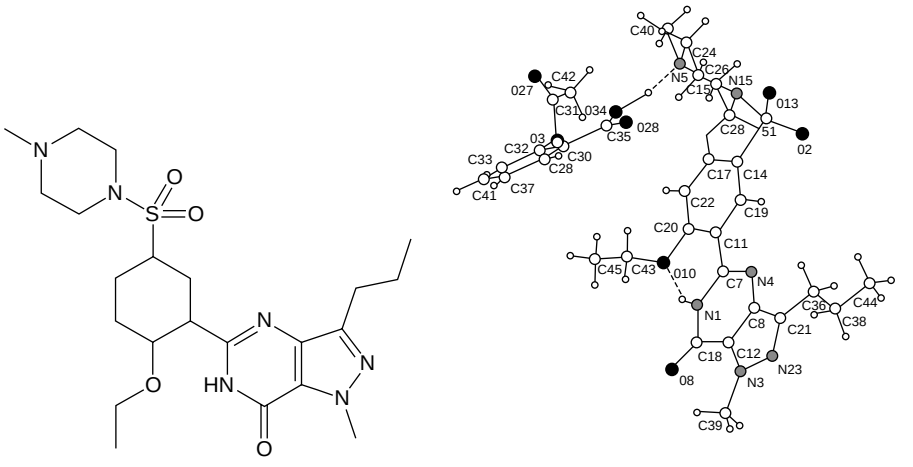

FIGURE 20 (**A**) Molecular structure of sildenafil. (**B**) Crystal structure of 1:1 sildenafil:acetyl salicylic acid co-crystal.

by single-crystal X-ray diffraction [Fig. 20(B)], and in addition, the composition of matter was confirmed by powder X-ray diffraction and infrared spectrometry. The melting point of the co-crystal is approximately 143°C, and it remains thermodynamically stable up to ca. 165°C. An intrinsic dissolution study in simulated gastric body fluid (pH = 1.2) shows that the co-crystal exhibits an intrinsic dissolution rate (IDR) of ca. 11.75 $mg \cdot min^{-1}\ cm^{-2}$ versus 6.64 $mg \cdot min^{-1}\ cm^{-2}$ for sildenafil citrate under the same conditions.

Pharmaceutical Co-crystals of 2-[4-(4-Chloro-2-Fluorophenoxy)Phenyl] Pyrimidine-4-Carboxamide (SCB), a Sodium Channel Blocker (49)

2-[4-(4-Chloro-2-fluorophenoxy)phenyl]pyrimidine-4-carboxamide (SCB) is a BCS class II drug that belongs to a class of sodium channel blockers and was developed as a potential drug candidate for the treatment or prevention of surgical, chronic, and neuropathic pain. SCB was observed to exhibit low in vitro dissolution, and upon oral administration to dogs it showed low in vivo plasma concentration. Efforts to increase the bioavailability of SCB by forming salts, solvates, hydrates, polymorphs, or amorphous material failed to produce a viable solid form for drug formulations. Hence, co-crystallization was used to improve the pharmaceutical properties of SCB. Co-crystal screening was carried out employing two methods: melt crystallization or highly saturated solution. A total of 26 carboxylic acids were screened out of which a co-crystal containing SCB and glutaric acid in 1:1 molecular ratio was identified and characterized by single-crystal X-ray analysis (Fig. 21), **5**. **5** can be scaled up in gram quantities, is non-hygroscopic, and chemically and physically stable to thermal stress.

The intrinsic dissolution rate profile suggests that the co-crystal increases the in vitro rate of dissolution by 18 times when compared to the pure API. Single-dose

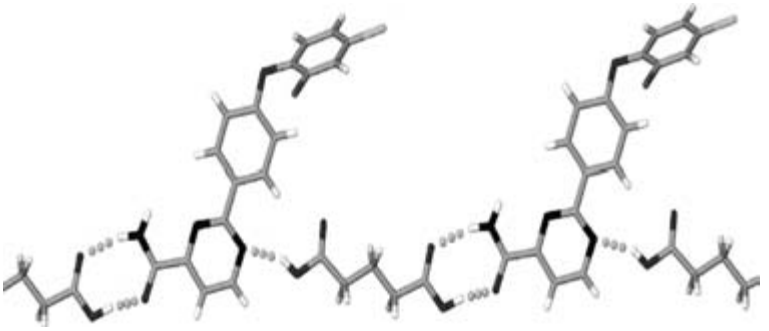

FIGURE 21 Hydrogen bonding in co-crystal **5** showing the interactions between the carboxylic acid groups of glutaric acid molecules and the amide and pyridine groups of the drug molecules, SCB.

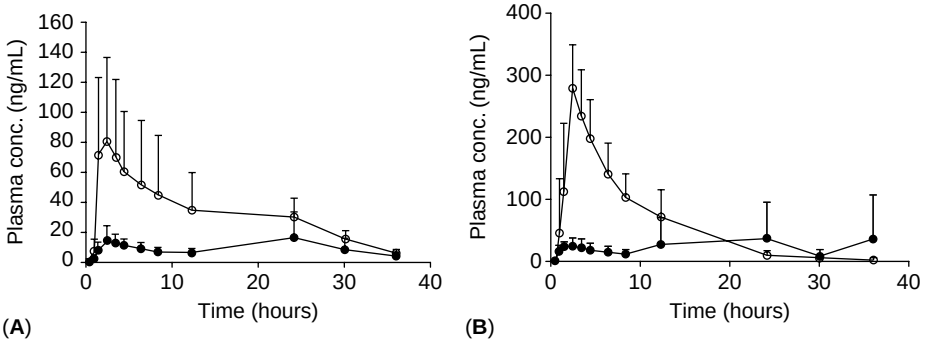

FIGURE 22 Dog plasma concentration with time for (**A**) 5 mg/kg dosing and (**B**) 50 mg/kg of API, SCB (solid circles) and co-crystal (open circles). Error bars show +1 standard deviation.

bioavailability studies on dogs confirmed that the co-crystal improved the plasma area under the curve (AUC) values by three times at both low (5 mg/kg) and high dose (50 mg/kg) as shown in Figure 22.

Pharmaceutical Co-crystals of "AMG 517" (102)

Transient receptor potential vanilloid 1 or TRPV1 is a nonselective ligand-gated cation channel that can be activated by a wide variety of external and internal stimuli such as a temperature greater than 43°C, an acidic medium or a neurotransmitter such as anandamide, or the capsaicin-active components in chilli pepper. TRPV1 receptors are found in central and peripheral nervous systems, and they are responsible for transmission and modulation of pain along with the integration of diverse painful stimuli. AMG 517 is a transient receptor potential vanilloid 1 antagonist that was developed by Amgen for the treatment of acute and chronic pain. The free base of AMG 517 is associated with problems such as insolubility in water and buffers at physiological pH. AMG 517 has three isolated forms: a monohydrate (stable for at

least three years at ambient temperature and humidity), a metastable nonsolvated form, and a stable free base. In addition numerous salts and solvates have been prepared, isolated, and characterized. However, the salts disproportionate in aqueous medium and convert into the hydrated form of AMG 517. Bak and coworkers (102) investigated 10 co-crystals of AMG 517 with the following carboxylic acids: sorbic acid, benzoic acid, *trans*-cinnamic acid, 2,5-dihydroxybenzoic acid, glutaric acid, glycolic acid, *trans*-2-hexanoic acid, 2-hydroxycaproic acid, L(+)-lactic acid, and L(+)-tartaric acid. The hydrogen bonding in two co-crystals is as shown in Figure 23. The physicochemical properties such as particle size, solubility, stability, hygroscopicity, thermal behavior, and structural characteristics of these co-crystals were studied in detail.

Solubility experiments on the AMG 517:sorbic acid co-crystal showed that the co-crystal has better initial solubility compared to AMG 517; however, it converts back to a form of the free base hydrate after prolonged slurrying in FaSIF (fasted simulated intestinal fluid, pH 6.8). Pharmacokinetic studies of the co-crystal in rats using 10% (w/v) Pluronic F1081 in OraPlus1 suspensions revealed that a 30 mg/kg dose in suspension had comparable exposure to a 500 mg/kg dose of the free base. Further solubility measurements on AMG 517 co-crystals with glutaric acid, glycolic acid, *trans*-2-hexanoic acid, lactic acid, and benzoic acid showed that the co-crystals reach a maximum solubility within 1–2 hours and, similar to the sorbic acid co-crystal, the dissolution profile indicates conversion of the co-crystals to AMG 517 hydrate.

Correlations between the melting point of the co-crystal formers and the co-crystals and between the melting point and solubility of the co-crystals were also addressed. The melting point of all co-crystals was between the co-crystal formers and AMG 517, and linear regression indicated that the melting points of co-crystal formers and co-crystals are directly proportional with 78% correlation. However, the melting point and solubility of the co-crystals are related with only 55% correlation.

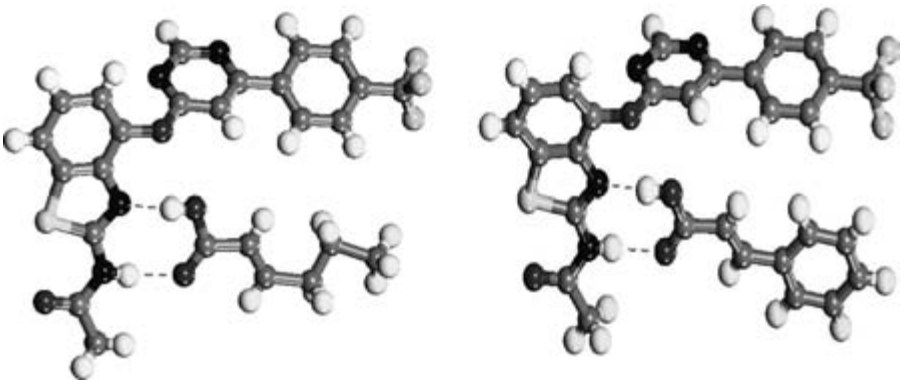

FIGURE 23 Molecular recognition between AMG 517 and (**A**) *trans*-cinnamic acid (**B**) *trans*-2-hexanoic acid.

Co-crystals of Melamine and Cyanuric acid (103)

In early 2007 there was a major pet food recall by the FDA based on the receipt of numerous complaints regarding the deaths of animals after ingestion of a variety of pet food products. It was reported that the majority of these deaths were associated with acute renal failure in these animals. Melamine, 2,4,6-triamino-1,3,5 triazine, was the primary suspect for contamination in the tainted pet food products because melamine had been intentionally added to raise the apparent protein content in the pet food. However, melamine is considered relatively nontoxic [LD_{50} values of 3100 mg/kg (rat male) and 3900 mg/kg (rat female)] and oral administration of 125 mg/kg body weight of melamine to dogs leads to diuretic effects but is not fatal. Indeed, the quantity of melamine observed in the pet food was not at the lethal dosage. In the course of the pet food recall investigation, cyanuric acid, another relatively nontoxic compound, was also identified in the pet food as a co-contaminant. Although melamine and cyanuric acid are relatively safe individually, no data could be found in the literature that determines the potential toxicity of melamine and cyanuric acid in combination. From the crystal engineering viewpoint, melamine and cyanuric acid (1:1 molar ratio) form an extensive two-dimensional networks in the solid state based on robust three-point molecular recognition (Fig. 24) and

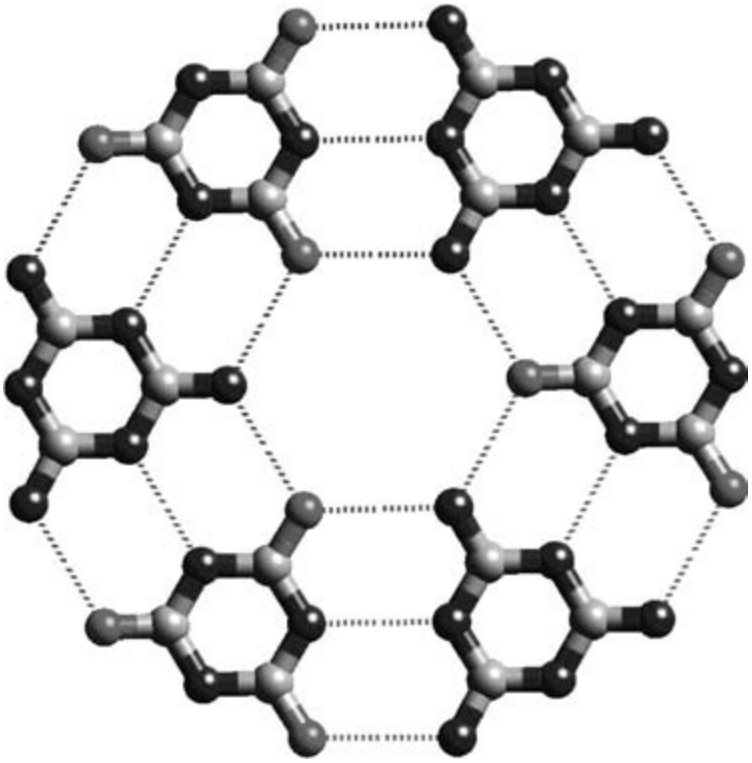

FIGURE 24 The rosette network formed between melamine and cyanuric acid.

the resulting melamine:cyanuric acid co-crystal is, perhaps unsurprisingly, highly insoluble in water.

Puschner et al. investigated the toxicity of melamine and cyanuric acid individually and also in combination when administered to cats, and demonstrated clinical pathologic changes, gross or histologic lesions, associated with the contaminants in the recalled pet food. The oral administration of 181 mg/kg body weight of melamine alone at 0.5% and 1% of their diet to three cats for 11 days did not show any evidence of renal failure. Similar results were obtained on administration of cyanuric acid alone in the diet at 0.2%, 0.5%, and 1% dosage respectively. However, it was observed that a single oral exposure of cats to the combination of melamine and cyanuric acid at a dosage as low as 32 mg/kg body weight leads to acute renal failure. A study conducted at the Bergh Memorial Animal Hospital in New York revealed that co-crystals blocked the tubes leading from the kidneys to the bladder in one cat. Thus, it seems clear that the formation of a low solubility co-crystal of melamine and cyanuric acid is responsible for these incidents. This case study of melamine:cyanuric acid co-crystals might be the first example of co-crystals altering clinically relevant physical properties in a negative manner.

POLYMORPHISM IN CO-CRYSTALS AND PHARMACEUTICAL CO-CRYSTALS

Polymorphism (19,104–105), the existence of different crystal forms of the same compound, is long recognized from a scientific perspective. Mitscherlich introduced the concept of isomorphism, an important development in structural chemistry, in 1819 (106), and in 1932 Wöhler and Liebig (107) described dimorphism of benzamide, perhaps the first example of a polymorphic organic substance. That polymorphism can impact physical properties is perhaps best exemplified in elements, where it is known as "allotropy," as exemplified by carbon, which exhibits three crystal forms with dramatically different physical properties: graphite, diamond, and fullerenes. The phenomenon of polymorphism is now well appreciated both academically and industrially because it impacts preparation and formulation of specialty chemicals, pharmaceuticals, dyes, explosives, and foods (108). McCrone's definition (109) of polymorphism, that is, "a solid crystalline phase of a given compound resulting from the possibility of at least two different arrangements of the molecules of that compound in the solid state," is apt in the context of this chapter's focus upon structural chemistry.

Crystallization of polymorphs is governed by a combination of thermodynamic and kinetic factors (110). The occurrence of polymorphs often follows Ostwald's rule of stages (111), which states that the meta-stable form is often obtained first and the stable form crystallizes subsequently. Depending upon the arrangement of molecules and/or conformation adopted by the functional groups present in the molecule, polymorphs may be classified into several categories: that is, conformational polymorphs (112), concomitant polymorphs (107,113) structural polymorphs (114), and configurational polymorphs (115). Nevertheless, a CSD analysis tabulated in Table 1 reveals that polymorphism is not prevalent in either single-component crystals (1,882/134,086) or in co-crystals (40/2,083).

This chapter focuses upon pharmaceutical co-crystals, and we present herein a structural analysis of selected co-crystals that exhibit polymorphism in addition to the polymorphic co-crystals of CBZ discussed earlier in the section "Pharmaceutical Co-crystals of Carbamzepine (Tegretol®)."

TABLE 1 Cambridge Structural Database Statistics of Polymorphic Single and Multicomponent Crystal Structures

	Number of entries	Percentage of organic structures
Organic crystal structures	186,053[a]	100[d]
Single-component molecular organic structures	134,086	72.1[d]
Single-component polymorphic structures	1,882[b]	1.4[e]
Hydrates	13,843	7.4[d]
Co-crystals	2,083[c]	1.1[d]
Polymorphic co-crystals	40	1.9[f]

CSD August 2008 update, 456,628 entries.
[a]Structures containing Na, Li, K, As were excluded.
[b]Only one refcode was counted for each polymorphic compound.
[c]Co-crystals sustained by strong hydrogen bonds.
[d]Percentages with respect to organic crystal structures only.
[e,f]Percentages with respect to 134,086 and 2083 sub-totals, respectively.

1:1 Co-crystals of Caffeine and Glutaric Acid (EXUQUJ–EXUQUJ01)

The crystal structures of the polymorphic forms of 1:1 co-crystals of caffeine and glutaric acid were described by Jones et al. (42) in 2004. Both crystal forms, rods and blocks, were obtained concomitantly from a solution containing a 1.3:1 ratio of caffeine and glutaric acid, respectively. The "rods" are monoclinic (Form I), whereas the "blocks" are triclinic (Form II). Both Forms I and II exhibit identical secondary architecture because they form sheets resulting from hydrogen bonds (O–H···N) between one of the –COOH moieties of glutaric acid and the free aromatic nitrogen atom (N_{arom}) of caffeine. The two polymorphs exhibit differences in the torsion angle of the methylene carbon atoms of glutaric acid (Fig. 25). The authors noted how solvent-drop grinding could be used to afford a co-crystal polymorph exclusively: dry grinding and solvent-drop grinding using nonpolar solvents such as *n*-hexane, cyclohexane, or heptane yielded only Form I; solvent-drop grinding using polar solvents such as chloroform, dichloromethane, acetonitrile, and water produced only Form II.

2:1 Co-crystals of 4-Cyanopyridine and 4,4′-Biphenol (TEHNAW–TEHNAW01)

Zaworotko et al. (116) reported that crystallization of a 2:1 ratio of 4-cyanopyridine and 4,4′-biphenol in methanol:ethyl acetate afforded concomitant polymorphs of the 2:1 co-crystal of 4-cyanopyridine and 4,4′-biphenol. The single-crystal X-ray structures revealed that Form I (irregular hexagonal plates) and Form II (parallelepiped plates) exhibit conformational differences in the 4,4′-biphenol molecules (Fig. 26), but O–H···N supramolecular heterosynthon sustain both forms, suggesting that O–H···N(pyridine) supramolecular heterosynthons are favored over competing O–H···N(cyano) supramolecular heterosynthons. Form I crystallized in $C2/c$ with half a 4,4′-biphenol molecule and one 4-cyanopyridine molecule in the asymmetric unit, whereas Form II crystallized in $P2_1/n$ with four 4-cyanopyridine and two 4,4′-biphenol molecules in the asymmetric unit. Form I can be obtained by dissolving Form II in MeOH, EtOAc, or acetone where Form II can be obtained by solvent drop grinding of the starting materials or Form I.

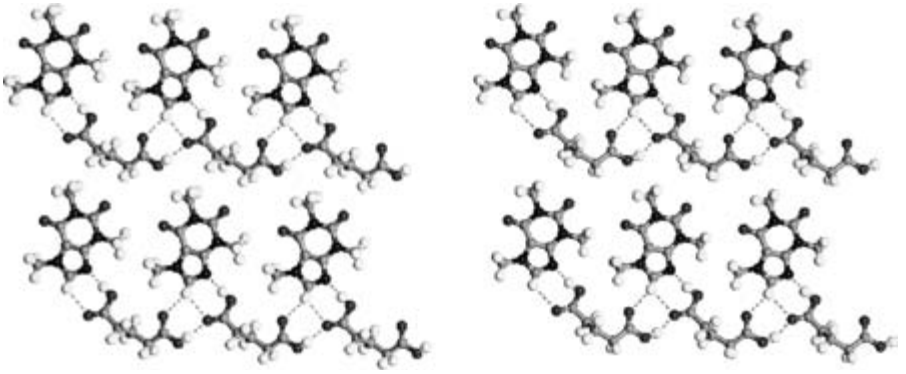

Form I Form II

FIGURE 25 Crystal structures of monoclinic (Form I) and triclinic (Form II) forms of caffeine:glutaric acid co-crystals. Although the crystal packing is similar there is a difference in the torsion angle of the methylene carbon atoms of glutaric acid.

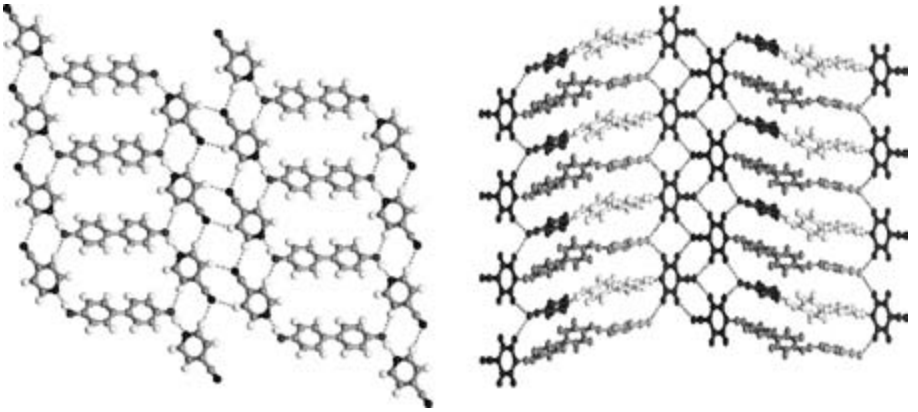

Form I Form II

FIGURE 26 Crystal packing of Form I and Form II of the 2:1 co-crystal of 4-cyanopyridine: 4,4′-biphenol.

1:1 Co-crystals of Hydroquinone/*p*-Benzoquinone (QUIDON–QUIDON02) (117–119)

Quinhydrone is a 1:1 co-crystal of hydroquinone and *p*-benzoquinone. It is the prototypal co-crystal that was first reported in 1844, and it is also the earliest entry of a co-crystal in the CSD for which atomic coordinates are available. Quinhydrone exists in two polymorphic crystal forms: monoclinic and triclinic. The monoclinic form ($P2_1/c$ space group, QUIDON02) was reported by Matsuda et al. in 1958.

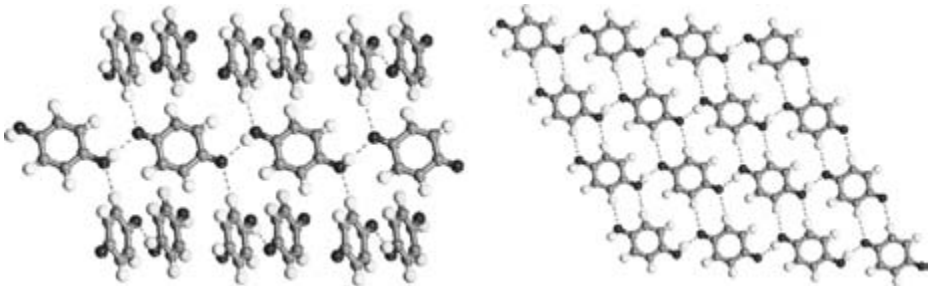

(**A**) (**B**)

FIGURE 27 Crystal structures of the (**A**) monoclinic and (**B**) triclinic forms of quinhydrone.

The crystal structure reveals that both hydroquinone and *p*-benzoquinone molecules reside on an inversion center generating linear tapes through O–H···O and C–H···O hydrogen bonds. Such tapes are further connected to generate a 3D network as illustrated in Figure 27(A). In the triclinic polymorph (*P*-1 space group, QUIDON), H-bonded tapes are also formed; however, the tapes are packed parallel to generate molecular sheets [Fig. 27(B)]. The crystal packing of Forms I and II is therefore different although the supramolecular synthons remain the same.

Polymorphism in the 1:1 Co-crystal of *N*,*N*-Bis(4-bromophenyl)melamine/5,5-Diethylbarbituric acid (JICTUK01–JICTUK10)

In 1994, Whitesides and coworkers (34) reported polymorphism in 1:1 co-crystals of *N*,*N-bis*(4-bromophenyl) melamine and 5,5-diethylbarbituric acid. Form I crystallized in a monoclinic crystal system ($P2_1/n$, JICTUK01), whereas Form II crystallized in a triclinic system (*P*-1, JICTUK10). Both polymorphs form linear tapes through three-point molecular recognition involving N–H···O and N–H···N hydrogen bonds. Once again, the same supramolecular synthons are observed in both crystal forms; however, the rotation of the phenyl ring along the C–N bond in Form II generates a different arrangement of linear tapes. (Fig. 28).

1:1 Co-crystals of Oxalic Acid and Iso-nicotinamide (ULAWAF01–ULAWAF02)

The crystal structures of the polymorphs of the 1:2 co-crystal of oxalic acid and iso-nicotinamide were reported by Wilson and coworkers in 2007 (120). The co-crystal exist in two forms: Form I crystallizes in the monoclinic space group $C2/c$ as earlier reported by Nangia and coworkers (75b), whereas Form II crystallizes in the triclinic space group *P*-1. These polymorphs can be obtained concomitantly from 1:1 ethanol:water. The fundamental difference between the two polymorphs is a *cis*/*trans* isomerism observed in the hydroxyl groups of oxalic acid. Form I exhibits the *cis*-configuration, whereas Form II contains the *trans*-configuration. The oxalic acid and iso-nicotinamide molecules form trimeric units sustained through O–H···N hydrogen bonds. These trimeric units are, in turn, connected through centrosymmetric amide dimers between iso-nicotinamide molecules, and thereby forming tapes that H-bond to form sheets. The overall crystal packing in both Form I and Form II can be described as stacked sheets (Fig. 29).

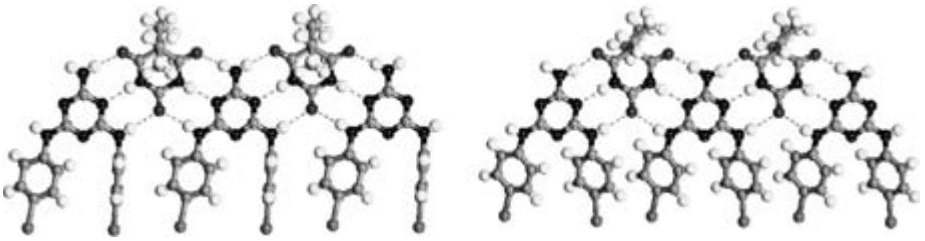

Form I Form II

(**A**) (**B**)

FIGURE 28 Linear tapes as observed by *N*,*N*-bis(4-bromophenyl)melamine and 5,5-diethylbarbituric acid co-crystals: (**A**) JICTUK01; (**B**) JICTUK10. The supramolecular synthons are identical in both forms and only salient difference between the structures lies with the orientation of the phenyl rings.

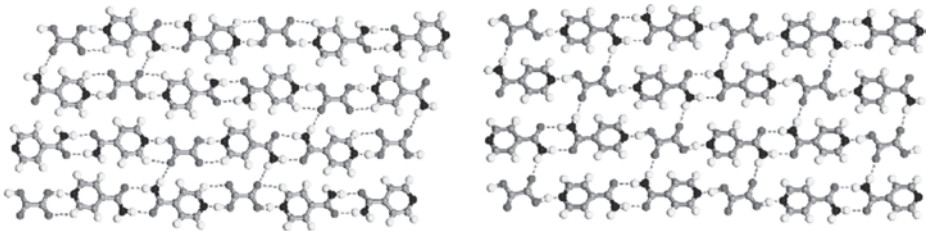

Form I Form II

(**A**) (**B**)

FIGURE 29 Crystal structures of Form (**A**) I and (**B**) Form II of the 1:1 oxalic acid:iso-nicotinamide co-crystal.

In summary, the series of polymorphic co-crystals presented herein is representative of the limited information within the CSD that addresses polymorphism in co-crystals and indicates that polymorphism in co-crystals in not typically the result of competing supramolecular synthons. However, the paucity of data precludes sweeping conclusions about polymorphism in co-crystals. That co-crystals are attracting wider interest means that there will likely be an increase in the number of systematic studies devoted to co-crystals and a corresponding increase in the number of polymorphic co-crystals. Intriguingly, this increase in the number of studies on co-crystals has afforded several recent reports of failed co-crystallizations that have instead resulted in new polymorphs of long known compounds such as benzidine and aspirin. Bernstein and coworkers (121) recently reported four new forms of benzidine obtained accidentally in the attempts to co-crystallize benzidine with different co-crystal formers. Zaworotko and coworkers (96b) first obtained Form II of aspirin during co-crystallization experiments involving aspirin and the antiseizure compound levetiracetam from hot acetonitrile. Such generation of new polymorphs could be a result of the creation of a new medium for crystallization via

the presence of co-crystal formers, and if so, it has implications for high-throughput screening as a methodology for discovering new polymorphs.

CONCLUSIONS

The pharmaceutical industry has only recently paid more than passing attention to pharmaceutical co-crystals, but there are several conclusions that can already be drawn:

- New pharmaceutical co-crystals should be patentable as novel crystal forms because their crystal structures are not obvious until prepared.
- New pharmaceutical co-crystals can be generated via rational design and multiple synthetic approaches for nearly all APIs by using crystal engineering strategies.
- Pharmaceutical co-crystals significantly diversify the number of crystal forms available for an API and always modify the physical properties of the API, thereby offering an opportunity to solve clinical problems through control of physicochemical properties of the API.

However, this does not mean that pharmaceutical co-crystals will become commonplace in marketed drug products because there remain practical handicaps that must be overcome such as the costs associated with the significant amounts of additional experimental research that are required and the risks associated with a patent and regulatory landscape that is presently in flux. As stated by Remenar (66), "If making a co-crystal of a specific molecule helps to enable an application or solve a problem, then it's the right thing to do, but you don't design a molecule in the real world simply because you are looking for a co-crystal strategy." This is probably a realistic assessment of where matters stand today in terms of pharmaceutical co-crystals and new drug development. However, there are certain niches where pharmaceutical co-crystals might be expected to find a role in drug development including high-throughput solid-state synthesis, new formulations of existing APIs, and processing of "difficult" APIs that are hard to crystallize and/or purify.

REFERENCES

1. Haleblian JK. Characterization of habits and crystalline modification of solids and their pharmaceutical applications. J Pharm Sci 1975; 64: 1269–88.
2. Byrn SR. Solid State Chemistry of Drugs, 2nd edn. SSCI Inc, 1999.
3. Salts: (a) Berge SM, Bighley LD, Monkhouse DC. Pharmaceutical salts. J Pharm Sci 1977; 66: 1–19. (b) Bastin RJ, Bowker MJ, Slater BJ. Salt selection and optimization procedures for pharmaceutical new chemical entities. Org Process Res Dev 2000; 4: 427–35 and references therein. (c) Gould PL. Salt selection for basic drugs. Int J Pharm 1986; 33: 201–17. (d) Banerjee R, Bhatt PM, Ravindra NV, et al. Saccharin salts of active pharmaceutical ingredients, their crystal structures, and increased water solubilities. Cryst Growth Des 2005; 5: 2299–309.
4. Hydrates/Solvates and polymorphs: (a) Remenar JF, MacPhee JM, Larson BK, et al. Salt selection and simultaneous polymorphism assessment via high-throughput crystallization: The case of Sertraline. Org Process Res Dev 2003; 7: 990–6. (b) Vishweshwar P, Beauchamp DA, Zaworotko MJ. An acetic acid solvate of trimesic acid that exhibits triple inclined interpenetration and mixed supramolecular homosynthons. Cryst Growth Des 2006; 6: 2429–31. (c) Banerjee R, Bhatt PM, Desiraju GR. Solvates of sildenafil saccharinate. A new host material. Cryst Growth Des 2006; 6: 1468–78. (d) Barnett SA,

Tocher DA, Vickers M. The solvates of o-acetamidobenzamide. CrystEngComm 2006; 8: 313–19. (e) Hosokawa T, Datta S, Sheth AR, et al. Isostructurality among five solvates of phenylbutazone. Cryst Growth Des 2004; 4: 1195–201.
5. Desiraju GR. Supramolecular synthons in crystal engineering – a new organic synthesis. Angew Chem Int Ed 1995; 34: 2311–27.
6. Lehn J-M. Supramolecular Chemistry: Concepts and Perspectives. Weinheim: VCH, 1995.
7. Atwood JL, Davies JED, MacNicol DD, et al., eds. Comprehensive Supramolecular Chemistry, Vol 6. Oxford: Pergamon, 1996.
8. MacDonald JC, Whitesides GM. Solid-state structures of hydrogen-bonded tapes based on cyclic secondary diamides. Chem Rev 1994; 94: 2383–420.
9. Schmidt GMJ. Photodimerization in the solid state. Pure Appl Chem 1971; 27: 647–78.
10. Etter MC. A new role for hydrogen-bond acceptors in influencing packing patterns of carboxylic acids and amides. J Am Chem Soc 1982; 104: 1095–6.
11. Desiraju GR. Crystal Engineering: The Design of Organic Solids. Amsterdam: Elsevier, 1989.
12. Dunitz JD. Phase transitions in molecular crystals from a chemical viewpoint. Pure Appl Chem 1991; 63: 177–85.
13. Mathias JP, Stoddart JF. Constructing a molecular LEGO set. Chem Soc Rev 1992; 21: 215–25.
14. Dunitz JD, Taylor R. Organic fluorine hardly ever accepts hydrogen bonds. Chem Eur J 1997; 3: 89–98.
15. Braga D. 15. Crystal engineering, Where from? Where to? Chem Commun 2003: 2751–4.
16. Moulton B, Zaworotko MJ. From molecules to crystal engineering: supramolecular isomerism and polymorphism in network solids. Chem Rev 2001; 101: 1629–58.
17. Tiekink ERT, Vittal JJ, eds. Frontiers in Crystal Engineering, Chichester, UK: Wiley, 2006.
18. Desiraju GR. Crystal engineering: a holistic view. Angew Chem Int Ed 2007; 46: 8342–56.
19. (a) Bernstein J. Polymorphism in Molecular Crystals. Oxford: Clarendon Press, 2002. (b) Hilfiker R. Polymorphism in the Pharmaceutical Industry. New York: Wiley VCH, 2006. (c) Special issue on polymorphism in crystals. Cryst Growth Des 2004; 4: 1085–444. (d) Special issue on pharmaceutical solid polymorphism in drug development and regulation. Adv Drug Delivery Rev 2004; 56: 235–418. (e) Brittain HG. Polymorphism in Pharmaceutical Solids. New York: Marcel Dekker Inc., 1999.
20. Amidon GL, Lennernas H, Shah VP, et al. A theoretical basis for a biopharmaceutic drug classification: the correlation of *in vitro* drug product dissolution and *in vivo* bioavailability. Pharm Res 1995; 12: 413–20.
21. Desiraju GR. Crystal and co-crystal. CrystEngComm 2003; 5: 466–7.
22. Dunitz JD. Crystal and co-crystal: a second opinion. CrystEngComm 2003; 4: 506.
23. Bond AD. What is a co-crystal? CrystEngComm 2007; 9: 833–4.
24. Aakeröy CB, Fasulo ME, Desper J. Cocrystal of salt: does it really matter? Mol Pharm 2007; 4: 317–22.
25. Stahly GP. Diversity in single- and multiple-component crystals. The search for the prevalence of polymorphs and cocrystals. Cryst Growth Des 2007; 7: 1007–26.
26. Zukerman-Schpector J, Tiekink ERT. What is a co-crystal? Zeit Fur Kristallogr 2008; 223: 233–4.
27. Parkin A, Gilmore CJ, Wilson CC. What is a co-crystal – and does it matter? Zeit Fur Kristallogr 2008: 223, 430.
28. Shan N, Zaworotko MJ. The role of cocrystals in pharmaceutical science. Drug Discov Today 2008; 13: 440–6.
29. (a) Aakeröy CB, Beatty AM, Helfrich BA. "Total synthesis" supramolecular style: design and hydrogen-bond-directed assembly of ternary supermolecules. Angew Chem Int Ed

2001; 40: 3240–2. (b) Aakeröy CB, Desper J, Helfrich BA. Heteromeric intermolecular interactions as synthetic tools for the formation of binary co-crystals. CrystEngComm 2004; 6: 19–24. (c) Aakeröy CB, Salmon DJ. Building co-crystals with molecular sense and supramolecular sensibility. CrystEngComm 2005; 7: 439–48. (d) Aakeröy CB, Hussain I, et al. Exploring the hydrogen-bond preference of N-H moieties in co-crystals assembled via O-H(Acid)…N(Py) intermolecular interactions. CrystEngComm 2007; 9: 46–54.
30. Ulrich J. Is melt crystallization a green technology? Cryst Growth Des 2004; 4: 879–90.
31. Almarsson Ö, Zaworotko MJ. Crystal Engineering of the composition of pharmaceutical phases. Do pharmaceutical co-crystals represent a new path to improved medicines? Chem Commun 2004: 1889–96.
32. Pepinsky R. Crystal engineering – a new concept in crystallography. Phys Rev 1955; 100: 971.
33. Etter MC. Hydrogen bonds as design elements in organic chemistry. J Phys Chem 1991; 95: 4601–10.
34. Zerkowski JA, MacDonald JC, Seto CT, et al. Design of organic structures in the solid state: molecular tapes based on the network of hydrogen bonds present in the cyanuric acid:melamine complex. J Am Chem Soc 1994; 116: 2382–91.
35. Desiraju GR, ed. Crystal Design: Structure and Function, New York: Wiley, 2003.
36. (a) Allen FH, Kennard O. Chem Des Automat News 1993; 8: 31–7. (b) Allen FH. The Cambridge Structural Database: a quarter of a million crystal structures and rising. Acta Crystallogr 2002; B58: 380–8.
37. Zerkowski JA, Seto CT, Whitesides GM, et al. Solid-state structures of 'Rosette' and 'Crinkled Tape' motifs derived from the cyanuric acid melamine lattice. J Am Chem Soc 1992; 114: 5473–5.
38. Vishweshwar P, McMahon JA, Bis JA, et al. Pharmaceutical co-crystals. J Pharma Sci 2006; 95: 499–516.
39. Special issue on pharmaceutical co-crystals. Mol Pharm 2007; 4: 299–486.
40. Wöhler F. Untersuchungen über das Chinon. Justus Liebigs Ann Chem 1844; 51: 153.
41. Shan N, Toda F, Jones W. Mechanochemistry and Co-crystal formation: effect of solvent on reaction kinetics. Chem Commun 2002: 2372–3.
42. Trask AV, Motherwell WDS, Jones W. Solvent-drop grinding: green polymorph control of cocrystallization. Chem Commun 2004; 10: 890–1.
43. Trask AV, Jones W. Crystal engineering of organic cocrystals by the solid-state grinding approach. Top Curr Chem 2005; 254: 41–70.
44. Karki S, Friscic T, Jones W, et al. Screening for pharmaceutical cocrystal hydrates via neat and liquid-assisted grinding. Mol Pharma 2007; 4: 347–54.
45. Childs SL, Rodríguez-Hornedo N, Reddy LS, et al. Screening strategies based on solubility and solution composition generate pharmaceutically acceptable cocrystals of carbamazepine. CrystEngComm 2008; 10: 856–64.
46. Rodriguez-Hornedo N, Nehm SJ, Seefeldt KF, et al. Reaction crystallization of pharmaceutical molecular complexes. Mol Pharma 2006; 3: 362–7.
47. Remenar JF, Morissette SL, Peterson ML, et al. Crystal engineering of novel cocrystals of a triazole drug with 1,4-dicarboxylic acids. J Am Chem Soc 2003; 125: 8456–7.
48. Childs SL, Chyall LJ, Dunlap JT, et al. Crystal Engineering Approach to Forming Cocrystals of Amine Hydrochlorides with Organic Acids. Molecular Complexes of Fluoxetine Hydrochloride with Benzoic, Succinic, and Fumaric Acids. J Am Chem Soc 2004; 126: 13335–42.
49. McNamara DP, Childs SL, Giordano J, et al. Use of a Glutaric Acid Cocrystal to Improve Oral Bioavailability of a Low Solubility API. Pharma Res 2006; 23: 1888–97.
50. Hickey MB, Peterson ML, Scoppettuolo LA, et al. Performance comparison of a co-crystal of Carbamazepine with marketed product. Eur J Pharma Biopharma 2007; 67: 112–9.
51. Trask AV, Motherwell WDS, Jones W. Pharmaceutical Cocrystallization: Engineering a Remedy for Caffeine Hydration. Cryst Growth Des 2005; 5: 1013–21.

52. Trask AV. An overview of pharmaceutical cocrystals as intellectual property. Mol Pharma 2007; 4: 301–9.
53. Lindenberg M, Kopp S, Dressman JB. Classification of orally administered drugs on the World Health Organization model list of essential medicines according to the biopharmaceutics classification system. Eur J Pharm Biopharm 2004; 58: 265–78.
54. Lobenberg R, Amidon GL. Modern bioavailability, bioequivalence and biopharmaceutics classification system. New scientific approaches to international regulatory standards. Eur J Pharm Biopharm 2000; 50: 3–12.
55. Kanfer I. Report on the international workshop on the biopharmaceutics classification system (BCS): scientific and regulatory aspects in practice. Pharm J Pharmaceut Sci 2002; 5: 1–4.
56. Ling AR, Baker JK. Halogen derivatives of quinine. Part III. Derivatives of quinhydrone. J Chem Soc Trans 1893; 63: 1314–27.
57. Anderson JS. Structure of organic molecular compounds. Nature 1937; 140: 583–4.
58. Pekker S, Kovats E, Oszlanyi G, et al. Rotor-stator molecular crystals of fullerenes with cubane. Nat Mater 2005; 4: 764–7.
59. (a) Hoogsteen K. The structure of crystals containing a hydrogen-bonded complex of 1-methylthymine and 9-methyladenine. Acta Crystallogr 1959; 12: 822–3. (b) Hoogsteen K. Crystal and molecular structure of a halogen-bonded complex between 1-methylthymine and 9-methyladenine. Acta Crystallogr 1963; 16: 907–16.
60. O'Brien EJ. Crystal structures of two complexes containing guanine and cytosine derivatives. Acta Crystallogr 1967; 23: 92–106.
61. Sivakova S, Rowan SJ. Nucleobases as supramolecular motifs. Chem Soc Rev 2005; 34: 9–21.
62. French patent: von Heyden F, et al. 1934; 769, 586.
63. Eli lilly patent: Amos JG, Indelicato JM, Pasini CE, et al. Bicyclic beta-lactam/paraben complexes. US5412094 (A1), JP7048383 (A), FI943081 (A), BR9402561 (A) and EP0637587 (B1), 1995.
64. Viagra-Aspirin patent: Zegarac M, Mestrovic E, Dumbovic A, et al. Pharmaceutically acceptable cocrystalline forms of sildenafil. WO 2007/080362 A1, 2007.
65. Caira MR. Sulfa drugs as model cocrystal formers. Mol Pharm 2007; 4: 310–6.
66. Thayer AM. Form and function: the choice of pharmaceutical crystalline form can be used to optimize drug properties, and cocrystals are emerging as new alternatives. C & E News 2007; 85: 17–30.
67. (a) Huang CM, Leiserowitz L, Schmidt GMJ. Molecular packing modes. Part XI. Crystal structures of the 2:1 complexes of benzamide with succinic acid and furamide with oxalic acid. J Chem Soc Perkins Trans 2 1973; 5: 503–8. (b) Aakeröy CB, Beatty AM, Helfrich BA. A high-yielding supramolecular reaction. J Am Chem Soc 2002; 124: 14425–32. (c) Pedireddi VR, Chatterjee S, Ranganathan A, et al. A study of supramolecular hydrogen bonded complexes formed by aliphatic dicarboxylic acids with azaaromatic donors. Tetrahedron 1998; 54: 9457–74. (d) Nguyen TL, Fowler FW, Lauher JW. Commensurate and incommensurate hydrogen bonds. An exercise in crystal engineering. J Am Chem Soc 2001; 123: 11057–64. (e) Walsh RDB, Bradner MW, Fleischman SG, et al. Crystal engineering of the composition of pharmaceutical phases. Chem Commun 2003: 186–7. (f) Bis JA, Vishweshwar P, Weyna D, et al. Hierarchy of supramolecular synthons: persistent hydroxyl...pyridine hydrogen bonds in cocrystals that contain a cyano acceptor. Mol Pharm 2007; 4: 401–16. (g) McMahon JA, Bis JA, Vishweshwar P, et al. Crystal engineering of the composition of pharmaceutical phases. 3 1. Primary amide supramolecular heterosynthons and their role in the design of pharmaceutical co-crystals. Fur Kristallogr 2005; 220: 340–50.
68. (a) Sudhakar P, Srivijaya R, Sreekanth BR, et al. Carboxylic acid-pyridine supramolecular heterocatemer in a co-crystal. J Mol Struc 2008; 885: 45–9. (b) Bhogala BR, Nangia A. Ternary and quaternary co-crystals of 1,3-*cis*,5-*cis*-cyclohexanetricarboxylic acid and

4,4′-bipyridines. New J Chem 2008; 32: 800–7. (c) Broker GA, Tiekink ERT. Co-crystal formation between 2,2′-dithiodibenzoic acid and each of 4,4′-bipyridine, *trans*-1,2-bis (4-pyridyl)ethene and 1,2-bis(4-pyridyl)ethane. CrystEngComm 2007; 9: 1096–109.
69. (a) Aakeröy CB, Desper J, Fasulo ME. Improving success rate of hydrogen-bond driven synthesis of co-crystals. CrystEngComm 2006; 8: 586–8. (b) Edwards MR, Jones W, Motherwell WDS. Cocrystal formation of 4-methyl and 4-chlorobenzamide with carboxylic acids: chloro/methyl interchange and crystal structure. CrystEngComm 2006; 8: 545–51.
70. Hosseini MW. Self assembly and generation of complexity. Chem Commun 2005: 5825–9.
71. Lindsey JS. Self-assembly in synthetic routes to molecular devices. Biological principles and chemical perspectives: a review. New J Chem 1991; 15: 153–80.
72. Mann S. Molecular tectonics in biomineralization and biomimetic materials chemistry. Nature 1993; 365, 499–505.
73. Calama MC, Timmerman P, Reinhoudt DN. Guest-templated selection and amplication of a receptor by noncovalent combinatorial synthesis. Angew Chem Int Ed 2000; 39: 755–8.
74. (a) Shattock TR, Arora KK, Peddy V, et al. Hierarchy of supramolecular synthons: persistent carboxylic acid...pyridine hydrogen bonds in cocrystals that also contain a hydroxyl moiety. Cryst Growth Des 2008; 8: 4533–45. (b) Aakeröy CB, Fasulo M, Schultheiss N, et al. Structural competition between hydrogen bonds and halogen bonds. J Am Chem Soc 2007; 129: 13772–3.
75. (a) Sharma CVK, Zaworotko MJ. X-Ray crystal structure of $C_6H_3(CO_2H)_3$-1,3,5·1.5 (4,4'-bipya): 'super trimesic acid' chicken-wire grid. Chem Commun 1996: 2655–6. (b) Vishweshear P, Nangia A, Lynch VM. Molecular complexes of homologous alkanedicarboxylic acids with isonicotinamide: X-ray crystal structures, hydrogen bond synthons, and melting point alternation. Cryst Growth Des 2003; 3: 783–90. (c) Shan N, Batchelor E, Jones W. Co-crystal structures of 4,7-phenanthroline and carboxylic acids: synthon competition and prediction. Tetrahedron Lett 2002; 43: 8721–5. (d) Arora KK, Pedireddi VR. A rational study of crystal engineering of supramolecular assemblies of 1,2,4,5-benzenetetracarboxylic acid. J Org Chem 2003; 68: 9177–85.
76. (a) Leiserowitz L, Nader F. The molecular packing modes and the hydrogen-bonding properties of amide:carboxylic acid complexes. Acta Crystallogr 1977; B33: 2719–33. (b) Reddy LS, Nangia A, Lynch VM. Phenyl-perfluorophenyl synthon mediated cocrystallization of carboxylic acids and amides. Cryst Growth Des 2004; 4: 89–94.
77. (a) Biradha K, Zaworotko MJ. A supramolecular analogue of cyclohexane sustained by aromatic C−H...π interactions: complexes of 1,3,5-trihydroxybenzene with substituted pyridines. J Am Chem Soc 1998; 120: 6431–2. (b) Papaefstathiou GS, MacGillivray LR. Discrete versus infinite molecular self-assembly: control in crystalline hydrogen-bonded assemblies based on resorcinol. Org Lett 2001; 3: 3835–8. (c) Vishweshwar P, Nangia A, Lynch VM. Supramolecular synthons in phenol-isonicotinamide adducts. CrystEngComm 2003; 5: 164–8.
78. Anastas PT, Warner JC. Green Chemistry: Theory and Practice, Oxford University Press, 1998.
79. Cannon AS, Warner JC. Noncovalent derivatization: green chemistry applications of crystal engineering. Cryst Growth Des 2002; 2: 255–7.
80. Foxman BM, Guarrera DJ, Taylor LD, et al. Environmentally benign synthesis using crystal engineering: steric accommodation in non-covalent derivatives of hydroquinones. Crystal Engineering 1998; 1: 109–18.
81. Taylor LD, Warner JC. US 5338644 A 19940816 Cont. of U.S., 5, 177262, 1994.
82. Etter MC, Frankenbach GM, Bernstein J. Solid-state nucleophilic aromatic substitution reaction of a carboxylic acid cocrystal. Tetrahedron Lett 1989; 30: 3617–20.

83. Cheney ML, McManus GJ, Perman JA, et al. The role of cocrystals in solid-state synthesis: cocrystal-controlled solid-state synthesis of imides. Cryst Growth Des 2007; 7: 616–17.
84. (a) Pasteur L. Ann Chim Phys 1848; 24: 442. (b) Pasteur L. Ann Chim Phys 1853; 38: 437. (c) Wheeler KA, Grove RC, Davis RE, Kassel WS. Rediscovering Pasteur's quisiracemates. Angew Chem Int Ed 2008; 47: 78–81.
85. Wallach O. Justus Liebigs Ann Chem 1895; 286: 90–143.
86. Samas B, Wang W, Godrej DB. 1:1 Cocrystal of (*S*)-3-(ammoniomethyl)-5-methylhexanoate and (*S*)-mandelic acid Acta Crystallogr 2007; E63: o3938.
87. (a) Teng MY, Sun J, Ma CA, et al. (*S*)-2-Hydroxy-2-phenylacetic acid-(*R*)-2-aminobutanoic acid-water (1/1/0.5). Acta Crystallogr 2006; E62: o2454–o2456. (b) Fischer E, Mouneyrat A. Ber Chem Ges 1900; 33: 2383. (c) Fischer E, Schoeller WA. Ann Chem 1907; 357: 1.
88. (a) Hu ZQ, Xu DJ, Xu YZ, et al. (*R*)-Mandelic acid (*S*)-alanine hemihydrate. (b) (*S*)-Alanine-(*S*)-mandelic acid (1/1). Acta Crystallogr 2002; C58: o612–o614. (b) Hu ZQ, Xu DJ, Xu YZ. Acta Crystallogr 2004; E60: o269–o271.
89. Higuchi T, Roy K. Study of possible complex formation between macromolecules and certain pharmaceuticals. I. Polyvinylpyrrolidone with sulfathiazole, procaine hydrochloride, sodium salicylate, benzyl penicillin, chloramphenicol, mandelic acid, caffeine, theophylline, and cortisone. J Am Pharm Assoc 1954; 43: 393–7.
90. Higuchi T, Roy K. Study of possible complex formation between macromolecules and certain pharmaceuticals. II. Polyvinylpyrrolidone with p-aminobenzoic acid, aminopyrine, benzoic acid, salicylic acid, p-hydroxybenzoic acid, m-hydroxybenzoic acid, citric acid, and Phenobarbital. J Am Pharm Assoc 1954; 43: 398–401.
91. CBZ four polymorphs: (a) Reboul JP, Cristau B, Soyfer JC, et al. 5H-dibenz[b,f]azépine-carboxamide-5 (carbamazépine). Acta Crystallogr 1981; B37: 1844. (b) Lowes MMJ, Cairo MR, Lotter AP, et al. Physicochemical properties and x-ray structural studies of the trigonal polymorph of carbamazepine. J Pharm Sci 1987; 76: 744. (c) Grzesiak AL, Lang M, Kim K, et al. Comparison of the four anhydrous polymorphs of carbamazepine and the crystal structure of form I. J Pharm Sci 2003; 92: 2260. (d) Lang M, Kampf JW, Matzger AJ. Form IV of carbamazepine. J Pharm Sci 2002; 91: 1186.
92. CBZ dihydrate: Gelbrich T, Hursthouse MB. Systematic investigation of the relationships between 25 crystal structures containing the carbamazepine molecule or a close analogue: a case study of the XPac method. CrystEngComm 2006; 8: 449.
93. CBZ solvates: (a) Chang CH, Yang DSC, Yoo CS, et al. The crystal structures of (*S*) and (*R*) baclofen and carbamazepine. Acta Crystallogr 1981; A37: c71. (b) Johnston A, Florence AJ, Kennedy AR. Carbamazepine furfural hemisolvate. Acta Crystallogr 2005; E61: o1777. (c) Johnston A, Florence AJ, Kennedy AR. Carbamazepine *N,N*-dimethylformamide solvate. Acta Crystallogr 2005; E61: o1509. (d) Lohani S, Zhang Y, Chyall LJ, et al. Carbamazepine-2,2,2-trifluoroethanol (1/1). Acta Crystallogr 2005; E61: o1310–o1312. (e) Fernandes P, Bardin J, Johnston A, et al. Carbamazepine trifluoroacetic acid solvate. (f) Solvent inclusion in the structural voids of form II carbamazepine: single-crystal X-ray diffraction, NMR spectroscopy and Hirshfeld surface analysis. Acta Crystallogr 2007; E63: o4269. (f) Fabbiani FPA, Byrne LT, McKinnon JJ, et al. CrystEngComm 2007; 9: 728. (g) Johnston A, Johnston BF, Kennedy AR, et al. Targeted crystallization of novel carbamazepine solvates based on a retrospective Random Forest classification. CrystEngComm 2008; 10: 23.
94. Ammonium salts: Reck G, Thiel W. Pharmazie 1991; 46: 509.
95. A solid solution with dihydrocarbamazepine: Florence AJ, Leech CK, Shankland N, et al. Control and prediction of packing motifs: a rare occurrence of carbamazepine in a catemeric configuration. CrystEngComm 2006; 8: 746.
96. Co-crystals (hydrates/solvates and polymorphs): (a) Fleischman SG, Kuduva SS, McMahon JA, et al. Crystal engineering of the composition of pharmaceutical phases:

multiple-component crystalline solids involving carbamazepine. Cryst Growth Des 2003; 9: 909. (b) Vishweshwar P, McMahon JA, Oliveira M, et al. The predictably elusive form II of aspirin. J Am Chem Soc 2005; 127: 16802. (c) Babu NJ, Reddy LS, Nangia A. Amide N-oxide heterosynthon and amide dimer homosynthon in cocrystals of carboxamide drugs and pyridine N-oxides. Mol Pharm 2007; 4: 417. (d) Porter III WW, Elie SC, Matzger AJ. Polymorphism in carbamazepine cocrystals. Cryst Growth Des 2008; 8: 14.

97. Hilfiker R, Berghausen J, Blatter F, et al. Polymorphism – integrated approach from high-throughput screening to crystallization optimization. J Ther Ana Calor 2003; 73: 429–40.
98. Seefeldt K, Miller J, Alvarez N, Rodriguez-Hornedo N. Crystallization pathways and kinetics of carbamazepine-nicotinamide cocrystals from the amorphous state by in situ thermomicroscopy, spectroscopy and calorimetry studies. J Pharma Sci 2007; 96: 1147–58.
99. Nehm SJ, Rodriguez-Spong B, Rodriguez-Hornedo N. Phase solubility diagrams of cocrystals are explained by solubility product and solution complexation. Cryst Growth Des 2006; 6: 592–600.
100. ter Horst JH, Cains PW. Co-crystal polymorphs from a solvent-mediated transformation. Cryst Growth Des 2008; 8: 2537–42.
101. (a) Peeteers J, Neeskens P, Tollenaere JP, et al. Characterization of the interaction of 2-hydroxypropyl-β-cyclodextrin with itraconazole at pH 2, 4, and 7. J Pharm Sci 2002; 91: 1414–22. (b) Francois M, Snoeckx E, Putteman P, et al. A mucoadhesive, cyclodextrin-based vaginal cream formulation of itraconazole. AAPS Pharma Sci 2003; 5: 1–5.
102. (a) Bak A, Gore A, Yanez E, et al. The co-crystal approach to improve the exposure of a water-insoluble compound: AMG 517 sorbic acid co-crystal characterization and pharmacokinetics. J Pharm Sci 2008; 97: 3942–56. (b) Stanton MK, Bak A. Physicochemical properties of pharmaceutical co-crystals: a case study of ten AMG 517 co-crystals. Cryst Growth Des 2008; 8: 3856–62.
103. (a) Puschner B, Poppenga RH, Lowenstine LJ, et al. Assessment of melamine and cyanuric acid toxicity in rats. J Vet Diagn Invest 2007; 19: 616–24. (b) Ranganathan A, Pedireddi VR, Rao CNR. Hydrothermal synthesis of organic channel structures: 1:1 hydrogen bonded adducts of melamine and cyanuric and trithiocyanuric acids. J Am Chem Soc 1999; 121: 1752–3.
104. Dunitz JD, Bernstein J. Disappearing polymorphs. Acc Chem Res 1995; 28: 193–200.
105. Davey RJ. Pizzas, polymorphs and pills. Chem Commun 2003: 1463–7.
106. Morrow SI. One hundred and fifty years of isomorphism. J Chem Edu 1969; 46: 580–4.
107. Wöhler F, Liebig J. Untersuchungen über das Radikal der Benzoesäure. Annal Pharm 1832; 3: 249–82.
108. Siegrist T, Kloc C, Schön JH, et al. Enhanced physical properties in a pentacene polymorph. Angew Chem Int Ed 2001; 40: 1732–6.
109. McCrone WC. Polymorphism in Physics and Chemistry of the Organic Solid State, Vol. II. In: Fox D, Labes MM, Weissberger A, eds. New York: Interscience, 1965: 725–67.
110. Caira MR. Crystalline polymorphism of organic compounds. Top Curr Chem 1998; 198: 163–208.
111. Ostwald W, Physikal Z. Studies on the formation and transformation of solid compounds: report I. Supersaturation and practicing cooling. Chem 1897; 22: 289.
112. (a) Boman CE, Herbertsson H, Oskarsson A. The crystal and molecular structure of a monoclinic phase of iminodiacetic acid. Acta Crystallogr 1974; B30: 378–82. (b) Bernstein J. Conformational polymorphism. III. The crystal and molecular structures of form II and form III of iminodiacetic acid. Acta Crystallogr 1979; B35: 360–6. (c) Graeber EJ, Morosin B. The crystal structures of 2,2', 4,4', 6,6'-hexanitroazobenzene (HNAB), forms I and II. Acta Crystallogr 1974; B30: 310–7.

113. David WIF, Shankland K, Pulham CR, et al. Polymorphism in benzamide. Angew Chem Int Ed 2005; 44: 7032–5.
114. Kalman A, Fabian L, Argay G, et al. Dipole-induced polymorphs of *trans*-2-hydroxycycloheptanecarboxylic acid with virtually the same unit cell. J Am Chem Soc 2003; 125: 34–5.
115. Matthews JH, Paul IC, Curtin DY. Configurational isomerism in crystalline forms of benzophenone anils. J Chem Soc Perkin Trans 1991; 2: 113–8.
116. Bis JA, Vishweshwar P, Middleton RA, et al. Concomitant and conformational polymorphism, conformational isomorphism, and phase relationships in 4-cyanopyridine + 4,4'-biphenol cocrystals. Cryst Growth Des 2006; 6: 1048–53.
117. Matsuda H, Osaki K, Nitta I. Crystal structure of quinhydrone, $C_{12}H_{10}O_4$. Bull Chem Soc Jpn 1958; 31: 611–20.
118. Sakurai T. On the refinement of the crystal structures of phenoquinone and monoclinic quinhydrone. Acta Crystallogr 1968; B24: 403–12.
119. Sakurai T. The crystal structure of the triclinic modification of quinhydrone. Acta Crystallogr 1965; B19: 320–30.
120. Schmidtmann M, Gutmann MJ, Middlemiss DS, et al. Towards proton transfer in hydrogen bonded molecular complexes: joint experimental and theoretical modeling and an energy scale for polymorphism. CrystEngComm 2007; 9: 743–5.
121. Rafilovich M, Bernstein J. Serendipity and four polymorphic structures of Benzidine, $C_{12}H_{12}N_2$. J Am Chem Soc 2006; 128: 12185–91.

9 Thermoanalytical and Crystallographic Methods

Sisir Bhattacharya*

Department of Pharmaceutics, University of Minnesota, Minneapolis, Minnesota, U.S.A.

Harry G. Brittain

Center for Pharmaceutical Physics, Milford, New Jersey, U.S.A.

Raj Suryanarayanan

Department of Pharmaceutics, University of Minnesota, Minneapolis, Minnesota, U.S.A.

INTRODUCTION

The different physical forms of a compound can exhibit pronounced differences in physicochemical properties. The term "physical form" encompasses polymorphs, solvates (also referred to as solvatomorphs), the non-crystalline (amorphous) form, and partially crystalline forms. Although numerous analytical techniques are available to characterize the physical forms of pharmaceutical compounds, this chapter will focus on thermal and crystallographic characterization techniques. While discussing the analytical techniques and their applications, we will use the term "polymorphism" in its broadest sense, with the understanding that with appropriate modifications, the techniques can often be extended for the characterization of the other physical forms of pharmaceuticals. Although crystallography (through crystal structure) provides the most definitive evidence of polymorphism, thermoanalytical, spectroscopic, and microscopic techniques are often used in a complementary fashion for the characterization of polymorphs.

Comprehensive and in-depth discussions of different thermoanalytical techniques can be found in the literature (1,2), and this chapter will specifically discuss the applications of thermoanalytical and crystallographic techniques in the characterization of pharmaceuticals. The specific thermoanalytical techniques to be discussed are differential scanning calorimetry (DSC), thermogravimetric analysis (TGA), and hot-stage microscopy (HSM). Several recent reviews and book chapters have covered this topic, and the examples presented are designed to complement the information in the literature (1–4). In the second part of the chapter, applications of X-ray powder diffractometry (XRD) (5,6) are provided. Finally, applications of variable-temperature XRD (VT-XRD) are discussed, specifically to monitor phase transitions as a function of temperature.

THERMOANALYTICAL TECHNIQUES

Thermal analysis methods can be conveniently defined as those techniques in which some property of the analyte is measured as a function of an externally applied temperature. In most applications, one effects a linear increase in the temperature of the sample while the property of interest is recorded on a continuous basis. Thermoanalytical methods are used to monitor endothermic processes (i.e., melting, boiling,

**Current affiliation*: Forest Laboratories, Inc., Commack, New York, U.S.A.

sublimation, vaporization, desolvation, solid–solid phase transitions, and chemical degradation) as well as exothermic processes (i.e., crystallization and oxidative decomposition). Thermal methods are routinely used for the characterization of polymorphs, and in light of the experimental simplicity, often constitute the first line of techniques used to understand the polymorphic space of a system.

Differential Scanning Calorimetry (DSC)

In DSC, which is the most widely used technique for thermal characterization of pharmaceuticals, the analyte is subjected to a controlled temperature program and the temperature and the heat flow associated with a thermally induced transition is measured.

DSC has been developed along two lines: power-compensation DSC and heat-flux DSC. In power-compensation DSC, separate heating elements are in contact with the sample and reference cells, with the rate of heating by these elements being controlled and measured. Thus the sample and reference are maintained at the same temperature and the heat flow required to accomplish this is measured. The other methodology is that of heat-flux DSC, where the sample and reference cells are heated by the same element, and one monitors the direction and magnitude of the heat being transferred between the two.

A detailed theory of DSC is outside the scope of this chapter and has been discussed elsewhere (1,2). Briefly, the basic principle behind a change in the baseline of a typical DSC plot (power vs. temperature), signifying a thermal event, is a change in the heat capacity of the system under investigation. The basic equation (4) describing the relationship between the heat flux (Q) associated with a thermal event and the heat capacity (C_p) of the system under investigation is given by:

$$(dQ/dt) = C_p(dT/dt) \quad (1)$$

where dQ/dt represents power at the constant heating or cooling rate, dT/dt. DSC plots are obtained as the differential rate of heating [in units of watts (joules/second) or calories/second] against temperature, and thus represent direct measures of the heat capacity of the sample. The area under a DSC peak is directly proportional to the heat absorbed or evolved by the thermal event, and integration of these peak areas yields the heat of reaction (in units of calories/seconds · gram or joules/seconds · gram).

The effectiveness of DSC to detect various polymorphic forms is illustrated in Figure 1 (7). Profiles 1, 2, and 3 (*from top*) show the reversible transitions between the enantiotropically related forms I and III. The fourth DSC curve shows the melting of form II followed by crystallization and melting of form I. The bottom DSC profile is a heating curve of a mixture of forms II and III, which shows the respective melting endotherms but no transition to form I. This was tentatively attributed to the absence of form I seeds in the mixture of forms II and III, which were concomitantly crystallized as opposed to the pure forms (profiles 1–4), which were crystallized separately using different methods.

Standard Reference Materials (SRMs) are available from the National Institute of Standards and Technology for calibration of temperature and enthalpy of fusion for differential scanning calorimeters. Indium (SRM 2232; melting temperature = 156.6°C; enthalpy of fusion = 28.5 J/g), tin (SRM 2220; melting point = 232.0°C; enthalpy of fusion = 60.2 J/g), and gallium (SRM 2234; melting temperature = 29.8°C;

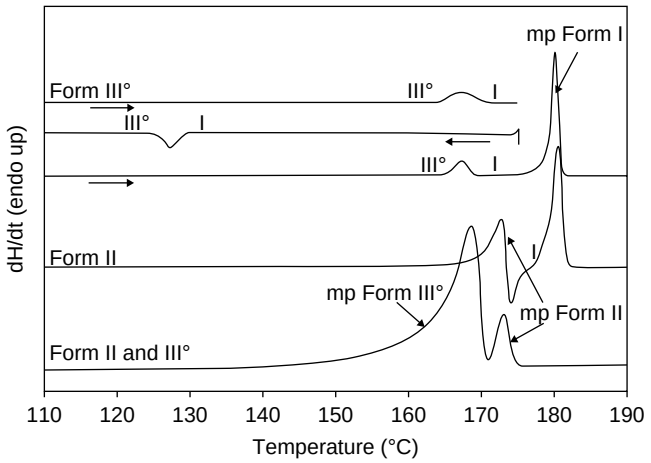

FIGURE 1 DSC profiles of cinacalcet hydrochloride polymorphs. The first (heating), second (cooling), and third (heating) profiles (*from top*) show the solid–solid transition (i.e., III° → I); the fourth profile shows melting of form II followed by crystallization and melting of form I; the fifth profile is a heating curve of a mixture of form II and form III° showing respective melting endotherms but no transition to form I signifying absence of form I seeds. *Note*: The direction of endotherm is *up*. *Source*: From Ref. (7).

enthalpy of fusion = 80.1 J/g) are suitable as calibration standards over the range of temperatures of interest in pharmaceutical analyses. Because DSC is also used at sub-ambient temperatures for the characterization of frozen solutions, mercury (SRM 2225; melting temperature = –38.9°C; enthalpy of fusion = 11.5 J/g) is a suitable calibration standard. Heat capacity calibration in a DSC is usually carried out with synthetic sapphire (SRM 720), copper (SRM RM5), polystyrene (SRM 705a), or molybdenum (SRM 781D2).

Depending on the protocol used for temperature programming, a DSC experiment could be classified as being conventional, modulated, or accelerated (also known as Hyper-DSC®). In the conventional mode, the heating rate is constant and typically ranges from 0.1°C/min to 20°C/min. The majority of DSC experiments are carried out in the conventional mode and may require optimization of the sample pan configuration (discussed later) and the experimental parameters to obtain the desired information (3). In Table 1, the effects of operational parameters are outlined.

In modulated DSC (MDSC), a changing (modulated) heating rate is superimposed on a constant average heating rate. The modulation is described by a frequency, determined by specific amplitude (±°C) and period (seconds), such as ±0.5°C every 60 seconds, with the choice of the amplitude and period being dictated by the nature of the transition (8–10). The advantage of MDSC over conventional DSC is that it can separate the reversible heat flow from the non-reversible heat flow (Fig. 2). Reversible heat flow corresponds to events that respond to the changing heating rate (e.g., heat capacity change, melting). On the other hand, non-reversible heat flow events (e.g., crystallization or decomposition) are not affected by changing heating rates.

TABLE 1 Influence of Operational Parameters on the Outcome of DSC Experimental Results

	Effects
Sample size	
Large	Advantages
	(i) Non-homogeneous samples
	(ii) Detects "weak" transitions
	Disadvantages
	(i) Broad peaks
	(ii) Temperature of the event may be inaccurate
	(iii) Poor resolution
	(iv) Requires slow heating rate
Small	Advantages
	(i) Sharp peaks
	(ii) Increased resolution
	(iii) Permits faster heating rate
	Disadvantages
	(i) Decreased sensitivity
Heating rate	
Fast	Advantages
	(i) Increased sensitivity
	Disadvantages
	(i) Decreased resolution
	(ii) Decreased temperature accuracy
Slow	Advantages
	(i) Increased resolution
	Disadvantages
	(i) Decreased sensitivity

Source: Adapted from Ref. (2).

MDSC has found limited utility in the characterization of polymorphs (11,12). However, the inherent capability of this technique to separate overlapping melting and crystallization events has been demonstrated for the polymorphs of tristearin (13,14). MDSC is especially suited for the characterization of amorphous materials (15,16), and has enabled the quantification of amorphous content in a partially crystalline material (17). Because crystallinity differences could affect material performance, it is important that analysts are aware of low levels of lattice disorder in highly crystalline materials that were brought about by processing and storage conditions. Saklatvala et al. investigated two batches of an investigational crystalline drug, which showed pronounced differences in their stability and water sorption profiles, and MDSC enabled detection and quantification of the amorphous content in the batch characterized by the lower chemical stability and the increased propensity to take up water (18).

Hyper-DSC® uses accelerated heating rates (up to 500°C/min) in order to selectively investigate phase transitions. The high heating rates result in selective inhibition of transitions that would normally take place over the longer timescales

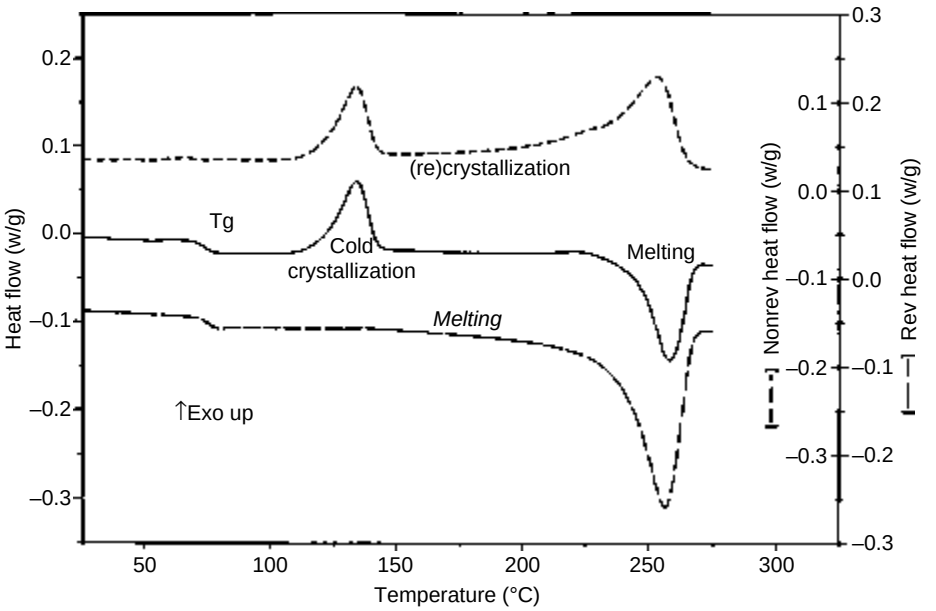

FIGURE 2 Modulated DSC profiles of quenched polyethylene terephthalate, showing the non-reversible (*uppermost trace*), total (*middle trace*), and reversible (*lowest trace*) heat flow curves. The exothermic recrystallization event is hardly discernible in the total heat flow but is prominent in the non-reversible heat flow. *Source*: From Ref. (66).

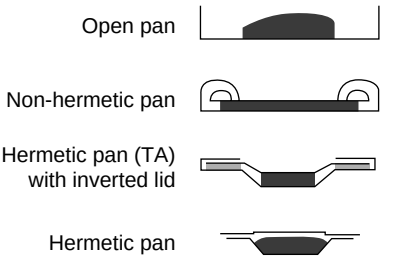

FIGURE 3 Diagrammatic representation of different DSC pan configurations. *Source*: From Ref. (9).

of conventional heating rates. A case in point are the polymorphs of carbamazepine, where a heating rate of 250°C/min was used to prevent simultaneous crystallization of form I during the melting of form III, thereby allowing determination of the enthalpy of fusion of form III (19).

In a typical DSC application, the sample is encapsulated in a pan and the lid is crimped, where the lid can be crimped either in a non-hermetic or in a hermetic manner (Fig. 3). In the hermetically crimped pan, a pinhole can be made in the lid to relieve pressure during the acquisition of the DSC curve. To minimize the head space, the lid can be inverted and then hermetically crimped.

The pan configuration can influence the outcome of a DSC experiment. This is especially true for solvates, because the desolvation kinetics, as well as the physical form of the product phase, can be profoundly influenced by the sample environment. In an open pan, there is no physical barrier to the escape of liberated solvent, and the purge gas (typically nitrogen) will facilitate removal of the liberated solvent. The reasonably unrestricted nature of a non-hermetically crimped pan will also permit ready escape of the liberated solvent. At the other extreme, the liberated solvent cannot escape in a hermetically crimped pan. In a sealed pan with a pinhole, the rate of vapor loss will become appreciable only when the vapor pressure exceeds atmospheric pressure. Different pan configurations, which result in varied desolvation conditions, have been used to generate different polymorphs of anhydrous carbamazepine and trehalose from their respective hydrates (20,21).

Pressure DSC (PDSC) enables DSC experiments to be carried out at elevated pressures as high as 1000 psi. PDSC is useful for the separation of overlapping dehydration and vaporization events that are observed following the dehydration of hydrates. Although the temperature of dehydration is likely to be unaffected by pressure, the boiling temperature of water is pressure dependent and can be ascertained from the Clausius–Clapeyron equation. In addition, the potential interaction of the liberated water with the anhydrous product phase can also be ascertained. Han and Suryanarayanan (22) used PDSC to successfully resolve overlapping dehydration and vaporization transitions observed when carbamazepine dihydrate was heated (Fig. 4, *upper left panel*). The conventional DSC of carbamazepine exhibited two overlapping endotherms over the temperature range of 85°C to 100°C, attributed to dehydration followed by vaporization, which were followed by the melting of non-solvated carbamazepine around 189°C. When the pressure was increased, only a single endotherm attributable to dehydration was observed at approximately 90°C. Interestingly, several thermal events were observed between the dehydration and the melting temperatures.

A limitation of DSC is that although it reveals the existence of thermally induced transitions, the nature of these transitions can be difficult to determine. In an effort to simulate the PDSC experiments, Han and Suryanarayanan (22) heated carbamazepine dihydrate in a "sealed" environment. Following dehydration, the released water caused an increase in pressure by being retained in the holder, although the pressure was uncontrolled. As shown in the *upper right panel* of Figure 4, the carbamazepine polymorphic transitions were further characterized by VT-XRD. The formation of β-carbamazepine at ~90°C was evident in the diffraction patterns on the basis of peaks observed at scattering angles of 13.1, 15.3, and 18.7° 2θ). Based on the disappearance of the characteristic peaks of carbamazepine dihydrate (at 8.9 and 12.3° 2θ), dehydration appeared to be complete by 100°C. Around 160°C, several characteristic peaks of γ-carbamazepine were observed, indicating a $\beta \rightarrow \gamma$ solid–solid phase transition. Based on the decrease in the intensities of the β-carbamazepine peaks, and the increase in the intensities of the γ-carbamazepine peaks, the $\beta \rightarrow \gamma$ phase transition was accelerated as the temperature was increased to 180°C. These VT-XRD results aided in the interpretation of the DSC results. When DSC was conducted under elevated pressure, usually four endotherms were observed. The first endotherm at ~90°C, as explained earlier, is attributed to dehydration. The two overlapping endotherms at ~120°C and 125°C are attributed to the $\beta \rightarrow \gamma$ carbamazepine phase transition and to the vaporization of water. The melting of γ-carbamazepine occurred at ~189°C. This scheme is

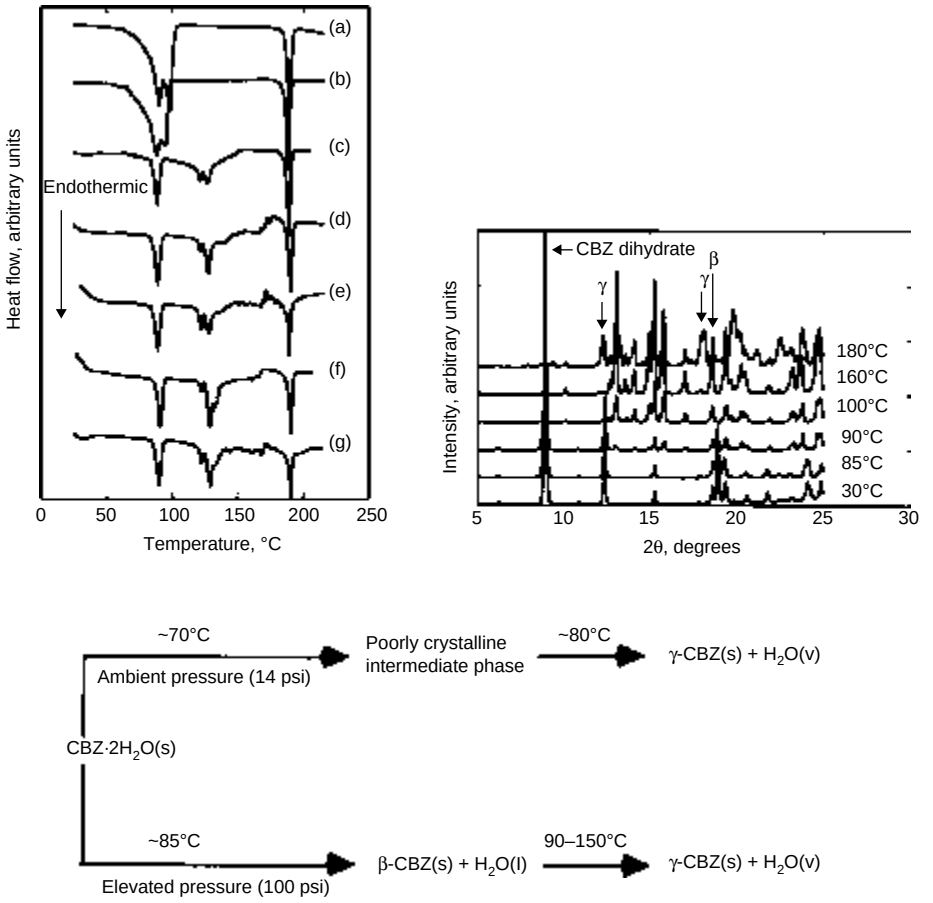

FIGURE 4 (*Upper left panel*) DSC of carbamazepine dihydrate at different pressures: (a) ambient pressure in conventional DSC cell, (b) ambient pressure in PDSC cell, (c) 100 psi, (d) 200 psi, (e) 300 psi, (f) 400 psi, (g) 600 psi. (*Upper right panel*) VT-XRD of carbamazepine dihydrate. Peaks characteristic of the dihydrate as well as anhydrous β and γ forms are shown. (*Lower panel*) Schematic showing carbamazepine dihydrate transitions under ambient and elevated pressures. *Source*: From Ref. (22).

illustrated in Figure 4 (*lower panel*) and shows the transitions of carbamazepine dihydrate at ambient and elevated pressures.

An emerging technique that could be considered as a variant of DSC is microthermal analysis, which combines the principles of DSC and scanning probe microscopy. Microthermal analysis was used to identify local regions of different polymorph content in a 50:50 mixture of two cimetidine polymorphs (23). This technique also has the potential to map a tablet surface for polymorph content uniformity.

Thermogravimetry

Thermogravimetry (TG, and also known as thermogravimetric analysis or TGA) is a technique where one uses a very sensitive balance to continuously determine the

weight of the analyte as a function of temperature or time. This simple technique provides valuable information that can aid in the identification and characterization of the thermal events associated with thermally induced reactions of solvates. For example, several hydrates of nedocromil sodium were identified and profiled using TG as one of the characterization tools (24). As the sample was heated, the weight loss occurred in a stepwise fashion, which facilitated calculation of the hydrate stoichiometries based on the percent weight loss at each step.

As discussed elsewhere in this book, there are different ways in which water can associate with solids. In authentic hydrates, water is incorporated in the crystal lattice, whereas in amorphous and partially crystalline materials, water can associate with disordered regions in the lattice. Water can also be adsorbed and also exist as "bulk water" in incompletely dried solids. TG analysis can also be used to distinguish between some of these states of water in solids. Compared with dehydration, desorption (adsorbed as well as bulk) typically occurs at lower temperatures, although these two processes can overlap. As shown in Figure 5, for carbamazepine dihydrate, when the TG experiment is carried out under isothermal conditions, there can be sequential loss of sorbed and lattice water (25).

TG analysis performed under isothermal conditions can be used to study the kinetics of phase transitions in solvatomorphs (26,27). Alkhamis et al. (26) carried out model-independent isoconversional analysis of the isothermal desolvation of the monohydrate and ethyl acetate solvate of fluconazole. One potential shortcoming of this technique is that a separate and direct technique might be required to confirm the cause of weight loss. In order to address this inadequacy, the TG instrument can be interfaced with additional instrumentation capable of identifying the vapor released upon heating. For example, TG has been used in combination with infrared absorption spectroscopy to understand the thermal behavior of a hydrate (28). In this study, two different thermal events resulting in weight loss were shown to be due to separate dehydration and decomposition processes.

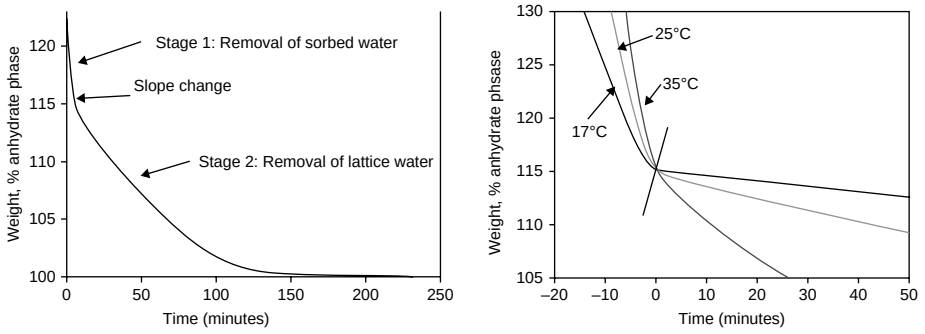

FIGURE 5 (*Left panel*) Dehydration of a wet sample of carbamazepine dihydrate at 0% RH (25°C). The plotted sample weight is based on the dry sample weight after complete dehydration. The first and second stages of dehydration are separated by the point of slope change. (*Right panel*) Effect of temperature on desorption and dehydration kinetics of carbamazepine dihydrate shown at three representative temperatures. For the purpose of comparison, the *x*-axis origin is the time point of transition from desorption to dehydration (point of slope change in left panel). *Source*: From Ref. (25).

Temperature calibration of TG instrumentation can be accomplished using melting point standards or the Curie point transition of a paramagnetic material (ASTM E1582) (29). Although not considered a "reference standard," calcium oxalate monohydrate is frequently used to validate the performance of a TG system (30).

Hot-Stage Microscopy

Visualization of solids using a microscope often provides unique insights not afforded by other techniques. The visual observation of the analyte, placed on a temperature controlled stage ("hot stage") of a microscope, forms the basis of HSM. For the characterization of polymorphs and solvates, HSM, with DSC and TG analyses, forms an optimal routine three-pronged approach. Vitez et al. (31) have briefly outlined the historical evolution of HSM from being merely a melting point determination tool to being an integral part of polymorph characterization. The practice and application of HSM has been reviewed and discussed in recent publications (3,32).

One of the primary advantages of HSM is the small amount of sample needed, which, given the limited availability of an active pharmaceutical ingredient (API) in the discovery phase, often represents a very important consideration. When characterizing solvates, the analyte is typically dispersed in silicone oil in order to aid in the visualization of the thermally induced release of any included solvent. As shown in Figure 6, a desolvation process is usually manifested by loss of transparency (perceived as a darkening of the crystals) (33), and in the formation of bubbles (specifically for hydrates) in the oil (34,35). Caution should be exercised in data interpretation because this observation could be potentially complicated by the release of entrapped air from the solids or by the simple presence of air bubbles in the dispersion medium. In addition, crystals may also darken as a result of decomposition.

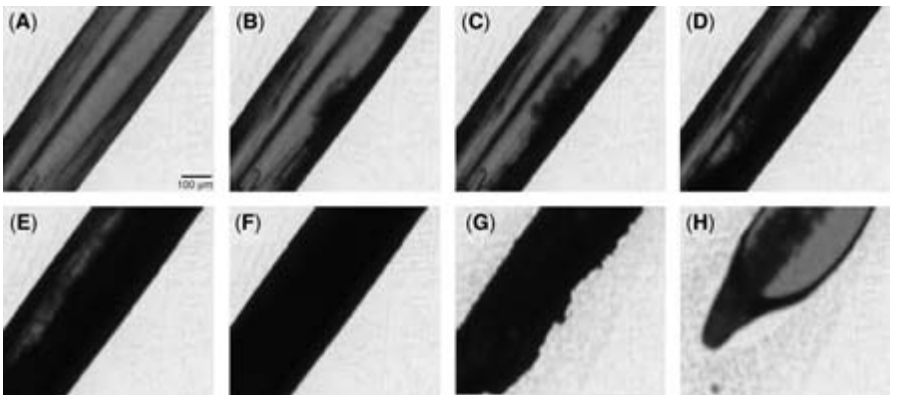

FIGURE 6 Hot-stage photomicrographs of toluene solvate of picryltoluidene, taken at various temperature values: (**A**) 25°C; (**B**) 35°C, onset of desolvation from crystal edges; (**C**) 45°C; (**D**) 55°C; (**E**) 65°C; (**F**) 80°C, completely desolvated anhydrous form; (**G**) 162.5°C, melting onset of the anhydrous form; (**H**) 163°C, remaining crystal of the anhydrous form in the melt. *Source*: From Ref. (33).

In some instances, desolvation may be accompanied by a change in crystal habit. For example, Tonder et al. used HSM to study the desolvation of different niclosamide solvates (36). Although the solvate crystals were characterized by different morphologies, desolvation resulted in the appearance of crystals having the same habit as that of the anhydrate form. In addition, the desolvated crystals were all observed to melt over the same temperature range as did the anhydrate, which was taken as confirming their transformation to the anhydrate phase.

Crystallization from the amorphous state can be demonstrated by the appearance of birefringence. In order to explain DSC observations, Bottom monitored the crystallization of a metastable spherulitic polymorph of sulfapyridine from the amorphous state through a solid-state phase transition to the stable needle-shaped form (12). Grooff et al. (37) used HSM as one of the tools to characterize crystallization of a metastable polymorph of nifedipine from the amorphous state. In this work, two other polymorphs were identified, and an enantiotropic relationship between two of the polymorphs was confirmed by direct observation of a reversible solid-state transition between the two crystal forms.

Microscope stage attachments are commercially available having a wide temperature range (less than –150°C to higher than 350°C) and excellent temperature stability (±0.1°C). In addition, most modern hot-stage systems are equipped with a high-resolution camera capable of rapid image collection, and which is controlled by a computer interface. All these accessories have drastically reduced the subjectivity associated with microscopy and have increased the efficiency of data collection. Consequently, HSM has evolved into one of the primary techniques that is used for the routine identification and characterization of pharmaceutical solids.

CRYSTALLOGRAPHIC CHARACTERIZATION TECHNIQUES

The technique of XRD is exceedingly important in the study of polymorphs and solvatomorphs because it represents the primary method whereby one can obtain fundamental information about the structure of a crystalline substance. The methodology is highly suited for the differentiation of crystal forms, as it would be only by pure coincidence that two compounds might form crystals having identical XRD patterns due to identical three-dimensional spacing of planes in all directions. One example of accidental isostructure is the trihydrate phases of ampicillin and amoxicillin (38), but such instances are uncommon. Typical applications of XRD methodology include the determination of crystal structures, evaluation of polymorphism and solvate structures, evaluation of degrees of crystallinity, and the study of phase transitions.

Every crystal consists of exceedingly small fundamental structural units, which are repeated indefinitely in all directions. In 1830, Hessel conducted a purely mathematical investigation of the possible types of symmetry for a solid figure bounded by planar faces, and deduced that only 32 symmetry groups were possible for such objects. The same conclusion was reached by Bravais in 1949, and Gadolin in 1867. These 32 crystallographic point groups are grouped into six crystal systems, denoted as triclinic, monoclinic, orthorhombic, tetragonal, trigonal, hexagonal, and cubic. Each crystal system is characterized by unique relationships existing among the crystal axes and the angles between these, and this information is summarized in Table 2.

TABLE 2 Characteristics of the Six Crystal Systems

System	Description
Cubic	Three axes of identical length (identified as a_1, a_2, and a_3) intersect at right angles.
Hexagonal	Four axes (three of which are identical in length, and denoted as a_1, a_2, and a_3) lie in a horizontal plane, and are inclined to one another at 120°. The fourth axis, c, is different in length from the others, and is perpendicular to the plane formed by the other three.
Tetragonal	Three axes (two of which are denoted as a_1 and a_2, and are identical in length) intersect at right angles. The third axis, c, is different in length with respect to a_1 and a_2.
Orthorhombic	Three axes of different lengths (denoted as a, b, and c) intersect at right angles. The choice of the vertical c axis is arbitrary.
Monoclinic	Three axes (denoted as a, b, and c) of unequal length intersect such that a and c lie at an oblique angle, and the b axis is perpendicular to the plane formed by the other two.
Triclinic	Three axes (denoted as a, b, and c) of unequal length intersect at three oblique angles.

Bragg (39) explained the diffraction of X rays by crystals using a model where the atoms of a crystal are regularly arranged in space, and that they can be regarded as lying in parallel sheets separated by a definite and defined distance. Then he showed that scattering centers arranged in a plane act like a mirror to X rays incident on them, so that constructive interference would occur in the direction of specular reflection. Within a given family of planes, defined by a Miller index of (hkl) and with an inter-planar distance d, each plane produces a specular reflectance of the incident beam. If the incident X rays are monochromatic (having wavelength equal to λ), then for an arbitrary glancing angle of θ, the reflections from successive planes are out of phase with one another. This yields destructive interference in the scattered beams. However, through the systematic variation of analysis angles, a set of values for θ can be found so that the path difference between X rays reflected by successive planes will be an integral number (n) of wavelengths, and then constructive interference would occur. One ultimately obtains the expression known as Bragg's law that explains the phenomenon:

$$2d\sin\theta = n\lambda \tag{2}$$

Unlike the diffraction of light by a ruled grating, the diffraction of X rays by a crystalline solid leads to constructive interference (i.e., reflection) only at critical Bragg angles. When reflection does occur, it is stated that the plane in question is reflecting in the nth order, or that one observes nth order diffraction for that particular crystal plane. Therefore, one will observe an X-ray scattering response for every plane defined by a unique Miller index of (hkl).

Single-Crystal X-Ray Diffractometry

Single-crystal XRD involves an assignment of the arrangement of atoms based on an electron density map generated by diffraction of a pure, regular, and adequately large crystal (40). Structural information derived from an XRD study of a single

crystal is the most fundamental description of a polymorph or solvatomorph, and helps to explain its physical properties.

Generally, polymorphic structures can be classified into one of two main categories. The first is associated with molecules that can only exist as a rigid grouping of atoms that can be stacked in different motifs to occupy the points of different lattices (i.e., packing polymorphism). One of the best-known instances of packing polymorphism is the allotropic system of carbon, namely graphite and diamond. As shown in Figure 7, in diamonds each carbon atom is tetrahedrally surrounded by four equidistant neighbors, and the tetrahedra are arranged to give a cubic unit cell. Graphite is composed of planar hexagonal nets of carbon atoms, which can be arranged to yield either a hexagonal unit cell (the α-form) or a rhombohedral unit cell (the β-form).

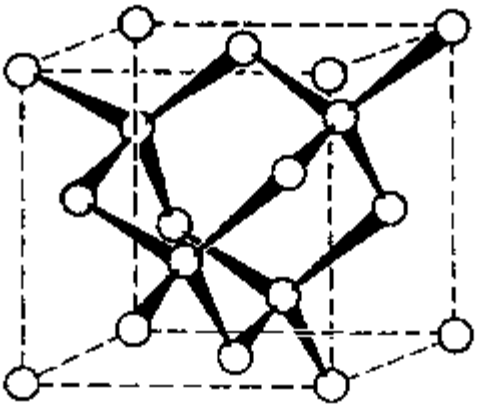

(**1**)

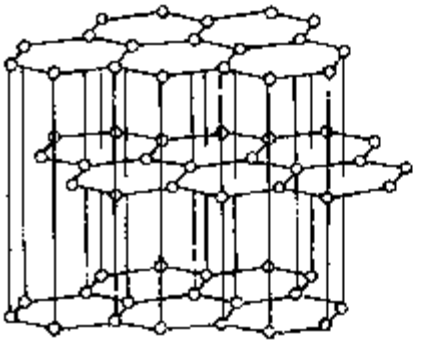

(**2a**)

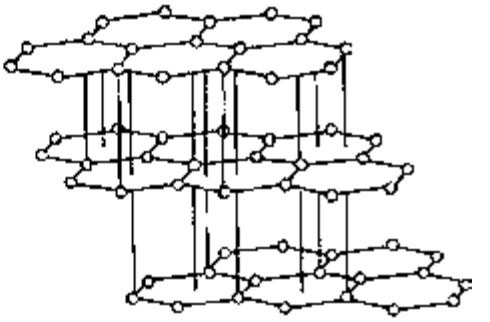

(**2b**)

FIGURE 7 Crystal structure of (**1**) diamond, showing the tetrahedral coordination of each carbon atom. Also shown are the crystal structures of the two polymorphs of graphite, specifically (**2a**) the hexagonal α-form, and (**2b**) the rhombohedral β-form.

The other category is associated with molecules that are capable of existing in conformationally different arrangements, each of which can crystallize in its own characteristic structure. This latter behavior has been termed conformational polymorphism (41), and the probucol system represents an extreme example of a compound where the polymorphism arises from the packing of different conformers (42). Although both polymorphs were found to be monoclinic, the unit cells belonged to different space groups and the molecular conformations of the title compound were quite different (Fig. 8). In form II, the C–S–C–S–C chain is extended,

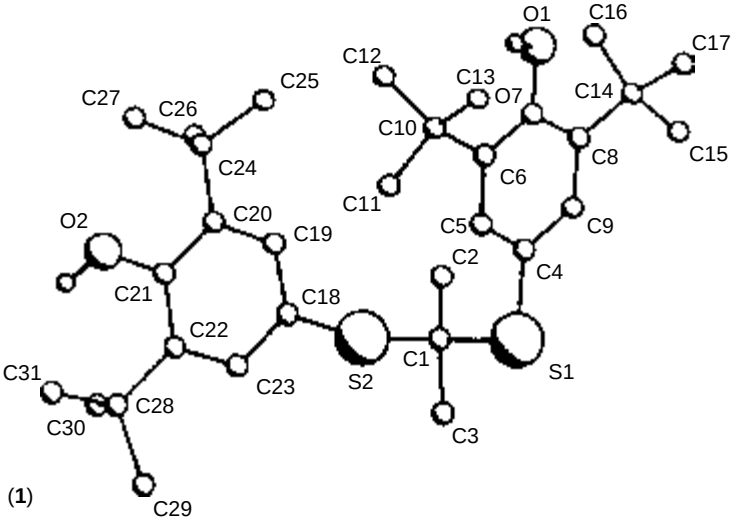

(**1**)

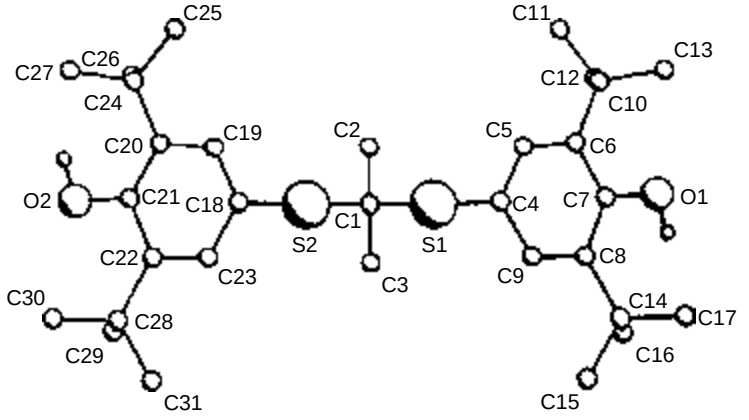

(**2**)

FIGURE 8 Conformation of the probucol molecule existing in **(1)** form I and in **(2)** form II. The figure was adapted from data contained in Ref. (42).

and the molecular symmetry approximates C_{2v}. This symmetry is lost in the structure of form I, where the torsion angles about the two C–S bonds deviate significantly from 180°. The extended conformer was shown to be less stable relative to the bent conformer, as simple grinding was sufficient to convert form II into form I.

Not all instances of conformational polymorphism are as dramatic as the probucol system, and often different conformers of a single sidechain are able to pack into different crystalline arrangements. For instance, the two polymorphs of *p*-(1*R*,3*S*)-3-thioanisoyl-1,2,2-trimethylcyclopentane carboxylic acid were found to be associated with different conformations of the carboxylate group (43). Torsion about a single C–N bond was shown to be the origin of the polymorphism detected for lomeridine dihydrochloride (44). Finally, relatively small differences in molecular conformation were detected for the two polymorphic and four solvated crystalline forms of spironlactone (45).

The analysis of single-crystal XRD data is divided into three parts (46–49). The first of these is the geometrical analysis, where one measures the exact spatial distribution of X-ray reflections and uses these to compute the size and shape of a unit cell. The second part entails a study of the intensities of the various reflections and uses this information to determine the atomic distribution within the unit cell. Finally, one looks at the X-ray diffraction pattern to deduce qualitative information about the quality of the crystal or the degree of order within the solid. This latter analysis may permit the adoption of certain assumptions that may aid in the solving of the crystalline structure.

A determination of the internal structure of a crystal requires the specification of the unit cell dimensions (axis lengths, and angles between these), and measurement of the intensities of the diffraction pattern of the crystal. For a given lattice, regardless of the content of the unit cell, the directions of reflection are the same. The experimental determination of these directions is used to deduce the reciprocal lattice of the crystal, which unambiguously yields the crystal lattice. In addition, the relative intensities diffracted by different planes depend on the contents of the unit cell. Their measurement leads to the determination of the crystal structure factor, and these data permit the determination of the atomic structure of crystals.

Crystallographic characterization of the physical form of an API may be used to understand its performance during pharmaceutical processing. One well-known case is that of polymorphic forms I and II of acetaminophen (also known as paracetamol). The crystal structures of both forms have been determined and the associated implications on their physical properties have been discussed (50). Monoclinic acetaminophen form I cannot be formulated into tablets by direct compression, but the presence of slip planes (illustrated in Fig. 9) in the orthorhombic form II allows its direct compression due to a plastic deformation process. This property is an immense advantage considering that direct compression is a cost-effective and time-efficient method of tablet production.

Crystallographic information is critical to understand dehydration of solvates that have channels in their crystal structures. As mentioned earlier, such solvatomorphs undergo desolvation under certain conditions, leading to the formation of isomorphic desolvates that tend to retain the three-dimensional structures of the parent compound (51,52).

Variable temperature and atmospheric-induced dehydration was characterized in form I of a small molecule developmental drug that was presented as a sodium salt and a trihydrate (53). It was shown that at 25°C, the compound lost 0.5% w/w

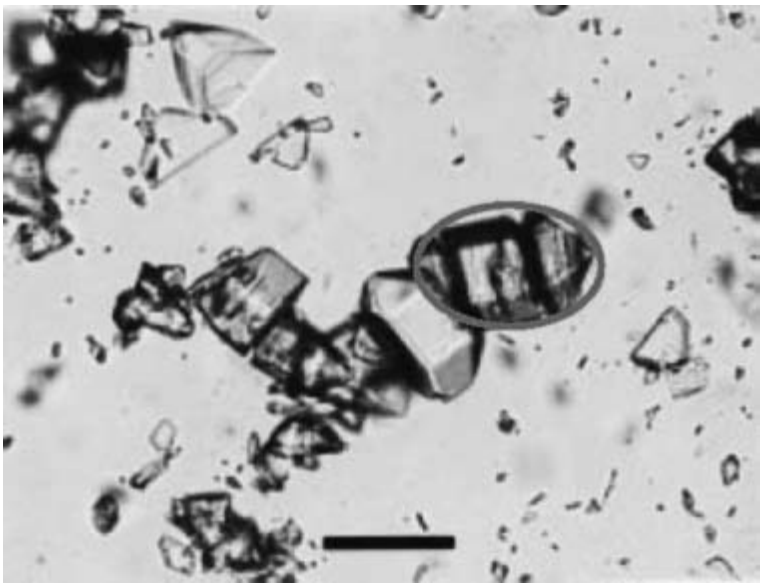

FIGURE 9 Pressure-induced formation of cleavages (*indicated by the ellipse*) in an acetaminophen form II crystal perpendicular to its length, showing the evidence of the existence of slip planes. *Source*: From Ref. (41).

water when the relative humidity was decreased from 90% to 15%, and that this water loss did not cause any change in the XRD pattern. A single-crystal XRD study revealed the existence of channels in the form I crystal structure (illustrated in Fig. 10), where one of the water molecules was weakly bound by hydrogen bonds and where the other two water molecules were bound to the sodium cation. Formation of the isomorphic dehydrate was attributed to the escape of some weakly bound water molecules through the channel, which did not compromise the integrity of the structure. Further decrease in relative humidity into the range of 5% to 15% resulted in a reversible phase transformation into form II, and at relativity humidities below 5%, XRD showed that the compound transformed into the semicrystalline form III. A combination of techniques was used to show that form II was formed as a result of the escape of both weakly and strongly bound water molecules, which caused a partial collapse of the channels. Further dehydration of the solid resulted in disordered anhydrate form III.

The interplay between intramolecular conformational flexibility and intermolecular hydrogen bonding may influence the properties of a polymorph (54), such as in the classic example of ritonavir (55). In 1998, the commercial form of this drug substance (tradename of Norvir®, and marketed as a semi-solid formulation contained in capsules) had to be reformulated because the newer lots failed to meet established dissolution specifications. This was attributed to the sudden appearance of a polymorph (form II), which was much less soluble than the parent polymorph (form I) in the hydro-alcoholic medium of the formulation. Single-crystal XRD studies showed that both the hydrogen bonding capability and the packing density of

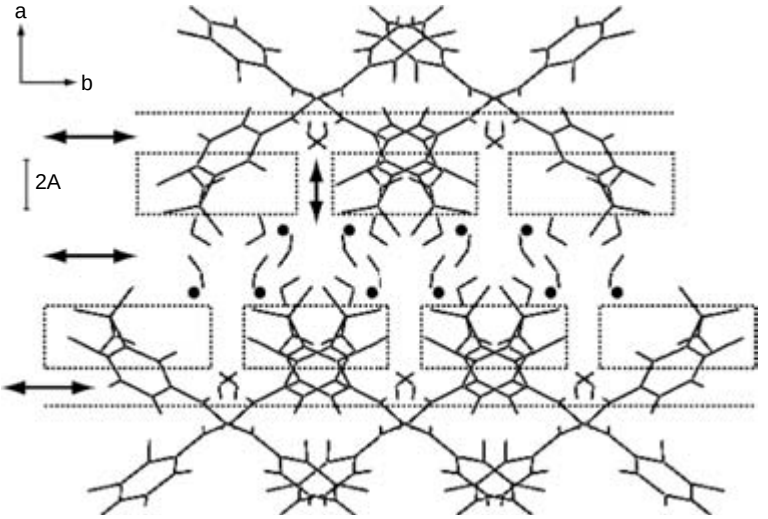

FIGURE 10 Top view along *c*-axis showing the crystal packing of form I of a developmental drug, the sodium salt of *N*-(3-(aminosulfonyl)-4-chloro-2-hydroxyphenyl)-*N*′-(2,3-dichlorophenyl) urea. Arrows indicate potential motion of water along the channels (*dashed lines*). Sodium atoms are represented by dark circles. *Source*: From Ref. (44).

form II was less than that of form I, which could be taken to suggest a greater stability of form I. However, the molecular conformation of ritonavir in form II was more favorable for crystal packing, and made this form the more stable polymorph.

It has been shown elsewhere that a thermodynamically stable polymorph may be characterized by the presence of unstable molecular conformations, such as the thermodynamically stable polymorph of oxybuprocaine hydrochloride, which was shown to have both stable and unstable molecular conformations in its crystalline forms (56).

X-Ray Powder Diffractometry

Although the solving of a crystal structure from an analysis of single-crystal diffraction provides the most fundamental structural understanding of polymorphic solids, the need for suitable single crystals and the degree of complexity associated with data analysis precludes this technique from being used on a routine basis for batch characterization. During routine synthesis, most drug substances are obtained as micro-crystalline powders, for which it is usually sufficient to establish only the physical form (usually polymorphic identity) of the solid, and to verify that the isolated compound is indeed of the desired structure. For these reasons, and in light of the experimental simplicity, the technique of XRD is the predominant tool for the study of polycrystalline materials (57–60), and is eminently suited for the routine characterization of polymorphs and solvates.

A properly prepared sample of a powdered solid will present a substantially random selection of all possible crystal faces and the diffraction patterns will therefore provide information regarding all possible spacings (atomic or molecular) in

the crystal lattice. To measure a powder pattern, a randomly oriented powdered sample is prepared in an effort to expose all the planes in the lattice. The scattering angle is determined by slowly rotating the sample and measuring the angle of diffracted X rays (typically using a scintillation detector) with respect to the angle of the incident beam. Alternatively, the angle between sample and source can be kept fixed, while moving the detector to determine the angles of the scattered radiation. Knowing the wavelength of the incident beam, the spacing between the planes (identified as the *d*-spacings) is calculated using Bragg's Law.

The XRD pattern will therefore consist of a series of peaks detected at characteristic scattering angles. These angles, and their relative intensities, can be correlated with the computed *d*-spacings to provide a full crystallographic characterization of the powdered sample. After indexing all the scattered lines, it is possible to derive unit cell dimensions from the powder pattern of the substance under analysis. For routine work, however, this latter analysis is not normally performed, and one typically compares the powder pattern of the analyte to that of reference materials to establish the polymorphic identity. Because every compound produces its own characteristic powder pattern owing to the unique crystal structure, powder XRD is clearly the most powerful and fundamental tool for polymorphic identity of an analyte.

The United States Pharmacopeia contains a general chapter on XRD (61), which sets the criterion that identity is established if the scattering angles in the powder patterns of the sample and reference standard agree to within the calibrated precision of the diffractometer. It is noted that it is generally sufficient that the scattering angles of the ten strongest reflections obtained for an analyte agree to within either ± 0.10 or $\pm 0.20^\circ$ 2θ, whichever is more appropriate for the diffractometer used. Older versions of the general test contained an additional criterion for relative intensities of the scattering peaks, but it has been noted that relative intensities may vary considerably from that of the reference standard, making it impossible to enforce a criterion based on the relative intensities of corresponding scattering peaks.

For identification purposes, it is usually convenient to identify the angles of the 10 most intense scattering peaks in a powder pattern, and to then list the accepted tolerance ranges of these based on the diffractometer used for the determinations. Useful tabulations of the XRD patterns of a number of compounds have been published by Koundourellis and coworkers, including 12 diuretics (62), 12 vasodilators (63), and 12 other commonly used drug substances (64).

The literature abounds with countless examples that illustrate how powder diffraction has been used to distinguish between polymorphs. It is safe to state that one could not publish the results of a phase characterization study without the inclusion of XRD data. Nowhere is this more crucial than in intellectual property controversies, where the different XRD patterns of polymorphs are used for patentability purposes. For example, two polymorphic forms of ibandronate sodium have been the subject of two United States patent applications (65), and although the XRD patterns of these are somewhat similar (Fig. 11), a sufficient number of differences in scattering peak angles exist so as to permit their identification. In the patent applications, some of the claims define the two polymorphs on the basis of five characteristic XRD scattering peaks, which enables one to tabulate the data and determine whether or not a given sample of ibandronate sodium is within the scope of these XRD claims.

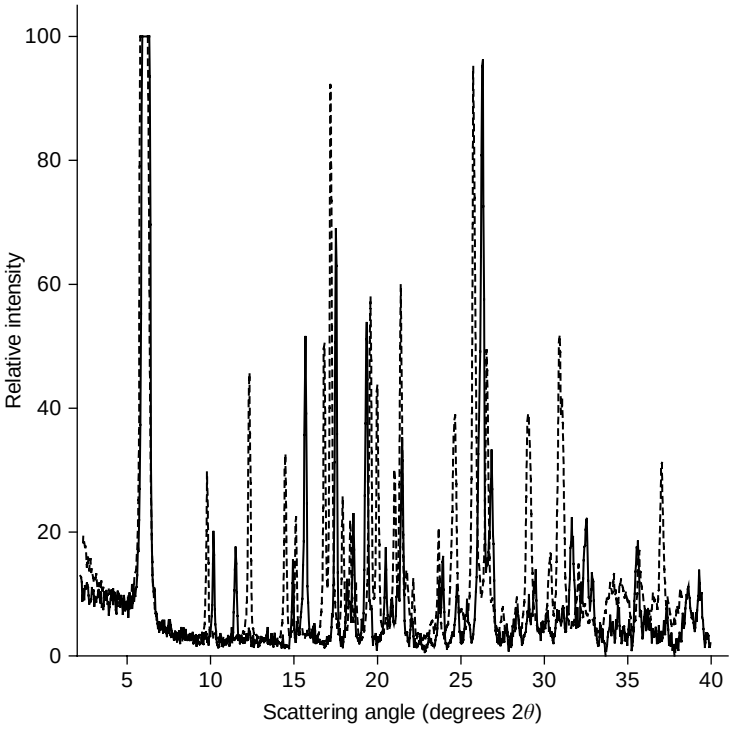

FIGURE 11 X-ray powder diffraction patterns of ibandronate sodium, Form A (*solid trace*) and Form B (*dashed trace*). The patterns have been adapted from data in United States patent applications 2006/0172975 and 2006/0172976 (65).

Once the characteristic XRD patterns of one or more analytes have been established, it is usually possible to develop methods for phase quantification. The methodology is based on the premise that each component will contribute to the overall scattering by an amount that is proportional to its weight fraction in a mixture, and that the powder pattern of each analyte contains one or more peaks whose scattering angle is unique to that analyte. Quantitative analysis typically requires the use of reference standards that contribute known scattering peaks at appropriate scattering intensities. This can be achieved through the use of internal standards, where one would mix reference materials such as elemental silicon or lithium fluoride into the sample matrix.

Although simple intensity correction techniques can be used to develop suitable quantitative XRD methods, the introduction of more sophisticated data acquisition and handling techniques can greatly improve the quality of the developed method. For instance, improvement of the powder pattern quality through use of the Rietveld method has been used to evaluate mixtures of two anhydrous polymorphs of carbamazepine and the dihydrate solvatomorph (66). The method of whole pattern analysis developed by Rietveld (67) has found widespread use in crystal structure refinement and in the quantitative analysis of complex mixtures.

Using this approach, the detection of analyte species was possible even when their concentration was less than 1% in the sample matrix. It was reported that good quantitation of analytes could be obtained in complex mixtures even without the requirement of calibration curves.

Well-characterized and stable (both physically and chemically) Standard Reference Materials are available from the National Institute of Standards and Technology (NIST) (68). These materials are used both to calibrate powder XRD equipment and to measure the instrument sensitivity. Silicon powder (SRM 640c) is typically used for the calibration of *d*-spacing or line position, and also can be used as an internal reference for quantitative applications. NIST SRM 674b is a set of four metal oxides (CeO_2, Cr_2O_3, TiO_2, and ZnO) that are also used as internal standards in quantitative work.

The use of parallel beam optics as a means for determining the polymorphic composition in powder compacts has been evaluated (69). In this study, compressed mixtures of known polymorphic composition were analyzed in transmission mode, and the data processed using profile fitting software. The advantage of using transmission, rather than reflectance, was that the results were not sensitive to the geometrical details of the compact surfaces, and that spurious effects associated with preferential orientation were minimized.

The effects of preferred orientation in XRD analysis can be highly significant, and are most often encountered when working with systems characterized by plate-like or tabular crystal morphologies. A viable XRD sample is one that is free from the deleterious effects of preferential orientation, and any sample packing effect that serves to introduce a non-random pattern of crystal faces can strongly affect the observed intensities and any quantitative results. The problem has been investigated for the three needle-like polymorphs of mannitol, and it was found that through the use of small particles, the preferential orientation effects were held to a minimum, enabling quantification of the polymorphs around the 1% level (70).

The use of powder XRD has been investigated to determine whether one may use pattern indexing as another tool for polymorph screening studies (71). In this work, data were collected on six compounds using two diffractometers that employed transmission geometry, primary monochromatic radiation, and a position-sensitive detector. The data were found to exhibit good angular resolution, and therefore lattice parameters were easily obtained using the indexing program DICYOL-91. The extent of preferred orientation in each pattern was estimated using the DASH implementation of the March–Dollase function. It was concluded that the combination of experimental techniques used would be highly effective compared to just one technique that would require a large number of samples per day with the aim of obtaining the type of high-quality data necessary for pattern recognition and indexing.

Practical complications associated with preferential orientation effects have been discussed in detail (72). A number of sample-packing methods were considered (vacuum free-fall, front-faced packing vs. rear-faced packing, etc.), but the best reduction in preferential orientation was achieved by using materials having small particles that were produced by milling. Through the use of sieving and milling, excellent linearity in diffraction peak area as a function of analyte concentration was attained. The authors deduced a protocol for development of a quantitative XRD method consisting of (a) calculation of the mass attenuation coefficient of the drug substance, (b) selection of appropriate diffraction peaks for quantification,

(c) evaluation of the loading technique for adequate sample size, (d) determination of whether preferred orientation effects can be eliminated through control of the sample particle size, (e) determination of appropriate milling conditions to obtain reproducibility in peak areas, and (f) generation of calibration curves from physical mixtures.

Profile-fitting analysis has been combined with powder XRD to develop a quantitative method to determine the relative amounts of two prazosin hydrochloride polymorphs in their powder mixtures (73). Powder patterns of the pure α- and δ-polymorphs were initially obtained, and then patterns of calibration samples containing the α-form at concentrations ranging from 0.5% to 10% w/w in bulk δ-form. As is evident from Figure 12, the α-form exhibits a strong scattering peak at 27.5° 2θ where the δ-form exhibits little scattering, thus making this peak suitable for use in developing a quantitative method for phase composition. Using mathematical profile fitting, the background intensity level of the δ-form and the integrated intensity of peaks due to the α-form were determined, enabling a detection limit of 0.5%.

Powder XRD and diffuse reflectance infrared absorption spectroscopy analyses were used to develop two independent quantitative phase composition methods

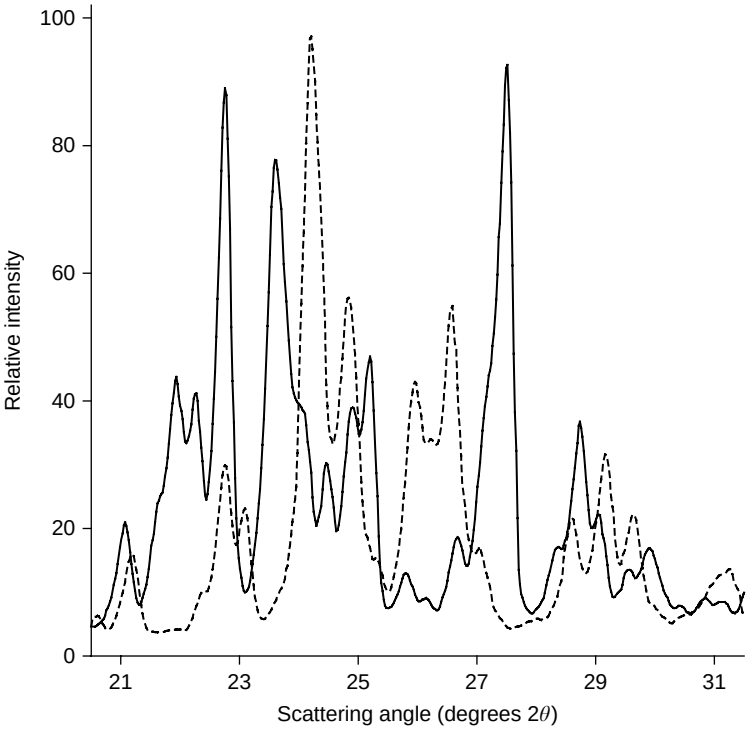

FIGURE 12 Expanded X-ray powder diffraction patterns of prazosin hydrochloride, α-form (*solid trace*) and δ-form (dashed trace), illustrating the peak at 27.5° 2θ that was used for quantitation purposes. The patterns have been adapted from data in Ref. (73).

for the determination of quantities of cefepime dihydrochloride dihydrate in samples of cefepime dihydrochloride monohydrate (74). For the XRD method, over a working concentration range 2.5% to 15% w/w, the limit of detection and quantification of the dihydrate in monohydrate were respectively 0.75% and 2.5% w/w. For the infrared method, a working range of 1.0% to 8.0% w/w was established with a minimum quantifiable level of 1.0% w/w and a limit of detection of 0.3% w/w dihydrate in monohydrate.

When reference samples of the pure amorphous and pure crystalline phases of a substance are available, calibration samples of known degrees of crystallinity can be prepared by mixing these reference samples. Establishment of a calibration curve (XRD response vs. degree of crystallinity) permits quantification of crystallinity in unknown samples. In one such study, a quantitative method was developed by beginning with commercially available crystalline digoxin and ball-milling of this substance to obtain various samples having various degrees of amorphous phase (75). Calibration mixtures were prepared as a variety of blends prepared from the 100% crystalline and 0% crystalline materials, and acceptable linearity and precision was obtained in the calibration curve of XRD intensity versus actual crystallinity.

In the absence of standard materials having known degree of crystallinity, one may determine the degree of crystallinity from the simple relation:

$$\mathrm{DOC} = (A_C/A_T)(100) \tag{3}$$

where A_C is the integrated intensity attributable to the crystalline regions, and A_T is the total diffracted intensity. The evaluation of A_C and A_T is illustrated in Figure 13, where the reported XRD pattern of lenalidomide Form H (76) is shown along with its associated amorphous background. One would obtain A_C as the sum of the areas of the peaks above the dashed line, whereas A_T would be measured as the total area under the curve.

Determination of Crystal Structures from Powder Diffraction Data

As discussed above, a powder pattern will consist of a series of peaks having varying intensities, detected at various scattering angles. Through the indexing process, the *d*-spacings computed from the values of the scattering angles are assigned to diffraction from the crystal planes defined by their Miller (*hkl*) indices to provide a full crystallographic characterization of the powdered sample. After the indexing procedure is complete, it is possible to derive unit cell dimensions and other crystallographic information from a high-resolution powder pattern of a substance, eventually developing an approximate structural model that can be refined against experimental powder XRD data (structure refinement) (77–81). This procedure is best conducted on diffraction data collected using a high-flux synchrotron source (82).

Of the three crystal forms of telmisartan, the structure of solvated Form C was determined using single-crystal XRD and the structures of non-solvated forms A and B were determined from high-resolution powder XRD data using the method of simulated annealing for structure solution followed by Rietveld refinement (83). With 13 degrees of freedom (three translational, three orientational, and seven torsion angles), the structure solution was accomplished in approximately two hours of computer time, demonstrating that the crystal packing and the molecular conformation

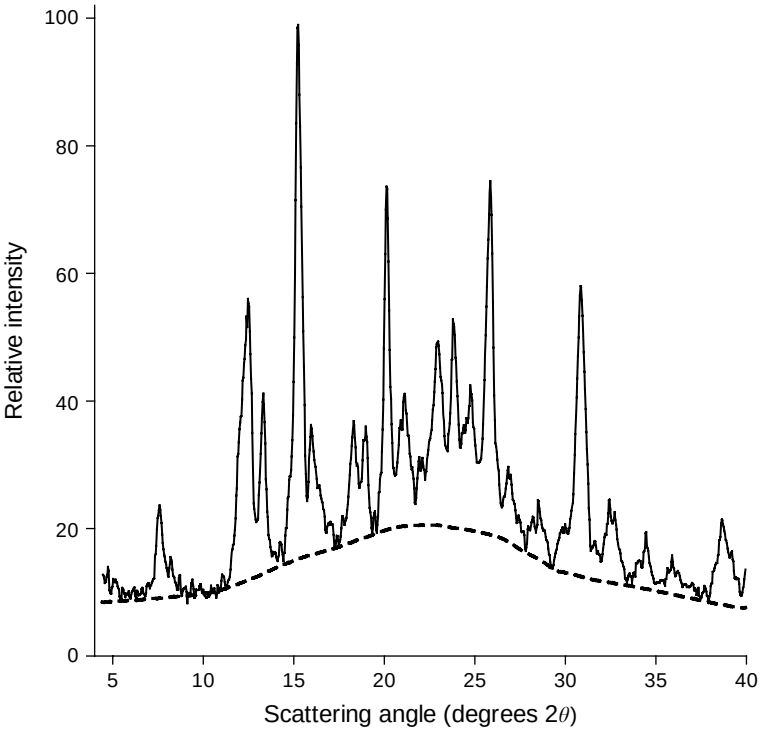

FIGURE 13 XRD pattern of lenalidomide form H (*solid trace*), and an estimation of the amorphous background (*dashed line*). The powder pattern of form H was adapted from data in Ref. (74).

of medium-sized pharmaceutical compounds could be solved quickly and routinely from high-resolution powder XRD data.

Other examples where structural properties have been derived from powder XRD data include enalapril maleate form II (84) and bupivacaine base (85).

Variable-Temperature X-Ray Diffractometry

XRD, performed on a hot stage, enables one to obtain powder patterns at elevated temperatures, and permits the deduction of structural assignments for thermally induced phase transformation reactions. By conducting VT-XRD studies, one can bring the system to conditions that had been indicated to be of interest during the conduct of thermal analysis studies. XRD systems equipped with hot-stage sample holders have been described, with this instrumentation being capable of obtaining powder patterns at temperatures of pharmaceutical interest (86,87). VT-XRD studies conducted under isothermal conditions can also be used for the calculation of activation energies of solid-state reactions.

VT-XRD is ideally suited to explain potentially complex solid-state transformations involving pharmaceutical hydrates. For example, Terakita et al. examined the dehydration behavior of calcium benzoate trihydrate, a system where the solid state transformations involved, in addition to crystalline and amorphous phases,

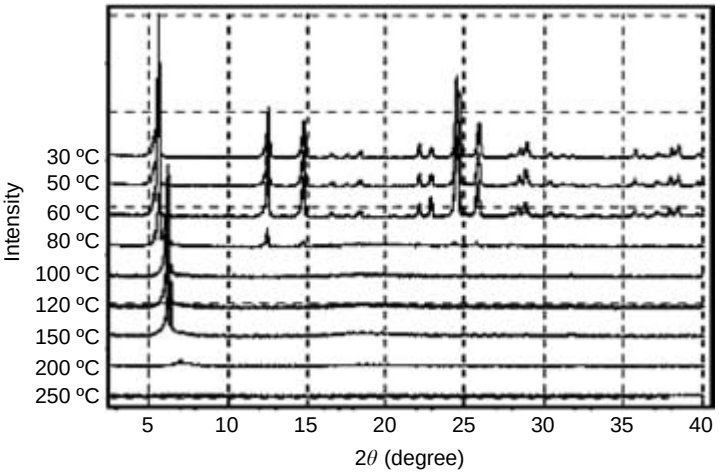

FIGURE 14 VT-XRD patterns obtained during the drying of calcium benzoate trihydrate, showing the gradual dehydration to a mesophase (100°C), which eventually culminated in the formation of an amorphous phase (250°C). *Source*: From Ref. (88).

a mesophase (88). As the temperature was increased, the trihydrate crystal form gradually formed a mesophase, as indicated by a sharp low-angle peak. As illustrated in Figure 14, further heating resulted in complete amorphization and the disappearance of all XRD peaks. A ground sample of the trihydrate was found to contain traces of calcium benzoate monohydrate, which was confirmed by VT-XRD to have formed by a recrystallization process. In this work, VT-XRD was shown to function both as an aid in the identification of crystalline phases, as well as in decoding the mechanism of their formation. Understanding such transformations and the knowledge of the conditions under which phase transitions occur, could aid in optimizing process parameters, such as the drying temperature of granules.

By virtue of their higher free energy compared to their more stable counterparts, metastable polymorphs of drug substances can significantly affect drug release from a dosage form. For example, theophylline monohydrate was observed by VT-XRD to dehydrate to the anhydrous form via an intermediate metastable anhydrate (89). The dissolution performance of tablets containing stable and metastable anhydrous theophylline was compared, where surprisingly the dissolution rate of the metastable form was found to be slower than that of the stable form. This phenomenon was shown to be due to the relatively rapid conversion of the metastable anhydrate form to the monohydrate form in the dissolution medium.

Isomorphic desolvates, formed by desolvation of solvates, represent the type of lattice structures that can be inherently unstable owing to their molecular packing. Consequently, such materials tend to be quite reactive and prone to instability, especially during their secondary processing into drug products (90). Miroshynk et al. used VT-XRD to investigate processing-induced phase transformations in erythromycin dihydrate (91). Dehydration resulted in shifts in the XRD peak positions, where some peaks shifted to higher angles owing to lattice expansion, whereas other peaks shifted to lower angular values as a result of lattice contraction.

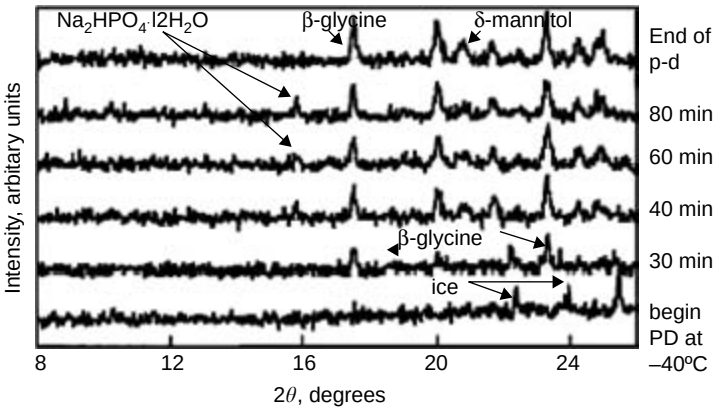

FIGURE 15 In situ VT-XRD patterns obtained during the primary drying (PD) of a frozen aqueous solution consisting of buffer salts, mannitol, and glycine. The solution was first cooled to –70°C at 2°C/min, which was then followed by heating to the primary drying temperature (–40°C) at 5°C/min. Primary drying was carried out for 4 hours. *Source*: From Ref. (92).

At higher temperatures, the XRD patterns indicated that the solids rearranged to form anhydrous erythromycin.

Although the typical use of VT-XRD is at elevated temperatures, the technique can also be used for work under sub-ambient conditions. For example, Pyne et al. characterized freeze-dried buffered aqueous systems of mannitol and glycine, and found that δ-mannitol and β-glycine crystallized during primary drying (92). By monitoring the intensities of the characteristic peaks of δ-mannitol and β-glycine both during primary and secondary drying, it was possible to determine the rate of crystallization of these solutes. Interestingly, one of the buffer salts, disodium hydrogen phosphate, crystallized as its dodecahydrate phase at the start of primary drying, but became dehydrated to an amorphous anhydrate at the end of the drying cycle (Fig. 15). It is important to note that conventional XRD of the final lyophile would not have revealed the crystallization of the buffer salt. The selective crystallization of disodium hydrogen phosphate only became evident by monitoring the phase transitions that took place *during* the freeze–drying process.

While attempting to simulate pharmaceutical processing steps, it is important to consider the effect of sample geometry on the phase transition kinetics. The relative quantities of stable and metastable anhydrous theophylline were found to be significantly different when theophylline monohydrate granules were dried in a microscale fluid bed dryer and in the sample stage of a powder X-ray diffractometer, with these differences being attributed primarily to differences in sample geometry (93). Although the VT-XRD sample bed was stationary, resulting in a slow drying rate, the sample in the fluid bed drier was dried rapidly due to fluidization.

XRD studies conducted at elevated temperatures can also be run under controlled water vapor pressures, using humidified nitrogen to control the vapor pressure. Han et al. proposed this technique to rapidly evaluate the physical stability of pharmaceutical hydrates, and studied the isothermal dehydration kinetics

of amoxicillin trihydrate at 68°C and at different water vapor pressures (94). The product they obtained was a poorly crystalline anhydrate. From these kinetic studies, the transition water vapor pressure of amoxicillin trihydrate was determined to be approximately 10.5 Torr at 68°C.

In addition to being extremely useful in the study of phase transformations, VT-XRD can also be used to obtain information on substance decomposition during a variable-temperature study. The commercially available form of aspartame is hemihydrate form II, which is known to transform into hemihydrate form I when milled, but a 2.5-hydrate species is also known (95,96). Through the use of VT-XRD, it was found that when either hydrate form was heated to 150°C, they dehydrated into the same anhydrous phase. Further heating of the anhydrate to 200°C resulted in a thermally induced cyclization, forming 3-(carboxymethyl)-6-benzyl-2, 5-dioxopiperazine. The 2.5-hydrate was shown to dehydrate to hemihydrate form II when heated to 70°C, and this dehydration product was shown to undergo the same decomposition sequence as directly crystallized hemihydrate form II.

REFERENCES

1. Wendlandt W. Thermal Analysis. New York: John Wiley & Sons, 1986.
2. Ford J, Timmins P. Pharmaceutical Thermal Analysis: Techniques and Applications. New York: E. Horwood, 1989.
3. Craig D. Pharmaceutical applications of DSC. In Thermal Analysis of Pharmaceuticals. In: Craig D, Reading M, eds. New York: CRC Press, 2006: 53–100.
4. Craig D. Characterization of polymorphic systems using thermal analysis. In: Polymorphism in the Pharmaceutical Industry. In: Hilfiker R, ed. Weinheim: Wiley-VCH, 2006: 43–79.
5. Jenkins R, Snyder RL. Introduction to X-Ray Powder Diffractometry. New York: John Wiley & Sons, 1996.
6. Suryanarayanan R. X-Ray powder diffractometry. In: Brittain HG, ed. Physical Characterization of Pharmaceutical Solids. New York: Marcel Dekker, 1995.
7. Braun DE, Tobbens DM, Kahlenberg V. Structural and thermodynamic features of crystal polymorphs of R-cinacalcet hydrochloride. Cryst Growth Des 2008; 8: 4109–19.
8. Coleman N, Craig D. Modulated temperature differential scanning calorimetry: a novel approach to pharmaceutical thermal analysis. Int J Pharm 1996; 135: 13–29.
9. Hill V, Craig D, Feely L. The effects of experimental parameters and calibration on MTDSC data. Int J Pharm 1999; 192: 21–32.
10. Simon S. Temperature-modulated differential scanning calorimetry: theory and application. Thermochim Acta 2001; 374: 55–71.
11. Kawakami K, Ida Y. Application of modulated-temperature DSC to the analysis of enantiotropically related polymorphic transitions. Thermochim Acta 2005; 427: 93–9.
12. Bottom R. The role of modulated temperature differential scanning calorimetry in the characterization of a drug molecule exhibiting polymorphic and glass forming tendencies. Int J Pharm 1999; 192: 47–53.
13. Singh S, Jalali A, Alden M. Modulated temperature differential scanning calorimetry for examination of tristearin polymorphism: I. Effect of operational parameters. J Am Oil Chem Soc 1999; 76: 499–505.
14. Singh S, Jalali A, Alden M. Modulated temperature differential scanning calorimetry for examination of tristearin polymorphism: 2. Isothermal crystallization of metastable forms. J Am Oil Chem Soc 1999; 76: 507–10.
15. Kaushal A, Bansal A. Thermodynamic behavior of glassy state of structurally related compounds. Eur J Pharm Biopharm 2008; 69: 1067–76.

16. Graeser K, Strachan C, Patterson J. Physicochemical properties and stability of two differently prepared amorphous forms of simvastatin. Cryst Growth Des 2008; 8: 128–35.
17. Guinot S, Leveiller F. The use of MTDSC to assess the amorphous phase content of a micronized drug substance. Int J Pharm 1999; 192: 63–75.
18. Saklatvala R, Royall P, Craig D. The detection of amorphous material in a nominally crystalline drug using modulated temperature DSC: a case study. Int J Pharm 1999; 192: 55–62.
19. McGregor C, Bines E. The use of high-speed differential scanning calorimetry (Hyper-DSCTM) in the study of pharmaceutical polymorphs. Int J Pharm 2008; 350: 48–52.
20. McMahon L, Timmins P, Williams A. Characterization of dihydrates prepared from carbamazepine polymorphs. J Pharm Sci 1996; 85: 1064–9.
21. Sussich F, Urbani R, Princivalle F. Polymorphic amorphous and crystalline forms of trehalose. J Am Chem Soc 1998; 120: 7893–9.
22. Han J, Suryanarayanan R. Applications of pressure differential scanning calorimetry in the study of pharmaceutical hydrates: I. Carbamazepine dihydrate. Int J Pharm 1997; 157: 209–18.
23. Sanders G, Roberts C, Danesh A. Discrimination of polymorphic forms of a drug product by localized thermal analysis. J Microsc 2000; 198: 77–81.
24. Khankari R, Chen L, Grant DJW. Physical characterization of nedocromil sodium hydrates. J Pharm Sci 1998; 87: 1052–61.
25. Surana R, Pyne A, Suryanarayanan R. Solid-vapor interactions: influence of environmental conditions on the dehydration of carbamazepine dihydrate. AAPS PharmSci 2003; 4: 1–10.
26. Alkhamis K, Salem M, Obaidat R. Comparison between dehydration and desolvation kinetics of fluconazole monohydrate and fluconazole ethyl acetate solvate using three different methods. J Pharm Sci 2006; 95: 859–70.
27. Miyazaki T, Sivaprakasam K, Tantry J, et al. Physical characterization of dibasic calcium phosphate dihydrate and anhydrate. J Pharm Sci 2009; 98: 905–16.
28. Rastogi S, Zamansky I, Roy S. Solid-state phase transitions of AG337, an antitumor agent. Pharm Dev Tech 1999; 4: 623–32.
29. Blaine RL, Fair PG. Estimate of the true magnetic transition temperatures for the ICTA reference materials GM761. Thermochim Acta 1983; 67: 233–40.
30. Hill JO. Thermogravimetric analysis. In Encyclopedia of Chemical Processing, Volume 5. In: Lee S, Lee L, eds. New York: CRC Press, 2006: 3009–22.
31. Vitez I, Newman A, Davidovich M. The evolution of hot-stage microscopy to aid solid-state characterizations of pharmaceutical solids. Thermochim Acta 1998; 324: 187–96.
32. Bernstein J. Polymorphism in Molecular Crystals. Clarendon: Oxford University Press, 2002.
33. Braun D, Gelbrich T, Jetti R. Colored polymorphs: thermochemical and structural features of N-picryl-p-toluidine polymorphs and solvates. Cryst Growth Des 2008; 8: 1977–89.
34. Zhu H, Grant DJW. Dehydration behavior of nedocromil magnesium pentahydrate. Int J Pharm 2001; 215: 251–62.
35. Zhu H. Dehydration behavior and structural characterization of the GW275919X monohydrate. Int J Pharm 2006; 315: 18–23.
36. Tonder E, Mahlatji M, Malan S. Preparation and physicochemical characterization of five niclosamide solvates and one hemisolvate. AAPS PharmSciTech 2004; 5: 1–10.
37. Grooff D, De Villiers M, Liebenberg W. Thermal methods for evaluating polymorphic transitions in nifedipine. Thermochim Acta 2007; 454: 33–42.
38. Boles MO, Girven RJ, Gane PAC. The structure of amoxicillin trihydrate and a comparison with the structures of ampicillin. Acta Cryst 1978; B34: 461–6.
39. Bragg WH, Bragg WL. X-Rays and Crystal Structure. London: G. Bell & Sons, 1918.

40. Cullity BD, Stock SR. Elements of X-Ray Diffraction. Upper Saddle River, NJ: Prentice Hall, 2001.
41. Bernstein J. Conformational polymorphism, chapter 13 in Organic Solid State Chemistry. In: Desiraju GR, ed. Amsterdam: Elsevier, 1987: 471–518.
42. Gerber JJ, Caira MR, Lötter AP. Structures of two conformational polymorphs of the cholesterol-lowering drug probucol. J Cryst Spect Res 1993; 23: 863–9.
43. Rambaud J, Bouassab A, Pauvert B, et al. Comparative study of the two polymorphic forms of p-(1R, 3S) 3-thioanisoyl-1, 2,2-trimethylcyclopentane carboxylic acid. J Pharm Sci 1993; 82: 1262–5.
44. Hiramatsu Y, Suzuki H, Kuchiki A, et al. X-ray structural studies of lomeridine dihydrochloride polymorphs. J Pharm Sci 1996; 85: 761–6.
45. Agafonov V, Legendre B, Rodier N, et al. Polymorphism of spironolactone. J Pharm Sci 1991; 80: 181–5.
46. Woolfson MM. X-Ray Crystallography. Cambridge: Cambridge University Press, 1970.
47. Stout GH, Jensen LH. X-Ray Structure Determination: A Practical Guide. New York: Macmillan Co, 1968.
48. Clegg W, Blake AJ, Gould RO, et al. Crystal Structure Analysis: Principles and Practice. New York: Oxford University Press, 2001.
49. Giacovazzo C. Fundamentals of Crystallography. New York: Oxford University Press, 2002.
50. Nichols G, Frampton C. Physicochemical characterization of the orthorhombic polymorph of paracetamol crystallized from solution. J Pharm Sci 1998; 87: 684–93.
51. Reutzel-Edens S, Kleemann R, Lewellen P. Crystal forms of LY334370 HCl: isolation, solid-state characterization, and physicochemical properties. J Pharm Sci 2003; 92: 1196–205.
52. Stephenson G, Groleau E, Kleemann R. Formation of isomorphic desolvates: creating a molecular vacuum. J Pharm Sci 1998; 87: 536–42.
53. Vogt F, Brum J, Katrincic L. Physical, crystallographic, and spectroscopic characterization of a crystalline pharmaceutical hydrate: understanding the role of water. Cryst Growth Des 2006; 6: 2333–54.
54. Nangia A. Conformational polymorphism in organic crystals. Acc Chem Res 2008; 41: 595–604.
55. Bauer J, Spanton S, Henry R. Ritonavir: an extraordinary example of conformational polymorphism. Pharm Res 2001; 18: 859–66.
56. Griesser U, Jetti R, Haddow M. Conformational polymorphism in oxybuprocaine hydrochloride. Cryst Growth Des 2008; 8: 44–56.
57. Klug HP, Alexander LE. X-ray Diffraction Procedures for Polycrystalline and Amorphous Materials, 2nd edn. New York: Wiley-Interscience, 1974.
58. Suryanarayanan R. X-ray Powder diffractometry, chapter 7 in Physical Characterization of Pharmaceutical Solids. In: Brittain HG, ed. New York: Marcel Dekker, 1995: 187–221.
59. Brittain HG. X-ray Diffraction of pharmaceutical materials, chapter 7, in Profiles of Drug Substances, Excipients, and Related Methodology, volume 30. In: Brittain HG, ed. Amsterdam: Elsevier Academic Press, 2003: 273–319.
60. Blachére JR, Brittain HG. X-ray diffraction methods for the characterization of solid pharmaceutical materials, Chapter 3.4, in Preformulation in Solid Dosage Form Development. In: Adeyeye MC, Brittain HG, eds. New York: Informa Healthcare Press, 2008: 229–52.
61. X-Ray Diffraction, General test <941>. United States Pharmacopoeia 32, Volume 1. Rockville, MD: The United States Pharmacopoeial Convention, 2009: 390–2.
62. Koundourellis JE, Markopolou CK, Underwood FA, et al. The x-ray characterization of 12 diuretics. J Chem Eng Data 1992; 37: 187–91.
63. Koundourellis JE, Malliou ET, Sullivan RAL, et al. X-ray characterization of 12 vasodilators in current use. J Chem Eng Data 1999; 44: 656–60.

64. Koundourellis JE, Malliou ET, Sullivan RAL, et al. X-ray powder diffraction data for 12 drugs in current use. J Chem Eng Data 2000; 45: 1001–6.
65. Eiermann U, Junghans B, Knipp B, et al. Ibandronate polymorph, United States Patent Applications 2006/0172975 and 2006/0172976, published August 3, 2006.
66. Iyengar SS, Phadnis NV, Suryanarayanan R. Quantitative analyses of complex pharmaceutical mixtures by the Rietveld metnod. Powder Diffraction 2001; 16: 20–4.
67. Rietveld HM. A profile refinement method for nuclear and magnetic structures. J Appl Crystallogr 1969; 2: 65–71.
68. https://srmors.nist.gov/tables/view_table.cfm?table=209-1.htm: Accessed: November 9, 2008.
69. Cao W, Bates S, Peck GE, et al. Quantitative determination of polymorphic composition in intact compacts by parallel-beam X-ray powder diffractometry. J Pharm Biomed Anal 2002; 30: 1111–19.
70. Campell Roberts SN, Williams AC, Grimsey IM, et al. Quantitative analysis of mannitol polymorphs. X-ray powder diffractometry: exploring preferred orientation effects. J Pharm Biomed Anal 2002; 28: 1149–59.
71. Florence AJ, Baumgartner B, Weston C, et al. Indexing powder patterns in physical form screening: instrumentation and data quality. J Pharm Sci 2003; 92: 1930–8.
72. Kidd WC, Varlashkin P, Li CY. The applicability of powder X-ray diffraction to the quantification of drug substance polymorphs using a model organic system. Powder Diffraction 1993; 8: 180–7.
73. Tanninen VP, Yliruusi J. X-ray powder diffraction profile fitting in quantitative determination of two polymorphs from their powder mixture. Int J Pharm 1992; 81: 169–77.
74. Bugay DE, Newman AW, Findlay WP. Quantitation of cefepime·2HCl dihydrate in cefepime·2HCl monohydrate by diffuse reflectance IR and powder X-ray diffraction techniques. J Pharm Biomed Anal 1996; 15: 49–61.
75. Black DB, Lovering EG. Estimation of the degree of crystallinity in digoxin by X-ray and infrared methods. J Pharm Pharmacol 1977; 29: 684–7.
76. Jaworsky MS, Chen RS-C, Muller GW, et al. Polymorphic forms of 3-(4-amino-1-oxo-1,3 dihydro-isoindol-2-yl)-piperidin-e-2,6-dione. United States Patent Application 2005/0096351, published May 5, 2005.
77. Poojary DM, Clearfield A. Application of X-ray powder diffraction techniques to the solution of unknown crystal structures. Acc Chem Res 1997; 30: 414–22.
78. Stephenson GA. Structure determination from conventional powder diffraction data: application to hydrates, hydrochloride salts, and metastable polymorphs. J Pharm Sci 2000; 89: 958–66.
79. Harris K, Tremayne M, Kariuki B. Contemporary advances in the use of powder X-ray diffraction for structure determination. Angew Chem Int Ed 2001; 40: 1626–51.
80. Harris KDM. New opportunities for structure determination of molecular materials directly from powder diffraction data. Cryst Growth Des 2003; 3: 887–95.
81. Habershon S, Cheung EY, Harris KDM, Johnston RL. Powder diffraction indexing as a pattern recognition problem: a new approach for unit cell determination based on an artificial neural network. J Phys Chem A 2004; 108: 711–16.
82. Cernik R, Louer D. Indexing unit cells from synchrotron X-ray powder diffraction data. J Appl Cryst 1993; 26: 277–80.
83. Dinnebier RE, Sieger P, Nar H, Shankland K, David WIF. Structural characterization of three crystalline modifications of telmisartan by single crystal and high-resolution X-ray powder diffraction. J Pharm Sci 2000; 89: 1465–79.
84. Kiang Y-H, Huq A, Stephens PW, et al. Structure determination of enalapril maleate form II from high-resolution X-ray powder diffraction data. J Pharm Sci 2003; 92: 1844–53.
85. Cheung EY, Harris KDM, Johnston RL, et al. Rationalizing the structural properties of bupivacaine base – a local anesthetic – directly from powder X-ray diffraction data. J Pharm Sci 2004; 93: 667–74.

86. Epple M, Cammenga HK. Investigation of solid state reactions and solid-solid phase transformations with time- and temperature-resolved X-ray diffractometry. Ber Bunsenges Phys Chem 1992; 96: 1774–8.
87. Conflant P, Guyot-Hermann A-M. Contribution of X-ray powder diffraction versus temperature to the solid state study of pharmaceutical raw materials. Eur J Pharm Biopharm 1994; 40: 388–92.
88. Terakita A, Byrn SR. Structure and physical stability of hydrates and thermotropic mesophase of calcium benzoate. J Pharm Sci 2006; 95: 1162–72.
89. Phadnis N, Suryanarayanan R. Polymorphism in anhydrous theophylline: implications on the dissolution rate of theophylline tablets. J Pharm Sci 1997; 86: 1256–63.
90. Govindarajan R, Suryanarayanan R. Processing induced phase transformations and their implications on pharmaceutical product quality, chapter 13 in Polymorphism in the Pharmaceutical Industry. In: Hilfiker R, ed. Weinheim: Wiley-VCH, 2006: 333–61.
91. Miroshnyk I, Khriachtchev L, Mirza S. Insight into thermally induced phase transformations of erythromycin A dihydrate. Cryst Growth Des 2006; 6: 369–74.
92. Pyne A, Chatterjee K, Suryanarayanan R. Solute crystallization in mannitol-glycine systems: implications on protein stabilization in freeze-dried formulations. J Pharm Sci 2003; 92: 2272–83.
93. Airaksinen S, Karjalainen M, Räsänen E. Comparison of the effects of two drying methods on polymorphism of theophylline. Int J Pharm 2004; 276: 129–41.
94. Han J, Suryanarayanan R. A method for the rapid evaluation of the physical stability of pharmaceutical hydrates. Thermochim Acta 1999; 329: 163–70.
95. Leung SS, Grant DJW. Solid state stability studies of model dipeptides: aspartame and aspartylphenylalanine. J Pharm Sci 1997; 86: 64–71.
96. Rastogi S, Zakrzewski M, Suryanarayanan R. Investigation of solid-state reactions using variable temperature X-ray powder diffractrometry. I. Aspartame hemihydrate. Pharm Res 2001; 18: 267–73.

10 Vibrational Spectroscopy

Harry G. Brittain
Center for Pharmaceutical Physics, Milford, New Jersey, U.S.A.

INTRODUCTION

In addition to the crystallographic techniques of X-ray diffraction and optical crystallography, methodologies based on molecular spectroscopy have become extremely important for the characterization of polymorphs and solvatomorphs (1). These methods become particularly useful when information must be obtained from a small amount of sample in a short period of time, and because most of the methods are non-destructive in nature, the analyzed material can be recycled for additional study once the measurements are complete. A number of techniques have been developed for the characterization of compounds in the solid state, and those based on probing the periodic motion of atoms and groups of atoms in molecules in solids will form the scope of this chapter.

The vibrational patterns existing in molecules are characterized by repetitious departures and returns about the center of gravity, and these correlated motions are termed the vibrational modes of the molecule. Energies associated with the lowest energy vibrational modes of a chemical compound will lie within the range of 400 to 4000 cm^{-1}, a spectral region of the electromagnetic spectrum denoted as the mid-infrared. Transitions among states associated with these vibrational modes can be observed directly through their absorbance in the mid-infrared region of the spectrum, or alternatively through an inelastic scattering of incident energy via the Raman effect. Transitions involving the excitation of multiple vibrational states are known as overtone bands or combination bands, and these are observed in the near-infrared (NIR) region of the spectrum (4000–13,350 cm^{-1}).

Infrared absorption spectroscopy is an enormously useful technique for the physical characterization of solids having pharmaceutical interest. When the crystallography of a given molecule sufficiently perturb the frequencies of vibrational modes relative to the energies of the modes for a free molecule, one can use changes in the spectra as a means to study the solid-state chemistry of the system. For example, being especially sensitive to changes in molecular conformation between different solid-state forms, infrared absorption spectra are frequently used to evaluate the polymorphic space of a drug substance system. In addition, the technology can be very useful in studies of solvent molecules contained within a solvatomorph.

The vibrational energy levels of a molecule in its solid form can also be evaluated using Raman spectroscopy. Because most compounds of pharmaceutical interest are characterized by low or no molecular symmetry, the same bands observed in the infrared absorption spectrum will also be observed in the Raman spectrum. However, the fundamentally different nature of the selection rules associated with the Raman effect leads to the existence of significant differences in intensity among peaks as measured by the two methods. In general, symmetric

vibrations and non-polar groups yield the most intense Raman scattering bands, whereas antisymmetric vibrations and polar groups yield the most intense infrared absorption bands.

The spectral features observed in the NIR region of the electromagnetic spectrum are associated with overtones and combinations of the same fundamental bands detected in infrared absorption or Raman spectroscopies. Some of the spectral features that have found the greatest utility are those functional groups that contain unique hydrogen atoms. For example, studies of water in solids can be easily performed through systematic characterization of the characteristic –OH band, usually observed around 5170 cm^{-1}. The determination of hydrate species in an anhydrous matrix can also be easily performed using near-IR analysis.

In this chapter, a brief overview of the necessary theoretical bases for all three types of vibrational spectroscopy will be presented, and it should be noted that more extensive details regarding molecular spectroscopy (2–6) and vibrational spectroscopy (7–17) are available. The utility of vibrational spectroscopy in the physical characterization of pharmaceutical compounds has been reviewed many times (18–32).

Motion of Atoms in Molecules

Because all forms of vibrational spectroscopy have their origin in the patterns of motion executed by the atoms and groups in the molecule, it is clear that the energies associated with these motions provide the basis to an understanding of the observed spectra. Consequently, it is appropriate to briefly consider the nature of these motions, and the manner in which energy can become distributed among the various modes. For this part of the discussion, the perturbing effects of other molecules in a condensed state will not be considered, but instead, only the state of a molecule will be considered, which is essentially free to move through space. The perturbing effects of the solid state on the vibrational properties of the component molecule in a crystal will be the focus of illustrative examples.

The number of degrees of freedom that any body may possess is related to the number of independent coordinates that are needed to specify its position in space. For instance, a sphere that is able to move randomly in space would require the specification of all three of the Cartesian coordinates (X, Y, and Z) to define its position. One therefore states that this free object has three degrees of freedom. However, if the object were constrained to move only in the *X*Y-plane, then the value of the Z-coordinate would be fixed and only the X and Y coordinates would have to be specified during the motion. In that case, the object would have only two degrees of freedom. If it is further required that the object move along a line in this plane, then one would only have to specify the coordinate along which the object moved (i.e., one degree of freedom).

If one now considers a molecule consisting of N atoms, it is clear that one must specify the three X, Y, and Z coordinates for each atom, and therefore, the total number of degrees of freedom possible for this molecule would be equal to $3N$. At the same time, the atoms in the molecule are bound, and this bonding will affect how the $3N$ degrees of freedom would be distributed among the different types of motion available to the molecule. In a molecule, each atom is not free to move independently of the others, but instead, the molecule must translate and rotate as a whole. For non-linear molecules, three degrees of freedom are associated with translational motion, and three more degrees of freedom are associated with

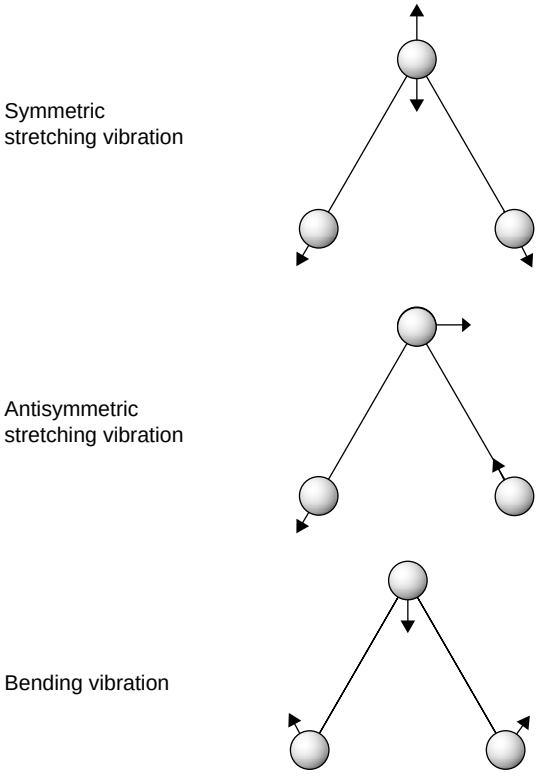

FIGURE 1 Motions of the atoms in each of the genuine vibrational modes of a nonlinear triatomic molecule.

rotational motion, so for polyatomic molecules consisting of N atoms, there will be $(3N - 6)$ degrees of freedom due to the various types of internal motion known as the vibrational modes.

Consider the case of a non-linear triatomic molecule, for which the number of authentic vibrations will therefore equal [3(3) – 6]. The three normal vibrational modes of motion are illustrated in Figure 1. To preserve the pure vibrational nature of the symmetric stretching motion, the central atom must move an equal amount in the direction opposite to the motion of the end atoms, so that the net result of the simultaneous motions of the end and central atoms is a symmetric stretching of the bonds. The atomic motions for the asymmetric stretching vibration gives rise to a compression of one bond and a stretching of the other bond, whereas the atomic motions for the bending vibration yield an opening and closing of the bond angle.

The Harmonic Oscillator Model and Spectroscopy Associated with Fundamental Vibrational Modes

A full understanding of vibrational spectroscopy requires a solution of the wave functions associated with vibrational motion, which are usually developed as quantum

mechanical expressions independent of the expressions for electronic motion. For a simple diatomic molecule, the Hamiltonian operator for nuclear motion is given by the sum of the kinetic and the potential energy operators, and so the Schrödinger equation for nuclear motion can be written as:

$$\{T_N + V(r)\}\boldsymbol{\psi} = E\boldsymbol{\psi} \tag{1}$$

where T_N is the kinetic energy operator, $V(r)$ is the potential energy function, and it is understood that $\boldsymbol{\psi}$ is the wave function for nuclear motion. For the diatomic molecule A-B, equation (1) becomes:

$$\frac{1}{m_A}\nabla_A{}^2\boldsymbol{\psi} + \frac{1}{m_B}\nabla_B{}^2\boldsymbol{\psi} + \frac{2}{\hbar^2}\{E - V(r)\}\boldsymbol{\psi} = 0 \tag{2}$$

where m_A and m_B are the masses of the two atoms comprising the molecule.

After elimination of terms associated with translation of the nuclei, the motion of the atoms is determined by the effect of the potential field directed along the internuclear axis. Mathematically, this situation is equivalent to that of a single particle moving in the field defined by $V(r)$, where the mass of this equivalent particle is given by the reduced mass (μ) of the two atoms:

$$\mu = \frac{m_A m_B}{m_A + m_B} \tag{3}$$

The wave equation now becomes:

$$\nabla^2\boldsymbol{\psi} + \frac{2\mu}{\hbar^2}\{E - V(r)\}\boldsymbol{\psi} = 0 \tag{4}$$

After the wave function is transformed into spherical polar coordinates, it can be factored into radial and angular functions that each consist of a single variable. The usual procedure is to define the radial distribution function, $\mathbf{S}(r)$, and after much work the radial portion of the wave equation becomes:

$$\frac{d\mathbf{S}}{dr^2} + \frac{2\mu}{\hbar^2}\{E - V(r)\}\mathbf{S} = 0 \tag{5}$$

Equation (5) cannot be considered further until one chooses a form for the potential function, but highly useful solutions are obtained if $V(r)$ is assumed to have the form associated with simple harmonic motion:

$$V(r) = \tfrac{1}{2}\, k\, r^2 \tag{6}$$

In equation (6), k is the force constant associated with the magnitude of the restoring force on the particle.

The mathematical solution to the harmonic oscillator wave function is beyond the scope of this chapter, but has been amply described in numerous texts on quantum mechanics (33–37). At the end of the process, one obtains expressions for the energies (E_V) of the vibrational wave functions that are functions of the reduced mass, the bond force constant, and a quantum number v for each wave function:

$$E_V = \eta\,\{k/\mu\}^{1/2}\,(v + \tfrac{1}{2}) \tag{7}$$

Because the classical vibrational frequency (υ_{OSC}) of a harmonic oscillator is:

$$\upsilon_{OSC} = (1/2\pi)\{k/\mu\}^{1/2} \tag{8}$$

it follows that the energies (in units of ergs) of the vibrational states are also equal to:

$$E_V = h\,\upsilon_{OSC}\,(v + 1/2) \tag{9}$$

It is more typical to express the energy of a given vibrational state in units of reciprocal centimeters (cm^{-1}), which is obtained by dividing equation (9) by the speed of light:

$$G_V = \frac{h\,\upsilon_{OSC}}{c}(v + 1/2) \tag{10}$$

Defining the oscillator energy as ω (in units of cm^{-1}), one obtains the expression:

$$G_V = \omega\,(v + 1/2) \tag{11}$$

For most molecules, ω will have values in the range of 200 to 4000 cm^{-1}.

In order for a molecule to absorb infrared energy to promote the system from the ground $E(v = 0)$ ground state to an excited $E(v \neq 0)$ excited states, the molecule must possess a permanent dipole moment. The intensity of this electric dipole transition is determined by the magnitude of the transition probability, $\mathbf{P}_{ij}$, which is calculated from the lower vibrational state ($\mathbf{S}_i$) to the upper vibrational state ($\mathbf{S}_j$):

$$\mathbf{P}_{ij} = \int S_i \boldsymbol{\mu} \mathbf{S}_j d\tau \tag{12}$$

For a molecule having a permanent dipole moment, it can be shown that equation (12) will equal zero unless the following harmonic oscillator selection rule is met:

$$\Delta v = \pm 1 \tag{13}$$

The energetics of vibrational energy levels is such that the ground vibrational state of a given molecule will be characterized by $v = 0$. The implication of the harmonic oscillator selection rule is that the only allowed vibrational transition would be $\mathbf{S}_0 \rightarrow \mathbf{S}_1$, which is known as the *fundamental* vibrational transition. In the harmonic oscillator model, transitions from $\mathbf{S}_0$ to higher excited states $\mathbf{S}_V$ are forbidden.

In the harmonic oscillator model, therefore, the energy of the $E(v = 0)$ state is given by:

$$E_0 = \frac{\hbar}{2}\{k/\mu\}^{1/2} \tag{14}$$

and the energy of the $E(v = 1)$ state is given by:

$$E_1 = \frac{3\hbar}{2}\{k/\mu\}^{1/2} \tag{15}$$

Therefore, energy of the ($v = 0$) → ($v = 1$) transition is given by:

$$E_1 - E_0 = \hbar \{k/\mu\}^{1/2} \tag{16}$$

or:

$$G_1 - G_0 = \omega \tag{17}$$

According to equation (17), the energy of a vibrational transition may be seen to be partially defined by the magnitude of the force constant (which is interpreted as a measure of the bond strength). In particular, it can be shown that one can calculate a value for the force constant of a harmonic oscillator using the relation:

$$k = \mu(4\pi^2\omega^2c^2) \tag{18}$$

where the reduced mass μ is give in units of grams/molecule, ω is in units of cm^{-1}, and the speed of light c equals 2.9979246×10^{10} cm/sec.

The energy of a vibrational transition is also dependent on the reduced mass of the atoms involved in the vibrational motion. Using the average bond stretching force constants of Wilson, Decius, and Cross [p. 175 of Ref. (17)], and the relation:

$$\omega = \frac{\{k/\mu\}^{1/2}}{2\pi c} \tag{19}$$

it is possible to calculate the transition energies for the fundamental vibrational transitions of some chemically relevant bond types. For instance, the energy of the C–H stretching mode is calculated to be 3444 cm^{-1}, and the energy of the C–C stretching mode is calculated to be 1189 cm^{-1}. In addition, the energy of the N–H stretching mode is calculated to be 3425 cm^{-1}, and the energy of the N–N stretching mode is calculated to be 1044 cm^{-1}. Finally, the energy of the O–H stretching mode is calculated to be 3737 cm^{-1}, and the energy of the C–C stretching mode is calculated to be 950 cm^{-1}.

From this analysis, the general trend emerges that the stretching frequencies of molecules containing a hydrogen atom will be much higher than the stretching frequencies of molecules that do not contain a hydrogen atom. The spectroscopic consequence of this trend (which will be developed further in forthcoming sections) is that vibrational transitions associated with atom–hydrogen stretching modes will be observed at much higher energies than will be the transitions of other functional groups.

Even for polyatomic molecules, the harmonic oscillator model can be adequately used to describe their fundamental vibrational transitions, because the vibrational spectra of complicated molecules can often be assumed to be summations of a number of harmonic oscillators. The concept of group frequencies is based on the fact that many vibrational wave functions are be essentially localized on the atoms of a functional group and its nearest neighbors. Because the bond force constants are fairly constant from molecule to molecule, and because the reduced masses often are comparable as well, it follows that the vibrational frequency of a given functional group is determined primarily by the identity of the atoms

involved. This concept has led to the concept of *group frequencies*, which have been summarized in several monographs (38–40).

Returning to the example of the non-linear triatomic molecule exhibiting three modes of vibration, the symmetric stretching mode will be identified as (v_1, the "scissors" bending mode as v_2, and the anti-symmetric stretching mode as v_3. Because the individual vibrational modes are independent of each other, the vibrational wave function describing the states of this non-linear triatomic molecule will be:

$$\psi\ (v_1, v_2, v_3) = \psi(v_1)\psi(v_2)\psi(v_3) \tag{20}$$

The ground state of this non-linear triatomic molecule will be characterized by $\psi(v_1)$, $\psi(v_2)$, and $\psi(v_3)$ each being in their respective $v = 0$ states, and its wave function will be abbreviated as ψ_{000}. The lowest energy excited states will be characterized by two of the $\psi(v_1)$, $\psi(v_2)$, or $\psi(v_3)$ functions each being in the $v = 0$ state and the third function being in the $v = 1$ state. These three possible excited states would be identified by the functions ψ_{100}, ψ_{010}, and ψ_{001}.

Because the harmonic oscillator selection rule is $\Delta v = \pm 1$, it follows that the only possible fundamental vibrational spectroscopic transitions for the non-linear triatomic molecule water are:

$$\psi_{000} \rightarrow \psi_{100} \text{ (the } v_1 \text{ mode)} \tag{21}$$

$$\psi_{000} \rightarrow \psi_{010} \text{ (the } v_2 \text{ mode)} \tag{22}$$

$$\psi_{000} \rightarrow \psi_{001} \text{ (the } v_3 \text{ mode)} \tag{23}$$

For water in the gas phase, it has been found that the energy of the ν_1 vibrational mode equals 3652 cm^{-1}, the energy of the ν_2 mode equals 3756 cm^{-1}, and the energy of the ν_3 mode equals 1545 cm^{-1}. However, as shown in Figure 2, in bulk water these frequencies are substantially shifted to 1634, 3262, and 3341 cm^{-1}, respectively, owing to the extensive degree of hydrogen bonding.

The Anharmonic Oscillator Model and Spectroscopy Associated with Overtones and Combinations of Fundamental Vibrational Modes

Because the harmonic oscillator selection rule states that only transitions for which $\Delta v = \pm 1$ are allowed, and because, the majority of molecules will be in the $v = 0$ state at room temperature, only fundamental transitions can be observed in either the infrared absorption or Raman spectra. A more realistic description of the energy level sequence can be achieved by using potential energy functions that allow for molecular distortion in excited vibrational states. The inclusion of anharmonic effects serves to weaken the $\Delta v = \pm 1$ selection rule, and permits transitions to higher quantum states. The development of appropriate technology has permitted the development of a wide variety of applications in the pharmaceutical and other industries.

The most widely used anharmonic potential energy function is the Morse potential:

$$V(r) = D_e[1 - e^{-a(r - re)}]^2 \tag{24}$$

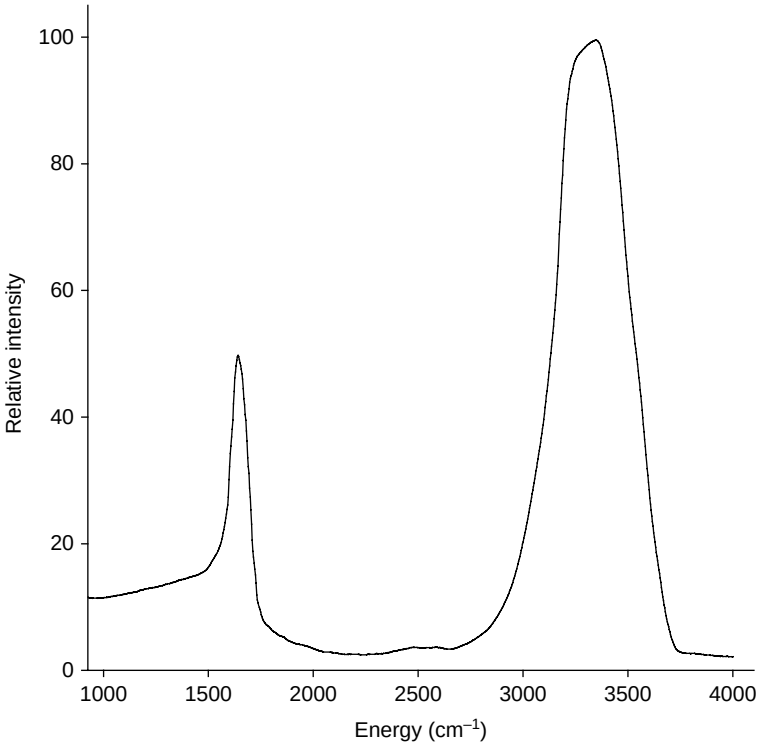

FIGURE 2 Infrared absorption spectrum of bulk water, obtained using the attenuated total reflectance sampling mode.

where D_e is the energy required to dissociate the bond. The rigorous approach would then be to substitute this form for the potential energy function back into the Hamiltonian equation, and to then solve the resulting Schrödinger equation in the usual manner. However, this approach is not trivial, and hence, more empirical approaches are usually taken.

A more practical approach toward vibrational spectroscopy is to expand the harmonic oscillator equation in an infinite power series based on $(v + ½)$ to include anharmonic effects:

$$G'_V = \omega_e(v + ½) - \omega_e X_e(v + ½)^2 + \omega_e Y_e(v + ½)^3 + ... \quad (25)$$

where ω_e is the harmonic oscillator constant, and where X_e and Y_e are anharmonic constants. The dissociation energy is given by the sum:

$$D_e = \sum \Delta G'(v + ½) \quad (26)$$

where the summation is performed over the range of $v = 0$ to the highest vibrational level for which the bond in the molecule is still intact. Usually the $\omega_e X_e$ term is

considerably larger than the $\omega_e Y_e$ term, and thus most experimentally determined vibrational spectra can be fitted to the simplified equation:

$$G'_V = \omega_e(v + ½) - \omega_e X_e(v + ½)^2 \tag{27}$$

For most molecules, the $\omega_e X_e$ term will be positive in character, so the separation between successively higher excited states will decrease as v increases. In this simplified model, the separation between the G'_V state and the G'_{V+1} state will be given by:

$$\Delta G'_V = \omega_e - \omega_e X_e(2v + 2) \tag{28}$$

In this simplified model of the anharmonic oscillator, the dissociation energy is given by:

$$D_e = \omega_e / 4X_e \tag{29}$$

Equation (28) indicates that progressions of experimentally observed vibrational transitions can be considered as being composed of a harmonic and an anharmonic part. But at ambient conditions the majority of molecules will be in the $v = 0$ state because the thermal energy available at 25°C is not sufficient to raise more than a few percent of molecules into the $v = 1$ state. This gives rise to the reality that for a transition from $v = 0$ to $v = 1$, the contribution from the anharmonic terms is relatively minor; therefore, fundamental transitions can be adequately treated using the harmonic oscillator model.

With the inclusion of anharmonic effects in vibrational energy states, the strict harmonic oscillator selection rule of $\Delta v = \pm 1$ becomes relaxed and transitions from the ground vibrational state to higher vibrationally excited states to gain some degree of allowedness. Because the overtone transitions can only take place through relaxation of the primary selection rule transitions, where $\Delta v = 2, 3, 4$, etc., will be less intense than the corresponding fundamental transition. Nevertheless, overtone transitions are easily detected, and are observed in the NIR region of the electromagnetic spectrum (41–45).

Returning to the non-linear triatomic molecule, once the effects of anharmonicity are factored into the transition moment calculations, almost any type of vibrational excitation becomes possible. One could observe sequences of simple *overtone* transitions, such as:

$$\Psi_{000} \rightarrow \Psi_{200}, \Psi_{300}, \Psi_{400}, \text{etc.} \tag{30}$$

$$\Psi_{000} \rightarrow \Psi_{020}, \Psi_{030}, \Psi_{040}, \text{etc.} \tag{31}$$

$$\Psi_{000} \rightarrow \Psi_{002}, \Psi_{003}, \Psi_{004}, \text{etc.} \tag{32}$$

or any one of a number of *combination* transitions, some of which can be written as:

$$\Psi_{000} \rightarrow \Psi_{110}, \Psi_{101}, \Psi_{011}, \text{etc.} \tag{33}$$

$$\Psi_{000} \rightarrow \Psi_{120}, \Psi_{201}, \Psi_{021}, \text{etc.} \tag{34}$$

TABLE 1 Overtone and Combination Vibrational Transitions of Water in the Vapor Phase

Upper State			Energy (cm^{-1})	Wavelength (nm)	Intensity
ν_1	ν_2	ν_3			
0	1	1	5,332.0	1875.5	Medium
0	2	1	6,874.0	1454.8	Weak
1	0	1	7,251.6	1379.0	Medium
1	1	1	8,807.1	1135.4	Strong
2	0	1	10,613.1	942.2	Strong
0	0	3	11,032.4	906.4	Medium
2	1	1	12,151.2	823.0	Medium
3	0	1	13,830.9	723.0	Weak
1	0	3	14,318.8	698.4	Weak

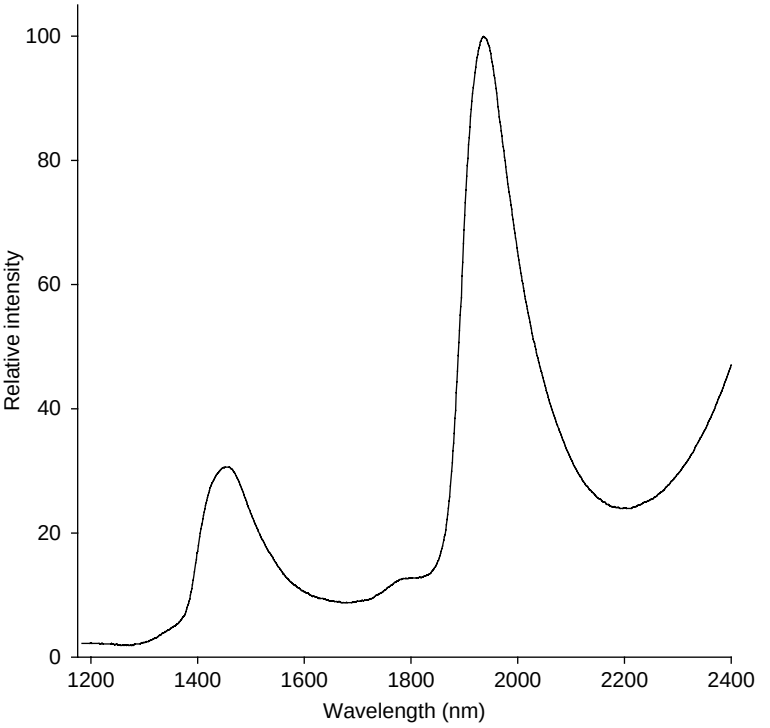

FIGURE 3 NIR absorption spectrum of bulk water, obtained using the reflectance sampling mode.

A summary of the overtone and combination bands of water in the vapor phase is given in Table 1, and a portion of its liquid phase absorption spectrum is shown in Figure 3. For bulk water, the moderate band observed at 1455 nm can be assigned to the $\psi_{000} \rightarrow \psi_{101}$ transition, the weak band at 1806 nm can be assigned to the $\psi_{000} \rightarrow \psi_{021}$ transition, and the strong band at 1936 nm can be assigned to the $\psi_{000} \rightarrow \psi_{011}$ transition.

INFRARED ABSORPTION SPECTROSCOPY FOR THE CHARACTERIZATION OF POLYMORPHS AND SOLVATOMORPHS

The acquisition of high-quality infrared spectra on solid materials has been made possible using Fourier transform technology, because the use of this methodology minimizes transmission and beam attenuation problems. Essentially all FTIR spectrometers use a Michelson interferometer, where infrared radiation entering the interferometer is split into two beams: one of which follows a path of fixed distance before being reflected back into the beam splitter, and the other traveling a variable distance before being recombined with the first beam. The recombination of these two beams yields an interference pattern, where the time-dependent constructive and destructive interferences have the effect of forming a cosine signal. Each component wavelength of the source yields a unique cosine wave, having a maximum at the zero pathlength difference (ZPD) and which decays with increasing distance from the ZPD. The radiation in the central image of the interference pattern impinges on the detector, and intensity variations in the recombined beam become measurable manifest as phase differences. If the component cosine waves can be resolved, then the contribution from individual wavelengths can be observed. The frequency domain spectrum is obtained from the interferogram by performing the Fourier transformation mathematical operation. More detailed descriptions of the components of a FTIR spectrophotometer are available (46–48).

Numerous modes of sampling may be used with FTIR spectrophotometers, although only a few of these are appropriate for the study of polymorphs and solvatomorphs. The classic alkali halide pellet method is probably the least useful for this type of work, as the sample may under so a solid-state transformation due to the pressure used to form the pellet, or one may encounter halide exchange between the KBr or KCl matrix and the sample (49). The use of mineral oil mulls avoids the problems noted for the pellet technique, but the mineral oil itself exhibits a number of intense absorption bands (2952, 2923, 2853, 1458, and 1376 cm^{-1}) that may overlap important absorption bands associated with the sample and obscure important spectral regions. Use of diffuse reflectance sampling avoids all of the problems just mentioned (50,51), but usually requires dilution of the analyte with either KBr or KCl at a level of 1% to 5% w/w. The diffuse reflectance technique lends itself to studies of polymorphic composition because it is non-invasive, its use causes no changes in polymorph character due to its inherent limited sample handling, and the technique can be used for quantitative purposes.

Probably the most useful sampling method for the study of polymorphs and solvatomorphs uses attenuated total reflectance accessories (52,53). In the ATR technique, infrared radiation is passed through a crystal at an angle less than the critical angle, which causes the light to undergo total internal reflection. At each such reflection, the radiation penetrates a small distance beyond the crystal surface, and if an analyte is in physical contact with the crystal, then the internally reflected

energy will be attenuated at those frequencies corresponding to changes in molecular vibrational states. The advantage of the ATR approach is that it requires effectively no sample preparation, because one simply clamps the analyte onto the surface of the crystal with moderate pressure to ensure a sufficient degree of optical contact. Because the internal reflectance process does not permit the infrared beam to pass very deeply into the sample, it is typical to determine the composition of an analyte up to a sampling depth in the range of 5 to 10 μm.

Not surprisingly, the sensitivity of infrared absorption spectroscopy to subtle changes in crystal structure have led to its application in a wide variety of investigations of polymorphic solids, often in conjunction with Raman spectroscopic studies. For example, FTIR spectra of different polymorphs of mepivacaine hydrochloride were obtained in Nujol mulls and via ATR sampling, with the ATR method providing better distinction between the polymorphs (54). This has been illustrated in Figure 4, where the infrared absorption spectra of mepivacaine hydrochloride (Form-II) is seen to be superior when obtained using the attenuated total reflectance

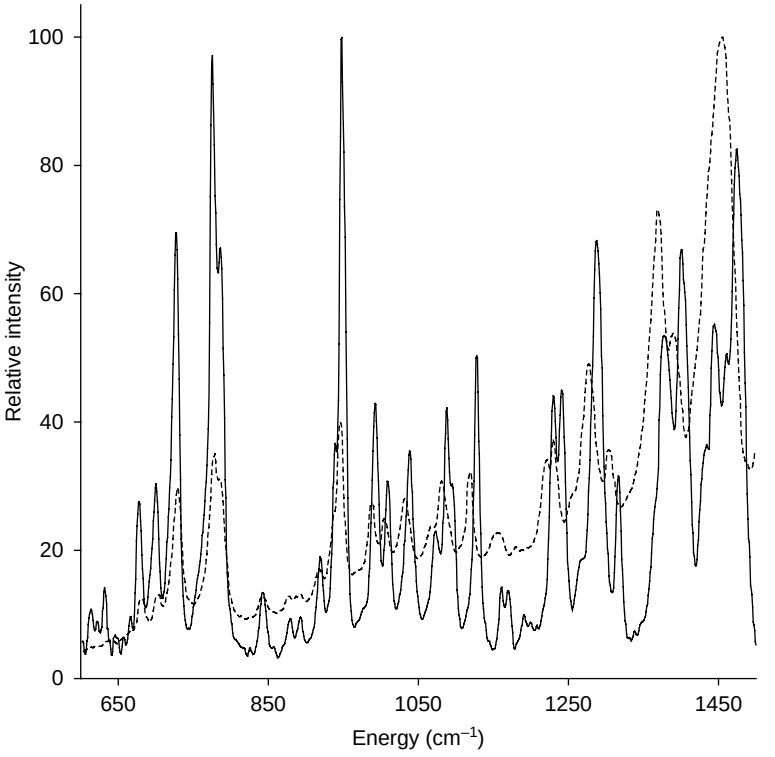

FIGURE 4 Infrared absorption spectra of mepivacaine hydrochloride, Form-II, obtained using the attenuated total reflectance (*solid trace*) and Nujol mull (*dashed trace*) sampling modes. Each spectrum has been normalized so that the relative intensity of the most intense band equals 100%, and the normalized spectra were generated from data given in Ref. (54).

sampling mode as opposed to a Nujol mull. When coupled with artificial neural network methods, a diffuse reflectance FTIR spectroscopic method was developed that permitted the simultaneous quantification of three polymorphs of carbamazepine in ternary mixtures (55).

FTIR–ATR spectroscopy was used to characterize the salt-induced crystallization of a metastable polymorph of flufenamic acid, and to characterize the product obtained after a subsequent interface-mediated polymorphic transition (56). The FTIR–ATR method was also used to characterize the fluconazole products obtained using the supercritical antisolvent process, with the technique being able to identify the polymorphic forms produced as a result of variation of operating conditions such as temperature, pressure, and solvent type (57). Three concomitant polymorphs of 1,3-bis(*m*-nitrophenyl)urea had been reported in 1899 as yellow prisms (the α-form), white needles (the β-form), and yellow tablets (the γ-form), and FTIR-microscopy was used during a more detailed investigation of the system (58). In this work, complete assignments for the absorption bands associated with hydroxyl, amide, nitro, and benzene-ring functional groups were developed in order to obtain a deeper understanding of the conformational differences in the molecules constituting the various crystal forms.

Five differently colored solid-state forms of 5-methyl-2-[(2-nitrophenyl) amino]-3-thiophenecarbonitrile, where the color of the polymorphic crystal forms is related to changes in the energies of molecular orbitals of the systems have been studied using infrared absorption spectroscopy (59). The spectra for three of the solid-state forms were characterized by frequency shifts originating from the structural differences, with the nitrile stretching frequency varying by approximately $10\,cm^{-1}$ each for the yellow, orange, and red solid-state forms of the compound. In a study of the amorphous salt formed by the co-precipitation of cimetidine and diflunisal, solid-state infrared absorption spectroscopy was used to prove the existence of the salt species (60). The prominent carbonyl absorption band observed at $1650\,cm^{-1}$ in crystalline diflunisal could not be observed in the spectrum of the amorphous salt, but a new peak was noted at $1580\,cm^{-1}$ that was assigned to an asymmetric stretching mode of a carboxylate group.

Diffuse reflectance sampling was used to study the anhydrates and hydrates of ampicillin and nitrofurantoin, with the presence of water in the hydrate crystal forms causing new bands to appear in the infrared absorption spectrum (61). On the other hand, FTIR spectroscopy was not useful in distinguishing between the hydrate forms of diclofenac sodium as the frequencies in the spectra of the polymorphic tetrahydrates were nearly identical, and only differed in band relative intensities (62). The utility of combined FTIR and solid-state ^{13}C nuclear magnetic resonance studies enabled the deduction that although the water molecules of topotecan hydrochloride trihydrate were intrinsic parts of the crystal lattice, the pentahydrate possessed additional structural channels where water could hydrogen bond to specific portions of the topotecan molecules (63).

Fluconazole has been isolated in a number of solvated and non-solvated forms, and infrared spectroscopy has proven to be an important tool in the characterization of these. In one study involving two non-solvated polymorphs (Forms I and II) and several solvatomorphs (the ¼-acetone solvate, a 1/7-benzene solvate, and a monohydrate), the infrared spectra of the different forms showed differentiation in bands associated with the triazole and 2,4-difluorobenzyl groups, and in the propane backbone (64). In another study, the diagnostic infrared spectral

characteristics of non-solvated Form-III and two solvatomorphs (the ¼-ethyl acetate solvate, and a monohydrate) were used to demonstrate the novelty of the new forms relative to those in the literature (65). In yet another work, the kinetics associated with the dehydration and desolvation of fluconazole solvatomorphs were studied by three physical methods, and then used to understand the mechanisms of the processes involved (66).

It has been found that the carbonyl frequency of niclosamide anhydrate and two of its monohydrates was particularly sensitive to the crystal form of the drug substance, and hence, infrared spectroscopy could be used to demonstrate the conformational state of the compound in the solvatomorphs (67). Similarly, infrared spectra obtained in the fingerprint and high-frequency regions for four non-solvated polymorphs of tenoxicam, and of its acetonitrile, dioxane, dimethyl formamide, ethyl acetate, acetone, and isopropanol solvates, facilitated a differentiation between the various crystal forms (68). A combination of thermogravimetric analysis and infrared absorption spectroscopy was used to develop a quantitative method for the determination of pantoprazole sodium monohydrate in bulk quantities of the sesquihydrate solvatomorph (69).

Because the pattern of vibrational modes is usually sufficiently perturbed by crystallographic differences, infrared absorption spectroscopy can be profitably used to study the phase transformation process between polymorphic forms of a substance. For example, infrared absorption spectroscopy has been used to study the solution-mediated phase transformation of metastable β-glycine to the stable α-phase, making use of disappearance of the weak band at 1660 cm^{-1} and shifts in energy for the anti-symmetric stretch of the carboxyl group (1580–1590 cm^{-1}), the deformation of the NH_3^+ group (1515–1500 cm^{-1}), and the O–C=O group bend (around 700 cm^{-1}) (70). In another work, characteristic absorption bands around 1145 to 1165 cm^{-1} were found to be useful in understanding the effect of experimental variables on the solution-mediated Form-II to Form-I phase transformation of buspirone hydrochloride (71).

Infrared spectroscopy has been used to follow the isothermal transformation of mefenamic acid Form-I into Form-II at a sufficient number of temperatures so as to calculate the activation energy for the process (72). The value of 71.6 kcal/mol, obtained using the infrared spectroscopic method, was significantly smaller than the previously reported value of 86.4 kcal/mol that had been determined using of differential scanning calorimetry. Conventional FTIR spectroscopy in conjunction with FTIR micro-spectroscopy has been used to study the polymorphic interconversion of famotidine metastable Form-B into stable Form-A during grinding in a ceramic mortar (73). The particle size reduction that resulted from the grinding process was also found to lead a decrease in the transition temperature for the Form-B to Form-A phase transformation.

Changes in infrared absorption spectra have also been used to study the phase transformation process between solvatomorphs. For example, granulation of anhydrous lactose with water results in conversion of the anhydrate phase to the monohydrate phase, as well as a change from the β-anomer to the α-anomer. Figure 5 shows the FTIR–ATR spectra obtained in the high-frequency region for different stages in the solution-mediated conversion of lactose anhydrate to lactose monohydrate phase of lactose monohydrate, where it is clear that the absorbance band at 3522 cm^{-1} could be used to follow the kinetics of formation of the monohydrate (74).

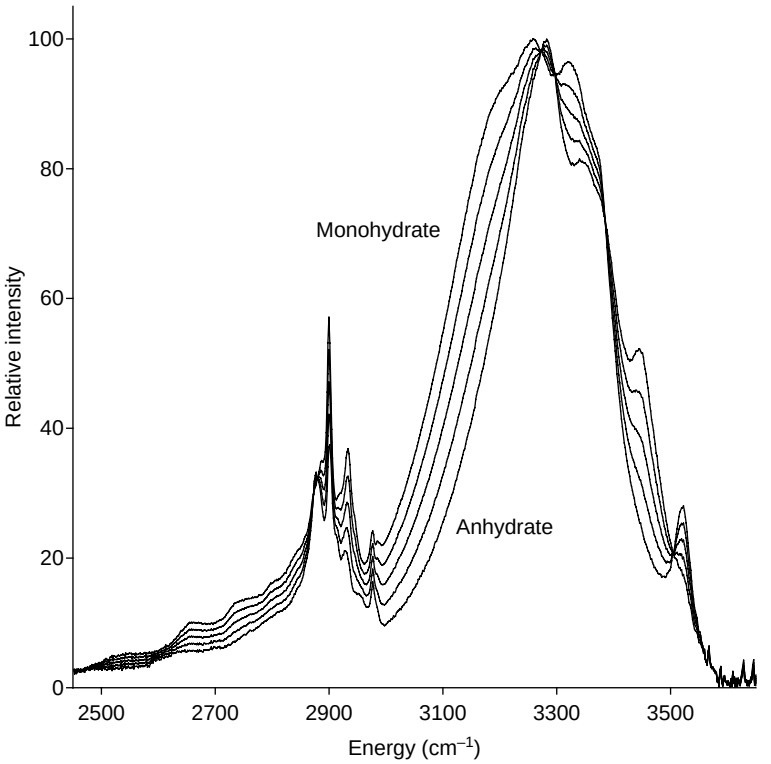

FIGURE 5 FTIR–ATR spectra obtained in the high-frequency region of lactose anhydrate (*lowest trace*), and during various stages of its solution-mediated phase transformation into the monohydrate phase (*uppermost trace*). H.G. Brittain, unpublished results (70).

Trehalose dihydrate undergoes a dehydration transition around 100°C, and the infrared spectra obtained during this process were found to change significantly over the 1500 to 1800 cm^{-1} region (75). For example, the band intensities at 1640 and 1687 cm^{-1} decreased sharply around 65°C, but remained relatively constant at higher temperatures. During the rehydration process where trehalose anhydrate became trehalose dihydrate, the liquid-like water became solid-like water over the same temperature range. It was postulated that this phase transition could be related to the protective effect of trehalose in preserving protein stability.

NIR SPECTROSCOPY FOR THE CHARACTERIZATION OF POLYMORPHS AND SOLVATOMORPHS

Because the energy separation of the ground vibrational state and the lowest vibrational excited states is large relative to kT at room temperature, molecules at ambient temperature will reside almost entirely in their ground vibrational states. According to the harmonic oscillator selection rule of $\Delta v = \pm 1$, only the fundamental vibrational transitions that are studied by ordinary infrared absorption spectroscopy

or Raman spectroscopy will be allowed. As long as the harmonic oscillator selection rules can be considered as being valid, vibrational transitions corresponding to $\Delta v = \pm 2$, $\Delta v = \pm 3$, $\Delta v = \pm 4$, etc., or combinations of these, are not allowed.

However, the harmonic oscillator model should be considered as being the first term in a solution of the vibrational Hamiltonian equation where the potential term can also include anharmonic effects. As discussed above, the strict $\Delta v = \pm 1$ selection rule can be relaxed by the inclusion of anharmonicity, and the relaxation of this fundamental selection rule enables the observation of transitions from the ground vibrational state to higher vibrationally excited states. However, because the fundamental selection rule is merely relaxed and not broken, these overtone transitions will generally be less intense than their fundamental transition.

The NIR region of the spectrum is generally considered to span 750 nm (13,350 cm^{-1}) to 2500 nm (4000 cm^{-1}). Through the design of appropriate instrumentation, the overtone and combination transitions can be detected and quantitated, with these being observed in the NIR region of the spectrum (76–83). In general, the spectral features of greatest utility entail overtone transitions associated with functional groups that contain unique hydrogen atoms. For example, NIR spectroscopy has been successfully used to develop methods for moisture determination, whole tablet assay, and powder blending (84–87). Owing to the usually broad nature of the absorption bands, the raw spectra themselves tend not to be most useful in the study of polymorphs and solvatomorphs, but when the spectra are differentiated and the resulting derivative spectra combined with multi-component analysis, real analytical utility emerges.

NIR spectroscopy has been shown to be capable of differentiating between polymorphs of sulfathiazole and sulfamethoxazole, as well as hydrates of ampicillin and lactose (88). For example, the raw absorption spectra of sulfathiazole Form-I and Form-III are shown in Figure 6 along with their corresponding second derivative spectra. It is evident that use of the derivative spectra eliminates the sloping baseline of the raw absorption spectra, readily identifying bands at 1376 and 1528 nm that were useful in differentiating between the polymorphic forms. These spectra differences were exploited to develop a quantitative analytical method for determination of the amount of Form-III in Form-I that was characterized by recovery errors less than 3%.

Although NIR spectroscopy can definitely be used as a means of polymorph identification, its real power lies in the ability of workers to readily develop quantitative assays for phase composition. The quantification of sulfathiazole Form-I and Form-III in binary mixtures was addressed in another work, here using univariate, multiple linear regression, and partial least-squares regression methods to generate the validation set (89). Quantitative methods for the two polymorphs of bicifadine hydrochloride have been developed using differential scanning calorimetry coupled with thermogravimetric analysis, X-ray powder diffraction, infrared absorption spectroscopy, and NIR spectroscopy, with the NIR methods being found to yield the best accuracy and ease of operation (90). The utility of Raman and NIR spectroscopies combined with multivariate analysis for the quantitation of ternary mixtures of α-, γ-, and amorphous indomethacin was investigated, with comparable root-mean-square errors of prediction being obtained for the two methods (91).

Distinctions between the solvated and non-solvated forms of a drug substance are often easy to detect using NIR spectroscopy, making the technique a valuable part of a multi-disciplinary study such as that carried out on the baclofen anhydrate

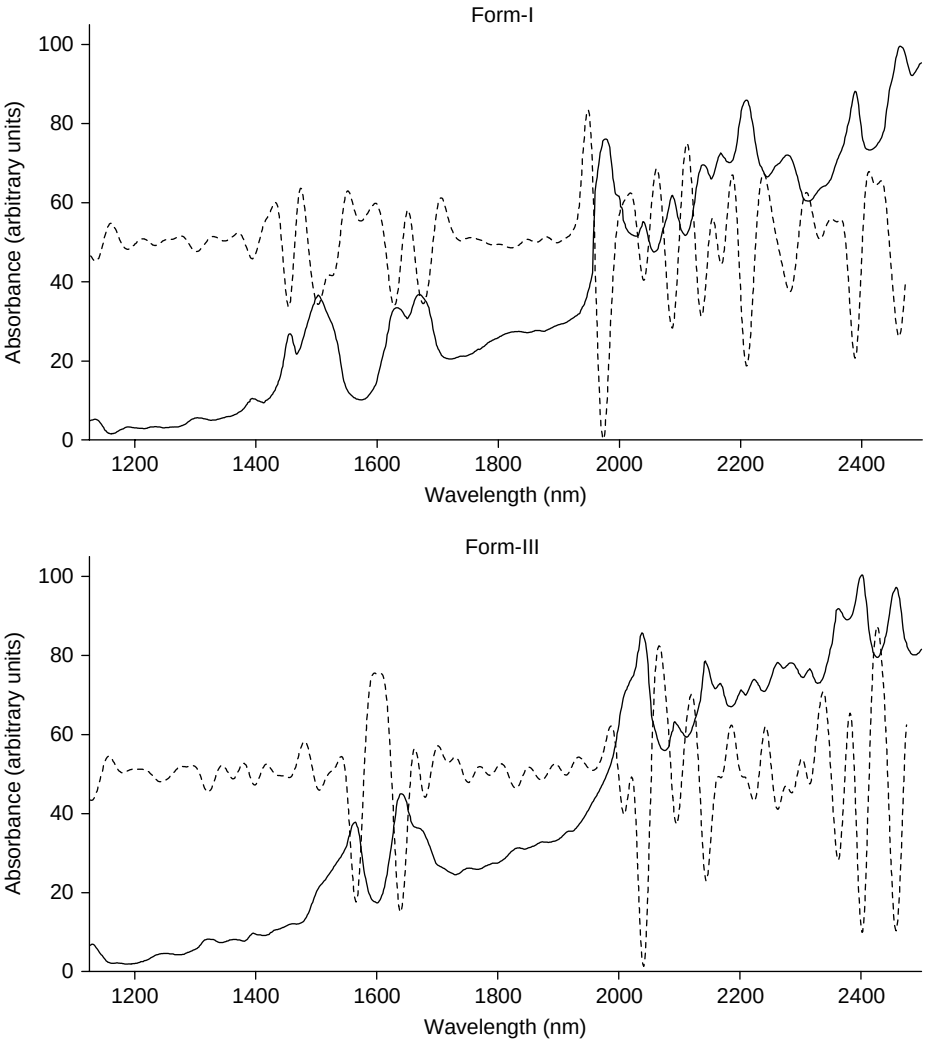

FIGURE 6 NIR spectra obtained for sulfathiazole Form-I (*upper spectra*) and Form-III), showing both the raw absorption spectrum (*solid traces*) and the corresponding second derivative spectrum (*dashed traces*) for each. The spectra are shown in arbitrary units, and have been adapted from Ref. (88).

and monohydrate (92). The factors associated with the quantitative analysis of anhydrate/hydrate powder mixtures have been discussed (93), and these issues illustrated in work establishing the phase boundaries in the anhydrate/hydrate system of caffeine (94). The interconversion between the anhydrate, monohydrate, and dihydrate forms of azithromycin have been studied, with the spectral region associated with the first overtone of water (1800–2200 nm) being most useful (95). In another work, the monohydrate/dihydrate composition of magnesium

stearate samples was established using NIR spectroscopy and multivariate calibration (96).

NIR spectroscopy was used to monitor the degree of conversion between the stable Form-A of a new chemical entity and the metastable Form-B produced at the elevated temperature and humidity conditions of its wet granulation (97). Because a reference method was not available for quantitation of Form-B in bulk quantities of Form-A, a calibration set was developed from the NIR spectra of the drug substance, the premix blend, and wet granulated samples, because narrow spectral regions unique to Form-B were found that were insensitive to differences in physical properties between the premix blend and wet granulation. The final univariate method was used for either for off-line, or for on-line, monitoring of phase conversion during the wet granulation process.

In-line NIR spectroscopy was used to demonstrate that the process-induced transformation of erythromycin A dihydrate to its dehydrated form did not take place easily during pellet manufacture via extrusion/spheronization and drying, although partial phase transformation was noted for pellets dried at 60°C (98). NIR spectroscopy was one of several techniques used to obtain quantitative determinations of phase compositions of a developmental compound in its bulk drug substance and in compressed tablets, with a partial least-squares regression algorithm being used to obtain good multivariate calibration (99).

TERAHERTZ SPECTROSCOPY FOR THE CHARACTERIZATION OF POLYMORPHS AND SOLVATOMORPHS

The ability to acquire absorption spectra in the far-infrared region of the spectrum (10–450 cm^{-1}) became much easier to obtain when dispersive technology was replaced by Fourier transform methodology. Initial applications of far-infrared spectroscopy included studies of pure rotational spectra, skeletal bending modes, molecular motion in four-, five-, six, and seven-membered rings, torsional vibrations, vibrational modes involving heavy atoms, and weak intermolecular interactions (100). Other investigational work involved studies of organic crystalline solids, where the translational and librational modes of molecular crystals below 250 cm^{-1} could be evaluated. In one such study, the four lattice modes of crystalline films of elemental nitrogen and carbon monoxide at 10 K were studied over the range of 20 to 250 cm^{-1}, and it was determined that although the translational modes were moderately strong, the librational modes were weak in intensity (101).

Fairly recently, it has been recognized that the developing field of terahertz (THz) spectroscopy can also be used to study low-frequency modes that hitherto had been the domain of far-infrared spectroscopy. Because 1 THz is equivalent to 33.33 cm^{-1}, it turns out that the spectral region of interest (i.e., 3–400 cm^{-1}) corresponds to frequencies of 0.09 to 12 THz. With the development of appropriate instrumentation, the technique has been applied to the study of a wide variety of materials (102,103), and has been used to study the crystallinity of materials having pharmaceutical interest (104–106). With the introduction of the attenuated total reflectance sampling mode (107), it is anticipated that application of THz spectroscopy to the characterization of polymorphs and solvatomorphs will become even more widespread.

The incident THz radiation is obtained as femtosecond pulses that are generated by the excitation of charge carriers in a semiconductor material through the

use of ultra-short pulses of light that is higher in energy than the bandgap of the semiconductor. These pulses can be detected with an ultra-fast antenna receiver, providing simultaneous amplitude and phase information over a wide frequency range in a single measurement. It is to be noted that this type of measurement is based on frequency (in the form of the instantaneous value of the electric field itself) and not on an intensity measurement of the type that would be used during the conduct of conventional far-infrared spectroscopy. The frequency-dependent absorption coefficient and index of refraction of the analyte are obtained from the attenuation, delay, and distortion of the femtosecond THz pulse transmitted through the sample. Additional details of the different modes of measurement technology are available in the book by Dexheimer (103).

The utility of pulsed THz spectroscopy as a tool for the differentiation of the two polymorphs or ranitidine hydrochloride has been demonstrated (108). As shown in Figure 7, the THz spectra of the two crystal forms are quite different, and the authors concluded that the region around 1.10 THz (36.7 cm^{-1}) was the most useful for identification of the polymorphic form contained in tablet formulations. It was also noted that the plastic bags commonly used for drug substance storage

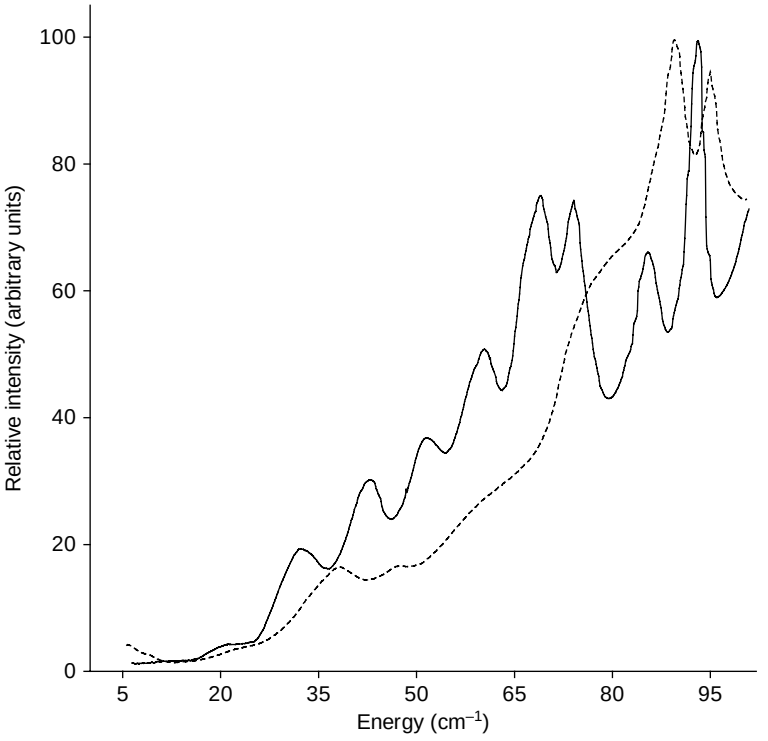

FIGURE 7 THz pulsed spectra of ranitidine hydrochloride, Form-I (*solid trace*), and Form-I (*dashed trace*). Each spectrum has been normalized so that the relative intensity of the most intense band equals 100%, and the normalized spectra were generated from data given in Ref. (104).

were transparent to THz radiation, thus making it possible to use the technology for substance identification without having to remove a sample for analysis.

The utility of pulsed THz spectroscopy for quantitative analysis of phase composition was demonstrated for various forms of carbamazepine, enalapril maleate, indomethacin, and fenoprofen calcium (109). Distinct THz spectra were measured for the various crystal forms owing to the unique patterns of lattice vibrations associated with each compound type and crystal form, and these differences were exploited to develop quantitative methods of analysis. Harmonic lattice dynamics calculations were performed on the four polymorphs of carbamazepine in order to derive assignments for the bands observed in the THz spectra, and to understand the observed trends in frequencies of similar hydrogen bond vibrations in the polymorphs (110). In fact, the sensitivity of THz spectroscopy toward differences between crystal structures has led to its inclusion as one of the identification tools in a polymorph screening study (111).

With the inclusion of a hot-stage in a THz spectrometer, acquisition of temperature-dependent spectra in real time could be used to study a variety of thermally induced phenomena. The methodology was first applied to a study of the phase transition of carbamazepine Form-III to Form-II, as well as the solid-state transformation under isothermal conditions below the melting point (112). When heated between 20°C and 160°C, the spectral features of Form-III broadened, decreased in intensity, and underwent a shift to lower energies. Further heating to 180°C led to melting of Form-III and recrystallization to Form-I, with the THz spectra reflecting the formation of the phase form. Sequences in the disappearance of Form-III spectral features, and in the appearance of Form-I features, indicated that the conversion mechanism entailed more than one step.

The far-infrared spectroscopic characteristics of five polymorphs of sulfathiazole have been studied by THz pulsed spectroscopy and thermal analysis, and then variable-temperature spectroscopic studies were conducted to monitor thermally induced phase transitions among the different forms (113). Time–domain THz spectroscopy was used to obtain the defining characteristics of two anhydrous polymorphs of theophylline and its monohydrate, and then variable-temperature studies were used to monitor phase transformations (114). Details of the phase transformation processes associated with the hydration and dehydration of theophylline have also been studied using THz pulsed spectroscopy (115).

THz time–domain spectroscopy has been used to study the anhydrous and hydrate forms of caffeine, theophylline, glucose, and ampicillin, with the aim of demonstrating the utility of this method as a process analytical tool in production and quality control (116). Crystallization and relaxation phenomena in amorphous carbamazepine have been studied using THz pulsed spectroscopy, and the technique was shown to be capable of determining glass transition temperatures (117).

Raman Spectroscopy for the Characterization of Polymorphs and Solvatomorphs

With the introduction of Fourier-transform methodology into measurement instrumentation, the use of Raman spectroscopy as a tool to solve problems having pharmaceutical interest has become widespread, and the technique is now as essential to the study of polymorphs and solvatomorphs as infrared absorption spectroscopy. Comparable to the use of attenuated total reflectance in FTIR spectroscopy, the sampling modes used in the acquisition of Raman spectra are non-destructive

in nature, and spectra can even be obtained in a non-invasive manner using fiber optics. Unlike diffuse reflectance sampling in FTIR spectroscopy, analytes are not required to be diluted with a spectroscopically inert filler before study. A number of detailed reviews are available regarding the use of Raman spectroscopy in areas of pharmaceutical interest (20–29,31,32).

When substances are irradiated with intense beams of monochromatic radiation, the majority of the photons are scattered at the same frequency as that of the incident beam (i.e., elastic or Rayleigh scattering). However, it has been found that a small amount of the incident light will also be scattered at non-resonant frequencies, some at frequencies more than and some at frequencies less than the frequency of the Rayleigh line. The differences in frequency between the incident radiation and the shifted frequencies correspond to the frequency of molecular vibrations of the molecules in the sample. The scattering peaks observed at lower frequencies relative to the Rayleigh line are known as the *Stokes* bands, and the scattering peaks observed at higher frequencies are known as the *anti-Stokes* bands. Owing to their stronger intensity, most Raman spectroscopic studies use only the Stokes peaks.

For those molecular systems having non-degenerate ground electronic states that are irradiated with intense beams of electromagnetic radiation whose energy does not permit a transition among electronic states, the theory states that the intensities of vibrational Raman transitions are determined by the matrix elements of the electronic polarizability. Therefore, only molecular transitions characterized by a change in polarizability will exhibit an allowed Raman transition. Because the magnitude of the frequency shifts of Raman bands relative to the frequency of the incident beam is determined by the energy differences of the associated vibrational states, the intensity of a given Raman band is related to the transition probability the transition, and as long as the harmonic oscillator model can be used to describe the system, the usual selection rule of $\Delta v = \pm 1$ will hold.

The intensity of scattered light will depend on the magnitude of the induced dipole moment, **P**, which can be defined in analogy with equation (12) for a transition between states *i* and *j* that are defined by the wavefunctions $\boldsymbol{\psi}_i$ and $\boldsymbol{\psi}_j$, and which is given by the matrix formed from the integrals:

$$\mathbf{P}_{ij} = \int \boldsymbol{\psi}_i \mathbf{P} \boldsymbol{\psi}_j \mathrm{d}\tau \tag{35}$$

The polarizability operator, **P**, being a matrix quantity, requires that the elements of transition moment along each of the Cartesian axes will be:

$$\mathbf{P}_{\mathrm{X}}^{\mathrm{ij}} = \mathbf{E}_{\mathrm{X}} \int \boldsymbol{\psi}_i \alpha_{\mathrm{XX}} \boldsymbol{\psi}_i \mathrm{d}\tau + \mathbf{E}_{\mathrm{Y}} \int \boldsymbol{\psi}_i \alpha_{\mathrm{XY}} \boldsymbol{\psi}_j \mathrm{d}\tau + \mathrm{E}_{\mathrm{Z}} \int \boldsymbol{\psi}_i \alpha_{\mathrm{XZ}} \boldsymbol{\psi}_j \mathrm{d}\tau \tag{36}$$

$$\mathbf{P}_{\mathrm{Y}}^{ij} = \mathbf{E}_{\mathrm{X}} \int \boldsymbol{\psi}_i \alpha_{\mathrm{YX}} \boldsymbol{\psi}_j \mathrm{d}\tau + \mathbf{E}_{\mathrm{Y}} \int \boldsymbol{\psi}_i \alpha_{\mathrm{YY}} \boldsymbol{\psi}_j \mathrm{d}\tau + \mathbf{E}_{\mathrm{Z}} \int \boldsymbol{\psi}_i \alpha_{\mathrm{YZ}} \boldsymbol{\psi}_j \mathrm{d}\tau \tag{37}$$

$$\mathbf{P}_{\mathrm{Z}}^{ij} = \mathbf{E}_{\mathrm{X}} \int \boldsymbol{\psi}_i \alpha_{\mathrm{ZX}} \boldsymbol{\psi}_i \mathrm{d}\tau + \mathbf{E}_{\mathrm{Y}} \int \boldsymbol{\psi}_i \alpha_{\mathrm{ZY}} \boldsymbol{\psi}_j \mathrm{d}\tau + \mathbf{E}_{\mathrm{Z}} \int \boldsymbol{\psi}_i \alpha_{\mathrm{ZZ}} \boldsymbol{\psi}_j \mathrm{d}\tau \tag{38}$$

$\mathbf{E}_{\mathrm{X}}$, $\mathbf{E}_{\mathrm{Y}}$, and $\mathbf{E}_{\mathrm{Z}}$ are the amplitudes of the incident electromagnetic radiation along each Cartesian direction.

The three diagonal matrix elements of the transition moment ($\int \boldsymbol{\psi}_i \alpha_{\mathrm{XX}} \boldsymbol{\psi}_i \mathrm{d}\tau$, $\int \boldsymbol{\psi}_i \alpha_{\mathrm{YY}} \boldsymbol{\psi}_j \mathrm{d}\tau$, and $\int \boldsymbol{\psi}_i \alpha_{\mathrm{ZZ}} \boldsymbol{\psi}_i \mathrm{d}\tau$) correspond to the Rayleigh scattering, whereas the six off-diagonal elements ($\int \boldsymbol{\psi}_i \alpha_{\mathrm{XY}} \boldsymbol{\psi}_j \mathrm{d}\tau$, $\int \boldsymbol{\psi}_i \alpha\alpha_{\mathrm{XZ}} \boldsymbol{\psi}_j \mathrm{d}\tau$, $\int \boldsymbol{\psi}_i \alpha_{\mathrm{YX}} \boldsymbol{\psi}_j \mathrm{d}\tau$, $\int \boldsymbol{\psi}_i \alpha_{\mathrm{YZ}} \boldsymbol{\psi}_j \mathrm{d}\tau$, $\int \boldsymbol{\psi}_i \alpha_{\mathrm{ZX}} \boldsymbol{\psi}_j \mathrm{d}\tau$, and $\int \boldsymbol{\psi}_i \alpha_{\mathrm{ZY}} \boldsymbol{\psi}_j \mathrm{d}\tau$) correspond to the Raman scattering. The $\boldsymbol{\psi}_i \rightarrow \boldsymbol{\psi}_j$ transition will be

Raman allowed if at least one of the six off-diagonal elements does not equal zero. Such determinations can be qualitatively made using symmetry-based group theory, but for low symmetry organic molecules all fundamental (i.e., $\Delta v = \pm 1$) Raman transitions will be allowed.

Although Raman spectra can be obtained using dispersive technology, the best spectra are acquired through the use of Fourier transform technology because FT-Raman systems can provide superior wavelength accuracy and minimization of any background fluorescence. In a typical system, a gas or diode laser is used to irradiate the sample, the sample is positioned in the laser beam, and the scattered radiation collected either in the 180° backscattering or the 90° right-angle configuration. The scattered photons are passed into an interferometer equipped with laser line filtering, and ultimately quantitated by a suitable detector. More detailed discussions of the spectrometer hardware can be found in the literature (13–16,118).

With appropriate collection optics, Raman spectroscopy can be performed on very small samples, with solid samples of approximately 25 to 50 mg often being merely filled into metal or glass sample holders. Samples that are darkly colored can present practical difficulties because such materials tend to absorb the exciting energy and degrade. In such cases, one must dissipate the heat, which can be accomplished by reducing the laser power or by spinning the sample to avoid the irradiation of a single point.

As in the case of infrared absorption spectroscopy, the bands in a Raman spectrum can be assigned through the use of group frequencies correlation tables. Significant insight can be obtained from the compilations of functional group vibrational frequencies associated with infrared absorption spectroscopy (38–40), but of greater utility is the compilation of group frequencies specific to Raman spectroscopy (119). Because the transition moment of a Raman transition depends on the magnitude of polarizability, it follows that the vibrational modes exhibiting the strongest intensities in a Raman spectrum will be those that are associated with functional groups that are characterized by high degrees of polarizability. Examples of such functionalities include the C–S, S–S, C–C, N=N, and C=C groups.

Although excitation of a given vibrational mode gives rise to infrared absorption bands and Raman scattering bands having identical frequencies, the fact that the infrared absorption process is an electric dipole transition and the Raman process is based on changes in polarizability leads to the observation of differences in relative spectral intensities for a given material. This is illustrated in Figure 8, where the infrared absorption and Raman spectra of racemic ibuprofen in the fingerprint region are compared (120). Most notable is the complete absence of a peak associated with the asymmetric C=O stretching mode in the Raman spectrum that is very prominent at 1707 cm^{-1} in the infrared absorption spectrum. Also noteworthy are the differing phenyl ring vibrational modes, one of which is observed at 779 cm^{-1} in the infrared absorption spectrum, and another which is observed at 827 cm^{-1} in the Raman spectrum.

As was the case for the other vibrational spectroscopic methods discussed above, Raman spectroscopy can be profitably used to study polymorphic and solvatomorphic solids when the differing crystal structures results in a perturbation of the pattern of molecular vibrations. This is often the case, but the question arises as to how different the energies of Raman peaks associated with the same group vibration in two different crystal forms should be in order to be useful. This question was addressed through the use of descriptive statistics and analysis of variance

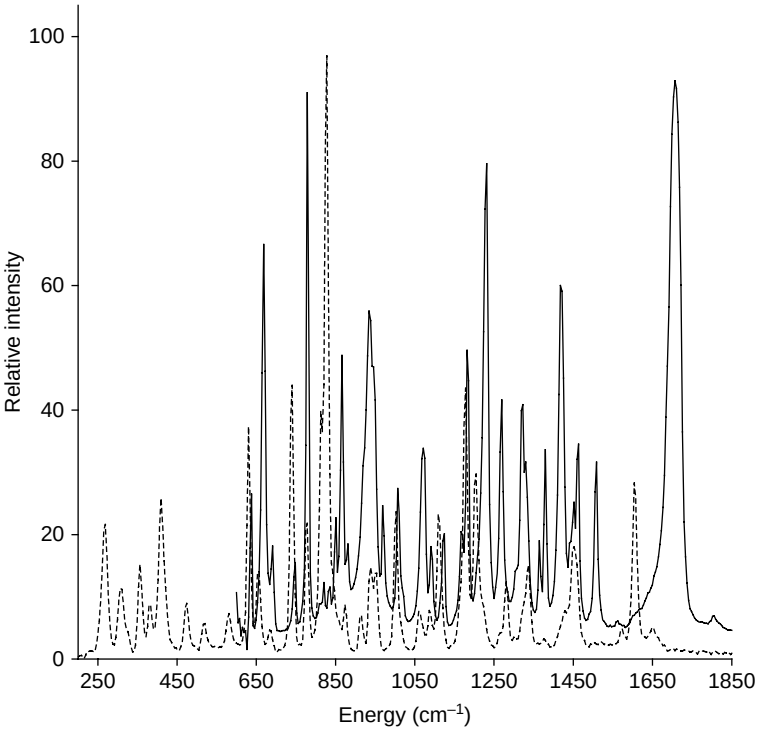

FIGURE 8 Fingerprint region infrared absorption spectrum of racemic ibuprofen (*solid trace*), and the fingerprint region Raman spectrum of the same compound (*dashed trace*). Each spectrum has been normalized so that the relative intensity of the most intense band equals 100%. H.G. Brittain, unpublished results (120).

methods for the development of a guideline that signify when Raman spectral differences could reliably signify the existence of different crystal structures for the same substance (121). From this analysis, it was proposed that the shift in the energy of a Raman peak would need to exceed 1.6 cm^{-1} to indicate the existence of polymorphism.

Nevertheless, the shifts commonly observed among polymorphic substances are frequently sufficiently large to permit the use of Raman spectroscopy as a triage method in screening protocols. In one such study, Raman spectroscopy was used to measure the amount of dissolved carbamazepine in a given solvent system, and subsequently to determine whether Form-I or Form-III crystallized upon cooling of the solutions (122). The advantage of the Raman method was that the analyses could be performed in sample volumes of 35 or 100 µL, and use of these small volumes allowed faster approaches to equilibrium through the use of smaller quantities of drug substance. The Raman method has been shown to be applicable to high-throughput studies conduced in multi-well plates (123) and in studies of epitaxial-induced crystallization (124).

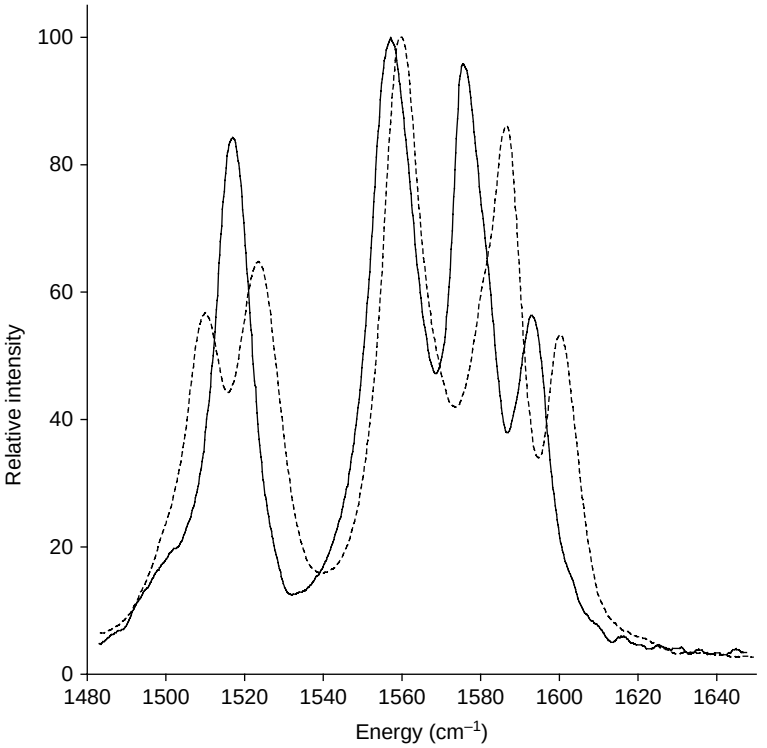

FIGURE 9 Raman spectra obtained in the high-frequency region for olanzapine Form-1 (*solid trace*) and Form-2 (*dashed trace*). Each spectrum has been normalized so that the relative intensity of the most intense band equals 100%, and the normalized spectra were generated from data given in Ref. (125).

A combination of infrared and Raman spectroscopic investigations was used to characterize two polymorphs of olanzapine, with spectral assignments being deduced for all observed bands in the two solid-state forms in order to obtain insight into the crystalline structures (125). As illustrated in Figure 9, the spectrum of Form-1 in the high-frequency region is characteristic of a hydrogen-bonded molecule, and the changes in the spectrum of Form-2 were determined to be consistent with atoms involved directly or indirectly to hydrogen bonds associated with the N–H group and not with any type of conformational difference between the molecules in the two crystal structures.

Schmidt has used Raman spectroscopy to study the polymorphic structures formed by benzocaine, butambene, and isobutambene as part of a program to characterize local anesthetic drugs having the general formula of lipo–CO–hyd, where the lipophilic end is mostly phenyl, CO is a negatively charged linkage (usually ester or amide), and the hydrophilic group (hyd) is usually a secondary or tertiary amine (126). Three polymorphs of sibenadet hydrochloride were found to exhibit varying degrees of dynamic disorder in a terminal phenyl group, with the

polymorphism being largely governed by skeletal symmetry changes rather than alterations in hydrogen-bonding patterns (127).

Raman spectroscopy has been found to be extremely useful for the quantitative analysis of phase composition. For example, two polymorphs of buspirone hydrochloride were characterized by a full range of techniques, with unique peaks in the Raman spectrum and chemometric analysis being used to develop quantitative methods for phase composition in mixtures of the two forms (128). A related approach was used to develop a quantitative method for the polymorphs of paracetamol in mixtures (129). An analytical method has been developed to determine the phase composition in mixtures of the two polymorphs of *N*-[5-chloro-4-[(4-chlorophenyl)cyanomethyl]-2-methylphenyl]-2-hydroxy-3,5-diiodobenzamide and its amorphous form, with these being quantitatively distinguished using Raman spectroscopy and a constrained linear regression model (130). The effect of particle size on quantitative phase determinations using Raman spectroscopy was studied for the case of flufenamic acid, noting that the intensity of Raman scattering tended to decrease with increasing particle size (131).

The use of X-ray powder diffraction in the study of amorphous solids is hampered by the lack of a useful response, but the vibrational transitions of such materials are still visible in both infrared absorption and Raman spectroscopies. Both techniques were used to evaluate the hydrogen-bonding patterns in a series of crystalline and amorphous dihydropyridine calcium channel blocker compounds, where it was learned that although significant variations existed in the various crystalline forms, similar patterns were detected for the amorphous states (132). The crystalline γ and amorphous modifications of indomethacin have been studied using vibrational spectroscopic and density functional theory computational methods, where it was deduced that the drug substance in the amorphate existed primarily in dimeric structures that were similar to those existing in the crystalline γ-form (133).

Raman spectroscopy has proven to be very useful as well in the study of the polymorphic content of drug substances in their formulations. For example, a detailed series of calibration samples was used to develop a method based on Raman spectroscopy for determination of the phase composition of the methyl ester of 5-*p*-fluoro-benzoyl-2-benzimidazolecarbamic acid in two formulations (134). The difficulty in this analysis lay in the fact that the drug substance was capable of existing in three polymorphic forms, and that a full statistical package based on the intensities of 78 selected bands was required to differentiate the forms.

The characterization of solvatomorphs by Raman spectroscopy is based on crystallographic effects on the energies of molecular vibrations. In addition to the known monohydrate and sesquihydrate crystal forms of pantoprazole sodium, two additional hydrate forms were studied using a full complement of spectroscopic characterization techniques, with both infrared absorption and Raman spectroscopies being capable of distinguishing between the various solvatomorphs (135). Four hydration states (an anhydrate, a monohydrate, a hemi-pentahydrate, and a variable hydrate containing fou to six waters) have been reported for risedronate sodium, with the Raman spectra of these forms being dominated by peaks associated with the substituted pyridine ring of the compound (136). Comparison of structures obtained by X-ray diffraction indicated the existence of strong intermolecular out-of-plane hydrogen bonding between the pyridine ring and an adjacent phosphate

group was capable of impacting the ring vibrational modes in the monohydrate and variable hydration forms.

Owing its ready adaptability as an in situ method of characterization, Raman spectroscopy has been shown to be useful in the study of solution-mediated phase transformation reactions. For example, a number of methods (including Raman spectroscopy) were used to follow the phase change of the metastable α-form of (*L*)-glutamic acid into its stable β-form, and as an aid develop the first-order kinetics for nucleation and growth kinetics of both polymorphs in a population balance model (137). The anhydrate/monohydrate equilibria of citric acid in aqueous solutions have been investigated with the aim of demonstrating the process analytical technology capabilities of in situ Raman spectroscopy (138). Flufenamic acid was used as the model system in a study of the use of in situ Raman spectroscopy as a method for the determination of transformation kinetics and transition temperatures, with good agreement being reported between results obtained by the spectroscopic method and those obtained using the more conventional van't Hoff approach (139).

The solution-mediated aqueous transformation of anhydrous carbamazepine to its dihydrate phase has proven to be a good model system for the use of Raman spectroscopy as a means to study the kinetics, because certain bands in the Raman spectra are diagnostic of the phase identity (Fig. 10). The thermodynamics associated with the system were studied in ethanol–water mixtures by measuring the solubility of both forms over the temperature range of 0°C to 60°C using a Raman immersion probe to establish the phase composition (140). In a related work, the Raman immersion probe was used to determine that crystallization of the stable form represented the rate-determining step (141). Raman spectroscopy was used to follow the kinetics associated with the conversion of the Form I, II, and II anhydrates to the dihydrate, where it was found that the morphology of the starting material seemed to determine the rates of reaction (142). The Raman technique, in combination with partial least squares regression analysis, was found to be the most robust method for the detection and quantification of mixtures of the carbamazepine solvatomorphs, with the possible biasing influences of particle size, morphology, mixing, and surface effects being evaluated (143).

Owing to its ease of acquisition, and non-invasive nature of sample handling, Raman spectroscopy has proven to be an ideal technique for the in situ study of thermally induced phase transformations. For example, variable-temperature Raman spectroscopy was used to study the low-temperature phase transitions in a biphenyl–fullerene single crystal, where three biphenyl vibrational modes and the C–H stretching mode were indicative of the phase transition, and changes in the planarity of the biphenyl molecule appeared to accompany the phase change (144). The behavior of most of the C_{60}–fullerene vibrational modes could be correlated with either of the transitions, indicating changes in its site symmetry. In contrast, Raman spectroscopy was used to demonstrate that single crystals of different polymorphs of pentacene did not undergo any phase transformation reactions over the temperature range of 79 K to 300 K (145).

Details of the phase transformation processes associated with the hydration and dehydration of theophylline have also been studied using Raman spectroscopy, because the bands in the high-frequency region were found to be especially sensitive toward the phase identity (146). The thermally induced dehydration of

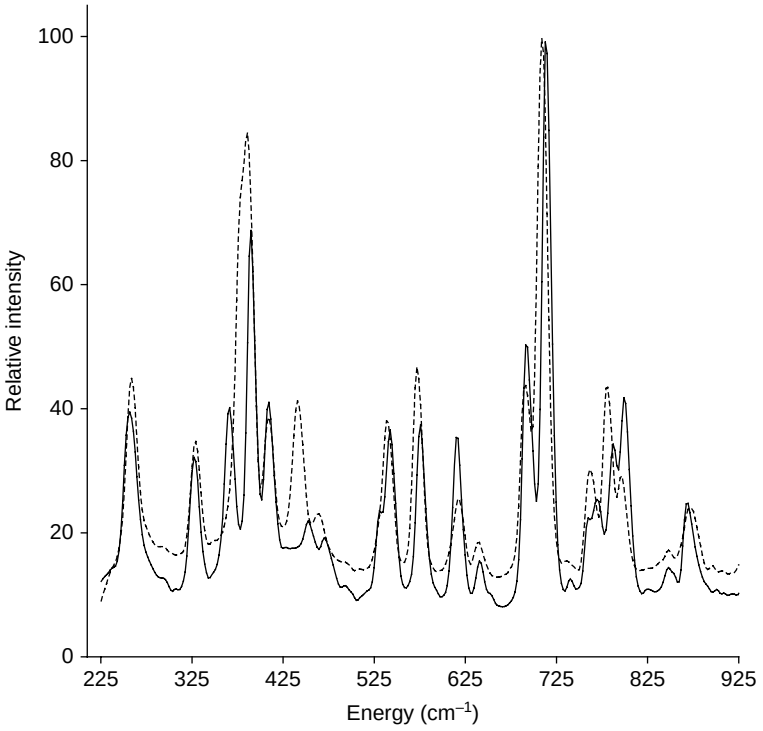

FIGURE 10 Raman spectra of carbamazepine anhydrate (*solid trace*) and carbamazepine dihydrate (*dashed trace*) over the lowest frequency region. Each spectrum has been normalized so that the relative intensity of the most intense band equals 100%. H.G. Brittain, unpublished results (120).

erythromycin A dihydrate has been studied using variable-temperature Raman spectroscopy, because the spectroscopic method was able to distinguish between the isomorphic dihydrate and its dehydrated product and being sufficiently responsive so as to be useful as an in-process technique for control over a drying process (147).

The use of principal component analysis and Raman spectroscopy in studies of the dehydration phenomena associated with various hydrated compounds, where it was found that the approach was effective in the fast screening of accumulated information, and its use facilitated the identification of critical temperatures or critical time points in the dehydration reactions (148). A Raman spectrometer interfaced with a moisture sorption gravimetric analyzer has been used to study modes of water–solid interactions in sulfaguanidine, cromolyn sodium, ranitidine hydrochloride, amorphous sucrose, and silica gel (149). Once again, principal components analysis was used to determine the genuine trends in the Raman data and facilitate the generation of information related the various types of interactions.

REFERENCES

1. Brittain HG. Spectroscopy of Pharmaceutical Solids. New York: Taylor & Francis, 2006.
2. Barrow GM. Molecular Spectroscopy. New York: McGraw-Hill, 1962.
3. King GW. Spectroscopy and Molecular Structure. New York: Holt, Rinehart and Winston, 1964.
4. Brittain EFH, George WO, Wells CHJ. Introduction to Molecular Spectroscopy. London: Academic Press, 1970.
5. Guillory WA. Introduction to Molecular Structure and Spectroscopy. Boston: Allyn and Bacon, 1977.
6. McHale JL. Molecular Spectroscopy. Upper Saddle River, NJ: Prentice Hall, 1999.
7. Rao CNR. Chemical Applications of Infrared Spectroscopy. New York: Academic Press, 1963.
8. Kendall DN. Applied Infrared Spectroscopy. New York: Reinhold Pub, 1966.
9. Conley RT. Infrared Spectroscopy. Boston, MA: Allyn and Bacon, 1966.
10. Colthup NB, Daly LH, Wiberley SE. Introduction to Infrared and Raman Spectroscopy, 2nd edition. London: Academic Press, 1975.
11. Nakanishi K, Solomon PH. Infrared Absorption Spectroscopy. San Francisco, CA: Holden-Day, 1977.
12. Bhagavantam S. Scattering of Light and the Raman Effect. New York: Chemical Publishing Co, 1942.
13. Grasselli JG, Snavely MK, Bulkin BJ. Chemical Applications of Raman Spectroscopy. New York: Wiley-Interscience, 1981.
14. Grasselli JG, Bulkin BJ. Analytical Raman Spectroscopy. New York: John Wiley & Sons, 1991.
15. Ferraro JR, Nakamoto K. Introductory Raman Spectroscopy. New York: Academic Press, 1994.
16. Lewis IR, Edwards HGM. Handbook of Raman Spectroscopy. New York: Marcel Dekker, 2001.
17. Wilson EB, Decius JC, Cross PC. Molecular Vibrations: The Theory of Infrared and Raman Vibrational Spectra. New York: McGraw-Hill Book Co, 1955.
18. Markovich RJ, Pidgeon C. Introduction to fourier transform infrared spectroscopy and applications in the pharmaceutical sciences. Pharm Res 1991; 8: 663–75.
19. Brittain HG, Bogdanowich SJ, Bugay DE, et al. Physical characterization of pharmaceutical solids. Pharm Res 1991; 8: 963–73.
20. Threlfall TL. Analysis of organic polymorphs. Analyst 1995; 120: 2435–60.
21. Bugay DE, Williams AC. Vibrational spectroscopy, chapter 3 in Physical Characterization of Pharmaceutical Solids. In: Brittain HG, ed. New York: Marcel Dekker, 1995: 59–91.
22. Brittain HG. Spectral methods for the characterization of polymorphs and solvates. J Pharm Sci 1997; 86: 405–12.
23. Findlay WP, Bugay DE. Utilization of fourier transform raman spectroscopy for the study of pharmaceutical crystal forms. J Pharm Biomed Anal 1998; 16: 921–30.
24. Brittain HG. Methods for the characterization of polymorphs and solvates, chapter 6 in Polymorphism in Pharmaceutical Solids. In: Brittain HG, ed. New York: Marcel Dekker, 1999: 227–78.
25. Bugay DE, Findlay WP. Pharmaceutical Excipients: Characterization by Raman IR and NMR Spectroscopy. New York: Marcel Dekker, 1999.
26. Frank CJ. Pharmaceutical applications of raman spectroscopy, chapter 6 in Analytical Applications of Raman Spectroscopy. In: Pelletier MJ, ed. Oxford: Blackwell Science, 1999: 224–75.
27. Brittain HG. Solid-state analysis, Chapter 3, in the Handbook of Pharmaceutical Analysis. In: Ahuja S, Scypinski S, eds. New York: Marcel Dekker, 2001: 57–84.

28. Bugay DE. Characterization of the solid-state: spectroscopic techniques. Adv Drug Del Rev 2001; 48: 43–65.
29. Brittain HG, Medek A. Polymorphic and solvatomorphic impurities, chapter 3 in Handbook of Isolation and Characterization of Impurities in Pharmaceuticals. In: Ahuja S, Alsante KM, eds. Academic Press, 2003: 39–73.
30. Bugay DE, Brittain HG. Infrared absorption spectroscopy, chapter 8, in Spectroscopy of Pharmaceutical Solids. In: Brittain HG, ed. New York: Taylor and Francis, 2006: 235–69.
31. Bugay DE, Brittain HG. Raman spectroscopy, chapter 9, in Spectroscopy of Pharmaceutical Solids. In: Brittain HG, ed. New York: Taylor and Francis, 2006: 271–312.
32. Brittain HG. Spectroscopic methods for the characterization of drug substances, chapter 3.5, in Preformulation in Solid Dosage Form Development. In: Adeyeye MC, Brittain HG, eds. New York: Informa Healthcare Press, 2008: 253–77.
33. Pauling L, Wilson EB. Introduction to Quantum Mechanics. New York: McGraw-Hill, 1935.
34. Eyring H, Walter J, Kimball GE. Quantum Chemistry. New York: John Wiley & Sons, 1944.
35. Kauzmann W. Quantum Chemistry. New York: Academic Press, 1957.
36. Davis JC. Advanced Physical Chemistry. New York: Ronald Press, 1965.
37. Levine IN. Quantum Chemistry. Boston: Allyn and Bacon, 1970.
38. Flett MC. Characteristic Frequencies of Groups in the Infra-Red. Amsterdam: Elsevier Pub, 1963.
39. Bellamy LJ. Advances in Infrared Group Frequencies. London: Methuen & Co, 1968.
40. Socrates G. Infrared and Raman Characteristic Group Frequencies – Tables and Charts, 3rd edn. Chichester: John Wiley & Sons, 2001.
41. Fearn T, Osborne BG. Near Infrared Spectroscopy in Food Analysis. Dublin, Ireland: Longman Scientific & Technical Pub, 1986.
42. Williams P, Norris K. Near-Infrared Technology in the Agricultural and Food Industries. Saint Paul, MN: American Association of Cereal Chemists, 2001.
43. Siesler HW, Ozaki Y, Kawata S, et al. Near-Infrared Spectroscopy: Principles, Instruments, Applications. Weinheim: Wiley-VCH Pub., 2002.
44. Burns DA, Ciurczak EW. Handbook of Near-Infrared Analysis, 2nd edn. New York: Marcel Dekker, 2001.
45. Ciurczak EW, Drennen JK. Pharmaceutical and Medical Applications of Near-Infrared Spectroscopy. New York: Marcel Dekker, 2002.
46. Anderson DH, Woodall NB. Infrared spectroscopy, chapter 1 in Physical Methods of Chemistry, volume I, part IIIB. In: Weissberger A, Rossiter BW, eds. New York: Wiley-Interscience, 1972: 1–84.
47. Griffiths PR, de Haseth JA. Fourier Transform Infrared Spectrometry. New York: John Wiley & Sons, 1986.
48. Fredericks P, Rintoul L, Coates J. Vibrational spectroscopy: instrumentation for infrared and Raman spectroscopy, chapter 7 in Ewing's Analytical Instrumentation Handbook, 3rd edn, Cazes J, ed. New York: Marcel Dekker, 2005: 163–238.
49. Mutha SC, Ludemann WB. Solid-state anomalies in IR spectra of compounds of pharmaceutical interest. J Pharm Sci 1976; 65: 1400–3.
50. Bugay DE, Newman AW, Findlay WP. Quantitation of cefepime dihydrochloride in cefepime dihydrochloride monohydrate by diffuse reflectance IR and powder X-ray diffraction techniques. J Pharm Biomed Anal 1996; 15: 49–61.
51. Culler SR. Diffuse Reflectance Spectroscopy: Sampling Techniques for Qualitative/Quantitative Analysis of Solids, in Practical Sampling Techniques for Infrared Analysis. In: Coleman PB, ed. Boca Raton, FL: CRC Press, 1993: 93–105.
52. Compton SV, Compton DAC. Optimization of data by internal reflectance spectroscopy, in Practical Sampling Techniques for Infrared Analysis. In: Coleman PB, ed. Boca Raton, FL: CRC Press, 1993: 55–92.

53. Urban MW. Attenuated Total Reflectance Spectroscopy of Polymers. Washington, DC: American Chemical society, 1996.
54. Giannellini V, Bambagiotti-Alberti M, Bartolucci G, et al. Solid-state study of mepivacaine hydrochloride. J Pharm Biomed Anal 2005; 39: 444–54.
55. Kipouros K, Kachrimanis K, Nikolakakis I, et al. Simultaneous quantification of carbamazepine crystal forms in ternary mixtures (I, III, and IV) by diffuse reflectance FTIR spectroscopy (DRIFTS) and multivariate calibration. J Pharm Sci 2006; 95: 2419–31.
56. Lee EH, Boerrigter SXM, Rumondor ACF, et al. Formation and solid-state characterization of a salt-induced metastable polymorph of flufenamic acid. Cryst Growth Des 2008; 8: 91–7.
57. Park HJ, Kim M-S, Lee S, et al. Recrystallization of fluconazole using the supercritical antisolvent (SAS) process. Int J Pharm 2007; 328: 152–60.
58. Rafilovich M, Bernstein J, Harris RK, et al. Groth's Original Concomitant Polymorphs Revisited. Cryst Growth Des 2005; 5: 2197–209.
59. Yu L, Stephenson GA, Mitchell CA, et al. Thermochemistry and conformational polymorphism of a hexamorphic crystal system. J Am Chem Soc 2000; 122: 585–91.
60. Yamamura S, Gotoh H, Sakamoto Y, et al. Physicochemical properties of amorphous salt of cimetidine and diflunisal system. Int J Pharm 2002; 241: 213–21.
61. Kojima T, Yamauchi Y, Onoue S, et al. Evaluation of hydrate formation of a pharmaceutical solid by using diffuse reflectance infrared fourier-transform spectroscopy. J Pharm Biomed Anal 2008; 46: 788–91.
62. Bartolomei M, Bertocchi P, Antoniella E, et al. Physicochemical characterization and intrinsic dissolution studies of a new hydrate form of diclofenac sodium: comparison with anhydrous form. J Pharm Biomed Anal 2006; 40: 1105–13.
63. Vogt FG, Dell'Orco PC, Diederich AM, et al. A study of variable hydration states in topotecan hydrochloride. J Pharm Biomed Anal 2006; 40: 1080–8.
64. Alkhamis KA, Obaidat AA, Nuseirat AF. Solid-state characterization of fluconazole. Pharm Dev Tech 2002; 7: 491–503.
65. Caira MR, Alkhamis KA, Obaidat RM. Preparation and crystal characterization of a polymorph, a monohydrate, and an ethyl acetate solvate of the antifungal fluconazole. J Pharm Sci 2004; 93: 601–11.
66. Alkhamis KA, Salem MS, Obaidat RM. Comparison between dehydration and desolvation kinetics of fluconazole monohydrate and fluconazole ethyl acetate solvate using three different methods. J Pharm Sci 2006; 95: 859–70.
67. van Tonder EC, Maleka TSP, Liebenberg W, et al. Preparation and physicochemical properties of niclosamide anhydrate and two monohydrates. Int J Pharm 2004; 269: 417–32.
68. Cantera RG, Leza MG, Bachiller CM. Solid phases of tenoxicam. J Pharm Sci 2002; 91: 2240–51.
69. Reddy VR, Rajmohan MA, Shilpa RL, et al. A novel quantification method of pantoprazole sodium monohydrate in sesquihydrate by thermogravimetric analyzer. J Pharm Biomed Anal 2007; 43: 1836–41.
70. Ferrari ES, Davey RJ, Cross WI, et al. Crystallization in polymorphic systems: the solution-mediated transformation of β to α glycine. Cryst Growth Des 2003; 3: 53–60.
71. Sheikhzadeh M, Murad S, Rohani S. Response surface analysis of solution-mediated polymorphic transformation of buspirone hydrochloride. J Pharm Biomed Anal 2007; 45: 227–36.
72. Gilpin RK, Zhou W. Infrared studies of the thermal conversion of mefenamic acid between polymorphic states. Vibrat Spectroscopy 2005; 37: 53–9.
73. Lin SY, Cheng WT, Wang SL. Thermodynamic and kinetic characterization of polymorphic transformation of famotidine during grinding. Int J Pharm 2006; 318: 86–91.

74. Brittain HG. unpublished results obtained at a resolution of 4 cm^{-1} using a Shimadzu model 8400S Fourier-transform infrared spectrometer, with each spectrum being obtained as the average of 40 individual spectra. The data were acquired using the attenuated total reflectance sampling mode, where the samples were clamped against the ZnSe crystal of a Pike MIRacleTM single reflection horizontal ATR sampling accessory.
75. Lin S-Y, Chien J-L. In vitro simulation of solid-solid dehydration, rehydration, and solidification of trehalose dihydrate using thermal and vibrational spectroscopic techniques. Pharm Res 2003; 20: 1926–31.
76. Fearn T, Osborne BG. Near Infrared Spectroscopy in Food Analysis. Dublin, Ireland: Longman Scientific & Technical Pub, 1986.
77. Williams P, Norris K. Near-Infrared Technology in the Agricultural and Food Industries. Saint Paul, MN: American Association of Cereal Chemists, 2001.
78. Siesler HW, Ozaki Y, Kawata S, Heise HM. Near-Infrared Spectroscopy: Principles, Instruments, Applications. Weinheim: Wiley-VCH Pub., 2002.
79. Burns DA, Ciurczak EW. Handbook of Near-Infrared Analysis, 2nd edn. New York: Marcel Dekker, 2001.
80. Ciurczak EW, Drennen JK. Pharmaceutical and Medical Applications of Near-Infrared Spectroscopy. New York: Marcel Dekker, 2002.
81. Cogdill RP, Drennen JK III. Near-Infrared spectroscopy, Chapter 10, in Spectroscopy of Pharmaceutical Solids. In: Brittain HG, ed. New York: Taylor & Francis, 2006: 313–412.
82. Ciurczak EW. Uses of Near-Infrared Spectroscopy in Pharmaceutical Analysis. Appl Spectrosc Rev 1987; 23: 147–63.
83. MacDonald BF, Prebble KA. Some applications of near-infrared reflectance analysis in the pharmaceutical industry. J Pharm Biomed Anal 1993; 11: 1077–85.
84. Roggo Y, Chalus P, Maurer L, Lema-Martinez C, et al. A review of near infrared spectroscopy and chemometrics in pharmaceutical technologies. J Pharm Biomed Anal 2007; 44: 683–700.
85. El-Hagrasy A, D'Amico F, Drennen JK III. A process analytical technology approach to near-infrared process control of pharmaceutical powder blending. Part I: D-optimal design for characterization of powder mixing and preliminary spectral data evaluation. J Pharm Sci 2006; 95: 392–406.
86. El-Hagrasy A, Delgado-Lopez M, Drennen JK III. A process analytical technology approach to near-infrared process control of pharmaceutical powder blending. Part II: qualitative near-infrared models for prediction of blend homogeneity. J Pharm Sci 2006; 95: 407–21.
87. El-Hagrasy A, Drennen JK III. A process analytical technology approach to near-infrared process control of pharmaceutical powder blending. Part III: quantitative near-infrared calibration for prediction of blend homogeneity and characterization of powder mixing kinetics. J Pharm Sci 2006; 95: 422–34.
88. Luner PE, Majuru S, Seyer JJ, et al. Quantifying crystalline form composition in binary powder mixtures using near-infrared reflectance spectroscopy. Pharm Dev Tech 2000; 5: 231–46.
89. Patel AD, Luner PE, Kemper MS. Low level determination of polymorph composition in physical mixtures by near-infrared reflectance spectroscopy. J Pharm Sci 2001; 90: 360–70.
90. McArdle P, Gilligan K, Cunningham D, et al. Determination of the polymorphic forms of bicifadine hydrochloride by differential scanning calorimetry–thermogravimetric analysis, X-ray powder diffraction, attenuated total reflectance–infrared spectroscopy, and attenuated total reflectance–near-infrared spectroscopy. Appl Spectrosc 2005; 59: 1365–71.
91. Heinz A, Savolainen M, Rades T, et al. Quantifying ternary mixtures of different solid-state forms of indomethacin by raman and near-infrared spectroscopy. Eur J Pharm Sci 2007; 32: 182–92.

92. Mirza S, Miroshnyk I, Rantanen J, et al. Solid-state properties and relationship between anhydrate and monohydrate of baclofen. J Pharm Sci 2007; 96: 2399–408.
93. Rantanen J, Wikström H, Rhea FE, et al. Improved understanding of factors contributing to quantification of anhydrate/hydrate powder mixtures. Appl Spectrosc 2005; 59: 942–51.
94. Krzyaniak JF, Williams GR, Ni N. Identification of phase boundaries in anhydrate/hydrate systems. J Pharm Sci 2007; 96: 1270–81.
95. Blanco M, Valdés D, Llorente I, et al. Application of NIR spectroscopy in polymorphic analysis: study of pseudo-polymorphs stability. J Pharm Sci 2005; 94: 1336–42.
96. Kauffman JF, Tumuluri V, Guo C, et al. Near-infrared spectroscopy of magnesium stearate hydrates and multivariate calibration of pseudo-polymorph composition. J Pharm Sci 2008; 97: 2757–67.
97. Li W, Worosila GD, Wang W, et al. Determination of polymorph conversion of an active pharmaceutical ingredient in wet granulation using NIR calibration models generated from the premix blends. J Pharm Sci 2005; 94: 2800–6.
98. Römer M, Heinämäki J, Miroshnyk I, et al. Phase transformations of erythromycin A dihydrate during pelletization and drying. Eur J Pharm Biopharm 2007; 67: 246–52.
99. Xie Y, Tao W, Morrison H, et al. Quantitative determination of solid-state forms of a pharmaceutical development compound in drug substance and tablets. Int J Pharm 2008; 362: 29–36.
100. Durig JR, Cox AW Jr. Current and past research in far-infrared interferometry, chapter 6 in Fourier Transform Infrared Spectroscopy, volume 1. In: Ferraro JE, Basile LJ, eds. New York: Academic Press, 1978: 215–74.
101. Friedmann H, Kimel S. Rotation-translation coupling spectrum of matrix-isolated diatomic molecules in the near and far infrared. J Chem Phys 1966; 44: 4359–60.
102. Beard MC, Turner GM, Schmuttenmaer CA. Terahertz spectroscopy. J Phys Chem B 2002; 106: 7146–59.
103. Dexheimer SL. Terahertz Spectroscopy: Principles and Applications. New York: Taylor and Francis, 2008.
104. Strachan CJ, Rades T, Newnham DA, et al. Using terahertz pulsed spectroscopy to study crystallinity of pharmaceutical materials. Chem Phys Lett 2004; 390: 20–4.
105. Zeitler JA, Rades T, Taday PF. Pharmaceutical and security applications of terahertz spectroscopy, chapter 8 in Terahertz Spectroscopy: Principles and Applications. In: Dexheimer SL, ed. New York: Taylor and Francis, 2008: 299–323.
106. Zeitler JA, Taday PF, Newnham DA, et al. Terahertz pulsed spectroscopy and imaging in the pharmaceutical setting. J Pharm Pharmacol 2007; 59: 209–23.
107. Newnham DA, Taday PF. Pulsed terahertz attenuated total reflection spectroscopy. Appl Spectrosc 2008; 62: 394–8.
108. Taday PF, Bradley IV, Arnone DD, et al. Using terahertz pulsed spectroscopy to study the crystalline structure of a drug: a case study of the polymorphs of ranitidine hydrochloride. J Pharm Sci 2003; 92: 831–8.
109. Strachan CJ, Taday PF, Newnham DA, et al. Using terahertz pulsed spectroscopy to quantify pharmaceutical polymorphism and crystallinity. J Pharm Sci 2005; 94: 837–46.
110. Day GM, Zeitler JA, Jones W, et al. Understanding the influence of polymorphism on phonon spectra: lattice dynamics calculations and terahertz spectroscopy of carbamazepine. J Phys Chem B 2006; 110: 447–56.
111. Aaltonen J, Strachan CJ, Pöllänen K, et al. Hyphenated spectroscopy as a polymorph screening tool. J Pharm Biomed Anal 2007; 44: 477–83.
112. Zeitler JA, Newnham DA, Taday PF, et al. Temperature dependent terahertz pulsed spectroscopy of carbamazepine. Thermochim Acta 2005; 436: 71–7.
113. Zeitler JA, Newnham DA, Taday PF, et al. Characterization of temperature-induced phase transformations in five polymorphic forms of sulfathiazole by terahertz pulsed spectroscopy and differential scanning calorimetry. J Pharm Sci 2006; 95: 2468–98.

114. Upadhya PC, Nguyen K, Shen YC, et al. Characterization of crystalline phase transformations in theophylline by time-domain terahertz spectroscopy. Spectrosc Lett 2006; 39: 215–24.
115. Zeitler JA, Kogermann K, Rantanen J, et al. Drug hydrate systems and dehydration processes studied by terahertz pulsed spectroscopy. Int J Pharm 2007; 344: 78–84.
116. Liu H-B, Chen Y, Zhang X-C. Characterization of anhydrous and hydrated pharmaceutical materials with THz time-domain spectroscopy. J Pharm Sci 2007; 96: 927–34.
117. Zeitler JA, Taday PF, Pepper M, et al. Relaxation and crystallization of amorphous carbamazepine studied by terahertz pulsed spectroscopy. J Pharm Sci 2007; 96: 2703–9.
118. Tobin MC. Laser Raman Spectroscopy. New York: Wiley-Interscience, 1971.
119. Dollish FR, Fateley WG, Bentley FF. Characteristic Raman Frequencies of Organic Compounds. New York: John Wiley & Sons, 1974.
120. Brittain HG. Unpublished results obtained for the infrared absorption spectrum of racemic ibuprofen obtained according to reference [74], and Raman spectrum obtained on this substance at a resolution of 5 cm^{-1} and using a Raman Systems model R-3000HR spectrometer (785 nm laser source). The data were acquired using front-face scattering from a thick powder bed contained in an aluminum sample holder.
121. Mehrens SM, Kale UJ, Qu X. Statistical analysis of differences in the raman spectra of polymorphs. J Pharm Sci 2005; 94: 1354–67.
122. Anquetil PA, Brenan CJH, Marcolli C, et al. Laser raman spectroscopic analysis of polymorphic forms in microliter fluid volumes. J Pharm Sci 2003; 92: 149–60.
123. Kojima T, Onoue S, Murase N, et al. Crystalline form information from multiwell plate salt screening by use of raman spectroscopy. Pharm Res 2006; 23: 806–12.
124. Grezesiak AL, Matzger AJ. New form discovery for the analgesics flurbiprofen and sulindac facilitated by polymer-induced heteronucleation. J Pharm Sci 2007; 96: 2978–86.
125. Ayala AP, Siesler HW, Boese R, et al. Solid-state characterization of olanzapine polymorphs using vibrational spectroscopy. Int J Pharm 2006; 326: 69–79.
126. Schmidt AC. Structural characteristics and crystal polymorphism of three local anesthetic bases. Int J Pharm 2005; 298: 186–97.
127. Cosgrove SD, Steele G, Austin TK, et al. Understanding the polymorphic behavior of sibenadet hydrochloride through detailed studies integrating structural and dynamical assessment. J Pharm Sci 2005; 94: 2403–15.
128. Sheikhzadeh M, Rohani S, Jutan A, et al. Solid-state characterization of buspirone hydrochloride polymorphs. Pharm Res 2006; 23: 1043–50.
129. Kachrimanis K, Braun DE, Greisser UJ. Quantitative analysis of paracetamol polymorphs in powder mixtures by FT-raman spectroscopy and PLS regression. J Pharm Biomed Anal 2007; 43: 407–12.
130. De Spiegeleer B, Baert B, Diericx N, et al. Assessment of the solid-state composition of an active salicylanilide compound by FT-raman spectroscopy. J Pharm Biomed Anal 2007; 44: 254–7.
131. Hu Y, Wikstrom H, Byrn SR, et al. Analysis of the effect of particle size on polymorphic quantitation by raman spectroscopy. Appl Spectrosc 2006; 60: 977–84.
132. Tang XC, Pikal MJ, Taylor LS. A spectroscopic investigation of hydrogen bond patterns in crystalline and amorphous phases in dihydropyridine calcium channel blockers. Pharm Res 2002; 19: 477–83.
133. Strachan CJ, Rades T, Gordon KC. A theoretical and spectroscopic study of γ-crystalline and amorphous indomethacin. J Pharm Pharmacol 2007; 59: 261–9.
134. De Spiegeleer B, Seghers D, Wieme R, et al. Determination of the relative amounts of three crystal forms of a benzimidazole drug in complex finished formulations by FT-Raman spectroscopy. J Pharm Biomed Anal 2005; 39: 275–80.
135. Zupančič V, Ograjšek N, Kotar-Jordan B, et al. Physical characterization of pantoprazole sodium hydrates. Int J Pharm 2005; 291: 59–68.

136. Redman-Furey N, Dicks M, Bigalow-Kern A, et al. Structural and analytical characterization of three hydrates and an anhydrate form of risedronate. J Pharm Sci 2005; 94: 893–911.
137. Schöll J, Bonalumi D, Vicum L, et al. In-situ monitoring and modeling of the solvent-mediated polymorphic transformation of L-glutamic acid. Cryst Growth Des 2006; 6: 881–91.
138. Caillet A, Puel F, Fevotte G. In-line monitoring of partial and overall solid concentration during solvent-mediated phase transition using raman spectroscopy. Int J Pharm 2006; 307: 201–8.
139. Hu Y, Wikström H, Byrn SR, et al. Estimation of the transition temperature for an enantiotropic polymorphic system from the transformation kinetics monitored using raman spectroscopy. J Pharm Biomed Anal 2007; 45: 546–51.
140. Qu H, Louhi-Kultanen M, Kallas J. Solubility and stability of anhydrate/hydrate in solvent mixtures. Int J Pharm 2006; 321: 101–7.
141. Qu H, Louhi-Kultanen M, Kallas J. Solvent-mediated phase transformation kinetics of an anhydrate/hydrate system. Cryst Growth Des 2006; 6: 2053–60.
142. Tian F, Zeitler JA, Strachan CJ, et al. Characterizing the conversion kinetics of carbamazepine polymorphs to the dihydrate in aqueous suspension using raman spectroscopy. J Pharm Biomed Anal 2006; 40: 271–80.
143. Tian F, Zhang F, Sandler N, et al. Influence of sample characteristics on quantification of carbamazepine hydrate formation by X-ray powder diffraction and raman spectroscopy. Eur J Pharm Biopharm 2007; 66: 466–74.
144. Palles D, Marucci A, Penicaud A, et al. Low-temperature phase transitions in a biphenyl-fullerene single crystal: a raman study. J Phys Chem B 2003; 107: 4904–11.
145. della Valle RG, Venuti E, Farina L, et al. Intramolecular and low-frequency intermolecular vibrations of pentacene polymorphs as a function of temperature. J Phys Chem B 2004; 108: 1822–6.
146. Amado AM, Nolasco MM, Ribeiro-Claro PJA. Probing pseudopolymorphic transitions in pharmaceutical solids using raman spectroscopy: hydration and dehydration of theophylline. J Pharm Sci 2007; 96: 1366–79.
147. Miroshnyk I, Kriachthev L, Mirza S, et al. Insight into thermally induced phase transformations of erythromycin A dihydrate. Cryst Growth Des 2006; 6: 369–74.
148. Jørgensen AC, Miroshnyk I, Karjalainen M, et al. Multivariate data analysis as a fast tool in evaluation of solid state phenomena. J Pharm Sci 2006; 95: 906–16.
149. Gift AD, Taylor LS. Hyphenation of raman spectroscopy with gravimetric analysis to interrogate water-solid interactions in pharmaceutical systems. J Pharm Biomed Anal 2007; 43: 14–26.

11 Solid-State Nuclear Magnetic Resonance Spectroscopy

Patrick A. Tishmack
SSCI, an Aptuit Company, West Lafayette, Indiana, U.S.A.

INTRODUCTION

Solid-state NMR (SSNMR) spectroscopy has been used to study polymorphism beginning with the analysis of hydroquinone by Ripmeester almost 30 years ago (1). The characterization of pharmaceutical polymorphs by SSNMR spectroscopy has become more common in the last 10 to 15 years as the technology has improved and NMR spectrometers have become easier to use, particularly for non-specialists. SSNMR spectroscopy provides unique information due to its selectivity and specificity compared to other analytical techniques, which makes it very valuable for characterization of pure compounds and well as mixtures.

SSNMR spectroscopy has also found an important role in establishing intellectual property in the pharmaceutical industry because it is critical to know the specific solid forms in which most drug substances exist. SSNMR spectroscopy tends to be the primary technique to establish the solid form of a drug in a formulated product due to its high specificity and relatively limited interference from excipients compared to X-ray powder diffraction (XRPD), and vibrational spectroscopy (IR or Raman). Therefore, it is prudent to have all solid forms characterized by SSNMR spectroscopy in addition to the typical XRPD data as part of a patent package. In general, ^{13}C cross-polarization magic angle spinning (CP/MAS) is sufficient for characterizing the solid form, but SSNMR spectroscopy of other nuclei might also be important for a particular drug.

A number of recent reviews have appeared about the use of SSNMR spectroscopy to analyze polymorphs and other solid forms (2–7). Three of the more extensive recent reviews covering many aspects of SSNMR spectroscopy of pharmaceutical compounds are by Harris (2), Medek (3), and Tishmack et al. (4). The reader is referred to the book chapter by Medek for a thorough review of many aspects of pharmaceutical SSNMR spectroscopy in addition to a theoretical discussion of NMR spectroscopy (3). The review by Harris is particularly interesting for solid-state structural determination, analysis of hydrates, and amorphous solids (2). The review by Tishmack et al. is a general overview of SSNMR spectroscopic analyses of pharmaceuticals through approximately 2002 (4).

In this chapter, the theory and applications of SSNMR spectroscopy will be discussed primarily in the context of pharmaceutical compounds. SSNMR spectroscopy is considered a necessary analytical characterization technique for every pharmaceutical solid that is marketed. The International Committee of Harmonization (ICH) specifically refers to SSNMR spectroscopy along with IR and Raman spectroscopic techniques as necessary for characterizing polymorphs in drug substances and drug products (8). It has been well established that characterization of pharmaceuticals generally requires multiple analytical techniques (e.g., diffraction, spectroscopy,

thermal analysis, microscopy, dissolution, etc.) to adequately understand their behavior with respect to production, stability, and bioavailability. Therefore, many of the literature references cited in this chapter use SSNMR spectroscopy as only one of several analytical techniques to study the compound(s) of interest to the authors. One of the difficulties in using SSNMR spectroscopy is that acquisition and interpretation of spectra usually requires a reasonably good understanding of the underlying physics. This may be the main reason that a relatively high percentage of the pharmaceutical literature examples use SSNMR spectroscopy as a secondary technique with minimal or even incorrect interpretation of the results. Hopefully this situation will improve in the future as SSNMR spectroscopy becomes even more powerful in analyzing solid materials.

The section on NMR theory in this chapter is not highly mathematical or extensive given that there are many excellent texts, reviews, and monographs on NMR theory that include details specific to SSNMR spectroscopy (9–23). Recent reviews by Baldus (9) and Reichert (10) cover general applications of SSNMR spectroscopy to many solid systems. Laws et al. wrote a particularly thorough review of SSNMR spectroscopy that is highly recommended (11). The SSNMR spectroscopy book by Duer is a useful reference for beginners and more advanced spectroscopists (12), and two older books are also excellent references for most aspects of SSNMR spectroscopy (13,14). The books by Friebolin (15), Chandrakumar (16), Harris (17), and Becker (18) are texts on general NMR spectroscopy with chapters devoted to the solid state. These books also provide reasonable reviews of the basic theory of NMR spectroscopy. Traficante's chapter is a basic introduction to NMR spectroscopy that is generally easy to understand (19). The older books by Carrington and McLachlan (20), Slichter (21), and Abragam (22) are fundamental resources on NMR spectroscopy with a much more mathematically detailed treatment of essentially every aspect of the quantum mechanical basis of the technique. Grant and Harris edit a large encyclopedia covering all aspects of NMR spectroscopy that is periodically updated with new information (23).

GENERAL THEORY OF NMR SPECTROSCOPY

NMR spectroscopy derives from the nuclear spin angular momentum, which is based on the number of protons and neutrons of an atom. Nuclear spin (I) is quantized in multiples of the Planck constant (h), $I = 0, 1/2, 1, 3/2, 2$, etc. Nuclei with even numbers of protons and neutrons have zero spin and thus no NMR signal such as ^{12}C and ^{16}O. Half integer nuclear spins result when the nucleus of an element has either an even or odd number of protons and an odd number for its mass. Integer nuclear spins result if a nucleus has an odd number of protons and an even mass. Most elements have a isotope that can be studied by NMR spectroscopy, but it is not always the isotope with the highest natural abundance. Unfortunately, nuclei with spins other than one-half have a quadrupole moment and thus an electric field gradient that will interact with the nuclear dipole moment and lead to broad peaks in most cases. Spin one-half nuclei such as ^{1}H, ^{13}C, ^{15}N, ^{19}F, and ^{31}P are studied most often because they have better resolution and sensitivity compared to quadrupolar nuclei. However, ^{13}C and ^{15}N have relatively low natural abundances (1.1% and 0.37%, respectively) and correspondingly lower sensitivity than the other commonly studied spin one-half nuclei. Some of the positive and negative aspects of NMR spectroscopy are summarized in Table 1.

TABLE 1 Summary of Some Advantages and Disadvantages of Solid-State NMR Spectroscopy

NMR property	Advantages	Disadvantages
High field strength	Better sensitivity. Possibly better resolution. Decreased effect of quadrupolar nuclei.	Longer T_1 relaxation times. Instrument cost and upkeep. Increased CSA effects. Increased anisotropic bulk magnetic susceptibility.
Very weak transition energies	Highest resolution spectroscopy. High specificity.	Lowest sensitivity spectroscopy. Larger samples may be required.
Multiple nuclei	High selectivity for compounds containing chosen nucleus.	Compounds without the chosen nucleus are not observed.
Signal is directly proportional to the number of nuclei producing it	Intrinsically quantitative technique.	Quantification efficiency depends on nuclear relaxation properties.
T_1 and $T_1\rho$ relaxation times	Dynamic and spatial properties can be measured.	Long T_1 increases total data collection time. A different T_1 for each nuclei or molecule requires careful optimization for each case particularly for mixtures.
T_2 relaxation time	Dynamic properties can be measured.	Short T_2 causes broader peak. Potential loss of signal during longer pulse sequences.
Chemical shift	Structural analyses are possible.	Difficult to predict accurately. Extensive overlap in complex molecules.
Coupling	Structural analyses are possible.	Complicates spectrum with peak broadening or splitting.
Quadrupolar nuclei	Comprise most of periodic table.	Not easy to observe due to broad peaks and rapid relaxation times. Special techniques may be required to obtain spectra.
Multi-dimensional NMR	Increased resolution. Correlations between multiple different nuclei possible. Bonding and spatial information for structural analyses.	Time consuming to obtain data. Significant skill usually required.

NMR active nuclei also have a magnetic quantum number (m_I), which has $2I + 1$ possible energy states (i.e., $m_I = I, I - 1, \ldots, -I$) that determine the orientations of the magnetic moments in a static magnetic field ($\mathbf{B_0}$). For a spin one-half nucleus, there are two possible energy states, $m_I = -½, +½$ that are either approximately anti-parallel or parallel to the magnetic field. Thhe nuclear magnetic moment (μ_0) is directly proportional to the nuclear spin: $\mu_0 = \gamma\hbar[I(I + 1)]^{½}$, where the spin angular momentum is $P = \hbar[I(I + 1)]^{½}$ and $\hbar = h/2\pi$ (Fig. 1). The magnetogyric ratio (γ) is a constant relating the magnetic moment to the spin angular momentum of a particular nucleus, and it determines the direction of precession of a magnetic moment in a magnetic field. The magnetic moment and spin angular momentum are usually aligned parallel to each other, but there are exceptions such as for ^{29}Si and ^{15}N. An anti-parallel orientation will affect certain NMR experiments such as those that involve the nuclear Overhauser effect (NOE) or CP. The interaction energy between the magnetic moment and the magnetic field is given by the equation: $E = -\mu_z\mathbf{B_0}$, and the energy difference between adjacent energy levels is $\Delta E = -\gamma\hbar\mathbf{B_0}$ or $\Delta E = h\nu$, where ν is the radiation frequency. Transitions occur between energy levels by applying the appropriate radiofrequency electromagnetic radiation given by the equation, $h\nu = |-\gamma\hbar\mathbf{B_0}\Delta m_I|$. The selection rule for transitions is $\Delta m_I = \pm 1$. Substituting in the appropriate values gives the resonance frequency or Larmor frequency of the nucleus, $\nu_L = |-\gamma\mathbf{B_0}/2\pi|$. The vertical bars in the equation mean absolute value to show that the Larmor frequency of a particular nucleus is always positive.

Electrons in molecules shield and deshield nuclei and lead to different resonant frequencies (chemical shifts) for each nucleus in a unique environment. The chemical shielding effect for a nucleus is, $\nu_i = \gamma\hbar\mathbf{B_0}(1 - \sigma_i)$, where σ_i is the shielding constant for the nucleus, and $\mathbf{B_0}$ is the applied magnetic field corrected for the effect of bulk magnetization, which depends on the shape of the sample and its bulk

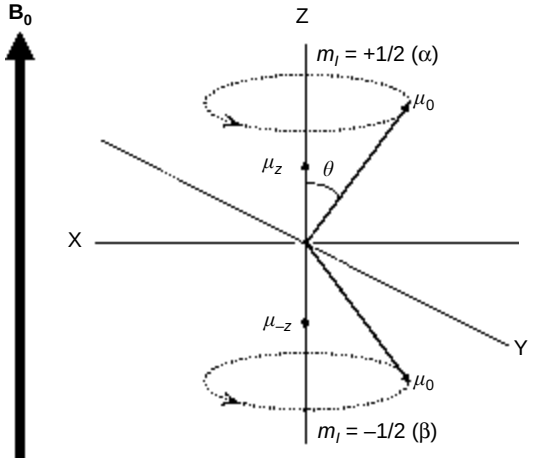

FIGURE 1 Spin one-half nuclear magnetic moments in a magnetic field ($\mathbf{B_0}$). The angle θ is 54.74° for spin one-half nuclei. μ_z is the *z*-component of the nuclear magnetic moments in $\mathbf{B_0}$. The α-state is lower energy and aligned parallel to $\mathbf{B_0}$, and the higher energy β-state is aligned anti-parallel to $\mathbf{B_0}$.

susceptibility. The electrons in molecular bonds also allow nuclear spins to interact or couple with each other, which results in fine splittings of the peaks produced by coupled spins. This is referred to as scalar coupling or J-coupling, and it is considered indirect because it is mediated by electrons. Dipolar coupling is referred to as direct coupling because it depends on the orientation and separation of nuclear dipoles that interact directly through space and not through bonding electrons. Dipolar coupling is a much stronger interaction than scalar coupling, and may cause significant peak broadening in solids. Dipolar coupling is not directly observed in NMR spectra of liquids or gases because it is averaged to zero by rapid motions. However, magnetic relaxation and the NOE rely on dipolar coupling, so it is a very important property for NMR structure determination in liquids. Other coupling mechanisms are also possible, but they are usually not important for spin one-half nuclei in common NMR samples.

The Boltzmann distribution of spins primarily determines the sensitivity for NMR spectroscopy. The NMR absorption and emission processes (i.e., transitions) between energy levels occur with equal probability, but the slight excess of spins in the lower energy state leads to absorption occurring more often. Each transition between energy states is a result of a spin flip from the α to β or β to α state. The equilibrium spin population ratio is: $n_\beta / n_\alpha = e^{-\Delta E/kT}$, where $n_{\alpha,\beta}$ are the spin populations in the α-state (lower energy) or β-state (higher energy) for the spin one-half case, k is the Boltzmann constant ($1.3806503 \times 10^{-23}$ J/K), ΔE is defined previously, γ for ^{1}H is 26.7515×10^7 rad·T^{-1}·s^{-1} and for ^{13}C is 6.7283×10^7 rad·T^{-1}·s^{-1}, the Planck constant ($\hbar = h/2\pi$) is $1.054571596 \times 10^{-34}$ J·s, and $\mathbf{B}_0$ is the magnetic field measured in tesla (kg·s^{-2}·A^{-1}) (24). In a magnetic field of 9.4 tesla at ambient temperature ($T \sim 298$ K), for every one million ^{1}H nuclei in the β-state, there will be one million and sixty-four in the α-state. The difference between the spin populations is graphed in Figure 2 for various magnetic field strengths represented by the corresponding ^{1}H frequency. The very small energy difference is the reason that NMR is inherently insensitive relative to other spectroscopic techniques. Low natural abundance also contributes to the decreased sensitivity of most nuclei relative to ^{1}H. A long T_1 relaxation time or short T_2 relaxation time for some nuclei may also adversely affect sensitivity. Relaxation properties will be discussed in more detail later. Dipolar coupling to the electric field gradient of quadrupolar nuclei or to unpaired electrons in paramagnetic systems can cause significant peak broadening and shifting that decreases the spectral resolution and also reduces the sensitivity. The weak transitions of NMR spectroscopy are also the reason that it has much higher resolution than any other spectroscopic techniques.

The magnetization vector in the positive z-axis (M_z) resulting from a summation of all the excess nuclear magnetic moments in the low energy state can be manipulated by modern NMR pulse sequences. Figure 3 shows what happens when a radiofrequency pulse (B_1) is applied perpendicular to M_z. M_z is equivalent to the equilibrium magnetization, M_0, when the time between pulses is sufficiently long to allow full relaxation of the particular nuclei being observed. The z component of the magnetization will rotate into the x–y plane if B_1 is applied for an appropriate length of time (i.e., a 90° pulse). The magnetization will then rotate in the x–y plane but not necessarily as a single vector, because each nucleus in a molecule may have a slightly different frequency (chemical shift) and may interact with other nuclei (coupling). This will break up the single magnetization vector into multiple vectors rotating at various rates orthogonally to the main field. The magnitude of each vector will also

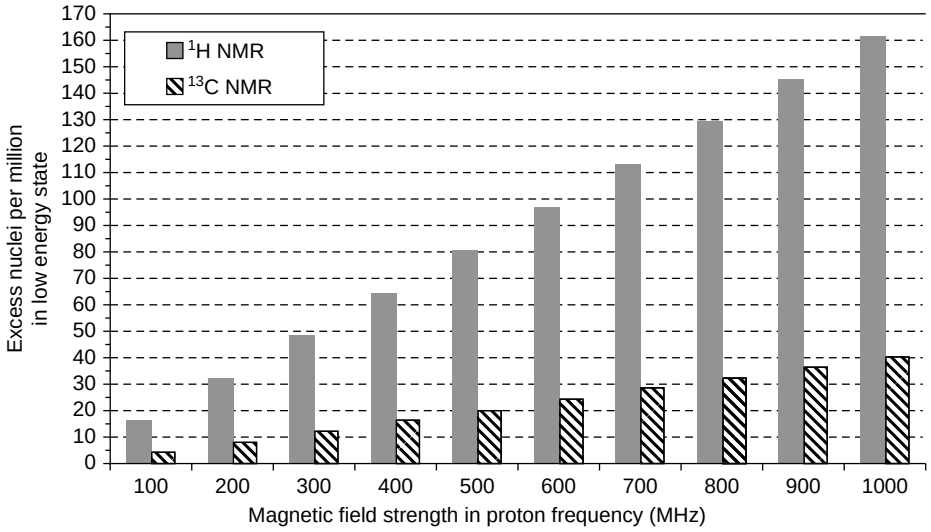

FIGURE 2 Bar graphs comparing the effect of the magnetic field strength on the number of excess nuclei in the lower energy state for two spin one-half nuclei. The effect of natural abundance is not taken into account for ^{13}C.

decrease over time due to interactions with electrons and nuclei in the sample that lead to relaxation. This is observed in the detector of the NMR spectrometer as a free induction decay (FID) where the signal intensity usually decays exponentially as the vectors dephase in the x–y plane due to random spin flips (T_2 relaxation) and as the equilibrium magnetization is re-established in the z-axis (T_1 relaxation) primarily through dipolar coupling. There is also another type of relaxation ($T_1\rho$) that occurs when the magnetization vector is continuously irradiated or spin-locked with a B_1 field that is typically in the kilohertz frequency region. The spin-lock is to achieve the Hartmann-Hahn matching condition, which is used in CP for solids or total correlation spectroscopy (TOCSY) and rotating frame Overhauser effect spectroscopy (ROESY) for liquids. In a solid, the time it takes for ^{13}C nuclei (or other low abundance nuclei) to be cross-polarized by ^{1}H nuclei (T_{CH}) is important because the ^{1}H $T_1\rho$ relaxation time determines how long the polarization will persist. Rapid ^{1}H $T_1\rho$ relaxation times may eliminate the sensitivity advantage that CP introduces. The ^{13}C T_1 and $T_1\rho$ relaxation times are usually not a significant factor for CP because they are almost always much longer than the ^{1}H relaxation times. The effects from relaxation due to the ^{1}H nuclei will occur long before those from ^{13}C nuclei can affect the magnetization. Accurate measurement of SSNMR relaxation times can be very important, and several of the most common techniques are compared by Frye (25). Figure 4 compares some of the effects of NMR parameters on the observed signal at various field strengths. Although it is generally beneficial to have a higher magnetic field strength, relaxation times may increase enough to adversely affect some samples and NMR experimental techniques. Higher field strength reduces the peak

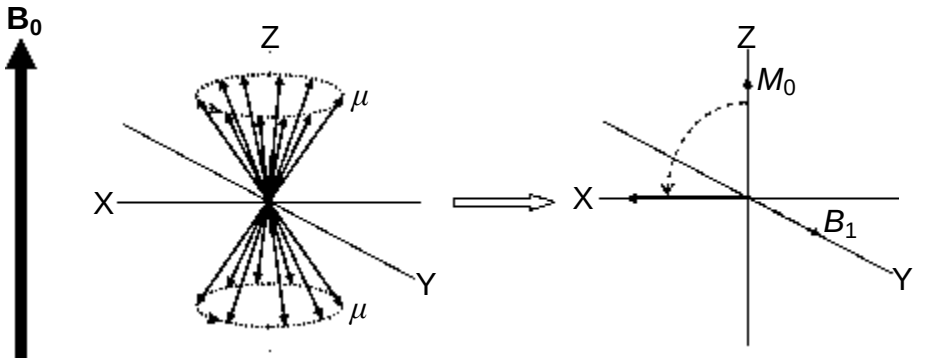

FIGURE 3 The magnetic moments for the excess nuclear spins in the lower energy state of a spin one-half nucleus in a magnetic field ($\mathbf{B_0}$) produce net magnetization (M_0) along the positive *z*-axis. A radiofrequency pulse (B_1) applied along the positive *y*-axis rotates the *z*-axis magnetization vector into the positive *x*-axis where it will begin to precess in the *x*,*y*-plane according to its Larmor frequency. If the nucleus exists in multiple unique environments as in a molecule, the magnetization vector will divide into vectors for each Larmor frequency corresponding to each chemical shift. Scalar coupling will also cause further separation of each vector in the *x*,*y*-plane, but usually this will be a much smaller effect because the frequency differences between peaks of multiplets are typically small relative to chemical shift differences.

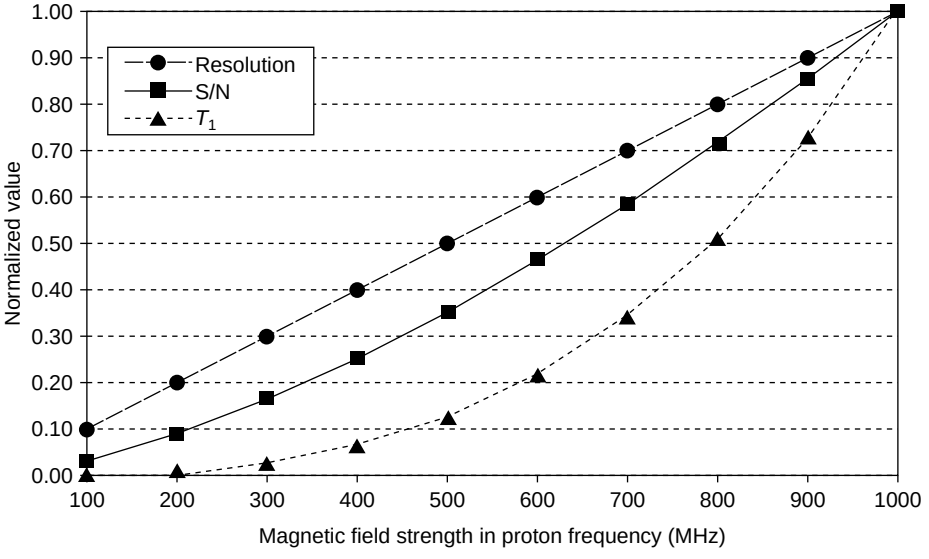

FIGURE 4 A graph of the effect of field strength on resolution, signal-to-noise ratio, and T_1 relaxation time. Although the resolution is expected to increase linearly with field strength, anisotropic bulk magnetic susceptibility, paramagnetic species, and quadrupolar coupling may significantly reduce this. In this comparison, the increase in the T_1 relaxation time has the largest deviation from linearity as the field strength increases.

broadening effect from quadrupolar nuclei, but it increases the longitudinal relaxation time (T_1) as well as the effects of chemical shielding anisotropy (CSA) and anisotropic bulk magnetic susceptibility (ABMS). These effects are particularly important for SSNMR spectroscopy.

SOLID-STATE NMR SPECTROSCOPY

NMR of solids presents significant problems compared to liquids. The rapid motions in liquids remove two effects that are largely responsible for the broad peaks typically observed in NMR spectra of solids: CSA and dipolar coupling. The T_2 relaxation time is also significantly shorter in solids, which increases the intrinsic peak widths. One of the main goals of SSNMR spectroscopy is to obtain spectra similar to what is observed for liquid-state NMR spectroscopy of the material in a solution. Figure 5 shows the structure of a simple organic molecule (DTPPAA) that has been used by the author to test pulse sequences for both liquid-state and SSNRMspectroscopy. The NMR spectra of DTPPAA are compared in Figure 6. Note that the chemical shifts are very close in the solid-state and liquid-state NMR spectra for DTPPAA with only one set of unresolved peaks (C14 and C17) in the SSNMR spectrum. This makes DTPPAA reasonably useful as a standard to test SSNMR pulse sequences and compare the results to the corresponding liquid-state NMR analyses. However, crystal packing forces and/or conformational changes will usually result in significant differences between liquid-state and SSNRMspectra.

For powdered solids, the nuclear magnetic moments are in fixed random orientations that result in broad peaks because both the CSA and dipolar coupling tensors have a $3\cos^2\theta - 1$ term, where θ is the angle of the tensor relative to the direction of $\mathbf{B_0}$. These phenomena will produce broad overlapped peaks in a SSNMR spectrum of a molecule with relatively few carbons. This would make SSNMR spectroscopy of limited use unless there was a means of reducing or eliminating the effects of CSA and dipolar coupling.

The isotropic component of chemical shielding averages to the isotropic frequency, ν_{iso}, in liquids due to rapid molecular motion, and the anisotropic component (CSA) vanishes. The CSA in solids depends on the orientation of nuclear magnetic moments with respect to the direction of $\mathbf{B_0}$. Nuclei of molecules in powdered solids have a distribution of parallel to perpendicular orientations relative to $\mathbf{B_0}$, and the peak shapes will depend on the crystallographic site symmetry at the nucleus (Fig. 7). Many different nuclei in a molecular solid will result in overlapping CSA patterns and a featureless spectrum with little useful information.

Dipolar coupling between spin one-half nuclei depends on the orientation of the dipolar vector between the nuclei relative to $\mathbf{B_0}$ as well as the distance between the nuclei. The distance dependence of dipolar coupling is very powerful for structural analysis of solids and partially ordered materials. The strength of the local field at each nucleus depends on the parallel to perpendicular orientations of dipolar vectors in the $\mathbf{B_0}$ field and gives rise to a distribution of resonance frequencies that produces peak shapes similar to axial CSA (Fig. 8). The two mirror image peaks are due to the two spin one-half transitions separated by the dipolar coupling constant (D_{CH}). The isotropic chemical shifts are identical for the two spin states and will be observed when the dipolar vector is at and angle of 54.74° relative to $\mathbf{B_0}$. There is no isotropic component of the dipolar coupling tensor, so it averages to zero in liquids due to rapid molecular motions, and has no direct effect on the spectrum. As for CSA,

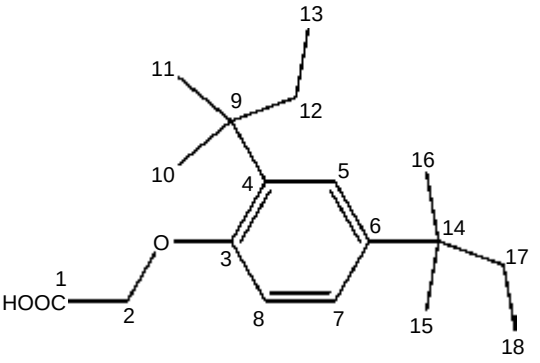

FIGURE 5 Chemical structure of (2,4-di-*tert*-pentylphenoxy)-acetic acid (DTPPAA) with numbering used for the assignments shown in Figure 6.

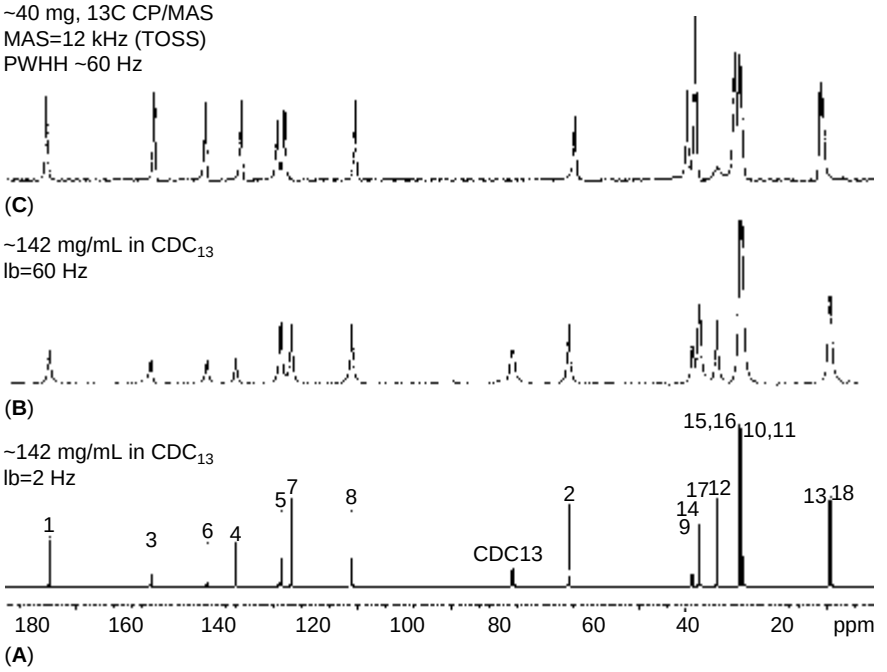

FIGURE 6 ^{13}C NMR spectra of DTPPAA at 9.4 T: (**A**) in $CDCl_3$ solution, (**B**) spectrum (**A**) with 60 Hz exponential multiplication, and (**C**) SSNMR spectroscopy of crystalline DTPPAA. The peak positions are similar for this molecule in the solid and liquid states. The peak labels in spectrum (**A**) are the resonance assignments for the structure in Figure 5. *Abbreviations*: CP/MAS, cross polarization magic angle spinning; TOSS, total side band suppression.

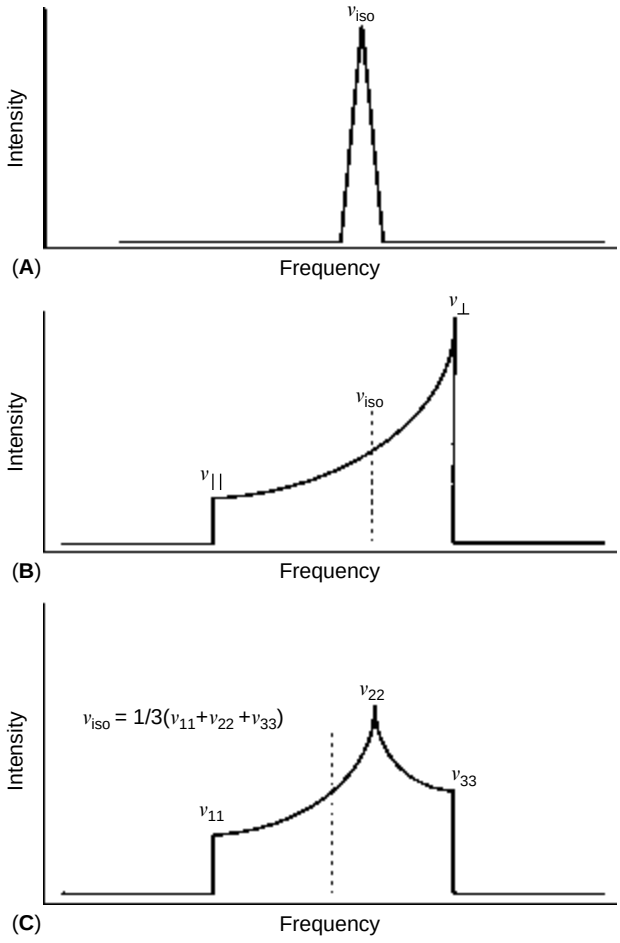

FIGURE 7 Representations of CSA powder patterns for (**A**) cubic, (**B**) axial, and (**C**) lower crystallographic site symmetry for a spin one-half nucleus relative to the magnetic field. Cubic symmetry results in only the isotropic frequency. For axial symmetry, the magnetic moment of the nucleus can vary between parallel and perpendicular orientations. The probability is much greater for a nuclear magnetic moment being in a perpendicular orientation, which results in the higher peak intensity for this case. The isotropic frequency for the axial case is a weighted average of the two extremes. The lower symmetry case results in a more complex peak shape, where υ_{22} will vary in position somewhere between the highest frequency (υ_{11}) and the lowest frequency (υ_{33}) with an isotropic frequency (υ_{iso}) as shown in the *bottom* diagram.

multiple dipolar coupled spins in a solid would result in many broad overlapped resonances and little useful information in the spectrum. Figure 9 shows the orientation dependence of dipolar coupling for two spin one-half nuclei in a solid. The results are similar for CSA except that only one peak will be present in each spectrum (i.e., the solid line spectrum of panel Fig. 9a and the corresponding peaks in Fig. 9b and c that align with frequencies for the parallel and perpendicular orientations.

The orientation dependence of CSA and dipolar coupling provides a means to reduce or eliminate their effects in SSNMR spectra. Andrew et al. discovered that rotating solid samples at 54.74° (the magic angle) relative to the magnetic field significantly reduced the peak widths in SSNMR spectra (26,27). Figure 10 shows the basic procedure for reducing CSA by rapid spinning at the magic angle, and it works essentially the same for dipolar coupling. In a powdered solid, all possible orientations of angles θ and β are present, but the angle of the rotor (θ_R) in the probe can be set by the operator.

Magic angle spinning (MAS) will cause modulations in the spectrum that extend out from the isotropic chemical shift position of each nucleus at integral multiples of the spinning speed. These spinning side bands move farther out and decrease in intensity as the spinning speed increases. The intensity of the isotropic peak increases with the spinning rate while the spinning side bands decrease until they are eliminated when the rate of rotation exceeds the CSA. An example of MAS for glycine (Fig. 11) is shown in Figure 12. Note the different CSA powder patterns for the carbonyl and methylene resonances in spectrum (a) of Figure 12. For ^{13}C SSNMR, the carbonyl resonance has a relatively large CSA (~150 ppm), whereas aliphatic carbons have significantly smaller CSA (~60 ppm). The CSA increases with field strength (e.g., for ^{13}C 100 ppm is ~10 kHz at 9.4 T and 15 kHz at 14.1 T), which means that faster spinning is required at higher field strengths to reduce the spinning side bands to the same extent. Smaller diameter rotors are required to achieve faster spinning speeds, but the reduced sample quantity results in lower sensitivity that may not be compensated by the higher field strength. If necessary, spinning side bands can be suppressed by using the total side band suppression (TOSS) technique first introduced by Dixon (28–33). In the typical four-pulse TOSS sequence, the 90° pulse width for the X-nucleus must be reasonably accurate for good suppression of the side bands. TOSS is particularly useful for removing overlapping side bands when the spinning speed is not fast enough to push them out past the peaks of

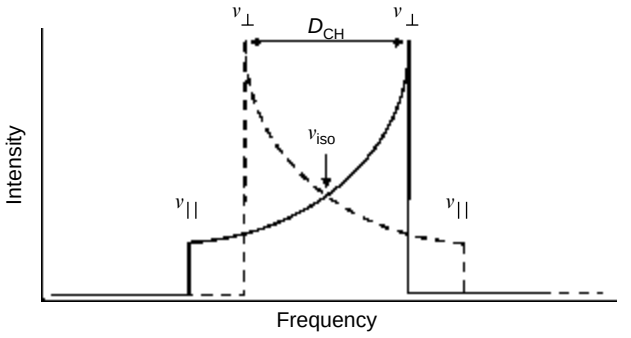

FIGURE 8 A diagram of a heteronuclear dipolar coupling powder pattern for the simple case of two coupled spins (e.g., ^1H and ^{13}C). The solid and dashed lines represent the two spin states for either of the spin one-half nuclei. Note the similarity of one peak of this pattern to the axial symmetry for CSA. The dipolar vectors also vary between the parallel and perpendicular orientations with respect to the magnetic field. The dipolar coupling constant is D_{CH}.

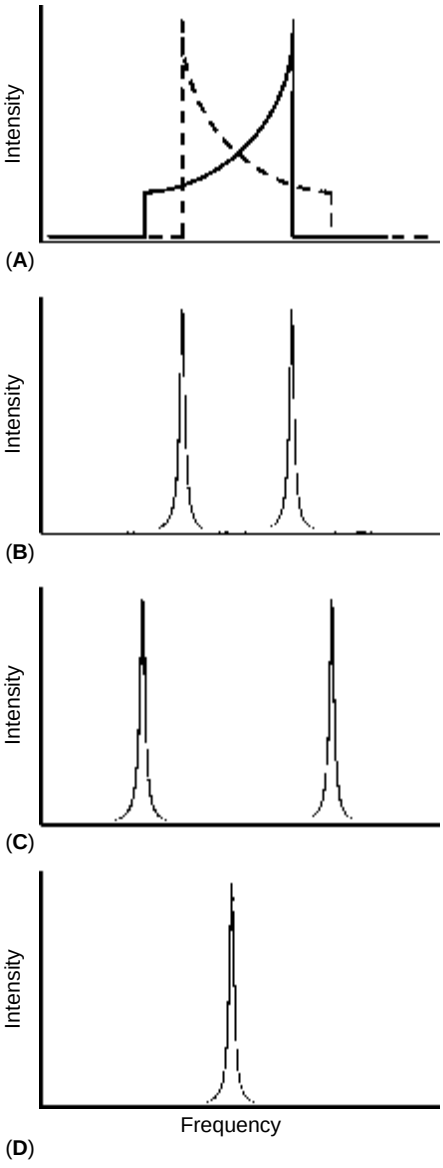

FIGURE 9 Representations of dipolar coupling for a two spin case: (**A**) powder pattern for randomly oriented dipolar vectors, (**B**) perpendicular orientation, (**C**) parallel orientation, (**D**) 54.74° orientation (the magic angle). Spectra (**B**)–(**D**) would be obtained for a single crystal positioned as specified.

interest such as with larger diameter rotors or at high magnetic field strengths. The ^{13}C CP/MAS spectrum (c) of Figure 6 was obtained with TOSS to eliminate potential overlap of the small isotropic peak at approximately 34 ppm with spinning side bands, which also helped confirm that it was a real peak.

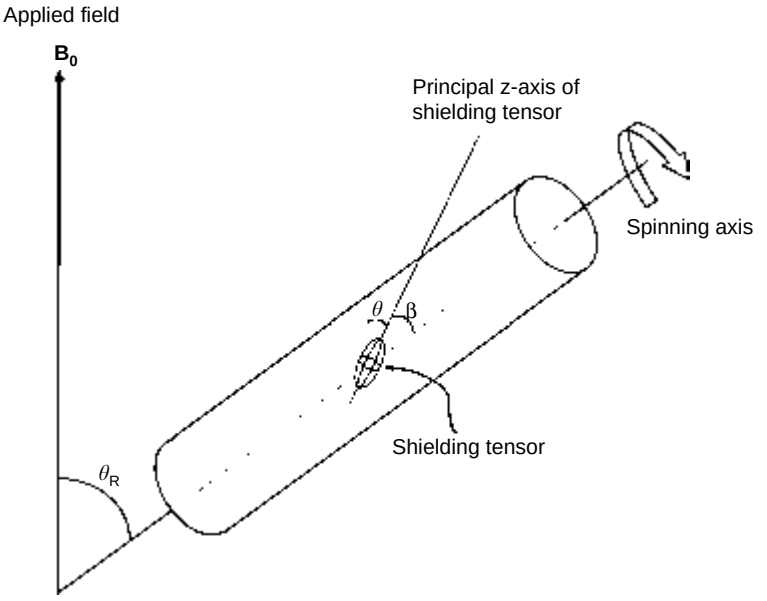

FIGURE 10 Spinning a sample rapidly at the magic angle (θ_R = 54.74°) will average the CSA (and the dipolar coupling) to zero because of $3\cos^2\theta - 1$ dependence of their orientation with respect to the magnetic field. Adapted from Ref. (12).

As with CSA, MAS will eliminate dipolar coupling only if it is significantly faster than the strength of the dipolar interaction (i.e., tens of kHz). Otherwise, it is scales the dipolar coupling in proportion to the spinning speed and gives broader peaks. MAS will usually remove the homonuclear dipolar coupling between ^{13}C nuclei because it is much weaker than $^{1}H/^{13}C$, $^{1}H/^{1}H$, $^{19}F/^{13}C$, or $^{19}F/^{1}H$ dipolar couplings (11). High-power ^{1}H decoupling is used to dramatically narrow the peaks in ^{13}C and ^{15}N detected SSNMR spectra. Simultaneous high-power ^{1}H and ^{19}F decoupling can also be used if both nuclei are present in the molecule of interest. Both scalar (through-bond) and dipolar (through-space) coupling are removed by decoupling. The decoupling power necessary to remove the dipolar interaction in solids is substantially greater than that used for broadband proton decoupling of the scalar coupling in liquid samples. Continuous wave decoupling was originally used, but dramatically improved results are possible with newer modulated techniques that will be discussed later.

Nuclei with low sensitivity (e.g., ^{13}C and ^{15}N) can be difficult to obtain spectra with good signal to noise in a reasonable time. Pines et al. first used the CP technique to increase the sensitivity of low natural abundance spins (34). This technique relies on dipolar coupling to transfer polarization from ^{1}H to ^{13}C nuclei, and its effectiveness is thus extremely dependent on the separation between the ^{1}H and ^{13}C nuclei in a solid. The enhancement of the ^{13}C signal is roughly proportional to the magnetogyric ratios of the nuclei. The high natural abundance and strong magnetic moment of protons results in an approximate four-fold enhancement of the ^{13}C signal or 10-fold enhancement of the ^{15}N signal. Because the ^{1}H T_1 relaxation time is

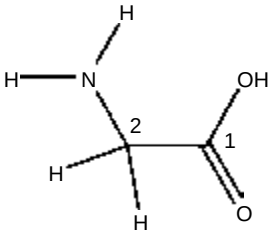

FIGURE 11 Chemical structure of the amino acid glycine.

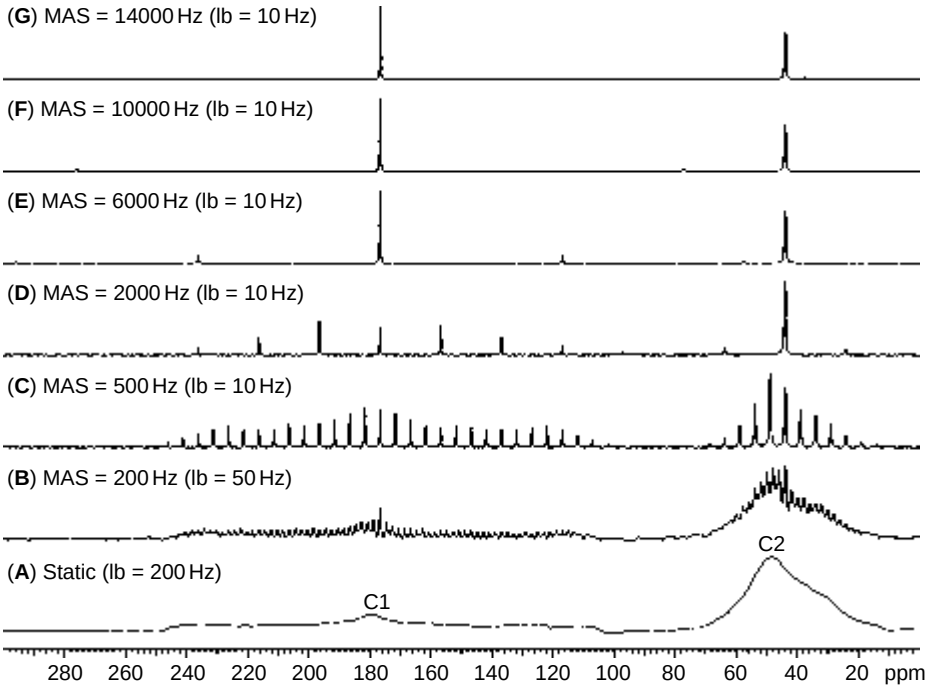

FIGURE 12 The effect of MAS on the ^{13}C SSNMR spectrum of glycine at 9.4 T. The peaks of the static pattern in (**A**) are broken up into spinning side bands that are separated by integral multiples of the spinning speed in spectra (**B**)–(**G**). The isotropic frequency is not readily apparent until the spinning speed is fast enough to reduce the spinning side bands significantly (2 kHz for methylene, 6 kHz for carbonyl). Note that the spinning side bands for the methylene resonance are essentially eliminated at 6 kHz because this is approximately equivalent to the CSA (60 ppm $\times$ 100 Hz/ppm = 6000 Hz). The spinning speed would need to be approximately 15 kHz to eliminate the spinning side bands for the carbonyl resonance, which has a CSA of ~150 ppm. *Abbreviation*: MAS, magic angle spinning.

usually much shorter than those of ^{13}C or ^{15}N, CP permits the acquisition of more scans in less time because the proton spin polarization determines how efficiently the X-nuclei are cross-polarized.

Stejskal and Shaefer first used a combination of magic angle spinning, high-power ^{1}H decoupling, and CP to obtain high-resolution ^{13}C SSNMR spectra (35,36). This CP/MAS technique is the standard procedure for obtaining high-resolution NMR spectra of solids. The effects of these three techniques on the ^{13}C SSNMR spectrum of glycine (Fig. 11) are shown in Figures 12 and 13. The CSA powder patterns are readily observed for the carbonyl and methylene carbon resonances of the static spectrum (a) of Figure 12. The enhancement due to CP is also apparent in spectra (b) and (d) of Figure 13. The high-power decoupling has the most dramatic effect on reducing the peak widths in the spectra (c) and (d) of Figure 13. An efficient modulated ^{1}H decoupling method [SPINAL-64 (57)] was used whenever decoupling was required because it is significantly better than the continuous wave decoupling procedure that was first used for ^{13}C CP/MAS spectra and is still used in many of the literature examples discussed in section "Solid-Form Characterization" on p. 398.

The basics of acquiring 1D SSNMR spectra has been demonstrated in an excellent article by Bryce et al., which is highly recommended to both novices and experienced NMR spectroscopists (37). Several things are important to clarify regarding this useful review. First, the authors state that glycine polymorphism may cause problems with using it as a standard for chemical shift referencing, CP, and sensitivity. However, the glycine polymorphs have such different relaxation properties, and it would not be difficult to determine if there was a polymorphic transformation in a glycine standard sample. The metastable α-glycine has significantly shorter relaxation times, which means that phase transformation is not likely to go unnoticed when obtaining SSNMR spectra (38). In this author's hands, the α-glycine polymorph appears to be stable for years under ambient storage conditions and in regular use as a ^{13}C CP/MAS SSNMR reference standard for signal-to-noise measurement, Hartmann-Hahn matching for CP, as a chemical shift reference, and to optimize ^{1}H decoupling (including at nonambient temperatures, –40°C to +80°C). The same sample of solid α-glycine has shown no detectable phase transformation or degradation affecting its ^{13}C CP/MAS spectrum for at least four years of regular use. Second, spectra C and D of Figure 7 in the review by Bryce et al. appear to be the same, which does not show the effect of two pulse phase modulated (TPPM) decoupling for spectrum D as the authors intended (37). Therefore, one should expect different results using the stated conditions. The peak for the methylene carbon of phenylacetic acid would actually be much like in spectrum B but with greater intensity due to the variable amplitude CP (VACP) in addition to the TPPM decoupling. The peak for the carbonyl resonance may not be narrowed as dramatically by TPPM, but it would likely be similar to what is shown in spectrum B of Figure 7 in the review by Bryce et al. (37).

Taylor has also written a more specific summary of the basic experimental set up procedures for ^{13}C CP/MAS SSNMR spectroscopy (39), and an interesting ^{13}C SSNMR spectroscopy study of the effect of low temperatures (–60°C) on the polymorphs of glycine (40). The changes in relaxation times (longer ^{1}H T_1 and shorter ^{1}H $T_1\rho$) for the glycine polymorphs at low temperature combine to make it significantly more difficult to acquire high sensitivity spectra in a reasonable amount of time. The carbonyl resonance is affected more dramatically because the magnitude of the changes in relaxation times is greater. This makes glycine somewhat problematic

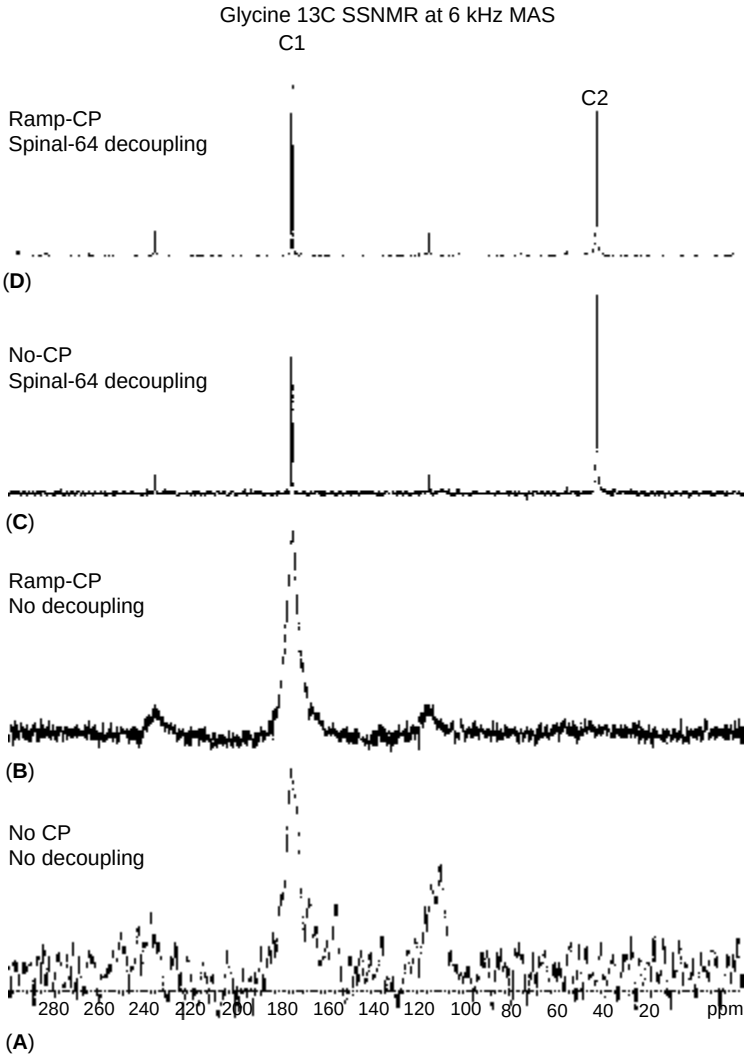

FIGURE 13 The effects of high-power ^{1}H decoupling and CP are shown for ^{13}C SSNMR spectra of glycine at 9.4 T and 6 kHz MAS. The MAS speed is too slow to reduce the dipolar coupling enough to observe the methylene resonance (C2) in spectra (**A**) and (**B**). CP dramatically increases the signal-to-noise ratio [compare spectra (**A**/**B**) or **C**/**D**)]. High-power ^{1}H decoupling is required to get the narrowest peaks in spectra (**C**) and (**D**). The apparent peak at approximately 115 ppm in spectrum (**A**) is due to the transmitter artifact partially overlapping a broad spinning side band combined with the very low signal-to-noise ratio of the spectrum. *Abbreviations*: CP, cross-polarization; MAS, magic angle spinning; RAMP-CP, ramped amplitude cross polarization; SSNMR, solid-state nuclear magnetic resonance.

as a reference standard to optimize the spectrometer at low-temperature conditions. However, this is not a significant problem in practice until the temperature is approximately –50°C, especially if amplitude- or frequency-modulated CP (41–48) and modulated decoupling are used (49–59).

Setting the magic angle accurately is obviously very important for obtaining the highest resolution SSNMR spectra. Frye and Maciel demonstrated the use of potassium bromide as a useful means of setting the magic angle for ^{13}C SSNMR spectroscopy (60). More recently, Antonijevic and Bodenhausen have used deuterated α-oxalic acid to set the magic angle to within 0.01° by minimizing the residual ^{2}H quadrupolar coupling (61). Barich et al. have shown that 3-methylglutaric acid (MGA) can be used to set the magic angle, optimize the Hartmann-Hahn match for CP, determine the signal-to-noise ratio, and as chemical shift reference for ^{13}C SSNMR spectroscopy (62). The two carboxylic acid carbonyl resonances for MGA are used to set the magic angle because carbonyl groups have a large CSA, which makes them very sensitive to the magic angle setting. However, adamantane is still the best molecule to use for optimizing the field homogeneity due to its very narrow ^{13}C SSNMR peak width (<0.05 ppm).

As noted earlier, SSNMR spectroscopy requires additional procedures compared to liquid-state NMR spectroscopy to obtain high-resolution spectra. The three procedures currently used are high-power ^{1}H decoupling, magic angle spinning, and CP. These have advanced in several ways since their inception. Magic angle spinning for spin one-half nuclei has been extended to double rotation (DOR) and dynamic angle spinning (DAS) for quadrupolar nuclei (63). Spinning speeds have also increased from several kHz when MAS was initially developed, to tens of kHz now. This is particularly helpful for ^{1}H and ^{19}F SSNMR, because these nuclei have strong dipolar coupling (40–50 kHz) compared to ^{13}C (10–20 kHz) and high natural abundance. Very fast spinning will reduce the dipolar coupling to give narrower peaks. High-power proton decoupling has progressed from continuous wave to various frequency and phase modulated decoupling methods (49–59). One of the best ^{1}H decoupling methods currently available for common use is the small phase incremental alternation (SPINAL-64) decoupling procedure (57), which is based on supercycles of the TPPM decoupling of Bennett et al. (59). TPPM decoupling itself was a dramatic improvement over existing decoupling techniques. CP has also advanced from the original continuous polarization to VACP and ramped amplitude (RAMP-CP) polarization techniques. RAMP-CP is more efficient than VACP and dramatically better than standard CP, particularly for rapidly spinning samples (>10 kHz). The result from using these techniques is higher sensitivity and resolution SSNMR spectra for all of the common nuclei. A minor drawback to using these modern techniques is that they require more complicated pulse sequences and additional effort to optimize them for obtaining spectra.

Temperature control for the sample is important for studying a variety of solid-state properties such as reactivity, relaxation properties, and molecular dynamics. Accurate temperatures in a SSNMR rotor have been significantly more difficult to obtain and determine than for liquids NMR (see Ref. (4) and references therein). Methanol or ethylene glycol is typically used for temperature calibration in liquid-state NMR spectroscopy, but they can work well for SSNMR spectroscopy in an appropriately sealed rotor. Antonijevic and Bodenhausen note that liquid methanol was used to calibrate the temperature in the rotor for their study (61). Methanol is used primarily for ambient and lower temperatures, whereas ethylene glycol is

used for ambient and higher temperatures. The overlap around room temperature is useful for connecting calibration curves for the entire temperature range of a probe. A significant advantage of using methanol and ethylene glycol is that only one or two samples are required to accurately determine an entire temperature calibration curve simply by measuring the frequency difference between the two peaks. The disadvantage is that a modified pulse sequence may be required to measure the temperature under similar CP/MAS conditions that will be used for solid samples. This is because the temperature calibration for either methanol or ethylene glycol must be determined with a ^{1}H pulse sequence, and liquids will not give NMR signals with CP as do solids.

SOLID-FORM CHARACTERIZATION

Molecular polymorphism can be divided into several types. Conformational polymorphism occurs when a molecule exists in two or more different conformations in a crystalline solid. Packing polymorphism occurs when a single conformation of a molecule is arranged in one of several unique orientations that have different long-range order. Polycrystalline powders are the typical samples for SSNMR spectroscopy and usually have a crystallite size in approximately the micrometer range (i.e., microcrystalline). Amorphous solids are essentially random arrangements of molecules, but they have some short-range order relative to each other because molecular motions are restricted in the solid state. Only the rapid tumbling of molecules in liquids or gases results in truly amorphous material. The molecules of amorphous solids can also have multiple conformations, which might suggest that these conformational differences would be observable by SSNMR spectroscopy or other techniques. However, the different conformations and the random spatial order of an amorphous solid tend to be indistinguishable by SSNMR spectroscopy because they have similar peak broadening effects on the spectrum. Nanocrystalline solids may also be distinguished from amorphous solids by SSNMR spectroscopy. Nanocrystallites will typically appear almost identical to microcrystallites or macrocrystallites (single crystals) by SSNMR spectroscopy using the typical CP/MAS technique. If nanocrystalline solids have significant disorder due to defects, they may be difficult to distinguish from amorphous solids.

The majority of the reports on polymorphism that are reviewed in this chapter were published within approximately the last eight years. Many published reports in the pharmaceutical literature use SSNMR spectroscopy as a secondary technique to analyze solid forms, and the interpretation tends to be rather minimal even when the results are quite interesting or potentially critical to a study. The complexity of NMR spectroscopy can be daunting at times, but the body of literature available on data acquisition and interpretation is extensive and reasonably easy to understand even for a novice (37,39). The value of SSNMR spectroscopy is significant for pharmaceutical solid-form analysis, and should be used to its greatest advantage as a complementary technique to XRPD, vibrational spectroscopy, microscopy, and thermal analyses. Hopefully, the examples provided in this chapter will demonstrate both the strengths and weaknesses of SSNMR spectroscopy in characterizing pharmaceutical solid forms.

Conformational polymorphism, where distinct conformations of a molecule result in different crystal forms, has been studied for decades (64,65). SSNMR spectroscopy is useful here because it is very sensitive to molecular conformations and

short-range order in solids. Griesser et al. studied conformational polymorphism in oxybuprocaine hydrochloride with spectroscopy, X-ray diffraction, and thermal analyses, and found it to have either a less stable bent conformation (U-type) or a more stable straight conformation (I-type) in the crystal forms (66). This local anesthetic drug has three polymorphs: modification I with one U-type conformer per asymmetric unit, modification III with two U-type conformers per asymmetric unit, and modification II° with one U-type and one I-type conformer in the asymmetric unit. Modification II° is the most stable polymorph below approximately 90°C, modification I is more stable above this temperature, whereas modification III is metastable over the temperature range studied. Both ^{13}C and ^{15}N SSNMR spectroscopy were useful in determining the number of molecules per asymmetric unit, and molecular mobility was studied using variable temperature analyses and the dipolar dephasing technique. The dipolar dephasing NMR experiment can be used to analyze molecular motion because dipolar coupling is reduced for more mobility for more mobile regions of a molecule.

Vogt et al. studied the two enantiotropic polymorphs of {4-(4-chloro-3-fluorophenyl)-2-[4-(methyloxy)phenyl]-1,3-thiazol-5-yl} acetic acid by ^{1}H, ^{13}C, ^{15}N, and ^{19}F SSNMR spectroscopy (67). A thorough SSNMR spectroscopy study was used to help understand the structures of each polymorph determined by X-ray diffraction. The solid-state transition temperature of the polymorphs was ~30°C. Form I was thermodynamically more stable below 35°C, but form II was more stable to milling and had lower hygroscopicity. The single-crystal structure of form I was determined, but form II did not produce suitable single crystals. The structure of form II was determined using XRPD, and various SSNMR spectroscopy analyses were used to provide additional restraints for the structure determination. Two 2D NMR pulse sequences that rely on dipolar coupling, ^{1}H DQ-BABA (double quantum back-to-back) and ^{1}H–^{13}C HETCOR (heteronuclear correlation), were used to determine conformational features of both polymorphs. The 2D PASS (phase-adjusted spinning sidebands) pulse sequence was used to determine chemical shielding tensors (CSTs) for ^{13}C resonances of form II to help refine the calculated structure. The orientation dependence of CSA is useful in providing unique structural details to support diffraction analyses. The authors suggest that, with additional work on other polymorphs, it may be possible to use SSNMR spectroscopy rather than the Burger–Ramberger IR rule for predicting the relative stability of polymorphs (68,69). The degree of peak overlap in the spectral region sensitive to hydrogen bonds is not nearly the problem for SSNMR spectroscopy as it is for IR spectroscopy. This study is an excellent example of using multinuclear, multidimensional SSNMR spectroscopy as a powerful technique to thoroughly characterize polymorphs. However, many of the analyses and the interpretation require a high level of expertise in NMR spectroscopy.

Maccaroni et al. studied the solid-state form interconversions for two linezolid (Fig. 14) polymorphs by ^{13}C SSNMR, XRPD, and thermal methods (70). Most of the SSNMR peaks were assigned for the two polymorphs by comparison to the ^{13}C NMR assignments of linezolid in a $CDCl_3$ solution. However, this procedure will not necessarily lead to correct assignments for the solid state unless the conformations are very similar or the electronic environment around each nucleus is coincidentally the same as shown for DTPPAA in Figure 6. It appears that the spectra of both polymorphs were acquired with the same parameters (e.g., contact time, pulse delay, number of scans), but form IV obviously has a longer ^{1}H T_1 relaxation time based on

the much lower signal-to-noise ratio in the spectrum (Fig. 15). The peak widths also are somewhat broader for form IV, which may result from unresolved peaks of two very similar molecules per asymmetric unit, as the authors state. The authors also note that the lowest frequency methyl carbon resonance of form IV is split into two peaks (nearly overlapping), which may be consistent with two molecules per asymmetric unit. However, this could also be explained by conformational exchange due to restricted rotation about the amide bond, which is quite well known for liquid-state NMR spectroscopy. The small symmetrical splitting of C2 (~170 ppm) in form II is likely due to conformational exchange rather than coupling to ^{14}N, because the quadrupolar broadening effect is not very large at this field strength (~9.4 T), and only some peak broadening is likely to be observed instead. The ^{13}C-^{14}N coupling usually produces asymmetrical splitting at lower field strengths where it is more readily observed (71–75). The ^{19}F atom directly bonded to the aromatic carbon (C9) produced significant broadening for this peak in the spectrum of form II due to the relatively strong scalar and dipolar coupling. The C8 resonance also shows broadening as do the C7 and C10 peaks to a lesser extent (Fig. 15). This is because ^{19}F decoupling is not commonly used simultaneously with ^{1}H decoupling for ^{13}C CP/MAS SSNMR spectroscopy unless the spectrometer and probe are specifically designed to do so. The MAS speed would need to be much faster than 7 kHz to reduce ^{19}F–^{13}C dipolar coupling significantly. The effect of ^{19}F coupling shows that for form II, C9 should be assigned to the broader peak at 154.9 ppm, and C6 should be assigned to the peak at 157.2 ppm. The C6 and C13–C16 resonances were apparently not observed for form IV supposedly because of broadening due to their proximity to oxygen and nitrogen in the molecule. However, the assignments for the C6 and C9 resonances are also swapped for form IV, which means that the C9 resonance is broadened (by ^{19}F coupling) into the baseline noise in this spectrum that already has a very low signal-to-noise ratio relative to the spectrum of form II (Fig. 15). This alternative interpretation of the spectrum of form IV is supported by the missing C13–C16 resonances (also broad in the spectrum of form II), which are likely broadened due to inefficient ^{1}H decoupling. Although the experimental details for the SSNMR spectroscopy data acquisition are very minimal in this report, it is quite likely that the older continuous wave ^{1}H decoupling scheme rather than one of the modern modulated decoupling methods was used to acquire the SSNMR spectra. The contact time (1 millisecond) is also relatively short, and may partly account for the low sensitivity of some quaternary carbons in the spectrum of form IV. The difficulties in correctly interpreting SSNMR spectra to compare solid forms can be reduced by using modern fast MAS and modulated decoupling or simultaneous ^{1}H and ^{19}F decoupling along with efficient CP. One or more of the various spectral editing methods would have been particularly useful in confirming the assignments in this case (76).

Two polymorphs of buspirone hydrochloride were compared using ^{1}H and ^{13}C SSNMR spectroscopy (observed and calculated values), XRPD, Fourier transform spectroscopy, infrared spectroscopy (FT-IR), and differential scanning calorimetry (DSC) (77). The single-crystal X-ray structure was determined for form I and found to be very similar to previous work. The authors used XRPD and DSC for quantitative analysis of mixtures of polymorphs and compared the results to previous quantitative FT-IR data. The XRPD patterns were difficult to use for quantification in this case. FT-IR spectroscopy gave superior quantitative data based on the summaries in Table 1 of their report (77), although the authors did not discuss

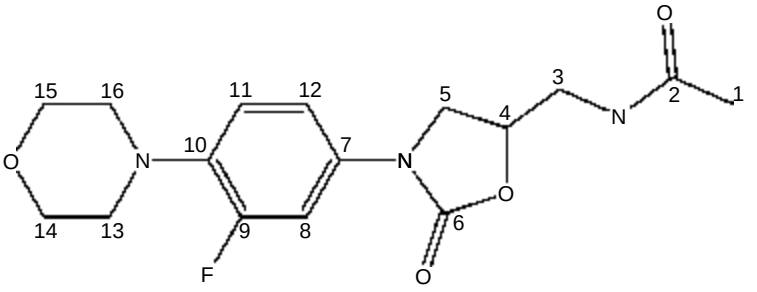

FIGURE 14 Chemical structure of linezolid. Adapted from Ref. (70).

this further. The ^{13}C SSNMR spectra clearly differentiated between the two forms, but form I appeared to have a longer ^{1}H relaxation time based on its relatively low signal-to-noise ratio. This may be why the authors were not able to obtain a ^{1}H SSNMR spectrum of form I, and also suggests that quantification by SSNMR spectroscopy may not be very practical in this case. The calculated ^{1}H and ^{13}C NMR chemical shifts were in generally good agreement with the observed values. The authors used the comparisons to determine which portions of buspirone hydrochloride had the greatest effect on the SSNMR spectroscopy differences observed for the two polymorphs. These comparisons with calculated chemical shifts are useful if the resonance assignments have not been previously obtained from a liquid-state NMR spectrum of the same molecule. Although calculated NMR chemical shifts have progressed greatly in recent years, it is still difficult to unambiguously determine them for cases when the molecular conformations are very close.

A recent study of donepezil hydrochloride used XRPD, SSNMR, vibrational spectroscopy, and thermal analyses to characterize five polymorphs, two hydrates, and an amorphous form (78). This work demonstrates the utility of multiple analytical techniques for characterizing pharmaceuticals. Unfortunately, each technique was not used to analyze every sample, which prevents a complete comparison of them. In general, the spectroscopic techniques could differentiate the solid forms. The authors apparently found three forms of a trihydate ("hydratemorphism") based on DSC, FT-IR, and water vapor sorption analyses. However, none of these hydrate forms were analyzed by any of the three most powerful solid-state techniques (XRPD, SSNMR spectroscopy, and Raman spectroscopy). These additional analyses would have greatly enhanced their case for "hydratemorphism." The authors also observed that hydrate I had slightly higher water content by Karl Fischer titration than a monohydrate, and one of three proposed reasons was that a small amount of amorphous material may cause this. The Karl Fischer results are explained by the observation of weak broad peaks in the SSNMR spectrum due to disordered material, and the XRPD pattern showed some diffuse scattering typical of disordered material. An interesting observation is that the carbonyl resonances in the ^{13}C SSNMR spectra are shifted to higher frequency for the hydrates, which is expected for hydrogen bonding with water.

Masuda et al. examined the α and γ forms of indomethacin by XRPD and ^{13}C CP/MAS SSNMR spectroscopy (79). They were able to determine that α-indomethacin

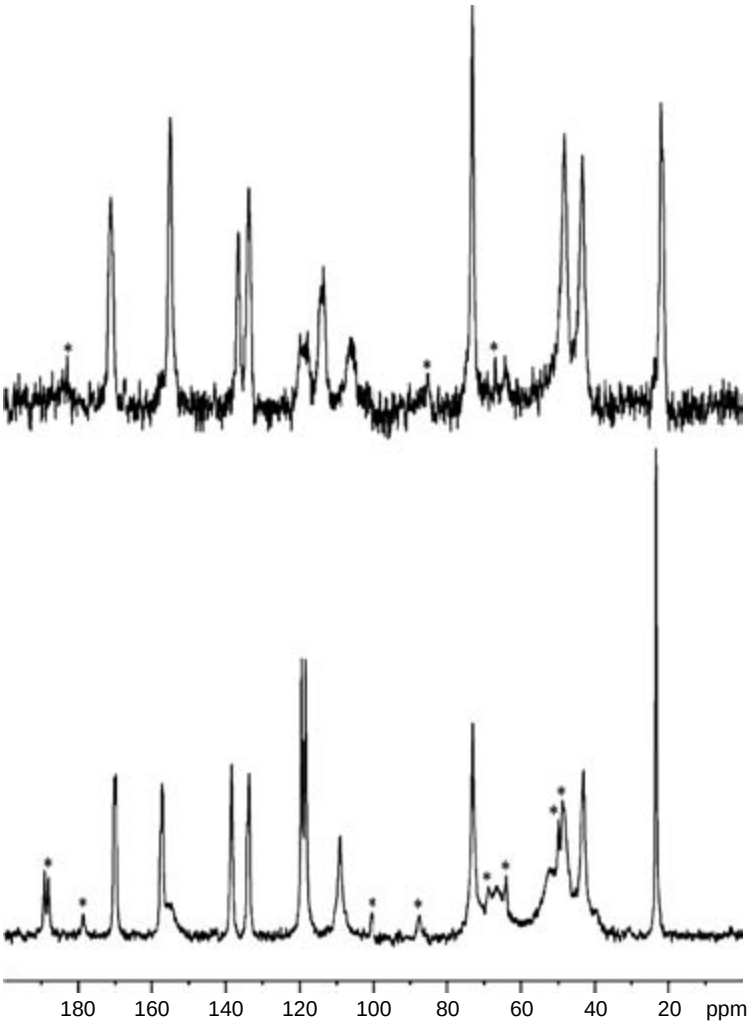

FIGURE 15 ^{13}C CP/MAS spectra of linezolid form II (*bottom*) and form IV (*top*) obtained at 9.4 T and 7 kHz MAS. Asterisks indicate spinning sidebands. Adapted from Ref. (70).

has three molecules per asymmetric unit while γ-indomethacin has only one based on the peak splitting (Fig. 16). However, the methoxy group (C12) and the aromatic carbon to which it was bonded (C5) of α-indomethacin also showed a slight splitting of the highest frequency peak at low temperature (203 K), which seemed inconsistent with three molecules per asymmetric unit. The variable temperature SSNMR analyses (at 203, 298, and 343 K) showed that this splitting was due to conformational exchange for one molecule in the asymmetric unit (Fig. 17). The flexible methoxy group (C12) of one molecule in the asymmetric unit is also in two slightly different conformations resulting in two nearly overlapping signals, and this apparently affects the aromatic carbon (C5) to which the methoxy group is bonded. The other

methyl group (C13) also shows some conformational flexibility, but it results in a broader peak rather than splitting. This is a good example of the sensitivity of SSNMR spectroscopy to molecular conformations of solid forms. Conformational flexibility is typically seen in an X-ray crystal structure as an enlarged thermal ellipsoid. The low temperature (<300 K) SSNMR spectrum shows that the methoxy carbon atom for one of the molecules in the asymmetric unit become "conformationally trapped" in one of two different environments. Above 300 K the methoxy group is apparently mobile enough to cause coalescence of the peaks. It was not clear from the report if temperature cycling or varying the cooling rate resulted in the same final spectrum at ambient temperature. This could demonstrate whether the two conformations became equally populated, or if they could be trapped unequally in the different conformations.

Apperley et al. also studied the solid forms of indomethacin as well as nifedipine by ^{1}H and ^{13}C SSNMR spectroscopy and ^{1}H T_1 and $T_1\rho$ relaxation analyses (80). The ^{13}C SSNMR spectroscopy peak widths of crystalline nifedipine were significantly narrower than for crystalline indomethacin, which suggests that molecular mobility is higher for nifedipine. The authors showed that amorphous nifedipine recrystallizes upon grinding while amorphous indomethacin does not. The onset points for the glass transition temperatures (T_g) of indomethacin and nifedipine are ~42°C and ~45°C, respectively. Nifedipine recrystallized at 55°C into a mixture of two different polymorphs (forms I and II), which converted almost completely to form I at 70°C.

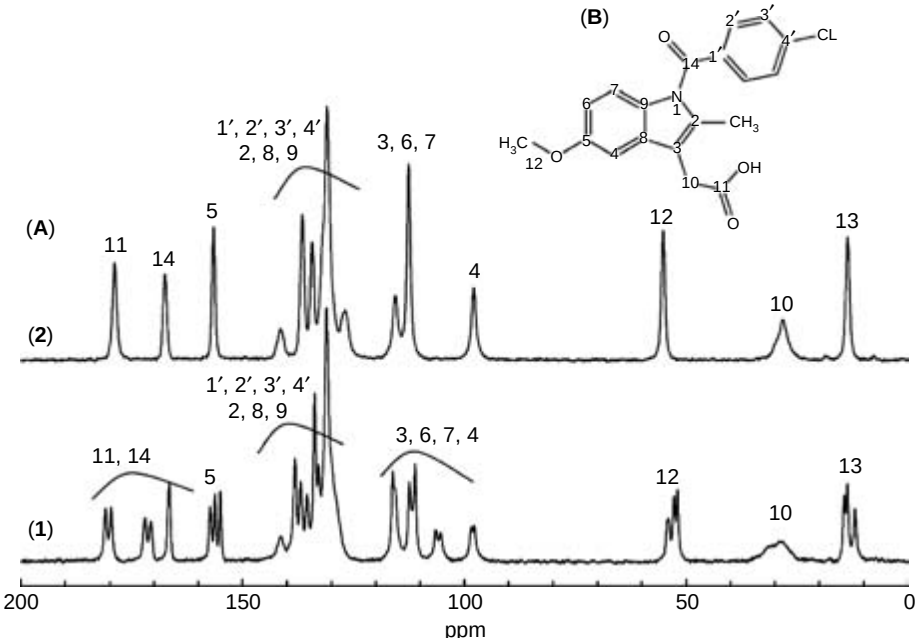

FIGURE 16 ^{13}C CP/MAS spectra of indomethacin at 9.4 T and 15 kHz MAS: (**A1**) α-form, (**A2**) γ-form, and (**B**) chemical structure of indomethacin. Adapted from Ref. (79).

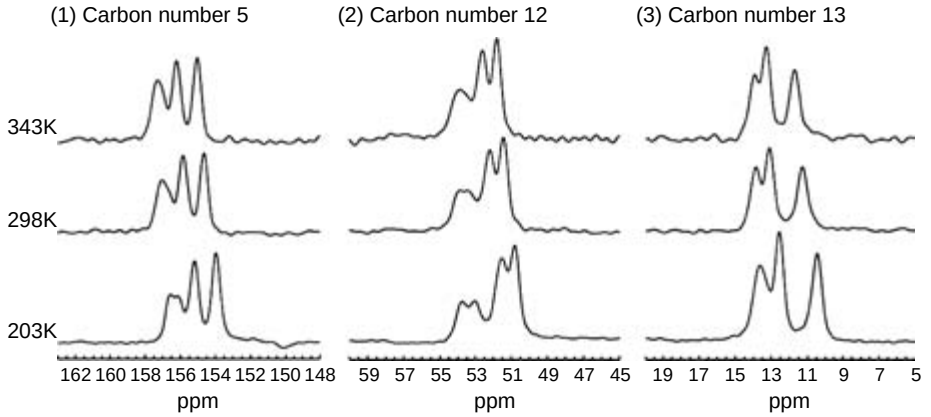

FIGURE 17 Expanded regions of the variable temperature ^{13}C CP/MAS spectra of α-indomethacin. The three groups of carbon resonances show conformational disorder for the highest frequency peak(s) in each region. The spectra also show that there are three molecules per asymmetric unit. Adapted from Ref. (79).

Nifedipine form II is a metastable polymorph. The ^{13}C SSNMR spectrum of amorphous indomethacin showed sharpening of peaks as the temperature was increased up to 80°C, but it did not recrystallize because the temperature was not increased high enough for this to occur in the ^{13}C SSNMR spectroscopy part of the study. The ^{1}H SSNMR spectra and relaxation measurements indicate that amorphous nifedipine has greater mobility below its glass transition temperature than indomethacin, and nifedipine tends to recrystallize first to a metastable form. The quadrupolar broadening effect of ^{35}Cl and ^{37}Cl was also examined in indomethacin at five different field strengths ranging from 4.7 to 18.8 T (50–200 MHz for ^{13}C). The quadrupole moment of both chlorine nuclides are much larger than for ^{14}N, which results in significantly more peak broadening as well as more complex splitting patterns. This can lead to much greater difficulty in SSNMR spectral interpretation for molecules having chlorine atoms unless high magnetic field strengths are used.

Schmidt et al. performed a series of studies on the polymorphism of local anesthetic drugs using spectroscopic, diffraction, microscopic, and thermal analyses (81–85). SSNMR spectroscopy was not a major part of any of these studies, but it provided unique complementary information for these compounds. In Part V (81), the authors showed ^{1}H SSNMR spectra in a study of hydrogen-bonding differences between modification II° and hydrated modification I, and ^{13}C SSNMR spectroscopy could easily differentiate modification II° from modification I and its hydrate. Modification I and its hydrate both appeared to have two molecules per asymmetric unit, which was confirmed by the single-crystal X-ray structures. Part IV (82) used ^{1}H, ^{13}C, and ^{15}N SSNMR spectroscopy to analyze polymorphism and molecular mobility in falicaine hydrochloride and isomorphic dyclonine hydrochloride. The SSNMR spectra showed that the polymorphs of both compounds have only one

molecule per asymmetric unit. Modification I of both falicaine hydrochloride and dyclonine hydrochloride had a significant amount of the corresponding modification II°. High-temperature ^{13}C SSNMR spectroscopy of the mixture of falicaine hydrochloride modifications I and II° showed that the aromatic ring is rotating at a rate that is intermediate on the NMR time scale at ambient temperature. This causes broadening of the protonated ring carbons for modification I such that they are not easily observed in the ^{13}C SSNMR spectrum. The authors state that a similar process is occurring for modification I in the dyclonine hydrochloride mixture, and this can be readily determined by the broad peaks near the baseline at the corresponding aromatic chemical shift positions in the ^{13}C CP/MAS spectrum. In Part VII (83), the author mentions that the ^{13}C SSNMR spectra of the three polymorphic systems did not have significant differences, although no spectra were shown for any of them. Only XRPD, thermal analyses, and microscopic data were shown for the polymorphs, but no IR, Raman, of SSNMR spectroscopic data was presented. A potentially interesting study would be to see if this were a series of polymorphs that can only be distinguished by specific analytical techniques. In Part VIII (84), the authors used ^{1}H and ^{13}C SSNMR spectroscopy to study several solid forms of hydroxyprocaine hydrochloride. The ^{1}H SSNMR spectroscopy was used to analyze the hydrogen bonding of the hydrate, and ^{13}C SSNMR spectroscopy was used to differentiate the two polymorphs and determine that the hydrate had two molecules per asymmetric unit. Part XI (85) also used ^{1}H SSNMR spectroscopy to study hydrogen-bonding differences for several hydrates. The relatively high chemical shifts of carboxylic acid protons made them useful for characterizing hydrogen bonds in several of these materials even though ^{1}H SSNMR peaks are typically very broad without very fast MAS or special pulse sequences like combined rotation and multiple pulse spectroscopy (CRAMPS).

Rubin-Preminger et al. studied polymorphs of ethambutol dihydrochloride diastereomers by single crystal X-ray diffraction, XRPD, SSNMR, and thermal analyses (86,87). The ^{13}C SSNMR spectroscopy was consistent with the crystal structure data showing that there was half a molecule per asymmetric unit for each form. Ethambutol dihydrochloride is a symmetrical molecule, and this property is maintained in the solid state resulting in the half molecule per asymmetric unit. The *S*,*S*-diastereomer has four polymorphs with two pairs that are enantiotropically related. The *R*,*S*-diastereomer has two enantiotropically related polymorphs. Variable temperature ^{13}C SSNMR spectroscopy of the *S*,*S*-diastereomer showed a solid-state phase transformation of a mixture of forms III and IV to form III at ~40°C and then back to form IV upon cooling again (87). A similar solid-state phase transformation occurs for form II to form I above ~70°C. The ^{13}C SSNMR spectra in these reports were very similar due to the similarity of the crystal structures for the polymorphs of each diastereomer. However, SSNMR spectroscopy was still sensitive and specific enough to easily distinguish the subtle differences among the solid forms.

Moynihan and O'Hare used IR, Raman, and SSNMR spectroscopic analyses to study two polymorphs of paracetamol (acetaminophen) (88). The authors note that IR and SSNMR spectra were useful for distinguishing the polymorphs, but the Raman spectra were not. The commercial form was monoclinic, and an orthorhombic form was produced as a mixture by melt quenching of the monoclinic material. A ^{13}C SSNMR spectrum of the orthorhombic form was obtained by subtracting the spectrum of the monoclinic form. The ^{13}C SSNMR spectra in this report use TOSS to suppress the spinning sidebands. The small out-of-phase peaks in each spectrum

are likely due to inefficient side band suppression from incorrectly setting the ^{13}C pulse width as noted in section "Solid-State NMR Spectroscopy" on p. 385.

Shaibat et al. used ^{13}C SSNMR spectroscopy to study polymorphs of the potential anti-leukemia compound Cu(II)(8-quinolinol)$_2$ (89). The paramagnetic copper atom increased the peak widths and shifted some of them to higher frequency for these molecules. The authors used relatively fast MAS of 20 kHz or more to decrease the peak broadening in the spectra. The interconversion of the polymorphs upon heating was also monitored by ^{13}C SSNMR. This study was a useful demonstration of SSNMR spectroscopy for characterizing molecular complexes having strong paramagnetic centers that cause peak broadening. Typically paramagnetic compounds have been very difficult to analyze by NMR spectroscopy because of the very broad peaks.

Enright et al. studied two anhydrous polymorphs of caffeine (Fig. 18) with single-crystal X-ray diffraction and SSNMR spectroscopy at low- and high-field strengths (90). The high-field ^{13}C CP/MAS SSNMR spectra had much better resolution compared to the low-field data because the interaction with the quadrupolar ^{14}N nucleus was dramatically reduced (Fig. 19). The anhydrous polymorphs appeared to be more disordered compared to the monohydrate, and the low-temperature anhydrous form had multiple molecules per asymmetric unit (Fig. 20). These results were confirmed by the single-crystal structures of each form.

Sheth et al. used ^{13}C SSNMR spectroscopy to study conversion of piroxicam polymorphs after cryogenically grinding them into "amorphous" solids (91). The "amorphous" material recrystallized to the original crystalline form during storage at 25°C and 0% relative humidity. This is not surprising given that forms I and II after cryogrinding for various times show different XRPD patterns for the most disordered forms, which are actually nanocrystalline piroxicam of the corresponding polymorph (92). The disordered nanocrystallites act as seeds for conversion back into larger crystallites of the same polymorph. SSNMR spectroscopy was not very useful in this case because the high degree of disorder in the cryoground samples resulted in broad peaks that masked the small amount of nanocrystalline material.

Harris et al. used ^{1}H and ^{13}C SSNMR spectroscopy to study the structures of four carbamazepine polymorphs, a dihydrate, and acetone and dioxane solvates (93).

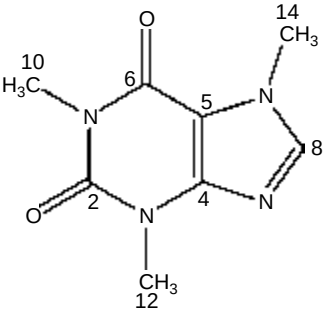

FIGURE 18 Chemical structure of caffeine with the numbering system as used for the assignments of Figure 19.

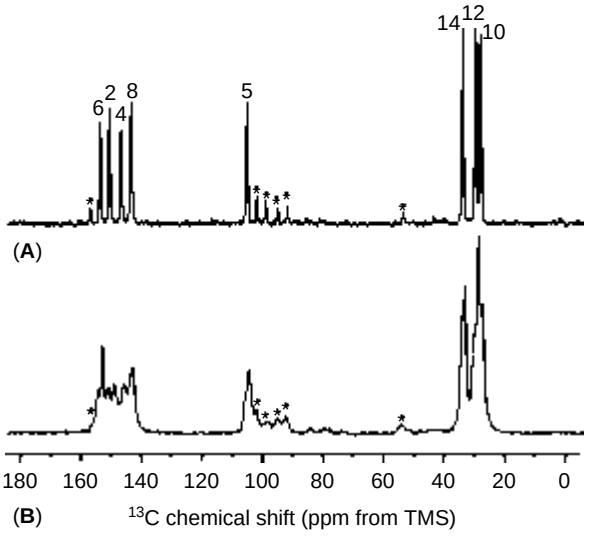

FIGURE 19 ^{13}C CP/MAS spectra of caffeine monohydrate: (**A**) 226.3 MHz (21.1 T) and 11.7 kHz MAS; (**B**) 50.3 MHz (4.7 T) and 2.6 kHz MAS. Asterisks indicate spinning sidebands. The assignments in spectrum (**A**) of the structure in Figure 18 are based on a spectrum obtained by liquid-state NMR spectroscopy. Adapted from Ref. (90).

The number of molecules per asymmetric unit was accurately determined for each case when compared to the crystal structures with only the triclinic form (with four molecules) having more than one. Computational analyses of the shielding constants of the P-monoclinic form were compared to the observed values and found to be reasonably close. The torsion angles for the P-monoclinic and trigonal forms of carbamazepine were also calculated and compared. The single-crystal X-ray structure of the dihydrate was also re-examined and determined to be monoclinic rather than orthorhombic as previous work had found, possibly due to micro-twinning.

Portieri et al. used ^{13}C and ^{15}N SSNMR, ^{1}H and ^{15}N T_1 and $T_1\rho$ relaxation data, and CSA to study polymorphs of sulfanilamide (94). The α, β, and γ forms were easily distinguished by ^{13}C SSNMR. The ^{1}H T_1 values for the α and γ forms were more than 10 times longer than for the β form, but the ^{1}H $T_1\rho$ values for the α and β forms were about twice as long as that of the γ form. This indicated that the solid-state molecular mobility was different for each polymorph. The authors note that the relaxation differences are large enough to result in potentially misleading information for mixtures of polymorphs. The peak intensities for the form with the shorter ^{1}H T_1 relaxation time may be relatively enhanced compared to the other if the SSNMR spectroscopy analyses are not set up to properly account for the differences. This is the reason that care should be used if one anticipates that mixtures of solid forms might be present in a sample to be analyzed by SSNMR spectroscopy. The ^{13}C SSNMR spectroscopy of each form obtained at this relatively low field strength (~50 MHz for ^{13}C) clearly showed the quadrupolar splitting of the carbon bonded to the quadrupolar ^{14}N nucleus. Selective ^{15}N-labeling at one of the two nitrogens was used to enable

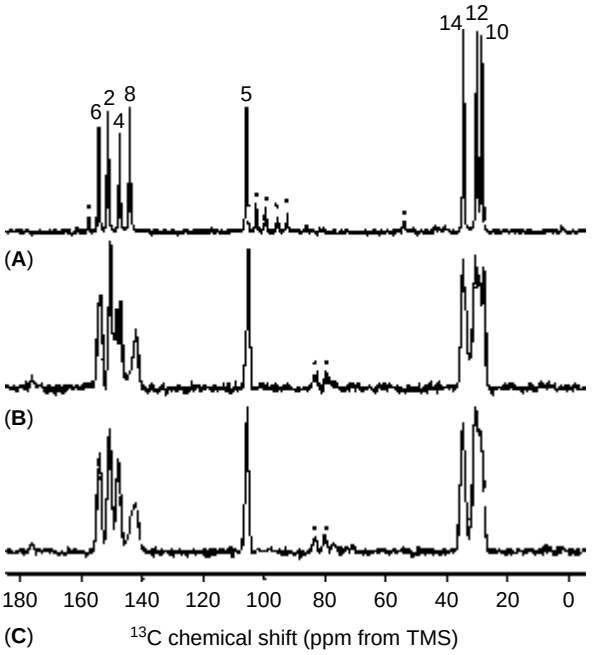

FIGURE 20 ^{13}C CP/MAS spectra of caffeine solid forms at 226.3 MHz (21.1 T): (**A**) caffeine monohydrate, (**B**) low-temperature anhydrous form, and (**C**) high-temperature anhydrous form. Asterisks indicate spinning sidebands. The spectra for the two anhydrous forms were acquired with 16 kHz MAS. Adapted from Ref. (90).

easier analysis of the nitrogen NMR parameters. The ^{15}N T_1 times for the secondary amine nitrogen in all three polymorphs were 100 seconds or longer as measured by the method of Torchia (95). The sulfonamide nitrogen T_1 relaxation times for all three polymorphs were less than three seconds. The $T_1\rho$ relaxation times for the secondary amine were 0.64 milliseconds for both the α and β forms, and 1.5 milliseconds for the γ form. The $T_1\rho$ relaxation times for the sulfonamide group were ~4 to 10 milliseconds. These results indicate that the mobility is substantially different in specific parts of this small molecule. The measured chemical shielding parameters were different for each nitrogen but almost the same among the three polymorphs. The calculated shielding parameters for ^{13}C and ^{15}N were reasonably useful for analyzing the differences in the polymorphs but also show that improvements in computational methods are still needed to accurately determine these values for detailed understanding of solid molecules.

Lee et al. used liquid-state ^{13}C NMR of several amphetamines to help assign the ^{13}C SSNMR spectra (96). The various amphetamines were easily distinguished by SSNMR spectroscopy. The authors also dry mixed 3,4-methylenedioxy-*N*-methylamphetamine-HCl [(*R*,*S*)-MDMA·HCl] with lactose monohydrate to mimic "Ecstasy" tablets. This simple mixing process involved rotating a vial of the two components without compression or shear forces, yet there was a very noticeable difference in the

^{13}C SSNMR spectrum compared to that of the pure drug. The authors noted shifts of about +5.5 ppm for C8 (methylene) and –6.2 ppm for C10 (methyl). Significant shifts of about 2.6 ppm for C1 and 1.3 ppm for C5 (both aromatic carbons) as well as a distinct increase in peak widths for the amphetamine in the mixture can also be seen in the spectra. A spectrum of pure lactose monohydrate was not shown for comparison, so the effect of mixing on it could not be determined. The authors also noted that the peaks shifted toward the positions of those observed in D_2O and attributed this to potential hydrogen bond formation in the solid mixture. The peak broadening may also be due to ABMS (138–140). However, the other amphetamines did not show similar spectral changes upon mixing with lactose monohydrate, so there appears to be a specific intermolecular interaction, such as hydrogen bonding, resulting in a conformational change that occurs with (*R*,*S*)-MDMA·HCl and causes both peak broadening and shifting.

Reutzel-Edens et al. used spectroscopic, diffraction, thermal, and water vapor sorption analyses to study three anhydrates, a dihydrate, and an acetic acid solvate of the developmental compound, LY33470 HCl (97). All of the forms had one molecule per asymmetric unit. An unusual observation was that form I had a much lower dissolution rate than the dihydrate. The liquid-state ^{13}C NMR spectrum was used to assign the peaks for the solid forms, but the peak shifting observed in the solid state was such that these assignments are tentative without supporting solid-state editing techniques or correlation spectroscopy. The peak of the fluorinated aromatic carbon was very near the amide carbonyl peak, and the large ^{19}F–^{13}C coupling constant (~150–375 Hz or ~1.5–3.7 ppm at 9.4 T field strength in this study) caused overlap with the amide resonance. The authors assigned three or four peaks in this region, although no more than two distinct peaks and a small shoulder were observable for any of the spectra they reported. The largest separation between the peaks above 160 ppm (excluding acetic acid) is about 3.3 ppm, which is within the range for ^{19}F–^{13}C coupling. The field strength used for the analyses was high enough that the proposed residual ^{13}C dipolar coupling to the quadrupolar ^{14}N nucleus of the amide group could not be responsible for this larger splitting, but may produce the shoulders observed for forms I, II, and the dihydrate. Restricted rotation about the amide bond is also a potential source of additional peaks that may be asymmetric depending on the conformational exchange rate. Therefore, the amide carbonyl and fluorinated aromatic carbon resonances appear to be overlapped with ambiguous chemical shift assignments without further information. A good example of the effects of ^{19}F–^{13}C coupling is shown for flurbiprofen by Antonioli and Hodgkinson (98).

Wang et al. studied four polymorphs of a fluorinated NK1 receptor agonist referred to as Compound A (Fig. 21) using variable temperature XRPD and ^{13}C SSNMR spectroscopy as well as differential scanning calorimetry, thermogravimetry, and microscopy (99). They found two sets of enantiotropically related polymorphs. Forms III and IV (Fig. 22) are the high-temperature polymorphs of forms I and II (Fig. 23), respectively. The highest frequency carbon resonance was due to the fluorinated aromatic carbon at ~160 to 165 ppm, which formed an asymmetrical doublet similar to that observed in the spectrum of LY334370 HCl (97) but without any possible overlap from amide carbonyl peaks or spinning side bands that could lead to misinterpretation (Figs. 22 and 23). The two trifluoromethyl carbon resonances (~120–130 ppm) were very broad in forms I and II (Fig. 23), but less so in forms III and IV (Fig. 22). The high-temperature forms of compound A appear to be conformational polymorphs of the low-temperature forms given the similarity of most

peak positions and the potential for flexibility for the methyl carbons and morpholine ring. The authors suggested that form I may have multiple molecules per asymmetric unit based on doublets at ~48 and ~100 ppm, but this could also be a conformational difference in the morpholine ring system (~48 ppm for N–CH_2 and ~100 ppm for O–CH–O) given that no other peak splittings were observed in the spectrum of form I to support this hypothesis. However, the spectrum of form II shows four peaks between 20 ppm and 30 ppm corresponding to the single methyl group, indicating that it is in four different environments in the unit cell (Fig. 23). This could result from conformational exchange for the mobile methyl group, but no variable temperature SSNMR spectra of form II were obtained to help clarify this.

Isotopic labeling is a very useful means of enhancing the sensitivity of NMR spectroscopy, particularly for biological molecules. It is used much less often for small molecules due to the difficulty in synthesizing molecules with isotopes at specific locations. Booy et al. specifically ^{13}C-labeled two ethynyl and one methyl carbon of a steroid (Org OD 14) as a means to enhance the sensitivity for detecting two polymorphs in formulations having 0.5% or 2.5% API loads (100). From the ^{13}C SSNMR spectra, form I had two molecules per asymmetric unit, and form II had one. Under the conditions used by the authors for ^{13}C SSNMR, the natural abundance steroid peaks were easily observed at 2.5% loading along with the much larger peaks from the isotopic labels. The polymorphic form was also readily determined from the natural abundance peaks at this loading level. For the 0.5% loading, the peaks of the natural abundance steroid were just visible above the noise in the baseline, and it was very difficult to determine the polymorphic form except by using the peaks of the labeled material. A spectrum of the pure labeled sample showed both sharp ethynyl carbon peaks overlapped on broader peaks, and this was also observed for

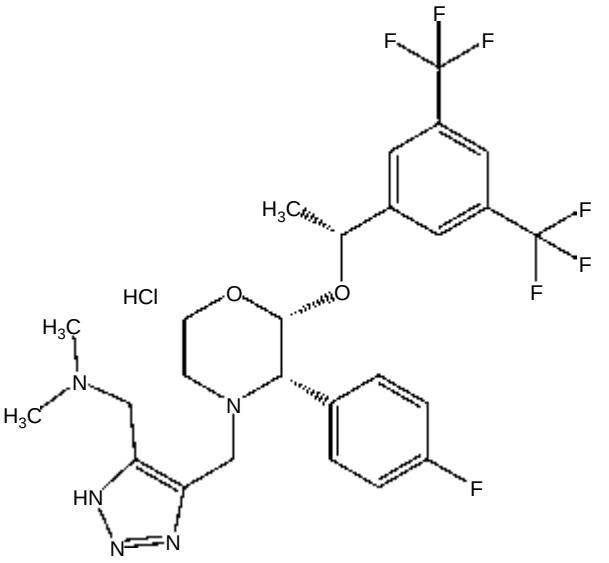

FIGURE 21 Chemical structure of Compound A. Adapted from Ref. (99).

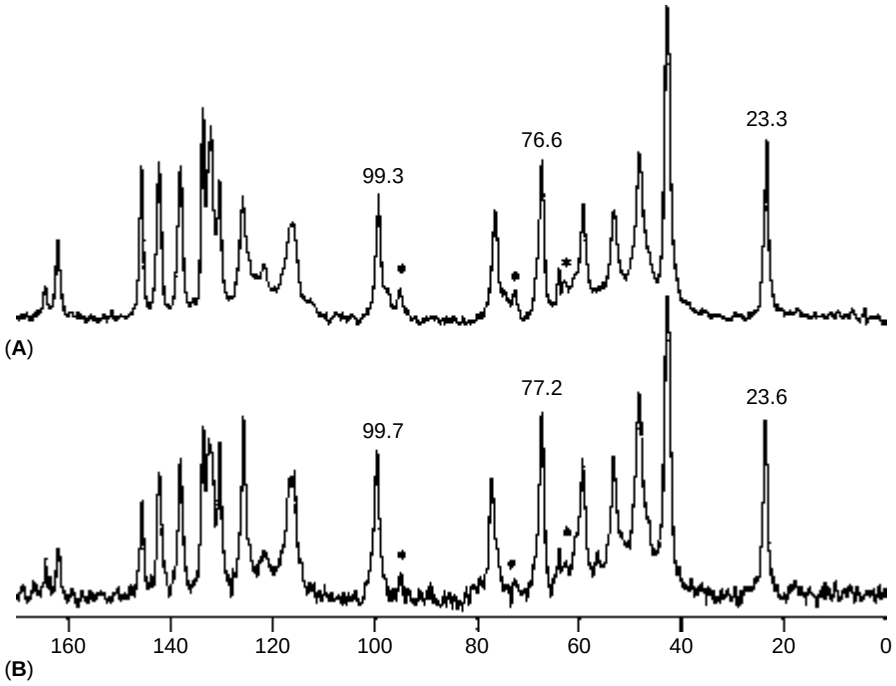

FIGURE 22 ^{13}C CP/MAS spectra of Compound A at 9.4 T and 7 kHz MAS: (**A**) form III and (**B**) form IV. Asterisks indicate spinning sidebands. Adapted from Ref. (99).

the spinning side bands. Although the authors attribute this to ^{13}C–^{13}C dipolar coupling, it is more likely due to some disordered ^{13}C-labeled material, because spinning at 8 kHz would dramatically reduce or eliminate the relatively small homonuclear ^{13}C coupling as noted in section "Solid-State NMR Spectroscopy" on p. 385. Synthetic isotopic labeling methods can be very useful for characterizing solid forms in low load formulations as long as the time and expense required for labeling the API is justified. It may eventually be a required technique if high potency pharmaceuticals become more prevalent as the current trend indicates.

Olejniczak et al. used 1D and 2D ^{13}C and ^{15}N SSNMR, CSA tensor analysis, and theoretical calculations to analyze polymorphs of *N*-benzoylphenylalanine (101). The carbonyl carbons were ^{13}C-labeled, and the amide nitrogen was ^{15}N-labeled. This permitted rapid 2D ^{1}H–^{13}C, ^{13}C–^{15}N, and ^{1}H–^{15}N HETCOR analyses of the molecule. CSA tensor analyses (^{13}C and ^{15}N) and $T_1\rho_H$ measurements were used to estimate the relative strengths of the hydrogen bonds. The authors noted that ^{15}N CSA tensor values were less reliable than the ^{13}C values for evaluating hydrogen bonding. The ^{15}N chemical shift tends to be very sensitive to the effects of chemical bonding and coupling, which makes them somewhat unpredictable even in relatively simple molecules. Polymorphs I and II each had two molecules per asymmetric unit. Polymorph III was only obtained as a mixture with one or more other polymorphs that were not isolated and studied. The isotopic labeling as done in this study can be further exploited for structural

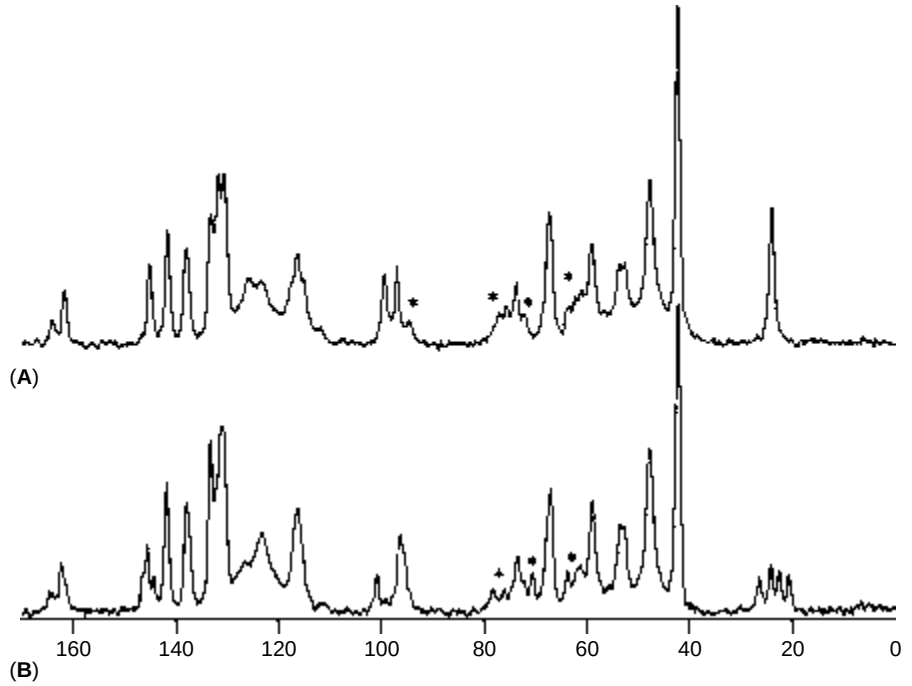

FIGURE 23 ^{13}C CP/MAS spectra of Compound A at 9.4 T and 7 kHz MAS: (**A**) form I and (**B**) form II. Asterisks indicate spinning sidebands. Adapted from Ref. (99).

analysis by using rotational echo double resonance (REDOR) to determine accurate internuclear distances within molecules (102,103).

Zhou et al. used both ^{1}H MAS and ^{2}H MAS SSNMR spectroscopy to study what they called "isotopomeric polymorphism" in a complex of pentachlorophenol with 4-methylpyridine (104). This complex could also be considered a co-crystal. They found that the fully protonated material only produces the triclinic polymorph with a strong hydrogen bond, whereas the 55% or 90% deuterated material forms the disordered monoclinic polymorph with a weaker hydrogen bond. The reason for deuterium causing weaker hydrogen bonding is not clear. It would be interesting to correlate the deuteron and proton covalent bond strengths with intermolecular hydrogen (or deuterium) bond strengths to determine what controls the resulting solid form. Neutron diffraction analyses and IR spectroscopy would be useful analytical techniques to study this further.

In some cases, SSNMR spectroscopy is more useful than XRPD in distinguishing solid forms. Othman et al. used ^{1}H and ^{13}C SSNMR spectroscopy (CP and direct polarization) and XRPD to study four polymorphs and four isomorphous solvate hydrates of finasteride (105). The solvate hydrates were readily distinguished by SSNMR spectroscopy but not by XRPD. The solvents in the crystal structures do not change the packing pattern significantly, but they influence the local electronic environments that affect the NMR chemical shifts. The solvent molecules (other than

water) also have unique chemical shifts that are observed in the SSNMR spectra. This study further emphasizes the need to use multiple analytical techniques when characterizing solid forms, because there is no reliable way to predict which analytical technique will be appropriate for properly characterizing solid materials. XRPD may be the gold standard for studying solid materials, but spectroscopic techniques provide unique data that complements or occasionally surpasses the value of XRPD.

Apperley et al. used ^{13}C and ^{15}N SSNMR spectroscopy to study hydrogen bonding in sildenafil citrate (active ingredient of Viagra™) upon exposure to water vapor (106). One of the citrate carbonyl peaks shifted to higher frequency upon exposure to water vapor over a seven-day period. The other two citrate carbonyl peaks did not change. The authors interpreted this as one citrate carboxyl group forming a hydrogen bond with water. The chemical shifts of the propyl and ethoxy groups of sildenafil also changed upon exposure to water vapor, which the authors suggest is due to water molecules occupying sites close to these groups and presumably changing the electronic environment surrounding these nuclei. However, the chemical shift changes may also result from modification of molecular mobility, and thus the conformations in the crystal, due to incorporation of water. The ^{15}N SSNMR spectroscopy chemical shifts of sildenafil varied by 0.2 to 1.5 ppm upon exposure to water vapor over seven days, which are relatively small changes that suggest weak interactions with the water molecules. The N2 and N3 nitrogens are bonded in sildenafil, which resulted in the typical 1:2 doublet peaks due to the interaction of the ^{15}N dipole with the electric field gradient of the ^{14}N nuclear quadrupole. The authors determined residual dipolar coupling constants of 33 Hz for $^{14}N3$–$^{15}N2$ and 37 Hz for $^{14}N2$–$^{15}N3$. The ^{15}N dipolar dephasing experiment showed that N26 was the only protonated nitrogen of sildenafil. The N5 peak was slightly suppressed by the dipolar dephasing experiment, which was interpreted to be a hydrogen bond at this position. The ^{13}C and ^{15}N SSNMR spectroscopy data are consistent with one citrate carbonyl donating a proton to N26 of sildenafil to form a salt, while a second citrate carbonyl is free to interact with water introduced into the sample. The third citrate carboxylate may have a pK_a that significantly reduces the exchange rate of its proton, which results in essentially no observed chemical shift changes for the corresponding carbonyl resonance upon exposure to water vapor.

Rafilovich et al. used a number of analytical techniques including ^{13}C SSNMR spectroscopy to study polymorphs of 1,3-bis(*m*-nitrophenyl)urea (107). This is the compound where concomitant polymorphs were first discovered. The authors found a new polymorph, designated δ, and a monohydrate that they believe was previously reported as the γ form. They were able to obtain only the β form as a pure phase. The α and δ forms have one molecule per asymmetric unit, and the monohydrate and β forms have half a molecule per asymmetric unit based on the X-ray diffraction data. This was generally supported by the ^{13}C SSNMR spectra. However, the spectrum of the α form did not show the expected 13 peaks, although the seven peaks observed were substantially broader than those in the spectra of the other forms. This may be indicative of some disorder in the crystal structure that may be sufficient to broaden the peaks and prevent observation of all of them. The authors were not able to obtain a ^{13}C SSNMR spectrum of the δ form, which was expected to show new peaks as a mixture with the β form. Only peaks from the β form were observed, so it was not certain whether any of the δ form was present or if it was indistinguishable from the β form. Small splittings for one peak due to ^{13}C dipolar coupling to the quadrupolar ^{14}N nucleus was observed for the monohydrate and β

forms that were analyzed at ~7.1 T but not for the α form that was analyzed at ~11.7 T, which is consistent with the field strength effect on dipolar coupling to quadrupolar nuclei. Some small chemical shift differences were observed in the ^{13}C SSNMR spectra that are consistent with the differences in hydrogen bonding among the polymorphs. An interesting result noted by the authors was the hydrogen bonding interactions observed for this molecule in acetone solution where a small amount of added water caused specific shifting of several peaks in the spectrum. This demonstrates that water specifically interacts with 1,3-bis(*m*-nitrophenyl)urea in the liquid-state, which is analogous to hydrates of solid forms.

Dong et al. prepared polymorphs of neotame anhydrate and studied them by XRPD, spectroscopy, microscopy, water vapor sorption, and thermal analyses (108). Forms A, D, F, and G were characterized more fully than the three forms that were more difficult to make in adequate quantities (B, C, and E). The polymorphs were readily distinguished by XRPD, FT-IR, and ^{13}C SSNMR spectroscopy. The ^{13}C SSNMR spectra of forms D and F had broader peaks, indicating some disordered material was present, which was also consistent with the XRPD data. Form D also appeared to have two polymorphs per asymmetric unit based on its ^{13}C SSNMR spectrum. The ^{13}C SSNMR spectra were obtained at a magnetic field strength of 7.1 T, so splitting due to dipolar coupling of ^{13}C with the ^{14}N nucleus was observed for the amide carbonyl resonance.

A recent brief communication by Griffin et al. demonstrated the use of ^{1}H double quantum combined rotation and multiple pulse (DQ CRAMPS (109)) NMR spectroscopy to distinguish the anhydrous and monohydrate pharmaceutical compounds in a tablet with $CaHPO_4 \cdot 2H_2O$ as the primary excipient (110). The identity of the compound and the loading level were not reported by the authors. However, the ^{1}H DQ CRAMPS analysis showed that the anhydrous form was present in the tablet, which would have been difficult to determine using 1D ^{1}H SSNMR due to overlap of some key resonances. The authors did not show a corresponding spectrum of the monohydrate in the same formulation, which would help validate this potentially useful technique.

Zhou and Rienstra used ^{1}H detected fast-MAS HETCOR to study acetaminophen and ibuprofen in tablet formulations (111). Fast MAS of 40 kHz was used with a 1.6 mm rotor that could hold about 6 mg of material. The fast MAS reduced the ^{1}H-^{1}H dipolar coupling without using homonuclear decoupling. A major advantage of this technique was that it did not require the tedious calibration procedures typical of CRAMPS experiments as used by Griffin et al. (110). The authors also used the technique to study hydrogen bonding and molecular motions. The ^{1}H detected HETCOR was much faster than the usual ^{13}C detected version particularly for acetaminophen (Fig. 24), which had a proton T_1 relaxation time about 30 times longer than that of ibuprofen (Fig. 25). The spectra in Figure 24 also show that it is important to acquire enough scans to obtain all of the correlations particularly for compounds with long relaxation times.

Harris et al. studied two anhydrates, a monohydrate, a higher hydrate, and an acetic acid solvate of terbutaline sulfate by ^{1}H, ^{13}C, and ^{15}N SSNMR spectroscopy as well as XRPD, single-crystal XRD (hydrates only), and thermal analyses (112). The ^{1}H and ^{13}C chemical shifts were also calculated and compared to the observed values. Modification A had broader ^{13}C SSNMR spectroscopy peaks that were attributed to disorder or crystal defects for this form, and it has only one molecule per asymmetric unit. Modification A also appeared to be contaminated with modification B. Based

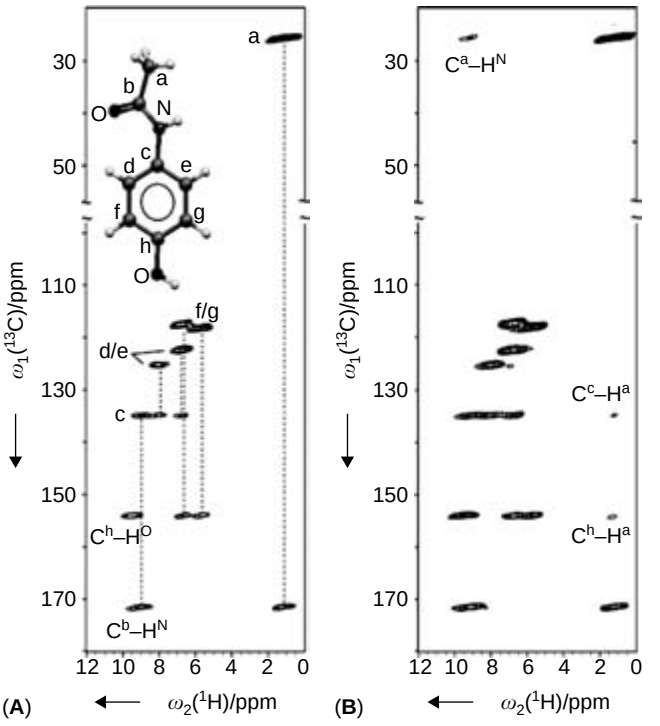

FIGURE 24 (**A**) ^{1}H detected ^{13}C–^{1}H HETCOR spectra at 17.6 T and 40 kHz MAS for 6 mg of a formulation containing 5.5 mg of acetaminophen (~93% load) with assignments for the labeled acetaminophen crystal structure shown in the inset of spectrum (**A**). Spectrum (**A**) was acquired in six hours with two scans per row, and spectrum (**B**) was acquired in 18 hours with six scans per row. The recycle delay for both spectra was 35 seconds. The ^{1}H T_1 relaxation time for acetaminophen was 63 seconds. Note the higher sensitivity in spectrum (**B**) that provided additional correlations. Adapted from Ref. (111).

on the peak splitting observed in their ^{13}C SSNMR spectra, modification B, the monohydrate, and the acetic acid solvate each have two molecules per asymmetric unit. The ^{13}C chemical shifts for each molecule in the asymmetric unit of modification B were computed, but the authors were not able to assign them to the independent molecules in this case. The ^{1}H SSNMR data and computational calculations indicated that strong hydrogen bonds may be present in all the forms, but further work is required to obtain better evidence for this.

Martin-Islán et al. used XRPD, FT-IR, ^{13}C SSNMR spectroscopy, and thermal analyses to study sodium pravastatin (113). The authors found a new polymorph (designated M) for this compound by very slow evaporation from a solution of 2-propanol. They also observed that sodium pravastatin tends to crystallize out as mixtures of multiple polymorphs (concomitant polymorphs). The polymorphs also tend to be disordered, which is typical of some statins due to the flexibility of the alkyl groups connected to the ring structures. Therefore, it is difficult to determine

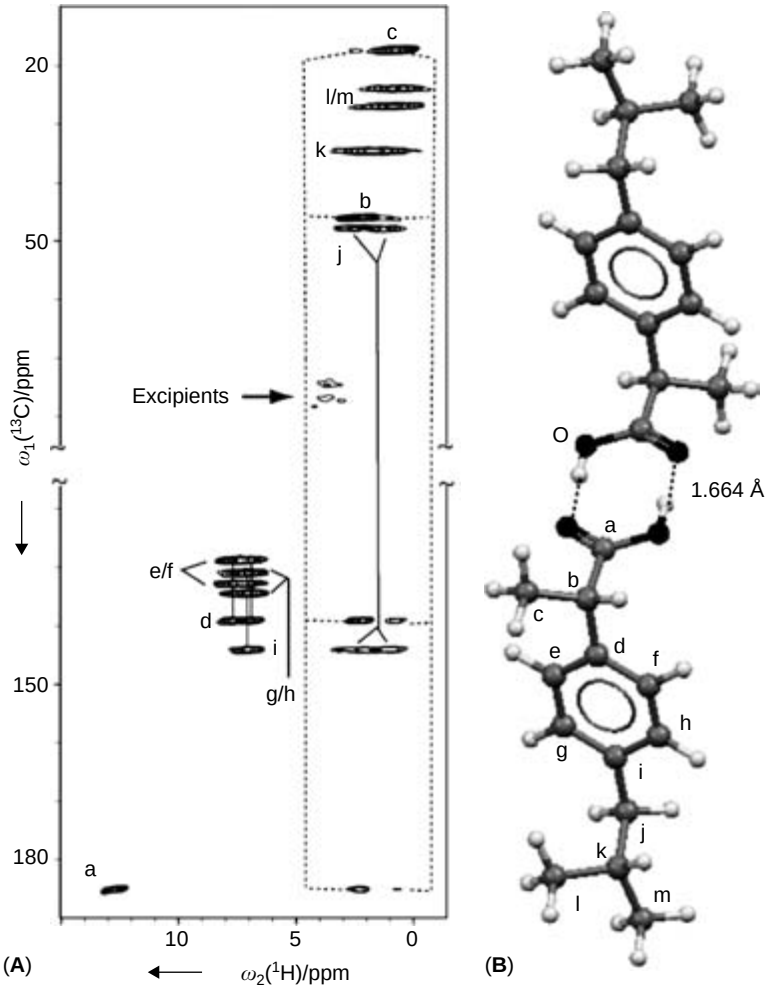

FIGURE 25 (**A**) ^{1}H detected ^{13}C–^{1}H HETCOR spectrum at 17.6 T and 40 kHz MAS for 6 mg of a formulation containing 3.8 mg of ibuprofen (~63% load) with assignments for the labeled ibuprofen crystal structure shown in (**B**). The spectrum was obtained in 33 minutes with two scans per row. The ^{1}H T_1 relaxation time for ibuprofen was 1.7 seconds. Adapted from Ref. (111).

the phase purity by most analytical methods unless truly pure phases can be obtained and compared. Without a crystal structure available for sodium pravastatin, no calculated XRPD patterns were possible. However, the authors used the crystal structure of *tert*-octylammonium pravastatin to build a model structure for sodium pravastatin, although they did not try to use this to calculate an XRPD pattern to compare with any of the forms they analyzed. The authors suggested that previously reported polymorphs of sodium pravastatin may actually be mixtures due to its propensity to crystallize out in multiple forms quite readily.

Maurin et al. studied two enantiotropically related polymorphs of roxifiban by XRPD, spectroscopy, and thermal analyses (114). The FT-IR spectra were essentially identical for both forms, and the FT-Raman spectra were almost indistinguishable. The standard DSC data for each form were the same, but the modulated DSC data showed some differences. The isothermal microcalorimetry data also showed differences between the two forms. The XRPD and ^{13}C SSNMR spectroscopy data easily differentiated both forms, although some peak regions were almost identical for the SSNMR spectra indicating that only part of the molecule experienced a change in electronic environment between the two polymorphs. Form I is the stable form above 132°C, and the *n*-butyl group of roxifiban showed splitting for three of the four aliphatic carbon resonances compared to form II. The splitting of the aliphatic resonances in the spectrum of form I is not necessarily indicative of two molecules per asymmetric unit because roxifiban has several amide groups that may have restricted rotation resulting in conformational exchange. Variable-temperature SSNMR spectroscopy would be useful in clarifying this issue, and single-crystal structures of both forms would show whether there was greater disorder for the aliphatic region of form I.

SSNMR Spectroscopy of Quadrupolar Nuclei in Pharmaceuticals

Several studies have shown that nuclear quadrupolar resonance (NQR) spectroscopy can be useful in analyzing polymorphs (115,116). Blinc et al. studied polymorphs of five sulfa drugs by using polarization enhancement of the ^{14}N NQR signal from protons (115). All of the drugs and their polymorphs were readily distinguished by this technique. Quantification was possible because the signal was directly proportional to the amount of sample that contains nitrogen, but it requires 10 mg or more of the compound in a sample. The authors also note that tablets can be analyzed without removing them from the bottle.

Pérez et al. used ^{35}Cl NQR spectroscopy without enhancement to analyze chlorpropamide and sodium diclofenac (116). Chlorpropamide had two polymorphs with one molecule per asymmetric unit in each, and variable temperature ^{35}Cl NQR spectroscopy revealed a third low-temperature form with a phase transition at –85°C. Quantification was also demonstrated in this study in which the limit of detection was near 10 mg and the limit of quantification limit was approximately 20 mg. NQR is not very useful with disordered or amorphous materials because the typically broad peaks even for crystalline materials become too broad to observe reliably.

NQR spectroscopy would not be a generally applicable technique for studying pharmaceuticals, but it can be useful in certain cases.

SSNMR Spectroscopy and Structure Determination

Structural determination in the solid state has been primarily done using diffraction techniques because of their atomic resolution. SSNMR spectroscopy is potentially very powerful for determining the conformation of a molecule in the solid state, but it is practically useless for determining long-range order in solids due to its strong dependence on the local electronic environment surrounding each nucleus. The conformations of molecules in the asymmetric unit and interactions with nearest neighbors provide useful information about different solid forms. There are numerous NMR pulse sequences used for structural determinations in liquid solutions, and some of them have been modified for use in the solid state. The orientationally

dependent properties of dipolar coupling and CSA have also been exploited to determine structure of solids at relatively high resolution. The various SSNMR spectroscopy techniques can also be applied to disordered solids to analyze their structures, although the broader peaks can make the data interpretation much more difficult. The rapid developments occurring in SSNMR spectroscopy will hopefully overcome some of the current limitations, particularly the broad peaks of ^{1}H SSNMR spectroscopy. Theoretical computations of chemical shifts in solid samples is also quite common as shown in several previous examples in section "Solid-Form Characterization" on p. 398, but improvements are required to obtain more accurate chemical shifts particularly for very similar conformations that may exist in the unit cell.

Harper et al. compared the ^{13}C detected HETCOR and 2D INADEQUATE experiments for analyzing the different molecules in the asymmetric units α-santonin, catechin, and calcium acetate (117). The resolution in the proton dimension of the HETCOR analysis tends to be low, which can make it difficult to assign the resonances appropriately. The ^{13}C–^{13}C INADEQUATE experiment has very low sensitivity (e.g., several days of data acquisition) but can show the carbon-to-carbon connections of a small molecule. Although the INADEQUATE experiment takes significantly longer than the HETCOR analysis, it usually has better resolution because there is no ^{1}H dimension.

Harris et al. used the refocused INADEQUATE (Figs. 26 and 27) and the HETCOR (Figs. 28 and 29) SSNMR spectroscopy experiments to determine most of the ^{1}H and ^{13}C resonance assignments for the two different molecules in the asymmetric unit for oxybuprocaine hydrochloride modification II° (118). This required a significant amount of data acquisition time as the INADEQUATE experiment took five days, whereas the HETCOR took 17 hours. The authors also observed unusually low chemical shifts for one of the ethyl amine groups ($CH_3CH_2NH^+$) that is likely due to the *γ-gauche* shielding effect.

Harper et al. used CST data to study a polymorph of paclitaxel with two molecules per asymmetric unit (119). Although they obtained useful data from the CST results for use with the XRPD structural refinement, they could not assign the specific peaks to one or the other molecule in the asymmetric unit. Paclitaxel is quite complex compared to most of the molecules so far discussed, which is why it is much more difficult to interpret it SSNMR spectra.

Harris et al. used the ^{13}C–^{13}C INADEQUATE experiment to assign the resonances of the two molecules in the asymmetric unit of the α form of testosterone (120). The SSNMR spectroscopy information was also used to test the accuracy of computed chemical shifts. Although the chemical shift calculations were reasonably close to the observed values, they were not accurate enough to differentiate between the molecules in the asymmetric unit.

Mifsud et al. used ^{1}H–^{1}H DQ-CRAMPS, ^{1}H–^{13}C INEPT-HSQC, and computation of ^{1}H and ^{13}C chemical shifts to study crystalline penicillin G (121). The resonance assignments were determined using through-space ^{1}H–^{1}H correlations from the DQ-CRAMPS technique and the through-bond ^{1}H–^{13}C correlations from the INEPT-HSQC technique. The computational results worked reasonably well for both ^{1}H and ^{13}C chemical shifts, although the aromatic resonances are probably the least reliable considering that five to six peaks are observed in a rather narrow chemical shift range. The variety of SSNMR techniques currently available allows one to analyze solids in many ways, which will lead to improved computational predictions of NMR properties and much better structural determinations of solids.

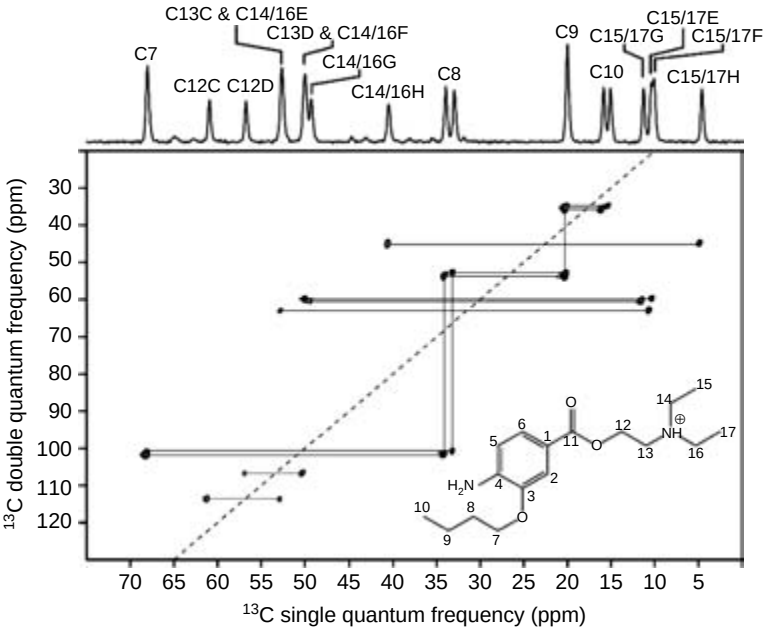

FIGURE 26 Solid-state ^{13}C INADEQUATE spectrum (low-frequency region) of oxybuprocaine hydrochloride (inset) modification II° at 11.7 T and 10 kHz MAS. The connections are shown for the two independent molecules in the asymmetric unit, and the ^{13}C resonance assignments are labeled in the 1D spectrum. Adapted from Ref. (118).

SSNMR Spectroscopy of Biopharmaceuticals

Biopharmaceuticals have been a rapid growth area in the pharmaceutical industry. Biopharmaceuticals are usually large molecules produced by living organisms, and most of those currently developed as pharmaceuticals tend to be proteins, particularly monoclonal antibodies. However, biopharmaceuticals can also be oligonucleotides, polysaccharides, and lipids with beneficial pharmacological properties. SSNMR spectroscopy is a very useful technique for studying crystalline and amorphous forms of proteins. Most pharmaceutical proteins are delivered in the lyophilized form primarily because protein crystals usually need a significant amount of liquid water to remain crystalline. The value of crystalline protein pharmaceutical formulations has been discussed in the literature (122). Production of crystalline formulation rather than the typical amorphous formulation may be beneficial for manipulating the stability or bioavailability of a biopharmaceutical.

Several studies have shown that SSNMR spectroscopy readily differentiates protein polymorphs (123,124). Five polymorphs of the protein GB1 (β1 immunoglobulin binding domain of protein G, 56 residues, ~6202 Da) were analyzed by ^{13}C SSNMR spectroscopy and XRPD (123). SSNMR spectroscopy showed the characteristic sharp peaks for the crystalline forms (Figs. 30 and 31). Although there was significant overlap due to the number of carbons in the molecule, the resolution was sufficient to easily identify the polymorphs.

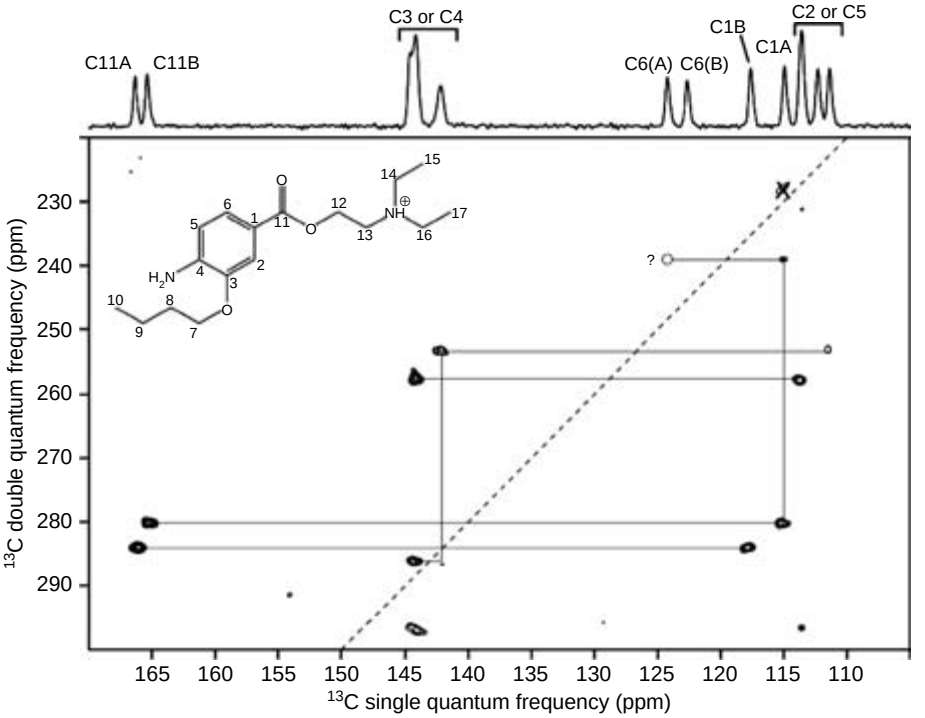

FIGURE 27 Solid-state ^{13}C INADEQUATE spectrum (high-frequency region) of oxybuprocaine hydrochloride (inset) modification II° at 11.7 T and 10 kHz MAS. The connections are shown for the two independent molecules in the asymmetric unit, and the ^{13}C resonance assignments are labeled in the 1D spectrum. Adapted from Ref. (118).

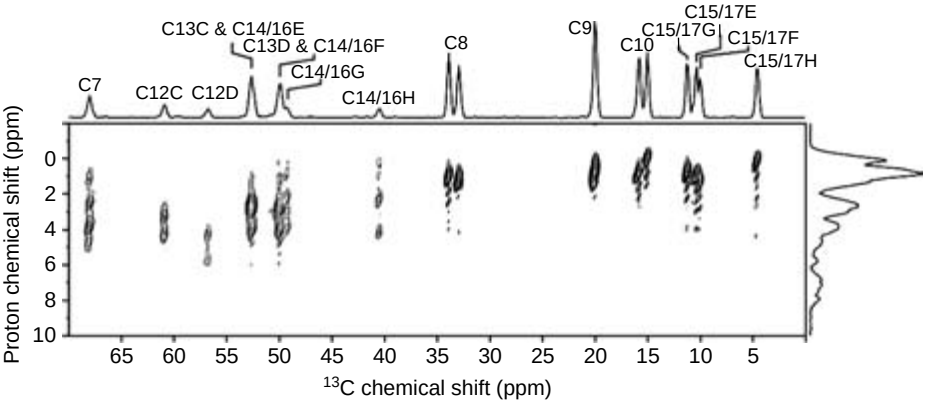

FIGURE 28 Solid-state ^{13}C–^{1}H HETCOR spectrum (low frequency region) of oxybuprocaine hydrochloride modification II° at 11.7 T and 10 kHz MAS. The ^{13}C resonance assignments are labeled in the 1D spectrum. Adapted from Ref. (118).

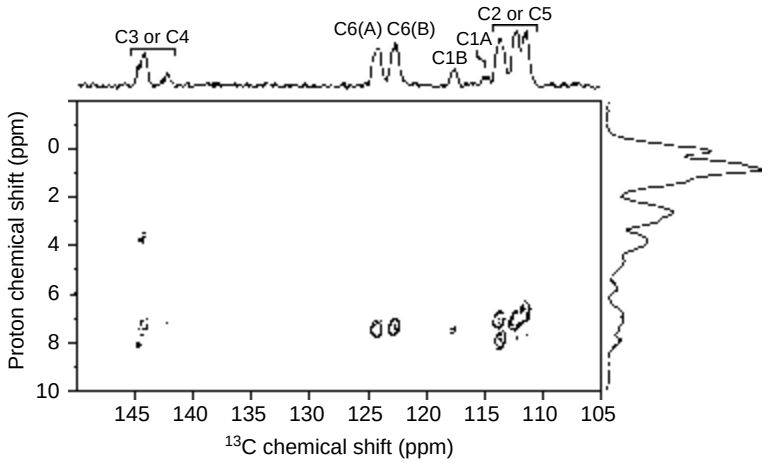

FIGURE 29 Solid-state ^{13}C–^{1}H HETCOR spectrum (high-frequency region) of oxybuprocaine hydrochloride modification II° at 11.7 T and 10 kHz MAS. The ^{13}C resonance assignments are labeled in the 1D spectrum. Adapted from Ref. (118).

Martin and Zilm analyzed five proteins with MW between ~8 and 56 kDa by ^{13}C SSNMR spectroscopy and XRPD (Figs. 32 and 33) (124). They showed that microcrystalline and nanocrystalline proteins produced essentially identical SSNMR spectra for cases where the nanocrystals were 100 nm or larger (Fig. 33). The authors also demonstrated some potentially useful procedures for making batch quantities of submicrometer size crystals and preparing small samples of wet crystals for SSNMR spectroscopy.

The need for molecular-level characterization of biopharmaceutical solids is likely to increase in the coming years as more of these molecules are developed to treat a wide variety of diseases. SSNMR spectroscopy of biopharmaceuticals may be a useful extension of liquid-state NMR spectroscopy of these large molecules. NMR spectroscopy of proteins, oligonucleotides, and polysaccharides in aqueous or organic solutions provides a detailed fingerprint of the molecule, which is a very powerful tool for comparing biopharmaceuticals. SSNMR spectroscopy is particularly useful for characterizing biopharmaceuticals because amorphous forms can be also analyzed and usually have unique spectra. Comparability of biologicals in the solid state has the potential to be a major application of SSNMR spectroscopy in pharmaceutical development.

Quantification with SSNMR Spectroscopy

The difficulties in performing quantitative SSNMR spectroscopy have been discussed by Harris (125). Stephenson et al. have reviewed quantitative X-ray diffraction, vibrational spectroscopy, and SSNMR spectroscopy (126). The main problem for quantitative SSNMR spectroscopy is ensuring that the relative peak areas are accurate for the components in the sample. For CP methods (e.g., ^{13}C CP/MAS) where the sensitivity enhancement is provided by ^{1}H to ^{13}C magnetization transfer, there are three main relaxation processes that need to be considered (127): (1) The CP time

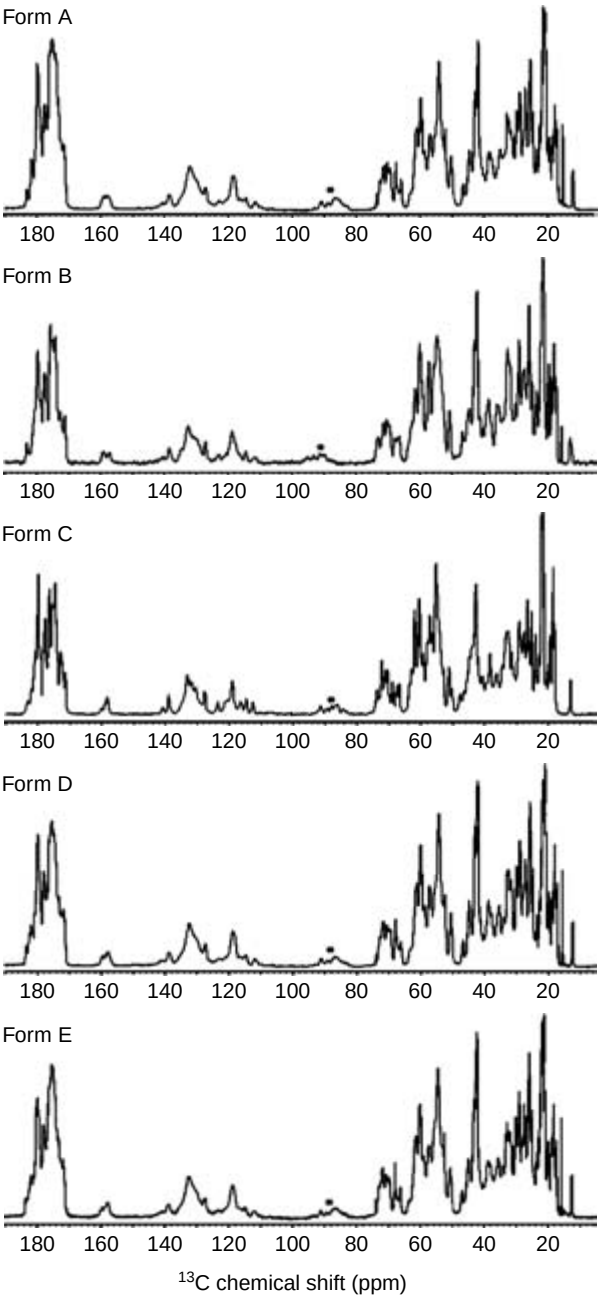

FIGURE 30 ^{13}C CP/MAS spectra of five forms of microcrystalline GB1. The spectra of forms A, D, and E were acquired at 11.7 T and 11.11 kHz MAS. The spectrum of form B was acquired at 14.1 T and 13.3 kHz MAS. The spectrum of form C was acquired at 17.6 T and 16.67 kHz MAS. Asterisks indicate spinning sidebands. Adapted from Ref. (123).

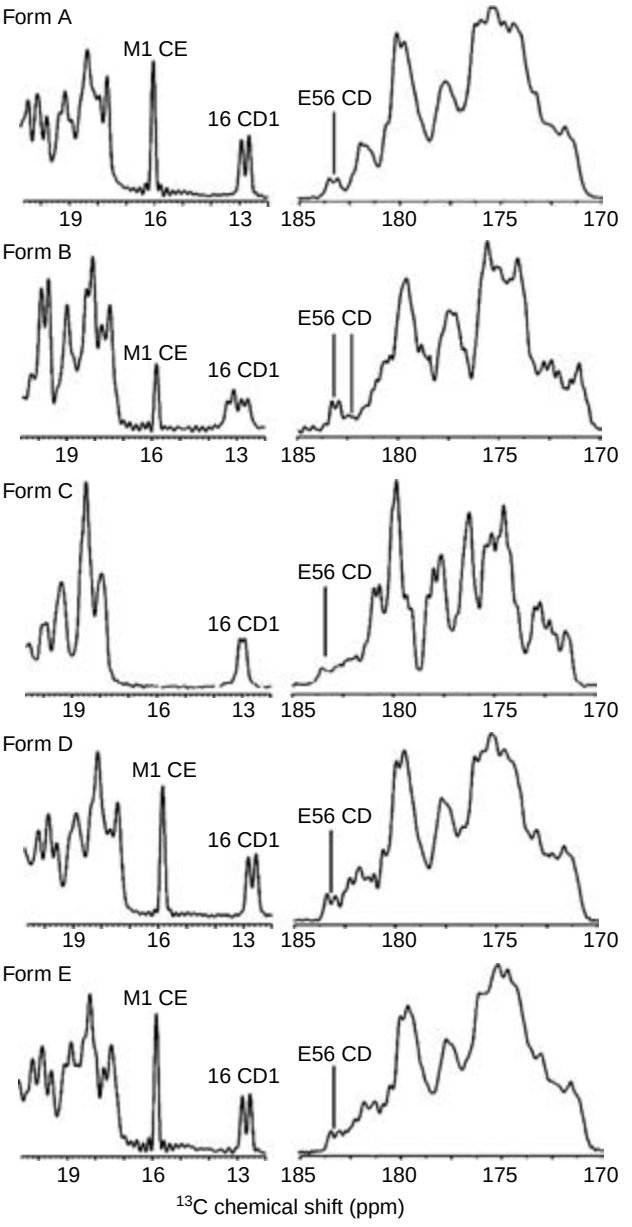

FIGURE 31 Expanded regions of the ^{13}C CP/MAS spectra of five forms of microcrystalline GB1. The carbonyl region is on the *right*, and the methyl region is on the *left*. Note that spectra of forms A, D, and E have similarities (labeled in each spectrum), but they are distinctly different and represent unique solid forms of GB1. Adapted from Ref. (123).

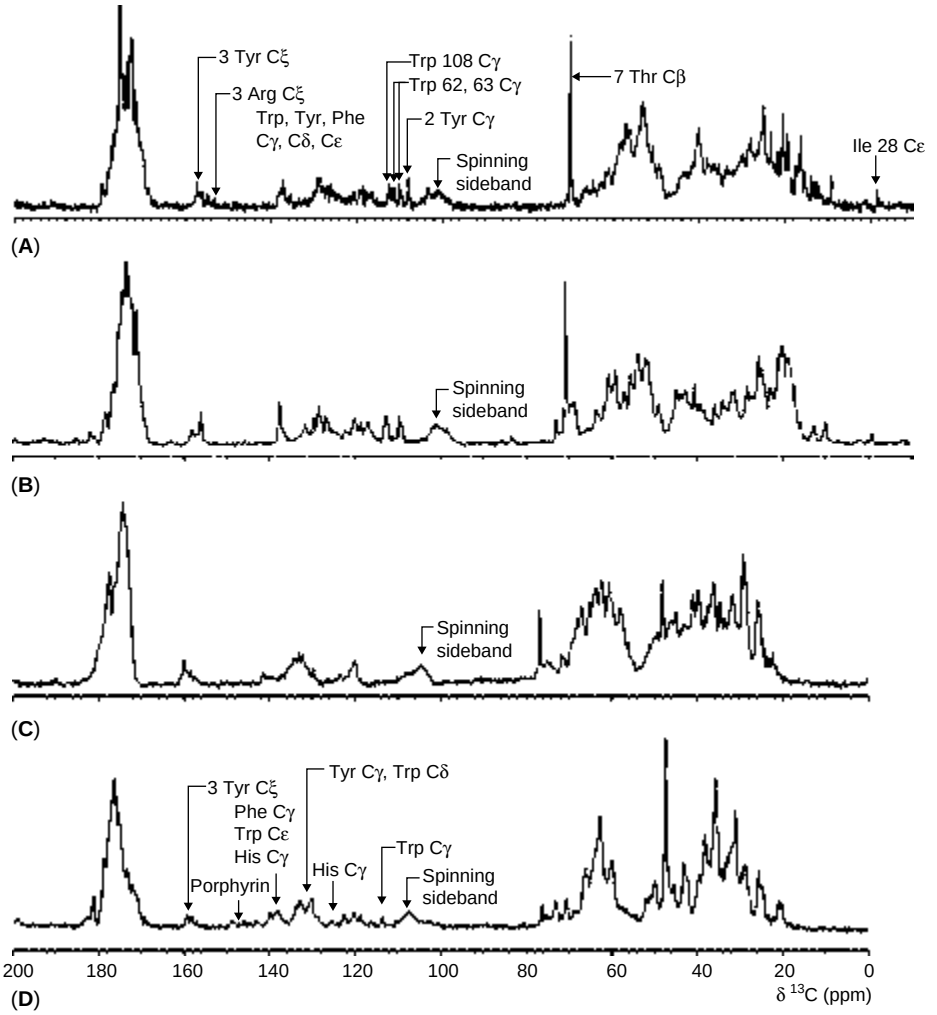

FIGURE 32 ^{13}C CP/MAS spectra of crystalline (**A**) lysozyme, (**B**) streptavidin, (**C**) ribonuclease A, and (**D**) cytochrome *c*. Some possible assignments are labeled. Adapted from Ref. (124).

(T_{CH}), (2) the rotating frame spin-lattice relaxation time for protons ($T_1\rho_H$), and (3) the spin-lattice relaxation time for protons (T_{1H}). The corresponding ^{13}C relaxation times ($T_1\rho_C$ and T_{1C}) usually to not have a significant effect on the observed signal for CP spectra. The T_{CH} determines how rapidly each carbon resonance gets enhanced by ^{1}H polarization transfer. Relatively immobile carbons with directly bonded protons will be polarized most rapidly. The $T_1\rho_H$ determines how rapidly the rotating frame ^{1}H magnetization decreases, and it competes with T_{CH} during the CP process. This means that if $T_1\rho_H$ is rapid, then T_{CH} will not be able to enhance some or all of the ^{13}C resonances sufficiently for CP to be useful. The T_{1H} determines how rapidly the equilibrium magnetization of each proton is re-established, and

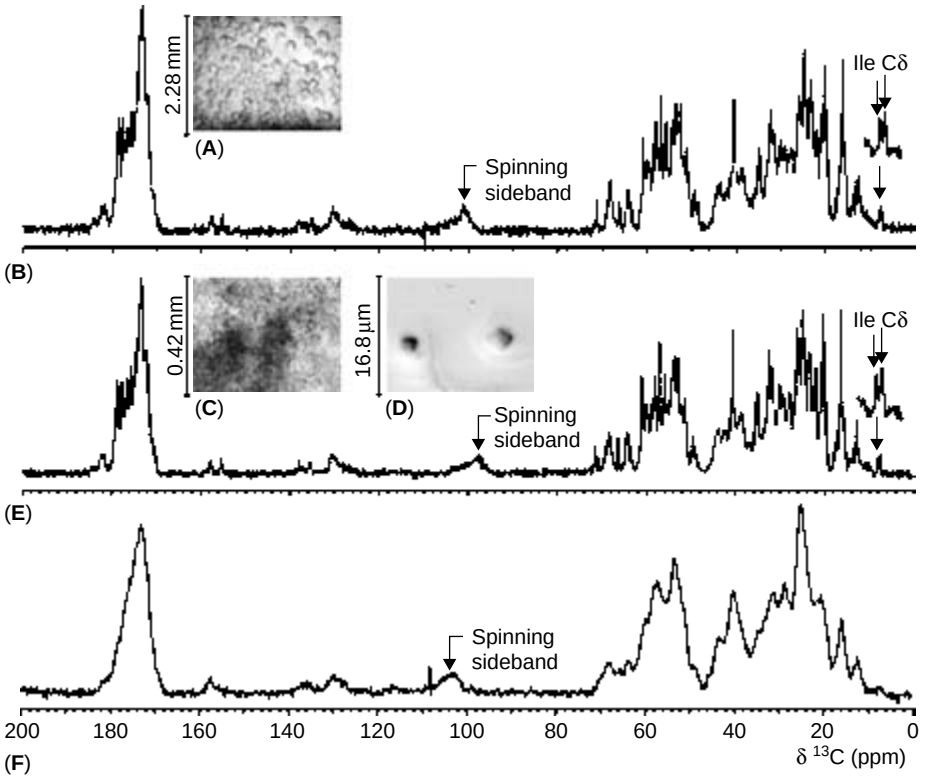

FIGURE 33 ^{13}C CP/MAS spectra of ubiquitin at 18.8 T and 14.5 kHz MAS: (**B**) microcrystalline protein, (**E**) nanocrystalline protein, and (**F**) lyophilized protein. Micrographs of the microcrystalline (**A**) and nanocrystalline (**C** and **D**) proteins are inset: (**A**) 5× magnified light microscope image of microcrystalline protein, (**B**) 225× magnified light microscope image of nanocrystalline protein, and (**C**) 4000× magnified electron microscope image of two larger crystallites in the nanocrystalline protein sample. Adapted from Ref. (124).

therefore, how long one must wait between pulses. Figure 34 shows how the length of the delay between pulses affects the recovery of magnetization. A delay of approximately three times the relevant T_1 value is required for greater than 90% of the magnetization to recover. Because protons are the most prevalent atom in pharmaceutical solids and have strong dipolar coupling, spin polarization will be rapidly distributed over the entire molecule (spin diffusion). Spin diffusion usually results in a single T_{1H} relaxation time for a compound. Even if an internal standard is used, some corrections would be necessary to obtain quantitative data from CP/MAS spectra due to the potential differences in relaxation times.

Direct polarization ^{13}C MAS experiments can be used for quantitative SSNMR analyses, but this requires waiting at least five times the T_{1C} between scans for greater than 99% of the magnetization to recover. Carbon-13 relaxation times can be several to many minutes long, making it impractical to obtain good signal averaging in a reasonable amount of time for many solid materials.

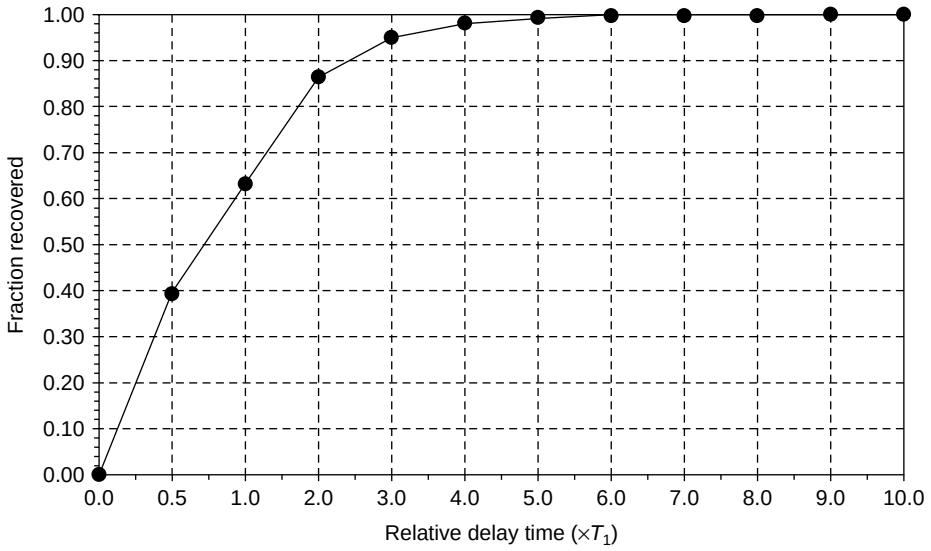

FIGURE 34 Recovery of magnetization (M_z) as a function of the amount of time allowed for relaxation.

Formoterol fumarate dihydrate was quantified at 0.45% in lactose by ^{13}C SSNMR, and the dihydrate to anhydrate ratio could be quantified to 2% in lactose (128). It is typical for quantification of polymorph mixtures to be more difficult than quantification of a single polymorph mixed with excipients because most active pharmaceutical compounds are well resolved from excipients but much less so from a polymorph.

Ziarelli et al. have discussed quantitative ^{13}C and ^{23}Na MAS SSNMR spectroscopy using an unusual external electronic signal (ERETIC™) as a quantification standard (129). They also show that using the center portion of the rotor is necessary to obtain the most accurate results, which has been previously discussed by Campbell et al. (130).

Offerdahl et al. quantified different forms of neotame by ^{13}C CP/MAS SSNMR spectroscopy (131). Their technique requires the determination of T_{CH} and $T_1\rho_H$ of the pure forms, obtaining spectra of mixtures using at least five different contact times that are $>5 \times T_{CH}$, and calculating the $T_1\rho_H$ for each component from a plot of the peak area versus contact time. The resulting graph gives a straight line with the y-intercept equal to the quantity of the particular component in the sample. The authors found a quantification limit of ~1% to 2%, and that both polymorphs contained a significant amount of amorphous material.

Miscellaneous Applications of SSNMR Spectroscopy

SSNMR spectroscopy can be used to analyze essentially any solid with NMR active nuclei. Small organic molecules are the typical compounds used for active pharmaceuticals, although larger proteins are being developed at a rapid rate.

Less commonly used as pharmaceuticals are carbohydrates, lipids, and nucleic acids. Tautomerization, ABMS, solid-state dynamics, hydrogen bonding, and pK_as can also be analyzed by SSNMR. All of these applications have potential uses in characterizing pharmaceutical solids, and some examples of these are discussed in this section.

Paradowska et al. studied seven crystalline methyl glycopyranosides by ^{13}C SSNMR spectroscopy and XRPD (132). Sugars tend to be structurally very similar and potentially difficult to differentiate by spectroscopic techniques. However, the ^{13}C SSNMR spectra were very different for each of the sugars in this study. One of the sugars had two molecules per asymmetric unit, whereas another was apparently contaminated with an unknown sugar that may have two molecules per asymmetric unit. The authors used XRPD and calculated patterns from the single-crystal structure to confirm the results from SSNMR spectroscopy.

Yoshinari et al. studied the effect of water on the β and δ polymorphs of mannitol by DSC, scanning electron microscopy (SEM), XRPD, FT-IR, ^{13}C SSNMR spectroscopy, and water vapor sorption analyses (133). SSNMR spectroscopy was used to confirm the δ polymorph because the crystal structure had not been obtained for it. Upon exposure of the δ polymorph to 97% relative humidity overnight, it completely converted to the β polymorph. The ^{1}H and ^{13}C T_1 relaxation times were obtained for the β and δ polymorphs. The ^{1}H T_1 relaxation time was quite long as is typical for sugars (~4 and ~8 minutes for β and δ, respectively), and the ^{13}C T_1 relaxation times were as much as 15 times longer than the ^{1}H T_1 relaxation times. Surprisingly, the authors used a very short relaxation delay (0.1 second) to obtain the ^{13}C SSNMR spectroscopy. This would require many more scans and more time to obtain useful data given that the relaxation delay was ~0.05% of shortest ^{1}H T_1, and 0.02% of the longest ^{1}H T_1(0). For most pure compounds with long ^{1}H T_1 relaxation times, a ^{13}C CP/MAS with an acceptable signal-to-noise ratio can be obtained using a relaxation delay of 0.5 to 1.0 times the ^{1}H T_1 relaxation time and relatively few scans (≤100). A very useful alternative for obtaining spectra of nuclei with long relaxation times is the flip-back pulse sequence (134).

Colsenet et al. used ^{13}C CST analysis and ^{1}H SSNMR spectroscopy to study hydrogen bonding in malonic acid by lyophilization of solutions at various pH values (135). The δ_{11}, δ_{22}, and δ_{iso} chemical shift tensor values had significant changes with pH, whereas the δ_{33} value did not change very much. The authors also calculated the pK_as of the carboxylate groups with ^{13}C SSNMR spectroscopy determinations of the acid to base ratios in the solid samples.

Mirmehrabi et al. used X-ray diffraction, ^{13}C SSNMR, FT-IR, scanning electron microscopy, and thermal analysis to study tautomerization in two forms of ranitidine hydrochloride (136). Tautomers undergo a configurational change in bonding to give a different isomer of the molecule, and these isomers exist in an equilibrium state among the various configurations depending on the conditions. This is in contrast to the more common conformational changes without bond breaking that lead to polymorphism. A change in protonation state is the most common tautomeric process because it requires less energy to break and reform bonds with electronegative atoms such as oxygen and nitrogen. The authors performed the ^{13}C SSNMR spectroscopy at 9.4 T with a 3.2 mm rotor and relatively fast MAS at 20 kHz. Both forms I and II appeared to have one molecule per asymmetric unit. The spectrum of form II showed significant peak broadening especially in the aliphatic region, which is consistent with a disordered crystalline solid. The single-crystal X-ray structure

confirmed the disorder in form II, but no crystal structure was obtained for form I because only small crystals (1–10 μm) could be grown. The higher degree of order in form I was obvious from the ^{13}C SSNMR spectra, although this was not confirmed by another technique in their study. The highest frequency carbon resonance (C15) was noticeably broader than the other resonances (particularly for form I) because C15 was bonded to two nitrogens. There was no asymmetrical splitting for this carbon resonance because the field strength was high enough to reduce the coupling with the ^{14}N quadrupole.

Novoa de Armas et al. studied two polymorphs of ranitidine base with XRPD, hot-stage microscopy, DSC, thermogravimetry, FT-IR spectroscopy, and ^{13}C SSNMR spectroscopy (137). The XRPD data was used to determine the crystal structure of forms I and II. The SSNMR spectra easily showed the differences between the solid forms, and that there was no indication of a mixture of tautomers as previously observed for the hydrochloride salt (136). The authors state that only X-ray crystallography can determine which tautomer is present, but SSNMR spectroscopy could also be used to do this, although it would probably be much more difficult. SSNMR analysis of the tautomers might require ^{15}N labeling for ^{15}N CP/MAS or REDOR analysis (102,103).

Barich et al. studied peak widths of ibuprofen in various formulations by ^{13}C SSNMR spectroscopy, XRPD, and SEM (138). The authors note that they could not make an amorphous form of ibuprofen, and it has no known polymorphs. The effect of ABMS was tested by mixing ibuprofen with materials that had different ABMS such as talc, hydroxypropyl methyl cellulose, and croscarmellose sodium (139,140). The concentration of the material and its particle size both affected the observed SSNMR peak widths of ibuprofen. The authors note that peak broadening observed after tableting may be due to reduction in the particle size or elimination of air from the voids. This is because air has much lower magnetic susceptibility than the surrounding solid. The authors also note that SSNMR spectroscopy can be used to study crystalline domain size, although they did not have any specific examples of this important issue in their report. The domain size of nanocrystalline materials is important for differentiating them from amorphous or disordered solids, such as solid dispersion formulations. The distance-dependent properties of NMR spectroscopy are particularly useful for studying domain sizes in solids, but this topic is outside the scope of this chapter.

Adam-Berret et al. used ^{13}C SSNMR spectroscopy to analyze the metastable α and stable β polymorphs of five triacylglycerols important in the food industry (141). The ^{1}H T_1 and T_2 relaxation times were determined a 9.4 T, whereas variable-temperature low-resolution time-domain NMR spectroscopy at 0.47 T was also used to measure the dipolar second moments of the polymorphs. They were able to distinguish the different triacyglycerol polymorphs by their different relaxation times (due to mobility differences) as well as by the chemical shift differences.

SSNMR spectroscopy can be a powerful analytical tool for partially ordered systems. Crowley et al. studied mesophases resulting from solid–solid transformations of lipids using variable-temperature ^{13}C SSNMR spectroscopy and T_1 relaxation times (142). They found that α-oleic acid and both forms of propranolol oleate were conformationally disordered crystalline phases.

Hughes and Harris used ^{13}C SSNMR spectroscopy to monitor crystallization of the α and γ polymorphs of ^{13}C-labeled glycine from H_2O and D_2O solutions (143). Both H_2O and D_2O show nucleation of α-glycine, but this converts to

γ-glycine for the D_2O solution (>80% within ~6 hours). The greater CP efficiency of α-glycine (~3-fold) was not a significant factor in observing the transformation, although the quantification would be unreliable without specifically accounting for the differences.

Xu and Harris monitored the dehydration of sodium acetate trihydrate during ^{13}C SSNMR spectroscopic analyses at several spinning rates, and confirmed the resulting solid form by XRPD (144). Their dehydration process produced form I from the trihydrate when all other studies had shown that the β form results from dehydration. A mixture of forms I and β are observed at lower spinning speed (3 kHz), and the ratio of form I increased at higher spinning speed (7 kHz). The final product after about five days was a mixture of forms I and β. Form I had previously been obtained by vacuum drying of the β form. However, the authors demonstrated with ^{13}C SSNMR spectroscopy that both form I and β are simultaneously produced during the drying process rather than an initial transformation of the trihydrate to the β form followed by dehydration to form I. Pure form β, obtained by dehydration, was also rotated at 3 and 7 kHz and did not convert to form I, which demonstrates that a transformation of form β to form I was not occurring.

SUMMARY

SSNMR spectroscopy is a versatile analytical technique for characterizing a wide variety of solid materials. Differentiating polymorphs is only one potential application, but it is critical to pharmaceutical development. SSNMR spectroscopy particularly stands out for mixture analysis, studying dynamic processes, and conformational analysis. It should be used routinely as one of the analytical techniques for characterizing pharmaceuticals as part of regulatory submissions. SSNMR spectroscopy is particularly suitable for patent applications of formulated pharmaceuticals because of its high specificity compared to XRPD or vibrational spectroscopy.

REFERENCES

1. Ripmeester JA. Application of solid state ^{13}C NMR to the Study of polymorphs, clathrates and complexes. Chem Phys Lett 1980; 74: 536–8.
2. Harris RK. NMR studies of organic polymorphs and solvates. Analyst 2006; 131: 351–73.
3. Medek A. Solid-state nuclear magnetic resonance spectrometry, Chapter 11 in Spectroscopy of Pharmaceutical Solids. In: Brittain HG, ed. New York: Taylor and Francis, 2006: 413–557.
4. Tishmack PA, Bugay DE, Byrn SR. Solid-state nuclear magnetic resonance spectroscopy — pharmaceutical applications. J Pharm Sci 2003; 92: 441–74.
5. Harris RK. Applications of solid-state NMR to pharmaceutical polymorphism and Related Matters. J Pharm Pharmacol 2007; 59: 225–39.
6. Berendt RT, Sperger DM, Isbester PK, et al. Solid-state NMR spectroscopy in pharmaceutical research and analysis. TRAC 2006; 25: 977–84.
7. Offerdahl TJ. Solid-state nuclear magnetic resonance spectroscopy for analyzing polymorphic drug forms and formulations. Pharm Tech 2006: 30: S25–S42.
8. U.S. Government. Q6A Specifications: Test Procedures and Acceptance Criteria for new drug substances and new drug products: chemical substances. Federal Register 1997; 62: 227, 62890–910.
9. Baldus M. Solid-state NMR spectroscopy: molecular structure and organization at the atomic level. Angew Chem Int Ed 2006; 45: 1186–8.

10. Reichert D. Solid-state NMR Spectroscopy and its application in analytical chemistry. Anal Bioanal Chem 2003; 376: 308–10.
11. Laws DD, Bitter H-ML, Jerschow A. Solid-state NMR spectroscopic methods in chemistry. Angew Chem Int Ed 2002; 41: 3096–139.
12. Duer MJ. Solid-State NMR Spectroscopy Principles and Applications. London: Blackwell Science Ltd, 2002.
13. Stejskal EO, Memory JD. High Resolution NMR in the Solid State. Fundamentals of CP/MAS. Oxford, U.K: Oxford University Press, 1994.
14. Jelinski LW, Melchior MT. High-Resolution NMR of Solids. In NMR Spectroscopy Techniques, 2nd edition. In: Bruch MD, ed. 1996: 417–85.
15. Friebolin H. Basic One- and Two-Dimensional NMR Spectroscopy, 4th edition. Wiley-VCH, 2005.
16. Chandrakumar N, Subramanian S. Modern Techniques in High-Resolution FT-NMR. New York: Springer Verlag, 1987.
17. Harris RK. Nuclear Magnetic Resonance Spectroscopy, A Physicochemical View. Essex, England: Longman Scientific and Technical, 1986.
18. Becker ED. High Resolution NMR, Theory and Chemical Applications, 3rd edition. San Diego: Academic Press, 2000.
19. Traficante DD. NMR concepts, in NMR Spectroscopy Techniques, 2nd edition, Chapter 1. In: Bruch MD, ed. New York: Marcel Dekker, 1996: 1–60.
20. Carrington AC, McLachlan AD. Introduction to Magnetic Resonance with Applications to Chemistry and Chemical Physics. New York: Harper and Row, 1967.
21. Slichter CP. Principles of Magnetic Resonance with Examples from Solid State Physics. New York: Harper and Row, 1963.
22. Abragam A. Principles of Nuclear Magnetism, International Series of Monographs on Physics, 32. Oxford, England: Oxford University Press, 1983.
23. Grant DM, Harris RK. Encyclopedia of Nuclear Magnetic Resonance. Hoboken, New Jersey: John Wiley & Sons, 1996 (updated 2002).
24. Fundamental Physical Constants – Complete Listing, from: http://physics.nist.gov/constants
25. Frye JS. Comparison of inversion-recovery methods for measuring longitudinal Relaxation rates. Concepts Magn Reson 1989; 1: 27–33.
26. Andrew ER, Bradbury A, Eades RG. Removal of dipolar broadening of nuclear magnetic resonance spectra of solids by specimen rotation. Nature 1959; 183: 1802–3.
27. Andrew ER. Magic angle spinning in solid state N.M.R. spectroscopy. Phil Trans R Soc Lond A 1981; 299: 505–20.
28. Dixon WT. Spinning-sideband-free and spinning-sideband-only NMR spectra in spinning samples. J Chem Phys 1982; 77: 1800–9.
29. Raleigh DP, Olejniczak ET, Griffin RG. Multiple-pulse NMR in inhomogeneously broadened rotating solids: theory of sideband suppression experiments. J Chem Phys 1988; 89: 1333–50.
30. Geen H, Bodenhausen G. Complete sideband suppression in magic angle spinning Solid-state suclear magnetic resonance for arbitrary chemical shift anisotropies. J Am Chem Soc 1993; 115: 1579–80.
31. Antzutkin ON, Song Z, Feng X, et al. Suppression of sidebands in magic-angle-spinning nuclear magnetic resonance: general principles and analytical solutions. J Chem Phys 1994; 100: 130–40.
32. Rienstra CM, Vega S, Griffin RG. Centerband intensity in sideband-suppressed magic-angle-spinning spectra. J Magn Reson 1996; A119: 256–9.
33. Antzutkin ON. Spinning manipulation in magic-angle-spinning nuclear magnetic resonance. Prog Nucl Magn Reson Spectr 1999; 35: 203–66.
34. Pines A, Gibby MG, Waugh JS. Proton-enhanced NMR of dilute spins in solids. J Chem Phys 1973; 59: 569–90.

35. Stejskal EO, Schaefer J. Magic-angle spinning and polarization transfer in proton-enhanced NMR. J Magn Reson 1977; 28: 105–12.
36. Schaefer J, Stejskal EO. Carbon-13 nuclear magnetic resonance of polymers spinning at the magic angle. J Am Chem Soc 1976; 98: 1031–2.
37. Bryce DL, Bernard GM, Gee M, et al. Practical aspects of modern routine solid-state multinuclear magnetic resonance spectroscopy: one dimensional experiments. Can J Anal Sci Spectr 2001; 46: 46–82.
38. Potrzebowski MJ, Tekely P, Dusausoy Y. Comment to 13C-NMR studies of α and γ polymorphs of glycine. Solid State Nucl Magn Reson 1998; 11: 253–7.
39. Taylor RE. Setting up 13C CP/MAS experiments. Concepts Magn Reson 2004; 22A: 37–49.
40. Taylor RE. 13C CP/MAS: application to glycine. Concepts Magn Reson A 2004; 22A: 78–89.
41. Metz G, Ziliox M, Smith SO. Towards quantitative CP-MAS NMR. Solid State Nucl Magn Reson 1996; 7: 155–60.
42. Metz G, Wu X, Smith SO. Ramped-amplitude cross polarization in magic-angle-spinning NMR. J Magn Reson A 1994; 110: 219–27.
43. Peersen OB, Wu X, Smith SO. Enhancement of CP-MAS signals by variable-amplitude cross polarization. Compensation for inhomogeneous B1 fields. J Magn Reson A 1994; 106: 127–31.
44. Peersen OB, Wu X, Kustanovich I, et al. Variable-amplitude cross-polarization MAS NMR. J Magn Reson A 1993; 104: 334–9.
45. Hediger S, Signer P, Tomaselli M, et al. A combination of slow and fast RF field modulation for improved cross polarization in solid-state MAS NMR. J Magn Reson 1997; 125: 291–301.
46. Fu R, Pelupessy P, Bodenhausen G. Freqency-modulated cross-polarization for fast magic angle spinning NMR at high fields: relaxing the hartmann-hahn condition. Chem Phys Lett 1997; 264: 63–9.
47. Baldus M, Geurts DG, Hediger S, et al. Efficient ^{15}N-^{13}C polarization transfer by adiabatic-passage hartmann-hahn cross polarization. J Magn Reson A 1996; 118: 140–4.
48. Hediger S, Meier BH, Ernst RR. Rotor-synchronized amplitude-modulated magnetic resonance spin-lock sequences for improved cross polarization under fast fagic angle sample spinning. J Chem Phys 1995; 102: 4000–11.
49. Ernst M, Samoson A, Meier GH. Low-power XiX decoupling in MAS NMR experiments. J Magn Reson 2003; 163: 332–9.
50. Detken A, Hardy EH, Ernst M, et al. Simple and efficient decoupling in magic-angle spinning solid-state NMR: the XiX scheme. Chem Phys Lett 2002; 356: 298–304.
51. De Paëpe G, Lesage A, Emsley L. The performance of phase modulated heteronuclear dipolar decoupling schemes in fast magic-angle-spinning nuclear magnetic resonance experiments. J Chem Phys 2003; 119: 4833–41.
52. De Paëpe G, Hodgkinson P, Emsley L. Improved heteronuclear decoupling schemes for solid-state magic angle spinning NMR by direct spectral optimization. Chem Phys Lett 2003; 376: 259–67.
53. Khitrin AK, Fujiwara T, Akutsu H. Phase-modulated heteronuclear decoupling in NMR of solids. J Magn Reson 2003; 162: 46–53.
54. Takegoshi K, Mizokami J, Terao T. 1H decoupling with third averaging in solid NMR. Chem Phys Lett 2001; 341: 540–4.
55. Bräuniger T, Wormald P, Hodgkinson P. Improved proton decoupling in NMR spectroscopy of crystalline solids using the SPINAL-64 sequence. Monat Chem 2002; 133: 1549–54.
56. Khitrin A, Fung BM. Design of heteronuclear decoupling sequence for solids. J Chem Phys 2000; 112: 2392–8.
57. Fung BM, Khitrin AK, Ermolaev K. An improved broadband decoupling sequence for liquid crystals and solids. J Magn Reson 2000; 142: 97–101.

58. Gan Z, Ernst RR. Frequency- and Phase-modulated heteronuclear decoupling in rotating solids. Solid State Nucl Magn Reson 1997; 8: 153–9.
59. Bennett A, Rienstra CM, Auger M, et al. Heteronuclear decoupling in rotating solids. J Chem Phys 1995; 103: 6951–8.
60. Frye JS, Maciel GE. Setting the magic angle using a quadrupolar nuclide. J Magn Reson 1982; 48: 125–31.
61. Antonijevic S, Bodenhausen G. High-resolution NMR spectroscopy by truly magic-angle spinning. Angew Chem Int Ed 2005; 44: 2935–8.
62. Barich DH, Gorman EM, Zell MT, et al. 3-methylgutaric acid as a 13C solid-state NMR standard. Solid State NMR 2006; 30: 125–9.
63. Wooten EW, Mueller KT, Pines A. New angles in nuclear magnetic resonance sample spinning. Acc Chem Res 1992; 25: 209–15.
64. Bernstein J. Conformational Polymorphism in Organic Solid State Chemistry. In: Desiraju GR. ed. Amsterdam: Elsevier, 1987: 471–518.
65. Nangia A. Conformational polymorphism in organic crystals. Acc Chem Res 2008; 41: 595–604.
66. Griesser UJ, Jetti RKR, Haddow MF, et al. Conformational polymorphism in oxybuprocaine hydrochloride. Cryst Growth Des 2008; 8: 44–56.
67. Vogt FG, Katrincic LM, Long ST, et al. Enantiotropically-related polymorphs of {4-(4-chloro-3-fluorophenyl)-2-[4-(methyloxy)phenyl]-1,3-thiazol-5-yl} acetic Acid: crystal structures and multinuclear solid-state NMR. J Pharm Sci 2008; 97: 4756–82.
68. Burger A, Ramberger R. On the polymorphism of pharmaceuticals and other molecular crystals. I. Theory of thermodynamic rules. Mikrochim Acta [Wien] 1979; II: 259–71.
69. Burger A, Ramberger R. On the polymorphism of pharmaceuticals and other molecular crystals. II. Applicability of thermodynamic rules. Mikrochim Acta [Wien] 1979; II: 273–316.
70. Maccaroni E, Alberti E, Malpezzi L, et al. Polymorphism of linezolid: a combined single-crystal, powder diffraction and NMR study. Int J Pharm 2008; 351: 144–51.
71. Naito A, Ganapathy S, McDowell CA. High resolution solid state ^{13}C NMR spectra of carbons bonded to nitrogen in a sample spinning at the sagic angle. J Chem Phys 1981; 74: 5393–7.
72. Zumbulyadis N, Henrichs PM, Young RH. Quadrupole effects in the magic-angle-spinning spectra of spin-1/2. Nuclei J Chem Phys 1981; 75: 1603–11.
73. Olivieri AC, Frydman L, Grasselli et al LE. Analysis of ^{13}C, ^{14}N residual dipolar decoupling in the ^{13}C CP/MAS NMR spectra of ribonucleosides. Magn Reson Chem 1988; 26: 281–6.
74. Ebrahimi M, Rossi P, Rogers C, et al. Dependence of ^{13}C NMR chemical shifts on conformations of RNA nucleosides and Nucleotides. J Magn Reson 2001; 150: 1–9.
75. Mooibroek S, Wasylishen RE. A carbon-13 nuclear magnetic resonance study of solid tetracyclines. Can J Chem 1987; 65: 357–62.
76. Zilm KW. Spectral editing techniques: hydrocarbon solids. In Encyclopedia of Nuclear Magnetic Resonance. In: Grant DM, Harris RK, eds. New York: John Wiley and Sons, 1996; 7: 4498–504.
77. Sheikhzadeh M, Rohani, S, Jutan A, et al. Quantitative and molecular analysis of buspirone hydrochloride polymorphs. J Pharm Sci 2007; 96: 569–83.
78. Vrbinc M, Jordan-Kotar B, Smrkolj J, et al. Characterization of physical forms of donepezil hydrochloride. Acta Chim Slov 2007; 54: 254–67.
79. Masuda K, Tabata S, Kono H, et al. Solid-state ^{13}C NMR of indomethacin polymorphism. Int J Pharm 2006; 318: 146–53.
80. Apperley DC, Forster AH, Fournier R, et al. Characterisation of indomethacin and nifedipine using variable-temperature solid-state NMR. Magn Reson Chem 2005; 43: 881–92.
81. Schmidt AC, Schwarz I, Mereiter K. Polymorphism and pseudopolymorphism of silicaine hydrochloride crystal polymorphism of local anaesthetic drugs, part V. J Pharm Sci 2006; 95: 1097–113.

82. Schmidt AC. Solid-state characterization of falicaine hydrochloride and isomorphic dyclonine hydrochloride part IV. crystal polymorphism of local anaesthetic drugs. Eur J Pharm Sci 2005; 25: 407–16.
83. Schmidt AC. Structural characteristics and crystal polymorphism of three local anaesthetic bases. crystal polymorphism of local anaesthetic drugs: part VII. Int J Pharm 2005; 298: 186–97.
84. Schmidt AC, Schwarz I. Solid state characterization of hydroxyprocaine hydrochloride. Crystal polymorphism of local anaesthetic drugs: part VIII. Int. J Mol Struct 2005; 748: 153–60.
85. Schmidt AC, Schwarz I. Solid-state characterization of non-stoichiometric hydrates of ester-type local anaesthetics. part XI. Crystal polymorphism of local anaesthetic drugs. Int J Pharm 2006; 320: 4–13.
86. Rubin-Preminger JM, Bernstein J, Harris RK, et al. [R,S]-ethambutol dihydrochloride: variable-temperature studies of a dimorphic system with very similar packing. J Pharm Sci 2004; 93: 2810–19.
87. Rubin-Preminger JM, Bernstein J, Harris RK, et al. Variable temperature studies of a polymorphic system comprising two pairs of enantiotropically related forms: [S,S]-ethambutol dihydrochloride. Cryst Growth Des 2004; 4: 431–9.
88. Moynihan HA, O'Hare IP. Spectroscopic characterization of the monoclinic and orthorhombic forms of paracetamol. Int J Pharm 2002; 247: 179–85.
89. Shaibat MA, Casablanca LB, Wickramasinghe NP, et al. Characterization of polymorphs and solid-state reactions for paramagnetic systems by ^{13}C solid-state NMR and ab initio Calculations. J Am Chem Soc 2007; 129: 10968–9.
90. Enright GD, Terskikh VV, Brouwer DH, et al. The structure of two anhydrous polymorphs of caffeine from single-crystal diffraction and ultrahigh-field solid-state ^{13}C NMR spectroscopy. Cryst Growth Des 2007; 7: 1406–10.
91. Sheth AR, Lubach JW, Munson EJ, et al. Mechanochromism of piroxicam accompanied by intermolecular proton transfer probed by spectroscopic methods and solid-phase changes. J Am Chem Soc 2005; 127: 6641–51.
92. Bates S, Zografi G, Engers D, et al. Analysis of amorphous and nanocrystalline solids from their X-ray diffraction patterns. J Pharm Res 2006; 23: 2333–49.
93. Harris RK, Ghi PY, Puschmann H, et al. Structural studies of the polymorphs of carbamazepine, its dihydrate, and two solvates. Org Proc Res Dev 2005; 9: 902–10.
94. Portieri A, Harris RK, Fletton RA, et al. Effects of polymorphic differences for sulfanilamide, as seen through ^{13}C and ^{15}N solid-state NMR, together with shielding calculations. Magn Reson Chem 2004; 42: 313–20.
95. Torchia DA. The measurement of proton-enhanced carbon-13 T1 values by a method which suppresses artifacts. J Magn Reson 1978, 30, 613–16.
96. Lee GSH, Taylor RC, Dawson M, et al. High-resolution solid state ^{13}C nuclear magnetic resonance spectra of 3,4-methylenedioxyamphetamine hydrochloride and related compounds and their mixtures with lactose. Solid State NMR 2000; 16: 225–37.
97. Reutzel-Edens SM, Kleemann RL, Lewellen PL, et al. Crystal forms of LY334370 HCl: isolation, solid-state characterization, and physicochemical properties. J Pharm Sci 2003; 92: 1196–205.
98. Antonioli G, Hodgkinson P. Resolution of ^{13}C-19F interactions in the ^{13}C NMR of spinning solids and liquid crystals. J Magn Reson 2004; 168: 124–31.
99. Wang Y, Wenslow RM, McCauley JA, et al. Polymorphic behavior of an NK1 receptor antagonist. Int J Pharm 2002; 243: 147–59.
100. Booy K-J, Weigerinck P, Vader J, et al. The use of 13C labeling to enhance the sensitivity of ^{13}C solid-state CPMAS NMR to study polymorphism in low dose solid formulations. J Pharm Sci 2005; 94: 458–63.
101. Olejniczak S, Mikula-Pacholczyk J, Hughes CE, et al. ^{15}N and ^{13}C high-resolution solid-state NMR study of the polymorphism of the L-enantiomer of N-benzoylphenylalanine. J Phys Chem B 2008; 112: 1586–93.

102. Jaroniec CP, Tounge BA, Rienstra CM, et al. Measurement of ^{13}C–^{15}N distances in uniformly ^{13}C labeled biomolecules: J-decoupled REDOR. J Am Chem Soc 1999; 121: 1023–8.
103. Schmidt-Rohr K, Hong M. Measurements of carbon to Amide-proton distances by C–H Dipolar recoupling with ^{15}N NMR detection. J Am Chem Soc 2003; 125: 5648–9.
104. Zhou J, Kye Y-S, Harbison GS. Isotopomeric polymorphism. J Am Chem Soc 2004; 126: 8392–3.
105. Othman A, Evans JSO, Evans IR, et al. Structural study of polymorphs and solvates of finasteride. J Pharm Sci 2007; 96: 1380–97.
106. Apperley DC, Basford PA, Dallman CI, et al. Nuclear magnetic resonance investigation of the interaction of water vapor with sildenafil citrate in the solid state. J Pharm Sci 2005; 94: 516–23.
107. Rafilovich M, Bernstein J, Harris RK, et al. Groth's original concomitant polymorphs revisited. Cryst Growth Des 2005; 5: 2197–209.
108. Dong Z, Padden BE, Salsbury JSW, et al. Neotame anhydrate polymorphs I: preparation and characterization. Pharm Res 2002; 19: 330–6.
109. Brown SP, Lesage A, Elena B, et al. Probing proton-proton proximities in the solid state: high-resolution two-dimensional 1H–1H double-quantum CRAMPS NMR spectroscopy. J Am Chem Soc 2004; 126: 13230–1.
110. Griffin JM, Martin DR, Brown SP. Distinguishing anhydrous and hydrous forms of an active pharmaceutical ingredient in a tablet formulation using solid-state NMR spectroscopy. Angew Chem Int Ed 2007; 46: 8036–8.
111. Zhou DH, Rienstra CM. Rapid analysis of organic compounds by proton-detected heteronuclear correlation NMR spectroscopy with 40 kHz magic-angle spinning. Angew Chem Int Ed 2008; 47: 7328–31.
112. Harris RK, Hodgkinson P, Larsson T, et al. Characterization of polymorphs and solvates of terbutaline sulfate. Cryst Growth Des 2008; 8: 80–90.
113. Martin-Islán AP, Cruzado MC, Asensio R, et al. Crystalline polymorphism and molecular structure of sodium pravastatin. J Phys Chem B 2006; 110: 26148–59.
114. Maurin MB, Vickery RD, Rabel SR, et al. Polymorphism of roxifiban. J Pharm Sci 2002; 91: 2599–604.
115. Blinc R, Seliger J, Zidanšek A, et al. ^{14}N nuclear quadrupole resonance of some sulfa drugs. Solid State Nucl Magn Reson 2006; 30: 61–8.
116. Pérez SC, Cerioni LL, Wolfenson AE, et al. Utilization of pure nuclear quadrupole resonance spectroscopy for the study of pharmaceutical crystal forms. Int J Pharm 2005; 298: 143–52.
117. Harper JK, Strohmeier M, Grant DM. Pursuing structure in microcrystalline solids with independent molecules in the unit cell using ^{1}H-^{13}C correlation data. J Magn Reson 2007; 189: 20–31.
118. Harris RK, Cadars S, Emsley L, et al. NMR crystallography of oxybuprocaine hydrochloride, modification II°. Phys Chem Chem Phys 2007; 9: 360–8.
119. Harper JK, Barich DH, Heider EM, et al. A Combined Solid-State NMR and X-ray Powder Diffraction Study of a Stable Polymorph of Paclitaxel. Cryst Growth Des 2005; 5: 1737–42.
120. Harris RK, Joyce SA, Pickard CJ, et al. Assigning carbon-13 NMR spectra to crystal structures by the INADEQUATE pulse sequence and first principles computation: a case study of two forms of testosterone. Phys Chem Chem Phys 2006; 8: 137–43.
121. Mifsud N, Elena B, Pickard CJ, et al. Assigning powders to crystal structures by high-resolution ^{1}H-^{1}H double quantum and ^{1}H-^{13}C J-INEPT solid-state NMR spectroscopy and first principles computation. A case study of penicillin. G Phys Chem Chem Phys 2006; 8: 3418–22.
122. Jen A, Merkle HP. Diamonds in the rough: protein crystals from aformulation perspective Pharm Res 2001; 18: 1483–8.

123. Frericks Schmidt HL, Sperling LJ, Gao YG, et al. Crystal polymorphism of protein GB1 examined by solid-state NMR spectroscopy and X-ray diffraction. J Phys Chem B 2007; 111: 14362–9.
124. Martin RW, Zilm KW. Preparation of protein nanocyrstals and their characterization by solid state NMR. J Magn Reson 2003; 165: 162–74.
125. Harris RK. Quantitative aspects of high-resolution solid-state nuclear magnetic resonance spectroscopy. Analyst 1985; 110: 649–55.
126. Stephenson GA, Forbes RA, Reutzel-Edens SM. Characterization of the solid state: quantitative issues. Adv Drug Delivery Rev 2001; 48: 67–90.
127. Kolodziejski W, Klinowski J. Kinetics of cross-polarization in solid-state NMR: a guide for chemists. Chem Rev 2002; 102: 613–28.
128. Apperley DC, Harris RK, Larrson T, et al. Quantitative nuclear magnetic resonance analysis of solid formoterol fumarate and Its dihydrate. J Pharm Sci 2003; 92: 2496–503.
129. Ziarelli F, Viel S, Sanchez S, et al. Precision and sensitivity optimization of quantitative measurements in solid state NMR. J Magn Reson 2007; 188: 260–6.
130. Campbell GC, Galya G, Beeler AJ, et al. Effect of RF inhomogeneity upon quantitative solid-state NMR measurements. J Magn Reson A 1995; 112: 225–8.
131. Offerdahl TJ, Salsbury JS, Dong Z, et al. Quantitation of crystalline and amorphous forms of anhydrous neotame using ^{13}C CPMAS NMR spectroscopy. J Pharm Sci 2005; 94: 2591–605.
132. Paradowska K, Gubica T, Termeriusz A, et al. 13C CP MAS NMR and crystal structure of methyl glycopyranosides. Carb RM,es 2008; 343: 2299–307.
133. Yoshinari T, Forbes RT, York P, et al. Moisture induced polymorphic transition of mannitol and Its morphological transformation. Int J Pharm 2002; 247: 69–77.
134. Tegenfeldt J, Haeberlen U. Cross polarization in solids with flip-back of I-spin magnetization. J Magn Reson 1979; 36: 453–7.
135. Colsenet R, Gardiennet C, Henry B, et al. A straightforward detection of deprotonated conformers of malonic acid by solid-state 13C NMR spectroscopy. Angew Chem Int Ed 2002; 41: 4743–5.
136. Mirmehrabi M, Rohani S, Murthy KSK, et al. Characterization of tautomeric forms of ranitidine hydrochloride: thermal analysis, solid-state NMR, X-ray. J Cryst Growth 2004; 260: 517–26.
137. Novoa de Armas H, Peeters OM, Blaton N, et al. Solid state characterization and crystal structure from X-ray powder diffraction of two polymorphic forms of ranitidine base. J Pharm Sci 2008; 98: 146–58.
138. Barich DH, Davis JM, Schieber LJ, et al. Investigation of solid-state NMR line widths of ibuprofen drug formulations. J Pharm Sci 2006; 95: 1586–94.
139. VanderHart DL. Magnetic susceptibility and high resolution NMR of liquids and solids, in Encyclopedia of NMR. In: Grant D, Harris R, eds. New York: John Wiley & Sons, 1996: 2938–46.
140. Samoson A, Tuherm T, Gan Z. High-Field high-speed MAS resolution enhancement in ^{1}H NMR spectroscopy of solids. Solid State NMR 2001; 20: 130–6.
141. Adam-Berret M, Rondeau-Mouro C, Riaublanc A, et al. Study of triacylglycerol polymorphs by nuclear magnetic resonance: effects of temperature and chain length on relaxation parameters. Magn Reson Chem 2008; 46: 550–7.
142. Crowley KJ, Forbes RT, York P, et al. Characterization of oleic acid and propranolol oleate mesomorphism using ^{13}C solid-state nuclear magnetic resonance spectroscopy (SSNMR). J Pharm Sci 2000; 89: 1286–95.
143. Hughes CE, Harris KDM. A technique for in situ monitoring of crystallization from solution by solid-state ^{13}C CPMAS NMR spectroscopy. J Phys Chem A 2008; 112: 6808–10.
144. Xu M, Harris KDM. Altering the polymorphic product distribution in a solid-state dehydration process by rapid sample rotation in solid-state NMR Probe. J Am Chem Soc 2005; 127: 10832–3.

12 Effects of Polymorphism and Solid-State Solvation on Solubility and Dissolution Rate

Harry G. Brittain
Center for Pharmaceutical Physics, Milford, New Jersey, U.S.A.
David J. R. Grant
College of Pharmacy, University of Minnesota, Minneapolis, Minnesota, U.S.A.
Paul B. Myrdal
College of Pharmacy, University of Arizona, Tucson, Arizona, U.S.A.

INTRODUCTION

It has now been amply demonstrated that the different lattice energies (and entropies) associated with different polymorphs or solvates give rise to measurable differences in the physical properties (density, color, hardness, refractive index, conductivity, melting point, enthalpy of fusion, vapor pressure, etc.). Even the explosive power of cyclotetramethylene-tetranitramine depends on which of its four polymorphs is being used (1). We have seen in previous chapters that the different lattice energies of polymorphs or solvates give rise to different solubilities and dissolution rates. If the solubilities of the various solid forms are sufficiently different, they can be very important during the processing of drug substances into drug products (2), and may have implications for the adsorption of the active drug from its dosage form (3). These concerns have led to an increased regulatory interest in the solid-state physics of drug substances, and in their characterization (4–10).

That the crystal structure can have a direct effect on the solubility of a solid can be understood using a simple model. For a solid to dissolve, the forces of attraction between solute and solvent molecules must overcome the attractive forces holding the solid intact and the solvent aggregates together. In other words, the solvation free energy released upon dissolution must exceed the lattice free energy of the solid plus the free energy of cavity formation in the solvent for the process to proceed spontaneously. The balance of the attractive and disruptive forces will determine the equilibrium solubility of the solid in question (which is an exponential function of the free energy change of the system). The enthalpy change and the increase in disorder of the system (i.e., the entropy change) determine the Ostwald free energy change. Because different lattice energies (and enthalpies) characterize different crystal structures, the solubility of different crystal polymorphs (or solvate species) must differ as well. Finally, the act of dissolution may be endothermic or exothermic in nature, so that measurements of solution calorimetry can be used to provide important information on the substance under study. The most common solvent media used in the characterization of polymorphs or solvates are liquids or liquid mixtures that give rise to liquid solutions of the solute (11) and that constitute the focus of this chapter.

The effect of polymorphism becomes especially critical on solubility because the rate of compound dissolution must also be dictated by the balance of attractive and

disruptive forces existing at the crystal–solvent interface. A solid having a higher lattice free energy (i.e., a less stable polymorph) will tend to dissolve faster, because the release of a higher amount of stored lattice free energy will increase the solubility and hence the driving force for dissolution. At the same time, each species would liberate (or consume) the same amount of solvation energy, because all dissolved species (of the same chemical identity) must be thermodynamically equivalent. The varying dissolution rates possible for different structures of the same drug entity can, in turn, lead to varying degrees of bioavailability for different polymorphs or solvates. To achieve bioequivalence for a given drug compound usually requires equivalent crystal structures in the drug substance, although exceptions are known to exist.

The dissolution rate and solubility in a solvent medium are one of the most important characteristics of a drug substance, because these quantities determine the bioavailability of the drug for its intended therapeutic use. Solubility is defined as the equilibrium concentration of the dissolved solid (the solute) in the solvent medium, and is ordinarily a function of temperature and pressure.

EQUILIBRIUM SOLUBILITY

The capacity of any system to form solutions has limits imposed by the phase rule of Gibbs:

$$F + P = C + 2 \tag{1}$$

where F is the number of degrees of freedom in a system consisting of C components with P phases. For a system of two components and two phases (e.g., solid and liquid) under the pressure of their own vapor and at constant temperature, F equals zero. If one of the phases consists solely of one component (a pure substance), the equilibrium solubility at constant temperature and pressure is a fixed quantity that is given as the amount of solute contained in the saturated solution in a unit amount of the solvent or solution.

For any case in which F is zero, a definite reproducible solubility equilibrium can be reached. Complete representation of the solubility relations is accomplished in the phase diagram, which gives the number, composition, and relative amounts of each phase present at any temperature in a sample containing the components in any specified proportion. Solubilities may therefore be expressed in any appropriate units of concentration, such as the quality of the solute dissolved (defined mass, number of moles) divided by the quantity either of the solvent (defined mass, volume, or number of moles) or of the solution (defined mass, volume, or number of moles). Jacques et al. have provided a compilation of the expressions for concentration and solubility (12).

Determination of Equilibrium Solubility

Methods for the determination of solubility have been thoroughly reviewed (11,13–15), especially with respect to the characterization of pharmaceutical solids (16). Solubility is normally highly dependent on temperature, so the temperature must be recorded for each solubility measurement in addition to the precise nature of the solvent and the solid phase at equilibrium. Plots of solubility against temperature are commonly used for characterizing pharmaceutical solids, and have been extensively discussed (11,17,18). Frequently (especially over a relatively

narrow temperature range), a linear relationship may be given either by a van't Hoff plot:

$$\ln X_2^{sat} = (-a/RT) + c' \tag{2}$$

or by a Hildebrand plot:

$$\ln X_2^{sat} = (b/R)\ln T + c'' \tag{3}$$

In equations (2) and (3), X_2^{sat} is the mole fraction solubility of the solid solute at an absolute temperature T, a is the apparent molar enthalpy of solution, b is the apparent molar entropy of solution, and c' and c'' are constants. The combined equation, attributed to Valentiner, has been used by Grant et al. (17) in the form:

$$\ln X_2^{sat} = (-a/RT) + (b/R)\ln T + c''' \tag{4}$$

This three-parameter equation enables solubility to be simulated and correlated quite accurately over a wide temperature range (e.g., 60°C).

As implied in the previous paragraph, the validity of the afore-mentioned equations requires that each crystal phase is stable with respect to the absence of any phase conversion during the determination of equilibrium solubility. Quite different methods of analysis must be considered if the substance under study is known to undergo a solution-mediated phase transformation.

Two general methods, the analytical method and the synthetic method (16), are available for determining solubility. In the analytical method, the temperature of equilibration is fixed, whereas the concentration of the solute in a saturated solution is determined at equilibrium by a suitable analytical procedure. The analytical method can be either the traditional, common batch agitation method, or the more recent flow column method. In the synthetic method, the composition of the solute–solvent system is fixed by appropriate addition and mixing of the solute and solvent, then the temperature at which the solid solute just dissolves or just crystallizes is carefully bracketed.

Another technique that has recently gained attention is that of the potentiometric titration method (19–21). The results of this technique have been favorably compared to that of the analytical shake flask method (20). In order to utilize this method a compound must be ionizable with some appreciable solubility. If compound solubility is too low, then cosolvents may be utilized; however, this complicates and can confound analysis. Fioritto et al. investigated the pH-metric method for determining the solubility and conversion of eight polymorphic compounds (22). Llinas et al. have used a potentiometric method referred to as the "chasing equilibrium" method (23) to determine the inter-conversion and solubility properties of hydrate polymorphs of sparfloxacin (24).

It is usually not difficult to determine the solubility of solids that are moderately soluble (greater than 1mg/mL), but the direct determination of solubilities much less than 1mg/mL is not straightforward. Problems such as slow equilibrium resulting from a low rate of dissolution, the influence of impurities, the apparent heterogeneity in the energy content of the crystalline solid (25), and analytical variability, can lead to large discrepancies in reported values. For example, reported values of the aqueous solubility of cholesterol range from 0.25 to 2600 mg/mL (26).

Metastable Solubility

Because only one member of a family of polymorphs or solvates can be the most thermodynamically stable form under a given set of environmental conditions defined by the phase rule, one frequently finds that one form spontaneously converts to another form during the time required to establish equilibrium solubility. The existence of an unexpected metastable solubility can lead to important (and possible undesirable) consequences. For digoxin, unexpectedly high solubility values and abnormally high dissolution rates have resulted in the overdosing of patients before the phenomenon of its solid-state phase conversion was properly understood and controlled (27). This phenomenon was caused by higher energy crystals resulting from a greater density of crystal defects rather than by polymorphism.

Any metastable phase will have a higher free energy than would a thermodynamically more stable phase, and will undergo a phase transformation to the more stable phase once the activation energy barrier is overcome. Often the barrier to phase transformation is merely the improbability of a suitable nucleation step. Hence, only fortuitously unfavorable kinetics permitted a determination of the equilibrium solubility of the various higher energy phases discussed in the preceding section.

Conversions of a metastable phase into a more stable phase may include the transformation of one polymorphic phase into another, the solvation of an anhydrous phase, the desolvation of a solvate phase, the transformation of an amorphous phase into a crystalline anhydrate or solvate phase, the degradation of a crystalline anhydrate or solvate phase to an amorphous phase, or in the case of digoxin, the conversion of imperfect (less crystalline, more amorphous) crystals with a high density of defects into more perfect (more crystalline) crystals with a lower density of defects. Although it is straightforward to determine the equilibrium solubility of a phase that stablizes with respect to conversion, the measurement of solubilities of metastable phases that are susceptible to conversion is not a trivial matter.

Because determinations of the solubility of solid materials are often made by suspending an excess of the compound in question in the chosen solvent or other dissolution medium, the application of this equilibrium method to a metastable phase will result in a determination of the solubility of the stable phase. One of the attempts to measure the solubility of a metastable polymorph was made by Milosovich, who developed a method based on the measurement of the intrinsic dissolution rates (IDR) and used it to deduce the relative solubilities of sulfathiazole Forms I and II (28). This method assumes that the IDR is proportional to the solubility, the proportionality constant being the transport rate constant that is constant under constant hydrodynamic conditions in a transport-controlled dissolution process. Nogami et al. have also used intrinsic dissolution rate models for characterizing compounds that have metastable states with relatively fast conversion times (29,30).

Ghosh and Grant have developed an extrapolation technique to determine the solubility of a crystalline solid that undergoes a phase change upon contact with a solvent medium (31). They proposed a thermodynamic cycle analogous to Hess's law, but based on free energies, and used this cycle to predict the theoretical solubility of solvates in water. In the model systems to which the technique was applied, good agreement was obtained between the solubility values measured

by equilibration (and derived from an extrapolation method in a mixed solvent system), and those derived from the extrapolation method and calculated by means of the thermodynamic cycle.

A light-scattering method has recently been described for the determination of the solubility of drugs, and its application to solubility evaluations of metastable phases has also been demonstrated (32). Using this technique to deduce solubility data for theophylline anhydrate (metastable with respect to the monohydrate phase in bulk water at room temperature), agreement with the most reliable literature data was excellent. The light-scattering method appears to be most useful in the determination of solubility data for metastable crystal phases in dissolution media in which they spontaneously and rapidly convert into a more stable crystal phase.

Because the solubility determination of metastable polymorphs is often challenging due to conversion kinetics, it is useful to pursue theoretical calculations based on pure component properties (e.g., transition temperatures, entropy, and enthalpy of melting). Indeed, the rigorous derivation of polymorph ideal solubility from first principals can be considered and is detailed elsewhere (18,33,34). A practical consideration when using the ideal solubility equation is to assume that polymorphs have similar heat capacity terms, and that the change in the heat capacity from the solid to the liquid state is negligible. Using these heat capacity assumptions, Mao et al. (34) have shown that for a monotropic polymorph system, the relationship between the solubility of polymorph 1 (X_1) and polymorph 2 (X_2) is,

$$\log \frac{X_1^{(i)}}{X_2^{(i)}} \approx \frac{\Delta H_{m2} - \Delta H_{m1}}{RT} + \frac{\Delta S_{m2} - \Delta S_{m1}}{R} \tag{5}$$

where ΔH_m and ΔS_m are the enthalpy and entropy of melting, respectively.

For the enantiotropic systems, the difference in solubility between two forms is

$$\ln \frac{X_1^{(i)}}{X_2^{(i)}} \approx \frac{\Delta S_t (T_t - T)}{RT} \tag{6}$$

where T_t is the transition temperature and ΔS_t is the entropy of transition.

Mao et al. found that the calculated solubility ratios based on good thermal data were in good agreement for representative enantiotropic and monotropic experimental data. From their work they provided a guide for calculating polymorph solubility ratios based on differential scanning calorimetry (DSC) thermal observations. A modified guide is given in Table 1.

Apparent Solubilities of Polymorphic Systems

The thermodynamic relationships examined in involving polymorphism and solubility has been applied to the methylprednisolone system (35). The solubilities of the two polymorphs of this steroid were determined at various temperatures in water, decyl alcohol, and dodecyl alcohol. Because the chemical potential and thermodynamic activity of the drug in the solid state and in each saturated solution is constant, the solubility ratios for the two forms (which may be found in Table 2) were found to be independent of the solvent. The enthalpy, entropy, and temperature

TABLE 1 Decision Scheme for Choosing a Solubility Ratio Equation Based on Different DSC Thermal Observations

Observations				Methodology		
Transition observed?	**Melting point**	**Heat of event[a]**	**Solubility**	**Relationship[b]**	**Transition temperature[a]**	**Equation[c]**
No	$T_2 > T_1$	$\Delta H_{m2} > \Delta H_{m1}$	$S_1 > S_2$	Monotropic	n.a.	Mono (M)
Yes	No T_1 T_2 seen	$\Delta H'_t$ seen No ΔH_{m1} ΔH_{m2} seen	$S_1 > S_2$	Enantiotropic	$T_t \leq T'_t$ $T_t < T$	Enant (E)
Yes	No T_1 T_2 seen	$\Delta H'_t$ seen No ΔH_{m1} ΔH_{m2} seen	$S_2 > S_1$	Enantiotropic	$T_t \leq T'_t$ $T < T_t$	Enant (E)
No	$T_2 > T_1$	$\Delta H_{m1} > \Delta H_{m2}$	$S_2 > S_1$	Enantiotropic	$T_t > T$	Mono (M)
No	$T_2 > T_1$	$\Delta H_{m1} > \Delta H_{m2}$	$S_1 > S_2$	Enantiotropic	$T_t < T$	Mono (M)

Adapted from Ref. (34).
[a]T_t is the equilibrium transition temperature and T'_t is the solid–solid transition temperature observed by DSC ($\Delta H'_t$ is the heat at T'_t).
[b]Relationship represents the actual thermodynamic relationship between the polymorphs.
[c]Equation refers to the equation that can be used in practice to estimate the solubility ratio based on the data observed.

TABLE 2 Equilibrium Solubility and Solubility Ratios of the Polymorphs of Methylprednisolone in Different Solvent Systems (35)

Temperature (°C)	**Solubility (mg/mL)**		
	Form I	**Form II**	**Solubility ratio (II/I)**
In Water			
30	0.09	0.15	1.67
39	0.12	0.20	1.67
49	0.16	0.26	1.63
60	0.21	0.33	1.57
72	0.30	0.43	1.43
84	0.43	0.55	1.28
In Decyl Alcohol			
30	2.9	4.8	1.66
39	3.5	5.7	1.63
49	4.3	6.9	1.60
60	5.5	8.6	1.56
72	8.3	11.9	1.43
84	–	–	–

of transition calculated from the data were 1600 cal/mol, 4.1 cal/K·mol, and 118°C, respectively.

Solubility determinations were used to characterize the polymorphism of 3-(((3-(2-(7-chloro-2-quinolinyl)-(*E*)-ethenyl)-phenyl)-((3-dimethylamino-3-oxopropyl)-thio)-methyl)-thio)-propanoic acid (36). The solubility of Form II was

TABLE 3 Equilibrium Solubility of Phenylbutazone Polymorphs, at Ambient Temperature in Different Solvent Systems (37)

Solvent system	Solubility (mg/mL)				
	I	II	IV	V	III
pH 7.5 Phosphate buffer	4.80	5.10	5.15	5.35	5.9
Above buffer with 0.05% Tween 80	4.50	4.85	4.95	5.10	5.52
Above buffer with 2.25% PEG 300	3.52	5.77	5.85	6.15	6.72

Note: The polymorphs are listed in order of increasing free energy at ambient temperature.

found to be higher than that of Form I in both isopropyl alcohol (IPA, solubility ratio approximately 1.7 from 5°C to 55°C) and in methyl ethyl ketone (MEK, solubility ratio approximately 1.9 from 5°C to 55°C), indicating that Form I is the thermodynamically stable form in the range of 5°C to 55°C. An analysis of the entropy contributions to the free energy of solution from the solubility results implied that the saturated IPA solutions were more disordered than were the corresponding MEK solutions, in turn, indicating the existence of stronger solute–solvent interactions in the MEK solution. This finding corroborated results determined for the enthalpy with respect to the relative idealities of the saturated solutions.

Phenylbutazone has been found capable of existing in five different polymorphic structures, characterized by different X-ray powder diffraction patterns and melting points (37). The equilibrium solubilities of all five polymorphs in three different solvent systems are summarized in Table 3. Form I exhibits the highest melting point (suggesting the least energetic structure at the elevated temperature), whereas its solubility is the lowest in each of the three solvent systems studied (actually demonstrating the lowest free energy). These findings indicate that Form I is the thermodynamically most stable polymorph both at room temperature and at the melting point (105°C). However, identification of the sequence of stability for the other forms at any particular temperature was not straightforward. Following one common convention, the polymorphs were numbered in the order of decreasing melting points, but the solubility data does not follow this order. This finding implies that the order of stability at room temperature is not the same as that at 100°C, and emphasizes that only measurements of solubility can predict the stability order at room temperature. If different polymorphs are not discovered in the same study, they are ordinarily numbered according to the order of discovery to avoid re-numbering those discovered earlier. Ostwald's rule of stages, discussed in Chapter 1, explains why metastable forms are often discovered first.

Gepirone hydrochloride was found to exist in at least three polymorphic forms, whose melting points were 180°C (Form I), 212°C (Form II), and 200°C (Form III) (38). Forms I and II, and Forms I and III, were deduced to be enantiotropic pairs in the sense that their G versus T curves crossed. Form III was found to be monotropic with respect to Form II, because the G versus T curves did not cross below their melting points, and because there was no temperature at which Form III was the most stable polymorph. The solubility data illustrated in Figure 1 were used to estimate a transition temperature of 74°C for the enantiotropic Forms I and II, whereas the reported enthalpy difference was 4.5 kcal/mot at 74°C and 2.54 kcal/mot at 25°C.

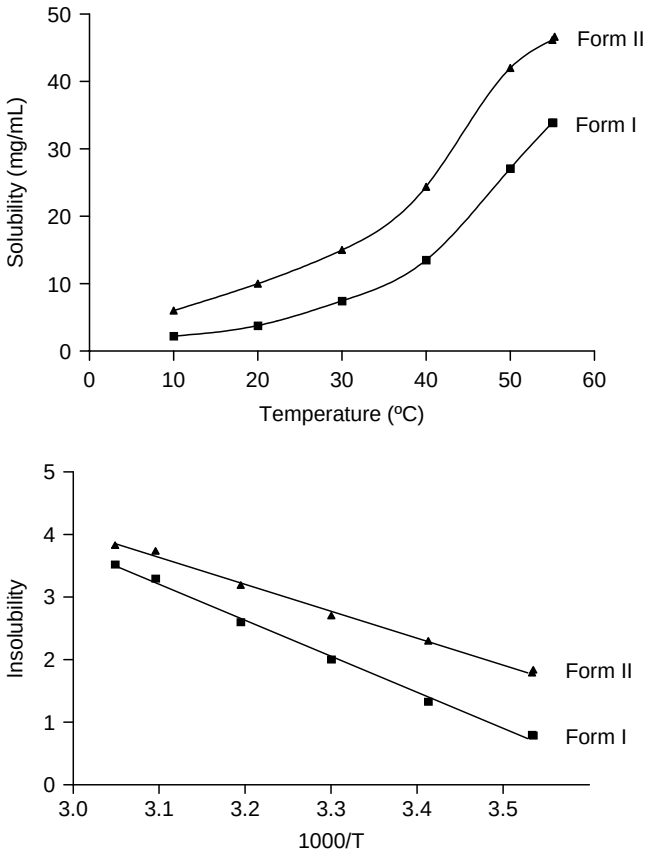

FIGURE 1 Temperature dependence of the equilibrium solubilities of two polymorphic forms of gepirone hydrochloride (38).

The most stable polymorph below 74°C was Form I, whereas Form II was the most stable above 74°C.

The effect of solvent composition on the solubility of polymorphs was investigated with cimetidine (39). Both forms exhibited almost identical melting points, but Form B was found to be less soluble than Form A, identifying it as the most stable polymorph at room temperature. The two forms were more soluble in mixed water–isopropanol solvents than in either of the pure solvents, reflecting the balance between the solvation of the molecules by water and isopropanol in determining the activity coefficient of the solute, and hence, the solubility. At constant temperature, the difference in the Gibbs free energy and the solubility ratio were constant, independent of the solvent system.

The equilibrium solubilities of two polymorphs of an experimental anti-viral compound were used to verify the results of solubility ratio predictions made on the basis of melting point and beat of fusion data (40). Even though the solubilities of Forms I and III were almost equal in three different solvent systems, the theoretically

calculated solubility ratio agreed excellently with the experimentally derived ratios in all of the solvent systems studied. The highest melting form (Form I) was found to be more soluble at room temperature, indicating that an enantiotropic relationship existed between Forms I and III.

It is well established that the temperature range of thermodynamic stability (and certain other quantities) can be determined from measurements of the equilibrium solubilities of the individual polymorphs (41). In one such study, the two polymorphic forms of 2-[[4-[[2-(1*H*-tetrazol-5-ylmethyl)-phenyl]-methoxy]-phenoxy] methyl]-quinoline were found to exhibit an enantiotropic relationship, because their *G* versus *T* curves intersected with Form I melting at a lower temperature than did Form II (42). Form I was determined to be the more thermodynamically stable form at room temperature, although the solubility of the two forms was fairly similar. The temperature dependence of the solubility ratio of the two polymorphs afforded the enthalpy of transition (Form II to Form I) as +0.9 kcal/mol, whereas the free energy change of this transition was –0.15 kcal/mol.

Aqueous suspensions of tolbutamide were reported to thicken to a nonpourable state after several weeks of occasional shaking, whereas samples of the same suspensions that were not shaken showed excellent stability after years of storage at ambient and elevated temperature (43). Examination by microscopy revealed that the thickening was due to partial conversion of the original plate-like tolbutamide crystals to very fine needle-shaped crystals. The new crystals were identified as a different polymorphic form, and did not correspond either to a solvate species or to crystals of a different habit. The crystalline conversion was observed to take place in a variety of solvents, the rate of conversion being faster in solvents where the drug exhibited appreciable solubility. Because the conversion rate in 1-octanol was relatively slow, use of this solvent permitted an accurate solubility ratio of 1.22 to be obtained (Form I being more soluble than Form III).

The polymorphism and phase interconversion of sulfamethoxydiazine (sulfameter) have been studied in detail (44). This compound can be obtained in three distinct crystalline polymorphs, with the metastable Form II being suggested for use in solid dosage forms on the basis of its greater solubility and bioavailability (45). However, the formulation of Form II in aqueous suspensions was judged inappropriate because of the fairly rapid rate of transformation to Form III. This behavior is illustrated in Figure 2, which shows that seeding of a Form II suspension with Form III crystals greatly accelerates the phase conversion. It was subsequently learned that phase conversion could be retarded by prior addition of various formulation additives, possibly permitting the development of a suspension containing the metastable Form II (46). Although there are many examples of the conversion of a metastable polymorph to a stable polymorph during the dissolution process, some of them seminal (47,48), the use of tailor-made additives to inhibit the crystallization of a more stable polymorph is relatively recent (49–52).

Table 4 provides a practical perspective of the differences in solubility that may be observed for compounds that exhibit different polymorphic states. The experimental data in Table 4 is a non-exhaustive list of solubility ratios (solubility of metastable/solubility of stable form) for 30 compounds abstracted from the scientific literature. When many of the reports offer solubilities at multiple equilibration temperatures, representative values nearest to 25–37°C are presented. Acemetacin, acetohexamide, cyclopenthiazide, and oxyclozamide on this list are the only compounds that show solubility ratios of greater than 3.0. Most metastable phases have

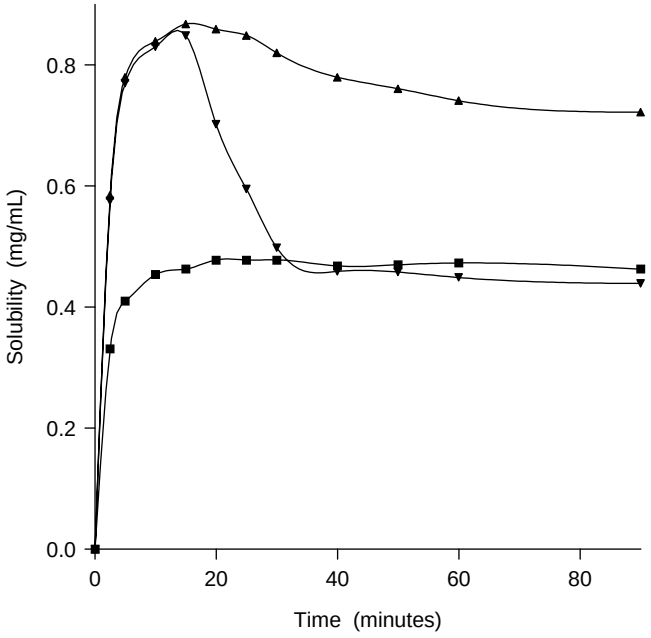

FIGURE 2 Effect on the solubility of sulfamethoxydiazine Form II by seeding with crystals of Form III. Shown are the dissolution profiles of Form II (-▲-), Form III (-■-), and Form II seeded with Form III after 20 minutes elapsed time (-▼-) (46).

apparent solubilities that are 25% to 100% greater than the polymorph with the lowest solubility. This results in a free energy of transition (ΔG_{tr}) of 132–410 cal/mol. As can be seen in the case of buspirone hydrochloride, the magnitudes of the solubilities vary considerably by solvent; however, because of the independence of the solubility ratio from the solvent identity, the ratio is virtually constant.

Pudipeddi and Serajuddin (81) have compiled 81 solubility ratios for 55 different drugs having polymorphic crystal forms, and their results are seen to parallel those of Table 4. Figure 3 combines the data from Table 4 with those of Pudipeddi and Serajuddin to offer a more comprehensive evaluation of observed solubility ratios. The 128 compounds utilized in Figure 3 are presented in order of increasing solubility ratios. Eighty-one percent of the polymorphs have solubility ratios between 1 and 2, whereas 9% of them have ratios greater than 3.5. Although these relative increases in solubility may be characterized as modest, for water-insoluble drugs exhibiting dissolution rate-limited absorption, this difference can be important for therapeutic activity.

Apparent Solubilities of Systems Having Solvate Phases

When the hydrates or solvates of a given compound are stable with respect to phase conversion in a solvent, the equilibrium solubility of these species can be used to characterize these systems. For instance, the equilibrium solubility of the trihydrate phase of ampicillin at 50°C is approximately 1.3 times that of the more stable

TABLE 4 Representative Examples of Solubility Differences Between Polymorphs

Drug	Solvent/Temp.	Solubilities	Ratio	Ref.
Acetohexamide	Distilled water 37°C	I 27 µg/mL II 32 µg/mL	II/I = 1.2	53
	0.1 N HCl 30°C	V 31.4 µg/mL IV 16.3 µg/mL III 10.4 µg/mL I 8.4 µg/mL	V/I = 3.7 IV/I = 1.9 III/I = 1.2	54
Acemetacin	Butanol 20°C	I 9.18 mM II 15.33 mM IV 19.00 mM V 25.65 mM III 43.44 mM	II/I = 1.7 IV/I = 2.1 V/I = 2.8 III/I = 4.7	55
Acetazolamide	pH 7 Phosphate buffer 25°C	A 2.04 mg/mL B 2.28 mg/mL	B/A = 1.1	56
Auranofin	25% aq. PEG 200 37°C	A 0.55 mg/mL B 1.35 mg/mL	B/A = 2.5	57
Benoxaprofen	pH 7 Phosphate buffer 25°C	I 230 µg/mL II 150 µg/mL	I/II = 1.5	58
Buspirone HCl	Distilled water 20°C	I 101.1 g/100 g II 190.0 g/100 g	II/I = 1.9	59
	Isopropanol 20°C	I 0.43 g/100 g II 0.80 g/100 g	II/I = 1.9	
	60:40 Water:isopropanol 20°C	I 84.93 g/100 g II 133.02 g/100 g	II/I = 1.6	
Carbamazepine	2-Propanol 26°C	I 11.16 mg/mL II 9.27 mg/mL	I/II = 1.2	60
{4-(4-Chloro-3-fluorophenyl)-2-[4-(methyloxy)phenyl]-1,3-thiazol-5-yl} acetic acid	Acetonitrile 8.9°C	I 10.6 mg/mL II 13.3 mg/mL	II/I = 1.2	61
	Acetonitrile 43.1°C	I 20.0 mg/mL II 16.0 mg/mL	I/II = 1.2	
Cyclopenthiazide	Distilled water 37°C	I 34.7 µg/mL II 61.8 µg/mL III 17.2 µg/mL	I/III = 2.0 II/III = 3.6	62
Difenoxin HCl	1% aq. tartaric acid 37°C	I 4.5 mg/100 mL II 3.1 mg/100 mL	I/II = 1.5	63
Famotidine	Methanol 37°C	B 11 mg/mL A 6 mg/mL	B/A = 1.8	64
Frusemide	pH 5 Acetate buffer 37°C	II 57.1 mg/100 mL I 35.2 mg/100 mL	II/I = 1.6	65
Gepirone HCl	*n*-Pentyl alcohol 20°C	II 10.01 mg/mL I 3.79 mg/mL	II/I = 2.6	38
Glibenclamide	Distilled water 37°C	II 1.06 mg/100 mL I 0.66 mg/100 mL	II/I = 1.6	66
Glycine	Distilled water 25°C	α 226.8 g·kg^{-1} γ 202.1 g·kg^{-1}	α/γ = 1.2	67
Indomethacin	Distilled water 35°C	α 0.87 mg/100 mL γ 0.69 mg/100 mL	α/γ = 1.3	68

(*Continued*)

TABLE 4 Representative Examples of Solubility Differences Between Polymorphs (*Continued*)

Drug	Solvent/Temp.	Solubilities	Ratio	Ref.
Mefloquine HCl	Distilled water 37°C	E 5.1 mg/mL D 4.3 mg/mL	E/D = 1.2	69
Meprobamate	Distilled water 25°C	II 6.2 mg/mL I 3.3 mg/mL	II/I = 1.9	70
MK571	Isopropyl alcohol 25°C Methyl ethyl ketone 25°C	II 0.390 mg/mL I 0.228 mg/mL II 2.40 mg/mL I 1.24 mg/mL	II/I = 1.7 II/I = 1.9	36
Nateglinide	pH 6.8 Phosphate buffered saline 25°C	H 1663.6 ug/mL B 1192.5 ug/mL S 1553.6 ug/mL	H/B = 1.4 S/B = 1.3	71
Nimodipine	Distilled water 25°C	I 0.036 mg/100 mL II 0.018 mg/100 mL	I/II = 2.0	72
5-Nor-Me	Ethanol 27.8°C	R 2.83 mg/mL O 3.06 mg/mL	O/R = 1.1	73
Oxyclozamide	0.1% aq. tween 80 25°C	III 109 ppm I 73 ppm I 28 ppm	III/I = 3.9 II/I = 2.6	74
Phenylbutazone	pH 7 Phosphate buffer 36°C	I 288.7 mg/100 mL II 279.9 mg/100 mL III 233.6 mg/100 mL IV 213.0 mg/100 mL	I/IV = 1.4 II/IV = 1.3 III/IV = 1.1	75
Phenobarbital	Distilled water 25°C	II-Ba 1.39 mg/mL II 1.28 mg/mL III-Cy 1.17 mg/mL	II-Ba/III = 1.2 II/III = 1.1	76
Piretanide	pH 1.2 37°C	B 13.3 mg/100 mL A 8.3 mg/100 mL	B/A = 1.6	77
Retinoic acid	30:70 Water:methanol 37°C	I 0.097 mg/100 mL II 0.129 mg/100 mL	II/I = 1.3	78
Seratrodast	pH 8 Phosphate buffer 25°C	I 0.543 mg/mL II 0.817 mg/mL	II/I = 1.5	56
Sulfanilamide	Ethanol 39–40°C	Ortho 21.4 g/1000 g Mono 14.0 g/1000 g	O/M = 1.5	79
Tolbutamide	Distilled water 37°C Octanol 30°C	I 14.61 mg/100 mL III 13.03 mg/100 mL I 23.54 mg/mL III 19.33 mg/mL	I/III = 1.1 I/III = 1.2	80

anhydrate phase at room temperature (82). However, below the transition temperature of 42°C, the anhydrate phase is more soluble and is therefore less stable. These relationships are illustrated in Figure 4.

Amiloride hydrochloride can be obtained in two polymorphic dihydrate forms, A and B (83). However, each solvate dehydrates around 115°C to 120°C, and the resulting anhydrous solids melt at the same temperature. However, form B was found to be slightly less soluble than form A between 5°C and 45°C, indicating that it is the thermodynamically stable form at room temperature. The temperature

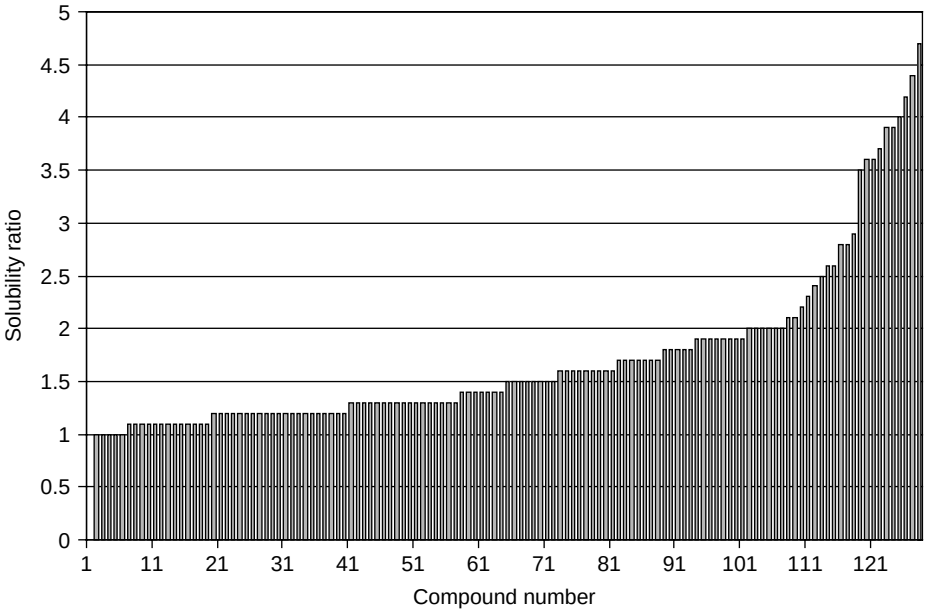

FIGURE 3 One hundred twenty-eight literature solubility ratios (metastable form/stable form) for polymorphic systems.

dependencies of the solubility data were processed by the van't Hoff equation to yield the apparent enthalpies of solution of the two polymorphic dihydrates.

The solubility of polymorphic solids derived from the anhydrate and monohydrate phases of tranilast crystals were evaluated, as were materials processed from them to enhance in vitro availability and micromeritic properties (84). Agglomerates of monohydrate phases I, II, or III were produced using different crystallization solvents and procedures. Monohydrate Form I transformed directly to the stable α-form upon dehydration, whereas Forms II and III dehydrated to the amorphous and β phases, respectively. The apparent equilibrium solubilities of monohydrate Form II and the amorphous form were much higher than those of the α and β forms due to their high surface energies. The solubilities of tranilast hydrate phases exceeded those of the anhydrate phases, which runs counter to the commonly observed trend and suggests that the anhydrate/hydrate transition temperatures are below the temperature of measurement. An analogous situation applies to the anhydrate and trihydrate phases of ampicillin (82) discussed above. The trihydrate phase is more soluble than the anhydrate phase at 50°C, because the transition temperature (42°C) is lower.

Carbamazepine is known to exist in both an anhydrate and a dihydrate form, with the anhydrate spontaneously transforming to the dihydrate upon contact with bulk liquid water (85). The anhydrous phase is reported to be practically insoluble in water, but this observation is difficult to confirm owing to its rapid transition to the dihydrate phase. The rates associated with the phase transformation process have been studied, and appear to follow first-order kinetics (86). Interestingly, the only difference in pharmacokinetics between the two forms was a slightly higher

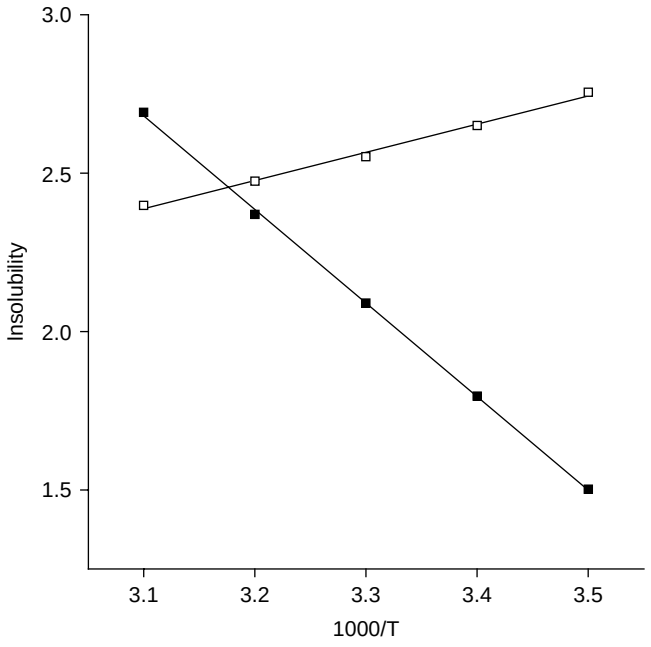

FIGURE 4 The van't Hoff plot for the anhydrate (-□-), and trihydrate (-■-) phases of ampicillin in water (82).

absorption rate for the dihydrate (87). The slower absorption of anhydrous carbamazepine was attributed to the rapid transformation to the dihydrate, accompanied by a fast growth in particle size. Comparison of the bioavailabilities of different polymorphs of a given drug suggest that significant differences are found only when the polymorphs differ significantly in Gibbs free energy deduced from the ratio of solubilities or intrinsic dissolution rates, as in the case of chloramphenicol palmitate.

A monohydrate phase of metronidazole benzoate exhibited solubility properties different from those of the commercially available anhydrous form (88). The monohydrate was found to be the thermodynamically stable form in water below 38°C. The enthalpy and entropy changes of transition for the conversion of the anhydrate to the monohydrate were determined to be –1200 cal/mol and –3.7 cal/K·mol, respectively. This transition was accompanied by a drastic increase in particle size, and caused physical instability of oral suspension formulations. These findings were taken to imply that any difference in bioavailability between the two forms could be attributed to changes in particle size distribution, and not to an inherent difference in the in vivo activity at body temperature.

Recognizing that the hydration state of a hydrate depends on the water activity, in the crystallization medium, Zhu and Grant investigated the influence of solution media on the physical stability of the anhydrate, trihydrate, and amorphous forms of ampicillin (89). The crystalline anhydrate was found to be kinetically stable in the sense that no change was detected by powder X-ray diffraction for at least five days in methanol/water solutions over the whole range of water activity ($a_v = 0$ for pure

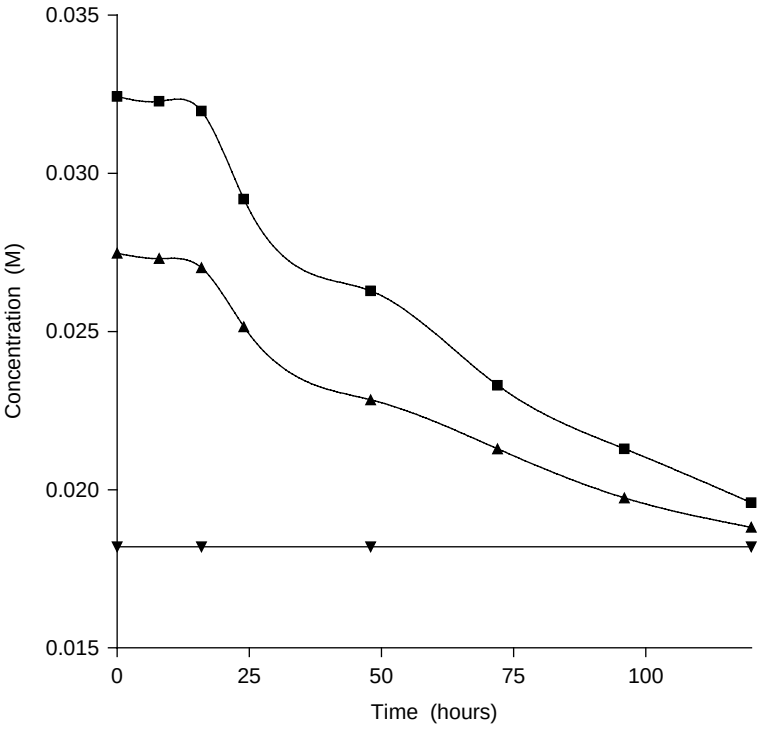

FIGURE 5 Conversion of ampicillin anhydrate to the trihydrate phase at various water activities after seeding with the trihydrate. Shown are the concentration–time data at a_w = 1.0 (-■-), a_w = 0.862 (-▲-), and a_w = 0.338 (-▼-). The curves were adapted from data originally presented in Ref. (89).

methanol to a_v = 1 for pure liquid water). However, addition of trihydrate seeds to ampicillin anhydrate suspended in methanol/water solutions at $a_v \geq 0.381$ resulted in the conversion of the anhydrate to the thermodynamically stable trihydrate. The trihydrate converted to the amorphous form at $a_w \leq 0.338$ in the absence of anhydrate seeds, but converted to the anhydrate phase at $a_w \leq 0.338$ when the suspension was seeded with the anhydrate. These trends are illustrated in Figure 5. The metastable amorphous form took up water progressively with increasing a_w from 0.000 to 0.338 in the methanol/water mixtures. The most significant finding of this work was that water activity was the major thermodynamic factor determining the nature of the solid phase of ampicillin, which crystallized from methanol/water mixtures.

Perhaps the most studied example of phase conversion in the presence of water concerns the anhydrate to monohydrate transition of theophylline. It had been noted in a very early work that the anhydrous phase would convert to the monohydrate phase within seconds of exposure of the former to bulk water (90). The conversion to the monohydrate phase was also demonstrated to take place during wet granulation (91), and could even occur in processed tablets stored under elevated humidity conditions (92). The difficulty in determining the equilibrium solubility of theophylline anhydrate is evident in the literature, which reports a wide range of values (93–95). Better success has been obtained in mixed solvent

TABLE 5 Representative Examples of Solubility Differences Between Solvated Systems

Drug	Solvent/Temp.	Crystal forms and solubilities	Ratio	Ref.
Ampicillin	Water Not given	Anhydrate 10.1 mg/mL Trihydrate 7.6 mg/mL	A/T = 1.3	99
Calcium gluceptate	Distilled water 22°C	Anhydrate 1.3 molal I (3.5 hydrate) 0.07 molal	A/I = 18.6	100
DMHP	Distilled water 25°C	DMHP anhydrate 0.109 M DMHP formate 0.894 M	F/A = 8.2	31
Formoterol fumarate	Water RT	A (anhydrate A) 4.7 mM B (anhydrate B) 3.5 mM C (anhydrate C) 7.5 mM D (dihydrate) 1.5 mM	A/D = 3.1 B/D = 2.3 C/D = 5.0	101
Furosemide	Water* 37°C	Dioxane solvate (X) 25.9 µg/mL DMF solvate (D) 24.7 µg/mL Form I anhydrate 19.8 µg/mL	X/A = 1.3 D/A = 1.2	102
GK-128	pH 4.0 acetate buffer 25°C	Anhydrate I 16.4 mg/mL Hemihydrate 9.3 mg/mL Monohydrate 7.6 mg/mL	A/M = 2.2 H/M = 1.2	103
Glibenclamide	Distilled water 37°C	Pentanol solvate 33.7 mg/100 mL Toluene solvate 2.5 mg/100 mL Form II nonsolvate 1.06 mg/100 m	P/II = 31.8 T/II = 2.4	66
Lamivudine	Distilled water 25°C Ethanol 25°C	I (0.2 hydrate) 84.9 mg/mL II (anhydrate) 98.1 mg/mL I (0.2 hydrate) 18.5 mg/mL II (anhydrate) 11.4 mg/mL	II/I = 1.2 I/II = 1.6	104
Mebendazole	Water Not given	DMA solvate (X) 5.82 µg/mL DMF solvate (D) 4.86 µg/mL Anhydrate 3.16 µg/mL	X/A = 1.8 D/A = 1.5	105
Paroxetine HCl	Distilled water 20°C	I (hemihydrate) 4.9 mg/mL II (anhydrate) 8.2 mg/mL	II/I = 1.7	106
Piroxicam	0.1 N HCl 25°C 0.1 N HCl 30°C	A (anhydrate) 11.90 mg/L B (monohydrate) 12.30 mg/L A (anhydrate) 10.58 mg/L B (monohydrate) 14.64 mg/L	B/A = 1.0 B/A = 1.4	107
Sulfamethoxazole	0.1 N HCl 25°C	A (anhydrate) 119.3 mg/100 mL B (monohydrate) 97.5 mg/100 mL	A/B = 1.2	108
Sparfloxacin	0.15 M KCl 25°C	A (anhydrate) 5600 µg/mL B (trihydrate) 167 µg/mL	A/B = 33.5	24
Theophylline	pH 6 phosphate buffer, 25°C	Anhydrate 12 mg/mL Monohydrate 6 mg/mL	A/M = 2.0	109

systems, as in the work of Zhu and Grant (97), analogous to the experiments with ampicillin (89). However, the data obtained in water-rich solutions was distorted by the formation of the monohydrate phase (96,97,98).

Table 5 provides literature solubility data for some representative solvated systems. The experimental data in Table 5 is a non-exhaustive list of solubility

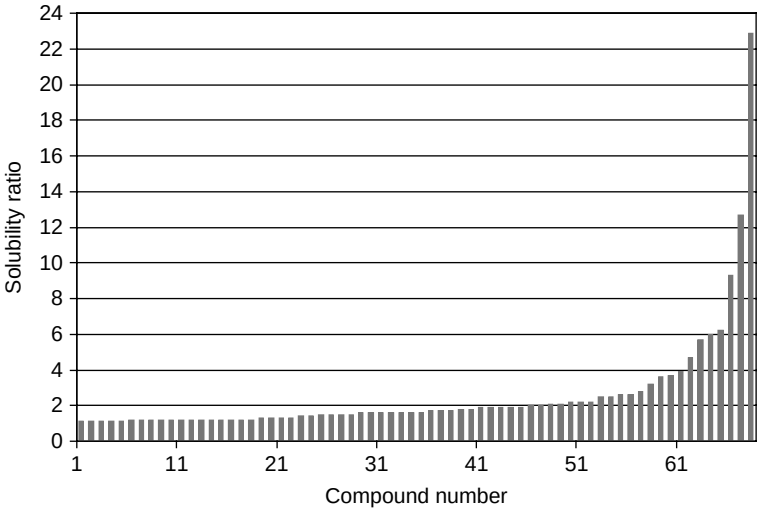

FIGURE 6 Sixty-eight literature solubility ratios (metastable form/stable form) for metastable solvated systems.

ratios (solubility of metastable/solubility of stable form) for 14 different compounds. In general, the solubility ratios for the solvated systems are greater than those of the polymorphic systems. In the case of glibenclamide and sparfloxacin, metastable solids have a 30-fold increase in solubility. Figure 6 combines the data from Table 5 and additional solvated system identified by Pudipeddi and Serajuddin (81). The 68 data points, representing 34 different compounds in Figure 6 are presented in order of increasing solubility ratios. Sixty-nine percent of the polymorphs have solubility ratios between 1 and 2, whereas 15% have ratios greater than 3.5.

SOLUTION CALORIMETRY

The practice of thermochemistry involves measurement of the heat absorbed or evolved when a chemical or physical reaction occurs. Such work entails the determination of the amount of heat, q, in the First Law of Thermodynamics:

$$dE = \delta q - \delta w \tag{7}$$

$$dH = \delta q + V dP \tag{8}$$

The usual practice for solution calorimetry is to conduct the studies at constant pressure, so that the enthalpy change equals either the heat evolved (for an exothermic change) or the heat absorbed (for an endothermic change). The principal chemical requirement for calorimetry is that the measured heat change must be assignable to a definite process, such as the dissolution of a solute in a solvent medium.

Enthalpies of Solution

When a solute is dissolved in a solvent to form a solution, there is almost always absorption or evolution of beat. According to the principle of Le Chatelier, substances that absorb heat as they dissolve must show an increase in solubility with an increase in temperature. Those that evolve heat upon dissolution must become less soluble at higher temperatures.

The heat change per mole of solute dissolved varies with the concentration, c, of the solution that is formed. It is useful to plot the total enthalpy change, ΔH, at constant temperature against the final molar concentration. This type of curve increases rapidly at low solute concentrations, but levels off at the point when the solution is saturated at the temperature of the experiment. The magnitude of the enthalpy change at a given concentration of solute divided by the corresponding number of moles of that solute dissolved represents the increase in enthalpy per mole of solute when it dissolves to form a solution of a particular concentration. This quantity is called the *molar integral heat of solution* at the given concentration. The integral heat of solution is approximately constant in dilute solution, but decreases as the final dissolved solute concentration increases.

For hydrated salts and salts that do not form stable hydrates, the integral heat of solution is ordinarily positive, meaning that heat is absorbed when these substances dissolve. When the anhydrous form of a salt capable of existing in a hydrated form dissolves, there is usually liberation of heat energy. This difference in behavior between hydrated and anhydrous forms of a given salt is attributed to the usual negative change in enthalpy (evolution of heat) associated with the hydration reaction.

Because the heat of solution of a solute varies with its final concentration, there must be a change of enthalpy when a solution is diluted by the addition of solvent. The *molar integral heat of dilution* is the change in enthalpy resulting when a solution containing one mole of a solute is diluted from one concentration to another. According to Hess's law, this change in enthalpy is equal to the difference between the integral heats of solution at the two concentrations.

The increase of enthalpy that takes place when one mole of solute is dissolved in a sufficiently large volume of solution (which has a particular composition), such that there is no appreciable change in the concentration, is the *molar differential heat of solution*. When stating a value for this quantity, the specified concentration and temperature must also be quoted. Because the differential heat of solution is almost constant in very dilute solutions, the molar differential and integral heats of solution are equal at infinite dilution. At higher concentrations, the differential heat of solution generally decreases as the concentration increases.

The *molar differential heat of dilution* may be defined as the heat change when one mole of solvent is added to a large volume of the solution at the specified concentration. The difference between the integral heats of solution at two different concentrations corresponds to the heat of dilution between these two concentrations. The heat of dilution at a specified concentration is normally obtained by plotting the molar heat of solution at various concentrations against the number of moles of solvent associated with a definite quantity of solute, and finding the slope of the curve at the point corresponding to that particular concentration. Because of the approximate constancy of the molar integral heat of solution at small concentrations, such a curve flattens out at high dilutions, and the differential heat of dilution then approaches zero.

The molar differential heats of solution and dilution are examples of partial molar properties, which are important thermodynamic quantities that must be used whenever systems of variable composition, such as solutions, are involved.

Principles Underlying Partial Molar Quantities

A solution that is deduced to be ideal of the chemical potential (μ_i) of every component is a linear function of the logarithm of its mole fraction (X_i), according to the relation:

$$\mu_i = \mu_i^* + RT \ln X_i \tag{9}$$

where μ_i^* is the (hypothetical or actual) value of μ_i when X_i equals unity, and is a function of temperature and pressure. A solution is termed ideal only if equation (9) applies to every component in a given range of composition (usually corresponding to dilute solutions), but it is not necessary that the relation apply to the whole range of composition. Any solution that is approximately ideal over the entire composition range is termed perfect solutions, although there are relatively few such solutions known. However, because a given solution may approach ideality over a limited composition range, it is worthwhile to develop the equations further.

When substance *i* is present both as a pure solid and as a component of an ideal solution, the condition of equilibrium may be stated as:

$$\mu_i^s = \mu_i^* + RT \ln X_i \tag{10}$$

where μ_i^s is the chemical potential of the pure solid, and X_i is the mole fraction in the solution. Rearranging, one finds:

$$\ln X_i = (\mu_i^s/RT) - (\mu_i^*/RT) \tag{11}$$

According to the phase rule, this two-component, two-phase, system is characterized by two degrees of freedom. One concludes that both the temperature and pressure of the solution can be varied independently. Because the pressure on the system is normally held fixed as that of the atmosphere during solubility studies, integration of equation (11) yields:

$$(\delta \ln X_i/\delta T)_P = (H_i - H_i^s)/RT^2 \tag{12}$$

H_i is the partial molar enthalpy of the component in the ideal solution, and H_i^s is its enthalpy per mole as the pure solid. The equation may therefore be rewritten as:

$$(\delta \ln X_i/\delta T)_P = \Delta H_i/RT^2 \tag{13}$$

where ΔH_i is the heat absorbed (at constant temperature and pressure) when one mole of the component dissolves in the ideal solution. As stated above this quantity is the differential heat of solution, and is given by:

$$\Delta H_i = H_i - H_i^s \tag{14}$$

Provided that the solution remains ideal up to $X_i = 1$, and because H_i is independent of composition in the region of ideality, H_i is the same as the enthalpy per mole of the pure liquid component. ΔH_i is equal to its molar heat of fusion, which was formerly termed the molar latent heat of fusion. It is noted, however, that these quantities refer to the temperature at which the solution having mole fraction X_i is in equilibrium with the pure solid.

If one now assumes that ΔH_i is independent of temperature over a narrow temperature range, then equation (13) can be integrated at constant pressure to yield:

$$\ln(X_1/X_2) = (\Delta H_i/R)\{(1/T_2) - (1/T_1)\} \tag{15}$$

where X_1 and X_2 refer to the solubilities (expressed as mole fractions) of the solute at temperatures T_1 and T_2, respectively. If equation (15) remains approximately valid up to a mole fraction of unity, this situation corresponds to that where pure liquid solute is in equilibrium with its own solid at the melting point. In that case, equation (15) yields:

$$\ln X = (\Delta H_i/R)\{(1/T_m) - (1/T)\} \tag{16}$$

where X is the solubility at temperature T, and T_m is the melting point of the solute. ΔH_i is the heat of solution, but by the nature of the assumptions that have been made is also equal to the latent heat of fusion (ΔH^f) of the pure solute.

Because the number of energy levels available to take up thermal energy is greater in the liquid state than in the solid state, the heat capacity of a liquid frequently exceeds that of the same substance in the solid state. As a result, ΔH^f must be assumed to be a function of temperature. If one assumes the change in heat capacity to be constant over the temperature range of interest, then one can use the relation:

$$\Delta H_i = \Delta H_R + \Delta C_p(T_i - T_R) \tag{17}$$

where ΔH_R is the heat of solution at some reference temperature, T_R. This situation has been treated by Grant and coworkers (17), who have provided the highly useful equation (8) for the treatment of solubility data over a wide range of temperature values. Equation (8) was originally derived by Valentiner by substituting the expression for ΔH_i [equation (17)] into the differential form of the van't Hoff [equation (13)], and integrating. In equation (8), a is equal to ΔH_R when T_R equals 0 K, while b is equal to ΔC_p.

The determination of solubility data over a defined temperature range can therefore be used to calculate the differential heat of solution of a given material. For instance, the data illustrated in the bottom half of Figure 1 indicate that equation (16) can be used to deduce a value for the molar differential heat of solution of gepirone. In addition, the fact that Forms I and II yield lines of different slopes indicates the existence of unique values of the molar differential heats of solution for the two polymorphs. One can subtract the differential heats of solution obtained for the two polymorphs to deduce the heat of transition (ΔH_T) between the two forms:

$$\Delta H_T = \Delta H_S{}^B - \Delta H_S{}^A \tag{18}$$

where ΔH_S^A and ΔH_S^B denote the differential heats of solution for polymorphs A and B, respectively.

The validity of the assumption regarding constancy in the heats of solution for a given substance with respect to temperature can be made by determining the enthalpy of fusion (ΔH_F) for the two forms, and then taking the difference between these:

$$\Delta H'_T = \Delta H_F^B - \Delta H_F^A \tag{19}$$

where $\Delta H'_T$ represents the heat of transition between forms A and B at the melting point. The extent of agreement between ΔH_T and $\Delta H'_T$ can be used to estimate the validity of the assumptions made.

For example, the heats of fusion and solution have been reported for the polymorphs of auranofin (57), and these are summarized in Table 6. The similarity of the heats of transition deduced in 95% ethanol (2.90 kcal/mol) and dimethylformamide (2.85 kcal/mol) with the heat of transition calculated at the melting point (3.20 kcal/mol) provides a fair estimation of the thermodynamics associated with this polymorphic system.

Because of the temperature dependence of the various phenomena under discussion, and because of the important role played by entropy, discussions based purely on enthalpy changes are necessarily incomplete. One can rearrange equation (9) to read:

$$\mu_i^* - \mu_i^s = -RT \ln X_i \tag{20}$$

where the left-hand side of the equation represents the difference in chemical potential between the chemical potential of i in its pure solid and the chemical potential of this species in the solution at a defined temperature and pressure. This difference in chemical potential is by definition the molar Gibbs free energy change associated with the dissolution of compound i, so one can write:

$$\Delta G_s = -RT \ln X_i \tag{21}$$

TABLE 6 Heats of Solution and Fusion Measured for the Polymorphs of Auranofin (57)

	Heat of solution, 95% ethanol (kcal/mol)	Heat of solution, dimethylformamide (kcal/mol)
Form A	12.42	5.57
Form B	9.52	2.72
Differential heat of solution	2.90	2.85
	Heat of fusion (kcal/mol)	
Form A	9.04	
Form B	5.85	
Differential heat of formation	3.20	

where ΔG_s is the molar Gibbs free energy of solution. By analogy with equation (12), the molar Gibbs free energy associated with the transformation of polymorph A to B is given by:

$$\Delta G_T = \Delta G_S^{\ B} - \Delta G_S^{\ A} \tag{22}$$

$$= RT \ln(X_A / X_B) \tag{23}$$

where X_A and X_B are the equilibrium solubilities of polymorphs A and B, respectively, expressed in units of mole fraction.

Finally, the entropy of solubility (ΔS_s) is obtained from the relation:

$$\Delta S_s = \{\Delta H_s - \Delta G_s\}/T \tag{24}$$

For basic thermodynamic understanding of the solubility behavior of a given substance, ΔG_s, ΔH_s, and ΔS_s must be determined. Similarly, a basic thermodynamic understanding of a polymorphic transition requires an evaluation of the quantities ΔG_T, ΔH_T, and ΔS_T associated with the phase transition.

To illustrate the importance of free energy changes, consider the solvate system formed by paroxetine hydrochloride, which can exist as a non-hygroscopic hemihydrate or as a hygroscopic anhydrate (106). The heat of transition between these two forms was evaluated both by DSC ($\Delta H'_T$ = 0.0 kJ/mol) and by solution calorimetry (ΔH_T = 0.1 kJ/mol), which would indicates that both forms are isoenthalpic. However, the free energy of transition (–1.25 kJ/mol) favors conversion of the anhydrate to the hemihydrate, and such phase conversion can be initiated by crystal compression or by seeding techniques. Because the two forms are essentially isoenthalpic, the entropy increase that accompanies the phase transformation is responsible for the decrease in free energy and may therefore be viewed as the driving force for the transition.

Methodology for Solution Calorimetry

Any calorimeter with a suitable mixing device and designed for use with liquids can be applied to determine heats of solution, dilution, or mixing. To obtain good precision in the determination of heats of solution requires careful attention to detail in the construction of the calorimeter. The dissolution of a solid may sometimes be a relatively slow process and requires efficient and uniform stirring. Substantial experimental precautions are ordinarily made to ensure that heat input from the stirrer mechanism is minimized.

Most solution calorimeters operate in the batch mode, and descriptions of such systems are readily found in the literature (110,111). The common practice is to use the batch solution calorimetric approach, in which mixing of the solute and the solvent is affected in a single step. Mixing can be accomplished either by breaking a bulb containing the pure solute, allowing the reactants to mix by displacing the seal separating the two reactants in the calorimeter reaction vessel, or by rotating the reaction vessel and allowing the reactants to mix (111). Although the batch calorimetric approach simplifies the data analysis, there are design problems associated with mixing of the reactants. Guillory and coworkers have described the use of a stainless steel ampoule whose design greatly facilitates batch solution calorimetric

analyses (112). This device was validated by measurement of the enthalpy of solution of potassium chloride in water, and the reproducibility of the method was demonstrated by determination of the enthalpy of solution of the two common polymorphic forms of chloramphenicol palmitate in 95% ethanol.

Applications of Solution Calorimetry

Solution calorimetric investigations may be classified into studies that focus entirely on enthalpic processes and studies that seek to understand the contribution of the enthalpy change to the free energy change of the system. Although the former can prove to be quite informative, only the latter permit the deduction of unequivocal thermodynamic conclusions about relative stability.

Although heats of solution data are frequently used to establish differences in enthalpy within a polymorphic system, they cannot be used to deduce accurately the relative phase stability. According to equation (12), the difference between the differential heats of solution of two polymorphs is a measure of the heat of transition (ΔH_T) between the two forms. Because enthalpy is a state function (Hess's Law), this difference must necessarily be independent of the solvent system used. However, conducting calorimetric measurements of the heats of solution of the polymorphs in more than one solvent provides an empirical verification of the assumptions made. For instance, ΔH_T values of two losartan polymorphs were found to be 1.72 kcal/mol in water and 1.76 kcal/mol in dimethylformamide (113). In a similar study with moricizine hydrochloride polymorphs, ΔH_T values of 1.0 and 0.9 kcal/mol were obtained from their dissolution in water and dimethylformamide, respectively (114). These two systems, which show good agreement, may be contrasted with that of enalapril maleate, where ΔH_T was determined to be 0.51 kcal/mol in methanol and 0.69 kcal/mol in acetone (115). Disagreements of this order (about 30%) suggest that some process, in addition to dissolution, is taking place in one or both solvents.

In systems characterized by the existence of more than one polymorph, the heats of solution have been used to deduce the order of stability. As explained above, the order of stability cannot be deduced from enthalpy changes but only from free energy changes. If the enthalpy change reflects the stability, then the polymorphic change is not driven by an increase in entropy, but by a decrease in enthalpy. The heat of solution measured for cyclopenthiazide Form III (3.58 kcal/mol) was significantly greater than the analogous values obtained for Form I (1.41 kcal/mol) or Form II (1.47 kcal/mol), identifying Form III as the polymorph with the greater enthalpy, but not necessarily the most stable polymorph at ambient temperature (62).

In the case of the anhydrate and hydrate phases of norfloxacin (116), the dihydrate phase was found to exhibit a relatively large endothermic heat of solution relative to either the anhydrate or the sesquihydrate. Both urapidil (117) and dehydroepiandrosterone (118) were found to exhibit complex polymorphic/solvate systems, but the relative enthalpy of these could be deduced through the use of solution calorimetry. As an example, the data reported for urapidil (117), which have been collected into Table 7, show that the form with the lowest heat of solution implies the highest enthalpy content, which would therefore be the least stable form. These deductions have merit because the rank order of enthalpy changes corresponded to that of the free energy changes.

It is invariably found that the amorphous form of a compound is less stable than its crystalline modification, in the sense that the amorphous form tends to

TABLE 7 Heats of Solution for the Various Polymorphs and Solvates of Urapidil (117)

Crystalline form	Heat of solution (kJ/mol)
Form I	21.96
Form II	24.26
Form III	22.98 (estimated)
Monohydrate	44.28
Trihydrate	53.50
Pentahydrate	69.16
Methanol solvate	48.39

crystallize spontaneously, indicating that the amorphous form has the greater Gibbs free energy. As discussed in Chapter 1, the amorphous form is more disordered, and must therefore have a greater entropy than does the crystalline form. Hence, the enthalpy of the amorphous form is also greater. The heat of solution of amorphous piretanide in water was found to be 12.7 kJ/mol, whereas the heat of solution associated with Form C was determined to be 32.8 kJ/mol (119). The authors calculated the heat of transformation associated with the amorphous-to-crystalline transition to be –20.1 kJ/mol. Any facile transformation of the two phases was obstructed by the significant activation energy (145.5 kJ/mol).

As emphasized above, a basic thermodynamic understanding of a polymorphic system requires a determination of the free energy difference between the various forms. The two polymorphs of 3-amino-1-(*m*-trifluoromethlyphenyl)-6-methyl-1*H*-pyridazin-4-one have been characterized by a variety of methods, among which solubility studies were used to evaluate the thermodynamics of the transition from Form I to Form II (120). At a temperature of 30°C, the enthalpy change for the phase transformation was determined to be –5.64 kJ/mol. From the solubility ratio of the two polymorphs, the free energy change was then calculated as –3.67 kJ/mol, which implies that the entropy change accompanying the transformation was –6.48 cal/K·mol. In this system, one encounters a phase change that is favored by the enthalpy term, but not favored by the entropy term. However, because the overall free energy change (ΔG_T) is negative, the process takes place spontaneously, provided that the molecules can overcome the activation energy barrier at a significant rate.

A similar situation has been described for the two polymorphic forms of 2-[[4-[[2-(1*H*-tetrazol-5-ylmethyl)phenyl]-methoxy]phenoxy]methyl]quinoline (42). The appreciable enthalpic driving force for the transformation of Form II to Form I (–0.91 kcal/mol) was found to be partially offset by the entropy of transformation (–2.6 cal/K·mol), resulting in a modest free energy difference between the two forms (–0.14 kcal/mol).

In other instances, an unfavorable enthalpy term was found to be compensated by a favorable entropy term, thus rendering negative the free energy change associated with a particular phase transformation. Latnivudine can be obtained in two forms, one of which is a 0.2-hydrate obtained from water or from methanol that contains water, and the other which is non-solvated and is obtained from many non-aqueous solvents (104). Form II was determined to be thermodynamically favored in the solid state. Solubility studies of both forms as a function of solvent

TABLE 8 Thermodynamic Parameters for Lamivudine in Various Solvents (104)

	Form I	Form II
Solvent = Water		
ΔG_{SOL} (cal/mol)	2990	2950
ΔH_{SOL}(cal/mol)	5720	5430
ΔS_{SOL}(cal/deg·mol)	9.2	8.3
Solvent = Ethanol		
ΔG_{SOL} (cal/mol)	3180	3460
ΔH_{SOL}(cal/mol)	5270	4740
ΔS_{SOL}(cal/deg·mol)	7.0	4.3
Solvent = *n*-Propanol		
ΔG_{SOL} (cal/mol)	3120	3610
ΔH_{SOL}(cal/mol)	5350	5000
ΔS_{SOL}(cal/deg·mol)	7.5	4.7

and temperature were used to determine whether entropy of enthalpy was the driving force for solubility. Solution calorimetric data indicated that Form I would be favored in all solvents studied on the basis of enthalpy alone (Table 8). In higher alcohols and other organic solvents, Form I exhibited a larger entropy of solution than did Form II, compensating for the unfavorable enthalpic factors and yielding an overall negative free energy for the phase change.

Shefter and Higuchi considered the thermodynamics associated with the anhydrate/hydrate equilibrium of theophylline and glutethimide (90). For both compounds, the free energy change for the transformation from the anhydrate to the hydrate was negative (hence, indicating a spontaneous process), the favorable enthalpy changes being mitigated by the unfavorable entropy changes. In this work, the free energy was calculated from the solubilities of the anhydrate and hydrate forms, whereas the enthalpy of solution was calculated from the temperature dependence of the solubility ratio using the van't Hoff equation. The entropy of solution was evaluated using equation (24).

A similar conclusion was reached regarding the relative stability of the monohydrate and anhydrate phases of metronidazole benzoate (88). The enthalpy term (–1.20 kcal/mol) favored conversion to the monohydrate, but the strong entropy term (–3.7 cal/K·mol) essentially offset this enthalpy change. At 25°C, the overall ΔG_T of the transition was still negative, favoring the monohydrates, but only barely so (–0.049 kcal/mol). This difference was judged to be too small to result in any detectable bioavailability differences.

KINETICS OF SOLUBILITY: DISSOLUTION RATES

Evaluation of the dissolution rates of drug substances from their dosage forms is extremely important in the development, formulation, and quality control of pharmaceutical agents (16,121–123). Such evaluation is especially important in the characterization of polymorphic systems owing to the possibility of bioavailability differences that may arise from differences in dissolution rate that may themselves arise from differences in solubility (4). The wide variety of methods for determining

the dissolution rates of solids may be categorized either as batch methods or as continuous-flow methods, for which detailed experimental protocols have been provided (124).

Factors Affecting Dissolution Rates

The dissolution rate of a solid may be defined as dm/dt, where m is the mass of solid dissolved at time t. To obtain dm/dt, the following equation, which defines concentration, must be differentiated:

$$m = Vc_b \tag{25}$$

In a batch dissolution method the analyzed concentration (c_b) of a well-stirred solution is representative of the entire volume (V) of the dissolution medium, so that:

$$dm/dt = V(dc_b/dt) \tag{26}$$

In a dissolution study, c_b will increase from its initial zero value until a limiting concentration is attained. Depending on the initial amount of solute presented for dissolution, the limiting concentration will be at the saturation level, or less than this.

Batch dissolution methods are simple to set up and to operate, are widely used, and may be carefully and reproducibly standardized. Nevertheless, they suffer from several disadvantages (16). The hydrodynamics are usually poorly characterized, a small change in dissolution rate will often create an undetectable and immeasurable perturbation in the dissolution time curve, and the solute concentration may not be uniform throughout the solution volume.

In a continuous flow method, the volume flow rate over the surface of the solid is given by dV/dt, so that differentiation of equation (25) leads to:

$$dm/dt = c_b(dV/dt) \tag{27}$$

where c_b is the concentration of drug dissolved in the solvent that has just passed over the surface of the solid drug.

Continuous-flow methods have the advantages that sink conditions may be easily achieved, and that a change in dissolution rate is reflected in a change in c_b (16). At the same time, they require a significant flow rate that may require relatively large volumes of dissolution medium. Should the solid be characterized by a low solubility and a slow dissolution rate, c_b will be small and a very sensitive analytical method would be required.

The diffusion layer theory is the most useful and best known model for transport-controlled dissolution, and satisfactorily accounts for the dissolution rates of most pharmaceutical solids. In this model, the dissolution rate is controlled by the rate of diffusion of solute molecules across a thin diffusion layer. With increasing distance from the surface of the solid, the solute concentration decreases in a non-linear manner across the diffusion layer. The dissolution process at steady state is described by the Noyes–Whitney equation:

$$dm/dt = k_D A(c_s - c) \tag{28}$$

where dm/dt is the dissolution rate, A is the surface area of the dissolving solid, c_s is the saturation solubility of the solid, and c is the concentration of solute in the bulk solution. The dissolution rate constant, k_D, is given by D/h, where D is the diffusion constant. The hydrodynamics of the dissolution process have been fully discussed by Levich (125).

It has been shown (16) that the dissolution rates of solids are determined or influenced by a number of factors, which may be summarized as follows:

1. Solubility of the solid, and the temperature.
2. Concentration in the bulk solution, if not under sink conditions.
3. Volume of the dissolution medium in a batch-type apparatus, or the volume flow rate in a continuous flow apparatus.
4. Wetted surface area, which consequently is normalized in measurements of intrinsic dissolution rate.
5. Conditions in the dissolution medium that, together with the nature of the dissolving solid, determine the dissolution mechanism.

The conditions in the dissolution medium that may influence the dissolution rate can be summarized as:

1. The rate of agitation, stirring, or flow of solvent, if the dissolution is transport-controlled, but not when the dissolution is reaction-controlled.
2. The diffusivity of the dissolved solute, if the dissolution is transport-controlled. The dissolution rate of a reaction-controlled system will be independent of the diffusivity.
3. The viscosity and density influence the dissolution rate if the dissolution is transport-controlled, but not if the dissolution is reaction-controlled.
4. The pH and buffer concentration (if the dissolving solid is acidic or basic), and the pKa values of the dissolving solid and of the buffer.
5. Complexation between the dissolving solute and an interactive ligand, or solubilization of the dissolving solute by a surface-active agent in solution. Each of these phenomena tends to increase the dissolution rate.

Applications of Dissolution Rate Studies to Polymorphs and Hydrates

Historically, batch-type dissolution rate studies of loose powders and compressed disks have played a major role in the characterization of essentially every polymorphic or solid-state solvated system (35,82,90). Stagner and Guillory used these two methods of dissolution to study the two polymorphs and the amorphous phase of iopanoic acid (126). As evident in the loose powder dissolution data illustrated in the *upper half* of Figure 7, the two polymorphs were found to be stable with respect to phase conversion, but the amorphous form rapidly converted to Form I under the dissolution conditions. In the powder dissolution studies, the initial solubilities of the different forms followed the same rank order as did their respective intrinsic dissolution rates, but the subsequent phase conversion of the amorphous form to the stable Form I appeared to change the order. The amorphous form demonstrated a 10-fold greater intrinsic dissolution rate relative to Form I, whereas the intrinsic dissolution rate of Form II was 1.5 times greater than that of Form I.

The nature of the dissolution medium can profoundly affect the shape of a dissolution profile. The relative rates of dissolution and the solubilities of the two polymorphs of 3-(3-hydroxy-3-methylbutylamino)-5-methyl-*as* triazino-[5,6-*b*]-indole

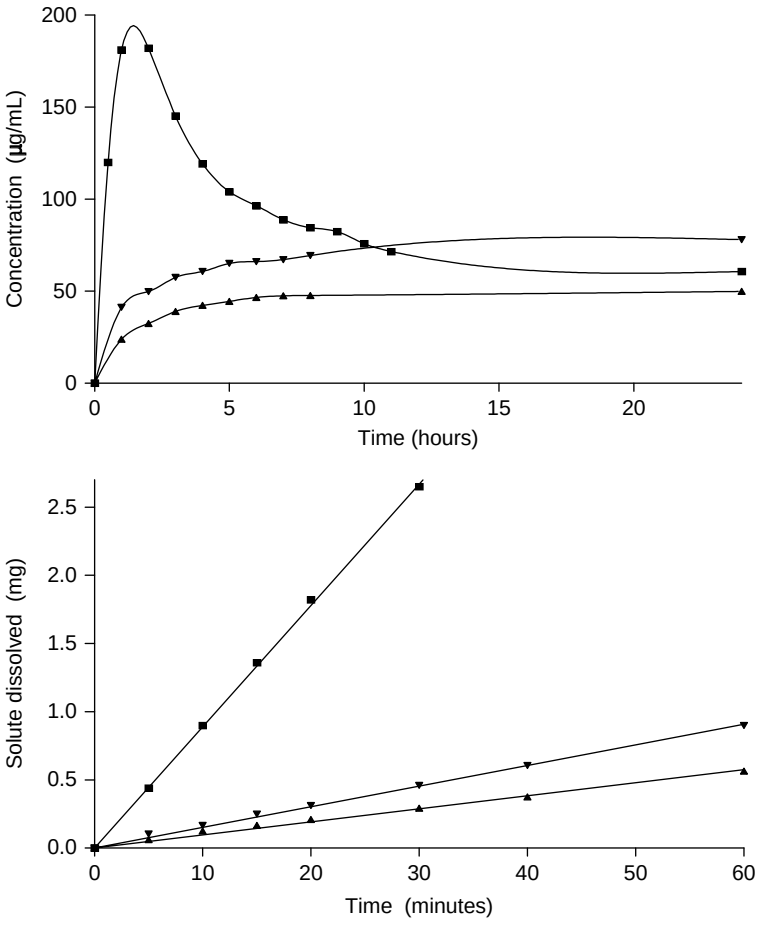

FIGURE 7 Loose powder dissolution (*upper set of traces*) and intrinsic dissolution (*lower set of traces*) profiles of iopanoic acid. Shown are the profiles of Form I (-▲-), Form II (-▼-), and the amorphous form (-■-). The plots were adapted from data originally presented in Ref. (126).

were determined in artificial gastric fluid, water, and 50% ethanol solution (127). In USP artificial gastric fluid, both polymorphic forms exhibited essentially identical dissolution rates. This behavior has been contrasted in Figure 8 with that observed in 50% aqueous ethanol, where Form II has a significantly more rapid dissolution rate than Form I. If the dissolution rate of a solid phase is determined by its solubility, as predicted by the Noyes–Whitney equation, the ratio of dissolution rates would equal the ratio of solubilities. Because this type of behavior was not observed for this triazinoindole drug, the different effects of the dissolution medium on the transport rate constant may be suspected.

The solubilities of the two polymorphs of difenoxin hydrochloride have been studied, as well as the solubility of tablets formed from mixtures of these

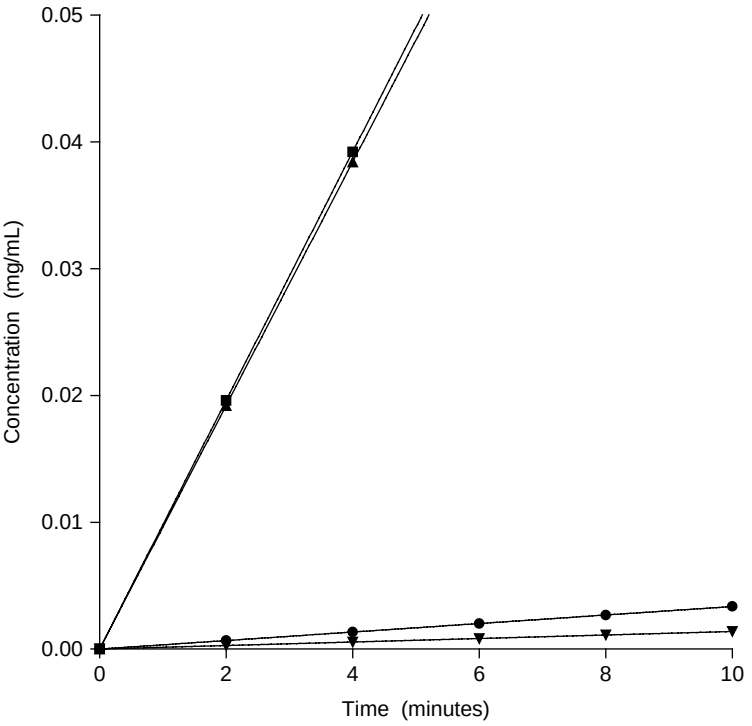

FIGURE 8 Initial stages of the dissolution of the two polymorphs of 3-(3-hydroxy-3-methylbutylamino)-5-methyl-*as* triazino-[5,6-*b*]-indole in different media. Shown are the profiles obtained for Form I (-■-) and Form II (-▲-) in simulated gastric fluid, as well as the profiles of Form I (-●-) and Form II (-▼-) in 50% aqueous ethanol. The traces were adapted from data originally presented in Ref. (127).

polymorphs (63). Form I was found to be more soluble than was Form II, and the solubilities of materials containing known proportions of Forms I and II reflected the differences in the solubilities of the pure forms. Likewise, the dissolution rate of difenoxin hydrochloride from tablets was determined by the ratio of Form I to Form II. In these studies, no solid-state transformation of the more soluble form to the less soluble form was observed. In addition, micronization proved to be a successful method for improving the dissolution of tablets prepared from the less soluble polymorph.

Stoltz and coworkers have conducted extensive studies on the dissolution properties of the hydrates and solvates of oxyphenbutazone (128,129). They compared the dissolution properties of the benzene and cyclohexane solvates with those of the monohydrate, hemihydrate, and anhydrate forms, and then compared their findings with results reported in the literature. The powder dissolution rates of the solvates proved to be comparable to those of the hemihydrate and the anhydrate, but superior to that of the monohydrate. This trend is illustrated in Figure 9, which confirms the usual observation that increasing degrees of hydration results in slower dissolution

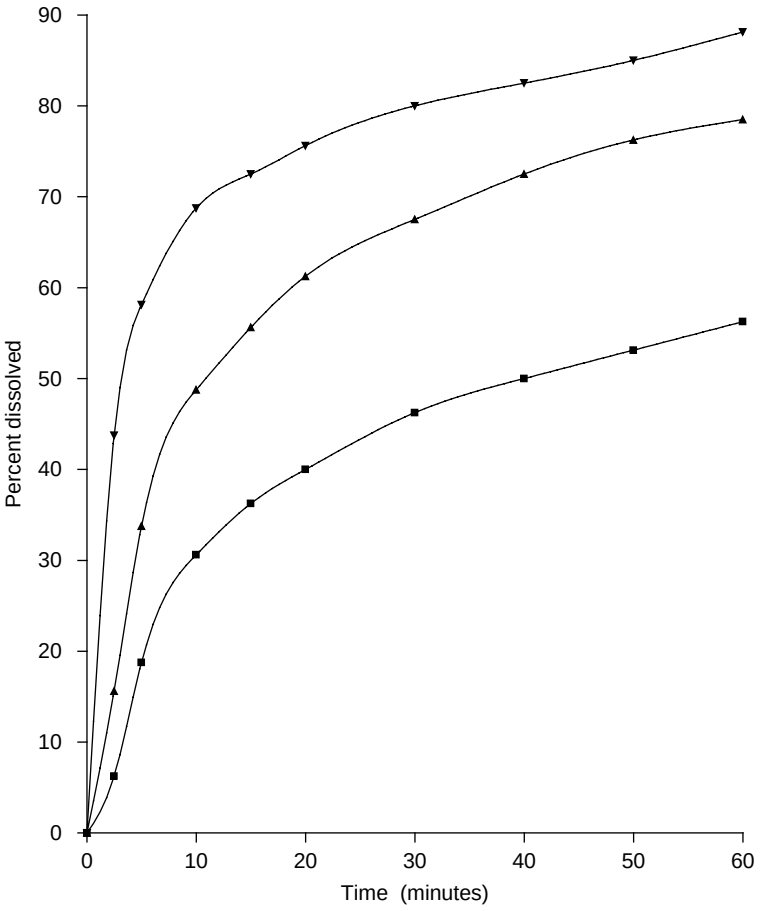

FIGURE 9 Powder dissolution profiles obtained for oxyphenbutazone anhydrate (-▼-), hemihydrate (-▲-), and monohydrate (-■-). The curves were adapted from data originally presented in Ref. (128).

rates. This observation differed from that previously reported by Matsuda and Kawaguchi, who reported powder dissolution rates in simulated intestinal fluid that were in the sequence hemihydrate > monohydrate > anhydrate (130). The reversed order in the dissolution rates of the former work (128) was attributed to the presence of a surfactant in the dissolution medium, which apparently overcame the hydrophobicity of the crystal surfaces of the anhydrate form. In terms of the Noyes–Whitney equation these results may be explained by the influence of the surface active agent in increasing either the wetted surface area, or the transport rate constant, or both quantities.

It has been noted from the earliest dissolution work (90) that, for many substances, the dissolution rate of an anhydrous phase usually exceeds that of any corresponding hydrate phase. These observations were explained by thermodynamics, where it was reasoned that the hydrates possessed less activity and

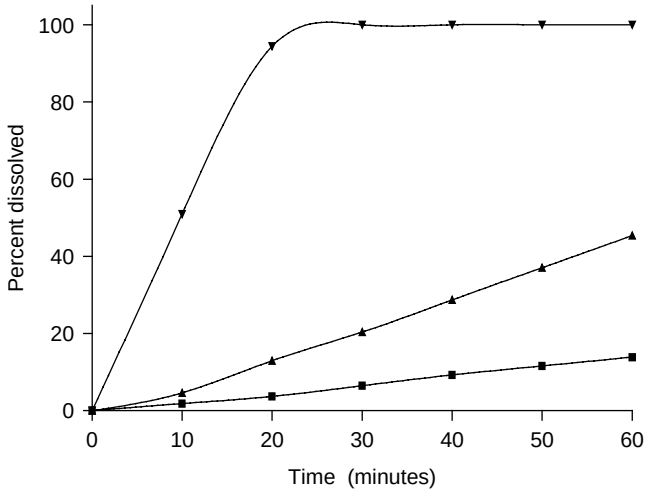

FIGURE 10 Dissolution profiles of erythromycin anhydrate (-■-), monohydrate (-▲-), and dihydrate (-▼-). The plots were adapted from data originally presented in Ref. (133).

would be in a more stable state relative to their anhydrous forms (131). This general rule was found to hold for the previously discussed anhydrate/hydrate phases of theophylline (93,95,97), ampicillin (89), metronidazone benzoate (88), carbamazepine (85,87), glutethimide (132), and oxyphenbutazone (129), as well as for many other systems not mentioned here. In addition, among the hydrates of urapidil, the solubility decreases with increasing crystal hydration (117).

Since the mid-1970s, a number of exceptions to the general rule have been found. For example, Figure 10 shows that the hydrate phases of erythromycin exhibit a reverse order of solubility where the dihydrate phase exhibits the fastest dissolution rate and highest equilibrium solubility (133). More recent examples include the magnesium, zinc, and calcium salts of nedocromil, for which the intrinsic dissolution rate increases with increasing water stoichiometry of their hydrates (134). The explanation for this behavior is that the transition temperatures between the hydrates are below the temperature of the dissolution measurements and decrease with increasing water stoichiometry of the hydrates. Consequently, the solubilities, and hence the intrinsic dissolution rates, increase with increasing stoichiometry of water in the hydrates. Acyclovir was recently found to be capable of forming a 3:2 drug/water hydrate phase, which exhibited an almost instantaneous dissolution relative to the more slowly dissolving anhydrous form (135). This latter finding implies a substantial difference in Gibbs free energy between the two forms.

Intrinsic Dissolution Rates

It should be recognized that the final concentration measured using the loose powder dissolution method is the equilibrium solubility, and that the initial stages of this dissolution are strongly affected by the particle size and surface area of the dissolving solids. For this reaction, many workers have chosen to study the dissolution

of compacted materials, where the particle size and surface area are regulated by the process of forming the compact.

In the disk method for conducting intrinsic dissolution studies, the powder is compressed in a die to produce a compact. One face of the disk is exposed to the dissolution medium, and rotated at a constant speed without wobble. The dissolution rate is determined as for a batch method, whereas the wetted surface area is simply the area of the disk exposed to the dissolution medium.

It is good practice to compare the powder X-ray diffraction patterns of the compacted solid and of the residual solid after the dissolution experiment with that of the original powder sample. In this manner, one may test for possible phase changes during compaction or dissolution.

The dissolution rate of a solid from a rotating disc is governed by the controlled hydrodynamics of the system, and has been treated theoretically by Levich (125). In this system, the intrinsic dissolution rate (J) may be calculated using either of the following relations:

$$J = 0.620D^{2/3}v^{-1/6}(c_s - c_b)\,\omega^{1/2} \tag{29}$$

or

$$J = 1.555D^{2/3}v^{-1/6}(c_s - c_b)W^{1/2} \tag{30}$$

where D is the diffusivity of the dissolved solute, ω is the angular velocity of the disc in radians per second, v is the kinematic viscosity of the fluid, c_b is the concentration of solute at time t during the dissolution study, and c_s is the equilibrium solubility of the solute. The dependence of J on $\omega^{1/2}$ has been verified experimentally (136).

Equations (29) or (30) enable the diffusivity of a solute to be measured. These relations assume the dissolution of only one diffusing species, but because most small organic molecules exhibit a similar diffusivity (of the order 10^{-5} cm^2/sec in water at 25°C), it follows that J depends on the 2/3 power of D. Consequently, the errors arising from several diffusing species only become significant if one or more species exhibit abnormal diffusivities. In fact, diffusivity is only weakly dependent on the molecular weight, so it is useful to estimate the diffusivity of a solute from that of a suitable standard of known diffusivity under the same conditions. In most cases, the diffusivity predictions agree quite well with those obtained experimentally (137).

Intrinsic Dissolution Rate Studies of Polymorphic and Hydrate Systems

Under constant hydrodynamic conditions, the intrinsic dissolution rate is usually proportional to the solubility of the dissolving solid. Consequently, in a polymorphic system, the most stable form will ordinarily exhibit the slowest intrinsic dissolution rate. For example, a variety of high-energy modifications of frusemide were produced, but the commercially available form was found to exhibit the longest dissolution times (138). Similar conclusions were reached regarding the four polymorphs of tegafur (139) and (*R*)-*N*-[3-[5-(4-fluorophenoxy)-2-furanyl]-1-methyl-2-propynyl]-*N*-hydroxyurea (140). However, it is possible that one of the less stable polymorphs of a compound can exhibit the slowest dissolution rate, as was noted in the case of diflunisal (141).

TABLE 9 Intrinsic Dissolution Rates for the Various Polymorphs of Aprazolam at Different Spindle Speeds (142)

Crystalline form	IDR, 50 RPM (μg/min/cm²)	IDR, 75 RPM (μg/min/cm²)
Form I	15.8	21.8
Form II	18.4	21.9
Form V	20.7	27.3

Intrinsic dissolution rate studies proved useful during the characterization of the two anhydrous polymorphs and one hydrate modification of alprazolam (142). The equilibrium solubility of the hydrate phase was invariably less than that of either anhydrate phase, although the actual values obtained were found to be strongly affected by pH. Interestingly, the intrinsic dissolution rate of the hydrate phase was higher than that of either anhydrate phase, with the anhydrous phases exhibiting equivalent dissolution rates. The IDR data of Table 9 reveal an interesting phenomenon, where discrimination between some polymorphs was noted at slower spindle speeds, but not at higher rates. Thus, if one is to use IDR rates as a means to determine the relative rates of solubilization of different rates, the effect of stirring speed must be investigated before the conclusions can be judged genuine.

Intrinsic dissolution rate investigations can become complicated when one or more of the studied polymorphs interconverts to another during the time of measurement. Sulfathiazole has been found to crystallize in three distinct polymorphic forms, two of which are unstable in contact with water (143) but which convert only slowly to the stable form (i.e., are kinetically stable) in the solid state. As may be seen in Figure 11, the initial intrinsic dissolution rates of these are all different, but as Forms I and II convert into Form III, the dissolved concentrations converge. Only the dissolution rate of Form III remains constant, which suggests that it is the thermodynamically stable form at room temperature. Aqueous suspensions of Forms I or II each converted into Form III over time, supporting the conclusions of the dissolution studies.

Suitable manipulation of the dissolution medium can sometimes inhibit the conversion of one polymorph to another during the dissolution process, thus permitting the measurement of otherwise unobtainable information. In studies on the polymorphs of sulfathiazole and methylprednisolone, Higuchi, who used various alcohols and additives in the dissolution medium to inhibit phase transformations, first employed this approach (144). Aguiar and Zeliner were able to thermodynamically characterize the polymorphs formed by chloramphenicol palmitate and mefenamic acid through the use of dissolution modifiers (145). Furthermore, the use of an aqueous ethanol medium containing 55.4% v/v ethanol yielded adequate solubility and integrity of the dissolving disc during studies conducted on digoxin (146).

One area of concern associated with intrinsic dissolution measurements is associated with the preparation of the solid disc by compaction of the drug particles. If a phase transformation is induced by compression, one might unintentionally measure the dissolution rate of a polymorph different from the intended one. This situation was encountered with phenylbutazone, where Form III was transformed to the most stable modification (Form IV) during the initial compression step (75).

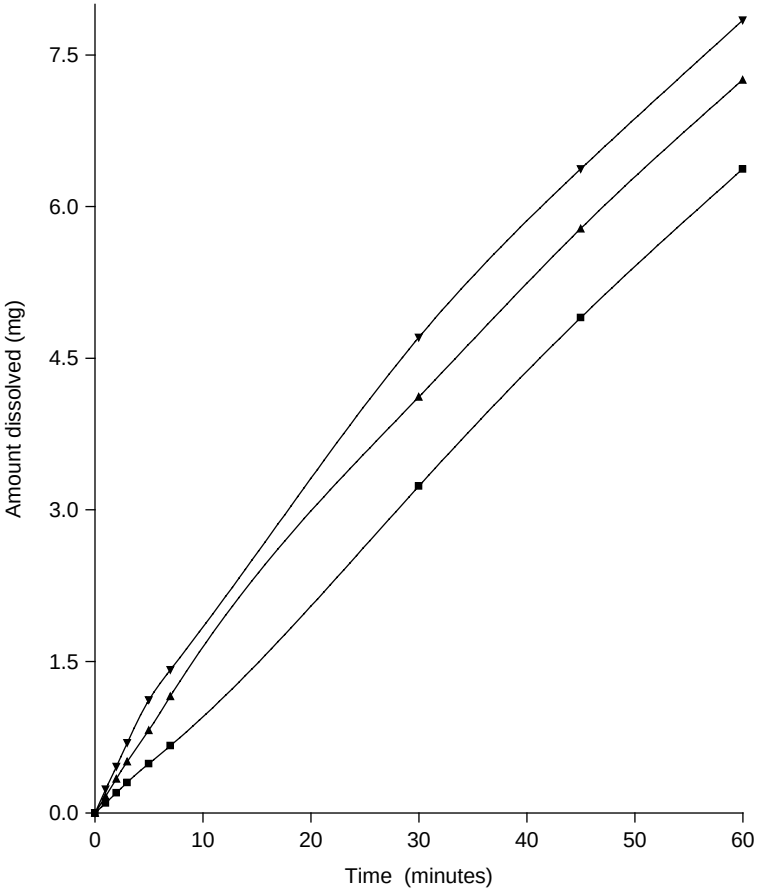

FIGURE 11 Dissolution profiles obtained for sulfathiazole Form I (-▲-), Form II (-▼-), and Form III (-■-) in water at 37°C. The figure has been adapted from data originally presented in Ref. (143).

One interesting note concerns the aqueous dissolution rates of solvate forms, where the solvent bound in the crystal lattice is not water. As noted earlier, the dissolution rate of an anhydrous phase normally exceeds that of any corresponding hydrate phase, but this relation is not usually applicable to other solvate species. It has been reported that the methanol solvate of urapidil exhibits a heat of solution approximately twice that of any of the anhydrate phases, and that it also exhibits the most rapid dissolution rate (147). Similarly, the pentanol and toluene solvates of glibenclainide exhibit significantly higher aqueous dissolution rates and aqueous equilibrium solubility values when compared to either of the two anhydrous polymorphs (66). The acetone and chloroform solvates of sulindac yielded intrinsic dissolution rates that were double those of the two anhydrate phases (148). These trends would imply that a non-aqueous solvate phase could be considered as being a high-energy form of the solid with respect to dissolution in water.

The most usual explanation of these phenomena is that the negative Gibbs free energy of mixing of the organic solvent, released during the dissolution of the solvate, contributes to the Gibbs free energy of solution, increasing the thermodynamic driving force for the dissolution process (90). This explanation, due to Shefter and Higuchi, was originally derived from observations on the higher dissolution rate of the pentanol solvate of succinylsulfathiazole than of the anhydrate (90). Prior addition of increasing concentrations of pentanol to the aqueous dissolution medium reduced the initial dissolution rate of the pentanol solvate. This reduction was attributed to a less favorable (less negative) Gibbs free energy of mixing of the released pentanol in the solution that already contained pentanol. In this way, the Gibbs free energy of solution was rendered less favorable (less negative), reducing the thermodynamic driving force for dissolution of the solvate. Thermodynamic characterization of the various steps in the dissolution of solvates and evaluation of their respective Gibbs free energies (and enthalpies) has been carried out by Ghosh and Grant (31).

CONSEQUENCES OF POLYMORPHISM AND SOLVATE FORMATION ON THE BIOAVAILABILITY OF DRUG SUBSTANCES

In those specific instances where the absorption rate of the active ingredient in a solid dosage form depends upon the rate of drug dissolution, the use of different polymorphs would be expected to affect the bioavailability. One can imagine the situation in which the use of a metastable polymorph would yield higher levels of a therapeutically active substance after administration owing to its higher solubility. This situation may be either advantageous or disadvantageous depending on whether the higher bioavailability is desirable or not. On the other hand, unrecognized polymorphism may result in unacceptable dose-to-dose variations in drug bioavailability, and certainly represents a drug formulation not under control.

The trihydrate/anhydrate system presented by ampicillin has received extensive attention, with conflicting conclusions from several investigations. In one early study, Poole and co-workers reported that the aqueous solubility of the anhydrate phase was 20% higher than that of the trihydrate form at 37°C (149). They also found that the time for 50% of the drug to dissolve in vitro was 7.5 and 45 minutes for the anhydrate and trihydrate forms, respectively (150). Using dogs and human subjects, these workers then determined in vivo blood levels, following separate administration of the two forms of the drug in oral suspensions or in capsules. The anhydrous form produced a higher maximum concentration of ampicillin (C_{max}) and an earlier time to reach maximum concentration (T_{max}) in the blood serum relative to the trihydrate form. This behavior was more pronounced in the suspension formulations. In addition, the area under the curve (AUC) was found to be greater with the anhydrous form, implying that the anhydrous form was more efficiently absorbed.

Since the early works just discussed, an interesting discussion on the comparative absorption of ampicillin has arisen. Some workers have concluded that suspensions and capsules containing ampicillin anhydrate exhibit superior bioavailabilities than analogous formulations made from the trihydrate (151,152). For instance, in a particularly well-controlled study, Ali and Farouk (152) obtained the clear-cut distinction between the anhydrate and the trihydrate, which is illustrated in Figure 12. However, others have found that capsules containing either form of

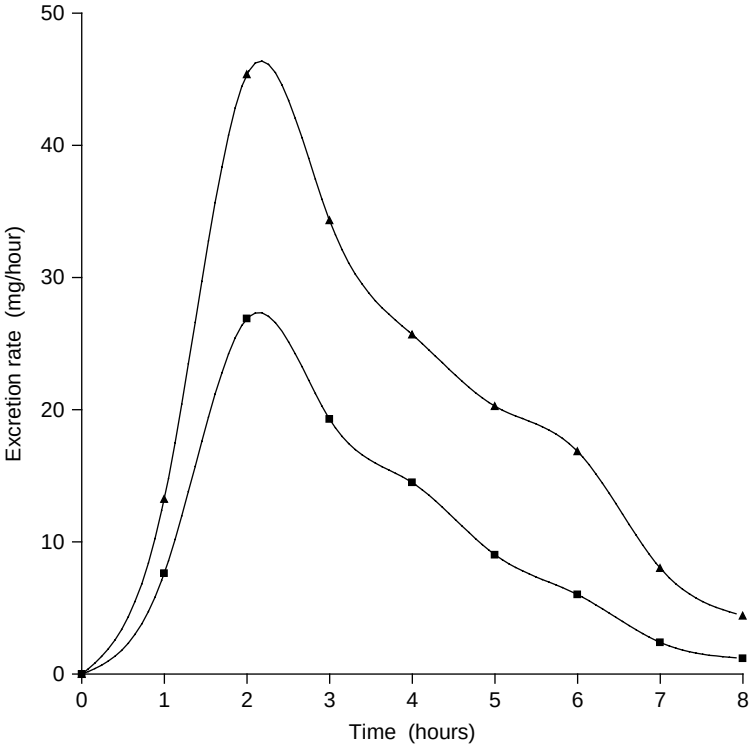

FIGURE 12 Ampicillin urinary excretion rates at various times after separate administration of the two forms. Shown are the profiles obtained for the anhydrate (-▲-) and trihydrate phases (-■-). The figure has been adapted from data provided in Ref. (152).

ampicillin yielded an essentially identical bioavailability (153–155). These conflicting observations indicate that the problem is strongly affected by the nature of the formulation used, and that the effects of compounding can overshadow the effects attributed to the crystalline state.

Chloramphenicol palmitate has been shown to exist in four crystal modifications, and the effect of two of these on the degree of drug absorption has been compared (156). After oral ingestion of Forms A and B, the highest mean blood levels were obtained with suspensions containing only Form B. In mixed dosage forms, the blood levels of the drug were found to bear an inverse relationship with the fraction of Form A. This finding explained the previous report, which noted that a particular suspension formulation of chloramphenicol palmitate exhibited an unsatisfactory therapeutic effect (157). A study of various commercial products indicated that the polymorphic state of the drug in this formulation was uncontrolled, consisting of mixtures of the active polymorph B and the inactive polymorph A.

Sulfamethoxydiazine has been shown to exist in a number of polymorphic forms, which exhibit different equilibrium solubilities and dissolution rates (158). Form II, the polymorph with the greater thermodynamic activity, was found to

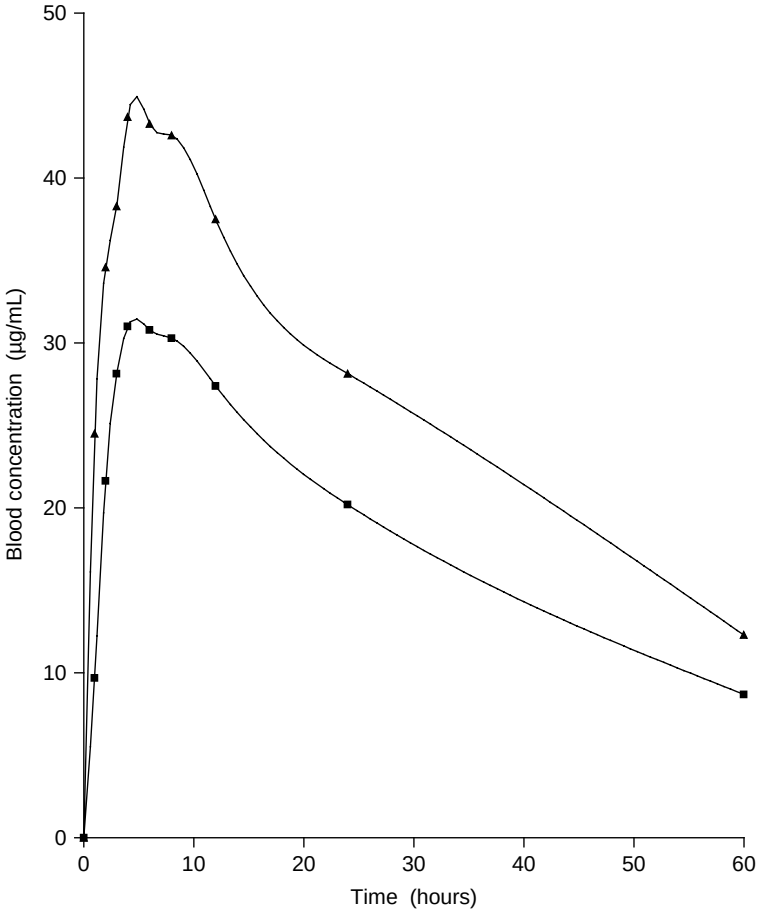

FIGURE 13 Mean concentrations of sulfamethoxydiazine in blood as influenced by the polymorphic state of the drug substance. Shown are the profiles of Form II (-▲-) and Form III (-■-). The figure has been adapted from data provided in Ref. (159).

yield higher blood concentration than those of Form III, which is stable in water (159). This relationship has been illustrated in Figure 13. Although the urinary excretion rates during the absorption phase confirmed the different drug absorption of the two forms as previously observed, the extent of absorption (as indicated by 72-hour excretion data) of the two forms was ultimately shown to be equivalent (160).

Fluprednisolone has been shown to exist in seven different solid phases, of which six were crystalline and one was amorphous (161). Of the crystalline phases, three were anhydrous, two were monohydrates, and one was a *tert*-butylamine solvate. The in vitro dissolution rates of the six crystalline phases of fluprednisolone were determined and compared with in vivo dissolution rates derived from pellet implants in rats (162). The agreement between the in vitro and in vivo dissolution

rates was found to be quite good, but the correlation with animal weight loss and adrenal gland atrophy was only fair. These results can be interpreted to indicate that, for fluprednisolone, differences in dissolution rates of the drug did not lead to measurable biological differences.

Erythromycin base is reported to exist in a number of structural forms, including an anhydrate, a dihydrate, and an amorphous form (163,164). The commercially available product appears to be a partially crystalline material, containing a significant amount of amorphous drug (165). From studies conducted in healthy volunteers, it was learned that the anhydrate and dihydrate phases were absorbed faster and more completely than was either the amorphous form or the commercially available form (166). These observations were reflected in two pharmaco-kinetic parameters (C_{max} and AUC).

Azlocillin sodium can be obtained either as a crystalline form or as an amorphous form, depending on the solvent and method used for its isolation (167). The antibacterial activity of this agent was tested against a large number of reference strains, and in most cases, the crystalline form exhibited less antibacterial activity than did the amorphous form. Interestingly, several of the tested microorganisms also proved to be resistant to the crystalline form.

Whether the different polymorphs or solvates of a given drug substance will lead to the existence of observable differences in the adsorption, metabolism, distribution, or elimination of the compound clearly cannot be predicted a priori at the present time. It is certainly likely that different crystal forms of highly soluble substances should be roughly bioequivalent, owing to the similarity of their dissolution rates. An effect associated with polymorphism that leads to a difference in bioavailability would be anticipated only for those drug substances whose absorption is determined by the dissolution rate. However, the literature indicates that, even in such cases, the situation is not completely clear. Consequently, when the existence of two or more polymorphs or solvates is demonstrated during the drug development process, wise investigators will determine those effects that could be associated with the drug crystal form and will modify their formulations accordingly.

REFERENCES

1. McCrone WC. Fusion Methods in Chemical Microscopy. New York: Interscience, 1957: 133.
2. Haleblian JK, McCrone WC. Pharmaceutical applications of polymorphism. J Pharm Sci 1969; 58: 911–29.
3. Higuchi WI, Lau PK, Higuchi T, et al. Polymorphism and drug availability. Solubility relationships in the methylprednisolone system. J Pharm Sci 1963; 52: 150–3.
4. Byrn S, Pfeiffer R, Ganey M, et al. Pharmaceutical solids: a strategic approach to regulatory considerations. Pharm Res 1995; 12: 945.
5. Q6A International Conference on Harmonization; Guidance on Q6A Specifications: Test Procedures and Acceptance Criteria for New Drug Substances. Federal Register 2000; 65: 83041–63.
6. Yu LX, Furness MS, Raw A, et al. Scientific considerations of pharmaceutical solid polymorphism in abbreviated new drug applications. Pharm Res 2003; 20: 531.
7. Snider DA, Addicks W, Owens W. Polymorphism in generic drug product development. Adv Drug Del Rev 2004; 56: 391–5.

8. Raw AS, Furness MS, Gill DS, et al. Regulatory considerations of pharmaceutical solid polymorphism in abbreviated new drug applications (ANDAs). Adv Drug Del Rev 2004; 56: 397–414.
9. Miller SPF, Raw AS, Andre S, et al. Scientific considerations of pharmaceutical solid polymorphism in regulatory applications, chapter 15 in Polymorphism in the Pharmaceutical Industry. In: Hilfiker R, ed. Wiley-VCH, 2006: 385–403.
10. Yu LX. Pharmaceutical quality by design: product and process development, understanding, and control. Pharm Res 2008; 25: 781–91.
11. Grant DJW, Higuchi T. Solubility Behavior of Organic Compounds, Vol. 21, Techniques of Chemistry. New York: John Wiley and Sons, 1990.
12. Jacques J, Collet A, Wilen SH. Enantiomers, Racemates and Resolutions. New York: Wiley, 1981: 168.
13. Mader WJ, Vold RD, Vold MJ. In Physical Methods of Organic Chemistry, 3rd ed. Vol. 1, Part I. In: Weissberger A, ed. New York: Interscience Publishers, 1959: 655–88.
14. Yalkowsky SH and Banerjee S. Aqueous Solubility Methods of Estimation for Organic Compounds. New York: Marcel Dekker, 1992: 149–54.
15. Brittain HG. Solubility methods for the characterization of new crystal forms, chapter 3.7 in Preformulation in Solid Dosage Form Development. In: Adeyeye MC, Brittain HG, eds. New York: Informa Healthcare, 2008: 323–46.
16. Grant DJW, Brittain HG. Solubility of pharmaceutical solids, chapter 11 in Physical Characterization of Pharmaceutical Solids. In: Brittain HG, ed. New York: Marcel Dekker, 1995: 321–86.
17. Grant DJW, Mehdizadeh M, Chow AH-L, et al. Non-linear van't Hoff solubility-temperature plots and their pharmaceutical interpretation. Int J Pharm 1984; 18: 25–38.
18. Bennema P, van Eupen J, van der Wolf BMA, et al. Solubility of molecular crystals: polymorphism in the light of solubility theory. Int J Pharm 2008; 351: 74–91.
19. Avdeef A, Berger CM, Brownell C. pH-metric solubility. 2: correlation between the acid-base titration and the saturation shake-flask solubility-pH methods. Pharm Res 2000; 17: 85–9.
20. Avdeef A, Berger CM. pH-metric solubility. 3. Dissolution titration template method for solubility determination. Eur J Pharm Sci 2001; 14: 281–91.
21. Avdeef A, Voloboy D, Foreman A. Comp Med Chem II 2006; 5: 399.
22. Fioritto AF, Bhattachar SN, Wesley JA. Solubility measurement of polymorphic compounds via the pH-metric titration technique. Int J Pharm 2007; 330: 105–13.
23. Stuart M, Box K. Chasing equilibrium: measuring the intrinsic solubility of weak acids and bases. Anal Chem 2005; 77: 983–90.
24. Llinás A, Burley JC, Prior TJ, et al. Concomitant hydrate polymorphism in the precipitation of sparfloxacin from aqueous solution. Cryst Growth Des 2008; 8: 114–18.
25. Higuchi T, Shih F-ML, Kimura T, et al. Solubility determination of barely aqueous-soluble organic solids. J Pharm Sci 1979; 68: 1267–72.
26. Bagley EB, Scigliano JM. Polymer solutions, chapter 16 in Solutions and Solubilities. Part II, Techniques of Chemistry, Vol. VIII. In: Dack MRJ, ed. New York: John Wiley, 1976: 437–85.
27. Chiou WL, Kyle LE. Differential thermal, solubility, and aging studies on various sources of digoxin and digitoxin powder: biopharmaceutical implications. J Pharm Sci 1979; 68: 1224–9.
28. Milosovich G. Determination of solubility of a metastable polymorph. J Pharm Sci 1964; 53: 484–7.
29. Nogami H, Nagai T, Suzuki A. Studies on powdered preparations. XVII. dissolution rate of sulfonamides by rotating disk method. Chem Pharm Bull 1966; 14: 329–38.
30. Nogami H, Nagai T, Yotsuyanagi T. Dissolution phenomena of organic medicinals involving simultaneous phase changes. Chem Pharm Bull 1969; 17: 499–509.

31. Ghosh S, Grant DJW. Determination of the solubilities of crystalline solids in solvent media that induce phase changes: solubilities of 1,2-dialkyl-3-hydroxy-4-pyridones and their formic acid solvates in formic acid and water. Int J Pharm 1995; 114: 185–96.
32. Brittain HG. A method for the determination of solubility of metastable crystal phases based on total light scattering. Langmuir 1996; 12: 601–4.
33. Gu C-H, Grant JW. Estimating the relative stability of polymorphs and hydrates from heats of solution and solubility data. J Pharm Sci 2001; 90: 1277–87.
34. Mao C, Pinal R, Morris KR. A quantitative model to evaluate solubility relationship of polymorphs from their thermal properties. Pharm Res 2005; 22: 1149.
35. Higuchi WI, Lau PK, Higuchi T, et al. Polymorphism and drug availability: solubility relationships in the methylprednisolone system. J Pharm Sci 1963; 52: 150–3.
36. Ghodbane S, McCauley JA. Study of the polymorphism of 3-(((3-(2-(7-chloro-2-quinolinyl)-(E)-ethenyl)phenyl) ((3-(dimethylamino-3-oxopropyl) thio) methyl)-thio) propanoic acid (MK571) by DSC, TG, XRPD and solubility measurements. Int J Pharm 1990; 59: 281–6.
37. Tuladhar MD, Carless JE, Summers MP. Thermal behavior and dissolution properties of phenylbutazone polymorphs. J Pharm Pharmacol 1983; 35: 208.
38. Behme RJ, Brooke D, Farney RF, et al. Characterization of polymorphism of gepirone hydrochloride. J Pharm Sci 1985; 74: 1041–6.
39. Sudo S, Sato K, Harano Y. J Chem Eng Japan 1991; 24: 237.
40. Rocco WL, Swanson JR. Win 63843 polymorphs: prediction of enantiotropy. Int J Pharm 1995; 117: 231–6.
41. Aguiar AJ, Zelmer JE. Dissolution behavior of polymorphs of chloramphenicol palmitate and mefenamic acid. J Pharm Sci 1969; 58: 983–7.
42. Carlton RA, Difeo TJ, Powner TH, et al. Preparation and characterization of polymorphs for an LTD4 antagonist, RG 12525. J Pharm Sci 1996; 85: 461–7.
43. Chiou EL, Anderson BD. Thermodynamic studies of tolbutamide polymorphs. J Pharm Sci 1984; 73: 1673–5.
44. Moustafa MA, Ebian AR, Khalil SA et al. Sulfamethoxydiazine crystal forms. J Pharm Pharmacol 1971; 23: 868.
45. Moustafa MA, Khalil SA, Ebian AR et al. Kinetics of interconversion of sulfamethoxydiazine crystal forms. J Pharm Pharmacol 1972; 24: 921.
46. Ebian AR, Moustafa MA, Khalil SA et al. Effect of additives on the kinetics of interconversion of sulfamethoxydiazine crystal forms. J Pharm Pharmacol 1973; 25: 13.
47. Levy G, Procknal JA. Dissolution rate studies on methylprednisolone polymorphs. J Pharm Sci 1964; 53: 656–8; Wurster DE, Taylor PW. Dissolution kinetics of certain crystalline forms of prednisolone. J Pharm Sci 1965; 54: 670–6.
48. Higuchi WI, Bernardo PD, Mehta SC. Polymorphism and drug availability II. Dissolution rate behavior of the polymorphic forms of sulfathiazole and methylprednisolone. J Pharm Sci 1967; 56: 200–7.
49. Addadi L, Berkovitch-Yellin Z, Weissbuch I, et al. Growth and dissolution of organic crystals with tailor-made inhibitors: implications in stereochemistry and materials science. Angew Chem Int Ed 1985; 24: 466–85.
50. Hulliger J. Chemistry and Crystal Growth. Angew Chem Int ed 1994; 33: 143–62.
51. Qu H, Louhi-Kultanen M, Kallas J. Additive effects on the solvent-mediated anhydrate/hydrate phase transformation in a mixed solvent. Cryst Growth Des 2007; 7: 724–9.
52. Skrdla PJ. Physicochemically relevant modeling of nucleation-and-growth kinetics: investigation of additive effects on the solvent-mediated phase transformation of carbamazepine. Cryst Growth Des 2008; 8: 4185–9.
53. Kuroda K, Yokoyama T, Umeda T, et al. Studies on drug nonequivalence. VI. Physicochemical studies on polymorphism of acetohexamide. Chem Pharm Bull 1978; 26: 2565–8.
54. Graf E, Beyer C, Abdallah O. Pharm Ind 1984; 46: 955.

55. Bruger A, Lettenbichler A. Pharmazie 1993; 48: 262.
56. Urakami K. Current Pharm Biotech 2005; 6: 193.
57. Lindenbaum S, Rattie ES, Zuber GE, et al. Polymorphism of auranofin. Int J Pharm 1985; 26: 123–32.
58. Umeda T, Matsuzawa A, Ohnishi N, et al. Physico-chemical properties and bioavailability of benoxaprofen polymorphs. Chem Pharm Bull 1984; 32: 1637–40.
59. Sheikhzadeh M, Rohani S, Taffish M, et al. Solubility analysis of buspirone hydrochloride polymorphs: measurements and prediction. Int J Pharm 2007; 338: 55–63.
60. Behme RJ, Brooke D. Heat of fusion measurement of a low melting polymorph of carbamazepine that undergoes multiple-phase changes during differential scanning calorimetry analysis. J Pharm Sci 1991; 80: 986–90.
61. Katrincic LM, Sun YT, Carlton RA, et al. Characterization, selection, and development of an orally dosed drug polymorph from an enantiotropically related system. Int J Pharm 2009; 366: 1–13.
62. Gerber JJ, van der Watt JG, Lötter AP. Physical characterization of solid forms of cyclopenthiazide. Int J Pharm 1991; 73: 137–45.
63. Walkling WD, Almond H, Paragamian V, et al. Difenoxin hydrochloride polymorphism. Int J Pharm 1979; 4: 39–46.
64. Lu J, Wang X-J, Yang X, et al. Polymorphism and crystallization of famotidine. Cryst Growth Des 2007; 7: 1590–8.
65. Doherty C, York P. Fresemide crystal forms; solid state and physicochemical analyses. Int J Pharm 1988; 47: 141–55.
66. Suleiman MS, Najib NM. Isolation and physicochemical characterization of solid forms of glibenclamide. Int J Pharm 1989; 50: 103–9.
67. Yang X, Wang X, Ching CB. Solubility of form α and form γ of glycine in aqueous solutions. J Chem Eng Data 2008; 53: 1133.
68. Kaneniwa N, Otsuka M, Hayashi T. Physicochemical characterization of indomethacin polymorphs and the transformation kinetics in ethanol. Chem Pharm Bull 1985; 33: 3447–5.
69. Kitamura S, Chang L-C, Guillory JK. Polymorphism of mefloquine hydrochloride. Int J Pharm 1994; 101: 127–44.
70. Clements JA, Popli SD. Can J Pharm Sci 1973; 8: 88.
71. Li Gang G, Xu Q-W, Li R, et al. Acta Chimica Sinica 2007; 65: 2817.
72. Gronenberg A, Keil B, Henck J-O. Processing effects on crystallinity of cephalexin: characterization by vacuum microbalance. Int J Pharm 1995; 118: 11–21.
73. Li H, Stowell JG, Borchardt TB, et al. Synthesis, conformational polymorphism, and construction of a G–T diagram of 2-[(2-Nitrophenyl)amino]-3-thiophenecarbonitrile. Cryst Growth Des 2006; 6: 11,2469.
74. Pearson JT, Varney G. The anomalous behavior of some oxyclozanide polymorphs. J Pharm Pharmacol 1973; 25: 62P.
75. Ibrahim HG, Pisano F, Bruno A. Polymorphism of phenylbutazone: properties and compressional behavior of crystals. J Pharm Sci 1977; 66: 669–73.
76. Kato Y, Okamoto Y, Nagasawa S, et al. New polymorphic forms of phenobarbital. Chem Pharm Bull 1984; 32: 4170–4.
77. Chikarishi Y, Sano A, Tsujiyama T, et al. Preparation of piretanide polymorphs and their physicochemical properties and dissolution behaviors. Chem Pharm Bull 1994; 42: 1123–8.
78. Caviglioli G, Pani M, Gatti P, et al. Study of retinoic acid polymorphism. J Pharm Sci 2006; 95: 2207–21.
79. Carstensen JT. Pharmaceutical principles of solid dosage forms. Lancaster, PA: Technomic Publishing Co, Inc, 1993: 133–149.
80. Rowe EL, Anderson BD. Thermodynamic studies of tolbutamide polymorphs. J Pharm Sci 1984; 73: 1673–5.

81. Pudipeddi M, Serajuddin ATM. Trends in solubility of polymorphs. J Pharm Sci 2005; 94: 929–39.
82. Poole JW, Bahal CK. Dissolution behavior and solubility of anhydrous and trihydrate forms of ampicillin. J Pharm Sci 1968; 57: 1945–8.
83. Jozwiakowski MJ, Williams SO, Hathaway RD. Relative physical stability of the solid forms of amiloride HCl. Int J Pharm 1993; 91: 195–207.
84. Kawashima Y, Niwa T, Takeuchi H, et al. Characterization of polymorphs of tranilast anhydrate and tranilast monohydrate when crystallized by two solvent change spherical crystallization techniques. J Pharm Sci 1991; 80: 472–8.
85. Laine E, Tuominen V, Ilvessalo P, et al. Formation of dihydrate from carbamazepine anhydrate in aqueous conditions. Int J Pharm 1984; 20: 307–14.
86. Young WWL, Suryanarayanan R. Kinetics of transition of anhydrous carbamazepine to carbamazepine dihydrate in aqueous suspensions. J Pharm Sci 1991; 80: 496–500.
87. Kahela P, Aaltonen R, Lewing E, et al. Pharmacokinetics and dissolution of two crystalline forms of carbamazepine. Int J Pharm 1983; 14: 103–12.
88. Annie Hoelgaard, Niels Moller. Hydrate formation of metronidazole benzoate in aqueous suspensions. Int J Pharm 1983; 15: 213–21.
89. Zhu H, Grant DJW. Influence of water activity in organic solvent + water mixtures on the nature of the crystallizing drug phase. 2. Ampicillin. Int J Pharm 1996; 139: 33–43.
90. Shefter E, Higuchi T. Dissolution behavior of crystalline solvated and nonsolvated forms of some pharmaceuticals. J Pharm Sci 1963; 52: 781–91.
91. Herman J, Remon JP, Visavarungroj N, et al. Formation of theophylline monohydrate during the pelletization of microcrystalline cellulose-anhydrous theophylline blends. Int J Pharm 1988; 42: 15–18.
92. Ando H, Ishii M, Kayano M, et al. Effect of moisture on crystallization of theophylline in tablets. Drug Dev Indust Pharm 1992; 18: 453–67.
93. Fokkens JG, van Amelsfoort JGM, de Blaey CJ, et al. A thermodynamic study of the solubility of theophylline and its hydrate. Int J Pharm 1983; 14: 79–93.
94. Bogardus JB. Crystalline anhydrous-hydrate phase changes of caffeine and theophylline in solvent-water mixtures. J Pharm Sci 1983; 72: 837–8.
95. de Smidt JH, Fokkens JG, Grijseels H, et al. Dissolution of theophylline monohydrate and anhydrous theophylline in buffer solutions. J Pharm Sci 1986; 75: 497–501.
96. Gould PL, Howard JR, Oldershaw GA. The effect of hydrate formation on the solubility of theophylline in binary aqueous cosolvent systems. Int J Pharm 1989; 51: 195–202.
97. Zhu H, Yuen C, Grant DJW. Influence of water activity in organic solvent + water mixtures on the nature of the crystallizing drug phase. 1. Theophylline. Int J Pharm 1996; 135: 151–60.
98. Otsuka N, Kaneniwa N, Otsuka K, et al. Effect of geometric factors on hydration kinetics of theophylline anhydrate tablets. J Pharm Sci 1992; 81: 1189–93.
99. Wells JI. Pharmaceutical preformulation: the physicochemical properties of drug substances. Chichester, United Kingdom: Ellis Horwood Ltd, 1988: 94–5.
100. Suryanarayanan R, Mitchell AG. Phase transitions of calcium gluceptate. Int J Pharm 1986; 32: 213–21.
101. Jarring K, Larsson T, Stensland B, et al. Thermodynamic stability and crystal structures for polymorphs and solvates of formoterol fumarate. J Pharm Sci 2006; 95: 1144–61.
102. Matsuda Y, Tatsumi E. J Pharmacobio-Dyn 1989; 12: s-38.
103. Ito S, Nishimura M, Kobayashi Y, et al. Characterization of polymorphs and hydrates of GK-128, a serotonin receptor antagonist. Int J Pharm 1997; 151: 133–43.
104. Jozwiakowski MJ, Nguyen NAT, Sisco JM, et al. Solubility behavior of lamivudine crystal forms in recrystallization solvents. J Pharm Sci 1996; 85: 193–9.
105. Kumar S, Chawla G, Sobhia ME, et al. Characterization of solid-state forms of mebendazole. Pharmazie 2008; 63: 136.
106. Buxton PC, Lynch IR, Roe JA. Solid-state forms of paroxetine hydrochloride. Int J Pharm 1988; 42: 135–43.

107. Kozjek F, Golic L, Zupet P, et al. Acta Pharm Jugosl 1985; 35: 275.
108. Abdallah O, El-Fattah SA. Pharm Ind 1984; 46: 970.
109. Rodriguez-Hornedo N, Lechuga-Ballesteros D, Wu H-J. Phase transition and heterogeneous/epitaxial nucleation of hydrated and anhydrous theophylline crystals. Int J Pharm 1992; 85: 149–62.
110. Sturtevant JM. Calorimetry, chapter 14 in Physical Methods of Organic Chemistry, 2nd edn. In: Weisssberger A, ed. New York: Interscience Pub, 1949: 817–27.
111. Hansen LD, Lewis EA, Eatough DJ. In Analytical Solution Calorimetry. In: Grime JK, ed. New York: John Wiley & Sons, 1985.
112. Winnike RA, Wurster DE, Guillory JK. A solid sampling device for use in batch solution calorimetry. Thermochim Acta 1988; 124: 99–108.
113. Wu L-S, Gerard C, Hussain MA. Thermal analysis and solution calorimetry studies on losartan polymorphs. Pharm Res 1993; 10: 1793–5.
114. Wu L-S, Torosian G, Sigvardson K, et al. Investigation of moricizine hydrochloride polymorphs. J Pharm Sci 1994; 83: 1404–6.
115. Ip DP, Brenner GS, Stevenson JM, et al. High resolution spectroscopic evidence and solution calorimetry studies on the polymorphs of enalapril maleate. Int J Pharm 1986; 28: 183–91.
116. Katdare AV, Ryan JA, Bavitz JF, et al. Characterization of hydrates of norfloxacin. Mikrochim. Acta 1986; III: 1.
117. Botha SA, Caira MR, Guillory JK, et al. Physical characterization of the hydrates of urapidil. J Pharm Sci 1988; 77: 444–51.
118. Chang L-C, Caira MR, Guillory JK. Solid state characterization of dehydroepiandrosterone. J Pharm Sci 1995; 84: 1169–79.
119. Chikaraishi Y, Otsuka M, Matsuda Y. Dissolution phenomenon of the piretanide amorphous form involving phase change. Chem Pharm Bull 1996; 44: 2111–15.
120. Chauvet A, Masse J, Ribet J-P, et al. Characterization of polymorphs and solvates of 3-amino-1-(m-trifluoro-methylphenyl)-6-methyl-1H-pyridazin-4-one. J Pharm Sci 1992; 81: 836–41.
121. Leeson LJ, Carstensen JT. Dissolution Technology. Washington DC: American Pharmaceutical Association, 1974.
122. Hanson R, Gray V. Handbook of Dissolution Testing, 3rd edn. Hockessin, Delaware: Dissolution Technologies, Inc, 2004.
123. Abdou HM. Dissolution, Bioavailability and Bioequivalence. Easton PA: Mack, 1989.
124. Dissolution, General Test <711>, United States Pharmacopoeia 32, volume 1. Rockville MD: United States Pharmacopoeial Convention, Inc, 2009: 263–71.
125. Levich VG. Physicochemical Hydrodynamics. Englewood Cliffs NJ: Prentice-Hall, 1962.
126. Stagner WC, Guillory JK. Physical characterization of solid iopanoic acid forms. J Pharm Sci 1979; 68: 1005–9.
127. Ravin LJ, Shami EG, Rattie E. Physical-chemical evaluation of 3-(3-hydroxy-3-methylbutylamino)-5-methyl-as, triazino [5,6-b] indole (SK&F 30097). J Pharm Sci 1970; 59: 1290–5.
128. Stoltz M, Lötter AP, van der Watt JG. Physical characterization of two oxyphenbutazone pseudopolymorphs. J Pharm Sci 1988; 77: 1047–9.
129. Stoltz M, Caira MR, Lötter AP, et al. Physical and structural comparison of oxyphenbutazone monohydrate and anhydrate. J Pharm Sci 1989; 78: 758–63.
130. Matsuda Y, Kawaguchi S. Physicochemical characterization of oxyphenbutazone and solid-state stability of its amorphous form under various temperature and humidity conditions. Chem Pharm Bull 1986; 34: 1289–98.
131. Yalkowsky SH. Techniques of Solubilization of Drugs. New York: Marcel Dekker, 1981: 160–80.
132. Khankari RK, Grant DJW. Pharmaceutical hydrates. Thermochim Acta 1995; 248: 61–79.

133. Allen PV, Rahn PD, Sarapu AC, et al. Physical characterization of erythromycin: anhydrate, monohydrate, and dihydrate crystalline solids. J Pharm Sci 1978; 67: 1087–93.
134. Zhu H, Khankari RK, Padden BE, et al. Physicochemical characterization of nedocromil bivalent metal salt hydrates. 1. Nedocromil magnesium. J Pharm Sci 1996; 85: 1026–34; Zhu H, Padden BE, Munson EJ, et al. Physicochemical characterization of nedocromil bivalent metal salt hydrates. 2. Nedocromil zinc. J Pharm Sci 1997; 86: 418–29; Zhu H, Halfen JA, Young VG, et al. Physicochemical characterization of nedocromil bivalent metal salt hydrates. 3. Nedocromil calcium. J Pharm Sci 1997; 86: 1439–47.
135. Kristl A, Srcic S, Vrecer F, et al. Polymorphism and pseudopolymorphism: influencing the dissolution properties of the guanine derivative acyclovir. Int J Pharm 1996; 139: 231–5.
136. Mooney KG, Mintun MA, Himmelstein KJ, et al. Dissolution kinetics of carboxylic acids I: effect of pH under unbuffered conditions. J Pharm Sci 1981; 70: 13–22.
137. Higuchi T, Dayal S, Pitman IH. Effects of solute – solvent complexation reactions on dissolution kinetics: testing of a model by using a concentration jump technique. J Pharm Sci 1972; 61: 695–700.
138. Doherty C, York P. Fresemide crystal forms; solid state and physicochemical analyses. Int J Pharm 1988; 47: 141–55.
139. Uchida T, Yonemochi E, Oguchi T, et al. Polymorphism of Tegafur: physico-chemical properties of four polymorphs. Chem Pharm Bull 1993; 41: 1632–5.
140. Li R, Mayer PT, Trivedi JS, et al. Polymorphism and crystallization behavior of abbott-79175, a second-generation 5-lipoxygenase inhibitor. J Pharm Sci 1996; 85: 773–80.
141. Martínez-Ohárriz MC, Martín C, Goñi MM, et al. Polymorphism of diflunisal: isolation and solid-state characteristics of a new crystal form. J Pharm Sci 1994; 83: 174–7.
142. Laihanen N, Muttonen E, Laaksonen M. Solubility and intrinsic dissolution rate of alprazolam crystal modifications. Pharm Dev Tech 1996; 1: 373–80.
143. Lagas M, Lerk CF. The polymorphism of sulphathiazole. Int J Pharm 1981; 8: 11–24.
144. Higuchi WI, Bernardo PD, Mehta SC. Polymorphism and drug availability II. Dissolution rate behavior of the polymorphic forms of sulfathiazole and methylprednisolone. J Pharm Sci 1967; 56: 200–7.
145. Aguiar AJ, Zelmer JE. Dissolution behavior of polymorphs of chloramphenicol palmitate and mefenamic acid. J Pharm Sci 1969; 58: 983–7.
146. Botha SA, Flanagan DR. Non-thermal methods in characterization of anhydrous digoxin and two digoxin hydrates. Int J Pharm 1992; 82: 195–204.
147. Botha SA, Caira MR, Guillory JK, et al. Physical characterization of the methanol solvate of urapidil. J Pharm Sci 1989; 78: 28–34.
148. Tros de Ilarduya MC, Martín C, Goñi MM, et al. Dissolution rate of polymorphs and two new pseudopolymorphs of sulindac. Drug Dev Indust Pharm 1997; 23: 1095–8.
149. Poole JW, Owen G, Silverio J, et al. Current Therap Res 1968; 10: 292.
150. Poole JW, Bahal CK. Dissolution behavior and solubility of anhydrous and trihydrate forms of ampicillin. J Pharm Sci 1968; 57: 1945–8.
151. MacLeod C, Rabin H, Ruedy J, et al. Can Med Assoc J 1972; 107: 203.
152. Ali AA, Farouk A. Comparative studies on the bioavailability of ampicillin anhydrate and trihydrate. Int J Pharm 1981; 9: 239–43.
153. Cabana BE, Willhite LE, Bierwagen ME. Antimicrob. Agents Chemotherap 1969; 9: 35.
154. Mayersohn M, Endrenyi L. Can Med Assoc J 1973; 109: 989.
155. Hill SA, Jones KH, Seager H, et al. Dissolution and bioavailability of the anhydrate and trihydrate forms of ampicillin. J Pharm Pharmacol 1975; 27: 594.
156. Aguiar AJ, Krc J, Kinkel AW, et al. Effect of polymorphism on the absorption of chloramphenicol from chloramphenicol palmitate. J Pharm Sci 1967; 56: 847–53.
157. Anderson CM. Aust J Pharm 1966; 47: S44.
158. Moustafa MA, Ebian AR, Khalil SA, et al. Sulfamethoxydiazine crystal forms. J Pharm Pharmacol 1971; 23: 868.

159. Khalil SA, Moustafa MA, Ebian AR, et al. GI absorption of two crystal forms of sulfameter in man. J Pharm Sci 1972; 61: 1615–17.
160. Khalafallah N, Khalil SA, Moustafa MA. Bioavailability determination of two crystal forms of sulfameter in humans from urinary excretion data. J Pharm Sci 1974; 63: 861–4.
161. Haleblian JK, Koda RT, Biles JA. Isolation and characterization of some solid phases of fluprednisolone. J Pharm Sci 1971; 60: 1485–8.
162. Haleblian JK, Koda RT, Biles JA. Comparison of dissolution rates of different crystalline phases of fluprednisolone by in vitro and in vivo methods. J Pharm Sci 1971; 60: 1488–91.
163. Allen PV, Rahn PD, Sarapu AC, et al. Physical characterization of erythromycin: anhydrate, monohydrate, and dihydrate crystalline solids. J Pharm Sci 1978; 67: 1087–93.
164. Fukumori Y, Fukuda T, Yamamoto Y, et al. Physical characterization of erythromycin dihydrate, anhydrate and amorphous solid and their dissolution properties. Chem Pharm Bull 1983; 31: 4029–39.
165. Murthy KS, Turner NA, Nesbitt RU, et al. Characterization of commercial lots of erythromycin base. Drug Dev Ind Pharm 1986; 12: 665–90.
166. Laine E, Kahela P, Rajala R, et al. Crystal forms and bioavailability of erythromycin. Int J Pharm 1987; 38: 33–8.
167. Kalinkova GN, Stoeva SV. Polymorphism of azlocillin sodium. Int J Pharm 1996; 135: 111–14.

13 Solid-State Phase Transformations

Harry G. Brittain
Center for Pharmaceutical Physics, Milford, New Jersey, U.S.A.

INTRODUCTION

Studies of the propensity of one polymorphic form of a substance to transform into a different polymorphic form are equally important to the pharmaceutical scientist as are studies designed to obtain the different forms and deduce methods for their preparation. It is not sufficient to be able to prepare a particular polymorphic state and develop conditions for its manufacture on a desirable scale because if that particular solid-state form is highly metastable then its maintenance in that form could prove to be problematic. Hence, determining the possible phase transformation pathways associated with the various polymorphs of a given substance is equally important to establishing the phase space of the crystal forms available to that substance.

The different types of polymorphic transformations that a system can undergo were set out by Buerger (1) as a means to understand the velocity of phase changes, and these were subsequently explained in a lucid manner by McCrone (2). These types were differentiated into the four categories of transformations of secondary coordination, transformations of disorder, transformations of first coordination, and transformations of bond type. As far as transitions among polymorphs are concerned, the most important processes are displacive transformations of secondary coordination (where the crystal lattice is deformed but not broken), and reconstructive transformations of secondary coordination (where the lattice framework is broken and re-formed into a new arrangement), and rotational transformations of disorder (where some intermolecular bonds are broken and re-formed to accommodate changes in the conformation of the constituent molecules).

At the molecular level, the different transformation types are manifested in two main distinguishable ways. When the molecules are constrained to exist as a rigid grouping of atoms, these may be stacked in different motifs to occupy the points of different lattices. This type of polymorphism has its origins in packing phenomena, and so is termed packing polymorphism. On the other hand, if the molecule in question is not rigidly constructed and can exist in distinct conformational states, then the additional possibility arises that each of these conformationally distinct modifications may crystallize in its own lattice structure. This latter behavior has been termed conformational polymorphism (3).

Byrn has summarize the scope of phase transformations from one solid phase to another as taking place between polymorphs, solvatomorphs of different stoichiometry, a non-solvated and a solvated form, and between amorphous and crystalline forms (4). He also extended the four-step mechanism for solid-state chemical reactions of Paul and Curtin (5) to suggest that solid–solid physical transitions that take place in the absence of solvent or vapor involve the four steps of molecular

loosening in the initial phase, followed by formation of an intermediate solid solution, nucleation of the new solid phase, and finally growth of the new phase.

In Chapter 2, covering the Phase Rule, it was noted that one may use the thermodynamic properties of the phases involved to specify a polymorphic system. Solid phases were defined as having a uniform structure and composition throughout, and were separated from other phases by defined boundaries. Solids will undergo a phase transition when a particular solid phase becomes unstable as a result of being placed in an undesirable set of environmental conditions. What phase alterations may occur is dictated by differences in free energy at the transition point associated with structural or compositional changes. During a phase transition, the free energy of the system remains constant, while the entropy, volume, and heat capacity undergo discontinuous changes.

Under a given set of environmental conditions that form a point or a zone in a phase diagram, the most stable polymorph will be the one having the lowest free energy. If some point on the phase diagram can be achieved experimentally so that the free energies of a more stable and a less stable phase are equal, then a reversible phase transition between these two may take place. This condition is termed enantiotropy, and the two phases are said to bear an enantiotropic relationship to each other. If however, the free energy of the metastable phase exceeds the free energy of the stable phase under all environmental conditions below the melting point of one of the phases, then any process that converts the metastable form into the stable form must be irreversible. This condition is termed monotropy, and the two phases are said to bear a monotropic relationship to each other. Consequently, absolute values for thermodynamic parameters are seen to be less important than are relationships predicting the relative stability of various phases of a polymorphic system.

Consider the pressure-temperature phase diagram illustrated in Figure 1 for a hypothetical substance capable of existing in two solid-state crystal phases that bear an enantiotropic relationship. The segment connected by points A and B defines the equilibrium conditions of sublimation between solid Form-I and the vapor state, while the B–C segment similarly defines the equilibrium conditions of sublimation between solid Form-II and the vapor state. The segment formed by points C and D defines the equilibrium conditions of vaporization and condensation between the molten substance and its vapor state. The E–C segment defines the equilibrium conditions of melting between Form-II and the liquid state, whereas the E–F segment defines the equilibrium conditions of melting between Form-I and the liquid state. Of particular interest is the segment formed by points B and E, which defines the equilibrium conditions of solid-state phase transformation between Form-I and Form-II.

Two categories of phase transformation can now be defined in terms of the phase diagram. One of these involves the simple exposure of a substance in a particular solid-state phase to a fixed pressure-temperature condition, which may or may not be within its zone of stability. If it is, then nothing will happen. However, if the conditions are such that the particular solid-state phase it is stable, then a phase change to a more stable phase would be anticipated. Another possibility would be to systematically vary either the pressure or the temperature of the system so that the substance moves from a state of stability into a state of instability, and then again a phase change to a more stable phase would be anticipated.

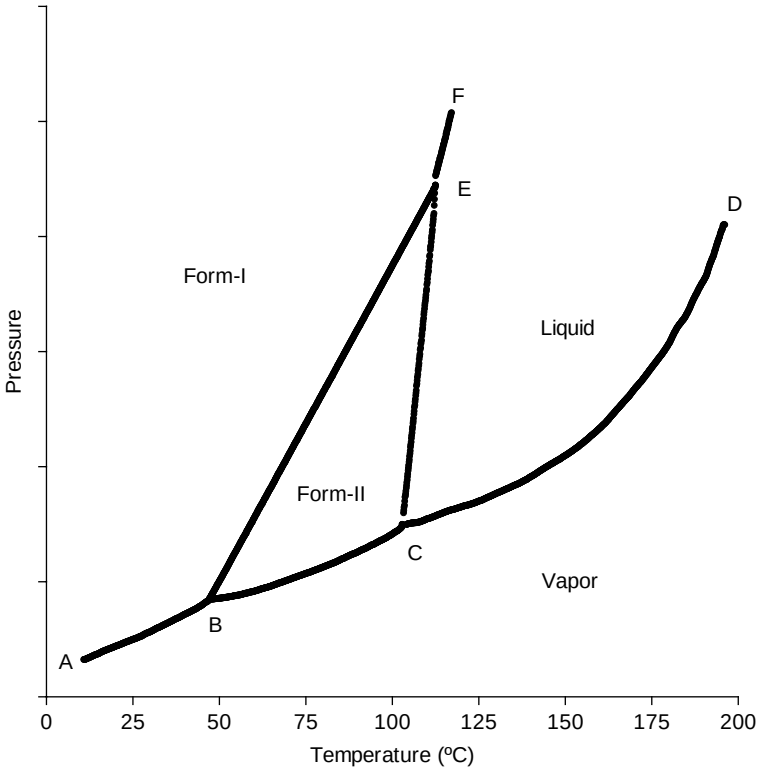

FIGURE 1 Complete phase diagram of a hypothetical enantiotropic system, illustrating the various regions of stability on a pressure–temperature diagram.

At this juncture, the specification of pressure becomes a critical parameter in the continued consideration of phase equilibria. It is a fact that the majority of experimental studies are conducted at ambient or atmospheric pressure, and this is especially true in pharmaceutical developmental studies of polymorph screening and crystal form stability. Therefore, the scope of reactions that might take place under the pre-determined ambient pressure condition becomes defined by where on the vertical pressure scale the value of ambient pressure happens to be. For the instance where temperature and pressure are fixed (e.g., in a simple solution-mediated phase transformation), the system should eventually adopt the phase identity that is stable at that particular temperature and ambient pressure.

For thermally initiated phase transformations, four distinct possibilities are presented for the hypothetical enantiotropic system of Figure 1. Figure 2 illustrates the situation where ambient pressure was such that a heating experiment would only cause the system to cross the A–B segment. Under these conditions, sublimation of Form-I would be the only observable phase transformation, and the lack of any stability of Form-II at that pressure condition would probably entirely preclude its discovery. If it happened that Form-II of the compound was somehow obtained during development, the nature of the phase diagram at this particular ambient

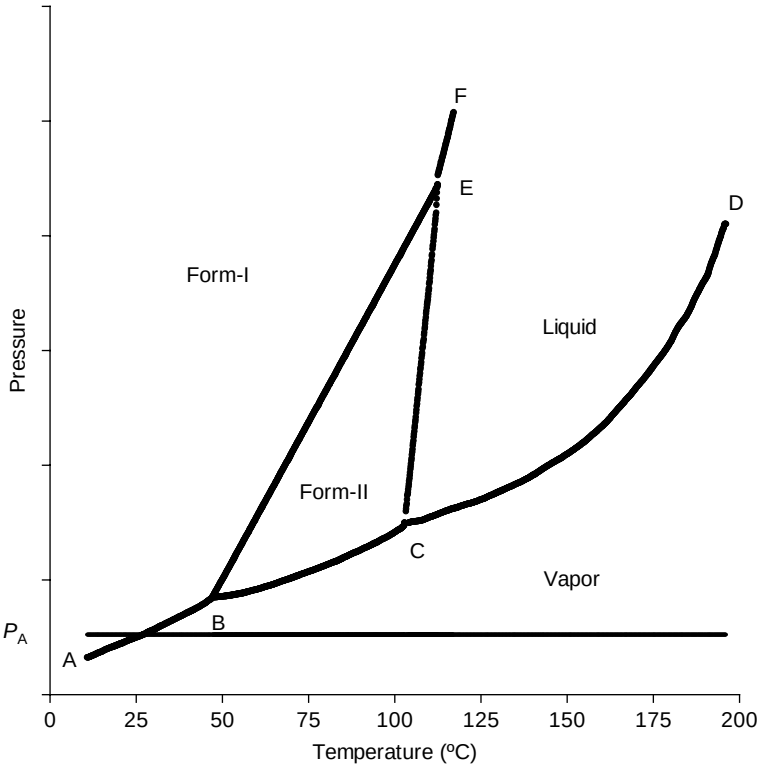

FIGURE 2 Phase diagram of the hypothetical enantiotropic system of Figure 1, illustrating the sublimation of Form-I that would be the only phase transformation if atmospheric pressure happened to equal P_A.

pressure might lead to the deduction of monotropic behavior rather than the correct enantiotropic relationship.

A more interesting condition is presented in Figure 3, where the ambient pressure is such that one could observe the solid-state phase transformation of Form-I into Form-II, followed by the sublimation of Form-II. For this particular pressure condition, the melting of either form under ambient conditions would not bean observed phenomenon. Figure 4 illustrates the situation most commonly considered as being characteristic of an enantiotropic system, namely, where one first observes the solid-state phase transformation of Form-I into Form-II, followed by the melting of Form-II, and the eventual volatilization of the liquid state formed by the melting process. Finally, Figure 5 illustrates the situation that would arise if most of the interesting zones in the phase diagram existed at pressures below atmospheric pressure, and at this pressure condition one could only observe the melting of Form-I and eventual volatilization of the resulting liquid state.

The intersection of segments A–B, B–E, and B–C forms a triple point at which the reversible transformation of the crystalline polymorphs can take place in equilibrium with their vapor phase. For an enantiotropic system, the triple point at B will be a stable and attainable value on the pressure–temperature phase diagram,

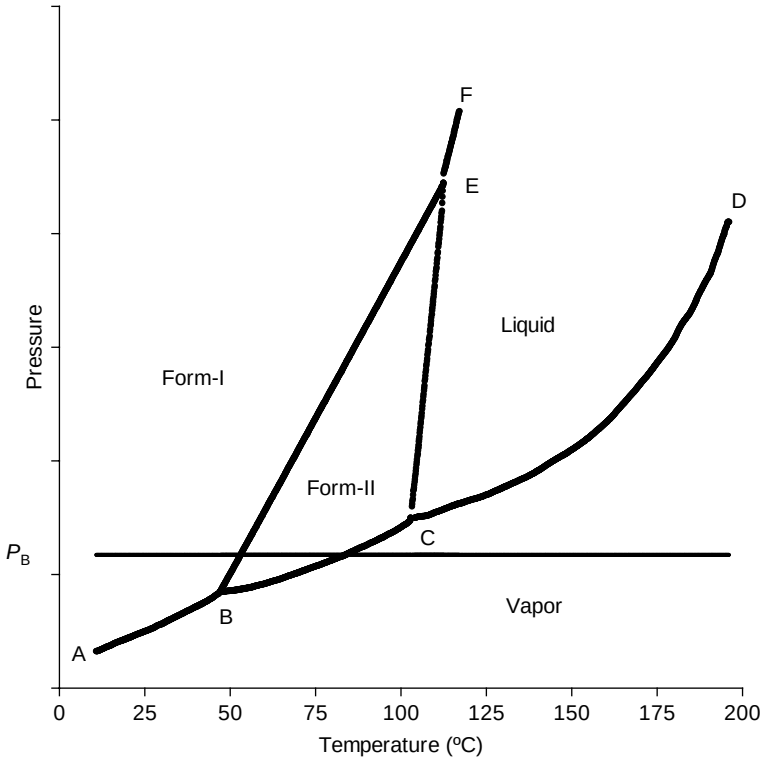

FIGURE 3 Phase diagram of the hypothetical enantiotropic system of Figure 1, illustrating the solid-state phase transformation of Form-I into Form-II, followed by the sublimation of Form-II that would be the phase transformations if atmospheric pressure happened to equal P_B.

and this transition point is a fundamental defining parameter of such a polymorphic system. In the vast majority studies that are conducted at atmospheric pressure, one merely measures an ordinary transition point that corresponds to a position somewhere along the B–E segment of the phase diagram, and which is given as the temperature at which the two polymorphic forms are in equilibrium for that pressure value. For a monotropic system, however, the triple point at B will not be attainable by experimental means as the melting of one of the polymorphic forms will take place at a temperature that is less than the triple point.

Adopting the accepted practice that experimental studies are almost exclusively conducted at ambient pressure, one may divide phase transformations into two categories. One of these is where the phase transformation is induced in a single phase purely by thermal means, with this type being exemplified by solid-to-solid phase changes or by thermally induced evolutions of a component into the vapor. The other category of phase transformation entails the transformation of an initial solid phase into a different solid phase by the intervention of a second phase, such as the sorption of a vapor phase component in a solid or a solution-mediated phase transformation.

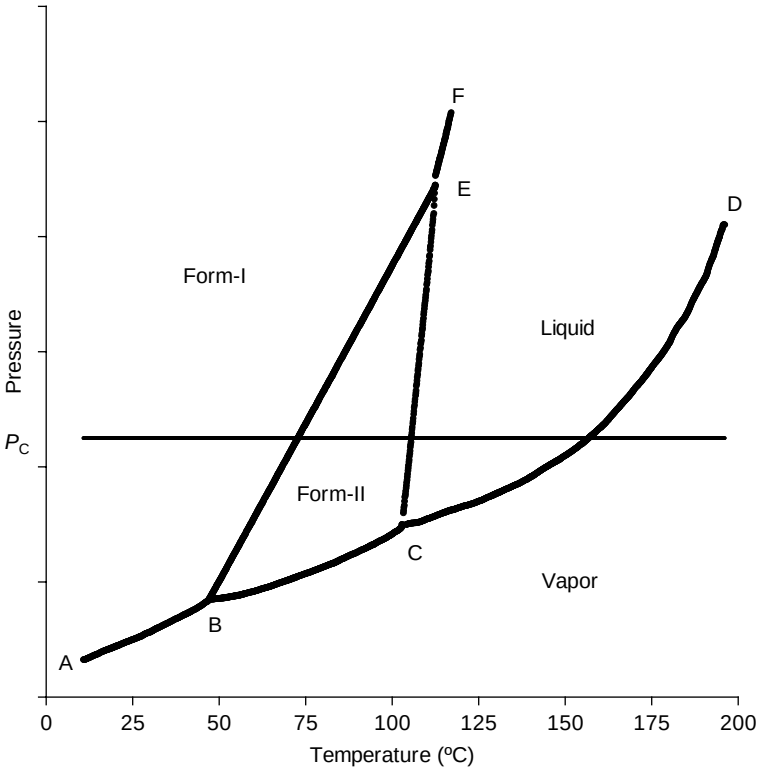

FIGURE 4 Phase diagram of the hypothetical enantiotropic system of Figure 1, illustrating the solid-state phase transformation of Form-I into Form-II, followed by the melting of Form-II and its subsequent volatilization of the liquid state that would be the phase transformations if atmospheric pressure happened to equal P_C.

THERMODYNAMICS OF PHASE TRANSITIONS

The relative stability of the various polymorphs for a given compound is determined by the respective Gibbs free energies (G) of the different forms, each of which is composed of an enthalpy (H) and an entropy (S) term:

$$G = H - TS \tag{1}$$

According to the Third Law of Thermodynamics, the entropy of a perfect, pure crystalline solid is zero at absolute zero, which determines the zero-point entropy of the system. The entropic term of equation (1) will generally increase more rapidly with increasing temperature than will the enthalpic term, and therefore the free energy of a substance will decrease with increasing temperature. Because each polymorphic form of a substance will exist in a distinctive crystal lattice, it is to be anticipated that the values of enthalpy, entropy, and free energy at a given temperature would be different among the various polymorphs. Thus, each polymorphic

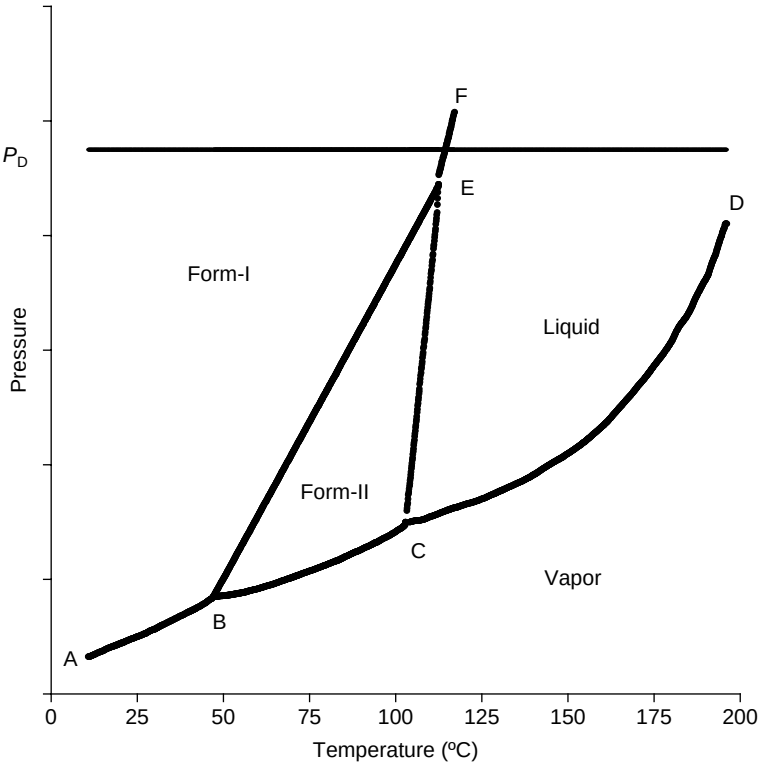

FIGURE 5 Phase diagram of the hypothetical enantiotropic system of Figure 1, illustrating the melting of Form-I and eventual volatilization of the resulting liquid state that would be the phase transformations if atmospheric pressure happened to equal P_D.

form of a substance will be characterized by a different temperature dependence of its Gibbs free energy.

The free energy curves of two hypothetical enantiotropic polymorphs are illustrated in Figure 6, as well as the free energy curve of the liquid (molten) state. In the figure, Form-1 is shown as having a lower free energy content over the lower temperature range, while Form-2 is shown to have a lower free energy over a higher temperature range. For such an enantiotropic system, a reversible transition between forms can be observed at the transition temperature where the free energy curves cross. The existence of enantiotropism in the system is indicated by the fact that the free energy curve for the liquid phase intersects the free energy curves for both polymorphs at a temperature that is higher than the temperature of the transition point. Because the temperature at which the curves intersect is dependent on the pressure of the system, this transition point is termed "ordinary" and is not a fundamental defining characteristic of the system as a triple point would be.

The free energy curves of two hypothetical monotropic polymorphs and their liquid state are illustrated in Figure 7, where now Form-1 is shown as always having a lower free energy content over the entire accessible temperature range. The free energy curve of the liquid state crosses the free energy curves of both polymorphs

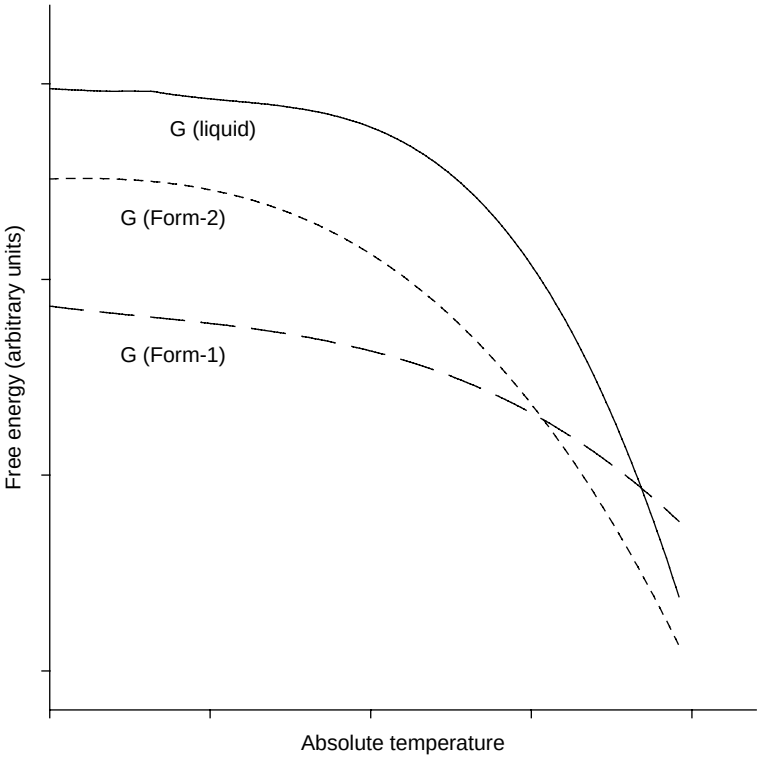

FIGURE 6 Temperature dependence of the free energy for two hypothetical enantiotropic polymorphic crystal forms and their liquid (molten) state.

at temperatures less than that of the transition point, and hence, there can be no temperature at which the two polymorphs would exhibit a reversible phase transition.

When a system undergoes a phase transformation, that change takes place at constant temperature, and the change in free energy of the transition is given by:

$$\Delta G_{TR} = \Delta H_{TR} - T\Delta S_{TR} \tag{2}$$

where ΔG_{TR} is the difference in free energy between the two forms, ΔH_{TR} is the enthalpy difference, and ΔS_{TR} is the entropy difference. A spontaneous process will be characterized by a decrease in the free energy of the system.

Consider the simple equilibrium between two solid-state phases, S_I and S_{II}, of a single component:

$$S_I \rightleftharpoons S_{II} \tag{3}$$

The change in free energy associated with this transformation process (ΔG_{TR}) will be given by:

$$\Delta G_{TR} = G_{S\text{-}I} - G_{S\text{-}II} \tag{4}$$

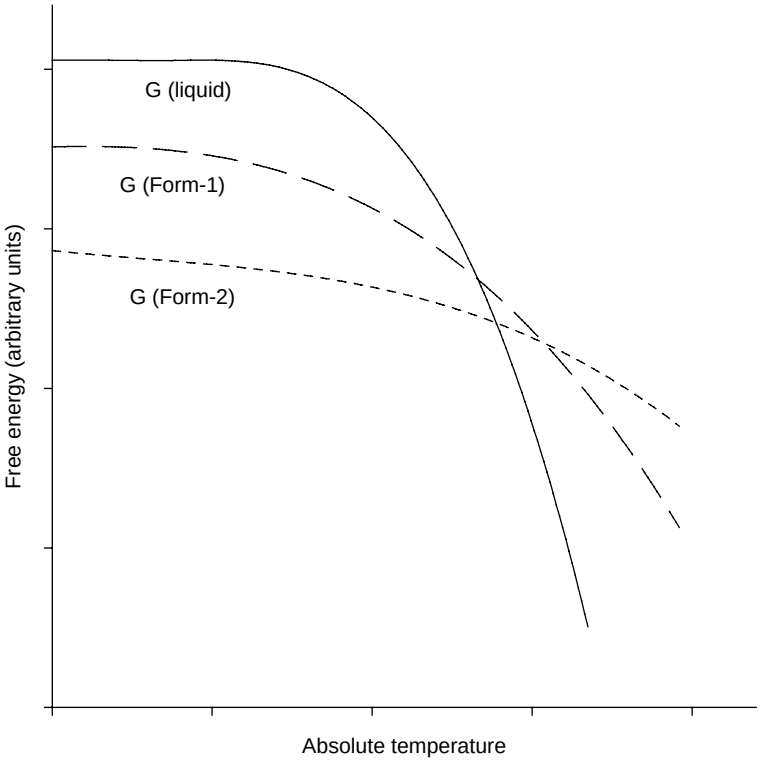

FIGURE 7 Temperature dependence of the free energy for two monotropic polymorphic crystal forms and their liquid (molten) state.

where $G_{S\text{-}I}$ and $G_{S\text{-}II}$ are the respective free energies of the two solid-state forms. The free energy of the Zth phase is determined by the magnitude of the free energy of that phase under standard conditions (G_Z^0) and the activity (a_Z) of that phase in the conditions under study:

$$G_Z = G_Z^0 + RT \ln(a_Z) \tag{5}$$

where R is the gas constant and T is the absolute temperature. Therefore, the free energy change associated with the phase transformation process is given by:

$$\Delta G_{TR} = \{G_{S\text{-}I}^0 + RT \ln(a_{S\text{-}I})\} - \{G_{S\text{-}II}^0 + RT \ln(a_{S\text{-}II})\} \tag{6}$$

defining ΔG_{TR}^0 as $G_{S\text{-}I}^0 - G_{S\text{-}II}^0$, one obtains:

$$\Delta G_{TR} = \Delta G_{TR}^0 + RT \ln(a_{S\text{-}I}/a_{S\text{-}II}) \tag{7}$$

Because the change in free energy corresponding to the phase transformation of equation (3) must equal zero at equilibrium, then:

$$\Delta G_{TR}{}^{0} = -RT \ln(a_{S\text{-}I}/a_{S\text{-}II}) \tag{8}$$

The activity ratio term of equation (8) is obviously the equilibrium constant of the phase transformation reaction:

$$K_{TR} = a_{S\text{-}I}/a_{S\text{-}II} \tag{9}$$

And therefore, equation (8) becomes:

$$\Delta G_{TR}{}^{0} = -RT \ln(K_{TR}) \tag{10}$$

It is to be emphasized that because the $\Delta G_{TR}{}^{0}$ term represents the free energy change at the standard state and is a constant factor referring to the two phases in their states of unit activity, the use of an empirically determined value of ΔG_{TR} at the ordinary transition point in place of $\Delta G_{TR}{}^{0}$ in equation (10) will not give a completely accurate value for the equilibrium constant of the phase transformation reaction. For example, because the activity of the Zth species is approximately proportional to its solubility, S_Z, in any given solvent under dilute conditions, one often writes an expression approximating the free energy difference between two polymorphic forms in terms of their respective equilibrium solubilities:

$$\Delta G_{TR} \sim -RT \ln(S_{S\text{-}I}/S_{S\text{-}I}) \tag{11}$$

Although equation (11) is only an approximation, the solubility ratio rule is a useful quantity in predicting and qualitative order of stability of two solid-state polymorphic forms.

Referring back to equation (10), one observed that the left-hand side refers to a process in which each of the reactants and products is in its standard state, and the right-hand side contains the variables T and K_{TR}. Continuing with the assumption of constant (i.e., ambient) pressure, it is possible to differentiate equation (10) with respect to temperature at constant pressure, obtaining:

$$\frac{\partial(\Delta G_{TR}{}^{0})}{\partial T} = -R \ln(K_{TR}) - RT \frac{\mathrm{d} \ln(K_{TR})}{\mathrm{d}T} \tag{12}$$

Multiplying equation (12) through by T, and substituting $\Delta G_{TR}{}^{0}$ for $-RT \ln(K_{TR})$ yields:

$$T \frac{\partial(\Delta G_{TR}{}^{0})}{\partial T} = -\Delta G_{TR}{}^{0} - RT^{2} \frac{\mathrm{d} \ln(K_{TR})}{\mathrm{d}T} \tag{13}$$

When all the phases in equilibrium are in their standard states, equation (2) becomes:

$$\Delta G_{TR}{}^{0} = \Delta H_{TR}{}^{0} - T\Delta S_{TR}{}^{0} \tag{14}$$

From to the First Law of Thermodynamics, it can be shown that:

$$\Delta G = V\Delta P - S\Delta T \tag{15}$$

At constant pressure, equation (15) simplifies to:

$$\Delta G = -S\Delta T \tag{16}$$

or:

$$\frac{\partial(\Delta G)}{\partial T} = -\Delta S \tag{17}$$

Upon substitution of the general relation (17) into equation (14) one obtains a form of the Gibbs–Helmholtz equation that pertains to the special case where all substances taking part in the phase transformation are in their standard states:

$$\Delta G_{\mathrm{TR}}{}^{0} = \Delta H_{\mathrm{TR}}{}^{0} + T\frac{\partial(\Delta G_{\mathrm{TR}}{}^{0})}{\partial T} \tag{18}$$

Because both equations (13) and (18) contain the $\Delta G_{\mathrm{TR}}{}^{0}$ term, one may derive the relation:

$$\Delta H_{\mathrm{TR}}{}^{0} = RT^{2}\frac{\mathrm{d}\ln(K_{\mathrm{TR}})}{\mathrm{d}T} \tag{19}$$

Equation (19) may be rearranged into the more familiar form known as the van't Hoff equation:

$$\frac{\Delta H_{\mathrm{TR}}{}^{0}}{RT^{2}} = \frac{\mathrm{d}\ln(K_{\mathrm{TR}})}{\mathrm{d}T} \tag{20}$$

In equation (20), $\Delta H_{\mathrm{TR}}{}^{0}$ is the change in enthalpy under standard state conditions for a phase transformation conducted at constant pressure.

It is known that the enthalpy change does not generally exhibit much variability as a function of pressure, and therefore, one may use the more general relation obtained by substituting ΔH_{TR} for $\Delta H_{\mathrm{TR}}{}^{0}$ without specifying the exact conditions to obtain:

$$\frac{\Delta H_{\mathrm{TR}}}{RT^{2}} = \frac{\mathrm{d}\ln(K_{\mathrm{TR}})}{\mathrm{d}T} \tag{21}$$

In practical terms, equation (21) predicts that if one were to plot $\ln(K_{\mathrm{TR}})$ against the absolute temperature, one would obtain a straight line whose slope at any temperature would be equal to $\Delta H_{\mathrm{TR}}/RT^{2}$. According to equation (21), K_{TR} must increase with temperature if ΔH_{TR} is positive, and K_{TR} must decrease with increasing temperature if ΔH_{TR} is negative.

Equation (21) must be integrated if it is to be used for practical calculations. If the enthalpy of phase transformation, ΔH_{TR}, is assumed to be constant over a small range of temperature, then a general integration of the van't Hoff equation yields:

$$\ln(K_{\mathrm{TR}}) = -\frac{\Delta H_{\mathrm{TR}}}{RT} + \text{constant} \tag{22}$$

or:

$$\log(K_{TR}) = -\frac{\Delta H_{TR}}{(2.303)RT} + \text{constant} \tag{23}$$

Another useful approach is to integrate the van't Hoff equation (21) between the definite temperature limits of T_1 and T_2, obtaining:

$$\frac{\log(K_{TR@T_2})}{\log(K_{TR@T_1})} = -\frac{\Delta H_{TR}}{(2.303)R}\left[\frac{1}{T_2} - \frac{1}{T_1}\right] \tag{24}$$

where and are the equilibrium constants at temperatures T_1 and T_2, respectively. When and ΔH_{TR} and R are given in units of calories, equation (24) becomes:

$$\frac{\log(K_{TR@T_2})}{\log(K_{TR@T_1})} = -\frac{\Delta H_{TR}}{(4.576)}\left[\frac{T_2 - T_1}{T_1 T_2}\right] \tag{25}$$

Using equation (25), it is possible to calculate the equilibrium constant at a different absolute temperature as long as the enthalpy of reaction is accurately known at another absolute temperature. Alternatively, if the equilibrium constants of the phase transformation have been determined at two temperatures, then one may calculate the enthalpy of the reaction. It should be emphasized that equation (25) is based on the approximation of a constant value of ΔH_{TR} over the temperature range of T_1 to T_2, and that exact calculations require one to make an allowance for any possible variation of the enthalpy of reaction with temperature.

Although one should base predictive rules on free energy principles rather than enthalpic considerations alone, a number of empirical rules have been proposed for the deduction of the relative order of stability of polymorphs and whether the interconversion processes are enantiotropic or monotropic nature (6–8). Among the better known of these is the *Heat of Transition Rule*, which states that if an endothermic transition is observed at some temperature, it may be assumed that there must be a transition point located at a lower temperature where the two forms bear an enantiotropic relationship. Conversely, if an exothermic transition is noted at some temperature, it may be assumed that there is no transition point located at a lower temperature. This, in turn, implies that either the two forms bear a monotropic relationship to each other, or that the transition temperature is higher than the temperature of the exotherm.

Another empirical rule is the *Heat of Fusion Rule*, which states that if the higher melting form has a lower heat of fusion relative to the lower melting form, then the two forms bear an enantiotropic relationship. Less well obeyed is the *Density Rule*, which states that the most dense form will be the most stable at absolute zero. Strictly speaking, the Density Rule is only properly applied to polymorphs of molecular solids where intramolecular hydrogen bonding is not a significant factor. The limitations of the thermodynamic rules of Burger and Ramberger have been discussed in several publications, and upgrades to these have been published (9–12).

PHASE TRANSFORMATIONS INITIATED WITHIN A SINGLE PHASE

As discussed above, thermally induced phase transformations most often correspond to those reactions where the pressure of the system is kept constant, and which is ordinarily ambient or atmospheric pressure. The pathways of these phase transformations then corresponds to a horizontal cut across a typical pressure–temperature phase diagram. Because this category of phase transformation is conducted at constant pressure, the equilibrium thermodynamics developed in the preceding section can often be used to obtain a deeper understanding of the processes involved.

It goes without saying that although thermodynamics tells one what must happen between now and the end of time, principles of thermodynamics cannot be used to deduce rates of phase transformation. A spontaneous reaction characterized by a negative value of ΔG_{TR} would be predicted to take place spontaneously, but if the activation energy for the process is substantial, the system may be locked into a metastable state. For such cases, only an outside intervention would serve to initiate the phase transformation.

Kawakami has discussed enantiotropically related transitions among polymorphs from an activation energy standpoint, pointing out that the kinetics of a reversible phase transformation may be impeded if the magnitude of the activation energy presents a barrier to the transformation (13). Phase transitions were categorized as being either kinetically reversible [i.e., those for which the transition temperature as measured by differential scanning calorimetry (DSC) was the same regardless of the direction of the temperature change] or as kinetically irreversible (i.e., those for which the transition temperature depended greatly on the direction of the temperature change). It was proposed that these distinctions should also be investigated during development, and that a mere definition of a phase change in a system as being monotropic or enantiotropic nature was insufficient.

Solid-to-Solid Phase Transformation

Of the four known polymorphs of (*S*,*S*)-ethambutol dihydrochloride, two have been found to bear an enantiotropic relationship during their thermally induced phase transformation (14). The phase transition was noted to transpire in the form of a rapidly moving front that passed through single crystals of the compound, and that left new crystals of the transformed substance. Using a hot-stage microscope, it was shown that crystallization from the melt (which took place at 124 ± 5°C) produced a thin film of Form-III that transformed to Form-IV upon cooling. On the other hand, Forms I and II could be reversibly interconverted about a temperature of 72°C.

DSC was used to study the phase interconversion associated with the α and β polymorphs of 2,4,5,6-tetrachloro-l,3-benzenedicarbonitile (chlorothalonil) (15). It was reported that the transition point for the endothermic $\alpha \rightarrow \beta$ transition was 150.5 ± 0.1°C, and that the phase transition was characterized by an enthalpy of 4.03 ± 0.03 kJ/mol and an activation energy of 650 ± 90 kJ/mol. Although fast kinetics were observed for the favorable $\alpha \rightarrow \beta$ transition, it was noted that even though the reverse $\beta \rightarrow \alpha$ transition could take place under appropriate conditions, the rate of this reaction was slow. Samples of the β form could be heated for several hours even at the transition temperature without formation of the α form as long as the relative humidity was maintained at a low value.

The number of non-solvated polymorphs of carbamazepine, and the ease of their interconversion, as led to the performance of a number of studies on this system. For example, in situ Raman spectroscopy has been used to study the kinetics associated with the solid-state transformation of Form-III into Form-I (16). The rate of transformation was monitored by measuring the relative intensities of peaks derived from two C–H bending modes, and the data subsequently fitted to various solid-state kinetic models. Arrhenius plots derived from the kinetic models yielded a range of 344 to 368 kJ/mol for the activation energy of the transition.

Temperature-dependent terahertz (THz) pulsed spectroscopy was used to study the phase transformation of carbamazepine Form-III into Form-II, as well as the solid-state transition that took place even under isothermal conditions below the melting point (17). Spectra reported for Form-I and Form-III are shown in Figure 8 along with the second-derivative spectra calculated from the original data. Although the zeroth-derivative spectra exhibit substantial differences, the second-derivative spectra of the two polymorphs are extremely different and permit ready identification of the two crystal forms. When Form-III was heated between 20°C and 160°C, the spectral features were observed to broaden and decrease in intensity, and eventually shifted to lower energies. Further heating the samples to 180°C led to melting and subsequent recrystallization to Form-I, which caused the THz absorption spectrum to change into that of the new form. Sequences in the disappearance of Form-III spectral features, and in the appearance of Form-I features, indicated that the conversion mechanism comprised more than one step.

A single-crystal to single-crystal phase transition was found to take place at 333 K for the α-polymorph of *ortho*-ethoxy-*trans*-cinnamic acid (18). Structures for this compound were determined at two temperatures above the transition point in addition to structures of the stabile form existing at lower temperatures. It was found that the phase transition involved a cooperative conformational transformation coupled with a shift in layers of the constituent molecules. The packing in the structures did not depend so much on the nature of the O–H···O and C–H···O interactions making up patterns of molecular ribbons as it depended on the nature of differing van der Waals forces in the polymorphs. Although the α and γ polymorphs could be crystallized from solutions, the high-temperature α′ form was only accessible from the thermally induced phase transformation.

The isothermal phase transformation of mefenamic acid Form-I into Form-II was studied using solid-state infrared spectroscopy at a sufficient number of temperatures that permitted calculation of the activation energy for the process (19). Although an activation energy of 86.4 kcal/mol had been determined using differential scanning calorimetry, the infrared method yielded a significantly smaller value of 71.6 kcal/mol. The discrepancy in results obtained by the spectroscopic and thermal methods was explained as a loss of analyte due to sublimation when samples of mefenamic acid were maintained at elevated temperatures in the DSC pans prior to measuring the exothermic event that was indicative of the Form-I content in a sample.

Mebendazole has been reported to exist in three different polymorphic forms in the solid state, with Form-C being the pharmaceutically preferred form because of its increased aqueous solubility. Variable-temperature X-ray powder diffraction has been used to study the transformation of metastable Form-C into stable Form-A, with this process taking place when the sample was heated above 180°C (20). The phase transformation was shown to be a first-order structural event that was

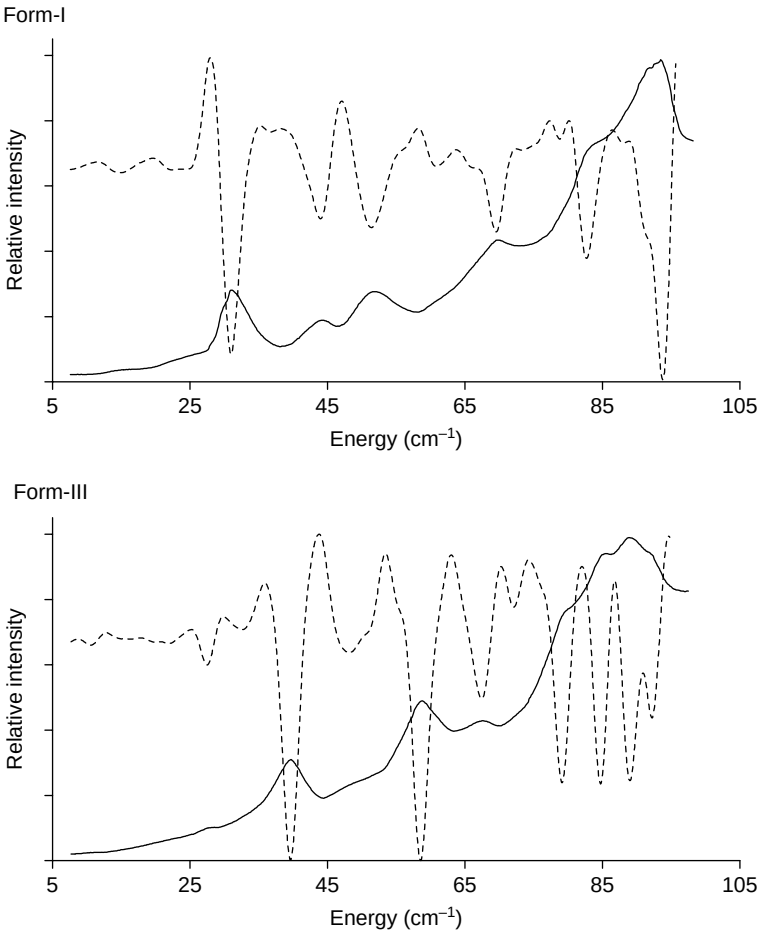

FIGURE 8 Terahertz absorption spectra obtained for carbamazepine Form-I (*upper spectra*) and Form-III (*lower spectra*), showing both the raw absorption spectrum (*solid traces*) and the corresponding second derivative spectrum (*dashed traces*) for each. The spectra are shown in arbitrary units, and have been adapted from Ref. (17).

characterized by an activation energy of 238 ± 16 kJ/mol. Compression of the metastable Form-C did not lead to the observation of any significant change in its crystal structure, indicating that the energy associated with the compaction process was insufficient to cause any measurable phase transformation.

The low-frequency vibrational modes of five polymorphs of sulfathiazole have been studied by THz pulsed spectroscopy and Raman spectroscopy, with the THz method being shown to be a rapid method of phase identification (21). Variable-temperature spectroscopic studies were contrasted with conventional thermal analysis measurements to develop structure–spectra correlations in order to understand the behavior of individual vibrational bands during the thermally

induced phase transitions between the different forms. Studies conducted at low heating rates in a special thermal transitiometer having high energetic sensitivity enabled a determination for the first time that theophylline Forms II and I were enantiotropically related, and that the phase transition between these forms took place at a temperature of 536.8 ± 2.2 K with an associated enthalpy change of 1.99 ± 0.09 kJ/mol (22).

The utility of on-line Raman spectroscopy as a sensitive method for the monitoring of transformation kinetics and the determination of transition temperatures was demonstrated using flufenamic acid as a model system (23). Transition temperatures deduced from use of the spectroscopic method were found to be in good agreement with results obtained using the more conventional van't Hoff computational approach. Because spectroscopic experiments can be followed on an extremely short time scale, such methodology was proposed for the study of rapidly converting systems where properties of the metastable forms might be difficult to accurately measure.

The Form-II to Form-I phase transformation of caffeine that takes place around 140°C has been studied using quasi-isothermal modulated temperature differential scanning calorimetry and microthermal analysis with the aim of developing a more complete understanding the physics of the process (24). In this work, a novel extension of the reduced temperature method was developed and applied to linear rising temperature data corresponding to the phase transition, with the analysis suggesting a close approximation to Arrhenius behavior. In addition, a heat transfer model that allows calculation of the thermal gradients within a hermetically sealed pan was described, and the combined approach allowed the characterization of the thermodynamics and kinetics of the transformation process as well as spatial identification of the distribution of the transformation in compressed systems.

Dehydration and Desolvation Phase Transformation

The performance of a dehydration or desolvation process frequently leads to the formation of a new crystalline state. For example, the initially crystallized dihydrate crystal form of naproxen sodium could be transformed into a monohydrate phase by dehydration of the dihydrate phase in a desiccator (maintained at 0% relative humidity) over a two-day period (25). It was also found that the anhydrate phase could be obtained from either the monohydrate or the dihydrate by drying the substance in an oven at 120°C for two hours. Thermal analysis data was used to demonstrate the existence of two types of water in the crystals of the dihydrate form, and that each could be separately removed at a characteristic temperature.

The dehydration of sodium naproxen dihydrate was further studied using X-ray powder diffraction and thermogravimetric analysis, confirming the observation that a monohydrate could be formed prior to generation of the anhydrate (26). Microscopic examination of dehydrating crystals revealed that dehydration along the *b*-axis of the crystals was most rapid owing to the presence of channels that could serve to facilitate water transport out of the lattice. In addition, large cracks formed during the dehydration process that were noted to form along the *b*-axis of the crystals, with this phenomenon being used to explain the observed significant shrinkage along the *c*-axis that accompanied the dehydration process.

Although thermal analysis and X-ray powder diffraction studies indicated that cefadroxil monohydrate appeared to undergo a relatively simple process

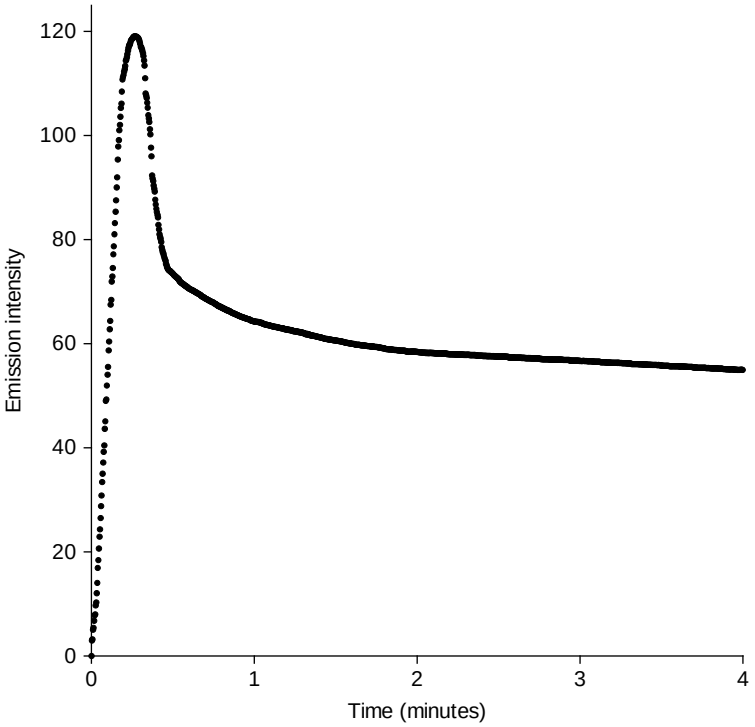

FIGURE 9 Early stages in the time dependence of the emission intensity (excitation at 350 nm, emission at 415 nm) of carbamazepine anhydrate Form-III slurried in water at 18.5°C, illustrating the rapid initial rise in emission intensity as the anhydrate material dissolved, and the decrease in intensity when the dihydrate phase nucleates and solid precipitate is formed. These zones are eventually followed by a gradual rise in intensity as the dihydrate phase content grows at the expense of the anhydrate phase content.

thermally induced dehydration, solid-state fluorescence spectroscopy studies pointed toward the existence of a cefadroxil hemihydrate that could be obtained by appropriate thermal dehydration (27). The fluorescence spectral results indicated the existence of two major photophysical pathways for delocalization of excitation in the cefadroxil monohydrate crystal, each of which could be selectively activated by irradiation with the proper excitation wavelength. As illustrated in Figure 9, one of the photophysical systems appeared to dominate the spectroscopy of the monohydrate, but was eliminated once the monohydrate was dehydrated to a hemihydrate. The other photophysical pathway existed in the monohydrate structure, and became the sole mechanism for observable fluorescence once the cefadroxil monohydrate was partially dehydrated to the hemihydrate.

Two-dimensional X-ray powder diffraction has been used to study the dehydration kinetics of theophylline monohydrate, as well as to investigate the effect of poly(vinylpyrrolidone) on the dehydration pathway and associated kinetics (28). The dehydration of the monohydrate was shown to yield either the anhydrate, or a metastable anhydrate that eventually transformed into the more stable anhydrate

form. The latter reaction had been previously implicated in dissolution failures associated with tablet hardening (29). Interestingly, the polymer was shown to be able to inhibit the dehydration reaction (especially at lower drying temperatures) in proportion to the poly(vinylpyrrolidone) concentration. Details of the phase transformation processes associated with the hydration and dehydration of theophylline have also been studied using Raman spectroscopy (30) and terahertz pulsed spectroscopy (31).

The thermally induced dehydration of erythromycin A dihydrate has been studied using in situ variable-temperature X-ray powder diffractometry and hot-stage Raman spectroscopy (32). The dehydration of the dihydrate form over the range of 40°C to 100°C led to the formation of an isomorphic non-hydrate, which could be melted around 135°C and eventually crystallized into the anhydrate phase at approximately 150°C. It was found that Raman spectroscopy could distinguish between the isostructural forms of erythromycin A, demonstrating its ability to be used as an in-process technique for control over a potential drying process.

The kinetics associated with the dehydration and desolvation of fluconazole solvatomorphs were studied by DSC, thermogravimetry, and X-ray powder diffraction, with the aim of understanding the kinetics and mechanisms associated with the desolvation processes (33). Statistical evaluation of the results indicated that the three-dimensional phase boundary reaction model provided the best fit for the fluconazole monohydrate dehydration data, whereas the three-dimensional diffusion model yielded the best fit for the fluconazole ethyl acetate solvatomorph desolvation data. Hydrogen-bond dissociation processes were found to have the largest effect on the magnitude of the activation energy of the dehydration process, whereas the activation energy for the ethyl acetate desolvation process appeared to be governed by factors associated with the constricted channels of the crystal.

The solid-state stability of five structurally related solvates of sulfameter have been studied using isothermal and nonisothermal thermogravimetry to understand the kinetics of their desolvation reaction (34). It was determined that the derived kinetic parameters could be correlated with structural features of the solid, and were not merely computed parameters that provided the best statistical fit to the data. The most appropriate solid-state reaction model correlated to single crystal structural features of the solvatomorphs where solvent molecules occupied cavities in the unit cell, indicating that the physical size of the solvent molecules and their desolvation activation energies depended on the cavity size within the crystal. It was also learned that isothermally and non-isothermally derived kinetic parameters did not agree, and that kinetic results obtained from the use of one method may not be extended to results obtained from the other.

The physicochemical behavior of trehalose dihydrate during storage under conditions of low relative humidity and ambient temperature was investigated using weight loss measurements, water content determinations, differential scanning calorimetry profiling, and X-ray powder diffraction analysis (35). It was shown that under these conditions, trehalose dihydrate could be dehydrated into its α polymorph, and this dehydration was accompanied by the formation of cracks on the surfaces of the particles These cracks set in prior to the completion of the dehydration process, and could not be fully reversed upon completion rehydration at a relative humidity of 50%. These findings have implications in the use of trehalose dihydrate as an excipient in carrier-based dry powder inhalation formulations because the surface properties of the excipient are essential to its proper behavior

and alterations resulting from processing or storage conditions could affect the way the excipient interacts with the drug substance.

In another work, the multi-disciplinary application of atomic force microscopy, dynamic vapor sorption, and near infrared spectroscopy was used to investigate the outer-layer and bulk kinetics of the dehydration of trehalose dihydrate under conditions of ambient temperature and low humidity (36). Use of the microscopic technique enabled the determination of the dehydration kinetics of the outer layers both directly and from bulk data, and it was reported that no significant differences between the outer layer dehydration kinetics could be gleaned using these methods. The microscopic method also permitted the analysis of bulk-only kinetics from the vapor sorption and spectroscopic data, suggesting that the combination of atomic force microscopy and bulk characterization techniques should facilitate the acquisition of a more complete understanding of the kinetics of certain solid-state reactions.

X-ray powder diffraction was used to study the progressive conversion of raffinose pentahydrate to its amorphous form by heating at 60°C over a period of 72 hours (37). The presence of defects in the crystalline structure and any amorphous content was determined using a total diffraction method where both the coherent long-range crystalline order and the incoherent short-range disorder components were modeled as a single system. The long-range crystal structure of the initial pentahydrate phase remained intact in residual crystalline material, although the *c*-axis of the unit cell underwent an abrupt change after two hours of drying with the loss of one to two water molecules. The remaining crystal structure gradually disappeared over the two- to eight-hour time period, with the diffuse scattering containing both amorphous and defect contributions. It was concluded that removal of the first two waters of hydration created defects, and that these defects aided in subsequent conversion to the amorphous state.

PHASE TRANSFORMATIONS CAUSED BY THE ACTION OF A SECOND PHASE

When a solid consisting of a single component interacts with another phase consisting of a different component, the number of variables required by the Phase Rule to specify the system increases. Besides the usual variables of temperature and pressure, a concentration factor must also be specified in order to simplify the phase diagram. For a solvent interacting with a solid, the additional factor will be the solubility of the solute in the solvent at a given temperature and pressure, and the magnitude of this solubility will strongly affect the kinetics and outcome of the phase conversion process. For a solid interacting with a vapor, the partial pressure of the interacting component in the vapor will generally be the dominant factor in determining the kinetics and type of product formed by sorption of that interacting component.

Solution-Mediated Phase Transformation

Because it is not likely that a solution-mediated phase transformation could be adequately described by equilibrium theory, one must consider the process more from a kinetic viewpoint than from a thermodynamic viewpoint. For instance, during investigational work designed to determine the polymorphic and solvatomorphic space for a compound, one typically first crystallizes the substance out of

a variety of solvents and under a variety of conditions. Very often, if conditions are appropriate for the nucleation of a metastable crystal form, one can then obtain bulk quantities of that polymorph through continued crystal growth as long as no other phase transformation reactions take place. The identity of the isolated crystal form frequently depends on the properties of the crystallization solvent, as well as on the mechanism whereby the supersaturation of the solute in the crystallizing solution is discharged (38).

Owing to its inherent range of chemical and physical properties, the crystallizing solvent often exerts a strong influence over the nature of packing or conformation polymorphism that can exist for a given compound. Solvents have been classified on the basis of their proton donating, proton accepting, and dipole interaction abilities (39), and also divided into classes according to their high-performance liquid chromatography (HPLC)-related properties (40). Additional information about solvent classifications is available in the compilation of Riddick and Bunger (41). Given the additional variability introduced into the phase diagram of a compound, there certainly exists a substantial probability that a kinetically controlled, non-thermodynamic, process could dominate in a system formed by a solid substance and its saturated solution.

It has been recognized since the earliest studies of Ostwald (42) that the phase diagram for solubility is more complicated than is most commonly envisioned. At a specified temperature and pressure, a supersaturated solution will not necessarily spontaneously adjust to the equilibrium condition required by the phase rule (i.e., the equilibrium solubility) unless the degree of supersaturation exceeds a certain critical value. The concentration region where supersaturation can be obtained without the spontaneous formation of crystal nuclei is termed the metastable zone, whereas the concentration region where the formation of crystal nuclei cannot be stopped is termed the labile zone.

Ostwald made a number of important observations regarding the relative stability of crystal forms, one of which is that the polymorph having the least stability tends to crystallize first, and another is that metastable crystal forms tend to convert into more stable crystal forms during the time they were suspended in solution. As he stated, "When a given chemical system is left in an unstable state, it tends to change not into the most stable form, but into the form the stability of which most nearly resembles its own; that is, into that transient stable modification whose formation from the original state is accomplished by the smallest loss of free energy" (14). The practical implication of the Rule of Stages is that if investigators want to isolate a metastable polymorph formed during a rapid discharge of supersaturation, they must quickly remove the precipitated solids from the crystallizing solution before it has a chance to transform into a new crystal form.

That kinetics plays the essential role in the course of solution-mediated phase transformations has been known for quite some time, and non-equilibrium thermodynamic approaches have been used to develop a theory to explain the phenomenon. The most notable of these is the work of Davey, who deduced that the kinetic theory suggested the existence of very different profiles for discharge of supersaturation for the extremes of growth-controlled and dissolution-controlled transformations (43,44). Davey used examples taken from the dyestuff and agrochemical fields to confirm that both types of process could occur under suitable circumstances. Around the same time, van Santen used an irreversible thermodynamic approach to show that the step rule of Ostwald served to minimize entropy production (45).

The significance of controlling both the mechanism and kinetics of particle growth during crystallization processes has been discussed, with the importance of nucleation control being emphasized (46). Microscopy was held to be an important interrogative tool for characterization work, stressing inverted optical microscopy (for the study of crystallization processes in situ, to monitor phase transformations in suspensions, to determine transformation times, and to measure crystal growth rates), electron microscopy (to characterize solute interactions with specific crystal faces, to identify nucleation and growth mechanisms, and to measure crystal growth rates), and atomic force microscopy (another in situ method for the study of crystallization processes).

One of the common procedures used to isolate quantities of a desired polymorphic form entails the introduction of seed crystals of the appropriate crystal form into a crystallizing solution where the solute concentration is in the metastable zone. The possibility that solution-mediated phase transformation processes could take place subsequent to the seeding step is very real, and as a result the seeding procedure has to be carefully investigated and controlled. These issues have been fully discussed, with particular emphasis being placed on the choice and preparation of seed crystals, the appropriate window for adding seed crystals in a crystallizing medium, the rate of crystallization and amount of added seed crystals, how to add the seed crystals, and how to scale up a seeded process (47).

One of the solution-mediated phase transformation systems that has been extensively studied is the formation of carbamazepine dihydrate from its various anhydrous polymorphs. For example, Raman spectroscopy has been used to study the kinetics of the conversion of the Forms I and II, and II anhydrates to the dihydrate in aqueous suspensions (48). In this work, it was found that the morphology of the starting material was a more important factor in determining the rates of reaction than was the actual phase identity of the starting material. In another study, electron microscopy was used in conjunction with Raman spectroscopy to study the conversion of single carbamazepine crystals to the dihydrate in water and in aqueous solutions, and it was shown that defect structures were a more important driving force for the conversion than was the identity of the crystal face where the hydration initially took place (49).

A Raman immersion probe was used to follow the anhydrate–dihydrate phase conversion of carbamazepine in ethanol–water mixtures as a function of both composition and temperature (50). The phase transformation was deduced to consist of a two-step process, with the first step consisting of dissolution of the anhydrate phase and the second step being crystallization of the dihydrate phase. Owing to the relatively slow kinetics of the crystallization, it was determined that crystallization of the dihydrate form represented the rate-determining step in the overall kinetics of phase transition. Through the use of mixed solvents, it was also determined that the phase transformation rates could be correlated with the deviation of the water activity in the solution from the equilibrium water activity value.

The effect of five different additives on the anhydrate-to-dihydrate transformation in ethanol–water mixtures were evaluated using an in-line Raman probe (51). Among other things, it was found that hydroxypropyl methylcellulose exhibited a strong inhibitory effect on the phase transformation, and that it also decreased the difference in solubility among the various crystal forms. In another study of the effect of excipients on the anhydrate-to-dihydrate phase transformation of carbamazepine, it was established that hydrogen bonding ability and sufficient

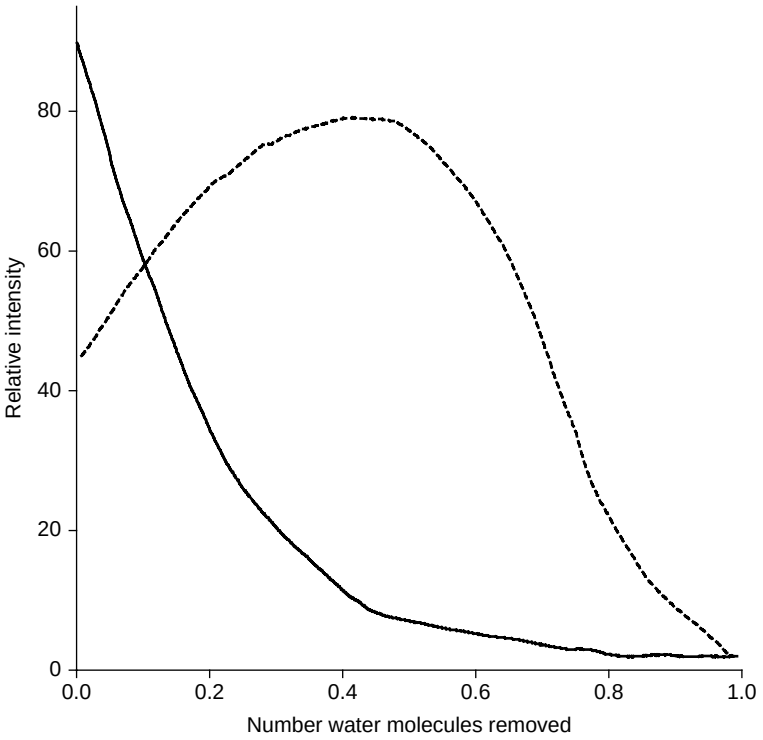

FIGURE 10 Dependence of cefadroxil fluorescence intensities as a function of the number of coordinated water molecules in isothermally heated samples. The intensity of the EX360–EM460 system is shown as the solid trace, whereas the intensity of the EX390–EM540 system is shown as the dashed trace.

hydrophobicity were important as factors influencing the inhibition activity of the excipients, although the relative importance of the two factors could not be established (52).

It has been found that both the anhydrous Form-III and dihydrate phases of carbamazepine exhibit fluorescence in the solid state (53). The fluorescence intensity associated with the dihydrate phase was determined to be significantly more intense than that associated with the anhydrate phase, and this difference was exploited to develop a method for study of the kinetics of the aqueous solution-mediated phase transformation between these forms. Figure 10 shows plots of the early stages in the time dependence of the emission intensity of carbamazepine anhydrate Form-III slurried in water at various at suspension concentrations. Each trace consisted of an initial rapid increase in emission intensity as the anhydrate material dissolved, followed by a decrease in intensity when the dihydrate phase nucleated and solid precipitate was formed, and finally a gradual rise in intensity as the dihydrate phase content grew at the expense of the anhydrate phase content. Studies were conducted at temperatures over the range of 18°C to 40°C, and it was found that the phase

transformation was adequately characterized by first-order reaction kinetics and an activation energy of 11.2 kcal/mol (47.4 cal/gram) for the phase conversion.

X-ray powder diffraction has been use to quantify the kinetics of the solution-mediated phase transformation of the metastable form of an active pharmaceutical ingredient to one of its more stable forms, and it was reported that the transformation rate could be influenced by the presence of structurally related, tailor-made, impurities (54). Modified attachment energy calculations were found to represent an effective indicator as to how likely a given impurity molecule would be incorporated in the growing crystal. In this work, it was proposed that the energetic calculations could facilitate the design of suitable molecules that would inhibit the crystallization of the stable form and therefore stabilize the metastable crystal form.

The kinetics associated with the phase conversion of mefenamic acid Form-II to Form-I was studied in three solvent systems and under high humidity conditions (55). As might be expected, the transformation was accelerated with increasing temperature, with the addition of seed crystals of the product phase, and with the degree of solubility in the suspending solvent system. The effect of a number of parameters on the solution-mediated Form-II to Form-I phase transformation of buspirone hydrochloride was studied with the aim of developing a response surface analysis in order to identify the more important factors affecting the polymorphic interconversion (56). The phase transformation of clopidogrel hydrogen sulfate Form-I into Form-II has been studied using in situ measurements of ultrasonic velocity, with the technique being able to provide information on the induction times and transformation rates for formation of the two polymorphs as well as effects of temperature and solvent composition (57).

Solution-mediated phase transformation reactions can play havoc with dissolution profile studies if they take place during the lifetime of the study, and any dissolution study of a metastable crystal form must take this possibility into account. Such phase transformations were studied for theophylline and nitrofurantoin using a channel flow intrinsic dissolution system, where the polymorphic form of the dissolving solid was continually monitored using Raman spectroscopy (58). It was concluded that knowing both the drug concentrations in the dissolution medium and the solid-state characterization provided a route to a deeper understanding of the phase transitions accompanying the dissolution. In a subsequent work, the solution-mediated phase transformation of theophylline anhydrate into the monohydrate were studied in rotating disc and channel flow cell dissolution devices with a particular aim of characterizing the kinetics of reactions taking place in both systems (59).

A rate enhancement effect due to secondary nucleation has been identified in the solution-mediated transformation of the α-phase of (*L*)-glutamic acid to its β-phase (60). In this study, the kinetics of the polymorphic transition were studied using optical microscopy combined with Fourier transform infrared, Raman, and ultraviolet absorption spectroscopies. In another work, four different in situ analytical techniques have been used to study the solvent-mediated $\alpha \rightarrow \beta$ phase transformation of (*L*)-glutamic acid, combined with a mathematical model based on population balance equations of equations describing the kinetics of nucleation and growth (61). This approach facilitated estimation of the nucleation and growth rates of the two polymorphs, profiling of the dissolution process, and a validation of the population balance model. On-line X-ray powder diffractometry has been

combined with a flow-through cell and a chemometric method to study the phase transformation between the metastable α-form and the stable β-form of (*L*)-glutamic acid (62). The interconversion processed were studied in slurries, and Arrhenius methods were used to determine that the activation energy of the process was 43.9 kJ/mol.

Phase Transformation Caused by Vapor Sorption

The interaction of solids with gases in the vapor phase represents another exceedingly important area of a crystal form screening protocol, and gains special importance when the interacting substance in the vapor is water and the product in the solid state is a hydrate. In its most basic form, the methodology is to simply expose solids pre-selected relative humidity conditions (usually through the use of saturated salt solutions) and to allow the solids to interact with the vapor for a sufficiently long time period for the equilibration to reach a steady state. After complete equilibration of the sample with the environment is obtained, one measures the water content and typically plots the total water content as a function of relative humidity. When a compound does not form a hydrate, a plot of water content against relative humidity will ordinarily consist of a simple concave-up type of plot. However, when a substance can form a stoichiometric hydrate, the hydrate will exhibit stability and a well-defined water content over a range of relative humidity values (63,64). It is a simple matter after that to use the measured water content to calculate the stoichiometry of the hydrate.

A wide range of additional experimentation can be performed using dynamic vapor sorption instrumentation, where a sample is subjected to varying conditions of humidity and temperature, and the gain or loss in mass of the sample is measured. Each measurement thus consists of a sorption isotherm, which contains information regarding the water content values during the process of adsorption at a constant temperature. The technology has been used to determine the critical relative humidity for the onset of moisture-induced phase transformation processes, and has proved to be especially useful in the characterization of trends in glass transition temperatures and crystallization processes in amorphous or partially amorphous substances (65).

A Raman spectrometer interfaced with a moisture sorption gravimetric analyzer has been used to study modes of water–solid interactions in sulfaguanidine, cromolyn sodium, ranitidine hydrochloride, amorphous sucrose, and silica gel (66). Principal components analysis was used to determine the trends in the Raman data, and the combination of instrumentation and data analysis facilitated the generation of information related the various types of interactions. For example, analysis using the various modeling routines on the humidity-dependent Raman spectra of cromolyn sodium enabled the conclusion that the spectral changes were most likely due to water-induced unit cell expansion, which in turn, provided increased flexibility in the structure allowing the two carboxylate groups to rotate away from each other.

The solvatomorphic space of the disodium salt of (*S*)-4-[[[1-(4-fluorophenyl)-3-(1-methylethyl)-1*H*-indol-2-yl]-ethynyl]-hydroxyphosphinyl]-3-hydroxybutanoic acid has been found to exceedingly rich, with the compound being able to form a multitude of hydrate forms upon exposure to various relative humidity environments (67). This developmental drug substance was found to exhibit rapid changes in moisture sorption (or desorption) when the environmental relative humidity was

altered, and the existence of an amorphous form, three crystalline hydrates, and a liquid crystalline phase were identified. Even so, it proved possible to formulate the substance into solid dosage forms by dry granulation as long as the relative humidity was kept below 52%. Interestingly, the dissolution rate of the substance from its formulations was found not to depend on the crystal form in the dosage form.

The three crystalline hydrates and liquid crystalline phase of this disodium salt of (*S*)-4-[[[1-(4-fluorophenyl)-3-(1-methylethyl)-1*H*-indol-2-yl]-ethynyl]-hydroxyphosphinyl]-3-hydroxybutanoic acid were also found to exhibit varying fluorescence properties as a result of the hydration condition in their respective solid states (68). The monohydrate Form-I was characterized by an excitation maximum at 345 nm and a fluorescence maximum at 371 nm. Form-II (a dihydrate) exhibited essentially equivalent spectral characteristics as did Form-I, except for a significant reduction in fluorescence intensity. The excitation maximum found for Form-III (effectively a hexahydrate) was found to shift to 400 nm, and the fluorescence shifted to 485 nm. This latter behavior is consistent with the formation of indole excimers in this phase, resulting from a stacking of the ring systems within the solid. Finally, upon binding of nine hydration waters, the structure relaxed into a liquid crystalline form that exhibited similar spectral characteristics to those of Form-III, but of greatly reduced intensity. The dependence of cefadroxil fluorescence intensities upon the number of coordinated water molecules in isothermally heated samples is shown in Figure 10.

Near-infrared spectroscopy was used to study the temperature dependence of the phase interconversion between the solvatomorphs of caffeine, with the rate of conversion being dependent on the difference between the observed relative humidity and the equilibrium water activity of the anhydrate/hydrate system (69). It was found that the phase boundary between caffeine anhydrate and the 4/5-hydrate existed at a relative humidity of 67% at 10°C, 74.5% at 25°C, and 86% at 40°C. Numerical fitting of these data enabled the deduction of a relationship that permitted the determination of the phase boundary at any temperature appropriate for a secondary processing process.

A monohydrate intermediate was implicated in the solid-state transition of theophylline metastable Form-III to the stable Form-II, with the transition being strongly affected by the environmental relative humidity (70). The transition between the anhydrates was found to be accelerated by increasing degrees of relative humidity, whereas elevated humidity levels inhibited the transition of the monohydrate to Form-II. The kinetics of the humidity-induced phase transformation from the anhydrate to the hydrate has been studied using Raman spectroscopy, where it was determined that although the anhydrate-to-monohydrate reaction proceeds as a single-step hydration process, the monohydrate-to-anhydrate is a two-step dehydration reaction (71). In this work, it was determined that the critical relative humidity for room temperature hydration of the anhydrate was approximately 79%. The effects of multi-chamber microscale fluid bed drying on the phase composition of theophylline drug products has been studied, indicating that drying a monohydrate starting material would produce the stable anhydrate phase that was contaminated with measurable quantities of the metastable anhydrous form (72).

The interaction of the anhydrate, dihydrate, hemi-pentahydrate, trihydrate, and pentahydrate solvatomorphs of norfloxacin with water have been studied with

the aim of understanding the particular zones of environmental stability as well as the propensity of each form to convert to another (73). Most of the forms converted to the pentahydrate at extremely high degrees of relative humidity, although the dihydrate resisted conversion. The pentahydrate itself proved to be fairly stable with respect to dehydration, only undergoing a desolvation reaction when the relative humidity was decreased below 20%, and the hemi-pentahydrate form was produced when the anhydrate was exposed to 75% relative humidity.

It has been observed that under conditions of high relative humidity, paracetamol Form-II that had been crystallized from ethanol transforms more rapidly into Form-I than did Form-II that had been crystallized from a molten state (74). Although it was determined that seed crystals of Form-I were present in product obtained when Form-II was obtained from a solution-phase process, their presence could not be used to entirely explain the difference in phase conversion rates. Grinding experiments indicated that a small amount of ethanol (less than 1%) remained in solution-grown product, and it was concluded that moisture sorption from the vapor phase triggered an ethanol-mediated growth of the existing Form-I nuclei.

An on-line process analytical approach was used to obtain a better understanding of the phase transformations experienced by erythromycin dihydrate during production of pellets by the extrusion-spheronization and drying process (75). Samples were taken after the blending, granulation, extrusion, and spheronization steps of the process during drying at 30°C or 60°C, and were characterized as to their near-infrared spectra and X-ray powder diffraction patterns. No change in phase composition was detected for product obtained by pelletization and drying at 30°C, but partial dehydration of the drug substance was observed for pellets dried at 60°C. Variable-temperature X-ray powder diffraction measurements carried out between 25°C and 200°C on initially wet pellets confirmed that erythromycin dihydrate underwent a thermally induced dehydration reaction at approximately 60°C.

REFERENCES

1. Buerger MJ. Crystallographic aspects of phase transformations, chapter 6 in Phase Transformations in Solids. In: Smoluchowski R, Mayer JE, Weyl WA, eds. New York: John Wilen & Sons, 1951: 183–211.
2. McCrone WC. Polymorphism, chapter 8 in Physics and Chemistry of the Organic Solid State. New York: Interscience Pub, 1965: 726–67.
3. Bernstein J. Conformational polymorphism, chapter 13 in Organic Solid State Chemistry. In: Desiraju GR, ed. Amsterdam: Elsevier, 1987: 471–518.
4. Byrn SR, Pfeiffer RR, Stowell JG. Physical transformations of crystalline solids, Part 4 in Solid-State Chemistry of Drugs, 2nd edn. West Lafayette: SSCI Inc, 1999: 259–60.
5. Paul IC, Curtin DY. Thermally induced organic reactions in the solid state. Acc Chem Res 1973; 6: 217–25.
6. Burger A, Ramberger R. On the polymorphism of pharmaceuticals and other molecular crystals. I. Theory of thermodynamic rules. Mikrochim Acta (Wien) 1979; II: 259–71.
7. Burger A, Ramberger R. On the polymorphism of pharmaceuticals and other molecular crystals. II. Applicability of thermodynamic rules. Mikrochim Acta (Wien) 1979; II: 273–316.
8. Burger A. Thermodynamic and other aspects of the polymorphism of drugs. Pharm Int 1982; 3: 158–63.
9. Yu L. Inferring thermodynamic stability relationship of polymorphs from melting data. J Pharm Sci 1995; 84: 966–74.

10. Giron D. Thermal analysis and calorimetric methods in the characterization of polymorphs and solvates. Thermochim Acta 1995; 248: 1–59.
11. Bernstein J. Fundamentals, chapter 2 in Polymorphism in Molecular Crystals. Oxford: Clarendon Press, 2002: 29–41.
12. Lohani S, Grant DJW. Thermodynamics of polymorphs, chapter 2 in Polymorphism in the Pharmaceutical Industry. Weinheim: Wiley-VCH, 2006: 21–42.
13. Kawakami K. Reversibility of enantiotropically related polymorphic transformations from a practical viewpoint: thermal analysis of kinetically reversible/irreversible polymorphic transformations. J Pharm Sci 2007; 96: 982–9.
14. Rubin-Preminger JM, Bernstein J, Harris RK, et al. Variable temperature studies of a polymorphic system comprising two pairs of enantiotropically related forms: (S,S)-ethambutol dihydrochloride. Cryst Growth Des 2004; 4: 431–9.
15. Rong HR, Gu H. Polymorphs of 2,4,5,6-tetrachloro-l,3-benzenedicarbonitile and their transformations. Thermochim Acta 2005; 428: 19–23.
16. O'Brien LE, Timmins P, Williams AC, et al. Use of in situ FT-raman spectroscopy to study the kinetics of the transformation of carbamazepine polymorphs. J Pharm Biomed Anal 2004; 36: 335–40.
17. Zeitler JA, Newnham DA, Taday PF, et al. Temperature dependent terahertz pulsed spectroscopy of carbamazepine. Thermochim Acta 2005; 436: 71–7.
18. Fernandes MA, Levendis DC, Schoening FRL. A new polymorph of ortho-ethoxy-trans-cinnamic acid: single-to-single-crystal phase transformation and mechanism. Acta Cryst 2004; B60: 300–14.
19. Gilpin RK, Zhou W. Infrared studies of the thermal conversion of mefenamic acid between polymorphic states. Vib Spectrosc 2005; 37: 53–9.
20. de Villiers MM, Terblanche RJ, Liebenberg W, et al. Variable-temperature X-ray powder diffraction analysis of the crystal transformation of the pharmaceutically preferred polymorph C of mebendazole. J Pharm Biomed Anal 2005; 38: 435–41.
21. Zeitler JA, Newham DA, Taday PF, et al. Characterization of temperature-induced phase transformations in five polymorphic forms of sulfathiazole by terahertz pulsed spectroscopy and differential scanning calorimetry. J Pharm Sci 2006; 95: 2468–98.
22. Legendre B, Randzio SL. Transitiometric analysis of solid-II / solid-I transition in anhydrous theophylline. Int J Pharm 2007; 343: 41–7.
23. Hu Y, Wikström H, Byrn SR, et al. Estimation of the transition temperature for an enantiotropic polymorphic system from the transformation kinetics monitored using raman spectroscopy. J Pharm Biomed Anal 2007; 45: 546–51.
24. Manduva R, Kett VL, Banks SR, et al. Calorimetric and spatial characterization of polymorphic transitions in caffeine using quasi-isothermal MTDSC and localized thermomechanical analysis. J Pharm Sci 2008; 97: 1285–300.
25. Kim Y-S, Rousseau RW. Characterization and solid-state transformations of the pseudo-polymorphic forms of sodium naproxen. Cryst Growth Des 2004; 4: 1211–16.
26. Kim YS, Paskow HC, Rousseau RW. Propagation of solid-state transformations by dehydration and stabilization of pseudopolymorphic crystals of sodium naproxen. Cryst Growth Des 2005; 5: 1623–32.
27. Brittain HG. Fluorescence studies of the dehydration of cefadroxil monohydrate. J Pharm Sci 2007; 96: 2757–64.
28. Nunes C, Mahendrasingam A, Suryanarayanan R. Investigation of the multi-step dehydration reaction of theophylline monohydrate using 2-dimensional powder X-ray diffractometry. Pharm Res 2006; 23: 2393–404.
29. Phadnis NV, Suryanarayanan R. Polymorphism in anhydrous theophylline – implications for the dissolution rate of theophylline tablets. J Pharm Sci 1997; 86: 1256–63.
30. Amado AM, Nolasco MM, Ribeiro-Claro PJA. Probing pseudopolymorphic transitions in pharmaceutical solids using raman spectroscopy: hydration and dehydration of theophylline. J Pharm Sci 2007; 96: 1366–79.

31. Zeitler JA, Kogermann K, Rantanen J, et al. Drug hydrate systems and dehydration processes studied by terahertz pulsed spectroscopy. Int J Pharm 2007; 344: 78–84.
32. Kriachthev L, Rantanen J, Yliruusi J. Insight into thermally induced phase transformations of erythromycin a dihydrate. Cryst Growth Des 2006; 6: 369–74.
33. Alkhamis KA, Salem MS, Obaidat RM. Comparison between dehydration and desolvation kinetics of fluconazole monohydrate and fluconazole ethyl acetate solvate using three different methods. J Pharm Sci 2006; 95: 859–70.
34. Khawam A, Flanagan DR. Desolvation kinetics of sulfameter solvates. J Pharm Sci 2008; 97: 2160–75.
35. Jones MD, Hooton JC, Dawson ML, et al. Dehydration of trehalose dihydrate at low relative humidity and ambient temperature. Int J Pharm 2006; 313: 87–98.
36. Jones MD, Beezer AE, Buckton G. Determination of outer layer and bulk dehydration kinetics of trehalose dihydrate using atomic force microscopy, gravimetric vapor sorption, and near infrared spectroscopy. J Pharm Sci 2008; 97: 4404–15.
37. Bates S, Kelly RC, Ivanisevic I, et al. Assessment of defects and amorphous structure produced in raffinose pentahydrate upon dehydration. J Pharm Sci 2007; 96: 1418–33.
38. Threlfall T. Crystallization of polymorphs: thermodynamic insight into the role of solvent. Org Proc Res Dev 2000; 4: 384–90.
39. Snyder LR. Classification of solvent properties of common liquids. J Chrom Sci 1978; 16: 223–41.
40. Sadek PC. The HPLC solvent guide. New York: John Wiley & Sons, 1996.
41. Riddick JA, Bunger WB. Organic solvents, 3rd edn. New York: Wiley-Interscience, 1970.
42. Ostwald W. Lehrbuch, volume 2. Leipzig: Engelmann Press, 1897.
43. Cardew PT, Davey RJ. The kinetics of solvent-mediated phase transformations. Proc Royal Soc London 1985; A398: 415–28.
44. Davey RJ, Cardew PT, McEwan D, et al. Rate controlling processes in solvent-mediated phase transformations. J Cryst Growth 1986; 79: 648–53.
45. van Santen RA. The ostwald step rule. J Phys Chem 1984; 88: 5768–9.
46. Rodríguez-Hornedo N, Murphy D. Significance of controlling crystallization mechanisms and kinetics in pharmaceutical systems. J Pharm Sci 1999; 88: 651–60.
47. Beckmann W. Seeding the desired polymorph: background, possibilities, limitations, and case studies. Org Proc Res Dev 2000; 4: 382–3.
48. Tian F, Zeitler JA, Strachan CJ, et al. Characterizing the conversion kinetics of carbamazepine polymorphs to the dihydrate in aqueous suspension using raman spectroscopy. J Pharm Biomed Anal 2006; 40: 271–80.
49. Tian F, Sandler N, Gordon KC, et al. Visualizing the conversion of carbamazepine in aqueous suspension with and without the presence of excipients: a single crystal study using sem and raman spectroscopy. Eur J Pharm Biopharm 2006; 64: 326–35.
50. Qu H, Louhi-Kultanen M, Rantanen J, et al. Solvent-mediated phase transformation kinetics of an anhydrate/hydrate system. Cryst Growth Des 2006; 6: 2053–60.
51. Qu H, Louhi-Kultanen M, Kallas J. Additive effects on the solvent-mediated anhydrate/hydrate phase transformation in a mixed solvent. Cryst Growth Des 2007; 7: 724–9.
52. Tian F, Saville DJ, Gordon K, et al. The influence of various excipients on the conversion kinetics of carbamazepine polymorphs in aqueous suspension. J Pharm Pharmacol 2007; 59: 193–201.
53. Brittain HG. Fluorescence studies of the transformation of carbamazepine anhydrate form-III to its dihydrate phase. J Pharm Sci 2004; 93: 375–83.
54. Mukuta T, Lee AY, Kawakami T, et al. Influence of impurities on the solution-mediated phase transformation of an active pharmaceutical ingredient. Cryst Growth Des 2005; 5: 1429–36.
55. Kato F, Otsuka M, Matsuda Y. Kinetic study of the transformation of mefenamic acid polymorphs in various solvents and under high humidity conditions. Int J Pharm 2006; 321: 18–26.

56. Sheikhzadeh M, Murad S, Rohani S. Response surface analysis of solution-mediated polymorphic transformation of buspirone hydrochloride. J Pharm Biomed Anal 2007; 45: 227–36.
57. Kim H-J, Kim K-J. In situ monitoring of polymorph transformation of clopidogrel hydrogen sulfate using measurement of ultrasonic velocity. J Pharm Sci 2008; 97: 4473–84.
58. Aaltonen J, Heinanan P, Peltonen L, et al. In situ measurement of solvent-mediated phase transformations during dissolution testing. J Pharm Sci 2006; 95: 2730–7.
59. Lehto P, Aaltonen J, Niemelä P, et al. Simultaneous measurement of liquid-phase and solid-phase transformation kinetics in rotating disc and channel flow cell dissolution devices. Int J Pharm 2008; 363: 66–72.
60. Ferrari ES, Davey RJ. Solution-mediated transformation of α to β L-glutamic acid: rate enhancement due to secondary nucleation. Cryst Growth Des 2004; 4: 1061–8.
61. Scholl J, Bonalumi D, Vicum L, et al. In situ monitoring and modeling of the solvent-mediated polymorphic transformation of L-glutamic acid. Cryst Growth Des 2006; 6: 881–91.
62. Dharmayat S, Hammond RB, Lai X, et al. An examination of the kinetics of the solution-mediated polymorphic phase transformation between α- and β-forms of L-glutamic acid as determined using online powder X-ray diffraction. Cryst Growth Des 2008; 8: 2205–16.
63. Morris KR, Rodriguez-Hornedo N. Encyclopedia of pharmaceutical technology, volume 7. New York: Marcel Dekker, 1993: 393–440.
64. Khankari RK, Grant DJW. Pharmaceutical hydrates. Thermochim Acta 1995; 248: 61–79.
65. Burnett DJ, Thielmann F, Booth J. Determining the critical relative humidity for moisture-induced phase transitions. Int J Pharm 2004; 287: 123–33.
66. Gift AD, Taylor LS. Hyphenation of raman spectroscopy with gravimetric analysis to interrogate water-solid interactions in pharmaceutical systems. J Pharm Biomed Anal 2007; 43: 14–26.
67. Morris KR, Newman AW, Bugay DE, et al. Characterization of humidity-dependent changes in crystal properties of a new HMG-CoA reductase inhibitor in support of its dosage form development. Int J Pharm 1994; 108: 195–206.
68. Brittain HG, Ranadive SA, Serajuddin ATM. Effect of humidity-dependent changes in crystal structure on the solid-state fluorescence properties of a new HMG-CoA reductase inhibitor. Pharm Res 1995; 12: 556–9.
69. Kryzyaniak JF, Williams GR, Ni N. Identification of phase boundaries in anhydrate/hydrate systems. J Pharm Sci 2007; 96: 1270–81.
70. Matsuo K, Matsuoka M. Solid-state polymorphic transition of theophylline anhydrate and humidity effect. Cryst Growth Des 2007; 7: 411–15.
71. Amado AM, Nolasco MM, Ribeiro-Claro PJA. Probing pseudopolymorphic transitions in pharmaceutical solids using raman spectroscopy: hydration and dehydration of theophylline. J Pharm Sci 2007; 96: 1366–79.
72. Airaksinen S, Karjalainen M, Räsänen E, et al. Comparison of the effects of two drying methods on polymorphism of theophylline. Int J Pharm 2004; 276: 129–41.
73. Chongharoen W, Byrn SR, Sutanthavibul N. Solid state interconversion between anhydrous norfloxacin and its hydrates. J Pharm Sci 2008; 97: 473–89.
74. Kachrimanis K, Fucke K, Noisternig M, et al. Effects of moisture and residual solvent on the phase stability of orthorhombic paracetamol. Pharm Res 2008; 25: 1440–9.
75. Römer M, Heinämäki J, Miroshnyk I, et al. Phase transformations of erythromycin a dihydrate during pelletization and drying. Eur J Pharm Biopharm 2007; 67: 246–52.

14 Effects of Pharmaceutical Processing on the Solid Form of Drug and Excipient Materials

Peter L. D. Wildfong
Duquesne University, Pittsburgh, Pennsylvania, U.S.A.

INTRODUCTION

The previous chapters in this book have considered the theories and thermodynamic bases behind the generation of different solid phases, as well as some of the principal analytical techniques used to characterize them. The volume of literature devoted to pharmaceutically relevant solid forms is sufficiently extensive to indicate its significance to formulation and development sciences. The role of solid form selection and solid materials characterization as an essential aspect of preformulation has been reinforced as an early step in a feed-forward drug product development scheme (1), and is consistent with worldwide regulatory guidance documents and the FDA's recent Critical Path Initiative.

Central to the present chapter is a review of current and historical research concerning the influence of primary processing (unit operations used to manufacture bulk drug substance) and secondary processing (unit operations used to manufacture drug product) on the solid form(s) of the materials involved. The importance of these phenomena is not isolated to the pharmaceutical industry, and several accounts can be found in the materials literature pertaining to the production and development of ceramic/inorganic (2–8) and metallic (9–14) composites, and food products (15). Inclusive of all processing- and materials-dependent industries, the occurrence of raw material solid form changes during manufacturing can have dramatic effects on product stability (chemical or physical), material workability and process efficiency (viability of downstream processing), product performance (alterations to composite behavior), and product failure (recalls owing to catastrophic failure or regulatory non-compliance). In the pharmaceutical industry, active pharmaceutical ingredient (API) phase changes induced during processing can result in unpredictable alterations in shelf-life and changes in relative bioavailability, leading to product recall and limiting patient access to important therapeutic products. Despite the importance of understanding these phenomena, many published studies are limited to characterizations of the phase changes without attempting to establish predictive patterns for their potential occurrence in new materials. The literature supporting other materials-dependent industries more often presents these phenomena at a fundamental level; however, transfer of these ideas to organic materials has been limited.

Importance of the Effects of Processing on Drug Product Viability and Stability

The importance of considering the influence of manufacturing on solid form is born of the need to ensure predictable drug product quality and performance. Solid-state

characterization is done early in development pipelines in order to identify the range of solid forms that a molecule might potentially exhibit (1,16–18). Identification of the most thermodynamically stable polymorph is performed with the mindset of preventing unanticipated physical changes to the API downstream, which, as classically demonstrated in the case of Ritonavir (19) led to a dramatic recall of a key therapeutic entity from the market, and a costly reformulation. The impact that form changes can have on drug products is the impetus behind the polymorph, solvate/hydrate, desolvated solvate, and amorphous substance decision trees presented in Byrn et al. (17,20), and various International Conference on Harmonization (ICH) and FDA guidance documents. At the heart of these decision trees are the essential questions: (1) does the solid material have the propensity to exist in more than one physical form, and (2) are the physicochemical properties of the forms sufficiently different from one another, that dosage form performance is affected? The significance of whether or not a molecule exists in multiple forms is tied to the impact its presence can have on a critical performance attribute, whether the change occurs during manufacturing (i.e., the ability to manipulate the API into a reproducibly homogeneous dosage form is altered) or as a drug product (i.e., the phase transition constitutes a significant alteration in the relative bioavailability of the API) (21).

The present chapter will examine solid form changes as a result of processing by looking at individual unit operations. Within this context, the over-arching sources of these transformations appear to fall into one of three categories: (1) exposure of materials to extensive mechanical stress, (2) exposure of materials to water (or other processing solvents), and (3) exposure of materials to temperature during processing. Overall, these three aspects are common to several steps in typical solid processing lines. The potential that a transformation may occur during manufacturing is, therefore, of importance to the industry.

The extent of transformation observed in any manufacturing environment will be highly variable depending on the time for which the material is exposed to the driving force. It could be argued that in many cases, materials encounter these driving forces for such limited durations (i.e., temperature or moisture excursions, short compaction dwell times, etc.) that transitions will occur on a scale to which the reproducibility of drug product performance is not compromised. Even if this argument was reflective of all current materials and processes, our present mechanistic understanding of process-induced transformations is very limited, and predictions of phase behavior are not yet possible.

The complex interplay between API and excipients that determines the performance of solid drug products is a major focus of current pharmaceutical research. A limitation of the body of literature concerning process-induced phase behavior in organic materials is that it is heavily skewed toward API. Excipients, many of which are derived from natural sources, often suffer from significant batch-to-batch, lot-to-lot, and vendor-to-vendor variability. It is not unreasonable to consider that the phase response of an excipient to a manufacturing environment might also be highly variable. Furthermore, whereas conclusions concerning API are based on purified materials, excipients (particularly naturally derived polymers) tend to be mixtures of molecules, adding an additional layer of complexity to their characterization, and making difficult the prediction of responses to different manufacturing environments. In short, there is still considerable work to be done in this field, if we are to move toward the "materials understanding" espoused by the FDA.

Recent Reviews on Mechanochemistry and Process-Induced Transformations

A survey of the literature suggests significant interest in process-induced transformation potential of pharmaceutical materials. Several reviews capture the pervasive nature of these phenomena, and list historical and current studies based on specific model compounds (22–27). Other reviews are dedicated to mechanistic and theoretical descriptions of processing and process control (28), which use compound-specific examples to argue mechanistic research (10,29–32). The present chapter will attempt to combine the two formats. In general, as pharmaceutical materials scientists look to the future, the boon of such research will only be realized as we attempt to construct a better understanding of these phenomena. As more mechanisms are elucidated and understood, the literature will begin to form a database, from which manufacturing and formulation decisions could be derived, ultimately leading to more predictable product performance, and consistent product quality.

PRODUCTION OF BULK DRUG SUBSTANCE

Upon identification of a candidate molecule, a potential API enters the development stream along two parallel pathways. On the drug product stream, preformulation, formulation, and process engineering are initiated in order to yield a dosage form. Parallel to this is a drug substance development stream in which process chemists are required to scale the synthesis and raw material production from milligram quantities through the various scales necessary to support the commensurate stages of product development. Although bench-top polymorph screens provide information on the variety of different forms that may be grown under numerous solvent and temperature conditions, the reaction times conducted at the industrial scale (as well as subsequent purification steps) oftentimes allow the system to establish thermodynamic equilibrium, resulting in the growth of the most stable form. Early in this development stream, however, high yield is often the primary focus, and the first scale-up opportunity may result in production of metastable phases.

Depending on the extent of process refinement that occurs during later stage raw material scale-up sequences, the opportunity for the appearance of the thermodynamically preferred form is considerable. Transformation in later development carries with it the burden for retesting of the drug substance, including alterations to the analytical profile, and expensive clinical or toxicological tests. Understanding the interplay of different processing steps involved in raw materials manufacturing, therefore, is very important in ensuring the phase purity of drug substance used throughout the product development stream, as well as the ultimate assurance that the same material can be produced beyond market approval, ad infinitum.

Solidification Processing

Crystallization occurs via the collective assembly of molecules into the periodic arrangements that will eventually define the structure and properties of the solid materials. This nucleation process templates the growth of the solid form that results from a given solidification process. Rigorous developments concerning the thermodynamics of crystallization can be found elsewhere (33–35).

Free energy arguments require the collective assembly of a finite number of molecules to form a critically-sized nucleus having a balance between the surface and volume free energies, such that growth to larger radii will result in a reduction in free energy of the system. Homogeneous nucleation from a recrystallization solvent can be described by equation (1):

$$\Delta G_{\text{crit}} = \frac{16\pi\gamma^3 v^2}{3(k_B T \ln S)^2} \tag{1}$$

where ΔG_{crit} represents the free energy change associated with forming a spherical nucleus having a critically-sized radius equal to r; γ is the interfacial energy owing to the incoherence between the surface of the growing particle and the mother liquor, v is the molecular volume, k_B is Boltzmann's constant, T is the recrystallization temperature, and S is the degree to which the growth medium is supersaturated. Practically speaking, the recrystallization temperature and degree supersaturation afford the greatest opportunity for the formation of differently arranged nuclear templates, which result in the growth of different phases. Depending on the system, the opportunity for local T and S excursions may favor the growth of different phases from the same molecules (34).

Ultimately, the homogeneous mechanism described above [equation (1)] is oversimplified, and as such, solidification via this mechanism is seldom observed in practice. More commonly heterogeneous mechanisms are invoked, which allow a reduction in the interfacial energy by allowing growth on the surfaces of impurities. This is mathematically represented by a shape factor, φ, defined in terms of the contact angle (θ) between the solid growth phase and the surface of impurities in the solvent [equation (2)].

$$\varphi = \frac{(2+\cos\theta)(1-\cos\theta)^2}{4} \tag{2}$$

This shape factor is a fractional multiplier, which can be used to relate the energy requirements of heterogeneous nucleation with homogeneous nucleation [equation (3)]:

$$\Delta G_{\text{hom}} = \varphi \cdot \Delta G_{\text{net}} \tag{3}$$

The reduction in free energy requirement offered by nucleation on impurity surfaces indicates why heterogeneous mechanisms are typically observed. This theory also supports the use of seed crystals (secondary nucleation) to direct pharmaceutical drug substance manufacturing. The addition of phase-pure particles of the desired solid form to the mother liquor provides a template for growth, as well as surfaces with which the API molecules should have perfect (or near perfect) coherence. This effectively drives the θ term of equation (2) (hence φ) to a value of zero, which implies that recrystallization in seeded systems should be highly favored and spontaneous. In the case of monotropically related polymorphs, seeding is expected to unambiguously result in growth of the stable form, whereas enantiotropically related pairs risk solvent-mediated transformations at temperatures below the transition temperature (34).

A well-controlled crystallization system should yield the desirable form, having had it introduced to the solvent as seed crystals. In contrast, inadvertent

seeding can be devastating to solidification processing, and result in the growth of undesired phases. This has been suggested to be the case in the now classic example of Ritonavir (19,36). The final drug product, *Norvir*, was released to the market in 1996 as a semisolid capsule formulation containing what was believed to be the most thermodynamically stable polymorph (Form I). In 1998, dissolution problems with the drug product prompted an investigation, which determined that transformation to a previously unknown, more thermodynamically stable polymorph (Form II) had occurred. The emergence of this much less soluble polymorph reduced the bioavailability of the marketed product, requiring a widespread recall. Attempts to isolate Form I at the US facilities failed, and a team of investigators was sent to Italy to determine whether or not any changes had been made to the bulk material manufacturing process. Shortly after the visiting scientists arrived, significant amounts of Form II began appearing at the Italian facility. This has been speculated to have been the result of an inadvertent transfer of Form II seeds from the US facility to the Italian facility, which after contaminating the Italian process, resulted in the observed growth of Phase II. This, of course, is also suggested to have been a coincidence, and that the spontaneous discovery of Form II was simply the unfortunate consequence of thermodynamics taking awhile to rear its ugly head.

Beyond recrystallization, bulk API manufacturing involves a series of filtrations, washes, and dryings, which may be required before the final solid material is ready for transfer to secondary operations. These are schematically illustrated in Figure 1. Conceivably, any of these steps could elicit an undesired phase change, the criticality of which depends substantially on the kinetics of the transformation and the duration of the process step. Excursions of *S* and *T* during recrystallization have been discussed briefly above. The time frame of crystallite exposure to the recrystallization solvent also carries with it the potential to cause a solvent-mediated transformation. In short, contact between the solvent and a metastable phase allows its re-dissolution followed by the independent nucleation and growth of the more stable polymorph. The kinetics of these transformations have been detailed by Cardew and Davey (37), but may occur during any of the solvent-dependent manufacturing steps (Fig. 1).

Also included in drug substance manufacturing is the removal of solvent by drying the purified solids (Fig. 1C). Akin to drying steps in drug product manufacturing, exposure of metastable solids to high temperatures hastens their solid-state conversion to more stable forms. Additionally, low-temperature stable enantiotropes dried at temperatures above their solid transition temperature (T_{tr}) may convert to the high temperature stable form, which could become kinetically trapped as a metastable phase when the temperature is removed. Further consideration will be given to drying in the section "Effects Due to Drying."

The last step indicated in Figure 1D is comminution, which is used to break up large, fused particles that result from the preceding steps, allowing the material to be better suited to secondary processing. The ubiquitous presence of milling in pharmaceutical processing and its potential for eliciting process-induced phase transformations merits considerable discussion. As such, comments on milling will be covered in the section "Effects of Particle Size Reduction."

Examples of Transformations During Drug Substance Manufacturing

At all levels, rigorous research has been performed to optimize process understanding, and fine-tune manufacturing control to ensure consistent *T* and *S* throughout

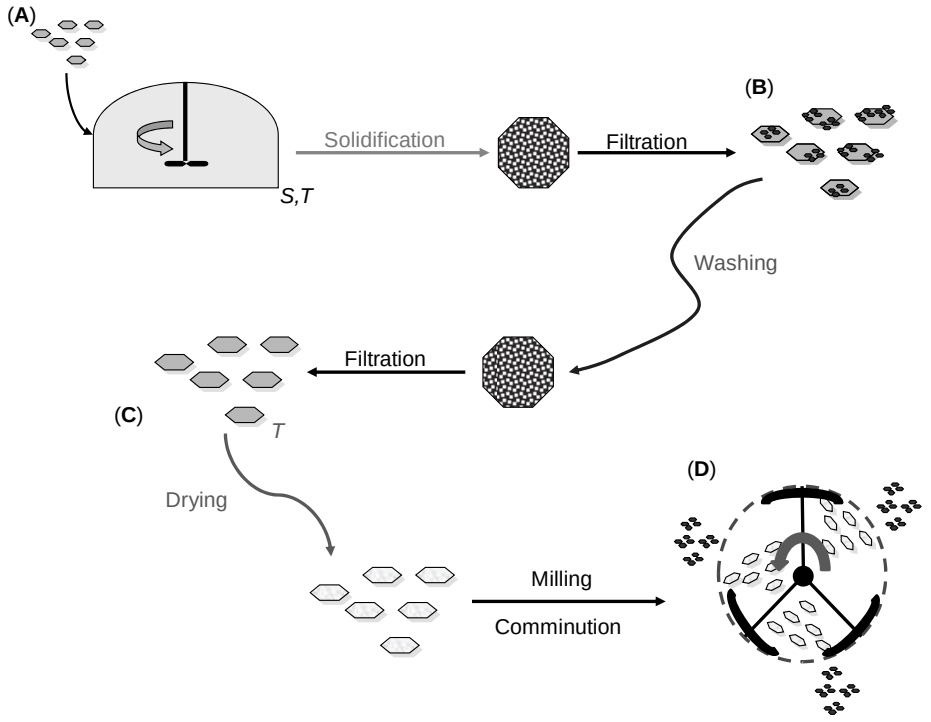

FIGURE 1 Solidification is accomplished via controlled *S* and *T*, used to establish favorable conditions. (**A**) Seed crystals may be added to facilitate recrystallization. (**B**) Filtered crystals may have poorly formed crystallites or impurities on their surfaces that need to be removed by washing in saturated mother liquor. (**C**) Residual solvent needs to be removed to complete purification by the application of temperature. (**D**) Dried materials are then subjected to milling for reduce particles to usable sizes/size distributions.

recrystallization. An excellent review, which discusses the importance of these controls is provided by Beckmann (34). Without such control we might expect excursions to result in the growth of unanticipated solid forms (alone or as mixtures with the desired phase). Gu et al. (38), and Zhang et al. (39), have both reported the influence of controlled processing conditions on the crystallization of polymorphs of sulfamerazine. It was found that the strength of interactions between the solvent and solute was a key determinant in the transformation rate, which was observed to be much slower in the solvent having the strongest hydrogen-bond donor propensity (38). Prior to these studies, the low-temperature stable Form II ($T_{tr,II \rightarrow I}$ is between 51°C and 54°C) had not been prepared in bulk quantities, owing to slow conversion rates in solution and in the solid state (39). Sulfamerazine provides a nice example of how Ostwald's Rule of Stages (33,40) can significantly influence the form yielded by a recrystallization process. Because there is a higher probability of forming the metastable form first (Form I), and the solvent-mediated conversion to Form II is observed to be exceedingly slow (39), except under highly controlled circumstances, growth of Form II should not be expected.

Because recrystallization also carries with it significant potential to yield undesirable solvatomorphs (hydrates, solvates, etc.), research focusing on predictions of the likelihood of this transformation is also central to the discussion of process-induced transformations. The temperature dependence of the transition point in concentration space is considerable, owing to a decreasing window of stability for anhydrate/desolvate with decreasing temperature (34). Hosokawa et al. (35) have used a chemo-informatic approach to study correlations between the molecular characteristics of various compounds and the solvents from which they were recrystallized. The authors completed a survey of the Cambridge Structural Database (CSD) to reveal that 6397 small molecule organic compounds had been crystallized from one of 15 solvents. Using 2D molecular descriptors to form a training dataset, priority rankings for each of the 15 solvents were satisfactorily predicted for randomly chosen test compounds.

Interest in rigorous control over the solidification process has seen its inclusion in recent process analytical technology (PAT) research. Non-invasive online measurement of solution concentration (supersaturation) has been demonstrated by Togkalidou (41,42). Additionally, interest in on-line monitoring and determining the kinetics of solid form changes during recrystallization has been done in an effort to provide a process that consistently results in the desired solid phase (43).

EFFECTS OF PARTICLE SIZE REDUCTION

As indicated above, the last step in bulk substance manufacturing is often milling, performed in order to generate raw materials having a reasonable (and uniform) particle size and particle size distribution. Comminution as a manufacturing step occurs throughout the pharmaceutical industry, and many processing streams require a high-shear particle sizing step, sometimes at multiple points in a given manufacturing line. Although milling mechanisms can be as varied as the different types of mills available for large-scale processing, particle size reduction and particle size distribution homogenization is accomplished by some combination of particle fracture and attrition. Depending on the equipment, the balance of these two mechanisms (and the applied stress state required to accomplish the task) can be substantially different. Although some effort may be taken to expose materials to "mild" processing conditions, particle size reduction by its very nature uses significant mechanical energy, carrying with it the potential to impose a change in physical form to the material. These changes can include polymorphic transformations, conversion to the amorphous state, dehydration, or some mixture of these transitions. The concern with these possible activated states rests in the nature of high energy forms, all of which have the potential to transform to more thermodynamically stable states over time.

Exploration of these phenomena throughout the materials literature often considers phase changes in response to extensive milling periods, during which the repeated exposure of materials to high-shear energy drives the transformations. Depending on the mill used at industrial scale, the duration for which the material is exposed to the stress is often short. The extent of transformations observed in academic modeling exercises may, therefore, be exacerbated relative to what is observed in practice. It is important to note, however, that uncontrolled transformations to high-energy solids can seriously compromise downstream manufacturing

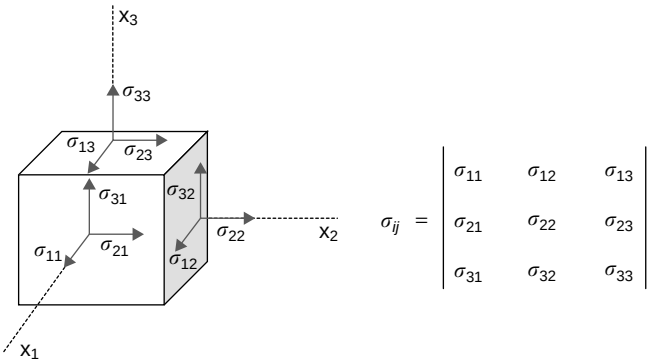

FIGURE 2 Assuming a right-handed coordinate system (x_1, x_2, x_3), the three-dimensional stress state experienced by a finite stress element can be represented by a second-rank tensor (σ_{ij}) consisting of normal ($i = j$) and shear ($i \neq j$) components.

and product performance; therefore, continued study of these mechanisms merits study.

Influence of Shear Stress on Physical Form

A solid body subjected to a mechanical load is forced to accommodate the applied stress in order to establish an energetically viable steady state (44). The application of stress typically results in a corresponding strain, the magnitude of which depends on the materials properties. Elastic strain (ε) is analogous to a simple Hooke's Law system, where deformation is directly proportional to an applied stress (σ), related by a material constant (Young's modulus, E).

$$\sigma = E\varepsilon \tag{4}$$

One-dimensional elastic responses [equation (4)], however, are insufficient to explain strain caused by the three-dimensional stress states typical of pharmaceutical processing. In such cases, stress needs to be considered as a combination of normal and transverse loads applied over areas of a finite stress element, whose description can be defined more appropriately by σ_{ij} (Fig. 2). Responses to a mechanical stress occur along the path of least resistance for the material, and can be broadly classified as either resulting in fracture or deformation.

Linear elastic fracture mechanics (*LEFM*) is rooted in pioneering work by Griffith (45), who determined that fracture occurs when the application of a critical stress (σ_f) applied normal to a flaw having length $2a$, is concentrated at the crack tip allowing crack propagation to become an energetically favorable route for stress dissipation [equation (5)].

$$\sigma_f = \sqrt{\frac{E2\gamma_{SV}}{\pi a}} \tag{5}$$

Although complex fracture mechanisms are expected in real systems (46), the heart of material fracture considers that as a is minimized, σ_f approaches unrealistic

magnitudes, which indicates that materials will have a fragmentation limit. Real particles that undergo milling are often polycrystalline aggregates for which the grain boundaries provide large flaws that require very little stress to facilitate fragmentation. Fracture of individual grains continues along cleavage plains (corresponding to the highest lattice *d*-spacing), across which the weakest interactions occur in a given crystal (47), or at defect sites (inherent consequence of growth) within the material (48).

Beyond the critical flaw size, continued application of mechanical energy forces the crystalline lattice to respond at a finer level of material structure. Small strain in the elastic regime causes displacement of atoms or molecules from their equilibrium lattice positions manifest as a potential energy increase as nuclei approach one another. Elastic responses are characterized by recovery of equilibrium positions as the stress is removed. Typical milling operations, however, will impose a stress state well beyond the elastic limit of the materials involved, where strain is not recoverable, and plastic deformation occurs.

Whereas elastic deformation is uniformly distributed throughout a crystal, plastic deformation may be localized as some of the energy is transferred from the applied load and lost to the formation or movement of lattice dislocations (44,49). The applied stress state (σ_{ij}) responsible for this deformation can be thought of as consisting of a hydrostatic component (equally resolved normal stresses and no shear components) and a deviatoric component (all non-hydrostatic stress components):

$$\sigma_{ij} = \begin{vmatrix} \sigma_{11} & 0 & 0 \\ 0 & \sigma_{22} & 0 \\ 0 & 0 & \sigma_{33} \end{vmatrix} + \sigma'_{ij} \tag{6}$$

Critically resolved shear stresses in this deviatoric component (σ'_{ij}) result in slip along structurally weak lattice planes by dislocation creation and movement (46).

The continuous dissipation of mechanical stress via this mechanism results in the accumulation of dislocations as the material is repeatedly deformed. Translation of dislocations through neighboring unit cells causes further lattice misalignments, which themselves migrate, inducing further translation in a chain reaction. Eventually, as the number of dislocations approaches a critical density, they interfere with the movement of one another (44,49). Structurally speaking, such a dislocation density can be envisioned as having perturbed the lattice to such an extent that the collective interactions that defined its periodicity are lost, regionally transforming the material to an amorphous solid (50,51).

Dislocations are incoherent with respect to the surrounding lattice. An increase in dislocation density (ρ_d) results in a positive free energy change owing to the accompanying strain. For a material having a known molar volume (M_V), the change in free energy required to incorporate a specific density of dislocations into a lattice (ΔG_d) can be approximated using equation (7):

$$\Delta G_d = \rho_d M_V \frac{b^2 \mu_s}{4\pi} \ln\left[\frac{2(\rho_d)^{-1/2}}{b}\right] \tag{7}$$

Reflected in this expression are material-specific properties: μ_s, the elastic shear modulus, and b, the magnitude of Burgers' vector. Application of significant and repeated shear stress during experimental milling has the potential to increase ρ_d to a critical value (ρ_{crit}), at which the periodicity of the lattice is completely lost, resulting in amorphization (52).

Assuming that the solid amorphous phase and the liquid phase are energetically similar (relative to the corresponding crystalline lattice), the free energy change associated with this transformation (ΔG_{am}) can be approximated by equation (8):

$$\Delta G_{am} = \left(\frac{\Delta H_f}{T_m}\right)(T_m - T_{expt}) \tag{8}$$

where ΔH_f is the heat of fusion, T_m is the melting temperature of the crystalline solid, and T_{expt} is the experimental milling temperature. If amorphization proceeds along this dislocation pathway, the critical dislocation density can be considered to be reached when ΔG_{am} is equal to ΔG_d (i.e., ρ_d is equal to ρ_{crit}).

$$\left(\frac{\Delta H_f}{T_m}\right)(T_m - T_{expt}) = \rho_{crit} M_V \frac{b^2 \mu_s}{4\pi} \ln\left[\frac{2(\rho_d)^{-1/2}}{b}\right] \tag{9}$$

The magnitude of ρ_{crit}, can be calculated for a material for which μ_s, b, and M_V are known. It is important to note that this structural argument recognizes that values of ρ_d must retain physical meaning; that is, their magnitudes are limited by some minimum achievable separation distance. Because dislocation density is defined in terms of the distance (d) between dislocations in a lattice:

$$d = \frac{1}{\sqrt{\rho_d}} \tag{10}$$

the proximity of dislocations relative to one another is restricted by the strain fields that surround them. As suggested in Wildfong et al. (53), estimates of a prohibitive value (above which ρ_d is meaningless), ρ^*, for molecular crystals based on strain field overlap should be approximately defined by equation (11):

$$\rho^* = \frac{1}{(2b)^2} \tag{11}$$

According to this model then, the potential of a crystalline material to be fully disordered by the application of high shear mechanical energy can be reasonably well predicted by solutions to equations (8) and (9), such that ΔG_{am} and ΔG_d are equal when $\rho_{crit} < \rho^*$.

This mechanism of mechanical disordering was investigated by Wildfong et al. (53). In a survey of seven pharmaceutically relevant materials, variables required to solve for ρ_{crit} [equation (9)] were measured or obtained from the literature and used to predict whether or not the material should completely transform to the amorphous state under continuous application of mechanical energy.

Of these seven materials, two were predicted to become completely disordered via this mechanism (sucrose and γ-indomethacin), while five were not. Each material was subjected to extensive cryogenic milling (T_{expt} controlled at 77 K), and periodically evaluated for complete amorphization using X-ray powder diffraction (XRPD) and differential scanning calorimetry (DSC). Experimental results confirmed the predictions regarding the disordering potential of sucrose and γ-indomethacin. Predicted resistance to amorphization for acetaminophen, aspirin, and salicylamide was also confirmed in these experiments, whereas the other two materials (proprietary compounds each subjected to a single three-hour milling experiment) provided predictions that conflicted with experimental observations. It was conceded by the authors that the model provided a first approach to predicting mechanical activation behavior, nonetheless resulting in data that merit further investigation and modeling.

Conversions to different crystalline phases are also supported by the deformation-dependent dislocation-mediated model described above, as suggested by Tromans and Meech (52). Here, rather than accumulation of defects to the extent at which lattices become completely aperiodic, ρ_{crit} raises the free energy commensurate with a metastable polymorph, allowing access to this higher energy state. At a structural level, the incorporation of dislocations is thought to provide sufficient mobility to lattice constituents that collective reassembly growth of another crystalline phase is permissible.

Temperature Accumulation During Milling Processes

A driving-force often suggested for solid-state transformations during milling is the accumulation of temperature (locally or sample-wide). It has long been held that owing to the relatively low T_m of organic solid materials, it is not unforeseeable that continuous application of mechanical energy could result in localized melting on the surfaces of particles, which either allows recrystallization to high energy forms, or is immediately quenched upon removal of impact stress, allowing surface vitrification.

The melt-quench hypothesis for milling-induced amorphization has been specifically addressed by Willart et al. (54,55), who performed extensive ball milling experiments on samples of lactose. Anhydrous α-lactose is a commonly used excipient, which shows a strong mutarotation to its β-anomer when melted. Otsuka et al. (56) had previously reported that extensive milling of α-lactose did result in substantial formation of β-lactose; however, their experiments were performed at 60% relative humidity (RH), and the adsorption of free water molecules by the amorphous lactose was suggested to be the cause for mutarotation, rather than the milling itself (54). In their experiments, Willart et al. (54) used a planetary ball mill (under dry nitrogen atmosphere) to grind samples of α-lactose, which were then evaluated using DSC, XRPD, and ^{1}H-NMR. Characterization of milled samples showed them to be nearly free of the β-anomer, whereas separate samples that were subjected to substantial heating did show a strong tendency to form β-lactose. Likewise, the authors reported that other amorphization routes for α-lactose, which inherently include heating or exposure to water (i.e., melt-quenching, lyophilization, and spray-drying) also result in substantial mutarotation (55). From these results, the authors concluded that the mechanically facilitated transition was driven by an unknown non-thermal mechanism.

The Role of Glass Transition Temperature (T_g) in Milling-Induced Amorphization

Given that transformation to the amorphous state is often the result of extensive milling, the glass transition temperature of the material is expected to play a role in the persistence of the resulting solid form. Descamps et al. (55) investigated the correlation between milling-induced amorphization and T_g by subjecting a small library of materials having known glass transitions (above and below the experimental temperature) to extensive comminution at room temperature. As summarized in Table 1, the materials milled at temperatures well below their T_g were observed to become fully amorphous, whereas those materials ground at temperatures above T_g were observed to undergo a conversion to a metastable polymorph (55). These data are supported by well-known observation concerning the stability and persistence of amorphous solids at temperatures relative to T_g. Trehalose, α-lactose, and budesonide were all ground at temperatures well below $T_g - T = 50$ K, a temperature reported as providing insufficient molecular mobility to allow collective reassembly of molecules and recrystallization (57). In contrast, the sorbitol and mannitol samples were ground at temperatures well above T_g, where mobility is substantially higher, and amorphous materials rapidly recrystallize. Note that all the polymorphic conversions observed in this example resulted in metastable crystalline phases, which implies recrystallization according to Ostwald's Rule of Stages.

The importance of T_g relative to milling temperature is further discussed by De Gusseme et al. (58), who performed ball milling experiments on fananserine (T_g = 19°C) at 25°C and 0°C. These authors found that both Forms III and IV of fananserine underwent a polymorphic conversion to metastable Form I when milled at 25°C ($T_{expt} > T_g$). In contrast, partial amorphization was observed when the same solid forms were ground at 0°C ($T_{expt} < T_g$).

Phase Transformations Owing to Desolvation During Milling

Another mechanism by which crystalline materials can be converted to amorphous solids by continuous grinding occurs via desolvation. In such instances comminution causes a loss of the water/solvent of crystallization. The structural void left by this loss is unable to support the applied stress state, and collapse to the amorphous state occurs. High-shear milling of carbamazepine has been used to demonstrate this phenomenon. In experiments conducted by Otsuka et al. (59), anhydrous Form I was subjected to extensive grinding in a centrifugal ball mill. Periodic evaluation of the DSC and XRPD data for samples milled over 1 to 24 hours under two separate humidity conditions (17% or 90%) did not show significant change. In contrast, at

TABLE 1 Summary of Experiments of Materials Milled Above and Below T_g

Material	T_g (°C)	Observation following extensive ball milling
Trehalose	120°C	Completely amorphous
α-Lactose	111°C	Completely amorphous
Budesonide	90°C	Completely amorphous
Γ-D-Sorbitol	0°C	Conversion to A-polymorph
Mannitol	13°C	β → α conversion (α → β re-conversion on storage) δ → α conversion (α → β re-conversion on storage)

Data summarized from Ref. (55).

both RH conditions the dihydrate (Form III) was observed to first transform to amorphous carbamazepine, which eventually recrystallized to Form I.

Further Examples of Phase Transformations Elicited During Milling

The pharmaceutical literature provides numerous further examples of pharmaceutical API and excipients that, when exposed to various extensive high-shear milling processes, undergo various solid state phase transformations. Many utilize traditional solid state characterization techniques to demonstrate the phase changes; at present, specific transformation mechanisms still remain an open point of discussion and topic for further research. Recognizing that this topic has received substantial attention over the past few decades, a *partial* list of several recent and historical comminution studies is provided in Table 2.

It should be noted that several of these transformations are observed to be incomplete (as evaluated, for the most part by XRPD and DSC). Whatever the specific mechanism eliciting the conversion, these changes occur via cumulative responses to the applied stress. This suggests that transitions induced by milling are likely to result in heterogeneous solid phases, in which the presence of lower energy solids drives conversions during continued milling, or during storage of the milled

TABLE 2 Summary of Some Reports of Polymorphism and Amorphization Induced by Milling

Material	Mill type	Observation
Caffeine (anhydrous) (60)	Ball mill	I → II transformation (metastable → stable)
Cortisone acetate (61)	Vibratory mill (cryogenic)	I → II transformation (complete, 10 min)
Salbutamol sulfate (62)	Air jet mill	Cryst → am (partial, <10%)
	Ball mill	Cryst → am (more substantial)
Sulfathiazole (23)	Ball mill	III → I transformation (partial cryst → am observed)
Piroxicam (23,63)	Ball mill (23)	Cryst → am (partial; discoloration) (23)
	Vibratory mill (cryogenic) (63)	I → am (complete; discoloration) (63) II → am (complete; discoloration) (63)
Cephalexin·H_2O (64,65)	Agate shaker mill	Cryst → am (complete, 3–4 hr) Persistence depends on %RH
Nitrofurantoin (66)	Centrifugal ball mill	Anh →·1H_2O II (75% RH) Anh → am (5%, 50% RH) 1H_2O I →·1H_2O II (50%, 75% RH)
Cimetidine (67)	Vibratory mill	B → A (substantial cryst → am) C → A (substantial cryst → am) A → D (with nucl.; substantial cryst → am)
Indomethacin (53,68)	Vibratory mill (cryogenic)	γ → am (53,68) α → am (68) δ → am (68) Methanolate → am (68) *t*-Butanolate (no transformation) (68)
Sucrose (53,69)	Centrifugal ball mill (69)	Cryst → am (complete) (69)
	Vibratory mill (cryogenic) (53)	Cryst → am (complete) (53)
Trehalose (55,70)	Planetary ball mill	Cryst → am (complete) (55,70)

material. This is supported by early experiments by Otsuka and Kaneniwa (71), who investigated the effects of seed crystals on the observed transformations of chloramphenicol palmitate during milling. In their experiments Form B was observed to convert to the more stable Form A after 150 minutes of grinding, whereas this transformation occurred much more quickly (40 minutes) when 1% of Form A seed crystals were added to the mill. Form C was observed to undergo rapid transformation to Form B (16 minutes), which continued to transform to A in the same time scale observed for unseeded B → A conversions. The conversion from C → B was accelerated in the presence of 1% B seeds, whereas the B → A conversion was left unaffected. Form C in the presence of 1% Form A seeds, however, was observed to undergo rapid C → B → A transformation in only 30 minutes of total grinding.

The influence of the limited presence of seeds in the above study, suggests that residual polymorphic memory has the potential to dramatically influence the physical stability of materials transformed via this route. Although several examples of direct crystal-to-amorphous transformations have been observed as a result of milling, at a structural level, it is easy to imagine that complete disruption of all molecules in the parent crystalline structure is unlikely, leaving some residual nanocrystalline regions (at the level of a few unit cells) that are undetectable via the XRPD and DSC methods typically employed to study these systems.

In a recent study by Lubach et al. (72), crystalline lactose was studied following the application of various processing routines (compaction, lyophilization, spray-drying, and cryogrinding). Consistent with previous reports on the response of lactose to grinding, the authors did observe amorphization of most of the sample, where conversion increased with increasing processing times. Unlike much of the mechanochemical literature, however, the conversion was evaluated using ^{1}H-ssNMR, which is better able to identify residual crystalline material in samples that would otherwise be considered amorphous via XRPD characterization.

This study also addressed mechanistic aspects of the observed amorphization process. The higher energy regions associated with defects in the crystalline material (locally amorphous solid) has higher molecular mobility, resulting in shorter proton spin-lattice relaxation times (proton T_1), as shown in Figure 3. This is meant to illustrate a large particle having no internal crystalline defects (slow-relaxing domain) surrounded by a fast-relaxing domain associated with the surface. As the particle is milled, the slow-relaxing domain is continuously broken down into smaller pieces, whereas region B experiences a commensurate increase as the specific surface area and surface defects of the material are both increased (72). This suggests that the progressive defect accumulation method proposed above (52,53) can be quantifiably observed using ^{1}H-ssNMR. Figure 3 also illustrates how nanocrystalline regions may be preserved in extensively milled samples. As discussed above [equation (5)] continued fracture of a material (continued reduction of the crystalline region in this case) requires increasing stress (σ_f) as critical flaw sizes (a) are reduced.

Consistent with the observations by Lubach et al. (72), it might be expected that a continuously milled sample would be largely converted to its amorphous phase (if such a transformation is permissible), however, the persistence of nanocrystalline regions in the sample may provide nucleation sites for subsequent recrystallization, reducing the physical stability of amorphous materials prepared by this route.

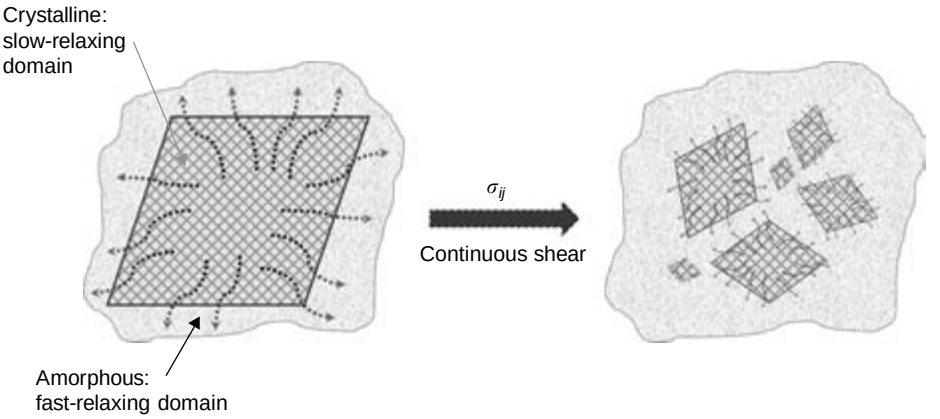

FIGURE 3 Schematic model illustrating how process-induced changes in crystalline systems affect relaxation and spin diffusion processes. Crystalline regions represent slow-relaxing domains, whereas amorphous regions represent fast-relaxing domains; dashed arrows represent magnetization transfer from crystalline to amorphous regions via spin diffusion. Figure modified after Ref. (72).

EFFECTS DUE TO GRANULATION METHODS

Depending on the characteristics of a given formulation, a granulation step may be required in order to improve the flow and consolidation properties of a blend as it proceeds into tableting. Regardless of the method, granulation serves primarily as a particle size enlargement and particle size distribution homogenization process. Approaches can be generally classified as wet or dry, either of which can potentially elicit a phase transformation during processing.

Dry Granulation

In dry granulation powders/powder blends are fed between two counter-rotating rolls under high pressure. Like tableting (see section "Effects Due to Compression"), consolidation occurs as particle surfaces are brought into intimate contact, allowing the formation of inter-particulate bonds. The emerging ribbon is fed through a series of sizing steps (breakers, mills), which are used to convert it into coarse granular particles (Fig. 4A).

If a finite stress element at the nip region (between the rolls) were considered (Fig. 4B), it could be described as experiencing considerable normal stress in the direction applied by the rolls (σ_{22}). Note also, smaller normal stresses (σ_{11}) resolved along the free edge of the ribbon, imposed by non-deforming material on both sides of the roll gap. Termed *plastic constraint*, this smaller compressive stress occurs because nearly all of the deformation proceeds along x_3, with very little mechanical energy transmitted laterally in x_1 (73). Commensurate shear stresses on the roll surfaces would also be expected, providing the source for dislocation generation and movement (deformation). As described above, high-shear stress states carry with them the opportunity to facilitate phase transformations.

Specific examples of transformations as a result of dry granulation are likely to be rarer. Roll-compaction research using single components is infrequent, as very

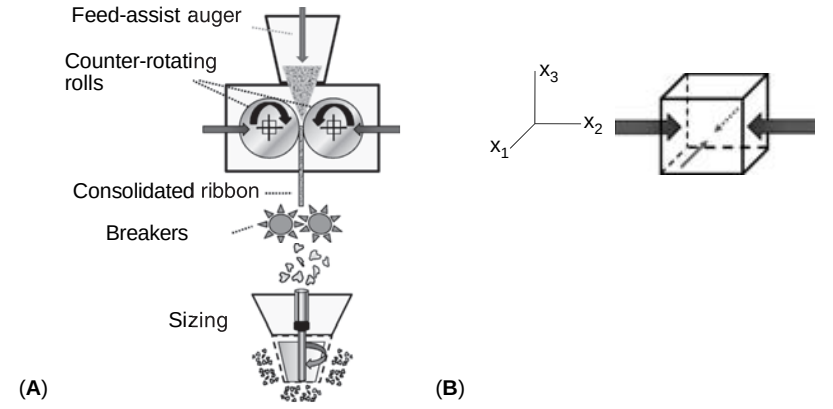

FIGURE 4 (**A**) Schematic representation of a dry granulation (roll-compaction/sizing) process. (**B**) Normal stresses on a finite stress element at the nip region between the rolls. Resolved shear stresses are also expected, particularly on the surfaces in direct contact with the rolls (shear arrows not shown above).

few materials have sufficient compactibility to generate ribbons. Furthermore, realistic, multi-component formulations are likely to contain excipients whose imminent compactibility allows significant dissipation of mechanical energy. As such, the extent of deformation-based transformations of API is reduced (or even eliminated). That said, transformations owing to this common manufacturing step have still been investigated. For example, Bozic et al. (74) observed partial amorphous conversion of mixtures of the antibiotic macrolide when combined with microcrystalline cellulose. Of the mixtures subjected to compression, slugging, and roll compaction, amorphization was observed for the two dry granulation methods, which the authors attributed to increased applications of mechanical stress relative to direct compression of the same mixtures.

Although milling is discussed above as a unit operation having considerable potential to elicit solid phase transformations (see section "Effects of Particle Size Reduction"), breaking and sizing used in dry granulation processes is done to convert the consolidated ribbon into coarse, free-flowing granules, having an overall larger particle size relative to the input powder blend. The dwell times and applied stress state of this particular milling step, therefore, dissipates most of the energy in particle fracture, reducing the probability that phase transformations may be seen in either of these particular steps.

Wet Granulation

As with dry granulation, the purpose of this manufacturing step is to facilitate particle size growth and particle size distribution homogenization in order to enable downstream processing. Currently, wet granulation is an approach used most widely to influence material handling properties (75). In wet granulation, an aqueous or hydroalcoholic binder solution (alone or with polymer) is added to a dynamic powder bed. The addition of binder solution to the powders promotes agglomeration as particles collide and surface films coalesce. The stages and theories of this

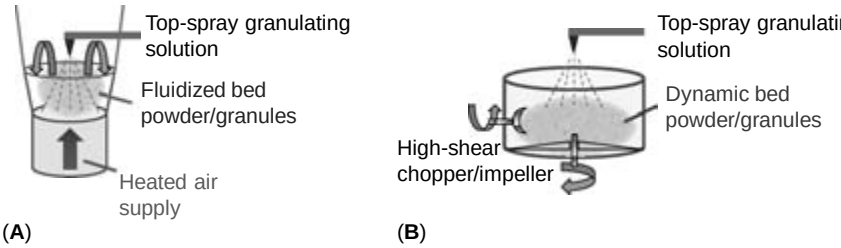

FIGURE 5 Schematic representation of (**A**) top-spray fluidized-bed granulation and (**B**) top-spray high-shear granulation.

process are classically treated elsewhere (75). Two major approaches used to accomplish this processing step are illustrated in Figure 5.

Top-spray fluidized bed granulation (Fig. 5A) applies the binder solution into a bed of particles entrained in a column of air. The particles adhere to one another as they collide in an airstream of defined velocity, temperature, and RH (76). Although liquid binders are involved, components sensitive to transitions in the presence of solvent may be less affected as it is continuously removed throughout the process. In fact, the opportunity for transformation may occur after solution addition is completed, when the fluidizing air temperature is increased to dry the granulated material (see section "Effects Due to Drying").

Top-spray high-shear granulation (Fig. 5B) employs a rotating impeller (~500 rpm) to mix the contents of the product bowl and spread the granulating solution as it is gradually added. A high speed chopper (~1000–3000 rpm) is used to break down the wet mass and facilitate granule formation (77). Although the rapidly moving blades may cause localized surface strain, the majority of the shear stress in the system is dissipated by the translational movement of particles. The major source of transformation potential in this system comes from the continuous exposure of the product to solvent. Owing to direct contact with the various solid components, the binder solution may cause spontaneous hydration/solvation of the crystalline materials, which has been shown to significantly affect the dissolution behavior of the eventual product, as reported for theophylline (78) and ciprofloxican (79).

Impact of Spontaneous Hydration Caused by Wet Granulation

Most wet granulation processes involve aqueous binder solutions, so hydration is expected to represent the majority of transformations observed as a result of this processing step. Chlorpromazine hydrochloride (Form II) has been observed to demonstrate severe lamination and capping when directly compressed, necessitating wet granulation of this API with ethanol and water in order to improve the compactibility of this API (80). Wet granulation is traditionally considered to be a secondary processing step whose intermediate product affords improved compaction behavior owing to properties of the granules themselves. In this particular case, solvent addition facilitated a phase transition from the starting material (Form II) to the more stable phase (Form I), whose specific lattice was more amenable to fracture and deformation processes.

Although the case of chlorpromazine hydrochloride illustrates a process-induced transformation that resulted in the improvement of product quality, unanticipated hydration can prove deleterious, as in the case of the anticonvulsant, carbamazepine. This particular API, which has received (and continues to receive) considerable attention, has been available in its generic form since 1986. In 1988, a recall of generic carbamazepine was issued for 53 different lots of the product. An independent study of three failed lots from this particular recall found that the products were not bioequivalent to the innovator product, or each other (81). Although the conclusions of this study were not specifically geared toward elucidating mechanistic causality, the authors did echo the findings of Wang et al. (82), who found that increased moisture content of tablets during storage was correlated to significant differences in both in vitro and in vivo performance profiles. In 1990, the FDA formally announced its recommendations to manufacturers that companies "change the products' packaging to keep out moisture" (83). Clinically, the consequences of moisture-exposed carbamazepine tablets have been reported to include reduced bioavailability and subsequent loss of seizure control (84). Specific studies concerning the effects of the crystal form of carbamazepine on bioavailability have shown that the administration of a 200 mg/body dose of the dihydrate form (in dogs) resulted in a significant reduction in area under the curve (AUC) (85). Ultimately, these studies suggest a link between carbamazepine solid form and in vivo response.

Otsuka et al. (86) reported that the phase behavior of carbamazepine was specifically influenced by the wet granulation process. In their experiments anhydrous Form I was granulated as a mixture of active with α-lactose monohydrate and corn starch in binder solutions containing hydroxypropyl cellulose (HPC) in either distilled water, 50% aqueous ethanol, or ethanol. The authors found that the mixtures experienced transformation from anhydrous Form I to the dihydrate form during granulation with the hydroalcoholic solution, whereas those mixtures granulated with pure water or pure ethanol did not undergo observable transformation. The authors also suggested that based on published studies for solvent-mediated transformation from Form I to dihydrate in aqueous suspensions, they expected approximately 76% dihydrate to result from the granulations, when substantially less was also observed. They suggested that the HPC used as a binder may have inhibited recrystallization of the dihydrate from solution.

In a follow-up paper, Otsuka et al. (87) investigated the effects of wet granulating different crystalline forms of carbamazepine. Forms I, II, III, and IV (dihydrate) were combined with α-lactose monohydrate and corn starch, and granulated with aqueous binders containing 5% HPC. After wet granulation with an aqueous binder, Forms I, II, and III were respectively observed to be 2.5%, 80.3%, and 35.2% transformed to the dihydrate. The authors also noted that when the wet mass was dried at 60°C, the water of crystallization was dehydrated from the structure, resulting in fine particles of anhydrous Form III.

In a further exploration of the influence of wet granulation on the solid form of carbamazepine, Wikström et al. (88) compared the transformation kinetics of the anhydrous monoclinic form of carbamazepine (CSD refcode: *CBMZPN10*) to the dihydrate when exposed to water as a slurry suspension (20 g H_2O/1 g anhydrous powder), a slurry seeded with 5% (w/w) dihydrate nuclei, and as a wet granulation (gradual addition of 0.5 g H_2O/1 g anhydrous powder, in a high-shear granulator). Complete conversion to the dihydrate was quantified (using Raman spectroscopy)

via all three types of exposure to water. The seeded slurry yielded 100% dihydrate after just 6 minutes of exposure, the unseeded slurry fully converted after 8 minutes of exposure, and the wet granulation showed 100% dihydrate formation after 10 minutes. Interestingly, there was no significant difference in induction time for any of the three processes, and nucleation and growth of the dihydrate was observed almost immediately upon exposure to water, regardless of the method. These data certainly confirm the risk associated with wet granulating a material such as anhydrous carbamazepine.

Continuous characterization of the solid state behavior of this molecule has provided further insight into to the likelihood of a deleterious transformation occurring during processing. Murphy et al. (89) studied the effects of lattice disorder on the solution-mediated phase transformation of anhydrous carbamazepine to its dihydrate form, and found that the kinetics and rate-controlling step for the transformation depended on the mechanical history of the material. Specifically, it was determined that grinding the anhydrous monoclinic polymorph of carbamazepine shortened the transformation times and changed the dependence of the transition from crystallization-limited to dissolution-limited. This was suggested to occur owing to disordered regions created during milling, which facilitate heterogeneous surface nucleation of the dihydrate form on the surface of the ground anhydrous polymorph. These findings would suggest that transformation to the dihydrate form during wet granulation could depend heavily on the processing steps occurring upstream of wet massing. Given the correlation of crystal form to therapeutic outcomes (84,85), this seems to be a case-in-point example of the importance of understanding and predicting these transformations.

Application of PAT for Monitoring Phase Conversions During Wet Granulation

As with many secondary manufacturing unit operations, the potential for physical form changes suggests the opportunity for real-time monitoring and process feedback as embraced by significant efforts to utilize PAT by various groups in academia, industry, and worldwide regulatory bodies. In a progression toward on-line monitoring of polymorphic conversions during wet granulation, off-line evaluations of the progressive hydration of both theophylline and caffeine (separately granulated using purified water) demonstrated the viability of appropriately processed Raman and near-infrared (NIR) spectroscopy (90). On-line Raman spectroscopy has also been demonstrated for real-time monitoring of hydration induced by wet granulation for several materials, as discussed in several papers by Wikström et al. (88,91,92).

The extent of an observable phase conversion will depend on the kinetics of the transformation process relative to the length of the process itself. Davis et al. (93) modeled the kinetics of the transformation between Forms I and III of flufenamic acid, a potent anti-inflammatory agent. The two forms are enantiotropes (having a transition temperature of 42°C), where Form III is the low-temperature stable polymorph. Both forms are easily dissolved in ethanol at 25°C, where the respective solubilities are 336.3 and 871 mg/mL for Forms III and I. In their experiments, flufenamic acid Form I was mixed with microcrystalline cellulose and granulated using ethanol. Phase changes were monitored online using a novel XRPD setup. As expected, metastable Form I underwent a solvent-mediated conversion to Form III during wet granulation at 25°C. Particularly important to the present discussion is

recognizing that the solvent-mediated conversion was still facilitated in the presence of adsorbed granulating fluid, which the authors calculated to be a total volume of 17 mL (distributed over a total dry mass of 124 g). Measured conversion data corresponded well with kinetic models, showing complete conversion of Form I to Form III during wet granulation after approximately two hours of continuous mixing.

It should be noted that in these experiments complete addition of the ethanol was accomplished at a rate of 5 mL/min over the first seven minutes of granulation time, reinforcing the notion that the extent of conversion is highly dependent on contact time with the solvent. This particular work, though, acknowledges the modeling approach as a means by which formulators and process engineers could predict the appropriate length of a granulation process that would result in minimal, moderate, or complete polymorphic conversion (93).

In their paper detailing factors influencing anhydrate to hydrate transformation during the wet granulation process, Wikström et al. (88) compare the conversion kinetics for five anhydrous materials (caffeine, carbamazepine, nitrofurantoin, sulfaguanidine, and theophylline) when exposed to water via three different methods. As described above for carbamazepine, each material was prepared as an aqueous slurry (20 g H_2O/1 g anhydrous powder), a seeded aqueous slurry (5% w/w hydrate crystals added to the starting material), and a wet mass generated by high shear granulation of the anhydrous powder by slow addition of purified water (0.5 g H_2O/1 g anhydrous powder). Eventual, complete conversion to the hydrated form of each material was observed, irrespective of the method of water exposure. Theophylline was completely transformed to the monoclinic monohydrate structure within three minutes by each of the three preparation methods, whereas caffeine (its structural analogue) underwent the slowest conversion to its hydrate in the slurry (12 minutes for complete conversion). Even in the seeded slurry and granulation experiments, the conversion kinetics for caffeine were still slower than for theophylline. Interestingly, sulfaguanidine was observed to undergo near instantaneous solvent-mediated growth of the hydrate structure, estimated by the authors as occurring in less than 30 seconds.

The transformation kinetics for nitrofurantoin in the above experiments were, perhaps the most interesting, where complete conversion took 180 minutes in the slurry, 60 minutes in the seeded slurry, and 50 minutes for wet granulated samples. A common structural element that has been described as a potential factor in identifying the risk of a solvent-mediated hydration occurring during wet granulation is the presence of distinctive channels within the crystal lattices of the anhydrous materials, via which solvent molecules can be absorbed and specifically incorporated. Of the compounds explored by Wikström et al. (88), four have known "channel hydrate" structures, whereas nitrofurantoin is known to form an isolated site hydrate. The manifestation of this structural difference seems to be most pronounced when comparing the observed kinetics for the solvent-mediated hydration conversions. The four channel structures completely transformed to their respective hydrates in relatively short time periods (ranging from less than 30 seconds to 12 minutes), whereas the shortest observed transformation time for nitrofurantoin was 50 minutes. The water addition routine that resulted in the most rapid transformation kinetics for nitrofurantoin corresponded to wet granulation experiments. The authors proposed that, despite significantly reduced volumes of H_2O (relative to other methods of exposure), the shear forces imposed by the high-shear granulator were sufficient

to produce secondary nuclei that were capable of initiating and propagating the transformation. In support of this hypothesis, it was noted that nitrofurantoin hydrate crystals were observed to grow as fine needles on the surfaces of the anhydrous particles. Fine needles would be easily fractured in a high shear bed, exposing the lattice hydration sites to contact with water, and enabling growth. In additional support of this idea, the authors noted that transition kinetics were observed to be greatly accelerated for pre-ground nitrofurantoin.

An interesting example from the literature suggests that transformations of materials from crystalline forms to an amorphous form may also be influenced by wet granulation. A study by Blanco et al. (94) used NIR spectroscopy to evaluate the transformation of dexketoprofen trometamol in both laboratory and production samples involving wet granulation. Two crystalline polymorphs of the molecule (termed A and B) were separately mixed with microcrystalline cellulose and wet massed at the laboratory scale by manually stirring in water to a total w/w content of 44%. Samples were subsequently dried and carefully ground into individual particles. Analyses of NIR signals (obtained from these granules) subjected to standard multivariate processing routines indicated that both A and B polymorphs, when wet granulated, transformed to a common form, which showed neither detectable diffraction peaks via XRPD nor endothermic events attributable to fusion of crystalline solids in DSC. The authors concluded, therefore, that wet granulation of either polymorph of dexketoprofen trometamol elicited a transformation to the amorphous form, which was not observed for the same material subjected to direct compression.

EFFECTS DUE TO DRYING

A solvent removal step is inevitably coupled with solvent-based secondary processes (wet granulation, recrystallization, etc.). Other chapters in this book have reviewed examples in which desolvation (mainly dehydration) results in conversions to anhydrous or amorphous solid forms. It is easily anticipated, therefore, that such transformations may be induced by the various methods used to dry pharmaceutical products and product intermediates. The greatest risk is associated with the adjustment of parameters that may be used to increase drying efficiency. If process optimization requires a temperature that exceeds T_{tr} for a pair of enantiotropically related polymorphs, these solids may be subject to a phase change. Alternatively, if the rate at which solvent is removed from a product is rapid, metastable forms may be kinetically trapped by the drying process.

Conventional Drying Methods

Tray drying is performed by placing moist material in coated trays, which are housed in chambers where controlled-temperature airflow is passed over and through product beds (Fig. 6A). Historically, tray drying was the most widely used method, but has largely been replaced by fluidized-bed drying processes. A slower process, tray drying does involve lengthy exposure of product to heat and moisture, which serves as a potential kinetic disadvantage where process-induced conversions are concerned.

In contrast, fluidized-bed drying is one of the most commonly used unit operations in the pharmaceutical industry. Often coupled with wet granulation, it uses the same equipment (Fig. 6A), and proceeds after binder solution addition is

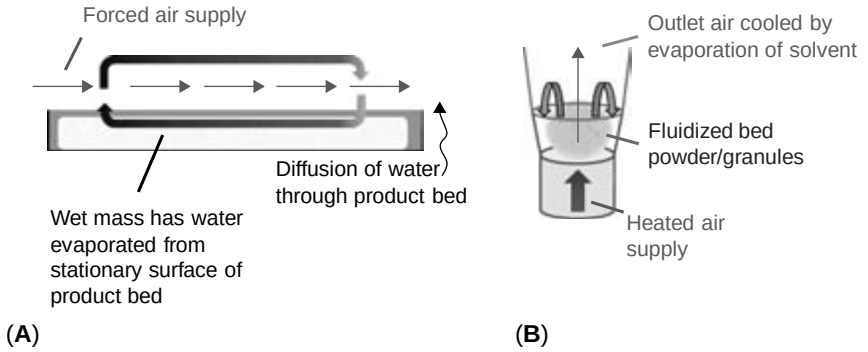
Forced air supply
Diffusion of water through product bed
Wet mass has water evaporated from stationary surface of product bed
(A)
Outlet air cooled by evaporation of solvent
Fluidized bed powder/granules
Heated air supply
(B)

FIGURE 6 Schematic representation of (**A**) tray drying and (**B**) fluidized-bed drying.

completed. Moist material is entrained in a warm, fluidizing air stream, allowing drying to sequentially proceed in two distinct phases (76). The first is heat transfer limited, and occurs as water evaporates from particle surfaces. The change in moisture content as a function of time (M_t) is linear during this phase and can be modeled by equation (12):

$$M_t = M_0 - kt \tag{12}$$

where M_0 is the initial moisture content, t is time, and k is a constant [equation (13)].

$$k = \frac{\rho_g}{\rho_s} \cdot \frac{C_{pg}(T_{inlet} - T_{exit})}{H_v} \cdot \frac{U_0}{(1-\varepsilon_m)L_m} \tag{13}$$

Established by well-known principles of process engineering, k considers the density of the gas (ρ_g) and the solid (ρ_s), the specific heat capacity of the gas at a constant pressure (C_{pg}), the inlet and exit air temperatures (T_{inlet} and T_{exit}, respectively), the latent heat of vaporization for water (H_v), the fluidizing stream velocity (U_0), the void fraction of a packed bed of solid material (ε_m), and the height of the bed (L_m). This constant [equation (13)] indicates that the heat transfer-limited phase will depend on the operating temperature and fluidizing air velocity.

The mass transfer-limited phase occurs once surface evaporation has ended, and continued drying proceeds by diffusion of water from particle cores. Here, M_t follows an exponential trend, approximated by equation (14).

$$M_t = M_\infty + M_0' \kappa e^{-\kappa t} \tag{14}$$

Here, M_0' represents the initial moisture content at the start of the mass transfer-limited phase, M_∞ is the endpoint moisture content, and κ is a geometric term summed over n terms in an infinite series [equation (15)]:

$$M_t = \frac{6}{\pi^2}\left[\sum_{n=1}^{\infty}\frac{1}{n^2}\exp\left(-n\pi^2\frac{D_m t}{R^2}\right)\right](M_0' - M_\infty) + M_\infty \tag{15}$$

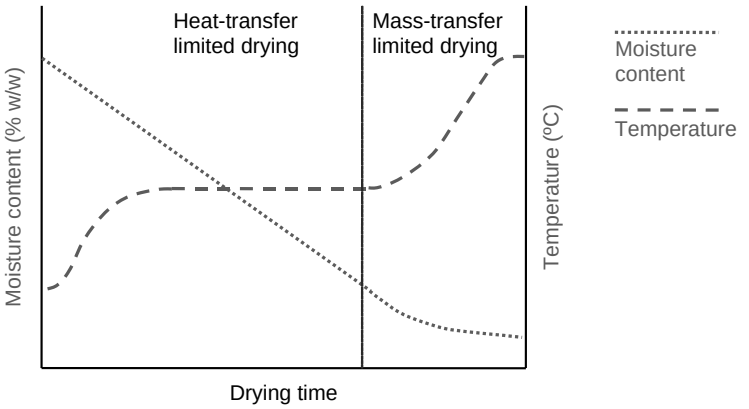

FIGURE 7 Schematic figure illustrating moisture content and outlet air stream temperature as a function of fluidized-bed drying time. The product temperature remains constant during heat transfer-limited (linear) drying, and sharply rises on transition to mass transfer-limited (exponential) drying.

where D_m is the diffusivity of water through the solid materials, R is the average particle radius, and all other terms are as defined above.

This two-stage model of fluid-bed drying is important to the present discussion particularly at the critical point in the process when drying switches from a heat transfer-limited mechanism to a mass transfer-limited mechanism. During the first phase, evaporative cooling protects the product from exposure to significant temperatures as energy is used to remove loosely bound surface water molecules. In contrast, the product bed temperature rapidly increases during the mass transfer-limited stage, running the risk of exposure to deleterious operating temperatures (Fig. 7).

A fast-drying technique has been suggested (95) that employs real-time feedback control to indicate the shift in mechanism between phases of drying. In this approach T_{inlet} is set above a critical operating temperature (i.e., solid-phase transition temperature for a pair of enantiotropes) during the heat transfer-limited phase. This is rationalized as safe, as the product would not actually experience this temperature as water is removed by evaporation. In anticipation of the drying mechanism changing to mass transfer-limited drying, T_{inlet} is reduced below the critical temperature until $M\infty$ is reached.

Kinetic Trapping of Metastable Polymorphs by Rapid Solvent Removal

In their work involving fluid bed drying of γ-glycine wet granulated with microcrystalline cellulose and water, Davis et al. (96) showed that rapid solvent removal lead to kinetic trapping of metastable α-glycine. Glycine can be recrystallized as one of three common crystalline phases (α, β, and γ) of which the γ-form is stable at room temperature. Given prolonged exposure to water during wet granulation, solvent-mediated conversion to the stable form at room temperature might be expected. Samples of granulate were dried at two separate temperatures (60°C and 80°C), both of which resulted in significant mass percent trapping of metastable α-glycine. The higher drying rate resulted in more extensive kinetic trapping of the

metastable α-phase. As would be expected, the stable form will dissolve in water at a rate proportional to its equilibrium solubility and the dissolution rate constant. The authors suggested that if the rate of solvent removal is much faster than the solution-mediated conversion to the stable form, the metastable polymorph may crystallize as drying progresses.

The risk of metastable phase trapping is considerably higher in fluid-bed operations, owing to more rapid and uniform solvent removal. As granulate is entrained in the fluidizing air, solvent can be quickly removed, and the degree of supersaturation (with respect to the metastable phase) in the available granulating fluid is expected to be higher, providing a larger thermodynamic driving force for rapid nucleation and growth of this form.

Dehydration and Desolvation During Drying

Another transformation anticipated as being the result of drying involves desolvation, specifically dehydration of hydrated crystalline lattices. Detailed mechanisms for dehydration and desolvation, as well as a thorough review of various examples is provided in Byrn et al. (20). Implications of the loss of crystallographically coordinated solvent molecules can include changes in dissolution rate, bioavailability, and stability of solid materials. For example, the non-stoichiometric hydrate of thiamine hydrochloride was observed to undergo a 5% unit cell volume reduction upon the loss of its water of hydration, but an increase in the free volume and molecular mobility of the dehydrated solid (97). From this, and numerous other studies, the ease with which a solid effloresces on heating has been highly correlated with specific structural features, including the presence and size of porous intracrystalline channels, the relative packing density of molecules in a given structure, the direction/orientation of solvent molecules relative to the direction/orientation of the host molecules, the number/strength of hydrogen bonds between the solvent and host, and the nature and extent of coordination of the solvent with cations in salts (20). Once again, the influence of defects within the lattice can be expected to play a role in the potential for dehydration, as their presence will affect the local structure associated with many of these factors. It might be expected, therefore, that depending on the preceding manufacturing steps, desolvation might be more favored during drying.

Airaksinen et al. (98) investigated the effects of two different drying methods on the resulting form changes of theophylline. In their work, anhydrous theophylline was granulated by the addition of purified water to the dry material in a planetary mixer. Fluidized-bed drying was performed using a multichamber microscale fluid-bed dryer (MMFD), while tray drying was simulated in situ in the variable temperature holder of a variable temperature (VT)-XRPD. Analysis of granules showed that drying of the monohydrate (Form II) at 30°C (dry air conditions) resulted in a mixture of forms, including Form II and two anhydrous polymorphs, Form I and Form I* (the dehydrated hydrate lattice observed by Phadnis and Suryanarayanan (99)). The extent of conversion to Form I* reached a maximum when the drying temperature was increased to 50°C. At 90°C, the maximum drying temperature, conversion of monohydrate to Form I* was decreased relative to 50°C drying; however, 35% (w/w) of Form I* still forms at this high temperature (Fig. 8).

In contrast, the same granules dried under ambient inlet air (~30% RH) at 30°C resulted in a XRPD pattern consistent with nearly 100% Form II (i.e., no dehydration

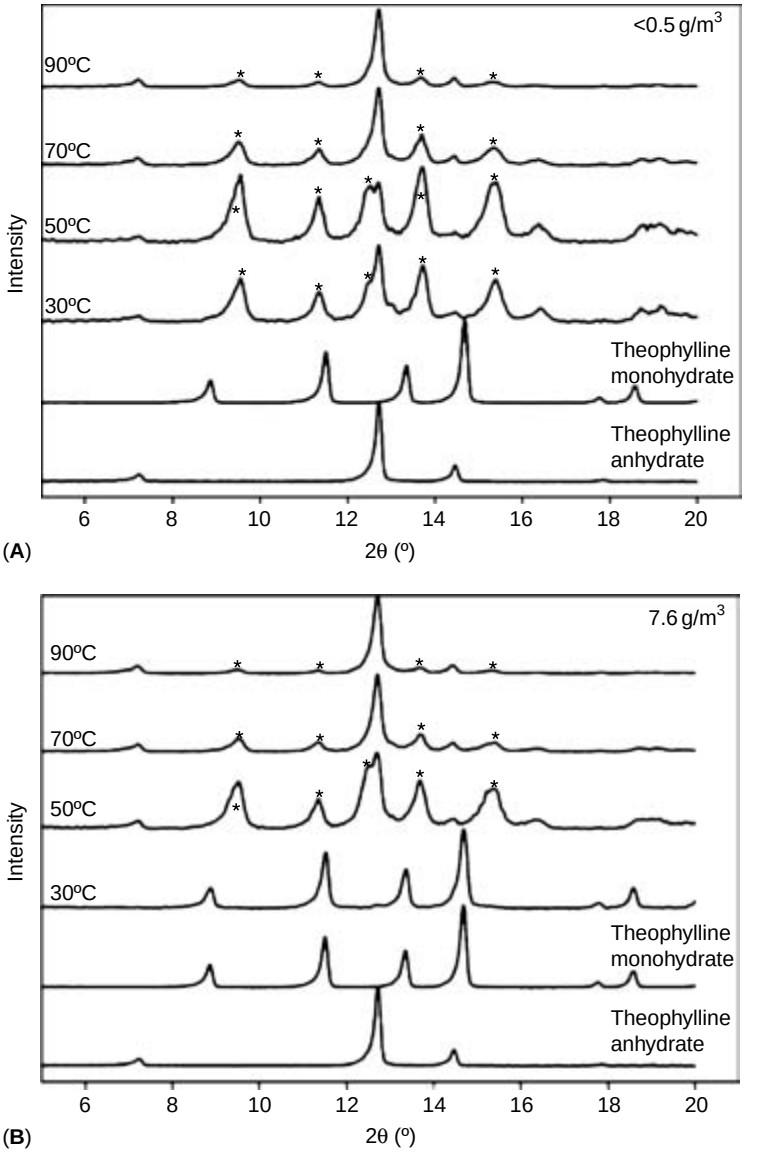

FIGURE 8 (**A**) XRPD patterns of theophylline granules dried using an MMFD at temperatures ranging from 30°C to 90°C using dry inlet air (<0.5 g/m³). (**B**) XRPD data for theophylline granules dried using an MMFD at temperatures ranging from 30°C to 90°C using ambient inlet air (7.6 g/m³). Peaks consistent with Form I* are indicated with (*). XRPD data for Form I (anhydrate) and Form II (monohydrate) are shown as controls. Reprinted from Ref. (98), with permission from Elsevier.

observed). At 40°C, nearly all of the Form II peaks were observed to disappear, and Form I* (dehydrated hydrate) reached its maximum level of conversion. With increasing drying temperatures, conversion to Form I* was observed to decrease with a commensurate increase in the stable anhydrate (Form I). It should be noted that although increasing temperatures did result in decreasing Form I*, at 90°C, 25% w/w Form I* was still observed (98).

The same authors simulated a tray drying experiment using the sample holder of a VT-XRPD, drying the Form II wet massed granules at temperatures ranging between 40°C and 70°C. At 40°C, a progressive reduction in monohydrate was observed over long drying times to a minimum plateau value of 5% w/w after 15 hours. The dehydrated hydrate (Form I*) reached a maximum conversion (40% w/w) after 75 minutes, with subsequent decline in its presence in the overall dried solid. Form I, the stable anhydrate also began to form immediately upon drying, ultimately resulting in granules having a distribution of approximately 75%, 20%, and 5% of Forms I, I*, and II after 15 hours of drying at this temperature. Granules dried at 50°C were observed to undergo faster initial conversions but resulted in the same ending composition as those dried at 40°C. At 60°C and 70°C, the monohydrate was observed to very rapidly dehydrate with commensurate increases in Forms I and I*. It should be noted, however, that formation of the dehydrated hydrate only occurred over the first 15 minutes, with eventual complete conversion of the granulated solid to Form I after five hours drying (98). Ultimately, both these experiments illustrate how drying conditions (specifically inlet air temperature and relative humidity) can influence the resulting forms of dried solid.

Collapse to Amorphous Solids on Dehydration

In addition to crystal-to-crystal form changes upon dehydration, many hydrates are known to become mechanically unstable as their waters of crystallization are removed, resulting in an inevitable a collapse to the amorphous state when dried. The rate of drying has been shown to affect the tendency to transform to the amorphous form as reported for trehalose dihydrate (100,101). Slow dehydration is reported to result in the formation of an anhydrous crystalline phase, whereas rapid dehydration promotes vitrification.

Raffinose pentahydrate is also known to collapse to its amorphous form upon dehydration. In a recent study by Bates et al. (102), it was shown quantitatively that initiation of the collapse to the amorphous state occurred by the formation of defects upon removal of the first two waters from the pentahydrate structure. Examination of the crystal structure of raffinose pentahydrate informs this behavior, as three of the water molecules act as both hydrogen bond donors and acceptors with raffinose, whereas the other two serve only as hydrogen bond donors: one with raffinose and one with water (Fig. 9). These more weakly bound water molecules are the first to leave the structure on drying, which was observed to be accompanied by a reduction in the *c*-lattice parameter. Curiously, the commensurate volume change is only equivalent to the loss of one water molecule, indicating some elastic recovery of the lattice. Pair distribution function (PDF) analysis of the XRPD pattern for the lower hydrate structure shows that the lattice remains isostructural with the pentahydrate, where the original space group is maintained. Subsequent loss of water from the structure creates defects (proposed to be site vacancies), which, once they reach a critical level, induce catastrophic collapse to the amorphous phase (102).

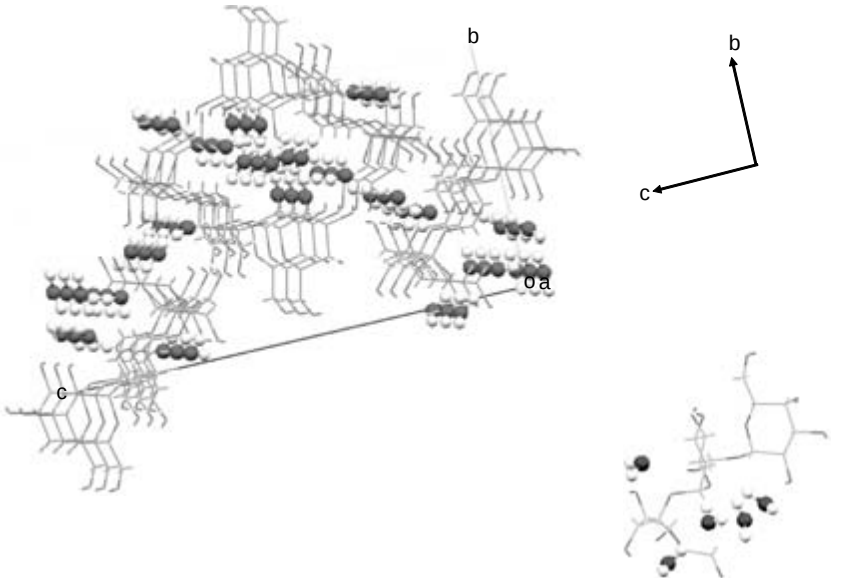

FIGURE 9 Single-crystal structure of raffinose pentahydrate (CSD refcode: *RAFINO01*) (103) packed along the *a*-parameter, showing the presence of distinct channels via which H_2O can leave the lattice upon dehydration. Note also that H_2O provides structural integrity to this lattice, which informs the observed mechanical instability upon drying.

In addition to conventional drying methods, spray drying, and lyophilization processes are routinely used in pharmaceutical manufacturing, and have been observed to cause solid state form changes.

Spray Drying

Spray drying is done by forming a concentrated solution or liquid dispersion of the agent to be dried in some volatile medium. The solution/dispersion is then atomized into droplets that are exposed to a heated atmosphere in order to accomplish rapid solvent removal (Fig. 10). The process yields a dry, free-flowing powder of fairly spherical particles having a relatively uniform diameter and size distribution. For example, the morphology of spray-dried lactose has been compared with that of the monohydrate and anhydrous phases of lactose, with significant differences being reported (104).

One advantage to this manufacturing step is the potential to control the resulting solid form via manipulation of the drying conditions. For example, the reported preparation of three different crystal forms of phenylbutazone from methylene chloride solution was accomplished by varying the drying temperature of the atomized droplets between 30°C and 120°C (105). The authors specifically noted that one of the polymorphs obtained from spray drying could not be isolated by any known crystallization procedure, and could only be produced using extremely slow solvent evaporation rates.

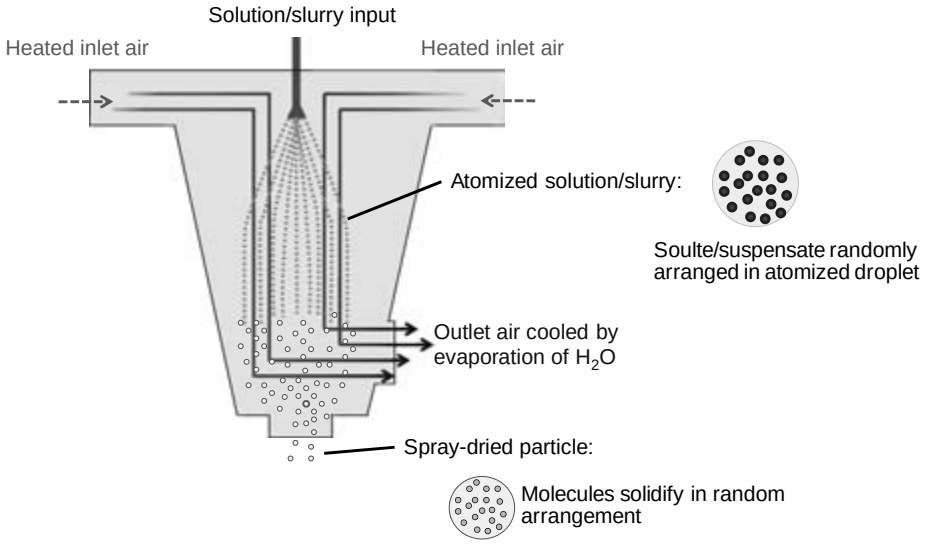

FIGURE 10 Schematic illustration of the spray-drying process. Heated air is passed over an atomized droplet containing solute or suspensate, and rapid evaporation of solvent results in formation of an amorphous solid product.

Spray drying has also been described as a method by which high-energy solids can be produced (106,107). Phenobarbitone has been isolated as a metastable polymorph (Form III) via spray drying (106), and hydroflumethiazide can be produced as amorphous solid by the same route (106). Amorphous lamotrigine mesylate has been prepared by spray drying, and was observed to be subject to recrystallization at moderate relative humidity (108).

Frequently, spray drying processes yield materials consisting of significant amounts of amorphous solid. As with other discussions involving amorphous solids, it is important to note that these materials are often observed to undergo unpredictable physical and chemical changes (109–111), which makes controlling their use in pharmaceutical drug products a topic of significant interest. The effect of various additives on the recrystallization of amorphous spray-dried lactose has been studied. Buckton and Darcy showed that the presence of magnesium stearate inhibited the recrystallization of amorphous lactose, whereas layers of microcrystalline cellulose in the spray-dried products could significantly delay the onset of recrystallization (112).

In a study of the behavior of amorphous salbutamol sulfate prepared by spray drying, Columbano et al. (113) observed rapid recrystallization upon exposure to moderately high RH (75%). Using a combination of dynamic vapor sorption and NIR spectroscopy, it was determined that the water that had been readily taken up by the amorphous solid, was expelled during crystallization but remained associated with the particle surfaces for several days.

Spray drying may also be used to encapsulate drug substances into excipient matrices; however, phase interconversions may still be possible in such environments. An example in which sulfamethoxazole Form I was microencapsulated with

cellulose acetate phthalate (CAP) and talc, colloidal silica, or montmorillonite clay by spray drying was shown to result in a transformation to Form II during the process (114). The formulation was shown to elicit an effect, where increasing amount of CAP led to increased conversion of the API to amorphous solid, whereas increased talc resulted in a greater extent of polymorphic conversion. In a subsequent study, the authors showed that no phase conversion was observed for formulations containing colloidal silica (115).

Lyophilization

Another drying process that commonly results in changes in material solid forms is freeze drying (interchangeably termed lyophilization). This approach is the most common way by which sterile powders for reconstitution/injection are prepared. During lyophilization the material to be dried is prepared as an aqueous solution or suspension, which is rapidly frozen. The frozen formulation is then exposed to vacuum and the ice is removed by sublimation. During the freezing step, most of the water is effectively separated from the solute as ice is formed. As freezing occurs, the solute becomes highly concentrated, forming a freeze concentrate that contains approximately 20% (w/w) water. Primary drying is then applied, which involves reduction of the pressure well below the vapor pressure of ice in order to drive sublimation. A secondary drying step is used to desorb water from the dried frozen concentrate, resulting in a final dried product (116). Because the lyophilized materials have minimal residual water (usually less than 1% of the initial mass from the solution) the materials are ordinarily hygroscopic and must be protected from adventitious water to prevent any unwanted phase transformations. In normal practice, the product that results from this process is amorphous, which, owing to the enhanced aqueous solubility of amorphous materials, is favorable for its subsequent reconstitution in solution (117). Consequently, the assessment of the potential for moisture-induced recrystallization of the lyophilized product is essential to its characterization.

Cefazolin sodium is capable of existing in a number of crystalline modifications, but the amorphous state is produced by the lyophilization process (118). The amorphous solid generated by lyophilization was observed to be physically stable at RH of less than 56%; however, recrystallization and conversion to the pentahydrate was observed above 75% RH. It is interesting to note that the hygroscopicity of the amorphous form was very similar to that observed for the dehydrated monohydrate or dehydrated α-form.

Excipients in lyophilized products may also undergo phase conversions during processing. Mannitol, which is commonly used as a bulking agent in lyophilized products, has a tendency to freeze dry as a combination of crystalline and amorphous solids. Because mannitol can exist in a number of crystal forms, slight variations in the lyophilization process can result in the generation of different solids. Within the course of the lyophilization process, an annealing step is often employed, which maintains the product at a temperature greater than the final freezing temperature to allow crystallization of the bulking agent. Here, the transformation to the excipient induced by the process is desired, as it facilitates better product stability on storage, owing to a reduced tendency of the solid to recrystallize. Process optimization with respect to annealing temperature and time is essential, and should occur prior to primary drying to avoid vial breakage. Formulations in which mannitol is used as a bulking agent should be annealed at approximately –20°C or

–25°C for longer than two hours to allow complete recrystallization of the excipient (116). The effect of surface-active agents on the composition of lyophilized mannitol formulations has been studied, and polysorbate 80 was found to affect both the crystal form and the degree of crystallinity in freeze-dried mannitol. When pure mannitol was lyophilized a mixture consisting of the α, β, and δ forms was observed, in various ratios. In the presence of polysorbate 80, however, generation of δ-mannitol is favored (119).

Protein therapeutic products oftentimes suffer from insufficient stability in aqueous solution and various approaches are used to dry the protein into a solid for reconstitution. In a series of papers, Abdul-Fattah et al. explored the impact of drying-induced variations on the physicochemical properties of a vaccine (live attenuated parainfluenza; *Medi 534*) (120), a monoclonal antibody (IgG_1) (121), and methionyl human growth hormone (Met-hgH) (122), to assess their influence on the stability of each of these products.

In the vaccine study, a sucrose-based formulation (formulated with and without Pluronic F-68 surfactant) was dried via lyophilization, spray drying, and foam drying. The specific surface area (SSA) of the vaccine produced by spray drying (without surfactant) was determined to be the highest ($2.8\,m^2/g$), and the lowest ($0.1\ m^2/g$) for the foam-dried formulations (with or without surfactant). Vaccine surface coverage estimated by electron spectroscopy for chemical analysis (ESCA) was predicted to be highest for spray-dried formulations (without surfactant) and lowest in foams containing surfactant. Stability studies on products prepared by all three methods indicated that freezing damaged both in-process and storage stability of the vaccine, regardless of whether or not the surfactant was used. Foam drying was determined to result in the best storage stability (both with and without surfactant), which was correlated with the low SSA and low vaccine surface coverage (120).

Sucrose-based IgG_1 formulations were dried via the same three methods (with and without the same hydrophilic nonionic surfactant used in the vaccine study), and similarly assessed. Both drying method and formulation were determined to have a significant effect on IgG_1 powders, including the storage stability. Spray-drying resulted in the highest SSA as well as the fewest perturbations in protein secondary structure. Foams having the highest sucrose content had the lowest SSA and protein surface accumulation, as well as the lowest molecular mobility, which was reflected in their highest relative physical stability. As with the vaccine experiments above, the freeze-dried formulations showed the poorest stability on storage, once again attributable to changes in protein secondary structure (121).

Formulations containing Met-hgH and various different stabilizers were dried using spray drying, freeze drying, and film drying, and characterized as above. Powders dried via the different methods were observed to have different morphologies, reflected in the different SSA values. In these experiments, film-drying resulted in the lowest SSA ($0.03\,m^2/g$) and lowest total protein surface accumulation. A loss of native protein structure showed a strong dependence on the stabilizer used in the formulation. The lower molecular weight stabilizers investigated (trehalose and stachyose) showed the best ability to maintain protein secondary structure across all three drying methods, regardless of whether or not a surfactant was used in the formulation. In contrast, the larger molecular weight polymers (dextran 40 and Ficoll 70) proved less able to preserve secondary structure, and

ultimately served as poor stabilizers for these formulations across the three drying methods (122).

EFFECTS DUE TO COMPRESSION

As with milling described above, the stress state required to form tablets from powders or granules involves the application of significant force. Some may assume that the solid forms of the materials remain consistent despite this harsh processing step, owing to the presence of softer excipients, which deform preferentially relative to harder, crystalline API. The difficulty with this statement is that it ignores that changes in the solid form of these softer excipients might, themselves, bear some impact on the drug product performance. Consider that the functional roles assigned to many excipients are highly variable, owing to inconsistencies in raw materials suppliers. Additionally, vague methods are often used for excipient characterization, which may or may not be adequately linked to the desired performance characteristics assigned them in the overall formulation. Given this variability and knowledge gap, it is no wonder that subtle or partial solid form changes at the excipient level have seldom been tied into dosage form performance issues. Certainly, the effect that phase changes have on the bioavailability of the API should be held important in the overall analytical scheme. From a materials standpoint, however, the stress state imposed on the formulation when it is compacted is capable of affecting many of the components, and it is the broader view of transformations with which this section is written.

Hydrostatic Stress States

Consolidation of solid materials under pressure in a closed-die system is rigorously termed *compaction*. The mechanisms by which materials yield to stress is broadly divided into fragmentation and deformation processes. It is reasonable to consider that under considerable load most materials will experience a combination of these responses in order to dissipate energy. Although terminology accompanying tableting often considers pressure to be the driving force for solid bond formation, it is more appropriate to view this load as a stress (σ_{ij}), containing both normal and shear components. Figure 11 below illustrates the difference in terminology, where the resolved stresses experienced by a finite stress element are considered.

In Figure 11A, the finite stress element is considered surrounded by a fluid, where all surfaces experience only normal loads of equivalent magnitude. This represents a special case of $\sigma_{ij} = P$, where $-\sigma_{11} = -\sigma_{22} = -\sigma_{33}$ and all σ_{ij} ($i \neq j$) are equal to zero (i.e., no resolved shear components).

$$\sigma_{ij} = \begin{vmatrix} -\sigma_{11} & 0 & 0 \\ 0 & -\sigma_{11} & 0 \\ 0 & 0 & -\sigma_{11} \end{vmatrix} = P \tag{16}$$

Termed hydrostatic pressure, access to a different crystal form via isothermal compression is possible if the coexistence line between the two phases has a negative slope (29). As the slope at any point along this boundary is described by the

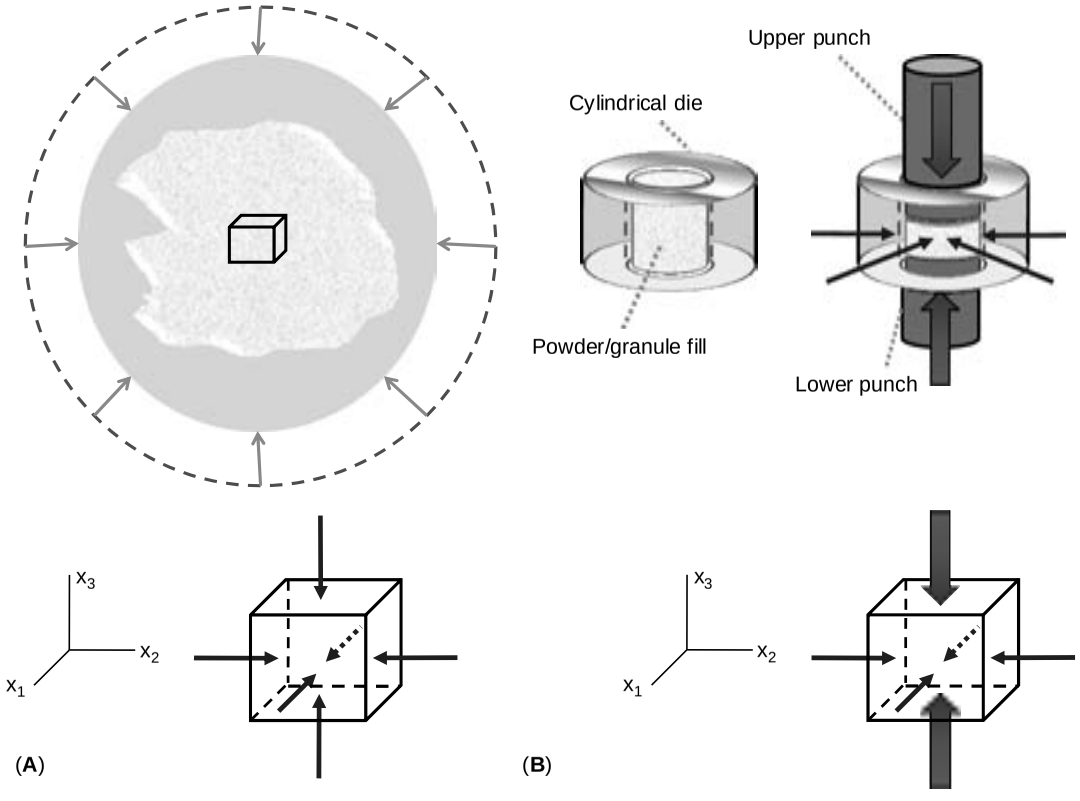

FIGURE 11 Differentiation between pressure and stress. In (**A**) a pressure is applied to a fluid in which a particle is suspended. Resolved stresses on a finite element within the particle are all normal and all equal. In (**B**) a pressure is applied to powders/granules in a cylindrical die. Stress is applied axially via the punches, whereas normal stresses are resolved radially as particles deform against the die walls. Shear stresses are resolved throughout as particles deform and rearrange (arrows not shown on stress element).

change in pressure with respect to the change in temperature, the following is true:

$$\left(\frac{\partial P}{\partial T}\right)_V = \left(\frac{\partial S}{\partial T}\right)_T \tag{17}$$

The change in entropy can also be expressed as follows:

$$\mathrm{d}S = \frac{\mathrm{d}q}{T} \tag{18}$$

where dq represents a reversible change in heat. During a phase transition, dq is equal to the enthalpy of transition (ΔH_{tr}), resulting in the following expression for transition entropy [equation (19)]:

$$\Delta S_{\mathrm{tr}} = \frac{\Delta H_{\mathrm{tr}}}{T} \tag{19}$$

Combining equations (17) and (19), the slope of the coexistence line results can be defined by:

$$\frac{\Delta P}{\Delta T} = \frac{\Delta S_{\mathrm{tr}}}{\Delta V_{\mathrm{tr}}} = \frac{\Delta H_{\mathrm{tr}}}{T\Delta V_{\mathrm{tr}}} \tag{20}$$

which is generally known as the Clausius–Clapeyron equation. Ordinarily, a transition from a stable phase to a metastable phase is accompanied by a volume expansion, which, if the transformation is endothermic, always results in a positive value for equation (20). Given $\sigma_{ij} = P$ above, it is difficult to imagine a volume expansion against the normal compressive stresses σ_{11}, σ_{22}, and σ_{33}. If, however, the more stable form is less dense than the metastable form, then ΔV_{tr} is negative, which coupled with an endothermic change in enthalpy, necessitates a negative slope to the coexistence curve, permitting a pressure-induced pathway to the metastable phase (Fig. 12). Such is the case in the example of the isothermal transition of PbO at high pressures, where the low temperature stable, tetragonal phase (litharge) is observed to transform to its more dense, high temperature stable, orthorhombic phase, enabled by a coexistence curve having a negative slope (123).

In their papers on the polymorphism of small molecule organic systems, Burger and Ramberger proposed a general density rule, stating: "If one modification of a molecular crystal has a lower density than the other, it may be assumed to be less stable at absolute zero (124)." At room temperature, however, the most stable polymorph may not necessarily have the highest density, most often owing to lattice stabilization by extensive hydrogen bonding (124). Such is the case for resorcinol, in which the low-temperature stable enantiotrope (α) is less dense than the high-temperature stable phase (β) (124,125). Equation (20) would predict a negative pressure-temperature coexistence (Fig. 12), which was experimentally confirmed by Yoshino et al. (126). The preceding development then provides rationale for the commonly observed phase transformation from α → β that occurs under hydrostatic pressures of approximately 0.5 GPa (127,128).

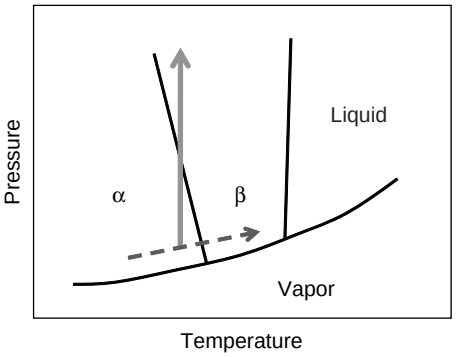

FIGURE 12 *P–T* phase diagram for a pair of enantiotropes (α, β) in which the low-temperature stable form has a smaller density than the high-temperature stable form. This necessitates that the coexistence curve between them has a negative slope, allowing isothermal, pressure-induced phase transformation from the stable to the metastable phase. Modified from Ref. (29).

Except under highly controlled circumstances, hydrostatic stress states are rare, and to some extent the shear-based deviatoric components will always occur in real deformation processing. Here, the stress state applied for consolidation includes significant resolved shear stresses, σ_{ij} $(i \neq j)$, as in Figure 11B, which occurs as particles rearrange and deform during consolidation.

$$\sigma_{ij} = \begin{vmatrix} -\sigma_{11} & -\sigma_{12} & -\sigma_{13} \\ -\sigma_{21} & -\sigma_{22} & -\sigma_{23} \\ -\sigma_{31} & -\sigma_{32} & -\sigma_{33} \end{vmatrix} \tag{21}$$

These shear components are responsible for dislocation propagation and translation, which is the structural basis for plastic deformation, and therefore, must be considered as being significant in this process. In fact, other industries also interested in process-induced phase transformations of their materials, have long identified that stress states involving shear components are capable of eliciting phase transformations at much lower applied stresses than purely hydrostatic applied states (3). For example, the phase transition from the anatase to the rutile form of TiO_2 has been observed during high energy milling under normal operating conditions (sub-GPa) (8). Under hydrostatic load, however, anatase does not undergo conversion until a pressure of 2.6 GPa has been applied, at which a different high-pressure phase results (129).

Similar observations have been made in pharmaceutically relevant systems, where an API that transforms under normal compaction pressures does not transform until significantly higher pressures when evaluated by analytical techniques involving diamond anvil sample cells (crystallites suspended in a fluid through which a hydrostatic pressure is transmitted). Such is the case for chlorpropamide Form A (see below for further discussion), which is known to undergo a facile transformation to its metastable phase (Form C) during compaction (130,131). When subjected to loads up to 5.5 GPa in a Merrill-Bassett diamond anvil cell, however,

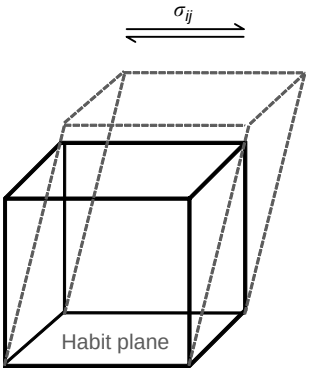

FIGURE 13 Parent and daughter phases of a martensitic transformation showing habit plane invariance with a shear facilitated dilatation.

and evaluated using high-resolution synchrotron X-ray powder diffraction, no evidence of the polymorphic transformation was observed (132).

Shear-Based Transformation Mechanisms

Shear-based mechanisms rely on the non-hydrostatic, shear components of σ_{ij} to overcome the energetic barriers associated with the shape change required by the transition. In general, shear-transforming systems share an invariant plane between the two phases and have a normal dilatational strain in the third direction (133). One commonly observed shear mechanism is the martensitic transformation found particularly in numerous metallic and ceramic materials. Martensitic transformations are diffusionless, proceeding by the simultaneous and cooperative movement of atoms over very small translational distances (134). These transformations often accompany conditions that promote extreme volume changes, such as stress states associated with extensive plastic deformation (135).

To allow the requisite coordinated movement of martensitic transformations, the transition requires that the product phase inherits the same composition, atomic order, and lattice defects of the parent phase. The transformation interface must contain one invariant line that remains undistorted and un-rotated by the strain, necessitating a structural relationship between the lattices of both phases. Within the habit plane, the invariant line remains common between the initial and final crystal phases (Fig. 13).

Experimental observations of three-dimensional martensite growth have indicated that growth normal to the habit plane is much slower than growth along the two directions in the habit plane (136). The crystallographic relationship between the parent and daughter phases also demands that both have a high degree of symmetry. As such, their occurrence in molecular organic systems is expected be less prominent than other mechanisms.

As with any solid state nucleation, it is necessary to overcome a free energy barrier to facilitate growth of the martensitic phase. Experimental observation has shown that the high energy associated with surfaces and grain boundaries does not contribute significantly to the initiation of martensitic transformations, rather the

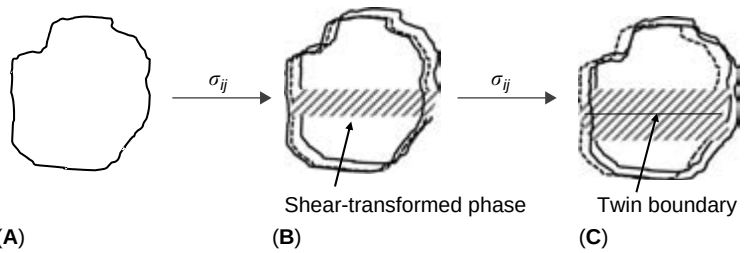

FIGURE 14 Schematic diagram illustrating martensitic transformation of a particle by formation of self-accommodating pairs of twinned planes. Continuous application of shear stress to the particles can lead to complete transformation by formation of successive twin regions. Figure modified after Ref. (134).

transformation most commonly starts at dislocations within the lattice of the parent phase (137). The energy change associated with a martensitic transformation is expressed below in equation (22):

$$\Delta G = A\gamma + V\Delta G_s - V\Delta G_V \tag{22}$$

Here, A is the surface area of the martensite phase, γ is the interfacial energy between the parent and daughter phases, V is the volume of the transformed phase, ΔG_V the free energy change associated with the volume change, and ΔG_s is the energy changed due to strain. The strain energy of the coherent interface between phases is the most important term influencing whether or not the free energy change associated with the transformation will be favorable. Homogeneous transformation of an entire grain via martensitic mechanism is energetically prohibitive; instead, slip or twinning along small parallel layers of paired unit cells (138) can accomplish the microstructural shape change using minimal strain energy (Fig. 14) (134).

Nucleation of these self-accommodating pairs requires growth of an initial template, the strain energy of which is greater than that associated with continued growth of the coupled layers (134). The shear component along the invariant plane is very high, increasing the contribution of the ΔG_s term to the thermodynamic spontaneity of this reaction. This may be the reason why dislocations serve as initiation sites of martensitic transformations. The strain imposed by the presence of a dislocation is likely greater than that imposed by the formation of a coherent interface between austenite and martensite, providing the energy gradient that initiates the reaction (137).

The most common geometry of a martensite growth phase occurs as thin, oblate spheroids whose strain energy can be estimated using equation (23) (134):

$$\Delta G_s = \frac{\mu_s}{(1-n)} \cdot \frac{\pi}{4} \cdot \left(\frac{t}{R}\right)\left[\Delta V^2 + \frac{(2-n)}{2}\varepsilon_\gamma^2\right] = \frac{t}{R} \cdot \psi \tag{23}$$

Here, μ_s is the elastic shear modulus, n is Poisson's ratio, R and t are, respectively, the radius of curvature and the thickness of the growth phase, and ΔV and ε_γ are the volume and shear components of strain required by the transformation. Substitution into equation (22) yields the following:

$$\Delta G = 2\pi R^2 t\gamma + \left(\frac{4\pi R^3 t}{3}\right)\left(\frac{t}{R}\right)\psi - \left(\frac{4\pi R^3 t}{3}\right)\Delta G_V \quad (24)$$

This expression clearly demonstrates the dependence of the transformation energy on the physical dimensions of the transformed phase. Compensation of the strain components in ψ, (ΔV and ε_y) by the application of an external stress, allows the strain energy to do work in the direction of the stress, reducing the overall free energy change needed to nucleate the new phase (134).

Martensitic transformations can be further classified into two sub-categories. Weak martensitic transformations can occur without the presence of dislocations, and are fully reversible. In contrast, reconstructive martensitic transformations are irreversible, and are accompanied by significant changes in microstructure, most notably the migration of dislocations through extensive deformation. The key difference between them appears to be the energy barrier against transformation. The parent and daughter phases involved in weak transformations both belong to symmetry groups that are related by a common, finite symmetry group (139), whereas it is unnecessary that the phases involved in reconstructive transformations be related in this way. As such, the energy barrier to accomplish the reconstructive symmetry change is as large as the energy barrier for the phase transformation itself, which is not the case for weak transformations, allowing them to be fully reversible (140). Common examples of reversible, weak martensitic transformations include shape memory alloys such as Nitinol (an alloy of Ni and Ti) used for numerous medical instruments and implants such as stents (141). Reconstructive martensitic transformations are those more traditionally seen in steels (135) or ceramics (134), which because of their reliance on dislocations for initiation and propagation, are not considered reversible (140).

Although no pharmaceutically relevant crystals have been specifically reported to undergo either type of martensitic transformation, this could easily be an inadvertent omission owing to terminology. The pharmaceutical materials literature is certainly full of examples of shear-based transformations of API occurring as a result of grinding or compaction. Few, if any, have explored specific indicators of structure, however, that may have facilitated the transformation. As martensitic classifications are indebted to specific evaluation of structure then, it is not surprising that this particular transformation mechanism has not been reported in the pharmaceutical literature. Although the authors do not specifically claim to have identified martensitic phase behavior for chlorpropamide, a structural investigation of two crystal forms of this antidiabetic molecule were concluded to undergo a specifically shear-based transformation (131).

Chlorpropamide is one of the most widely studied API that undergoes compaction-induced transformations. Two of its enantiotropes have been observed to undergo a facile solid-state phase transformation when exposed to moderate mechanical stress, which has been reported in several studies (130,131,142,143). Following the naming convention adopted by Simmons (144), these two crystalline phases are termed Form A and Form C, respectively, representing the low-temperature and high-temperature stable polymorphs. An early observation of this transformation was published by Ueda et al. (142), who observed that Form C was converted to Form A when compacted at 2 tons/cm^2 (196 MPa) during the preparation of disks for use in intrinsic dissolution studies. These observations were further

investigated by Otsuka et al. (130), who demonstrated that consolidation of Form A at 196 MPa resulted in compacts consisting of a mixture of both Form A and Form C. Likewise, consolidation of pure Form C at the same applied stress resulted in a similar mixture of forms. These studies indicate that the stress involved in routine tablet manufacturing is capable of eliciting an interconversion between these two phases of chlorpropamide. Given the apparent bi-directionality of the transformation it has been suggested that the application of pressure induces conversion to a disordered intermediate from which either form is capable of recrystallizing (130). In a subsequent publication, however, compacts formed under similar pressures were sectioned and analyzed by DSC for persistent amorphous content, and none was observed (131).

A more recent study of chlorpropamide polymorphs, specifically addresses the crystal structure of Forms A and C, finding them to be very similar (Fig. 15). In the figure, visual comparison of the two polymorphs is facilitated by setting the unit cells for both forms in equivalent orientations. As described in Wildfong et al. (131), when the respective unit cells are scaled to equal dimensions, the fractional coordinates of the four molecules in either of the two structures have identical relative positions. Transformation, therefore, only requires a torsion and minimal translation of the molecules to interconvert between the two phases.

The ease with which the two phases are allowed to interconvert was described as a function of the structural similarity between the two forms, and facilitated specifically by the shear components in the applied stress state. This claim was emphasized by experiments in which both Form A and Form C were exposed to

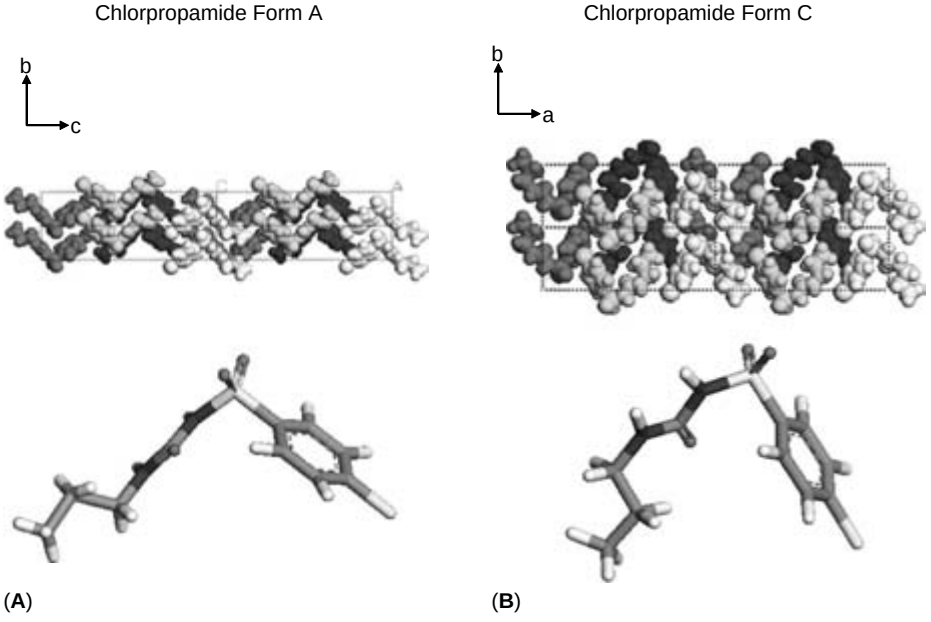

FIGURE 15 Comparison of packing models and asymmetric unit for (**A**) chlorpropamide Form A and (**B**) chlorpropamide Form C.

significant hydrostatic pressures without observed transformation. Evaluation of the two crystal structures indicated a common slip plane, which when exposed to shear stresses during compaction were proposed to allow sufficient lattice distortion to permit the observed phase interconversion (131).

Further Examples of Phase Transformations Elicited During Milling

As with milling, numerous examples of compression-induced phase transformations are reported throughout the pharmaceutical literature. Once again, recognizing that this topic has received considerable attention, Table 3 contains a *partial* list of recent and historical studies.

TABLE 3 Summary of Some Reports of Polymorphism Induced During Tableting or by the Application of Hydrostatic Pressure

Material	Compression experiment	Observation
Piroxicam (145)		$\alpha \rightarrow \beta$ (tablets prepared to RTS 9 kg/cm^2) $\beta \rightarrow$ no tfm observed
Anhydrous caffeine (60,146)	Instrumented single-punch machine (60,146) Mixed w. maltodextrin (60)	I $\rightarrow$ II ($\sigma \sim 50$ MPa; $G_{II} < G_I$) (60) A $\rightarrow$ B (~25% at 150 MPa; $G_B < G_A$) (146)
Maprotiline·HCl (146)	Instrumented single-punch machine	III $\rightarrow$ II (~45% at 200 MPa; $G_{II} < G_{III}$) I $\rightarrow$ no tfm observed
Sulfabenzamide (146)	Instrumented single-punch machine	B $\rightarrow$ A (σ = 50–350 MPa; $G_A < G_B$)
L-Serine (147)	Hydrostatic diamond anvil cell	I $\rightarrow$ II (σ = 5.3 GPa) II $\rightarrow$ III (σ = 7.8 GPa)
Phenol (148)	Hydrostatic diamond anvil cell	Monoclinic (I) $\rightarrow$ monoclinic (II) (σ = 0.16 GPa)
Phenylbutazone (149–151) *Note*: Polymorph nomenclature highly variable among sources	Single station pellet press (149–151)	III $\rightarrow$II (σ = 1 ton/cm^2; $G_{II} < G_{III}$) (149) C $\rightarrow$A (~5.6% at 216 MPa; $G_C < G_A$) (150) D $\rightarrow$ A (~2.2% at 216 MPa; $G_D < G_A$) (150) E $\rightarrow$ A (~1.8% at 216 MPa; $G_E < G_A$) (150) III $\rightarrow$ IV ($\sigma \sim$ 310–398 MPa; $G_{IV} < G_{III}$) (151) II $\rightarrow$ IV,? ($\sigma \sim$ 310–398 MPa; $G_{IV} < G_{II}$) (151)
Glycine (152,153)	Hydrostatic diamond anvil cell	$\beta \rightarrow \beta'$ (σ = 0.8 GPa) (152) $\gamma \rightarrow \delta$ (σ = 2.73–7.85 GPa; partial tfm) (153)
Acetaminophen (154)	Hydrostatic diamond anvil cell	I $\rightarrow$ II (σ = 4 GPa; partial tfm)
Chlorpropamide (130–132,143,155–157)	Single-station eccentric tableting machine (130,143,155,156) Bench-top hydraulic press (131,157) Hydrostatic diamond anvil cell (132)	A $\leftrightarrow$ C [interconversion (130,131,143,155–157); $G_A < G_C$; not observed under hydrostatic load (132)] A $\rightarrow$ C (σ_{crit} = 10.5 MPa; $G_A < G_C$) (157) C $\rightarrow$ A (σ_{crit} = 10.5 MPa; $G_A < G_C$) (157)

? the authors suggested the possibility of transformation to an unnamed polymorph.
Abbreviation: tfm, transformation.

Analysis of Phase Transformations in Intact Tablets

Characterization (and quantification) of phase transitions induced during consolidation of powders can prove to be analytically challenging. Historical examples from the literature generally involve reversion of compacts back to powders via trituration, a step that carries with it the risk of inducing further transformation. Spectroscopy techniques have been used to evaluate various physicochemical properties of intact tablets (158–162). It should be noted, however, that these techniques are limited in their ability to penetrate intact tablets deeply, significantly limiting the volume of interrogation.

XRPD provides an excellent means for observing transformations, owing to the unique diffraction by different polymorphs. In order to evaluate pharmaceutical systems in their consolidated context, XRPD methods for intact compacts have been developed (131,157,163–165). XRPD analysis of intact tablets in traditional Bragg-Brentano (reflectance) settings, however, can result in significant optics and sample-related geometry errors. Often manifest as diffraction peak offsets (166), these could be easily mistaken as the formation of "new phases," if not corrected for. Although mass attenuation coefficients of organic solid materials do result in some degree of "sample transparency," (166) it can be expected that the volume of interrogation for an intact tablet would still be incomplete. As such, transmission XRPD offers a means by which diffraction signal can be collected from the entire tablet volume, significantly improving quantitative statistics for intact, consolidated systems. The use of parallel-beam XRPD, compensated for signal attenuation owing to sample thickness and solid fraction was used to specifically quantify the chlorpropamide A ↔ C interconversion discussed above, having sensitivity down to 2.0% (w/w) of Form A in a matrix of Form C (157). Combinations of quantitative X-ray diffractometry with multivariate analysis techniques has proven effective in further improving the sensitivity and selectivity of intact compact transmission XRPD data, in particular, for multicomponent systems more akin to those that might be analyzed for transformations in an industrial setting (165).

Effects of Different Crystal Forms on Tableting Properties

The effect of polymorphism on mechanical properties is well known, owing to the differences in response of elements of internal crystalline structure to mechanical stress. Various examples are reviewed in Singhal and Curatolo (167). Sun and Grant (168) demonstrated that the internal crystal structure holds considerable influence over the mechanical properties of L-lysine monohydrochloride dihydrate. In their study, crystals were grown in prismatic and plate-shaped habits by adjusting the composition of the crystallization solvent. These crystals, known to have a distinct slip system operating on (001) were observed to form stronger compacts when the plate-shaped crystals were used (relative to compacts prepared from the prismatic crystals). The observed difference was attributed to the probable orientation of (001) relative to the principle load axis in compression (Fig. 16). As shown in Figure 16A, the compressive load is oriented perpendicular to the orientation of the slip planes, whereas in Figure 16B the load is parallel to the slip planes.

The critically resolved shear stress (τ_{cr}) needed to initiate deformation within a slip plane can be described by Schmid's Law [equation (25)]:

$$\tau_{cr} = \sigma \cdot \cos(\alpha)\cos(\beta) \tag{25}$$

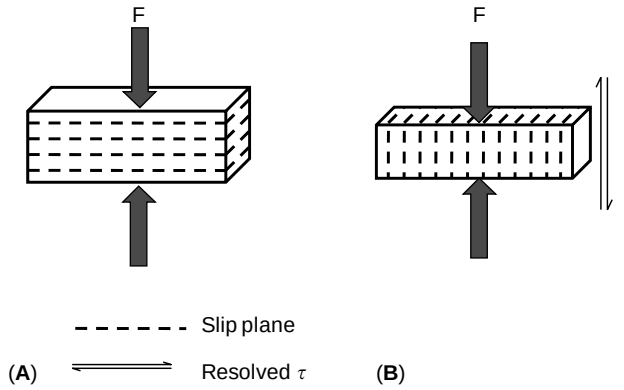

FIGURE 16 Resolved shear stress (τ; σ_{ij}, where $i \neq j$) relative to principal load for (**A**) slip planes oriented perpendicular to compressive load, and (**B**) slip planes oriented parallel to compressive load. Figure modified after Ref. (168).

where α is the angle between the slip plane normal and the applied load (σ), and β is the angle between the slip plane and σ (46). In Figure 16A $\alpha = \beta = 90°$ (i.e., $\cos(\alpha)\cos(\beta) = 0$), suggesting that crystals exactly oriented in this way would experience no resolved shear stress in the slip plane, and be unlikely to deform. In contrast, Figure 16B has $\alpha = \beta = 0°$, (i.e., $\cos(\alpha)\cos(\beta) = 1$), suggesting that τ_{cr} is maximized in this orientation. In Sun and Grant, the authors argued that the most probable orientation of the prism-shaped crystals of L-lysine monohydrochloride dihydrate was similar to Figure 16A, whereas that of the plate-shaped crystals was similar to Figure 16B. The maximally resolved shear experienced by the plate-shaped crystals was suggested to enable more extensive deformation and the formation of a greater interparticulate bond area, which supports the observed compaction behavior (168). Although this example maintains a consistent solid form of the model material (only habit is varied), it is easy to visualize how activation/inactivation of slip systems in different polymorphs would significantly impact the mechanical behavior of a material.

The poor compressibility of acetaminophen (paracetamol) has been well documented (169–173). As such, acetaminophen for direct compression is often compounded with more compactable excipients (i.e., gelatin, polyvinylpyrrolidone, starch, or starch derivatives). A chemically pure acetaminophen suitable for direct compression would constitute a better compendia article, motivating the search for a new polymorph. A new phase (orthorhombic; Form II) was recrystallized from dioxane, and its crystals were found to have slip planes, which better facilitated deformation (174). Although the orthorhombic form is metastable with respect to the monoclinic form (marketed; Form I), the dissolution rates for the two forms were found to be sufficiently similar that questions as to the relative bioavailability of the two forms would likely prove meaningless.

Compressive deformation studies were conducted on single crystals of α-lactose, using mechanical strength and acoustic emission analyses to characterize differences in the deformation behavior of α-lactose monohydrate relative to anhydrous β-lactose (56). The α-lactose monohydrate crystals were found to exhibit

greater mechanical strength than did the anhydrous α-lactose crystals. The acoustic emission data showed that the fragmentation process of the monohydrate phase was acoustically more active and energetic. Amplitude distribution analysis of the acoustic signals further confirmed that the nature of fragmentation during the deformation of the two types of lactose was different. This was attributed to fundamental differences in the internal crystal structure of the two lactose phases.

Forms A, B, and F of phenobarbital were individually consolidated using a compaction simulator, and evaluated for the effects of crystalline form on the compression mechanism and resulting compact characteristics (175). Form A was found to form stronger compacts than Form B, which in turn, formed stronger compacts than Form F. Cooper–Eaton analysis (176) was used to assess pore reduction during compaction (at 196 MPa) in terms of the balance between particle rearrangement (phase I) and fragmentation/deformation (phase II). Form A was found to be more resistant to phase I-type pore reduction than either B and F (which themselves showed very similar phase I behavior), suggesting that the friction between the die wall and particles of Form A was larger than for particles of either B or F. In contrast, during phase II-type pore reduction, Form A progressed further than either Form B or Form F, which correlated with the observation that Form A also had the highest compression energy relative to the other two polymorphs (175).

SUMMARY

Several of the common processing steps used in primary and secondary manufacturing of pharmaceutical drug substances and drug products are capable of eliciting phase transformations of the solid materials involved. Important parameters in drug substance manufacturing include: prolonged processing times owing to batch size or purity requirements, a lengthy final recrystallization step for the purposes of purity, yield, or particle considerations (size, morphology, etc.), drying conditions, and milling to improve raw material characteristics needed for secondary processing steps. In any of these steps, crystal forms having small energy differences between them may result in conversion to, or growth of, undesired polymorphic forms, desolvated (or solvated) substance, or conversion to an amorphous product.

On the drug product side, API in its desired solid form is combined with excipients via a series of harsh secondary processing steps in the effort to make a reproducibly functional drug product. In solid dosage form manufacturing, one of the first opportunities for crystal form changes to occur is during milling, where the application of considerable shear stress to the solid, and extensive fracture and deformation, results in energy changes at the structural level, which may be manifest as polymorphic changes, desolvation, or significant disordering. Wet Granulation and drying mainly risk inducing transformations that involve solvent incorporation or loss, particularly with respect to water molecules. Exposure to aqueous binder solutions during granulation may mediate conversions to thermodynamically stable forms, whereas dehydration during drying may result in lattice collapse and formation of an amorphous solid. Tableting and dry granulation mainly run the risk of inducing transformations to high-energy polymorphs, which persist upon the removal of the multi-axial high-shear stress state imposed during compaction.

The primary goal of any pharmaceutical company is to manufacture a drug product that conforms to reproducible quality standards. Central to this goal for

solid products is selection of an API solid form that will remain unaltered throughout processing, shipping, storage, and product life. For the most part, it is desirable to identify and select the most thermodynamically stable phase as early as possible (preferably during the first scale-up of drug substance production) so that all downstream toxicology, pharmacokinetics, and clinical studies may be conducted using the form likely to be present in the commercial product. Prudent drug development will also consider the impact of processing on the properties of various excipients included in formulations, where subtle (or significant) changes to their solid forms may also result in unanticipated or unpredictable performance attributes of the drug product. In the end, multidisciplinary studies that investigate the likelihood of form changes any time during the handling of formulation materials is important to ensure the consistency of the final drug product. Fortunately, the wide variety of available characterization methods makes it possible to detect even very subtle changes in solid materials as they are processed. A successful approach to problem solving will require collaborative research by process, formulation, and analytical scientists. Although problems in development can often occur at the most inopportune time, the judicious use of information previously gathered from properly designed studies, and rigorous efforts to embrace more complete materials understanding espoused by worldwide regulatory bodies, should lead to ever-improving development paradigms that enable higher quality pharmaceutical products.

REFERENCES

1. Sun CC. Materials science tetrahedron – a useful tool for pharmaceutical research and development. J Pharm Sci 2009; 98: 1744–9.
2. Nagai T, Kagi H, Yamanaka T. The first observation of a pressure-induced phase transition and compression behavior of kalcinite ($KHCO_3$) at room temperature. Solid State Comm 2002; 123: 371–4.
3. Sharma SM, Sikka SK. Pressure induced amorphization of materials. Prog Mater Sci 1996; 40: 1–77.
4. Andryushkova OV, et al. Effect of mechanical activation on phase transformations in transition aluminas. Solid State Ionics 1997; 101–3: 647–53.
5. Hemley RJ, et al. Pressure-induced amorphization of crystalline silica. Nature 1988; 334: 53–4.
6. Katzke H, Schlogl R. Mechanism of the morphotropic transformation between the rutile and corundum structural types. Acta Cryst 2003; B59: 456–62.
7. Bose P, Pradhan SK, Sen S. Rietveld analysis of polymorphic transformations of ball milled anatase TiO_2. Mater Chem Phys 2003; 80: 73–81.
8. Ren R, Yang Z, Shaw LL. Polymorphic transformation and powder characteristics of TiO_2 during high energy milling. J Mater Sci 2000; 35: 6015–26.
9. Fujii Y, Kowaka M, Onodera A. The pressure-induced metallic amorphous state of SnI_4: I. A novel crystal-to-amorphous transition studied by X-ray scattering. J Phys C Solid State Phys 1985; 18: 789–97.
10. Johnson WL. Thermodynamic and kinetic aspects of the crystal to glass transfomration in metallic materials. Prog Mater Sci 1986; 30: 81–134.
11. Koch CC. Amorphization reactions during mechanical alloying/milling of metallic powders. React Solids 1989; 8: 283–97.
12. Schwartz RB, Koch CC. Formation of amorphous alloys by the mechanical alloying of crystalline powders of pure metals and powders of intermetallics. Appl Phys Lett 1986; 49: 146–8.
13. Samwer K. Amorphisation in solid metallic systems. Phys Reports 1988; 161: 1–41.

14. Imamura K, Senna M. Difference between mechanochemical and thermal processes of polymorphic transformation of ZnS and PbO Mater Res Bull 1984; 19: 59–65.
15. Mazzanti G, et al. Novel shear-induced phases in cocoa butter. Cryst Growth Des 2004; 4: 409–11.
16. Vippagunta SR, Brittain HG, Grant DJW. Crystalline solids. Adv Drug Del Rev 2001; 48: 3–26.
17. Byrn SR, et al. Pharmaceutical solids: a strategic approach to regulatory considerations. Pharm Res 1995; 12: 945–54.
18. Byrn SR, et al. Solid-state pharmaceutical chemistry. Chem Materials 1994; 6: 1148–58.
19. Chemburkar SR, et al. Dealing with the impact of ritonavir polymorphs on the late stages of bulk drug process development. Org Proc Res Dev 2000; 4: 413–17.
20. Byrn SR, Pfeiffer RR, Stowell JG. Solid-State Chemistry of Drugs, 2nd ed. West Lafayette, IN: SSCI-Inc., 1999: 574.
21. Grant DJW, Byrn SR. A timely re-examination of drug polymorphism in pharmaceutical development and regulation. Adv Drug Del Rev 2004; 56: 237–9.
22. Brittain HG. Effects of mechanical processing on phase composition. J Pharm Sci 2002; 91: 1573–80.
23. Shakhtshneider TP. Phase transformations and stabilization of metastable states of molecular crystals under mechanical activation. Solid State Ionics 1997; 101–3: 851–6.
24. Boldyrev VV. Mechanochemical modification and synthesis of drugs. J Mater Sci 2004; 39: 5117–20.
25. Caira MR. Crystalline polymorphism of organic compounds. Topics Curr Chem 1998; 198: 163–208.
26. Brittain HG. Polymorphism and solvatomorphism 2005. J Pharm Sci 2007; 96: 705–28.
27. Brittain HG. Polymorphism and solvatomorphism 2006. J Pharm Sci 2008; 97: 3611–36.
28. Morris KR, et al. Advances in pharmaceutical materials and processing. Pharm Sci Tech Today 1998; 1: 235–45.
29. Morris KR, et al. Theoretical approaches to physical transformations of active pharmaceutical ingredients during manufacturing processes. Adv Drug Del Rev 2001; 48: 91–114.
30. Boldyrev VV. Mechanical activation of solids and its application to technology. J Chim Phys 1986; 83: 821–9.
31. Boldyrev VV, Tkacova K. Mechanochemistry of solids: past, present, and prospects. J Mater Synth Proc 2000; 8: 121–32.
32. Willart JF, Descamps M. Solid state amorphization of pharmaceuticals. Molec Pharmaceut 2008; 5: 905–20.
33. Mullin JW. Crystallization, 4th Ed. ed. New York: Butterworth-Heinemann, 2001: 594.
34. Beckmann W. Crystallization of pharmaceutical compounds – polymorphs, pseudo-polymorphs and particle formation. Eng Life Sci 2003; 3: 113–20.
35. Hosokawa K, Goto J, Hirayama N. Prediction of solvents suitable for crystallization of small organic molecules. Chem Pharm Bull 2005; 53: 1296–9.
36. Datta S, Grant DJW. Crystal structures of drugs: advances in determination, prediction and engineering. Nature Rev Drug Disc 2004; 3: 42–57.
37. Cardew PT, Davey RJ. The kinetics of solvent-mediated phase transformations. Proc Royal Soc Lond 1985; A398: 415–28.
38. Gu C-H, Young V Jr, Grant DJW. Polymorph screening: influence of solvents on the rate of solvent-mediated polymorphic transformation. J Pharm Sci 2001; 90: 1878–90.
39. Zhang GGZ, et al. Crystallization and transitions of sulfamerazine polymorphs. J Pharm Sci 2002; 91: 1089–100.
40. Ostwald W. The formation and changes of solids. Z Physik Chem 1897; 22: 289–330.
41. Togkalidou T, et al. Solute concentration prediction using chemometrics and ATR-FTIR spectroscopy. J Cryst Growth 2001; 231: 534–43.

42. Togkalidou T, et al. Solution concentration prediction for pharmaceutical crystallization processes using robust chemometrics and ATR-FTIR spectroscopy. Org Proc Res Dev 2002; 6: 317–22.
43. Wang F, et al. An investigation of solvent-mediated polymorphic transformation of progesterone using in situ Raman spectroscopy. Org Proc Res Dev 2000; 4: 391–5.
44. Hüttenrauch R, Fricke S, Zielke P. Mechanical activation of pharmaceutical systems. Pharm Res 1985; 6: 302–6.
45. Griffith AA. The phenomena of rupture and flow in solids. Phil Trans Royal Soc London 1921; A221: 163–98.
46. Bowman K. Mechanical Behavior of Materials. Hoboken, NJ: John Wiley & Sons, Inc., 2004: 334.
47. Osborn JC, et al. Prediction of Slip Planes in Molecular Crystals by Molecular Modeling. Cambridge, UK: In 14th International Symposium on Industrial Crystallization, 1999.
48. Juhasz AZ. Aspects of mechanochemical activation in terms of comminution theory. Coll Surf A Physicochem Eng Aspects 1998; 141: 449–62.
49. Hiestand EN. Mechanics and Physical Principles for Powders and Compacts, 2nd ed. Foundations of Pharmaceutical Sciences. In: JG Stowell, ed. West Lafayette, IN: SSCI, Inc., 2002: 110.
50. Fecht HJ. Defect-induced melting and solid-state amorphization. Nature 1992; 356: 133–5.
51. Fecht HJ, Johnson WL. Entropy and enthalpy catastrophe as a stability limit for crystalline material. Nature 1988; 334: 50–1.
52. Tromans D, Meech JA. Enhanced dissolution of minerals: stored energy, amorphism and mechanical activation. Miner Eng 2001; 14: 1359–77.
53. Wildfong PLD, et al. Towards an understanding of the structurally based potential for mechanically activated disordering of small molecule organic crystals. J Pharm Sci 2006; 95: 2645–56.
54. Willart JF, et al. Athermal character of the solid state amorphization of lactose induced by ball milling. Solid State Comm 2004; 132: 693–6.
55. Descamps M, et al. Transformation of pharmaceutical compounds upon milling and comilling: the role of T_g. J Pharm Sci 2007; 96: 1398–407.
56. Otsuka M, et al. Isomerization of lactose in solid-state by mechanical stress during grinding. J Pharm Pharmacol 1991; 43: 148–53.
57. Hancock BC, Shamblin SL, Zografi G. Molecular mobility of amorphous pharmaceutical solids below their glass transition temperatures. Pharm Res 1995; 12: 799–806.
58. De Gusseme A, et al. Ordering and disordering of molecular solids upon mechanical milling: the case of fananserine. J Pharm Sci 2008; 97: 5000–12.
59. Otsuka M, Ofusa T, Matsuda Y. Effect of environmental humidity on the transformation pathway of carbamazepine polymorphic modifications during grinding. Coll Surf B Biointerfaces 1999; 13: 263–73.
60. Pirttimäki J, et al. Effects of grinding and compression on crystal structure of anhydrous caffeine. Int J Pharm 1993; 95: 93–9.
61. Gubskaya AV, et al. Effect of cryogrinding on physico-chemical properties of drugs. II. cortisone acetate: particles sizes and polymorphic transition. Drug Dev Ind Pharm 1995; 21: 1965–74.
62. Brodka-Pfeiffer K, et al. Influence of mechanical activation on the physical stability of salbutamol sulphate. Eur J Pharm Biopharm 2003; 56: 393–400.
63. Sheth AR, et al. Mechanochromism of piroxicam accompanied by intermolecular proton transfer probed by spectroscopic methods and solid-phase changes. J Am Chem Soc 2005; 127: 6641–51.
64. Otsuka M, Kaneniwa N. Effect of grinding on the degree of crystallinity of cephalexin powder. Chem Pharm Bull 1983; 31: 4489–95.
65. Otsuka M, Kaneniwa N. Effects of grinding on the physicochemical properties of cephalexin powder. Chem Pharm Bull 1984; 32: 1071–9.

66. Otsuka M, Matsuda Y. Effect of environmental humidity on the transformation pathway of nitrofurantoin modifications during grinding and the physicochemical properties of ground products. J Pharm Pharmacol 1993; 45: 406–13.
67. Bauer-Brandl A. Polymorphic transitions of cimetidine during manufacture of solid dosage forms. Int J Pharm 1996; 140: 195–206.
68. Crowley KJ, Zografi G. Cryogenic grinding of indomethacin polymorphs and solvates: assessment of amorphous phase formation and amorphous phase physical stability. J Pharm Sci 2002; 91: 492–507.
69. Font J, Muntasell J, Cesari E. Amorphization of organic compounds by ball milling. Mater Res Bull 1997; 32: 1691–6.
70. Willart JF, et al. Direct crystal to glass transformation of trehalose induced by ball milling. Solid State Comm 2001; 119: 501–5.
71. Otsuka M, Kaneniwa N. Effect of seed crystals on solid-state transformation of polymorphs of chloramphenicol palmitate during grinding. J Pharm Sci 1985; 75: 506–11.
72. Lubach JW, et al. Investigation of the effects of pharmaceutical processing upon solid-state NMR relaxation times and implications to solid-state formulation stability. J Pharm Sci 2007; 96: 777–87.
73. Hosford WF, Caddell RM. Metal Forming: Mechanics and Metallurgy, 2nd ed. Upper Saddle River, NJ: Prentice Hall, 1993.
74. Bozic DZ, Dreu R, Vrecer F. Influcence of dry granulation on compactibility and capping tendency of macrolide antibiotic formulation. Int J Pharm 2008; 357: 44–54.
75. Parikh DM, ed. Handbook of Pharmaceutical Granulation Technology, 2nd ed. New York: Taylor & Francis, 2005: 623.
76. Kunii D, Levenspiel O. Fluidization Engineering, 2nd ed. Boston: Butterworth-Heinemann, 1991: 491.
77. Gokhale R, Sun Y, Shukla AJ. High-Shear Granulation, in Handbook of Pharmaceutical Granulation Technology. In: Parikh DM, Editor. New York: Taylor & Francis, 2005: 191–228.
78. Tantry JS, Tank J, Suryanarayanan R. Processing-induced phase transitions of theophylline – implications on dissolution of theophylline tablets. J Pharm Sci 2007; 96: 1434–44.
79. Li X, Zhi F, Hu Y. Investigation of excipient and processing on solid phase transformation and dissolution of ciprofloxacin. Int J Pharm 2007; 328: 177–82.
80. Wong MWY, Mitchell AG. Physicochemical characterization of a phase change produced during the wet granulation of chlorpromazine hydrochloride and its effects on tableting. Int J Pharm 1992; 88: 261–73.
81. Meyer MC, et al. The bioequivalence of carbamazepine tablets with a history of clinical failures. Pharm Res 1992; 9: 1612–6.
82. Wang JT, et al. Effects of humidity and temperature on in vitro performance of carbamazepine tablets. Pharm Res 1990; 9(Suppl): S143.
83. Shaffer M. FDA Finds Moisture Causes Epilepsy Pill to Weaken. 1990. [cited 02/27/1990]; Available from: http://www.fda.gov/bbs/topics/NEWS/NEW00071.html
84. Bell WL, Crawford IL, Shiu GK. Reduced bioavailability of moisture-exposed carbamazepine resulting in status epilepticus. Epilepsia 1993; 34: 1102–4.
85. Kobayashi Y, et al. Physicochemical properties and bioavailability of carbamazepine polymorphs and dihydrate. Int J Pharm 2000; 193: 137–46.
86. Otsuka M, Hasegawa H, Matsuda Y. Effect of polymorphic transformation during the extrusion-granulation process on the pharmaceutical properties of carbamazepine granules. Chem Pharm Bull 1997; 45: 894–8.
87. Otsuka M, Hasegawa H, Matsuda Y. Effect of polymorphic forms of bulk powders on pharmaceutical properties of carbamazepine granules. Chem Pharm Bull 1999; 47: 852–6.

88. Wikström H, et al. Toward an understanding of the factors influencing anhydrate-to-hydrate transformation kinetics in aqueous environments. Cryst Growth Des 2008; 8: 2684–93.
89. Murphy D, et al. Solution-mediated phase transformation of anhydrous to dihydrate carbamazepine and the effect of lattice disorder. Int J Pharm 2002; 246: 121–34.
90. Jorgensen A, et al. Hydrate formation during wet granulation studied by spectroscopic methods and multivariate analysis. Pharm Res 2002; 19: 1285–91.
91. Wikström H, Carroll WJ, Taylor LS. Manipulating theophylline monohydrate formation during high-shear wet granulation through improved understanding of the role of pharmaceutical excipients. Pharm Res 2008; 25: 923–35.
92. Wikström H, Marsac PJ, Taylor LS. In-line monitoring of hydrate formation during wet granulation using raman spectroscopy. J Pharm Sci 2005; 94: 209–19.
93. Davis TD, et al. In situ monitoring of wet granulation using online X-ray powder diffraction. Pharm Res 2003; 20: 1851–7.
94. Blanco M, et al. Near infrared spectroscopy in the study of polymorphic transformations. Anal Chim Acta 2006; 567: 262–8.
95. Wildfong PLD, et al. Accelerated fluid bed drying using nir monitoring and phenomenological modeling: method assessment and formulation suitability. J Pharm Sci 2002; 91: 631–9.
96. Davis TD, et al. Modeling and monitoring of polymorphic transformation during the drying phase of wet granulation. Pharm Res 2004; 21: 860–6.
97. Te RL, et al. X-ray diffraction and solid-state nmr investigation of the single-crystal to single-crystal dehydration of thiamine hydrochloride monohydrate. Cryst Growth Des 2003; 3: 997–1004.
98. Airaksinen S, et al. Comparison of the effects of two drying methods on polymorphism of theophylline. Int J Pharm 2004; 276: 129–41.
99. Phadnis NV, Suryanarayanan R. Polymorphism in anhydrous theophylline – implications on the dissolution rate of theophylline tablets. J Pharm Sci 1997; 86: 1256–63.
100. Taylor LS, York P. Effect of particle size and temperature on the dehydration kinetics of trehalose dihydrate. Int J Pharm 1998; 167: 215–21.
101. Willart JF, et al. Vitrification and polymorphism of trehalose induced by dehydration of trehalose dehydrate. J Phys Chem B 2002; 106: 3365–70.
102. Bates S, et al. Assessment of defects and amorphous structure produced in raffinose pentahydrate upon dehydration. J Pharm Sci 2007; 96: 1418–33.
103. Jeffrey GA, Huang D-b. The hydrogen bonding in the crystal structure of raffinose pentahydrate. Carbohydr Res 1990; 206: 173–82.
104. Brittain HG, et al. Physical Characterization of Pharmaceutical Solids. Pharm Res 1991; 8: 963–73.
105. Matsuda Y, et al. Physicochemical characterization of spray-dried phenylbutazone polymorphs. J Pharm Sci 1984; 73: 173–9.
106. Corrigan OI, Sabra K, Holohan EM. Physicochemical properties of spray dried drugs: phenobarbitone and hydroflumethiazide. Drug Dev Ind Pharm 1983; 9: 1–20.
107. Hancock BC, Zografi G. Characteristics and significance of the amorphous state in pharmaceutical systems. J Pharm Sci 1997; 86: 1–12.
108. Scmitt E, Davis CW, Long ST. Moisture-dependent crystallization of amorphous lamotrigine mesylate. J Pharm Sci 1996; 85: 1215–9.
109. Yu L. Amorphous pharmaceutical solids: preparation, characterization, and stabilization. Adv Drug Del Rev 2001; 48: 27–42.
110. Shalaev EY, Shalaeva M, Zografi G. The effect of disorder on the chemical reactivity of an organic solid, tetraglycine methyl ester: change of the reaction mechanism. J Pharm Sci 2002; 91: 584–93.
111. Hilden LR, Morris KR. Prediction of the relaxation behavior of amorphous pharmaceutical compounds. I. Master curves concept and practice. J Pharm Sci 2003; 92: 1464–72.

112. Buckton G, Darcy P. The influence of additives on the recrystallisation of amorphous spray dried lactose. Int J Pharm 1995; 121: 81–7.
113. Columbano A, Buckton G, Wikeley. A study of the crystallisation of amorphous salbutamol sulphate using water vapour sorption and near infrared spectroscopy. Int J Pharm 2002; 237: 171–8.
114. Takenaka H, Kawashima Y, Lin SY. Polymorphism of spray-dried microencapsulated sulfamethoxazole with cellulose acetate phthalate and colloidal silica, montmorillonite, or talc. J Pharm Sci 1981; 70: 1256–60.
115. Kawashima Y, Lin SY, Takenaka H. Polymorphism and drug release behavior of spray-dried microcapsules of sulfamethoxazole with polysaccharide gum and colloidal silica. Drug Dev Ind Pharm 1983; 9: 1445–63.
116. Tang X, Pikal MJ. Design of freez-drying processes for pharmaceuticals: practical advice. Pharm Res 2004; 21: 191–200.
117. Hancock BC, Parks M. What is the true solubility advantage for amorphous pharmaceuticals? Pharm Res 2000; 17: 397–404.
118. Osawa T, Kamat MS, DeLuca P. Hygroscopicity of cefazolin sodium: application to evaluate the crystallinity of freeze-dried products. Pharm Res 1988; 5: 421–5.
119. Haikala R, et al. Polymorphic changes of mannitol during freeze-drying: effect of surface-active agents. PDA J Pharm Sci Tech 1997; 51: 96–101.
120. Abdul-Fattah AM, et al. Drying-induced variations in physico-chemical properties of amorphous pharmaceuticals and their impact on stability II: stability of a vaccine. Pharm Res 2007; 24: 715–27.
121. Abdul-Fattah AM, et al. Drying-induced variations in physico-chemical properties of amorphous pharmaceuticals and their impact on stability (I): stability of a monoclonal antibody. J Pharm Sci 2007; 96: 1983–2008.
122. Abdul-Fattah AM, et al. The impact of drying method and formulation on the phycial properties and stability of methionyl human growth hormone in the amorphous solid state. J Pharm Sci 2008; 97: 163–184.
123. White WB, Dachille F, Roy AP. High-pressure-high-temperature polymorphism of the oxides of lead. J Am Chem Soc 1961; 44: 170–4.
124. Burger A, Ramberger R. On the polymorphism of pharmaceuticals and other molecular crystals I: theory of thermodynamic rules. Mikrochim Acta 1979; II: 259–71.
125. Burger A, Ramberger R. On the polymorphism of pharmaceuticals and other molecular crystals. II. mikrochim acta 1979; II: 273–316.
126. Yoshino M, et al. Contribution of hydrogen bonds to equilibrium a transition of resorcinol. J Phys Chem A 1999; 103: 2775–83.
127. Sharma SM, et al. High pressure phase transitions in organic solids I: a-b transition in resorcinol. Pramana J Phys 1985; 25: 75–9.
128. Deb SK, Rekha MA, Roy AP. Raman-scattering study of high-pressure phase transition and amorphization of resorcinol. Phys Rev B 1993; 47: 11491–4.
129. Wang Z, et al. X-ray diffraction study on pressure-induced phase transformations in nanocrystalline anatase/rutile (TiO_2). J Phys Condens Matter 2001; 13: 8317–23.
130. Otsuka M, Matsumoto T, Kaneniwa N. Effects of the mechanical energy of multi-tableting compression on the polymorphic transformations of chlorpropamide. J Pharm Pharmacol 1989; 41: 665–9.
131. Wildfong PLD, et al. Demonstration of a shear-based solid-state phase transformation in a small molecular organic system: chlorpropamide. J Pharm Sci 2007; 96: 1100–13.
132. Boldyreva EV, Dmitriev V, Hancock BC. Effect of pressure up to 5.5 GPa on dry powder samples of chlorpropamide form-A. Int J Pharm 2006; 327: 51–7.
133. Delaey L. Diffusionless Transformations, in Phase Transformations in Materials. In: Cahn RW, Haasen P, Kramer EJ, Editors. New York: VCH Publishers, Inc., 1991: 648.
134. Kelly PM, Rose LRF. The martensitic transformation in ceramics – its role in transformation toughening. Prog Mater Sci 2002; 47: 463–557.

135. Christian JW. The Theory of Transformations in Metals and Alloys, 2nd ed. New York, NY: Pergamon Press, 1975: 586.
136. Tang M, et al. One-dimensional model of martensitic transformations. Acta Mater 2002; 50: 467–74.
137. Porter DA, Easterling KE. Phase Transformations in Metals and Alloys, 1st ed. Wokingham, UK: Van Nostrand Reinhold (UK), 1981: 446.
138. Bhadeshia HKDH. Martensitic Transformation, in Encyclopedia of Materials Science: Science and Technology. In: Buschow K, et al. Editors. New York, NY: Pergamon Press, 2001: 5203–6.
139. Ericksen JL. Weak Martensitic transformations in bravais lattices. Arch Ration Mech Anal 1989; 107: 23–36.
140. Bhattacharya K, et al. Crystal symmetry and the reversibility of martensitic transformations. Nature 2004; 428: 55–9.
141. Pelton AR, Russell SM, DiCello J. The physical metallurgy of nitinol for medical applications. JOM 2003; 55: 33–7.
142. Ueda H, Nambu N, Nagai T. Dissolution behavior of chlorpropamide polymorphs. Chem Pharm Bull 1984; 32: 244–50.
143. Otsuka M, et al. Effect of compression temperature on the consolidation mechanism of chlorpropamide polymorphs. J Pharm Sci 1995; 84: 614–8.
144. Simmons DL, Ranz RJ, Gyanchandani ND. Polymorphism in pharmaceuticals III. chlorpropamide. Can J Pharm Sci 1973; 8: 125–7.
145. Gahn GA, Lalla JK. Effect of compressional forces on piroxicam polymorhps. J Pharm Pharmacol 1992; 44: 678–81.
146. Chan HK, Doelker E. Polymorphic transformation of some drugs under compression. Drug Dev Ind Pharm 1985; 11: 315–32.
147. Boldyreva EV, et al. Pressure-induced phase transitions in crystalline L-serine studied by single-crystal and high-resolution powder X-ray diffraction. Chem Phys Lett 2006; 429: 474–8.
148. Allan DR, et al. Pressure-induced polymorphism in phenol. Acta Cryst B 2002; 58: 1018–24.
149. Matsunaga J, Nambu N, Nagai T. Polymorphism of phenylbutazone. Chem Pharm Bull 1976; 24: 1169–72.
150. Tuladhar MD, Carless JE, Summers MP. Thermal behaviour and dissolution properties of phenylbutazone polymorphs. J Pharm Pharmacol 1983; 35: 208–14.
151. Ibrahim HG, Pisano F, Bruno A. Polymorphism of phenylbutazone: properties and compressional behavior of crystals. J Pharm Sci 1977; 66: 669–73.
152. Tumanov NA, Boldyreva EV, Ahsbahs H. Structure solution and refinement from powder or single-crystal diffraction data? Pros and cons: An example of the high-pressure b′-polymorph of glycine. Powder Diffr 2008; 23: 307–16.
153. Boldyreva EV, et al. Effect of hydrostatic pressure on the g-polymorph of glycine. 1. A polymorphic transition into a new d-form. Z Kristallogr 2005; 220: 50–7.
154. Boldyreva EV, et al. Effect of high pressure on the polymorphs of paracetamol. J Therm Anal Calorim 2002; 68: 437–52.
155. Matsumoto T, et al. Effects of temperature and pressure during compression on polymorphic transformation and crushing strength of chlorpropamide tablets. J Pharm Pharmacol 1991; 43: 74–8.
156. Otsuka M, Matsuda Y. Effects of environmental temperature and compression energy on polymorphic transformation during tabletting. Drug Dev Ind Pharm 1993; 19: 2241–69.
157. Wildfong PLD, et al. Quantitative determination of polymorphic composition in intact compacts by parallel-beam X-ray powder diffractometry II. Data correction for analysis of phase transformations as a function of pressure. J Pharm Biomed Anal 2005; 39: 1–7.
158. Cogdill RP, Drennen JK. Near-Infrared Spectroscopy, in Spectroscopy of Pharmaceutical Solids. In: Brittain HG, Editor. New York, NY: Taylor & Francis, 2006: 313–412.

159. Kirsch JD, Drennen JK. Nondestructive tablet hardness testing by near-infrared spectroscopy: a new and robust spectral best-fit algorithm. J Pharm Biomed Anal 1999; 19: 351–62.
160. Morisseau KM, Rhodes CT. Near-infrared spectroscopy as a nondestructive alternative to conventional tablet hardness testing. Pharm Res 1997; 14: 108–11.
161. Otsuka M, Yamane I. Prediction of tablet hardness based on near infrared spectra of raw mixed powders by chemometrics. J Pharm Sci 2006; 95: 1425–33.
162. Ebube NK, et al. Application of near-infrared spectroscopy for nondestructive analysis of Avicel powders and tablets. Pharm Dev Technol 1999; 4: 19–26.
163. Phadnis NV, Cavatur K, Suryanarayanan R. Identification of drugs in pharmaceutical dosage forms by X-ray powder diffractometry. J Pharm Biomed Anal 1997; 15: 929–43.
164. Cao W, et al. Quantitative determination of polymorphic composition in intact compacts by parallel-beam X-ray powder diffractometry. J Pharm Biomed Anal 2002; 30: 1111–9.
165. Moore MD, et al. The use of net analyte signal orthogonalization in the separation of multi-component diffraction patterns obtained from X-ray powder diffraction of intact compacts. J Pharm Biomed Anal 2008; 47: 238–47.
166. Jenkins R, Snyder RL. Introduction to X-ray Powder Diffractometry. Chemical Analysis: A Series of Monographs on Analytical Chemistry and Its Applications. In: Winefordner JD, ed. New York, NY: Wiley Interscience, 1996: 403.
167. Singhal D, Curatolo W. Drug polymorphism and dosage form design: a practical perspective. Adv Drug Del Rev 2004; 56: 335–47.
168. Sun CC, Grant DJW. Influence of crystal shape on the tableting performance of L-lysine monohydrochloride dihydrate. J Pharm Sci 2001; 90: 569–79.
169. Garekani HA, et al. Effect of compression force, compression speed, and particle size on the compression properties of paracetamol. Drug Dev Ind Pharm 2001; 27: 935–42.
170. Krycer I, Pope DG, Hersey JA. The prediction of paracetamol capping tendencies. J Pharm Pharmacol 1982; 34: 802–4.
171. Malamataris S, Bin-Baie S, Pilpel N. Plasto-elasticity and tableting of paracetamol, avicel and other powders. J Pharm Pharmacol 1984; 36: 616–17.
172. Duncan-Hewitt WC, Weatherly GC. Evaluating the hardness, Young's modulus and fracture toughness of some pharmaceutical crystals using microindentation techniques. J Mater Sci Lett 1989; 8: 1350–2.
173. Lin M-C, Duncan-Hewitt WC. Deformation kinetics of acetaminophen crystals. Int J Pharm 1994; 106: 187–200.
174. Di Martino P, et al. A new pure paracetamol for direct compression: the orthorhombic form. Int J Pharm 1996; 128: 1–8.
175. Otsuka M, Nakanishi M, Matsuda Y. Effects of crystalline form on the tableting compression mechanism of phenobarbital polymorphs. Drug Dev Ind Pharm 1999; 25: 205–15.
176. Cooper AR, Eaton LE. Compaction behavior of several ceramic powders. J Am Ceram Soc 1962; 45: 97–101.

15 Structural Aspects of Molecular Dissymmetry

Harry G. Brittain
Center for Pharmaceutical Physics, Milford, New Jersey, U.S.A.

INTRODUCTION

The molecular chirality associated with an optically active molecule is frequently manifested in the crystallography of the compound, and one often encounters a type of polymorphism between racemic mixtures and resolved enantiomers where the two species crystallize in different space groups (1). Because the historical development of optical activity was greatly aided by systematic studies of the habits of enantiomorphic crystals, the concepts of molecular dissymmetry, crystallography, and chirality are inexorably linked. As with any other solid, these materials can be characterized on the basis of their crystal structures and through an understanding of their melting point phase diagrams.

It has become abundantly clear that the stereoselective actions associated with the enantiomeric constituents of a racemic drug can differ markedly in their pharmacodynamic or pharmacokinetic properties (2–5). These factors can lead to much concern, especially if a drug containing a potentially resolvable center is marketed as a racemic mixture. This situation is not invariably bad, but it is clear that a racemate should not be administered when a clear-cut advantage exists with the use of a resolved enantiomer (6). An excellent discussion regarding the possible selection of a resolved enantiomer over a racemate, from both a practical and regulatory viewpoint, has been provided by De Camp (7).

When the mirror images of a compound are not superimposable, these mirror images are denoted as enantiomers. Numerous techniques exist that permit the physical separation of enantiomers in a mixture (8), and such methodologies have become important in the large-scale preparation of separated enantiomers for pharmaceutical purposes. Individual enantiomeric molecules are completely equivalent in their molecular properties, with the exception of their interaction with circularly polarized light. An equimolar mixture of two enantiomers is termed a racemic mixture. The generally accepted configurational nomenclature for tetrahedral carbon enantiomers was devised by Cahn, Ingold, and Prelog, and is based on sequencing rules (9). Enantiomers are identified as being either *R* or *S*, depending on the direction (clockwise or counterclockwise) of substituents after they have been arranged according to increasing atomic mass. Compounds containing more than one center of dissymmetry are identified as diastereomers, and in compounds containing n dissymmetric centers the number of diastereomers will equal 2^n.

Although not quite fitting the formal definition of polymorphic solids, the relationship between racemic mixtures and resolved enantiomers presents an intriguing parallel. By virtue of symmetry constraints, a resolved enantiomer must crystallize in a non-centrosymmetric space group. Racemic mixtures are under no

analogous constraint, but over 90% of all racemic mixtures (which are merely equimolar mixtures of the enantiomers) are found to crystallize in a centrosymmetric space group (10). This consequence of molecular dissymmetry results in the situation where differing crystal structures can be obtained for the same chemical compound, depending only on the degree of resolution. It is therefore appropriate to explore the relation between molecular and crystallographic chirality, and to examine some of the consequences of these relationships.

ENANTIOMER AND RACEMATE CRYSTAL STRUCTURES

A relatively small number of the possible crystallographic lattice symmetries are available for the crystals of separated enantiomers, because these must crystallize in a lattice structure that does not contain inverse elements of symmetry. Out of the 230 possible space groups belonging to the 32 crystal classes, only 66 space groups within 11 crystal classes are non-centrosymmetric and can accommodate homochiral sets of enantiomers. Racemates are permitted to crystallize in any of the 230 space groups, and are not restricted to crystallizing in a centrosymmetric group. It has been found that most racemates crystallize into a group that possesses some elements of inverse symmetry. As will be discussed later, racemic mixtures occasionally crystallize in an enantiomorphic lattice system, and this system results in a spontaneous resolution of the enantiomers upon crystallization.

A symmetry element is defined as an operation that when performed on an object, results in a new orientation of that object that is indistinguishable from and superimposable on the original. There are five main classes of symmetry operations: (a) the identity operation (an operation that places the object back into its original orientation), (b) proper rotation (rotation of an object about an axis by some angle), (c) reflection plane (reflection of each part of an object through a plane bisecting the object), (d) center of inversion (reflection of every part of an object through a point at the center of the object), and (e) improper rotation (a proper rotation combined with either an inversion center or a reflection plane). Every object possesses some element or elements of symmetry, even if this is only the identity operation.

The rigorous group theoretical requirement for the existence of chirality in a crystal or a molecule is that no improper rotation elements be present. This definition is often trivialized to require the absence of either a reflection plane or a center of inversion in an object, but these two operations are actually the two simplest improper rotation symmetry elements. It is important to note that a chiral object need not be totally devoid of symmetry (i.e., be asymmetric), but that it merely be dissymmetric (i.e., containing no improper rotation symmetry elements). The tetrahedral carbon atom bound to four different substituents may be asymmetric, but the reason it represents a site of chirality is by virtue of dissymmetry.

Jacques has evaluated the compilations published by various authors, and has reported that 70–90% of homochiral enantiomers crystallize in the $P2_12_12_1$ or $P2_1$ space groups (10). The most frequently encountered chiral space group, $P2_12_12_1$, is orthorhombic, with the unit cell commonly consisting of four homochiral molecules that are related to each other by three binary screw axes. Practically all of the other homochiral enantiomers crystallize in the monoclinic $P2_1$ space group, which is characterized by a plane of symmetry and a twofold axis. The unit cell generally contains two molecules related by a binary screw axis.

Jacques has also concluded that among the 164 space groups possessing at least one element of inverse symmetry, it is found that 60–80% of racemic compounds crystallize in either the $P2_1c$, $C2/c$, or $P\bar{1}$ space groups (10). The most common group is monoclinic $P2_1c$, and whose unit cell contains two each of the opposite enantiomers related to one another by a center of symmetry and a binary screw axis.

A chirality classification of crystal structures that distinguishes between homochiral (type-A), heterochiral (type-B), and achiral (type-C) lattice types has been provided by Zorkii et al. (11), and expanded by Mason (12). In the type-A structure, the molecules occupy a homochiral system, or a system of equivalent lattice positions. Secondary symmetry elements (e.g., inversion centers, mirror or glide planes, or higher order inversion axes) are precluded in type-A lattices. In the racemic type-B lattice, the molecules occupy heterochiral systems of equivalent positions and opposite enantiomers antipodal are related by secondary lattice symmetry operations. In type-C structures, the molecules occupy achiral systems of equivalent positions, and each molecule is located either on an inversion center, on a mirror plane, or on a special position of a higher order inversion axis. If there are two or more independent sets of equivalent positions in a crystal lattice, the type-D lattice becomes feasible. This structure consists of one set of type-B and another of type-C, but is not commonly encountered. Of the 5000 crystal structures studied, 28.4% were classified as being type-A, 55.6% were of type-B, 15.7% belong were of type-C, and only 0.3% were considered as being type-D.

A detailed discussion of crystal packing and the resulting space groups has been given by Kitaigorodskii (13). This approach assumes that molecular crystals are assemblages for which compactness tends toward the maximum, which is compatible with the molecular geometry. He defined a packing coefficient as vZ/V, where v is the volume of the molecule, V is the volume of the cell, and Z is the number of molecules in the unit cell. In this way, the space-filling or packing coefficient in crystals always lies between 0.65 and 0.77, which is of the same order as the regular packing of spheres or ellipsoids. Molecules whose structures cause an inability to attain a packing coefficient at least equal to 0.6 are not found to crystallize, and these compounds can only form glasses from the melt. In order to fill space in the most compact manner with objects of indeterminate geometry, the lattice must be populated in a compact fashion. There are only a limited number of two-dimensional arrays in which an object may reside in contact with six neighbors, which is necessary for the optimal packing of a molecular assembly. It has been concluded that the binary screw axis is highly conducive toward efficient packing. In the final analysis, the limited possible combinations of stacking leads to a limited number of space groups that fulfill the requirements of three-dimensional close-packing (13).

The close-pack criterion for crystal stability generally yields lower free energies for a structure composed of a racemic assembly over that composed of homochiral molecules. This view has been expressed in the empirical rule of Wallach (14), which states that the combination of two opposite enantiomers to form a racemate is accompanied by a volume contraction. As might be expected, there are many exceptions to this rule, and these have been discussed in a systematic manner (15). The modification to Wallach's rule contributed by Walden (16) is more generally valid, and states that if an enantiomer has a lower melting point than its corresponding racemate, then the crystals of the latter will have the higher density.

RELATIONSHIP BETWEEN MACROSCOPIC AND MICROSCOPIC STRUCTURES AS ILLUSTRATED BY QUARTZ AND ITS NON-SUPERIMPOSABLE HEMIHEDRAL CRYSTAL FACES

The most appropriate point to begin a discussion of molecular and crystallographic chirality is to discuss the case of quartz. The morphology of a quartz crystal is that of a hexagonal prism, where each end is capped by a hexagonal pyramid. This geometrical figure is highly symmetrical, and possesses 24 symmetry elements of various types. It was noted by Hauy at the beginning of the nineteenth century that quartz crystals contained many small facets that considerably reduced the overall symmetry (17). These facets were found only on alternate corners of the crystal, and were therefore described as being hemihedral. As shown in Figure 1, the distribution of these hemihedral faces gives rise to two forms of quartz, identified at the time as being either left- or right-handed (18). It was noted that the two forms of quartz were mirror images of each other, and that no amount of positioning or orientation permitted the superimposition of one form onto the other. For instance, on a right-handed crystal the *s* trigonal pyramid lies to the right of the *m* face, which is below the predominating positive rhombohedron, *r*. On a left-handed crystal, the *s* trigonal pyramid lies to the left of the *m* face below the *r* rhombohedron.

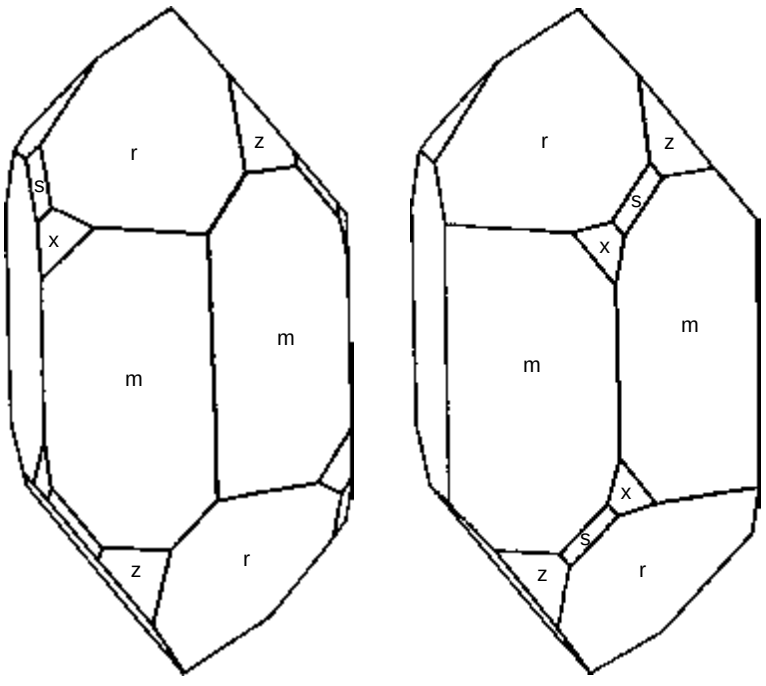

FIGURE 1 Crystal morphologies of levorotary (**A**) and dextrorotatory (**B**) quartz crystals, which can be readily distinguished by the relative placement of the hemihedral facets. The figure was adapted from Ref. (11).

The first complete determinations of the simple β-quartz structure were made by Bragg (19) and Wyckoff (20), who reported that each silicon atom was surrounded by four oxygen atoms, two which were above and two of which were below the silicon atom. The tetrahedral groups were found to arrange in spirals, each of which twisted in a definite manner. Thus, all the spirals of left-handed quartz twist in one way, and all the spirals of right-handed quartz twist in the other way. The left-handed modification belongs to the enantiomorphic space group $C3_12$, while the right-handed modification belongs to the mirror image space group $C3_22$.

Herschel investigated the optical properties of quartz slabs, which were cut perpendicular to the long crystal axis (17). He found that crystals cut from left-handed quartz would invariably rotate the plane of linearly polarized light in a clockwise fashion, while crystals cut from right-handed quartz rotated the plane of linearly polarized light in a counterclockwise direction. Elsewhere, Biot was performing extensive studies on the optical rotatory properties of certain compounds dissolved in fluid solutions, and it was at this time that the connection between optical activity and crystallographic properties was made.

Observations of this type were extremely important to Pasteur in that they permitted him to deduce requirements for chirality. He connected the concept of non-superimposable mirror images with the existence of chirality. Because quartz loses its optical rotatory power when dissolved or melted, he inferred that it was a helical arrangement of molecules in this particular solid that conveyed the given properties (17). He also understood that solids could possess certain elements of symmetry and still exhibit optical activity (i.e., chirality), and therefore coined the term "dissymmetry" to describe materials whose mirror images were not superimposable on each other.

The twinning of quartz crystals can yield interesting structures. In the extreme case, the complete interpenetration of left- and right-handed structures can yield a crystal whose morphology is devoid of non-superimposable hemihedral faces (Fig. 2). As would be expected, no optical activity is observable from crystal slabs cut from this type of quartz structure (21). Complete interpenetration would yield equal numbers of left-handed and right-handed spirals within the same crystal, with the optical effect of one type canceling the effect of the other. A more common occurrence is the so-called Dauphiné twin, which consists of a partial crystal interpenetration of differently handed quartz crystals (Fig. 2). In this latter instance, one can find separate regions of opposite crystal chirality existing within the same twinned structure. In one sense, the instance of twinned quartz crystals can be considered to be a prototypical racemic mixture. The understanding of optical effects in quartz permitted Pasteur to develop important conclusions about the chirality of other crystal systems, and in turn, about individual molecules.

RELATION OF MOLECULAR DISSYMMETRY AND THE CRYSTALLOGRAPHY OF TARTRATES

Crystalline quartz is one of those unique materials whose fundamental molecular units are achiral, but which are forced to adopt a chiral configuration by virtue of the crystal structure. The proof of this lies in the observation what when dissolved or melted, quartz loses its ability to rotate the plane of linearly polarized light. The fusion/solubilization process serves to destroy the spiral arrangement of the crystal, and the isotropic fluid that results contains no residual optical activity.

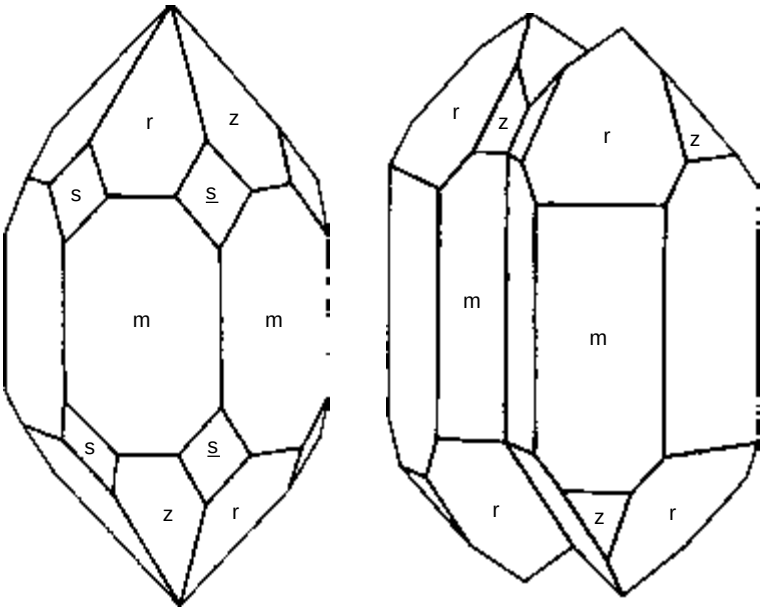

FIGURE 2 Examples of twinned quartz crystals, illustrating the lack of hemihedral facets in a completely interpenetrating crystal (**A**), and the existence of oppositely-handed quartz crystals in a single twinned structure (**B**). The figure was adapted from Ref. (14).

Early in the study of optical activity, it was learned that many organic compounds did not lose their ability to interact with polarized light even after being melted or dissolved in a solvent. A significant number of these optically active materials could be obtained as crystals that exhibited non-superimposable hemihedral crystal facets. As discussed above, Pasteur used the term "dissymmetry" to describe situations that were distinguished by the existence of non-superimposable mirror images. Pasteur understood that in the case of quartz, the dissymmetry was a result solely attributable to the nature of the crystal structure, and that destruction of the structure eliminated the dissymmetry. He realized, however, that organic molecules that remained optically active even after dissolution or fusion must possess an inherent molecular dissymmetry. The remarkable nature of these postulates is that Pasteur made his proposals prior to the general acceptance of the tetrahedral nature of carbon valency.

The development of molecular dissymmetry as an understood property was inescapably linked to optical and structural crystallography (1), and with tartaric acid and its salts providing the best illustrations. Tartaric acid was discovered by Scheele in 1769, in conjunction with wine-making, and numerous studies on its optical activity were carried out by Biot (17). Perplexing scientists of that era was a compound known as racemic acid, and whose name was derived from the Latin

Racemas, or raisin. This compound was shown by Gay Lussac to have an identical elemental analysis as tartaric acid, but which exhibited significantly different physical properties. For example, the melting point of tartaric acid is 168–170°C, while the melting point of racemic acid is 206°C. The solid density of tartaric acid (1.760 g/mL) exceeds that of racemic acid (1.697 g/mL), as does the water solubility (1390 g/L for tartaric acid compared to 206 g/L for racemic acid). Most importantly, Biot conclusively demonstrated that racemic acid was not optically active (17).

Pasteur studied the crystals of both tartaric and racemic acids, and found that although tartrate crystals contained non-superimposable hemihedral facets, racemate crystals did not. Examples of the ideal crystal morphologies of these crystal forms are shown in Figure 3. Pasteur subsequently proved the relationship between tartaric and racemic acids by mixing equal amounts of tartrate crystals having left-handed and right-handed hemihedrism, and crystallizing out a tartrate substance whose crystal morphology was completely indistinguishable from that of racemate crystals isolated in the same manner (17).

Although Pasteur was able to deduce many important conclusions using optical crystallography as his main tool, structural crystallography has the ability to go much further. It has been established that tartaric acid contains two centers of dissymmetry, with the naturally obtained optically active acid having the (*R*,*R*)-configuration (23). Enantiomerically pure tartaric acid crystallizes as an anhydrate phase in the monoclinic class (space group $P2_1$), with the unit cell containing two molecules (24,25). The reported crystallographic data are a = 7.715 Å, b = 6.004 Å, c = 6.231 Å, and β = 100.1° (25).

Racemic acid has now been shown to consist of an equimolar mixture of (*R*,*R*)-tartaric acid and the unnatural (*S*,*S*)-enantiomer, and is obtained as a monohydrate species. The compound crystallizes in the triclinic class (space group $P\bar{1}$, with the unit cell consisting of one molecule of (*R*,*R*)-tartaric acid, one molecule of (*S*,*S*)-tartaric acid, and two water molecules (26). This heterochiral unit cell is significantly different from the homochiral unit cell, and a = 8.06 Å, b = 9.60 Å, c = 4.85 Å, α = 70.4°, β = 97.2°, and γ = 112.5°. The unit cell of racemic acid contains a center of symmetry, whereas the unit cell of tartaric does not.

The molecular conformation of the tartaric acid is not significantly different in the tartrate and racemate structures, but the different modes of molecular packing lead to the existence of the two very different crystal structures (see Fig. 4 for a comparison). For the tartaric acid anhydrate crystal, the molecular planes are held directly together by a complicated network of intermolecular hydrogen bonds (25). The hydrogen bonding pattern in the racemic acid monohydrate crystal is very different, with the molecules being bound into columns that are linked up to form sheets (26).

Another acid was occasionally encountered in the French wine-making industry, which was chemically identical to the tartaric and racemic acids, but which exhibited a completely different range of physical properties. It did not exhibit optical activity, not could it be resolved into components that were themselves optically active (17). The solid exhibited a melting point of 159–160°C, a density of 1.737 g/mL, and a solubility of 1250 g/L (22). Pasteur was ultimately able to obtain quantities of this acid as a by-product from the heating of tartaric acid in the presence of basic substances.

It was ultimately learned that this non-resolvable, optically inactive, form of tartaric acid was the *meso*-form, and that it contained two centers of oppositely

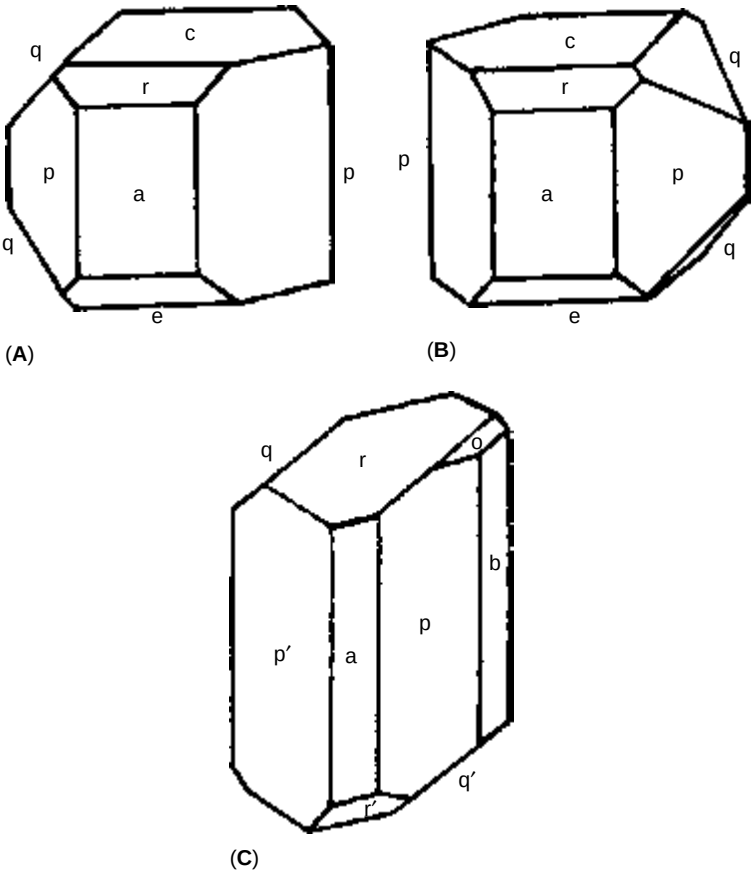

FIGURE 3 Crystals of tartaric acid, obtained under conditions yielding the hemihedral facets distinctive of the levorotatory (**A**) and dextrorotatory (**B**) forms. Also shown is the crystal morphology of racemic tartaric acid (**C**). The figure was adapted from Ref. (17).

senses dissymmetry in the same molecule. This compound has been found to crystallize in four distinct modifications, two of which are polymorphic anhydrates and two of which are polymorphic monohydrates (27). Triclinic *meso*-tartaric acid monohydrate crystallizes in the $P\bar{1}$ space group with two molecules in the unit cell, and $a = 5.516$ Å, $b = 9.220$ Å, $c = 7.330$ Å, $\alpha = 115.11°$, $\beta = 93.62°$, and $\gamma = 93.64°$.

The monoclinic monohydrate contains four molecules in the unit cell and crystallizes in the $P2_1c$ space group, with $a = 5.215$ Å, $b = 5.019$ Å, $c = 25.92$ Å, and $\beta = 99.77.2°$. The triclinic anhydrate crystallizes in the $P\bar{1}$ space group with two molecules in the unit cell, and $a = 9.459$ Å, $b = 6.464$ Å, $c = 5.396$ Å, $\alpha = 68.99°$, $\beta = 76.36°$, and $\gamma = 75.77°$. Finally, the orthorhombic anhydrate crystallizes in the $Pbn2_1$ space group with 16 molecules in the unit cell, and $a = 19.05$ Å, $b = 9.88$ Å, and $c = 12.16$ Å.

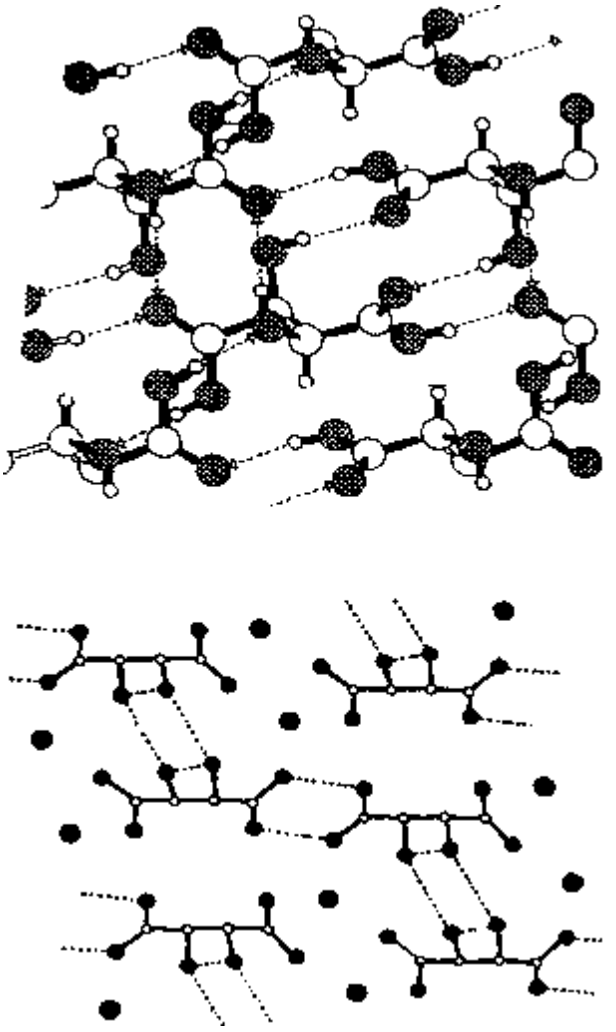

FIGURE 4 Comparison of the molecular packing in crystals of enantiomerically pure (*top*) and racemic (*bottom*) tartaric acids. The figure was adapted from data contained in Refs. (25) and (26).

In the triclinic *meso*-tartaric acid structures, the relative positions most of the non-hydrogen atoms of the molecule are approximately equivalent with those of the corresponding atoms of racemic acid. As mentioned earlier, one of the important linkages in the racemic acid structure is a square system of hydrogen bonds between hydroxyl groups on four molecules, which forms columns parallel to the *c*-axis (26). Analogous squares are formed in the *meso*-tartaric acid structures. In the

structure of racemic acid, one carboxyl group of the molecule is directly linked with a carboxyl group of a centro-symmetrically related molecule, and the other carboxyl group is indirectly connected with a counterpart through water molecules. The first type of linkage is found at one side of the molecule in the triclinic anhydrate form of *meso*-tartaric acid, whereas the second type is found at one side of the molecule in the triclinic hydrate structure. In the monoclinic hydrate, one side of the molecule takes part in a carboxylic acid dimer configuration, but the linkage through water molecules at the other side of the molecule is a less common mutation of the hydrated links found in other cases. Evidently the geometry of *meso*-tartaric acid does not permit an ideal three-dimensional arrangement to exist with both types of intermolecular linkages present.

Undoubtedly, Pasteur's most widely known work in the area of molecular dissymmetry and crystallography came about during his study of the salts of tartaric acid (17). In studies concerning the mixed 1:1 sodium/ammonium salts of tartaric and racemic acids, Mitscherlich has previously reported that both salts exhibited completely identical properties. This finding contradicted the growing body of evidence that optically active and inactive forms of the same chemical species should exhibit different physical properties. Pasteur found that sodium ammonium tartrate crystallized with the presence of non-superimposable hemihedral facets, but was surprised to learn that crystals of sodium ammonium racemate contained non-superimposable hemihedral facets as well. Upon closer examination, Pasteur found that half of the crystals of sodium ammonium racemate exhibited hemihedral facets that spiraled to the left, whereas the other half exhibited hemihedral facets that spiraled to the right. He was able to manually separate the left-handed crystals from the right-handed ones, and found that these separated forms were optically active upon dissolution. Drawings of these crystal habits are provided in Figure 5.

The explanation to Pasteur's experiments is that sodium ammonium salt prepared from racemic tartaric acid crystallizes in the orthorhombic $P2_12_12_1$, space group, and contains four molecules in the unit cell (28). This particular crystal class is non-centrosymmetric, and as a result, individual crystals are optically active. In fact, efficient growth of this tartrate salt only takes place if all of the (*R*,*R*)-tartrate molecules crystallize in one ensemble of crystals, and if all of the (*S*,*S*)-tartrate molecules crystallize in another ensemble. When formed below a temperature of 26°C, the preferred molecular packing does not permit the intermingling of the enantiomers to yield a true a racemic crystal. The crystallization of sodium ammonium tartrate below 26°C results in a spontaneous resolution of the substance into physically separable enantiomers. Interestingly, a different polymorph forms above 26°C, which requires a completely different packing pattern, and which allows for the formation of a racemic modification of sodium ammonium tartrate.

A series of half neutralized salts of tartaric acid are also found to crystallize in the orthorhombic $P2_12_12_1$, space group (all containing four molecules in the unit cell), and are thus potentially resolvable by a mechanical separation. Ammonium hydrogen tartrate is found to crystallize with $a = 7.648$ Å, $b = 11.066$ Å, and $c = 7.843$ Å (29). Sodium hydrogen tartrate crystallizes with $a = 8.663$ Å, $b = 10.583$ Å, and $c = 7.228$ Å, whereas potassium hydrogen tartrate crystallizes with $a = 7.782$ Å, $b = 10.643$ Å, and $c = 7.608$ Å (30). Finally, rubidium hydrogen tartrate is found to crystallize with $a = 7.923$ Å, $b = 10.988$ Å, and $c = 7.653$ Å (31).

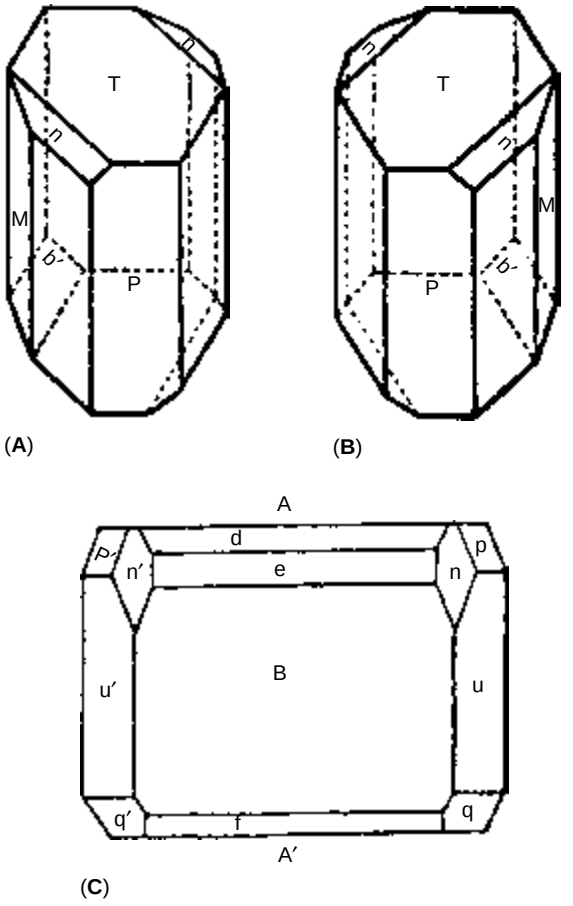

FIGURE 5 Crystals of sodium ammonium tartrate, obtained under conditions yielding the hemihedral facets distinctive of the levorotatory (**A**) and dextrorotatory (**B**) forms. Also shown is the crystal morphology of racemic sodium ammonium tartrate (**C**). The figure was adapted from Ref. (17).

PHYSICAL CHARACTERISTICS OF RACEMIC MIXTURES OF DISSYMMETRIC SOLIDS

The early work of Pasteur clearly demonstrated the possibility that racemic compounds were actually mixtures, and that these mixtures could be separated into their component enantiomers using either physical or chemical means. Although some compounds could be separated by direct crystallization into chiral crystals, the majority of organic compounds required some type of chemical reaction in order to effect a separation of the enantiomers. Compounds separable by the direct

crystallization method were termed *conglomerates*, whereas compounds separable subsequent to their derivatization were termed *racemates*. Much work has gone into the investigation of these two types of dissymmetric solids, and it is appropriate to conduct a more detailed exposition of some of the structural aspects of these systems.

Conglomerate Systems

Conglomerate solids are characterized by the presence of a single enantiomer within the unit cell of the crystal, even when the solid is obtained through crystallization of a racemic or partially resolved mixture. These solids consist of separate crystals, each of which consists entirely of one enantiomer or its mirror image, and which may be separated solely on the basis of their physical properties. The small-scale resolution of dissymmetric compounds crystallizing as conglomerates can be straight forward because the resolution step takes place spontaneously with the crystallization step. The key to a successful resolution by direct crystallization lies in the means used to physically separate the crystals containing the opposite enantiomers. Jacques and coworkers have provided extensive summaries of the methods whereby direct crystallization can be used to effect the resolution of a racemic mixture (10,32).

The first method is the classical technique of Pasteur, and this entails the mechanical separation of enantiomorphic crystals that are formed simultaneously while the mother liquor remains racemic. Enantiomer separation by this particular method can be extremely time-consuming, and not possible to perform unless the crystals form with recognizable chiral features (such as well-defined hemihedral faces). Nevertheless, this procedure is often the method of choice to obtain the first seed crystals required for the scale-up of the resolution process through direct crystallization. When a particular system has been shown to be a conglomerate, and the crystals are not sufficiently distinct so as to be separated, polarimetry or circular dichroism spectroscopy can often be used to establish the chirality of the enantiomer.

Even a few seed crystals, mechanically separated, can be used to produce larger quantities of resolved enantiomerically pure material. A second method of resolution by direct crystallization involves the localized crystallization of each enantiomer from a racemic, supersaturated solution. With the crystallizing solution within the metastable zone, oppositely handed, enantiomerically pure, seed crystals of the compound are placed in geographically distant locations in the crystallization vessel. These serve as nuclei for the further crystallization of the like enantiomer, and enantiomerically resolved product grows in the seeded locations. This procedure has been used to obtain both enantiomers of methadone, where approximately 50% total yield of enantiomerically pure material can be obtained (33). An apparatus has been described that permits the more automated use of localized crystallization, and that has successfully been used to separate the enantiomers of hydrobenzoin (34).

Enantiomer separation may be practiced on the large industrial scale using the procedure known as resolution by entrainment (35). The method is based on the condition that the solubility of a given enantiomer is less than that of the corresponding racemate. To begin, a solution is prepared that contains a slight excess of one enantiomer. Crystallization is induced (usually with the aid of appropriate seed crystals), whereupon the desired enantiomer is obtained as a solid and the mother

liquor is enriched in the other isomer. In a second crystallization step, the other enantiomer is obtained. The method can be applied to any racemic mixture that crystallizes as a conglomerate, and the main complication that can arise is when the compound exhibits polymorphism. In that case, the entrainment procedure must be carefully designed so as to generate only the desired crystal form.

Resolution by entrainment is best illustrated through the use of an example, and the bench-scale resolution of hydrobenzoin (32) is an excellent example. About 1100 mg of racemic material was initially dissolved along with 370 mg of (–)-hydrobenzoin in 85 g of 95% ethanol, and the solution cooled to 15°C. Then 10 mg of the (–)-isomer was added as seeds, and crystals were allowed to form. After 20 minutes, 870 mg of (–)-hydrobenzoin was recovered. 870 mg of racemic hydrobenzoin was then dissolved with heating, the resulting solution cooled to 15°C, and seeded with 10 mg of the (+)-isomer; 900 mg of (+)-hydrobenzoin was recovered at this time. The process was cycled 15 times, and ultimately yielded 6.5 g of (–)-hydrobenzoin and 5.7 g of (–)-hydrobenzoin. Each isomer was obtained as approximately 97% enantiomerically pure.

Jacques and coworkers have provided compilations of the known conglomerate systems, identifying at the time approximately 250 organic compounds (36). This relatively small number represents only about 10% of the number of chiral compounds for which resolutions have been published, and represents the major limitation to enantiomer resolution by direct crystallization. It has been noted that substitution of additional functionalities onto the achiral portion of a compound can sometimes also yield a conglomerate system. For example, although mandelic acid and many of its derivatives crystallize as racemic mixtures, *ortho*-chloromandelic acid is obtained as a conglomerate (37). Interestingly, both the *meta*- and *para*-chloromandelic acids crystallize as racemates.

This seemingly randomness of conglomerate formation has been explained through examinations of the thermodynamics of these systems. The stability of true racemic solids is defined by the free energy change associated with the process of combining the *R*-enantiomer with the *S*-enantiomer to produce the *R*,*S*-enantiomeric solid. This has been calculated to be in the range of 0 to –2 kcal/mol, and is roughly proportional to the difference in melting points between the racemate and the resolved enantiomers (38). In most cases, the free energy associated with the formation of racemates is exothermic, owing to the positive nature of the enthalpies and entropies of formation. In those cases where the melting point of the racemic mixture is at least 20 degrees lower than the melting points of the separated enantiomers, one generally obtains a conglomerate system.

The use of crystal structure prediction in the evaluation of systems for their tendency toward spontaneous resolution has been explored (39). Using a gas phase conformational search to locate low-energy conformations, the possible crystal structures of 5-hydroxymethyl-2-oxazolidinone and 4-hydroxymethyl-2-oxazolidinone assembled from these conformations have been predicted. For both compounds, the racemate was predicted to have the lowest energy, with the energy difference between the lowest energy racemic structure and the lowest energy separated enantiomer structure being in the range of 0.2 to 0.9 kcal/mol. The authors noted that as the accuracy of lattice energy calculations becomes more accurate, it should become possible to predict whether a chiral molecule will crystallize in a space group where its racemate or conglomerate nature would be expressed.

Because conglomerate systems consist of totally independent formed enantiomer crystals, and are physical mixtures of the enantiomer components, these constitute a binary system. Such binary mixtures are easily described by the phase rule, and can be characterized by their melting point phase diagrams (10). Because the components of a conglomerate racemate will melt independently at the same temperature, the material will exhibit the melting phenomena of a pure substance. One would therefore observe the existence of a eutectic point in the melting point phase diagram that would be located at exactly the racemic composition. For a partially resolved conglomerate system, one can separate out the enantiomer present in excess simply by heating the sample to a temperature just above the melting point of the racemate, and then collecting the crystalline excess of the residual enantiomer.

The liquidus line of a phase diagram can be calculated using the Schröder–Van Laar equation:

$$\ln X_i = (\Delta H^F/R)\{(1/T_P) - (1/T_i)\}$$

where X_i is the ith mole fraction of one of the enantiomers, ΔH^F is the molar heat of fusion of the pure enantiomer, T_P is the melting point of the pure enantiomer, and T_i is the melting point of the substance having mole fraction X_i.

An example of the type of melting point phase diagram that may be obtained for a conglomerate system is shown in Figure 6, which illustrates one half of the phase diagram reported for 4,4′-dimethyl-8,9,10-trinor-spiro-2,2′-bornane (40). Below the eutectic temperature of 67°C, the system exists as a mixture of solid *D*-enantiomer and *L*-enantiomer. At the exact composition of the racemic mixture ($X = 0.5$), the system will exist entirely in the liquid phase above the eutectic temperature. At mole fractions where the amount of *L*-enantiomer exceeds that of the *D*-enantiomer, the system will exist as an equilibrium mixture of racemic liquid and solid *L*-enantiomer. As required by the phase diagram of a conglomerate, the eutectic temperature is the lowest temperature attainable where any liquid phase can exist in equilibrium with any solid phase. For the 4,4′-dimethyl-8,9,10-trinor-spiro-2,2′-bornane system, an excellent fit of the data according to the Schröder–Van Laar equation was obtained, yielding $\Delta H^F = 5.9$ kcal/mol and $T_P = 95$°C.

An alternate approach for the characterization of conglomerate systems is through the use of ternary phase diagrams, where one component is the solvent and the solubility of the substance is used as the observable parameter (10,32). A racemic mixture will be more soluble than are the separated enantiomers, and the rule of Meyerhoffer states that a conglomerate will have a solubility that is twice the solubility of the resolved enantiomer (41). This situation arises because ideally the mole fraction of an independent constituent in a liquid depends only on the enthalpy of fusion and melting point of the substance, and because according to the Schröder–Van Laar equation the solubility of one enantiomer cannot affect the solubility of the other. Jacques and Gabard have examined the solubilities of a number of conglomerate systems, and have largely confirmed the double solubility rule (42). A selection of their results obtained for substances, which are not dissociated in solution, is presented in Table 1.

A theoretical explanation has been developed to explain the effect of chiral impurities on the crystallization rates of the enantiomorphic components of a conglomerate system (43). The theory provides the time required to complete the crystallization of the separated enantiomers, suggests that one might be able to

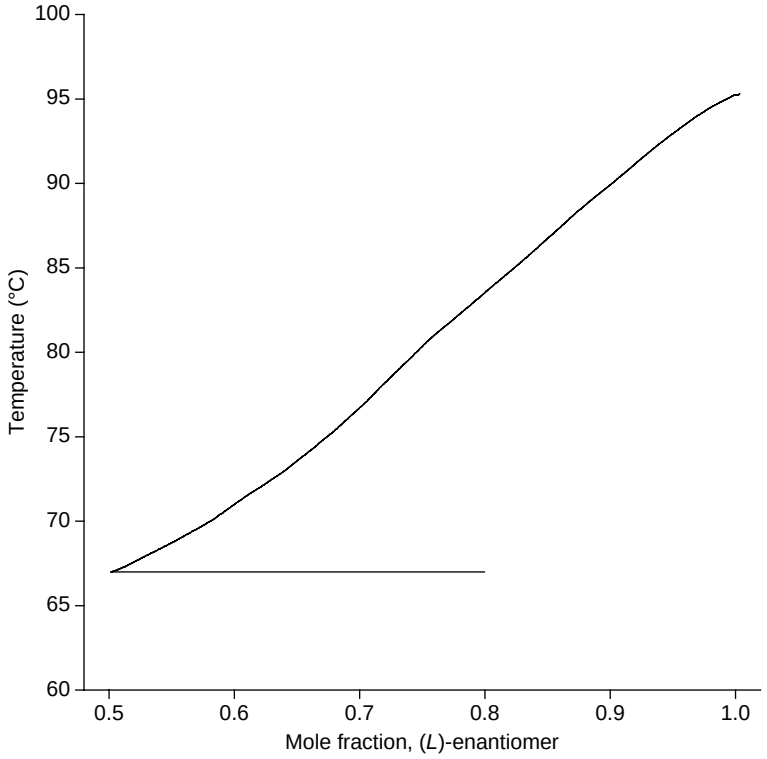

FIGURE 6 Portion of the melting point phase diagram obtained for the crystalline conglomerate formed by 4,4′-dimethyl-8,9,10-trinor-spiro-2,2′-bornane. The figure was adapted from data contained in Ref. (40).

TABLE 1 Solubilities of Separated Enantiomers and Racemic Mixtures of Conglomerate Materials

Compound	System	Solubility of separated enantiomer (g/100 mL)	Solubility of racemic mixture (g/100 mL)	Ratio of racemate solubility to enantiomer solubility
Asparagine	Water (25°C)	2.69	5.61	2.16
(α-Naphtoxy)-2-propionamide	Acetone (25°C)	1.38	2.24	2.08
p-Nitrophenylamino propanediol	Methanol (25°C)	1.63	3.35	2.14
N-acetyl-leucine	Acetone (25°C)	1.86	4.12	2.13
N-acetyl-glutamic acid	Water (25°C)	4.14	8.28	2.12
Diacetyldiamide	Water (35.5°C)	12.4	23.7	2.14
3,5-Dinitrobenzoate-lysine	Water (30°C)	6.96	13.17	1.99

obtain an enantiomerically pure product even if the chiral impurity was less than enantiomerically pure, and even provides information regarding the particle size distribution. The model was tested on the crystallization of (*D*,*L*)-glutamic acid that was carried out in the presence of a resolved (*L*)-lysine impurity.

Racemate Systems

Racemate solids are characterized by the presence of equimolar amounts of both enantiomers within the unit cell of the crystal. Materials of this type will crystallize within a centrosymmetric space group, which will necessarily be different from the non-centrosymmetric space group of the separated enantiomers. As a result, the range of physical properties associated with a heterochiral solid must be completely different from those of the homochiral solid. For instance, the melting point of the exact racemic mixture may be greater than or less than that of the separated enantiomers, and there is no general rule that can be invoked to provide a reliable prediction of melting point behavior. The basic problem is that the phase diagram of a racemate system exhibits two eutectic minima, and crystallization at those conditions yields a racemic mixture and not enantiomerically pure product.

Racemates can only be separated after the performance of a derivatization reaction with a suitable chiral reagent, and where the resulting diastereomers (often identified in the literature as the *p-salt* and the *n-salt*) exhibit a phase diagram that contains only a single minimum. In general, this minimum will not be located at the exact racemic composition, but will instead be observed at some other concentration value. In fact, for the p-salt to be separated from the n-salt in a single crystallization step, the position of the eutectic should be substantially removed from the equimolar point. However, if the eutectic point should happen by accident to be close to the equimolar point, then the phase diagram would closely resemble that of a conglomerate. In that particular instance, it would be possible to devise an entrainment procedure for the separation of the p- and n-salts. This possibility has been demonstrated by the preferential crystallization of 4-methylpiperidinium hydrogen (*R*,*S*)-succinate (44).

The procedure most commonly used to alter the crystallization thermodynamics of true racemate systems involves the formation of dissociable diastereomer species (45). These are most often simple salts formed between electron-pair donors and electron-pair acceptors. For instance, the first resolving agents introduced for acidic enantiomers were alkaloid compounds, and hydroxy-acids were used for the resolution of basic enantiomers. This type of resolution procedure has been known since the time of Pasteur, and extensive tables of resolving agents and procedures are available (46,47).

As an example, consider the specific case where a racemic acid is to be resolved through the use of a basic resolving agent. The first step of the resolution procedure involves formation of the p- and n-diastereomeric salts:

Racemic Mixture		*Resolving Agent*		*Diastereomer Salts*
(+)R-COOH				(+)R-COO-NH_3-R′(+)
	+	2NH_2-R′(+)	→	
(–)R-COOH				(–)R-COO-NH_3-R′(+)

According to convention (48), the (*R*,*R*) and (*S*,*S*) diastereomers are termed the p-salts, and the (*R*,*S*) and (*S*,*R*) diastereomers are identified as the n salts. In the example used above, the (+)R-COO-NH_3-R′(+) diastereomer would correspond to the p-salt, and the (–)R-COO-NH_3-R′(+) diastereomer would be the n-salt. In the usual practice, the p- and n-salts are separated by fractional crystallization, and the success of the resolution process is critically related to this crystallization step.

As mentioned earlier, the desirable effect of derivatization is to transform the undesirable thermodynamics of a racemate system into those more amenable for direct separation of the diastereomers. One way to look at the process is that the act of derivatization alters the phase diagram from containing the double eutectic of the racemate system into a pseudo-conglomerate phase diagram exhibiting only one eutectic. For example, the enantiomers of phenylsuccinic acid can be separated after formation of the proline salt (49), and an example of the solubility phase diagram reported for the 1:2 phenylsuccinate/proline salt is shown in Figure 7. In this work, it was found that the degree of resolution for the salt having the 1:2 stoichiometry was only minimally affected by temperature, but that separation of the 1:1 stoichiometric phenylsuccinate/proline salt was strongly affected by temperature. These findings illustrate the strong need for obtaining the phase diagram when designing enantiomeric separations, because the efficiency of the process can be strongly affected by environmental factors.

For instance, the aqueous solubility of the n-salt of α-methylbenzylamine mandelate has been reported as 49.1 g/L, and the solubility of the p-salt as 180 g/L (50). However, the relative solubilities of the p- and n-salt pairs is greatly affected by the choice of temperature or solvent system, and the pathway of the diastereomer separation can easily be manipulated by variations in experimental conditions.

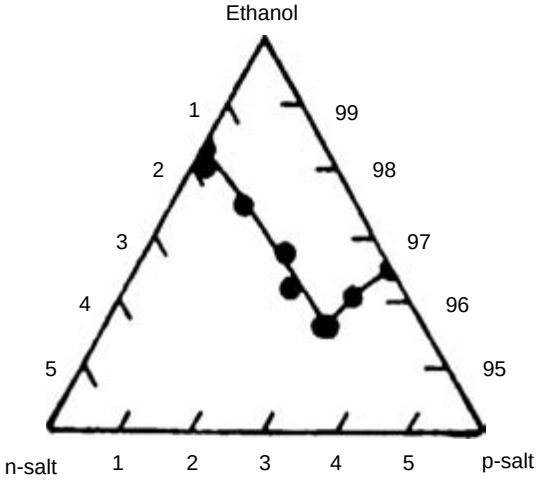

FIGURE 7 Solubility phase diagram reported for the diastereomer system (1:2 stoichiometry) formed by (±)-phenylsuccinic acid and (–)-proline, using ethanol as the solvent system. The figure was adapted from data contained in Ref. (47).

In fact, it is possible to preferentially crystallize either the p- or n-salt depending on the range of parameters used.

The chiral discrimination existing in the diastereomer systems formed by ephedrine and various mandelic acids has been studied in great detail, using a variety of spectroscopic and structural tools. Although significant differences in the solubilities of the n- and p-salts obtained after reaction of ephedrine with mandelic acid were known to exist, both salts were found to crystallize in the same monoclinic space group with crystal structures that were isosteric (51). In subsequent work, it was shown that the crystalline diastereomer salts formed by (*R*)-mandelic acid formed a more compact repeating pattern (with higher melting points and enthalpies of fusion) than did analogous salts formed by (*S*)-mandelic acid (52). It was deduced that the subtle chiral discriminations led to the existence of different hydrogen-bonding modes, which in turn, became manifest in a variety of other physical properties.

There is no doubt that the crystallographic differences between the diastereomers generated during derivatization directly affect the outcome of the resolution process. For example, when (*D*,*L*)-phenylglycine was resolved with (*S*)-camphor-10-sulfonic acid, the n-salt was isolated in 45.7% yield and having an enantiomeric purity of 98.8% (53). The less soluble n-salt exhibited a higher melting point and enthalpy of fusion than did the p-salt, which was found to be freely soluble. The crystal structure of the n-salt exhibited a dense structure containing alternating phenylglycine cation and camphor sulfonate anion layers, whereas the structure of the p-salt exhibited a coarser structure with vacancy layers between the anion and cation planes. These differences in crystal structure directly led to the differing physical properties of the diastereomeric salts that caused the enantiomeric resolution to be so successful.

Distinctions in hydrogen-bonding networks were noted during studies of the structures formed by α-amino acids and (*S*)-phenylethanesulfonic acid (54), and the differences noted for the two salts formed between *p*-hydroxyphenylglycine and the resolving agent are shown in Figure 8. In another work, the diastereomers formed during the resolution of (*R*,*S*)-mandelic acid with *R*-2-*tert*-butyl-3-methylimidazoldin-4-one were characterized by varying networks of hydrogen bonding, whereas the conformations of the molecular species were relatively equivalent (55).

Depending on the details of the lattice dynamics, there is no restriction regarding the ability of a given pair of p- and n-salts to crystallize in the same or in different space groups. For example, in the diastereomeric system formed by α-methylbenzylamine and hydratropic acid, the p-salt was found to crystallize in the $P2_1$ space group, whereas the n-salt crystallized in the $P2_12_12_1$ space group (56). Although the conformations of the constituent species in the two crystal forms were reported to be similar, the mode of molecular packing that led to the structure of the individual crystals was very different.

This latter behavior differs from that observed in the crystalline diastereomers of mandelic acid with 1-phenylethylamine (57). Here, the n-salt crystallized in the triclinic $P\bar{1}$ space group, whereas the p-salt crystallized in the monoclinic $P2_1$ space group. The crystallographic structures of the two diastereomers revealed the existence of fairly equivalent hydrogen-bonding patterns, but at the same time substantially different conformations for the two molecular ions making up the donor–acceptor complex were noted. These structural differences became manifest in the relative solubilities of the two diastereomers, where the aqueous solubility of the p-salt was much less than that of the n-salt.

n-Salt: (*R*)-HPG – (*S*)-PES

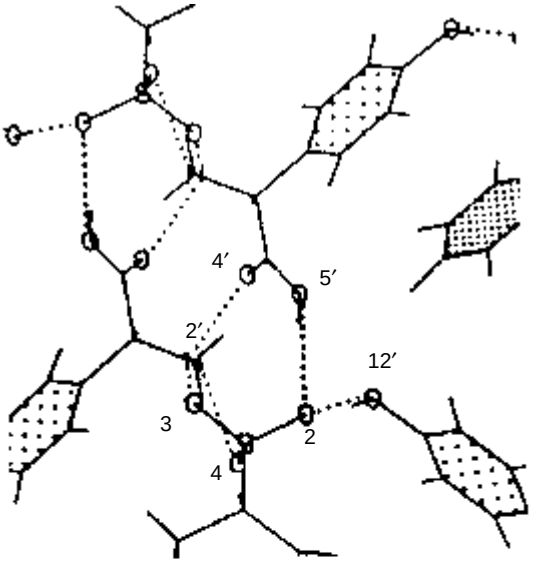

p-Salt: (*S*)-HPG – (*S*)-PES

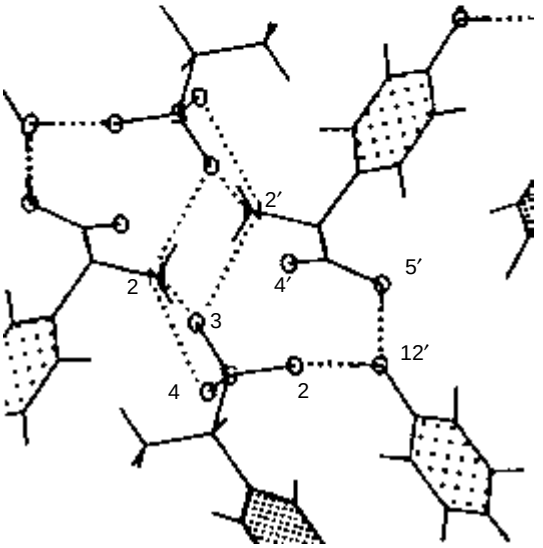

FIGURE 8 Details of the hydrogen bonding existing in crystals of the diastereomeric salts formed between the enantiomers of *p*-hydroxyphenylglycine (HPG) and (*S*)-1-phenylethanesulfonic acid (PES). The figure was adapted from data contained in Ref. (54).

Once either the p-salt or the n-salt (or both) is successfully crystallized, the diastereomer salt is usually dissociated and the resolving agent separated. In the specific instance of acid resolution, the diastereomeric salt is efficiently cleaved by means of a hydrolysis reaction:

Separated Diastereomers	+	*Hydrolysis Agent*	→	*Separated Enantiomers*
(+)R-COO-NH_3-R′(+)	+	HCl	→	(+)R-COOH + (+)R′-NH_3Cl
(–)R-COO-NH_3-R′(+)	+	HCl	→	(–)R-COOH + (+)R′-NH_3Cl

The diastereomer cleavage must be simple, selective, take place in quantitative yield, must not racemize the resolved compound, and must leave the resolving agent in a form that is easily recovered. The recovery is usually effected by precipitation or extraction of the resolving agent. One important criterion in the choice of a resolving agent is the ease by which it may be dissociated and removed from the compound being resolved (45).

Racemate Systems Turned into Conglomerate Systems

Although the frequency of conglomerate-forming systems is fairly small for organic compounds, a statistical analysis of more than 500 salts has demonstrated that the probability of observing spontaneous resolution is two or three times higher for salts of the same organic compounds (58). The possibility has been further demonstrated through studies of the crystallization of achiral dicarboxylic acids with α-phenethylamine, where racemates were obtained for the salts with hydrogen malonate and hydrogen phthalate, but a conglomerate was obtained for the hydrogen succinate salt (59). In a subsequent work, it was concluded that conglomerate formation took place when the protonated and deprotonated carboxylic acid groups formed hydrogen-bonded chains rather than forming intermolecular hydrogen-bonded dimers in the crystal (60).

To illustrate how a racemate system can be turned into a conglomerate system, we will consider the example of ibuprofen, or 2-(4-isobutylphenyl)propanoic acid. The single crystal structures of enantiomerically pure (61) and racemic (62) ibuprofen have been published, and the crystallographic properties of the respective unit cells are summarized in Table 2. Using the published details of the two unit cells, the powder diffraction patterns of the enantiomerically pure and racemate forms were calculated, and these are shown in Figure 9. As would be expected, these are quite different in their character. The racemic mixture of ibuprofen has been shown to be a racemate (63), and consequently, the resolution of the compound into its enantiomers typically proceeds through the conventional route of diastereomer separation (64).

The physical and structural properties of ibuprofen are dominated by the chemistry of the carboxylate group, for which the p*K*a has been determined to be 4.45 (65). As would be anticipated for a carboxylic acid compound, the solubility of

TABLE 2 Crystallographic Data for (*S*)-Ibuprofen and (*R*,*S*)-Ibuprofen

	(*S*)-ibuprofen	**(*R*,*S*)-ibuprofen**
Crystal class	Monoclinic	Monoclinic
Space group	$P2_1$	$P2_1/c$
Unit cell lengths	$a = 12.462$ Å	$a = 14.667$ Å
	$b = 8.035$ Å	$b = 7.886$ Å
	$c = 13.539$ Å	$c = 10.730$ Å
Unit cell angles	$\alpha = 90°$	$\alpha = 90°$
	$\beta = 112.89°$	$\beta = 99.362°$
	$\gamma = 90°$	$\gamma = 90°$
Molecules in unit cell	4	4
Cell volume	1248.8 Å^3	1165.6 Å^3
Density	1.10 g/mL	1.175 g/mL
Reference	61	62

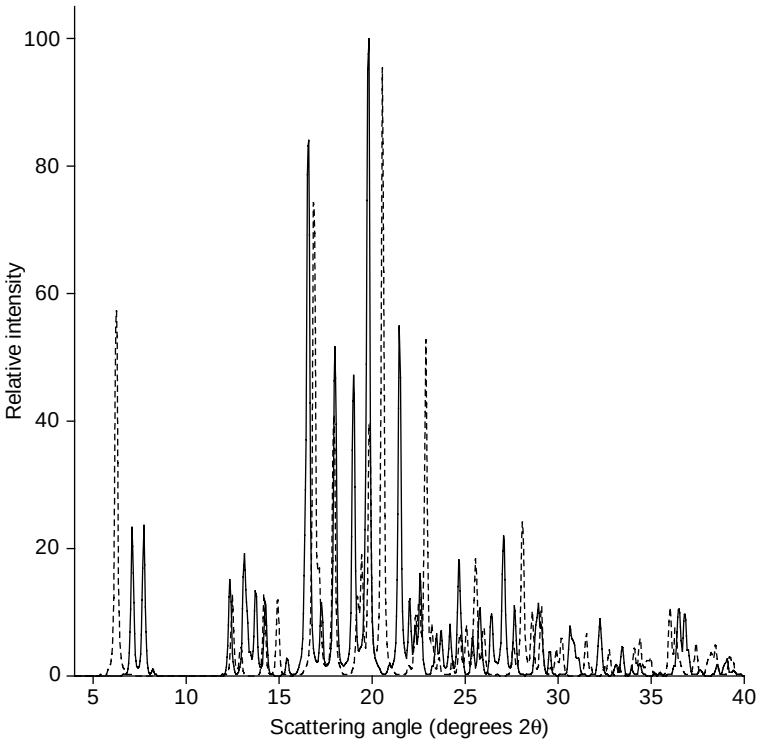

FIGURE 9 X-ray powder diffraction patterns calculated from the published crystal structures of (*S*)-ibuprofen [solid trace; Ref. (61)] and (*R*,*S*)-ibuprofen [dashed trace; Ref. (62)].

the free acid is very low owing to its hydrophobic character, but once the solution pH is raised above neutral anionic ibuprofen becomes very soluble. Tromethamine (2-amino-2-(hydroxymethyl)propane-1,3-diol) is a basic substance, and has been found to form salt species with ibuprofen (66). The X-ray powder diffraction patterns of the (*S*)-ibuprofen/tromethamine and (*R*,*S*)-ibuprofen/tromethamine salts are shown in Figure 10, where it may be noted that the respective diffraction patterns are equivalent.

Because the respective diastereomers of a conglomerate system would crystallize in the same space group, it follows that equivalence in diffraction patterns for the tromethamine salts of (*S*)-ibuprofen and (*R*,*S*)-ibuprofen ibuprofen identifies these as constituting a conglomerate system. The structural equivalence of the ibuprofen–tromethamine salts is further demonstrated by the equivalence of their other physical properties. For example, the differential scanning calorimetry thermograms of the salts are effectively the same, with the (*S*)-ibuprofen salt exhibiting a melting endotherm at 158.4°C (enthalpy of fusion of 159.1 J/g) and the (*R*,*S*)-ibuprofen salt having a melting endotherm at 158.9°C (enthalpy of fusion of 160.2 J/g) (66).

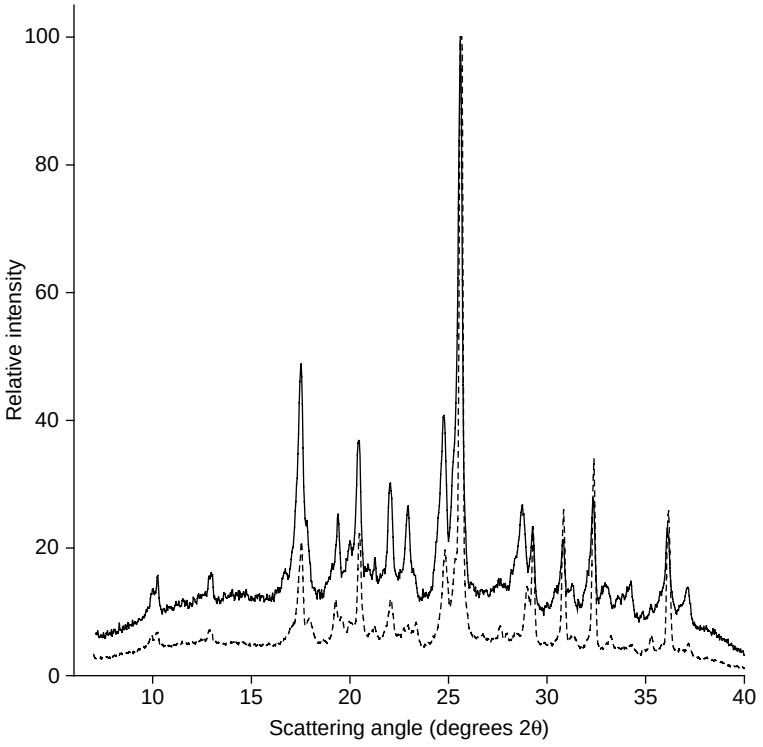

FIGURE 10 X-ray powder diffraction patterns obtained for the tromethamine salts with (*S*)-ibuprofen (solid trace) and (*R*,*S*)-ibuprofen (dashed trace) (HG Brittain, unpublished results).

Because the crystal structures of the (*S*)-ibuprofen/tromethamine and (*R*,*S*)-ibuprofen/tromethamine salts are effectively the same, one would anticipate that the solid-state spectra of these compounds would also be equivalent. This is evident in the infrared absorption and Raman spectra shown in Figure 11, where there is no discernable difference in the respective spectra of the various tromethamine salts prepared from the enantiomerically pure and racemic ibuprofen.

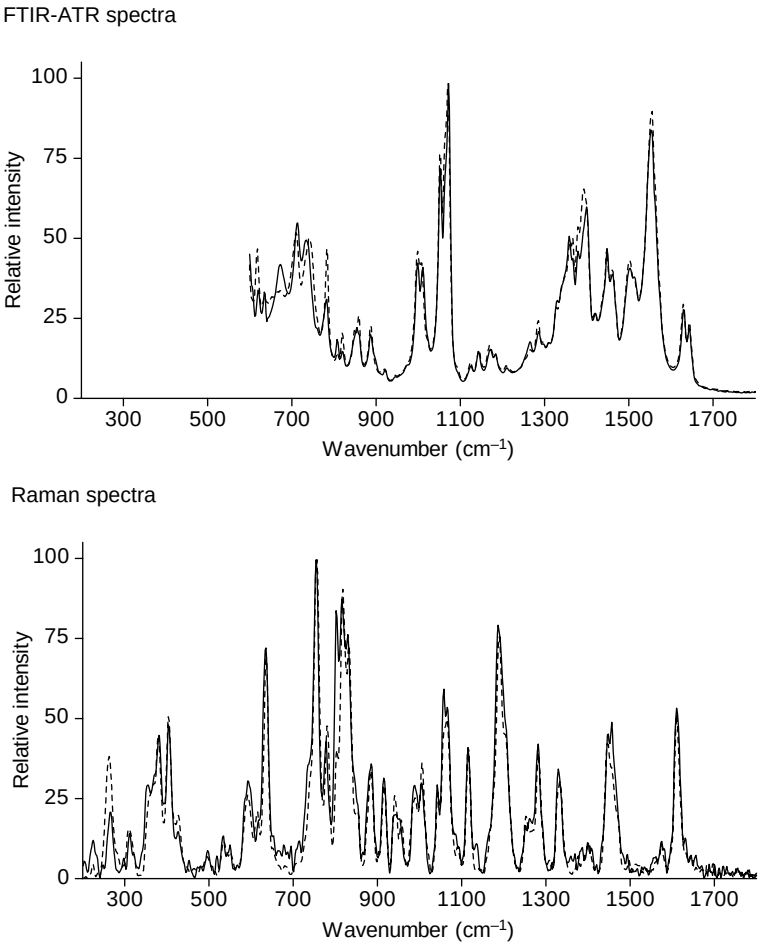

FIGURE 11 Fingerprint region infrared absorption and Raman spectra of the tromethamine salts with (*S*)-ibuprofen (solid trace) and (*R*,*S*)-ibuprofen (dashed trace) (HG Brittain, unpublished results).

SUMMARY

Observations on the chirality of crystals made it possible for Pasteur and others to identify dissymmetry as the true origin of optical activity, as the molecular chirality associated with a given compound proved to be directly observable in the crystallography of that compound. The crystallographic consequences of the molecular dissymmetry caused the existence of observable differences in a variety of physical properties, such as the melting point, solubility, and spectroscopy of such species. Although the majority of chiral molecules can only be resolved through the formation and separation of dissociable diastereomers, many chiral molecules have been observed to exhibit the property of spontaneously resolution upon crystallization, and the resulting enantiomorphic crystals may be physically separated.

With more and more therapeutic agents being administered as resolved enantiomers, methods for isolation of the desired dissymmetric species will be in constant development. Determination of the melting point or solubility phase diagram becomes a key element to the development process, because one can use this information to identify the agent in question as being either a conglomerate or a racemate. Should the compound happen to crystallize as a conglomerate, then enantiomer separation by direct crystallization could represent the cost-effective route. Compounds identified as racemates would necessarily require separation by the formation of dissociable diastereomers. Of course, when the compound in question can be synthesized directly with the proper enantiomeric composition, the need to conduct a resolution procedure evaporates. It should never be forgotten, however, that even when asymmetric synthesis is the chosen route, an investigation into the relationship between chirality and crystallography is essential to having an understanding of the molecular system.

REFERENCES

1. Brittain HG. Crystallographic consequences of molecular dissymmetry. Pharm Res 1990; 7: 683–90.
2. Wainer IW, Drayer DE. Drug Stereochemistry: Analytical Methods and Pharmacology. New York: Marcel Dekker, 1988.
3. Testa B, Trager WF. Racemates versus enantiomers in drug development. Chirality 1990; 2: 129–33.
4. Li ZJ, Grant DJW. Relationship between physical properties and crystal structures of chiral drugs. J Pharm Sci 1997; 86: 1073–8.
5. Fassihi AR. Racemates and enantiomers in drug development. Int J Pharm 1993; 92: 1–14.
6. Smith RL, Caldwell J. Racemates: towards a new year resolution. Trends Pharmacol Sci 1988; 9: 75–7.
7. De Camp WH. The FDA perspective on the development of stereoisomers. Chirality 1989; 1: 2–6.
8. Newman P. Optical Resolution Procedures for Chemical Compounds, Volumes 1–3. New York: Manhattan College Press, 1984.
9. Cahn RS, Ingold CK, Prelog V. Specification of molecular chirality. Angew Chem Int Ed Engl 1966; 5: 385–415.
10. Jacques J, Collet A, Wilen SH. Enantiomers, Racemates, and Resolutions. New York: John Wiley & Sons, 1981.
11. Zorkii PM, Razumaeva AE, Belsky VK. The systematization of molecular crystal structures. Acta Cryst 1977; A33: 1001–4.

12. Mason SF. Molecular Optical Activity and the Chiral Discriminations. Cambridge: Cambridge University Press, 1982: 165–6.
13. Kitaigorodskii AI. Molecular Crystals and Molecules. New York: Academic Press, 1973.
14. Wallach G. Annalen 1895; 286: 140.
15. Brock CP, Schweizer WB, Dunitz JD. On the validity of Wallach's rule: on the density and stability of racemic crystals compared with their chiral counterparts. J Am Chem Soc 1991; 113: 9811–20.
16. Walden P. Chem Ber 1896; 29: 1692.
17. For an excellent introduction into the early work involving chirality and crystallography, see Lowry TM. Optical Rotatory Power. London: Longmans, Green, & Co, 1935: 25–36.
18. Dana ES, Ford WE. A Textbook of Mineralogy. New York: John Wiley & Sons, 1922: 470.
19. Bragg WH, Gibbs RE. The structure of α and β quartz. Proc Roy Soc 1925; A109: 405–27.
20. Wyckoff RWG. Am J Sci 1926; 11: 101.
21. Frondel C. The System of Mineralogy, Volume III. New York: John Wiley & Sons, 1962: 75–98.
22. The Merck Index, 14th ed. In: O'Neil MJ, Heckelman PE, Koch CB, Roman KJ, eds. Rahway, NJ: Merck & Co. Inc., 2006: 9069.
23. Klyne W, Buckingham J. Atlas of Stereochemistry, 2nd ed. New York: Oxford University Press, 1978: 6.
24. Stern F, Beevers CA. The crystal structure of tartaric acid. Acta Cryst 1950; 3: 341–6.
25. Okaya Y, Stemple RR, Kay MI. Refinement of the structure of D-tartaric acid by X-ray and neutron diffraction. Acta Cryst 1966; 21: 237–43.
26. Parry GS. The crystal structure of hydrate racemic acid. Acta Cryst 1951; 4: 131–8.
27. Bootsma GA, Schoone JC. Crystal structures of mesotartaric acid. Acta Cryst 1967; 22: 522–32.
28. Brozek Z, Stadnicka K. Structure of sodium ammonium (+)-tartrate tetrahydrate at 200, 151 and 120 K. Acta Cryst 1994; B50: 59–68.
29. van Bommel AJ, Bijvoet JM. The crystal structure of ammonium hydrogen D-tartrate. Acta Cryst 1958; 11: 61–70.
30. Kubozone Y, Hirano A, Nagasawa S, Maeda H, Kashino S. Structures of sodium hydrogen L-tartrate monohydrate and potassium hydrogen L-tartrate. Bull Chem Soc Jap 1993; 66: 2166–73.
31. Templeton LK, Templeton DH. Structure of rubidium hydrogen (+)-tartrate. Acta Cryst 1989; C45: 675–6.
32. Collet A, Brienne M-J, Jacques J. Optical resolution by direct crystallization of enantiomer mixtures. Chem Rev 1980; 80: 215–30.
33. Zaugg HE. A mechanical resolution of DL-methadone base. J Am Chem Soc 1955; 77: 910.
34. Brugidou J, Christol H, Sales R. Bull Soc Chim France 1974: 2033.
35. Amiard G. Sur le dedoublement direct de la threonine, par entrainement. Bull Soc Chim France 1956: 447–51.
36. Collet A, Brienne M-J, Jacques J. Dédoublements spontanés et conglomérats d'énantiomères. Bull Soc Chim France 1972: 127–42; Étude des mélanges d'antipodes optiques. XIII. Compléments à dédoublements spontanés. ibid 1977: 494–8.
37. Collet A, Jacques J. Étude des mélanges d'antipodes Optiques. V. Acides mandéliques substitués. Bull Soc Chim France 1973: 3330–4.
38. Leclercq M, Collet A, Jacques J. Étude des mélanges d'antipodes optiques. XII. Mesure de la stabilite des racemiques vrais. Tetrahedron 1976; 32: 821–8.
39. Gourlay MD, Kendrick J, Leusen FJJ. Rationalization of racemate resolution: predicting spontaneous resolution through crystal structure prediction. Cryst Growth Des 2007; 7: 56–63.
40. Lajzerowicz-Bonneteau J, Lajzerowicz J, Bordeaux D. Phase separation: statics and dynamics in a racemic molecular solid solution. Phys Rev B 1986; 34: 6453–63.

41. Meyerhoffer W. Stereochemische Notizen. Ber Dtsch Chem Ges 1904; 37: 2604–10.
42. Jacques J, Gabard J. Étude des mélanges d'antipodes optiques. III. Diagrammes de solubilité pour les divers types de racémiques. Bull Soc Chim France 1972: 342–50.
43. Kondepudi DK, Crook KE. Theory of conglomerate crystallization in the presence of chiral impurities. Cryst Growth Des 2005; 5: 2173–9.
44. Shiraiwa T, Ohki Y, Sado Y, Miyazaki H, Kurokawa H. Optical resolution by preferential crystallization of 4-methylpiperidinium hydrogen (RS)-phenylsuccinate. Chirality 1994; 6: 202–6.
45. Wilen SH. Resolving agents and resolutions in organic chemistry. Topics in Stereochemistry 1971; 6: 107–76.
46. Wilen SH. Tables of Resolving Agents and Optical Resolutions. South Bend, IN: University of Notre Dame Press, 1972.
47. Newman P. Optical Resolution Procedures for Chemical Compounds, in three volumes. Riverdale, NY: Optical Resolution Information Center, 1984.
48. Ugi I. Use of diastereomers avoids the ambiguities of the threo, erythro nomenclature. Z Naturforsch 1965; 20B: 405–21.
49. Shiraiwa T, Sado Y, Fujii S, Nakamura M, Kurokawa H. Optical resolution of (±)-phenylsuccinic acid by using (–)-proline as resolving agent. Bull Chem Soc Jap 1987; 60: 824–6.
50. Ingersoll AW, Babcock SH, Burns FB. Solubility relationships among optically isomeric salts. III. The mandelates and α-bromocamphor-π-sulfonates of α-phenylethyl mine and α-p-tolylethylamine. J Am Chem Soc 1933; 55: 411–16.
51. Valente EJ, Zubkowski J, Egglestron DS. Discrimination in eesolving aystems I: ephedrine-mandelic acid. Chirality 1992; 4: 494–504.
52. Valente EJ, Miller CW, Zubkowski J, Egglestron DS, Shui X. Discrimination in resolving Systems II: ephedrine-substituted mandelic acids. Chirality 1995; 7: 652–76.
53. Hiramatsu H, Okamura K, Tsujioka I, Yamada S-I, Yoshioka R. Crystal structure–solubility relationships in optical resolution by diastereomeric salt formation of DL-phenylglycine with (1S)-(+)-camphor-10-sulfonic acid. J Chem Soc Perkin Trans 2000; 2: 2121–8.
54. Yoshioka R, Ohtsuki O, Da-Te T, Okamura K, Senuma M. Optical resolution, characterization, and X-ray crystal structures of diastereomeric salts of chiral amino acids with (S)-(–)-1-phenylethanesulfonic acid. Bull Chem Soc Jap 1994; 67: 3012–20.
55. Acs M, Novotny-Bregger E, Simon K, Argay G. Structural aspects of optical resolutions. Optical resolution of (R,S)-mandelic acid. DSC and X-ray studies of the diastereoisomeric salts. J Chem Soc Perkin Trans 1992; 2: 2011–17.
56. Brianso MC. Structures atomiques et moléculaires des sels diastéréoisomères des α-phényl-α-méthylacétates d'α-phényl-éthylammonium p et n. Acta Cryst 1976; B32: 3040–5.
57. Lopez de Diego H. Crystal structure of (S)-1-phenylethylammonium (R)-mandelate and a comparison of diastereomeric mandelate salts of 1-phenylethylamine. Acta Chem Scand 1994; 48: 306–11.
58. Jacques J, Leclercq M, Brienne M-J. La formation de sels augmente-t-elle la fréquence des dédoublements spontanés. Tetrahedron 1981; 37: 1727–33.
59. Kozma D, Böcskei Z, Simon K, Fogassy E. Racemic compound formation-conglomerate formation. Part 1. Structural and thermoanalytical study of hydrogen manonate, hydrogen phthalate, and hydrogen succinate of α-phenylethylamine. J Chem Soc Perkin Trans 1994; 2, 1883–6.
60. Böcskei Z, Kassai C, Simon K, Fogassy E, Kozma D. Racemic compound formation-conglomerate formation. Part 3. Investigation of the acidic salts of α-phenylethylamine by achiral dicarboxylic acids. Optical resolution by preferential crystallization and a structural study of (R)-α-phenylethylammonium hydrogen itaconate. J Chem Soc Perkin Trans 1996; 2: 1511–15.

61. Freer AA, Bunyan JM, Shankland N, Sheen DB. Structure of (S)-(+)-ibuprofen. Acta Cryst 1993; C49: 1378–80.
62. Shankland N, Wilson CC, Florence AJ, Cox PJ. Refinement of ibuprofen at 100 K by single-crystal pulsed neutron diffraction. Acta Cryst 1997; C53: 951–4.
63. Dwivedi SK, Sattari S, Jamali F, Mitchell AG. ibuprofen racemate and enantiomers: phase diagram, solubility, and thermodynamic studies. Int J Pharm 1992; 87: 95–104.
64. Effers EJ, Plum BJ, Ariaans GJA, et al. New Resolving Bases for Ibuprofen and Mandelic Acid: Qualification by Binary Phase Diagrams. Tetrahedron: Assymmetry 1997; 8: 4047–57.
65. Prankerd RJ. Critical compilation of pKa values for pharmaceutical substances, in Profiles of Drug Substances, Excipients, and Related Methodology, volume 33. In: Brittain HG, ed. Amsterdam: Elsevier-Academic Press, 2007: 221.
66. Brittain HG. Unpublished results.

16 Amorphous Solids

Lynne S. Taylor

Department of Industrial and Physical Pharmacy, School of Pharmacy and Pharmaceutical Sciences, Purdue University, West Lafayette, Indiana, U.S.A.

Sheri L. Shamblin

Pfizer Global Research and Development, Pfizer, Inc., Groton, Connecticut, U.S.A.

INTRODUCTION

Amorphous solids are an integral part of pharmaceutical research and development, and thus, an understanding of amorphous solids in relation to crystalline solids and liquids is essential. This is self-evident when a drug is intentionally made amorphous to increase bioavailability, or an amorphous polymer or excipient is purposely incorporated into a pharmaceutical product to provide elegance, and improve performance or stability. What may be less obvious is the potential for amorphous solids to be formed during processing of drugs and excipient into dosage forms, or for amorphous regions to exist in nominally crystalline materials. This requires an understanding of the how amorphous materials can be formed, the persistence of any amorphous solids during manufacturing, and the potential for subsequent physical or chemical change during storage.

Historically, the majority of marketed amorphous products were those produced by freeze drying and intended for parenteral administration. In recent years, there has been an increase in the number of oral dosage forms containing the drug in the amorphous form, mainly as a means to improve bioavailability, and examples are listed in Table 1.

The importance of the amorphous state to pharmaceutical development, either by design or as a result of its unintentional presence, is increasingly being recognized, and this has fueled considerable research effort. Pharmaceutical research in this area has been aided by the fact that amorphous solids are very important in metallurgy, polymer science, food science, cryobiology, and ceramics among others. Many of the concepts developed in other fields have been translated to pharmaceutical materials, although it should be recognized that a number of key differences exist between many of the aforementioned classes of materials and small molecule organic amorphous solids. An understanding of the important differences between pharmaceutical amorphous materials and other well-characterized classes of materials (e.g., polymer, metals, ionic glasses) has been the focus of much of the research conducted with pharmaceutical amorphous solids. Amorphous solids have very different properties from their crystalline counterparts, and a review of the structure and thermodynamics of amorphous materials is provided in the next section.

TABLE 1 Examples of Products Containing Drug Substance in Its Amorphous Form

Product	Drug substance	Reason for amorphous form
Accolate	Zafirlukast	Bioavailability
Cefetin	Cefuroxime axetil	Bioavailability
Mefoxin	Cefoxitin	Dissolution (sterile) (USP)
Accupril	Quinapril HCl	Unstable solvate
Rezulin	Troglitazone	Bioavailability
Sporanox	Itraconazole	Bioavailability
Intelence	Etravirine	Bioavailability
Indocin	Indomethacin	Biavailability (PDR)
Pancrease MT	Pancrelipase	Does not crystallize, peptide (PDR)
Erythromycin ethylsuccinate	Erythromycin ethylsuccinate	Bioavailability (USP)
Singulair	Montelukast sodium	Unknown (PDR)
Viracept	Nelfinavir	Bioavailability
Kaletra	Lopinavir/ritonavir	Bioavailability

Source: Taken from Ref. (1) and the current United States Pharmacopeia–National Formulary (USP31-NF26) and Physician's Desk Reference (PDR).

THE AMORPHOUS STATE AS A CONDENSED PHASE

In common with crystalline solids and liquids, amorphous materials fall into the category of condensed phases. In general terms, their ability to demonstrate both liquid-like and solid-like behavior is what makes amorphous materials of interest pharmaceutically. In the simplest terms, it is temperature that controls the properties of the amorphous state. The relationship between temperature and the molecular structure and macroscopic properties of amorphous solids is central to understanding the unique properties of these materials, and under what circumstances an amorphous material can be compared to a solid or a liquid. The importance of temperature to the macroscopic behavior and the underlying molecular level structure will be addressed in much greater depth throughout this chapter.

The feature that distinguishes the amorphous "solid" from a crystalline solid is the absence of repeat three-dimensional order that persists over long length scales (i.e., many, many molecules). Amorphous solids do show short-range order (2), and in many cases the short-range order is similar to that seen in a liquid. Essentially, this means that nearest neighbor interactions are maximized in the amorphous solid where possible, to obtain a local minimum in the free energy. The short-range order found in amorphous substances stems from packing of the molecules to form nearest neighbor interactions through van der Waals interactions, hydrogen bonding, or electrostatic interactions, and the local packing may or may not be similar to the short-range order found in the crystalline counterpart. The locally favored structure is not periodic over long distances. Thus, amorphous materials are isotropic over longer length scales, whereas most organic crystals display directionally dependent properties as a result of their three-dimensional order.

Accompanying the more random arrangement of molecules in amorphous materials is a higher free volume compared to a crystalline solid. Free volume can be determined quantitatively by the difference in the total volume and the molecular volume as defined using van der Waals radii. For an amorphous material, greater

	Crystalline solid	Amorphous	Liquid	Gas
Molecular order		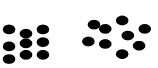		
	Short and long range	Short range	Short range	none
Specific volume	increasing →			
Molecular mobility	increasing →			

FIGURE 1 Comparison of molecular order, specific volume, and molecular mobility in different phases.

free volume translates to molecular motions that are otherwise restricted in a crystalline solid. It is this greater free volume and enhanced molecular mobility that leads to liquid-like behavior in an amorphous solid at temperatures well below the crystal-to-liquid transition temperature (T_m).

A summary of how the nearest neighbor interactions, molecular order, and free volume for an amorphous solid compare and contrast to other condensed phases (crystals and liquids) and the gas phase is provided in Figure 1. The combination of some nearest neighbor interactions, absence of long-range molecular order, and a greater free volume and higher molecular mobility play a very important role in determining the macroscopic properties that are unique to an amorphous solid. For example, the viscosity, mechanical strength, and even color can be distinctly different for the amorphous form compared to the crystal or liquid forms.

THE GLASS TRANSITION

Amorphous solids undergo a unique transition, the glass transition (glass-to-supercooled liquid), which distinguishes them from crystalline solids that undergo a melt transition (crystal-to-liquid). This transition is important because it indicates the temperature range where the amorphous material transitions from a rigid, brittle glass (e.g., glass bead) to one that resembles a very viscous liquid (e.g., molten lava or asphalt on a warm day). Below T_g, the amorphous solid is called a glass, and above T_g, it is a supercooled liquid. The glass transition is reversible, and therefore occurs during heating of the glass, or during cooling of a supercooled liquid. Macroscopic and thermodynamic properties such as viscosity, mechanical strength, enthalpy, and volume, undergo distinctive changes in the region of the glass transition. These changes are indicative of differences in the modes of molecular motion that are accessible in these two temperature regimes. Above T_g, modes of motion that require diffusion of a molecular segment or entire molecules are increasingly more accessible with increasing free volume. For polymers, these are the molecular motions associated with polymer backbone mobility, or the α-relaxation processes. Such motions are typically restricted below T_g. In the glass, the modes of molecular motions are usually restricted to vibration, rotation, and diffusion through rotation. The motions that persist below T_g in polymeric glasses are primarily due to motions in the side chains, with little or no contribution from the polymer main chain.

In polymers these molecular motions have been referred to collectively as the β-relaxation process (3,4). Although the classification of modes of molecular motions as α and β in different temperature regimes has its origin in the characterization of the molecular dynamics in polymers, the glass transition represent a distinction between very subtle but important modes of motion below T_g, and those above T_g leading to diffusion.

Glass formation, also called vitrification, occurs during cooling of an equilibrium supercooled liquid when molecular rearrangement in response to decreasing temperature is no longer possible. With decreasing temperature the modes of molecular motions are increasingly restricted, leading to the eventual "freezing in" of a structure and configuration that no longer represents an equilibrium state. With continued cooling below T_g, the nearest neighbor interactions do not represent the lowest free energy possible for a supercooled liquid, and the free volume is greater than expected for an equilibrium supercooled liquid. The glass transition represents a point where the time scales for molecular motion coincide with and eventually exceed the rate of cooling. Therefore, the temperature where this transition occurs depends on the rate of cooling.

Very fast cooling will yield a higher glass transition temperature than slower cooling of the same supercooled liquid, as has been illustrated schematically in Figure 2. This sensitivity of T_g to cooling rate, or the time scale of measurement means that T_g values measured using different experimental techniques can be different. The glass transition measured using dilatometry, calorimetry, or nuclear magnetic resonance (NMR) spectroscopy will be different due to the sensitivity of these techniques to different modes of motions that require a unique length of time to take place. This characteristic time for a particular motion, or collection of motions is sometimes referred to as the time scale for molecular motion or the characteristic relaxation time. Because T_g represents a coincidence of the time scales of molecular

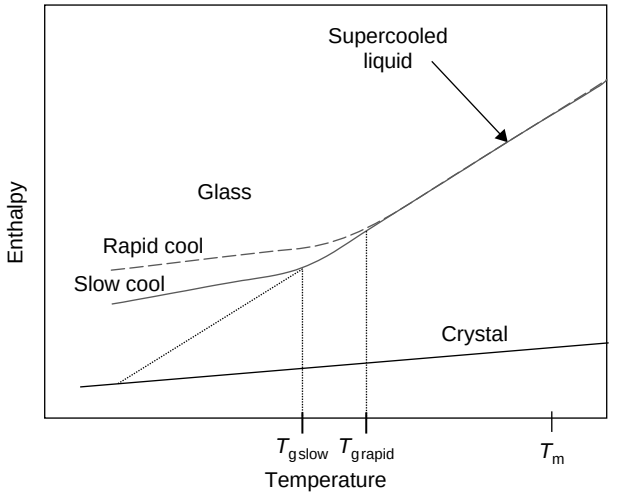

FIGURE 2 The dependence of the glass transition on cooling rate.

motion and the time scale detected by the experiment, it is appropriate to think about the glass transition as a "region" of temperatures, rather than a single temperature.

The glass transition can be measured by heating a glass, or cooling a supercooled liquid. One of the most common techniques used to measure the glass transition in pharmaceutical systems is differential scanning calorimetry (DSC) (5,6). Because non-isothermal calorimeters are optimized for measurement of thermal events during heating, T_g values determined by DSC are usually measured during heating. Measurement of T_g using DSC at a heating rate of 10°C/min has been equated to a time scales for molecular motion on the order of several hundred seconds based on the concept of the "coincidence" of molecular motion and experimental time scale. Comparisons of the viscosity at temperatures close to the T_g values measured by DSC suggest that T_g is an "isoviscous" state within the range of 10^{10} to 10^{12} Pa s (7). DSC is only one of many techniques for measuring T_g, and is commonly used for pharmaceutical materials because of the availability in many academic and industrial laboratories. The use of different techniques for measuring molecular mobility will be discussed later in this chapter.

THERMODYNAMICS

The absence of long-range molecular order in amorphous solids translates to a greater free energy in comparison to a crystalline reference state (Fig. 3). As a liquid is cooled below the melt temperature, there is a reduction in volume and degree of molecular motion as expected, as governed by the thermal expansion coefficient unique to the supercooled liquid. When the rate of cooling exceeds the rate of molecular rearrangement necessary to maintain the thermodynamic properties consistent with the supercooled liquid, a glass is formed. The sudden loss of certain modes of molecular motion at T_g leads to a change in the temperature dependence

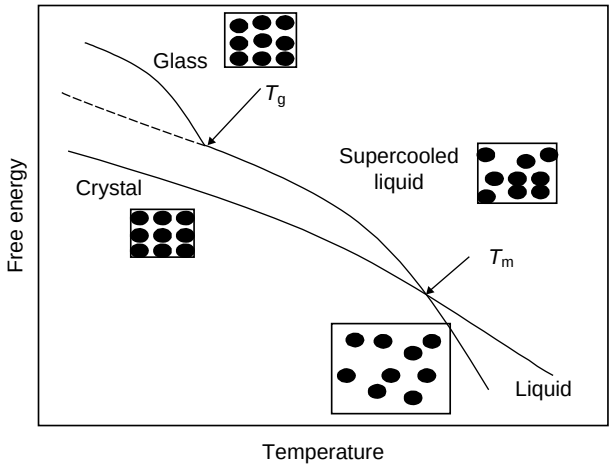

FIGURE 3 Free energy of the amorphous state in comparison to a crystal, including the supercooled liquid and glass regions.

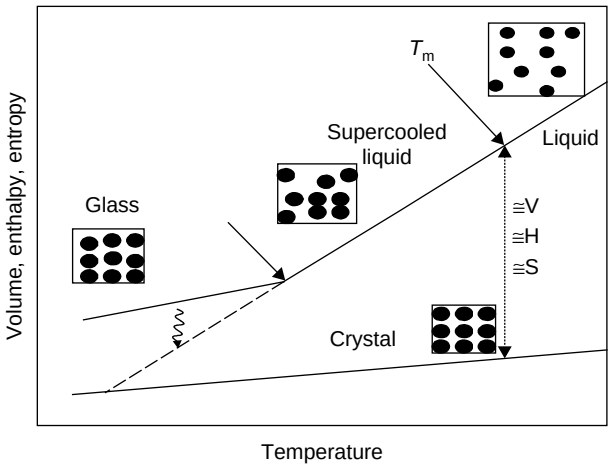

FIGURE 4 Volume, enthalpy, and entropy of the amorphous state in comparison to a crystal, including the supercooled liquid and glass regions.

of the thermodynamic functions of volume, enthalpy, and entropy as shown in Figure 4. Because this transition has a kinetic component (it depends on how it is measured) to the divergence of enthalpy, entropy, and volume at the glass transition, T_g is often referred to as a "pseudo" second-order phase change. Unlike a first-order phase transition (e.g., crystal-to-liquid), which by definition has discontinuous change in the aforementioned thermodynamic properties at the transition, the enthalpy is continuous for a second-order phase transition (Fig. 4). The continuity in the thermodynamic properties such as enthalpy, entropy, and volume at the glass transition temperature is important to its measurement using DSC and dilatometry. At the glass transition, the thermodynamic properties obtained by taking the second derivative of free energy (heat capacity and thermal expansion) are discontinuous, as shown in Figure 5.

Below T_g, the thermodynamic properties of the glass are in excess of those of the crystal and the theoretical supercooled liquid that was obtained by cooling infinitely slowly to maintain equilibrium. The enthalpy for a theoretical supercooled liquid that remains in equilibrium below T_g is shown in Figure 5 as the dashed line, which is simply an extrapolation of the thermodynamic properties of a supercooled liquid in a temperature region where equilibrium is possible. Even though the glass is very solid-like with respect to its viscosity and mechanical properties, there is sufficient free volume such as to allow molecular motions that enable molecular rearrangements. Over time, these rearrangements lead to structural relaxation of the glass to a lower free energy state approaching that of the infinitely slowly cooled supercooled liquid. The excess or "free" volume available in the amorphous solid is reflected by the higher specific volume of the amorphous form in comparison to the crystal (8,9) as shown in Table 2.

The process by which a glass transforms toward a more energetically favorable state is called structural relaxation. Thus, strictly speaking, a thermodynamic description of a glass is not possible due to the time-dependent nature of the glass

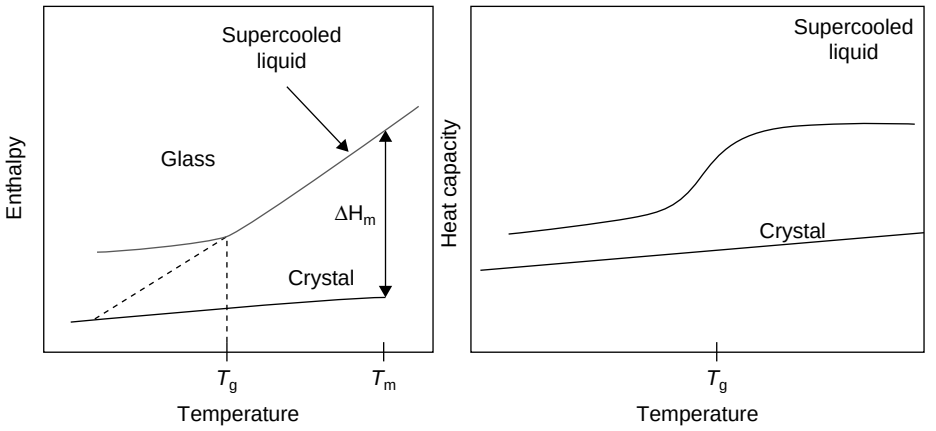

FIGURE 5 The enthalpy and heat capacity measured by DSC as a function of temperature in the region of the glass transition temperature.

TABLE 2 Differences in Specific Volumes of Crystalline and Amorphous Forms

Material	Crystal-specific volume (mL/g)	Amorphous-specific volume (mL/g)	Excess volume in amorphous form (%)
Indomethacin	0.72	0.75	4.0
Sucrose	0.63	0.7	10.0
Trehalose	0.62	0.68	8.8
Drug "a"	0.75	0.76	1.5

resulting from the evolution to a more energetically favorable state. Although both the glass and supercooled liquid are non-equilibrium states relative to the crystal, above T_g, the supercooled liquid is still ergodic. For an ergodic system, the time and space distributions averaged over time are equal; thus, an ergodic system is effectively "unchanged" over time. In contrast, the glass is transitional and non-ergodic. The changes in time and space at the molecular level are reflected thermodynamically by decreases in enthalpy and volume. These changes in the thermodynamic properties can be detected experimentally and used to provide a more accurate thermodynamic description of the non-ergodic glassy state. One such approach is the concept of fictive temperature, T_f, which defines a non-ergodic glass in terms of the supercooled liquid. The supercooled liquid, although only theoretically possible at temperatures below T_g, serves as an unchanging or erogodic reference state.

Another complexity in a thermodynamic description of the amorphous state is the observation that the extrapolation of the entropy of the equilibrium supercooled liquid to lower temperatures eventually leads to a value equal to that of the crystal (Fig. 4). Further extrapolation of the entropy of the theoretical supercooled liquid would violate the Second Law of Thermodynamics. This violation occurs

with the implication that the supercooled liquid would be lower in entropy than the thermodynamically most stable crystalline form. The temperature where this theoretical thermodynamic crisis occurs is called the Kauzmann temperature, T_K, after Kauzmann who first recognized this dilemma (10). The so-called Kauzmann Paradox has been reconciled by invoking the T_K as the true T_g, a second-order transition that prevents thermodynamic crisis in the theoretical supercooled liquid formed with infinitely slow cooling. Although the origin of the Kauzmann temperature is based on thermodynamics, it has provided the basis for a kinetic interpretation of the temperature where the enhanced molecular mobility in an amorphous material is no longer present. One final note, the ability to cool slowly enough to produce an ergodic liquid at temperatures near T_K, and so far below the crystal-liquid transition, is nearly impossible in practice. However, because a thermodynamic description of a glass depends somewhat on the thermodynamic properties of the theoretical supercooled liquid, this thermodynamic impossibility has been widely discussed and debated in attempt to reconcile the problem.

The time-dependent nature of glasses below T_g has important implications for pharmaceutical product quality and elegance, such as cracking or crazing in film coatings and shrinkage of lyophilized cakes. The measurement of structural relaxation as a measure of molecular mobility will be discussed in more detail later within this chapter.

THE MEANING OF SOLUBILITY FOR AMORPHOUS SOLIDS

The excess thermodynamic properties of amorphous solids discussed above explain why the dissolution of an amorphous solid frequently leads to a higher solution concentration than that obtained for a corresponding crystalline solid. The amorphous solid is characterized by less favorable cohesive intermolecular interactions, and therefore dissolves more readily. If the resulting solution concentration is higher than the equilibrium solubility of a crystal form, the solution is said to be supersaturated with respect to that phase, and there is a thermodynamic driving force for crystallization. Although low levels of supersaturation can often be maintained for long time periods, above a certain threshold concentration, nucleation and crystal growth will occur, resulting in depletion of the solution concentration until the thermodynamic solubility is reached.

Just as a true thermodynamic description of the amorphous state is not possible, the equilibrium solubility for an amorphous solid cannot be measured. However, various approaches, each involving certain assumptions, can be used to approximate the theoretical maximum solution concentration. Predictions of amorphous "solubility" are based on estimations of the free energy difference between the amorphous and crystalline solids, ΔG_c, which in turn, can be related to the amorphous:crystalline solubility ratio as shown in equation (1). Thus, it is necessary to know the solubility of the crystalline phase.

$$\Delta G_c = RT \ln \frac{a_{\text{amorphous}}}{a_{\text{crystalline}}} \approx RT \ln \frac{S_{\text{amorphous}}}{S_{\text{crystalline}}} \tag{1}$$

where R is the gas constant, T is temperature, a is the activity, and S is solubility. Depending on the level of rigor required, various methods are available to estimate

ΔG_c. For example, if the melting temperature (T_m) and heat of fusion of the crystalline form (ΔH_f) are known, the Hoffman equation [equation (2)] can be used.

$$\Delta G_c = \Delta H_f \frac{(T_m - T)T}{T_m^2} \tag{2}$$

It is important to realize that using the amorphous form to enhance solubility can be a double-edged sword in that the higher the amorphous:crystalline solubility ratio (and hence the greater the potential advantage), the greater the thermodynamic driving force for crystallization and the higher the probability of drug substance crystallization. Thus, although dissolution rate advantages are frequently seen for amorphous systems, these are not always of the expected magnitude due to drug substance recrystallization from solution (11,12). An example of a dissolution profile of an amorphous solid is shown in Figure 6. The solution concentration initially increases with time, reaches a maximum, and then decreases toward the equilibrium solution concentration of the stable crystalline form. The decrease in solution concentration can be accounted for by crystallization.

In addition to drug substance recrystallization from the supersaturated solution generated by dissolution of the amorphous solid, the amorphous solid itself can recrystallize. On contact with the dissolution medium, water will be absorbed into the amorphous matrix and will increase molecular mobility. The increased molecular mobility will favor crystallization of the hydrated amorphous solid. As a result of crystallization from either the solution phase or from the amorphous solid, it is

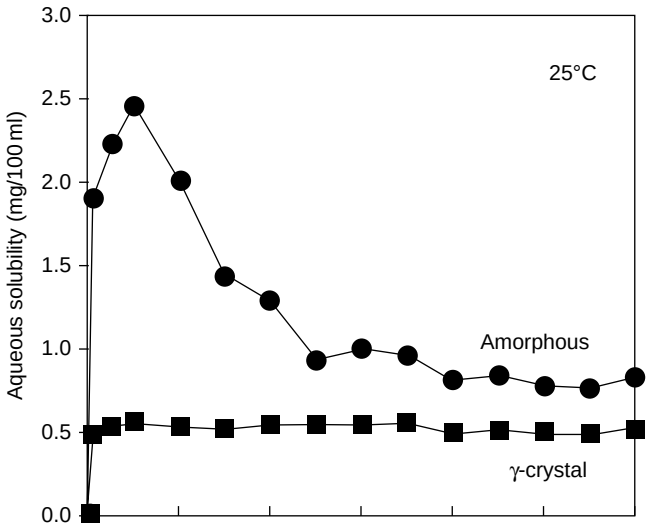

FIGURE 6 Solution concentration versus time profile for amorphous indomethacin compared to the thermodynamically stable crystal form. Figure adapted from Ref. (12) and reproduced with kind permission of Springer Science and Business Media.

very difficult to reproducibly measure the solution concentration generated by an amorphous solid, and the experimentally measured value may be very different from predicted values. Figure 7 shows the predicted and measured solution concentrations for three amorphous solids, and illustrates that the measured values are substantially lower than the predicted values for the reasons discussed above.

MATERIAL AND MECHANICAL PROPERTIES

Like crystalline materials, the mechanical and material properties of amorphous materials will depend on the molecular level structure, as well as macroscopic properties such as particle size. When defined in rheological terms, amorphous materials are viscoelastic, consistent with the ability to behave both like an elastic solid and a viscous liquid. The ability for an amorphous material to flow in response to an applied stress reflects the molecular flexibility as a result of greater free volume and results in viscous behavior. However, unlike a strictly viscous liquid, amorphous materials can undergo a fast deformation and recovery process, or "push back," in response to an applied stress. This resistance to stress is a solid-like behavior and results from nearest neighbor interactions that are increasingly more important to the mechanical properties of the amorphous solid with decreasing temperature. Thus, the viscoelastic response of amorphous materials is very dependent on temperature. At higher temperatures, a greater degree of molecular mobility results in a more viscous response to applied stress. This ability to flow also leads to the higher ductility characteristic of many polymers above T_g. As temperatures approach T_g the restriction of molecular motion translates to a resistance to flow in response to applied stress. Thus, below T_g the glass is more "elastic" than "viscous" in comparison to the same material at higher temperatures. With decreasing temperature and a reduction in molecular motion, an amorphous material also becomes more brittle.

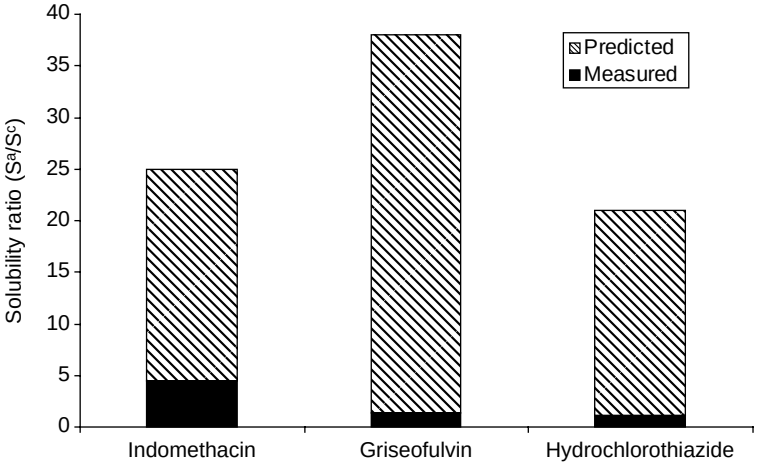

FIGURE 7 Comparison of the predicted amorphous:crystalline solubility ratio with that experimentally observed. The plots were constructed from data originally presented in Ref. (12).

Below T_g, an amorphous material will be more brittle and more solid-like (resist flow in response to applied stress) than the same solid above T_g, but less brittle and more likely to flow under applied stress than a crystalline material.

Although the molecular order and mobility are important to the mechanical and rheological performance of a condensed phase, particle properties are also extremely important to the behavior of powders, even for amorphous materials. For example, a direct comparison of the dynamic indentation hardness and tensile strength of amorphous and crystalline forms of a drug substance showed that the amorphous form below T_g was the more solid-like, more brittle, and less ductile of the two (8). It is likely that differences in the mean particle sizes, particle size distributions, bulk specific volumes, or specific surface areas lead to differences in the mechanical properties of the two forms, but not differences at the molecular level (i.e., mobility, free volume, degree of long-range order).

The unique mechanical properties of amorphous materials are relevant in many pharmaceutical applications. In comparison to crystalline or partially crystalline materials (e.g., microcrystalline cellulose) amorphous polymeric excipients are more ductile (13) and exhibit lower tensile strength during compression (14). Higher ductility may be needed to improve the compressibility of a very brittle drug, but may lead to a lower tensile strength. The integrity of film coatings is also related to the mechanical and rheological properties of the film-forming polymer. Reduction in the tendency of films to crack can be achieved by the addition of a plasticizer that increases molecular mobility and results in formation of a less brittle, more viscous-than-elastic film.

FORMATION OF AMORPHOUS SOLIDS

Amorphous solids may be formed intentionally by employing specific techniques such as spray drying or precipitation from solution, or unintentionally during various processing operations. Figure 8 provides an overview of different ways of making amorphous solids.

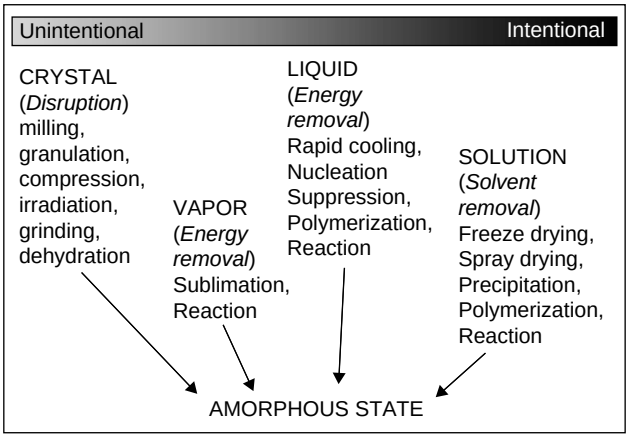

FIGURE 8 Schematic illustration of the different ways in which amorphous materials can be formed.

For freeze-dried products, the crystalline or amorphous nature of the product can sometimes be controlled through the freeze–drying cycle. Cooling of a drug solution below any eutectic melting temperatures and glass transition temperatures followed by drying at these temperatures will favor the formation of amorphous solids. The addition of crystallization inhibitors such as poly(vinylpyrrolidone) (PVP) or dextran will also increase the likelihood of producing amorphous material. For intentional production of solid dosage forms containing an amorphous drug, the two routes most generally employed are spray drying and melt extrusion. Critical parameters for both processes include the processing temperature, nature of the solvent, rate of solvent removal, and the use of polymeric crystallization inhibitors. When attempting to generate amorphous materials for characterization and assessment, the most common methods are melt quenching for heat-stable compounds, freeze drying for water soluble compounds, and spray drying or precipitation for compounds soluble in organic solvents.

In terms of unintentional production of amorphous material during processing operations, the following routes are possible. First, if the crystalline material dissolves to any extent in a processing solvent, then recrystallization may not occur on drying, particularly if there are excipients present that act as crystallization inhibitors. For example, water-soluble compounds can dissolve during aqueous granulation, and recrystallization may not occur following drying, particularly if polymeric additives used as binders are effective crystallization inhibitors (15). Second, a hydrate or a solvate may be dehydrated during processing, leading to an amorphous compound. Examples of hydrates/solvates that can form amorphous solids following desolvation include raffinose pentahydrate (16), trehalose dihydrate (17), and carbamazepine dihydrate (18).

Third, disproportionation of salts on exposure to aqueous conditions can lead to precipitation of the amorphous form of the unionized compound. For example, it was observed that when the hydrochloride salt of an experimental compound was subjected to aqueous wet granulation, partial conversion to the amorphous free base occurred (19). Fourth, high energy processes such as milling and micronization can generate disordered material. The level of disorder introduced by comminution processes can be small and difficult to detect, although it can have a profound impact on powder properties and chemical stability. It was noted that that micronization of albuterol sulfate followed by storage at moderate relative humidities resulted in agglomeration of particles as a result of crystal bridges formed following recrystallization of amorphous domains (20).

For many compounds, a high degree of disorder is produced by comminution processes, and samples can become X-ray amorphous following grinding or milling. Examples include indomethacin (21), sucrose (9), digoxin (22), and ursodeoxycholic acid (23). Because it is well recognized that some materials form and remain as amorphous solids more easily than others, factors affecting glass forming ability and glass stability will be discussed below.

FACTORS INFLUENCING GLASS-FORMING ABILITY

It is well known that some compounds more easily form amorphous solids than do others. Thus, some compounds crystallize on cooling from a melt, whereas others do not and form amorphous solid in the process. Likewise, some compounds are amorphous after spray drying, whereas others are crystalline. In principle, it is possible to

make any heat-stable compound amorphous if it can be cooled from the melt faster than the time frame required for crystallization. However, if the required cooling rate is higher than experimentally attainable, a crystalline solid will result. An example of a system that crystallizes with slow cooling, but which can be made amorphous with rapid cooling, is shown in Figure 9, where DSC thermograms of carbamazepine are shown. The sample was heated to its melting point, and then cooled either slowly (2°C/min) or rapidly (20°C/min). The slowly cooled sample crystallized during cooling, as evidenced by an exothermic event during the cooling cycle and an absence of a glass transition event during heating. In contrast, the fast-cooled sample does not have any exothermic events during cooling, and has a glass transition event during reheating, indicating that it was cooled sufficiently fast to avoid crystallization.

The viscosity of a material at its melting temperature, and the rate of increase in the viscosity with decreasing temperature, are important material properties that will also influence glass-forming ability (24,25). A liquid with a high viscosity will have a greater kinetic barrier to nucleation and crystal growth. However, the thermodynamic barriers to nucleation and crystal growth are also important factors, and will also influence the crystallization tendency. It has been suggested that liquids with short range order very different from the nearest neighbor interactions in the crystal will be more resistant to crystallization (25,26). Likewise, molecules with a high configurational entropy would also be expected to be more resistant to crystallization (27).

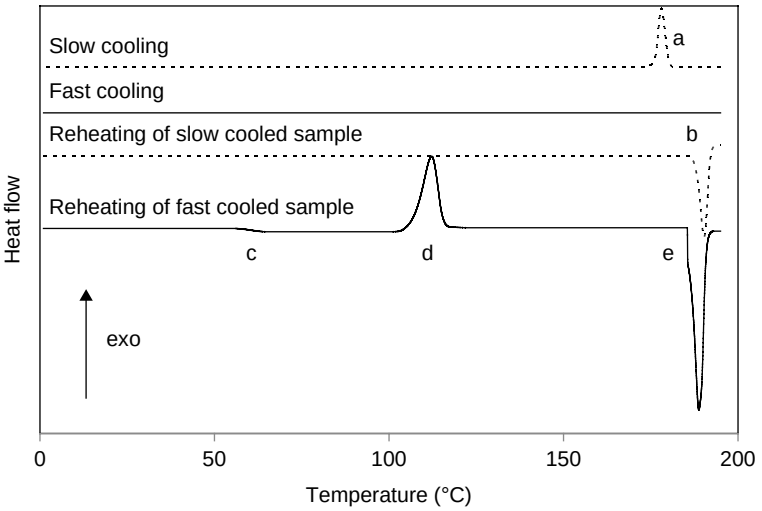

FIGURE 9 Dependence of carbamazepine crystallization behavior on cooling rate as measured using DSC. A sample cooled slowly from the melt shows a crystallization exotherm during the cooling cycle (event a). When this sample is reheated, the crystallized solid melts (event b). A sample cooled at a faster rate does not show an exothermic crystallization event. When the fast cooled sample is reheated, a T_g event is seen (event c) followed by a recrystallization endotherm (event d) and melting of the crystallized material (event e). The slow cooling rate was 2°C/min and the fast cooling rate was 20°C/min.

When considering glass-forming ability, it has been observed that the $T_g/T_m \approx 2/3$ "rule" holds for many pharmaceutical compounds, where this ratio has consistently been found to be between 0.65 and 0.8 for glass-forming pharmaceutical systems. However, it has been argued that this "rule" only holds because substances with high values of T_g/T_m do not crystallize (T_m cannot be measured), and substances with low values of T_g/T_m do not form a glass (T_g cannot be measured); thus, any values that can be measured will fall within a certain range (24). Although this "rule" is empirically based, it provides a useful means to estimate the expected temperature range for a glass transition event based on the melting point of the crystalline counterpart.

Although it is perhaps intuitive that compounds that do not readily form glasses will also crystallize more rapidly from the glassy state, very little data exists to support this idea, particularly for organic systems. Clearly, this would be an important link to establish because glass-forming ability could then be used as a screening technique to assess the potential of a compound to remain as an amorphous solid. Factors influencing crystallization from amorphous solids are discussed in more detail later in this chapter.

METHODS FOR DETECTION AND CHARACTERIZATION OF AMORPHOUS SOLIDS

In this section, a brief overview of methods available to detect and characterize amorphous solids will be provided. A greater level of detail can be found elsewhere (9,28–31).

For pharmaceutical systems, DSC is typically the favored technique for determination of the glass transition temperature, although this parameter can also be measured with many other techniques including dielectric spectroscopy, thermally stimulated current spectroscopy, rheometry, and dynamic mechanical analysis. DSC is also used to assess other aspects of amorphous materials, including crystallization tendency and molecular mobility.

X-ray powder diffraction (XRPD) is frequently used to assess if a material is amorphous or crystalline. Because amorphous materials only have short-range order, X rays are scattered incoherently so that one observes only a characteristic halo pattern. The term "X-ray amorphous" is used to indicate the absence of detectable Bragg diffraction peaks; however, different disordered states may lead to incoherent scattering of X rays, so other techniques or a closer examination of the scattering data should be used to confirm the exact nature of the system (2). Currently, pharmaceutical applications of XRPD are increasing in sophistication with the use of peak broadening effects to determine crystallite size, and pairwise distribution functions to gain more insight into the structure in disordered materials (32). XRPD is also a very valuable technique to quantify the extent of crystallinity in a solid with sophisticated data analysis methods such as whole pattern fitting being employed to increase the sensitivity (33).

Solid-state NMR spectroscopy has been used with great success to interrogate molecular mobility in single component and multi-component amorphous solids (34,35), as well as for quantitation of amorphous material (36). Dielectric spectroscopy has also been used widely to study dynamics in glasses and supercooled liquids (37–39). Vibrational spectroscopy provides a means to probe intermolecular

interactions in amorphous materials (40), as well as for detection and quantification of amorphous content (41). Additional techniques found to be useful for detection and quantification of low levels of amorphous content include isothermal microcalorimetry (42–44) and vapor (either water or an organic solvent) sorption (9,45). More details about specific techniques will be given in later sections that deal specifically with the assessment of molecular mobility.

TEMPERATURE DEPENDENCE OF MOLECULAR MOBILITY

With increasing temperature, there is an increase in free volume, and hence, an increase in molecular mobility. The overall increase in molecular mobility reflects an increase in frequency for a particular type of motion (e.g., rotation about an axis) and an increase in the occurrence of motions that may have been restricted at lower temperatures (e.g., diffusion, polymer backbone mobility). In a normal liquid, above the crystal-to-liquid transition, the dependence of molecular motions, including diffusion, on temperature can be described in terms of an activated process. Thus, molecular mobility and processes dependent on molecular motion are well described by the Arrhenius equation. However, this is not the case for many amorphous materials, as illustrated in Figure 10, which shows the viscosity for the supercooled liquids that represent many classes of materials. The deviation from Arrhenius behavior has been called "fragile" behavior. In contrast to "strong" supercooled liquids, such as SiO_2, fragile liquids characteristically show more extreme changes in molecular structure and dynamics for a given change in temperature. The fragility of a supercooled liquid is a measure of the sensitivity of its structure and dynamics to thermal fluctuations. Fragile behavior has been explained by heterogeneity in the structure (and hence dynamics) inherent to many disordered system (46–48), and the need for cooperative motions of many molecules in highly viscous systems.

For many materials there appears to be a return to Arrhenius behavior in the glassy state (50,51). This is shown in Figure 11 as a sharp transition for the purpose of illustrating a point. In reality, this transition tends to be a more gradual return to an Arrhenius temperature dependence near and below T_g, as evidenced by measurements of ionic conductivity in glasses near T_g (50) and relaxation times in pharmaceutical glasses measured using solid-state NMR spectrometry (52).

Many mathematical descriptions of the non-Arrhenius temperature dependence of dynamic processes in supercooled liquids have been invoked, and vary greatly with respect to physical and theoretical significance. The Vogel–Tamman–Fulcher (VTF) equation [equation (3)] is one that is has been used most frequently to describe a given dynamic process.

$$\tau(T) = A\exp\left(\frac{DT_0}{T - T_0}\right) \tag{3}$$

This equation describes the relaxation time constant, τ, as a function of temperature in terms of three parameters, A, D, and T_0. The VTF equation has been ascribed physical meaning when the pre-exponential term A is assigned a value of ~10^{-14} seconds (which approximates the time scale for lattice vibrations), when D corresponds to the strength parameter, and when T_0 represents the temperature where a particular motion effectively ceases to occur. The strength parameter D is inversely related to fragility, with lower D values corresponding to more fragile behavior.

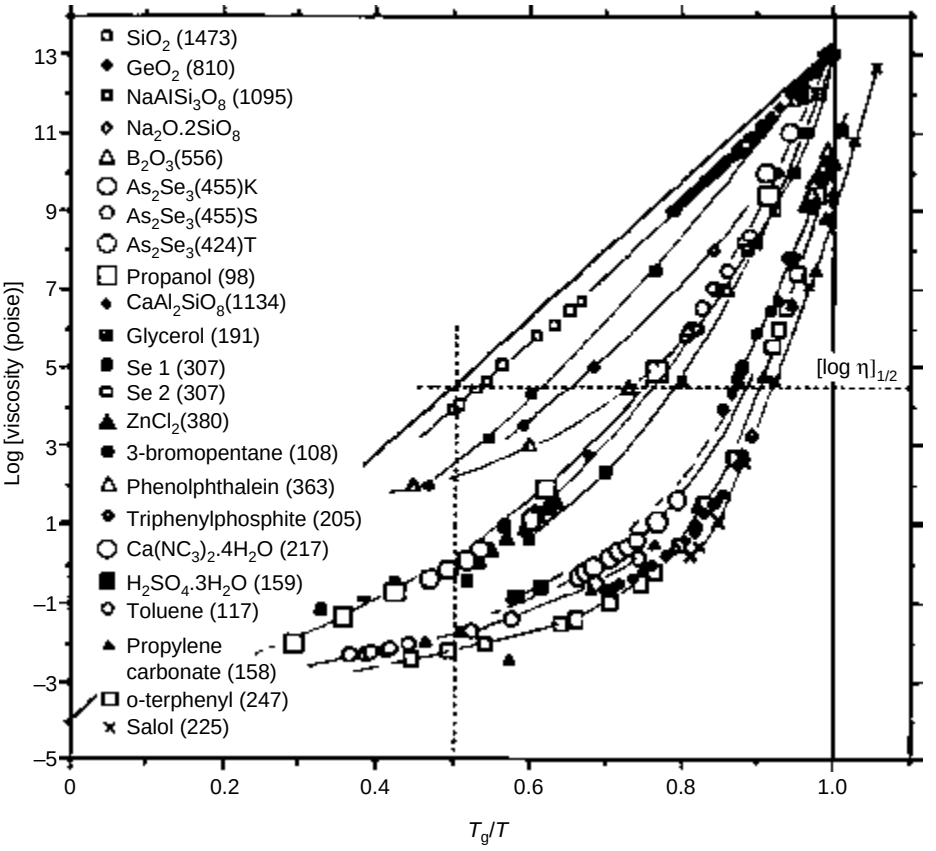

FIGURE 10 Range of temperature dependencies of viscosity on temperature for supercooled liquids. Figure reproduced from Ref. (49) with the kind permission of the Nature Publishing Group.

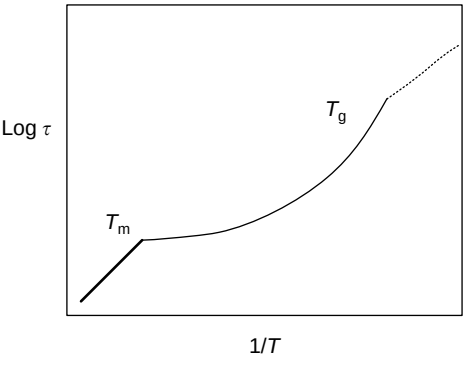

FIGURE 11 Schematic description of the relationship between relaxation time and temperature that is observed in amorphous materials.

The value of T_0 has been equated to the Kauzmann temperature, defined as the temperature where extrapolated thermodynamic properties of a supercooled liquid are equal to those for the crystal. The Kauzmann temperature, as described previously, is sometimes recognized as the true glass transition.

The VTF equation has been used to describe the temperature dependence of molecular motion in pharmaceutical amorphous solids (39,53,54), with D values typically ranging from 9 to 13, and values of T_0 that usually are 40 to 100 K below the calorimetric T_g. The temperature dependence of molecular motions and related macroscopic properties is very complex due to the heterogeneity in the structure and dynamics present in supercooled liquids and glasses. The spatial and temporal heterogeneity has important implications for establishing stability–temperature relationships in pharmaceutical drugs and excipients using accelerated temperature regimens. Over narrow ranges of temperatures, molecular mobility and processes that are dependent on molecular mobility may show an Arrhenius dependence on temperature. However, in studying molecular mobility, and physicochemical properties or processes that require molecular motion, the complex dependence of molecular mobility on temperature and time should be considered, and may require different approaches to assess pharmaceutical product quality and stability.

MEASUREMENT OF MOLECULAR MOBILITY

The time scales for molecular motion in amorphous materials have been characterized using a number of techniques. The most common techniques include measurement of viscosity, the use of solid-state NMR to obtain relaxation times (52,55–57), dielectric relaxation (38,58–60), and calorimetric measures of enthalpy relaxation (61–63). It is important to consider that the various experimental techniques measure different molecular motions that occur over very different time scales. Therefore, molecular mobility measurements must be considered in the context of the relaxation process being measured and caution applied when trying to compare data obtained with different techniques. Thus, the use of several experimental techniques is required to measure molecular motions that occur over a range of time scales (and temperatures). The potential for crystallization of the supercooled liquid is one of the challenges in measuring molecular mobility in amorphous solids, particularly above T_g. Thus, there is very limited data for pharmaceutically relevant amorphous solids.

TIME DEPENDENCE IN THE STRUCTURE AND DYNAMICS OF GLASSES

As discussed previously, a glass that is formed by very rapid cooling will have a higher T_g value. In addition, a glass formed by rapid cooling will have greater enthalpy and volume compared with one formed by slower cooling. This was illustrated in Figure 2, which shows the enthalpy and volume of glasses with different cooling rates in comparison to a theoretical supercooled liquid formed by very slow cooling. The tendency for any glass to evolve to a lower free energy state is accompanied by a reduction in enthalpy, volume, and the degree of molecular mobility over time (53). This process is called structural relaxation, and refers to collective molecular motions, which include rotation, rotational-diffusion, and some limited diffusion of molecules, leading to a more energetically favorable structure.

Structural relaxation has been studied in many pharmaceutical glasses using calorimetry, dielectric relaxation, and solid-state NMR. Measurements of molecular

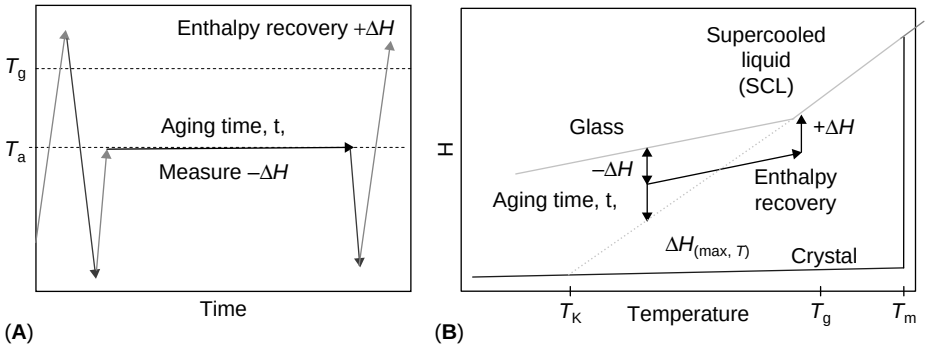

FIGURE 12 Schematic descriptions of (**A**) of the aging experiment used for measuring structural relaxation in glasses, and (**B**) the enthalpy loss accompanying structural relaxation during aging and the enthalpy recovery process of an aged glass during heating through T_g.

mobility in pharmaceutically relevant glasses have contributed to a broad understanding the molecular mobility below T_g, and have revealed the complexity in the molecular dynamics below T_g. Generally the temperature range that molecular mobility in glasses can be analyzed is limited to 40–50°C below T_g. Incidentally, this temperature limit for many materials is close to estimates of T_K. The limitation in the range of temperatures where glass dynamics can be measured is due primarily to eventual slowing down of motions and structural relaxation to the point that they cannot be detected over practical time scales.

A commonly used technique for measuring molecular mobility in glasses is the use of calorimetry to detect the loss in enthalpy that accompanies structural relaxation (62,63). As a macroscopic measure of molecular mobility this has limitations. Unlike solid-state NMR, which can focus on motions associated with specific chemical functionalities within a molecule, this technique captures the summation of many different modes of motion. However, the technique is straightforward, is able to distinguish between mobility in different materials, and uses readily available equipment. The loss in enthalpy during structural relaxation can be detected directly using a highly sensitive isothermal microcalorimeter (63,64), or indirectly using differential scanning calorimetry to measure enthalpy recovery following controlled aging of a newly formed glasses (62).

Knowing the thermal history of a glass is the first step in characterization of molecular dynamics and structure below T_g. Thermal history refers to the "conditioning" of a glass, whether done purposefully or unintentionally, and is a record of the exposure of the glass to different temperatures. A newly formed glass will have a faster rate of structural relaxation, or greater degree of molecular mobility compared to one that has a thermal history that includes some "aging." The purposeful aging of glasses has been important to understanding of structure and dynamics in glasses. Aging experiments begin with a freshly formed glass that is held isothermally for different lengths of time. A schematic representation of the aging experiment is shown in Figure 12. The loss in enthalpy can be monitored continually using isothermal calorimetry during the aging process. Alternatively, this loss in enthalpy is

measured by first cooling the aged glass to a low temperature to stop further relaxation, and then reheating through the glass transition to measure enthalpy recovery at T_g (Fig. 12B). The enthalpy "recovered" at T_g on heating is a close approximation of the enthalpy loss that occurred during aging of the glass. The rate of enthalpy loss, as measured by enthalpy recovery using DSC, is a measure of mobility below T_g.

The use of a DSC aging experiment, such as shown in Figure 12, to measure the enthalpy recovery, relies on the assumption that continued structural changes and further loss in enthalpy during quenching of an aged glass and subsequent heating to measure enthalpy recovery are minimal. The size of the endothermic peak observed during heating by DSC in the region of the glass transition is directly proportional to the enthalpy loss that occurred during aging, as shown in Figure 13. The change in enthalpy measured with time reflects the extent to which the newly formed glass evolved to a more relaxed glass, with properties more similar to a supercooled liquid.

The measurement of enthalpy changes associated with structural relaxation alone can detect relative differences for a single material as a function of thermal history, temperature, and time. However, more quantitative measures of mobility that also allow the comparison of the mobility to other materials are made possible by calculating structural relaxation times. Because of the complexity in the structure and dynamics of amorphous solids, relaxation processes are not exponential. Thus, the Kohlrausch–Williams–Watt (KWW) equation, which can describe non-exponential relaxation phenomena, must be employed. The KWW equation has two relaxation time constants, τ_{KWW} (the average relaxation time constant) and β (a parameter that accounts for the degree of non-exponentiality in the dynamics). These two parameters describe the relaxation of a glass as function time, t. The enthalpy changes in an aged glass, $\Delta H(t)$, like those detected by DSC as shown Figure 13, can be converted to a fractional extent of relaxation, ϕ, using equation (4). Here, the difference in enthalpy for the newly formed glass and that of the theoretical supercooled liquid

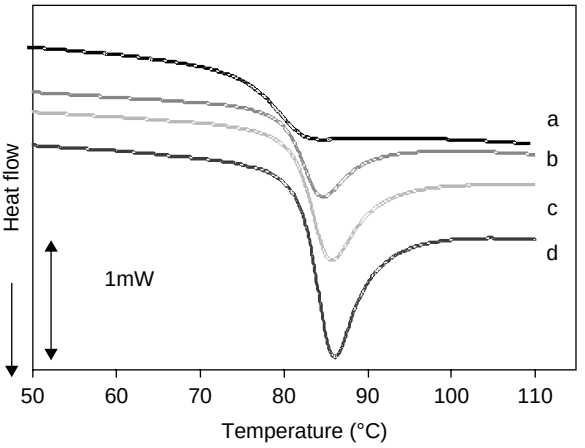

FIGURE 13 Enthalpy recovery for an aged glass as a function of aging time: a = initial, b = 2 hours, c = 8 hours, and d = 16 hours.

(ΔH_∞) is used to represent a fully relaxed state. Similar forms of the KWW equation have been used to determine relaxation times for dielectric relaxation (38,59).

$$\phi(t) = 1 - \left(\frac{\Delta H(t)}{\Delta H_\infty} \right) \approx \exp\left[-\left(\frac{t}{\tau_{KWW}} \right)^{\beta} \right] \tag{4}$$

The non-exponential behavior in amorphous solids is due in part to the spatial and dynamic heterogeneity of an ensemble of molecules. Thus, the two parameters in the KWW equation are a measure of the average time scale for molecular motion, τ_{KWW}, and the distribution of relaxation time as reflected in the value of β. The value of the β-term in KWW ranges from 0 to 1, and reflects a broader distribution as the number decreases from a value of unity. When β is equal to unity, the equation collapses to that describing an exponential relaxation, and suggests homogeneous molecular dynamics.

The use of aging experiments to measure structural relaxation, and to determine relaxation times, has been used extensively to understand the implication of these processes to the mechanical and rheological properties of polymers (3,7). Aging in polymeric glasses has been correlated to mechanical properties such as tensile strength. Studies with pharmaceutical polymers and drugs have also shown volume reduction associated with structural relaxation in an amorphous drug, indomethacin, below T_g (62). Systematic aging of glasses as a function of time and temperature can be used to compare the molecular mobility of different drugs and excipients (62,65,66), the difference between amorphous drug and a mixture of drug and polymer (67), and how the molecular mobility changes with time (53).

In the last decade there has been an effort to study molecular mobility in amorphous materials, including the structural relaxation behavior in glasses in an attempt to understand the tendencies for crystallization and enhanced chemical reactivity in amorphous systems. While the correlation of macroscopic measures of mobility, such as the enthalpy and volume changes associated with structural relaxation, to processes such as film shrinkage or cake collapse may be somewhat straightforward, this may not be the case with the more complex processes of crystallization and chemical reactivity. The molecular motions that are required for both crystallization and chemical reactivity are likely to be more subtle in nature compared to those that contribute to the mechanical and rheological properties (68,69) Furthermore, there are other factors that may be equally or more important to chemical reactivity and crystallization than simply the types and degrees of molecular motions. The crystallization and chemical reactivity of amorphous systems, including the role that molecular mobility plays in these processes, will be discussed in more depth later in this chapter.

CRYSTALLIZATION FROM AMORPHOUS SOLIDS: THEORETICAL ASPECTS

A major concern for amorphous drugs is their tendency to crystallize when heated, when exposed to high relative humidities, or when simply stored for long periods of time. The thermodynamic driving force for crystallization from an amorphous solid arises from the higher free energy of the amorphous system relative to that of the crystal for all temperatures lower than the equilibrium melting point. This driving force increases with the degree of undercooling; thus, the further from the crystal

melting temperature, the greater the driving force for crystallization. The difference in Gibbs free energy between the supercooled liquid and crystalline phases, ΔG, is given by equation (5):

$$\Delta G(T) = \Delta H(T) - T\Delta S(T) \tag{5}$$

and can be estimated at a particular temperature from the enthalpy of fusion (ΔH_{fus}), the entropy of fusion (ΔS_{fus}), the melting temperature, T_m, and ΔC_p, the heat capacity difference between the supercooled liquid and the crystal (i.e., $C_p^l - C_p^c$), as a function of temperature as shown in equations (6) and (7).

$$\Delta H(T) = \Delta H_{fus} + \int_{T_m}^{T} \Delta C_p \mathrm{d}T \tag{6}$$

$$\Delta S(T) = \Delta S_{fus} + \int_{T_m}^{T} \frac{\Delta C_p}{T} \mathrm{d}T \tag{7}$$

When heat capacity data is not available, equations such as the Hoffman equation (70) [equation (2), discussed earlier] can be used to approximate ΔG at a given temperature.

Figure 14 shows how the thermodynamic driving force changes as a function of temperature for felodipine and nifedipine, as calculated using either the Hoffman equation or by using the heat capacity differences between the liquid and the crystal in conjunction with equations (5) to (7) (68). It is apparent from Figure 14 that nifedipine has a larger driving force for crystallization and that the driving force increases as the temperature decreases below the crystal melting point.

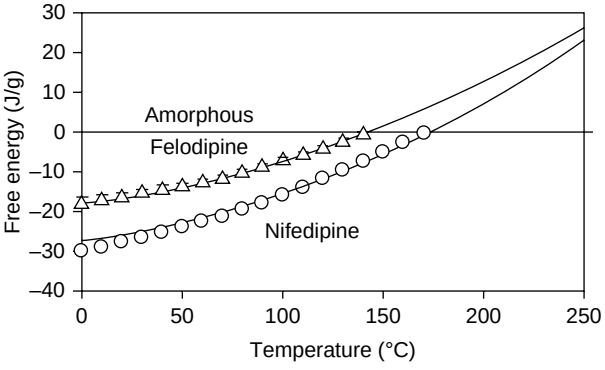

FIGURE 14 Free energy difference between liquid and crystalline forms of felodipine and nifedipine as a function of temperature. The data points were generated using equations (5) to (7) where the heat capacity of crystalline and liquid forms were determined experimentally. The solid lines were determined using the Hoffman equation [equation (2)]. The figure has been reproduced from Ref. (68) with kind permission of Springer Science and Business Media.

Although the thermodynamic driving force increases with decreasing temperature, molecular mobility decreases on cooling, thereby increasing the kinetic barrier to crystallization. The kinetic barrier to crystallization is a consequence of the high viscosity and decreased molecular mobility of supercooled liquids and glassy systems, and is obviously strongly temperature dependent, as discussed in detail above. Consequently, there is a balance between the thermodynamic driving force for nucleation and growth, which increases with decreasing temperature, and kinetic factors, and which become less favorable as the temperature is reduced due to restricted molecular mobility. This leads to a theoretical maximum rate of crystallization at a temperature between the melting point, T_m and the glass transition temperature, T_g (71).

For bulk crystallization of a drug substance to occur, nuclei of the new phase must first form and then these must grow into crystals. It is therefore relevant to consider theoretical models for nucleation and growth from supercooled liquids and glasses. A classical nucleation theory has been developed to describe factors influencing nucleation kinetics from supercooled liquids (72). In this model, the rate of nucleation is governed by the free energy change occurring on formation of a nucleus of critical size, ΔG^* and the activation energy for transport of a molecule from the amorphous phase to the nucleus, ΔG_a (72).

$$I = A \exp\frac{-(\Delta G^* + \Delta G_a)}{kT} \tag{8}$$

Here, A is a constant, k is the Boltzmann constant, and T is temperature. ΔG^* represents the balance between the energy penalty associated with creating a new surface, ΔG_S, and the favorable reduction in free energy associated with forming a crystalline phase, ΔGv.

Once a stable nucleus has been formed, an increase in the mass of crystalline material is achieved by crystal growth. Crystal growth from a disordered phase is generally considered to be a first-order phase change that occurs at an interface and proceeds by propagation of the interface through the sample. Crystal growth from viscous liquids is often described by the normal crystal growth model (73).

$$u = \frac{k}{\eta}\left[1 - \exp\left(-\frac{\Delta G}{RT}\right)\right] \tag{9}$$

where ΔG is the free energy difference between the liquid and crystalline forms, k is a temperature independent constant, and η is the viscosity. A typical growth rate as a function of temperature profile for an organic material is shown in Figure 15.

Close to the melting temperature where the molecular mobility is high, the rate of crystal growth depends on the thermodynamic driving force for crystallization, which in turn, is related to the degree of undercooling from the equilibrium melting point. The growth rate passes through a maximum and then decreases. When the degree of undercooling is large, the growth rate is under kinetic control, that is, controlled by molecular mobility. It is typically assumed that reorientation of the molecule and breaking of intermolecular interactions present in the supercooled liquid are necessary before the molecule can be incorporated onto the crystal face. Most crystal growth models assume that these processes are similar to the process of self-diffusion, which in turn, is inversely proportional to viscosity (73).

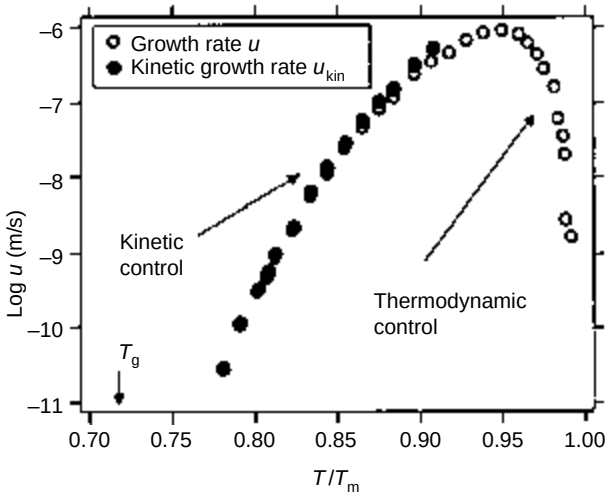

FIGURE 15 Experimental crystal growth rates for supercooled tris(naphthylbenzene) (74). The figure was reproduced from Ref. (75) with the kind permission of the American Institute of Physics.

Crystal growth models invoking a relationship between the growth rate and bulk viscosity appear to be an oversimplification for some supercooled liquids. Recent analyses suggest that, for fragile liquids, there is a breakdown in scaling between the viscosity and growth rate, particularly in the deeply supercooled region. Thus, the crystal growth rate is faster than would be predicted based on the viscosity (75). In addition, a new mode of growth has been observed for some organic glass formers, whereby the growth rates are discontinuous with temperature and increase as the glass transition temperature is approached (76–79). This mode of growth has been termed glass-crystal (GC) growth, and is thought to involve a diffusionless process. Figure 16 shows an example of a system that displays a change in the mode of growth as T_g is approached. It is apparent the growth rate abruptly increases by more than two orders of magnitude and no longer correlates with the self-diffusion coefficient (D). Furthermore, the increase in growth rate persists into the glassy region.

MOLECULAR MOBILITY AND CRYSTALLIZATION RATES

It is clear from the preceding discussion that both nucleation and crystal growth in deeply supercooled liquids (i.e., those cooled far below the equilibrium melting temperature of the crystal) and glasses are highly dependent on the molecular mobility. In attempting to relate various measurements of molecular mobility to crystallization tendency, it is important to recall that supercooled liquids and glasses are spatially heterogeneous, and that there are many different types of molecular motion. Thus, it is very difficult to predict crystallization kinetics using simple measurements of molecular mobility, although several attempts have been made to do so.

The complexity of attempting these types of predictions is illustrated by the work of Bhugra et al. (80). These workers measured the crystallization onset times

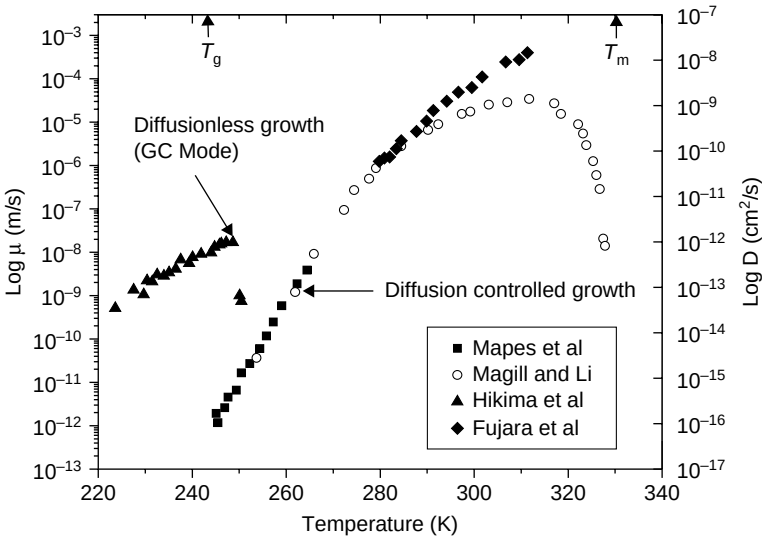

FIGURE 16 Crystal growth rate as a function of temperature for supercooled *o*-terphenyl liquid. The figure was adapted from Ref. (77).

and crystal growth rates of several compounds in addition to measuring molecular mobility above and below T_g. The techniques used to measure molecular mobility included DSC and isothermal microcalorimetry for the glasses and dielectric spectroscopy for supercooled liquids, whereas crystallization onset times and growth rates were measured using polarized light microscopy. The authors found that crystallization onset times coupled with dielectric spectroscopy relaxation times, albeit with coupling coefficients of less than one (implying that the molecular motions associated with the relaxation time measurements are not identical to those involved in dictating the crystallization onset times) for some, but not all compounds above T_g. Below T_g, successful prediction of crystallization onset time from relaxation times was hard to achieve. These results highlight that there is currently no robust method available for measuring a surrogate for crystallization tendency and using this method to predict crystallization rates. These results are perhaps not surprising, because it currently not well understood which modes of molecular mobility are important for crystallization, particularly in glasses. In addition, crystallization from supercooled liquids and glasses is complicated by the different kinetics of surface and bulk molecular assembly processes in addition to temperature dependent growth mechanisms (75,77,81).

Another complexity that makes crystallization prediction difficult is the well-known impact of sample preparation and handling on crystallization tendency. Samples prepared by melt quenching have been found to be more resistant to crystallization than samples rendered X-ray amorphous through milling of crystalline material (21). Even samples prepared by melt quenching can have different recrystallization tendencies depending on how they are handled post-melt quenching.

For example, it has been observed that milled melt-quenched samples crystallize much more readily than do unmilled samples (82). It has been suggested that mechanical stress such as milling introduces "high energy sites" or nuclei, which can lead to crystallization.

Another factor that needs to be considered is the importance of the surface area of the powder to the phenomenon of surface crystallization. It has been demonstrated that the growth rate of crystals at the surface is much faster than the bulk growth rate (81). The implication of this observation is that solids with a higher surface area may be more prone to crystallization, and thus this might be one reason that milled samples crystallize faster.

As described above, it is very difficult to predict the crystallization tendency of amorphous solids, and therefore, experimental measurements of physical stability need to be made. Crystallization rates are normally measured using techniques such as XRPD, DSC, or spectroscopy. Given that crystallization may be slow under ambient conditions, it is obviously desirable to use accelerated stability testing conditions to evaluate the crystallization potential of an amorphous formulations. There are several factors that may complicate extrapolations of crystallization rates at high temperatures/relative humidities to ambient conditions. The crystal phase resulting from devitrification may not be the same for the different experimental conditions. For example, indomethacin crystallizes predominantly as the gamma polymorph at lower temperatures and relative humidities, and as the alpha form at higher temperatures and relative humidities (83,84).

In addition, the temperature dependence of the crystallization rate may not follow a simple Arrhenius-type relationship. This may result from crystallization of different polymorphs as mentioned above or from a non-Arrhenius dependence of molecular mobility on temperature as discussed earlier. Additional factors that have to be considered are changes in growth mechanism close to T_g as discussed previously and the effects of water content, which will be discussed in more detail below.

Based on the preceding discussion, it is clearly very difficult to predict precise crystallization rates under a given set of experimental conditions either from data obtained under accelerated stability conditions or from some experimentally measured property of the amorphous solid. However, given that different compounds have very different crystallization tendencies, it is still useful to assess crystallization tendency under a variety of conditions. Clearly, a compound that is stable under extreme conditions will be a viable candidate for formulation in an amorphous state. For compounds having a moderate tendency to crystallize, a measure of the effect of moisture and temperature on crystallization tendencies may help to determine if packaging could reduce the crystallization tendency and provide storage stability.

STABILIZATION AGAINST CRYSTALLIZATION: AMORPHOUS SOLID DISPERSION TECHNOLOGY

Single-component amorphous drugs often display physical instability over the intended shelf life of the product, and so polymeric crystallization inhibitors are frequently added to improve the physical stability. In order to be an effective inhibitor of bulk crystallization, the polymer must form an intimate mixture with the drug substance, resulting in a miscible, single-phase, amorphous solid dispersion. Molecular mixtures of amorphous solids are also generated in freeze-dried

biological products where sugars are added to improve the stability of proteins, and for polymeric film coatings where small molecules are added to the coating to act as plasticizers and to improve mechanical properties.

Several methods can be used to prepare amorphous solid dispersions, which involve destroying the crystal structure of the drug and mixing the resultant liquid with the polymer. One common method entails dissolution of crystalline drug and polymer in a solvent, followed by drug substance solvent removal. This process is typically carried out using techniques such as rotary evaporation, spray drying, freeze drying, air drying, or vacuum oven drying. Another common method entails heating the crystalline drug and polymer mixture to a temperature above the melting point of the drug and processing the mixed molten mass by means of melt extrusion. It has also been reported that solid dispersions can sometimes be prepared by co-milling the drug and the polymer (85). If crystallization is avoided during the preparation stage, and the drug and polymer remain intimately mixed, the system is said to have formed a miscible, single-phase, amorphous solid dispersion.

If miscibility is achieved, the behavior of the drug in the solid dispersion will be altered relative to that of the pure amorphous drug, and the properties of the solid dispersion will depend on the individual component properties as well as on the composition. There are several polymers that can be used to form solid dispersions, although it has been observed that some drug–polymer combinations are miscible whereas other systems are immiscible. From a theoretical perspective, molecular level mixing will only be achieved if the intermolecular interactions between the drug and the polymer are sufficiently favorable to overcome the cohesive interactions in the pure amorphous phases and crystallization of either component is avoided.

Derivatized cellulose polymers such as hydroxypropyl methylcellulose and the vinylpyrrolidone family of polymers [including poly(vinylpyrrolidone) and poly(vinyl-pyrrolidone-co-vinyl acetate)] have been found to be miscible with a variety of drug substances. In contrast, polymers or drugs containing strong cohesive interactions may not mix with chemically dissimilar components. For example, the ionic polymer, Eudragit E100 (which is a cationic methacrylate polymer), is only partially miscible with the itraconazole (86). Ibuprofen has been found to be largely immiscible with dextran (87), which is able to form extensive cohesive hydrogen bonding interactions.

ESTABLISHING MISCIBILITY

Determining the miscibility of the binary system can be challenging. For miscible systems, it would be expected that the glass transition temperature of the amorphous mixture is intermediate to that of the pure component T_g values. Thus, if a high T_g polymer is mixed with a low T_g drug substance, the T_g of the dispersion will increase with an increasing amount of polymer. An example is shown in Figure 17, where the T_g as a function of polymer concentration is shown for the felodipine–PVP solid dispersion system.

Assuming that two components are miscible, there are theoretical ways to predict the T_g of the mixture as a function of composition. The Gordon–Taylor equation is one of the most commonly used approaches for pharmaceutical systems (89), and assumes that the two components are miscible at all compositions and that the free volumes of the components are additive (90). The T_g of mixture, T_{g12}, is then defined as

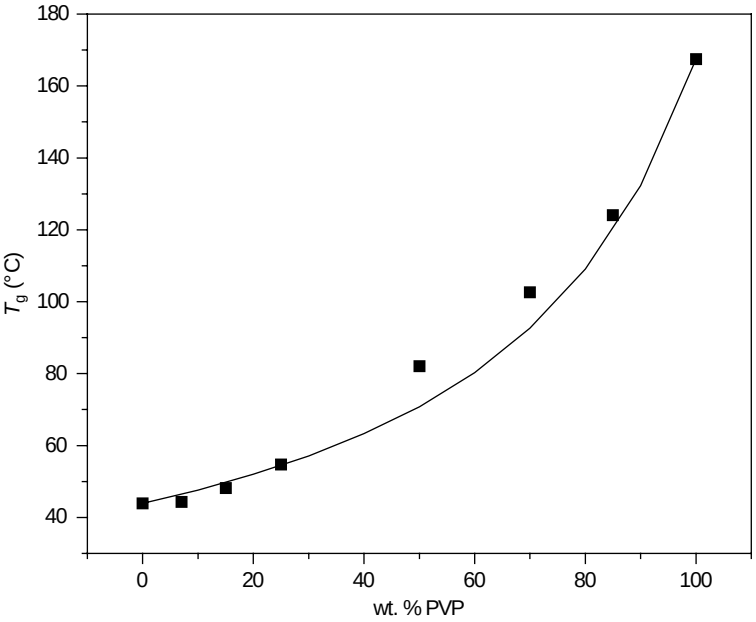

FIGURE 17 Glass transition temperature of solid dispersions of felodipine and PVP as a function of PVP concentration, with the solid line showing T_g as predicted using the Gordon–Taylor equation. The figure has been adapted from data presented originally in Ref. (88).

$$T_{g12} = \frac{w_1 T_{g1} + K w_2 T_{g2}}{w_1 + K w_2} \tag{10}$$

where w_1 and w_2 are the weight fractions of each component, T_{g1} and T_{g2} are the respective glass transition temperatures, and K is a constant. It can be seen from Figure 17 that the Gordon–Taylor equation yields reasonably good predictions for the T_g of dispersions of felodipine and PVP. However, application of this equation for other systems may either overestimate or underestimate T_g for binary mixtures (67,91).

Because DSC is widely used to measure T_g, it is also one of the most common methods used to establish miscibility, although there are certain limitations. DSC is obviously not a good method to evaluate miscibility if the T_g of each component is very similar, or if the T_g of one or both components is hard to determine. Furthermore, due to the non-isothermal nature of DSC, changes in the sample can occur during heating which may make results difficult to interpret.

T_g is not the only property that will change when a miscible mixture is formed, and solid-state NMR has also been used to investigate miscibility (92). This is a very elegant approach, because by measuring different relaxation times, some estimate of the length scale of domains can be achieved. The basis of this technique is that the relaxation time of the solid dispersion will be mono-exponential (but different from the mono-exponential relaxation profiles of the

individual amorphous materials), whereas a phase separated system will be bi-exponential. Using nifedipine as the model drug, Aso and coworkers found that the T_1 and $T_{1\rho}$ relaxation times were mono-exponential for HMPC and PVP dispersions (92). In contrast, dispersions with α,β-poly(*N*-5-hydroxypentyl)-L-aspartamide were mono-exponential for the T_1 relaxation times but bi-exponential for $T_{1\rho}$ relaxation measurements. It was concluded that the latter system was phase separated into two amorphous phases whereby the size of the phase separated domains was between 5 and 50 nm.

Vibrational spectroscopy has been used extensively to study intermolecular interactions between drugs and polymers (40). This technique is most useful for systems that can form specific (hydrogen bonding) interactions between the drug and the polymer. The formation of drug–polymer hydrogen bonding interactions is evidence of the close contact between the drug and the polymer, and hence, molecular level mixing.

XRPD/scattering has also been employed to probe miscibility in solid dispersions (93). Amorphous materials scatter X rays in a way that is dependent on the local packing arrangement. In a miscible solid dispersion, the nearest neighbor and the nearest nearest neighbor interactions should be different from in each of the pure components. Therefore, the X-ray scattering pattern of the miscible solid dispersion should be different from a weighted average of the individual diffraction patterns (93). In other words, it should not be possible to construct the scattering pattern of the miscible dispersion using the scattering patterns of the individual amorphous components.

IMPROVED PERFORMANCE OF MISCIBLE SOLID DISPERSIONS

The physical stability of miscible solid dispersions is typically enhanced relative to the amorphous drug alone; that is, the crystallization tendency is considerably reduced. Thus, by forming an intimately mixed solid dispersion, a product with an adequate shelf life can often be achieved even when the drug alone recrystallizes within a few days. The crystallization rate of an amorphous solid dispersion is complex and will depend on several factors, including the crystallization tendency of the drug alone (68), the storage temperature (94), the water content (95), and the amount and type of polymer used (95,96). The mechanism by which polymers retard crystallization is currently not well understood, but important factors likely include the increased T_g in the presence of the polymer, decreased molecular mobility, disruption of drug self-association by the polymer, and a reduced thermodynamic driving force for crystallization.

Amorphous solid dispersions often provide enhanced dissolution when compared to the amorphous drug alone. An example of this behavior is shown in Figure 18, where it can be seen that both the maximum solution concentrations and area under the curves are much larger for the solid dispersions than for the pure amorphous drug.

INTERACTION OF MOISTURE WITH AMORPHOUS SOLIDS

Amorphous solids can interact with moisture via two mechanisms, one of which is adsorption of the water molecules at the surface, and the other of which is absorption of water into the bulk structure. Absorption is possible due to the lower density

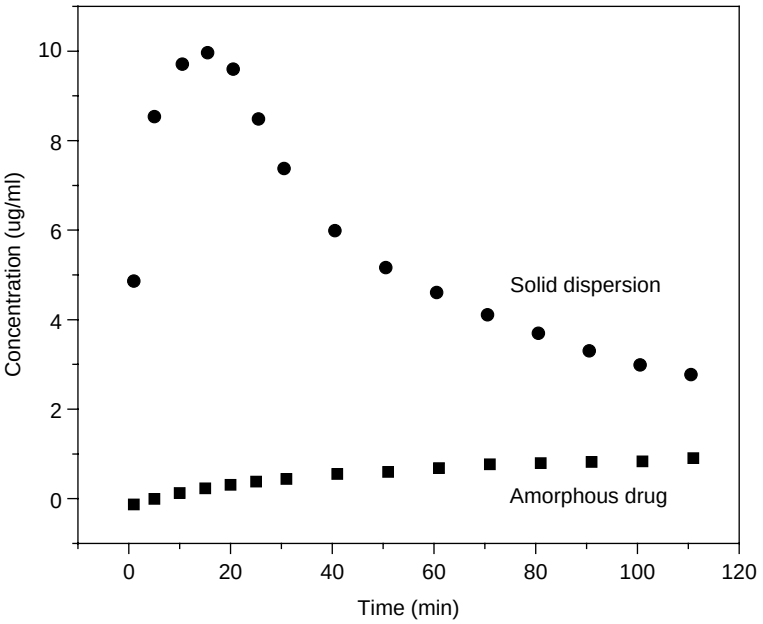

FIGURE 18 Dissolution profile of amorphous felodipine compared to that of an amorphous solid dispersion containing 50% PVP.

structure of amorphous solids whereby the free volume facilitates the sorption of water molecules, and hence, amorphous solids typically absorb considerably more water than to their crystalline counterparts. This is illustrated in Figure 19, where the moisture sorption profile of crystalline indomethacin is compared with that of its amorphous solid (84). It can be seen that the water content of the amorphous solid increases continuously with an increase in relative humidity.

The amount of moisture sorbed by an amorphous solid will depend to a large degree on the chemistry of the compound, with hydrophilic compounds sorbing considerably more moisture than hydrophobic compounds. The amount of moisture sorbed will also depend on temperature, relative humidity, the presence of any crystalline regions, and the mass of sample (rather than the surface area which is relevant for surface adsorption). An example is shown in Figure 20, where the moisture sorption profile of the hydrophilic amorphous polymer, PVP, is compared with that of the hydrophobic amorphous polymer, poly(vinyl acetate). Moisture sorption by amorphous materials is complex, altering both the thermodynamics and kinetics of the system, and may lead to crystallization as well as increased chemical reactivity.

Because of its low glass transition temperature, water is a well-known plasticizer of amorphous solids. The glass transition temperature of water has been reported to somewhere between –137°C (97) and –108°C (98). Plasticizers change a number of material properties, and will decrease mechanical strength, viscosity, T_g, and increase

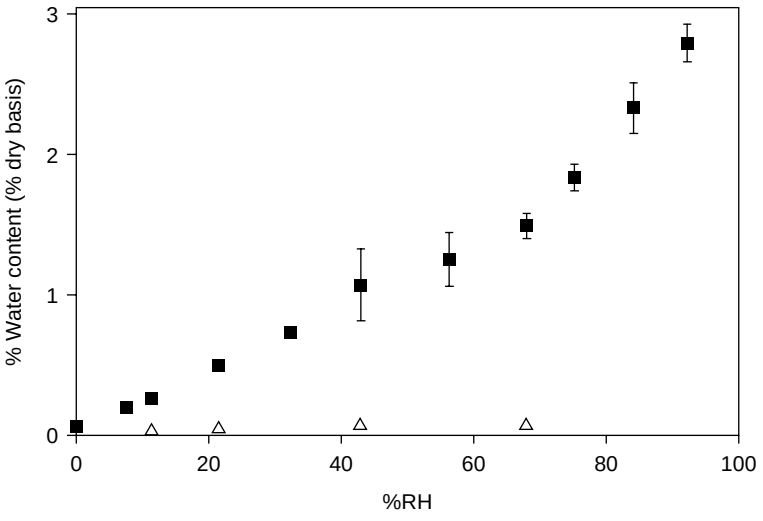

FIGURE 19 Moisture sorption profile for amorphous (squares) and crystalline (triangles) indomethacin. The figure was adapted from Ref. (84).

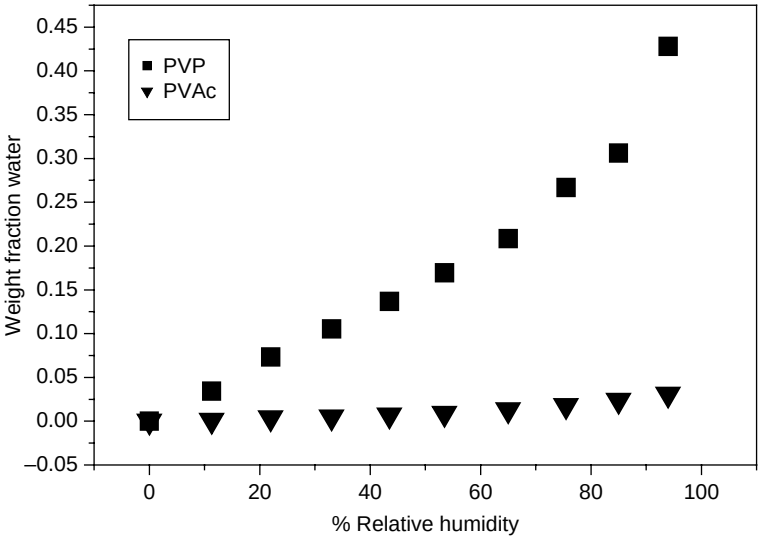

FIGURE 20 Moisture sorption profile of a hydrophilic amorphous polymer, poly(vinylpyrrolidone), compared with that of a hydrophobic amorphous polymer, poly(vinyl acetate).

molecular mobility, the tendency for crystallization, and chemical reactivity. The extent of plasticization of amorphous solids by water is usually reflected by the magnitude of the decrease in the glass transition temperature of a system. Figure 21 shows a plot of T_g against water content for the PVP–water system.

It is apparent that absorption of water results in a marked decrease in the glass transition temperature. At high relative humidities, the glass transition temperature of PVP is reduced to below room temperature, and the sample becomes a supercooled liquid rather than a glass. For samples where the T_g is reduced to below the storage temperature, profound changes in appearance can result due to the increased molecular mobility, which can lead to sample collapse, flow, and crystallization. Indeed, highly plasticized samples often appear liquid-like, although it is important to recognize that this phenomenon is fundamentally different from the deliquescence transition experienced by certain crystalline solids. Although water is a known plasticizer, it is interesting to note that at very low concentrations it can actually act as an anti-plasticizer, increasing, for example, mechanical strength (100).

Because of its profound impact on the kinetics of chemical and physical transformations in amorphous materials, it is important to consider the effects (of even small amounts) of water. Indomethacin is a hydrophobic molecule, and hence, the amorphous solid only absorbs small amounts of moisture, as shown in Figure 19. However, dielectric and shear relaxation time measurements indicate that even these low levels of moisture have a very large influence on the molecular mobility, with large increases being observed for water contents of 1–2% (39). This, in turn, leads to a reduced glass transition temperature and a much faster crystallization rate when compared to the dry solid (101).

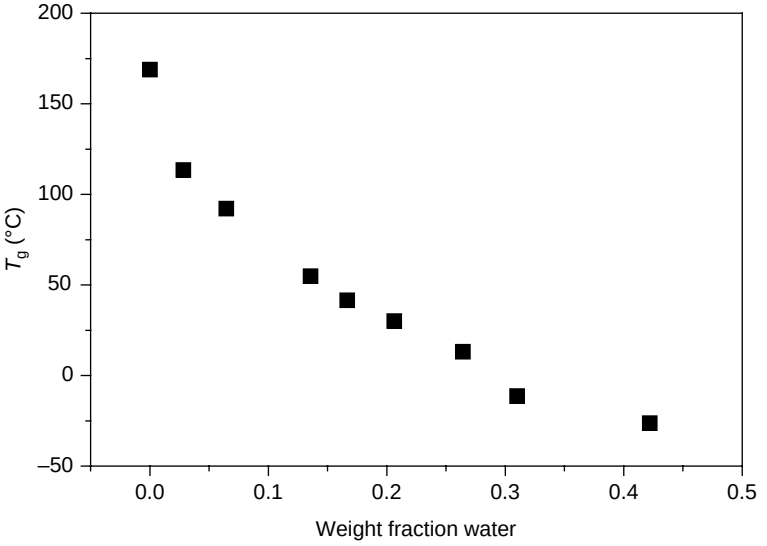

FIGURE 21 Glass transition temperature of poly(vinylpyrrolidone) as a function of water content. The figure has been adapted from data presented originally in Ref. (99).

Absorption of water vapor has been found to promote the crystallization of many organic materials, and this crystallization may even take place during measurement of the moisture sorption isotherm. A classic example is that of sucrose. When the moisture sorption profile of amorphous sucrose is measured, the mass is observed to increase with relative humidity and then abruptly decrease (Fig. 22). The abrupt decrease occurs because the amorphous sample crystallizes to a denser solid that cannot accommodate the water molecules in its internal structure (sucrose does not form a hydrate). This process leads to expulsion of the water, and a decrease in sample mass with increasing relative humidity.

The thermodynamics of moisture sorption by amorphous solids can be described by the well known Flory–Huggins theory and modifications thereof, in particular, the Vrentas model. These models were initially developed to describe highly non-ideal polymer solutions (103–105), and have been subsequently applied to investigating the interaction of water vapor with a variety of amorphous pharmaceutical systems (106–108). The Flory–Huggins equation is:

$$\ln\left(\frac{p}{p_0}\right) = \ln f_1 + \left(1 - \frac{1}{x_{12}}\right) f_2 + \chi_{12} f_2^{\,2} \tag{11}$$

In this form, the equation describes the relationship between the partial pressure (p) of water vapor and the volume fraction of water absorbed by the sample. p_0 is the vapor pressure of pure water, ϕ_1 is the volume fraction of water, ϕ_2 is the volume fraction of the amorphous solid, x_{12} is the relative molecular volume of the two components, and χ_{12} is the Flory–Huggins interaction parameter between the water and

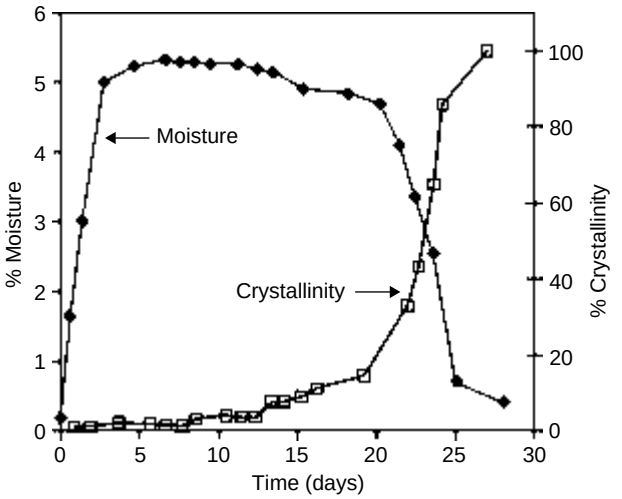

FIGURE 22 Moisture sorption profile for initially amorphous sucrose as a function of time during exposure to 30% RH, together with the corresponding degree of crystallinity. The figure was adapted from Ref. (102).

the amorphous solid. The interaction parameter is a measure of the chemical affinity between water and the amorphous solid. Thus, hydrophobic compounds such as indomethacin have large, positive interaction parameters around 3 (107), whereas more hydrophilic substances such as sucrose and poly(vinylpyrrolidone) have values around 0.5 (108).

In the model proposed by Vrentas and Vrentas (109), an additional term, f, is added to account for the fact that water molecules absorbed into amorphous solids can lead to non-ideal volumetric changes, and hence, an additional free energy change beyond that predicted by the Flory–Huggins equation. The complete mathematical statement of the Vrentas–Vrentas model is thus:

$$\ln\left(\frac{p}{p_0}\right) = \ln\phi_1 + \left(1 - \frac{1}{x_{12}}\right)\phi_2 + \chi_{12}\phi_2^{\,2} + f \tag{12}$$

where

$$f = M_1 W_2^2 \left[\frac{\Delta C_p^{1\to g}}{RT}\right]\left[\frac{dT_g}{dW_1}\right]\left[\frac{T}{T_g} - 1\right] \quad \text{for } T < T_g$$

and

$$f = 0 \quad \text{for } T > T_g,$$

and this equation will be identical to the Flory–Huggins equation. Thus, interpretations of water absorption isotherms for amorphous solids exhibiting Type II isotherms must take into account both chemical binding and the effects of water on the structure of the solid (plasticization).

CHEMICAL REACTIVITY IN AMORPHOUS SOLIDS

The chemical reactivity of amorphous solids, including cephalosporin drugs (64,110,111), peptides (112,113), and proteins (114–116), is well documented. In general, amorphous solids show greater chemical reactivity when compared to crystals, which is due in part to the enhanced degree of molecular mobility. In addition, nearest neighbor interactions that may not be possible in the more ordered structure of a crystal may increase the potential for intra-molecular and inter-molecular chemical reactions. One of the earliest documented examples of the enhanced chemical reactivity of an amorphous drug is that of cefoxitin sodium, as shown in Figure 23 (110).

Even in nominally crystalline drugs, chemical reactions are likely initiated at defect sites in the crystal lattice (117) where molecular motions are enhanced. In addition, high energy sites have the potential to interact with water vapor that can further increase mobility, and in turn, chemical reactivity, through its plasticizing effects. It has been shown that high energy processing (such as milling) of drugs or drug products promotes chemical reactivity (118–121). This enhancement in chemical reactivity may be due in part to the increased surface area associated with particle size reduction. However, it is possible that application of high shear rates to the

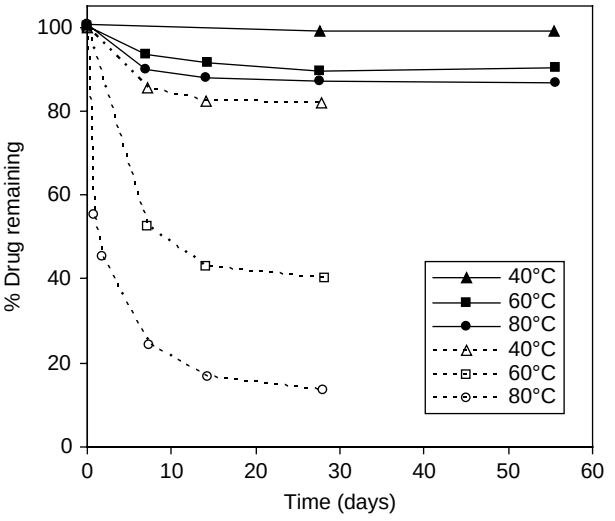

FIGURE 23 Degradation of crystalline cefoxitin sodium (filled symbols, solid lines) and amorphous cefoxitin sodium (open symbols, dashed lines). The figure has been adapted from data presented originally in Ref. (110).

crystal surface may lead to some disruption of the long-range molecular order leading to greater free volume and enhanced molecular mobility.

The formation of an amorphous phase, either intentionally (e.g., by spray drying) or unintentionally (e.g., during milling or compaction of powders), typically increases the rate or extent of chemical reactions. In several cases, the formation of amorphous regions within a crystal, or complete conversion to an amorphous form leads to a different degradation mechanism. A change in reaction mechanism for tetraglycine methyl ester from a methyl ester transfer to a polycondensation reaction was observed in samples that were milled to produce amorphous regions (113). In another example, amorphous ethacrynate sodium was shown to react to form a dimer, which is a reaction pathway that has been observed in concentrated solutions but not in the crystal (111,122). In both of these examples, the availability of molecular configurations or modes of motions in the amorphous solid, that were otherwise restricted in the crystalline state, promote chemical reactions.

The occurrence of chemical reactions in amorphous solids that also take place in a liquid state but not the crystal, strongly suggest that enhanced molecular mobility relative to that in the crystal plays a significant role in chemical instability in the amorphous phase. Strickly and Anderson showed an increase in the rate of reaction and the number of degradation pathways for human insulin, a highly disordered globular protein, with increasing moisture content (123). The observation that the reaction rate of the human insulin approaches values observed in solution with increasing water content is consistent with the observation that water increases molecular dynamics in proteins in the same way that it plasticizes polymers and small drug molecules (115).

It is worthwhile to note, that although chemical reactivity in amorphous solids is enhanced relative to the crystalline state, it is still likely to be much less compared to that of the solution. Thus, the formation of an amorphous solid may provide a strategy for improving stability for drugs intended for dosing as liquids. Drugs, peptides, and proteins intended for parenteral applications are often prepared as amorphous solids that are later reconstituted to a liquid form prior to dosing provided that both physical and chemical stability can be maintained over practical pharmaceutical time scales.

The tendency of amorphous materials to absorb water plays an important role in the reactivity of amorphous drugs. Although the increased molecular mobility alone may render the amorphous form of a drug more chemically unstable than the crystal, the potential for the amorphous form to absorb more water than the crystalline form as described earlier in this chapter, can further promote chemical reactivity. The effect of water on the degradation of human insulin provided earlier illustrates the importance of molecular mobility as moderated by the presence of water.

According to Shalaev and Zografi, water can play one of four roles in promoting chemical reactivity in amorphous systems: a reactant, a product, plasticizer, or as a reaction medium (124). The versatility of water alone makes it a critical participant in many types of reactions. In addition, the ubiquitous nature of water, in combination with its ability to plasticize almost any amorphous drug, peptide, or protein, makes water a culprit in the chemical degradation of many amorphous drugs. The ability of water to promote the cyclization of quinapril hydrocholoride to diketopiperazine (112) through its ability to plasticize the drug is illustrated in Figure 24. With increasing water content, the glass transition is lowered, reflecting an overall greater mobility, which is also reflected in the T_1 relaxation time of the C_{21} carbon as measured by solid-state NMR. Accompanying this increase in mobility of the carbon is an increased rate in the cyclization reaction.

Recently there has been a strong effort in the pharmaceutical field to establish correlations between the degree of molecular mobility and chemical reactivity with a view toward being able to predict chemical instability, improving experimental approaches for accelerated stability testing of amorphous drugs and excipients, and to provide the understanding needed to reduce chemical instability through the addition of polymers or by formation of complexes. There has been some success in making correlations between the degree of molecular mobility and chemical reactivity (38,65,69). However, this is a very challenging area for research. The spatial and temporal heterogeneity present in the amorphous state that leads to a distribution of relaxation times (47,125,126), and also a distribution of chemical degradation rates (38) makes correlation between the time scales for molecular motion and chemical change extremely difficult. Furthermore, many of the techniques that measure molecular mobility are more "macroscopic," and measure an ensemble of molecules.

Thus, the relevance of enthalpy changes in glasses, dielectric relaxation processes, or the changes in viscosity as a function of temperatures near to T_g to the chemical processes is not clear, even when the reaction is known to have significant requirements for molecular mobility, such as the intra- or inter-molecular mobility required for intra-molecular cyclization, protein aggregation, or the formation of a dimer. Here it is important to return to the example of the cyclization reaction for quinapril hydrochloride provided earlier to emphasize that the observed

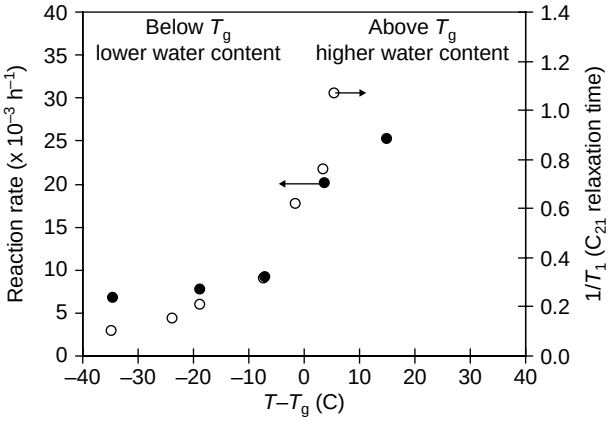

FIGURE 24 The rates of cyclization and T_1 relaxation times of the C_{21} carbon measured by solid-state NMR for amorphous quinapril hydrochloride as a function of temperature scale to T_g. The figure has been adapted from data presented originally in Ref. (112).

correlation between molecular mobility and chemical reactivity is likely due to the measurement of the relaxation time for a specific functional group.

In general, the ability to correlate molecular mobility to a chemical reaction is likely related to the ability to measure the motions relevant to the process of interest (127). Recent work by Cicerone and workers have suggested that, in glasses, it is the very fastest motions that contribute to chemical reactivity, and that these motions may not be represented by the relaxation time constants obtained by measuring enthalpy relaxation in glasses (128,129). Thus, there is limit in the ability to establish correlations between chemical change and molecular mobility, unless there is an understanding of how molecular motions leading to chemical change are coupled to those detected by NMR, enthalpy relaxation, or other measures of molecular mobility.

At this time there is not sufficient understanding of molecular dynamics in the amorphous state as a function of temperature and humidity to make accurate predictions about the chemical stability, even when measurement of mobility is made under conditions relevant to storage and handling. The best approach for assessing the potential for chemical changes to compromise the quality and safety of an amorphous drug form is to study the chemical stability of the amorphous drug as a function of temperature and relative humidity while concurrently considering the effects of these stressors on the properties of amorphous solids.

METHODS FOR IMPROVING CHEMICAL STABILITY OF AMORPHOUS DRUGS

One of the most straightforward ways to reduce the tendency for chemical instability is to protect the amorphous drug from moisture using packaging that creates a barrier to moisture. As described earlier, because of the ability for water to play many roles in promoting chemical change, the protection of the amorphous system from moisture should be the first line of defense. Another strategy is to reduce the storage temperature so that the system is further away from the glass transition region.

The formation of amorphous molecular dispersions has also been shown to improve the chemical stability of reactive drugs and peptides.

The formation of solid dispersions of cefoxitin sodium and ethacrynate sodium with sugars and polymers reduced the reaction rate compared the drug alone (69). Although the mechanism by which a second component can reduce the reactivity of an amorphous drug is not always well understood, it is likely due to some combination of dilution of the drug–drug interactions, reduction of overall molecular mobility, and/or the formation of adhesive interactions between components in a mixture.

The ability to improve the chemical stability of a drug through formation of an intimate molecular mixture will depend upon the mechanism for the chemical reaction, and the miscibility of the two components. The mechanism of the chemical reaction is likely to be the most important factor that determines if the stability of a drug can be successfully improved by formation of an amorphous molecular dispersion. The ability to slow reactions that require diffusion of molecular segments or entire molecules such as dimer formation or aggregation in proteins, by formation of a dispersion has been somewhat successful (65,69). In contrast, the ability to slow reactions that only require intermolecular conformation changes, or reactions with molecular oxygen or water, which have very high mobility, is more challenging. The formation of inclusion complexes with a cyclodextrin has also been shown to reduce the chemical reactivity of amorphous quinapril (130). This type of approach may be successful depending on the binding constant between a drug and cyclodextrin, and the nature of the reaction.

SUMMARY

The unique properties of amorphous solids that provide both the desirable attributes (e.g., enhanced dissolution rate) and liabilities (e.g., increased hygroscopicity, tendency for chemical reactivity) can be attributed to both molecular level structure and macroscopic properties. Molecular order in amorphous solids is more random than in crystalline solids. In macroscopic terms, the free volume, molecular mobility, and viscosity of amorphous solids are intermediate to those for a crystalline solid or a liquid, and are very dependent on temperature. Higher free energy in the amorphous solid compared to a crystal creates the potential for crystallization, and the disordered structure promotes the potential for mixing with a second component. The tendency for crystallization is governed primarily by two factors, namely, the degree of molecular mobility and the thermodynamic driving force for crystallization (which is related to the degree of undercooling relative to the crystal-to-liquid transition temperature). However, there are many subtle factors that can influence the nucleation and crystal growth in amorphous solids, making measurement and prediction of crystallization very challenging. The potential for an amorphous solid to form a miscible mixture as a means of reducing free energy leads to the absorption of vapor and the formation of molecular mixtures with other compatible amorphous solids. The formation of a molecular mixture is one of the key strategies for reducing the potential for crystallization.

Chemical reactivity in amorphous solids tends to be intermediate to that observed for the crystalline and liquids states. The enhanced reactivity compared to the crystalline solids arises in part as a result of the increased molecular mobility of amorphous solids. Understanding the enhanced chemical reactivity in the

amorphous solids is important for understanding chemical reactivity in nominally crystalline solids, which very likely takes place in disordered regions. The ability to correlate chemical reactivity and molecular mobility in amorphous solids is often hampered by the complexity of the molecular structure and dynamics in amorphous systems, and the ability to measure motions specifically related to the chemical reaction. However, an understanding of which factors can affect mobility, such as temperature, moisture sorption, and mixing with a second component can help to improve chemical stability in amorphous solids such that adequate storage stability for pharmaceutical applications can be realized.

REFERENCES

1. Hancock BC. Disordered drug delivery: destiny, dynamics and the deborah number. J Pharm Pharmacol 2002; 54: 737–46.
2. Bates S, Zografi G, Engers D, et al. Analysis of amorphous and nanocrystalline solids from their X-ray diffraction patterns. Pharm Res 2006; 23: 2333–49.
3. Boyer RF. Dependence of mechanical properties on molecular motion in polymers. Polym Eng Sci 1968; 8: 161–85.
4. Boyer RF. Mechanical motions in amorphous and semi-crystalline polymers. Polymer 1976; 17: 996–1008.
5. Richardson MJ. Thermal analysis. In: Boothand C, Price C, eds. Comprehensive Polymer Science, Vol. 1. New York: Pergamon Press, 1989: 867–901.
6. Ford JL, Timmins P. Pharmaceutical thermal analysis: techniques and applications. New York: John Wiley & Sons, 1989.
7. Ferry JD. Viscoelastic properties of polymers. New York: John Wiley & Sons Inc., 1980.
8. Hancock BC, Carlson GT, Ladipo DD, Langdon BA, Mullarney MP. Comparison of the mechanical properties of the crystalline and amorphous forms of a drug substance. Int J Pharm 2002; 241: 73–85.
9. Saleki-Gerhardt A, Ahlneck C, Zografi G. Assessment of disorder in crystalline solids. Int J Pharm 1994; 101: 237–47.
10. Kauzmann W. The nature of the glassy state and the behaviour of liquids at low temperatures. Chem Rev 1948; 43: 219–56.
11. Savolainen M, Kogermann K, Heinz A, et al. Better understanding of dissolution behaviour of amorphous drugs by in situ solid-state analysis using Raman spectroscopy. Eur J Pharm Biopharm 2009; 71: 71–9.
12. Hancock BC, Parks M. What is the true solubility advantage for amorphous pharmaceuticals? Pharm Res 2000; 17: 397–404.
13. Al-Angari AA, Kennerley JW, Newton JM. The compaction properties of polyethylene glycols. J Pharm Pharmacol 1985; 37: 151–3.
14. Sheskey PJ, Hendren J. The effects of roll compaction equipment variables, granulation technique, and HPMC polymer level on a controlled-release matrix model drug formulation. Pharm Tech 1999; 23: 90–106.
15. Wardrop J, Law D, Qiu Y, et al. Influence of solid phase and formulation processing on stability of Abbott-232 tablet formulations. J Pharm Sci 2006; 95: 2380–92.
16. Saleki-Gerhardt A, Stowell JG, Byrn SR, Zografi G. Hydration and dehydration of crystalline and amorphous forms of raffinose. J Pharm Sci 1995; 84: 318–23.
17. Taylor LS, York P. Characterization of the phase transitions of trehalose dihydrate on heating and subsequent dehydration. J Pharm Sci 1998; 87: 347–55.
18. Li YH, Han J, Zhang GGZ, Grant DJW, Suryanarayanan R. In situ dehydration of carbamazepine dihydrate: a novel technique to prepare amorphous anhydrous carbamazepine. Pharm Dev Technol 2000; 5: 257–66.

19. Williams AC, Cooper VB, Thomas L, et al. Evaluation of drug physical form during granulation, tabletting and storage. Int J Pharm 2004; 275: 29–39.
20. Ward GH, Schultz RK. Process-induced crystallinity changes in albuterol sulfate and its effect of powder physical stability. Pharm Res 1995; 12: 773–9.
21. Crowley KJ, Zografi G. Cryogenic grinding of indomethacin polymorphs and solvates: assessment of amorphous phase formation and amorphous phase physical stability. J Pharm Sci 2002; 91: 492–507.
22. Florence AT, Salole EG, Stenlake JB. The effect of particle size reduction on digoxin crystal properties. Communications, J Pharm Pharmac 1974; 26: 479–80.
23. Yonemochi E, Ueno Y, Ohmae T, et al. Evaluation of amorphous ursodeoxycholic acid by thermal methods. Pharm Res 1997; 14: 798–803.
24. Alba-Simionesco C, Fan J, Angell CA. Thermodynamic aspects of the glass transition phenomenon. II. Molecular liquids with variable interactions. J Chem Phys 1999; 110: 5262–72.
25. Turnbull D, Cohen MH. Reconstructive transformation and formation of glass. J Chem Phys 1958; 29: 1049–54.
26. Tanaka H. Two-order-parameter model of the liquid-glass transition. I. Relation between glass transition and crystallization. J Non-Cryst Solids 2005; 351: 3371–84.
27. Zhou DL, Zhang GGZ, Law D, Grant DJW, Schmitt EA. Physical stability of amorphous pharmaceuticals: importance of configurational thermodynamic quantities and molecular mobility. J Pharm Sci 2002; 91: 1863–72.
28. Shah B, Kakumanu VK, Bansal AK. Analytical techniques for quantification of amorphous/crystalline phases in pharmaceutical solids. J Pharm Sci 2006; 95: 1641–65.
29. Buckton G, Darcy P. Assessment of disorder in crystalline powders - a review of analytical techniques and their application. Int J Pharm 1999; 179: 141–58.
30. Lehto VP, Tenho M, Vaha-Heikkila K, et al. The comparison of seven different methods to quantify the amorphous content of spray dried lactose. Powder Technol 2006; 167: 85–93.
31. Yu L. Amorphous pharmaceutical solids: preparation, characterization and stabilization. Adv Drug Deliver Rev 2001; 48: 27–42.
32. Bates S, Kelly RC, Ivanisevic I, et al. Assessment of defects and amorphous structure produced in raffinose pentahydrate upon dehydration. J Pharm Sci 2007; 96: 1418–33.
33. Chen XM, Bates S, Morris KR. Quantifying amorphous content of lactose using parallel beam X- ray powder diffraction and whole pattern fitting. J Pharm Biomed Anal 2001; 26: 63–72.
34. Aso Y, Yoshioka S. Molecular mobility of nifedipine-PVP and phenobarbital-PVP solid dispersions as measured by C-13-NMR spin-lattice relaxation time. J Pharm Sci 2006; 95: 318–25.
35. Aso Y, Yoshioka S, Kojima S. Relationship between the crystallization rates of amorphous nifedipine, phenobarbital, and flopropione, and their molecular mobility as measured by their enthalpy relaxation and H-1 NMR relaxation times. J Pharm Sci 2000; 89: 408–16.
36. Offerdahl TJ, Salsbury JS, Dong ZD, et al. Quantitation of crystalline and amorphous forms of anhydrous neotame using C-13 CPMAS NMR spectroscopy. J Pharm Sci 2005; 94: 2591–605.
37. Carpentier L, Decressain R, Desprez S, Descamps M. Dynamics of the amorphous and crystalline alpha, gamma-phases of indomethacin. J Phys Chem B 2006; 110: 457–64.
38. Johari GP, Kim S, Shanker RM. Dielectric relaxation and crystallization of ultraviscous melt and glassy states of aspirin, ibuprofen, progesterone, and quinidine. J Pharm Sci 2007; 96: 1159–75.
39. Andronis V, Zografi G. The molecular mobility of supercooled amorphous indomethacin as a function of temperature and relative humidity. Pharm Res 1998; 15: 835–42.
40. Taylor LS, Zografi G. Spectroscopic characterization of interactions between PVP and indomethacin in amorphous molecular dispersions. Pharm Res 1997; 14: 1691–8.

41. Taylor LS, Zografi G. The quantitative analysis of crystallinity using FT-Raman spectroscopy. Pharm Res 1998; 15: 755–61.
42. Sebhatu T, Angberg M, Ahlneck C. Assessment of the degree of disorder in crystalline solids by isothermal microcalorimetry. Int J Pharm 1994; 104: 135–44.
43. Ahmed H, Buckton G, Rawlins DA. The use of isothermal microcalorimetry in the study of small degrees of amorphous content of a hydrophobic powder. Int J Pharm 1996; 130: 195–201.
44. Briggner LE, Buckton G, Bystrom K, Darcy P. The use of isothermal microcalorimetry in the study of changes in crystallinity induced during the processing of powders. Int J Pharm 1994; 105: 125–35.
45. Mackin L, Zanon R, Park JM, et al. Quantification of low levels (<10%) of amorphous content in micronised active batches using dynamic vapour sorption and isothermal microcalorimetry. Int J Pharm 2002; 231: 227–36.
46. Bohmer R, Ngai KL, Angell CA, Plazek DJ. Nonexponential relaxations in strong and fragile glass formers. J Phys Chem 1993; 99: 4201–9.
47. Ediger MD. Spatially heterogeneous dynamics in supercooled liquids. Annu Rev Phys Chem 2000; 51: 99–128.
48. Ediger MD, Angell CA, Nagel SR. Supercooled liquids and glasses. J Phys Chem 1996; 100: 13200–12.
49. Martinez LM, Angell CA. A thermodynamic connection to the fragility of glass-forming liquids. Nature 2001; 410: 663–7.
50. Angell CA, Ngai KL, McKenna GB, McMillan PF, Martin SW. Relaxation in glassforming liquids and amorphous solids. J Appl Phys 2000; 88: 3113–57.
51. Yoshioka S, Aso Y. Correlations between molecular mobility and chemical stability during storage of amorphous pharmaceuticals. J Pharm Sci 2007; 96: 960–81.
52. Yoshioka S. Molecular mobility of freeze-dried formulations as determined by NMR relaxation, and its effect on storage stability. In: Reyand L, May JC eds., Freeze-drying/lyophilization of Pharmaceutical and Biological Products, Vol. 137. New York, USA: Informa Healthcare, 2004: 187–212.
53. Shamblin SL, Tang X, Chang L, Hancock BC, Pikal MJ. Characterization of the time scales of molecular motion in pharmaceutically important glasses. J Phys Chem B 1999; 103: 4113–21.
54. Tong P, Zografi G. Solid-state characteristics of amorphous sodium indomethacin. Pharm Res 1999; 16: 1186–92.
55. Luthra SA, Pikal MJ, Utz M. Solid state 13C NMR investigation of impact of annealing in lyophilized glasses. J Pharm Sci 2008; 97: 4336–46.
56. Oksanen CA, Zografi G. Molecular mobility in mixtures of absorbed water and solid poly(vinylpyrrolidone). Pharm Res 1993; 10: 791–9.
57. Yoshioka S, Aso Y. Glass transition-related changes in molecular mobility below glass transition temperature of freeze-dried formulations, as measured by dielectric spectroscopy and solid state nuclear magnetic resonance. J Pharm Sci 2005; 94: 275–87.
58. Abdul-Fattah AM, Dellerman KM, Bogner RH, Pikal MJ. The effect of annealing on the stability of amorphous solids: chemical stability of freeze-dried moxalactam. J Pharm Sci 2007; 96: 1237–50.
59. Duddu SP, Sokoloski TD. Dielectric analysis in the characterization of amorphous pharmaceutical solids. 1. Molecular mobility in poly(vinylpyrrolidone)-water systems in the glassy state. J Pharm Sci 1995; 84: 773–6.
60. Noel TR, Parker R, Ring SG. Effect of molecular structure and water content on the dielectric relaxation behaviour of amorphous low molecular weight carbohydrates above and below their glass transition. Carbohyd Res 2000; 329: 839–45.
61. Bhugra C, Shmeis R, Krill SL, Pikal MJ. Different measures of molecular mobility: comparison between calorimetric and thermally stimulated current relaxation times below T_g and correlation with dielectric relaxation times above T_g. J Pharm Sci 2008; 97: 4498–515.

62. Hancock BC, Shamblin SL, Zografi G. The molecular mobility of amorphous pharmaceutical solids below their glass transition temperatures. Pharm Res 1995; 12: 799–806.
63. Liu J, Rigsbee DR, Stotz C, Pikal MJ. Dynamics of pharmaceutical amorphous solids: the study of enthalpy relaxation by isothermal microcalorimetry. J Pharm Sci 2002; 91: 1853–62.
64. Pikal MJ, Dellerman KM. Stability testing of pharmaceuticals by high-sensitivity isothermal calorimetry at 25°C: cephalosporins in the solid and aqueous solution states. Int J Pharm 1989; 50: 233–52.
65. Chang L, Shepherd D, Sun J, et al. Mechanism of protein stabilization by sugars during freeze-drying and storage: native structure preservation, specific interaction, and/or immobilization in a glassy matrix? J Pharm Sci 2005; 94: 1427–44.
66. Luthra SA, Hodge IM, Pikal MJ. Investigation of the impact of annealing on global molecular mobility in glasses: optimization for stabilization of amorphous pharmaceuticals. J Pharm Sci 2008; 97: 3865–82.
67. Shamblin SL, Taylor LS, Zografi G. Mixing behavior of colyophilized binary systems. J Pharm Sci 1998; 87: 694–701.
68. Marsac PJ, Konno H, Taylor LS. A comparison of the physical stability of amorphous felodipine and nifedipine systems. Pharm Res 2006; 23: 2306–16.
69. Shamblin SL, Hancock BC, Pikal MJ. Coupling between chemical reactivity and structural relaxation in pharmaceutical glasses. Pharm Res 2006; 23: 2254–68.
70. Hoffman JD. Thermodynamic driving force in nucleation and growth processes. J Chem Phys 1958; 29: 1192–3.
71. Jolley EI. The microstructure of photographic gelatin binders. Photogr Sci Eng 1970; 14: 169–77.
72. Turnbull D, Fisher JC. Rate of nucleation in condensed systems. J Chem Phys 1949; 17: 71–3.
73. Uhlmann DR, Uhlmann EV. Crystal Growth and Melting in Glass-Forming Systems, A View from 1992. In: Weinberg MC, ed., Nucleation and Crystallization in Liquids and Glasses, Vol. 30. Westerville, Ohio: American Ceramic Society, 1993.
74. Magill JH, Plazek DJ. Physical properties of aromatic hydrocarbons. II. Solidification behavior of 1,3,5-tri-a-napthylbenzene. J Chem Phys 1967; 46: 3757–69.
75. Ediger MD, Harrowell P, Yu L. Crystal growth kinetics exhibit a fragility-dependent decoupling from viscosity. J Chem Phys 2008; 128.
76. Wu T, Yu L. Origin of enhanced crystal growth kinetics near T-g probed with indomethacin polymorphs. J Phys Chem B 2006; 110: 15694–9.
77. Sun Y, Xi H, Ediger MD, Yu L. Diffusionless crystal growth from glass has precursor in equilibrium liquid. J Phys Chem B 2008; 112: 661–4.
78. Ishida H, Wu TA, Yu LA. Sudden rise of crystal growth rate of nifedipine near T-g without and with polyvinylpyrrolidone. J Pharm Sci 2007; 96: 1131–8.
79. Hikima T, Adachi Y, Hanaya M, Oguni M. Determination of potentially homogeneous-nucleation-based crystallization in o-terphernyl and an interpretation of the nucleation-enhancement mechanism. Phys Rev B 1995; 52: 3900–8.
80. Bhugra C, Shmeis R, Krill SL, Pikal MJ. Prediction of onset of crystallization from experimental relaxation times. II. Comparison between predicted and experimental onset times. J Pharm Sci 2008; 97: 455–72.
81. Wu T, Yu L. Surface crystallization of indomethacin below T-g. Pharm Res 2006; 23: 2350–5.
82. Bhugra C, Shmeis R, Pikal MJ. Role of mechanical stress in crystallization and relaxation behavior of amorphous indomethacin. J Pharm Sci 2008; 97: 4446–58.
83. Andronis V, Zografi G. Crystal nucleation and growth of indomethacin polymorphs from the amorphous state. J Non-Cryst Solids 2000; 271: 236–48.
84. Andronis V, Yoshioka M, Zografi G. Effects of sorbed water on the crystallization of indomethacin from the amorphous state. J Pharm Sci 1997; 86: 346–57.
85. Shakhtshneider TP, Danede F, Capet F, et al. Grinding of drugs with pharmaceutical excipients at cryogenic temperatures. J Therm Anal Calorim 2007; 89: 709–15.

86. Six K, Leuner C, Dressman J, et al. Thermal properties of hot-stage extrudates of itraconazole and eudragit E100 – phase separation and polymorphism. J Therm Anal Calorim 2002; 68: 591–601.
87. Greenhalgh DJ, Williams AC, Timmins P, York P. Solubility parameters as predictors of miscibility in solid dispersions. J Pharm Sci 1999; 88: 1182–90.
88. Konno H, Taylor LS. Influence of different polymers on the crystallization tendency of molecularly dispersed amorphous felodipine. J Pharm Sci 2006; 95: 2692–705.
89. Hancock BC, Zografi G. Characteristics and signficance of the amorphous state in pharmaceutical systems. J Pharm Sci 1997; 86: 1–12.
90. Gordon M, Taylor JS. Ideal co-polymers and the second order transitions of synthetic rubbers 1. Non-crystalline co-polymers. J Appl Chem 1952; 2: 493–500.
91. Tong P, Zografi G. A study of amorphous molecular dispersions of indomethacin and its sodium salt. J Pharm Sci 2001; 90: 1991–2004.
92. Aso Y, Yoshioka S, Miyazaki T, et al. Miscibility of nifedipine and hydrophilic polymers as measured by H-1-NMR spin-lattice relaxation. Chem Pharm Bul 2007; 55: 1227–31.
93. Newman A, Engers D, Bates S, et al. Characterization of amorphous drug substance: polymer mixtures using X-ray powder diffraction. J Pharm Sci 2008; 97: 4840–56.
94. Miyazaki T, Yoshioka S, Aso Y, Kojima S. Ability of polyvinylpyrrolidone and polyacrylic acid to inhibit the crystallization of amorphous acetaminophen. J Pharm Sci 2004; 93: 2710–7.
95. Konno H, Taylor LS. Ability of different polymers to inhibit the crystallization of amorphous felodipine in the presence of moisture. Pharm Res 2008; 25: 969–78.
96. Yoshioka M, Hancock BC, Zografi G. Inhibition of indomethacin crystallization in poly(vinylpyrrolidone) coprecipitates. J Pharm Sci 1995; 84: 983–6.
97. Johari GP, Astl G, Mayer E. Enthalpy relaxation of glassy water. J Chem Phys 1990; 92: 809–10.
98. Velikov V, Borick S, Angell CA. The glass transition of water, based on hyperquenching experiments. Science 2001; 294: 2335–8.
99. Taylor LS, Langkilde FW, Zografi G. Fourier transform Raman spectroscopic study of the interaction of water vapor with amorphous polymers. J Pharm Sci 2001; 90: 888–901.
100. Seow CC, Cheah PB, Chang YP. Antiplasticization by water in reduced-moisture food systems. J Food Sci 1999; 64: 576–81.
101. Andronis V, Yoshioka M, Zografi G. Effects of sorbed water on the crystallization of indomethacin from the amorphous state. J Pharm Sci 1997; 86: 346–51.
102. Makower B, Dye WB. Equilibrium moisture content and crystallization of amorphous sucrose and glucose. Agr Food Chem 1956; 4: 72–7.
103. Flory PJ. Principles of polymer chemistry. Ithaca: Cornell University Press, 1953.
104. Vrentas JS, Duda JL. Diffuson in polymer-solvent systems. 2. A predictive theory for the dependence of diffusion coefficients on temperature, concentration and molecular weight. J Polym Sci (Polymer Physics Edition) 1977; 15: 417–39.
105. Vrentas JS, Duda JL. Diffusion in polymer-solvent systems. 1. Reexamination of the free-volume theory. J Polym Sci (Polym Phys Edition) 1977; 15: 403–16.
106. Hancock BC, Zografi G. The use of solution theories for predicting water vapor absorption by amorphous pharmaceutical solids: a test of the Flory-Huggins and Vrentas models. Pharm Res 1993; 10: 1262–7.
107. Crowley KJ, Zografi G. Water vapor absorption into amorphous hydrophobic drug/poly(vinylpyrrolidone) dispersions. J Pharm Sci 2002; 91: 2150–65.
108. Zhang J, Zografi G. Water vapor absorption into amorphous sucrose-poly(vinyl pyrrolidone) and trehalose-poly(vinyl pyrrolidone) mixtures. J Pharm Sci 2001; 90: 1375–85.
109. Vrentas JS, Vrentas CM. Sorption in glassy-polymers. Macromol 1991; 24: 2404–12.

110. Oberholzer ER, Brenner GS. Cefoxitin sodium: solution and solid state chemical stability studies. J Pharm Sci 1979; 68: 836–66.
111. Yarwood R, Collett J. The influence of storage on the crystalline structure of freeze dried sodium ethacrynate. Drug Dev Ind Pharm 1985; 11: 461–72.
112. Byrn SR, Xu W, Newman AW. Chemical reactivity in solid-state pharmaceuticals: formulation implications. Adv Drug Deliver Rev 2001; 48: 115–36.
113. Shalaev E, Shalaeva M, Zografi G. The effect of disorder on the chemical reactivity of an organic solid, tetraglycine methyl ester: change of the reaction mechanism. J Pharm Sci 2002; 91: 584–93.
114. Hageman MJ. Water vapor sorption and solid state stability of proteins. In: Manning MC, ed., Stability of Protein Pharmaceuticals Part A: Chemical and Physical Pathways of Protein Degradation. New York, USA: Plenum Press, 1992: 273–309.
115. Hill JJ, Shalaev EY, Zografi G. Thermodynamic and dynamic factors involved in the stability of native protein structure in amorphous solids in relation to levels of hydration [Review]. J Pharm Sci 2005; 94: 1636–67.
116. Nail SL, Jiang S, Chongprasert S, Knopp SA. Fundamentals of freeze-drying. Pharmaceutical Biotechnology 2002; 14: 281–360.
117. Byrn SR. Solid State Chemistry of Drugs. New York: Academic Press, 1982.
118. Chieng N, Zujovic Z, Bowmaker G, Rades T, Saville D. Effect of milling conditions on the solid-state conversion of ranitidine hydrochloride form 1. Int J Pharm 2006; 327: 36.
119. Fukuoka E, Makita M, Yamamura S, Yoshihashi Y. Solid-state reaction between sulfacetamide and phthalic anhydride by grinding. Chem Pharm Bull 1994; 72: 1342–4.
120. Huttenrauch R, Fricke S, Zielke P. Mechanical activation of pharmaceutical systems. Pharm Res 1985: 302–6.
121. Waltersson J, Lundgren P. The effect of mechanical comminution on drug stability. Acta Pharm Suecica 1985; 22: 291–300.
122. Phillips AJ, Yarwood RJ, Collett JH. Thermal analysis of freeze dried products. Anal Proc 1986; 23: 394–5.
123. Strickley RG, Anderson BD. Solid-state stability of human insulin I. Mechanism and the effect of water on the kinetics of degradation in lyophiles from pH 2–5 solutions. Pharm Res 1996; 13: 1142–53.
124. Shalaev EY, Zografi G. How does residual water affect the solid-state degradation of drugs in the amorphous state? J Pharm Sci 1996; 85: 1137–41.
125. Cicerone MT, Kimbler N. Growth of dynamic heterogeneities during physical aging of high enthalpy glasses. Abstracts of Papers, 220th ACS National Meeting. Washington, DC, United States, August 20–24, 2000:PHYS-554 (2000).
126. Shamblin SL, Hancock BC, Dupuis Y, Pikal MJ. Interpretation of relaxation time constants for amorphous pharmaceutical systems. J Pharm Sci 2000; 89: 417–27.
127. Yoshioka S, Aso Y. Correlations between molecular mobility and chemical stability during storage of amorphous pharmaceuticals. J Pharm Sci 1997; 96: 960–81.
128. Cicerone MT, Soles CL. Fast dynamics and stabilization of proteins: binary glasses of trehalose and glycerol. Biophys J 2004; 86: 3836–45.
129. Cicerone MT, Soles CL, Chowdhuri Z, Pikal MJ, Chang L. Fast dynamics as a diagnostic for excipients in preservation of dried proteins. Am Pharm Rev 2005; 8: 22, 24–7.
130. Li J, Guo Y, Zografi G. Effects of a citrate buffer system on the solid-state chemical stability of lyophilized quinapril preparations. Pharm Res 2002; 19: 20–6.

Index

Note: Page numbers in *italics* indicate figures or tables.

2-[(2-nitrophenyl) amino]-3-thiophene-carbonitrile, 225–226
14 Bravais lattices, 188
^{13}C and ^{15}N SSNMR spectroscopy, 14
^{13}C and ^{23}Na MAS SSNMR spectroscopy, 426
^{13}C CP/MAS SSNMR spectroscopy, 401, 426
^{13}C SSNMR spectroscopy, 395, 400, 403, 404, 406, 413, 414, 428
4-cyanopyridine and 4,4′-biphenol, 306
5-fluorouracil, 64, 69
^{1}H SSNMR spectroscopy, 405, 406, 414
5-Methyl-2-[(2-nitrophenyl) amino]-3-thiophenecarbonitrile (ROY), 221–225
^{15}N SSNMR spectroscopy, 399, 413, 414
3-oxauracil, 68

A-/B-lattice, 189
Acetaminophen (paracetamol), 53, 331, 550
Active pharmaceutical ingredients (APIs), 76, 282, 510
Activity, 9
Allotropy, 305
α-form, 1
AMG 517, 302
Amorphization process, 523
Amorphous APIs, 82
Amorphous solids, 587–588, *588*
  chemical reactivity, 619–622, *620*, *622*
  chemical stability, 622–623
  as condensed phase, 588–589, *589*
  crystallization, 606–609, *609*, *610*
    rates, 609–611
    stabilization against, 611–612
  detection and characterization, 600–601
  different ways in which amorphous materials can be formed, 597
  examples of products containing drug substance in, 588
  factors influencing glass-forming ability, 598–600, *599*
  formation, *597*, 597–598
  glass transition, 589–591, *590*
  material and mechanical properties, 596–597
  miscibility, 612–614, *613*, *615*
  miscible solid dispersions, 614
  moisture interaction, 614–619, *616–618*
  molecular mobility, 609–611
    measurement, 603
    temperature dependence, 601–603, *602*
  solubility, 594–596, *595*, *596*
  structure and dynamics of glasses, 603–606, *604–605*
  thermodynamics, *591–593*, 591–594
  thermodynamics of moisture sorption by, 618
  water as plasticizer, 615–616
Amorphous "solubility," predictions, 594
Amorphous *vs.* crystalline solid, 588
  differences in specific volumes of, 593
  free energy of, 591
  volume, enthalpy, and entropy of, 592
Ampicillin, 49
Ampicillin trihydrate, 254
Analytical and synthetic method, 438
Anhydrous α-lactose, 520
Anti-stokes bands, 367
Antisolvent crystallization
  in pharmaceuticals, 101
Arrested crystallization, 67
Arrhenius behavior, 601
Aspirin, 53, 60
Automated parallel crystallization, *153*, *154*
  automated preparation of solutions, 155
  completeness, 156–157, *157*
  examples, 157–159, *159*, *160*, *161*, *162*
  experimental design, 154
  inducing crystallization, 156
  information management and process control, 154–155

Automated parallel crystallization (*Cont.*)
isolation of solid, 156
small-scale semi-automated crystallization, 159–161, *163*
Avrami-Erofeev model, 266
Axial glide, 191
Azlocillin sodium, 473

β-form, 1
B-relaxation process, 590
Biopharmaceuticals, 419
Body-centered-cubic cell, 189
Bragg's law, 328
Bulk drug substance, production of
examples of transformations, 514–516
solidification processing, 512–514, *515*

Caffeine and glutaric acid, 306
CalculateSimilarity, 53
Calteridol calcium, 261
Cambridge Crystallographic Database, 226
Cambridge Structural Database (CSD), 53, 235
Capillary crystallization, 120
Capillary transmission instrument geometry, 166
Carbamazepine, 142, 207–208, 246, 268, 290–297, 448, 527
Cephradine, 250
Channel hydrates, 250
Chasing equilibrium method, 438
Chiral resolution, 289
Chirality in crystal, existence of, 561
Chloramphenicol palmitate, 471
Chlorpropamide polymorphs, 547
Cilansetron hydrochloride, 252
Circular dichroism spectroscopy, 571
Clausius–Clapeyron equation, 29, 30, 31, 33, 35, 323, 542
Co-crystal former, 286
Co-crystal preparation, 123
grinding, 109–113
Köfler mixed fusion method, 108
solution crystallization, 113
Co-crystals, 81, 283–284, 287
advantages, 82
applications, 289–291
design, 286–288, *287*
history, 284–285, *285*
history of pharmaceutical, 286, *287*
pharmaceutical, 283
preparation, *288*, 288–289
relevance, 289–291, *290*
Co-crystals and pharmaceutical co-crystals, polymorphism in
4-cyanopyridine and 4,4′-biphenol, 306, *307*
caffeine and glutaric acid, 306, *307*
hydroquinone/*p*-benzoquinone, 307–308, *308*
N,*N-bis* (4-bromophenyl) melamine and 5,5-diethylbarbituric acid, 308, *309*
oxalic acid and iso-nicotinamide, 308–310, *309*
Comminution, 514, 516, 598
Compack methodology, 53
Compaction, 540
Compaction-induced transformations, 546
Complex crystal energy landscape, 69–70
Complexes, 285
Component, 25
Compression, effects due to, 540
Compression effects
effects of crystal forms, 549–551, *550*
hydrostatic stress states, 540–544, *541*, *543*
phase transformations, *548*, 548–549
shear-based mechanisms, *544–545*, 544–548, *547*
Compressive deformation, 550
Computational method, 52
errors in crystal structure, 57
Concomitant crystallization, 18
Concomitant polymorphs, 18
Condensed transition point, 32, 36
"Conditioning" of glass, 604
Conditions, 4
Conformational polymorphism, 199, 210, 330, 398, 481
Conglomerate materials, racemic mixtures of, 574
Conglomerate solids, 571
Conglomerate systems, characterization of, 573
Conglomerates, 570–571, 571
Continuous-flow methods, 461
Cooling crystallization, 90
advantages, 89
metastable zone, 90, *91*
principles, 89
unstable polymorphs, 92, *93*
Copper chloride dihydrate, 42
CP/MAS, 395, 398
Crashing out, 102
Crissy platform, 158
Critical nucleus, 15
Cromolyn, 257
Cryogenic grinding, 112
Cryogenic milling, 520

Cryohydric point, 238
Crystal, elastic *vs.* plastic deformation, 518
Crystal classes, 186, *187*
Crystal energies, calculation of
  free energies and other properties, 63–64
  lattice energy evaluation
    electronic structure modelling, 58–59, *59*
    force fields, 59–60
    monomer + model, *59*, 60–63, *61*
Crystal energy landscapes, 67, 141
  complex, *68*, 69–70
  disorder, 70–71
  interchangeable, *68*, 70–71
  monomorphic, 67–68, *68*
  predictive, *68*, 69
Crystal engineering, 288
Crystal growth, 608
Crystal structure, lattice theory of
  14 Bravais lattices, 187–189, *190*
  230 space groups, 189–192
  unit cell, 186, *187*
    symmetry operations, 186–187
Crystal structure modelling, 57
  force fields, 59
  induction energy, 61–62
  lattice energy, 59
Crystal structure prediction (CSP), 64–67, *66*, 141
Crystal structures
  chirality classification of, 562
  spheres of differing sizes, 194–195, *195*
  spheres of equivalent size, 192–194, *193*
Crystalline conglomerate
  portion of melting point phase diagram obtained for, 574
Crystalline phase, solubility of, 594
Crystalline quartz, 564
Crystallization, 512
Crystallization and polymorphic transformation methods
  capillary crystallization, 120
  desolvation of hydrates and solvatomorphs, 118–119
  slurrying, 116–117
  thermal methods, 113–116, *114*
  ultrasound, 119–120
  use of additives, 117–118
Crystallization from melts, 107–109
Crystallization from solution
  antisolvent, *101*, 101–106, *104–105*
  cooling, 89–93, *90–93*
  evaporative, *100*, 100–101
  functions, 89
  principles, 88–89
  reactive, *106*, 106–107
  seeded, 96–100, *98*
  solvent effects, 93–96, *95*, *97*, *98*
Crystallization methods, 87, 88, 141, 142–144
Crystallographic characterization techniques, 318, 327–328, *328*
  crystal structures determination, 338–339
  single-crystal XRD, 328–333, *329*, *330*, *332*, *333*
  VT-XRD, 339–342, *340*, *341*
  X-ray powder diffractometry, 333–338, *335*, *337*, *339*
Crystallographic space group, 189
CrystalMax platform, 157
Cubic close packing, 192, *193*

Dauphiné twin, 564
Deformation, applied stress state, 518
Deformation-dependent dislocation-mediated model, 520
Degree of crystallinity, 338
Degrees of freedom, 25
Dehydration kinetics, 264, 266
Dehydration process, 266
Deliquescence, 43
Density functional theory, 58
Density Rule, 14
Derivatization, desirable effect of, 576
Design of Experiments (DOE) approaches, 154
Desolvated solvates, 44, 118
Desolvation, 521
Desolvation and dehydration phenomena
  dehydration and hydrate class, 264–265, *266*
  particle size and crystal morphology, 265–267
Desolvation of solvatomorphs, 118
Deviatoric component, 518
Diagonal glide, 191
Diamond anvil sample cells, 543
Diamond glide, 191
Diastereomer species, 575
Diastereomer system
  chiral discrimination existing in, 577
  solubility phase diagram reported for, 576
Diastereomeric salts
  hydrogen bonding existing in crystals of, 578
Diastereomers, 560
Dielectric relaxation processes, 621
Differential scanning calorimetry, 13, 109, 114, 205, 319, 591, 600
  limitation, 323

Diffraction amorphous, 166
Diffraction of X rays, 328
Diffraction pattern quality, 167
Diffuse reflectance sampling, 359
Diffusion, 87–88
Diffusion layer theory, 461
Dimorphism, 1
  of benzamide, 305
Dipolar coupling, 385
Direct polarization 13 C MAS, 425
Disappearing polymorphs, 77, 99
Dislocation density, 519
Dislocations, 518
Dissociation pressure, 42
Dissolution rate of solid, 461
Dissolution rates, 460
  applications, 462–466, *463–466*
  determination, 462
  factors affecting, 461–462
  intrinsic, 466–470, *468–469*, *471*
Dissymmetry, 561, 564, 565
Droloxifene citrate, 121
Drug product viability and stability
  effects of processing, 510–511
Drug products, impact of form
    changes on, 511
Drug substance development stream, 512
Drying
  effects, 530
  effects of drying methods on form changes
    of theophylline, 533
Drying effects
  collapse to amorphous solids, 535–536
  conventional methods, 530–532, *531*, *532*
  dehydration and desolvation, 533–535,
    534, *536*
  kinetic trapping of metastable polymorphs,
    532–533
  lyophilization, 538–540
  spray drying, 536–538, *537*

Electronic structure methods, 58–59
Electrostatic model, 60
Enantiomer
  and racemate crystal structures, 561–562
Enantiomer separation, 571
  classical technique (Pasteur), 571
  localized crystallization from racemic,
    supersaturated solution, 571
  resolution by entrainment, 571–572
Enantiomers, 560
  solubilities of, and racemic mixtures of
    conglomerate materials, 574
Enantiotropy, 11, 94, 482
Enantiotropy and monotropy, 10–15, *11–12*, *13*,
    37, 37–39, *38*, 196
Endothermic reaction, 5
Energy, 3
Enthalpy, 5
Enthalpy of formation, 6
Enthalpy of reaction, 5
Enthalpy of vaporization, 6
Entropy, 6, 542
  transition, 542
Entropy of Fusion Rule, 14
Epitaxial crystallization, 19
Equation of state, 4
Equilibrium, 26
Equilibrium solubility, 46
  determination, 437–438
  metastable solubility, 439–440, *441*
  polymorphic systems, 440–445, *441–443*,
    445–448
  solvate phases, 445–452, *449–450*, *451*, *452*
Equilibrium theory, 499
Equilibrium thermodynamics of stoichiometric
    hydrates, 238
Erythromycin, 473
Erythromycin A
  crystal structure, 247
Essential space group operations, 191
Ethambutol dihydrochloride, 405
Eutectic, 46
Evaporative crystallization, 100, *100*, 151
Exothermic reaction, 5
Exp-6 model, 59
Experimental space, 142, *143*
Extensive/intensive properties, 4

F-lattice, 189
Far-infrared spectroscopy, 365
Feed-forward drug product development
    scheme, 510
Finite stress element, 517
First law of thermodynamics, 4, 452
Flory–Huggins theory, 618
Flufenamic acid, 217–218
Fluidized-bed drying processes, 530, 531
  two-stage model of, 532
Fluoxetine HCl, 297–299
Fluprednisolone, 472
Force fields, 59–60
Fossil relic, 69
Fragile behavior, 601
Free energy, 6–7
Freezing point, 46
FTIR spectrometers, 357, 359, 360
FTIR–ATR spectroscopy, 359

Fugacity, 9
Fundamental vibrational transition, 351
Fusion curve, 31

Gas Antisolvent Crystallization (GAS)
  operating principle, 105
Gauche conformation, 201
Generally regarded as safe (GRAS)
    compounds, 286
Gibbs Phase Rule, 90
Glass-crystal (GC) growth, 609
Glass formation, 590. *See also* Vitrification
Glass transition
  dependence on cooling rate, 590
  enthalpy and heat capacity in
    region of, 593
Glass transition, 589–590
Glass transition temperature, 521
  experiments of materials milled
    above, 521
Glide plane, 191
Glide/screw operations, 191
Global optimization strategies, 171–172
Gordon–Taylor equation, 127
Granulation methods
  dry, 524–525, *525*
  wet, 525–526, *526*
    PAT application, 528–530
    spontaneous hydration, 526–528
Granulation step, 524
Green chemistry approaches, 289
Grinding, 109, 111
Group frequencies, 353

Harmonic model, 64
Harmonic oscillator model, 352, 362, 367
Hartree–Fock approximation, 58
Heat of Fusion Rule, 13
Heat of Transition Rule, 13, 492
Heteromolecular crystals, 285
Hexagonal close packing, 192
High-throughput crystallization,
    139–140, *141*
Hoffman equation, 595
Homogeneous nucleation, 513
Homogeneous nucleation from
    recrystallization, 513
Hooke's Law system, 517
Hotstage microscopy (HSM), 318, 326–327
  advantages, 326
Hydrates
  channel, 253–259, *254*, *256*, *258–259*
  isolated site, 250–253, *251–253*
  metal ion-associated, 259–263, *260–262*
Hydration/dehydration
  structural aspects, 263
Hydrostatic component, 518
Hydrostatic pressure, 540
Hygroscopicity, 127
Hyper-DSC®, 321

Ibuprofen, 257
  physical and structural properties of,
    579–581
Infrared absorption process, 368
Infrared absorption spectroscopy, 337, 347,
    357–361
Internal energy, 4
International Committee of Harmonization
    ICH), 381
Intramolecular dispersion, 63
Iodoanilinium picrate, 202–204
Isedronate, 259
Isolated site hydrates, 250
Isomorphism, 305
Isothermal thermogravimetric analysis, 263
Isotopic labeling, 410
Isotopomeric polymorphism, 412
Itraconazole, 299–300

Kauzmann temperature, 594, 603
Kinetically impaired equilibria
  pressure–temperature relations, 40–41
  suspended phase transformations, 39–40
Kohlrausch–Williams–Watt (KWW)
    equation, 605

Labile zone, 500
Lattice, 186
Lattice energy, 58
Lattice translation operation, 186
Law of Definite Proportions, 25
Law of Stages, 18
Le Chatelier's Principle, 29, 30, 31, 34, 453
Light-scattering method, 440
Linear elastic fracture mechanics (*LEFM*), 517
Liquid/solid dosing, 155, 158
Liquid-state NMR spectroscopy, 388, 397,
    400, 421
Liquidus line of phase diagram, 573
Lomeridine dihydrochloride, 218–220
Low-temperature form, 243
Lyophilization, 538–540

Machine imaging systems, 163
Magic angle spinning (MAS), 391
Magnetogyric ratio, 384
Mannitol, 538

Martensitic transformation, 544, 546
  energy change associated with, 545
  geometry of, 545
Mechanochemical methods, 109–113, *110*
Mechanochemistry, 113
  and process-induced transformations, 512
Melamine and cyanuric acid, 304–305
Melt crystallization, 107
  principles, 108
Melt-quench hypothesis for milling-induced amorphization, 520
Melting points, 32
Meso -tartaric acid structures, 568
Metal ion-associated hydrates, 250
Metastable polymorphs, 20, 21
Metastable zone, 19, 500
Metastable zone width (MZW), 90, 91
Meyerhoffer states, rule of, 573
Milling, 516
  polymorphism and amorphization induced by, 522
Modulated DSC (MDSC), 320–321
Molar differential heat of dilution, 453
Molar differential heat of solution, 453
Molar integral heat of solution, 453
Molar latent heat of fusion, 455
Molecular dissymmetry
  structural aspects, 560–561
  and tartrate crystals, 564–570, *567*, *568*, *570*
Molecular Dynamics simulations, 64, 69
Molecular polymorphism, 398
Mometasone furoate, 255
Monomer + model approach, 58, 60–63
Monomorphic crystal energy landscape, 67–68
Monotropy, 11, 38, 482
  phase diagram, 38
Multiple-primitive unit cells, 188
Multivariate analysis, 156, 164

Near infrared (NIR) spectroscopy, 272, 505
Nedocromil, 260
Nifedipine form II, 404
NIR spectroscopy, 361–364
NIST SRM 674b, 336
Nitrofurantoin, 205–206
Nitrofurantoin, transformation kinetics for, 529
NMR spectroscopy, 382–388, *383*, *384*, *386*, *387*
N,*N*-*bis* (4-bromophenyl) melamine and 5,5-diethylbarbituric acid, 308
Non-covalent derivatization, 289
Non-ergodic glass, 593
Non-essential space group operations, 191
Non-stoichiometric solvatomorphs, 233
Non-superimposable hemihedral crystal faces, *563*, 563–564, *565*
Noyes–Whitney equation, 461
Nuclear quadrupolar resonance (NQR) spectroscopy, 417
Nucleation, 117
  and crystal growth, 15–19, *17*
  process, 512
  theory, 15, 608

Olanzapine, 251
On-line Raman spectroscopy, 528
Optical microscopy, 162
Ordinary transition point, 8
Organic molecular compounds, 285
Organic molecule solvates
  channel-type, 246–249, *248*
  discrete position, 244–246, *245*
Ostwald ripening, 18
Ostwald's Rule of Stages, 515
Oxalic acid and isonicotinamide, 308

P-lattice, 188
P-methyl-*N*-(*p*-methylbenzylidine) aniline, 212–213
P-(*N*-chlorobenzylidene)-*p* -chloroaniline, 210–212
P-salts, 576
Packing coefficient, 562
Packing polymorphism, 199, 329, 398, 481
Paracetamol, 208. *See* Acetaminophen (paracetamol)
  crystalline forms, 244
  monoclinic polymorph, 20
Paracetamol (Acetaminophen), 208–209
Parallel crystallization, 176
Particle size analysis, 267
Particle size reduction, effects of
  glass transition temperature, 521, *521*
  phase transformations, 521–524, *522*, *524*
  shear stress, *517*, 517–520
  temperature accumulation, 520
Pasteur crystallization, 289
Pawley fit, 71, 168
PCA analysis, 164
Perfect solutions, 454
PH alteration, 107
Pharmaceutical co-crystals, 283–284
Pharmaceutical co-crystals (case studies)
  2-[4-(4-Chloro-2-fluorophenoxy)phenyl] pyrimidine-4-carboxamide (SCB), 301–302, *301–302*
  AMG 517, 302–303, *303*
  carbamazepine (Tegretol®), *292*, *293*
    isonicotinamide, 296–297, *297*, *298*

nicotinamide, 292–295, *293–295*
polymorphs, 296, *297*
saccharin, *295*, 295–296
fluoxetine hydrochloride (Prozacâ), 297–299, *299*
history, 286
itraconazole (Sporanox®), 299–300, *300*
melamine and cyanuric acid, *304*, 304–305
sildenafil (Viagra®), 300–301, *301*
Phase rule, 24, 26–27
components, 25
degrees of freedom, 25–26
phases, 25
Phase transitions
second phase
solution-mediated, 499–504, *502*
single phase
dehydration and desolvation, 496–499, *497*
solid-to-solid, 493–496, *495*
thermodynamics, 486–492, *488–489*
vapor sorption, 504–506
Phases, comparison of molecular order, specific volume, and molecular mobility, 589
Phenylbutazone
crystal structures, 246
Physical form, 318
Physical form diversity
automated parallel crystallization, 144–148, *145*, *146–147*, *148*
crystallization methods, 142–144
maximizing number, 142, *143*
solution crystallization
agitation, 152
anti-solvent addition, 152
desolvation of solvates, 152–153
evaporation, 151–152
solvent and solvent selection, 148–150, *149*, *150*
supersaturation, 150–151
suspensions, 152
temperature, 151
time scales and rate of crystallization, 151
use of additives, 152
Physical form screening, *164*
crystal packing analysis, 176
microscopy and imaging, 162–163
physicochemical characterization, 176
Raman spectroscopy, 163–164
single crystal diffraction, 174–176
XRPD
instrumentation, 165–166, *166*
sample characterization, 166–167, *168*, *169*
sample identification, 167
SDPD, 170–171, *171*
SDPD using global optimization, *171*, 171–174, *172*, *173*
variable temperature, 174, *175*
vs. single-crystal structure, 167–170, *170*
Planar hydrates, 199
Plane-polarized light microscopy, 162–163
Plastic constraint, 524
Plasticizer, 615, 617
Polarization, 61
Polymorph screening, 89, 94, 100
antisolvent addition, 104
Polymorphic systems, *2*, *3*
thermodynamics, 3–10, *7*, *8*
Polymorphism, 1, 76, 233, 305, 318
acetaminophen, 53, *54*
aspirin, 53, *55*, 60
eniluracil, 53, *56*, 70
Polymorphism, structural theory of
related lattices, 197–198
unrelated lattices, 196–197
Polymorphism and solvate formation, 470–473, *472*
Polymorphism in molecular crystals
different molecular conformations
5-Methyl-2-[(2-nitrophenyl)amino]-3-thiophenecarbonitrile (ROY), 221–224, *222*, *223*, *225*, *226*
flufenamic acid, 217–218, *219*
lomeridine dihydrochloride, 218–220, *219*, *220*
p-methyl-N-(p-methylbenzylidine) aniline, 212–213, *213*
p-(N-chlorobenzylidene)-p-chloroaniline, 210–212, *211*, *212*
probucol, 213–215, *214*, *215*
spironolactone, *216*, 216–217
other conformational polymorphic systems, 224–226
similar molecular conformations
carbamazepine, *207*, 207–208
iodoanilinium picrate, *202*, 202–204, *203*
nitrofurantoin, 205–206, *206*
paracetamol, *208*, 208–209
resorcinol, 199–200, *200*
sulfamerazine, 200–201, *201*
sulfathiazole, 204–205, *205*
Polymorphs, 53, 67, 76
different physical properties, 2, *3*
disappearing and reappearing, 19–21, 225
ground-state, 76–77

Polymorphs and solvatomorphs characterization
infrared absorption spectroscopy, 357–361, *358*, *361*
NIR spectroscopy, 361–364, *363*
Raman spectroscopy, 366–373, *369*, *370*, *373*
terahertz spectroscopy, 364–366, *365*
PolySNAP, 167
Poly(vinylpyrrolidone) (PVP), 598
Position-sensitive detectors (PSD), 165
Potential energy, 3
Potentiometric titration method, 438
Predictive energy landscape, 69
Pressure DSC (PDSC), 323
Pressure *vs.* stress, 540
Probucol, 213–215
Process analytical technology (PAT) research, 516
Profile-fitting analysis, 337
Progressive defect accumulation method, 523
Prohibitive value, for molecular crystals, 519
"Pseudo" second-order phase change, 592
Pseudopolymorphism, 1

Quartz crystal, morphology of, 563
Quartz crystals, twinned, 564
Quinhydrone, 307–308

Racemates, 571, 575
alter crystallization thermodynamics of, 571, 575
of ibuprofen, 579
Racemic acid, 565–566
Racemic mixture, 560–561
Racemic mixtures, physical characteristics of, *574*
conglomerate systems, 571–575, *574*
racemate systems, 575–582, *576*, *578*, *580*, *581–582*
Racemic solids, stability of, 572
Raffinose pentahydrate, 535
single-crystal structure of, 536
Raman microprobe systems, 164
Raman spectroscopy, 163, 272, 366–373, 372, 496
advantages, 163–164
Reaction crystallization, 106, 293
Recrystallization, 512–513
bulk API manufacturing beyond, 514
of glycine, 532
yeilding, undesirable solvatomorphs, 516
Reflection geometry, 165
Relative humidity, 240
Relaxation time constant, 601
Resolution by entrainment, 571–572
Resolution procedure, 575
Resolved shear stress, 550
Resorcinol, 199–200
Rietveld refinement, 168, 174
Ritonavir, 514
(R,S)-Ibuprofen
crystallographic data for, 580
X-ray powder diffraction patterns obtained for tromethamine salts, 581
(R,S)-ibuprofen
infrared absorption and Raman spectra of tromethamine salts with, 582
Rule of stages, 78, 305

(S)-ibuprofen
crystal structures of, 580
crystallographic data for, 580
infrared absorption and Raman spectra of tromethamine salts with, 582
X-ray powder diffraction patterns obtained for tromethamine salts, 581
Salt formers, 286
Salt preparation and screening, 122–123
Scalar coupling/J-coupling, 385
Schmid's law, 549
Screw axis, 191
Screw operation, 191
Seed crystals *vs.* direct pharmaceutical drug substance manufacturing, 513
Seeding crystallization, 96
disappearing polymorphs, 99
principles, 99
product size distributions, 98–99
Seeding techniques, 19, 20
Separated enantiomers
solubilities of, and racemic mixtures of conglomerate materials, 574
Shear-based mechanisms, 544
Shear-based transformation mechanisms, 544–548
Sildenafil, 300–301
Sildenafil citrate, 286
Single-crystal diffraction, 172
Single-crystal structure determination, 172–173
Single-crystal XRD, 102, 174, 328, 331, 332
Six crystal systems, 327, *328*
Slurrying, 116
competitive, 117
unseeded, 116–117
Sodium ammonium tartrate, crystals of, 570
Sodium channel blocker, 301–302

Solid drug products, performance of, 511
Solid form changes
  sources of, 511
Solid-form characterization, 398–417, *401–404*, *406–408*, *410–412*, *415–416*
Solid forms
  characteristics, 76–87, *78–86*
  methods for producing, 87–88, *88*
    crystallization, 87
  preparation
    co-crystals, 123
    salts, 122–123, *124*
    solvatomorphs, 120–122
    and stabilization of amorphous forms, 123–130, *126–130*
Solid phases, 482
Solid-state fluorescence spectroscopy, 265
Solid-state NMR spectroscopy, 381, 388–398, *389–394*, *396*, 603
  advantages and disadvantages, *383*
  applications, 426–429
  biopharmaceuticals, 419–421, *424*, *425*
  quadrupolar nuclei, 417
  quantification, 421–426, *426*
  structure determination, 417–419, *419–423*
Solid-state phase transformations, 481–486, *483–487*
Solid-state polymorphism, 34
Solid-state polymorphism and phase rule
  condensed transition point, 35–36, *36*
  enantiotropy and monotropy, 37–39
  transition point, 34–35, *35*
Solid-state synthesis, 289
Solid–liquid–solid phase transformation, 241
Solubility, 46, 437
Solubility Rule, 14
Solution calorimetry
  applications, 458–460, *459*, *460*
  enthalpies of solution, 453–454
  methodology, 457–458
  partial molar quantities principles, 454–457, *456*
Solution-mediated phase transformations, 268
Solvates, 78, *78*
Solvatomorphic systems, 237
  structural aspects of, *236*, *237*
  thermodynamics of, 237–243, *239*, *240*, *242*
Solvatomorphism, 2, 41, 233
Solvatomorphs, 78, 79, 233, 318
  of organic solvents, 233–234
  relative stabilities, 241
Solvatomorphs, behavior of
  kinetics of transformation, 276
  processing induced transitions, 267–268
    particle size reduction, 269–271, *270*
    solution-mediated transformations, 268–269, *269*
    wet granulation and subsequent drying, 271–273, *273*
  transitions in final product, 273–275, *275*
Solvent-drop grinding, 109, *110*, 123, 289
Solvent effects
  polymorph selection, 94–96
Solvent-mediated transformation, 99
Space-filling model, 57
Space group, 189.
    See also Crystallographic space group
Space group symmetry operations, 191
SpecScreen xHTS system, 158
Sphere packing model, 192
Spironolactone, 216–217
Spray drying, 536–538
  advantage, 536
Stable and metastable polymorphs, 20
Stacked sheets, 308
Standard Reference Materials (SRMs), 319
Stoichiometric solvatomorphs, 233
Stokes bands, 367
Structural relaxation, 592–593, 603
Structure comparison tools, 52–56, *54–56*
Structure determination from powder data (SDPD) methods, 166
Sublimation, 115
Sublimation curve, 29
Sulfamerazine, 200–201, 515
Sulfamethoxydiazine, 471
Sulfathiazole, 204–205, 245
Supercooled liquid, 593
Supramolecular heterosynthons, 288
Supramolecular synthons, 288
Suspended phase transformations, 39
Symmetry element, 187, 561
Symmetry operations, 187
Systems of one component, 45
  characteristics of univariant systems
    liquid/vapor equilibria, *28*, 28–29
    solid/liquid equilibria, 30–32, *31*
    solid/vapor equilibria, 29–30, *30*
  triple points, 32–34, *33*
Systems of two components
  kinetically impaired equilibria, 47–49
  solid/liquid/vapor equilibria, 45
  solid/solution equilibria, 45–47, *47*, *48*
  solid/vapor equilibria
    desolvated solvates, 44–45
    multiple solvation state systems, 43–44, *44*
    single solvation state systems, *42*, 42–43

Tableting, polymorphism induced during, 548
Tartaric acid, 566
  crystals of, 567
Temperature, 4
Terahertz spectroscopy, 364–366
Theophylline monohydrate dehydration, 265, 274
Thermal analysis, 318
Thermal fusion methods, 108
Thermal history, 604
Thermoanalytical techniques, 318
  DSC, 319–324, *320*, *321*, *322*, *324*
  hot-stage microscopy, *326*, 326–327
  thermogravimetry, 324–326, *325*
Thermochemistry, 5
Thermocycling, 116
Thermodynamically stable polymorph, identification, 511
Thermodynamics of moisture sorption, 618
Thermogravimetric analysis (TGA), 318
Thermogravimetry, 324
Thiazide diuretic compound hydrochlorothiazide, 245–246
Third Law of Thermodynamics, 486
Top-spray fluidized bed granulation, 526
Top-spray high-shear granulation, 526
Topetecan hydrochloride, 256
Total side band suppression (TOSS), 391
Transformation, extent of, depending factors, 511
Transition entropy, 542
Transition point, 32, 34
Transition temperature, 243. *See also* Low-temperature form
Tray drying, 530, 531
Triamcinolone diacetate, 247
Triclinic *meso* -tartaric acid structures, 568
Trihydrate, 49
Triple point, 32, 33
Tromethamine, 581
Tromethamine salts
  IR absorption and Raman spectra with (S)-ibuprofen and (R,S)-ibuprofen, 582
  XRPD patterns obtained with (S)-ibuprofen and (R, S)-ibuprofen, 581
TRPV1, 302
True solvates, 78, 79
Twinned quartz crystals, 564

Unit cell, 186
Unit cell parameters, *2*
Univariant system, 26, 45

Vaccine, impact of drying on the physicochemical properties, 539
Van't Hoff equation, 491
Vapor pressure of hydrate, 238
Vaporization curve, 28
Variable-temperature X-ray diffractometry, 339–342
Variance, 26
Vibrational modes, 347, 349
Vibrational spectroscopy
  anharmonic oscillator model, 353–357, *356*
  harmonic oscillator model, 349–353, *354*
  motion of atoms in molecules, 348–349, *349*
Viscoelastic, 596
Vitrification, 590

Wallach's rule, 562
Water, 234
Wet granulation, 271
Work function, 6

X-ray amorphous, 600
X-ray crystallography, 1
X-ray powder diffractometry (XRD), 164–165, 333–338, 499, 503, 520, 600
  applications, 327
  polymorphs and solvatomorphs, 327
  profile-fitting analysis, 337
  protocol, 336–337
  sample analysis, 165
X-rays, 185
Xpac methodology, 54
XRPD, 549

Pharmaceutical Science and Technology

about the book...

Using clear and practical examples, ***Polymorphism in Pharmaceutical Solids, Second Edition*** presents a complete examination of polymorphic behavior in pharmaceutical development.

Ideal for pharmaceutical development scientists and graduate students in pharmaceutical science, this updated edition includes:

- **new chapters**—on the latest developments and methods in the field that give pharmaceutical development scientists the up-to-date information they need to successfully implement new drug development techniques and methods
- **expert editorship**—from Dr. Harry G. Brittain, whose vast experience and knowledge of the pharmaceutical industry provides readers with the authoritative advice they need and trust
- **comprehensive content**—that includes information appropriate for all levels of expertise in the field, from experienced pharmaceutical scientists to graduate students in physical pharmacy
- **200 high quality illustrations**—that present readers with a visual blueprint to the methods and techniques involved in polymorphism and solvatomorphism

about the editor...

HARRY G. BRITTAIN is Institute Director, Center for Pharmaceutical Physics, Milford, New Jersey, USA. Dr. Brittain's former positions include Vice President for Pharmaceutical Development at Discovery Laboratories, Inc. and Director of Pharmaceutical Development at Ohmeda, Inc. He has also held faculty positions at Ferrum College and Seton Hall University, and has served as Adjunct Professor at Rutgers University and Lehigh University. He has authored more than 300 research publications and book chapters, and has presented numerous invited lectures and short courses in pharmaceutics. Dr. Brittain is Associate Editor for the *Journal of Pharmaceutical Sciences* and serves on the editorial boards of *Pharmaceutical Research* and *AAPS PharmSciTech.* He is also Editor for the book series *Profiles of Drug Substances, Excipients, and Related Technology.* Dr. Brittain is Fellow of the American Association of Pharmaceutical Scientists and presently serves as Chairman of the United States Pharmacopeia expert committee on Excipient Monograph Content. He is also on the Organic and Pharmaceutical subcommittee of the International Centre for Diffraction data.

Printed in the United States of America

H7321

ISBN 978-142007321-8

90003

9 781420 073218

informa
healthcare
www.informahealthcare.com

52 Vanderbilt Avenue
New York, NY 10017

Telephone House
69-77 Paul Street
London EC2A 4LQ, UK